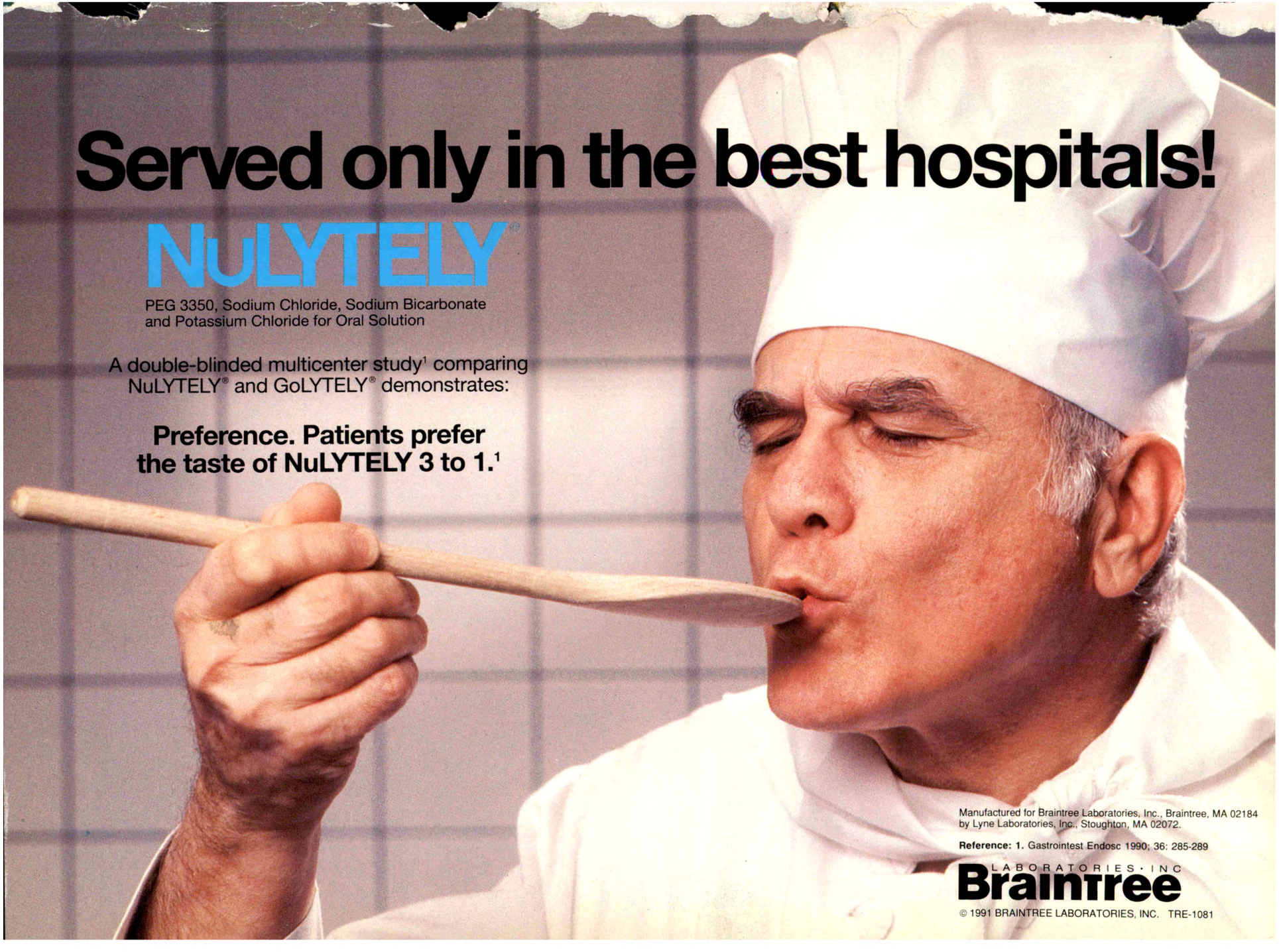
ank-HS1755-36-P0244169
12 11/92
112
V.36
36

AJR

American
Journal of
Roentgenology

September 1991


Served only in the best hospitals!
NuLYTELY®
PEG 3350, Sodium Chloride, Sodium Bicarbonate
and Potassium Chloride for Oral Solution
A double-blinded multicenter study[1] comparing
NuLYTELY® and GoLYTELY® demonstrates:
Preference. Patients prefer
the taste of NuLYTELY 3 to 1.[1]
Manufactured for Braintree Laboratories, Inc., Braintree, MA 02184
by Lyne Laboratories, Inc., Stoughton, MA 02072.
Reference: 1. Gastrointest Endosc 1990; 36: 285-289
LABORATORIES · INC
Braintree
© 1991 BRAINTREE LABORATORIES, INC. TRE-1081

Official Journal of the American Roentgen Ray Society

AJR

American Journal of Roentgenology
Diagnostic Imaging and Related Sciences

Editor-In-Chief	Robert N. Berk, *La Jolla, California* *University of California, San Diego* *School of Medicine and Medical Center*
Editor Emeritus	Melvin M. Figley, *Seattle, Washington*
Associate Editor	Karim Valji, *San Diego, California*
Consulting Editor	Michael S. Huckman, *Chicago, Illinois*
Statistician	Charles C. Berry, *San Diego, California*

P 24469

Editorial Board

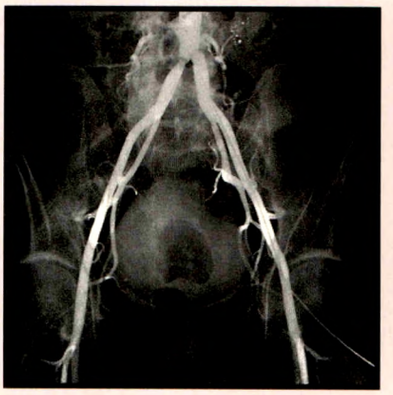
John R. Amberg	John R. Hesselink	Peter M. Ronai
Ithamar Aviad	Charles B. Higgins	Sjef H. J. Ruijs
Mark E. Baker	Melvyn T. Korobkin	Stuart S. Sagel
Lawrence W. Bassett	Faye C. Laing	David J. Sartoris
Michael A. Bettmann	Thomas L. Lawson	Stefan C. Schatzki
Felix S. Chew	Robert G. Levitt	William P. Shuman
N. Reed Dunnick	Bruce L. McClennan	Edward A. Sickles
David K. Edwards	Richard P. Moser	Barry A. Siegel
Ronald G. Evens	Albert A. Moss	David D. Stark
David S. Feigin	Jeffrey H. Newhouse	Edward T. Stewart
Sandra K. Fernbach	Donald L. Resnick	Murali Sundaram
Richard H. Gold	Stewart R. Reuter	Eric vanSonnenberg
William R. Hendee	Charles A. Rohrmann, Jr.	Robert K. Zeman

Editorial Staff: Margaret Levene, *managing editor*; Katie L. Spiller, Barbara Rose, Barbara L. Halliburton, and Janine Anderson, *manuscript editors*; Nancy Rydbeck, *office manager*; Sheri Smith, *administrative assistant*; Linda J. Waggoner, *administrative secretary*

AJR, AMERICAN JOURNAL OF ROENTGENOLOGY (ISSN 0361 803X) is the official journal of the American Roentgen Ray Society and is published monthly by Williams & Wilkins, 428 E. Preston St., Baltimore, MD 21202. Annual dues include $50 for journal subscription. Second-class postage paid at Baltimore, MD, and at additional mailing offices. Postmaster, send address changes (Form 3579) to AJR, 428 E. Preston St., Baltimore, MD 21202. Subscription rates $125 ($180 foreign); institutions $135 ($190 foreign); in training $25 ($80 foreign); single copy $18 ($22 foreign). The GST number for Canadian subscribers is 123394371. Airmail rates furnished on request. Indexed by *Current Contents* and *Index Medicus*. Copyright © 1991 by American Roentgen Ray Society.
0361–803X/90$3.00

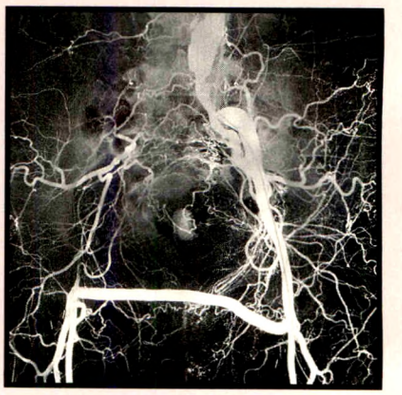
EGLESTON LIBRARY

The Comfortable Choice for Angiography









Gundersen Clinic: Because where you practice is as important as what you practice.

The Gundersen tradition: state-of-the-art medical care delivered by a highly qualified group of medical and dental specialists. And what sets our professionals apart from other medical staffs? Teamwork.

We are seeking General Radiologists to join our staff of 17 Radiologists who provide outreach services to those patients who visit our multiple branch community clinics in Iowa, Minnesota and Wisconsin, as well as provide care to patients in our full service main clinic in La Crosse. Last year, 139,412 radiographic examinations were performed throughout our system. It's the best of both worlds where you can combine sophisticated technology with one-on-one involvement in primary care.

Become part of the Gundersen tradition as we enter our second century serving the needs of 70,000 families through over 702,000 patient visits each year. You'll also enjoy an outstanding quality of life, competitive salaries and benefits, an excellent continuing education program and pension plan. Send your CV or **call Tim Skinner, Manager, Physician Recruitment, COLLECT, at 1-608-782-7300 ext. 6673.** An equal opportunity employer.

1891 - 1991

Gundersen Clinic, Ltd.

1836 South Avenue
Dept. KK-9
La Crosse, Wisconsin 54601

Duke University

Staff Radiologists

DUKE UNIVERSITY MEDICAL CENTER is seeking qualified candidates for staff positions in the Department of Diagnostic Radiology. Currently there are a limited number of staff positions available in the following sections: General Diagnostic Radiology, Pediatric Radiology, Chest Radiology, Musculoskeletal Radiology, Vascular - Interventional.

We offer an excellent salary and benefits package. The Radiology department is state-of-the-art in diagnostic imaging with diverse resources available for clinical, teaching, and academic pursuits. Staff members have guaranteed academic time and research support. Interested Board Certified Radiologists with appropriate experience should submit letters of inquiry to Office of the Chairman, Department of Radiology, Box 3808, Duke University Medical Center, Erwin Road, Durham, North Carolina 27710.

NEURORADIOLOGIST

Temple University Hospital and School of Medicine is searching for a third Neuroradiologist at the rank of Assistant Professor. The candidate should have fellowship training in Neuroradiology, be board-certified, qualify for senior membership in the Society of Neuroradiology, and have experience in invasive neuroradiology procedures. Candidate should have skills in resident and medical student teaching as well as in patient care. A candidate with a research background is preferable.

The Department is currently adding two new CT scanners and a state of the art 1.5 tesla MRI unit. An excellent angiographic facility is also available.

Candidates should contact **Francis J. Shea, M.D., Professor & Acting Chairperson, Department of Diagnostic Imaging, TEMPLE UNIVERSITY SCHOOL OF MEDICINE, Broad & Ontario Streets, Philadelphia, PA 19140.**

Temple University is an Affirmative Action, Equal Opportunity Educator and Employer.

Choose TEMPLE UNIVERSITY

University of Miami School of Medicine Chairman, Department of Radiology

The University of Miami School of Medicine is seeking qualified applicants for the position of Professor and Chairman of the Department of Radiology. The duties include serving as Chief of Radiology at Jackson Memorial Hospital, the major teaching hospital of one of the largest and busiest medical centers in the nation.

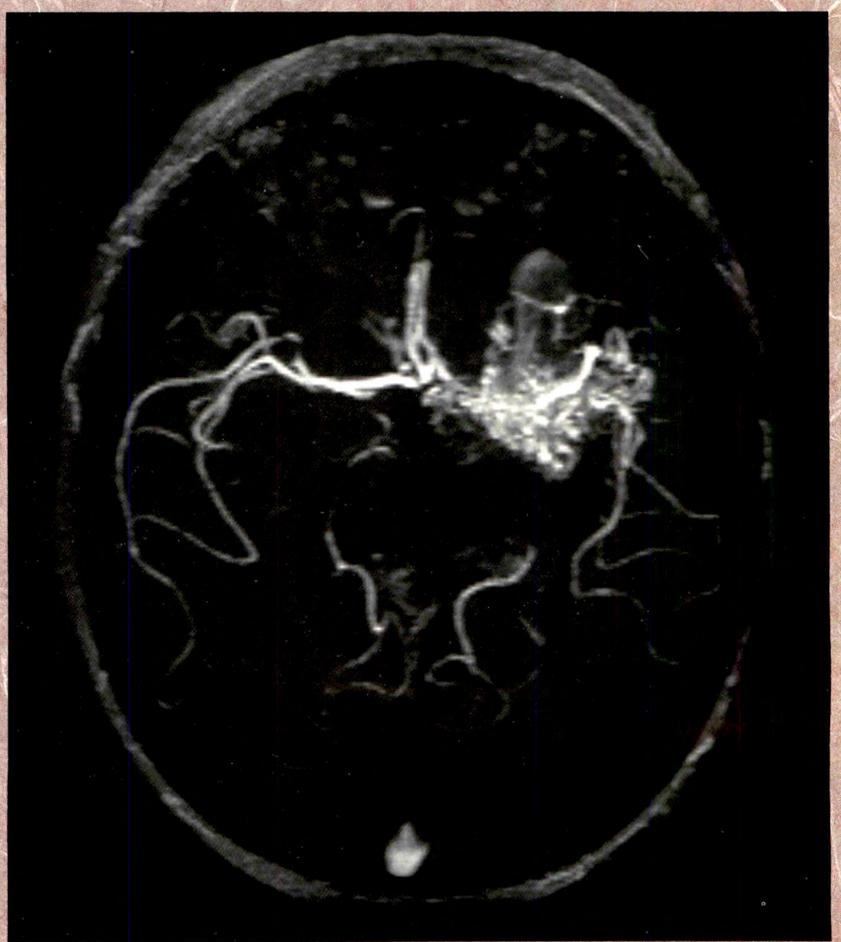
In addition to a strong academic record and clinical skills, we seek a person who is interested and able to lead a complex and busy patient care service. Facilities include a state-of-the-art MRI Center, a large and expanding unit at Jackson Memorial Hospital and a smaller facility at the University of Miami Hospital and Clinics. The Department currently has 42 full-time faculty members, who excel in teaching and clinical service. Radiology is regularly recognized by our medical students as one of our strongest teaching services and the Residency Training Program is outstanding.

Board Certification in Radiology is required, as is eligibility for licensure by the State of Florida.

Applicants should send Curriculum Vitae to:

W. Jarrard Goodwin, Jr., M.D.
Chairman, Radiology Search Committee
Department of Otolaryngology (D-48)
University of Miami School of Medicine
P.O. Box 016960
Miami, Florida 33101

The University of Miami is an equal opportunity/affirmative action employer.



MR vascular image demonstrating an arteriovenous malformation

MR

© 1990 General Electric Company 1573A

Get the most complete picture.

Now you can easily perform comprehensive, routine vascular imaging studies with MR.

GE's new multi-sequence vascular package (MVP) makes it possible.

Paired with our standard shielded gradients (which virtually eliminate gradient-induced artifacts), this package offers the most complete range of MR vascular acquisition methods available—including:

- **2D phase contrast.** For directional and velocity information, without contrast injections. Excellent for head, carotids, portal and hepatic veins.
- **3D phase contrast.** Providing high-resolution imaging of slow flow in tortuous vessels and intracranial arteries.
- **3D time-of-flight.** For a faster exam, well-suited for capturing the Circle of Willis, arterial/venous malformations, and other small volumes of fast flow.
- **2D time-of-flight.** Offering venous or arterial selection—for quick evaluation of occlusions and slow flow in the carotids, as well as venous evaluation in the legs and pelvis.
- **And 2D phase contrast with cine acquisition.** Allowing assessment of alterations in hemodynamic conditions during the cardiac cycle with the Cine Plus option.

For more information on GE's MR multi-sequence vascular package (MVP), call 1-800-433-5566.



2D phase contrast



3D phase contrast



3D time-of-flight



2D time-of-flight



2D phase contrast with cine

GE Medical Systems

AJR Business and Subscriber Information

The American Roentgen Ray Society

AJR, American Journal of Roentgenology, is published monthly to disseminate research on current developments in the radiologic sciences and commentary on topics related to radiology. It is published by the American Roentgen Ray Society, 1891 Preston White Dr., Reston, VA 22091; (703) 648-8992. Inquiries regarding society business, the annual ARRS meeting, and membership should be addressed to the Society at the above address.

Correspondence Concerning the *AJR*

Correspondence regarding display (not classified) advertising, subscriptions, address changes, reprints, and permission requests should be addressed to Williams & Wilkins, 428 E. Preston St., Baltimore, MD 21202; (301) 528–4000.

Correspondence regarding editorial matters and classified advertising should be addressed to Editorial Office, AJR, 2223 Avenida de la Playa, Ste. 103, La Jolla, CA 92037-3218; telephone (619) 459-2229; FAX (619) 459-8814. For information on manuscript submission, see Guidelines for Authors, pages A23–A25

Subscriber Information

Subscription requests and inquiries should be sent to Williams & Wilkins, 428 E. Preston St., Baltimore, MD 21202. ARRS annual dues include $50 for journal subscription. Subscription rates are as follows: nonmembers, $125/year ($180 foreign); institutions, $135 ($190 foreign); nonmember in-training, $25 ($80 foreign). Single copies of the Journal may be purchased for $18 ($22 foreign). Airmail rates will be furnished on request. The GST number for Canadian subscribers is 123394371.

Call toll-free, 1-800-638-6423 (in Maryland call 1-800-638-4007), with subscription questions or problems. Please have the mailing label from your latest issue available when you call.

If a subscriber receives a damaged copy of the *AJR* or fails to receive an issue, the subscriber should notify Williams & Wilkins (428 E. Preston St., Baltimore, MD 21202) within 60 days of publication (90 days for foreign subscribers) and that issue will be replaced.

Change of address information should be sent to Williams & Wilkins, 428 E. Preston St., Baltimore, MD 21202. Allow 90 days for address changes.

Copyrights, Permissions, and Reprints

The American Roentgen Ray Society holds the copyright for all material published in the *AJR*. No part of this publication may be reproduced without permission from the ARRS. Requests for such permission should be addressed to Williams & Wilkins, 428 E. Preston St., Baltimore, MD 21202.

For reprints of a particular article, please contact the author designated in the footnotes for that article.

Indexes

The *AJR* provides volume and yearly indexes (subject and author) in the June and December issues each year. *AJR* articles are also indexed in *Current Contents*, *Index Medicus*, and the cumulative index published by *Radiology*.

AJR Guidelines for Authors

Address new and revised manuscripts, correspondence, and classified ads to the Editor:

AJR Editorial Office
2223 Avenida de la Playa, Suite 103
La Jolla, CA 92037-3218
Telephone: (619) 459-2229; FAX: (619) 459-8814

Inquiries regarding subscriptions, display advertising, reprints, or permission to republish *AJR* material should be addressed to the publisher:

The Williams & Wilkins Co.
428 E. Preston St.
Baltimore, MD 21202 Telephone: 1-800-638-6423

The *AJR* publishes original contributions to the advancement of medical diagnosis and treatment. Submitted manuscripts should not contain previously published material and should not be under consideration for publication elsewhere.

Manuscript decisions are based on peer review. Reviewers receive manuscripts without title pages to ensure an unbiased review. Statements made in the article, including changes made by the Editor or manuscript editor, are the responsibility of the author and not of the *AJR* or its publisher. Authors will be sent the edited manuscript, galley proof, and proofs of illustrations. If the corresponding author will be unavailable to review galleys, arrangements should be made for a coauthor or colleague to read and return the proof.

The following guidelines are based on instructions set forth in the **Uniform Requirements for Manuscripts Submitted to Biomedical Journals** (*Ann Intern Med* **1988;**108:258–265). Articles will be edited, however, to conform to the individual style of AJR.

General Guidelines for Major Papers

Abstract. Clearly state (in 200 words or less) the purpose, methods, results, and conclusions of the study. Include actual data.

Introduction. Briefly describe the purpose of the investigation and explain why it is important.

Methods. Describe the research plan, the materials (or subjects), and the methods used, in that order. Explain in detail how disease was confirmed and how subjectivity in observations was controlled.

Results. Present results in a clear, logical sequence. If tables are used, do not duplicate tabular data in text, but do describe important trends and points.

Discussion. Describe the limitations of the research plan, materials (or subjects), and methods, considering both the purpose and the outcome of the study. When results differ from those of previous investigators, explain the discrepancy.

AUTHOR'S CHECKLIST

For priority handling, complete the following checklist, sign the copyright form on the reverse side of this page, and include both with the manuscript.

_____ Two copies of the manuscript (the original and a photocopy) and two complete sets of figures are submitted. One copy has been retained by the author.

_____ If appropriate, *AJR* Guidelines for case reports, technical notes, pictorial essays, or letters to the Editor have been followed. (See page A25.)

_____ The manuscript, including references, figure legends, and tables, is typed double-spaced on 8½ × 11 in. (21.6 × 27.9 cm) *nonerasable* paper. Right-hand margins are not justified.

_____ All manuscript pages are numbered consecutively beginning with the abstract. Authors' names do not appear on the manuscript pages.

_____ The manuscript is organized as follows: title page, blind title page (title only), abstract, introduction, methods, results, discussion, acknowledgments, references, tables, figure legends, and figures.

_____ Informed consent has been obtained from patients who participated in clinical investigations. If experiments were performed on animals, authors complied with NIH guidelines for use of laboratory animals.

_____ Use of unfamiliar acronyms and abbrevations is kept to a minimum. When abbreviations are used they are defined at first mention, followed by the abbreviation in parentheses.

_____ Metric measurements are used throughout, or the metric equivalent is given in parentheses.

_____ Names and locations (city and state only) of manufacturers are given for equipment and nongeneric drugs.

Title Page

_____ The following information is given: title of article; names and complete addresses (including zip code) of all authors; current addresses of authors who have moved since study; acknowledgment of grant or other assistance. The corresponding author is clearly identified, and a current address, phone number, and FAX number are given.

_____ A blind title page is included in each copy of the manuscript, giving only the title (without the authors' names) for use in the review process.

Abstract

_____ An abstract of approximately 200 words concisely states the purpose, methods, and results of the study in one paragraph. Actual data are included. Conclusions are stated in a second, summary paragraph.

_____ No abbreviations or reference citations are used.

References

_____ References (not to exceed 35) are typed double-spaced starting on a separate page and are **numbered consecutively in the order in which they appear in the text**.

_____ All references are cited in the text and are enclosed in brackets and typed on line with the text (not superscript).

_____ Unpublished data are not cited in the reference list, but are cited parenthetically in the text, for example, (Smith DJ, personal communication), (Smith DJ, unpublished data). This includes papers submitted, but not yet accepted, for publication.

_____ Papers presented at a meeting are not cited in the reference list, but are cited parenthetically in the text (e.g., Smith DJ et al., presented at the annual meeting of the American Roentgen Ray Society, May 1990). After first mention, use (Smith DJ et al., ARRS meeting, May 1990).

_____ Inclusive page numbers (e.g., 333–335) are given for all references.

_____ Journal names are abbreviated according to *Index Medicus*.

_____ Style and punctuation of references follow the format illustrated in the following examples (all authors are listed when six or fewer; when seven or more authors, the first three are listed, followed by "et al."):

Journal article

1. Long RS, Roe EW, Wu EU, et al. Membrane oxygenation: radiographic appearance. *AJR* **1986**;146:1257–1260

Book

2. Smith LW, Cohen AR. *Pathology of tumors*, 6th ed. Baltimore: Williams & Wilkins, **1977**:100–109

Chapter in a book

3. Breon AJ. Serum monitors of bone metastasis. In: Clark SA, ed. *Bone metastases*. Baltimore: Williams & Wilkins, **1983**:165–180

Tables

_____ Each table is typed double-spaced on a separate page without vertical or horizontal rules; each has a short, descriptive title. Tables do not exceed two pages in length and contain at least four lines of data.

_____ Tables are numbered in the order in which they are cited in the text.

_____ Abbreviations are defined in an explanatory note below each table.

_____ Tables are self-explanatory and do not duplicate data given in the text or figures.

_____ All arithmetic (percentages, totals, differences) has been double checked for accuracy, and tabular data agree with data given in the text.

Figures and Legends

_____ Two complete sets of original figures are submitted unmounted in labeled envelopes.

_____ Figures are clean, unscratched, 5 × 7 in. (13 × 18 cm) glossy prints with **white borders.** A separate print is submitted for each figure *part*.

_____ All figure parts relating to one patient have the same figure number.

_____ Each figure is labeled on the back with the figure number and an arrow indicating "top." For black-and-white figures, labeling is done on a gummed label, which is then affixed to the back of the print. **Never** use labels on **color** figures, but write figure number on the back lightly in pencil. *Never* use ink on front or back of any figures.

_____ Author's names are *not* written on the backs of figures.

_____ Only removable (rub-on) arrows and letters are used on the figures. Symbols are uniform in size and style and are not broken or cracked.

_____ Images are uniform in size and magnification.

_____ Line drawings are done in black ink on a white background. They are professional in quality, and all use the same size type. (Only glossy prints are acceptable.)

_____ Written permission has been obtained for use of all previously published illustrations (and copies of permission letters are included), and an appropriate credit line is given in the legends.

_____ Legends are typed double-spaced, and figure numbers correspond with the order in which the figures are cited in the text.

Transfer of Copyright Agreement, Conflict of Interest Acknowledgment, Certification of Coauthors, and Exclusive Publication Statement

Complete copyright to the article entitled: _____

_____

is hereby transferred to the American Roentgen Ray Society (for United States government employees to the extent transferable), effective if and when the article is accepted for publication in the *American Journal of Roentgenology*. In the case of the authors who are officers or employees of the United States government, the American Roentgen Ray Society recognizes that works prepared by officers or employees of the United States government as part of their official government duties are in the public domain.

Authors reserve all proprietary rights other than copyright, such as patent rights and the right to use all or part of this article in future works of their own. The authors retain the right of replication, subject only to crediting the original source of publication and receiving written permission from the publisher.

Authors guarantee that this manuscript contains no matter that is libelous or otherwise unlawful, invades individual privacy, or infringes any proprietary rights.

Authors understand that they will receive no royalty or other compensation from the American Roentgen Ray Society or the publisher.

Authors guarantee that the editor has been or will be informed of any proprietary or commercial interest or conflicts of interest the authors may have that relate directly or indirectly to the subject of this article.

All authors certify that they have made substantive and specific intellectual contributions to the article and assume public responsibility for its content.

Finally, the authors certify that none of the material in this manuscript has been published previously or is currently under consideration for publication elsewhere.

_____	_____	_____
First author/date	Second author	Third author
_____	_____	_____
Fourth author	Fifth author	Sixth author

This agreement must be signed by all authors in order for the manuscript to be published.

Case Reports

A case report is a brief description of a special case that provides a message that transcends the individual patient.

Format. There is no abstract. The introduction should be a short paragraph giving the general background and the specific interest of the case. No more than one case should be described in detail (similar ones can be mentioned briefly in the discussion). Emphasis should be on the radiologic aspects; clinical information must be limited to that necessary to provide a background for the radiology. The discussion should be succinct and should focus on the specific message and relevance of radiologic methods. A review of the literature is not appropriate.

Length. Maximum of five double-spaced, typewritten pages, including the references but not the title page or figure legends.

References. Maximum of eight.

Figures. Maximum of four, unless the text is shortened accordingly. Legends must not repeat the text.

Tables and Acknowledgments. Not appropriate in case reports.

Technical Notes

A technical note is a brief description of a specific technique or procedure, modification of a technique, or equipment of interest to radiologists.

Format. No abstract, headings, or subheadings are required. If headings are used, they should be a combination of "Case Report," "Materials and Methods," "Results," and "Discussion." A brief one-paragraph introduction should be included to give the general background. Discussion should be limited to the specific message, including the uses of the technique or equipment. Literature reviews and lengthy case reports are not appropriate.

Length. Maximum of five double-spaced, typewritten pages, including the references but not the title page or figure legends.

References. Maximum of eight.

Figures. Maximum of two, unless the text is shortened accordingly.

Tables and Acknowledgments. Not appropriate in technical notes.

Pictorial Essays

A pictorial essay is an article that conveys its message through illustrations and their legends. Unlike other *AJR* articles, which are based on original research, pictorial essays serve primarily as teaching tools, like exhibits at a scientific meeting. They are not encyclopedic book chapters. The abstract should be a short, introductory paragraph.

Length. Maximum of four double-spaced, typewritten pages, including the references but not the title page or figure legends.

References. Maximum of four.

Figures. Maximum of 30 figure *parts*. Number should be as few as necessary to convey the message of the paper.

Tables and Acknowledgments. Not appropriate in pictorial essays.

Letters to the Editor and Replies

Letters to the Editor and Replies should offer objective and constructive criticism of published articles. Letters may also discuss matters of general interest to radiologists. Do not end a letter with a hand-written signature.

Format. All letters should be typed double-spaced on nonletterhead paper, with no greeting or salutation. Name and affiliation should appear at the end of the letter. Titles for letters should be short and pertinent. The title for a reply is simply "Reply."

Length. Maximum of two double-spaced, typewritten pages, including references.

References. Maximum of four.

Figures. Maximum of two.

Tables and Acknowledgments. Not appropriate in Letters to the Editor and Replies.

Opinions, Commentaries, and Perspectives

Opinions, commentaries, and perspectives are special articles dealing with controversial topics or issues of special concern to radiologists.

Format. Include a title page but no abstract. Headings may be used to break up the text.

Length. Maximum of five double-spaced, typewritten pages.

References. Maximum of five.

Tables and Figures. Maximum of four.

Computer Page Articles

Articles published on the computer page deal with practical computer applications to radiology.

Format. Include a title page and an abstract.

Length. Maximum of eight double-spaced, typewritten pages.

References. Maximum of five.

Figures and Tables. Maximum of five. Computer printouts are not acceptable. Figures must be submitted as 5 × 7 in. glossy prints.



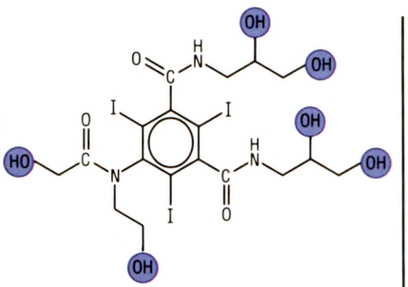
All submissions to the *AJR* must be accompanied by a completed copy of the Author's Checklist and the signed Copyright Agreement.


R O M M A L L

The friendlier molecule and its pattern of protection

The toxic portion of the contrast agent molecule is the iodinated benzene ring. In modern contrast agents, the ring is sheltered by hydroxyl groups arranged around it. If the arrangement is less than optimal, it can leave "holes" in the structure.

The Optiray® molecular structure provides a superior pattern of protection from the benzene ring with six hydroxyl groups arranged symmetrically around it.[1] In addition, Optiray has no hydrophobic (lipid-soluble) methyl group as in iopamidol and iohexol molecules. These are the reasons why one investigator has called Optiray the "friendlier" contrast media molecule.[1]



Balanced distribution of hydroxyl (OH) groups creates a pattern of protection around the toxic iodinated benzene ring.

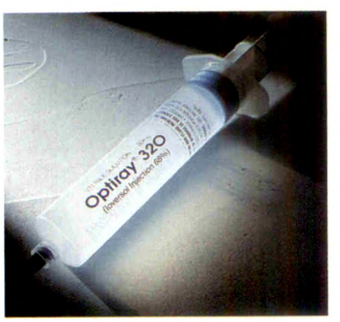
With Optiray, you can expect a very low incidence of individual, drug-related adverse reactions.[2] Optiray also offers the safety, convenience, and cost-efficiency of the single-dose Ultraject® prefilled syringe. With all these advantages, shouldn't Optiray's friendlier molecule be your choice in a nonionic contrast agent? For more information, contact your Mallinckrodt Medical representative or call us toll free at (800) 325-3688.

All nonionic iodinated contrast media currently available inhibit blood coagulation, in vitro, less than ionic contrast media. Clotting has been reported when blood remains in contact with syringes containing nonionic contrast media. Therefore, meticulous intravascular administration technique is necessary to minimize thromboembolic events.

Please see adjacent brief summary of prescribing information.

References:

1. McClennan BL. Ionic and nonionic iodinated contrast media: evolution and strategies for use. *AJR.* 1990; 155:225-233.
2. Benamor M, Aten EM, McElvany KD, et al. Ioversol clinical safety summary. *Invest Radiol.* 1989;24 (suppl 1):S67-S72.



Nonionic

OPTIRAY®

(ioversol)

The friendlier molecule

OPTIRAY® 160 240 320
(Ioversol Injection)

DESCRIPTION: Each milliliter of OPTIRAY 160 (ioversol injection 34%) provides 339 mg of ioversol with 3.6 mg of tromethamine as a buffer and 0.2 mg of edetate calcium disodium as a stabilizer. OPTIRAY 160 provides 16% (160 mg/mL) organically bound iodine.

Each milliliter of OPTIRAY 240 (ioversol injection 51%) provides 509 mg of ioversol with 3.6 mg of tromethamine as a buffer and 0.2 mg of edetate calcium disodium as a stabilizer. OPTIRAY 240 provides 24% (240 mg/mL) organically bound iodine.

Each milliliter of OPTIRAY 320 (ioversol injection 68%) provides 678 mg of ioversol with 3.6 mg of tromethamine as a buffer and 0.2 mg of edetate calcium disodium as a stabilizer. OPTIRAY 320 provides 32% (320 mg/mL) organically bound iodine.

CONTRAINDICATIONS: None.

WARNINGS: Nonionic iodinated contrast media inhibit blood coagulation, in vitro, less than ionic contrast media. Clotting has been reported when blood remains in contact with syringes containing nonionic contrast media.

Serious, rarely fatal, thromboembolic events causing myocardial infarction and stroke have been reported during angiographic procedures with both ionic and nonionic contrast media. Therefore, meticulous intravascular administration technique is necessary, particularly during angiographic procedures, to minimize thromboembolic events. Numerous factors, including length of procedure, catheter and syringe material, underlying disease state and concomitant medications may contribute to the development of thromboembolic events. For these reasons, meticulous angiographic techniques are recommended including close attention to guidewire and catheter manipulation, use of manifold systems and/or three-way stopcocks, frequent catheter flushing with heparinized saline solutions and minimizing the length of the procedure. The use of plastic syringes in place of glass syringes has been reported to decrease but not eliminate the likelihood of in vitro clotting.

Serious or fatal reactions have been associated with the administration of iodine-containing radiopaque media. It is of utmost importance to be completely prepared to treat any contrast medium reaction.

As with any contrast medium, serious neurologic sequelae, including permanent paralysis, can occur following cerebral arteriography, selective spinal arteriography and arteriography of vessels supplying the spinal cord. A cause-effect relationship to the contrast medium has not been established since the patients' pre-existing condition and procedural technique are causative factors in themselves. The arterial injection of a contrast medium should never be made following the administration of vasopressors since they strongly potentiate neurologic effects.

Caution must be exercised in patients with severely impaired renal function, combined renal and hepatic disease, severe thyrotoxicosis, myelomatosis, or anuria, particularly when large doses are administered.

Intravascularly administered iodine-containing radiopaque media are potentially hazardous in patients with multiple myeloma or other paraproteinemia, particularly in those with therapeutically resistant anuria. Myeloma occurs most commonly in persons over age 40. Although neither the contrast agent nor dehydration has been proved separately to be the cause of anuria in myelomatous patients, it has been speculated that the combination of both may be causative. The risk in myelomatous patients is not a contraindication to the procedure; however, special precautions, including maintenance of normal hydration and close monitoring, are required. Partial dehydration in the preparation of these patients prior to injection is not recommended since this may predispose the patient to precipitation of the myeloma protein.

Administration of radiopaque materials to patients known or suspected of having pheochromocytoma should be performed with extreme caution. If, in the opinion of the physician, the possible benefits of such procedures outweigh the considered risks, the procedures may be performed; however, the amount of radiopaque medium injected should be kept to an absolute minimum. The blood pressure should be assessed throughout the procedure, and measures for treatment of a hypertensive crisis should be available.

Contrast media may promote sickling in individuals who are homozygous for sickle cell disease when administered intravascularly.

Reports of thyroid storm following the intravascular use of iodinated radiopaque agents in patients with hyperthyroidism or with an autonomously functioning thyroid nodule, suggest that this additional risk be evaluated in such patients before use of any contrast medium.

PRECAUTIONS: *General:* Diagnostic procedures which involve the use of iodinated intravascular contrast agents should be carried out under the direction of personnel skilled and experienced in the particular procedure to be performed. A fully equipped emergency cart, or equivalent supplies and equipment, and personnel competent in recognizing and treating adverse reactions of all types should always be available. Since severe delayed reactions have been known to occur, emergency facilities and competent personnel should be available for at least 30 to 60 minutes after administration.

Preparatory dehydration is dangerous and may contribute to acute renal failure in patients with advanced vascular disease, diabetic patients, and in susceptible non-diabetic patients (often elderly with pre-existing renal disease). *Patients should be well hydrated prior to and following the administration of OPTIRAY.*

The possibility of a reaction, including serious, life-threatening, fatal, anaphylactoid or cardiovascular reactions, should always be considered (See ADVERSE REACTIONS). Increased risk is associated with a history of previous reaction to a contrast medium, a known sensitivity to iodine and known allergies (i.e., bronchial asthma, hay fever and food allergies) or hypersensitivities.

The occurrence of severe idiosyncratic reactions has prompted the use of several pretesting methods. However, pretesting cannot be relied upon to predict severe reactions and may itself be hazardous to the patient. It is suggested that a thorough medical history with emphasis on allergy and hypersensitivity, prior to the injection of any contrast medium, may be more accurate than pretesting in predicting potential adverse reactions. A positive history of allergies or hypersensitivity does not arbitrarily contraindicate the use of a contrast agent when a diagnostic procedure is thought essential, but caution should be exercised. Premedication with antihistamines or corticosteroids to avoid or minimize possible allergic reactions in such patients should be considered. Reports indicate that such pretreatment does not prevent serious life-threatening reactions, but may reduce both their incidence and severity.

General anesthesia may be indicated in the performance of some procedures in selected patients; however, a higher incidence of adverse reactions has been reported in these patients, and may be attributable to the inability of the patient to identify untoward symptoms or to the hypotensive effect of anesthesia which can prolong the circulation time and increase the duration of exposure to the contrast agent.

In angiographic procedures, the possibility of dislodging plaques or damaging or perforating the vessel wall should be considered during catheter manipulations and contrast medium injection. Test injections to insure proper catheter placement are suggested.

Angiography should be avoided whenever possible in patients with homocystinuria because of the risk of inducing thrombosis and embolism.

Patients with congestive heart failure should be observed for several hours following the procedure to detect delayed hemodynamic disturbances which may be associated with a transitory increase in the circulating osmotic load.

Selective coronary arteriography should be performed only in selected patients and those in whom the expected benefits outweigh the procedural risk. The inherent risks of angiocardiography in patients with chronic pulmonary emphysema must be weighed against the necessity for performing this procedure.

Extreme caution during injection of a contrast medium is necessary to avoid extravasation. This is especially important in patients with severe arterial or venous disease.

Drug Interactions: Renal toxicity has been reported in a few patients with liver dysfunction who were given oral cholecystographic agents followed by intravascular contrast agents. Administration of any intravascular contrast agent should therefore be postponed in patients who have recently received a cholecystographic contrast agent.

Other drugs should not be mixed with ioversol injection.

Drug Laboratory Test Interactions: The results of PBI and radioactive iodine uptake studies, which depend on iodine estimation, will not accurately reflect thyroid function for up to 16 days following administration of iodinated contrast media. However, thyroid function tests not depending on iodine estimations, e.g., T3 resin uptake and total or free thyroxine (T4) assays are not affected.

Carcinogenesis, Mutagenesis, Impairment of Fertility: No long term animal studies have been performed to evaluate carcinogenic potential. However, animal studies suggest that this drug is not mutagenic and does not affect fertility.

Pregnancy Category B: No teratogenic effects attributable to ioversol have been observed in teratology studies performed in animals. There are, however, no adequate and well controlled studies in pregnant women. It is not known whether ioversol crosses the placental barrier or reaches fetal tissues. However, many injectable contrast agents cross the placental barrier in humans and appear to enter fetal tissue passively. Because animal teratology studies are not always predictive of human response, this drug should be used during pregnancy only if clearly needed. X-ray procedures involve a certain risk related to the exposure of the fetus.

Nursing Mothers: It is not known whether ioversol is excreted in human milk. However, many injectable contrast agents are excreted unchanged in human milk. Although it has not been established that serious adverse reactions occur in nursing infants, caution should be exercised when intravascular contrast media are administered to nursing women because of potential adverse reactions, and consideration should be given to temporarily discontinuing nursing.

Pediatric Use: Safety and effectiveness in children have not been established.

ADVERSE REACTIONS: Adverse reactions following the use of OPTIRAY formulations are usually mild to moderate, of short duration and resolve spontaneously (without treatment). However, serious, life-threatening and fatal reactions, mostly of cardiovascular origin, have been associated with the administration of iodine-containing contrast media.

Injections of contrast media are often associated with sensations of warmth and pain. In controlled double-blind clinical studies, significantly less warmth and pain were associated with the injection of OPTIRAY than with iothalamate meglumine, diatrizoate meglumine, and diatrizoate meglumine and diatrizoate sodium.

When OPTIRAY 320 is used for coronary arteriography and ventriculography in double-blind clinical trials, electrocardiographic and hemodynamic changes occur with less frequency and severity with ioversol injection than with diatrizoate meglumine and diatrizoate sodium.

Following coronary artery and left ventricular injection, electrocardiographic parameters were affected less with OPTIRAY (ioversol injection) than with diatrizoate meglumine and diatrizoate sodium injection. These parameters included the following: bradycardia, tachycardia, T-wave amplitude, ST depression and ST elevation.

OPTIRAY has also been shown to cause fewer changes in cardiac function and systemic blood pressure than conventional ionic media. These include cardiac output, left ventricular systolic and end-diastolic pressure, right ventricular systolic and pulmonary artery systolic pressures and decreases in systolic and diastolic blood pressures.

The following table of incidence of reactions is based upon clinical trials with OPTIRAY formulations in over 1100 patients. This listing includes all adverse reactions which were coincidental to the administration of ioversol regardless of their direct attributability to the drug or the procedure. Adverse reactions are listed by organ system and in decreasing order of occurrence. Significantly more severe reactions are listed before others in a system regardless of frequency.

Adverse Reactions

System	> 1%	≤ 1%
Cardiovascular	none	angina pectoris hypotension vascular spasm bradycardia conduction defect false aneurysm hypertension transient arrhythmia vascular trauma
Digestive	none	nausea vomiting
Nervous	none	cerebral infarct headache blurred vision vertigo lightheadedness vasovagal reaction disorientation dysphasia paresthesia visual hallucination
Respiratory	none	laryngeal edema nasal congestion sneezing coughing hypoxia
Skin	none	periorbital edema urticaria facial edema flush pruritus
Miscellaneous	none	extravasation shaking chills bad taste general pain

Regardless of the contrast medium employed, the overall incidence of serious adverse reaction is higher with coronary arteriography than with other procedures. Cardiac decompensation, serious arrhythmias, myocardial ischemia or myocardial infarction may occur during coronary arteriography and left ventriculography.

General Adverse Reactions to Contrast Media

The following adverse reactions are possible with any parenterally administered iodinated contrast medium. Severe life-threatening reactions and fatalities, mostly of cardiovascular origin, have occurred. Most deaths occur during injection or 5 to 10 minutes later; the main feature being cardiac arrest with cardiovascular disease as the main aggravating factor. Isolated reports of hypotensive collapse and shock are found in the literature. Based upon clinical literature, reported deaths from the administration of conventional iodinated contrast agents range from 6.6 per 1 million (0.00066 percent) to 1 in 10,000 patients (0.01 percent).

The reported incidence of adverse reactions to contrast media in patients with a history of allergy is twice that of the general population. Patients with a history of previous reactions to a contrast medium are three times more susceptible than other patients. However, sensitivity to contrast media does not appear to increase with repeated examinations.

Adverse reactions to injectable contrast media fall into two categories: chemotoxic reactions and idiosyncratic reactions.

Chemotoxic reactions result from the physicochemical properties of the contrast medium, the dose and the speed of injection. All hemodynamic disturbances and injuries to organs or vessels perfused by the contrast medium are included in this category.

Idiosyncratic reactions include all other reactions. They occur more frequently in patients 20 to 40 years old. Idiosyncratic reactions may or may not be dependent on the dose injected, the speed of injection, the mode of injection and the radiographic procedure. Idiosyncratic reactions are subdivided into minor, intermediate and severe. The minor reactions are self-limited and of short duration; the severe reactions are life-threatening and treatment is urgent and mandatory.

In addition to the adverse reactions reported for ioversol, the following additional adverse reactions have been reported with the use of other contrast agents and are possible with any water soluble, iodinated contrast agent.

Nervous: muscular spasm, convulsions, aphasia, syncope, paralysis, visual field losses which are usually transient but may be permanent, coma and death.

Cardiovascular: angioneurotic edema, peripheral edema, vasodilation, thrombosis and rarely thrombophlebitis, disseminated intravascular coagulation and shock.

Skin: maculopapular rash, erythema, conjunctival symptoms, ecchymosis and tissue necrosis.

Respiratory: choking, dyspnea, wheezing which may be an initial manifestation of more severe and infrequent reactions including asthmatic attack, laryngospasm and brochospasm, pulmonary edema, apnea and cyanosis. Rarely these allergic-type reactions can progress into anaphylaxis with loss of consciousness, coma, severe cardiovascular disturbances and death.

Miscellaneous: hyperthermia, temporary anuria or other nephropathy.

Other reactions may also occur with the use of any contrast agent as a consequence of the procedural hazard; these include hemorrhage or pseudoaneurysms at the puncture site, brachial plexus palsy following axillary artery injections, chest pain, myocardial infarction, and transient changes in hepatorenal chemistry tests. Arterial thrombosis, displacement of arterial plaques, venous thrombosis, dissection of the coronary vessels and transient sinus arrest are rare complications.

In cerebral arteriography, cardiovascular reactions that may occur with some frequency are bradycardia and either an increase or decrease in systemic blood pressure. Neurological reactions that may occur are: seizures, drowsiness, transient paresis, and mild disturbances in vision.

Central nervous system reactions with OPTIRAY in controlled clinical studies in cerebral arteriography that occurred with frequencies greater than 1% were: vertigo (4%) and blurred vision (3%).

In aortography, depending on the technique employed, the risks of this procedure also include the following: injury to the aorta and neighboring organs, pleural puncture, renal damage including infarction and acute tubular necrosis with oliguria and anuria, retroperitoneal hemorrhage from the translumbar approach and spinal cord injury and pathology associated with the syndrome of transverse myelitis. Under conditions of slowed aortic circulation there is an increased likelihood for aortography to cause muscle spasm. Occasional serious neurologic complications, including paraplegia, have also been reported in patients with aortoiliac obstruction, femoral artery obstruction, abdominal compression, hypotension, hypertension, spinal anesthesia, and injection of vasopressors to increase contrast. In these patients the concentration, volume, and number of repeat injections of the medium should be maintained at a minimum with appropriate intervals between injections. The position of the patient and catheter tip should be carefully monitored.

Entry of a large aortic dose into the renal artery may cause, even in the absence of symptoms, albuminuria, hematuria, and an elevated creatinine and urea nitrogen. Rapid and complete return of function usually follows.

Cardiovascular system reactions with OPTIRAY in controlled clinical studies in coronary arteriography with left ventriculography that occurred with frequencies greater than 1% were: angina (1.2%) and nausea (1.2%).

PRECAUTIONS FOR SPECIFIC PROCEDURES:

Cerebral Arteriography

Extreme caution is advised in patients with advanced arteriosclerosis, severe hypertension, cardiac decompensation, senility, recent cerebral thrombosis or embolism, and migraine.

Peripheral Arteriography

Pulsation should be present in the artery to be injected. In thromboangiitis obliterans, or ascending infection associated with severe ischemia, angiography should be performed with extreme caution, if at all.

Coronary Arteriography and Left Ventriculography

Mandatory prerequisites to the procedure are specialized personnel, ECG monitoring apparatus and adequate facilities for immediate resuscitation and cardioversion. Electrocardiograms and vital signs should be routinely monitored throughout the procedure.

Venography

Special care is required when venography is performed in patients with suspected thrombosis, phlebitis, severe ischemic disease, local infection or a totally obstructed venous system. In order to minimize extravasation during injection, fluoroscopy is recommended.

OVERDOSAGE: The adverse effects of overdosage are life-threatening and affect mainly the pulmonary and cardiovascular system. Treatment of an overdosage is directed toward the support of all vital functions, and prompt institution of symptomatic therapy.

Ioversol does not bind to plasma or serum protein and is therefore, dialyzable.

The intravenous LD_{50} values (gI/kg) for ioversol in animals were: 17 (mice), and 15 (rats).

DOSAGE AND ADMINISTRATION: Details on dosage are provided in the package insert. CONSULT FULL PACKAGE INSERT BEFORE USE.

MALLINCKRODT®

Changing the look of medicine.™

© 1991 Mallinckrodt Medical, Inc. 4/91 MI22377

RADIOLOGY PRACTICE OPPORTUNITIES

Practice opportunity for 5 radiologists at a 1000-bed, major teaching hospital located within the New York City metropolitan area. There is an affiliated, off-site imaging center opening Jan. 1, 1992.

NEURORADIOLOGIST: New York state medical license, board certification, fellowship training, MRI, CT, angiography, and myelography experience necessary.

DIAGNOSTIC RADIOLOGIST WITH MRI EXPERIENCE: New York state medical license, board certification, fellowship training in neuro MRI, body MRI, orthopedic MRI, CT, and ultrasound necessary. In addition to a fellowship, previous experience in an imaging center is a plus.

DIAGNOSTIC RADIOLOGIST WITH IMAGING BACKGROUND: New York state medical license, board certification, fellowship training, MRI, CT, and ultrasound experience necessary. Experience in CT and ultrasound-guided procedures a plus.

DIAGNOSTIC RADIOLOGIST WITH MAMMOGRAPHY EXPERIENCE: New York state medical license, board certification/eligibility, with specific experience, expertise, and training in mammography and breast localization procedures.

GENERAL DIAGNOSTIC RADIOLOGIST: New York state medical license, board certification/eligibility with experience in all conventional and routine diagnostic radiology modalities.

Our dept. performs 150,000 procedures/yr, including ultrasound, CT, angiography, interventional radiology, mammography and breast localizations, neuroradiology, and all basic and routine radiographic studies. Staffing in our dept. consists of 13 full-time staff radiologists, including 2 in the subdivision of nuclear medicine and 1 in the subdivision of radiation therapy.

Attractive salaries are being offered, which will be commensurate with the level of experience. An extensive comprehensive benefits package, including vacation and conference time, is being offered. The imaging center opening in Jan. 1992 will include MRI, CT, ultrasound, mammography, and R&F.

Please respond in confidence with CV, which should include potential d... of availability, to **Director of Radiology, The Brookdale Hospital Medical Center, Linden Blvd., at Brookdale Plaza, Brooklyn, NY 11212-3198.**

RADIOLOGIST

The University of California, San Francisco and its affiliate, VA Medical Center, Fresno, seek a full-time radiologist. Responsibilities will include teaching and supervising residents in general radiology, as well as subspecialty such as MRI, CT, or interventional radiology.

Qualifications include board certification in radiology and interest, skill, and background in clinical instruction and interest in research. Though candidates at all levels will be considered, the position is ideal for a recent graduate starting an academic career.

The central California location offers pleasant living conditions for family life with affordable housing, good schools, and ready access to both coastal and mountain recreational areas.

Address inquiries and send c.v. to:

Malcolm F. Anderson, M.D.
Chief, Department of Radiology
2615 E. Clinton Ave. (114)
Fresno, CA 93703
209-228-5328

UCSF is an AA/EOE, M/F/H/V.

Columbia University

Neuroradiologist

Harlem Hospital Center, an affiliate of Columbia University, has a full time position for a BC Neuroradiologist with knowledge of special and interventional procedures. Academic appointment to the faculty of Columbia University. Professionals interested in this position should send CV to: Dr. Jan Smulewicz, Director of Radiology, Harlem Hospital Center, 506 Lenox Avenue, New York, NY 10037. We take affirmative action to ensure equal opportunity.

You learn from your experience with

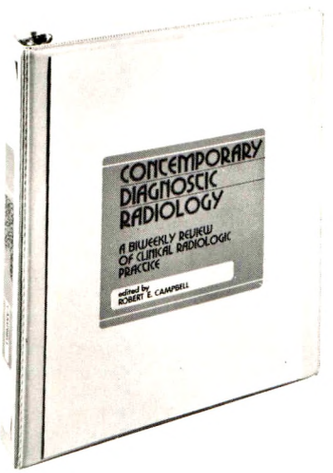
CONTEMPORARY DIAGNOSTIC RADIOLOGY

Editor: **Robert E. Campbell, M.D.**

A Biweekly Review of Clinical Radiologic Practice—26 issues a year!

One of your toughest jobs is keeping up with the many new developments that affect radiology. That's why you want **Contemporary Diagnostic Radiology**... an effective and convenient way to perfect your skills and maintain your professional status.

Contemporary Diagnostic Radiology is designed as a continuing education program that lets you work at your own pace. Every two weeks you'll receive an issue that covers a single topic or procedure in detail. Read the information and study the clearly reproduced radiographs—and then, if you choose, respond to a comprehensive examination in the strictest confidence. You set the pace.
Each biweekly lesson brings you pertinent review of the basics in bone radiology... gastrointestinal radiology... pediatric radiology... genitourinary radiology... MR imaging... and all of the topics you want to know more about.



Contemporary Diagnostic Radiology works *two ways*. You may choose to subscribe to the non-scoring version, receiving every issue as an important element of your professional reading. The scoring version, however, supplements your reading and computer-coded examinations with confidential result responses, making you eligible for Continuing Medical Education credits co-sponsored by the University of Pennsylvania School of Medicine.

"As an organization for continuing medical education, the University of Pennsylvania School of Medicine designates this continuing medical education activity as meeting the criteria for 1 credit hour per bi-weekly issue in Category I for Educational Materials for the Physician's Recognition Award of the American Medical Association provided it has been completed according to instructions."

You can begin this ongoing program **today. Contemporary Diagnostic Radiology** is a year-round program, so you can join at any time. To begin your lessons, just fill out the enclosed card and return it to us. Or call **FREE** 1-800-638-6423 from anywhere in the U.S. or Canada. You'll find that **Contemporary Diagnostic Radiology** is the most efficient and inexpensive way to keep up with your dynamic field.

Williams & Wilkins

P.O. Box 23291
Baltimore, Maryland 21203-9990

Broadway House
2-6 Fulham Broadway
London SW6 1AA England

clip & mail

CONTEMPORARY DIAGNOSTIC RADIOLOGY

☐ **Yes!** I want to keep pace in my field! Begin my 26-issue subscription:
☐ Send me the scoring version ($240)
☐ Send me the non-scoring version ($197)
☐ Send me the resident non-scoring version* ($120)
(add $57 for optional airmail delivery outside the U.S.; in Canada, also add 7% GST.)
☐ new subscription ☐ renewal

name

address

city/state/zip

payment options
☐ payment enclosed ☐ bill me
☐ American Express ☐ MasterCard ☐ VISA

printed in USA

card # expiration date

signature/P.O. #

Maryland residents add 5% sales tax. Subscriptions outside the U.S. must be prepaid in U.S. dollars only. Rates valid through October 31, 1991. Please allow 8 weeks for delivery of your first issue, up to 16 weeks for surface delivery outside the U.S. Optional airmail rates add $57 per subscription.

***Residents** are eligible for the special in-training rate for up to three years. When requesting this rate, please include training status and institution.

Don't forget: you can order with a **TOLL-FREE** call to 1-800-638-6423 from anywhere in the U.S. or Canada.

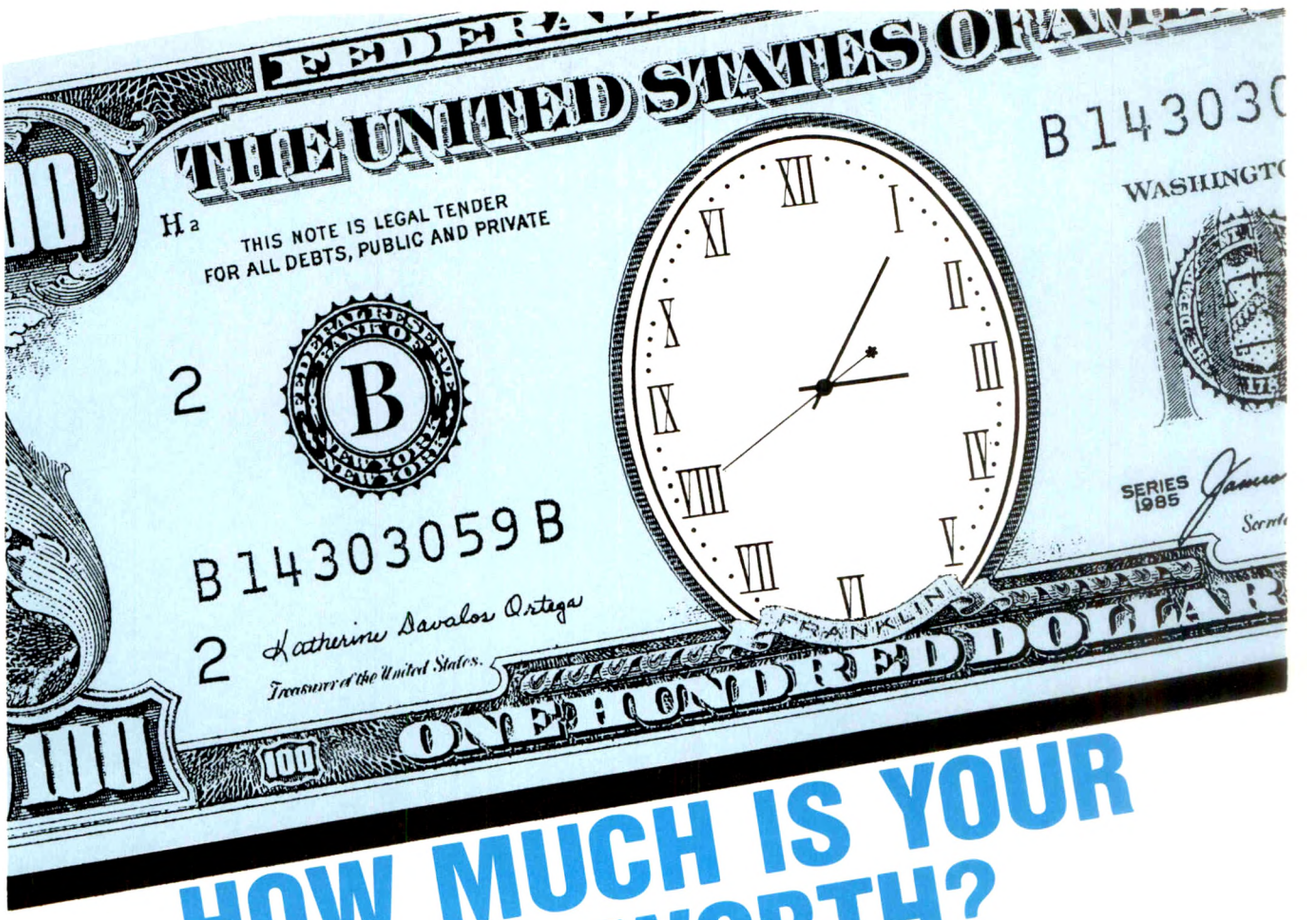
Williams & Wilkins

P.O. Box 23291
Baltimore, Maryland 21203-9990

Broadway House
2-6 Fulham Broadway
London SW6 1AA England

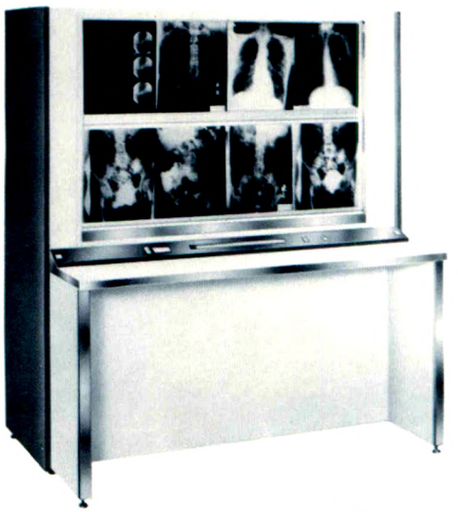
CDR 52740

J1091S01



HOW MUCH IS YOUR TIME WORTH?

If, like most Radiologists, you spend 30% or more of your day **handling** films, let us show you how S & S Motorized Viewers eliminate those COSTLY WASTED HOURS!

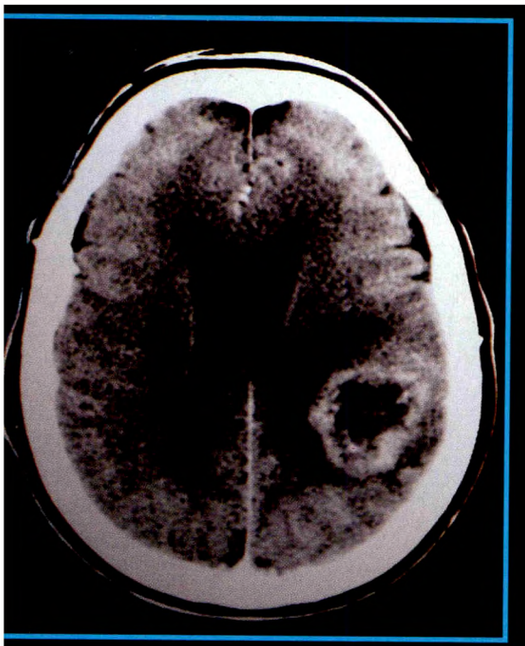


Model MV216

- From 48 up to 324 14" x 17" films can be pre-loaded and stored in proper sequence to be recalled when needed for viewing in as little as 7 seconds—by simply pressing a button!
- All 12 models feature illumination brighter than most other viewers, plus individual panel light controls which promote viewer concentration and increase reading efficiency.
- Some models feature an optional "floating bright spot" which illuminates dense area —at the touch of a button.
- Optional remote controls eliminate need to stand directly in front of viewer to operate it.
- Smaller capacity units on casters provide room-to-room mobility as needed.
- Specially dedicated models are also available for MAMMOGRAPHY, ULTRASOUND, CT and NUCLEAR FILM VIEWING.

Ideal for Teaching, Lecturing or Consultation, S & S Motorized Viewers turn waste into efficiency. **How much is YOUR time worth?** Call S & S or your local x-ray dealer **today.**

S & S X-RAY PRODUCTS INC.
1101 Linwood Street
Brooklyn, NY 11208
800/347-XRAY
718/649-8500
FAX 718/257-0219



NOW IN CT



SOON IN MR

Winthrop has earned universal leadership in nonionic contrast media for CT. Look to us again in MR. For the overall quality of our products, our people, and our commitment to serve. Qualities that help radiology choose Winthrop contrast media first. Now in CT, and soon in MR.

Winthrop
PHARMACEUTICALS

DIAGNOSTIC IMAGING DIVISION

LEADERSHIP IN NONIONIC CONTRAST MEDIA

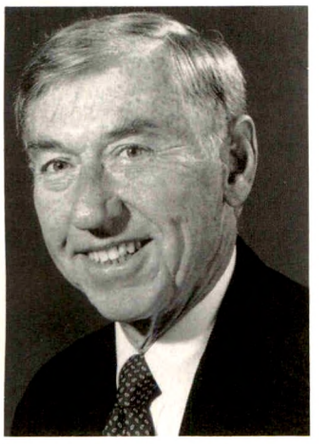
© 1991 Winthrop Pharmaceuticals

63-MAO82

ARRS Presidential Address

Reflections on Radiology as a Career

John A. Kirkpatrick, Jr.[1]



My message this morning is one that gives me great pleasure to deliver: it is a reminder of our good fortune in contributing to society as radiologists, and of our three roles—clinical care, teaching, and research. These roles have daily import in the life of every radiologist, whether in his or her office, in a community hospital, or in an academic setting. Every one of our many daily (often considered routine) interactions carries with it an element of each role. It is important, at a time when radiologists seem to be beset by conflicts with their clinical colleagues and with governments, to reflect on these and to acknowledge with appreciation the efforts of those in leadership positions, who as they vigorously pursue the goals of radiology, deserve our active support and participation.

Clinical Care

Interest in radiology is unprecedented at this time. Often the best graduates of medical schools are selecting it as their life's work. Radiology has become a true clinical specialty that encompasses hands-on medical care and surgical intervention. Combine this with tools that defy the imagination in respect to their ability to define anatomy, study function, and probe the very chemical constituents of tissue and one has a powerful and awesome armamentarium in the pursuit of accurate diagnosis with maximal benefit to the patient. This also mandates the evaluation of these tools as they relate to diagnosis, therapy, and the well-being of the patient. I in no way wish to take anything from the great clinicians—internists, pediatricians, or surgeons—but as Dr. Harry Mellins (personal communcation) has said so well, "The radiologist perceives a shadow, sees a lesion and imagines the man. The bedside clinician sees a man, perceives the signs and imagines the lesion. They practice from the outside in, and we practice from the inside out. Both are clinicians for, in truth, there is no other kind of doctor worthy of the name."

In our department at Children's Hospital, over 75% of the examinations are plain films and fluoroscopy—chest, abdomen, skeleton, gastrointestinal, genitourinary, and so on. These studies are the bridge between the radiologist and the clinician, a bridge that leads to the best care of the patient. A study may confirm the clinical diagnosis (not a trivial matter) or reveal the unexpected, but it also permits characterization beyond the realms of the stethoscope and of palpating or percussing fingers: "Yes, there is consolidation, but also a small amount of fluid, an element of atelectasis, and a mass; there is a fracture, but it is comminuted, pathologic, or through a growth plate." From these routine studies come the indications for the remaining 25%: sonography, CT, MR imaging, nuclear medicine, or radiologic intervention (vascular or nonvascular).

In a sense, the radiologist in a hospital is a gatekeeper; in an office, a vital step toward the next decision—antibiotics, bed rest, home care, hospitalization, or referral to a clinical specialist. He or she is also a communicator, a role necessary for the best care of patients and through which specialized contributions to diagnosis and treatment are anticipated and expected. Harvard Dean Henry Rosovsky said, "Communication is a special form of accountability" [1]. Our accountability is to our patients and to referring physicians.

Presented at the annual meeting of the American Roentgen Ray Society, Boston, MA, May 1991.

[1] Department of Radiology, Harvard Medical School and Children's Hospital, 300 Longwood Ave., Boston, MA 02115. Address reprint requests to J. A. Kirkpatrick, Jr.

AJR **157:447–448, September 1991** 0361–803X/91/1573–0447 © American Roentgen Ray Society

Education

We are teachers, but we are students first. Otherwise, why would we be here today? Why would our journals list pages of courses and seminars each month? Why would our personal libraries be so extensive and our journals so eagerly read in this country and abroad? At a recent meeting of the International Diagnostic Course in Davos, Switzerland, the meeting place for registrants between seminars was a huge area devoted to the sale of books and journals—some general, some technique-related, and some devoted to a small but significant anatomic area. One had to stand in line to peruse the offerings, so anxious were the participants for information and for reading material in their specialty.

There is another facet of education practiced daily by radiologists that is so routine and so commonplace that it is apt to be overlooked, in fact almost denigrated. In our normal interactions with students, residents, fellows, and colleagues, teaching is a serious part of our professional skill as radiologists. Can one discuss a chest radiograph without pointing out why the lobe is atelectatic, that is, the elevation of the fissure and the hilum? Is not the correlation of radiographs with the clinical assessment or pathologic findings an educational exercise? We work in a spotlight, and our endeavors are educational in nature. Like our surgical colleagues, we do procedures, the outcome of which is apparent to all. In order to have arrived at this point of ever-increasing clinical responsibilities, there has been an educational process that has led to collegial trust and to the development of many of our practices. Our aims in the development of quality-improvement plans speak clearly to our continuing efforts in self-evaluation. Fortunately, our images and reports are permanent and available for review, analysis, and study.

I am struck by the educational role that we continue to play in the development of MR imaging. As a technique, it was, and is, something to be learned, as is its application to diagnosis. As a clinical tool, its role must be brought to our colleagues—why T1 images show fat better than T2 images do, etc. This is an act of teaching performed daily, generously and instinctively. Think of surgical conferences, neurology seminars, and the dozens of daily interactions we have with clinicians. These interactions truly make us consultants, able to communicate that next step with shared confidence. Perhaps some might say that such educational activities contribute to turf wars, but so be it; it is the nature of the specialty and those of us who practice it. The goal is to learn more and temper technical understanding with the wisdom of experience and concern for the patient. One cannot forget the enormous efforts of the American College of Radiology in continuing medical education started over two decades ago.

Research

One tends to think of research as being confined to the laboratory. On the one hand, there is undoubtedly the need for an increased understanding of molecular biology as the future of MR imaging is planned. On the other, as Dr. James Thrall once commented to me, "Research in radiology is truly the understanding and application of the interaction of energy with tissue." We see this in the application of each imaging technique to the study of disease and, we hope, to the development of more sophisticated therapy. Dr. Benjamin Felson, in his Caldwell lecture, "Armchair Research and the Practicing Radiologist," [2] reminded us of the importance of collecting, collating, and documenting our clinical material; of the careful follow-up of personal cases through the department of pathology, the medical record room, the clinicians, or through direct contact with patients; and finally, of putting pen to paper to make these observations available to radiologic colleagues and clinicians. One need only peruse the program of this, the 91st meeting of the American Roentgen Ray Society, to realize the spectrum of research. One hundred and eighty-eight papers, a categorical course, 59 instructional courses, a symposium concerned with imaging of the breast, and 256 scientific exhibits are available, all provided by radiologists for radiologists. Each contribution has been obtained through careful observation. Each is derivative, from the laboratory, through protocols, but always with a view to learning something new and passing it on freely and with enthusiasm.

A dictionary definition of research is "studious inquiry; usually critical and exhaustive investigation of experimentation having for its aim the revision of accepted conclusions in the light of newly discovered facts" [1]. Because of the unstinting efforts of a number of our organizations and radiologic leaders, an added dimension to radiologic research is becoming a reality, a niche at the National Institutes of Health (NIH) that promises increasing support for radiologic research. As reported by Dr. Charles Putman, the NIH will create an autonomous intramural research laboratory on the main NIH campus. This will allow an identified focus in the training of radiologists for careers devoted to scientific pursuits. Further, the American Roentgen Ray Society, the Radiological Society of North America, and the Association of University Radiologists are embarking on renewed and expanded efforts in research and education.

So, although radiology still has problems (i.e., radiology by nonradiologists, turf wars waged about compensation), as outlined in the March 1991 *American College of Radiology Bulletin*, I am optimistic about our future as we support societal, legislative, and institutional efforts to bolster the status of radiology and also as we consider our clinical, educational, and research efforts and advances during the 92 years the American Roentgen Ray Society has been in existence. It should be a fine future, when we consider the innate intelligence, curiosity, and abilities of our students, trainees, and young associates and the advances in technology that have made us hands-on physicians as well as privileged users and evaluators of the most advanced technology.

I am proud to accept the presidency of this august society and to be associated with such an exciting and innovative specialty and with such outstanding colleagues. I thank you all for the great honor you have bestowed on me today.

REFERENCES

1. Rosovsky H. *The university: an owner's manual*. New York: Norton, **1990**
2. Felson B. Armchair research and the practicing radiologist (Caldwell Lecture). *AJR* **1986**;147:881–890

Review

Imaging of Vascular Complications Associated with Renal Transplants

Gerald D. Dodd III,[1] Mitchell E. Tublin, Ajit Shah, and Albert B. Zajko

Vascular complications associated with renal transplants are a significant cause of graft dysfunction. The most common complications are arterial and venous stenoses and thromboses and intrarenal and extrarenal arteriovenous fistulas and pseudoaneurysms. Although angiography is the imaging gold standard for the diagnosis of these disorders, Doppler sonography, scintigraphy, and occasionally CT are capable of detecting them. An awareness of the different imaging appearances of each complication will aid in their early detection and treatment. In this review, we present this information and provide a perspective on the relative roles of these techniques in the detection of vascular complications from renal transplants.

Vascular complications associated with renal transplants are a significant cause of graft dysfunction. They are reported to occur in up to 10% of transplantation patients, with the most common types being arterial and venous stenoses and thromboses and intrarenal and extrarenal arteriovenous fistulas (AVFs) and pseudoaneurysms [1–4]. If detected early, many are amenable to graft-sparing surgical or radiologic intervention. However, the clinical presentation of these lesions is often ambiguous, and imaging is required to differentiate them from the more common nonvascular causes of dysfunction. Although angiography is the accepted gold standard for the imaging diagnosis of these disorders, it is often the more routine imaging techniques, such as sonography, nuclear medicine, or sometimes CT that are the first to detect their presence. Therefore, early diagnosis of these complications requires a knowledge of their different appearances with each imaging technique.

In this review, we discuss the spectrum and varied imaging appearances of vascular complications associated with renal transplants.

Vascular Anatomy of the Normal Transplant

Accurate diagnosis of vascular complications in renal transplantation requires a thorough understanding of the postoperative vascular anatomy [4, 5]. There are two main types of arterial anastomoses, the choice of which is guided by the type of allograft available for transplantation. Cadaver kidneys are usually harvested with an intact main renal artery and an attached portion of aorta. The piece of aorta is trimmed to a circular or oval configuration (Carrel patch) and then sutured end to side to the external iliac artery of the recipient (Figs. 1A and 1B). Living donor kidneys cannot be harvested with a portion of aorta. Therefore, the main renal artery of the donor is sutured either directly end to side to the recipient's external iliac artery or sometimes end to end to the recipient's internal iliac artery. Venous anastomoses are almost always performed end to side to the recipient's external iliac vein (Fig. 1C).

Received February 25, 1991; accepted after revision April 30, 1991.

[1] All authors: Department of Radiology, University of Pittsburgh Medical Center, Presbyterian University Hospital, DeSoto at O'Hara St., Pittsburgh, PA 15213. Address reprint requests to G. D. Dodd III.

AJR 157:449–459, September 1991 0361–803X/91/1573–0449 © American Roentgen Ray Society

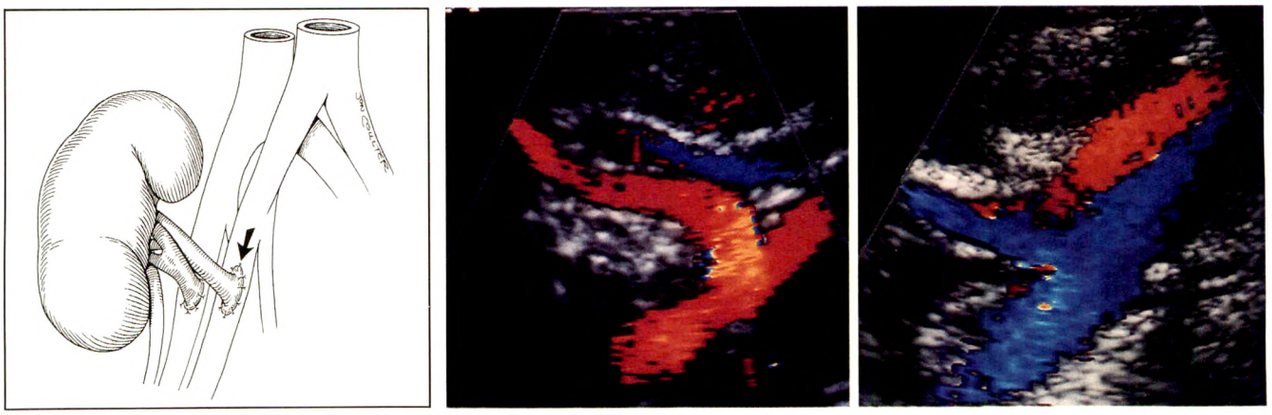


Fig. 1.—Vascular anatomy of normal renal transplant.
***A*, Anatomic diagram shows typical end-to-side anastomosis of main renal artery and vein to external iliac artery and vein. Note Carrel patch (*arrow*).**
***B*, Color Doppler sonogram shows end-to-side anastomosis of main renal artery to external iliac artery. Flow within artery (*red areas*) is toward transducer.**
***C*, Color Doppler sonogram shows end-to-side anastomosis of main renal vein to external iliac vein. Flow within vein (*blue areas*) is away from transducer.**

Imaging Techniques

Sonography

Conventional sonography should be performed on all renal grafts prior to a Doppler sonographic examination. Although it is of limited usefulness in the diagnosis of many vascular complications, conventional sonography will occasionally detect specific anatomic abnormalities suggestive of a vascular complication, as well as nonvascular causes of graft dysfunction.

The most appropriate use of Doppler sonography for the detection of vascular complications consists of screening the graft and associated vascular structures with color Doppler sonography followed by a duplex Doppler sonographic evaluation of any detected color Doppler abnormalities. This approach is based on the fact that color Doppler sonography, because of its ability to sample a long segment of one or more vessels at a time and display flow in vessels invisible to gray-scale sonography, is faster and less likely to miss vascular complications than is duplex Doppler sonography. However, color Doppler sonography is unable to accurately quantify flow disturbances. Thus, all flow abnormalities detected by color Doppler sonography must be quantified by duplex Doppler sonography [6, 7].

Effective Doppler sonographic screening requires appropriate adjustment of the Doppler controls. For most transplant vascular applications, both color and duplex Doppler imaging should be performed with the lowest filter setting, maximal gain without background noise, and smallest scale that will accommodate the highest normal peak velocities without aliasing. The choice of colors used to display vascular flow (the color map) should conform to the convention that flow toward the transducer be displayed as red and flow away from the transducer be displayed as blue (Figs. 1B and 1C). It is extremely helpful if the peak velocities of the antegrade and retrograde flows are displayed in colors different from each other and different from the reds and blues used to display slower flow. A color map of this design will allow rapid recognition of color aliasing indicative of abnormally increased velocities. Additional specific duplex Doppler controls that should be adjusted include gate size (which should be between 3 and 5 mm) and angle correction (which should be adjusted when quantifying peak flow) [7–9].

It is important to note that a Doppler signal can be displayed in terms of frequency shift (kHz) or velocity (m/sec). Both are equally accurate and intimately related, as demonstrated in the Doppler formula [9]:

$$\text{Frequency shift} = \frac{2 \times \text{Doppler frequency} \times \text{flow velocity} \times \cos\theta}{\text{velocity of sound}};$$

however, there is a significant difference in the way the two are reported on a sonographic CRT screen. With all other variables held constant, the reported frequency shift varies with changes in the insonating Doppler frequency, whereas the reported flow velocity remains constant. This is important to keep in mind when reviewing published Doppler criteria used in the diagnosis of specific vascular complications. If criteria are reported in terms of frequency shift, to remain valid, they must be adjusted for Doppler insonating frequencies of individual probes.

Scintigraphy

A variety of radionuclides can be used to image vascular complications associated with renal transplants. An in-depth discussion concerning the relative merits of each isotope is beyond the scope of this review. Suffice it to say that the most common agent in use, ^{99m}Tc-DTPA, is adequate for the

detection of most vascular complications in renal transplants. Image acquisition, which should begin immediately after venous injection of the isotope, should include a flow phase (one image per second for 60 sec) for the depiction of vascular anatomy and a functional phase (one image every 30 sec for 30 min) for the depiction of renal parenchyma and urinary drainage. Analysis of the images can be either qualitative or quantitative, depending on personal preference. Either is adequate for the detection of the majority of vascular complications [10].

Angiography

Arteriographic evaluation of renal transplants is usually performed with intraarterial digital subtraction techniques and dilute contrast material. In this way the study can be completed with the smallest amount of contrast material. In general, 4- to 5-French catheters are used for most studies. A contralateral femoral arterial approach is used for the evaluation of renal allografts anastomosed to the internal iliac artery. For end-to-side anastomoses to the external iliac artery, an ipsilateral or contralateral approach is used, depending on the indication for the examination. Image acquisition rates should include an early rapid phase for arterial anatomy and a prolonged slower phase for parenchymal and venous anatomy [11, 12].

Vascular Complications

Renal Artery Stenosis

Arterial stenoses, with a reported prevalence of approximately 10%, are the most common vascular complications of renal transplants [1, 2, 13, 14]. They usually occur within the first 3 years after transplantation and are more common in grafts from cadavers, especially those of young donors, than in grafts from living donors [4, 15, 16]. The hallmark of a significant stenosis is hypertension. However, up to 80% of transplant recipients may exhibit hypertension unrelated to arterial stenosis. Therefore, suspicion of a stenosis is reserved for patients with specific hypertensive profiles, such as newly developed or progressive hypertension, marked hypertension resistant to medical therapy, hypertension with graft dysfunction in the absence of rejection, or hypertension in the presence of a systolic bruit audible over the graft [2, 4]. Invasive therapy (surgical or radiologic) for stenoses is reserved for patients whose hypertension is uncontrolled by intensive medical therapy or who have significant renal failure in the absence of other causes of dysfunction [13, 15, 17, 18].

Three main types of stenoses have been described: anastomotic, distal donor, and recipient artery. Anastomotic stenoses occur more frequently in end-to-end anastomoses, distal stenoses occur more frequently in end-to-side anastomoses, and recipient artery stenoses occur equally in both types. Anastomotic lesions are primarily short-segment stenoses, composed of variable amounts of intimal fibrosis and calcium, that have been ascribed to surgical difficulties such as tight sutures, incomplete intimal approximation, excessive vessel length, twisting of the vascular pedicle, and large discrepancies in donor and recipient arterial size. Distal donor stenoses are single or multiple long-segment stenoses, composed primarily of diffuse intimal hyperplasia, that are caused by hemodynamic turbulence distal to the anastomosis, intimal injury caused by the graft perfusion catheter, or excessive dissection around the main renal artery that results in destruction of the vasa vasorum. Both anastomotic and distal donor stenoses may also be caused by rejection. Recipient stenoses are uncommon and usually due to either native atherosclerotic disease or intraoperative clamp injury [1, 2, 4, 5, 13, 14].

Imaging techniques useful in the diagnosis of stenoses include duplex Doppler imaging, color Doppler imaging, and angiography. Scintigraphy is of questionable usefulness, and MR angiography has not yet been evaluated.

Duplex and color Doppler sonography.—The use of Doppler sonography in the detection of arterial stenosis in renal transplants is quite similar to its use in the evaluation of carotid arterial disease. In both, the vessels of interest are insonated throughout their extent, looking for abnormally elevated peak velocities and turbulent flow indicative of stenosis. Specific criteria denoting significant stenosis have been established for each application. The most reproducible criteria for renal transplants were published by Taylor et al. [19]. Using a 3-MHz transducer, they found that significant stenoses (those requiring intervention) were associated with peak Doppler shifts greater than 7.5 kHz (2 m/sec) at the stenosis and turbulence in the immediate poststenotic segment. Their criteria were substantiated by a prospective study performed by Snider et al. [20], in which 16 of 17 significant stenoses (>50% luminal narrowing) in 32 transplants were correctly identified, for an overall sensitivity of 94% and specificity of 87%. The results of these and other studies indicate that duplex Doppler sonography can be used to identify significant stenoses.

The success of this technique depends on direct insonation of the stenosis. As stenoses occur in different locations in both the main and segmental renal arteries, these vessels must be insonated throughout their entirety. Unfortunately, visualization of these vessels is often quite difficult. Thus, the duplex Doppler examination is commonly a prolonged and tedious procedure in which the arteries are located by a trial-and-error method. If portions of the vessels are skipped, stenoses cannot be excluded.

Color Doppler sonography, with its larger field of view and ability to detect vessels invisible to gray-scale sonography, is both faster and less likely to miss a stenosis than is duplex Doppler. With properly adjusted color controls, the abnormally increased velocities associated with stenoses appear as regions of focal aliasing (Fig. 2A). Once located, these regions can be examined with duplex Doppler sonography to determine the nature and severity of the flow disturbance (Fig. 2B).

The combination of these Doppler techniques provides a very sensitive method for the detection of arterial stenoses. Unlike angiography, they are essentially risk-free procedures and thus can be used together as a screening tool. If a Doppler study is of reasonable quality and no significant flow abnormalities have been identified, then significant stenoses can be excluded with a relatively high degree of confidence. If a strong clinical suggestion of stenosis persists, then an-

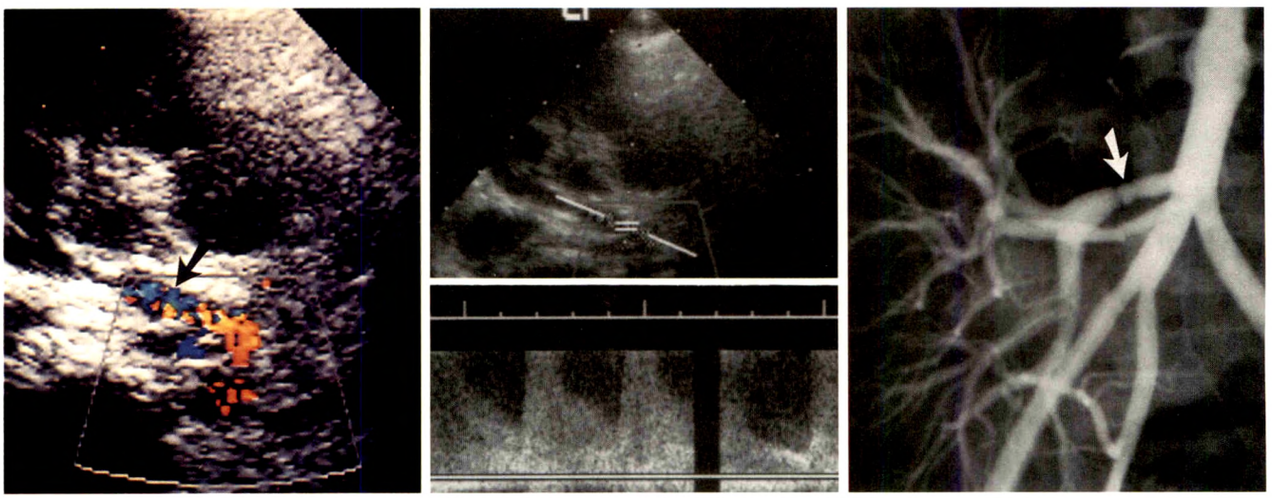


Fig. 2.—Renal arterial stenosis.

***A*, Color Doppler sonogram of end-to-side anastomosis of main renal artery to aorta in a child shows high-velocity blue green aliasing (*arrow*) within stenotic segment of donor main renal artery 2 cm distal to anastomosis.**

***B*, Duplex Doppler spectrum at region of color aliasing shows peak velocities greater than 6 m/sec (23 kHz) with marked spectral turbulence consistent with a significant stenosis.**

***C*, Arteriogram of dual end-to-side anastomosis shows stenosis (*arrow*) of cephalic donor main renal artery 2 cm distal to anastomosis. Hypertension resolved after balloon dilatation of stenosis.**

giography should be performed to exclude an undetected stenosis of a segmental or accessory renal artery [6]. All flow disturbances that meet or exceed the criteria of Taylor et al. [19] should be evaluated by angiography so that the severity of the lesions can be graded and false-positive results excluded.

Scintigraphy.—In routine transplant scintigraphy, the effects of arterial stenosis are indistinguishable from those of rejection and cyclosporine toxicity. All cause a progressive decrease in renal perfusion and function that can be identified on serial imaging [10]. It is usually only after the clinical exclusion (by percutaneous biopsy) of rejection and cyclosporine toxicity that the diagnosis of stenosis is suspected. Recent reports claim that scintigraphy done before and after the administration of captopril can detect native renal artery stenoses with a high degree of confidence [21]. However, these claims have yet to be substantiated in renal transplants [22].

Angiography.—Angiography is accepted as the most accurate imaging technique for the evaluation of renal artery stenoses. It clearly depicts the three types of stenoses described and is considered the gold standard for quantification of degree of stenosis and demonstration of multiple stenoses (Fig. 2C). It rarely produces false-positive results from overlapping vessels obscuring stenoses.

Renal Artery Thrombosis

Thrombosis of the main renal artery occurs in less than 1% of renal transplantation patients [2, 4]. It is usually an acute event in the early postoperative period (<1 month), and invariably results in graft loss. Hyperacute and acute rejection are by far its most common causes. However, intraoperative intimal trauma, faulty intimal approximation, wide disparity in vessel size, end-to-end anastomoses, vascular kinking, hypotension, hypercoaguable states, cyclosporine, and atherosclerotic emboli have all been cited as precipitators of thrombosis [23–25]. Thrombosis of the main renal artery has also been reported to occur in transplants as a result of acquired stenosis [26]. Although most cases require nephrectomy, there is at least one case report of successful reperfusion after the use of selective intraarterial thrombolytic drugs [26].

Segmental renal artery thrombosis is clinically less obvious than is main renal artery thrombosis. In our experience, symptoms may be absent or consist of graft tenderness, decreased function, or hematuria. Most limited infarcts result in a focal scar rather than complete graft loss.

The diagnosis of segmental or main renal artery thrombosis requires detection of absent arterial flow. Duplex Doppler sonography, color Doppler sonography, scintigraphy, and angiography all can provide this information.

Duplex and color Doppler sonography.—In the presence of an occlusive arterial thrombus, neither duplex nor color Doppler sonography will detect flow in the arterial branches distal to the occlusion [6, 19]. Venous flow likewise will be absent. As long as the Doppler equipment is functioning properly, these findings are highly specific for renal artery thrombosis. However, false-positive readings of renal artery thrombosis can be created if the Doppler equipment is poorly calibrated, or in rare cases with high-grade stenosis and minimal flow. False-positive readings caused by equipment problems can be prevented by using the adjacent iliac vessels to check for malfunction and to adjust the Doppler settings. Color Doppler

sonography, because of its larger field of insonation, is more likely to detect segmental infarcts than is duplex Doppler sonography [6]. Thrombosis of the main renal artery should be detected equally well by both techniques.

Scintigraphy.—The scintigraphic findings of renal artery thrombosis are fairly specific [10, 27]. The absence of renal arterial flow prevents visualization of a normal scintigraphic nephrogram. In addition, a large avascular kidney in the pelvis produces a focal ipsilateral decrease in isotope intensity that is less than the background intensity of the contralateral side (Fig. 3A). This "cold spot" is highly suggestive of an infarcted kidney; however, hyperacute or accelerated rejection can cause a similar appearance.

Segmental arterial thromboses produce persistent intrarenal photopenic defects that are classically wedge shaped [10]. Although their appearance is fairly specific, other causes of focal photopenic areas such as hematomas, abscesses, and cysts should be included in the differential diagnosis.

Angiography.—The angiographic findings of an occlusive thrombus vary depending on its location and extent. If the thrombus extends to or near the origin of the vessel, then the vessel will not be visible except for perhaps minimal irregularity at its origin or filling of a small stump [28]. Occasionally, contrast material will surround a portion of a partially occlusive thrombus and cause a filling defect within the lumen of the artery (Fig. 3B). In all cases of occlusive thrombus, the parenchyma in the distribution of the occluded vessel is not visualized.

Intrarenal Arteriovenous Fistulas and Pseudoaneurysms

Intrarenal AVFs and pseudoaneurysms are almost exclusively the result of trauma induced during percutaneous needle biopsy. AVFs occur with simultaneous laceration of adjacent arteries and veins, whereas pseudoaneurysms result from isolated arterial laceration. Injury of any of the renal hila or parenchymal vessels from segmental to arcuate may lead to their formation. The prevalence of these lesions has been reported as 1–18% [29–31]. This wide discrepancy is most likely due to their predominantly benign and asymptomatic course. Most AVFs and pseudoaneurysms are small and resolve spontaneously. AVFs that produce symptoms do so when they become large enough to cause decreased renal perfusion via marked arteriovenous shunting, or when they communicate with the caliceal system and produce hematuria. Pseudoaneurysms cause symptoms when they rupture into the perinephric space or renal collecting system [32]. In light of their predominantly benign nature, repair of AVFs and pseudoaneurysms is indicated only when they become symptomatic or large. The majority of these lesions can be treated effectively by percutaneous transcatheter embolization [32–34].

Imaging techniques applicable to the diagnosis of AVFs and pseudoaneurysms are duplex Doppler sonography, color Doppler sonography, and angiography. Scintigraphy can be used to detect some large pseudoaneurysms and AVFs but not to resolve smaller lesions.

Duplex and color Doppler sonography.— The duplex Doppler findings of both AVFs and pseudoaneurysms are fairly specific [19, 35]. AVFs exhibit high-velocity low-impedance arterial waveforms with associated arterialized venous tracings (Figs. 4A and 4B). Pseudoaneurysms show highly turbulent pulsatile flow in their central lumen with classic "machinelike" to-and-fro flow at their neck. The actual flow at the neck is variable, with only very narrow orifices showing classic machinelike to-and-fro flow. The spectral aberrations of both AVFs and pseudoaneurysms are always localized to a portion of the kidney, with "normal" hemodynamics in the remaining parenchymal vessels. Most AVFs are invisible to gray-scale sonography, whereas most pseudoaneurysms are identified as focal cysts. Thus, duplex Doppler detection of AVFs is limited to a blind, hunt-and-peck method, whereas detection of pseudoaneurysms requires only insonation of apparent renal cysts. Color Doppler sonography, owing to its wide field of view, greatly increases the detection of AVFs [6, 36, 37].

The color appearance of AVFs depends on their size. Small lesions appear as focal areas of color aliasing that reflect increased arterial velocities. Larger lesions produce considerable perifistula tissue vibration that causes a focal flurry of disorganized color at normal Doppler settings (vibration detection depends on sensitivity of color Doppler sonography and thus may not be detected by some machines). With



Fig. 3.—Renal arterial thrombosis.
***A*, Renal scintigram of thrombosed renal artery in dual renal transplant shows absent nephrogram with cold spot (*arrows*) in caudal transplant bed located between normally functioning cephalic renal transplant (*arrowhead*) and bladder.**
***B*, Arteriogram of end-to-end anastomosis of main renal artery to internal iliac artery shows anastomotic stenosis (*arrow*) with abundant intraluminal thrombus (*arrowheads*) distal to stenosis. (Reprinted with permission from Zajko et al. [26]).**

P24469

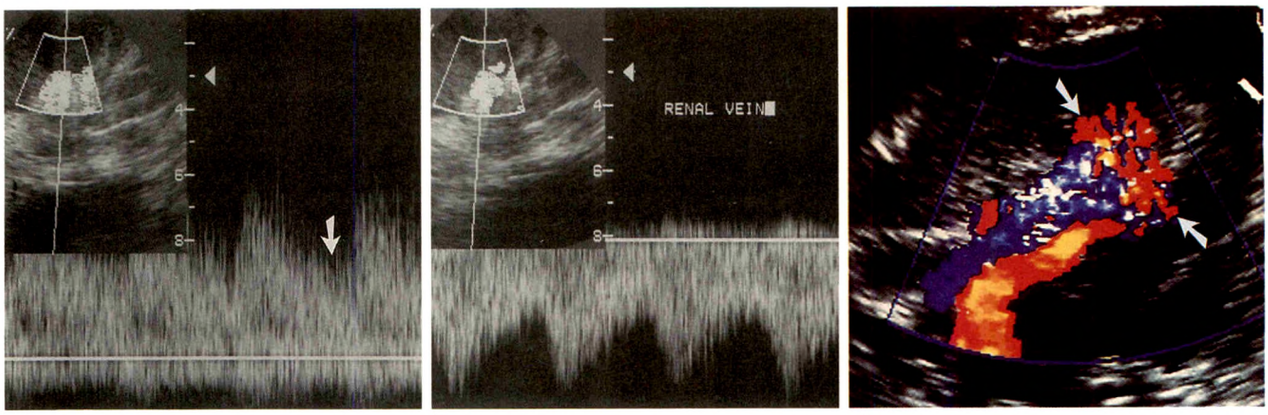


Fig. 4.—Doppler sonography of intrarenal arteriovenous fistula (AVF).
A, Duplex Doppler spectrum of AVF feeding artery in lower pole shows high-velocity, low-impedance flow. Diastolic flow (*arrow*) is increased. Doppler of arterial flow elsewhere in kidney (*not shown*) demonstrated normal flow with decreased velocity and lower diastolic flow.
B, Duplex Doppler spectrum of AVF draining vein shows arterialized venous flow.
C, Color Doppler sonogram of AVF shows prominent feeding artery (*red areas*), draining vein (*blue areas*), and region of fistula (*arrows*).

adjustment of wall filters and color scales, the feeding artery and draining vein of large AVFs may be visualized [6, 36, 37] (Fig. 4C). Regardless of size, AVFs detected by color Doppler sonography should be verified with duplex Doppler sonography to exclude confusion with similar color aberrations that may be caused by segmental stenoses or focally prominent normal vessels [37].

Pseudoaneurysms are demonstrated equally well by duplex and color Doppler sonography. The color appearance of a pseudoaneurysm consists of disorganized color flow within an apparent cyst, with the same surrounding parenchymal vibration color as is seen with AVFs [6, 35, 37] (Fig. 5). Close interrogation may reveal the communicating neck, which appears as alternating jets of forward and reverse color. The color appearance of a pseudoaneurysm is virtually diagnostic. However, both the color and duplex findings may be confusing in the rare instance in which a pseudoaneurysm communicates with an AVF. In this situation, the aneurysmal cyst will exhibit both a feeding artery and an arterialized draining vein.

Scintigraphy.—Intrarenal AVFs cannot be visualized directly by scintigraphy. Rather, their presence can be suggested with a high degree of certainty if premature isotope activity is detected within the inferior vena cava during the flow phase of the study (Fig. 6). After the flow phase, they become invisible. Large intrarenal pseudoaneurysms are detectable as focal hot spots that appear in the early flow phase and often persist into the functional phase of the study. Their appearance is diagnostic [27].

Angiography.—Angiography is considered the most sensitive technique for the detection of AVFs and pseudoaneurysms. The diagnostic finding of an AVF consists of early visualization of a renal vein during the arterial phase (Fig. 7). The extent of early venous opacification is directly related to the size of the AVF; the larger the lesion, the earlier and more extensive the venous opacification. A pseudoaneurysm appears as a spherical extravascular collection of contrast material that opacifies during the arterial phase and often persists into the late venous phase. Venous opacification is usually normal, except in the rare instance in which a pseudoaneurysm communicates with an AVF (Fig. 8). The degree of opacification of a pseudoaneurysm depends on the size of its neck and the amount of thrombus within its lumen. Pseudoaneurysms may exhibit heterogeneous opacification owing to luminal thrombus [29].

Extrarenal Arteriovenous Fistulas and Pseudoaneurysms

Extrarenal pseudoaneurysms and AVFs are less common and usually have a different cause and worse prognosis than their intrarenal counterparts do. They are commonly asymptomatic and found as unsuspected lesions on imaging studies performed for unrelated reasons. Occasionally they cause renal dysfunction by excessive arteriovenous shunting or direct compression of the main renal artery. The most serious complication of these lesions is exsanguination due to spontaneous rupture of a pseudoaneurysm. The severity of this complication makes extrarenal pseudoaneurysms a relative clinical emergency requiring timely intervention [38–40].

Faulty vascular reconstruction is the most common cause of both extrarenal pseudoaneurysms and AVFs. Less common causes are erroneous percutaneous biopsies and perigraft infection [41–43]. When these lesions are due to surgical defects or infection, they are usually located at the surgical anastomosis. Those due to biopsy can occur anywhere along the main renal or iliac vessels. When pseudoaneurysms are infected, both the PA and the renal transplant must be resected.

Extrarenal pseudoaneurysms may be diagnosed definitively by duplex Doppler sonography, color Doppler sonography, and angiography, and may be suggested by scintigraphy and contrast-enhanced CT. The diagnosis of extrarenal AVFs is

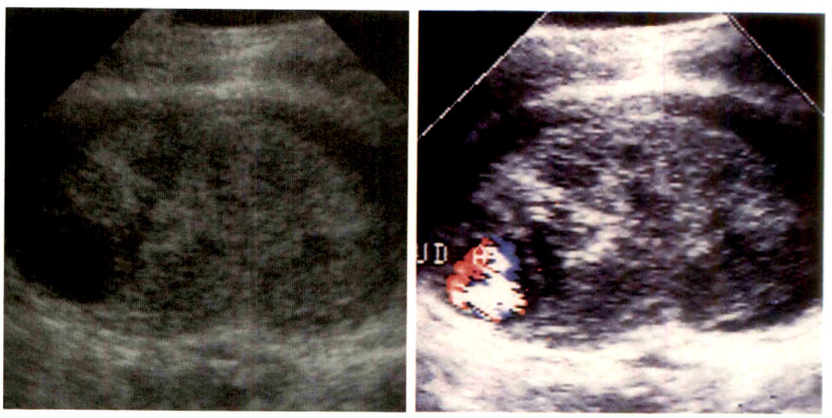


Fig. 5.—Sonography of intrarenal pseudoaneurysm.
A, Gray-scale sonogram of intrarenal pseudoaneurysm shows apparent "simple cyst."
B, Color Doppler sonogram of same pseudoaneurysm shows obvious flow within cyst.

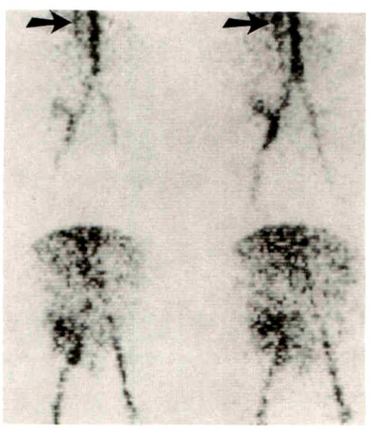


Fig. 6.—Renal scintigram of arteriovenous fistula shows premature isotope activity in inferior vena cava (*arrows*) during early flow phase. Inferior vena cava is not visible in later flow phase.

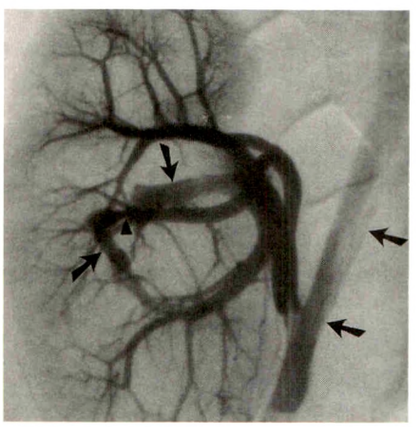


Fig. 7.—Arteriogram of intrarenal arteriovenous fistula shows diagnostic early visualization of renal and external iliac veins (*arrows*), as well as fistula (*arrowhead*).

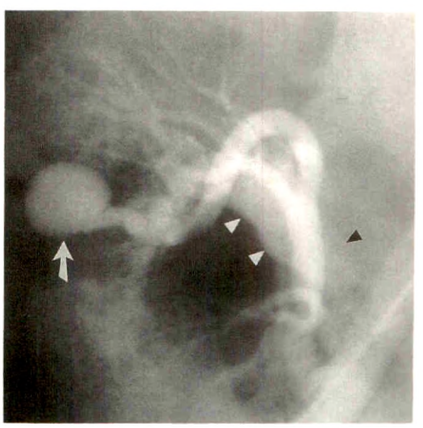
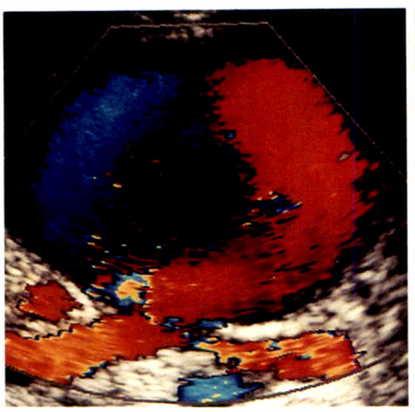


Fig. 8.—Arteriogram of intrarenal pseudoaneurysm shows diagnostic spherical collection of contrast material (*arrow*). Early venous opacification (*arrowheads*) is due to concomitant arteriovenous fistula.

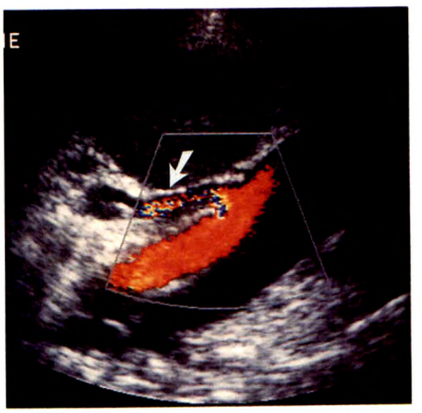
best made by angiography, but can be suspected by duplex Doppler sonography, color Doppler sonography, and scintigraphy. CT cannot detect AVFs.

Duplex and color Doppler sonography.—Extrarenal pseudoaneurysms appear as predominantly anechoic, spherical, paranephric fluid collections that exhibit Doppler characteristics identical to those of intrarenal pseudoaneurysms [2] (Fig. 9). Unless they are insonated they can be mistaken for other paranephric fluid collections such as lymphoceles and seromas. In our experience, extrarenal AVFs exhibit Doppler characteristics similar to those of their intrarenal counterparts. However, recognition of the extrarenal lesions is more difficult because of involvement of larger common vessels. In main renal arteries, the increased velocity and turbulence that occur in AVF feeding arteries can be easily mistaken for the abnormal hemodynamics of the more common arterial stenosis (Fig. 10). Recognition of the associated increased diastolic flow of an AVF will suggest the correct diagnosis. Confirmation can usually be obtained with detection of an adjacent arterialized draining vein. However, because the fistulized vein is a main common vein, the arterialization will be diffuse rather than focal, as occurs with intrarenal AVFs. This diffuse venous pulsation can be confusing because it also occurs in normal transplanted kidneys. Thus, the diagnosis of an extrarenal AVF requires careful evaluation of both the arterial and venous Doppler spectra. Absence of either characteristic spectrum should suggest an alternative diagnosis.

Scintigraphy.—Except for location, the scintigraphic features of these lesions are identical to those of intrarenal pseudoaneurysms and AVFs. In fact, intra- and extrarenal AVFs are nearly impossible to distinguish from each other. The appearance of extrarenal pseudoaneurysms is fairly diagnostic. However, because of location they can be confused with focal urine leaks. The two are differentiated by recognition of the early- or flow-phase appearance of a pseudoaneurysm (Fig. 11) vs the delayed or functional phase appearance of a urine leak. Pseudoaneurysms also tend to wash out sooner than urinomas do [27].



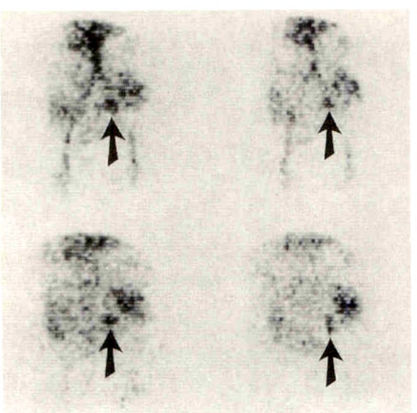
9



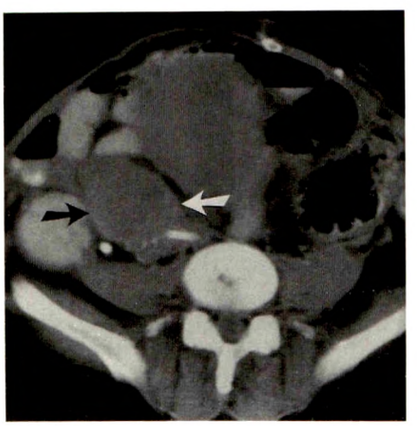
10

Fig. 9.—Color Doppler sonogram of large anastomotic extrarenal pseudoaneurysm shows swirling flow.

Fig. 10.—Color Doppler sonogram of extrarenal arteriovenous fistula (AVF) shows high-velocity color aliasing of main renal artery (*arrow*). Duplex Doppler spectrum obtained in region of AVF color aliasing (*not shown*) showed high-velocity, low-impedance arterial flow similar to Doppler spectrum in Fig. 4A. Doppler spectrum of main renal vein (*not shown*) showed venous arterialization similar to Doppler spectrum in Fig. 4B.



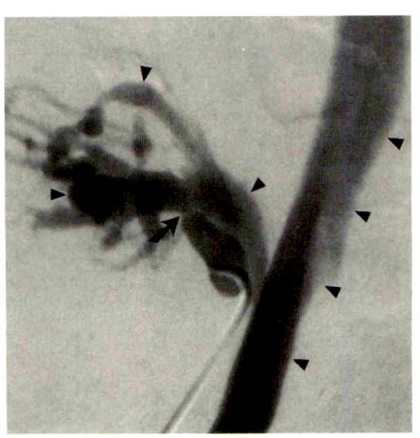
11



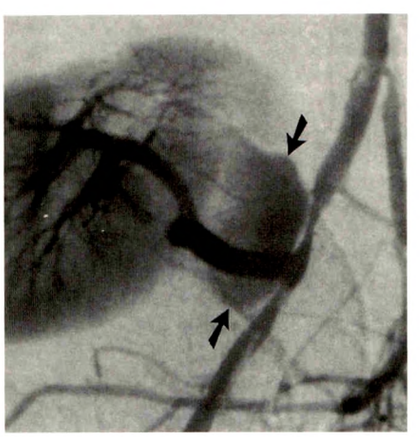
12

Fig. 11.—Renal scintigram of extrarenal pseudoaneurysm shows focal extrarenal accumulation of isotope (*arrows*) throughout flow phase.

Fig. 12.—Unenhanced CT scan of extrarenal pseudoaneurysm shows pseudoaneurysm as a mass with soft-tissue attenuation (*arrows*) contiguous with external iliac vessels and medial to lower pole of renal transplant.



13



14

Fig. 13.—Arteriogram of extrarenal arteriovenous fistula (AVF), with catheter tip in main renal artery, shows AVF (*arrow*) 2 cm distal to tip, with predominantly venous opacification (*arrowheads*) during early arterial injection.

Fig. 14.—Arteriogram of extrarenal pseudoaneurysm shows elliptical collection of contrast material (*arrows*) adjacent to end-to-side anastomosis. Note compression of external iliac artery by pseudoaneurysm.

CT.—Extrarenal pseudoaneurysms appear on CT as spherical, low-attenuation paranephric fluid collections (Fig. 12) that exhibit marked vascular contrast enhancement [44]. Their appearance is fairly characteristic, but should be confirmed with angiography or sonography.

Angiography.—Except for location, the angiographic appearances of extrarenal and intrarenal AVFs and pseudoaneurysms are identical (Figs. 13 and 14).

Renal Vein Thrombosis and Stenosis

Renal vein thrombosis is a rare complication of transplantation (0–4%) that mostly occurs in the early postoperative

period [1, 2, 4]. Symptoms are usually abrupt in onset and consist of graft tenderness, swelling, oliguria, proteinuria, and decreased renal function. Predisposing factors include hypovolemia, faulty surgical technique, propagation of ipsilateral common femoral or iliac deep venous thrombosis, and renal vein compression by postoperative fluid collections (hematoma, lymphocele, urinoma, abscess). Several investigators have also noted an increased rate of renal vein thrombosis in left lower quadrant allografts that has been attributed to compression of the left common iliac vein between the sacral promontory and the right common iliac artery [45].

Early diagnosis of renal vein thrombosis is paramount because prompt thrombectomy may restore graft function. However, most cases remain undetected, with prolonged venous stasis and thrombosis leading to graft loss. A few cases of delayed renal vein thrombosis due to chronic rejection have been treated successfully with anticoagulation and selective renal vein thrombolytic therapy [2].

Renal vein stenosis is a rare complication of transplantation about which little has been written. In our experience, its recognition is significant because, if discovered early and repaired, its deleterious effects on graft function are completely reversible. We have seen renal vein stenosis caused by perivascular fibrosis and compression by adjacent perinephric fluid collections.

Doppler sonography and venography can be used to diagnose renal vein thrombosis and stenosis. Scintigraphic studies can be suggestive of renal vein thrombosis but cannot detect renal vein stenosis. CT is useless for the diagnosis of both entities.

Duplex and color Doppler sonography.—Renal vein thrombi are rarely visualized by gray-scale sonography. Instead, the allograft can appear normal or enlarged, with decreased parenchymal echogenicity and nonvisualized renal veins [46, 47]. The duplex Doppler findings of renal vein thrombosis consist of absent renal venous flow and reversed plateauing diastolic arterial flow [48–50] (Fig. 15). When these two Doppler findings occur simultaneously, they are virtually diagnostic of renal vein thrombosis. Color Doppler sonography, although capable of demonstrating absent venous flow, lacks diagnostic specificity because of its inability to detect the altered arterial flow.

Venous stenoses are readily detected by color Doppler sonography as regions of focal aliasing that reflect the increased velocities associated with stenosis [19] (Fig. 16). Duplex insonation of these regions confirms and quantifies the velocity increases. Unfortunately, no information has been published correlating degree of accelerated velocities to degree of venous stenosis. We have found that velocities greater than three to four times those in the prestenotic segments are highly suggestive of significant stenoses.

Scintigraphy.—The scintigraphic findings of renal vein thrombosis are difficult to differentiate from other causes of decreased perfusion and function. The exact appearance depends on the degree and age of the thrombus. Myerly and Kirchner [51] have reported that absence of a nephrogram without a cold spot (i.e., isotope intensity of transplant bed equal to the background intensity of the contralateral pelvis) is characteristic of renal vein thrombosis. The absence of the cold spot implies that renal perfusion is present but markedly diminished. Other causes such as rejection can cause a similar appearance; however, the identification of this finding as an acute event in a series of scintigrams warrants immediate clinical attention.

Angiography.—The arteriographic findings of renal vein thrombosis (pulsatile arterial flow, delayed nephrogram, and delayed clearance of contrast material) are mostly nonspecific, indistinguishable from those of rejection. It is uncommon to visualize a venous thrombus during the venous phase of arteriography. The angiographic diagnosis of renal vein throm-

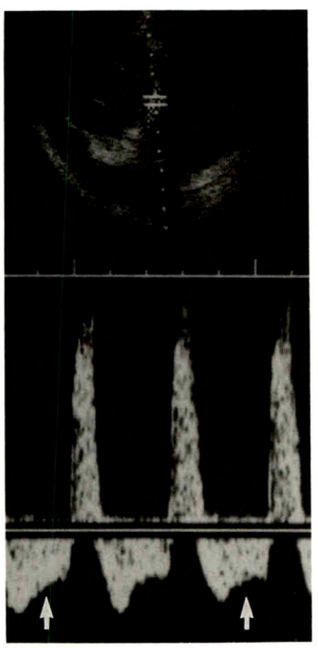


Fig. 15.—Duplex Doppler spectrum of main renal artery in a patient with renal vein thrombosis shows reversed plateauing diastolic flow (*arrows*). Venous flow was absent. Combination of these findings is highly suggestive of renal vein thrombosis.

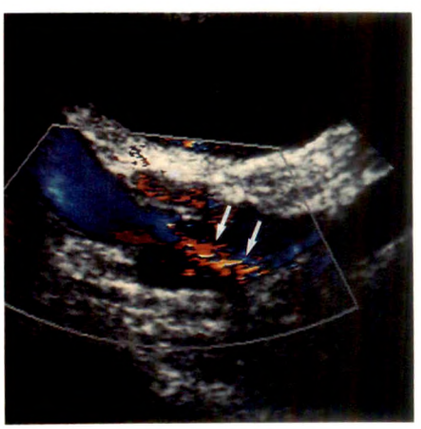


Fig. 16.—Color Doppler sonogram of stenosis of main renal vein just proximal to anastomosis with external iliac vein shows high-velocity color aliasing (*arrows*) within a perivascular hypoechoic mass. Duplex Doppler spectrum of main renal vein at level of color aliasing (*not shown*) demonstrated high-velocity flow, approximately six times greater than flow above or below region of aliasing, highly suggestive of significant stenosis.

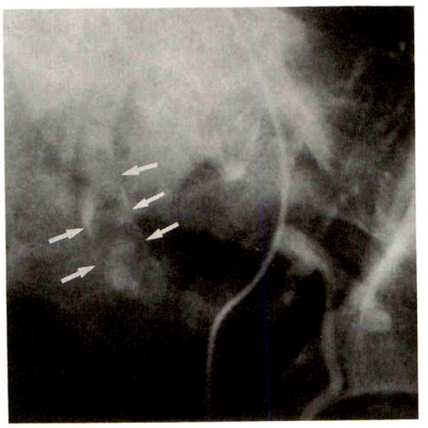


Fig. 17.—Venous-phase arteriogram of main renal vein thrombosis shows serpentine filling defect (*arrows*).

bosis and stenosis usually requires direct venography of the main renal vein [52]. Renal vein thrombi have the same appearance as any other venous thrombi. They appear as intraluminal filling defects, either occlusive with abrupt vascular terminations or nonocclusive with intraluminal filling defects (Fig. 17). Renal vein stenoses appear as focal venous narrowing, the significance of which is obvious if the stenoses are high grade. However, less severe stenoses are more difficult to interpret and must be correlated with the clinical signs and symptoms.

Conclusions

In this review, we have presented the clinical and imaging spectrum of vascular complications associated with renal transplants. Since many of these lesions are detected incidentally, radiologists need to be familiar with their varied appearance with different imaging techniques (Doppler sonography, scintigraphy, CT, and angiography). However, some of these techniques lack sensitivity, and thus should not be used to screen patients for vascular complications.

Screening of patients strongly suspected of having a vascular complication should be performed with Doppler sonography or angiography. All vascular complications except nonocclusive arterial and venous thromboses can be effectively detected and excluded with high-quality Doppler sonography. However, if the results of the Doppler examination are equivocal, the study suboptimal, or the sonographer inexperienced, angiography should be performed to adequately evaluate the patient. While small asymptomatic intrarenal AVFs and pseudoaneurysms detected by Doppler sonography need not be confirmed by angiography, all other vascular complications should be confirmed.

A thorough understanding of the clinical and imaging characteristics of vascular complications associated with renal transplants should increase the timeliness of their detection and decrease their associated morbidity and mortality.

ACKNOWLEDGMENTS

We thank the sonographers of the Presbyterian University Hospital sonography laboratory for the sonograms used in this manuscript and Rochelle Hornfeck for help in manuscript preparation.

REFERENCES

1. Jordan ML, Cook GT, Cardella CJ. Ten years of experience with vascular complications in renal transplantation. *J Urol* **1982**;128:689–692
2. Palleschi J, Novick AC, Braun WE, Magnusson MO. Vascular complications of renal transplantation. *Urology* **1980**;16:61–67
3. Hohnke C, Abendroth D, Schleibner S, Land W. Vascular complications in 1,200 kidney transplantations. *Transplant Proc* **1987**;19:3691–3692
4. Rijksen JFWB, Koolen MI, Walaszewski JE, Terpstra JL, Vink M. Vascular complications in 400 consecutive renal allograft transplants. *J Cardiovasc Surg (Torino)* **1982**;23:91–98
5. Honto D, Simmons R. Renal transplantation: clinical considerations in organ transplantation. *Radiol Clin North Am* **1987**;25:239–248
6. Grenier N, Douws C, Morel D, et al. Detection of vascular complications in renal allografts with color Doppler flow imaging. *Radiology* **1991**;178:217–223
7. Mitchell DG. Color Doppler imaging: principles, limitations and artifacts. *Radiology* **1990**;177:1–10
8. Needleman L, Kurtz AB. Doppler evaluation of the renal transplant. *JCU* **1987**;15:661–673
9. Taylor KJW, Holland S. Doppler US. Part I: Basic principles, instrumentation and pitfalls. *Radiology* **1990**;174:297–307
10. Kirchner PT, Rosenthall L. Renal transplant evaluation. *Semin Nucl Med* **1982**;12:370–378
11. Gedroyc WMW, Reidy JF, Saxton HM. Arteriography of renal transplantation. *Clin Radiol* **1987**;38:239–243
12. Picus D, Neeley JP, McClennan BL, Weyman PJ, Heiken JP. Intraarterial digital subtraction angiography of renal transplants. *AJR* **1985**;145:93–96
13. Roberts JP, Ascher NL, Fryd DS, et al. Transplant renal artery stenosis. *Transplantation* **1989**;4:580–583
14. Munda R, Alexander WJ, Miller S, First MR, Fidler JP. Renal allograft artery stenosis. *Am J Surg* **1977**;134:400–403
15. Barth MO, Gagnadoux MF, Mareschal JL, et al. Angioplasty of renal transplant artery stenosis in children. *Pediatr Radiol* **1989**;19:383–387
16. Stanley P, Malekzadeh M, Diament MJ. Posttransplant renal artery stenosis: angiographic study in 32 children. *AJR* **1987**;148:487–490
17. Grossman RA, DaFoe DC, Shoenfeld RB, et al. Percutaneous transluminal angioplasty treatment of renal transplant artery stenosis. *Transplantation* **1982**;34:339–343
18. Raynaud A, Bedrossian J, Remy P, Brisset JM, Angel CY, Gaux JC. Percutaneous transluminal angioplasty of renal transplant arterial stenosis. *AJR* **1986**;146:853–857
19. Taylor KJW, Morse SS, Rigsby CM, Bia M, Schiff M. Vascular complications in renal allografts: detection with duplex Doppler ultrasound. *Radiology* **1987**;162:31–38
20. Snider JF, Hunter DW, Moradian GP, Castañeda-Zuñiga WR, Letourneau JG. Transplant renal artery stenosis: evaluation with duplex sonography. *Radiology* **1989**;172:1027–1030
21. Chen CC, Hoffer PB, Vahjen G, et al. Patients at high risk for renal artery stenosis: a simple method of renal scintigraphic analysis with Tc-99m DTPA and captopril. *Radiology* **1990**;176:365–370
22. Miach PJ, Ernest D, McKay J, Dawborn JK. Renography with captopril in renal transplant recipients. *Transplant Proc* **1989**;21(1):1953–1954
23. Scott Samara EN, Voss BL, Pederson JA. Renal artery thrombosis associated with elevated cyclosporin levels: a case report and review of the literature. *Transplant Proc* **1988**;20:119–123
24. Rigotti P, Flechner SM, Van Buren CT, Payne WT, Kahan BD. Increased incidence of renal allograft thrombosis under a cyclosporin immunosuppression. *Surgery* **1986**;71:38–41
25. Aujla ND, Greenberg A, Banner BF, Johnston JR, Tzakis AG. Atheroembolic involvement of renal allografts. *Am J Kidney Dis* **1989**;12:329–332

26. Zajko AB, McLean GK, Grossman RA, et al. Percutaneous transluminal angioplasty and fibrinolytic therapy for renal allograft arterial stenosis and thrombosis. *Transplantation* **1982**;33:447–450
27. Manier SM, Van Nostrand D, Kyle RW. Primer and atlas for renal transplant scintigraphy: flow, Tc-99m DTPA, I-131, Hippuran. *Clin Nucl Med* **1985**; 10:118–133
28. Kaude JV, Hawkins IF. Renal transplantation. In: Abrams HL, ed. *Abrams angiography: vascular and interventional radiology*. Boston: Little, Brown, **1983**:1365–1391
29. Bennett AR, Wiener SN. Intrarenal arteriovenous fistula and aneurysm: a complication of percutaneous renal biopsy. *AJR* **1965**;95:372–382
30. Altebarmakian VK, Guthinger WP, Yakub YN, Gutierrez OH, Linke CA. Percutaneous kidney biopsies: complications and their management. *Urology* **1981**;18:118–122
31. Wickre CG, Golper TA. Complications of percutaneous needle biopsy of the kidney. *Am J Nephrol* **1982**;2:173–178
32. Benoit G, Charpentier B, Roche A, Bellamy J, Mohamedi D, Fries D. Arteriocalyceal fistula after grafted kidney biopsy: successful management by selective catheter embolization. *Urology* **1984**;24:487–490
33. Baquero A, Morris MC, Cope C, Raja R, Bannett AD. Selective embolization of vascular complications following renal biopsy of the transplant kidney. *Transplant Proc* **1985**;27:1751–1754
34. Wallace S, Schwarten D, Smith D, Gerson L, Davis L. Intrarenal AV fistulas: trans-catheter steel coil occlusion. *J Urol* **1978**;120:282–286
35. Weissman J, Giyanani VL, Landreneau MD, Kilpatrick JS. Postbiopsy arterial pseudoaneurysm in a renal allograft: detection by duplex sonography. *J Ultrasound Med* **1988**;7:515–518
36. Hubsch PJS, Mostbeck G, Barton PP, et al. Evaluation of arteriovenous fistulas and pseudoaneurysms in renal allografts following percutaneous needle biopsy: color coded Doppler sonography vs duplex Doppler sonography. *J Ultrasound Med* **1990**;9:95–100
37. Middleton WD, Kellman GM, Melson GL, Madrazo BL. Post biopsy renal transplant arteriovenous fistulas: color Doppler versus US characteristics. *Radiology* **1989**;171:253–257
38. Renigers SA, Spigos DG. Pseudoaneurysm of the arterial anastomosis in a renal transplant. *AJR* **1978**;131:525–526
39. Mulderije ED, Berden JHM, Buskens FGM, Raaijmakers PAM, Rosenbusch G. False and true aneurysms of the renal artery after kidney transplantation: a report of two cases. *Br J Radiol* **1985**;58:896–899
40. Pigott JP, Sharp WV. Arteriovenous fistula involving a transplant kidney: brief communications. *Transplantation* **1987**;44:1
41. Salahudeen AK, Sellars L, Srinivasa Merthy LN, et al. Extrarenal arteriovenous fistula: an unusual complication of percutaneous renal transplant biopsy. *Nephron* **1984**;37:64–65
42. Tobben PJ, Zajko AB, Sumkin JH, et al. Pseudoaneurysms complicating organ transplantation: roles of CT, duplex sonography, and angiography. *Radiology* **1988**;169:65–70
43. Kyriakides GK, Simmons RL, Najarian JS. Mycotic aneurysms in transplant patients. *Arch Surg* **1976**;3:472–476
44. Raval B, Balsara V, Kim E. Computed tomography detection of transplant renal artery pseudoaneurysm. *J Comput Tomogr* **1985**;9:149–151
45. Sorensen BL, Hald T, Nissen HM. Silent iliac compression syndrome. *Scand J Urol Nephrol* **1972**;15:75–77
46. Braun B, Weilemann LS, Weigand W. Ultrasonographic demonstration of renal vein thrombosis. *Radiology* **1989**;138:157–158
47. Rosenfield AT, Zeman RK, Cronan JJ, Taylor KJW. Ultrasound in experimental and clinical renal vein thrombosis. *Radiology* **1980**;137:735–741
48. Reuther G, Wanjura D, Bauer H. Acute renal vein thrombosis in renal allografts: detection with duplex Doppler ultrasound. *Radiology* **1989**;170:557–558
49. Kaveggia LP, Parrella RR, Grant EG, et al. Duplex Doppler sonography in renal allografts: the significance of reversed flow in diastole. *AJR* **1990**;155:295–298
50. Warshauer DM, Taylor KJW, Bia MJ, et al. Unusual causes of increased vascular impedance in renal transplants: duplex Doppler evaluation. *Radiology* **1988**;169:367–370
51. Myerly KF, Kirchner PT. Renal scintigraphic findings in a case of transplant renal vein thrombosis. *Clin Nucl Med* **1988**;13:426–429
52. Clark RA, Colley DP. Radiological evaluation of renal vein thrombosis. *Crit Rev Diagn Imaging* **1980**;13:337–388

AJR

AMERICAN JOURNAL OF ROENTGENOLOGY

MELVIN M. FIGLEY FELLOWSHIPS IN RADIOLOGY JOURNALISM 1992

The American Roentgen Ray Society announces two one-month fellowships in radiology journalism in the La Jolla editorial office of the AJR. Board-certified radiologists with special academic promise are invited to apply.

PURPOSE

The purpose of the fellowship is (1) to stimulate bright young radiologists to continue with an academic career, to accelerate their progress, and to stimulate their interest in good radiology journalism and (2) to improve the quality of radiology journals by teaching the fundamentals of medical journalism to academicians, training manuscript reviewers and future editors, and providing core teachers of medical journalism in radiology departments around the country.

CURRICULUM

The fellows will be taught the fundamentals of medical writing, manuscript preparation, peer review, manuscript editing, the ethics of scientific journalism, and journal publication and printing in personal tutorials given by the AJR editors and editorial staff through hands-on experience in the editorial office. They will visit Williams & Wilkins in Baltimore to observe the publication and printing process.

STIPEND

The successful candidates will each be awarded $10,000, which includes the cost of travel to La Jolla and Baltimore, living expenses for the month, and an honorarium.

APPLICATIONS

Candidates should apply in writing to Robert N. Berk, M.D., Editor-in-Chief, AJR Editorial Office, 2223 Avenida de la Playa, Suite 103, La Jolla, CA 92037. The letter must include a curriculum vitae and a description of the candidate's goals during the fellowship. Letters of recommendation from his or her department chairman and one other senior person are required. Deadline for receipt of applications is Nov. 1, 1991. The successful candidates will be notified Dec. 2, 1991.

Diffuse Pulmonary Alveolar Hemorrhage After Bone Marrow Transplantation: Radiographic Findings in 39 Patients

Robert J. Witte[1]
Jud W. Gurney[1]
Richard A. Robbins[2]
James Linder[3]
Stephen I. Rennard[2]
Mark Arneson[4]
William P. Vaughan[4]
Elizabeth C. Reed[4]
Karel A. Dicke[4]

Diffuse alveolar hemorrhage is a life-threatening complication after bone marrow transplantation. We investigated the radiographic abnormalities that occurred in 39 transplantation patients with a diagnosis of diffuse alveolar hemorrhage and correlated the findings with the patients' clinical course. The initial radiographic abnormalities after diffuse alveolar hemorrhage developed an average of 11 days after bone marrow transplantation, and the radiographic abnormalities preceded the clinical diagnosis by an average of 3 days. Twenty-seven patients initially had bilateral radiographic abnormalities; 10 initially had unilateral abnormalities (seven in the right lung, three in the left lung). Two patients had normal chest radiographs throughout their clinical course. All 37 patients with radiographic abnormalities had abnormalities involving the central portion of the lung, primarily the middle and lower lung zones. The initial radiographic pattern was interstitial in 27 and alveolar in 10. In 24 patients, radiographic abnormalities were initially judged to be mild; three were severe from the onset. Radiographic abnormalities rapidly worsened in most patients over 6 days. In 30 patients, diffuse bilateral radiographic abnormalities involving all lung zones developed. Eleven patients persisted in having only interstitial radiographic abnormalities; 26 had a confluent alveolar pattern. At the height of radiographic abnormalities, 27 cases were judged to be severe, and only one case was judged to be mild. The mortality rate in patients with diffuse alveolar hemorrhage was 77%.

The radiographic abnormalities of diffuse alveolar hemorrhage are nonspecific and usually precede the clinical diagnosis. The clinical course after hemorrhage is short, often resulting in death.

AJR **157:461–464, September 1991**

Received February 19, 1991; accepted after revision April 10, 1991.

Presented at the annual meeting of the American Roentgen Ray Society, Washington, DC, May 1990.

[1] Department of Radiology, University of Nebraska Medical Center, 600 S. 42nd St., Omaha, NE 68198-1045. Address reprint requests to J. W. Gurney.

[2] Pulmonary and Critical Care Section, Department of Internal Medicine, University of Nebraska Medical Center, Omaha, NE 68198-1045.

[3] Department of Pathology, University of Nebraska Medical Center, Omaha, NE 68195-1045.

[4] Hematology and Oncology Section, Department of Internal Medicine, University of Nebraska Medical Center, Omaha, NE 68195-1045.

0361–803X/91/1573–0461
© American Roentgen Ray Society

Pulmonary complications are common after bone marrow transplantation and include opportunistic infection, cardiac and noncardiac pulmonary edema, drug and radiation toxicity, and metastatic spread of tumor [1, 2]. Diffuse alveolar hemorrhage (DAH) is another newly described complication occurring in transplantation patients [3]. The radiographic abnormalities that occur with DAH in bone marrow transplantation patients have not previously been described. It was our purpose to review the radiographic abnormalities that occur with DAH and correlate these with the patient's clinical course.

Materials and Methods

Patients

The hospital records and chest radiographs of 39 bone marrow transplant recipients with a discharge diagnosis of DAH were reviewed from a total of 288 patients. Autologous bone marrow transplantations were performed for a variety of medical conditions in the patients in whom DAH eventually developed, including 15 patients with non-Hodgkin lymphoma, nine with Hodgkin lymphoma, six with breast carcinoma, three with melanoma, two with sarcoma, two with ovarian carcinoma, one with aplastic anemia, and one with acute myelogenous

leukemia. The average age of the patients with DAH was 41 years (range, 16–68 years). There were 21 women and 18 men.

Autopsies were performed in 21 (70%) of the 30 patients who died. DAH was the primary cause of death or significantly contributed to the cause of death in 19 (90%) of the 21 patients. At autopsy, the lungs were found to have scattered areas of hemorrhage. Microscopic examination of the lungs revealed intraalveolar hemorrhage. Reactive epithelial cells were often present, but no pathogens were identified.

Diagnosis of DAH

DAH was diagnosed on the basis of the findings from bronchoalveolar lavage when the lavage fluid became progressively bloodier with each aliquot aspirated from separate subsegments of the lung. DAH was diagnosed only when other conditions known to result in hemorrhage were excluded [3, 4].

Radiographs

We reviewed the chest radiographs of all patients in whom DAH was diagnosed, beginning with the pretreatment film and all films after transplantation. In most patients, portable films were obtained daily. The films were reviewed by two radiologists unaware of the time of bronchoscopy or the date of the diagnosis of DAH. The radiographs were reviewed independently by each radiologist and the findings were agreed on by consensus. Serial radiographs were analyzed for the following: (1) the initial pattern of pulmonary involvement (i.e., interstitial or alveolar), the distribution within the chest, and the pattern's severity; (2) the time between bone marrow transplantation and initial radiographic abnormality and the time between the initial radiographic abnormality and bronchoscopic diagnosis of DAH; (3) the time between the initial radiographic abnormality and the radiograph showing the most severe radiographic abnormality; and (4) other radiographic abnormalities that developed, such as pleural effusions or cardiomegaly.

An interstitial pattern was defined as one in which reticular or small nodular opacities predominated, or in which the vessel margins became indistinct. An alveolar pattern was defined as one in which acinar opacification with air bronchograms predominated. The distribution of radiographic abnormalities was categorized into two regions: (1) central or peripheral and (2) upper, middle, and lower zones. This distribution was determined by reference to the midpoint of the interlobar pulmonary artery. A central region was within a 4-cm radius from the artery and a peripheral region was from this 4-cm edge to the edge of the lung. Mirror-image regions were used for the left lung. The lower zone was a horizontal region from 3 cm below the midpoint of the interlobar pulmonary artery to the base of the lung; the middle zone was a horizontal region from 3 cm below to 3 cm above the interlobar pulmonary artery; the upper zone was a horizontal region from 3 cm above the interlobar pulmonary artery to the lung apex. Mirror-image boundaries were used in the left lung. Severity was graded as mild if the normal pulmonary arteries in the lung were easily identified but their borders were indistinct, moderate if the arteries were partially obscured but still visible, and severe if the arteries were completely obscured.

Results

The initial radiographic abnormalities were seen an average of 10.6 ± 8.5 days after bone marrow transplantation (range, 0–31 days) and preceded the diagnosis by bronchoalveolar lavage by an average of 3.4 ± 4.6 days (range, 0–24 days). The syndrome progressed rapidly, and the chest radiographs had the most severe radiographic abnormalities an average of 5.9 ± 6.5 days after the initial radiographic abnormalities were identified (range, 0–27 days).

Of the 39 patients, two had normal findings on chest radiographs. Of the remaining 37 patients, 27 had initial bilateral radiographic abnormalities, seven had abnormalities initially limited to the right lung, and three had abnormalities initially limited to the left lung.

The regional involvement was more common in the central and lower lung (Figs. 1 and 2). All 37 patients with abnormal radiographs had initial involvement of the central lung. In 12 (32%) of these 37 patients, the radiographic abnormalities extended to the peripheral lung. There were no patients with initial radiographic abnormalities limited to the peripheral lung. Twenty-two patients (59%) had involvement of the upper lung. In five patients (14%), this region was the only one involved. Twenty-nine patients (78%) had involvement of the middle lung, and 31 patients (84%) had involvement of the lower lung. A total of four patients (11%) had initial bilateral radiographic abnormalities involving all lung zones.

From their initial radiographic presentation, most patients developed diffuse radiographic abnormalities in the lungs (Figs. 1 and 2). Thirty patients developed diffuse bilateral radiographic abnormalities involving all lung zones, three patients had persistent unilateral involvement of the right lung, and four patients had bilateral involvement of middle and lower lung zones. No patients had unilateral involvement of the left lung.

The initial radiographic pattern was interstitial in 27 patients (73%) and alveolar in 10 patients (27%). At peak, 11 patients (30%) persisted in having only interstitial radiographic abnormalities and 26 patients (70%) had radiographic abnormalities that progressed to an alveolar pattern. Initially, 24 patients (65%) had radiographic abnormalities that were mild, 10 (27%) were moderate, and three (8%) were severe. Only one patient (3%) had peak radiographic abnormalities that were mild, nine (24%) had moderate abnormalities, and 27 (73%) had severe abnormalities.

Other radiographic findings included pleural effusions in five patients (14%) and mild cardiomegaly in seven patients (19%). None of the patients with pleural effusions had cardiomegaly.

Of the 37 patients whose radiographs were abnormal, 23 (62%) had no radiographic evidence of resolution, eight (22%) had partial resolution, and six (16%) resolved completely. The clinical outcome of patients with DAH was poor. Thirty died (77%) and nine recovered.

Discussion

DAH is a serious complication in patients undergoing bone marrow transplantation. The clinical signs and symptoms are nonspecific—most patients have hypoxia and dyspnea. Interestingly, hemoptysis is uncommon [3].

The cause of DAH is unknown. Several factors are thought to contribute to its pathogenesis, including radiation toxicity, drug toxicity, and WBC influx into the lung [3]. Patients with DAH have a higher prevalence of chest irradiation, either

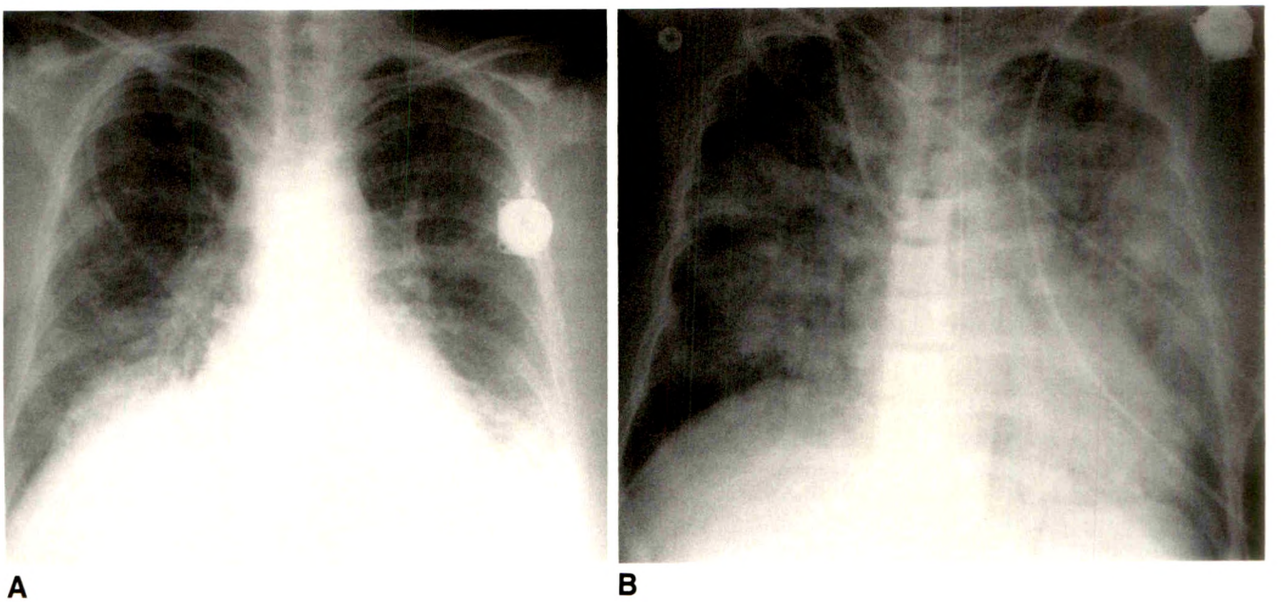


Fig. 1.—Chest radiographs in a 37-year-old woman with breast carcinoma.
A, Severe interstitial prominence is present in central lung and also involves middle and lower lungs 11 days after bone marrow transplantation.
B, 5 days later, there has been a progression to alveolar pattern and extension to all regions of lung.

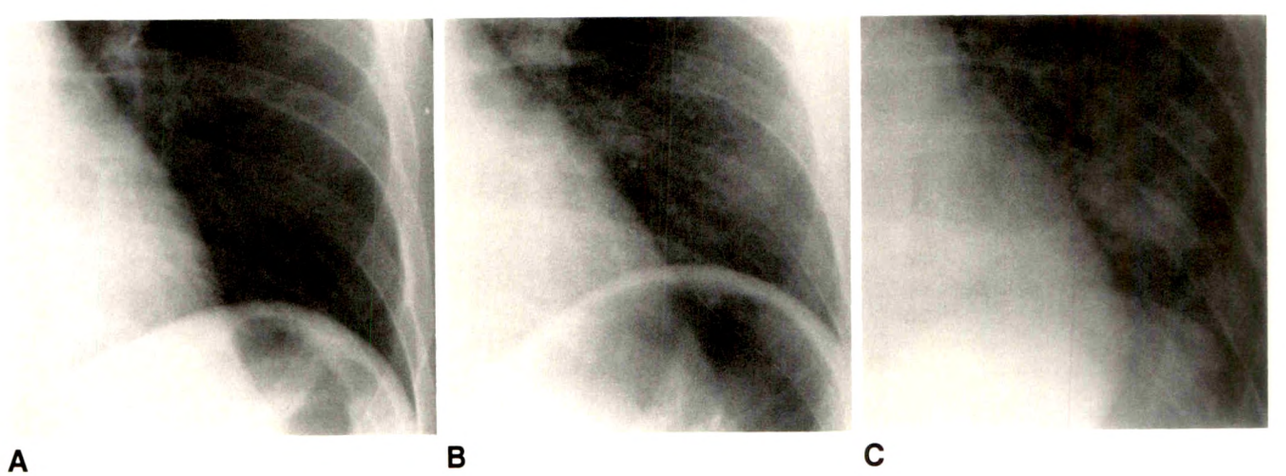


Fig. 2.—Chest radiographs in a 45-year-old man with melanoma.
A, Baseline radiograph coned to left base shows no abnormalities.
B, 11 days after bone marrow transplantation, vessels are now indistinct centrally.
C, 8 days later, a severe alveolar pattern is present extending to lung periphery.

whole body, chest, or mediastinal irradiation before bone marrow transplantation [1–3]. Treatment consists of platelet administration, and recently, high-dose steroids have shown promise in reducing the high mortality rate associated with this syndrome (Armitage JA, unpublished observations).

We found the radiographic abnormalities in DAH to be nonspecific. The findings associated with hemorrhage in the bone marrow transplantation population do not differ from descriptions of hemorrhage that occurs in other conditions [5, 6]. Most patients initially exhibited a mild interstitial or alveolar pattern in the central and lower lung zones. This is indistinguishable from pulmonary edema or opportunistic infection, other common complications after bone marrow transplantation. In addition, cardiomegaly and pleural effusions were occasionally seen in patients with DAH; these findings are usually suggestive of pulmonary edema. Although

DAH was usually a bilateral process, an initial unilateral abnormality, which could be easily confused with opportunistic infection, was sometimes seen (10 cases, 27%). Characteristically, DAH was fulminant, with rapid progression during 6 days to a diffuse, severe alveolar pattern. This mirrored the clinical course, in which 77% died. Although clinical signs and symptoms and the radiographic time course may help in the evaluation of the transplant recipient with diffuse pulmonary abnormalities, ultimately bronchoscopy or open lung biopsy is needed for differentiation.

The reported prevalence of hemorrhage after bone marrow transplantation varies. Pagani et al. [7] found one case of pulmonary hemorrhage out of 35 children after bone marrow transplantation. Cordonnier et al. [1] found a prevalence of 7% in 130 patients after bone marrow transplantation, and Crawford et al. [8] found an 8% prevalence. In our population of patients, 14% of the patients undergoing transplantation suffered DAH.

It has been speculated that DAH may be related to idiopathic interstitial pneumonitis [3, 8–10]. Both have a similar prevalence, time of onset after bone marrow transplantation (within the first 7 weeks after bone marrow transplantation), and a high mortality rate. Histologically, nonspecific inflammatory changes are seen in idiopathic interstitial pneumonitis; however, hemorrhage has not been specifically mentioned. Whether the two disorders represent the same entity is unknown [9, 10].

Radiographic abnormalities of DAH usually occur within the first 2 weeks after transplantation and rapidly progress to severely involve both lungs. The findings, however, are nonspecific and are identical to the findings in pulmonary edema and infection.

ACKNOWLEDGMENTS

We thank Mary Wilke for manuscript preparation. We also thank the UNMC Bone Marrow Transplant Pulmonary Study Group for their assistance in this study.

REFERENCES

1. Cordonnier C, Bernaudin J-F, Bierling P, Huet Y, Vernant J-P. Pulmonary complications occurring after bone marrow transplantation. *Cancer* **1986**;58:1047–1054
2. Krowka MJ, Rosenow EC, Hoagland HC. Pulmonary complications of bone marrow transplantation. *Chest* **1985**;87:237–246
3. Robbins RA, Linder J, Stahl MG, et al. Diffuse alveolar hemorrhage in autologous bone marrow transplant recipients. *Am J Med* **1989**;87:511–518
4. Linder J, Robbins R, Rennard S. Cytologic criteria for diffuse alveolar hemorrhage. *Acta Cytol* **1988**;32:763
5. Albelda SM, Gefter WB, Epstein DM, Miller WT. Diffuse pulmonary hemorrhage: a review and classification. *Radiology* **1985**;154:289–297
6. Palmer PES, Finley TN, Drew WL, Golde DW. Radiographic aspects of occult pulmonary haemorrhage. *Clin Radiol* **1978**;29:139–143
7. Pagani JJ, Kangarloo H, Gyepes MT, Feig SA, Falk PM. Radiographic manifestations of bone marrow transplantation in children. *AJR* **1979**;132:883–890
8. Crawford SW, Hackman RC, Clark JG. Open lung biopsy: diagnosis of diffuse pulmonary infiltrates after bone marrow transplantation. *Chest* **1988**;94:949–953
9. Cardozo BL, Hagenbeek A. Interstitial pneumonitis following bone marrow transplantation: pathogenesis and therapeutic considerations. *Eur J Cancer Clin Oncol* **1985**;21:43–51
10. Meyers JD, Flournoy N, Thomas ED. Nonbacterial pneumonia after allogeneic marrow transplantation: a review of ten year's experience. *Rev Infect Dis* **1982**;4:1119–1132

Motion Artifact Simulating Aortic Dissection on CT

M. Alan Burns[1]
Paul L. Molina
Fernando R. Gutierrez
Stuart S. Sagel

We recently imaged two patients clinically suspected of having aortic dissection whose contrast-enhanced CT examinations, obtained on a new scanner with a 1-sec scanning time, showed findings suggesting an ascending aortic dissection. The subsequent clinical course and evaluation implied that the CT findings were predominantly artifactual. We identified identical artifacts in 18% of 50 consecutive contrast-enhanced CT examinations performed for a variety of indications on the same scanner. The double-lumen artifact, simulating an intimal flap, occurs in the proximal ascending aorta and is limited to one or two contiguous transaxial images. The artifact was not detected on two other CT units. We believe the artifact arises from motion of the aortic wall and the surrounding pericardial recesses during image acquisition.

***AJR* 157:465–467, September 1991**

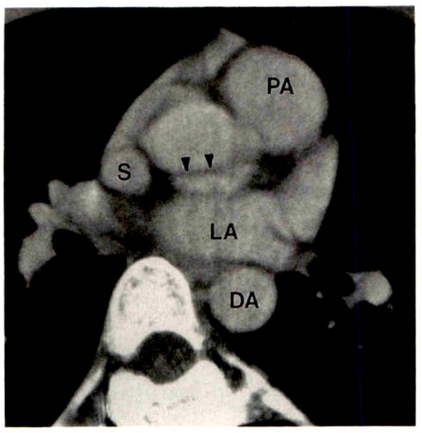
Contrast-enhanced CT is an effective method for diagnosing aortic dissection [1–6]. The examination is fast, noninvasive, and often supplies sufficient information for angiography to be avoided [6]. The CT diagnosis of dissection rests on identifying an intimal flap or a thrombosed false lumen surrounding the true lumen [7]. However, several pitfalls exist that may simulate an intimal flap or false channel. The left brachiocephalic vein, thickened pleura, streak artifacts, pericardial recesses, and atherosclerotic aneurysms with thrombus have all been described as potential causes of false-positive examinations [7, 8]. We describe another pitfall in the CT diagnosis of ascending aortic dissection, almost certainly due to motion artifact created by fast (1-sec scanning time) CT scanners.

We recently encountered two patients who were suspected clinically of having aortic dissection. The first, a 34-year-old woman with Marfan syndrome, had chest pain radiating into her back. Findings on posteroanterior and lateral chest radiographs were normal. Bolus contrast-enhanced dynamic scanning performed on a Somatom Plus (Siemens Medical Systems, Iselin, NJ), a continuously-rotating CT system with a 1-sec scanning time, suggested an intimal flap in the proximal ascending aorta on two contiguous 10-mm sections (Fig. 1). However, findings on aortography done immediately afterward were normal. The patient's chest pain resolved, and she has remained asymptomatic during a 5-month follow-up. Several weeks after this first case, a 45-year-old woman with a history of hypertension described similar symptoms of chest pain radiating into her back. Findings on chest radiographs and electrocardiograms were normal. Dynamic scanning with bolus contrast enhancement, again performed on the Somatom Plus, suggested circumferential dissection of the proximal ascending aorta (Fig. 2). Findings on a second examination on a Somatom DRH (Siemens Medical Systems, Iselin, NJ), a CT scanner with a 5-sec scanning time, and an MR examination of the aorta immediately afterward, were normal. Clinical follow-up in this patient also revealed resolution of symptoms.

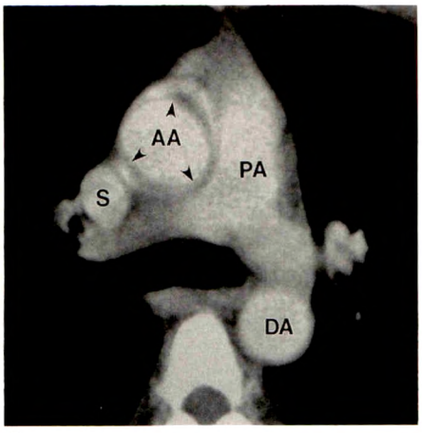
Received March 11, 1991; accepted after revision April 25, 1991.

[1] All authors: Mallinckrodt Institute of Radiology, Washington University School of Medicine, 510 S. Kingshighway Blvd., St. Louis, MO 63110. Address reprint requests to P. L. Molina.

0361–803X/91/1573–0465
© American Roentgen Ray Society



1



2

Fig. 1.—34-year-old woman with Marfan syndrome and chest pain. Contrast-enhanced image from Somatom Plus CT scanner at level of left atrium (LA) suggests an intimal flap (*arrowheads*) in ascending aorta. Numerous streak artifacts are seen arising from metallic fixation rods in thoracic spine. Findings on aortogram obtained immediately afterward were normal. S = superior vena cava; PA = pulmonary artery; DA = descending aorta.

Fig. 2.—45-year-old hypertensive woman with chest pain radiating into her back. Contrast-enhanced image from Somatom Plus CT scanner suggests circumferential dissection (*arrowheads*) of ascending aorta (AA). Findings on a second examination on a Somatom DRH CT scanner (5-sec scanning interval) and MR examination of aorta were normal. S = superior vena cava; PA = pulmonary artery; DA = descending aorta.

Our experience with these patients prompted further investigation of the prevalence, characteristic CT features, and potential causes of this artifact simulating dissection of the ascending aorta.

Materials and Methods

Fifty consecutive dynamic contrast-enhanced chest CT examinations from a 6-month interval (January–June, 1990) performed on a Somatom Plus CT scanner for a variety of nonselected indications (i.e., lymphoma follow-up, lung cancer staging) were reviewed together by two observers. Twenty randomly selected unenhanced chest CT scans done on the Somatom Plus during this same period also were examined. To assess the frequency of the artifact in a slower CT scanner, we reviewed 20 contrast-enhanced and 20 unenhanced randomly selected chest CT studies from a Somatom DRH CT scanner. To evaluate the frequency of the artifact in another fast CT scanner from a different vendor, we then reviewed 20 randomly selected contrast-enhanced CT scans of the chest obtained on a Quick Hilight CT scanner (GE Medical Systems, Milwaukee, WI; 1.2- to 1.3-sec scanning time). All studies included contiguous images from the base of the heart through the aortic arch using 8- to 10-mm section thickness. Contrast enhancement was provided by bolus IV infusion of 100–150 ml of contrast medium.

Studies were interpreted as positive if images showed an apparent intimal flap and/or double lumen of the ascending aorta (Figs. 1 and 2). On studies showing these findings, note was also made of the extent of the artifact and the presence or absence of any associated CT findings such as mediastinal or pericardial hemorrhage.

Results

Ten percent (two of 20) of unenhanced and 18% (nine of 50) of contrast-enhanced chest CT scans done on the Somatom Plus exhibited the artifact. Thirteen patients had both contrast-enhanced and unenhanced CT studies on the Somatom Plus. Of these, in one patient the artifact was visible on both contrast-enhanced and unenhanced examinations. In another patient, the artifact was visible on the unenhanced study, but not on the contrast-enhanced examination. In the remaining 11 patients with both unenhanced and contrast-enhanced CT scans done on the Somatom Plus, the scans did not show the artifact.

In all studies exhibiting this artifact, it was limited to one or two contiguous sections near the aortic root. None of these studies had any other evidence of aortic dissection, mediastinal hemorrhage, or pericardial hemorrhage.

The artifact was not detected on any CT scans done on either the Somatom DRH or GE Quick Hilight CT scanners.

Discussion

The exact cause of the artifact in our cases remains uncertain. We believe the artifact arises from motion of the aortic wall and the surrounding superior pericardial recesses during image acquisition. In our first index case, the apparent contrast-filled false lumen along the posterior margin of the ascending aorta (Fig. 1) probably represents pseudoenhancement of the retroaortic recess of the superior pericardial space. In a previous article describing the pitfall of the superior pericardial recesses simulating aortic dissection on CT, the authors reported that the recess often appeared to enhance after administration of contrast material, possibly as a result of volume averaging with contiguous structures [8].

Several cases of the artifact observed in our study are not adequately explained by this single mechanism of pseudoenhancement of the superior pericardial recesses. The pericardial recesses do not typically extend into the space between the left lateral aortic root and the main pulmonary artery. Yet in the scan shown in Figure 3A, an apparent "intimal flap" extends along the left lateral aortic wall, where it abuts the main pulmonary artery. This finding suggests that motion of another structure, the aortic wall itself, generates the artifact in some cases. Lung parenchymal window settings of the same image (Fig. 3B) confirm motion of the aortic wall as evidenced by blurring of the interface between the right lateral aortic wall and the adjacent lung.

In another case (Fig. 4), aortic wall motion produces a double-wall artifact in a patient with a calcified ascending aorta. This type of motion artifact has been described for the

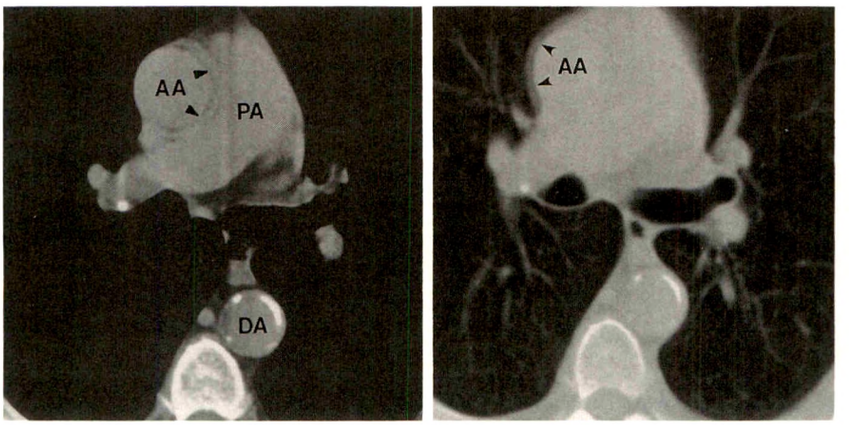


Fig. 3.—*A*, Unenhanced CT scan obtained on Somatom Plus CT scanner in a patient with a suspected pulmonary nodule simulates dissection (*arrowheads*) of ascending aorta (AA), with extension along left lateral aortic wall where it abuts main pulmonary artery (PA). DA = descending aorta.

***B*, Corresponding CT scan with lung parenchymal window settings (width 2000 H, center −600 H) shows blurring of right lateral aortic wall (*arrowheads*), compatible with motion. Motion-induced blurring is also apparent in right lung parenchyma next to ascending aorta.**

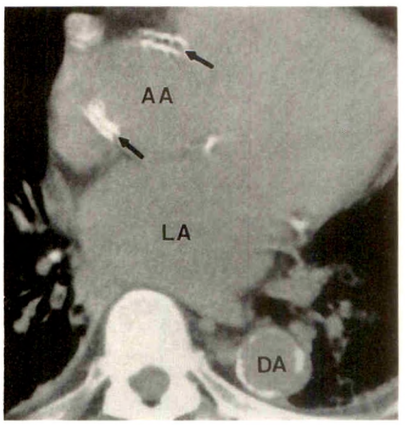


Fig. 4.—Motion of a calcified proximal ascending aorta. Unenhanced CT scan in a patient with severe coronary artery disease shows double-aortic-wall artifact (*arrows*) in a calcified proximal ascending aorta (AA) caused by wall motion during image acquisition. LA = left atrium; DA = descending aorta.

pulmonary fissures, because of movement during image acquisition [9]. Similarly, if image acquisition occurs during the period of maximal aortic wall motion from end diastole to end systole, the image generated may display a portion of the aortic wall in both systole and diastole. This process could produce double-wall artifacts such as those seen in Figures 3 and 4. An earlier publication regarding the Somatom Plus CT scanner attributes the artifact we saw to motion of the aortic wall during the cardiac cycle [10]. The longer 5-sec scanning interval of the Somatom DRH would not be expected to produce this artifact because image acquisition occurs over several cardiac cycles, with averaging of motion resulting in slightly blurred interfaces rather than distinct double-wall artifacts.

We were surprised that the 1.2- to 1.3-sec scanning time of the GE Quick Hilight CT scanner did not produce the artifact. Differences in vendor-specific CT reconstruction algorithms are one possible explanation for our findings. Recently, one of our authors observed an identical artifact of the ascending aorta on images from the I.Q. Premier CT scanner (Picker International, Cleveland, OH; 1-sec scanning time).

Our observations support motion of either the superior pericardial recesses or the aortic wall itself, or a combination of both mechanisms, as the cause of the artifact. The pattern is so typical that it should be possible to categorize correctly these findings as artifactual in most patients considered clinically at risk for dissection. Apparent "intimal flaps" and/or "double lumens" occur in the aortic root and are confined to one or two contiguous slices. The findings do not extend into the aortic arch or descending aorta. No associated findings, such as mediastinal or pericardial hemorrhage, suggest dissection. The newer, fast CT scanners markedly decrease motion artifact, but may introduce a new, potentially misleading artifact of the proximal ascending aorta, which should be added to the list of potential causes of false-positive diagnosis of aortic dissection on CT.

REFERENCES

1. Vasile N, Mathier D, Keita K, Lellouche D, Bloch G, Cachera JP. Computed tomography of thoracic aortic dissection: accuracy and pitfalls. *J Comput Assist Tomogr* **1986**;10(2):211–215
2. Heiberg E, Wolverson M, Sundaram M, Connors J, Susman N. CT findings in thoracic aortic dissection. *AJR* **1981**;136:13–17
3. Godwin DJ, Herfkins RL, Skioldebrand CG, Federle MP, Lipton MJ. Evaluation of dissections and aneurysms of the thoracic aorta by conventional and dynamic CT scanning. *Radiology* **1980**;136:125–133
4. Gross SC, Barr I, Eyler WR, Fareed K, Goldstein S. Computed tomography in dissection of the thoracic aorta. *Radiology* **1980**;136:135–139
5. Larde D, Belloir C, Vasile N, Frija J, Ferrane J. Computed tomography of aortic dissection. *Radiology* **1980**;136:147–151
6. Thorsen MK, San Dretto MA, Lawson TL, Foley WD, Smith DF, Berland LL. Dissecting aortic aneurysms: accuracy of computed tomographic diagnosis. *Radiology* **1983**;148:773–777
7. Godwin DJ, Breiman RS, Speckman JM. Problems and pitfalls in the evaluation of thoracic aortic dissection by computed tomography. *J Comput Assist Tomogr* **1982**;6:750–756
8. Chiles C, Baker ME, Silverman PM. Superior pericardial recess simulating aortic dissection on computed tomography. *J Comput Assist Tomogr* **1986**;10:421–423
9. Mayo JR, Muller NL, Henkelman MR. The double-fissure sign: a motion artifact on thin-section CT scans. *Radiology* **1987**;165:580–581
10. Dixon AK, Flower CDR. The Somatom Plus in the mediastinum: preliminary observations. In: Fuchs WA, ed. *Advances in CT*. New York: Springer-Verlag, **1990**:186–189

Mediastinal Thymolipoma

Felix S. Chew[1] and Ralph Weissleder

An abnormality was found incidentally on the chest radiograph of a 49-year-old woman admitted for wrist surgery. The mediastinal contour was broad and had an abnormal density projected over the left pulmonary artery (Fig. 1). Chest CT showed a fatty mass adjacent to the thymus. The mass extended caudad along the ascending aorta and the left cardiac margin for 6 cm. The chest radiographs and CT scans were otherwise unremarkable. Because the differential diagnosis included liposarcoma, surgical resection was performed. The lesion was fatty and encapsulated. Microscopy revealed mature adipose tissue with normal thymic tissue interspersed. The final pathologic diagnosis was thymolipoma.

Thymolipomas are unusual benign mediastinal tumors composed of thymic and adipose tissue. The imaging characteristics are those of fat [1, 2], although the thymic tissue may appear as islands of soft-tissue density within the fat. Arising in the anterior mediastinum at the level of the thymus gland, these soft and pliable tumors droop inferiorly as they enlarge and are said to slump onto the diaphragm, accommodating themselves to the spaces between the lungs and the heart, diaphragm, or anterior mediastinum [3]. Their pendulous, elongated, teardrop shape leaves the anterior clear space unencumbered on the lateral chest film. They may simulate cardiomegaly on the frontal chest film. Because they are asymptomatic until marked mass effect occurs, thymolipomas often become large, sometimes weighing several kilograms at the time of excision.

Thymolipomas are uncommon, accounting for approximately 5% of all thymic tumors. Most are discovered incidentally. In a very few cases, myasthenia gravis is a concurrent condition, but the association is weak and is probably coincidental [4]. When treated at all, the treatment is surgical resection. They do not recur.

REFERENCES

1. Faerber EN, Balsara RK, Shidlow DV, Marmon LM, Zaeri N. Thymolipoma: computed tomographic appearances. *Pediatr Radiol* **1990**;20:196–197
2. Shirkhoda A, Chasen MH, Eftekhari F, Goldman AM, Decaro LF. MR imaging of mediastinal thymolipoma. *J Comput Asst Tomogr* **1987**;11:364–365
3. Teplick JG, Nedwich A, Haskin ME. Roentgenographic features of thymolipoma. *AJR* **1973**;117:873–877
4. Pan CH, Chiang CY, Chen SS. Thymolipoma in patients with myasthenia gravis: report of two cases and a review. *Acta Neurol Scand* **1988**;78:16–21

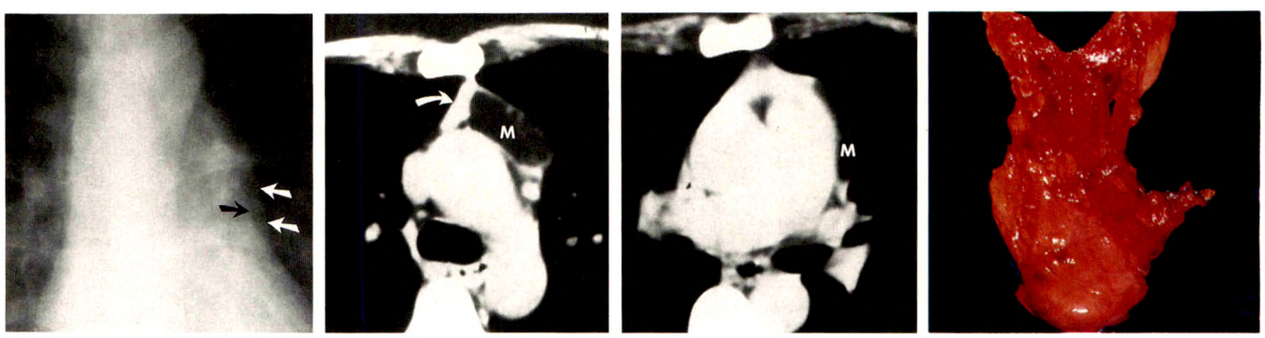


Fig. 1.—Mediastinal thymolipoma.
***A*, Detail of chest radiograph shows an abnormal density (*white arrows*) projected over left pulmonary artery (*black arrow*).**
***B*, CT scan at level of aortic arch shows an anterior fatty mass (M) adjacent to thymus (*arrow*).**
***C*, CT scan at level of left pulmonary artery shows fatty mass (M) that showed as abnormal density on plain film (*A*).**
***D*, An encapsulated fatty mass with interspersed thymic tissue was found at surgery. Note pendulous, elongated, teardrop shape.**

From the weekly radiologic-pathologic correlation conferences conducted by Jack Wittenberg. Pathology editor: Andrew E. Rosenberg. Radiology editors: Felix S. Chew, Daniel P. Barboriak, William E. Palmer, Daniel I. Rosenthal.

[1] Both authors: Department of Radiology, Massachusetts General Hospital and Harvard Medical School, 32 Fruit St., Boston, MA 02114. Address reprint requests to F. S. Chew.

Commentary

Current Status of Mediastinal Sonography in the Posttreatment Evaluation of Patients with Lymphoma

Stephen I. Marglin,[1] Faye C. Laing,[2] and Ronald A. Castellino[3]

In the recent *AJR* article, "Value of Sonography in Monitoring the Therapeutic Response of Mediastinal Lymphoma: Comparison with Chest Radiography and CT," Wernecke et al. describe the results of mediastinal sonography in 40 consecutive patients with a diagnosis of lymphoma [1–3]. Twenty-nine patients had Hodgkin disease, and 11 suffered from one of the non-Hodgkin lymphomas. Scans were obtained by using both a suprasternal and a parasternal approach and were correlated with the patients' clinical course and with the results of other imaging tests. On the basis of this experience, the authors drew the following conclusions: (1) All mediastinal nodes that are detectable by sonography should be considered abnormal, that is, either malignant or inflammatory. (2) Mediastinal nodes that remain or become hypoechoic after treatment should be viewed as highly suggestive of viable tumor. (3) Chest radiographs are less sensitive than mediastinal sonography is to the presence of residual tumor and/or tumor progression. (4) Sonography offers a more accurate method for monitoring the therapeutic response of mediastinal lymphomas than does conventional radiography. (5) Sonography appears to offer better prognostic information than CT because it provides information that goes beyond simple measurements of the dimensions of mediastinal lymph nodes.

As suggested by Dr. Ferris Hall's letter in this issue of the Journal [2], this manuscript is both provocative and perplexing. It is provocative, in part, because the information is novel and unexpected and also because the approach appears to offer promise for better treatment of patients. It is perplexing because mediastinal sonography is, to the best of our knowledge, rarely used in the current practice of oncologic radiology in the United States, and because it is unclear where, if at all, mediastinal sonography should fit among our diagnostic tools. In attempting to understand these issues more completely, we have chosen to focus our discussion on an analysis of the following three questions: (1) Are the authors' conclusions plausible? (2) Are the approach and the authors' conclusions likely to be generalizable to other medical centers? (3) Is the approach relevant to the treatment of patients with Hodgkin disease or one of the non-Hodgkin lymphomas?

A considerable body of information already exists to support the conclusion that lymphoma (and other forms of neoplasia) can readily exist in lymph nodes that are of normal size. A somewhat smaller literature attests to the fact that neither CT nor MR imaging can consistently be used to distinguish these nonenlarged, neoplastic lymph nodes from similarly sized nodes that do not contain tumor. Wernecke et al. contend that sonography, presumably because of the quality of the information contained in textural echoes, offers promise in this area—although they readily admit that the limited number of cases in this preliminary study is insufficient to draw confident conclusions. Can this position be regarded as plausible? Based on our analysis, accepting the fact that we have no personal experience with the use of sonography for this purpose, the answer would have to be yes. The authors also address the acknowledged limitations of conventional chest radiographs, drawing specific attention to the fact that mediastinal abnormalities cannot be detected until a distortion of one of the pleuromediastinal reflections has occurred. Again, the arguments on behalf of mediastinal sonography appear to be, at the very least, plausible.

What then of the question of whether the results achieved by these investigators can be generalized or extended to other sonographers and medical centers. This question is somewhat more difficult to answer. Although mediastinal sonography via the jugular fossa was originally proposed by Goldberg [4] in 1971, little enthusiasm or interest attended this suggestion during the next 15 years. Beginning in 1986, Wernecke et al. published five articles [1, 5–8] dealing with the technical aspects and potential benefits of mediastinal sonography—each exhibiting a high degree of dedication and what appears to be meticulous attention to detail. Our impression from reading these articles is that most, if not all, of the examinations were interpreted by either one person or per-

This article is a commentary on the letter-to-the-editor by Hall [2].

[1]Department of Radiology (SB-05), University of Washington Medical Center, Seattle, WA 98195. Address reprint requests to S. I. Marglin.
[2]Department of Ultrasound, Swedish Hospital Medical Center, Seattle, WA 98195.
[3]Department of Medical Imaging, Memorial Sloan-Kettering Cancer Center, 1275 York Ave., New York, NY 10021.

AJR 157:469–470, September 1991 0361–803X/91/1573–0469 © American Roentgen Ray Society

haps a limited group of experts. This, in conjunction with the relative paucity of supporting data from other sonographers throughout the world [9–16] prompts us to view the question of potential generalizability with some caution. Although our dispositions are generally inclined to be optimistic, we would be remiss if we did not explicitly emphasize the need for further validation of the authors' excellent results by other skilled sonographers.

Dr. Hall [2] correctly points out that "mediastinal sonography would seem to be more labor and physician intensive, more operator dependent, more difficult to compare with previous and subsequent examinations, and less useful for assessment of certain areas" than CT. Although these observations are undoubtedly true, and although they will undoubtedly have some bearing on the enthusiasm with which radiologists approach this technique, we offer only the rejoinder that in situations in which the information obtained is of sufficient clinical importance, "the pain may be worth the gain."

If we then assume that (1) sonography, at least in the hands of dedicated and skillful investigators, may be capable of visualizing superior mediastinal lymph nodes more accurately than conventional chest radiographs and (2) that the information obtained may permit accurate prognostication, does it necessarily follow that mediastinal sonography will soon become an integral component in the posttreatment follow-up of patients with lymphomas? In our opinion, a prudent answer to this question is "not necessarily." Currently available information is, as yet, insufficient to predict whether the results of mediastinal sonography are likely to have a salutary, measurable effect on treatment of patients—and whether other examinations might now be eliminated.

We would be disinclined to eliminate standard frontal and lateral chest radiographs from the posttreatment evaluation of patients with lymphomas. Although a concern regarding the possibility of mediastinal relapse or recurrence is perfectly legitimate, other issues that pertain to infection and treatment-related complications are also of great significance. Chest radiography, although admittedly less than optimally sensitive to the presence and viability of mediastinal lymph nodes, does provide important information about the status of the entire thorax, at a relatively low cost and at a relatively low dose of radiation. It does not seem practical to replace chest radiography with mediastinal sonography, which assesses only a limited portion of the mediastinum and thorax.

There are, however, certain occasions after initial treatment when important decisions are made concerning the need for additional treatment. We could easily envision a role for mediastinal sonography at these junctures, for example, to distinguish residual fibrosis from viable tumor, but probably more as an adjunct to other imaging studies than as a replacement for those that are already being done.

In closing this discussion, it is important to remember that Hodgkin disease and the non-Hodgkin lymphomas, although they share certain obvious similarities, are also quite different. Hodgkin disease manifests a predictable spread from one lymph node group to the next contiguous group. For those patients who initially have mediastinal disease (85%) who are then treated with radiation (with or without chemotherapy), the likelihood is high that the mediastinal nodes will be sterilized. Relapses are therefore more likely to occur outside the initial treatment field than within it. Put differently, the original sites of involvement, well imaged with mediastinal sonography, are not the most likely sites of recurrence. Hodgkin disease is also a disease with a very favorable prognosis. Approximately 75% of Hodgkins patients will be cured of their neoplasm [17]. It is not immediately apparent that mediastinal sonography will improve on these results.

Patients with one of the many non-Hodgkin lymphomas, on the other hand, are less likely to have localized disease, and are less likely to be cured. For these patients, recurrence of tumor often occurs at the sites of original bulk disease. Non-Hodgkin lymphoma can be monitored in many ways, including abdominal CT and analyses of the patients' bone marrow.

Conclusions

The recent series of articles by Wernecke et al. [1, 5–8] give ample evidence of what is possible in the hands of skillful and dedicated investigators. The issues of generalizability and of how, if at all, this approach is likely to be used, remain unanswered. We believe that there is reason to be cautiously optimistic, and we await the results of other investigators.

REFERENCES

1. Wernecke K, Vassallo P, Hoffmann G, et al. Value of sonography in monitoring the therapeutic response of mediastinal lymphoma: comparison with chest radiography and CT. *AJR* **1991**;156:265–272
2. Hall FM. Sonography for mediastinal lymphoma (letter). *AJR* **1991**;157:644
3. Wernecke K, Vassallo P, Peters PE. Reply. To: Hall FM. Sonography for mediastinal lymphoma (letter). *AJR* **1991**;157:644
4. Goldberg B. Suprasternal ultrasonography. *JAMA* **1971**;15:245–250
5. Wernecke K, Peters PE, Galanski M. Mediastinal tumors: evaluation with suprasternal sonography. *Radiology* **1986**;159:405–409
6. Wernecke K, Poetter R, Peters PE, Koch P. Parasternal mediastinal sonography: sensitivity in the detection of anterior mediastinal and subcarinal tumors. *AJR* **1988**;150:1021–1026
7. Wernecke K, Vassallo P, Peters PE, von Bassewitz DB. Mediastinal tumors: biopsy under US guidance. *Radiology* **1989**;172:473–476
8. Wernecke K, Vassallo P, Poetter R, Lueckener HG, Peters PE. Mediastinal tumors: sensitivity of detection with sonography compared with CT and radiography. *Radiology* **1990**;175:137–143
9. Ikezoe J, Morimoto S, Arisawa J, et al. Ultrasonography of mediastinal teratoma. *JCU* **1986**;14:513–520
10. Lemaitre L, Marconi V, Avni F, Remy J. The sonographic evaluation of normal thymus in infants and children. *Eur J Radiol* **1987**;7:130–136
11. Lemaitre L, Leclerc F, Marconi V, Taboureau O, Avni FE, Remy J. Ultrasonographic findings in thymic lymphoma in children. *Eur J Radiol* **1987**;7:125–129
12. Liu P, Daneman A, Stringer DA. Real-time sonography of mediastinal and juxtamediastinal masses in infants and children. *Can Assoc Radiol J* **1988**;39:198–203
13. Marx MV, Cunningham JJ. Sonographic findings in mediastinal embryonal carcinoma. *J Ultrasound Med* **1986**;5:41–43
14. Pedersen OM, Aasen TB, Gulsvik A. Fine needle aspiration biopsy of mediastinal and peripheral pulmonary masses guided by real-time sonography. *Chest* **1986**;89:504–508
15. Saito T, Kobayashi H, Sugama Y, et al. [Usefulness of ultrasonic-guided needle biopsy in the diagnosis of mediastinal lesions.] *Nippon Kyobu Shikkan Gakkai Zasshi* **1987**;25:334–340
16. Saito T, Kobayashi H, Sugama Y, Tamaki S, Kawai T, Kitamura S. Ultrasonically guided needle biopsy in the diagnosis of mediastinal masses. *Am Rev Respir Dis* **1988**;138:679–684
17. Rosenberg SA. Hodgkin's disease: challenges for the future. *Cancer Res* **1989**;49:767–769

Case Report

Torsion of the Upper Lobe of the Lung After Surgery: Findings on Pulmonary Angiography

Peter L. Munk,[1] A. Dale Vellet,[1] and Charles Zwirewich[2]

Torsion of a pulmonary lobe is an infrequently encountered complication of thoracic surgery [1–5]. The diagnosis must be made quickly, because prompt therapy is required. The radiographic and CT findings of pulmonary torsion are well recognized, but to our knowledge, only one example of pulmonary angiography performed in a patient with pulmonary torsion has appeared in the literature [5].

Case Report

A 32-year-old woman involved in a motor vehicle accident had a deceleration injury to the chest. Marked mediastinal widening was noted, and the diagnosis of aortic rupture was made on angiography at another hospital. The left lung was normal at that time. The patient underwent successful repair of the aorta. The initial postoperative course was unremarkable; however, within 1 day of surgery, persisting left upper lobe opacification was noted on a chest radiograph (Fig. 1A). The patient's oxygenation remained poor, and evidence of sepsis was noted with confirmation by blood cultures. CT showed dense consolidation of the left upper lobe with air bronchograms. In retrospect, possible fusiform tapering of the proximal segment of the upper lobe bronchus and artery could be observed (Fig. 1B). Approximately 12 days after surgery, a gradual decrease in oxygenation was noted, and pulmonary embolism was suspected clinically. Pulmonary angiography was performed with selective injection of the left main pulmonary artery (Figs. 1C–1E). Lateral and oblique views showed that the branches in the left lower lobe were unremarkable; however, marked decrease in caliber was noted, with sluggish filling of the branches in the left upper lobe and no opacification of upper lobe pulmonary veins, even on delayed films. Venous phase images showed retrograde filling of the upper lobe venous stump, which had a tapered appearance. Near the origin of the left upper lobe pulmonary artery, fusiform tapering of the vessel, which had an apparent ectopic origin from the left main pulmonary artery, was noted. Clearance of contrast material in arterial branches of the left upper lobe was markedly delayed. On the basis of the pulmonary angiogram, torsion of the left upper lobe was suggested; the patient immediately underwent bronchoscopy, which confirmed this finding. During thoracotomy later the same day, infarction of the left upper lobe was diagnosed and lobectomy was performed. The patient subsequently made a satisfactory recovery.

Discussion

A variety of causes of pulmonary torsion have been reported, principally as case reports in the literature. Most cases have been reported subsequent to pulmonary resection or blunt trauma, although examples have been reported in association with diaphragmatic hernia and pneumothorax [6–8]. Fortunately, intraoperative and postoperative torsion is rare. Thoracic surgeons are well aware of the occurrence of this complication, and some recommend anchoring the remaining lobes after lobectomy in order to prevent torsion from occurring. In order for torsion of a lobe to occur, the pulmonary fissures must be complete. Incision of the pulmonary ligament during surgery also facilitates torsion [1, 3, 5].

In our patient, the length of time torsion was present is unclear; it may have dated from the surgery 2 weeks before, although instances of posttraumatic or postoperative torsion are said to be associated with grave clinical signs and symptoms (unlike spontaneous torsion, which is seldom symptomatic) [3].

On plain radiographs, decrease in lobar volume and consolidation are the most frequently noted findings. The hilum may be displaced, and the orientation of the pulmonary vasculature may be abnormal. The pulmonary veins may also appear engorged in the affected lobe owing to compromise of drainage [3]. Consolidation is usually identified on plain radiographs and CT scans, but is a nonspecific feature. However, at times, twisting of the bronchus and accompanying artery may be recognized as a tapered occlusion on CT, although this was not confidently observed in this case [3]. After administration of contrast material, slow flow within a partially obstructed lobar pulmonary artery may be identified as hyperdense lobar vascularity on delayed scans. Partial lobar torsion may be recognized when the lobar bronchovascular architecture, particularly the bronchial tree, demonstrates inversion. Bronchography also has been used to arrive at the diagnosis [2, 3], as is shown in our case and one other [5]. As noted by Marchena et al. [5], the oblique view on

Received March 18, 1991; accepted after revision April 19, 1991.

[1] Department of Diagnostic Radiology and Nuclear Medicine, University Hospital and University of Western Ontario, P.O. Box 5339, London, Ontario, N6A 5A5, Canada.

[2] Department of Radiology, Vancouver General Hospital and University of British Columbia, Vancouver, B.C., V5Z 1M9 Canada.

 0361–803X/91/1573–0471 © American Roentgen Ray Society

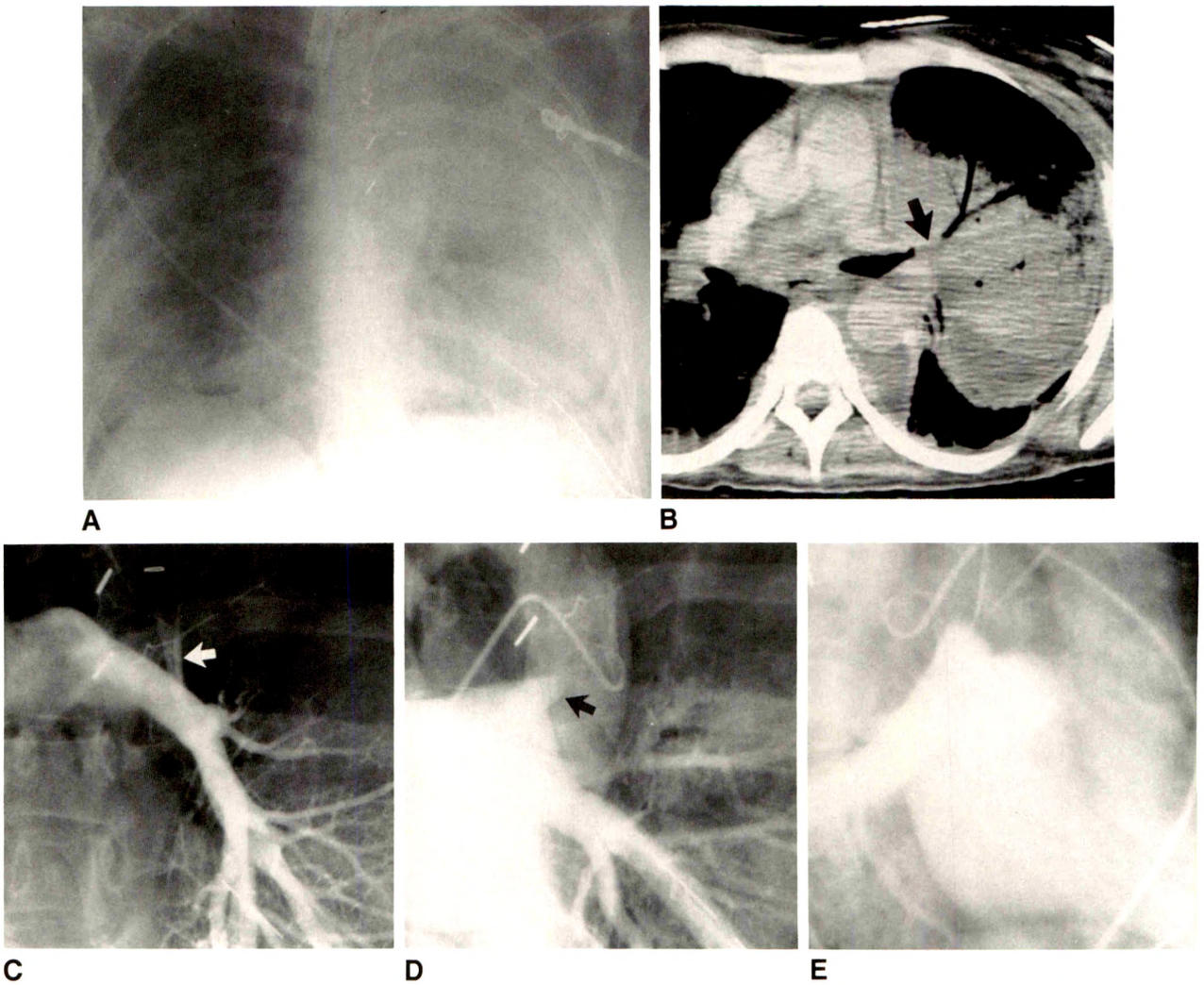


Fig. 1.—*A*, Chest radiograph 1 day before angiography shows extensive opacification throughout left hemithorax, especially around left upper lobe.
***B*, CT scan obtained 2 days before angiography shows dense consolidation (*arrow*) of most of left upper lobe. In retrospect, interruption of left upper lobe bronchus most likely represents torqued bronchial vascular stem to left upper lobe, although this was not appreciated prospectively.**
***C*, 10° left anterior oblique projection from selective left pulmonary angiogram, early arterial phase. Upper lobe vessels (*arrow*) take an unusually medial course and are markedly attenuated (compare with lower lobe).**
***D*, Venous phase from same study. Left upper lobe vein is seen only as a retrograde filling (*arrow*).**
***E*, Later image from same study. Marked blood flow stasis is apparent. Upper lobe arteries are still filled, and rest of lung is already in venous phase.**

angiography shows the relevant findings especially well, although we found the diagnosis could also be made on the anteroposterior projection. This diagnosis may also be arrived at via bronchoscopy, because abnormal orientation of the bronchi may be observed as well as obstruction of the bronchial lumen.

This case is unusual because the diagnosis was not initially entertained and was made only after pulmonary angiography for suspected pulmonary embolism. Both the slow filling of the upper lobe vessels and the fusiform tapering of the vessel at the site of torsion were strongly suggestive of this specific diagnosis. In most instances, pulmonary angiography would certainly not be required to make this diagnosis; however, should these findings be observed, a specific diagnosis can be made confidently.

REFERENCES

1. Oddi MA, Traugott RC, Will RJ, Simmons RA, Treasure RL, Schuchmann GF. Unrecognized intraoperative torsion of the lung. *Surgery* **1980**;89:390–393
2. Cervantes-Perez P. Recognizing pulmonary torsion (letter). *Chest* **1988**;93:444–446
3. Felson B. Lung torsion: radiographic findings in nine cases. *Radiology* **1987**;162:631–638
4. Pinstein ML, Winer-Muram H, Eastridge C, Scott R. Middle lobe torsion following right upper lobectomy. *Radiology* **1985**;155:580
5. Marchena E, Futterman L, Wozniak P, et al. Pulmonary artery torsion: a potentially lethal complication after orthotopic heart transplantation. *J Heart Transplant* **1989**;8:499–502
6. Berkman YM. Uncomplicated torsion of the right upper lobe secondary to spontaneous pneumothorax. *Chest* **1985**;87:695–697
7. Huang T-Y, Cho S-R. Torsion of the lung without trauma. *Radiology* **1979**;132:25–26
8. Berkman YM, Yankelvitz D, Davis SD, Zanzonico P. Torsion of the upper lobe in pneumothorax. *Radiology* **1989**;178:447–449

The American College of Radiology Mammography Accreditation Program

Robert McLelland[1]
R. Edward Hendrick[2]
Marie D. Zinninger[3]
Pamela A. Wilcox[3]

This article discusses the background, goals, criteria, current results, impact, and future directions of the American College of Radiology's (ACR's) Mammography Accreditation Program. To date, approximately one half of the mammographic units in the United States have voluntarily applied for accreditation through the ACR program, with approximately one quarter of the units in the United States now accredited. Application rates have increased steadily since the start of the program in August 1987. The equipment performance criteria and professional criteria defined and employed in the ACR Mammography Accreditation Program have been adopted as standards for the performance of screening mammography by the ACR and have served as a basis for quality assurance standards in state and federal legislation on mammography.

AJR 157:473–479, September 1991

Background to the American College of Radiology's Mammography Accreditation Program

Demand for screening mammography has increased dramatically [1, 2] for several reasons: breast cancer is the most common cancer in women and second only to lung cancer as a cause of death from cancer; mammography can detect breast cancer earlier, before a lesion can be palpated, and can significantly reduce the mortality rate from this disease [3–5]; and early diagnosis offers women breast-conserving treatment options. Earlier detection of breast cancers requires dedicated equipment, careful positioning, adequate compression, optimal technical factors, careful processing, and accurate interpretation [6, 7].

During the early to mid 1980s, dedicated mammographic equipment became readily available and widely used [8]. At that time, many radiologists believed that the use of modern, dedicated mammographic equipment was all that was needed to ensure optimal image quality at low radiation dose. However, during the mid to late 1980s, several findings raised doubts about the validity of this assumption [9–13].

The Nationwide Evaluation of X-ray Trends (NEXT) study conducted in 1985 surveyed 232 mammography facilities across the United States [9, 10]. The findings of the NEXT-85 study, published in 1987, showed wide variations in image quality and radiation dose, even from dedicated mammography units. Another study, conducted by Galkin et al. [11] in 1986, surveyed 29 dedicated screen-film mammography units as part of a Breast Cancer Screening Awareness project in the Philadelphia area. Their results, published in 1988, showed a tenfold range of average glandular radiation doses from mammography (a dose ranging from 26 mrad [0.26 mGy] to 260 mrad [2.6 mGy] from a single exposure to a typical breast thickness), a variation in image quality from site to site, and a significant variation in processor performance from day to day at nearly half (41%) of the sites surveyed.

A further impetus to develop the American College of Radiology's (ACR) Mammography Accreditation Program was the interest of the American Cancer Society

Received June 1, 1990; accepted after revision April 9, 1991.

Note.—The members of the ACR Breast Task Force are Gerald D. Dodd (chairman), Franklin S. Alcorn, James D. Cox, Stephen A. Feig, William R. Hendee, Robert V. P. Hutter, Harold J. Lasky, Robert McLelland, Thomas F. Meaney, Tearle L. Meyer, Helmut A. Mueller, Alan H. Robbins, Jonathan L. Stolz, and Raymond L. Tanner.

[1] Department of Radiology, The University of North Carolina at Chapel Hill, Third Floor–CB#7510, The North Carolina Memorial Hospital, Chapel Hill, NC 27599-7510. Address reprint requests to R. McLelland.

[2] Department of Radiology, University of Colorado Health Sciences Center, 4200 East 9 Ave., Denver, CO 80262.

[3] The American College of Radiology, 1891 Preston White Dr., Reston, VA 22091.

0361–803X/91/1573–0473
© American Roentgen Ray Society

(ACS) in promoting mammographic screening among asymptomatic women. When the ACS decided to embark on its Breast Cancer Awareness Screening Campaign several years ago, a joint ACS-ACR Committee on Mammographic Screening was formed to assist implementation of the program. Concerns were raised regarding the capacity of radiologists to respond appropriately to the increased demand for screening mammography. The quality and accuracy of interpretation of mammographic images were major issues of concern, which led to the concept of the ACR Mammography Accreditation Program.

A voluntary accreditation process for the practice of general radiology has been offered by the ACR since 1966. In 1986, the newly constituted ACR Breast Task Force, using the precedent and framework developed by the departmental process, and after extensive deliberations with diagnostic radiologists and physicists, instituted a voluntary Mammography Accreditation Program. Seed money was provided by a grant from the ACS, and design and pilot testing began in the fall of 1986. The first sites applied for accreditation in August 1987 [12, 13]. In order to increase speed and to limit costs, the Mammography Accreditation Program is conducted entirely by mail.

Goals of the Program

The goals of the ACR Mammography Accreditation Program are to establish standards of quality for mammography, to provide a mechanism for radiologists voluntarily to compare their own performance with national standards, to collect and disseminate data on the current practice of mammography, to encourage quality assurance practices in mammography, and to ensure reproducibly high-quality images at low radiation dose to the patient. The program has been designed to make the accreditation process instructive, encouraging voluntary compliance while pointing out potential deficiencies in a mammography practice.

Design of the Program

The ACR Mammography Accreditation Program consists of four distinct phases. The first phase involves completion of a comprehensive survey questionnaire concerning (1) the practice setting (hospital, office, mobile van, or other), number of mammograms per month, proportions of symptomatic and asymptomatic patients, and other breast imaging procedures used at the site; (2) personnel (radiologists, technologists, diagnostic radiologic physicists) and their training, certification, and experience; (3) equipment—mammographic unit manufacturer, model number and specifications (tube target material, filtration, focal spot size or sizes, phototimer, compression device, grid, half-value layer, magnification), recording system (film/screen, xeromammographic), and processor (manufacturer, model number, chemistry, time and temperature, dedicated or not); (4) mammographic technique—routine number of views, peak kilovoltage setting (kVp), tube current (mA), time settings, grid, and phototimer use; (5) quality-control practices—responsibility (radiologist, physicist, technologist, or service person) and frequency of monitoring average glandular radiation dose, phantom image quality, half-value layer, kVp accuracy, mA linearity, timer accuracy, focal spot size, phototimer performance, grid alignment, screen quality control, and processor testing; (6) medical history obtained from the patient—including symptoms and signs, personal and family history of breast cancer (especially in premenopausal first-degree relatives), previous mammography, any breast surgery or augmentation, and pregnancies; (7) physical examination (who performs it, their training and experience), instruction in breast self-examination; (8) reporting and follow-up mechanisms; and (9) policy for retention of mammograms.

Applications are reviewed by quality assurance professionals and trained assistants working under the direction of the Mammography Accreditation Committee. After review of the survey response, sites are told whether they may proceed to the next phases of the application process. If sites fail to meet criteria, an explanation is provided and sites may reapply after correcting deficiencies.

The second phase of this voluntary accreditation process involves physical testing of the entire mammographic imaging chain: radiographic equipment, factors related to technique, image receptors, processing, overall image quality, half-value layer, and average glandular dose to a typical breast. This is done by having the applicant make test images of a specially designed breast phantom embedded with test objects simulating various-sized masses, spicules, and calcifications, ranging from sizes that should be easily visible to invisible in the phantom image. The phantom image is interpreted independently by three medical physicists certified by the American Board of Radiology (ABR); image scores are averaged for each type of test object. In the same exposure made to evaluate image quality, a thermoluminescent dosimeter strip is exposed to measure entrance exposure and half-value layer, from which the average glandular breast dose is calculated [14]. The applicant must purchase the breast phantom and use it or another acceptable mammography phantom as part of an ongoing quality-control program. To pass this second phase of accreditation testing, the site must separately pass each of the criteria: mass visualization, spicule visualization, calcification visualization, and adequately low average glandular dose.

The third phase of the accreditation process is a peer review evaluation of clinical images. The site is requested to submit typical normal studies of two patients, one with fatty breasts and one with dense breasts. These are reviewed independently by two ABR-certified diagnostic radiologists experienced in clinical mammography. The evaluation of clinical images covers patient positioning, compression, film densities, image resolution, contrast, noise, examination identification, and artifacts. Those radiologists reviewing the clinical images have been instructed in a systematic protocol to minimize individual differences. If any aspect of the clinical image evaluation is inadequate, the site fails the accreditation process.

The last phase of evaluation examines further the regular quality-control practices at the site, particularly those related to processor performance. Each site is requested to submit the last 30 days of quality-control records for mammography

equipment, including the processor. Sites must test and maintain records of daily processor quality control, including sensitometric testing of average density, contrast, base plus fog, and developer temperature. Sites failing to adequately monitor processor performance or sites with processors showing excessive variations in measured parameters fail this portion of the accreditation process.

Each site receives a report of the results of all four phases of accreditation testing, along with a pass or fail result. All sites receive the comments of all reviewers along with guidelines to improve image quality further. Sites failing to meet criteria of the accreditation program also receive comments on the most likely causes of deficiencies. After correcting deficiencies, the site may apply for reevaluation for a small additional fee.

Sites passing the ACR Mammography Accreditation Program remain accredited for 3 years. During that period, annual updates of the status of the site are required, including the annual physicist's calibration report, processor data, and any personnel or equipment changes that have occurred. If any significant equipment changes are made at a facility, the image and dose evaluations must be repeated. To remain accredited, sites must reapply for accreditation every 3 years and meet the same criteria as new applicants.

Criteria of the Program

The criteria of the ACR Mammography Accreditation Program include both technical performance criteria and professional practice criteria. These criteria are consistent with the *ACR Standards for the Performance of Screening Mammography* [15], adopted at the ACR annual meeting in 1990.

The initial survey questionnaire monitors standards including the qualifications of personnel involved in the practice of mammography, the design of equipment used for mammography, and the quality-control practices used at the mammography site.

Standards for each physician interpreting mammograms at an ACR-accredited site require that the physician be certified in diagnostic radiology by the ABR or by the American Osteopathic Board of Radiology, or have received 2 months of full-time documented formal training in the interpretation of mammograms, including instruction in medical radiation physics, radiation effects, and radiation protection. In addition to these requirements, the physician must interpret mammograms regularly, with a recommendation that the physician interpret or review a minimum of 480 mammograms per year. The physician also must participate regularly in continuing education specifically in mammography, with at least 40 hr continuing Medical Education (category I or II) credits in mammography prior to accreditation and at least 15 hr every 3 years thereafter.

It is recommended that the radiologic physicist who inspects the mammography system be certified by the ABR in radiologic physics or diagnostic radiologic physics. It is required that all radiologic technologists performing mammography at an accredited site be certified by the American Registry of Radiologic Technologists (ARRT) and/or possess unrestricted state licensure. In addition, the mammographic technologist must perform mammography on a regular basis; must be competent in breast positioning and compression; and must be knowledgeable about technical factors, radiation safety, radiation protection, and quality control in mammography. To implement these goals, the ARRT, with the assistance of the ACR, is developing a special competency examination for mammography. Qualified registered technologists will be eligible for this examination.

Equipment used for mammography at accredited sites must be designed specifically (or in the case of xeromammography, properly modified) for mammography, with appropriate breast compression devices and, for screen/film systems, a removable grid. Film processors should have developer time and temperature settings appropriate for the specific type of film and chemistry being used for screen/film mammography, with adequate volume to maintain proper chemical replenishment; a dedicated mammographic processor is recommended.

A quality-control program must be in place, with procedure manuals and logs maintained in compliance with the recently published *ACR Mammography Quality Control Manuals* [16].

Performance standards monitored by the clinical image assessment include a qualitative assessment of image quality, patient positioning, film identification, and image artifacts.

Performance standards monitored by the phantom image and dosimetry measurements include a quantitative assessment of image quality and mean glandular breast dose. Quantitative image quality criteria require that accredited sites be able to visualize the largest four fibers (with diameters of 1.56, 1.12, 0.89, and 0.75 mm), the largest three microcalcification groups (with individual speck diameters of 0.54, 0.40, and 0.32 mm), and the largest three masses (with thicknesses of 2.0, 1.0, and 0.75 mm) in the RMI-156 Mammographic Phantom. The phantom image also must be free of significant artifacts. The dose criterion is that a single view should produce a mean glandular dose of less than 400 mrad (4 mGy), regardless of the type of image receptor. This criterion is consistent with the recommendation of *Report No. 85* of the National Council on Radiation Protection that the mean glandular dose of a two-view mammogram be less than 800 mrad (8 mGy) [6].

Processor quality-control data must indicate monitoring of developer temperature and resultant film speed, contrast, and base plus fog levels every workday. Film speed, as determined by a mid-density difference, and contrast, as determined by a density difference, must remain within ± 0.15, and base plus fog must remain within ± 0.05, of initial 5-day averages to demonstrate adequate processor control.

Other program standards concerning professional quality assurance, the mammography report, film retention, and self-referral are contained in the *ACR Standards for Screening Mammography*, recently distributed to all ACR members.

Results of the Program

The ACR Mammography Accreditation Program began in August 1987. Between initiation and April 15, 1991, 4717 sites with 5745 mammography units have applied for accred-

itation. This represents more than half of the estimated 10,000 mammography units in the United States. Of those applicants, 2954 units have completed the full evaluation process. The large difference between the number of applicants and the number of units that have completed the accreditation process (a difference of 2791 units) reflects the large number of units that are currently obtaining accreditation, a process that typically takes 4–6 months from initial application to completion.

On the first attempt, 2068 (70%) of the 2954 units that completed the process passed the full accreditation review. Of the 886 units failing on the first attempt, more than one half (609 units) reapplied for accreditation after correcting deficiencies, and 533 (88%) of these passed on the second application. This brings the total number of accredited units to 2601, approximately one quarter of the mammography units in the United States.

Among the 886 units failing the accreditation program on the first attempt, 368 (42%) failed on the basis of phantom image quality, 324 (37%) failed on the basis of clinical image quality, and 115 (13%) failed both the phantom and clinical image evaluation. Another 64 units (7%) failed because of excessive glandular dose. Fifteen units (1%) failed because of processor problems, some in combination with image quality deficiencies, although this number is artificially low because inclusion of processor testing as a pass/fail criteria did not begin until June 1990.

Data collected from the site survey questionnaire, phantom and clinical image tests, dosimetry measurements, and processor quality-control tests in the ACR Mammography Accreditation Program provide the most extensive data available on the practice of mammography in the United States.

Tables 1 and 2 present image quality and dose data by image receptor type for units that had completed the accreditation process through April 15, 1991. It should be noted that xeromammographic image receptor units constitute only 9.4% of the total number of units that have completed the accreditation process. Table 1 indicates only slight differences in image quality scores averaged over all units of a given image receptor type. Screen/film image receptors with grids score slightly higher than nongrid screen/film image receptors for each type of test object; xeromammographic systems score slightly higher in the demonstration of fibers, and screen/film systems scored higher for masses.

TABLE 1: Average Phantom Image Scores for Visualization of Test Objects

Unit/Object	Score[a]		
	Mean	Median	Range
Film/screen, nongrid			
Fibers	3.97	4.0	2.2–5.0
Specks	2.87	2.8	2.0–4.2
Masses	3.53	3.7	1.3–4.3
Film/screen, grid			
Fibers	4.30	4.3	0.8–5.4
Specks	3.24	3.2	2.0–5.0
Masses	3.70	3.8	0.3–4.8
Xeromammographic			
Fibers	4.51	4.5	2.2–5.5
Specks	3.12	3.0	2.0–4.8
Masses	3.42	3.5	1.2–4.5

[a] The score is the number of fibers, specks, or masses visualized (actual totals of 6, 5, and 5, respectively).

TABLE 2: Average Doses of Radiation for Glandular Breasts by Type of Image Receptor

Image Receptor	Dose (mrad)		
	Mean	Median	Range
Film/screen, nongrid	73	62	12–275
Film/screen, grid	138	130	15–599
Xeromammographic	305	290	132–890

Table 2 indicates that there is a distinct difference among doses averaged over all units with a given type of image receptor. Nongrid screen/film systems deliver, on average, approximately one half the mean glandular dose of screen/film systems with a grid, whereas xeromammographic image receptor systems deliver, on average, approximately twice the mean glandular dose of screen/film systems with a grid.

Tables 1 and 2 demonstrate that there are wide ranges in image quality and average glandular dose from site to site among applicants to the accreditation program [13, 17]. Even among dedicated mammographic equipment with the same type of image receptor (screen/film without grid, screen/film with grid, or xeromammography), there is wide variation in image quality and dose, with no statistically significant correlation between image quality and dose parameters [13].

Table 3 presents the distribution of failure rates by image receptor type for sites failing the phantom image quality evaluation. The table demonstrates a similarly high failure rate among sites that used nongrid screen/film image receptors and xeromammographic image receptors (19%); a substantially lower failure rate (5%) occurred among sites that use screen/film image receptors with a grid for the 4.5-cm-thick breast simulated by the phantom.

Tables 4 and 5 present failure rates for phantom and clinical image quality by the type of facility and by volume (number of mammograms performed per month). Table 4 indicates that image quality failure rates for mammography units sited in hospitals, private offices, multispecialty clinics, and multiple settings are not significantly different, ranging from 11% to 15%, whereas failure rates for mobile units are significantly higher (23%). Table 5 indicates that a more significant factor correlating with the quality of the mammographic image is the number of mammograms performed at the site. A clear inverse relationship exists between the failure rate of the site and the number of mammographic examinations performed at the site.

Discussion

A surprising result of the ACR Mammography Accreditation Program is that, since its inception, the failure rate among first-time applicants has remained consistently high, ranging between 28% and 30%. This is surprising in part because

TABLE 3: Phantom Image Failure Rates by Type of Image Receptor

Image Receptor	Total No. of Units	No. with Inadequate Phantom Images (%)
Film/screen, nongrid	124	23 (19)
Film/screen, grid	2551	139 (5)
Xeromammographic	279	54 (19)
Total	2954	216 (7)

TABLE 4: Number of Applications and Failure Rates by Type of Facility

Type of Facility	No. of Applications	No. of Completed Applications	No. Failing (%)
Hospital	2072	1288	195 (15)
Private office	1668	1215	143 (12)
Multispecialty clinic	492	277	36 (13)
Mobile unit	177	111	27 (24)
Multiple settings	105	40	4 (10)
Other settings	203	102	15 (15)
Total	4717	3033	420 (14)

Note.—Failures result from phantom or clinical image evaluations or both.

TABLE 5: Number of Applications and Failure Rates by Volume of Facility

No. of Mammographic Studies/Month	No. of Applicants	No. of Completed Applications	No. of Failures (%)
0–50	525	291	76 (26)
51–100	904	520	113 (22)
101–200	1492	949	118 (12)
201–300	768	510	62 (12)
301–400	457	345	26 (8)
401–500	253	180	16 (9)
501 or more	318	238	9 (4)
Total	4717	3033	420 (14)

Note.—Failures result from phantom or clinical image evaluations or both.

application to the program is voluntary, and sites voluntarily applying generally believe that they meet or exceed the standards of the program. The current 30% failure rate among first-time applicants suggests that even among sites that believe they are performing good mammography, improvement is needed. The 30% failure rate also suggests that establishing national standards and comparing the performance of individual sites with those standards is beneficial. The much lower failure rate of 12% among applicants that failed the program on their first attempt suggests that sites improve their performance once deficiencies are pointed out.

Another surprising result, pointed out previously [13], is the wide ranges in image quality and dose that exist in the current practice of mammography among applicant sites. Clearly, use of a dedicated mammographic unit and a particular type of image receptor is not sufficient to ensure adequate image quality. The data acquired in conducting the Mammography Accreditation Program have confirmed the early suspicions that led to the creation of the accreditation program in the first place. The lack of correlation between dose and image-quality parameters suggests that the wide ranges in image quality and dose from site to site are not intentional or due to the desire to increase image quality at the expense of higher dose, but the result of uncontrolled factors such as the performance of the processor at the site.

The significantly lower failure rate of phantoms at sites that use screen/film image receptors with a grid (Table 3) indicates that the choice of imaging technique is an important one. Failure to use a grid in imaging a breast compressed to 4.5 cm thick or greater permits significant additional scatter, reducing the detection of low-contrast structures in the breast. In a phantom, a xeromammographic image receptor fails to show low-density masses as effectively as a screen/film image receptor with a grid shows them. This is because xeromammographic image receptors rely on edge enhancement rather than large differences in area density as the primary contrast mechanism, and malignant masses tend not to have well-defined edges.

The results presented in Tables 4 and 5 indicate that there is no clear correlation between quality and the practice setting of a radiology-based mammographic practice, whereas there is a clear correlation between quality and the number of mammograms obtained at a mammographic site within a given time. This result is consistent with the findings of a recent survey conducted by the General Accounting Office on behalf of the Department of Health and Human Services that showed a correlation between the volume of patients and the quality assurance practices at mammography sites [18].

Impact of the Program

Increasingly, ACR accreditation is being recognized by radiologists as a means of quality improvement. The ability to compare one's own mammographic practice with a national standard, while not always a pleasant experience at the time, offers the opportunity to validate the superior aspects of one's practice and to identify areas that need improvement.

Similarly, national organizations interested in ensuring high-quality mammography, such as the ACS, the Centers for Disease Control (CDC), and the National Cancer Institute (NCI), as well as the public, are recognizing the ACR Mammography Accreditation Program as a demonstration of high-quality standards in the practice of mammography. Both the ACS and NCI are using ACR accreditation as a basis for recommending mammography sites to women seeking screening mammography.

Most states have passed laws requiring insurance coverage and reimbursement for mammography, including screening [19]. A few states, such as Michigan and New Mexico, have legislated quality assurance standards. In those states, facilities accredited by the ACR are deemed as meeting quality assurance requirements. In some other states and regions, such as Kentucky and Washington, DC, insurance companies such as Blue Cross–Blue Shield are requiring ACR accreditation as a prerequisite to reimbursement for mammography.

The Medicare coverage of screening mammography passed during the frenetic last few days of the 1990 Congress provides for Medicare coverage of screening mammography after January 1, 1991. The legislation provides for reimbursement of up to $55 per screening mammogram for women who qualify for Medicare. This provides mammography screening every other year to approximately 17 million women aged 65 and over. Approximately 1.5 million disabled women between the ages of 35 and 64 also are covered: those aged 35–39 qualify for coverage of a single baseline mammogram; those aged 40–49 qualify for coverage of screening every 2 years, and those aged 50–64 qualify for coverage of annual screening under Medicare. Women at higher risk may be screened more frequently.

Medicare coverage of screening mammography requires extensive quality assurance measures for each participating mammographic site, duplicating many of the quality assurance standards of the ACR and many of the requirements of the ACR Mammography Accreditation Program. While the mechanisms are still being worked out to ensure that sites seeking Medicare reimbursement meet quality standards, one possible scenario is that the ACR apply for "deemed" status from the Health Care Financing Administration (HCFA). With deemed status, an ACR-accredited mammographic site would submit evidence of accreditation to demonstrate that the site meets HCFA quality assurance standards.

A second piece of national legislation on quality assurance in mammography, the Breast Cancer Safety Screening Act, was introduced in October 1990 in the United States Senate by Senator Brock Adams and in the House of Representatives by Congresswoman Pat Schroeder. The bill failed to pass during the 1990 legislative session, but will be reintroduced in 1991. The bill would require every mammographic unit in the United States to be accredited through an approved national accreditation program such as the ACR accreditation program. Since the ACR Mammography Accreditation Program is the only national accreditation program for the practice of mammography, the legislation appears to provide a national mandate for ACR accreditation. However, if passed, implementation of the bill would be left to the Secretary of Health and Human Services. The potential impact of this legislation is unclear.

Future Plans for the ACR Mammography Accreditation Program

The evaluation of the clinical image, phantom image, dosimetry, and processor of mammographic sites ensures the technical quality of mammography. Criteria in each of these areas are being reviewed regularly. Criteria that are likely to be revised during the next year include clinical image evaluation, phantom image evaluation, maximum breast dose, and film labeling.

The proposed Medicare quality assurance legislation requires that only dedicated radiographic equipment be used for mammography. In light of this change, the Mammography Accreditation Program will soon reconsider equipment criteria to restrict accreditation to sites that use dedicated radiographic equipment for mammography, eliminating the possibility of sites that use modified conventional radiographic systems with xeromammographic image receptors.

The current accreditation requirement of regular quality assurance practices at accredited sites should help ensure that technical quality remains high over the period of accreditation. Recently, the ACR Committee on Quality Assurance in Mammography produced a set of quality control manuals for mammography, funded in part by the ACS. These consist of "cookbook-like" manuals for the radiologist, physicist, and radiologic technologist, defining the roles of each person in maintaining consistent high quality in the practice of mammography [16]. A cooperative agreement between the ACR and the CDC is currently funding further development of quality assurance methods and the pilot testing of programs to educate radiologists, physicists, and technologists on the importance of their role in mammographic quality assurance.

Although the question of technical quality is addressed directly by the Mammography Accreditation Program, the question of quality of image interpretation is addressed only indirectly, through an assessment of training, certification, experience, and continuing education of the radiologist. In 1990, the ABR made breast imaging a separate and comprehensive part of its examinations for certification, including a basis for failure. For radiologists whose training predates the introduction of mammography into residency programs, the ACR has developed an extensive continuing education program under the auspices of the Commission on Education and its Committees on Breast Imaging, ACR Symposia, and Continuing Evaluation in Postgraduate Education. The ACR standards for the performance of screening mammography serve as a guideline for necessary minimal educational requirements.

There is a need for a software/ledger program for data collection, including follow-up information for results and accuracy determinations. This is being studied by the ACR and should include the option of a simple, user-friendly format. This could provide radiologists with a patient tracking system and useful follow-up data for quality assurance [7].

In terms of numbers of voluntary participants, the ACR Mammography Accreditation Program has been the most successful accreditation program ever established in radiology. The voluntary application for accreditation of approximately half of the mammographic units in the United States is good evidence of the acceptance of such programs by the radiologic community. Conceivably, the Mammography Accreditation Program could serve as a model for quality assurance in other areas of diagnostic radiology.

Although the success of the ACR Mammography Accreditation Program is encouraging, the task of improving the quality of mammography is not complete [20]. Radiologists must be encouraged to implement meaningful quality assurance procedures, devoting the necessary personnel, time, and attention to the task of evaluating and improving quality on an ongoing basis. Radiologists, physicists, and mammographic technologists must continue to update their skills and their knowledge of mammography, including all areas of quality assurance. More continuing education programs specifically for mammography must be developed and implemented for each of these three groups.

REFERENCES

1. McLelland R. The politics of mammography. *Radiol Clin North Am* **1992**;30(1) (in press)
2. Tabar L. Control of breast cancer through screening mammography. *Radiology* **1990**;174:655–656
3. Shapiro S. The status of breast cancer screening: a quarter century of research. *World J Surg* **1989**;13:9–18
4. Feig SA. Decreased breast cancer mortality through mammographic screening: results of clinical trials. *Radiology* **1988**;167:659–665
5. McLelland R. Low-cost mass screening with mammography as a means of reducing overall mortality from breast cancer. *Radiol Clin North Am* **1987**;25:1007–1013
6. Rothenberg LN, ed. *NCRP Report No. 85. Mammography: a user's guide.* Bethesda, MD: National Council on Radiation Protection and Measurement, **1986**
7. McLelland R. Challenges and progress with mammography. *Cancer* **1989**;64:2664–2666
8. Haus AG. Technologic improvements in screen-film mammography. *Radiology* **1990**;174:628–637
9. Reuter FG. Preliminary report—NEXT-85. In: *National Conference on Radiation Control. Proceedings of the 18th annual conference of Radiation Control Program Directors.* Frankfort, KY: Conference on Radiation Control Program Directors (CRCPD publication 86-2), **1986**:111–120
10. Conway BJ, McCrohan JL, Reuter FG, et al. Mammography in the eighties. *Radiology* **1990**;177:335–339
11. Galkin BM, Feig SA, Muir HD. The technical quality of mammography in centers participating in a regional breast cancer awareness program. *Radiographics* **1988**;8:133–145
12. Hendrick RE, Haus AG, Hubbard LB, et al. American College of Radiology accreditation program for mammographic screening sites: physical evaluation criteria. *Radiology* **1987**;165(P):209
13. Hendrick RE. Standardization of image quality and radiation dose in mammography. *Radiology* **1990**;174:648–656
14. Stanton L, Villafana T, Day JL, Lightfoot DA. Dosage evaluation in mammography. *Radiology* **1984**;150:577–584
15. American College of Radiology. *ACR standards for the performance of screening mammography.* Reston, VA: American College of Radiology, **1990**
16. McLelland R, Gray JE, McCrohan J, et al. *ACR mammography quality control manuals.* Reston, VA: American College of Radiology, **1990**
17. Hendrick RE. *Current status of the American College of Radiology's mammography accreditation program.* In: *National Conference on Radiation Control. Proceedings of the 21st annual conference of Radiation Control Program Directors.* Frankfort, KY: Conference on Radiation Control Program Directors (CRCPD publication 89-4), **1989**:27–44
18. United States General Accounting Office. *Screening mammography: low-cost services do not compromise quality.* Washington, DC: United States General Accounting Office (report HRD 90-32), **1990**
19. Thompson GB, Kessler LG, Bass LP. Breast cancer screening legislation in the United States: a commentary. *Am J Public Health* **1989**;79:1541–1543
20. McLelland R. Supply and quality of screening mammography: a radiologist's view. *Ann Intern Med* **1990**;113:490-491

Book Review

Detection and Treatment of Early Breast Cancer. By Ian Fentiman. Philadelphia: Lippincott, 272 pp., 1990. $69.50

Should a radiologist buy a medical text of 272 pages that devotes less than three pages to mammography and less than two pages to sonographic study of the breast? It depends on the radiologist. If you already have a strong practice and background in breast diagnosis and feel up on the latest in the controversies surrounding mammography, diagnosis, screening, and techniques, the price of this book is decidedly worth it, as it deals in detail with issues of sure clinical importance to you. As an expert, you will note the interest and additional discussion on screening, surgical techniques, radiation implant therapy, adjunct therapy, and theories of risk and recurrence. Other topics include male breast cancer and psychologic strategies.

An especially strong chapter discusses the possible causes of breast cancer. What is the current risk associated with obesity, use of caffeine, radiation, or benign breast disease? What are oncogenes, and why is everyone talking about them? If such topics are of interest to you, then you should buy this text.

This work originated in London. The author, Ian S. Fentiman, is a prestigious consultant surgeon in the United Kingdom. The book is, as expected, well written and a joy to read—a job well done. Illustrated with clinical charts and photographs of anatomic and surgical pathologic specimens, the text flows logically from one idea to another. Conclusions and data when in doubt are presented with the competing up-to-date references. Dr. Fentiman discusses such topics openly, and because this is a text written by only one author, repetition of ideas or topics is avoided.

Should you buy this book if you are only occasionally or not at all involved in mammographic interpretation? Probably not. It does not have enough mammograms to hone the skills needed. Should residents buy this volume? Again, probably not. It is best to have the residency's program librarian buy it for residents to peruse as needed and let the residents save their salary for other necessities (like loan payments).

The author has succeeded in coming through on his prefaced promise to "write a cohesive account" of early breast cancer. In conclusion, this medical text is an excellent and worthwhile purchase for radiologists who have selected mammography as a focus of their skills. It should also find its way into most institutions' library list of purchases.

Michael Crade
Long Beach Memorial Medical Center
Long Beach, CA 90801-1428

Self-Referred Mammography Patients: Analysis of Patients' Characteristics

Handel E. Reynolds[1]
Valerie P. Jackson

Among mammography patients, a small but growing group of highly motivated women refer themselves directly for screening without the suggestion of their physicians. We surveyed 485 patients during a 3-month period to study how self-referred mammography patients differ from physician-referred patients. Self-referred patients were more likely than physician-referred patients to have a family income of more than $30,000 per year, to be college graduates, and to consider their health as good or excellent. A large percentage of self-referred patients performed other health-promoting practices, but were not significantly more likely to do these than were physician-referred patients. Women who referred themselves were more likely to have a friend with breast cancer and to believe that cancer could be cured. They expressed much less worry about radiation exposure and were more likely to consider $50.00 an appropriate charge for a screening mammogram. By far, the greatest motivator for self-referred patients was health promotion and disease prevention.

Self-referred mammography patients tend to be wealthier, more educated, and less concerned about the cost and radiation dose of mammography when compared with physician-referred mammography patients.

***AJR* 157:481–484, September 1991**

Breast cancer is the second leading cause of cancer death among women, claiming approximately 40,000 lives in the United States annually [1]. Screening mammography can reduce the mortality rate of this disease by as much as 50% [2]. Further, at least 90% of patients can be cured if the disease is detected in stage I or lower [3]. Despite these facts, very few eligible women are being screened regularly. A 1986 Gallup–American Cancer Society poll found that only 43% of women over 40 years old had ever had a mammogram, and only 28% had had a screening mammogram [4].

One of the major barriers to the use of screening mammography is the lack of general acceptance of the procedure by primary care physicians. A recent survey of primary care physicians conducted by the American Cancer Society regarding attitudes toward screening recommendations revealed that only 37% of the physicians followed the American Cancer Society recommendation with their eligible patients [5].

Given this reluctance by physicians, and the heightened public awareness about breast cancer and screening mammography, radiologists are faced with an increasing number of highly motivated women who directly refer themselves for screening. Radiologists need to better understand the motivation of this group so that their needs can be best served and so that they can possibly be used as a model to improve compliance among all women. This study examines the characteristics and attitudes of self-referred mammography patients compared with physician-referred patients.

Received January 22, 1991; accepted after revision April 22, 1991.

[1] Both authors: Department of Radiology, Indiana University Medical Center, University Hospital X98, 926 W. Michigan St., Indianapolis, IN 46223.

0361–803X/91/1573–0481
© American Roentgen Ray Society

Subjects and Methods

All patients who underwent mammography during a 3-month period were asked to complete a two-page questionnaire while waiting for their examination. Our breast imaging center is located in a large outpatient building attached to a county general hospital. Although a large proportion of our patients are elderly, minority, and/or indigent, we also see a number of women from other socioeconomic groups.

The survey questions explored five areas of potential differences between self-referred and physician-referred patients. The first area was demographics (age, race, marital status, employment status, family income, and educational level). The second concerned use of other health-promoting practices (breast self-examination, physician breast examination, routine medical checkups, Pap smears, prior mammography). Patients were also asked to rate their health as excellent, good, fair, or poor. Third, we asked about knowledge of, experience with, and attitudes toward cancer (could the patient identify heart disease as the commonest cause of death in the United States from a list of causes of death, did the patient have a family member or friend with breast cancer, did the patient believe that cancer could be cured or that early treatment of cancer affects the outcome). Fourth, we wanted to know the motivation for undergoing mammography (health maintenance, influence of the media, breast cancer in a family member or friend, encouragement by family or friend, encouragement by physician, fear that she may have cancer). Fifth, potential barriers to the examination (fear of radiation exposure and cost of mammography) were sought. Patients were asked to rate their fear of radiation exposure: very worried, a little worried, not worried, or unsure. Finally, patients were asked to choose a reasonable cost for a mammogram: $25, $50, $75, or $100.

For continuous measures, the self- and physician-referred groups were compared by using Student's t tests. Categorical measures were compared by using chi-square tests. When contingency tables were sparse, data were collapsed into 2 × 2 tables, and Fisher's exact tests (two-tailed) were performed.

Results

Approximately 40% of all of our patients complied, yielding 485 completed forms. Of these, 437 were physician-referred and 48 were self-referred patients.

Patients in both groups were similar in age and racial makeup; most were in their late forties (mean ages: self-referred, 47; physician-referred, 48) and white (self-referred, 73%; physician-referred, 62%). Self-referred patients were more likely to be married than were physician-referred patients (51% vs 36%, $p = .05$). There was no significant difference in employment status. Sixty percent of self-referred patients worked outside the home compared with 48% for those referred by physicians ($p = .12$). Physician-referred patients tended to have family incomes of less than $15,000 per year (58%), whereas self-referred women usually had family incomes over $15,000 per year (66%, $p = .01$). Approximately one third of patients in both groups were high school graduates. Physician-referred patients were more likely to have not attended high school (24% vs 9% for self-referred patients), whereas self-referred patients were more likely to be college graduates than were those referred by physicians (30% vs 19%, $p = .08$).

Eighty-three percent of self-referred patients regarded their health as excellent or good compared with 56% of physician-referred patients ($p = .001$). No significant differences were found in the use of other early detection practices among patients in one group vs the other. Approximately two thirds of patients in both groups practiced each of the early detection methods tested, with the exception of mammography. Just over 55% of patients in both groups had had a prior mammogram.

The most common cause of death was correctly identified by 59% of self-referred patients compared with 46% of physician-referred patients ($p = .14$). In terms of experience, no real difference was seen in the occurrence of breast cancer among family members in one group vs the other (self-referred, 37%; physician-referred, 28%; $p = .23$). Self-referred patients, however, were much more likely to have a friend with breast cancer than were physician-referred patients (80% vs 51%, $p < .001$). The vast majority of patients in both groups believed in the curability of cancer (self-referred, 95%; physician-referred, 84%; $p = .05$) and the efficacy of early treatment (self-referred, 100%; physician-referred, 97%; $p = .38$).

Sixty-two percent of self-referred patients stated that health maintenance was the primary motivator in their decision to undergo mammography. Twelve percent were worried that they may have breast cancer, and 18% were encouraged by their physician.

Regarding fear of radiation exposure, no difference was found in the distribution of concerns of self-referred and physician-referred patients in the four categories. If the data are analyzed according to "not worried" vs the other three choices, a significant difference (self-referred, 61%; physician-referred, 44%; $p = .03$) is found, with self-referred patients expressing less worry about the potential effects of radiation exposure from a mammogram. Twenty-three percent of self-referred patients and 24% of physician-referred patients stated that they were unsure of the effects of radiation from a mammogram. Regarding cost, self-referred patients were more likely to choose $50 as a reasonable cost for a mammogram, as opposed to physician-referred patients, who were more likely to choose $25.

Discussion

Self-referred patients were more likely to have a family income of greater than $30,000 per year and to have completed college than were physician-referred patients. This pattern has been noted before [6]. Several explanations for this are possible, including that better-educated women are more likely to be well read and informed about current screening recommendations. Further, women who are socioeconomically advantaged are more likely than disadvantaged women to seek health care that they will have to pay for out of pocket, as is the case with screening mammography in Indiana.

A slight difference was found in marital status, with self-referred patients more likely to be married than physician-referred patients. Having a spouse is likely to increase family

income. As a social group, widows are often elderly and poor, and the rate of widowhood was much lower among self-referred patients (6% vs 18%).

Self-referred patients gave a generally more optimistic rating of their health than did physician-referred patients. More than 80% regarded their health as good or excellent, compared with 56% of physician-referred patients. None of the self-referred patients regarded their health as poor.

Prior studies have shown that self-referred mammography patients are more likely to use other early detection practices [6]. Our study showed no significant difference between the two groups in this area. This most likely reflects much more public awareness of early detection and slightly more emphasis placed on prevention by the medical profession. McCusker and Morrow [7] showed that among women with personal physicians, use of early detection techniques depends, in large measure, on the emphasis placed on such techniques by their physicians.

It is encouraging that approximately two thirds of patients in each group reported doing regular breast self-examination, and two thirds of these did it monthly. Slightly more than two thirds have regular physician breast examinations and the vast majority of these have one per year. Two thirds reported having regular Pap smears. Thus, these women have a fairly high level of compliance with current American Cancer Society recommendations.

We found no significant difference in the ability of patients in the two groups to accurately choose heart disease as the most common cause of death in the United States today. Earlier studies had indicated that self-referred mammography patients were, in general, more knowledgable on health issues than were physician-referred patients and more likely to answer questions such as this correctly [6]. Our findings may be due to increased public awareness of health issues, heart disease in particular.

Approximately one third of patients in both groups reported having a family member with breast cancer. Self-referred patients, however, were much more likely to have a friend with breast cancer than were physician-referred patients (80% vs 51%, $p < .001$). This is probably an important factor in the decision to obtain a mammogram.

Both groups overwhelmingly believed that cancer could be cured. There is the suggestion of a trend, however, with self-referred patients believing in the curability of cancer more than did physician-referred patients ($p = .05$). This also probably plays a role in the decision to undergo mammography. Almost uniformly, both groups believed that early treatment affects the outcome of cancer.

The desire to maintain good health was the stated major motivator for a women to refer herself for a mammogram. Other factors most likely influenced the decision, such as having a friend with breast cancer. However, it is important to note that women do not refer themselves for screening mammography out of fear that they might have cancer (12%), but rather out of a genuine desire to promote health, believing that cancer can be cured, especially if detected early.

Several studies have shown that the greatest barrier to compliance with screening guidelines is the lack of recommendation of the procedure by primary care physicians to their patients [8–10]. Some barriers are patient related. Commonly cited among these are fear of radiation exposure and cost. When questioned about radiation exposure, there was no difference in the overall distribution of concerns of physician- and self-referred patients in the four categories: very worried, a little worried, not worried, and unsure. If the data are collapsed into a 2×2 table and analyzed according to not worried vs all other choices, there is a significant difference ($p = .03$), with self-referred patients more likely than physician-referred patients to be not worried. Thus, this potential barrier is probably less among self-referred patients than among physician-referred patients. About one fourth of each group stated that they were unsure of the effects of radiation exposure from a mammogram. These women, as well as those who were very worried about radiation, are obvious targets for educational campaigns.

On the subject of cost, both groups were clustered around the $25–$50 range. Self-referred patients, being of slightly higher socioeconomic level, were more likely to choose $50 as an appropriate fee for a screening mammogram (54% vs 34%, $p = .03$) than were physician-referred patients.

Several limitations of this study need to be addressed. First, the overall sample size is small, and in particular, the number of self-referred patients is very small, being only about 10% of the total. This naturally affects the applicability of these data on a larger scale. Second, only about 40% of our patients completed the questionnaire, and we know nothing about the 60% of women who declined. Therefore, it is possible that a significant selection bias was introduced. Third, the results of the question regarding the opinion of patients on a reasonable cost for mammography are probably biased owing to the patients' knowledge of the cost of a mammogram at our facility. It is probably unreasonable to expect patients to choose anything higher than the price they will have to pay.

The National Cancer Institute has set a goal of mammography screening of 80% of eligible women by the year 2000 [11]. Although the attitude of primary physicians to screening mammography has been improving in the past few years [5], this is a very slow process. If the goal is to be reached, women will have to be targeted directly with educational campaigns stressing the importance of early detection. The cost must be kept at a minimum, because in many parts of the country the cost of screening mammography is borne by the patient.

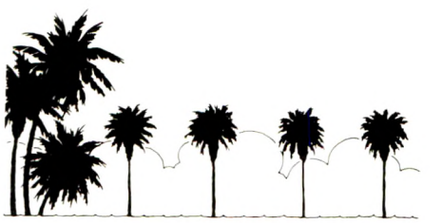
In summary, a few differences exist between self- and physician-referred mammography patients. For the most part, however, these groups are rather similar. With increased public education and price moderation, more patients of all socioeconomic levels are likely to request regular screening mammography.

ACKNOWLEDGMENTS

We thank Lorrie Kalasinski and Barry Katz, Division of Biostatistics, for assistance in the statistical analysis of the data.

REFERENCES

1. Silverberg E, Boring C, Squires T. Cancer statistics, 1990. *CA* **1990**;40: 9–28
2. Feig SA. Decreased breast cancer mortality through mammographic screening: results of clinical trials. *Radiology* **1988**;167:659–665
3. Wertheimer MD, Costanza ME, Dodson TF, D'Orsi C, Pastides H, Zapka JG. Increasing the effort toward breast cancer detection. *JAMA* **1986**;255:1311–1315
4. Gallup Organization, Inc. *1986 Survey of awareness and use of mammograms: American Cancer Society*. Princeton, NJ: Gallup Organization Inc., **1987**
5. American Cancer Society. 1989 Survey of physicians' attitudes and practices in early cancer detection. *CA* **1990**;40:77–101
6. Hobbs P, Smith A. Acceptors and rejecters of an invitation to undergo breast screening compared with those who referred themselves. *J Epidemiol Community Health* **1980**;34:19–22
7. McCusker J, Morrow GR. Factors related to the use of cancer early detection techniques. *Prev Med* **1980**;9:388–397
8. Fox SA, Baum JK, Klos DS, Tsou CV. Breast cancer screening: the underuse of mammography. *Radiology* **1985**;156:607–611
9. Fox S, Klos DS, Tsou CV. Underuse of screening mammography by family physicians. *Radiology* **1988**;166:431–433
10. Rimer BK, Keintz MK, Kessler HB, Engstrom PF, Rosan JR. Why women resist screening mammography: patient related barriers. *Radiology* **1989**;172:243–246
11. Greenwald P, Sondik EJ. *Cancer control objectives for the nation: 1985–2000*. Washington, DC: National Cancer Institute, **1986** (NCI Monographs 1986 No. 2. NIH publication No. 86-2880)



Scientific Program (200 papers)
Instructional Courses (60 hours)
Categorical Course on Neuroradiology
The Caldwell Lecture
Award Papers
Scientific Exhibits
Social, Golf, and Tennis Programs
Guest Programs

Come to the American Roentgen Ray Society

92nd

ANNUAL MEETING

Orlando, FL

Marriott's Orlando World Center
May 10–15, 1992

Altered Gallbladder Contractility After Extracorporeal Shock-Wave Cholecystolithotripsy

Brijendra Rawat[1]
J. Stephen Fache
H. Joachim Burhenne

Change in gallbladder contractility after biliary extracorporeal shock-wave lithotripsy (ESWL) may significantly influence the clearance of fragments after successful gallstone fragmentation. We assessed changes in gallbladder contractility in response to an oral fatty meal in 50 patients 1 month after biliary ESWL (all fragments were smaller than 3 mm) and also in a separate group of 10 patients 3 months after complete clearance of fragments. The prevalence of persistent lumen-obliterating contraction of the gallbladder after biliary ESWL also was analyzed in 325 patients. Gallbladder contractility remained unchanged in 30, increased in nine, and decreased in 11 of the 50 patients. The average reduction in the fasting gallbladder volume after lithotripsy was 28% ($p < .001$). Gallbladder contractility remained unchanged 3 months after complete clearance of fragments in six of 10 patients studied separately. A decrease ($n = 2$) or increase ($n = 2$) in contractility was seen in the remaining patients. No significant difference occurred in the average ejection fraction of the gallbladder before lithotripsy and after complete clearance of the fragments. Thirty-four of the 325 patients who have so far undergone biliary ESWL had a completely contracted gallbladder with no lumen visible on sonography. The gallbladder returned to a relaxed state in half of these patients within 1–9 months.

Thus, biliary ESWL did not significantly alter gallbladder contractility in 60% of patients. A significant reduction in the volume of the fasting gallbladder occurred after lithotripsy. Successful clearance of fragments did not improve the contractility of stone-bearing gallbladders in the majority of patients.

AJR 157:485–489, September 1991

Biliary extracorporeal shock-wave lithotripsy (ESWL) has emerged as a safe and effective nonsurgical alternative in the management of selected patients with symptomatic gallbladder calculi [1, 2]. Use of adjuvant oral bile acids with biliary ESWL has become the standard practice [3, 4]. At our institution, we do not use bile acids to dissolve residual fragments. Lithotripsy is performed as definitive therapy for the treatment of selected cases of gallbladder stones. Spontaneous passage of the fragments is the only mechanism of clearance of fragments and presumably depends on adequate contraction of the gallbladder. Any change in gallbladder contractility may significantly influence the clearance of fragments in our patient group. In this context, it is notable that oral bile acids are thought to diminish the contractility of the gallbladder [5, 6]. The effect of extracorporeal shock waves on gallbladder contractility is not completely understood, and to date only one relevant article [7] has been published. We present our data on the effects of biliary ESWL on the contractility of the gallbladder.

Subjects and Methods

This study was divided into three parts. In the first part, gallbladder contractility was assessed sonographically in 50 consecutive consenting patients 1 month after they had

Received January 28, 1991; accepted after revision April 8, 1991.

Presented at the annual meeting of the American Roentgen Ray Society, Boston, MA, May 1991.

[1] All authors: Department of Radiology, University of British Columbia and Vancouver General Hospital, 855 W. 12th Ave., Vancouver, B.C., Canada V5Z 1M9. Address reprint requests to H. J. Burhenne.

0361–803X/91/1573–0485
© American Roentgen Ray Society

TABLE 1: Results of Gallbladder Contraction Studies in Two Groups of Patients Before and After Biliary Extracorporeal Shock-Wave Lithotripsy (ESWL)

Study Group/Interval	Gallbladder Volume (ml)		
	Fasting	Residual	Change
Group 1 (n = 50)			
Before lithotripsy	34.2 ± 7.0 (8.0–70)	11.3 ± 4.5 (4.0–37)	64.0 ± 4.0 (25.0–88)
1 month after successful fragmentation	24.5 ± 8.9[a] (3.8–80)	9.6 ± 10.0 (1.5–80)	59.0 ± 15.0[b] (0–94)
Group 2 (n = 10)			
Before lithotripsy	27.3 ± 7.0 (8.0–50)	8.0 ± 3.4 (4.0–13)	67.0 ± 4.0 (43.0–80)
3 months after fragment clearance	23.8 ± 6.4[c] (5.0–37)	7.8 ± 3.5 (3.0–14)	66.0 ± 4.0[b] (37.0–85)

Note.—Values are means ± SD; ranges are in parentheses. Group 1 comprised 50 patients studied before biliary ESWL and 1 month after successful fragmentation; group 2 comprised 10 patients studied before biliary ESWL and 3 months after fragment clearance.

[a] Significantly different from value before lithotripsy ($p < .001$).

[b] Not significantly different from value before lithotripsy ($p > .5$).

[c] Not significantly different from value before lithotripsy ($p > .2$).

shock-wave fragmentation of symptomatic gallbladder calculi (no fragments were larger than 3 mm). This was compared with the prelithotripsy measurement of gallbladder contraction, performed by a similar method, as required by our biliary lithotripsy protocol. An oral fatty meal (60 ml of Neocholex, Horner, Montreal, Canada) diluted with an equal amount of water was used to induce gallbladder contraction. Each subject fasted for a minimum of 12 hr before sonographic examination. The greatest axial length of the gallbladder in the sagittal plane was recorded. The transducer was then rotated 90° to obtain the image of the short axis of the gallbladder, and the greatest transverse and anteroposterior dimensions were recorded. The approximate volume of the gallbladder was then determined by the ellipsoid method, as described previously [8, 9]. The gallbladder volume was determined again 45–60 min after administration of the oral fatty meal. The contraction of the gallbladder was expressed as the percentage of change (ejection fraction); the volume before the fatty meal was used as the index value. The difference between contraction values before and after lithotripsy was expressed as a percentage; contraction before lithotripsy was used as the index value. Statistical analysis was done with the assumption that the measured gallbladder volumes were distributed approximately normally about their true value. When the delta method [10] was used, the variance of the ejection fraction was approximately four times the coefficient of variation of the measured gallbladder volumes. When published data on the accuracy of measurement of gallbladder volume were used, which indicated that the coefficient of variation was approximately 10% [11], the calculated standard deviation of the ejection fraction was 20%. Thus, an observed difference of 20% or less between ejection fractions before and after lithotripsy was considered not significant.

In the second part of the study, gallbladder contraction was assessed in 10 patients 3 months after successful clearance of residual fragments. A comparison was then made with gallbladder contraction values obtained before lithotripsy in order to determine if any change in gallbladder contractility occurred after successful treatment of gallbladder disease. Statistical analysis and comparison of data were performed by using the paired t test. A p value of .05 or less was considered statistically significant.

In the third part of the study, follow-up sonographic examinations performed after lithotripsy in all patients in our program were reviewed to determine the prevalence of persistent complete obliteration of the gallbladder lumen.

A Lithostar Plus lithotriptor (Siemens, Erlangen, Germany) was used for stone fragmentation. Technical details and the lithotripsy protocol have been described [2, 12]. The number of shock waves administered ranged from 2000 to 20,000 (average, 10,500).

Results

In the first part of the study, assessment of gallbladder contractility after lithotripsy, the ejection fraction of the gallbladder was 64 ± 4% and 59 ± 15% before and after lithotripsy, respectively (Table 1). The difference between these two values is not significant ($p > .5$). The ejection fraction of the gallbladder after lithotripsy was unchanged in 30 patients (60%), increased in nine patients (18%), and decreased in 11 patients (22%). In six of the 11 patients in whom the ejection fraction decreased, the gallbladder showed no response to a fatty meal after lithotripsy (Fig. 1A). Thus, a 100% loss of ejection fraction occurred in these six patients. ^{99m}Tc-*N*-(2,6-dimethylphenyl-carbamoyl-methyl) iminodiacetic acid (HIDA) scans were obtained later in five of these six patients to rule out cystic duct obstruction and to assess gallbladder contraction in response to IV cholecystokinin. The cystic duct was patent and the gallbladder failed to contract in response to cholecystokinin in these five patients. One patient had undergone surgery because of recurrent biliary colic.

The average volume of the gallbladder after fasting and before lithotripsy was 34.2 ± 7.0 ml (range, 8–70 ml). This decreased to 24.5 ± 8.9 ml (range, 3.8–80.0 ml) after lithotripsy (Table 1). Thus, the average reduction after lithotripsy was 28%, which is statistically significant ($p < .001$). No correlation was found between the number of shocks administered and the degree of alteration in contraction of the gallbladder.

In the second part of the study, assessment of gallbladder contractility after complete clearance of all fragments, the ejection fraction of the gallbladder was unchanged in six patients, increased in two, and decreased in two 3 months after complete clearance of residual fragments (Fig. 1B). No

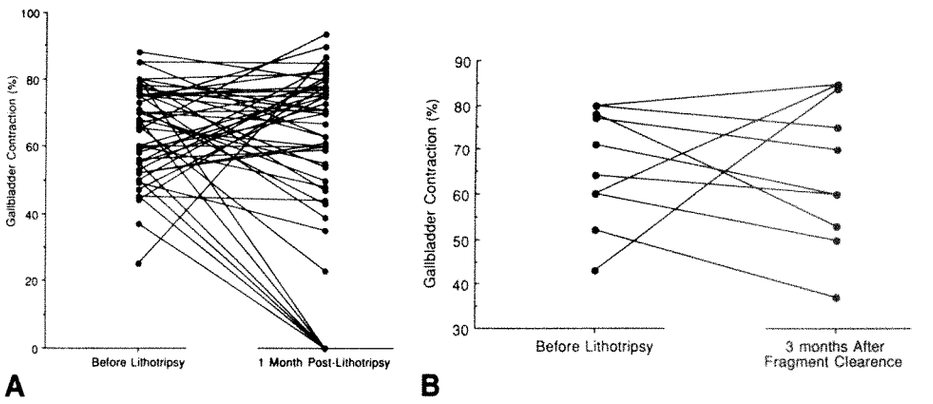


Fig. 1.—*A*, Graph showing gallbladder contraction before and 1 month after lithotripsy in 50 patients. Contractility was unchanged in 30 patients, increased in nine, and decreased in five. Gallbladder contractility was lost in six patients.

***B*, Graph showing gallbladder contraction before and 3 months after complete clearance of fragments in 10 patients. Gallbladder contraction was unchanged in six patients, increased in two, and decreased in the remaining two.**

significant difference was found in the average ejection fraction of the gallbladder determined before lithotripsy and again after complete clearance of the gallstone fragments ($p > .5$, Table 1). Unlike in the first part of the study, no significant difference was seen in the volume of the gallbladder after fasting and before lithotripsy and after clearance of fragments ($p > .2$).

For the third and final part of the study, the prevalence of complete obliteration of the gallbladder lumen was analyzed in 325 patients with symptomatic gallbladder calculi who had thus far undergone lithotripsy. Thirty-four patients (10%) had a completely contracted gallbladder within 2 days to 3 months of the first lithotripsy session. No gallbladder lumen was visible on sonograms in these patients. The gallbladder lumen opened in 18 of these patients within 1–9 months (Fig. 2). In the remaining 16 patients, the gallbladder still was contracted during follow-up examinations at 2–15 months.

Discussion

Extracorporeally administered shock waves can cause structural damage in various organs, including the kidney [13], liver [14], and gallbladder [15]. Traumatic changes in the kidney in turn can lead to functional impairment in the form of diminished effective renal plasma flow. Reduction in this flow may be one of the predisposing factors responsible for the reported occurrence of systemic arterial hypertension in patients with renal stones who are treated with ESWL [16]. Gallbladder function can be assessed radiologically with the demonstration of the ability of the gallbladder mucosa to concentrate bile and radiologic contrast material (concentrating ability) and the contraction of the gallbladder in response to a fatty meal (motor function). Previous investigations [7, 17] have found that both of these functions remain unaltered after biliary ESWL with electrohydraulically generated shock waves. These investigators, however, administered a limited number of shock waves (average, <2000) to the gallbladder calculi. We administered on average 10,500 electromagnetically generated shock waves per patient; however, differences in the shock-wave characteristics and the shock-wave generator designs of different manufacturers make it difficult to directly compare the number of shock waves administered. No report is available to date that has investigated change in the contractility of the gallbladder when larger numbers of shock waves are administered. Our study shows that gallbladder contraction did not change significantly in the majority of patients after lithotripsy. However, in a small subgroup of patients, the gallbladder lost its contracting ability after administration of shock waves. ^{99m}Tc-HIDA scanning showed a patent cystic duct in these patients. The direct traumatic effects of shock waves to the gallbladder musculature may lead to atony. One of these six patients had undergone surgery because of repeated attacks of biliary colic. The gallbladder showed focal areas of hemorrhage in the mucosa and changes of chronic cholecystitis. Long-term retention of fragments might be expected in these patients.

Several reports [18, 19] have shown diminished gallbladder emptying in patients with gallbladder calculi. This impairment in gallbladder contractility might be a primary phenomenon that predisposes to nucleation and subsequent development of gallstones [20, 21], or the presence of gallstones may cause chronic inflammation of the gallbladder wall with a corresponding reduction in its contractility. Our study shows that the contractility of 10 stone-bearing gallbladders did not improve after successful removal of stones by lithotripsy. This observation is in accordance with the findings of other investigators [7] and could be interpreted as supporting the hypothesis that defective gallbladder motility leads to formation of gallstones. Conversely, traumatic fibrosis of the gallbladder after lithotripsy may prevent restoration of gallbladder contractility that otherwise might occur after stone removal. Shaffer [5] has observed a partial but significant restoration of gallbladder motility after successful (and presumably nontraumatic) dissolution of gallbladder stones with oral bile-acid therapy. We presume that lithogenicity remains at best unaltered after biliary ESWL, and the rate of gallstone recurrence after ESWL is expected to be at least that of recurrence after bile-acid therapy. Recurrence of calculi after successful dissolution with bile acids occurs at a rate of approximately 10% per year for the first 5 years [22].

We have observed a 10% prevalence of prolonged complete obliteration of the gallbladder lumen in 325 patients who have undergone biliary ESWL. The obliteration of the lumen generally is preceded by an acute biliary colic-type pain.

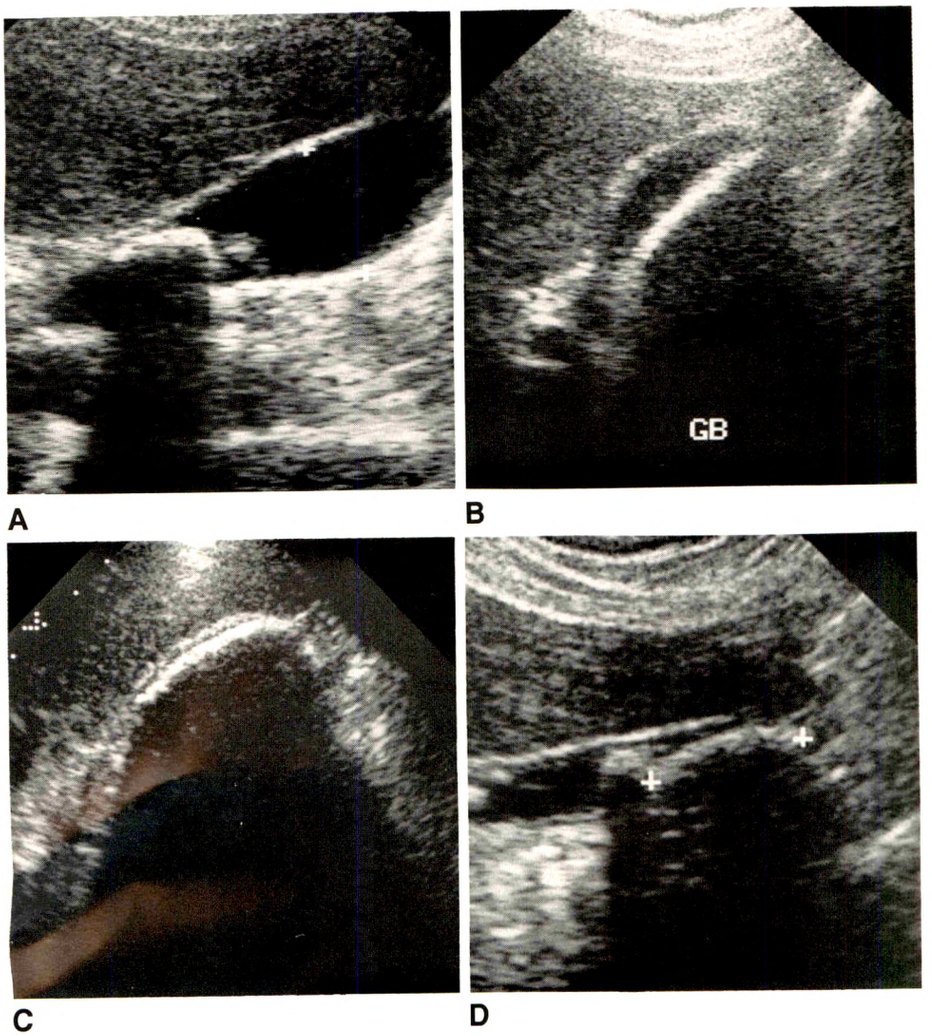


Fig. 2.—Contraction of gallbladder after lithotripsy.

***A* and *B*, Sonograms obtained before lithotripsy (*A*) and after two sessions (*B*) show successful fragmentation of two stones.**

***C*, Sonogram obtained 1 month after *B* shows gallbladder completely contracted.**

***D*, Sonogram obtained 8 months after *C* shows gallbladder is relaxed. Fragments were clumped together in a group of three or four because of prolonged contraction of gallbladder.**

Subsequently, the patient remains relatively symptom-free, presumably with a noncontracting "silent" gallbladder. Sonographic imaging and targeting of the fragments become difficult during this period. If lithotripsy is performed at this time, the gallbladder lumen may open again, indicating muscular contraction rather than fixed fibrosis in those cases. We also have observed spontaneous opening of the gallbladder lumen in some patients. This occurred at intervals ranging from 2 to 9 months after obliteration of the gallbladder lumen.

In conclusion, biliary ESWL with electromagnetically generated shock waves did not produce significant change in the contractility of the gallbladder in the majority of patients. A significant reduction in the volume of the gallbladder after fasting occurred after lithotripsy. This reduction in volume was not observed in those patients in whom clearance of stone fragments was complete. Successful clearance of the fragments did not improve the motility of stone-bearing gallbladders.

ACKNOWLEDGMENT

We thank Betty Fowler for help in manuscript preparation.

REFERENCES

1. Sackmann M, Delius M, Sauerbruch T, et al. Shockwave lithotripsy of gallbladder stones: the first 175 patients. *N Engl J Med* **1988**;318: 393–397
2. Burhenne HJ, Becker CD, Malone DE, Rawat B, Fache JS. Biliary lithotripsy: early observations in 106 patients. Work in progress. *Radiology* **1989**;171:363–367
3. Ponchon T, Barkun A. Experimental and clinical studies on extracorporeal shock wave biliary lithotripsy: the Lyon experience. In: Burhenne HJ, Paumgartner G, Ferrucci JT, eds. *Biliary lithotripsy II*. Chicago: Year Book Medical, **1990**:83–87
4. Ell C, Kerzel W, Schneider JT, Domschke W, Hahn EG. Piezoelectric lithotripsy of gallbladder stones: the Erlangen experience. In: Burhenne HJ, Paumgartner G, Ferrucci JT, eds. *Biliary lithotripsy II*. Chicago: Year Book Medical, **1990**:93–95

5. Shaffer EA. Influence of bile acid therapy on gallbladder function. In: Burhenne HJ, Paumgartner G, Ferrucci JT, eds. *Biliary lithotripsy II*. Chicago: Year Book Medical, **1990**:143–149
6. Howard P, Murphy GM, Dowling RH. Effects of chenodoxy (CDCA) and ursocholic acids (UCA) on gallbladder (GB) emptying (abstr). *Gut* **1985**;26:A1124
7. Spengler U, Sackmann M, Sauerbruch T, Holl J, Paumgartner G. Gallbladder motility before and after extracorporeal shockwave lithotripsy. *Gastroenterology* **1989**;96:860–863
8. Dodds WJ, Groh WJ, Darweesh RMA, Lawson TL, Kishk SMA, Kern MK. Sonographic measurement of gallbladder volume. *AJR* **1985**;145:1009–1011
9. Kishk SMA, Darweesh RMA, Dodds WJ, et al. Sonographic evaluation of resting gallbladder volume and postprandial emptying in patients with gallstones. *AJR* **1987**;148:875–879
10. Cochran WG. *Sampling techniques*, 2nd ed. New York: Wiley, **1963**:30–31
11. Everson GT, Braverman DZ, Johnson ML, Kern F. A critical evaluation of real-time ultrasonography for the study of gallbladder volume and contraction. *Gastroenterology* **1980**;79:40–46
12. Rawat B, Fache JS, Burhenne HJ. Biliary lithotripsy with the Siemens Lithostar Plus overhead module. *J Lithotripsy Stone Dis* **1990**;2:111–116
13. Rubin JI, Arger PH, Pollack HM, et al. Kidney changes after extracorporeal shockwave lithotripsy: CT evaluation. *Radiology* **1987**;162:21–24
14. McGrath FP, Lee SH, Gibney RG, Burhenne HJ. Hepatic subcapsular hematoma: an unusual complication of biliary lithotripsy. *AJR* **1990**;154:1015–1016
15. Delius M, Brendel W. In vivo parameters of gallstone fragmentation: experimental basis. In: Ferrucci JT, Delius M, Burhenne HJ, eds. *Biliary lithotripsy*. Chicago: Year Book Medical, **1989**:49–58
16. Williams CM, Kaude JV, Newman RC, Peterson JC, Thomas WC. Extracorporeal shock-wave lithotripsy: long-term complications. *AJR* **1988**;150:311–315
17. Burnett D, Ertan A, Jones R, et al. Use of external shockwave lithotripsy and adjuvant ursodiol for treatment of radiolucent gallstones: a national multicenter study. *Dig Dis Sci* **1989**;34:1011–1015
18. Fisher RS, Stelzer F, Rock E, Malmud LS. Abnormal gallbladder emptying in patients with gallstones. *Dig Dis Sci* **1982**;23:1019–1024
19. Forgacs IC, Maisey MN, Murphy GM, Dowling RH. Influence of gallstones and ursodeoxycholic acid therapy on gallbladder emptying. *Gastroenterology* **1984**;87:299–307
20. LaMorte WW, Schoetz DJ, Birkett DH, Williams LF. The role of the gallbladder in the pathogenesis of cholesterol gallstones. *Gastroenterology* **1979**;77:580–592
21. Shaffer EA, Small DM. Gallstone disease: pathogenesis and management. *Curr Probl Surg* **1976**;13:1–72
22. O'Donnel LDJ, Heaton KW. Recurrence and re-recurrence of gallstones after medical dissolutions: a long-term follow up. *Gut* **1988**;29:655–658

Book Review

The Radiologic Clinics of North America. Interventional Radiology of the Biliary Tract. Guest editor: H. Joachim Burhenne. Philadelphia: Saunders, November 1990;28(6):1139–1313. $25; by subscription, 6 issues annually for $93

H. Joachim Burhenne, the editor of this issue of *The Radiologic Clinics of North America*, begins with an absolutely fascinating history of interventional radiology of the biliary tract. As he was prominently involved in much of that history, he is in the perfect position to review the myriad details of this rich background. A second introductory paper sets the stage for the rest of the volume by reviewing all the nonsurgical interventional radiologic alternatives to cholecystectomy.

Subsequently, more focused papers review interventional gallbladder procedures and transcholecystic interventions. Newer techniques in interventional biliary radiology are included in papers on such topics as percutaneous balloon dilatation of benign strictures, plastic and metal biliary stents, and intraductal radiation therapy for neoplasm. The tremendous growth of new knowledge in dealing with gallbladder and biliary calculi is well covered. Articles include information on fine-caliber cholangioscopy, intra- and extracorporeal biliary lithotripsy, and interventional ablation of the gallbladder.

This is a timely and comprehensive collection of articles. I recommend it highly to all radiologists. *The Radiologic Clinics of North America* has continued its long tradition of providing comprehensive reviews of interesting and rapidly changing fields of radiology.

Robert A. Clark
H. Lee Moffitt Cancer Center and Research Institute
Tampa, FL 33682-0179

Case Report

Placement of a Metallic Biliary Endoprosthesis via Cholecystostomy

Steven L. Dawson,[1] Mark J. Girard, Sanjay Saini, and Peter R. Mueller

Relief of bile duct obstruction can be accomplished by surgical or percutaneous cholecystostomy. Subsequent conversion to internal drainage with an endoprosthesis is difficult because of the manipulations and dilatation necessary to traverse the cystic duct. Recently, metallic biliary endoprostheses with a small-caliber delivery system that requires limited dilatation and can be inserted through small tracks have become available. We present a patient who had transcystic duct placement of a metallic endoprosthesis in the common bile duct for malignant obstruction due to metastatic breast cancer.

Case Report

A 48-year-old woman with a history of metastatic breast carcinoma had obstructive jaundice of 6 weeks' duration. A laparotomy revealed an unresectable peripancreatic mass extending to the porta hepatis. Although the mass obstructed the common bile duct below the insertion of the cystic duct, neither choledochojejunostomy nor hepaticojejunostomy could be performed. Biliary drainage was accomplished by surgical placement of a 24-French cholecystostomy catheter. Cholangiography showed a patent cystic duct with complete obstruction of the distal common bile duct (Fig. 1A). The cholecystostomy tube was removed over a guidewire, and a 24-French Amplatz sheath was inserted in order to preserve the cholecystostomy track. A 6.5-French Cobra-1 catheter was placed at the proximal turn of the cystic duct (Fig. 1B). A Tracker-18 system (Target Therapeutics, San Jose, CA) was placed coaxially through the Cobra-1 catheter. A steerable 0.016-in. (0.41 mm) guidewire was used in conjunction with the 3.0-French catheter to negotiate the cystic duct; the small caliber of the catheter system allowed immediate passage through the obstruction (Fig. 1C). With the 3.0-French catheter in the duodenum, an exchange was made for a 5-French H1 catheter (Cook, Inc., Bloomington, IN), which was easily placed through the obstruction over the 3.0-French Tracker catheter. An Amplatz 0.038-in. (0.97 mm) Extra Stiff guidewire (Cook, Inc.) was placed through the 5-French catheter, which was then removed, and the malignant stricture was then dilated with a 9-French VanAndel catheter (Cook, Inc.). A 7-French, 10-mm-diameter, 68-mm-long Wallstent (Schneider USA, Minneapolis, MN) was placed without difficulty (Figs. 1D and 1E). A 20-French Foley cholecystostomy tube was left for follow-up cholangiography. This tube was removed 1 week later, when cholangiography showed a widely patent endoprosthesis.

Discussion

Gallbladder drainage can be an effective alternative to transhepatic drainage in patients with obstruction of the common bile duct [1]. However, this alternative leaves the patient with a permanent external catheter. Insertion of a biliary endoprosthesis by using the gallbladder for access has not previously been reported. The limiting factor has been placement of a 14- to 16-French catheter through the cystic duct.

Interventional procedures through the gallbladder have traditionally been more difficult than those through the liver because of the cystic duct and valves of Heister interposed between the initial entry point and the final working location. In this case, even a large-caliber cystic duct proved to be difficult to negotiate with standard size 5- to 6.5-French

Received January 31, 1991; accepted after revision March 12, 1991.

[1] All authors: Department of Radiology, Massachusetts General Hospital and Harvard Medical School, Fruit St., Boston, MA 02114. Address reprint requests to P. R. Mueller.

AJR 157:491–493, September 1991 0361–803X/91/1573–0491 © American Roentgen Ray Society

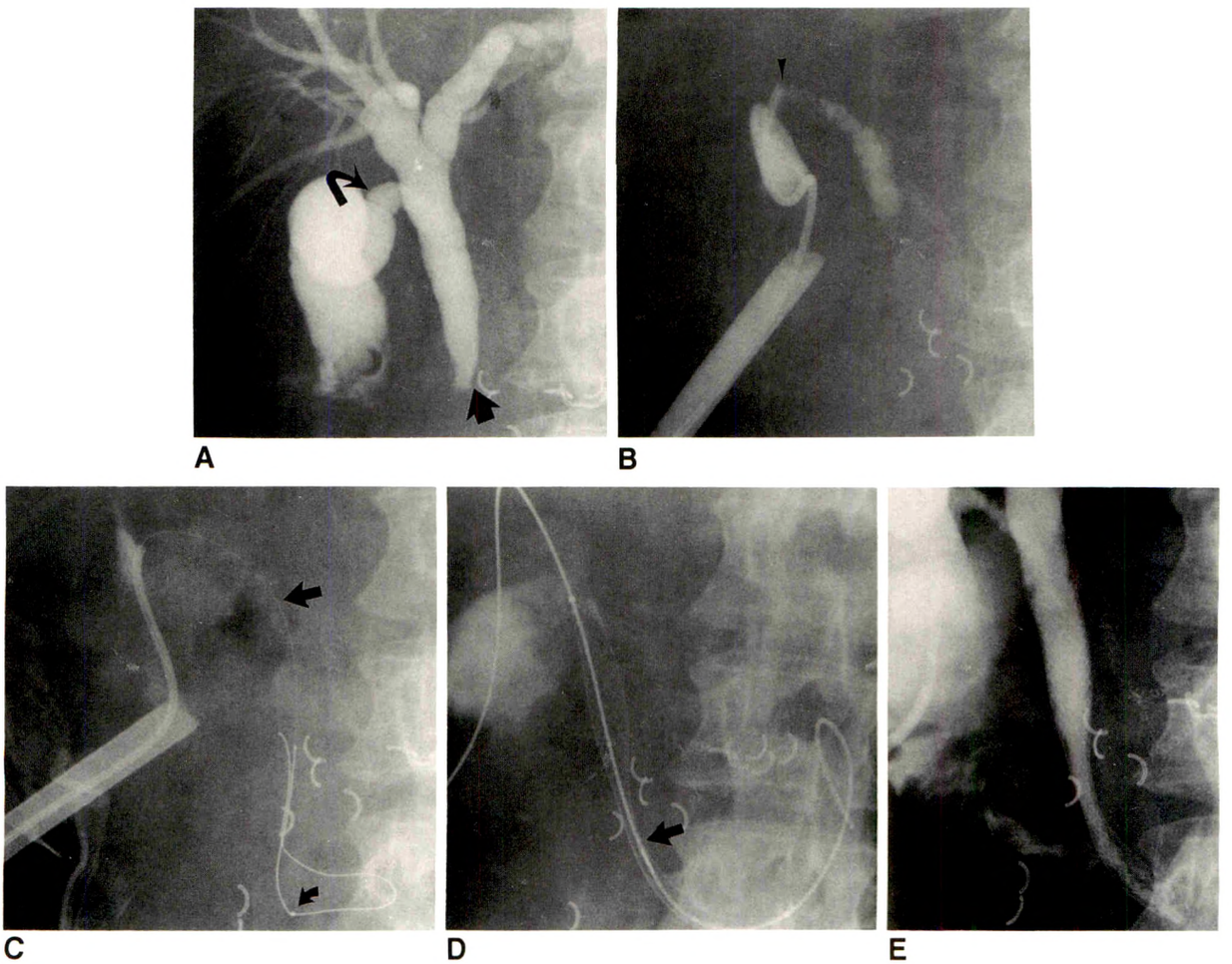


Fig. 1.—*A*, Preliminary cholangiogram obtained through surgical cholecystostomy tube. Distal common bile duct (*straight arrow*) is completely obstructed with a very tortuous, large-caliber cystic duct (*curved arrow*).

***B*, Selective cystic duct injection via 6.5-French Cobra-1 catheter that has been placed through a 24-French sheath, preserving access through surgical cholecystostomy track. Cobra catheter tip has been negotiated to first turn of double-S cystic duct configuration (*arrowhead*). Valves of Heister are clearly seen and made initial cystic duct catheterization attempts difficult.**

C, Through Cobra-1 catheter, Tracker 0.016-in. (0.41 mm) guidewire (*straight arrow*) and catheter have been placed through cystic duct and advanced beyond obstruction of common bile duct. Opaque marker of the Tracker catheter tip (*curved arrow*) can be seen in duodenum.

***D*, Spot film after placement of Wallstent endoprosthesis over an Extra Stiff Amplatz guidewire. Endoprosthesis has adequate length above and below obstructing lesion, but tumor continues to narrow distal portion of stent (*arrow*).**

***E*, Final cholangiogram via percutaneous cholecystostomy tube that has been placed through surgical track. Flow of contrast material through endoprosthesis is demonstrated, and some residual narrowing is at level of obstructing mass. Contrast material flowed freely through obstruction at low injection pressures, and a Foley cholecystostomy tube was left as a safety catheter.**

catheters and 0.018-in. (0.46 mm) to 0.038-in. (0.97 mm) guidewires, as well as various hydrophilic Terumo glidewires (Medi-tech, Watertown, MA).

The Tracker system uses a very fine, platinum-tipped, soft guidewire of 0.013 in. (0.33 mm) diameter at the tip, tapered to 0.016 in. (0.41 mm) diameter along the working shaft. The wire is designed to be used with a special catheter that is 2.2-French at the narrowest outside diameter, 2.7-French at the opaque metallic marker in the tip, and 3.0-French along the working length. The entire system fits within sturdier 5-French and larger catheters. These catheters can be placed close to the area of maximal narrowing, and the Tracker system can be used to negotiate extremely tortuous narrowed vessels, ducts, or ureters. In this patient, the use of this system allowed placement of the endoprosthesis via an existing track, a procedure that otherwise would have been impossible. We are currently working with manufacturers to develop a torquable 3-French catheter that is more affordable than the Tracker system, but a similar catheter was not available at the time of this case.

The Wallstent endoprosthesis uses a compressed, elongated, fine stainless steel mesh stent, which is delivered inside a 7-French catheter [2–4]. The endoprosthesis is 10 cm long in its compressed state, but shortens as it expands after deployment to a nominal final length of 68 mm, with a nominal 10-mm internal diameter. If necessary to improve drainage,

the stent diameter can be enlarged to 10 mm by balloon dilatation of any residual narrowing. The duct should ideally be dilated before stent insertion, but if marked narrowing persists after placement, dilatation has been performed with the stent in place. After placement, the diameter of the stent frequently continues to increase for several days, even without balloon dilatation, as the metallic mesh seeks to resume its unconstrained diameter. The introducer system and compressed metallic stent are sufficiently pliable that the catheter can be negotiated around acute angles over a stiff guidewire.

In this patient, a traditional transhepatic approach could have been performed with the surgical cholecystostomy for biliary opacification, or alternatively, a standard de novo transhepatic approach could have been used. However, any transhepatic procedure would have required a new puncture and dilatation of the track, with risk of increased morbidity. By using the existing surgical tube for access, we were able to drain the system transcholecystically without the need for two temporary tubes. The single cholecystostomy safety catheter was removed within days of endoprosthesis placement.

To our knowledge, this is the first report of endoprosthesis placement via a transcholecystic approach. The use of a highly torquable guidewire and extremely small catheter combination such as the Tracker system may open this pathway to further interventions in the common bile duct when intrahepatic duct access is not possible. In addition, the Wallstent endoprosthesis permits a flexible large-lumen stent to be placed through a track that is smaller than the standard initial 8.3-French drainage catheter.

REFERENCES

1. VanSonnenberg E, D'Agostino H, Casola G, Varney R, Taggart S, May S. The benefits of percutaneous cholecystostomy for decompression of selected cases of obstructive jaundice. *Radiology* **1990**;176:15–18
2. Gillams A, Dick R, Dooley J, Wallsten H, El-Din A. Self-expandable stainless steel braided endoprosthesis for biliary strictures. *Radiology* **1990**; 174:137–140
3. Lammer J, Klein G, Kleinert R, Haussegger K, Einspieler R. Obstructive jaundice: use of expandable metal endoprosthesis for biliary drainage. *Radiology* **1990**;177:789–792
4. La Berge J, Doherty M, Gordon R, Ring E. Hilar malignancy: treatment with an expandable metallic transhepatic biliary stent. *Radiology* **1990**;177:793–797

Videotape Review

RSNA Today, Vol. 4, No. 5. Oak Brook, IL: The Radiological Society of North America, 1990. $55; by subscription, 6 issues annually at $185 for RSNA members and $225 for nonmembers (VHS videotape)

This videotape covers four separate topics and is moderated by William J. Casarella. The first topic, "Imaging Insights: Breast Calcifications—Parenchymal or Dermal?" is presented by Edward A. Sickles. Dr. Sickles discusses the mammographic differentiation between dermal calcifications, which are benign, and parenchymal calcifications, which may be malignant. The location of calcifications in the breast, their typical appearances, and the methods of proving their dermal location ("dead reckoning" and "BB guidance") are discussed, and illustrative cases are presented. The efficacy of a presentation on this one specific aspect of mammography is to be questioned, although the presentation is clear, and, of course, Dr. Sickles is a well-known expert in this field.

The second part, "Thoracic Drainage Procedures," is presented by Eric vanSonnenberg. This is a thorough and well-presented review of all aspects of interventional drainage of empyema and abscess collections in the lung, pleura, and mediastinum and of treatment for pneumothorax. Dr. vanSonnenberg discusses the types of collections to be drained, how the procedure is guided, and techniques and equipment used in the diagnosis and drainage of these pathologic entities. The failures and limitations of previously used surgical techniques are discussed also. All of these factors are related to a previously completed study of 150 patients, including the results of the study and the complications and failure rates to be expected with these procedures. The presentation is comprehensive, and the illustrative cases are clearly presented and are instructive.

The third part, "Imaging Insights: Perienteric Changes—Signs and Significance in Abdominal CT," is presented by Alec J. Megibow. The CT changes in the perienteric fat are presented for both inflammatory and neoplastic diseases. The thickening and increased density of mesenteric and fascial planes in diverticulitis, appendicitis, and pancreatitis are discussed for the inflammatory lesions, and the added perivascular and soft-tissue extensions and masses are discussed for the neoplastic lesions. The accompanying case presentations are clearly displayed and are quite helpful. This presentation is excellent and should be useful to radiologists interested in body CT.

The fourth part, "The Battered Child," is presented by Paul K. Kleinman and Nancy Genieser. After a brief historical review of Dr. Caffey's original description of what is now known as the battered child syndrome, Dr. Kleinman discusses the skeletal findings thereof. The various degrees of specificity of several findings are illustrated, from those that are highly specific (i.e., metaphyseal corner and bucket-handle fractures) to those that are common and highly nonspecific. The mechanism of injury and techniques of filming are described, and each finding is clearly demonstrated by using an illustrative case. Dr. Genieser then discusses the CNS findings in the battered child syndrome, including the various types of skull fractures, the methods of radiologic workup (i.e., plain films, CT, MR), the intracranial manifestations, and the mechanism of injury. Radiographs and surgical-pathologic examples are shown for several typical entities. A presentation such as this, on a topic of such broad-based interest to general radiologists, is a virtual must, for both education and review.

Although I found the first topic rather restrictive in scope, the overall quality of the tape is excellent. Intermixing topics of interest to interventionalists with ones of interest to noninterventionalists may, however, limit the audience of interest for this tape.

Hano A. Siegel
Mercy Hospital
San Diego, CA 92103

Perspective

Primary Sclerosing Cholangitis: A Modified Classification of Cholangiographic Findings

Charles B. L. M. Majoie,[1] Jacques W. A. J. Reeders,[1] Joost B. Sanders,[2] Kees Huibregtse,[2] and Peter L. M. Jansen[2]

Primary sclerosing cholangitis (PSC) is a disease characterized by obliterative inflammatory fibrosis usually affecting both the intrahepatic and extrahepatic portions of the biliary tree. Cholangiography is the accepted method for making the diagnosis. Histologic findings can be highly suggestive of PSC, particularly when concentric periductal fibrosis is present (one third of patients), but the findings are usually nondiagnostic [1].

The cholangiographic appearance of PSC includes a broad spectrum of features [2]. On the basis of a study of these features in 40 patients with PSC, we classified the abnormalities into three types of intrahepatic and four types of extrahepatic abnormalities depending on the extent of bile duct narrowing, the severity of narrowing, contour abnormalities, and prestenotic dilatation. In this article, we present a modified classification and discuss the clinical implications of each class.

Cholangiograms Analyzed

Adequate cholangiograms were available in 40 patients, 27 men and 13 women 20–73 years old (mean, 43 years). Those patients with choledocholithiasis and operative trauma were excluded. Malignancy was excluded by a clinical follow-up of at least 2 years. The diagnosis of PSC was made by using a combination of clinical, cholangiographic, and liver biopsy findings. Alkaline phosphatase levels were elevated in all patients; they were three times the upper limit of normal in 63%. In 29 patients, the aspartate aminotransferase level was elevated, and in all patients the alanine aminotransferase level was increased. The total serum bilirubin level was raised in 17 patients. Eighteen patients had liver biopsies, all of which showed histologic changes compatible with PSC.

Classification

A classification of the cholangiographic findings in a series of 19 patients with PSC was first presented by Li-Yeng and Goldberg [2]. We made a minor modification in this scheme (Table 1). Li-Yeng and Goldberg proposed four types of intrahepatic and four types of extrahepatic bile duct involvement. In their classification of intrahepatic involvement, type I consisted of minor irregularities of duct contour and local narrowing with prestenotic dilatation, type II consisted of threadlike narrowing alternating with normal caliber of bile ducts or slight dilatation, type III was characterized by multiple strictures with saccular dilatations, and type IV consisted of advanced ductal narrowing with resultant lack of filling of the peripheral ducts. We found the distinction between types I and II to be of limited use, because they are difficult to differentiate and have the same clinical implications. Therefore, we propose three types of intrahepatic duct involvement that can be distinguished without difficulty. Type I intrahepatic duct involvement is characterized by multiple strictures and normal caliber of bile ducts or minimal dilatation (nine cases, 23%; Fig. 1). In type II, intrahepatic ducts show multiple

Received January 29, 1991; accepted after revision April 5, 1991.

[1] Department of Diagnostic Radiology, Academic Medical Center, University of Amsterdam, Meibergdreef 9, 1105 AZ Amsterdam Z.O., the Netherlands. Address reprint requests to C. B. L. M. Majoie.

[2] Department of Gastroenterology, Academic Medical Center, University of Amsterdam, 1105 AZ Amsterdam Z.O., the Netherlands.

AJR 157:495–497, September 1991 0361–803X/91/1573–0495 © American Roentgen Ray Society

TABLE 1: Classification of Cholangiographic Findings in Primary Sclerosing Cholangitis

Type of Duct Involvement/ Classification	Cholangiographic Abnormalities
Intrahepatic	
I	Multiple strictures; normal caliber of bile ducts or minimal dilation
II	Multiple strictures, saccular dilatations, decreased arborization
III	Only central branches filled despite adequate filling pressure; severe pruning
Extrahepatic	
I	Slight irregularities of duct contour; no stenosis
II	Segmental stenosis
III	Stenosis of almost entire length of duct
IV	Extremely irregular margin; diverticulumlike outpouchings

strictures, saccular dilatations, and decreased arborization (22 cases, 55%; Fig. 2). Type III intrahepatic duct involvement is characterized by severe pruning and only central branches filled, despite adequate filling pressure (six cases, 15%; Fig. 3).

The extrahepatic types of bile duct involvement were as presented by Li-Yeng and Goldberg [2]. Four (10%) patients showed type I extrahepatic duct involvement (Fig. 4). Type II was demonstrated in 13 patients (33%; Fig. 5), type III in five patients (13%; Fig. 6), and type IV in 16 patients (40%; Figs. 7 and 8).

The intrahepatic ducts were involved in 37 cases and the extrahepatic ducts in 38 cases. In 35 cases (88%), both intra- and extrahepatic ducts were affected. In three cases, only the extrahepatic bile duct showed abnormalities, and in two cases, only the intrahepatic bile ducts were abnormal. Intrahepatic type II abnormalities were usually seen in combination with extrahepatic type II or IV abnormalities. The different types of intra- and extrahepatic bile duct involvement were equally distributed in the patients with and without inflammatory bowel disease. Patients with inflammatory bowel disease could not be distinguished cholangiographically from other PSC patients. This finding is consistent with previous reports [2, 3].

Clinical Implications

In type I intrahepatic duct involvement, differentiation has to be made from primary biliary cirrhosis. Primary biliary cirrhosis can be differentiated clinically from PSC. Primary biliary cirrhosis is a disease of young women with histologic signs of nonsuppurative cholangitis and the presence of high titers of antimitochondrial antibodies in the blood. The extrahepatic bile ducts are not affected in this disease. In PSC, there is a marked male predominance, most patients have ulcerative colitis, and serologic markers are absent or present in low titers. Both the intrahepatic and extrahepatic bile ducts are usually affected in PSC [3].

Type II intrahepatic duct involvement is considered pathognomonic of PSC [3]. In type III intrahepatic duct involvement, differentiation from diffuse sclerosing cholangiocarcinoma may be difficult. Because the peripheral ducts are not filled in type III disease, CT is indicated to evaluate the extent of intrahepatic duct involvement [4].

In types II and III extrahepatic duct involvement, differentiation from cholangiocarcinoma is also difficult, especially when the intrahepatic ductal system is not involved. We noted this pattern in only one patient. Extensive dilatation of intrahepatic ducts is more often seen in carcinoma and is uncommon in PSC. However, cholangiocarcinoma must be considered when there is stenosis of the extrahepatic duct, and a biopsy may be needed to exclude it. Type IV extrahepatic duct involvement is pathognomonic of PSC [3].

PSC may itself be predisposed to malignant change, and the possibility of malignancy must be considered during initial presentation and follow-up. Sudden worsening of jaundice should raise the possibility of development of cholangiocar-

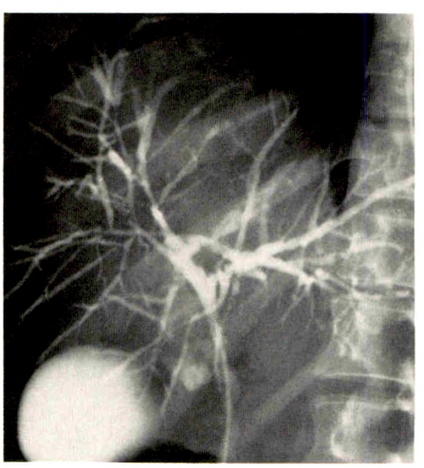


Fig. 1.—Type I intrahepatic duct involvement. Endoscopic retrograde cholangiogram shows multiple strictures and normal caliber of bile ducts or minimal dilatation.

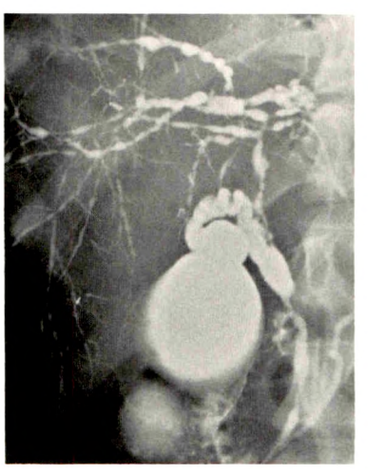


Fig. 2.—Type II intrahepatic duct involvement. Endoscopic retrograde cholangiogram shows multiple short, bandlike strictures; saccular dilatations; and decreased arborization.

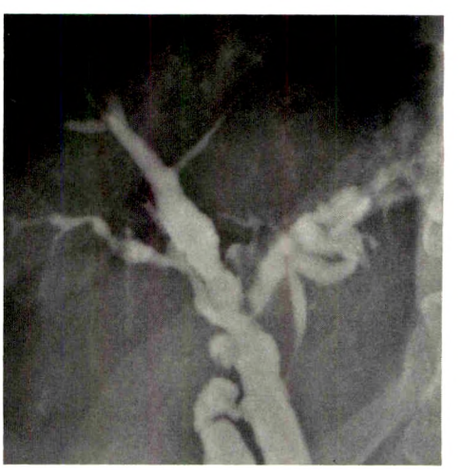


Fig. 3.—Type III intrahepatic duct involvement. Endoscopic retrograde cholangiogram shows severe pruning with only central branches filled, despite adequate filling pressure.

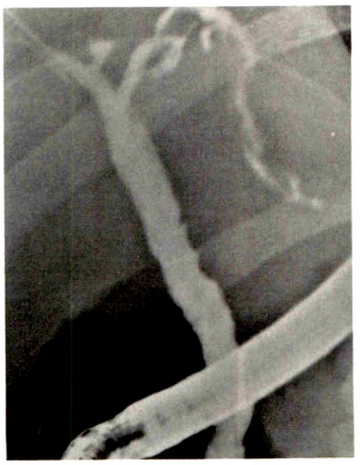


Fig. 4.—Type I extrahepatic duct involvement. Endoscopic retrograde cholangiogram shows slight irregularities of duct contour without stenosis.

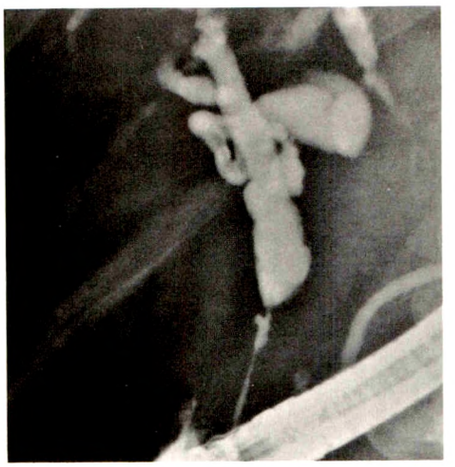
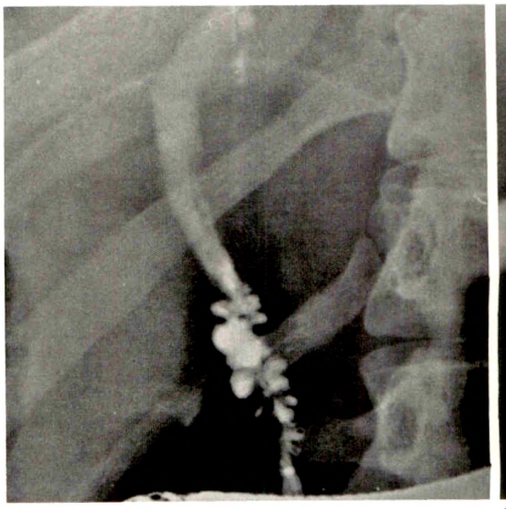


Fig. 5.—Type II extrahepatic duct involvement. Endoscopic retrograde cholangiogram shows severe segmental stenosis.

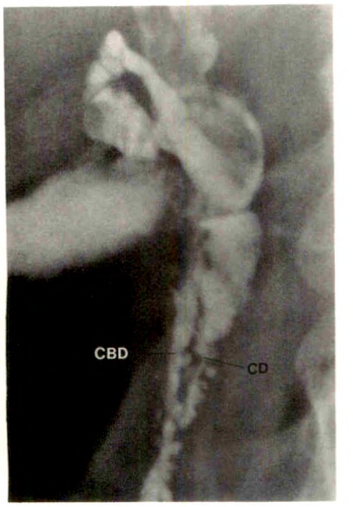


Fig. 6.—Type III extrahepatic duct involvement. Endoscopic retrograde cholangiogram shows stenosis of almost entire length of common bile duct.

Fig. 7.—Type IV extrahepatic duct involvement. Endoscopic retrograde cholangiogram shows an extremely irregular margin with diverticulumlike outpouchings.



7



8

Fig. 8.—Type IV extrahepatic duct involvement. Endoscopic retrograde cholangiogram shows tiny diverticulumlike outpouchings of cystic duct (CD) and common bile duct (CBD).

cinoma in PSC. Cholangiographic findings suggestive of the development of cholangiocarcinoma in patients with PSC have been reported previously [5]. Findings included markedly dilated ducts, presence of a polypoid mass larger than 1 cm in diameter, and progressive stricture formation or duct dilatation. In PSC uncomplicated by malignancy, the cholangiographic appearance frequently remains static for years. In our series, 10 patients were followed up by endoscopic retrograde cholangiography for periods of 22–100 months. In eight, the types of intra-and extrahepatic duct involvement remained the same. No evidence of malignancy was found by clinical follow-up for another 2 years in these cases.

Conclusions

Cholangiography is the mainstay in the diagnosis of PSC. Several types of radiologic abnormalities can be recognized. In our opinion these abnormalities can be subdivided into three intrahepatic and four extrahepatic patterns with different clinical implications. This classification helps in diagnosing PSC. Whether and how the various abnormalities are correlated with the stage of clinical disease, or whether they have any prognostic value, remains to be investigated.

REFERENCES

1. Chapman RWG, Marborgh BA, Rhodes JM, et al. Primary sclerosing cholangitis: a review of its clinical features, cholangiography and hepatic histology. *Gut* **1980**;21:870–877
2. Li-Yeng C, Goldberg HI. Sclerosing cholangitis: broad spectrum of radiographic features. *Gastrointest Radiol* **1984**;9:39–47
3. MacCarty RL, LaRusso NF, Wiesner RH, Ludwig J. Primary sclerosing cholangitis: findings on cholangiography and pancreatography. *Radiology* **1983**;149:39–44
4. Teefey SA, Baron RL, Rohrmann CA, Shuman WP, Freeny PC. Sclerosing cholangitis: CT findings. *Radiology* **1988**;169:635–649
5. MacCarty RL, LaRusso NF, May GR, et al. Cholangiocarcinoma complicating primary sclerosing cholangitis: cholangiographic appearances. *Radiology* **1985**;156:43–46

Book Review

Atlas of Roentgenographic Measurement, 6th ed. By Theodore E. Keats. St. Louis: Mosby–Year Book, 710 pp., 1990. $89.95

Like Rocky and Rambo, and, yes, *Gray's Anatomy*, some things go on forever. And so they should. For they have become lore. A classic is defined as a work often discussed but seldom read. Not so with Keats's atlas (nee Lusted and Keats, 1959). Just the other day I was reviewing emergency department films with a first-year resident and had occasion to discuss the following with respect to measurements: the optic foramen, the acetabular angle, the sella turcica, scoliosis, and the interpedicular spaces, to mention just a few. All of these require some idea of normal dimensions.

The sixth edition of this atlas is expanded, expounded, and exhaustive. It has charts, graphs, numbers, sketches, and a few faded radiographs. Pelvimetry and fetometry are covered, with plain films and sonograms, for 59 pages. Renal measurements are covered in 19 pages (for an update on the statistic, see Gourtsoyiannis et al., "The Thickness of the Renal Parenchyma Decreases with Age," *AJR* 1990;155:541–544, and Cohen et al., "Ovarian Volumes Measured by US: Bigger Than We Think," *Radiology* 1990;177:19–192). Numbers and norms will continue to play a role as new techniques are searched for better understanding of anomalies; for an example, see Kurtz et al., "Usefulness of a Short Femur in the in Utero Detection of Skeletal Dysplasias," *Radiology* 1990;177:197–200.

The sixth edition continues to use an organ-related format: CNS, skeletal, gastrointestinal, genitourinary, and so forth. The index is adequate, and each topic is amply supported with references from the current literature. Line drawings and charts are crisp and simple to follow. The binding appears durable. What may seem esoteric to some (muscle cylinder ratio in infancy, measurement of the auditory ossicles) or out of date (esophageal displacement by left atrium, localization of the pineal gland) may be bread and butter to others. The newer techniques are well represented by Doppler imaging, MR, and CT. For the life of me, I can never remember the axial measurements of the foot for the determination of congenital abnormalities (funny-looking feet). I suspect that like me, most old timers are "eyeballers," but it is comforting to have all this information readily available and in one place for reference. The scope of the graphs and charts are commendable. Just to give you some idea, they include "Fat Thickness in the Neonatal Small Left Colon Syndrome," "Measurement of Recording of Flow Velocity in Basal Cerebral Arteries by Doppler Ultrasound," "Normal Left Heart Dimension by MR," "Measurement of the Size of Cervical and Retro-pharyngeal Lymph Nodes by CT," and "Echocardiographic measurements in normal subjects from infancy to old age."

The preface to the second edition (1967) quotes Lord Kelvin, "I often say that when you can measure what you are speaking about, and express it in numbers, you know something about it, but when you can not express it in numbers, your knowledge is of a meager and unsatisfactory kind . . ." If I had my way, I would see to it that every newcomer became familiar with this atlas. Perhaps it would go a long way to help solve the "Beginning Resident Syndrome" (Keats, *Appl Radiol*, June 1990). Don't leave home without it.

Murray A. Rosenberg
Easton, CT 06612

Case Report

MR Demonstration of Edema Adjacent to a Liver Metastasis: Pathologic Correlation

Michael J. Lee,[1] Sanjay Saini,[1] Carolyn C. Compton,[2] and Ronald A. Malt[3]

T2-weighted MR images of liver metastases occasionally show a perilesional increase in signal intensity in the form of a ring (halo) or wedge (pyramid). This perilesional increase in signal intensity makes tumors appear larger on T2-weighted images than on T1-weighted images (Fig. 1) [1] (Cohen EK et al. and Simeone JF et al., presented at the annual meeting of the Society for Magnetic Resonance Imaging in Medicine, 1989). In a radiologic-pathologic study, Cohen et al. (Cohen EK et al., SMRM meeting, 1989) found viable tumor cells surrounding the lesion seen on MR images and ascribed the ringlike area of high signal intensity to perilesional invasion by tumor cells. Other authors [1] (Simeone JF et al., SMRM meeting, 1989), however, have claimed that this area of high signal intensity may be due to peritumoral edema. To date, no pathologic proof of edema in surrounding normal liver has been reported. This report provides histologic confirmation of peritumoral edema in a patient with a wedge-shaped area of high signal intensity surrounding a colonic liver metastasis shown on T2-weighted MR images.

Case Report

A 62-year-old man had dull pain in the right upper quadrant, 2 years after having an anterior resection for rectal carcinoma. He had no other physical findings or pertinent history. Contrast-enhanced CT showed a solitary 4.5-cm, low-attenuation mass in the periphery of the right lobe of the liver without any peripheral high- or low-density rings. MR imaging was performed for tissue characterization. T1-weighted, spin-echo (275/14 [TR/TE]) and multiecho T2-weighted, spin-echo (2350/60, 120, 180) images were obtained on a mid-field-strength (0.6 T) MR unit (Teslacon, GE Medical Systems, Milwaukee, WI). The T1-weighted MR image confirmed the CT finding of a single 4.5-cm lesion of low signal intensity in the right lobe of the liver in direct contiguity with a branch of the right portal vein (Fig. 1A). T2-weighted images showed a wedge-shaped perilesional area of high signal intensity that obscured and substantially increased the apparent size of the lesion (Fig. 1B). Percutaneous biopsy confirmed the presence of colonic metastasis. An extended right hepatectomy was performed, after which the patient made an uneventful recovery.

Examination of the resected specimen showed a solitary yellow-tan tumor mass 4.5 × 4.5 × 4.0 cm, corresponding to the size of the lesion on T1-weighted MR images, surrounded by a rim of pale discolored liver tissue approximately 1 cm wide. Microscopic examination showed a moderately to well-differentiated adenocarcinoma with an abundant sclerotic tumor stroma and patchy central necrosis. The periphery of the lesion was demarcated from normal liver by a border of immature stroma approximately 1 mm thick (Fig. 1C). The hepatic parenchyma surrounding the tumor showed portal inflammation, portal fibrosis with focal portal-to-portal bridging fibrosis, mild fatty change, marked sinusoidal dilatation (Fig. 1C), and hepatic edema as evidenced by expansion of the space of Disse (Fig. 1D). These changes were observed throughout the zone of liver adjacent to the advancing edge of the metastatic lesion, correlating with the peritumoral halo of increased signal intensity on T2-weighted MR images.

Discussion

A peritumoral halo of increased signal intensity on T2-weighted MR images is a well-described finding on MR im-

Received February 25, 1991; accepted after revision April 10, 1991.
[1] Department of Radiology, Massachusetts General Hospital and Harvard Medical School, Fruit St., Boston, MA 02114. Address reprint requests to S. Saini.
[2] Department of Pathology, Massachusetts General Hospital and Harvard Medical School, Fruit St., Boston, MA 02114.
[3] Department of Surgery, Massachusetts General Hospital and Harvard Medical School, Fruit St., Boston, MA 02114.

AJR 157:499–501, September 1991 0361–803X/91/1573–0499 © American Roentgen Ray Society

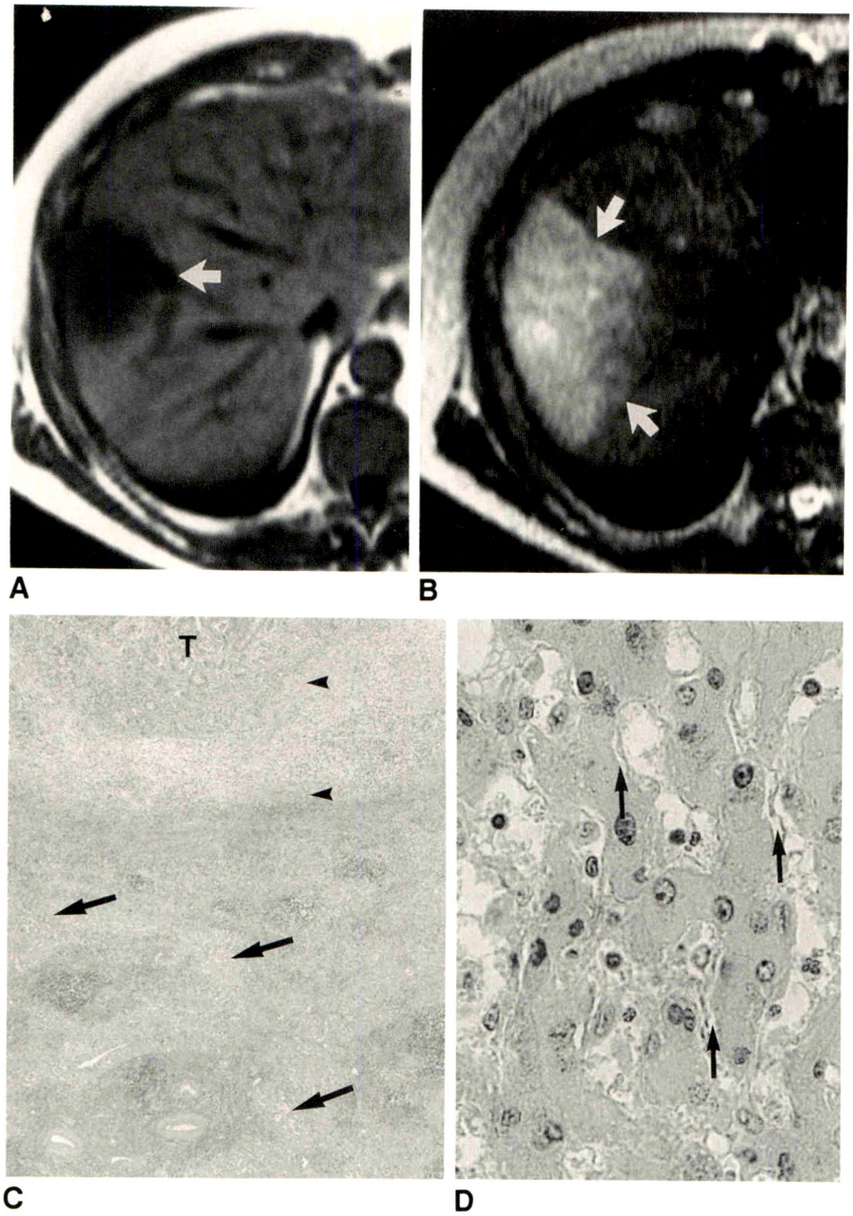


Fig. 1.—62-year-old man with surgically proved colonic metastasis.

A, T1-weighted (275/14) MR image shows peripheral round, hypointense metastasis abutting a branch of right portal vein (*arrow*).

B, T2-weighted (2350/180) MR image shows marked increase in size of tumor due to peritumoral wedge-shaped increase in signal intensity. Histologic examination confirmed peritumoral edema with sinusoidal dilatation and edema in space of Disse.

C, Low-power (original magnification ×25) photomicrograph of histologic section shows metastatic tumor (T) is well demarcated from surrounding liver parenchyma by an edematous band of immature stroma (*arrowheads*). Liver adjacent to lesion shows marked sinusoidal dilatation (*arrows*) and inflammation of portal tracts.

D, High-power (original magnification ×200) photomicrograph of histologic section shows spaces of Disse, which are the conduits for lymph flow from liver lobules to lymphatic vessels of the portal tracts, are dilated because of edema (*arrows*). In absence of liver edema, these spaces are not visible on light microscopy.

aging of brain and soft-tissue neoplasms [2, 3]. A peritumoral area of increased signal intensity also may occur with hepatic abscesses, in which case it is known to be associated with sinusoidal dilatation and edema [4]. Perilesional halos of increased signal intensity on MR imaging also have been described in diffuse cancer, focal hepatitis, and liver metastases, particularly in those from colonic primary tumors (Cohen EK et al., SMRM meeting, 1989). The cause of this phenomenon is controversial. Some authors have claimed that this halo appearance, when found with metastatic lesions, is due to perilesional infiltration by tumor cells (Cohen EK et al., SMRM meeting, 1989). Our case supports the theory that the peritumoral wedge appearance may be due to peritumoral edema and not to peritumoral infiltration by tumor cells. Careful histologic examination of the resected specimen from our patient showed sinusoidal dilatation and marked edema in the space of Disse without evidence of perilesional tumor cells (Figs. 1C and 1D).

The space of Disse lies between the sinusoidal wall and the outer sinusoidal surface of the hepatocyte and extends between hepatocytes in a labyrinthine fashion. This space is not normally discernible in biopsy material when light microscopy is used, but it may be seen in postmortem livers when the hepatocytes shrink away from the sinusoids, making the space of Disse visible [5]. Sinusoidal congestion and dilatation lead to free extravasation of plasma into the space of Disse. We hypothesize that the sinusoidal congestion and resultant increased tissue water due to the extravasated plasma in the

space of Disse lead to the perilesional wedge-shaped area of increased signal intensity seen on T2-weighted MR images. The increased sensitivity of MR, compared with other imaging techniques, in detecting edema patterns can be explained by its increased sensitivity to tissue water.

It is known that hepatic metastases can produce either peritumoral sinusoidal congestion or compression [6]. Peritumoral compression of sinusoids is seen on contrast-enhanced CT as a low-density perilesional ring; sinusoidal congestion is seen as a more common, high-density ring [6]. The peritumoral halo of increased signal intensity on MR imaging most likely corresponds to the high-density ring seen on contrast-enhanced CT. However, the wedge-shaped distribution of perilesional edema seen with MR imaging has not been seen with other imaging techniques. Although wedge-shaped perfusion abnormalities may occur during CT angiography, we believe that these have a different pathogenesis. Perfusion defects seen during CT angiography may have many causes, but all appear to be related to altered flow dynamics in the hepatic arterial tree [7, 8]. On the other hand, we hypothesize that the wedge distribution of peritumoral increased signal intensity seen on T2-weighted MR images may be explained by obstruction of portal blood and lymph drainage, leading to sinusoidal congestion and edema, by a downstream metastasis. In our patient, the metastatic tumor deposit is directly contiguous with a branch of the right portal vein (Fig. 1A), and although there is no CT portographic or angiographic proof, the tumor may be occluding a segmental branch of this portal vein.

Proper interpretation of these edema patterns on MR imaging is important for staging of surgically resectable liver metastases. However, in order to document fully that the wedge-shaped peritumoral MR high-signal-intensity pattern is due to edema and that the halo is due to perilesional infiltration by tumor cells, a larger study with pathologic correlation is necessary.

REFERENCES

1. Wittenberg J, Stark DD, Forman BH, et al. Differentiation of hepatic metastases from hepatic hemangiomas and cysts by using MR imaging. *AJR* **1988**;151:79–84
2. Brant-Zawadzki M, Bartkowski HM, Oriendah DA, et al. NMR in experimental cerebral edema: value of T1 and T2 calculations. *AJNR* **1984**;5: 125–129
3. Beltran J, Simon DC, Katz W, Weis LD. Increased MR signal intensity in skeletal muscle adjacent to malignant tumors: pathologic correlation and clinical relevance. *Radiology* **1987**;162:251–255
4. Weissleder R, Saini S, Stark DD, et al. Pyogenic liver abscess: contrast-enhanced MR imaging in rats. *AJR* **1988**;150:115–120
5. MacSween RNM, Scothorne RJ. Developmental anatomy and normal structure. In: McSween NMR, Anthony PP, Scheurer PJ, eds. *Pathology of the liver*. New York: Churchill Livingstone, **1979**:1–32
6. Lin G, Boijsen E, Hagerstrand I, Lunderquist A. Microvascular architecture of small liver metastases in man: a correlation between microfil vascular preparations and histologic sections. *Invest Radiol* **1984**;19:296–302
7. Freeney PC, Marks WM. Hepatic perfusion abnormalities during CT angiography: detection and interpretation. *Radiology* **1986**;159:685–691
8. Itai Y, Moss AA, Goldberg HI. Transient hepatic attenuation difference of lobar or segmental distribution detected by dynamic computed tomography. *Radiology* **1982**;144:835–839

Forthcoming Articles

REVIEW ARTICLES

Hysterosalpingography in the '90s. *Yoder IC, Hall DA*

Percutaneous biopsy of skeletal lesions. *Kattapuram SV, Rosenthal DI*

Percutaneous procedures for the diagnosis and treatment of lower back pain: diskography, facet injection, and epidural injection. *El-Khoury GY, Renfrew DL*

THORACIC RADIOLOGY

Chronic diffuse infiltrative lung disease: comparison of diagnostic accuracy of high-resolution and conventional CT. *Leung AN, Staples CA, Müller NL*

Paraquat poisoning: findings on chest radiography and CT in 42 patients. *Im J-G, Lee KS, Han MC, Kim SJ, Kim IO*

Diagnosis and localization of laceration of the thoracic duct: usefulness of lymphangiography and CT. *Sachs PB, Zelch MG, Rice TW, Geisinger MA, Risius B, Lammert GK*

Pictorial essay. Normal anatomy of the thoracic inlet as seen on transaxial MR images. *Spring BI, Schiebler ML*

BREAST RADIOLOGY

Localization and needle aspiration of breast lesions: complications in 370 cases. *Helvie MA, Ikeda DM, Adler DD*

Phylloides tumor: results of mammography, sonography, and aspiration cytology in nine cases. *Buchberger W, Strasser K, Heim K, Müller E, Schröcksnadel H*

GASTROINTESTINAL RADIOLOGY

Value of dual-energy CT to differentiate focal fatty infiltration of the liver from low-density masses. *Raptopoulos V, Karellas A, Bernstein J, Reale FR, Constantinou C, Zawacki JK*

Differentiation between hemangiomas and metastases of the liver with ultrafast MR imaging: preliminary results with T2 calculations. *Goldberg MA, Saini S, Hahn PF, Egglin TK, Mueller PR*

Detection of hepatic masses in patients with carcinoma: comparative sensitivities of sonography, CT, and MR imaging. *Wernecke K, Rummeny E, Bongartz G, et al.*

Pictorial essay. MR imaging of hydatid disease. *von Sinner W, te Strake L, Clark D, Sharif H*

Gallstone lithotripsy: results when number of stones is excluded as criterion for treatment. *Zeman RK, Davros WJ, Goldberg JA, et al*

Gallbladder contractility: variation in normal subjects. *Donald JJ, Fache JS, Buckley AR, Burhenne HJ*

Pictorial essay. rCT appearance of splenic injuries managed nonoperatively. *Do HM, Cronan JJ*

The value of barium as a gastrointestinal contrast agent in MR imaging: a comparison study in normal volunteers. *Ros PR, Steinman RM, Torres GM, et al.*

Enteral feeding tubes: placement with fluoroscopy and endoscopy. *Ott DJ, Mattox HE, Gelfand DW, Chen MYM, Wu WC*

Case report. Systemic *Yersinia enterocolitica* infection associated with iron overload and deferoxamine therapy. *Abcarian PW, Demas BE*

MUSCULOSKELETAL RADIOLOGY

Indications for radiography in patients with acute ankle injuries: role of the physical examination. *Auletta AG, Conway WF, Hayes CW, Guisto DF, Gervin AS*

Pictorial essay. Sonography of the normal elbow. *Barr LL, Babcock DS*

Diagnosis of osteomyelitis in the presence of soft-tissue infection and radiographic evidence of osseous abnormalities: value of leukocyte scintigraphy. *Jacobson AF, Harley JD, Lipsky BA, Pecoraro RE*

Pictorial essay. Abnormalities of the foot in patients with diabetes mellitus: findings on MR imaging. *Moore TE, Yuh WTC, Kathol MH, El-Khoury GY, Corson JD*

Case report. Septic arthritis of the hip: a complication of a rectal tear associated with pelvic fractures. *Magen AB, Moser RP Jr, Woomert CA, Guidici MAI*

GENITOURINARY RADIOLOGY

Percutaneous biopsy of left adrenal masses: prevalence of pancreatitis after anterior approach. *Kane NM, Korobkin M, Francis IR, Quint LE, Cascade PN*

Case report. Castleman disease of the adrenal gland: MR imaging features. *Debatin JF, Spritzer CE, Dunnick NR*

Case report. Cystic carcinoma of the prostate: findings on transrectal sonography. *Llewellyn CH, Holthaus LH*

Case report. Diagnosis of gestational trophoblastic disease: value of endovaginal color Doppler flow sonography. *Desai RK, Desberg AL*

PEDIATRIC RADIOLOGY

Response of osteosarcoma and Ewing sarcoma to chemotherapy: imaging evaluation. *Fletcher BD*

Case report. Distal aortopulmonary window with aortic origin of the right pulmonary artery and interruption of the aortic arch (Berry syndrome): diagnosis by MR imaging. *Yoo S-J, Choi HY, Park I-S, Hong CY, Song MG, Kim SH*

NEURORADIOLOGY

Pictorial essay. Sonography of the eye. *Munk PL, Vellet AD, Levin M, Lin DTC, Collyer RT*

Optimizing brain MR imaging protocols with gadopentetate dimeglumine: enhancement of intracranial lesions on spin-density- and T2-weighted images. *Wessbecher FW, Maravilla KR, Dalley RW*

Intracerebral gangliogliomas in patients with partial complex seizures: CT and MR imaging findings. *Tampieri D, Moumdjian R, Melanson D, Ethier R*

MR imaging of reversible cyclosporin A–induced neurotoxicity. *Truwit CL, Denaro CP, Lake JR, DeMarco T*

Value of subtraction images in the detection of hemorrhagic brain lesions on contrast-enhanced MR scans. *Hanna SL, Langston JW, Gronemeyer SA*

Neurologic involvement in Behcet disease: imaging findings in 16 patients. *Banna M, El-Ramahi K*

VASCULAR RADIOLOGY

Transfemoral venous catheterization through IVC filters: results in seven cases. *Hansen ME, Geller SC, Yucel EK, Egglin TK, Waltman AC*

Technical note. Percutaneous retrieval of an embolized arterial sheath. *Marcuzzi DW, Chisholm RJ*

MEETING NEWS

Meeting news. Ninth annual meeting and postgraduate course: Society of Thoracic Radiology, May 1991. *Whalen E*

Pictorial Essay

Endorectal Sonography in the Evaluation of Rectal and Perirectal Disease

Edward W. St. Ville,[1] S. Zafar H. Jafri,[1] Beatrice L. Madrazo,[1] Duane G. Mezwa,[1] Robert L. Bree,[2] and Barbara F. Rosenberg[3]

Endorectal sonography initially was developed for evaluation of the prostate and now has been adapted for evaluation of rectal and perirectal disease. We used endorectal sonography to evaluate a spectrum of diseases, including primary and recurrent rectal carcinoma, metastases, villous adenoma, leiomyosarcoma, endometriosis, sacrococcygeal teratoma, chordoma, retroperitoneal cystic hamartoma, pelvic lipomatosis, diverticulitis, and perirectal abscess. The technique has been useful in localization of perirectal abscesses and in sonographically guided biopsy of perirectal masses. Knowledge of normal sonographic anatomy of the rectum is essential in the evaluation of rectal and perirectal disease. In this essay, we describe the technique of endorectal sonography and illustrate the sonographic findings in a variety of diseases.

The rectum and perirectal space are the sites of numerous diseases, both benign and malignant. Because of the anatomic detail provided by endorectal sonography, it is useful for the evaluation of the direction of spread of rectal disease, depth of tumor penetration, and assessment of invasion of adjacent viscera [1, 2]. The technique provides accurate definition of the layers of the rectal wall and perirectal soft

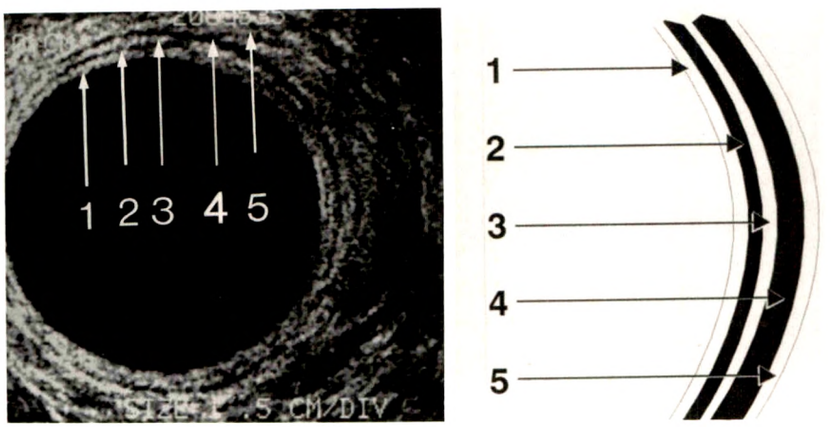


Fig. 1.—Sonogram and drawing show five layers of normal rectum: (1) interface between balloon and mucosa, (2) deep mucosa and muscularis mucosa, (3) interface between submucosa and muscularis propria, (4) muscularis propria, and (5) interface between muscularis propria and perirectal fat.

Received January 24, 1991; accepted after revision April 17, 1991.
Presented at the annual meeting of the American Roentgen Ray Society, Washington, DC, May 1990.
[1] Department of Diagnostic Radiology, William Beaumont Hospital, 3601 W. Thirteen Mile Rd., Royal Oak, MI 48073. Address reprint requests to S. Z. H. Jafri.
[2] Department of Diagnostic Radiology, Veterans Administration Hospital, 2215 Fuller Rd., Ann Arbor, MI 48105.
[3] Department of Surgical Pathology, William Beaumont Hospital, Royal Oak, MI 48073.

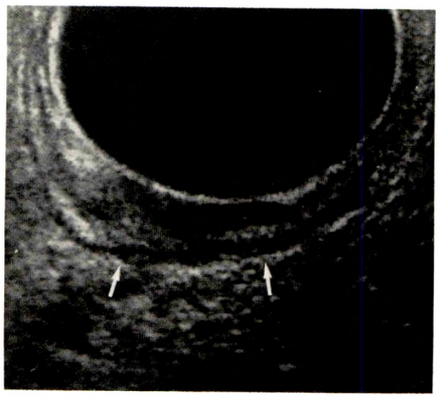


Fig. 2.—Primary rectal carcinoma confined to rectal wall. Endorectal sonogram shows a well-defined hypoechoic lesion confined to muscularis propria (*arrows*).

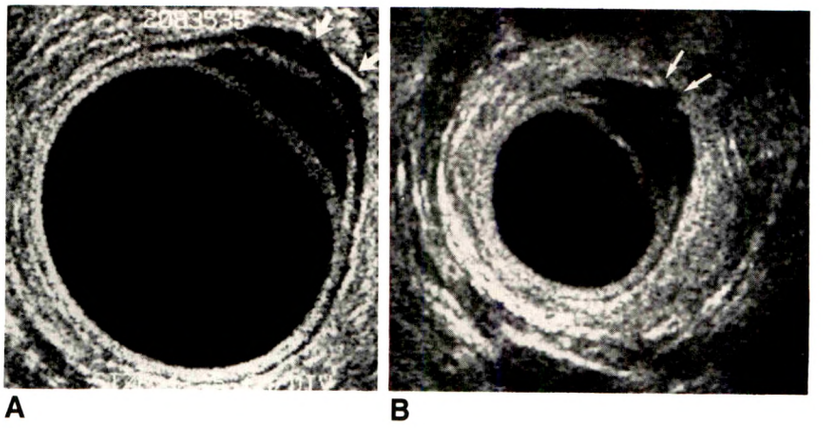


Fig. 3.—Primary rectal carcinoma with local invasion.

A, Sonogram shows soft-tissue mass with muscularis propria in left anterolateral wall of rectum (*arrows*).

B, Sonogram obtained at a higher level reveals mass, which appears to disrupt muscularis propria (*arrows*) and invade perirectal fat planes.

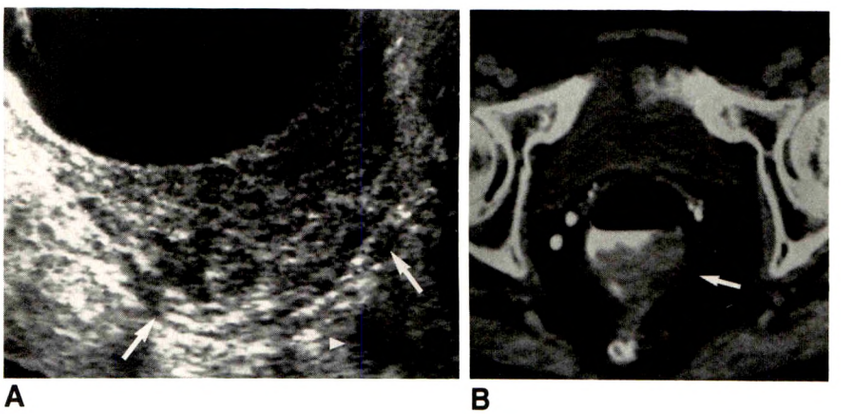


Fig. 4.—Primary rectal carcinoma with local invasion.

A, Endorectal sonogram shows a well-defined mass of mixed echogenicity in posterior wall of rectum that disrupts muscularis layer and invades perirectal fat (*arrows*). A well-defined hypoechoic area (*arrowhead*) represents extension of tumor to a perirectal lymph node.

B, CT scan at same level shows a soft-tissue mass in posterior rectal wall with extension into perirectal fat (*arrow*). Microscopic section revealed invasive mucin-producing adenocarcinoma of rectum with extension into perirectal fat.

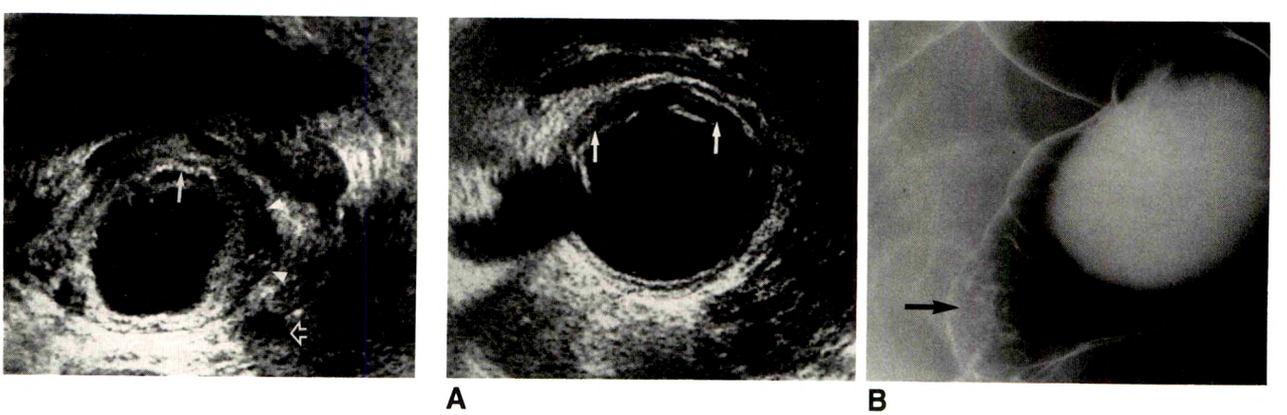


Fig. 5.—Recurrent rectal carcinoma. Sonogram obtained after abdominoperineal resection shows diffuse thickening of rectal wall and disruption of muscularis propria (*arrowheads*). Enlarged perirectal lymph nodes also were identified (*open arrow*). Surgical suture is present in anterior rectal wall (*solid arrow*). Biopsy revealed recurrent rectal carcinoma.

Fig. 6.—Villous adenoma.

A, Endorectal sonogram shows a well-defined area of mixed echogenicity contained within muscularis propria layer in anterior rectal wall (*arrows*).

B, Air-contrast barium enema shows marked mucosal irregularity in anterior rectal wall (*arrow*). Microscopic section of resected specimen showed characteristic frondlike appearance of villous adenoma.

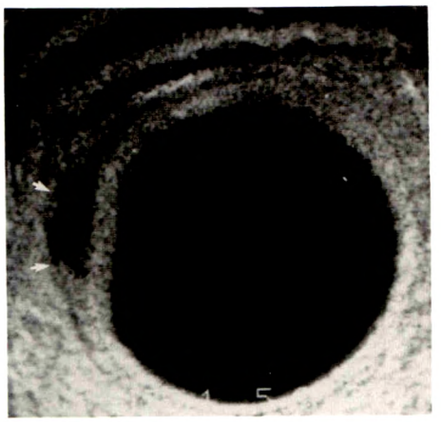


Fig. 7.—Leiomyosarcoma. Endorectal sonogram obtained at level of palpable rectal mass in a patient with chronic active ulcerative colitis shows a uniform hypoechoic lesion limited by muscularis propria layer (*arrows*). Microscopic section revealed a discrete area of malignant spindle cell proliferation corresponding to a 1.5-cm leiomyosarcoma found in gross pathologic specimen. This neoplasm was confined to muscularis propria. Overlying submucosa and mucosa are obliterated as a result of chronic active ulcerative colitis.

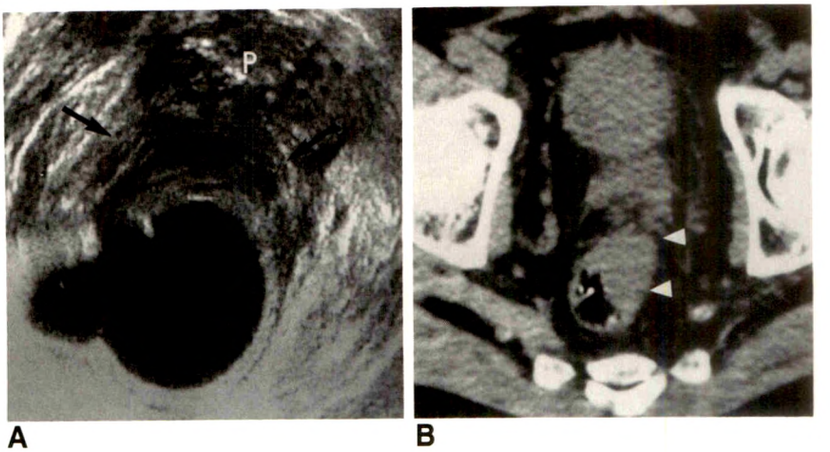


Fig. 8.—Carcinoma of prostate.

A, Sonogram shows large, poorly defined hypoechoic mass disrupting perirectal soft-tissue planes anteriorly between prostate (P) and rectum (*arrows*).

B, CT scan at same level shows a soft-tissue mass posteriorly between prostate and perirectal soft-tissue planes with extension into anterior rectal wall (*arrowheads*). Diagnosis of carcinoma was confirmed by results of transrectal biopsy.

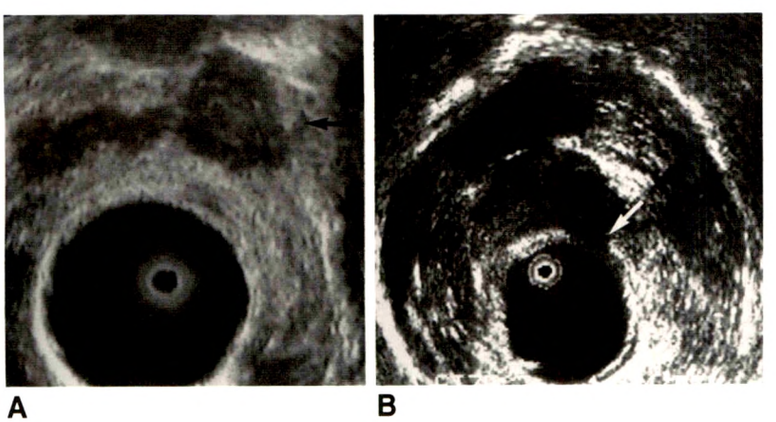


Fig. 9.—Malignant melanoma.

A, Endorectal sonogram shows a hypoechoic mass in left seminal vesicle (*arrow*) in a patient with malignant melanoma.

B, Sonogram obtained at a lower level shows a well-defined hypoechoic metastasis in left lobe of prostate that disrupts and invades anterior rectal wall (*arrow*).

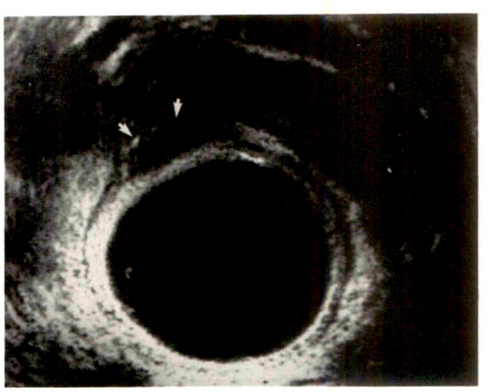
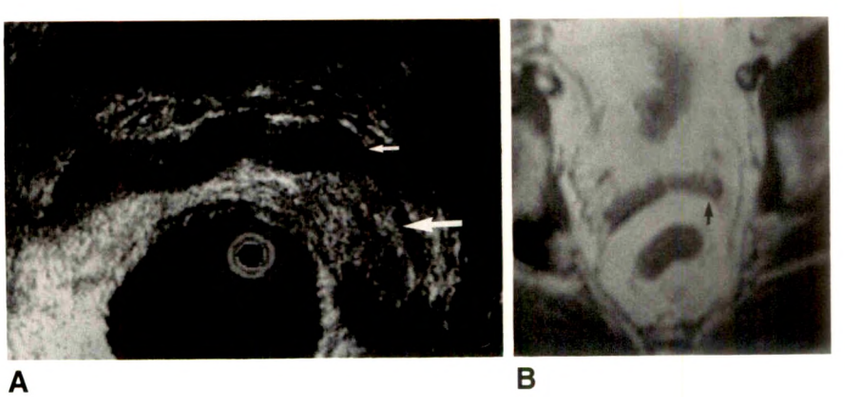


Fig. 10.—Endometriosis. Sonogram shows a well-demarcated area (*arrows*) interposed between muscularis propria and mucosa. Lesion is confined by and does not extend beyond muscularis propria. Histologic examination showed a focus of endometriosis, which was delimited by muscularis propria.

Fig. 11.—Lipomatosis.

A, Sonogram shows pelvic lipomatosis with perirectal deposition of fat causing anterior displacement of left seminal vesicle (*small arrow*). Note asymmetry of echo texture of perirectal tissue between seminal vesicle and rectum, with decreased echogenicity on left (*large arrow*) simulating a mass.

B, T1-weighted MR image of pelvis shows a uniform circumferential ring of increased signal intensity in perirectal soft tissues consistent with lipomatosis. Note more anterior location of left seminal vesicle relative to right (*arrow*). No masses were identified.



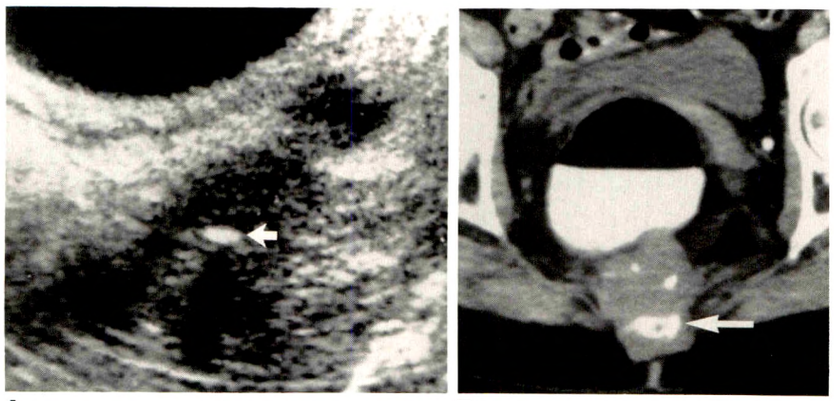


Fig. 12.—Chordoma.
A, Endorectal sonogram shows a complex mass posteriorly that lies outside rectal wall. Mass is mostly hypoechoic and poorly defined and contains several bright reflectors (*arrow*) caused by tiny calcifications.
B, CT scan at same level shows soft-tissue mass posterior to rectum that contains tiny calcifications and appears to extend into coccyx (*arrow*).

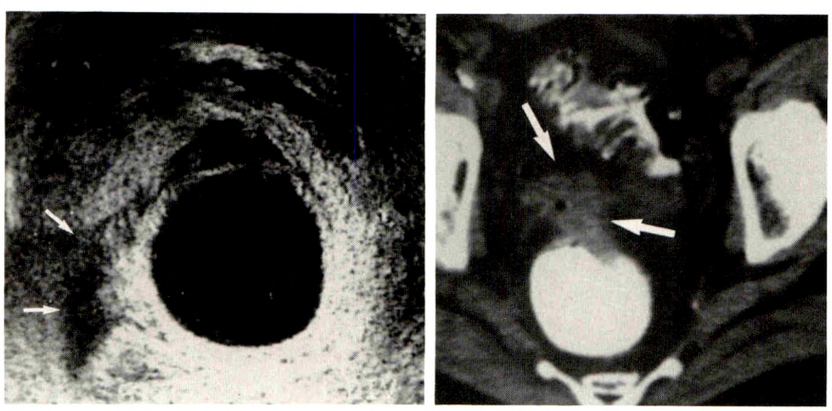


Fig. 13.—Diverticulitis.
A, Sonogram shows hypoechoic area in anterior rectal wall outside muscularis propria. Fluid extends into perirectal soft tissues (*arrows*).
B, CT scan of pelvis confirms edema and thickening of wall of rectosigmoid colon (*arrows*).

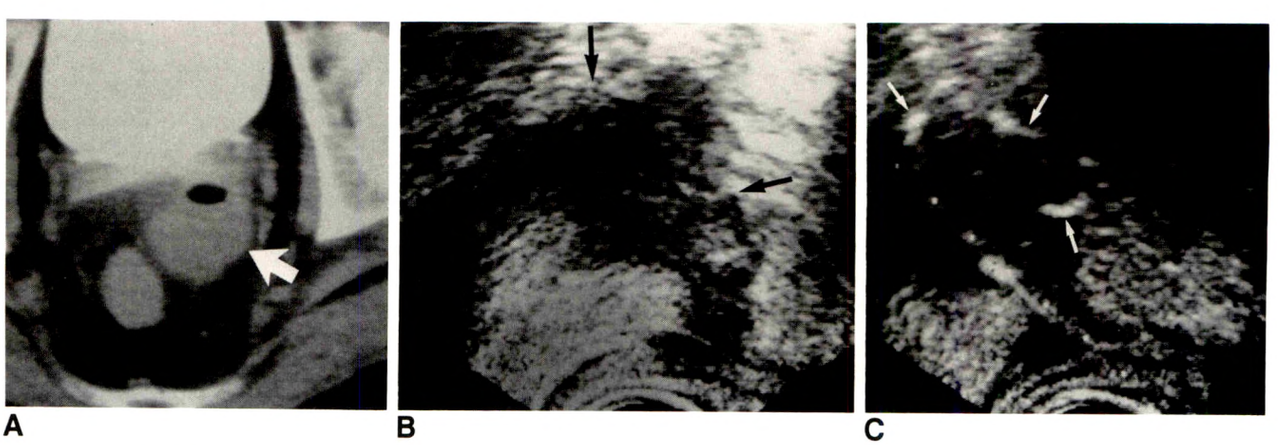


Fig. 14.—Perirectal abscess.
A, CT scan in a patient with inflammatory bowel disease shows perirectal abscess anterior to rectum (*arrow*) that could not be found during surgery.
B, Endorectal sonogram obtained after surgery shows a poorly defined hypoechoic area anterior to rectum (*arrows*).
C, Under sonographic guidance, a guidewire (*arrows*) was inserted and secured to skin. Surgery was repeated, and guidewire was used successfully to locate abscess cavity.

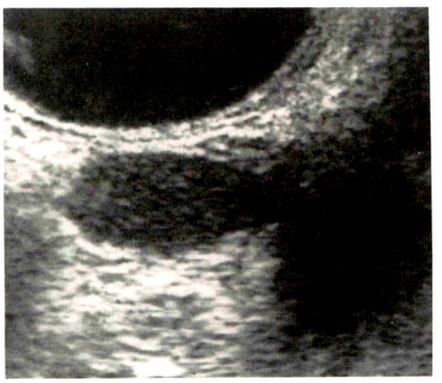
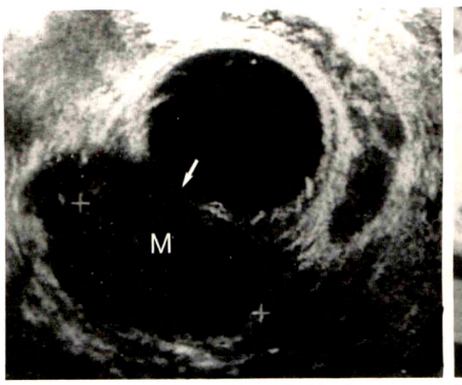


Fig. 15.—Sacrococcygeal teratoma. Endorectal sonogram shows a well-defined hypoechoic mass, with acoustic enhancement outside posterior rectal wall.





A B

Fig. 16.—Retroperitoneal cystic hamartoma (tailgut cyst).
A, Sonogram shows a homogeneous well-circumscribed hypoechoic mass (M) compressing rectum (*arrow*).
B, CT scan at level of tailgut cyst (*arrow*) correlates with endorectal sonogram, revealing a perirectal soft-tissue mass (M) in presacral space that narrows rectal lumen.

tissues (Fig. 1). Anatomic changes caused by soft-tissue masses, cysts, calcification, and fluid collections can be detected. In this essay, we describe the technique of endorectal sonography and illustrate the sonographic findings in a variety of diseases. Pathologic verification of sonographic findings was available in all cases.

Technique

An axial, transversely oriented radial scanner (model 1850, Brüel & Kjaer, Copenhagen, Denmark) is used most commonly. The total length of the rigid probe with the transducer is 24 cm. The transducer rotates at a rate of two to three cycles per second. Scanning radial to the long axis of the rectal probe provides a 360° display of the rectum and surrounding tissues.

The transducer, covered by a disposable latex sheath and lubricated with a scanning gel, is introduced into the rectum. A minimum luminal diameter of 25 mm is necessary to insert the probe. The sheath is filled with 60 ml of degassed water to provide an acoustic window. Images routinely are obtained at 1-cm intervals from approximately 2–15 cm above the anus, which is the usual maximal depth of insertion. The transducer also can be inserted via a rectoscope to evaluate the rectum. During simultaneous withdrawal of the probe and the rectoscope, the region of interest is scanned in a stepwise fashion. Depending on the extent of the lesion, the examination takes 10–15 min.

Sonographic Anatomy of the Normal Rectum

When a 7-MHz transducer is used, sonograms show five layers in the rectal wall; three are hyperechoic and two are hypoechoic. The first echogenic line corresponds to the interface between the water balloon and the mucosa. The innermost hypoechoic line represents the deep mucosa and muscularis mucosa. The third and most echogenic line is produced by the submucosa. The outer, wider hypoechoic line delineates only the muscularis propria. This is of clinical importance because it defines a sonographic criterion for determining intramural or extramural invasion. The most peripheral line, the fifth echogenic line, corresponds to the interface between the muscularis propria and perirectal fat.

Sonographic Findings in Rectal and Perirectal Disease

Endorectal sonography initially was developed for evaluation of carcinoma of the prostate and recently has been adapted for staging of rectal carcinoma and evaluating a spectrum of benign and malignant rectal and perirectal conditions [3]. Rectal carcinoma appears on endorectal sonograms as a low-echogenicity lesion that abruptly interrupts the normal sequence of layers (Figs. 2 and 3). In order to stage the tumor precisely, it is necessary to determine the relationship between the neoplasm and the outer hypoechoic layer (muscularis propria). When no infiltration has taken place, this layer has a smooth regular course and is separated by the thin echogenic line of submucosa. Disappearance of submucosa may indicate infiltration of the muscularis propria. This pattern is most difficult to determine. Tumor with minimal extrarectal spread could therefore be understaged also. Extension into the perirectal fat is represented by the interruption of the muscularis propria by the neoplasm (Fig. 4). In addition, infiltration into the adjoining pelvic organs and perirectal lymph nodes should be sought.

Lymphadenopathy caused by metastases or lymph-node hyperplasia resulting from local sepsis commonly is seen with endorectal sonography. When no lymph nodes are visible in

metastases is low [4]. The enlarged nodes may be hyperechoic and hypoechoic. Hyperechoic lymph nodes are enlarged because of nonspecific inflammatory change. When enlarged lymph nodes are hypoechoic, metastases are most likely, although nonspecific inflammation cannot be excluded.

Preoperative assessment of the depth of tumor invasion is important in the treatment of rectal carcinoma, particularly when local excision is being considered. A major value of endorectal sonography is to determine the depth of tumor invasion. The procedure can be used to detect local recurrence after low anterior resection or local excision. Extent of primary or recurrent tumor infiltration is defined more exactly with endorectal sonography than with CT (Fig. 5). The high spatial resolution of endorectal sonography also has proved useful in characterizing the nature and extent of numerous rectal and perirectal disease entities. Endorectal sonography shows villous adenoma (Fig. 6), leiomyosarcoma (Fig. 7), metastases (Figs. 8 and 9), endometriosis (Fig. 10), and pelvic lipomatosis (Fig. 11) as nonspecific, solid masses within the rectal wall and perirectal soft tissues. Calcification within a chordoma (Fig. 12) and perirectal fluid collections seen in diverticulitis and perirectal abscess can be demonstrated (Figs. 13 and 14). Sacrococcygeal teratoma (Fig. 15) and retroperitoneal cystic hamartoma (Fig. 16) are seen as well-circumscribed masses outside of the rectal wall. Endorectal sonography also has been useful for localization of perirectal abscess and needle biopsy of perirectal masses.

REFERENCES

1. Orrom WJ, Wong WD, Rothenberger DA, Jensen LL, Goldberg SM. Endorectal ultrasound in the preoperative staging of rectal tumors: a learning experience. *Dis Colon Rectum* **1990**;33:654–659
2. Konishi F, Ugajin H, Kanazawa K. Endorectal ultrasonography with a 7.5 MHz linear array scanner for the assessment of invasion of rectal carcinoma. *Int J Colorectal Dis* **1990**;5:15–20
3. Beynon J, Foy DM, Temple LN, Channer JL, Virgee J, Mortenson NJ. The endosonic appearances of normal colon and rectum. *Dis Colon Rectum* **1986**;29:810–813
4. Glaser F, Schlag P, Herfarth C. Endorectal ultrasonography for the assessments of invasion of rectal tumors and lymph node involvement. *Br J Surg* **1990**;77:883–887

LIST OF BOOK AND VIDEOTAPE REVIEWS

480 **Detection and Treatment of Early Breast Cancer.** *Fentiman I*
490 **The Radiologic Clinics of North America. Interventional Radiology of the Biliary Tract.** *Burhenne HJ, ed.*
494 **RSNA Today, Vol. 4, No, 5.** *Casarella WJ, moderator*
498 **Atlas of Roentgenographic Measurement, 6th ed.** *Keats TE*
516 **Magnetic Resonance Imaging of Carcinoma of the Urinary Bladder.** *Barentsz JO, Debruyne FMJ, Ruijs SHJ*
520 **Textbook of Uroradiology.** *Dunnick NR, McCallum RW, Sandler CM*
526 **MRI of the Musculoskeletal System, 2nd ed.** *Berquist TH, ed.*
532 **The Language of Fractures, 2nd ed.** *Schultz RJ*
544 **Obstetrics and Gynecology.** *Berman MC, ed.*
584 **Neuroradiology Test and Syllabus.** *Weinberg PE, section ed.*
602 **Gamuts and Pearls in MRI.** *Pomeranz SJ*
608 **A Short Textbook of Clinical Imaging.** *Sutton D, Young JWR, eds.*

Transurethral Balloon Dilatation of the Prostatic Urethra: Effectiveness in Highly Selected Patients with Prostatism

Neil F. Wasserman[1]
Pratap K. Reddy[2]
Gang Zhang[2]
Deepak A. Kapoor[2]
Patricia Berg[2]

Transurethral balloon dilatation of the prostate has been shown to be a safe and potentially effective alternative to surgery in the treatment of benign prostatic hyperplasia, with a 66% success rate in relatively unselected patients. This study hypothesized that more careful patient selection might result in a significantly better rate of improvement. Ninety-one subjects with symptoms and signs of prostatism attributable to benign prostatic hyperplasia were studied. Group 1 comprised 42 patients with an initial mean symptom score of 16.8, residual urine of 249 ml, maximal flow rate of 7.9 ml/sec, and nomogram of maximal flow rate of −1.5. Group 2 comprised 49 less symptomatic patients with an initial mean symptom score of 14.5, residual urine of 105 ml, maximal flow rate of 10.7 ml/sec, and nomogram of maximal flow rate of −0.8. The difference in mean age and prostate size between groups was not statistically significant, but differences in baseline symptom score, residual urine, maximal flow rate, and nomogram of maximal flow rate were significant ($p < .04$). Transurethral balloon dilatation of the prostate was performed under local anesthesia or IV sedation and analgesia with single- or double-balloon catheters with maximal diameters of 25–30 mm inflated to 2.5–4.0 atmospheres pressure for 10 min. Patients were followed up with repeat symptom scoring, uroflometry, and measurement of residual urine. After a mean follow-up of 22 months (range, 6–48 months), an improvement in symptom score was seen in 80% of group 2 patients compared with 43% in group 1. Improvement in symptom scores was statistically significant in both groups ($p < .04$).

We conclude that transurethral balloon dilatation of the prostate is more effective in patients with more moderate symptoms and with less marked signs of obstruction than in patients with more marked prostatism.

AJR 157:509–512, September 1991

Transurethral balloon catheter dilatation of the prostate (TUDP) has been shown to be a safe and potentially effective alternative to surgery in the treatment of moderately severe benign prostatic hyperplasia (BPH) [1]. In relatively unselected patients, including some with very large prostates, mild median lobe enlargement, and urinary retention, significant relief of symptoms was demonstrated in 66% [1]. TUDP has been found to be less successful in patients with acute or chronic retention, dominant median lobe hyperplasia, or manifestations of more severe bladder outlet obstruction (Machan LS et al., presented at the annual meeting of the Radiological Society of North America, November 1989) [1]. Because of low risk and low initial cost compared with surgery, there may be a temptation to apply TUDP nonselectively as the first treatment for symptoms of bladder outlet obstruction. The potential for this kind of misuse has been pointed out recently [2, 3]. We hypothesized that more careful selection of patients for treatment by TUDP might result in a significantly greater rate of clinical improvement and allow us to apply this new technique more thoughtfully to those who would most benefit.

Subjects and Methods

Ninety-one patients with symptoms of prostatism attributable to BPH were studied, including 73 patients previously reported [1] but now having had longer follow-ups and 18

Received November 26, 1990; accepted after revision April 16, 1991.

[1] Department of Radiology (114), Department of Veterans Affairs Medical Center, One Veterans Dr., Minneapolis, MN 55417. Address reprint requests to N. F. Wasserman.

[2] Department of Urology, Department of Veterans Affairs Medical Center, Minneapolis, MN 55417.

0361–803X/91/1573–0509
© American Roentgen Ray Society

new patients. Preliminary screening exclusions included age less than 55 years, neurogenic bladder, nonambulatory condition, prior prostatic surgery, history of prostatic cancer, previous pelvic radiation, ethanol abuse, psychiatric disorder, severe respiratory disease, and estimated prostatic weight greater than 100 g. The mean age of the patients was 70 years (range, 59–95 years). The diagnosis of BPH was made on the basis of physical examination, symptom scoring with the Madsen and Iversen scale [4], urinalysis and culture, cystoscopy, uroflometry, catheterized residual urine, and cystourethrography. If the diagnosis of obstruction was in doubt, invasive urodynamic studies were done to determine the presence of significant obstruction. Additional laboratory measurements included RBC count, coagulation time, and levels of prostate-specific antigen and prostatic acid phosphatase. Transrectal sonography of the prostate was performed in 38 patients when that technique became available to us, and prostatic volume-equivalent weight was calculated by using a formula based on the ellipsoid model (width × height × length × 0.5).

The symptom scoring system allows a maximal score of 27, which is weighted toward obstructive symptoms [1, 4]. Symptom scoring was done by a research nurse who did all preliminary and follow-up interviews of patients. All patients had symptom scores between 8 and 24. Patients with scores less than 8 were considered minimally symptomatic and excluded from the study. Those with scores between 8 and 20 were considered moderately symptomatic and those with scores greater than 20 were considered severely symptomatic.

Maximal urine flow (Q_{max}) was measured by using a standard urine collection funnel in a commode into which the patients voided from the seated position. The urine passes from the collection funnel through a flowmeter, which is connected to a strip chart that produces a flow curve until voiding ceases. The peak of this curve is subtracted from the baseline and is taken as Q_{max}. Normal Q_{max} is a function of age. In our population of patients, values lower than 10 ml/sec are abnormal and values 10–15 ml/sec may be abnormal.

Q_{max} was corrected for total starting bladder volume by measuring the volume voided and residual urine and then using the nomogram developed by Jørgensen et al. [5], which was selected because it is based on flow data in asymptomatic men with a mean age that approximates the mean age of our patients. The nomogram value of Q_{max} shows where the Q_{max} lies relative to the mean and plus or minus two standard deviations from the mean [1, 5].

Patients with renal azotemia, an abnormal rectal digital examination (including prostatitis, suggestive prostatic nodule, or rectal mass), or intractable urinary tract infection were excluded from this study. Cystoscopic or radiologic evidence of urethral stricture, bladder cancer, bladder stone, or diverticulum also resulted in exclusion.

Eighty-one patients were prospectively divided into two groups. In addition, our first 10 patients were retrospectively assigned to one of these groups on the basis of the same clinical criteria as the other patients.

Group 1 comprised 42 patients who were considered suboptimal candidates for TUDP, including eight with symptom scores greater than 20, seven with complete urinary retention, nine with residual urine greater than 350 ml, 10 with prominent median lobe hyperplasia, 12 who were considered to have moderately severe obstruction but were at high risk for surgery, and one with Parkinson disease plus BPH. Several patients had more than one of these conditions.

Group 2 comprised 49 patients with symptom scores between 8 and 20 and residual urine less than or equal to 350 ml with no prior or current episode of retention who were considered to have less severe obstruction and to be excellent candidates for TUDP. The results of the selection process are shown in Table 1, which establishes the ability of our measuring instruments to separate patients into two distinct statistically significant groups.

This study was approved by our human experimentation committee. After the experimental nature of the TUDP procedure was fully explained to each subject, a special informed consent form was signed.

TABLE 1: Mean Baseline Values in 91 Patients with Symptoms of Prostatism Attributable to Benign Prostatic Hyperplasia

Variable	Group 1 ($n = 42$)	Group 2 ($n = 49$)	p Value[a]
Age (years)	71	64	<.06
Weight of prostate (g)	30	25	<.71
Symptom score	16.8	14.5	<.004
Residual urine (ml)	249	105	<.001
Maximal urine flow (ml/sec)	7.9	10.7	<.02
Nomogram of maximal urine flow	−1.5	−0.8	<.04

Note.—Patients in group 1 had more severe urethral obstruction than did patients in group 2.

[a] Unpaired two-tailed t test.

TUDP was performed with the patient either under IV sedation and analgesia or paraprostatic block with 1% xylocaine. Details of our balloon dilatation techniques have been reported [1]. The prostates of the first 38 patients were dilated by using a single-balloon catheter with an outside diameter of 25–27 mm (Medi-Tech, Boston Scientific, Watertown, MA). The remaining 53 prostates were dilated with a double-balloon catheter with an outer diameter of 30 mm (American Medical Systems, Minnetonka, MN). Patients were followed up 1 week and 1 month later and quarterly for 1 year, then semiannually with repeated symptom scoring, uroflometry, and measurement of residual urine. For purposes of this study, a decrease in symptom score was used as the criterion for improvement.

Differences within groups were analyzed for significance with the two-tailed paired t test after establishing the normal distribution of the data. The unpaired two-tailed t test and test of z were used to evaluate differences between groups. Statistical significance was regarded as $p < .05$.

Results

The mean follow-up was 22 months (range, 6–48 months). The mean follow-ups of patients in groups 1 and 2 were 27 and 16 months, respectively (Fig. 1). Symptoms improved in 43% of patients in group 1, compared with 80% in group 2 (Table 2). Most of the treatment failures occurred within the first 6 months. The decline in symptom scores was strongly significant for patients in groups 1 and 2 for the first 18 months ($p < .001$) and still significant 2 years later ($p < .04$, Fig. 2). The magnitude of this drop in symptom score after TUDP was significantly greater in group 2 than in group 1 during the first 9 months ($p < .02$) and sustained at 12 and 18 months, although not at a statistically significant level (Fig. 2). Notice that the improvement attained in group 2 was consistently in the minimally symptomatic range below a score of 8. Mean decreases in symptom scores for groups 1 and 2 were 7.5 (45%) and 7.7 (53%), respectively.

Sustainable statistically significant ($p < .04$) improvements in Q_{max} and nomogram of Q_{max} were demonstrated as a result of TUDP in group 1 only (Fig. 3). However, the improvements in urine flow and residual urine otherwise seen generally were

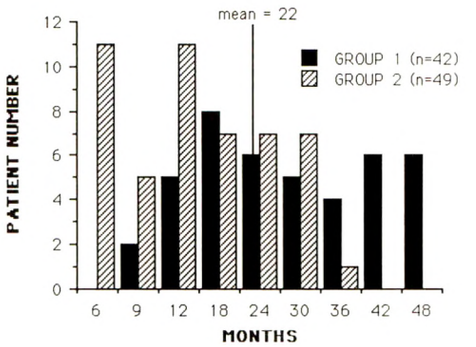


Fig. 1.—Follow-up intervals in 42 patients with more severe obstruction of the urethra (group 1) and in 49 patients with less severe obstruction (group 2).

TABLE 2: Outcome of Transurethral Balloon Dilatation of the Prostate in Two Groups of Patients with Benign Prostatic Hyperplasia

Outcome	No. (%)		
	Group 1	Group 2	Total
Improved	18 (43)	39 (80)	57 (63)
Unimproved			
Prostatectomy	15	5	20
Retention	5	1	6
Worse symptom score	1	4	5
Stable symptom score	2	0	2
Stent	1	0	1
Subtotal	24 (57)	10 (20)	34 (37)
Total	42	49	91

Note.—Patients in group 1 had more severe urethral obstruction than did those in group 2. Follow-ups ranged from 6 to 48 months (mean, 22 months).

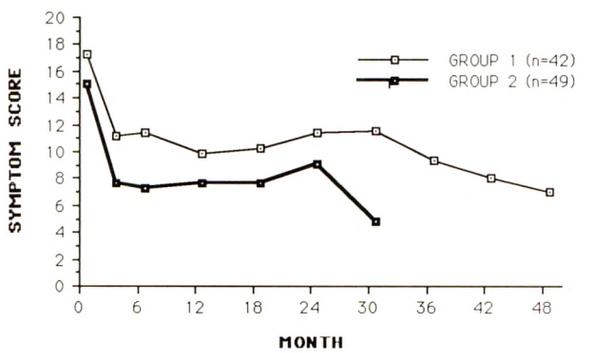


Fig. 2.—Improvement in symptom score in 42 patients with more severe obstruction of the urethra (group 1) and in 49 patients with less severe obstruction (group 2). Note sustained effect of transurethral balloon dilatation of the prostate in both groups, but symptom scores fall into minimal range (below 8) for group 2 only. Highest possible symptom score was 27. Scores between 8 and 20 were considered moderately symptomatic; those above 20 were considered severely symptomatic.

not statistically significant. The magnitude of this change between the groups also was not significant.

Outcome as a function of mean baseline symptom score, residual urine, Q_{max}, nomogram of Q_{max} is shown in Figure 4, which suggests that baseline residual urine less than 150 ml and nomogram of Q_{max} below −2.0 are associated with successful outcome in 83% and 90% of cases, respectively. Baseline symptom score and uncorrected Q_{max} were of no predictive value.

Discussion

Our previous study [1] focused on the general hypothesis that TUDP was a safe and potentially effective alternative treatment strategy for BPH in a mixed population of patients with moderate to severe prostatism. Although it was apparent that symptom scores in patients with baseline residual urine less than 150 ml improved as a result of TUDP more frequently (83%) than did those with residual urine greater than 150 ml (52%), no other baseline measurements emerged as having potential as predictors for success in this pooled population. Because we had prospectively assigned most patients into categories meeting more selective and less selective criteria, we thought that a disjunctive reanalysis of the original total group with the addition of subsequent similarly selected patients might further define measurable predictors for successful treatment of BPH with TUDP.

Results of selection show that groups 1 and 2 were matched for age and prostatic size but differed in degree of obstruction. Patients in group 1 manifested greater symptoms and objective signs of infravesical obstruction than did patients in group 2 (Table 1). The difference in symptomatic response to TUDP expressed as a percentage was statistically significant between the two groups ($p < .01$, Table 2). Patients in group 2 with more moderate obstruction benefited to a greater degree (80%) than did those in group 1 with more severe obstruction (43%). There was also a trend, although not at a statistically significant level, toward improvement in uroflow values and residual urine.

These data can be compared with those of Bruskewitz et al. [6] and Nielsen et al. [7], who used the same symptom scoring system and uroflow measurements before and after treatment of BPH with transurethral prostatectomy. Their patients, with baseline mean symptom scores and Q_{max} almost identical to those of our patients, showed improvement in symptom scores at 12 and 36 months of 84% and 75%, respectively.

Measured differences between groups 1 and 2 in our study could not be explained by bias due to variation in catheter design or balloon caliber, which were equally distributed in the two groups. Nor could the difference be attributed to improvement in skill by the authors, because the distributions of entry dates of patients in groups 1 and 2 during the course of the study period were relatively comparable.

As therapeutic successes occurred in each group, the pooled data from both groups were analyzed for variables associated with improvement in symptom scores after TUDP. When patients were sorted into groups that were improved and unimproved after TUDP, baseline symptom scores and Q_{max} failed to show a pattern predictive of successful result. However, baseline residual urine correlated strongly with

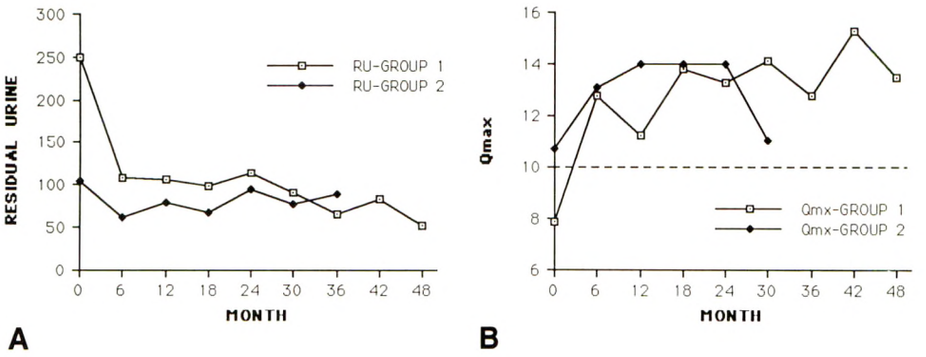


Fig. 3.—*A* and *B*, Mean improvement in residual urine (RU) volume in milliliters (*A*) and maximal urine flow (Q_{max}, Q_{mx}) in ml/sec (*B*) in patients with more severe urethral obstruction (group 1) and in patients with less severe obstruction (group 2) after transurethral balloon dilatation of the prostate.

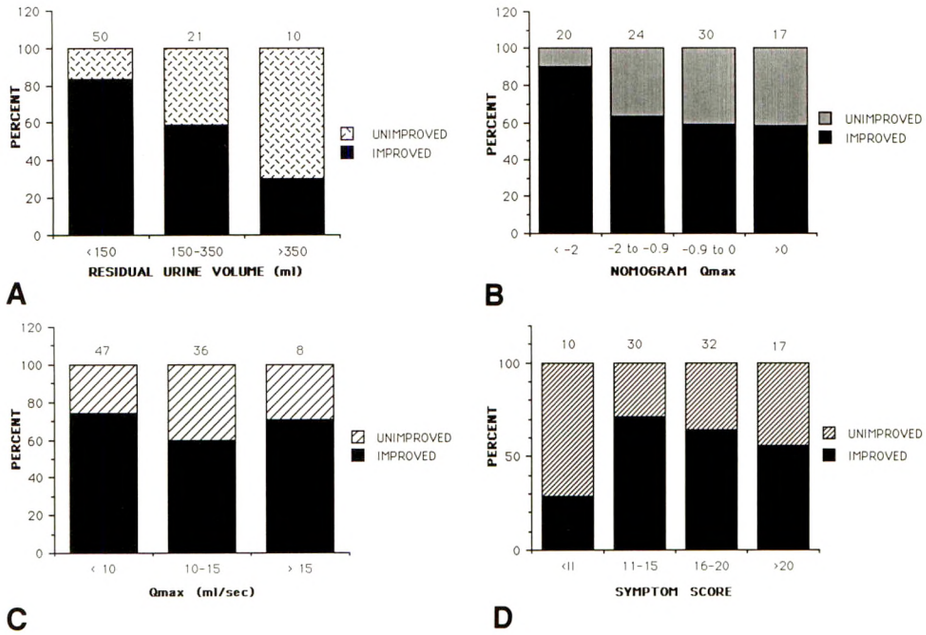


Fig. 4.—*A–D*, Outcome as a function of mean baseline residual urine volume (*A*), nomogram of maximal urine flow (Q_{max}) (*B*), maximal urine flow (*C*), and symptom score (*D*). The numbers of subjects in each category are indicated above the bars. Note the relative predictive values of residual urine under 150 ml and nomogram Q_{max} below −2.0.

success, because 83% of patients with residual urine less than 150 ml (43 patients) and 59% of those with residual urine less than 350 ml (55 patients) improved after TUDP (Fig. 4). A nomogram value of Q_{max} below −2.0 also was associated with significant improvement in 90% of patients.

Some might question the interest of diagnostic and interventional radiologists in the issues raised in this article, because it is not directly about imaging nor is it about the development and assessment of new technology. This report is about the understanding and application of assessment techniques outside the usual discipline of radiology to optimize the therapeutic results of an intervention initially developed by radiologists. Radiologists serve their patients and the medical community better if they extend the limits of their interests and understanding to overlap those of their clinical colleagues [8–10].

We conclude that it is possible to improve the success of TUDP significantly by careful selection of patients with symptom scoring, uroflometry, physical examination, laboratory tests, sonography, and cystoscopy to exclude those with severe obstruction, infection, very large prostates, and dominant median lobe hyperplasia. We predict the best results will occur in patients with symptom scores below 20 who have prostates weighing less than 40 g, little or no median lobe hyperplasia, and residual urine less than 150 ml or nomogram of Q_{max} below −2.0.

REFERENCES

1. Wasserman NF, Reddy PK, Zhang G, Berg P. Experimental management of benign prostatic hyperplasia by transurethral balloon dilatation of the prostate: preliminary results in 73 humans. *Radiology* **1990**;177:485–494
2. Pollack H. Balloon dilation of the prostate: effective treatment or dilatory tactic. *Radiology* **1990**;178:331–333
3. Wasserman NF. The devil in Dr. Pollack: defending our souls. *Radiology* **1990**;178:333–334
4. Madsen PO, Iversen P. A point system for selecting operative candidates. In: Hillman F, ed. *Benign prostatic hypertrophy*. New York: Springer-Verlag, **1983**:763–765
5. Jørgensen JB, Jensen KM-E, Bille-Brahe NE, Mogensen P. Uroflowmetry in asymptomatic elderly males. *Br J Urol* **1986**;58:300–395
6. Bruskewitz RC, Larsen EH, Madsen PO, Dørflinger T. Three year follow-up of urinary symptoms after transurethral resection of the prostate. *J Urol* **1986**;136:613–615
7. Nielsen KT, Christensen MM, Madsen PO, Bruskewitz RC. Symptom analysis and uroflowmetry 7 years after transurethral resection of the prostate. *J Urol* **1989**;142:1251–1253
8. Meaney TF. The decline of diagnostic radiology: call to action. *Radiology* **1989**;172:889–892
9. Holman L. The research that radiologists do: perspective based on a survey of the literature. *Radiology* **1990**;176:329–332
10. Northway WH Jr. Research in departments of diagnostic radiology: a question of method limitation. *Radiology* **1989**;171:873–875

Case Report

Iliac Artery Stenosis Causing Renal Allograft–Mediated Hypertension: Angiographic Diagnosis and Treatment

John B. Weigele[1]

Renovascular hypertension due to transplant renal artery stenosis is well recognized, variably reported in 2% to 25% of allografts [1–3]. Most stenoses occur at or near the surgical anastomosis [1, 3]. Intimal hyperplasia, probably due to both rejection and endothelial trauma, is considered the most common cause [3]. The resultant hypertension is often quite difficult to treat medically. Graft function may be compromised or threatened. Favorable results with percutaneous transluminal angioplasty (PTA) have been reported by most groups [1, 3], although some have had lower success rates [4].

As older persons are accepted as transplantation candidates, and as the recipient population ages, it follows that occlusive atherosclerosis of the native aortoiliac system will be present or will develop proximal to the graft. Intimal hyperplasia also may develop after the surgical manipulation. This report presents three patients in whom transplant renovascular hypertension developed because of a proximal, flow-limiting iliac artery stenosis. Angiographic diagnosis and treatment are discussed.

Case Report

A 44-year-old woman with a long-standing history of hypertension and cigarette smoking underwent cadaveric kidney transplantation for end-stage renal disease associated with nephrosclerosis. Although the function of the transplanted kidney was adequate (serum creatinine level ranged from 1.0 to 1.5 mg/dl [90–130 μmol/l]), the patient's hypertension immediately became more difficult to control. Five antihypertensive medications were required. Ten weeks after transplantation, the patient was examined angiographically for a suspected transplant renal artery stenosis. On preangiographic examination, femoral pulses were markedly asymmetric and significantly diminished on the side of the allograft. A pelvic arteriogram showed a 90% or greater stenosis of the proximal right common iliac artery above the transplant anastomosis (Fig. 1A).

PTA with high-pressure kissing balloons resulted in a widely patent common iliac artery. No residual arterial pressure gradient was seen. The patient had an immediate, marked clinical response. Good blood pressure control was subsequently maintained with two antihypertensive medications. The glomerular filtration rate measured by renal scan was markedly improved, from a pre-PTA computer-estimated rate of 0.8 ml/min to 35.5 ml/min after the angioplasty.

Two years after the successful PTA, femoral artery Doppler waveforms raised the question of restenosis, although the patient's blood pressure control and renal function were relatively stable. A second arteriogram showed an insignificant 25% stenosis without a pressure gradient in the right common iliac artery (Fig. 1B).

Discussion

Although the usual cause of allograft-mediated renovascular hypertension is a stenosis involving the transplant renal artery [1–4], this case shows that the flow-limiting lesion can be in the proximal native aortoiliac system.

Two similar cases have occurred. A 62-year-old woman with a history of hypertension and carotid artery stenosis received an allograft from a living relative for end-stage renal disease associated with "nephritis." Blood pressure control progressively worsened in the 5 months after transplantation, requiring two medications in increasing dosages. The serum

Received February 25, 1991; accepted after revision April 16, 1991.
[1] Department of Radiology, Hospital of the University of Pennsylvania, 3400 Spruce St., Philadelphia, PA 19104-4283. Address reprint requests to J. B. Weigele.

 0361–803X/91/1573–0513 © American Roentgen Ray Society

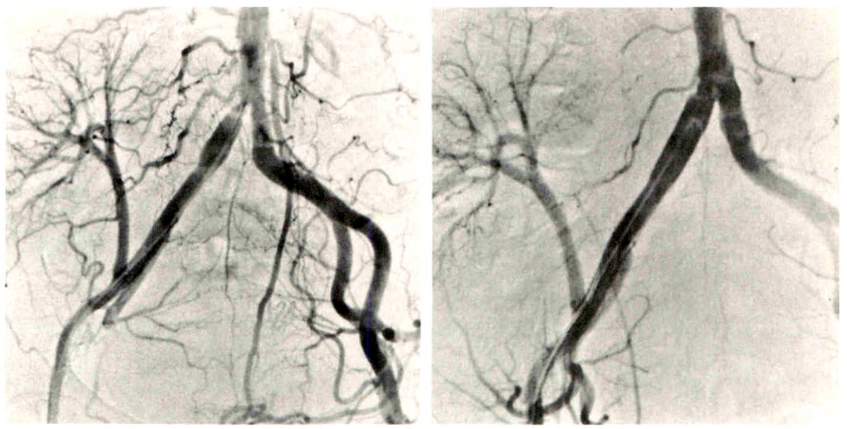


Fig. 1.—*A*, Angiogram shows eccentric high-grade stenosis originating in right common iliac artery. Extensive cross-pelvic collaterals from inferior mesenteric and internal iliac arteries. Widely patent transplant renal artery anastomosed end-to-side to external iliac artery.

B, Follow-up angiogram 2 years after percutaneous transluminal angioplasty shows site is widely patent and previous cross-pelvic collaterals are absent.

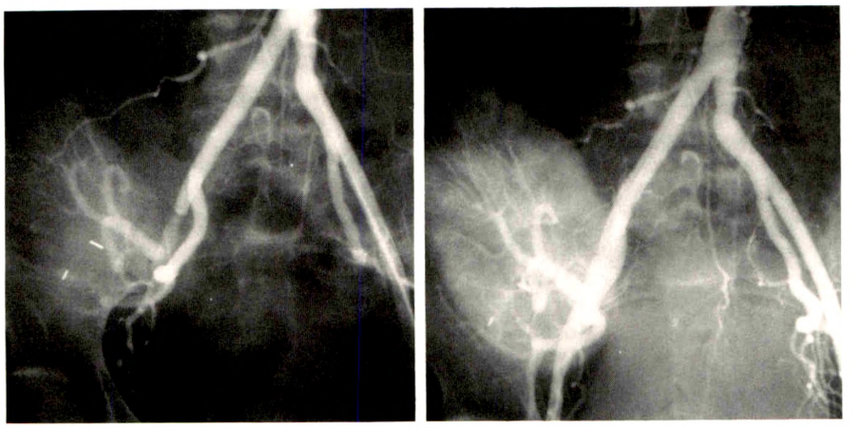


Fig. 2.—*A*, Angiogram shows weblike stenosis several centimeters proximal to a widely patent end-to-side renal transplant anastomosis.

B, Angiogram after percutaneous transluminal angioplasty shows stenosis has been effaced.

creatinine level remained stable (1.4 mg/dl [120 μmol/l]). An arteriogram obtained 5 months after transplantation showed a high-grade bandlike stenosis of the proximal external iliac artery just above the wide-open transplant anastomosis (Fig. 2A). PTA was performed, with a cosmetically acceptable result (Fig. 2B). The femoral pulse was immediately stronger. Right pedal pulses, which had been absent, were newly palpable. After the successful PTA, she was normotensive on one medication. During the subsequent year, the patient was admitted for two episodes of rejection; however, the angioplasty site remained patent on examination.

The third patient, a 37-year-old woman 4 years after cadaveric renal transplantation for end-stage renal disease from membranous glomerulonephritis had worsening hypertension while taking atenolol and a mild increase in serum creatinine level (1.6 mg/dl [140 μmol/l]). She had a history of a myocardial infarction and was a long-standing cigarette smoker. A pelvic arteriogram revealed a high-grade atherosclerotic stenosis of the proximal right iliac artery, above the widely patent transplant renal artery. A successful PTA resulted in immediate improvement in blood pressure control and her atenolol treatment was discontinued. In retrospect, the patient had reported a history of progressive claudication in the right leg. No clinical evidence of recurrence is evident 3 years later. The ankle-brachial index has been 1.0 since the angioplasty.

Several distinct scenarios are represented by these cases. In the first patient, a graft was placed distal to a preexisting iliac stenosis. Renovascular hypertension developed immediately after surgery. The second patient had progressively worsening hypertension in the first few months after transplantation. She had a stenosis with an appearance and location most consistent with intimal hyperplasia from a surgical clamp injury. In the final patient, progressive hypertension and concomitant claudication in the right leg developed years after transplantation from an evolving atherosclerotic stenosis.

These cases illustrate the need for clinical evaluation for occlusive aortoiliac disease before and after transplantation.

Transplantation candidates should be questioned for claudication. Examination should include peripheral pulse status and ankle-brachial indices. Duplex Doppler sonography and femoral artery Doppler waveform analysis may resolve questionable cases [5, 6]. Angiography may be required in some instances. Transplant recipients in whom renovascular hypertension develops should have a similar noninvasive assessment. Angiographic examination of patients with renovascular hypertension after transplantation should include evaluation of the infrarenal abdominal aorta and iliac artery as well as the transplant renal artery.

In this report, all three iliac artery stenoses were successfully treated by angioplasty. Iliac artery PTA has been well documented to have initial technical success rates (90–95%) and 3- to 5-year patency rates (75–90%) comparable to the rates with surgery, with lower morbidity and mortality rates [7, 8]. Angioplasty is, therefore, the appropriate initial treatment for iliac artery stenoses that cause transplant renovascular hypertension.

REFERENCES

1. Greenstein S, Verstandig A, McLean GK, et al. Percutaneous transluminal angioplasty: the procedure of choice in the hypertensive renal allograft recipient with renal artery stenosis. *Transplantation* **1987**;43:29–32
2. Luke RG. Hypertension in renal transplant recipients. *Kidney Int* **1987**;31:1024–1037
3. Sniderman KW, Sprayregen S, Sos TA, et al. Percutaneous transluminal dilatation in renal transplant arterial stenosis. *Transplantation* **1980**;30:440–444
4. Roberts JP, Ascher NL, Fryd DS, et al. Transplant renal artery stenosis. *Transplantation* **1989**;48:580–583
5. Langsfeld M, Nepute J, Hershey FB, et al. The use of deep duplex scanning to predict hemodynamically significant aortoiliac stenoses. *J Vasc Surg* **1988**;7:395–399
6. Sawchuk AP, Flanigan DP, Tober JC, et al. A rapid, accurate, noninvasive technique for diagnosing critical and subcritical stenoses in aortoiliac arteries. *J Vasc Surg* **1990**;12:158–167
7. Van Andel G. Transluminal iliac angioplasty: long-term results. *Radiology* **1980**;135:607–611
8. Brothers TE, Greenfield LJ. Long-term results of aortoiliac reconstruction. *J Vasc Intervent Radiol* **1990**;1:49–55

American Roentgen Ray Society
Residents' Award Papers, 1992

The ARRS announces competition for the 1992 President's Award and two Executive Council Awards for the best papers concerning the clinical application of the radiologic sciences.

Awards

The winner of the President's Award will receive a certificate and a $2000 prize. The winners of the two Executive Council Awards will each be given a certificate and a prize of $1000. The winners will be announced on March 16, 1992. Winning papers will be presented at the ARRS annual meeting at Marriott's Orlando World Center, Orlando, FL, May 10–15, 1992. Winning papers will be submitted for early publication in the *American Journal of Roentgenology*. All other papers will be returned to the authors.

Regulations

Eligibility is limited to residents or fellows in radiology who have not yet completed 4 years of approved training in a radiologic discipline. A letter from the resident's department chairman attesting to this status must accompany the manuscript. The resident must be the sole or senior author and be responsible for all or most of the project.

Submitted manuscripts must not exceed 5000 words and have no more than 10 illustrations. Four copies of the manuscript and illustrations are required. Submitted manuscripts should not contain previously presented or published material and should not be under consideration for publication elsewhere.

Deadline for submissions is February 14, 1992. Send papers to

Nancy O. Whitley, M.D.
Chairman, Committee on Education & Research
American Roentgen Ray Society
Department of Radiology
University of Maryland Medical Systems Hospital
22 S. Greene St.
Baltimore, MD 21201

Book Review

Magnetic Resonance Imaging of Carcinoma of the Urinary Bladder. By Jelle O. Barentsz, Frans M. J. Debruyne, and Sjef H. J. Ruijs. Boston: Kluwer, 121 pp., 1990. $120

Written by two radiologists and a urologist, this short monograph is targeted to radiologists, urologists, and oncologists who are interested in the radiologic staging of carcinoma of the bladder. The book consists of seven chapters: (1) a general discussion of clinical and non-MR methods of staging bladder carcinoma; (2) a general introduction to MR imaging; (3) a discussion of technical aspects of MR specifically pertaining to the bladder; (4) a pelvic anatomic–MR imaging atlas; (5) results of staging 134 patients by using MR compared with cystectomy (40 patients); clinical staging, CT, and lymphography (43 patients), and clinical staging (51 patients); (6) a discussion of the results of chapter 5; and (7) an outline of the book.

The quality of the illustrations is good to excellent, except that many of the findings on T1-weighted images are nearly invisible because of either poor photography or poor windowing. The quality of the cover, binding, and paper is first-rate. The price is reasonable. The references are all at the end of the book and are current through 1988.

The nine color plates are on separate pages and unnecessarily increase the cost of the book. The discussion of general MR principles is really no longer necessary. The chapter on technique specific to the bladder is excellent. The translation into English causes some unusual terminology, but the text is always readily comprehensible.

Basically this text is a long journal article. Its appeal is extremely limited because of its narrow focus and exorbitant price ($1 per page). I can recommend it only to someone with money to spend who wishes to supplement knowledge gleaned from a general body MR text without the bother of collecting recent journal articles.

Arnold C. Friedman
Temple University Hospital
Philadelphia, PA 19140

Case Report

Bilateral Testicular Infarction Caused by Epididymitis

David J. Eisner,[1] Stanford M. Goldman,[1] John Petronis,[2] and Steven H. Millmond[1]

Testicular infarction is most commonly associated with acute testicular torsion. We present a unique case of bilateral testicular infarction caused by severe nonresolving bilateral epididymitis. Several unilateral cases have been reported before. Knowledge of this potential complication of epididymitis allows recognition of early testicular ischemia and may result in testicular salvage [1–3].

Case Report

A 65-year-old man came to the emergency department complaining of urgency and decreased urinary output. Sonography showed obstructive hydronephrosis due to prostatic enlargement. After treatment with an indwelling urethral catheter for 2 weeks, a transurethral prostatectomy was performed.

Two weeks after being discharged, the patient returned complaining of bilateral scrotal pain and swelling. Bilateral epididymal enlargement and tenderness were noted on physical examination. The clinical diagnosis was acute bilateral epididymitis. No imaging studies were performed at that time.

Initially, the patient was treated with IV ampicillin and gentamicin. A urine culture obtained on admission revealed a *Pseudomonas aeruginosa* strain resistant to gentamicin. Therefore, his antibiotic regimen was switched to oral ciprofloxacin and IV tobramycin.

On the seventh hospital day, the scrotum and epididymal areas remained swollen. A testicular sonogram, obtained to rule out an abscess, showed bilateral epididymal enlargement with loss of soft-tissue planes. Bilateral hydroceles with a few septa were identified. Both testicles appeared normal without evidence of an abscess (Fig. 1A). Neither Doppler sonography nor scintigraphy were performed at this time. A diagnosis of bilateral epididymitis without orchitis was made.

By the 14th hospital day, physical examination revealed partial resolution of the scrotal swelling. However, progressive thickening and inflammation of the spermatic cords and epididymides were noted. Another emergent sonogram, obtained to determine a cause for the progressive changes, showed partial resolution of the bilateral hydroceles. The testicular parenchyma now had definite new areas of inhomogeneity bilaterally (Fig. 1B). Epididymal enlargement with loss of soft-tissue planes persisted (Fig. 1C).

In order to determine whether the inhomogeneous echo pattern was due to testicular infarction or orchitis, the patient was sent immediately for a radionuclide scan of the testicles. The flow images showed increased activity within the scrotum on early images (Fig. 1D) and on delayed scans. Large, round, focal areas of diminished radiotracer activity were seen centrally on both sides of the scrotum, surrounded by a rim of hyperemia consistent with bilateral testicular infarction (Fig. 1E).

When surgery was performed, the spermatic cords were found to be thickened, but no torsion was evident. The testicles were thought to be unsalvable. A bilateral orchiectomy was performed.

Pathologic examination revealed advanced bilateral infarcted testicles with marked fibrosis of the epididymides, spermatic cords, and tunica albuginea. On microscopic examination, extensive vascular thromboses involving the numerous veins and arteries supplying the testes were noted. On microscopic and gross examination of the spermatic cords, no evidence was found of recent or past torsion.

Discussion

Epididymitis is a recognized complication of prostatectomy. Preoperative catheterization and urinary tract infection after

Received February 14, 1991; accepted after revision April 12, 1991.
[1] Department of Radiology, Francis Scott Key Medical Center, 4940 Eastern Ave., Baltimore, MD 21224. Address reprint requests to D. J. Eisner.
[2] Division of Nuclear Medicine, Department of Radiology, Francis Scott Key Medical Center, 4940 Eastern Ave., Baltimore, MD 21224.

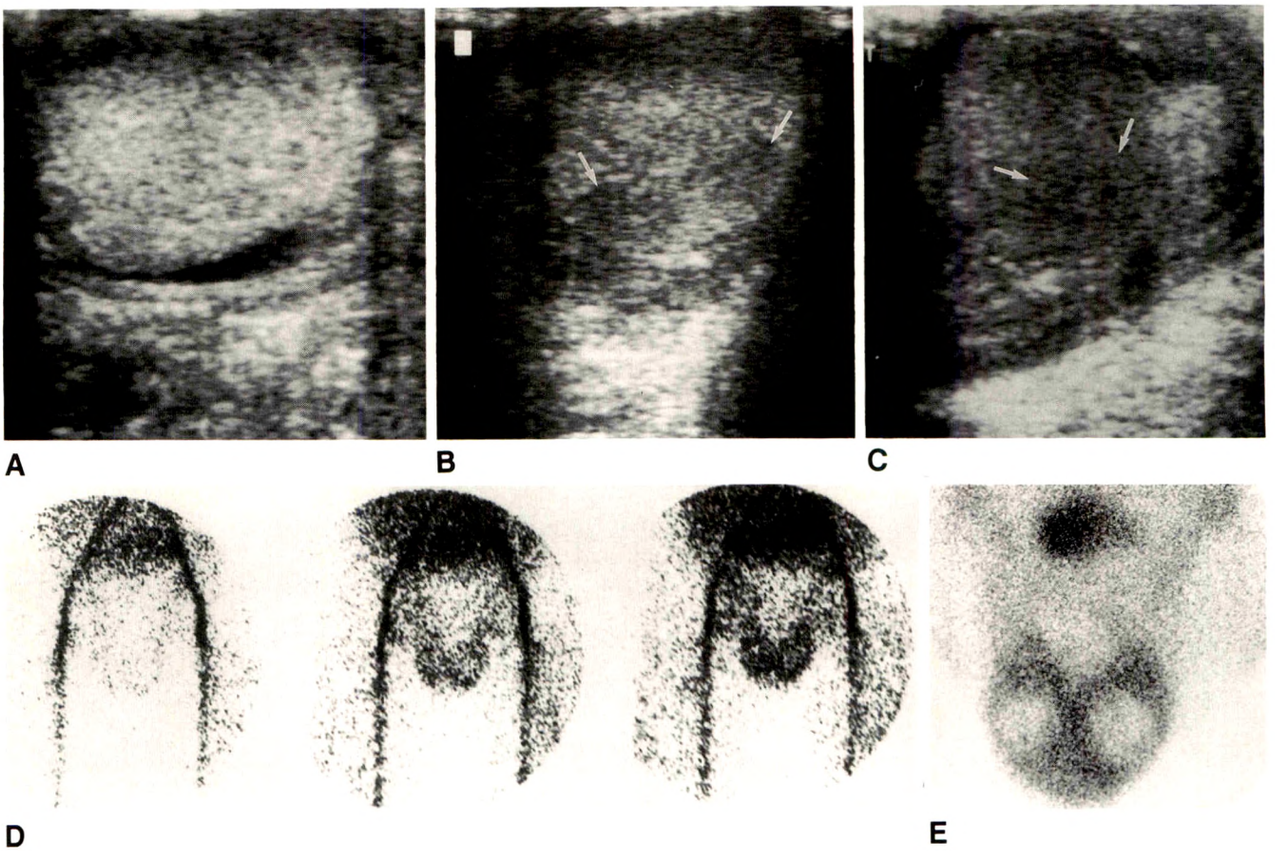


Fig. 1.—Fibrotic epididymis and infarcted testicle.
A, Initial sonogram shows homogeneous testicular parenchyma. A hydrocele is noted posteriorly.
B and *C*, Sonograms obtained on same day as orchiectomy show new echolucent areas in testicular parenchyma (*arrows* in *B*), and testicular inhomogeneity (*arrows* in *C*), echogenic areas within the epididymis, and loss of normal soft-tissue planes that separate epididymis and testicle.
D, Early scintigraphic flow images show markedly increased flow to scrotal regions bilaterally.
E, Tissue-phase scintigram shows increased peritesticular activity with bilateral central regions of diminished activity.

prostatectomy are associated with an increased prevalence of epididymitis [4]. Urethrovasal reflux is one path by which the epididymitis may occur [5] and probably was the cause for the epididymitis in our case. The vas deferens is the continuation of the canal of the tail of the epididymis; it courses through the spermatic cord and eventually forms the ejaculatory duct, which opens into the prostatic urethra. The major blood supply of the testicle includes the testicular and deferential arteries within the spermatic cord, which continue as capsular arteries within the tunica albuginea, and these, finally, branch into intratesticular arteries. Venous drainage is by superficial and deep veins of the testis anastomosing along the posterior testis (passing medial to the head of the epididymis), and these receive branches from epididymal veins. The resulting convoluted venous plexus is called the pampiniform plexus—this forms the greater mass of the spermatic cord.

Infarction after epididymitis is probably due to edema compromising venous drainage, which leads to thrombosis. Most often, the thrombosis develops at the level of the pampiniform plexus (the edema causes increased compression within the relatively rigid tissues that envelop the spermatic cord); however, testicular hypoperfusion may originate more distally by direct involvement of the draining testicular veins with inflammation extending out of the epididymis [2].

It is important to be aware of several clinical situations in which testicular ischemia may result from epididymitis. These include (1) patients with severe nonresolving epididymitis despite appropriate conservative treatment; (2) testicular pain of sudden onset developing in patients who initially improved with antibiotics [1]; (3) patients with a history of recurrent epididymitis who have acute epididymitis; (4) patients in whom tenderness and palpable thickening of the spermatic cord develop or persist during treatment of the epididymitis; and (5) patients with increasing febrile episodes while taking suitable medication [3]. In our case, situations (1) and (3) were present.

In the past, testicular hypoperfusion was diagnosed primarily by scintigraphy. Recently, both conventional duplex Doppler and color Doppler sonography have been used to assess testicular flow.

Testicular scintigraphy of uncomplicated epididymitis shows increased flow to the involved side, whereas the static

images show increased uptake in the region of the epididymis. However, testicular ischemia is characterized by diminished flow to the testicle, and on static images, little or no uptake in the testicle. The usual cause of this is testicular torsion. The hypoperfused testicle resulting from epididymitis has decreased flow to the testicle, whereas peripheral flow in the scrotum is increased. Therefore, static images show increased uptake in the epididymis and scrotum, with an area of diminished radiotracer activity corresponding to the testicle, as shown in this case [6].

Conventional duplex sonography may not be the best way to diagnose testicular ischemia. Pulsed Doppler imaging is most helpful when blood flow is definitely established. It is less satisfactory when flow cannot be clearly established, because imaging of the small, slow-flow, intratesticular vessels is technically difficult [7].

Intratesticular blood flow is much easier to show on color Doppler sonography in the normal testis. Failure to identify intratesticular blood flow is a reliable indicator of testicular hypoperfusion.

Doppler sonographic assessment of blood flow, with or without color, has an added advantage over scintigraphy. Simultaneous use of gray-scale and Doppler sonography allows better evaluation of the status of the testicular and epididymal parenchyma.

Gray-scale sonography alone is not sufficient to identify early testicular ischemia. Furthermore, in the later stages of testicular ischemia, the findings are nonspecific and cannot be differentiated from a number of other entities that can cause testicular inhomogeneity [8]. However, this testicular inhomogeneity is an important secondary observation that supports the Doppler findings.

In summary, the first reported case of bilateral testicular infarction caused by epididymitis is reported. Recognition that testicular ischemia can complicate severe epididymitis should prompt timely assessment of testicular perfusion; ideally this will result in testicular salvage. The diagnosis can be made, as in our case, with a combination of gray-scale sonography and scintigraphy.

REFERENCES

1. Vordermark JS, Favila M. Testicular necrosis: a preventable complication of epididymitis. *J Urol* **1982**;128:1322–1324
2. Rencken RK, Du Plessis DJ, De Haas LS. Venous infarction of the testis—a cause of non-response to conservative therapy in epididymo-orchitis: a case report. *S Afr Med J* **1990**;78:337–338
3. Costas S, Van Blerk PJP. Incision of the external inguinal ring in acute epididymitis. *Br J Urol* **1973**;45:555–558
4. Fujita K, Kimura T, Saito K, Kitagawa M, et al. Epididymitis after transurethral prostatectomy. *Clin Ther* **1988**;10:56–59
5. Carlton CE, Leader AJ. The cystourethrographic demonstration of retrograde urinary flow in the vas deferens as a cause of epididymitis. *J Urol* **1960**;84:123–125
6. Vordermark JS, Buck AS, Brown SR, Tuttle WK. The testicular scan: use in diagnosis and management of acute epididymitis. *JAMA* **1981**; 245:2512–2514
7. Middleton WD, Melson GL. Testicular ischemia: color Doppler sonographic findings in five patients. *AJR* **1989**;152:1237–1239
8. Bird K, Rosenfield AT, Taylor KJW. Ultrasonography in testicular torsion. *Radiology* **1983**;147:527–534

Book Review

Textbook of Uroradiology. By N. Reed Dunnick, Ronald W. McCallum, and Carl M. Sandler. Baltimore: Williams & Wilkins, 505 pp., 1991. $125

For several years an up-to-date textbook on radiology of the urinary tract was not available. Residents interested in surveying the entire field were referred to the appropriate sections of general radiology textbooks or to a number of review articles from different sources. In 1990, this changed brilliantly with the publication of Pollack's *Clinical Urography*, an encyclopedic three-volume atlas and textbook of urologic imaging. However, that work is more a definitive reference source than a concise volume that can be read cover to cover in a convenient period, and it certainly is too costly to be purchased by the average radiology resident. As the preface to *Textbook of Uroradiology* states, the standard of "what one ought to know," rather than "what there is to know," was applied to this more modest volume. The authors have succeeded in producing a comprehensive, one-volume text that integrates all aspects of uroradiology in adults.

The volume has 22 chapters and a detailed, easy-to-use index. No specific references are cited in the text itself, but a useful and up-to-date list of suggested readings is appended at the end of each chapter. References as recent as 1990 are included. The anatomy, embryology, and congenital anomalies of the urinary tract are described in chapters 1 and 2. Chapter 3 is an overview of the diagnostic imaging techniques discussed and illustrated in subsequent chapters. Chapter 4 covers urographic contrast material, including pertinent functional renal anatomy, physiology, and reactions to contrast media and their treatment. Chapters 5 to 11 describe imaging of renal disorders: cystic disease, tumors, inflammatory disease, vascular diseases, renal hypertension, nephrocalcinosis and nephrolithiasis, and the pelvicaliceal system. Urinary tract trauma is the subject of chapter 12. Chapters 13 to 19 cover the nonrenal structures of the urinary tract: adrenal gland, ureter, urinary bladder, neurogenic bladder, prostate and seminal vesicles, urethra and penis, and scrotum and contents. Chapter 20 covers renal failure and medical renal disease. Chapter 21 is about renal transplantation, and the final chapter is an overview of interventional uroradiology.

The distribution of chapters within the book is puzzling. It would be more consistent and logical to place the chapter on interventional uroradiology with the early chapter on examination techniques, rather than at the end of the book after the chapters on specific urinary tract diseases and disorders in which many of these interventional techniques are discussed and the underlying condition for which the procedure is indicated. Similarly, the chapters on renal failure and renal transplantation more logically would be grouped with the other chapters dealing with renal diseases, rather than after the chapters on the lower urinary tract.

The book is easy to carry and easy to read. The quality of the binding, paper, and printing is excellent. The text is written in short declarative sentences, without imaginative flourishes but in a style that is uniform and reader friendly. Although care is taken not to elaborate all sides of every controversial topic, the discussions of contrast-induced acute renal dysfunction and the arguments for complete vs selective use of low-osmolar contrast media are admirable reviews of complex subjects. The discussion of endorectal sonography in the evaluation of prostatic disease is up-to-date, informative, and nicely balanced. Unfortunately, the recent multiinstitutional study emphasizing the limitations of transabdominal MR and endorectal sonography in staging prostatic cancer was published too late for inclusion in this book. The illustrations are numerous but not exhaustive; no attempt was made to create a comprehensive atlas of radiologic images. Most of the CT scans, MR images, and sonograms are from state-of-the-art equipment, an unusual feat for a radiologic textbook. Several pertinent examples of MR images obtained by using limited flip-angle techniques with gradient-echo sequences are included. The overall quality of the illustrations is exceptional, and even the choice of superimposed letters and arrows shows careful attention to size, boldness, and location on the prints. The size of the illustrations is uniformly optimal except for many of the adrenal CT scans, which are disproportionately and unnecessarily larger than most of the others.

Despite the book's initial printing and distribution in late 1990, many significant publications from 1990 are listed in the suggested readings and, more surprisingly, are discussed in the body of the text. Notable among them is Katayama's landmark study comparing the type and rate of adverse reactions to both ionic and nonionic contrast media. Inevitably some important recent advances are not included, among them are Platt's recent studies suggesting an important role for duplex Doppler sonographic evaluation of intrarenal arteries in the differentiation of obstructive vs nonobstructive hydronephrosis. Other interesting concepts not discussed include Kunin's work suggesting that an extracapsular renal hematoma confined by perinephric space septations can be indistinguishable from a subcapsular hematoma on CT scans.

I enthusiastically recommend this book to all radiologists and urologists. It belongs in all radiology, urology, and medical school or hospital libraries. It can be read cover to cover as an introduction to the field or as a review before specialty board examinations. It accurately and admirably summarizes the current status of urinary tract imaging and intervention. It clearly fills a need different from that served by Pollack's three-volume text. Two other new textbooks of uroradiology, one by Amis and Newhouse and one by Barbaric, have also just been published; they are likely to be similar in scope to, and inevitably will be compared with, this outstanding achievement by Dunnick, McCallum, and Sandler.

Melvyn Korobkin
University of Michigan Medical Center
Ann Arbor, MI 48109-0030

Technical Note

Insertion of the Simon Nitinol Caval Filter: Value of the Antecubital Vein Approach

Ducksoo Kim,[1] Bertrand W. Schlam,[1] David H. Porter,[1] and Morris Simon[1,2]

The Simon nitinol vena caval filter (Nitinol Medical Technologies, Woburn, MA) was successfully placed via an antecubital vein in five patients in whom other access routes were not suitable. The antecubital approach is a new alternative for placement of the filter and avoids complications associated with punctures of veins in the groin or neck.

Subjects and Methods

Five patients, three men and two women (mean age, 67 years; range, 52–92 years) had deep venous thrombosis of the lower extremities and were referred for caval filter placement because of contraindications to anticoagulation. Femoral routes for insertion of a caval filter were not used because of thrombi in both femoral veins documented sonographically or thrombi encroaching into the inferior vena cava from iliac veins (documented by venacavography). Catheterization of the jugular vein was prevented by severe orthopnea in three patients, by a wish not to disturb an indwelling jugular chemotherapy catheter in one patient, and by one patient's specific request to avoid jugular puncture.

The standard Simon nitinol filter jugular kit can be used for the antecubital approach without changing the technique of filter release. With the patient supine, lying as flat as possible, the right or left arm is supinated and abducted 40 degrees. A tourniquet or blood pressure cuff (inflated to just above diastolic pressure) is placed as high on the arm as possible. We prefer the medial branch of the large straight basilic vein along the ulnar aspect of the arm, because the cephalic vein along the lateral radial aspect of the arm is often smaller and intersects the axillary vein at a right angle. After elevating the skin to avoid injuring the superficial vein, a 4-mm scalpel nick is made with a number 11 blade in the overlying skin. Venipuncture with a 19-gauge ultra-thin single-wall angiographic needle permits introduction of a 0.035-in. (0.89 mm), 180-cm guidewire into the arm vein. By using conventional angiographic technique, a catheter and guidewire are manipulated through the central veins into the inferior vena cava (IVC). The 9-French (outer diameter) Simon nitinol filter introducer is passed over the guidewire into the lower IVC, then inferior venacavography is performed, and the filter is placed. When needed, contrast material is injected, with fluoroscopic guidance, road mapping, and slight alterations in arm position facilitating passage of the guidewire and catheter. Initial use of a hydrophilic, angled-tip guidewire (Glidewire, Medi-tech/Boston Scientific, Watertown, MA) aids negotiation through tortuous veins and seems less prone to induce venous spasm.

Unlike in the lower extremity, venous blood in the upper extremity is drained predominantly by superficial veins, which are larger than the deep veins, simplifying catheterization. However, the deep venous system of the arm can be entered by puncturing one of the two paired brachial veins formed by the confluence of the radial and ulnar veins at the elbow. The brachial veins parallel the brachial artery and are entered by palpating the brachial pulse and passing the needle medial to the artery. The deep paired brachial veins, although more difficult to access, combine with the basilic vein at the lower border of the pectoralis major muscle to form the axillary vein, providing a straight, direct route to the subclavian and central veins.

Variations, including duplication or accessory veins of the cephalic, axillary, or subclavian veins occur; however, these are unlikely to prevent successful catheterization. The size relationship between the basilic and the cephalic veins is reciprocal, with the basilic vein usually larger, but the 9-French Simon nitinol introducer is less than 3 mm in outer diameter and can be accommodated by most veins. We used the cephalic vein in two of our cases, one of which required introduc-

Received March 8, 1991; accepted after revision April 2, 1991.
[1]Department of Radiology, Beth Israel Hospital, Harvard Medical School, 330 Brookline Ave., Boston, MA 02215. Address reprint requests to D. Kim.
[2] Nitinol Medical Technologies, Inc., 175-P New Boston St., Woburn, MA 01801.

 0361–803X/91/1573–0521 © American Roentgen Ray Society

tion of a stiff exchange wire (Amplatz stiff exchange, 0.035-in. diameter, 260 cm, Cook Co., Bloomington, IN) to straighten the junction of cephalic and axillary veins before introducing the sheath. In the other patient, a right-angle tip catheter was needed to steer the guidewire into the subclavian vein toward the superior vena cava instead of returning toward the arm. These manipulations were routine and resulted in minimal delay.

Discussion

A new generation of vena caval filters with low-profile delivery systems is now available. These filters include the titanium Greenfield filter (Medi-tech/Boston Scientific), the bird's nest filter (Cook Co.), the LGM Venatech filter (L. G. Medical, Chassenveil, France), and the Simon nitinol filter (Nitinol Medical Technologies). The delivery sheaths' outer diameters are 14.3-, 14.0-, 12.0-, and 9.0-French, respectively [1]. All can be placed percutaneously via femoral or internal jugular routes, but some manufacturers' insertion instructions restrict venous access routes. For example, the new titanium Greenfield filter insertion instructions state, "Warnings—Do not attempt a left side insertion unless all other attempts are impossible. Sheath kinking or insertion difficulties may result due to tortuous left-sided anatomy" [2]. Many patients with an indication for filter placement have femoral vein thrombosis and relative contraindications to the jugular approach, such as jugular venous occlusion or severe orthopnea.

When standard femoral or jugular approaches are not available, the Simon nitinol filter offers several technical advantages. Although it is cooled during its passage through the introducer, the nitinol wire alloy is soft and flexible, allowing it to negotiate acute angles. The nitinol filter remains soft until it is extruded into the warm blood in the vena cava. Therefore, a rigid filter carrier capsule is not necessary. This flexibility results in the smallest-profile introducer system of any IVC filter [3]. These advantages enable placement via right or left internal or external jugular vein, right or left femoral vein, or antecubital veins of either arm.

Although the right common femoral approach remains the shortest and fastest route for IVC filter placement, the antecubital approach is an excellent alternative when conventional routes are compromised, or when early ambulation is necessary. One patient, an outpatient in an oncology practice, expressed a strong wish to minimize time in the hospital and avoid possible complications of jugular puncture. The antecubital approach enabled us to meet his request easily. In practice, we have found the antecubital approach from either arm is technically easier and more acceptable to patients than are approaches via the external or internal jugular vein. The external jugular vein approach for caval filter placement was introduced recently [4, 5]; however, it has many of the same technical limitations as the internal jugular vein approach, such as positioning of the patient supine or with the head slightly down to distend the vein before puncture. This position caused significant orthopnea in three of our patients. Patients' discomfort, both direct and psychological, entailed in the jugular approach is avoided by the antecubital route, as are the complications of inadvertent puncture of the carotid artery and pneumothorax.

We believe the small Simon nitinol introducer may reduce the occurrence of iatrogenic venous thrombosis at the access site, but in any case, thrombosis of an antecubital vein is less serious for the patient than is thrombosis of the common femoral or internal jugular vein. Thrombotic occlusion of the access vein has not occurred during the short follow-up of these five patients, nor has bleeding or hematoma. Bleeding is easily controlled by direct pressure at the puncture site. We do not discontinue heparin before filter insertion because of anticipated ease of control at the antecubital access site.

The current jugular delivery system is just long enough to accommodate most patients of average height. We have recommended production of longer antecubital introducer systems suitable for use in taller patients.

REFERENCES

1. Dorfman GS. Percutaneous inferior vena caval filters. *Radiology* **1990**;174:987–992
2. Instructions for Use. Titanium Greenfield Vena Cava Filter with 12 French Introducer System. Watertown, MA: Medi-tech/Boston Scientific Corp., **1990**:4
3. Simon M, Athanasoulis CA, Kim D, et al. Simon nitinol inferior vena cava filter: initial experience. *Radiology* **1989**;172:99–103
4. McCowan TC, Ferris EJ, Carver DK, Harshfield D. Use of external jugular vein as a route for percutaneous inferior vena caval filter placement. *Radiology* **1990**;176:527–530
5. Kim D, Siegel JB, Porter DH, Simon M. Vena caval placement via the external jugular vein. *AJR* **1990**;155:898–899

Cervical Paraspinal Calcification in Collagen Vascular Diseases

Mark E. Schweitzer[1,2]
Vinicio Cervilla[1]
B. J. Manaster[3]
Judy Gerharter[1]
Murray Dalinka[4]
Wallace W. Peck[5]
Donald Resnick[1]

Although soft-tissue calcification is common in collagen vascular disease, paraspinal calcification in the cervical spine has not been described before. We studied five women with large, lobulated, predominantly homogeneous calcific masses centered on synovial articulations in the neck. Changes consisting of either osteolysis or erosions were evident. All patients had radiculopathy, focal pain, or stiffness. In two patients, the presence of hydroxyapatite crystals was confirmed on biopsy.

Symptomatic cervical paraspinal calcifications in patients with collagen vascular disease cause large soft-tissue masses that mimic tumoral calcinosis.

AJR 157:523–525, September 1991

Collagen vascular disorders are a diverse group of diseases that affect the supporting tissues of the body. Musculoskeletal involvement, especially soft-tissue calcification in the hands, is common and well recognized.

Calcification in the soft tissues adjacent to the spine is unusual. It frequently causes focal pain [1], weakness [2], or radiculopathy [3]. The calcification may decrease range of motion [4].

A recent report [5] described the occurrence of paraspinal and intraspinal calcification in the thoracic spine in a patient with progressive systemic sclerosis. To our knowledge, calcification of the cervical spine in patients with collagen vascular disorders has not been reported previously.

Materials and Methods

During the past 3 years, we saw five patients who had calcification in the cervical region in association with collagen vascular disorders. The age range of the patients was 54 to 65 years (mean age, 63 years). All five patients were women. The radiographs, CT scans, MR images, and scintigrams from all five patients were examined retrospectively. The patients' medical records were reviewed for presence and type of symptoms, and laboratory data were reviewed to exclude metabolic diseases that may affect calcium metabolism. The images were evaluated for the appearance, location, and extent of the calcific masses, and the adjacent articulations were assessed.

Results

The calcific masses were large and extended over several vertebral levels. They were centered at synovial articulations: the apophyseal joints in four patients (Figs. 1 and 2) and the anterior and posterior median atlantoaxial joints in one (Fig. 3). The underlying articulations were abnormal in all cases. Three patients had extensive osteolysis around the joints (Fig. 2B). In the remaining two patients, bone erosions were apparent. In one of these patients, the erosions appeared to be caused by a pressure effect from the masses. In the other patient, the erosions

Received February 4, 1991; accepted after revision April 23, 1991.

Presented at the annual meeting of the American Roentgen Ray Society, Boston, MA, May 1991.

This work was supported in part by VA Grant #SA306.

[1] Department of Radiology, Veterans Affairs Medical Center (VAMC), 3350 La Jolla Village Dr., San Diego, CA 92161, and University of California, San Diego, Medical Center, San Diego, CA 92103. Address reprint requests to D. Resnick at the VAMC.

[2] Present address: Department of Radiology, Thomas Jefferson University Hospital, Philadelphia, PA 19107.

[3] Department of Radiology, University of Utah Medical Center, Salt Lake City, UT 84132.

[4] Department of Radiology, Hospital of University of Pennsylvania, 3400 Spruce St., Philadelphia, PA 19104.

[5] Department of Radiology, St. Joseph's Hospital, Orange, CA 92668.

0361–803X/91/1573–0523
© American Roentgen Ray Society

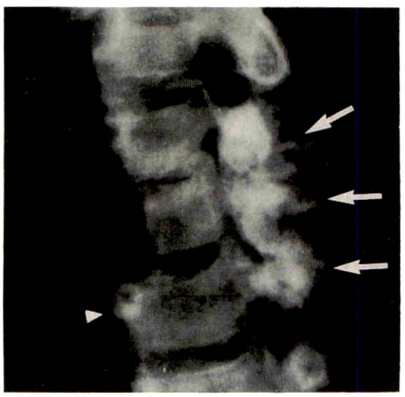
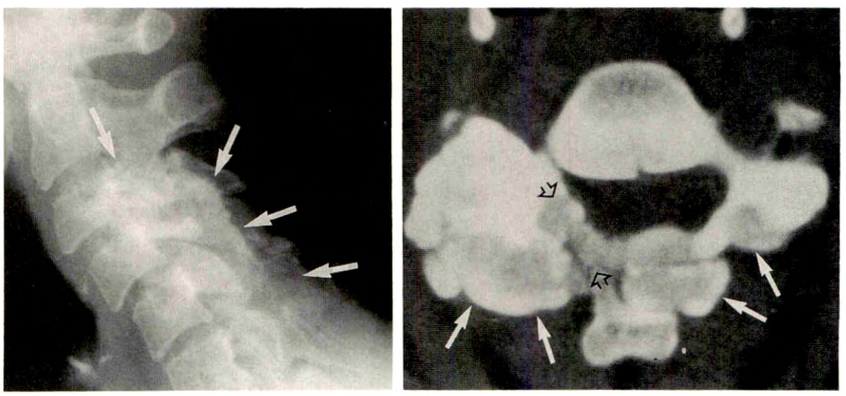


Fig. 1.—65-year-old woman with a 10-year history of progressive systemic sclerosis with characteristic dermal, esophageal, and polyarticular disease. Oblique radiograph of cervical spine shows right-sided parapophyseal calcifications at C3–C4, C4–C5, and C5–C6 (*arrows*). Left-sided calcification is visible at C5–C6 (arrowhead). Calcification is homogeneous centrally with punctate areas in periphery.

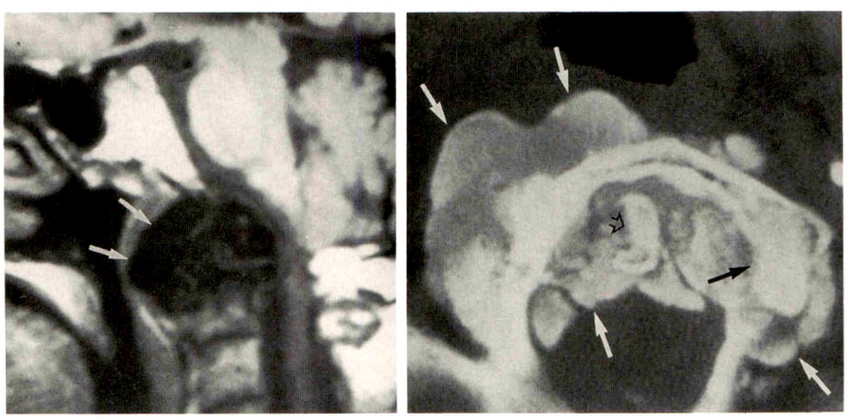


A B

Fig. 2.—56-year-old woman with progressive systemic sclerosis had decreased range of motion in cervical spine.

A, Lateral cervical radiograph shows calcific masses about apophyseal joints of C3–C4, C4–C5, and C5–C6 (*arrows*).

B, CT scan shows bilateral calcific masses (*white arrows*). Right-sided mass is larger, and osteolysis of right apophyseal joint and lamina (*black arrows*) is present. Calcific mass is lobulated and homogeneous.



A B

Fig. 3.—63-year-old woman with seizures.

A, MR image shows a large area of signal void around odontoid process (*arrows*).

B, CT scan shows an extensive lobulated mass surrounding dens and atlas (*white arrows*). Right side of dens is eroded (*open black arrow*), and erosions (*solid black arrow*) of atlas are present. Mass is lobulated and homogeneous centrally. Note somewhat punctate-appearing calcific areas in periphery on right side. Clinical evaluation indicated systemic lupus erythematosus.

appeared to be caused by synovial inflammation (Fig. 3B). Calcification was lobulated and homogeneous. In three patients, however, small punctate calcific regions were noted in the periphery of the larger lobulated mass (Figs. 1 and 3B).

All patients were symptomatic. Three patients had radiculopathy, three had local pain, and three had neck stiffness. In two patients, the masses were sampled by biopsy, and the specimens contained crystals of hydroxyapatite. Two patients had the masses resected. In these two, symptoms resolved.

Metabolic disorders of calcium metabolism were excluded in all patients. In four of the patients, progressive systemic sclerosis was diagnosed on the basis of typical rheumatologic criteria. In one patient, the diagnosis of systemic lupus erythematosus was made because of the presence of an elevated antinuclear antibody titer, elevated erythrocyte sedimentation rate, and characteristic findings on radiographs.

Discussion

Musculoskeletal involvement is common in collagen vascular diseases, including progressive systemic sclerosis, systemic lupus erythematosus, dermatomyositis, and polymyositis. Among the most significant radiologic findings of this involvement is soft-tissue calcification. In progressive systemic sclerosis, involvement of the hands and wrists is most frequent, with calcified deposits located in the subcutaneous tissues and around joints. These periarticular deposits may form large tumoral masses. In systemic lupus erythematosus, the calcifications most frequently involve the lower extremity. Polymyositis and dermatomyositis may be associated with calcification of the intramuscular fascial planes and subcutaneous tissue. Calcification about the spine, however, has not been frequently described in any of

these disorders, although in a recent report [5] paravertebral calcification in the thoracic region was noted in a patient with progressive systemic sclerosis. Paracervical calcifications appear to be a previously unrecognized manifestation of collagen vascular disease. However, osteolysis in the cervical spine has been reported [6] in cases of progressive systemic sclerosis in which the images, in retrospect, also show such paravertebral calcification.

Calcification in the spine is known to occur in several disorders other than collagen vascular diseases, particularly in association with crystal deposition diseases and diffuse idiopathic skeletal hyperostosis. In calcium pyrophosphate dihydrate (CPPD) crystal deposition disease, calcific deposits may be seen in the intervertebral disks, the posterior longitudinal and interspinous ligaments, and the ligamentum flavum [7]. Less frequently, calcifications similar to those noted in our patients with collagen vascular disease have been observed in CPPD crystal deposition disease. Idiopathic calcification of the ligamentum flavum or, less frequently, other spinal ligaments, may be noted, especially in elderly women [8]. In addition, calcifications may surround the odontoid process and cause severe upper cervical pain; the resulting appearance has been termed the crowned dens syndrome [9]. Its cause is not clear.

Our observations confirm that paraspinal cervical calcification may be observed in collagen vascular diseases. We identified five cases among the approximately 300 patients with collagen vascular diseases we have seen in the past 10 years. These resultant calcific deposits were significantly larger than those occurring in CPPD crystal deposition disease, idiopathic ligamentous calcification, or the crowned dens syndrome. These masses are similar to the masses of tumoral calcinosis that occur in the appendicular skeleton in progressive systemic sclerosis. Because the calcific deposits in our cases were large, their site of origin was difficult to determine. The masses appeared to be centered on synovial articulations (the apophyseal joints in four cases and the anterior and posterior median atlantoaxial joints in one case). These deposits initially may have represented intraarticular or periarticular calcifications. They subsequently appear to have extended from the joints to adjacent tissues. The affected synovial joints also were abnormal. Three showed severe osteolysis, and two showed more limited bone erosions; in one patient, the erosion appeared to represent a pressure effect, and in the other two cases, articular erosions similar to those occurring in inflammatory arthritis were observed.

Two of the patients who had surgery had crystals of calcium hydroxyapatite. It has been suggested that soft-tissue calcification begins with the deposition of CPPD crystals, which convert to crystals of hydroxyapatite beginning in the center of the deposit [10]. The radiologic findings in our case are similar to those of deposition of hydroxyapatite elsewhere in the body. The masses were homogeneous and lobulated. In two patients, however, the periphery of the masses resembled CPPD deposits more than deposits of hydroxyapatite.

All patients were symptomatic. Two complained of local pain, discomfort, and stiffness. These findings appear to be attributable to limited motion and mass effect caused by the calcifications. In one patient, the symptoms resolved when the mass was removed. Three patients complained of radiculopathy. In these patients, the mass caused neural foraminal stenosis with nerve-root impingement. One patient complained of diffuse weakness.

ACKNOWLEDGMENTS

We thank Lee Rogers and Al Nemcek from Northwestern University Medical School in Chicago, and Morrie Kricun from the Hospital of the University of Pennsylvania, Philadelphia, for contribution of case material.

REFERENCES

1. Yamishita Y, Takahashi M, Matsuno Y, et al. Spinal cord compression due to ossification of ligaments: MR imaging. *Radiology* **1990**;175:843–848
2. Ogata M, Ishikawa K, Ohira T. Cervical myelopathy in pseudogout. *J Bone Joint Surg [Am]* **1984**;66-A:1301–1303
3. Kawaro N, Yoshida S, Takashi O, Yada K, Sasaki K, Takashi M. Cervical radiculomyelopathy caused by deposition of calcium pyrophosphate dihydrate crystals in the ligamenta flava. *J Neurosurg* **1980**;52:270–282
4. Berghausen EJ, Balogh K, Landis WS, Lee DD, Wright AM. Cervical myelopathy attributable to pseudogout. *Clin Orthop* **1987**;214:217–221
5. Walden CA, Gilbert P, Rogers LF, Hendrix RW. Case report 620. *Skeletal Radiol* **1990**;19:377–378
6. Haverbush TJ, Wilde AH, Hawk WA, Scherbel AL. Osteolysis of the ribs and cervical spine in progressive systemic sclerosis. *J Bone Joint Surg [Am]* **1974**;56-A:637–640
7. Resnick D, Pineda C. Vertebral involvement in calcium pyrophosphate dihydrate crystal deposition disease. *Radiology* **1984**;153:55–60
8. Nakajina K, Miyaoka M, Suwe A, Nakzato T, Ishi S. Cervical radiculomyelopathy due to calcification of the ligamenta falva. *Surg Neurol* **1984**;21:479–488
9. Bouvet JP, LeParc JM, Michalski B, Berlahrache C, Auguier L. Acute neck pain due to calcification surrounding the odontoid process: the crowned dens syndrome. *Arthritis Rheum* **1985**;28:1417–1420
10. Kawaro N, Matasur T, Miyazawa S, et al. Calcium pyrophosphate dihydrate crystal deposition disease in the cervical ligamentum flavum. *J Neurosurg* **1988**;68:613–620

Book Review

MRI of the Musculoskeletal System, 2nd ed. Edited by Thomas H. Berquist. New York: Raven, 545 pp., 1990. $130

This text is a major revision of a much smaller book, published in 1987, titled *Magnetic Resonance of the Musculoskeletal System.* Since 1987, dramatic advances have occurred in MR imaging—the result of technological improvements in both hardware and software. In turn, these improvements have resulted in an increasingly important role for MR in the radiologic evaluation of musculoskeletal disorders. These exciting technical advances and the resulting broader clinical applications of musculoskeletal MR are the basis for the second edition (with minimal change in title) of this textbook.

The text is divided into 15 chapters; Dr. Berquist is the author of eight and a coauthor of an additional two. His "authorship," rather than mere "editorship," adds a positive cohesiveness to the text, particularly considering his recognized expertise in the field of musculoskeletal MR. The first three chapters are "Basic Principles and Terminology of Magnetic Resonance Imaging," "Interpretation of Magnetic Resonance Images," and "General Technical Considerations in Musculoskeletal MRI." When compared with the first edition, the first chapter of this edition is a major revision, including new authors. On the other hand, chapter 2 has only minimal changes from the 1987 version, and chapter 3 includes many of the same illustrations in both editions. Some of the duplication is reasonable, but an attempt could have been made in chapters 2 and 3 to include "new and improved" images. Finally, the first three chapters constitute approximately 15% of the text. It is hoped that the chapters on basic principles and technical considerations of MR will soon be incorporated exclusively into technical MR books, thereby allowing expansion of the amount of clinical material covered in a single book.

Chapters 4–11 of the second edition are devoted to anatomic regions: temporomandibular joint; the spine; pelvis, hips, and thighs; the knee; foot, ankle, and calf; shoulder and arm; elbow and forearm; and hand and wrist. Essentially, all of this information was added since the first edition. These chapters begin with a useful outline; major categories are technique, anatomy, pitfalls, applications, and references. The technique section includes sequential MR images, each of which is accompanied by a line drawing showing the plane of section corresponding to the MR image. In each of these chapters, the appropriate pulse sequence, slice thickness, matrix, field of view, and image time are listed in a concise table. Although there are as many different techniques for performing musculoskeletal MR as there are different magnets, it is nevertheless extremely helpful to learn the "tricks" of the experts.

The sections devoted to anatomy are extremely well done and are subdivided into osseous, muscular, and neurovascular anatomy. Some illustrative MR images should be included in this section, however. The applications section provides discussions and MR examples of specific diseases. For example, in chapter 6, "Pelvis, Hips, and Thighs," the applications section addresses the following entities: osteonecrosis, transient osteoporosis or edema, trauma, neoplasms, arthropathies, infection, and disorders in infants and children.

Chapters 12–15 address musculoskeletal neoplasms, musculoskeletal infection, diffuse marrow diseases, and miscellaneous conditions (e.g., myopathies, arthropathies, and pediatric and congenital disorders). A valid criticism of the text is the underuse of correlation of plain radiographs with the MR images, particularly with regard to examples of musculoskeletal neoplasms and infection. Bone tumors are best "named" from the radiograph, whereas MR is best suited for determining the extent of disease. Unfortunately, when interpreting the MR images, far too many radiologists fail to correlate the high-tech MR images with the low-tech radiographs, particularly when the former are obtained at a free-standing or outpatient facility. For instance, when the authors show three images of a Ewing sarcoma of the humerus, the teaching value of the case is significantly diminished by the absence of a radiograph for correlation. The scarcity of radiographs is additionally frustrating because a moderate amount of wasted, blank space surrounds many of the illustrations.

Overall, this textbook is packed with useful information. The illustrations are sharp, the paper is of high quality, and the reference lists are complete. This text is highly recommended for all physicians (oncologists, orthopedic surgeons, and radiologists) who are interested in MR of the musculoskeletal system. Even during the preparation of this review, I have referred to my copy of the book countless times as a clinical reference. This text is clearly one of the best available sources on MR of the musculoskeletal system. Such a great improvement was made between 1987 and 1990 that I am already eagerly awaiting 1993 and the third edition of this book.

Richard P. Moser, Jr.
Penn State University Hospital
The Milton S. Hershey Medical Center
Hershey, PA 17033

Diagnosis of Osteomyelitis of the Foot in Diabetic Patients: Value of ^{111}In-Leukocyte Scintigraphy

George Larcos[1]
Manuel L. Brown[1,2]
Ross T. Sutton[3]

The noninvasive diagnosis of osteomyelitis of the foot in diabetic patients with currently available radiologic and radionuclide imaging techniques is often difficult. Recently, ^{111}In-labeled leukocyte scintigraphy has been proposed as an attractive alternative. Accordingly, we retrospectively reviewed 51 ^{111}In-labeled leukocyte scans, 49 technetium-99m bone scans, and 49 plain radiographs obtained in 51 adults with diabetes in whom osteomyelitis of the foot was suspected. The sensitivity and specificity of these techniques were evaluated in all patients, as well as in a subgroup of 11 patients with neuroarthropathy. Results with ^{111}In-labeled leukocyte scans were also examined in subsets of patients with soft-tissue ulcers (n = 35) and those receiving antibiotics during investigation (n = 20). Confirmation or exclusion of osteomyelitis was made surgically in 28 patients and clinically in 23. Fourteen patients had osteomyelitis. Bone scans were most sensitive (93%) but least specific (43%); plain radiographs were most specific (83%) but least sensitive (43%). ^{111}In-labeled leukocyte scans were both sensitive (79%) and specific (78%), and remained useful in patients with neuroarthropathy, soft-tissue ulcers, and antibiotic treatment. Poor spatial resolution contributed to the false-negative and false-positive ^{111}In-labeled leukocyte scans, suggesting that this technique should not be interpreted independent of other tests.

^{111}In-labeled leukocyte scans are a valuable diagnostic tool for the diagnosis of pedal osteomyelitis in diabetic patients.

***AJR* 157:527–531, September 1991**

Diabetic patients in whom osteomyelitis of the foot is suspected pose a common yet formidable diagnostic problem [1]. Coexisting disorders such as peripheral vascular disease, cellulitis, and neuroarthropathy obscure the clinical and radiologic manifestations of osteomyelitis [1, 2]. An inaccurate diagnosis is associated with deleterious consequences [3]. Plain radiographs, ^{99m}Tc-methylene diphosphonate (MDP) scans, and ^{67}Ga-citrate scans are widely considered to have limited diagnostic accuracy [1, 3–5]. Recently, several investigators [6–14] reported favorable results in osteomyelitis when ^{111}In-labeled leukocytes were used. However, most of these series have contained few patients with diabetes mellitus, and the conclusions regarding the usefulness of ^{111}In-WBC scanning in neuroarthropathy have been conflicting [4, 8, 9, 15]. Further, diabetics often have soft-tissue ulcers or are receiving antibiotics during investigation, yet there is a paucity of information regarding the potential limitations imposed by these factors on results with ^{111}In-WBC scintigraphy. Initial evaluation of CT scanning [16] and MR imaging [17] have been promising, but both are more expensive than scintigraphy [3] and their respective roles in imaging strategies are at present undefined [1].

The purpose of this study was to determine the usefulness of ^{111}In-WBC scintigraphy in a large heterogeneous group of diabetic patients referred for investigation of possible pedal osteomyelitis. The value of this test was also assessed in subsets of patients with advanced neuroarthropathy, current antibiotic therapy, and foot ulcers. Further, since ^{111}In-WBCs may localize falsely at sites of

Received January 28, 1991; accepted after revision April 17, 1991.

[1] Section of Nuclear Medicine, Mayo Clinic and Mayo Foundation, Rochester, MN 55905.

[2] Present address: Division of Nuclear Medicine, Department of Radiology, University of Pittsburgh Medical Center, Desoto at O'Hara Sts., Pittsburgh, PA 15213. Address reprint requests to M. L. Brown.

[3] Department of Diagnostic Radiology, Mayo Clinic and Mayo Foundation, Rochester, MN 55905.

0361–803X/91/1573–0527
© American Roentgen Ray Society

hyperemia and noninfective inflammation [8], we tested the interpretative criterion requiring uptake to be of proportionately greater intensity than ^{99m}Tc-MDP to indicate osteomyelitis.

Materials and Methods

During the 5 years from April 1985 to March 1990, 76 adults with insulin- or noninsulin-dependent diabetes mellitus underwent ^{111}In-WBC scintigraphy for suspected pedal osteomyelitis. Fifty-one patients were selected in whom a final diagnosis was proved by either surgery (bone biopsy or culture, or deep wound culture during debridement) or clinical follow-up in the outpatient department. Accordingly, 51 ^{111}In-WBC scans, 49 ^{99m}Tc-MDP scans, and 49 plain radiographs were reviewed. The studies of the remaining 25 patients were excluded from analysis because treatment was subsequently undertaken at other institutions, with no correspondence regarding outcome (n = 20), or these patients had multisystem disorders with inadequate documentation for the foot (n = 5).

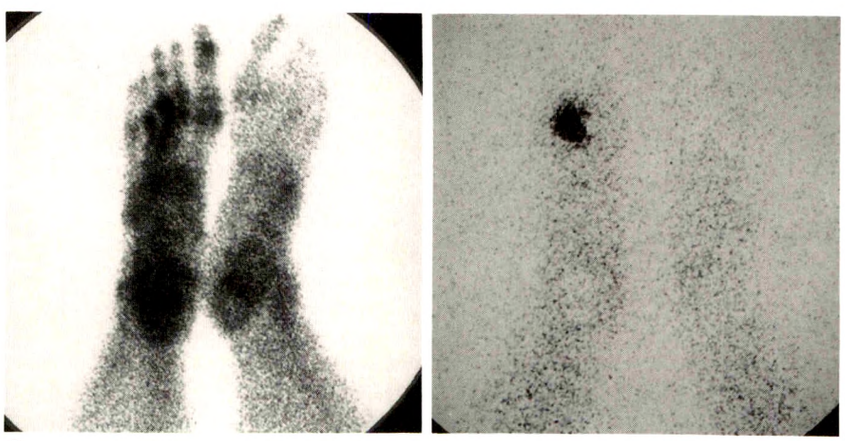
The study group included 31 men and 20 women with a mean age of 62 years (range, 30–88). The majority of patients (n = 49) had diabetes mellitus for at least 12 months; however, the remaining two subjects were diagnosed only 1 month before examination for osteomyelitis. The mean duration of diabetes was 14 years. Thirty-five patients had ulcers adjacent to suspected areas of osteomyelitis. Twenty patients were receiving antibiotics at the time of investigation; treatment in 11 had been discontinued at least 2 days before the ^{111}In-WBC study (mean, 7 days), whereas 20 patients were not started on antibiotics until after the completion of noninvasive tests. The presence or absence of osteomyelitis was established by surgery in 28 patients and by a clinical follow-up of at least 2 months (range, 2–50 months; mean, 26 months) in the rest. Patients who were diagnosed by clinical means were considered not to have osteomyelitis if their signs and symptoms responded to topical therapy and/or a brief (less than 2 weeks) course of antibiotics with no subsequent relapse. Culture of sinus tract specimens was considered indeterminate for osteomyelitis and was not used for diagnosis [3]. Bone cultures or biopsies were obtained only after surgical debridement of soft-tissue ulcers or infection [3].

The ^{111}In-WBC scan was obtained with ^{111}In-oxine according to modification [18] of the method of Thakur et al. [19]. After preparation of the cells, 18 MBq (470 μCi) of labeled leukocytes was reinjected. Images were obtained at 24 hr by using one of a number of large-field-of-view gamma cameras (Siemens 7500 Orbiter, General Electric 400T or 500 Maxi), all equipped with a medium-energy collimator. Multiple views of the feet were acquired for 10 min with symmetric 20% windows placed around the 173- and 247-keV photopeaks of ^{111}In. The three-phase bone scan was conducted after the IV injection of approximately 800 MBq (21 mCi) of ^{99m}Tc-MDP. The dynamic phase was acquired by using consecutive 5-sec/frame images in the plantar or anterior projection in order to visualize optimally the area of interest. Blood-pool and delayed 3-hr scans of both feet were obtained for 500,000 counts, each in multiple projections. All images were obtained by using the same gamma camera equipped with a low-energy all-purpose collimator and a 20% window centered symmetrically over 140 keV.

The ^{111}In-WBC and ^{99m}Tc-MDP scans were usually obtained on the same day (n = 47) and in all cases within 6 days of each other (n = 49). When the tests were performed on the same day, the ^{111}In-WBC scan was acquired before injection of ^{99m}Tc-MDP. Foot radiographs were taken on average within 8 days of these scans (range, 0–58). The mean interval between the radionuclide studies and surgical correlation (when available) was 5 days (range, 0–41).

The radionuclide scans and radiographs were analyzed retrospectively by two experienced observers who had no knowledge of the final diagnosis. Limited clinical information (e.g., site of suspected infection) was made available to the readers. The observers were asked to code studies as positive or negative for osteomyelitis. The ^{111}In-WBC scan was considered abnormal if focal accumulation of radionuclide activity in bone exceeded background radioactivity. Uptake was determined to be in bone or soft tissue by comparison with the bone scan images. The three-phase bone scan was considered indicative of osteomyelitis according to previously described criteria [20]. In brief, focal arterial hyperemia associated with increased uptake of radionuclide by bone on delayed views was considered positive. Osteomyelitis was diagnosed on the basis of radiographs when (1) bone destruction was present alone or in combination with soft-tissue swelling or osteopenia or periosteal reaction, or (2) localized osteopenia or periosteal reaction occurred in the absence of fracture or neuropathic joint disease. The presence of significant neuroarthropathy also was recorded, as this may influence the sensitivity and specificity of ^{111}In-WBC scans.

Finally, two authors reviewed scans in all patients in whom uptake of ^{111}In-WBC and ^{99m}Tc-MDP occurred in identical areas of bone, in order to determine whether the relative uptake could distinguish between infection and "reactive" hyperemia. This was assessed



A B

Fig. 1.—*A*, ^{99m}Tc-MDP scan in plantar projection shows uptake in right third and fourth metatarsophalangeal joints of a 47-year-old insulin-dependent diabetic patient with chronic plantar ulcer.

***B*, Corresponding ^{111}In-WBC scan shows intense activity at this site. Osteomyelitis was confirmed at surgery.**

TABLE 1: Sensitivity and Specificity of ^{111}In-WBC and ^{99m}Tc-MDP Scans and Radiographs in the Diagnosis of Pedal Osteomyelitis in Diabetic Patients

Group/Study	No. of Patients (%)	
	Sensitivity	Specificity
All patients		
^{111}In-WBC	11/14 (79)	29/37 (78)
^{99m}Tc-MDP	13/14 (93)	15/35 (43)
Radiograph	6/14 (43)	29/35 (83)
Neuroarthropathy		
^{111}In-WBC	1/1 (100)	7/10 (70)
^{99m}Tc-MDP	1/1 (100)	2/10 (20)
Radiograph	0/1 (0)	8/10 (80)
Antibiotics		
^{111}In-WBC	4/5 (80)	11/15 (73)
Soft-tissue ulcers		
^{111}In-WBC	11/13 (85)	17/22 (77)

Note.—Sensitivity = true positive/(true positive + false negative); specificity = true negative/(true negative + false positive).

qualitatively by visually comparing for each agent the maximal uptake of radionuclide in diseased bone relative to background radioactivity.

Results

Osteomyelitis of the foot was diagnosed in 14 patients. Eleven of these 14 cases were identified correctly by using ^{111}In-WBC scanning (Fig. 1). In one patient with a false-negative study, uptake of ^{111}In-WBC was noted in the foot but was considered to be in soft tissues. The radiograph and bone scan were also unremarkable in this patient, but at surgery a sinus tract leading to an infected left second metatarsal head was identified. In the other two patients, the bone scan was positive at sites of chronic infection (left ankle and great toe, respectively), whereas the ^{111}In-WBC scans were normal. At surgery, necrotic bone was resected and cultured. In one case, no pathogenic microorganisms were grown; however, histologic examination showed changes consistent with chronic osteomyelitis (Fig. 2).

Of the 37 patients without osteomyelitis, there were 29 true-negative and eight false-positive ^{111}In-WBC studies. Of the latter, surgical correlation was available in five. In three of these, there were soft-tissue microabscesses that on the ^{111}In-WBC scan had been incorrectly ascribed to bone; in the other two cases, no bone or soft-tissue infection was present. The ^{99m}Tc-MDP scan was most sensitive but least specific for osteomyelitis, whereas radiographs were specific but insensitive (Table 1).

Eleven patients had neuropathic joint disease on radiographs. The ^{111}In-WBC scan was both sensitive and relatively specific for osteomyelitis in this group (Fig. 3). However, the ^{99m}Tc-MDP scans and radiographs lacked specificity and sensitivity, respectively. ^{111}In-WBC scintigraphy was also sensitive and specific in patients with soft-tissue ulcers and in those subjects receiving antibiotics during investigation (Table 1).

The results for 13 in whom ^{111}In-WBC and ^{99m}Tc-MDP uptake occurred concordantly in bone were analyzed separately. Uptake of ^{111}In-WBCs was proportionately greater than uptake of ^{99m}Tc-MDP in eight of nine patients in whom osteomyelitis was confirmed (89% sensitivity). However, two of four patients without osteomyelitis also had this feature (50% specificity).

Discussion

Pedal osteomyelitis is a common complication of diabetes, occurring in up to 15% of patients [3]. Early detection reduces the likelihood of chronic osteomyelitis [3]. However, owing to

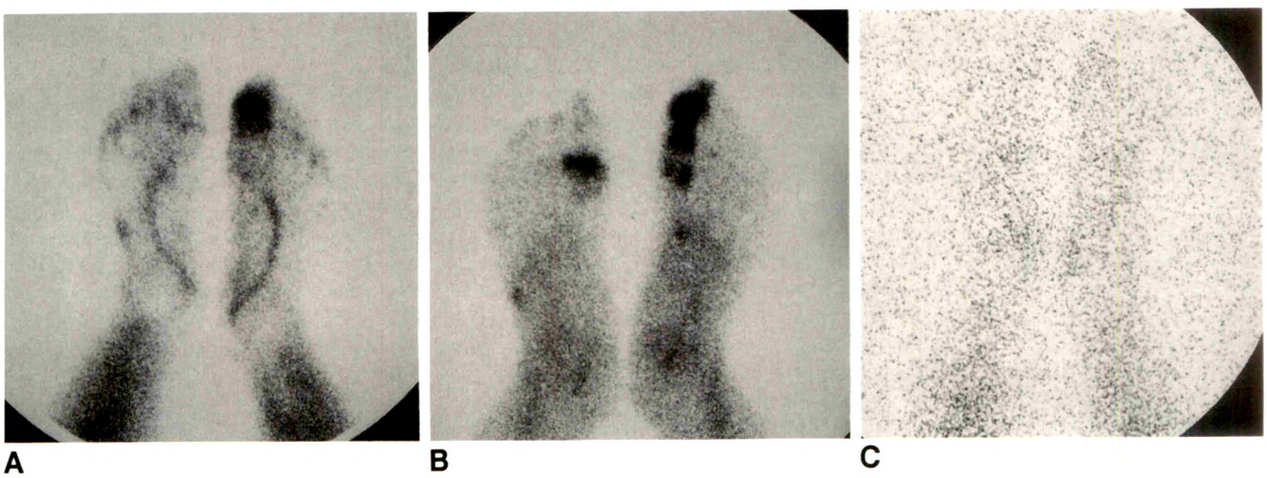
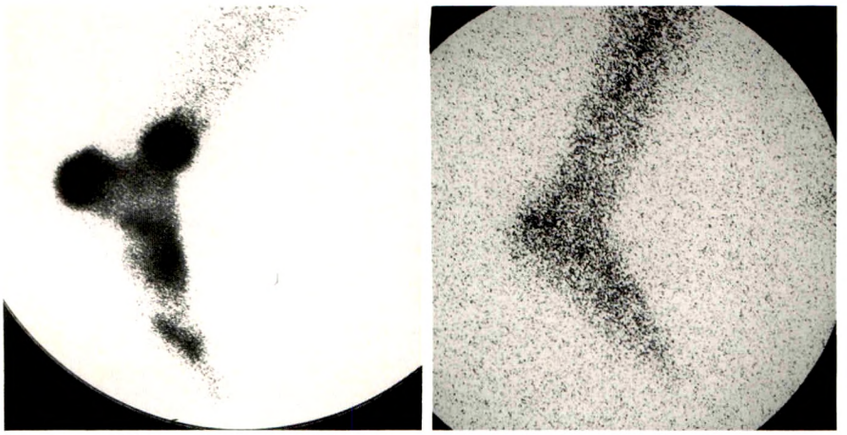


Fig. 2.—65-year-old man with chronic pain and cellulitis of left great toe. Plain radiograph (*not shown*) revealed lytic changes in distal aspect of proximal first phalanx. This was considered indicative of osteomyelitis.

***A* and *B*, ^{99m}Tc-MDP blood pool (*A*) and delayed (*B*) plantar views were interpreted as positive for osteomyelitis.**

***C*, Corresponding ^{111}In-WBC scan shows no abnormality. However, histologic examination of resected necrotic bone showed changes consistent with chronic osteomyelitis, indicating that ^{111}In-WBC scan was falsely negative.**



A B

Fig. 3.—30-year-old woman with insulin-dependent diabetes mellitus and neuroarthropathy had acute pain in right forefoot.

***A*, Right lateral projection of ^{99m}Tc-MDP scan shows intense uptake of radionuclide in several foot joints.**

***B*, Corresponding ^{111}In-WBC scan is unremarkable, suggesting no evidence of infection. The patient responded to conservative therapy and has remained well for more than 4 years, thus confirming true-negative status of ^{111}In-WBC scan.**

superimposed abnormalities such as neuropathic joint disease, trauma, and chronic soft-tissue change, confident diagnosis made on the basis of plain radiographs or ^{99m}Tc-MDP or ^{67}Ga scans is difficult [1, 4, 5]. Our data show that ^{111}In-labeled leukocytes are sensitive and specific for osteomyelitis of the foot. Further, the value of this imaging technique is preserved in patients with neuroarthropathy, patients with soft-tissue ulcers, and those receiving antibiotics during investigation. A small minority have false-negative and false-positive studies, which suggests that a high index of suspicion and prudent use of other noninvasive tests remain essential. The differential uptake of ^{111}In-WBC and ^{99m}Tc-MDP in a small group of patients in our series did not improve specificity further.

The sensitivity of ^{111}In-WBC scintigraphy in our series (79%) was less than that found in previous investigations. Splittgerber et al. [13] reviewed six diabetic patients with neuroarthropathy and/or osteomyelitis and reported a sensitivity of 100%. Two larger series [8, 9] also reported no false-negative ^{111}In-WBC scans. However, the high prevalence of osteomyelitis may have contributed to these results, at least in one study [8]. Incorrect localization of ^{111}In-WBC uptake to soft tissues rather than bone was a factor in one false-negative study in our group. In the other two patients with false-negative ^{111}In-WBC scans, necrotic bone was identified at surgery; avascularity and tissue necrosis may have contributed to reduced sensitivity in these cases, as has been suggested previously [8]. In our study, the gold standard for osteomyelitis in 14 patients was either histologic confirmation of osteomyelitis or the growth of pathogenic microorganisms from bone biopsy specimens or culture material. However, Wheat [3] has emphasized that diabetic neuroarthropathy may be difficult to distinguish histologically from chronic osteomyelitis. Indeed, in one of our false-negative ^{111}In-WBC scans, resected bone was reported to show changes consistent with chronic osteomyelitis, but no microorganisms were grown.

The relative number of false-positive ^{111}In-WBC studies in our series (specificity, 78%) was similar to previous reports. In three of our patients, this occurred because the poor spatial resolution of the ^{111}In-WBC scan made it difficult to distinguish between uptake in bone and adjacent soft tissue, a factor noted by others [8, 9, 12]. Another important cause of false-positive studies in our series was the presence of advanced neuroarthropathy on the radiograph. Of 11 patients with such changes, uptake of ^{111}In-WBC without evidence of infection was demonstrated in three. By contrast, in a recent series of diabetic patients [8], ^{111}In-WBC scintigraphy was 100% specific in eight patients with neuropathic joint disease. Another group [9] also concluded that sites of uninfected neuroarthropathy did not accumulate ^{111}In-WBCs. Early (3- to 4-hr) simultaneous imaging of ^{99m}Tc-MDP and ^{111}In-WBC may contribute to false-positive studies in neuroarthropathy by virtue of "crossover" activity (^{99m}Tc into the lower ^{111}In photopeak) [9]. However, in our series, ^{111}In-WBC scintigraphy was always performed before injection of ^{99m}Tc-MDP. A recent study [15] of 14 patients with Charcot joint associated with peripheral neuropathy showed that progressive neuroarthropathy of recent onset could not be distinguished from osteomyelitis on ^{111}In-WBC scans. The authors postulated that stress fractures at such locations that are occult on radiographs may be the mechanism for uptake of ^{111}In-WBCs. Consequently, we believe that accurate diagnosis of osteomyelitis in patients with neuropathic joint disease requires careful interpretation of the ^{111}In-WBC scan in combination with other imaging techniques. Serial radiographs may serve an important adjunctive role.

Hyperemia and sterile inflammation have also been reported to cause accumulation of ^{111}In-labeled leukocytes [8], a feature that may limit the usefulness of this test. Hyperemia contributes to this phenomenon, presumably because the cell-labeling process involves not only leukocytes but also erythrocytes and platelets [21]. Accordingly, we evaluated the hypothesis that only ^{111}In-WBC uptake proportionately greater than that of ^{99m}Tc-MDP indicated osteomyelitis. Although eight of nine patients with this scintigraphic finding had osteomyelitis (89% sensitivity), two of four patients without osteomyelitis also had a similar pattern (50% specificity). Thus, our preliminary findings suggest that the differential uptake of ^{111}In-WBC and ^{99m}Tc-MDP may not be helpful in discriminating between infection and nonspecific localization

of leukocytes. However, these data were based on visual analysis and, therefore, are inherently limited. Confirmation from others who used a quantitative method may be valuable.

Other factors that potentially may limit ^{111}In-WBC accuracy include antibiotic therapy and coexisting soft-tissue ulcers. In our series, sensitivity and specificity were 80% and 73% (antibiotics) and 85% and 77% (ulcers), respectively. Our experience with antibiotics confirms a previous report [22] indicating that the sensitivity of ^{111}In-WBC scintigraphy was unaffected by such treatment. Osteomyelitis may complicate foot ulcers in 15% of diabetics [3]. Our data, based on a large subset of 35 patients, show that ^{111}In-WBC scans remain valuable in this setting.

Our study had several important limitations. The retrospective evaluation of patients referred for diagnosis and treatment at a tertiary care center contributed to selection bias. Although we are uncertain of the outcome, 25 patients excluded from analysis owing to management elsewhere were less likely to have had osteomyelitis. Nevertheless, the prevalence of osteomyelitis in our series was relatively small (only 14 of 51 patients). Review of scans from patients examined during a period of 5 years introduces a potential for significant discrepancy in image quality. However, our examination protocol and gamma cameras were largely unaltered during this time. Further, although we encountered minor dissimilarities in image quality, no patients were excluded from analysis on the basis of a technically suboptimal study. In routine practice, studies are interpreted in conjunction with one another, and detailed clinical data are often available. Thus, the sensitivity and specificity of ^{111}In-WBC scans in our series may be an underestimation. Also, as the ^{99m}Tc-MDP scan was acquired after the patient had been injected with ^{111}In-WBCs, the 140-keV photopeak of ^{99m}Tc may have included some crossover of activity from the lower-energy peak of ^{111}In. However, data from our laboratory indicate that, owing to a discrepancy in counting rates, this contribution is insignificant (<2% of 500,000 counts acquired in the ^{99m}Tc photopeak are actually due to ^{111}In).

The disadvantages of ^{111}In-WBC scintigraphy include the need for long cell-preparation time (contributing to its expense relative to other radionuclide imaging techniques), low radioactivity administered (poor spatial resolution), and relatively long interval (24 hr) before views are obtained. However, experimentation with imaging at earlier times (3–4 hr) has been discouraging [12]. CT and MR can be performed more rapidly than ^{111}In-WBC scintigraphy. Altered marrow density or signal intensity indicates osteomyelitis, allowing detection at an earlier stage by these techniques [16, 17]. However, other processes such as acute trauma and soft-tissue disease may mimic these changes, thus reducing specificity [3, 17]. Although preliminary data on these alternative imaging techniques have been promising, further studies are required.

In conclusion, ^{111}In-WBC scanning is sensitive and specific in the detection of osteomyelitis of the foot in patients who have diabetes and offers distinct advantages over other currently used techniques. Further, ^{111}In-WBC scintigraphy is useful in patients with neuroarthropathy, soft-tissue ulcers, and antibiotic treatment. However, because of poor counting statistics, ^{111}In-WBC scans should be interpreted cautiously if correlative tests such as ^{99m}Tc-MDP scans and plain radiographs are unavailable.

ACKNOWLEDGMENT

We thank Rose Busta for secretarial support.

REFERENCES

1. Zlatkin MB, Pathria M, Sartoris DJ, Resnick D. The diabetic foot. *Radiol Clin North Am* **1987**;25:1095–1105
2. Zeiger LS, Fox IM. Use of indium-111–labeled white blood cells in the diagnosis of diabetic foot infections. *J Foot Surg* **1990**;29:46–51
3. Wheat J. Diagnostic strategies in osteomyelitis. Am J Med **1985**; 78(6B):218–224
4. Techner LM, Eiser CA, Laine W. Indium-111 imaging in osteomyelitis and neuroarthropathy. *J Am Podiatr Med Assoc* **1986**;76:23–29
5. Eisenberg B, Wrege SS, Altman MI, Moore JW. Bone scan: indium-WBC correlation in the diagnosis of osteomyelitis of the foot. *J Foot Surg* **1989**;28:532–536
6. Hartshorne MF, Peters V. Nuclear medicine applications for the diabetic foot. *Clin Podiatr Med Surg* **1987**;4:361–375
7. Simon WH, Joseph WS. Clinical imaging with indium 111 oxine-labeled leukocyte scan: review and case report. *Clin Podiatr Med Surg* **1988**;5:329–340
8. Keenan AM, Tindel NL, Alavi A. Diagnosis of pedal osteomyelitis in diabetic patients using current scintigraphic techniques. *Arch Intern Med* **1989**;149:2262–2266
9. Schauwecker DS, Park HM, Burt RW, Mock BH, Wellman HN. Combined bone scintigraphy and indium-111 leukocyte scans in neuropathic foot disease. *J Nucl Med* **1988**;29:1651–1655
10. Schauwecker DS. Osteomyelitis: diagnosis with In-111–labeled leukocytes. *Radiology* **1989**;171:141–146
11. McCarthy K, Velchik MG, Alavi A, Mandell GA, Esterhai JL, Goll S. Indium-111–labeled white blood cells in the detection of osteomyelitis complicated by a pre-existing condition. *J Nucl Med* **1988**;29:1015–1021
12. Maurer AH, Millmond SH, Knight LC, et al. Infection in diabetic osteoarthropathy: use of indium-labeled leukocytes for diagnosis. *Radiology* **1986**;161:221–225
13. Splittgerber GF, Spiegelhoff DR, Buggy BP. Combined leukocyte and bone imaging used to evaluate diabetic osteoarthropathy and osteomyelitis. *Clin Nucl Med* **1989**;14:156–160
14. Merkel KD, Brown ML, Dewanjee MK, Fitzgerald RH. Comparison of indium-labeled-leukocyte imaging with sequential technetium-gallium scanning in diagnosis of low-grade musculoskeletal sepsis. *J Bone Joint Surg [Am]* **1985**;67A:465–476
15. Seabold JE, Flickinger FW, Kao SCS, et al. Indium-111–leukocyte/technetium-99m–MDP bone and magnetic resonance imaging: difficulty of diagnosing osteomyelitis in patients with neuropathic osteoarthropathy. *J Nucl Med* **1990**;31:549–556
16. Williamson BRJ, Teates CD, Phillips CD, Croft BY. Computed tomography as a diagnostic aid in diabetic and other problem feet. *Clin Imaging* **1989**;13:159–163
17. Yuh WTC, Corson JD, Baraniewski HM, et al. Osteomyelitis of the foot in diabetic patients: evaluation with plain film, ^{99m}Tc-MDP bone scintigraphy, and MR imaging. *AJR* **1989**;152:795–800
18. Magnuson JE, Brown ML, Hauser MF, Berquist TH, Fitzgerald RH, Klee GG. In-111–labeled leukocyte scintigraphy in suspected orthopedic prosthesis infection: comparison with other imaging modalities. *Radiology* **1988**;168:235–239
19. Thakur ML, Lavender JP, Arnot RN, Silvester DJ, Segal AW. Indium-111–labeled autologous leukocytes in man. *J Nucl Med* **1977**;18:1012–1019
20. Seldin DW, Heiken JP, Feldman F, Alderson PO. Effect of soft-tissue pathology on detection of pedal osteomyelitis in diabetics. *J Nucl Med* **1985**;26:988–993
21. Wahner-Roedler DL. Multifocal skeletal uptake of labeled leukocytes: infection versus tumor metastasis. *J Nucl Med* **1990**;31:1543–1547
22. Datz FL, Thorne DA, Taylor A. Evaluation of factors that could potentially decrease the sensitivity of the In-111–labeled leukocyte scan (abstr). *J Nucl Med* **1986**;27:914–915

Book Review

The Language of Fractures, 2nd ed. By Robert Jordon Schultz. Baltimore: Williams & Wilkins, 333 pp., 1990. $49.95

This text is primarily an introduction to skeletal trauma. The author aims to provide the reader with a logical understanding of the more common orthopedic terminology used to define the routine radiologic features of traumatic lesions of the axial and appendicular skeleton. The text is aimed at both undergraduates and postgraduates. The second edition is divided into four basic chapters: foundation of fracture vocabulary, application of vocabulary to specific regions, fracture eponyms, and fractures that are not fractures.

In the first chapter, the author provides an overview of normal osseous anatomy and embryologic development before methodically discussing the basic biomechanics and classification of bone and joint injuries. Various fundamental descriptors that define the features of these traumatic deformities as seen on radiographs are logically discussed. Numerous examples of routine radiographs are supplemented, where necessary, by line drawings used to provide the reader with an elementary understanding of the pathoanatomy of skeletal injury in adults and in infants and children. The process of normal fracture healing and the complications of osseous union are also briefly mentioned. Fundamental concepts are reemphasized in the spot reviews at the end of each section.

Having established these basic concepts and a common vocabulary, the author then reviews the normal osteoarticular anatomy of each major region of the axial and appendicular skeleton. The more commonly occurring fractures and dislocations of each region are discussed with respect to their mechanism of injury, radiologic appearance, and particular classification. Some of the more common complications are mentioned briefly. Line drawings are often used to accentuate the anatomic and pathologic features.

The third chapter on fracture eponyms is ordered alphabetically and certainly allows ready reference. Radiographs are supplemented with specific descriptions obtained from the original articles, which are referenced alphabetically in the bibliography. However, accurate descriptions of the various injuries are preferable to the use of eponyms.

Chapter 4 covers some of the more common anatomic variants seen on radiographs that can simulate fractures. The present availability of specific more comprehensive atlases of such normal anatomic variants limits the usefulness of this chapter.

Overall, the text has a logical, clear presentation and is easy to read. The numerous radiographs and the many line drawings contribute most to the length of the book. Spot reviews do help emphasize essential concepts. Use of different case material in the pictorial quizzes at the end of the various sections would make the exercises more challenging. In my copy, the quality of some of the reproductions is less than optimal, and one of the figures is upside-down. Two figures are reversed. The legends have a couple of typographic errors. For the novice reader, interpretation of the images is made more difficult by the lack of appropriate figure annotation.

It is impossible for a book of this size to be inclusive. However, only a single paragraph is devoted to postoperative assessments of fractures, and little mention is made of basic orthopedic splints or implants. Terminology used in discussing internal fixation is not adequately addressed. The role of cross-sectional imaging in defining traumatic deformity in complex anatomic regions such as the spine and the pelvis is not mentioned. The bibliography is primarily devoted to chapter 3.

Despite these deficits, the author does succeed in providing a concise basic overview of the fundamentals of skeletal trauma. The reader is clearly instructed on how to appropriately describe the essential features of a skeletal injury as seen on routine radiographs. Therefore, this text should be required reading for all radiology residents. General radiologists may find this book a useful review in basic description, and therefore it should be available in departmental libraries.

Brian A. Howard
University of Toronto, Sunnybrook Medical Centre
Toronto, Ontario, Canada M4N 3M5

Photostimulable Phosphor Digital Radiography of the Extremities: Diagnostic Accuracy Compared with Conventional Radiography

Anthony J. Wilson[1]
F. A. Mann
William A. Murphy, Jr.
Barbara S. Monsees
Margaret R. Linn

A direct comparison was made between digital and conventional radiographs to assess the relative accuracy of a photostimulable phosphor digital imaging system in detecting and localizing minor trauma in the extremities. Matched sets of images were obtained on 103 patients who came to the emergency department for radiographs of the hand, wrist, foot, or ankle. One set was obtained with a conventional screen/film system. The other set was obtained with photostimulable phosphor digital cassettes. The two sets of images of each patient were independently interpreted by three radiologists in a blinded fashion. The findings of each of these three readers were compared with the consensus opinion of two different radiologists. Receiver-operating-characteristic (ROC) curves were plotted for each of the three readers, areas under the curves were calculated, and true-positive fractions were determined at false-positive fractions of 0.1. Although no significant differences in the areas under the ROC curves for the two imaging systems were detected, conventional radiography showed a slight advantage. However, when true-positive fractions for fracture detection were compared at false-positive fractions of 0.1 a statistically significant difference was shown, with conventional screen/film radiography being more sensitive.

This study raises questions about the use of currently available photostimulable phosphor systems for imaging trauma of the extremities and suggests that those systems should not be used exclusively.

AJR 157:533–538, September 1991

Photostimulable phosphor digital radiography (PPDR) was first developed in Japan [1] and has been the subject of a number of technical [1–7] and clinical [7–18] studies. These reports have compared PPDR with conventional screen/film radiography, describing a much greater dynamic range with PPDR, but lower spatial resolution than with conventional radiography. The technique has been in limited use in a variety of settings including emergency departments [7, 8]. Although several authors have studied the efficacy of this technique for chest [9–12], spine [13, 14], breast [15, 16], and abdominal radiography [17, 18], few investigative results have been published regarding musculoskeletal applications of the system [13, 19, 20]. We were concerned that a system, promoted to replace the gold standard of conventional radiography, is being used in clinical settings for which it has not been adequately validated. Before using PPDR for extremity imaging in our own emergency department, we thought that a study was necessary to compare this technique directly with the established standard of conventional radiography.

The purpose of this study was to compare directly the diagnostic accuracy of the PPDR system with our existing conventional screen/film combination for extremity imaging in an emergency department setting. As a wide range of extremity disorders are seen in the emergency department, it seemed appropriate to use cases from the full spectrum of these. The question to be answered was: Is PPDR a satisfactory alternative to conventional radiography, or does the known loss in

Received March 11, 1991; accepted after revision April 29, 1991.

Presented at the annual meeting of the American Roentgen Ray Society, Washington, DC, May 1990.

[1] All authors: Mallinckrodt Institute of Radiology, Washington University School of Medicine, St. Louis, MO 63110. Address reprint requests to A. J. Wilson.

0361–803X/91/1573–0533
© American Roentgen Ray Society

spatial resolution with PPDR have a measurable adverse affect on diagnostic efficacy?

Materials and Methods

Study Design

Observer performance with paired photostimulable phosphor images and with conventional radiographs was compared by using data from three readers. A consensus panel was used to establish the reference standard.

Study Group

Cases for this study were recruited from our urban emergency department (65,000 annual visits). Patients having hand, wrist, foot, and ankle examinations, on weekdays between 8 a.m. and 4 p.m., were offered the opportunity to participate in the study. Patients with life-threatening disorders, pregnant patients, children, and patients with impaired mental status were not studied. The study protocol was approved by our institutional review board.

Image Acquisition

Matched pairs of conventional and PPDR images of the extremities of 103 patients were obtained. After informed consent was obtained, the examination requested by the referring physician was performed with Lanex fine screens and T-Mat G film (Eastman Kodak Company, Rochester, NY). The examination was then repeated by the same technologist by using Philips Computed Radiography (PCR) 8 × 10 in. (20 × 25 cm) cassettes (Philips Medical Systems, Shelton, CT) with the same X-ray tube and generator, the same exposure factors, and the same projections (Fig. 1). The hand, foot, and ankle examinations included three views: frontal, lateral, and oblique. The wrist examinations included four views: posteroanterior, ulnar deviation, lateral, and oblique.

The PCR system installed in our institution produces images on film and has no video display capability. The images produced are printed onto film by using standardized postprocessing parameters selected before imaging. These parameters were changed from those originally supplied by the manufacturer and were optimized for each type of examination in the study. Minimal edge enhancement was used, as excessive enhancement has been shown to decrease detectability of cortical defects [20]. The factors used were designed to make the final images mimic conventional radiographs as closely as possible. The PCR image may be stored on a laser disk for archival purposes and additional postprocessing, but this does not occur automatically. All of the images in this study were stored on disk.

High-definition 8 × 10 in. PCR cassettes were selected because these have higher spatial resolution than the larger PCR cassettes [5]. The 8 × 10 cassettes also present the viewer with a single full-sized image on film, whereas the larger sizes (10 × 12, 14 × 14, 14 × 17) produce two reduced-size images per film, one of which usually has a high degree of digital edge enhancement. The option of two images on the film is not available for 8 × 10 cassettes. Thus the 8 × 10 cassettes produce images much closer in appearance to conventional film than do the other cassette sizes. PPDR images obtained on 8 × 10 cassettes have a 2510 × 2000 matrix, producing a pixel size of 0.1 mm and spatial resolution of 5 line pairs per millimeter (lp/mm) [5]. This is clearly less than the resolution of 14 lp/mm claimed by the manufacturer for the screen/film system used in this study [Kodak, personal communication].

Reference Standard

As the study group consisted of patients in the emergency department for whom reliable follow-up was difficult to obtain, and because there was no other logical gold standard for diagnosis, the radiologic "truth" was established from the images alone. To establish truth, two experienced musculoskeletal radiologists performed a pilot study. Initially, each set of images was studied alone, then the conventional and digital image sets were studied together, and finally a consensus was achieved between the two radiologists by discussion of differences of opinion. Although focusing on minor trauma, this truth included 14 separate categories of positive findings (Table 1). Arthritic alterations were further subdivided into cartilage loss, erosions, osteophytes, and other arthritic changes.

Image Evaluation

Three other radiologists then interpreted each set of images, without access to clinical information. The experience level and

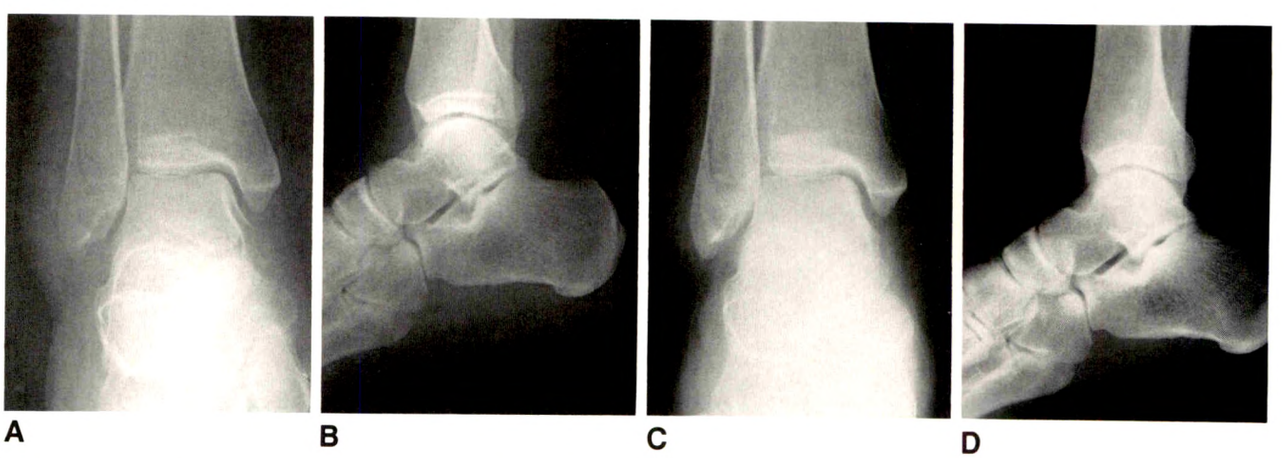


Fig. 1.—Computed (*A*, *B*) and conventional (*C*, *D*) radiographs of an ankle showing lateral and posterior malleolar fractures with soft-tissue swelling laterally. Although fractures are readily visible on both sets of radiographs, increased dynamic range of computed images makes both soft tissues and densest bony areas easier to see.

TABLE 1: Range and Number of Abnormalities Recorded

Type of Abnormality	No. of Cases
Fractures	31
Arthritic changes	28
Soft-tissue swelling	28
Nonarticular bony spurs	14
Generalized osteopenia	12
Dislocations	6
Vascular calcifications	5
Lacerations/ulcerations	5
Foreign bodies	4
Tumors	2
Arthrodeses	2
Amputations	2
Medullary infarct	1
Total	140

subspecialty expertise of the three readers varied: One was an experienced musculoskeletal radiologist, one an experienced general radiologist, and one a musculoskeletal fellow less than 6 months after completion of residency. A separate data sheet was provided for each reader for each set of images (206 sheets per reader). The data sheet required a positive response to each of the radiographic features (Table 1) using a five-point confidence score (1 = definitely normal, 2 = probably normal, 3 = possibly abnormal, 4 = probably abnormal, 5 = definitely abnormal). The location of each finding was recorded with free text.

The digital and conventional examinations of each case were presented at four separate sittings in a 2-month period, with digital and conventional examinations mixed in equal quantities during each reading session. The digital and conventional examinations of each case were presented at different times. All conventional and digital images were presented on film. Each reader had access to only one copy of each digital image and did not have the opportunity to alter window level and width or to perform any other postprocessing. Finally, to estimate intrareader variance, each of the three radiologists was asked to look at 30 of the examinations a second time, several weeks after the initial readings. These 30 examinations were randomly selected; 15 were conventional radiographs and 15 were PCR images.

Statistical Methods

Statistical data were generated and comparisons made, for each reader, for fractures (n = 31) and for the combined data of all of the 14 findings listed in Table 1 (n = 140). Receiver-operating-characteristic (ROC) curves (Figs. 2 and 3) for the performance of each reader with conventional radiography and PPDR were generated from the confidence scores by using a personal computer–based program (CORROC 2, Metz et al., University of Chicago, Chicago, IL). Comparisons of true-positive fractions (TPF) at a false-positive fraction (FPF) of 0.10 for each reader were tested for significance, using critical ratios (Table 2) [21]. The value of 0.10 was chosen for the FPF because it reflects the reported utility in routine diagnostic settings [22].

Results

Of the 103 matched pairs of images, there were 26 feet, 25 ankles, 25 hands, 14 fingers, and 13 wrists. There were 50 women and 53 men, from 19 to 85 years old, with a mean age of 40 years.

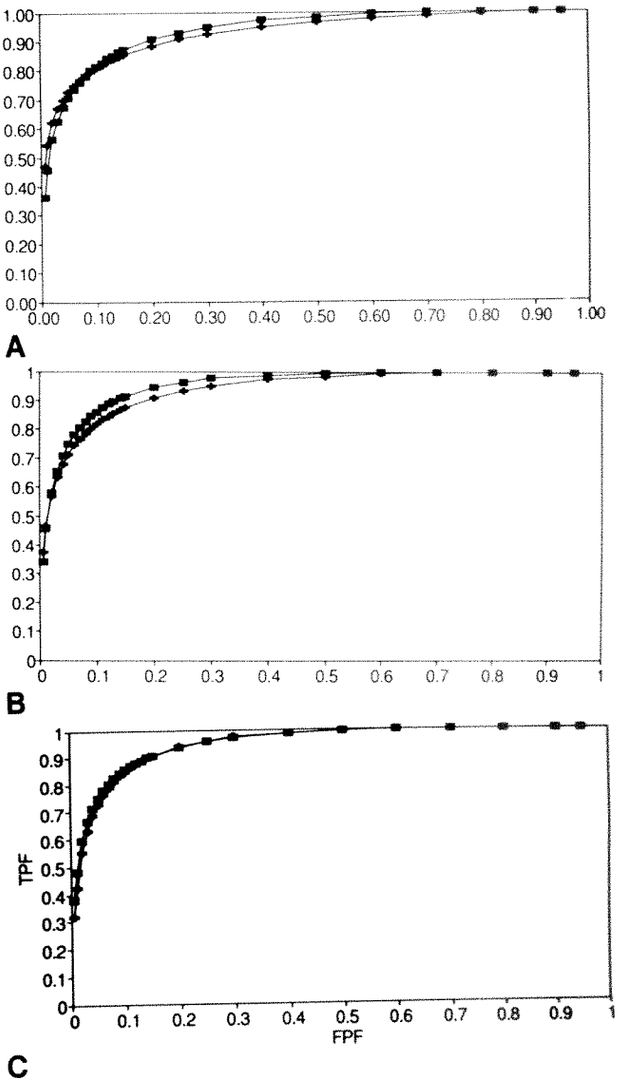


Fig. 2.—Receiver-operating-characteristic curves for combined data for reader 1 (*A*), reader 2 (*B*), and reader 3 (*C*). Shaded boxes = plain film, black crosses = digital radiograph.

The ROC curves plotted for the combined categories (Fig. 2) yielded an area under each curve (A_z) as shown in Table 3. No significant difference in A_z was shown for any of the readers. These curves were closely matched for all three readers. The ROC curves derived for fractures alone (Fig. 3) yielded A_z values as listed in Table 3. Again no significant difference was found between the paired A_z values. Despite a lack of any statistical difference, the curves show conventional radiography to have a better overall performance than PPDR had for all readers for both fractures and combined data.

Using the methods of Hanley and McNeil [23, 24], we compared A_zs between each observer's readings of the first and last 20 cases, and we found almost no difference for readers 1 and 2, but a moderate reduction for reader 3. Thus, no evidence exists of either learning effect or case maldistribution. Similarly, comparison between the first and second

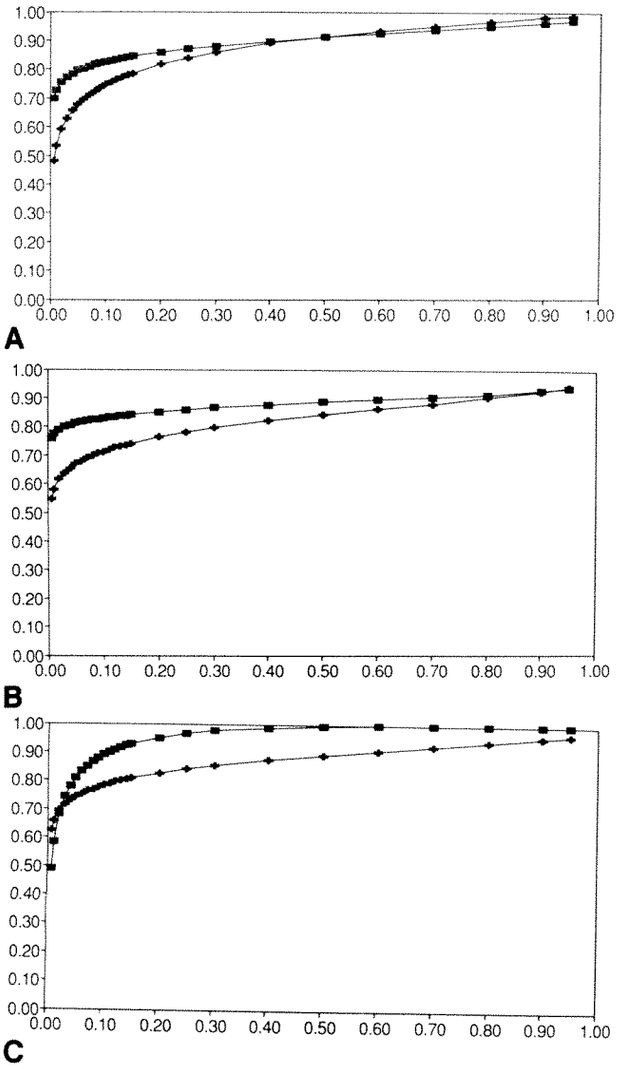


Fig. 3.—Receiver-operating-characteristic curves for fractures for reader 1 (*A*), reader 2 (*B*), and reader 3 (*C*). Shaded boxes = plain film, black crosses = digital radiograph.

TABLE 2: True-Positive Fractions at False-Positive Fraction of 0.10

	Reader No. 1	Reader No. 2	Reader No. 3
Combined data			
Film/screen radiographs	0.8145	0.8610	0.8560
Computed radiographs	0.8084	0.8177	0.8503
Fractures			
Film/screen radiographs	0.8256	0.8330	0.8899
Computed radiographs	0.7457	0.7123	0.7829

readings of the 30 randomly selected cases showed no difference for reader 1, a moderate difference for reader 2, and a marked difference for reader 3. It should be noted that reader 3 was also the least experienced radiologist. The magnitude of the intrareader differences for readers 2 and 3 was greater than their intertechnique differences. This weakens our ability to recognize small, but real, differences between techniques in this study.

TABLE 3: Areas Under Receiver-Operating-Characteristic Curves

	Reader No. 1	Reader No. 2	Reader No. 3
Combined data			
Film/screen radiographs	0.9374	0.9534	0.9517
Computed radiographs	0.9281	0.9382	0.9504
	(p = .6079)	(p = .5121)	(p = .9352)
Fractures			
Film/screen radiographs	0.9004	0.8810	0.9618
Computed radiographs	0.8842	0.8280	0.8788
	(p = .8085)	(p = .6063)	(p = .2062)

As the shapes of the ROC curves for PPDR and SFR differ (i.e., all but one of the ROC curves cross; Figs. 2 and 3), we thought a direct comparison of TPFs at FPF 0.10 (Table 2) would be a more meaningful method of assessment than A_zs [21]. Although these showed no significant difference for the combined categories ($p > .5$), a significant difference was shown for fractures for all readers ($p = .04$, 95% confidence interval, TPF = 0.722 to 0.772).

Discussion

Our study shows PPDR in acute minor trauma to be less accurate than is conventional screen/film radiography. Although this difference is statistically significant, we doubt that it has major clinical significance. Close cooperation between clinician and radiologist, careful clinical examination, and the selective use of conventional radiographs in appropriate patients should result in reliable detection of subtle fractures when PPDR is used as the primary imaging technique.

We failed to show a statistically significant difference between the two techniques, using ROC curves and comparing A_z values. However, when looking only at FPFs of 0.10, we see a significant difference for fracture detection, with conventional radiography being superior. We believe that the latter method is the better method when applied to these data [21].

This study has several strengths: The study cases were all paired, which is an efficient experimental method to detect small, but real, differences in diagnostic accuracy. The range of abnormalities seen represents an important and common disease spectrum. The readers, while all competent radiologists, had a range of skill levels representative of those found among subspecialists and general radiologists. Finally, the image parameters used for the PPDR images were optimized for the different anatomic areas studied.

On the other hand, the study has at least two weaknesses: We demonstrated a large intrareader variance and we used the images themselves to establish "radiographic truth," in the absence of any better gold standard. Both of these shortcomings should decrease the sensitivity of this study to small differences between the two imaging techniques. As we believe that the clinical impact of our demonstrated difference between PPDR and conventional radiography is small,

and that it can be compensated for during clinical practice, we do not believe that these weaknesses are critical.

The potential advantages of PPDR over conventional radiography have been reported by others [1–18] and include: greater dynamic range than film, ability to correct for exposure errors with a resultant decreased rate of repeated examinations, ability to apply postprocessing algorithms (such as edge enhancement), and ability to transmit images almost instantaneously to remote viewing areas. The major disadvantage of PPDR is a measurable loss of spatial resolution as compared with standard radiography extremity systems. Evaluation of the spatial resolution requirements for musculoskeletal imaging by using conventional radiographs that have been optically digitized has suggested that some fine detail may be lost at matrix sizes similar to the size used by the current PPDR systems (2510 × 2000) [25–27].

PPDR images have a potential advantage over digitized conventional radiographs. The latter cannot present any data that were not on the original conventional film. On the other hand, an image that was initially acquired by a digital system may indeed contain data that could not be captured on a single exposure by the lower dynamic range of the screen/film system or data that may have been lost through incorrect exposure. For example, two conventional radiographs of a hand may be necessary to reveal soft-tissue detail in the fingertips and bony detail in the distal radius, whereas both anatomic areas can be displayed on the same digital image (Fig. 4). It is therefore possible that a PPDR image may present data to the reader that are simply not present on a conventional radiograph obtained under similar conditions. Conversely, the digital image may contain less data, as a result of the decreased spatial resolution, electronic noise, or data manipulation after imaging.

Previous studies, using digitized conventional films [25–27], have suggested that a pixel size smaller than 0.2 mm is necessary for detection of fine bone detail on digital radiographs. The PCR 8 × 10 cassettes achieve a pixel size of 0.1 mm, but this resolution is still inferior to that achieved with conventional screen/film systems in current use. Our intent was to test the diagnostic efficacy of a method of direct digital acquisition in a demanding clinical setting and to determine whether or not the lesser spatial resolution of the system, as compared with conventional screen/film radiography, was an obvious handicap. We believe that the case mix obtained in this study is representative of the extremity cases in our emergency department during an average week, and should therefore have provided a realistic test.

As a significant difference in fracture detection was shown for all readers at 0.10 FPF, there may indeed be a clinically significant difference between PPDR and conventional radiography. Further, a semiquantitative review of the literature has revealed that, although statistically significant differences have not been shown between the two imaging methods, conventional radiography generally outperforms PPDR. We have failed to show that PPDR is equal to traditional film/screen systems and feel that if PPDR is used as the primary imaging method for acute trauma to the extremities, conventional radiography should still be available.

More extensive testing with larger groups of patients with more focused ranges of examinations and abnormalities is necessary to evaluate more completely the effectiveness of this technique for extremity imaging. Particular attention must be paid to the detection of subtle fractures. We are concerned that the spatial resolution of currently available photostimulable phosphor systems may be insufficient for such systems to completely replace state-of-the-art film/screen radiography.

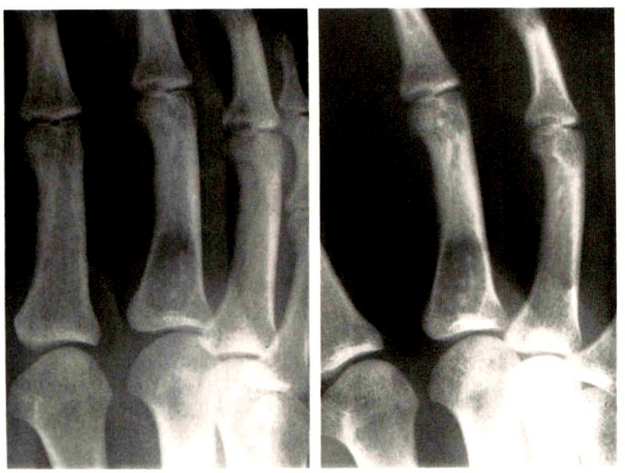


Fig. 4.—*A* and *B*, Computed (*A*) and conventional (*B*) radiographs of an enchondroma in a proximal phalanx. Although both images show tumor well, soft tissues are more visible on computed radiograph.

REFERENCES

1. Sonoda M, Takano M, Miyahara J, Kato H. Computed radiography utilizing scanning laser stimulated luminescence. *Radiology* **1983**;148:833–838
2. Kato H, Miyahara J, Takano M. New computed radiography using scanning laser stimulated luminescence. *Neurosurg Rev* **1985**;8:53–62
3. Higashida Y, Moribe N, Hirata Y, et al. Computed radiography utilizing laser-stimulated luminescence: detectability of simulated low-contrast radiographic objects. *Comput Med Imaging Graph* **1988**;12:137–145
4. Fuhrman CR, Gur D, Schaetzing R. High-resolution digital imaging with storage phosphors. *J Thorac Imaging* **1990**;5:21–30
5. Blume H. PCR technical review. Shelton CT: Philips Medical Systems, Issue #1; April **1989**:1–14
6. Sherrier RH, Chotas GH, Johnson GA, Chiles C, Ravin CE. Image optimization in a computed-radiography/photostimulable-phosphor system. *J Digital Imaging* **1989**;2:212–219
7. Hillman BJ, Fajardo LL. Clinical assessment of phosphor-plate computed radiography: equipment strategy and methods. *J Digital Imaging* **1989**;2:220–227
8. Kangarloo H, Capek P, Barbaric Z, et al. Two-year clinical experience with a computed radiography system. *AJR* **1988**;151:605–608
9. Kogutt MS, Jones JP, Perkins DP. Low-dose digital computed radiography in pediatric chest imaging. *AJR* **1988**;151:775–779
10. Margin SI, Rowberg AH, Godwin JD. Preliminary experience with portable digital imaging for intensive care radiography. *J Thorac Imag* **1990**;5:49–54
11. Schaefer CM, Greene R, Oestmann JW, et al. Digital storage phosphor imaging versus conventional film radiography in CT-documented chest disease. *Radiology* **1990**;174:207–210
12. Schaeffer CM, Greene R, Hall DA, et al. Mediastinal abnormalities: detection with storage phosphor digital radiography. *Radiology* **1991**;178:169–173
13. Pettersson H, Aspelin P, Bousen E, Herrlin K, Egund N. Digital radiography

of the spine, large bones and joints using stimulable phosphor. *Acta Radiol* **1988**;29:267–271
14. Yang PJ, Seeley GW, Carmody RF, Seeger JF, Yoshino MT, Mockbee B. Conventional vs computed radiography: evaluation of myelography. *AJNR* **1988**;9:165–168
15. Chan HP, Vyborny CJ, MacMahon H, Metz CE, Doi K, Sickles EA. Digital mammography ROC studies of the effects of pixel size and unsharp-mask filtering on the detection of subtle microcalcifications. *Invest Radiol* **1987**;22:581–589
16. Oestmann JW, Kopans D, Hall DA, McCarthy KA, Rubens JR, Greene R. A comparison of digitized storage phosphors and conventional mammography in the detection of malignant microcalcifications. *Invest Radiol* **1988**;23:725–728
17. Aspelin P, Petterson H, Bousen E. Digital radiography using laser stimulated luminescence for evaluation of urinary calcifications. *Acta Radiol* **1988**;29:277–284
18. Lee KR, Chang J, Murphey MD, et al. Computed radiographic imaging in pediatric examinations. *Appl Radiol* **1990**;19:27–34
19. Nakano Y, Hiraoka T, Togashi K, et al. Direct radiographic magnification with computed radiography. *AJR* **1987**;148:569–573
20. Prokop M, Galanski M, Oestmann JW, et al. Storage phosphor versus screen-film radiography: effect of varying exposure factors and unsharp mask filtering on the detectability of cortical bone defects. *Radiology* **1990**;177:109–113
21. Swets JA, Picket RM. *Evaluation of diagnostic systems*. New York: Academic Press, **1982**:38–39
22. Swets JA, Swets JB. ROC approach to cost-benefit analysis. *Proceedings of sixth conference on computer applications in radiology*. New York: IEEE, **1979**:203–206
23. Hanley JA, McNeil BJ. The meaning and use of the area under a receiver operating characteristic (ROC) curve. *Radiology* **1982**;143:29–36
24. Hanley JA, McNeil BJ. A method of comparing the areas under receiver operating characteristic curves derived from the same cases. *Radiology* **1983**;148:839–843
25. Murphey MD. Digital skeletal radiography: spatial resolution requirements for detection of subperiosteal resorption. *AJR* **1989**;152:541–546
26. Murphey MD, Bramble JM, Cook LT, Martin NL, Dwyer SJ. Nondisplaced fractures: spatial resolution requirements for detection with digital skeletal imaging. *Radiology* **1990**;174:865–870
27. Wegryn SA Piraino DW, Richmond BJ, et al. Comparison of digital and conventional musculoskeletal radiography: an observer performance study. *Radiology* **1990**;175:225–228

Radiology Outreach Foundation

The Radiology Outreach Foundation (ROF) is a nonprofit corporation whose goal is to help disadvantaged countries improve their health care by providing radiology equipment, books, consultation, education, and training to their practitioners. This assistance is on an application basis that is independent of political, ethnic, or religious orientation of the grantee. It depends on the need of the people and the ability of the ROF to meet that need. The ROF is approved by the U.S. Internal Revenue Service as a tax-exempt organization. It is endorsed by the following radiologic societies: American Association of Women Radiologists, American College of Radiology, American Roentgen Ray Society, Association of University Radiologists, Radiological Society of North America, Society of Chairmen of Academic Radiology Departments, Society for Pediatric Radiology, European Society of Pediatric Radiology.

All donations to the ROF are tax deductible. Persons who would like to contribute financially to the ROF, would be interested in being a visiting professor, would like to send books or journals to any of the institutions supported by the ROF, or would like further information about the ROF should write to Charles A. Gooding, M.D., President, Radiology Outreach Foundation, 3415 Sacramento St., San Francisco, CA 94118 USA.

Diagnosis of Acute Pyelonephritis in Children: Comparison of Sonography and ^{99m}Tc-DMSA Scintigraphy

Eythor Björgvinsson[1,2]
Massoud Majd[1]
Kathleen Dunne Eggli[1,3]

Ninety-one children 1 week to 10 years old with culture-documented febrile urinary tract infection were evaluated with renal sonography and renal cortical scintigraphy by using ^{99m}Tc-labeled dimercaptosuccinic acid (DMSA). On the basis of previous experimental studies, DMSA scintigraphy was used as the standard of reference for the diagnosis of acute pyelonephritis. The DMSA scans showed changes consistent with acute pyelonephritis in 63% (57/91) of the patients. Sonograms showed changes consistent with acute pyelonephritis in 24% (22/91) of the whole group and in only 39% (22/57) of the patients with scintigraphically documented acute pyelonephritis. Pertinent sonographic findings were areas of increased cortical echogenicity in 14 patients and decreased echogenicity in eight, including three patients with renal abscesses. Dilatation of the renal collecting system was noted in nine patients and renal enlargement was noted in three.

We conclude that renal sonography is a relatively insensitive test for the detection of acute inflammatory changes of renal cortex. Therefore, it should not be used as the primary imaging technique for the diagnosis of acute pyelonephritis. However, sonography is a useful technique in evaluating the nature of the defects seen on the DMSA scan and in detecting obstructive uropathies that may be associated with urinary tract infections.

AJR 157:539–543, September 1991

Sonography has been evaluated as one of the imaging techniques for differentiating acute pyelonephritis from lower urinary tract infection (UTI). In these studies, clinical and laboratory variables have been used as the standard of reference [1–3]. Recent clinical studies have shown that the diagnosis of acute pyelonephritis in children based on these commonly used clinical and laboratory parameters is unreliable [4, 5]. Experimental animal studies have shown that renal cortical scintigraphy with ^{99m}Tc-labeled dimercaptosuccinic acid (DMSA) is very sensitive and reliable for the detection and localization of acute pyelonephritis [6, 7]. The purpose of this study was to evaluate the accuracy of sonography in the diagnosis of acute pyelonephritis by using ^{99m}Tc-DMSA scintigraphy as the standard of reference.

Subjects and Methods

This is a combined prospective study from Children's Hospital of Washington, DC, and Landakot's Hospital of Reykjavík, Iceland. All patients with culture-documented febrile UTI who were hospitalized at Children's Hospital from August 1985 to January 1986 or at Landakot's Hospital from June 1989 to June 1990 and were referred to us for imaging workup were included in the study. The criteria for positive urine culture were growth of a single organism with a colony count of more than 10^5 colony-forming units/ml on a clean catch specimen or more than 10^4 colony-forming units/ml on a specimen obtained by catheterization or suprapubic aspiration.

The renal sonograms and DMSA scans were obtained within 72 hr of admission. The renal

Received November 9, 1990; accepted after revision April 22, 1991.

[1] Department of Diagnostic Imaging and Radiology, Children's National Medical Center, 111 Michigan Ave., N.W., Washington, DC 20010-2970. Address reprint requests to M. Majd.

[2] Present address: Department of Radiology, Landakot Hospital, 101 Reykjavík, Iceland.

[3] Present address: Department of Radiology, Milton S. Hershey Medical Center, 500 University Dr., Hershey, PA 17033.

0361–803X/91/1573–0539
© American Roentgen Ray Society

cortical scans were obtained 2–3 hr after an IV injection of ^{99m}Tc-DMSA in a dose of 50 μCi (1.85 MBq)/kg (minimum, 300 μCi [11.10 MBq]). High-resolution, magnified images of the kidneys in posterior and posterior oblique projections were obtained routinely by using a gamma camera equipped with a pinhole collimator. The sonographic examinations were performed on computerized sonographic units equipped with 3.5- and 5.0-MHz transducers. The renal sonograms were interpreted without the knowledge of the DMSA scan findings.

The criteria for the diagnosis of acute pyelonephritis by DMSA scintigraphy were the presence of one or more areas of decreased cortical uptake with preservation of renal outline, even if faint. The criteria for the diagnosis of acute pyelonephritis by sonography were the presence of one or more areas of increased or decreased cortical echogenicity and/or loss of corticomedullary differentiation, with or without focal or diffuse renal enlargement.

Voiding cystography was also performed in 87 cases. The cystograms in the Washington, DC, study (21 cases) were obtained before the patients were discharged from the hospital, and in the Reykjavík study, 4–6 weeks after the treatment of acute infection.

Results

The population of patients consisted of 91 children, 22 in Washington (14 black and eight white) and 69 in Reykjavík (all white). There were 62 girls and 29 boys 1 week to 10 years old (mean, 2.7 years; median, 1.5 years). The organisms isolated from the urine cultures were *Escherichia coli* in 89, *Staphylococcus* in one and *Salmonella* in one.

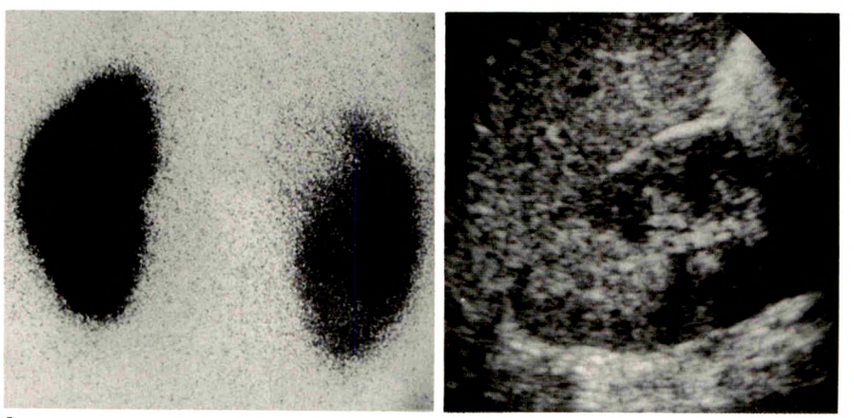
The DMSA scan showed changes consistent with acute pyelonephritis in 63% (57/91) of the patients (Reykjavík, 64%; Washington, DC, 59%). The involvement was unilateral in 43 and bilateral in 14 patients. The lesions were unifocal in 32 patients and multifocal in 25. Vesicoureteral reflux was noted in 34% (30/87) of the whole group (Reykjavík, 33%; Washington, DC, 38%), but in 45% (25/55) of the patients with DMSA scintigraphic findings of acute pyelonephritis (Reykjavík, 44%; Washington, DC, 50%). Five children with vesicoureteral reflux had normal DMSA scans. In the Washington, DC, study, reflux was seen in 29% (4/14) of black and in 57% (4/7) of white children.

Sonographic changes consistent with acute pyelonephritis were seen in 24% (22/91) of the entire group (Reykjavík, 24%; Washington, DC, 23%) and in only 39% (22/57) (Reykjavík, 39%; Washington, DC, 38%) of the patients with scintigraphically documented acute pyelonephritis. The abnormalities were unilateral in 20 patients and bilateral in two; they were unifocal in 15 and multifocal in seven. The sonograms showed one or more areas of increased cortical echogenicity (Fig. 1) in 14 patients and decreased echogenicity in eight, including three with renal abscesses (Fig. 2). Diffuse renal enlargement was seen in three patients with abnormal cortical echogenicity. Dilatation of the collecting system was noted in nine patients, all of whom had DMSA scintigraphic evidence of acute pyelonephritis. However, only five of them had abnormal cortical echogenicity on sonography. Therefore, abnormal sonographic findings (changes of acute pyelonephritis and/or dilatation of the renal collection system) were found in 46% of the patients with scintigraphically documented pyelonephritis. Six of nine patients with sonographic findings of dilatation of the renal collecting system had vesicoureteral reflux. The remaining three patients, including one patient with obstruction of the ureteropelvic junction, had no evidence of reflux.

Discussion

UTI may be limited to the bladder (cystitis) or upper collecting systems (ureteritis, pyelitis), or may involve the renal parenchyma (pyelonephritis). Acute pyelonephritis is a major cause of morbidity in children with UTI and can result in irreversible renal scarring. Well-recognized late sequelae of pyelonephritic scarring include hypertension, hyposthenuria, proteinuria, and chronic renal failure [8, 9]. Clinical and experimental studies have demonstrated that renal scarring can be prevented or diminished by early diagnosis and aggressive treatment of acute pyelonephritis [10–12]. Therefore, accurate diagnosis of acute pyelonephritis has significant clinical relevance.

The differentiation of acute pyelonephritis from lower UTI based on classic clinical and laboratory findings may be difficult, especially in children [4, 5, 13]. Various laboratory techniques, including measurements of serum levels of C-reactive protein, urinary beta$_2$-microglobulin excretion, anti-



A B

Fig. 1.—Acute pyelonephritis involving upper pole of right kidney in a 6-year-old girl with 3-day history of fever and flank pain.

***A*, Posterior view of ^{99m}Tc-DMSA scan shows large area of decreased cortical uptake in upper pole of right kidney.**

***B*, Longitudinal sonogram of right kidney shows triangular area of increased echogenicity corresponding to area of decreased cortical uptake on DMSA scan.**

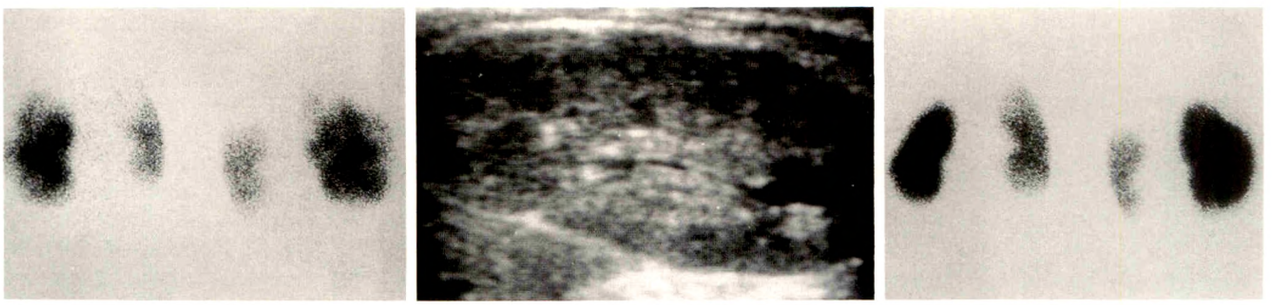


Fig. 2.—Multifocal bilateral pyelonephritis in a 3-month-old boy with a 6-week history of intermittent fever.
***A*, Magnified posterior oblique ^{99m}Tc-DMSA images of kidneys show bilateral cortical defects more severe on right side.**
***B*, Longitudinal sonogram of right kidney selected from a series of longitudinal and transverse sonograms of both kidneys shows no abnormal echogenicity in region of cortical defects. Sonograms of left kidney (*not shown*) were also normal.**
***C*, Follow-up ^{99m}Tc-DMSA scan obtained 5 months later shows complete resolution of cortical defects on left side and evidence of cortical scarring of upper and lower poles on right side.**

body-coated bacteria in the urine sediment, and urinary lactic dehydrogenase levels, have been reported. For a variety of reasons, including unreliability and/or nonavailability, these have not gained widespread acceptance for the evaluation of children with acute UTI [14]. Split-ureteral catheterization or bladder washout studies may accurately localize infection to the upper or lower urinary tract, but they are invasive. Furthermore, none of these techniques provide any information regarding renal function or extent of parenchymal involvement during acute pyelonephritis.

Several imaging techniques been evaluated as a means of differentiating acute pyelonephritis from lower UTI. Excretory urography has a very low sensitivity for the diagnosis of acute pyelonephritis. CT is probably a sensitive and effective technique for documenting the nature and extent of parenchymal involvement, and particularly for the evaluation of the perinephric space. However, its routine use in the evaluation of children with UTI is not practical [2, 15]. Radionuclide imaging procedures that use ^{67}Ga-citrate or ^{111}In-labeled leukocytes may be very reliable in the diagnosis of acute pyelonephritis [16, 17]. These imaging procedures, however, result in a high dose of absorbed radiation, require 24–48 hr to perform, and more importantly do not provide any information about the function and morphology of the kidneys. Therefore, they are poorly suited for routine use in the evaluation of children with febrile UTI. The role of MR imaging in the diagnosis of acute pyelonephritis is unclear [18]. Recent clinical studies have shown renal cortical scintigraphy with ^{99m}Tc-labeled glucoheptonate or DMSA to be significantly more sensitive than excretory urography and renal sonography in the detection of renal parenchymal involvement [3, 19, 20]. In these clinical reports, the various imaging techniques have been retrospectively compared with clinical signs and symptoms and routine laboratory studies. However, these same clinical signs and symptoms have been shown to have poor correlation to direct localization studies, such as the bladder washout test [13].

To our knowledge, the only imaging technique that has been evaluated in experimentally induced acute pyelonephritis in an animal model is ^{99m}Tc-DMSA renal cortical scintigraphy [6, 7]. In one study, unilateral vesicoureteral reflux of infected urine was surgically induced in 22 piglets. DMSA scans were obtained at 1 week (in nine piglets) or 2 weeks (13 piglets) after the introduction of bacteria into the bladder. Subsequently the piglets were sacrificed and the kidneys were examined for histopathologic evidence of acute pyelonephritis. The location and extent of pyelonephritic lesions found on histopathologic examination were compared with DMSA findings in a blinded fashion. Of the 22 kidneys subjected to vesicoureteral reflux of infected urine, 15 had histopathologic evidence of acute pyelonephritis. DMSA scans showed scintigraphic evidence of acute pyelonephritis in 13 of 15 kidneys (sensitivity, 87%). The two kidneys in which inflammation was not detected on the scans had only minimal microscopic foci of inflammatory cells and were grossly normal. There were no false-positive scans in any of the 22 experimental kidneys (specificity, 100%). There was an overall 94% agreement between the DMSA scan and histopathologic findings for the detection of individual lesions [6]. Thus, DMSA renal cortical scintigraphy is a highly sensitive and reliable technique for the detection and localization of experimental acute pyelonephritis. Therefore, at present, DMSA scanning appears to be the best clinically applicable standard of reference for the diagnosis of acute pyelonephritis and for the evaluation of the sensitivity and specificity of other imaging techniques.

^{99m}Tc-DMSA is an excellent renal cortical imaging agent. About 60% of the administered dose is tightly bound to the proximal tubular cells, and only a small amount is slowly excreted in the urine. DMSA allows visualization of renal parenchyma without interference from retained tracer in the collecting systems. ^{99m}Tc-glucoheptonate is cleared by both glomerular filtration and cortical fixation. About 20% of the administered dose is firmly bound to the tubular cells. Therefore, delayed imaging provides visualization of the renal cortex similar to that of DMSA images. Most of the administered dose is excreted in the urine, allowing moderately good visualization of the renal collecting systems. This additional information provided by glucoheptonate makes it the agent preferred by some. However, the status of the collecting systems is best evaluated on the renal sonogram, which is usually obtained in conjunction with the renal scan. There is

often some hepatobiliary excretion of glucoheptonate, particularly in infants. Tracer in the gallbladder or small bowel may superimpose on the right kidney. Concerns have been expressed regarding a higher absorbed dose of radiation with DMSA. It is true that the radiation to the cortex of the kidneys is three times higher with DMSA as compared with glucoheptonate, but this is due to cortical fixation of a larger fraction of DMSA. Therefore, the administered dose of DMSA can be one third that of glucoheptonate. With this adjustment in the administered dose, total DMSA retained in the kidney and resultant renal radiation doses are equal to those of glucoheptonate, but owing to the accumulation of a smaller amount of DMSA in the bladder, the gonadal radiation dose is significantly less. Therefore, we prefer to use DMSA, particularly in infants and young children.

Changes consistent with acute pyelonephritis were seen on the DMSA cortical scan in 63% of children in our study group. This is in agreement with the 66% positive rate found in another prospective study of children with febrile UTI [4]. It is interesting to note that in a study of 28 adult patients with a clinical diagnosis of acute pyelonephritis, similar results were obtained with CT [2]. We demonstrated vesicoureteral reflux in only 45% of the patients with DMSA scintigraphic findings of acute pyelonephritis, indicating that acute pyelonephritis in the absence of vesicoureteral reflux is common. This is in agreement with other recent reports [4, 5].

In our study, sonographic changes consistent with acute pyelonephritis were found in 39% (22/57) of the children with scintigraphically documented acute pyelonephritis (Figs. 1 and 2). This is in close agreement with the 45% (8/18) positive rate for sonography in 18 adults with CT evidence of acute pyelonephritis [2]. Sonograms underestimated the number and extent of pyelonephritic lesions in the majority of cases as compared with DMSA scans, but they provided additional diagnostic information in patients with renal abscesses or obstruction of the ureteropelvic junction.

In our study, the sonographic diagnosis of acute pyelonephritis was based on changes in cortical echogenicity. We found increased cortical echogenicity in 14 patients and decreased echogenicity in eight, including three with renal abscesses (Figs. 1 and 3). These findings are similar to the previously described sonographic findings in acute pyelonephritis, except for a higher frequency of increased echogenicity in our series [3, 20, 21].

Diffuse renal enlargement has been reported as a reliable sonographic sign of acute pyelonephritis in children [1]. In our study, focal or diffuse renal enlargement was found only in association with altered echogenicity. In one patient, focal enlargement of the upper pole of the kidney with normal echogenicity on sonograms was initially interpreted as positive. The first DMSA scan showed a prominent upper pole with normal cortical uptake, which was interpreted as a normal variant. The follow-up DMSA scan after 4 weeks and a follow-up sonogram after 5 months remained unchanged. Therefore, enlargement of the kidney with normal echogenicity may not be a reliable sign of acute pyelonephritis.

Various degrees of dilatation of the renal collecting system were noted on sonograms in nine patients, all of whom had scintigraphic evidence of acute pyelonephritis. Six of these patients had vesicoureteral reflux, and one had obstruction of the ureteropelvic junction. Mild dilatation of the collecting systems in the remaining two patients probably was due to atony caused by infection [20].

These data show that sonography has a low sensitivity for the detection of acute inflammatory changes of renal cortex. Therefore, it is not the optimal imaging technique for the diagnosis of acute pyelonephritis. However, sonography is very useful in characterizing the defects seen on the DMSA

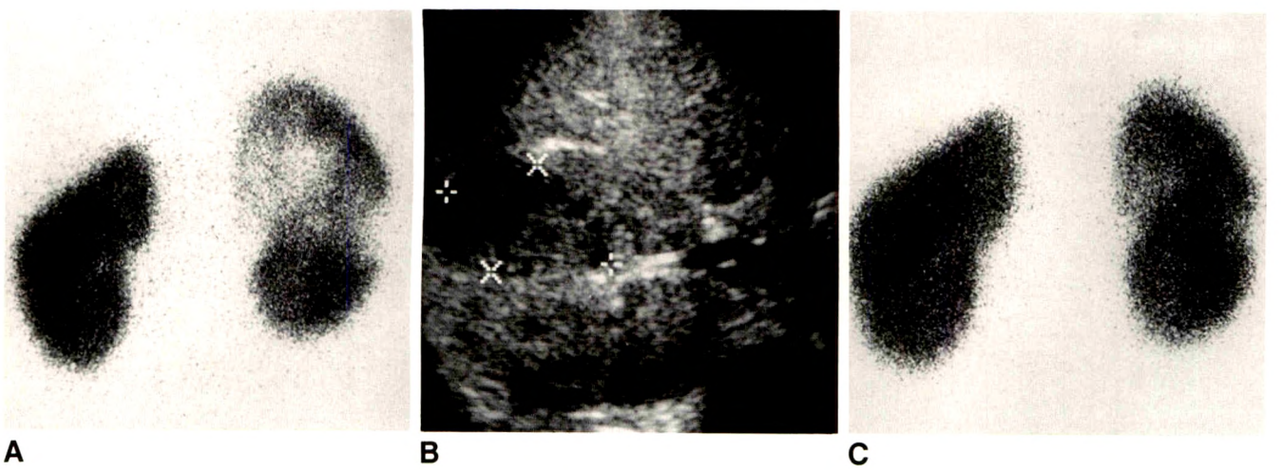


Fig. 3.—Right renal abscesses in a 7½-year-old girl with 4-day history of fever, chills, and right flank pain.
A, Posterior image of ^{99m}Tc-DMSA scan shows enlargement of upper two thirds of right kidney associated with at least two large areas of decreased cortical uptake.
B, Representative transverse sonogram of right kidney shows one of two abscesses. Other abscess was seen on other images (*not shown*).
C, Follow-up ^{99m}Tc-DMSA scan obtained 2 months later shows marked improvement in right renal defects and return of kidney to normal size. This patient was treated with antibiotics with no surgical intervention.

cortical scan and in detecting obstructive uropathies that may be associated with UTI.

REFERENCES

1. Dinkel E, Orth S, Dittrich M, Schulte-Wisserman H. Renal sonography in the differentiation of upper from lower urinary tract infection. *AJR* **1986**;146:775–780
2. June CH, Browning MD, Smith LP, et al. Ultrasonography and computed tomography in severe urinary tract infection. *Arch Intern Med* **1985**;145:841–845
3. Traisman ES, Conway JJ, Traisman HS, et al. The localization of urinary tract infection with ^{99m}Tc-glucoheptonate scintigraphy. *Pediatr Radiol* **1986**;16:403–406
4. Majd M, Rushton HG, Jantausch B, Wiedermann BL. Relationship of vesicoureteral reflux, P-fimbriated *E. coli* and acute pyelonephritis in children with febrile urinary tract infection. *J Pediatr* (in press)
5. Tappin DM, Murphy AV, Mocan MH, et al. A prospective study of children with first acute symptomatic *E. coli* urinary tract infection. *Acta Paediatr Scand* **1989**;78:723–729
6. Rushton HG, Majd M, Chandra R, Yim D. Evaluation of ^{99m}Tc technetium-dimer-capto-succinic acid renal scans in experimental acute pyelonephritis in piglets. *J Urol* **1988**;140:1169–1174
7. Parkhouse HF, Godley ML, Cooper J, Risdon RA, Ransley PG. Renal imaging with ^{99m}Tc-labelled DMSA in the detection of acute pyelonephritis: an experimental study in the pig. *Nucl Med Commun* **1989**;10:63–70
8. Torres VE, Velosa JA, Holley KE, Kelalis PP, Stickler GB, Kurtz SB. The progression of vesicoureteral reflux nephropathy. *Ann Intern Med* **1980**;92:776–784
9. Jacobson SH, Eklof O, Eriksson CG, Lins LE, Tidgren B, Winberg J. Development of hypertension and uremia after pyelonephritis in childhood: 27 year follow up. *BMJ* **1989**;299:703–706
10. Winberg J, Bollgren I, Kallenius G, Mollby R, Svenson SB. Clinical pyelonephritis and focal renal scarring. A selected review of pathogenesis, prevention, and prognosis. *Pediatr Clin North Am* **1982**;29:801–814
11. Ransley PG, Risdon RA. Reflux nephropathy: effects of antimicrobial therapy on the evolution of the early pyelonephritic scar. *Kidney Int* **1981**;20:733–742
12. Glauser MP, Lyons JM, Braude AI. Prevention of chronic experimental pyelonephritis by suppression of acute suppuration. *J Clin Invest* **1978**;61:403–407
13. Busch R, Huland H. Correlation of symptoms and results of direct bacterial localization in patients with urinary tract infections. *J Urol* **1984**;132:282–285
14. Sheldon CA, Gonzalez R. Differentiation of upper and lower urinary tract infections: how and when? *Med Clin North Am* **1984**;68:321–333
15. Montgomery P, Kuhn JP, Afshani E. CT evaluation of severe renal inflammatory disease in children. *Pediatr Radiol* **1987**;17:216–222
16. Mendez G Jr, Morillo G, Alonso M, et al. Gallium-67 radionuclide imaging in acute pyelonephritis. *AJR* **1980**;134:17–22
17. Fawcett HD, Goodwin DA, Lantieri RL. In-111 leukocyte scanning in inflammatory renal disease. *Clin Nucl Med* **1981**;6:237–241
18. Raynaud C, Tran-Dinh S, Bourguignon M, Syrota A, et al. Acute pyelonephritis in children. Preliminary results obtained with NMR imaging. *Contrib Nephrol* **1987**;56:129–134
19. Handmaker H. Nuclear renal imaging in acute pyelonephritis. *Semin Nucl Med* **1982**;12:246–253
20. Sty JR, Wells RG, Starshak RJ, Schroeder BA. Imaging in acute renal infection in children. *AJR* **1987**;148:471–477
21. Lee JKT, McClennan BL, Melson GL, Stanley RJ. Acute focal bacterial nephritis: emphasis on gray-scale sonography and computed tomography. *AJR* **1980**;135:87–92

Book Review

Obstetrics and Gynecology. (Vol 1. in Diagnostic Medical Sonography. A Guide to Clinical Practice.) Edited by Mimi C. Berman. Philadelphia: Lippincott, 768 pp., 1991. $85

This is a remarkable book. Many excellent and authoritative texts have already been written on sonography in obstetrics and gynecology. However, this latest addition manages to provide a fresh and innovative approach to standard subjects and challenges the reader with thoughtful reviews of controversial issues not covered in other books. The novel approach is probably related to the fact that 34 of the 58 contributors to this volume are sonographic technologists, not physicians. Judging from their titles, most of the authors are heavily involved in teaching. All have produced practical, concise yet comprehensive chapters. Normal anatomy, underemphasized in many books, is well described and nicely portrayed by both high-quality line drawings and excellent sonograms. Sonographic techniques are well integrated with descriptions of clinical principles and interpretive criteria, giving each chapter a problem-oriented approach to sonographic diagnosis. The latest sonographic techniques are encompassed, including transvaginal sonography; Doppler evaluation of uterine and adnexal blood flow; and the use of sonography to guide invasive procedures such as cordocentesis, fetal transfusion, and chorionic villus sampling. This is the first of a series of three volumes on diagnostic medical sonography. Volume 2 will cover echocardiography, and volume 3 will cover the abdomen. Each volume will be edited by a different person.

Volume 1 consists of 38 chapters organized into four parts. Part 1 covers the basic principles of sonographic techniques in obstetrics and gynecology. Part 2 has 10 chapters on gynecologic sonography. Embryology, congenital anomalies, and benign and malignant diseases are covered. Unique and pertinent chapters review gynecologic sonography in children and the role of sonography in the management of infertility and contraception. Part 3 covers obstetric sonography in 21 chapters, including embryology and the evaluation of normal and abnormal pregnancy and fetal anatomy. Particularly valuable contributions are chapters on the effect of maternal disease in pregnancy, pelvic masses in pregnancy, and the use of sonography for amniocentesis and chorionic villus sampling. Part 4 consists of six distinctive chapters covering technical and psychosocial topics. Of particular interest are discussions of controversies and ethical issues in obstetric and gynecologic sonography and sonographer support of maternal-fetal bonding.

More than 600 sonograms are included. All are of high quality and were obtained by using modern sonographic equipment. The sonograms are supplemented by excellent schematics, line diagrams, and summary tables. The composite is an exceptionally functional and useful text that will serve well not only as a standard reference for physicians and sonographers but also as an excellent study guide for students of the art of sonographic examination.

William E. Brant
University of California, Davis Medical Center
Sacramento, CA 95817

Normal Length of Fetal Kidneys: Sonographic Study in 397 Obstetric Patients

Harris L. Cohen[1,2]
James Cooper[1]
Peter Eisenberg[1]
Francine S. Mandel[3]
Beth R. Gross[1]
Mitchell A. Goldman[1]
Eyal Barzel[2]
Keith F. Rawlinson[4]

This study was done to measure normal lengths of fetal kidneys sonographically during pregnancy. Knowledge of these measurements may allow earlier diagnosis of a variety of abnormalities. The greatest length of each of 498 kidneys in 397 consecutive fetuses between 18 and 41 weeks gestation was measured on sonograms. Gestational ages were determined by last menstrual period and biometry; significant discrepancies led to case exclusion. Abnormal fetuses, twins, offspring of diabetic mothers, and fetuses with renal pelvic dilatation of 4 mm or greater were excluded to avoid any questionable measurements. The results show that mean lengths are greater and confidence intervals are wider than previously reported. Renal lengths are similar to those reported in premature and full-term neonates. Strong correlation exists between renal length and gestational age, determined by biparietal diameter, femoral length, and abdominal circumference, and an average of the three. No significant difference was found between right and left renal lengths in fetuses in whom both kidneys were imaged. Average renal lengths are significantly different when compared across the range of gestational ages ($p < .001$). No correlation is seen ($r = .00$) between parental height or weight and fetal renal length.

Our results show that fetal renal lengths are longer than previously reported.

***AJR* 157:545–548, September 1991**

An accurate baseline of the lengths of normal fetal kidneys is necessary to diagnose fetal abnormalities associated with abnormal kidney size. Accurate measurements also may be helpful in determinations of gestational age, particularly when the mother's last menstrual period is unknown and routine methods used to determine gestational age give conflicting results.

Current radiology textbooks [1–3] refer to the measurements provided by Bertagnoli et al. [4]. Because our measurements have been consistently larger than theirs, we did this study to determine the normal length of the fetal kidney at various gestational ages.

Material and Methods

The fetal kidneys of 397 consecutive women examined at various stages of pregnancy at Kings County Hospital, Brooklyn, NY, between November 1987 and October 1988, and at North Shore University Hospital-Cornell University Medical College between November 1988 and November 1990 were evaluated for greatest length. We measured from outer to outer margin as did Bertagnoli et al. [4].

These lengths were analyzed in relationship to gestational ages determined on the basis of biparietal diameter (BPD), femoral length (FL), abdominal circumference (AC), and an average of those three gestational ages in weeks, which we termed *average weeks* or AVW. These measurements were correlated with gestational ages determined on the basis of last menstrual period (LMP) and, in a few cases, crown-rump length (CRL). Renal lengths were excluded from the study if discrepancies between the ages determined by biometry and those by LMP were greater than ±2 weeks for gestational ages less than 30 weeks or greater than ±3 weeks for gestational ages of 30 weeks or more.

Received February 5, 1991; accepted after revision April 23, 1991.

[1] Division of Ultrasound, Department of Radiology, North Shore University Hospital–Cornell University Medical College, Manhasset, NY 11030. Address reprint requests to H. L. Cohen, 78 Grove Ave., Cedarhurst, NY 11516.

[2] Department of Radiology, State University of New York Health Science Center at Brooklyn, Brooklyn, NY 11203.

[3] Division of Biostatistics, Department of Research, North Shore University Hospital–Cornell University Medical College, Manhasset, NY 11030.

[4] Division of Maternal-Fetal Medicine, Department of Obstetrics and Gynecology, North Shore University Hospital–Cornell University Medical College, Manhasset, NY 11030.

0361–803X/91/1573–0545
© American Roentgen Ray Society

The longest renal lengths also were assessed in relationship to maternal and paternal heights and weights and reported sonographic measurements of renal length in neonates [5–8].

Our goal was to measure normal fetal renal lengths in a group of fetuses with no known anatomic or chromosomal abnormality and no known reason to have an abnormal renal length. Patients were excluded from the study if they had sonographic (>90th percentile for estimated fetal weights according to LMP dates) or birth evidence of being large for gestational age, or sonographic (<10th percentile for estimated fetal weights according to LMP, oligohydramnios, or FL/AC ratio ≥ 23.5) or birth evidence of having intrauterine growth retardation. Infants of diabetic mothers were excluded. Only singleton pregnancies were used. Only those kidneys for which a complete outline could be imaged were included. Unclear adrenal or renal borders, abnormal renal morphology, and renal pelvic dilatation greater than 4 mm in anteroposterior diameter were grounds for excluding the measurement. We used the last criteria, despite the fact that dilatations as great as 1 cm may be found in fetuses who at birth have no evidence of renal obstruction or vesicoureteral reflux [9], because we wished to avoid any suggestion of falsely long kidney measurements due to dilatation.

Measurements were obtained with a DRF 400 (Diasonics, Milpitas, CA), the ATL Ultramark 4 and 9 (Advanced Technology Laboratories, Bothell, WA), and the Acuson 128 (Acuson, Mountainview, CA).

Information was obtained about maternal height and weight before pregnancy and about paternal height and weight. Gestational ages were determined by using Hadlock's chart of predicted fetal measurements at specific menstrual weeks for BPD and FL and his gestational age/abdominal circumference chart for AC [10]. If the cephalic index was beyond two standard deviations of normal (<70 or >86), the BPD was excluded [11]. This was done to decrease the known significant variation in determinations of gestational age on the basis of BPD, especially in the third trimester. Hadlock et al. [12] noted an improvement in the high variability of third-trimester biometric measurements to ±2.3–2.4 weeks when a mean measurement of BPD, FL, AC, and head circumference was used. We averaged gestational ages obtained by BPD, FL, and AC. Although we did not measure head circumference in many of our cases, removal of BPD measurements when there was an abnormal cephalic index would logically suggest a similar limitation to the variability of our mean lengths.

Statistical analyses were conducted by using the SAS software package (SAS Institute, Cary, NC). Because the lengths of left and right fetal kidneys were found to be significantly correlated ($r = .91$) with each other in the subset of patients in whom both right and left fetal kidneys could be measured adequately ($n = 101$), it was necessary to determine if this might affect results. As we found no significant difference between mean lengths of left and right kidneys in this subset and as the lengths were highly correlated, results were similar whether we examined (1) paired kidneys with measurements of left and right kidneys separated, (2) paired kidneys with lengths of left and right kidneys combined, or (3) all kidneys (paired or not) with measurements combined. We chose the third approach to maximize our use of the data with no apparent bias.

An analysis of variance was used to compare mean renal lengths for each week of gestational age (weeks 18–41). Pearson product moment correlation coefficients were used to measure the degree of relationship among the various biometric gestational age measurements. Partial correlation was used to determine the relationship between parental height and weight and renal length when age was controlled for.

Results

Lengths of 498 fetal kidneys were measured in 397 pregnant women. In 101 fetuses, both the right and left kidney were imaged adequately and measured. The Pearson correlation coefficient for the length of the right kidney compared with that of the left kidney was 0.91.

We found a strong correlation between kidney length and gestational age as predicted by BPD ($r = .81$), FL ($r = .82$), AC ($r = .80$), and AVW ($r = .82$). Extremely strong correlation was found between each of the three component measurements (BPD weeks, FL weeks, or AC weeks) and AVW ($r = .99$). These measurements are not statistically different, and each can be used to correlate renal length.

Mean renal lengths, their standard deviations, and 95% confidence intervals are presented for each week of gestation from 18 weeks to 41 weeks determined by AVW (Table 1). A significant difference in the average fetal renal length is found when lengths are compared across the 18 to 41 week range of gestational ages ($p < .001$).

No correlation was found between fetal renal length and father's height ($r = .00$), father's weight ($r = .00$), mother's height ($r = .00$), and mother's prepregnancy weight ($r = .00$) when a partial correlation was performed and gestational age was partialled out.

Although not all fetuses in this study were born in the institutions where their sonographic examinations were done, to the best of our knowledge, none of them had abnormal kidneys as neonates.

Discussion

It is helpful to know normal lengths of fetal kidneys in order to diagnose fetal renal abnormalities. This in particularly true

TABLE 1: Mean Renal Lengths for Various Gestational Ages

Gestational Age (weeks)	Mean Length (cm)	SD	95% CI	*n*
18	2.2	0.3	1.6–2.8	14
19	2.3	0.4	1.5–3.1	23
20	2.6	0.4	1.8–3.4	22
21	2.7	0.3	2.1–3.2	20
22	2.7	0.3	2.0–3.4	18
23	3.0	0.4	2.2–3.7	13
24	3.1	0.6	1.9–4.4	13
25	3.3	0.4	2.5–4.2	9
26	3.4	0.4	2.4–4.4	9
27	3.5	0.4	2.7–4.4	15
28	3.4	0.4	2.6–4.2	19
29	3.6	0.7	2.3–4.8	12
30	3.8	0.4	2.9–4.6	24
31	3.7	0.5	2.8–4.6	23
32	4.1	0.5	3.1–5.1	23
33	4.0	0.3	3.3–4.7	28
34	4.2	0.4	3.3–5.0	36
35	4.2	0.5	3.2–5.2	17
36	4.2	0.4	3.3–5.0	36
37	4.2	0.4	3.3–5.1	40
38	4.4	0.6	3.2–5.6	32
39	4.2	0.3	3.5–4.8	17
40	4.3	0.5	3.2–5.3	10
41	4.5	0.3	3.9–5.1	4

Note.—Gestational age is an average of the gestational ages in weeks determined on the basis of biparietal diameter, femoral length, and abdominal circumference. SD = standard deviation, 95% CI = 95% confidence interval, *n* = number of fetuses. A t distribution was used when $n < 30$.

if the echogenicity is apparently normal, which may occur in some early cases of polycystic disease of the kidney. Knowledge of normal renal length can be helpful in early determinations of nephromegaly or hypoplasia [13].

The kidney is imaged in 90% of fetuses between 17 and 22 weeks [14]. Maternal obesity can hinder imaging [15]. As the pregnancy progresses, increased echogenicity from increasing perinephric fat is said to make them more visible by allowing easier separation of the kidney from its surrounding soft tissues [1]. However, exact measurements continue to be hindered by uncertainty of renal end points especially at the upper pole, if hidden by fetal ribs or obscured by the adrenal gland [14, 15].

Improved resolution with current machinery and transducers seems to make this less of an issue. Identification of the kidneys' borders and the adrenal gland and distinction of the adrenal gland from the kidney is easier (Fig. 1). Improvements in sonographic technology may be the key factor resulting in our larger measurements as compared with the earlier (1981–1983) studies [4, 13, 14]. The current ease of renal identification makes it easier to determine a foreshortened renal measurement (e.g., by noting asymmetry of the visualized pyramids in relationship to the imaged kidney) and therefore allows the examiner to image a truer (longer) length by subtly adjusting the angle of the transducer.

Unless the fetus is prone with its back facing the transducer, usually only the borders of the near kidney can be imaged adequately. We attempted to be strict with our border visualization before accepting a measurement so as to decrease the possibility of incorrect, especially falsely elevated, measurements.

Kurtz and Goldberg [1], in their review of studies of obstetric measurements, noted only two earlier studies of fetal kidney length that used real-time equipment. Both those studies [4, 13] showed measurements smaller than ours. The work by Bertagnoli et al. [4] and their chart were recommended. Their mean and standard deviations appear to be at the lowest point of our 95% confidence intervals (Fig. 2). The

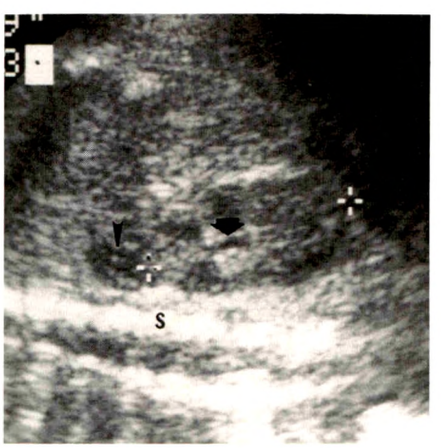


Fig. 1.—Longitudinal sonogram of fetal kidney and adrenal gland at paravertebral position shows minimal central pyelectasis (*arrow*). Upside-down V-shaped structure superior to kidney is adrenal gland (*arrowhead*). Cursors mark off kidney borders for measurement. S = spine.

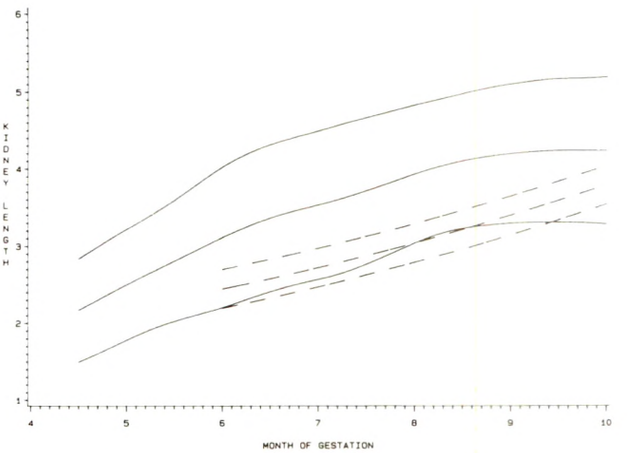


Fig. 2.—Plot of kidney length vs gestational age. Our measurements (*solid lines*) are compared with those of Bertagnoli et al. [4] (*broken lines*). Central lines represent mean. Superior and inferior lines represent two standard deviations of mean. Plot has been smoothed by using cubic-spline interpolation.

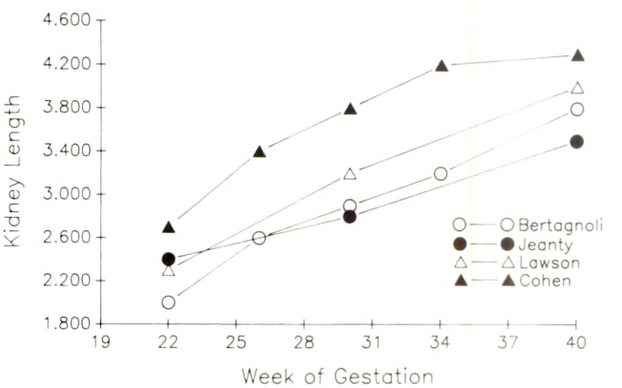


Fig. 3.—Plot of kidney length vs gestational age. Measurements of kidney length at several points within pregnancy obtained by Bertagnoli et al. [4], Jeanty et al. [13], and Lawson et al. [14] are compared with our (Cohen et al.) larger measurements.

referenced articles showed, as did we, that mean length increases with gestational age. The study of Lawson et al. [14], using articulated arm scanning, showed measurements of 3.2 cm at 30 weeks and measurements of 4.2–4.3 cm at term, which are closer to our measurements. Figure 3 is a graphic representation of our measurements at various weeks of gestation compared with those of the aforementioned authors.

Although renal dilatation as great as 10 mm may be considered physiologic and normal [9, 15–17], we arbitrarily decided to exclude kidneys with anteroposterior pelvic measurements greater than 4 mm. We did so in order to avoid the possibility of considering pelvic dilatation, even if physiologic, a reason for the longer lengths that we measured.

To confirm our measurements, we correlated our figures with published neonatal studies. Rosenbaum et al. [6] noted the mean renal length in neonates (0–1 week) as 4.48 cm with a 0.31-cm standard deviation. Han and Babcock [7]

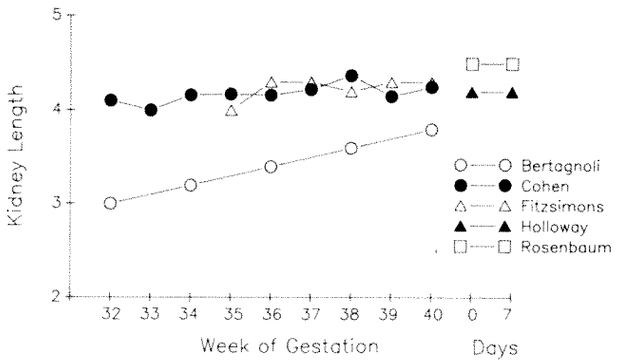


Fig. 4.—Plot of kidney length vs age. Our measurements in late pregnancy are compared with fetal measurements of Bertagnoli et al. [4] and premature neonatal measurements of Fitzsimons [5]. Measurements by Holloway et al. [18] and Rosenbaum et al. [6] in first week after birth are used for reference.

noted measurements of 3.9–5.9 cm in neonates. Fitzsimons' measurements of neonatal kidneys among premature infants whose gestational age was determined by menstrual history, fetal sonographic measurements, or maturity assessment were similar to those of our fetuses of equivalent gestational age (Fig. 4). Both our measurements and those of Fitzsimons showed little difference in the renal length measurements between weeks 35 and 40. We have no explanation for this finding. Although we do not have birth weights of all fetuses for comparison, Erwin et al. [19] found mean neonatal renal lengths to be 4.8 cm for those greater than 3500 g and 4.5 cm for those between 3.0 and 3.5 kg, numbers similar to those of our older fetuses and larger than those of Bertagnoli et al. Holloway et al. [18] noted neonatal (0–7 days) mean renal lengths to be 4.3 cm (SD, 0.48 on left side, 0.44 on right side) in males and between 4.1 and 4.2 cm for females. These measurements are similar to our length of 4.3 cm (SD, 0.5) at 40 weeks gestation. The study by Chiara et al. [8] of term and preterm neonates showed that the average kidney length was 4.0 cm (SD, 0.7). Gestational ages were determined by maternal dates and Dubowitz assessment; mean measurements and (upper limit measurements) obtained from their graph were 4.4 cm (5.0 cm) at 38 weeks and 4.8 cm (5.4 cm) at 41 weeks [8].

In conclusion, gestational age is related to renal length. Our mean lengths are longer than those of earlier reports, yet are consistent with neonatal measurements in other published studies. Parental height and weight cannot be used to predict fetal or neonatal renal length. Fetal renal lengths may aid in confirming other questionable biometric measurements of gestational age.

ACKNOWLEDGMENTS

We thank Dara Muller, Cheryl Jacoby, Lauri Federbush, Maria Clifford, Maureen Parcell, Donna Denicola, and Kathrin Sakni for their sonographic expertise; Martin Lesser for his biostatistical guidance; Dennis Skahil for his photographic expertise; and Sandra W. Cohen, Karl Drehobl, and Lauren E. Cohen for their computer consultations.

REFERENCES

1. Kurtz A, Goldberg B. *Obstetrical measurements in ultrasound: a reference manual.* Chicago: Year Book Medical, **1988**:88–92
2. Kurtz A, Goldberg B. Fetal body measurements. In: Goldberg B, Kurtz A, eds. *Atlas of body measurements.* Chicago: Year Book Medical, **1990**: 332–333
3. Mahony B. The genitourinary system. In: Callen PW, ed. *Ultrasonography in obstetrics and gynecology*, 2nd ed. Philadelphia: Saunders, **1988**:256
4. Bertagnoli L, Lalatta F, Gallicchio R, et al. Quantitative characterization of the growth of the fetal kidney. *JCU* **1983**;11:349–356
5. Fitzsimons R. Kidney length in the newborn measured by ultrasound. *Acta Paediatr Scand* **1983**;72:885–887
6. Rosenbaum D, Korngold E, Teele R. Sonographic assessment of renal lengths in normal children. *AJR* **1984**;142:467–469
7. Han B, Babcock D. Sonographic measurements and appearance of normal kidneys in children. *AJR* **1985**;145:611–616
8. Chiara A, Chirico G, Barbarini M, DeVecchi E, Rondini G. Ultrasonic evaluation of kidney length in term and preterm infants. *Eur J Pediatr* **1989**;149:94–95
9. Grignon A, Filion R, Filiatrault D, et al. Urinary tract dilatation in utero: classification and clinical applications. *Radiology* **1986**;160:645–647
10. Athey PA, Hadlock FP. *Ultrasound in obstetrics and gynecology*, 2nd ed. St Louis: Mobsy, **1985**:323–325
11. Hadlock F, Deter R, Carpenter R, Park S. Estimating fetal age: effect of head shape on BPD. *AJR* **1981**;137:83–85
12. Hadlock F, Deter R, Harrist R, Park S. Estimating fetal age: computer-assisted analysis of fetal growth parameters. *Radiology* **1984**;152: 497–501
13. Jeanty P, Dramaix-Wilmet M, Elkhazen N, Hubinot C, van Regemorter N. Measurement of fetal kidney growth on ultrasound. *Radiology* **1982**;144:159–162
14. Lawson T, Foley W, Berland L, Clark K. Ultrasonic evaluation of fetal kidneys: analysis of normal size and frequency of visualization as related to stage of pregnancy. *Radiology* **1981**;138:153–156
15. Sagi I, Vagman I, David M, et al. Fetal kidney size related to gestational age. *Gynecol Obstet Invest* **1987**;23:1–4
16. Hoddick W, Filly R, Mahony B, Callen P. Minimal fetal renal pyelectasis. *J Ultrasound Med* **1985**;4:85–89
17. Arger P, Coleman B, Mintz M, et al. Routine fetal genitourinary tract screening. *Radiology* **1985**;156:485–489
18. Holloway H, Jones T, Robinson A, Harpen M, Wiseman H. Sonographic determination of renal volumes in normal neonates. *Pediatr Radiol* **1983**;13:212–214
19. Erwin B, Carrol B, Muller H. Sonographic assessment of neonatal renal parameters. *J Ultrasound Med* **1985**;4:217–220

Benign Hemorrhagic Adrenocortical Macrocysts in Beckwith-Wiedemann Syndrome

Roy G. K. McCauley[1]
J. B. Beckwith[2]
E. R. Elias[3]
E. N. Faerber[4]
L. H. Prewitt, Jr.[5]
W. E. Berdon[6]

A new pseudotumorous lesion found in the adrenal cortex of six infants with Beckwith-Wiedemann syndrome is described. These cystic masses were discovered either prenatally by using sonography or early in the neonatal period as palpable flank masses. Imaging studies, including sonography and CT, could not confidently exclude malignancy. After the masses were removed surgically, histologic examination showed them all to be benign hemorrhagic macrocysts within the capsule or permanent cortex (in contrast to neonatal adrenal hemorrhage, which usually occurs more centrally in the fetal cortex). The cysts were as large as 8 cm in diameter, and in one case a solitary cyst was predominant. Hemihypertrophy was present in all cases. Four of the six lesions were right-sided, and there was a male-female ratio of 5:1.

Benign hemorrhagic adrenocortical macrocysts are a cause of abdominal mass in the fetus and neonate with Beckwith-Wiedemann syndrome.

***AJR* 157:549–552, September 1991**

The previously reported major features of Beckwith-Wiedemann syndrome (BWS) include macroglossia, abdominal wall defects, visceromegaly, gigantism, hemihypertrophy, hypoglycemia, ear creases, nevus flammeus, adrenal cytomegaly, midface hypoplasia, and association with various tumors [1–4]. Incomplete forms of BWS in which only two or three of these features are present also occur [5]. The prevalence of associated benign and malignant tumors ranges from 7.5% to 11.0% [1, 4, 5].

We report six cases of BWS in which tumorlike abdominal masses were discovered in the first few weeks after birth. After surgical removal, these were all shown histologically to be benign hemorrhagic macrocystic lesions of the adrenal gland. This represents a previously unreported cause of abdominal mass in the fetus and neonate.

Materials and Methods

Six cases of BWS were seen at five separate institutions over a period of 12 years. The prevalence of BWS has been estimated at 1:13,700 [6]. All of the lesions in our cases were removed shortly after birth, except for one (case 6), in which surgery was performed at 7 weeks of age.

Case Reports

Case 1

Prenatal sonography revealed a cystic lesion in the fetus's right flank that was easily palpated after birth. The male neonate also had macroglossia, umbilical hernia, and hemihypertrophy. The position of the mass, next to the upper part of the right kidney, was confirmed by sonography (Fig. 1A) and CT (Fig. 1B), which also showed fluid/fluid levels within the

Received January 2, 1991; accepted after revision April 9, 1991.

[1] Department of Radiology, New England Medical Center, 750 Washington St., NEMC #165, Boston, MA 02111. Address reprint requests to R. G. K. McCauley.

[2] Department of Pathology, Children's Hospital, 1056 E. 19th Ave., Box B120, Denver, CO 80218.

[3] Department of Pediatrics, New England Medical Center, Boston, MA 02111.

[4] Department of Radiology, St. Christopher's Hospital, Erie Ave. at Front St., Philadelphia, PA 19134.

[5] Department of Radiology, Minneapolis Children's Medical Center, 2525 Chicago Ave., Minneapolis, MN 55404.

[6] Department of Radiology, Babies Hospital, Broadway and 167th St., New York, NY 10032.

0361–803X/91/1573–0549
© American Roentgen Ray Society

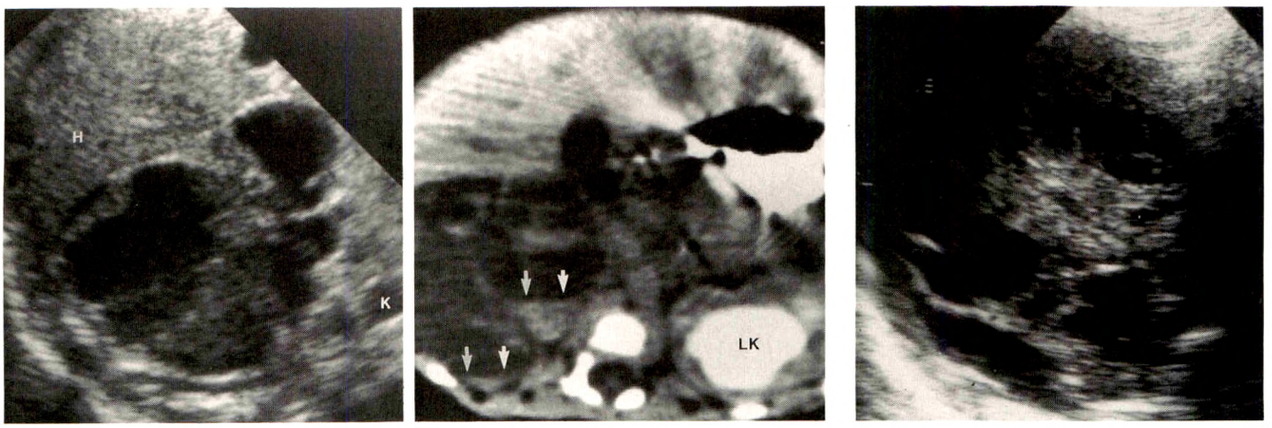


Fig. 1.—Case 1. *A*, Oblique sonogram through right suprarenal area. Hypoechoic cystic changes are shown within solid mass between right upper kidney (K) and liver (H).

***B*, Axial CT scan through right suprarenal area. Large, multicystic mass with thin-walled cysts is shown. Fluid/fluid levels are shown within several cysts; more dependent fluid is of higher attenuation (*arrows*). Incidental note was made of bilateral hydronephrosis; dilatation in left kidney (LK) is shown here.**

Fig. 2.—Case 2. Oblique sonogram of right suprarenal area. Large, complex mass with hypoechoic cystic contents is shown.

cysts. A grapelike cluster of cysts up to 6 cm in diameter arising in the right adrenal gland was removed during surgery. Histologic findings were adrenal nodules containing hemorrhagic cysts lined by hemosiderin accumulation. Focal microcystic change in the permanent cortex was noted with adrenocortical cytomegaly. The patient was well 4 years after surgery.

Case 2

A mass in the patient's right flank was noted on prenatal sonography. At birth, this male neonate had hemihypertrophy, left-sided hemimacroglossia, hypoglycemia, and hepatomegaly. Sonography (Fig. 2) and CT showed a complex multicystic mass. At surgery, a 430-g, mainly cystic suprarenal mass with discrete areas of solid tissue was removed. Histologic findings were cortical cytomegaly in the provisional cortex, macrocystic change in the cortex with acute hemorrhage, and microcystic change in the definitive cortex. A left adrenal adenoma developed when the patient was 8 months old and was removed.

Case 3

As a neonate, this girl had left-sided hemimacroglossia, hypoglycemia, hepatomegaly, and a palpable rubbery 3-cm mass in the left flank. Arteriography showed a large avascular mass displacing the left kidney downward. Sonography showed a complex 3- by 5-cm suprarenal mass. A cystic mass in the left adrenal gland was removed during surgery. The cysts contained watery serosanguineous fluid. Histologic findings were remnants of adrenal cortex, epithelium-lined cystic spaces, macrocysts containing blood, and adrenal cytomegaly (Fig. 3).

Case 4

At birth this large male neonate had hypoglycemia, supraventricular tachycardia, and a palpable mass in the left flank; left-sided hemihypertrophy had developed by 2 months of age. Excretory urography with tomography showed a suprarenal mass of uncertain origin, and sonography showed a complex left suprarenal mass. CT revealed a partly cystic mass. During surgery, the left adrenal gland was removed. The gland had multiple cysts, 0.1 to 1.7 cm in diameter, attached to its capsule. Histologic findings were variously sized cysts attached to the capsule and within the permanent cortex, some containing RBCs. Interstitial hemorrhage and adrenocortical cytomegaly were noted. The patient did well initially, but subsequently developed a Wilms tumor at 29 months of age and eventually died.

Case 5

This full-term male neonate had right-sided hemihypertrophy at birth with a palpable right-sided midabdominal mass. Sonography showed a complex right-sided multicystic mass in the suprarenal area. CT confirmed these appearances. A 6- by 4- by 4-cm multicystic mass attached to the right adrenal gland was removed surgically. Histologic findings were adrenocortical cytomegaly with multiple hemorrhagic adrenal cysts. The patient was well 3 years after surgery.

Case 6

Prenatal sonography showed an upper abdominal mass that was palpable on the right side at birth. Mild left-sided hemihypertrophy was present. Sonography showed a multilocular cystic mass in the upper kidney or adrenal gland. CT showed a multicystic mass, with one cyst predominant, in the right suprarenal area. At 7 weeks of age, an 8- by 6- by 5-cm encapsulated multiloculated mass and the right adrenal gland were removed. Histologic sections revealed multilocular hemorrhagic cysts in the adrenal gland without evidence of tumor. The child was well 3 years after surgery.

Results

In the six cases reported here, sonography revealed complex suprarenal masses (Fig. 1) that contained cystic and solid components; three of them were detected prenatally. CT confirmed that the masses were partly cystic and partly solid.

In case 1 (Fig. 1B), CT showed that there were fluid-fluid levels due to heavier blood products layering beneath less dense serumlike fluid.

It is of interest that within this group of six patients, other tumors developed in two (33%). One was a Wilms tumor with a fatal outcome and the other an adrenal adenoma. This is a much higher rate of association than in BWS cases in general, although it is similar to the prevalence in those with BWS who also have hemihypertrophy [1].

Five of the six cases were in male infants, with no obvious explanation for this male preponderance, as the reported prevalence of BWS in males and females is not significantly different [1]. Four of the six lesions were right sided, but with the small number of cases involved, this right-side preponderance may have occurred by chance. Hemihypertrophy is described in 30% of cases of BWS [1], yet hemihypertrophy was present in all six cases of benign hemorrhagic macrocystic lesion.

Discussion

Patients with BWS should be examined regularly (initially every 3 months) for the occurrence of associated tumors. This is performed clinically and by various imaging tests—most notably sonography. Sonography is excellent for screening the kidneys, adrenal glands, and liver for tumor formation. When necessary, further evaluation can be done with CT or MR imaging. Recently it has been recommended that these patients have routine screening chest radiographs because of the increased frequency of neural crest tumors found in the thorax [7].

Neuroblastoma, adrenal cortical carcinoma, and Wilms tumor all may have cystic components and appear morphologically similar on imaging studies. Therefore, a complex suprarenal mass should be considered potentially malignant. An exception to this rule is the single cystic or partially cystic adrenal lesion that is suspected clinically to be neonatal adrenal hemorrhage. Neonatal adrenal hemorrhage may initially appear as a hyperechoic mass on sonography, but within a few days or less progresses to a hypoechoic cystlike lesion as liquefaction occurs [8]. Neonatal adrenal hemorrhage is most often unilocular, but septa can be seen within the cavity. As time progresses, the cystic hematoma becomes smaller and eventually shrinks away, leaving a small calcified scar. There is often a history of stress before the hemorrhage and a sudden drop in hematocrit. These clinical features did not appear to be prominent in most of the six cases reported here, although case 4 was noted to have a hematocrit of 22% and hypoglycemia was present in cases 2–4. One definite case of neonatal adrenal hemorrhage in a child with BWS has been documented [9], as have two other possible cases [10].

The spectrum of adrenal abnormality previously described in BWS includes cortical hyperplasia, fetal cortical cytomegaly, cortical microcysts, and tumors [2, 4, 11]. The type and prevalence of benign and malignant tumors described in association with complete BWS or partial BWS are very similar, with nephroblastoma and adrenocortical carcinoma accounting for most of the cases. Other tumors reported include hepatoblastoma, neuroblastoma, glioblastoma (of the brainstem), rhabdomyosarcoma (of the orbit), fibrous hamartoma of the heart, umbilical myxoma, retroperitoneal ganglioneuroma, and carcinoid of the appendix [5, 10]. The benign hemorrhagic macrocystic lesion described here enlarges this spectrum.

Microscopic cortical microcysts are a consistent finding in the adrenal gland of BWS patients, as was emphasized and illustrated in 1969 [2]. These cysts usually occur in the outer portion of the cortex and are lined by adrenocortical epithelium. Usually they are either empty or contain proteinaceous, cell-free fluid (Fig. 3A).

Similar cysts may normally occur early in development, and their occurrence later in gestation has been described as an apparent result of stress or maternal steroid use [12, 13]. Their significance in patients with BWS currently is unknown. In adrenal glands of patients with BWS, these cysts are usually minute, but some accumulate either fluid or blood in their lumens, expanding to the grossly visible range. Foci of necrosis are commonly seen in the lining of the larger cysts (Fig. 3B), and in some, the lining epithelium is entirely lost.

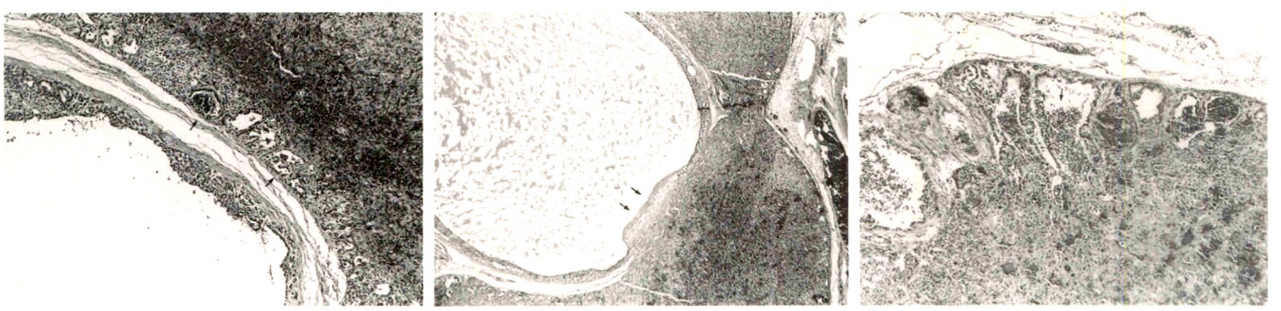


Fig. 3.—Case 3. *A*, High-power photomicrograph shows large cyst lined by adrenocortical epithelium. Multiple smaller cysts are seen in adjacent outer cortex (*arrows*). These nonhemorrhagic cysts are not seen in the more common neonatal adrenal hemorrhage.

***B*, Low-power photomicrograph of adrenal cortex shows a microcyst filled with proteinaceous material with focal necrosis of epithelial lining (*arrows*).**

***C*, High-power photomicrograph shows characteristic superficial cortical location of microcysts. Most cystic spaces in this field are filled with blood (*arrow*). Superficial location of these hemorrhagic cysts differs from the deeper location of neonatal adrenal hemorrhage.**

Fresh or old hemorrhage can be seen in cysts with apparently intact linings and in those with focal or complete destruction of the lining epithelium. We postulate that hemorrhage may result from either of the following two processes:

1. Hemorrhage is commonly seen in the fetal adrenal cortex in BWS cases, possibly as a sequela of the process of regression of the abnormal fetal cortex of these patients. This hemorrhage often dissects peripherally into the permanent cortex, where it apparently disrupts the walls of the cyst and enters the cyst cavities (Fig. 3C).

2. Focal necrosis of cyst linings is seen frequently in these specimens. This possibly results from increasing fluid accumulation with local pressure effects. These necrotic foci could easily lead to hemorrhage into the cystic spaces. It seems possible for a vicious cycle to develop, in which hemorrhage leads to extension of the destructive process, which leads in turn to new sites of hemorrhage, as may be seen in aneurysmal bone cysts.

Once hemorrhage has been initiated, repeated episodes can cause progressive enlargement of the cysts and coalescence of adjacent cysts. Organization with fibrosis, hemosiderin deposition, and calcification are late sequelae of this process.

The lesions herein described differ in several ways from the more commonly seen neonatal adrenal hemorrhage. The cortical cysts that are a fundamental component of these lesions are not observed in neonatal adrenal hemorrhage. Furthermore, neonatal adrenal hemorrhage characteristically arises in the fetal cortex or deeper portions of the permanent cortex, whereas the lesions we are describing characteristically involve the most superficial regions of the permanent cortex, and only the larger lesions extend to the level of the fetal cortex or juxtamedullary region.

Theoretically these cystic hemorrhagic lesions could regress spontaneously. Because they cannot be clearly distinguished from tumor, all lesions in our cases have been surgically removed.

In summary, a benign hemorrhagic macrocystic lesion is described, expanding the spectrum of adrenal disease in patients with BWS. This lesion is a new cause of abdominal mass and should be considered in the affected fetus and neonate.

REFERENCES

1. Pettenati MJ, Haines JL, Higgins RR, Wappner RS, Palmer CG, Weaver DD. Wiedemann-Beckwith syndrome: presentation of clinical and cytogenetic data on 22 new cases and review of the literature. *Hum Genet* **1986**;74:143–154
2. Beckwith JB. Macroglossia, omphalocele, adrenal cytomegaly, gigantism, and hyperplastic visceromegaly. *Birth Defects* **1969**;5:188–196
3. Wiedemann HR. Complexe malformatif familial avec hernie ombilicale et macroglossie—"un syndrome nouveau"? *J Genet Hum* **1964**;13:223–232
4. Wiedemann HR. Tumors and hemihypertrophy associated with Wiedemann-Beckwith syndrome. *Eur J Pediatr* **1983**;141:129
5. Sotelo-Avila C, Gonzalez-Crussi F, Fowler JW. Complete and incomplete forms of Beckwith-Wiedemann syndrome: their oncogenic potential. *J Pediatr* **1980**;96:47–50
6. Thornburn MJ, Wright ES, Miller CG, et al. Exomphalos–macroglossia–gigantism syndrome in Jamaican infants. *Am J Dis Child* **1970**;119:316–321
7. Sirinelli D, Silberman B, Baudon JJ, Sinnassamy P, Gruner M, Montagne JP. Beckwith-Wiedemann syndrome and neural crest tumors. A report of two cases. *Pediatr Radiol* **1989**;19:242–245
8. Metreweli C, Garel L, Montagne JP. Echographic aspects of neonatal adrenal hemorrhage. *Ann Radiol* (Paris) **1981**;24:13–17
9. Pignatti CB, Maggiore G, Bianchi E, Magrini U, Ripamonte L. Adrenal hemorrhage in a newborn with Beckwith-Wiedemann syndrome. *Am J Dis Child* **1978**;132:1142–1143
10. Ichiba Y, Aoyama K. Adrenal calcification in Beckwith-Wiedemann syndrome. *Am J Dis Child* **1977**;131:1296–1297
11. Emery LG, Shields M, Shah NR, Garbes A. Neuroblastoma associated with Beckwith-Wiedemann syndrome. *Cancer* **1983**;52:176–179
12. Oppenheimer EH. Cyst formation in the outer adrenal cortex. Studies in the human fetus and newborn. *Arch Pathol Lab Med* **1969**;87:653–659
13. De Sa DJ. Stress response and its relationship to cystic (pseudofollicular) change in the definitive cortex of the adrenal gland in stillborn infants. *Arch Dis Child* **1978**;53:769–776

Parotid Enlargement in Children Seropositive for Human Immunodeficiency Virus: Imaging Findings

Nina Soberman[1]
John C. Leonidas[1]
Walter E. Berdon[2]
Vincent Bonagura[3]
Jack O. Haller[4]
Mark Posner[3]
Louis Mandel[5]

We investigated the clinical, immunologic, and imaging features of parotid enlargement in 10 children seropositive for human immunodeficiency virus (HIV) who were infected prenatally. In seven patients, sonography revealed many small hypoechoic areas suggestive of lymphoid infiltration. In three older children, large anechoic areas suggesting lymphoepithelial cysts were present. The lesions probably represent generalized lymphoid infiltration akin to pulmonary lymphoid hyperplasia, although only two of our patients had radiologic evidence of pulmonary lymphoid hyperplasia. Four of five of the children with parotid enlargement who had immunologic studies were phenotypically HLA-DR5, an immunophenotype associated with improved immune response, occurring in less than one in four in the normal population. This suggests that painless parotid enlargement may be a good prognostic sign in HIV-seropositive children.

Parotid enlargement was found in 10 HIV-positive children from 6 months to 11 years old. All except one were infected prenatally.

AJR 157:553–556, September 1991

Parotid enlargement in association with human immunodeficiency virus (HIV) infection has been found in both adults and children [1–8]. CT and MR imaging findings have been described in parotid disease of HIV-infected adults, emphasizing benign lymphoepithelial proliferation as the underlying cause of parotid enlargement [6, 9, 10]. These patients generally have a milder clinical course [6, 8–10]. Although parotid enlargement has been recognized in HIV-seropositive children [2, 11, 12], only recently Goddart et al. [8] described sonographic findings of enlarged parotid glands in four African children.

We examined the prevalence, clinical significance, and imaging characteristics of parotid swelling in HIV-seropositive children seen in two pediatric centers in New York City so that we could draw attention to a relatively common manifestation of HIV infection in this age group. We focus on the imaging appearance of the parotid gland, primarily on sonography, and have attempted to correlate parotid involvement with the immune status of these patients.

Materials and Methods

Ten patients between 6 months and 11 years old (mean, 5 years) with documented HIV infection and clinically evident parotid enlargement were seen at the Schneider Children's Hospital at Long Island Jewish Medical Center and Babies Hospital at Columbia-Presbyterian Medical Center between July 1988 and June 1990. Both facilities serve the New York metropolitan area. These 10 children came from a group of about 100 young HIV-positive patients and represent approximately 10% of all seropositive children currently followed up at these institutions. Thus, the rate of parotid involvement in pediatric HIV infection may actually be higher. There were six boys and four girls. HIV infection was congenital in all patients, who were born to drug-addicted mothers, although in one patient transfusion at the age of 2 may have been responsible.

Received October 29, 1989; accepted after revision April 9, 1991.

[1] Department of Radiology, Schneider Children's Hospital, Long Island Jewish Medical Center, Albert Einstein College of Medicine, New Hyde Park, NY 11042. Address reprint requests to J. C. Leonidas.

[2] Department of Radiology, Babies Hospital, Columbia-Presbyterian Medical Center, Broadway and 167th St., New York, NY 10032.

[3] Department of Pediatrics, Division of Allergy/Immunology, Schneider Children's Hospital, Long Island Jewish Medical Center, Albert Einstein College of Medicine, New Hyde Park, NY 11042.

[4] Department of Radiology, Kings County Hospital, State University of New York, Downstate Medical Center, 450 Clarkson Ave., Box 1208, Brooklyn, NY 11203-2098.

[5] Department of Dentistry, Columbia-Presbyterian Medical Center, 622 W. 168th St., New York, NY 10032.

0361–803X/91/1573–0553
© American Roentgen Ray Society

All patients were evaluated with sonography. Images were obtained with 5-MHz linear transducers (Acuson, Mountain View, CA). One child had a sialogram followed by CT with 5-mm axial images obtained at 5-mm intervals. All patients had chest radiographs, and three had CT scans of the chest with 10-mm slice thickness at 10-mm intervals followed by 1.5-mm slices at 15-mm intervals by using bone algorithms (high-resolution CT). One patient had MR imaging of the parotid gland (Siemens 1.0-T Magnetom). Five patients had comprehensive immunologic studies. Biopsy material was not obtained from any of our patients.

Results

In only one instance was parotid swelling the initial manifestation of HIV infection. This 6-month-old infant was initially thought to have mumps. When the parotid swelling persisted much longer than expected, further examination revealed evidence of HIV infection. The parotid swelling eventually regressed spontaneously. Of the remaining nine children, three were found to be HIV-seropositive after multiple infections and six had HIV testing because a parent or sibling had AIDS. Parotid enlargement in these nine patients appeared 4 months to 4.5 years after the diagnosis of HIV infection (Table 1).

Two main sonographic patterns were observed. The first and most common pattern, seen in seven (70%) of 10 children, consisted of diffuse small (1- to 4-mm) to medium-sized (5- to 8-mm) hypoechoic or anechoic areas, highly concentrated throughout a grossly enlarged gland (Fig. 1). The normal architecture was preserved in most of these glands. On MR, performed in one patient, these lesions behaved as high-water-content areas with low signal intensity on T1-weighted images (650/17 [TR/TE]) and increased intensity on T2-weighted images (2000/60; Fig. 1).

The second pattern, present in three of 10 patients, consisted sonographically of large anechoic areas almost totally replacing the gland with only minimal residual parotid parenchyma visualized (Fig. 2). In one of these patients (No. 10), foci of increased echogenicity with sharp posterior shadowing consistent with calcification were present within the large anechoic areas. A sialogram showed large cysts communicating with a nondilated ductal system (Fig. 3).

Chest radiography revealed findings consistent with pulmonary lymphoid hyperplasia (PLH) in only two patients (Table 1). Three children with normal findings on chest radiographs had high-resolution CT, which also failed to reveal PLH (Table 1).

Follow-up clinical examinations of our patients have shown no change in the degree of parotid enlargement for a period of 4–18 months. In one instance, parotid masses regressed spontaneously (Case No. 6).

Antibodies reactive with the Epstein-Barr virus were found in all those tested (Cases 1–5). Class II phenotyping was performed on four of these patients and revealed three patients with DR5 [13, 14].

Discussion

Recent reports have emphasized that many adults with biopsy-proved lymphoepithelial infiltration of the parotid gland have been free of symptoms at the time of presentation and

TABLE 1: Clinical, Epidemiologic, and Imaging Findings of Human Immunodeficiency Virus (HIV)-Positive Children with Parotid Enlargement

Patient No.	Sex	Age at Presentation with Parotid Enlargement	Race[a]	Age at Diagnosis of HIV Infection	Clinical Status Other Than Parotid Enlargement	Sonography[b]	PLH[c]
1	F	10 yr	B	6.0 yr	Asymptomatic	L	No[d]
2	M	6 yr	H	1.5 yr	Recurrent bacterial infections	L	No
3	M	7 yr	H	3.5 yr	Opportunistic infections	S[e]	Yes
4	M	6 yr	H	3.0 yr	Recurrent bacterial infections	S	No[d]
5	F	3 yr	B	2.0 yr	Asymptomatic	S	No[d]
6	M	6 mo	B	0.5 yr	Asymptomatic	S	No
7	F	8 mo	B	0.2 yr	Asymptomatic	S	No
8	M	2 yr	B	1.0 yr	Asymptomatic	S	No
9	M	4 yr	B	1.0 yr	Asymptomatic	S	No
10	M	11 yr	B	7.0 yr	Asymptomatic	L + CA[f]	Yes

[a] B = Black, H = Hispanic.

[b] L = large cystic areas, S = small hypoechoic areas, CA = calcification.

[c] PLH = pulmonary lymphoid hyperplasia.

[d] No PLH on high-resolution CT either.

[e] MR imaging showed markedly enlarged parotid glands with multiple lesions with low signal on T1-weighted images and high signal on T2-weighted images.

[f] CT showed large cysts with calcification. Sialography showed cysts communicating with ducts.

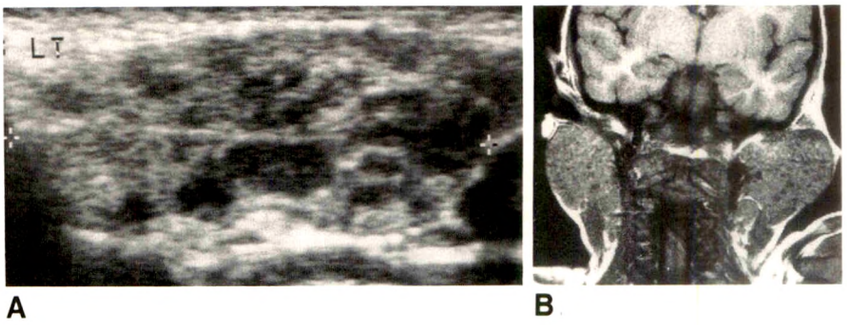


Fig. 1.—7-year-old girl with massive bilateral parotid enlargement.

A, Longitudinal sonogram of left parotid gland shows an enlarged gland with multiple hypoechoic areas consistent with what have been described as lymphoepithelial lesions.

B, Coronal T1-weighted (650/17) MR image shows massive bilateral parotid enlargement containing many small low-signal areas.

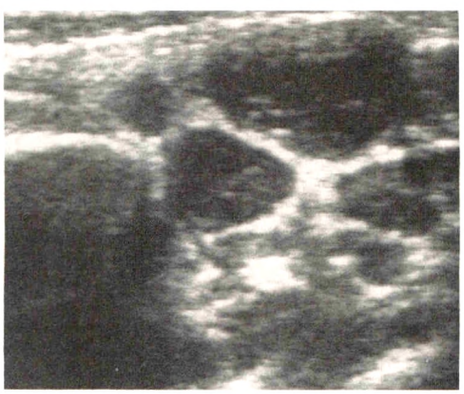


Fig. 2.—10-year-old black girl with chronic parotid enlargement. Longitudinal sonogram of left parotid gland reveals an enlarged gland almost entirely replaced with large cystlike lesions.

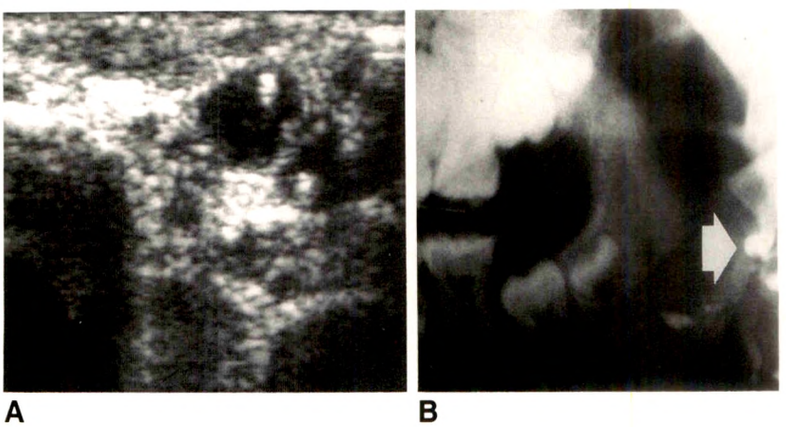


Fig. 3.—*A*, Longitudinal sonogram of enlarged parotid glands in 11-year-old girl shows cystic areas with central bright foci of calcification. Each gland had multiple cysts, most with calcifications.

B, Sialogram shows filling of cysts with contrast material (*arrow*).

were only subsequently found to be HIV seropositive. In general, this group has been free of opportunistic infections. Therefore, in adults the finding of chronic parotid enlargement is significant in that it should suggest the diagnosis of HIV infection [1, 4, 6, 9, 10, 15]. Furthermore, it may indicate a milder clinical course.

We found parotid swelling of various degrees in approximately 10% of HIV-positive children examined in two major health care facilities in New York. This 10% rate may not be accurate, however, because parotid enlargement is at times inconspicuous clinically.

The imaging characteristics of our patients are similar to those described in HIV-seropositive adults on whom biopsy material is available, although limited in numbers. Histologic findings are those of germinal lymphoid hyperplasia containing, in many instances, salivary epithelial elements and cysts (lymphoepithelial cysts) [3, 5, 6, 10, 15, 16]. The epithelial elements are probably related to the embryogenesis of the parotid gland and periparotid tissues, which results in epithelial inclusions in both intraparotid and periparotid lymph nodes [15, 16]. An alternative theory is ductal obstruction caused by lymphocytic infiltration [16]; however, a sialogram obtained in patient 10 (Table 1) revealed no ductal obstruction. Small lesions were generally seen on sonograms of our younger patients, whereas larger "cysts" were seen among older children, suggesting, perhaps, a sequential evolution of these lesions. The sonographic appearance of the small lesions is consistent with hyperplastic lymphoid tissue and is probably similar to the pulmonary abnormality known as lymphocytic interstitial pneumonia or PLH [11, 12]. Their sonographic appearance is consistent with hyperplastic lymphoid tissue. The larger anechoic lesions most likely represent lymphoepithelial cysts.

All the children who had comprehensive immunologic evaluation (Cases 1–5, Table 1) had evidence of antibodies reactive with Epstein-Barr virus, which has been associated with the development of PLH [12]; yet only one of these patients had evidence of PLH on radiologic evaluation. Unlike previous reports [8, 12], no correlation between parotid enlargement and PLH could be shown in this small group of patients.

In adults, parotid enlargement has been found to be associated with the HLA DR5 phenotype, increased CD8+ lymphocytosis, and histologic evidence of PLH [17]. This association may be true for children with parotid enlargement also, as three (75%) of the four children who were tested expressed the HLA DR5 phenotype and showed increased absolute numbers of CD8+ T cells. The finding may be significant considering that the prevalence of HLA DR5 in the general population is only 20% for whites and 25% for blacks [18].

Our study is limited by the small population of patients and the lack of histologic confirmation of the sonographic findings. Such information is difficult to obtain ethically because parotid enlargement does not require biopsy. We wish to emphasize the identical imaging characteristics of the parotid enlargement in adults and children with HIV infection. Parotid enlargement occurs frequently in children and may be associated with a milder clinical course and the lack of detectable PLH.

REFERENCES

1. Ryan JR, Joachim HL, Marmer J, Loubeau JM. Acquired immune deficiency syndrome-related lymphadenopathies presenting in the salivary gland lymph nodes. *Arch Otolaryngol Head Neck Surg* **1985**;111:554–556
2. Colebunders R, Francis H, Mann JM, et al. Parotid swelling during human immunodeficiency virus infection. *Arch Otolaryngol Head Neck Surg* **1988**;114:330–332
3. Kornstein MJ, Parker GA, Mills AS. Immunohistology of the benign lymphoepithelial lesion in AIDS-related lymphadenopathy. *Hum Pathol* **1988**;19:1359–1361
4. Shaha A, Thelmo W, Jaffe BM. Is parotid lymphadenopathy a new disease or part of AIDS? *Am J Surg* **1988**;156:297–300
5. Finfer MD, Schinella RA, Rothstein SG, Persky MS. Cystic parotid lesions in patients at risk for the acquired immunodeficiency syndrome. *Arch Otolaryngol Head Neck Surg* **1988**;114:1290–1294
6. Holliday RA, Cohen WA, Schinella SG, Persky MS, Jacobs JM, Som PM. Benign lymphoepithelial parotid cysts and hyperplastic cervical adenopathy in AIDS-risk patients: a new CT appearance. *Radiology* **1988**;168:439–441
7. Williams MA. Head and neck findings in pediatric acquired immune deficiency syndrome. *Laryngoscope* **1987**;97:713–716
8. Goddart D, Francois A, Ninane J, et al. Parotid gland abnormality found in children seropositive for the human immunodeficiency virus (HIV). *Pediatr Radiol* **1990**;20:355–357
9. Chapnik JS, Noyek AM, Berris B, et al. Parotid gland enlargement in HIV infection: clinical/imaging findings. *J Otolaryngol* **1990**;19:189–194
10. Tunkel DE, Loury MC, Fox CH, Goins MA, Johns ME. Bilateral parotid enlargement in HIV-seropositive patients. *Laryngoscope* **1989**;99:590–595
11. Rubinstein A, Sicklick M, Gupta A, et al. Acquired immunodeficiency with reversed T4/T8 ratios in infants born to promiscuous and drug-addicted mothers. *JAMA* **1983**;249:2350–2356
12. Rubinstein A, Morecki R, Silverman B, et al. Pulmonary disease in children with acquired immune deficiency syndrome and AIDS-related complex. *J Pediatr* **1986**;108:498–503
13. Bodmer WF, Bodmer JC. Cytofluorochromasia for HLA-A,B,C and DR typing. In: *NIAID manual of tissue typing techniques*. NIH Publication 1979-80;80:545. Washington DC: U.S. Govt Printing Office, **1979**
14. Danilovs J, Terasaki PI, Park S, Ayoub G. B lymphocyte isolation by thrombin-nylon wool. In: Terasaki PI, ed. *Histocompatibility testing*. Los Angeles: UCLA Tissue Typing Laboratory, **1980**
15. Smith FB, Rajdeo H, Panesar N, Bhuta K, Stahl R. Benign lymphoepithelial lesion of the parotid gland in intravenous drug users. *Arch Pathol Lab Med* **1988**;112:742–745
16. Shugar JMA, Som PM, Jacobson AL, et al. Multicentric parotid cysts and cervical adenopathy in AIDS patients. A newly recognized entity: CT and MRI manifestations. *Laryngoscope* **1988**;98:772–775
17. Itescu S, Brancato LJ, Buxbaum J, et al. A diffuse infiltrative CD8 lymphocytosis syndrome in human immunodeficiency virus (HIV) infection: a host immune response associated with HLA DR5. *Ann Intern Med* **1990**;112:3–10
18. Joint report. Histocompatibility testing 1980. In: Terasaki PI, ed. *Histocompatibility testing*. Los Angeles: UCLA Tissue Typing Laboratory, **1980**

Case Report

Goitrous Cretinism Manifesting as Newborn Stridor: CT Evaluation

Robert J. Optican,[1] Keith S. White,[2] and Eric L. Effmann[3]

Retropharyngeal masses can be an important cause of respiratory distress in neonates and infants. Causes vary with age, but include retropharyngeal abscess, cystic hygroma, neuroblastoma, hemangiona, branchial cleft cyst, hematoma, and hypothyroidism. Hypothyroidism is one cause of a neonatal retropharyngeal mass that has previously been attributed to soft-tissue myxedema [1]. Experience with a recent case shows that an enlarged thyroid gland can compress the airway.

Case Report

The patient is a full-term, 3815-g female neonate. The patient's mother had no history of thyroid abnormality and did not take any medication during the pregnancy. Two days after birth, the patient was noted to have a high-pitched cry with stridorous respirations. Lateral radiographs of the neck showed retropharyngeal thickening (Fig. 1A), which was confirmed on fluoroscopic examination. Physical examination was unremarkable. Sonography was requested, but the examination was limited by poor access. CT of the neck, done 4 days after birth, showed an enhancing, "double-barrelled" retrotracheal mass extending from the craniocervical junction to the thoracic inlet (Fig. 1B). The mass was continuous with the thyroid isthmus and was thought to represent thyroid tissue. Three-dimensional reconstruction confirmed that this mass encircled the trachea and pharynx (Fig. 1C). A ^{99m}Tc-thyroid scan showed uptake in an area corresponding to the mass identified on CT.

Synthroid (levothyroxine sodium) supplementation was instituted on the basis of the radiologic findings. Analysis of serum samples drawn on day 5 confirmed low thyroxine levels (T_4 index was 1.9; normal in neonates is 9.3–26.6) with correspondingly high levels of thyroid-stimulating hormone (>60 mU/l, normal in neonates is 3–12 mU/ml). Two days after treatment was started, the stridor resolved. The results of the State Health Department's thyroid screening confirmed the hospital laboratory findings, but were not available until 4 weeks later. Follow-up examination 5 months later showed the patient's thyroid-stimulating hormone and thyroxine levels to be within the normal range. Her height, weight, and development were within normal limits.

Discussion

Embryologically, the thyroid gland forms from three constituents: a median anlage forms as a diverticulum from the base of the tongue (foramen cecum) and fuses with two lateral anlagen from the fifth branchial pouch. The thyroid components descend in anatomic relationship to the developing heart. Abnormalities in this relationship lead to ectopy. The lateral lobes of the thyroid gland normally lie between the trachea (anteromedially) and the carotid sheath (posterolaterally). The unusual posterior location of the lateral lobes in this case is presumed to be due in part to their pathologic enlargement. The massive nature of the lobes is presumably due to dyshormonogenesis and compensatory glandular hypertrophy. Histologic proof was unattainable in our case.

Among the causes for a retropharyngeal mass in neonates, thyroid causes are often overlooked because of the usual

Received February 4, 1991; accepted after revision April 10, 1991.
[1] Department of Radiology, Box 3808, Duke University Medical Center, Durham, NC 27710. Address reprint requests to R. J. Optican.
[2] Department of Radiology, Children's Hospital Medical Center, Cincinnati, OH 45229.
[3] Department of Radiology, Children's Hospital Medical Center, Seattle, WA 98105.

AJR **157:557–558, September 1991** 0361–803X/91/1573–0557 © American Roentgen Ray Society

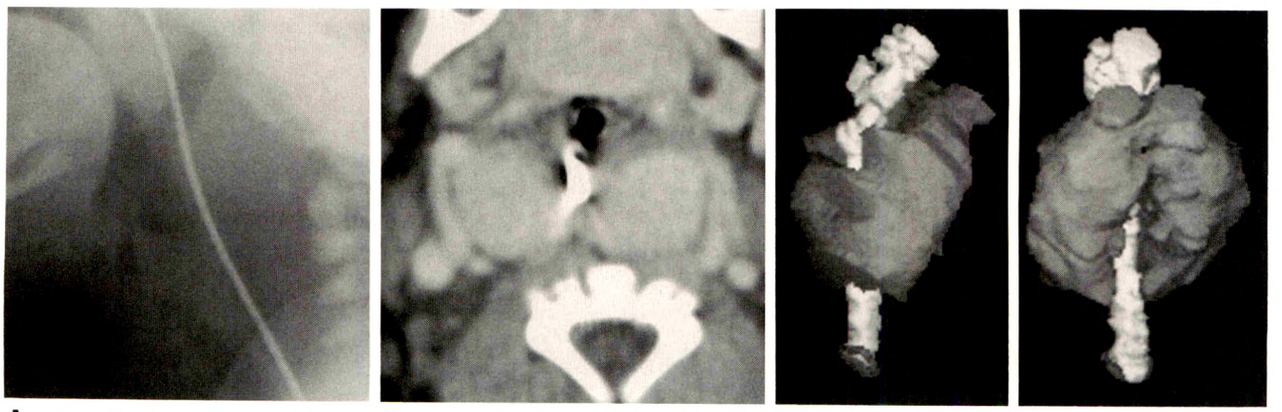


Fig. 1.—*A*, Lateral radiograph shows thickening of retropharyngeal soft tissues. Fluoroscopy confirmed constancy of this finding.
***B*, Transaxial CT scan of neck shows a bilobed, enhancing retropharyngeal mass. Each lobe is positioned between hypopharynx medially and respective carotid sheath laterally. A nasogastric tube causes some streak artifact.**
***C* and *D*, Computer-generated three-dimensional CT reconstruction of goiter encircling airway. Left anterior oblique view (*C*) shows thyroid isthmus anteriorly. Left posterior oblique view (*D*) shows large lateral lobes posterior to airway. Lobes abut each other superiorly.**

lack of overt signs of hypothyroidism. The most common causes of neonatal hypothyroidism (a congenitally aplastic, hypoplastic, or malfunctioning ectopic gland) usually do not cause symptoms of tracheal compression. Defects in thyroid hormone synthesis (i.e., goitrous cretinism) account for most of the remaining causes and may have mass effect on the trachea because of compensatory glandular hypertrophy. Other causes of neonatal hypothyroidism include iodine deficiency, maternal medication, and pituitary disease; these do not usually cause tracheal compression.

Normal thyroid tissue can usually be distinguished on CT examination because of its location (superior aspect usually near the inferior aspect of the cricoid cartilage) and density. The density of normal thyroid tissue on unenhanced scans is greater than that of soft tissue because of the thyroid gland's high iodine content. Normal thyroid tissue density is also higher on enhanced scans owing to its rich vascular supply. Abnormal masses of thyroid origin can be distinguished as such by their attenuation value and by their continuity with the thyroid gland [2]. Both of these criteria were present in this case.

Scintigraphy confirmed the identity of the mass found on CT before the results of biochemical testing were available. In cases of suspected neonatal hypothyroidism, scintigraphy is considered the gold standard by which the anatomic diagnosis of neonatal hypothyroidism is made [3].

Retropharyngeal thickening in association with neonatal hypothyroidism has been described before [1]. McCook and Felman [4] reported two cases of a retropharyngeal mass in association with infantile hypothyroidism. Most published reports implicate myxedematous soft-tissue swelling as the cause of retropharyngeal thickening. Histologically, myxedema represents connective tissue accumulation of hyaluronic acid, associated with excess sodium, water, and albumin [5]. This case demonstrates the goiter itself to be a cause of retropharyngeal soft-tissue thickening. We believe that some of the previously reported cases of retropharyngeal thickening associated with neonatal hypothyroidism may have actually been unrecognized goiters.

Diagnostic imaging information is important clinically. Scintigraphy often confirms the diagnosis before biochemical results are available, allowing earlier treatment. With early treatment, many infants can expect to attain normal IQ, height, and weight. Also, treatment can help alleviate symptoms of mass effect. Lastly, parents of infants with goiters due to dyshormonogenesis (usually an autosomal recessive condition) should be aware of the chances of disease in future offspring.

REFERENCES

1. Grunebaum M, Moskowitz G. The retropharyngeal soft tissues in young infants with hypothyroidism. *AJR* **1970**;108:543–545
2. Siegel MJ, St. Amour TE. Neck. In: Siegel MJ, ed. *Pediatric body CT*. New York: Churchill Livingstone, **1988**:293–311
3. Wells RG, Sty JR, Duck SC. Technetium 99m pertechnetate thyroid scintigraphy: congenital hypothyroid screening. *Pediatr Radiol* **1986**; 16:368–373
4. McCook TA, Felman AH. Retropharyngeal masses in infants and young children. *Am J Dis Child* **1979**;133:41–43
5. Kohn LD. Connective tissue. In: Ingbar S, Braverman L, eds. *Werner's the thyroid*. Philadelphia: Lippincott, **1986**:1128–1129



Pictorial Essay

Biological Classification of Soft-Tissue Vascular Anomalies: MR Correlation

James S. Meyer,[1,2] Fredric A. Hoffer,[1] Patrick D. Barnes,[1] and John B. Mulliken[3]

When vascular anomalies are separated into the infantile hemangiomas and vascular malformations in a biological classification system, the MR appearances based on features of flow-related and static tissue are unique and consistent.

MR imaging has proved useful for delineating the extent of vascular anomalies when applied to arteriovenous malformations (AVMs) [1] or lymphatic malformations [2]. However, the term hemangioma is often used generically, and in the past has been used to describe a combination of infantile hemangiomata and venous malformations with confusing radiologic findings [3]. The biological classification of vascular anomalies proposed by Mulliken et al. [4, 5] is based on cellular turnover, histology, natural history, and physical findings. It clearly separates hemangiomas of infancy (tumors with an early proliferative and later involuting stage) from vascular malformations: capillary, lymphatic, venous, arterial, or combined (e.g., capillary venous, lymphaticovenous, AVM). This classification has been useful clinically [5], has been correlated with angiography [6], and recently has been adopted for interventional radiology [7]. It is the official nomenclature for the International Workshop for the Study of Vascular Anomalies [5].

Materials and Methods

MR examinations were performed between 1988 and 1990 in 23 patients with vascular anomalies classified by the biological system and histologic correlation. Five patients 0–3 years old had hemangiomas, three patients 7–13 years old had AVMs, three patients 4–25 years old had venous malformations, six patients 0–9 years old had lymphatic malformations, and six patients 8–21 years old had lymphaticovenous malformations.

MR was performed on a 1.5-T General Electric Signa unit with a combination of sequences including T1-weighted longitudinal spin-echo (SE), 400–600/15–20 (TR/TE), and T2-weighted axial SE, 2000/20–30,80, with presaturation superiorly and inferiorly. On the SE presaturation sequences, the protons flowing rapidly into the imaging volume were presaturated and therefore appeared as flow voids relative to the unaffected slow-flow blood or stationary tissues that were in the volume. A gradient-recalled echo (GRE) axial sequence with gradient-moment nulling was also obtained as single-slice gradient-recalled acquisition in the steady state (GRASS), GRE 33/13/30° (TR/TE/flip angle), or multiplanar GRE, GRE 450–750/13/30°. On GRE sequences with gradient-moment nulling, the rapidly flowing protons are rephased and appear as a very intense signal, especially with GRASS [8]. Anomalies demonstrating vascular flow voids on SE presaturation images and vascular high-intensity flow enhancement on GRE images with gradient-moment nulling were designated high-flow anomalies, while those not showing vascular flow voids on SE

Received January 14, 1991; accepted after revision April 9, 1991.
Presented at the annual meeting of Society for Pediatric Radiology, Cincinnati, OH, April 1990.
[1] Department of Radiology, The Children's Hospital and Harvard Medical School, 300 Longwood Ave., Boston, MA 02115. Address reprint requests to F. A. Hoffer.
[2] Present address: Department of Radiology, Children's Hospital of Philadelphia, Philadelphia, PA 19104.
[3] Division of Plastic Surgery, The Children's Hospital and Harvard Medical School, Boston, MA 02115.

AJR **157:559–564, September 1991** 0361–803X/91/1573–0559 © American Roentgen Ray Society



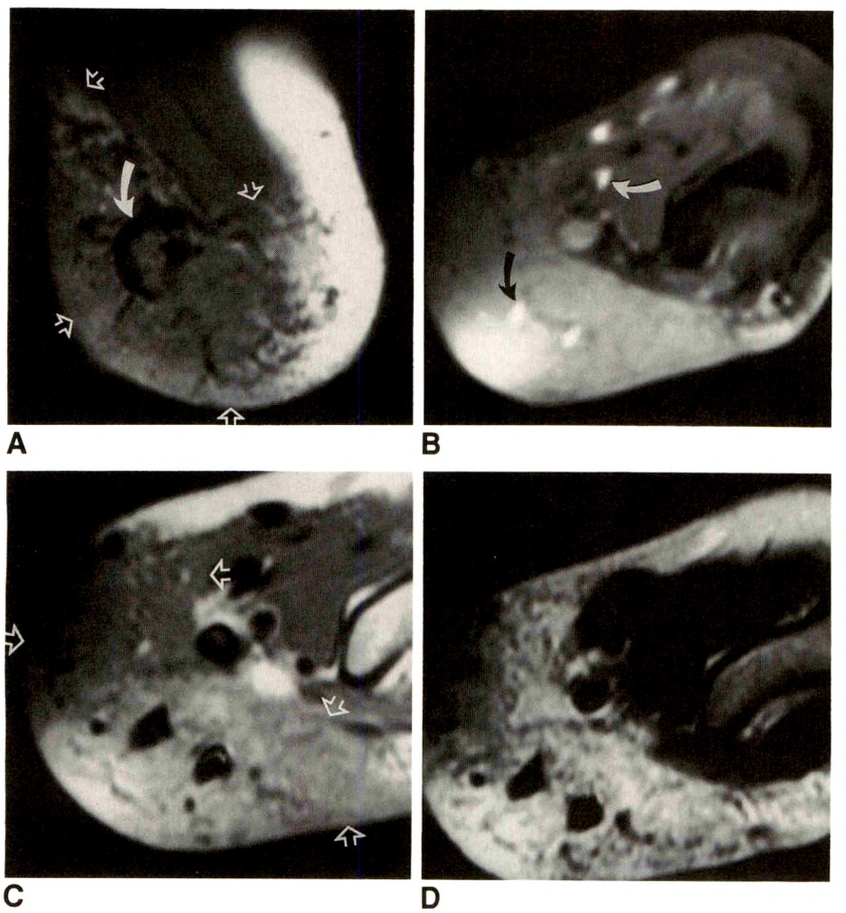


Fig. 1.—3-year-old boy with large hemangioma of left upper arm.

***A,* Sagittal T1-weighted SE presaturation MR image shows intermediate intensity of tumor parenchyma (*open arrows*) containing vascular flow voids (*solid arrow*).**

***B,* Corresponding axial multiplanar GRE image with gradient-moment nulling shows high-signal vessels (*arrows*) within and about tumor.**

***C,* Axial proton-density SE presaturation image shows intermediate-intensity tumor parenchyma (*arrows*) and vascular flow voids.**

***D,* Axial T2-weighted SE presaturation image shows high-intensity tumor parenchyma and vascular flow voids. Lesion was totally resected owing to recurrent venous thrombosis and pain.**

presaturation images were labeled low-flow anomalies. Gadopentetate dimeglumine was administered immediately before the last T1-weighted SE presaturation sequence in five cases.

Results

Hemangiomas

All five hemangiomas were high flow (Figs. 1, 2A, and 2B). In two patients who were treated with an antiangiogenesis agent (a medication that inhibits vascular proliferation), high-flow characteristics (Fig. 2C) in the lesion were less distinct. All hemangiomas had solid tissue, which was of intermediate intensity on T1-weighted SE presaturation images and bright on T2-weighted SE presaturation images. The one patient with Kasabach-Merritt syndrome (thrombocytopenic coagulopathy), who was studied early, had a diffuse infiltrative or edemalike pattern (Fig. 2). Contrast material, however, helped to differentiate the enhancing hemangioma tissue from edema.

Arteriovenous Malformations

The three AVMs had an MR appearance of high flow (Figs. 3 and 4) with flow voids on SE presaturation images, but only two had vascular flow enhancement on GRE images with gradient-moment nulling. One small AVM was dark on GRE images with gradient-moment nulling perhaps from turbulent flow. AVMs were differentiated from hemangiomas by their lack of solid-tissue abnormality (none were bright on T2-weighted SE presaturation images).

Venous Malformations

Three venous malformations have been studied, all of which manifested slow flow (Fig. 5). The typical pattern was of a less intense signal from the venous space on GRE images with gradient-moment nulling than on the very bright T2-weighted SE presaturation images. All of the venous malformations were of intermediate intensity, slightly more intense than muscle on T1-weighted SE presaturation images. Contrast material was administered in one patient, and the venous channels enhanced (Fig. 6).

Lymphatic Malformations

There were six cases of lymphatic malformations, all of which manifested slow flow. Two were cystic (Figs. 7 and 8). The cystic portions were low intensity when compared with

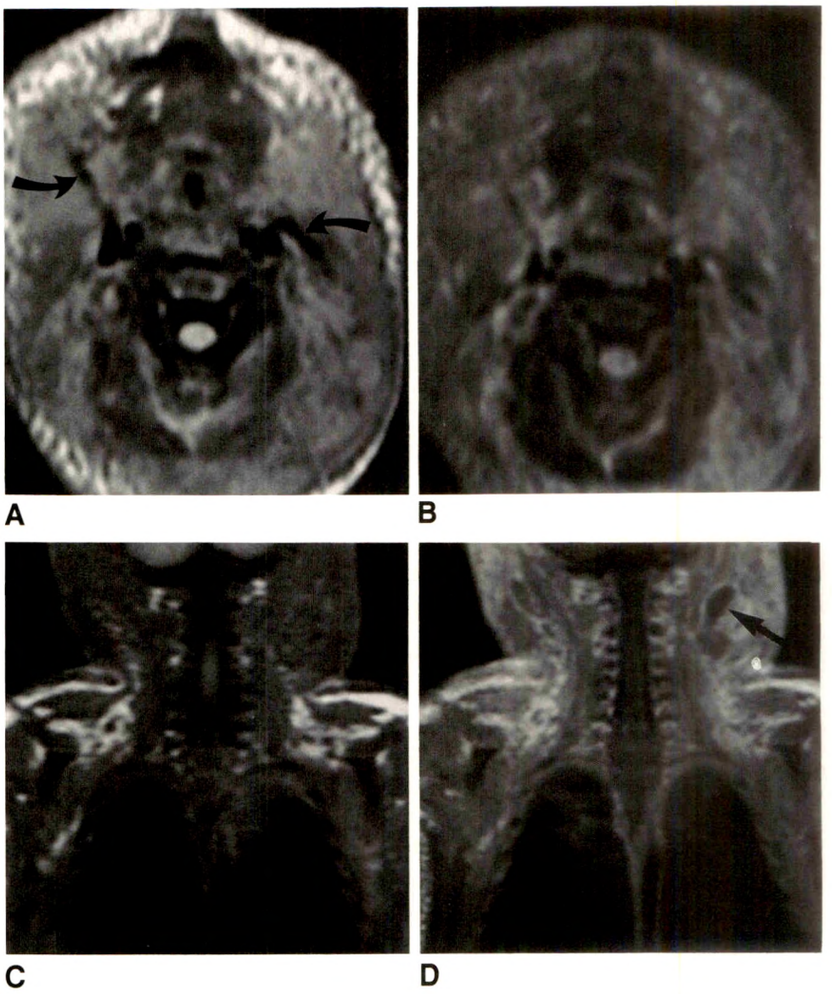


Fig. 2.—10-day-old girl with Kasabach-Merritt syndrome has extensive and rapidly growing hemangioma of neck and upper chest.

A, Axial proton-density SE presaturation MR image shows flow voids (*arrows*) and intermediate-intensity soft tissue, which infiltrates and replaces a portion of subcutaneous fat (edema pattern).

B, Axial T2-weighted SE presaturation image shows mild brightening of signal from hemangioma.

C, Coronal T1-weighted SE presaturation image 2 weeks after *A* and *B*, after treatment with antiangiogenesis factor, shows essentially no change in diffuse infiltrating process, but flow voids are not as prominent.

D, Gadopentetate-dimeglumine enhancement further delineates diffuse hemangioma. Nonenhancing area correlated with finding of fibrin thrombi (*arrow*) on histology. The patient died despite aggressive medical therapy.

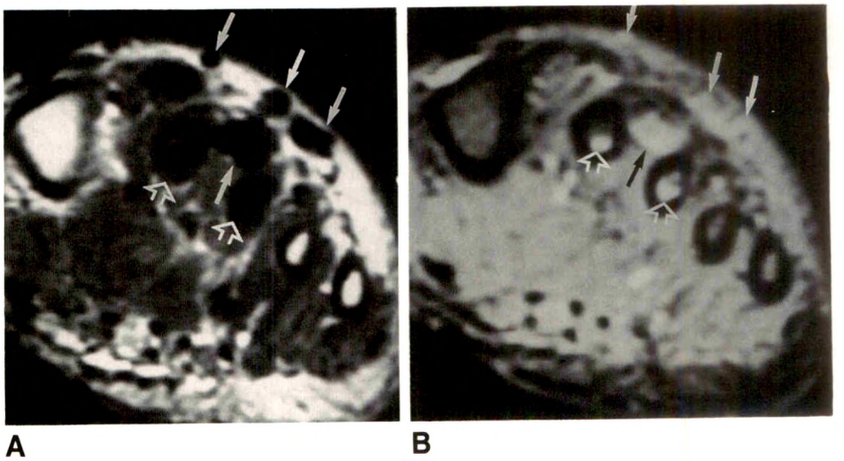


Fig. 3.—11-year-old girl with an arteriovenous malformation of the foot.

A, Axial T2-weighted SE presaturation MR image shows vascular flow voids in second and third metatarsal bones (*open arrows*) and in subcutaneous and cutaneous tissues (*solid arrows*).

B, Corresponding axial multiplanar GRE image with gradient-moment nulling shows vascular intensities (*arrows*) in same areas. Arteriovenous malformation has since been resected and recurred several times.

muscle on T1-weighted SE presaturation images and did not enhance with gadopentetate dimeglumine (Fig. 8). The other four lymphatic malformations were made predominantly of septa rather than cystic spaces. All lymphatic malformations were bright on T2-weighted SE presaturation images. Hemorrhage was present in one case (Fig. 9).

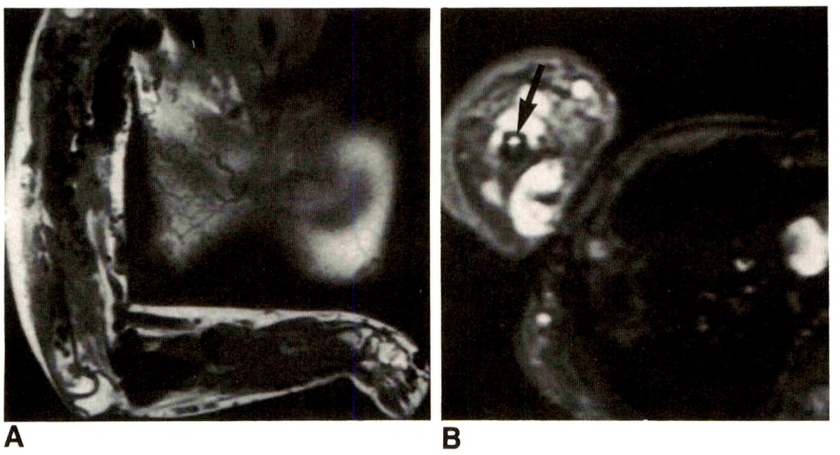


Fig. 4.—14-year-old girl with a chronic debilitating arteriovenous malformation of the right arm.
A, Coronal oblique T1-weighted SE presaturation MR image shows diffuse flow voids, mainly of proximal arm and chest.
B, Axial GRASS image with gradient-moment nulling shows vascular flow enhancement of large vessels within soft tissues and within medullary cavity of humerus (*arrow*).

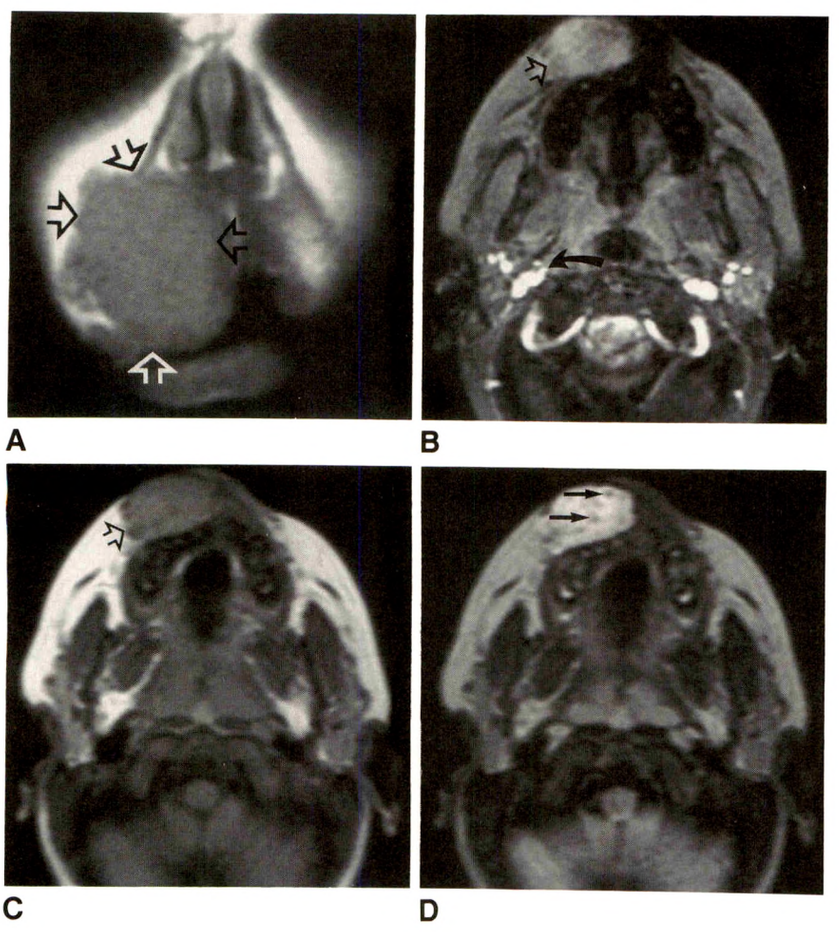


Fig. 5.—4-year-old boy with compressible blue venous malformation of right upper lip.
A, Coronal T1-weighted SE presaturation MR image shows intermediate-intensity lesion (*arrows*) with no flow voids.
B, Axial GRASS image with gradient-moment nulling shows intermediate-intensity lesion (*open arrow*) and high-intensity flow in normal vessels outside malformation (*solid arrow*).
C, Axial proton-density SE presaturation image shows intermediate-intensity homogeneous lesion (*arrow*).
D, Axial T2-weighted SE presaturation image shows high-intensity mass containing low-intensity punctate areas (*arrows*) suggesting early calcification or hemosiderin deposition. Note displacement of teeth posterior to mass. This venous malformation was later sclerosed, then resected.

Lymphaticovenous Malformations

The lymphaticovenous malformation is a combined malformation with both lymphatic and venous channels. All six of these malformations had slow-flow characteristics on MR. They shared other characteristics with the lymphatic and venous malformations, such as having a fibrofatty matrix (two venous malformations, four lymphatic malformations, four lymphaticovenous malformations) (Fig. 10). The venous component of the lymphaticovenous malformation enhanced (Fig. 11) in the two cases in which gadopentetate dimeglumine was administered.

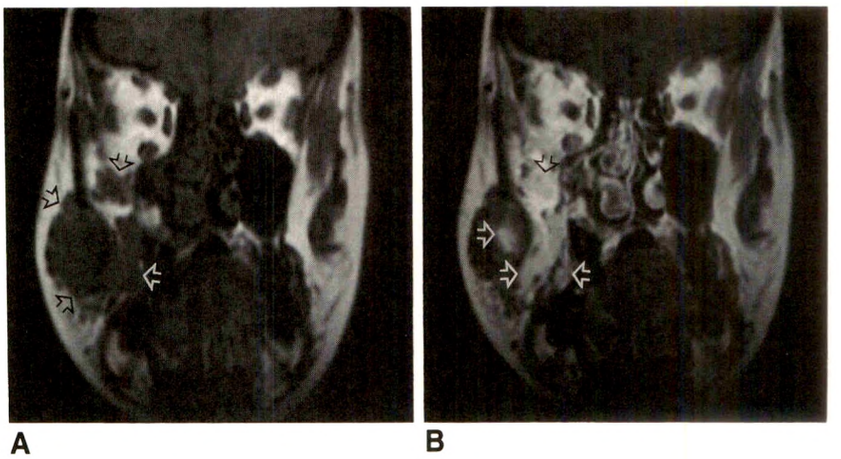


Fig. 6.—25-year-old woman with compressible venous malformation of right side of face.

A, Coronal T1-weighted SE presaturation MR image shows intermediate-intensity lesions (*arrows*) slightly brighter than tongue.

B, Gadopentetate dimeglumine provides enhancement of venous channels of malformation (*arrows*).



Fig. 7.—3-week-old boy with massive lymphatic malformation involving left side of neck, chest, and upper extremity. Coronal T1-weighted SE presaturation MR image shows large cystic areas (*arrows*) of low intensity. Malformation was later partially resected.

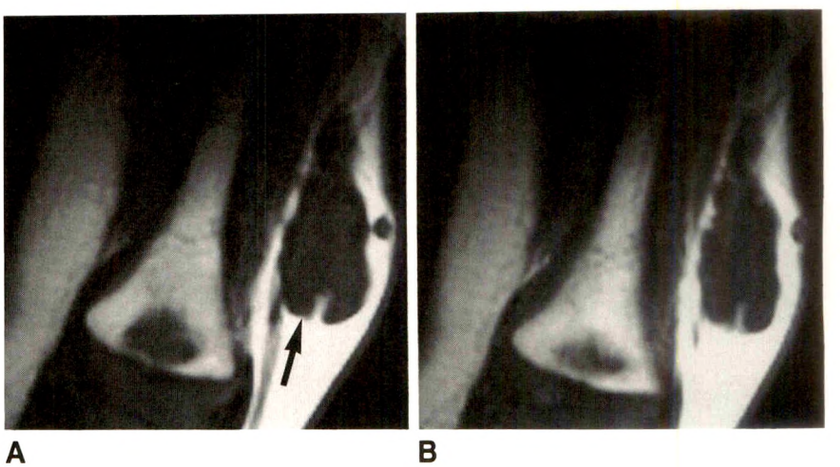


Fig. 8.—2-year-old boy with small fluctuant lymphatic malformation in medial upper arm.

A, Coronal T1-weighted SE presaturation MR image shows a subcutaneous low-intensity lesion (*arrow*).

B, Enhancement occurs in septa only. The malformation was later resected.

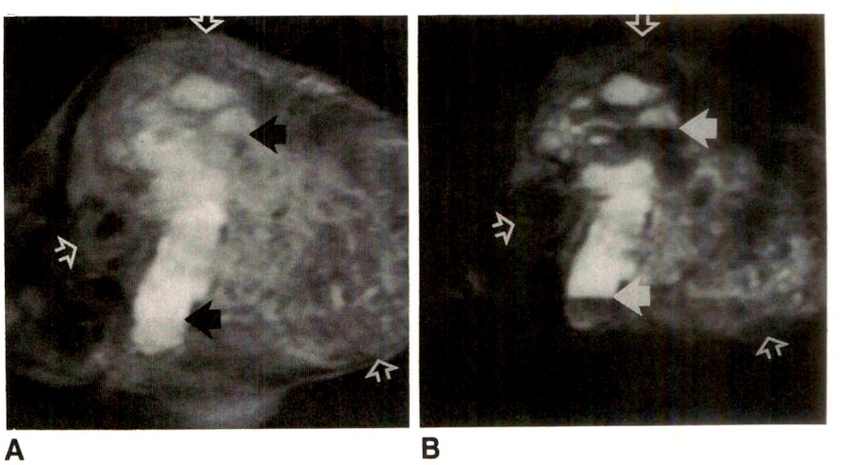


Fig. 9.—2-year-old girl with a large lymphatic malformation of left side of face, tongue, and floor of mouth.

A, Axial proton-density SE presaturation MR image shows large lesion (*open arrows*) containing fluid-fluid levels (*solid arrows*) with areas of high and intermediate intensity.

B, Corresponding axial T2-weighted SE presaturation image shows lesion (*open arrows*) and fluid-fluid levels (*solid arrows*). Upper high-intensity fluid levels probably represent serum or methemoglobin. Lower fluid areas are darker than in *A* and probably represent clot or hemosiderin.

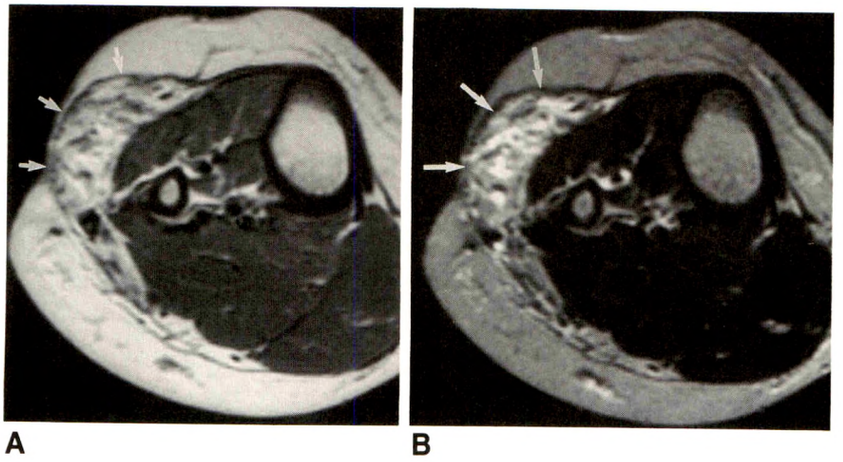


Fig. 10.—8-year-old girl with a lymphaticovenous malformation of leg.

A, Axial proton-density SE presaturation MR image shows lesion (*arrows*) containing areas of high, intermediate, and low intensity.

B, Corresponding axial T2-weighted SE presaturation image shows lesion (*arrows*) with high-intensity areas of blood or lymph (intermediate intensity in *A*). Intermediate-intensity areas represent fat (high intensity in *A*). Low-intensity areas represent fibrous septa (low intensity in *A*).

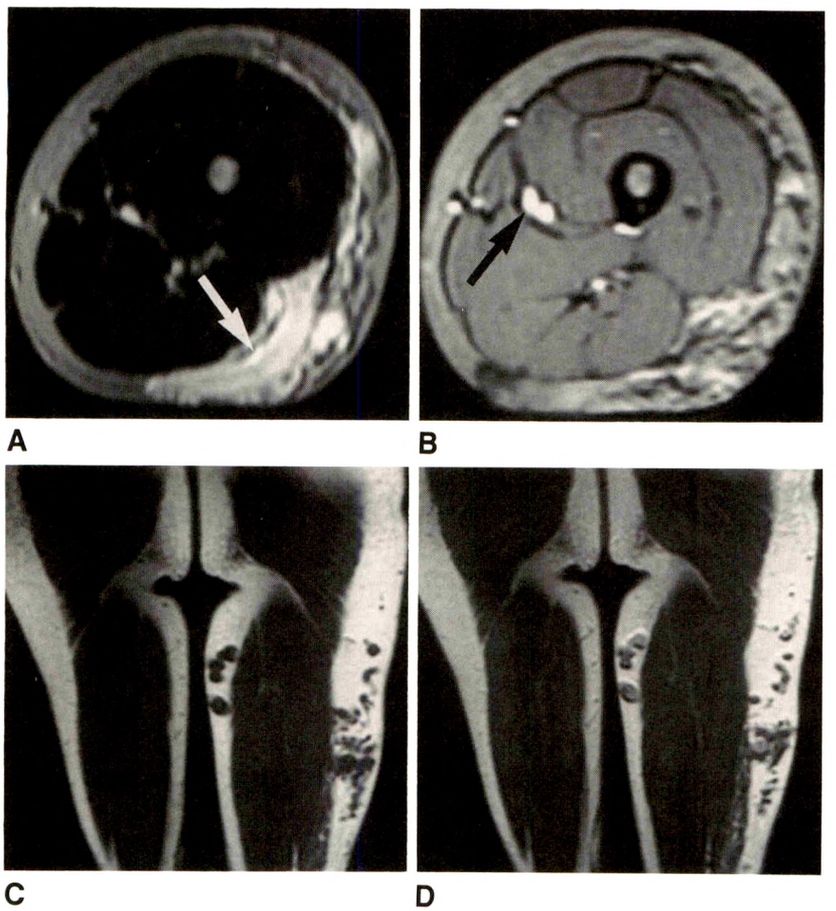


Fig. 11.—16-year-old boy with lymphaticovenous malformation of left leg.

A, Axial T2-weighted SE MR image shows high-signal malformation (*arrow*) of subcutaneous tissue in left leg.

B, Axial GRASS image with gradient-moment nulling shows normal-sized high-flow vessels (*arrow*) and no flow enhancement of lesion.

C, Coronal T1-weighted SE presaturation image shows low to intermediate intensity within subcutaneous fat of left thigh.

D, Gadopentetate dimeglumine enhances venous but not lymphatic component of malformation.

REFERENCES

1. Cohen JM, Weinreb JC, Redman HC. Arteriovenous malformations of the extremities: MR imaging. *Radiology* **1986**;158:475–479
2. Siegel MJ, Glazer HS, St. Amour TE, Rosenthal DD. Lymphangiomas in children: MR imaging. *Radiology* **1989**;170:467–470
3. Kaplan PA, Williams SM. Mucocutaneous and peripheral soft-tissue hemangiomas: MR imaging. *Radiology* **1987**;163:163–166
4. Mulliken JB, Glowacki J. Hemangiomas and vascular malformations in infants and children: a classification based on endothelial characteristics. *Plast Reconstr Surg* **1982**;69:412–420
5. Mulliken JB, Young AE. *Vascular birthmarks: hemangiomas and malformations*. Philadelphia: Saunders, **1988**:483
6. Burrows PE, Mulliken JB, Fellows KE, Strand RD. Childhood hemangiomas and vascular malformations: angiographic differentiation. *AJR* **1983**; 141:483–488
7. Yakes WF, Luethke JM, Parker SH, et al. Ethanol embolization of vascular malformations. *RadioGraphics* **1990**;10:787–796
8. Evans AJ, Hedlund LW, Herfkens RJ, et al. Evaluation of steady and pulsatile flow with dynamic MR using limited flip angles and gradient refocused echoes. *Magn Reson Imaging* **1987**;5:475–482

MR Imaging of Cerebral Ischemia:
Findings in the First 24 Hours

William T. C. Yuh[1]
Martin R. Crain[1]
Daniel J. Loes[1]
George M. Greene[2]
Tony J. Ryals[1]
Yutaka Sato[1]

MR changes of cerebral ischemia have been shown to occur as early as 1–2 hr after vessel occlusion in experimental models of stroke. However, the MR findings in the early stages of ischemic stroke in the clinical population have not been well established. We studied 41 lesions in 39 patients in whom MR was performed within the first 24 hr after onset of ischemic symptoms. Twenty-five lesions were studied with gadopentetate dimeglumine. Vascular flow-related abnormalities, including absence of normal flow void and presence of arterial enhancement, were the earliest MR findings, detected within minutes of onset. Morphologic changes (brain swelling) on T1-weighted images without signal changes on T2-weighted images could be detected within the first few hours. Signal changes were not usually found before 8 hr on T2-weighted images or before 16 hr on T1-weighted images. In contrast to the absence of parenchymal enhancement typically found in cortical infarctions in the first 24 hr, a few lesions (including transient occlusions, partial occlusions, and isolated watershed infarctions) exhibited early, exaggerated parenchymal enhancement.

We conclude that signal changes may not be reliable in detecting ischemic stroke within the first 8 hr after onset. Vascular abnormalities, when present, are the most reliable and earliest findings. Other MR findings of early ischemic stroke, including morphologic changes and early, exaggerated parenchymal enhancement, may also precede signal changes. Paramagnetic contrast administration often provides valuable information in the detection and evaluation of acute ischemia.

AJNR 12:621–629, July/August 1991; *AJR* 157:565–573, September 1991

The diagnosis of acute stroke in its very early stages by clinical and radiologic methods can be difficult. An early diagnosis of ischemia might allow prompt initiation of treatment aimed at reducing morbidity and mortality and also enable the ongoing assessment of treatment. MR imaging has been shown to be more sensitive than CT in the detection of acute cerebral ischemia (either completed infarct or transient deficit) within the first 72 hr [1–8]. Abnormal MR findings with and without paramagnetic contrast enhancement have also been reported as early as 1–2 hr after onset of vessel occlusion in experimental models of stroke [9–12]. However, the early MR findings of acute stroke in the clinical population have not been well established. Because there are anatomic and physiologic differences between species, the temporal development of ischemic changes in the experimental animal model may differ from that of the human clinical population. The purposes of this study were to examine the earliest MR findings of clinical cerebral ischemia and their temporal progression using unenhanced and enhanced imaging. We also attempted to understand how these changes may reflect underlying pathophysiologic mechanisms in acute cerebral ischemia.

Materials and Methods

All patients who had an MR examination within 24 hr after the onset of ischemic symptoms between November 1988 and February 1990 were evaluated retrospectively. Chosen for

Received July 12, 1990; revision requested November 1, 1990; revision received December 19, 1990; accepted January 1, 1991.

[1] Department of Radiology, The University of Iowa College of Medicine, Iowa City, IA 52242. Address reprint requests to W. T. C. Yuh.

[2] Department of Neurosurgery, The University of Iowa College of Medicine, Iowa City, IA 52242.

0361–803X/91/1573–0565
© American Roentgen Ray Society

TABLE 1: Time of MR After Onset of Cerebral Ischemia and MR Findings at Each Time Interval in 39 Patients

Time After Onset (hr)	No. of Lesions	Absent Flow Void	Arterial Enhancement[a]	Morphologic Changes on T1-Weighted Images	Signal Changes on T1-Weighted Images	Signal Changes on T2-Weighted Images	Parenchymal Enhancement[a]
0–2	8	3	1/4	4	0	0	2/4
2–4	3	2	2/2	2	0	1	0/2
4–8	5[b]	3	4/5	4	2	4[b]	0/5
8–12	2	0	1/1	1	1	2	0/1
12–18	5	1	2/3	4	2	3	1/3
18–24	18	5	6/10	12	10	17	2/10
Total	41	14	16/25	27	15	27	5/25

[a] Expressed as number of lesions with abnormal enhancement per total number receiving gadopentetate dimeglumine at that time interval.
[b] Three of five lesions in this interval were not examined until 8 hr after onset.

inclusion in the final study group were all patients who had positive MR findings in a distribution that corresponded with an initial history and physical examination strongly suggestive of cerebral ischemia. In order to accurately determine the temporal appearance and progression of MR findings, asymptomatic patients (obviously without a time of onset) were excluded from the study group. Also excluded from consideration were patients with clinical signs or symptoms but without corresponding MR abnormalities, owing to the variability in degree of clinical suspicion of ischemia and the resultant lack of specificity of the diagnosis. Forty-one ischemic lesions in 39 patients were studied. Each of two patients had two separate clinical ischemic events that corresponded to separate anatomic lesions on MR images. The timing of onset (either the acute onset of ischemic symptoms in a previously asymptomatic patient or rapid progression of symptoms in a patient with intermittent ischemic symptoms) was determined from the best available clinical history. Patients whose MR examination was performed more than 24 hr after onset of symptoms or whose initial MR or CT examination revealed hemorrhagic infarct were also excluded.

Patients ranged in age from 22 to 91 years (mean, 57 years). Twenty-three were men and 16 were women. Seven patients were imaged after developing neurologic signs due to an iatrogenic cause, including cerebral angiography (three), cardiovascular surgery (two), percutaneous occlusion of the internal carotid artery for treatment of an aneurysm (one), and failed test occlusion of the internal carotid artery (one). Twenty-five lesions were studied with contrast material.

Scans were reviewed retrospectively by two radiologists without knowledge of the duration of ischemic symptoms. Lesions were categorized as cortical when the distribution involved the cortex predominantly and as noncortical when confined primarily to deep white or noncortical gray structures. Special attention was given to the absence of normal flow-void phenomenon and to the presence of any abnormal signal intensity changes, brain morphologic changes (e.g., swelling), and abnormal arterial or parenchymal contrast enhancement. Abnormal arterial enhancement was defined as asymmetric enhancement of arterial structures on short TR spin-echo pulse sequences.

All examinations were performed on either a 0.5-T (Picker International, Highland Heights, OH) or a 1.5-T (General Electric, Milwaukee, WI) superconductive scanner. At least one T1-weighted, 350–700/20–26 (TR/TE), and one T2-weighted (2000–2500/80–100) spin-echo pulse sequence was obtained with 3–10 mm slice thickness. Multiecho pulse sequences were included in all T2-weighted examinations performed at 1.5 T. There was a 10–50% slice gap in the examinations performed at the higher field strength. At least two orthogonal planes were imaged. Extra pulse sequences and planes of imaging were added depending on the individual case. Any patient receiving contrast material was imaged immediately after an IV injection of 0.1 mmol/kg of gadopentetate dimeglumine (Magnevist, Berlex Laboratories, Inc., Wayne, NJ). Postcontrast T1-weighted imaging (without gradient moment nulling) was performed with pulse parameters and imaging planes identical with those of the precontrast T1-weighted sequences.

TABLE 2: MR Findings in Acute Cerebral Ischemia

Mechanism	MR Finding	Possible Causes	Estimated Time[a] (hr)
Flow kinetics	Absent flow	Slow flow; occlusion	Early
	Arterial enhancement	Accentuation of flow derangement	Early
Biophysiologic	T1 morphologic change	Cytotoxic edema (free water)	2–4
	T2 signal change	BBB breakdown; vasogenic edema; macromolecular binding	8
	T1 signal change	BBB breakdown; vasogenic edema; macromolecular binding	16–24
Combination	Delayed parenchymal enhancement[b]	Impaired delivery of significant contrast agent	>24[c]
	Early exaggerated enhancement[d]	Intact delivery of contrast agent; BBB leakage; focal hyperemia	2–4[d]

Note.—BBB = blood-brain barrier.
[a] Time at which findings generally could first be detected by available MR examinations; this does not necessarily imply the exact time of onset.
[b] Typical finding in completed cortical infarctions.
[c] Usually not detected before 5–7 days.
[d] Found in a few cases with transient or partial occlusions and in watershed infarctions.

Results

The temporal distribution of MR examinations after the onset of symptoms and the individual MR findings in each time interval are summarized in Table 1. MR was obtained within the first 4 hr in 11 lesions. Twenty-five lesions were cortical and 16 were noncortical. Table 2 summarizes the early MR findings of ischemia and the estimated time at which they could be detected.

Abnormal Vascular Findings

The earliest MR findings detected in acute cerebral ischemia were vascular abnormalities in major intracranial vessels, including the absence of normal flow-void phenomenon and/

or the presence of arterial enhancement (Fig. 1A). The earliest findings were seen in a patient who had a cardiac arrest during the MR examination. Absence of normal flow void was seen within 8 min of the last documented normal flow void on an earlier pulse sequence (Fig. 2). Most (22 of 41) of the lesions imaged in the first 24 hr were associated with vascular abnormalities (Fig. 1A); eight showed both absence of flow void and arterial enhancement, eight showed only arterial enhancement, and the remaining six lesions showing absence of flow void were not studied with contrast material. Vascular abnormalities were detected in three of eight lesions evaluated in the first 2 hr and in more than half of the total lesions evaluated by 4 hr (six of 11) and by 6 hr (seven of 13).

An absence of normal flow void in a major intracranial artery was detected in association with 14 lesions. Eight lesions were in internal carotid/middle cerebral artery distributions (Fig. 3) and six were in the vertebrobasilar system (Fig. 4).

Arterial enhancement was found in association with 16 of the 25 lesions studied with contrast MR within the first 24 hr (Fig. 5). Thirteen of the 16 were in a cortical distribution. Arterial enhancement was seen in one of four lesions evaluated in the first 2 hr, in two lesions evaluated between 2 and 4 hr, and in one of two lesions evaluated between 4 and 6 hr. No arterial enhancement was seen within the first 24 hr in any case of isolated supratentorial noncortical infarction.

Five patients who received contrast material in our series also underwent cerebral angiography within 24 hr of the MR examination. Of the three in whom arterial enhancement was detected, two demonstrated slow antegrade flow in the middle cerebral artery at angiography (one case of nonoccluding intraluminal clot and one case of moyamoya disease). The third showed proximal occlusion of the middle cerebral artery with delayed retrograde filling of distal middle cerebral branches via leptomeningeal collaterals. The two other patients who had angiography within 24 hr of the MR examination included one person with a failed test occlusion of the internal carotid artery before MR and one person whose aneurysm was successfully treated by balloon occlusion of the internal carotid. In both cases, MR failed to demonstrate arterial enhancement.

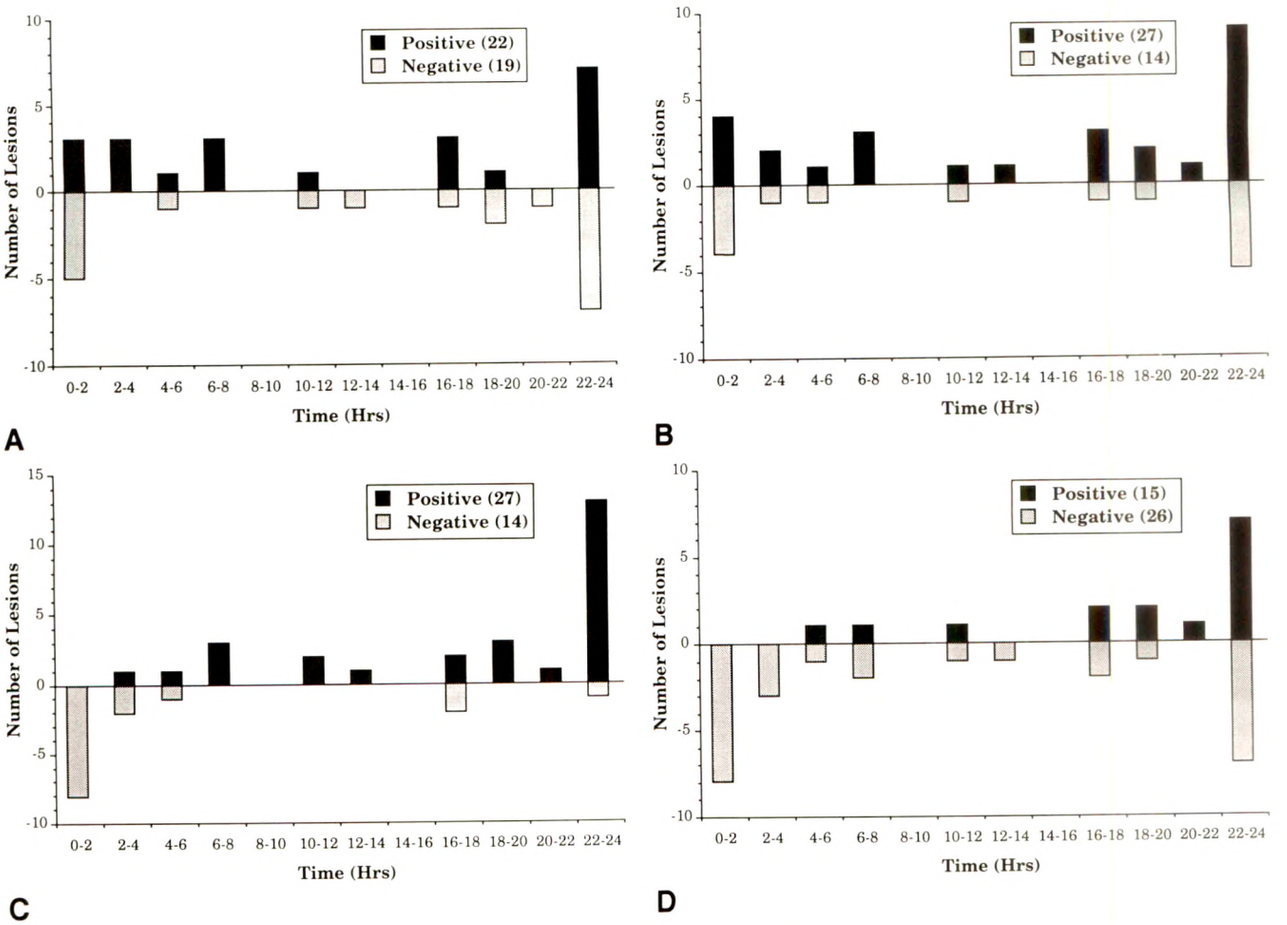


Fig. 1.—Temporal distribution of MR findings within first 24 hr after onset of ischemic symptoms.
A, Positive vascular findings in first 24 hr. Vascular findings include absence of flow void and/or presence of arterial enhancement.
B, T1 morphology in first 24 hr. Morphologic change is defined as evidence of brain swelling demonstrated by T1-weighted images.
C, T2 signal changes in first 24 hr. T2 signal change refers to abnormally high signal intensity of brain parenchyma.
D, T1 signal changes in first 24 hr. T1 signal change refers to abnormally low signal intensity of brain parenchyma.

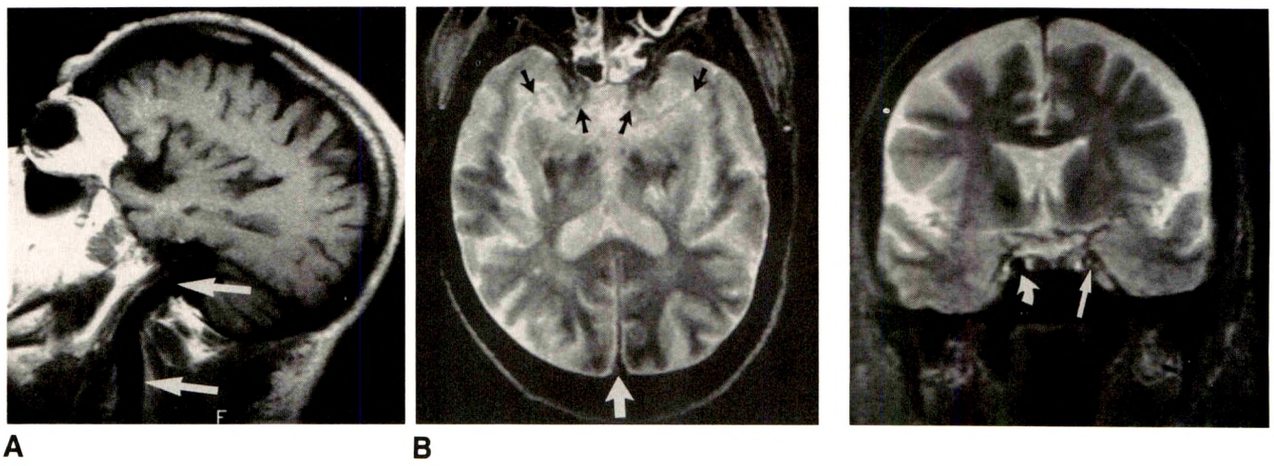


Fig. 2.—71-year-old man who had a cardiac arrest during MR examination.
A, Initial parasagittal T1-weighted image (400/20) shows flow-void phenomenon within jugular vein (*arrows*).
B, Axial T2-weighted image (2000/100) obtained 8 min later shows absence of flow-void phenomenon within middle cerebral and distal internal carotid arteries (*small black arrows*) and in superior sagittal sinus (*large white arrow*). Note old stroke in left thalamic region.

Fig. 3.—63-year-old man with acute onset of diminished vision in left eye. Coronal T2-weighted image (2000/100) obtained 18 hr after onset shows absence of flow-void phenomenon in left internal carotid artery (*straight arrow*). Note normal right internal carotid artery (*curved arrow*).

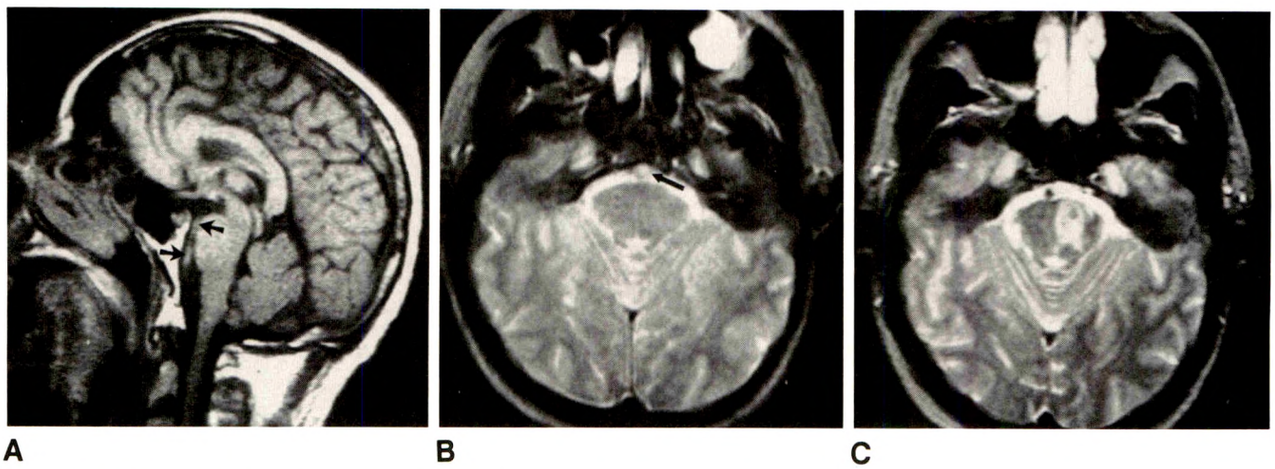


Fig. 4.—50-year-old man with symptoms of brainstem ischemia.
A, Parasagittal T1-weighted image (350/26) obtained 4 hr after onset shows linear signal isointense with brain in prepontine region (*arrows*) along course of basilar artery, suggesting intraluminal clot.
B, Axial T2-weighted image (2000/100) shows absence of flow void in basilar artery (*arrow*). No apparent T2 signal abnormality is detected within the pons at this time.
C, Repeat axial T2-weighted image (2000/100) obtained 48 hr later shows the interval development of ischemic changes in the pons.

Morphologic Changes

Morphologic changes caused by tissue swelling were found in most (27 of 41) of the lesions studied in the first 24 hr after the onset of symptoms (Fig. 1B). Morphologic changes were detected in at least half of the lesions imaged by 2 hr (four of eight), between 2 and 4 hr (two of three), and between 4 and 6 hr (one of two). Swelling was detected either by gross enlargement of structures or more often by distortion of normal adjacent structures. These morphologic changes were best seen on T1-weighted scans. Rapid development of massive parenchymal swelling over the course of 1 hr was documented in two patients. This occurred before the appearance of signal changes on T1- or T2-weighted images (Fig. 6).

Morphologic changes occurred frequently in cortical lesions (20 of 25), where swelling was best demonstrated by obliteration of cortical sulci. Morphologic changes in isolated noncortical lesions, including those in the deep white matter, noncortical gray matter, and brainstem, were detected less often (only seven of 16) and were also not as obvious. When noncortical swelling was detected, this was usually manifested by distortion of the ventricular system or by brainstem swelling.

It is of note that morphologic changes on T1-weighted images could be detected in all lesions associated with arterial

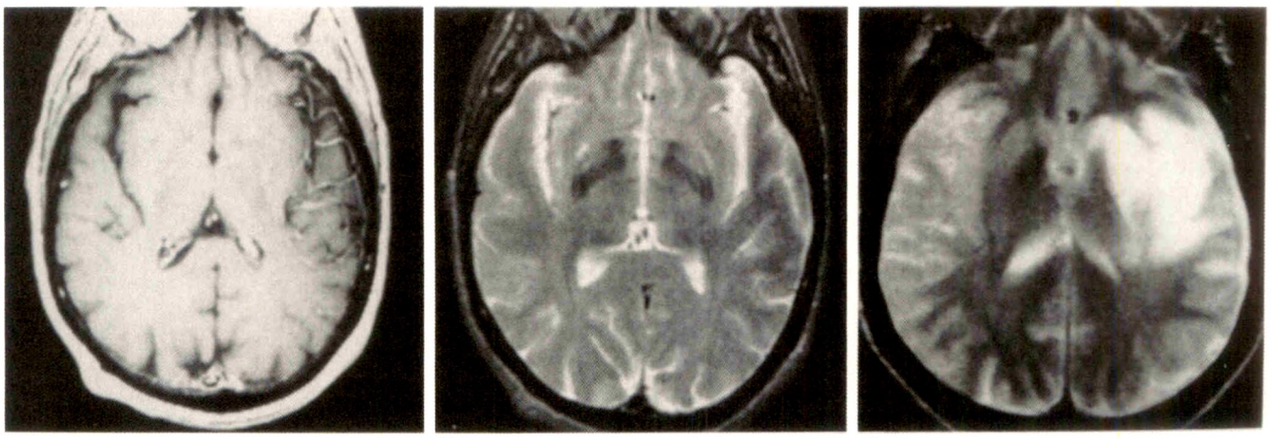


Fig. 5.—62-year-old man with acute left hemispheric stroke symptoms.
***A*, Axial T1-weighted contrast-enhanced image (700/20) obtained 3 hr after onset shows abnormal arterial enhancement in distribution of left middle cerebral artery. No abnormal parenchymal enhancement is noted.**
***B*, Axial T2-weighted image (2200/90) at corresponding level shows no parenchymal T2 signal changes at this time.**
***C*, Axial T2-weighted image (2000/100) obtained 24 hr later shows extensive T2 signal changes consistent with ischemia of the left middle cerebral artery.**

enhancement. However, vascular enhancement was frequently more obvious.

Signal Changes

Signal changes on T1- and T2-weighted images were usually not detected within the first few hours of symptoms. Most (11 of 13) of the lesions evaluated before 8 hr after onset showed no signal abnormality on T2-weighted images, whereas most (25 of 28) of the lesions evaluated from 8 to 24 hr demonstrated such abnormalities (Fig. 1C). Therefore, signal changes on T2-weighted images were not usually present until 8 hr after onset of cerebral ischemia. Although one lesion did show signal abnormality on T2-weighted images obtained at 4 hr, the exact time of onset may have been more than 4 hr, because the patient was first noted to have symptoms of stroke when he awoke.

Evaluation of the scans for signal abnormalities included a review of both long TR/short TE (proton density) and long TR/long TE images. Although small cortical lesions were frequently depicted better by proton density images and deep noncortical lesions were more easily seen on long TR/long TE images, all lesions seen on long TR images could be seen on short and long TE images.

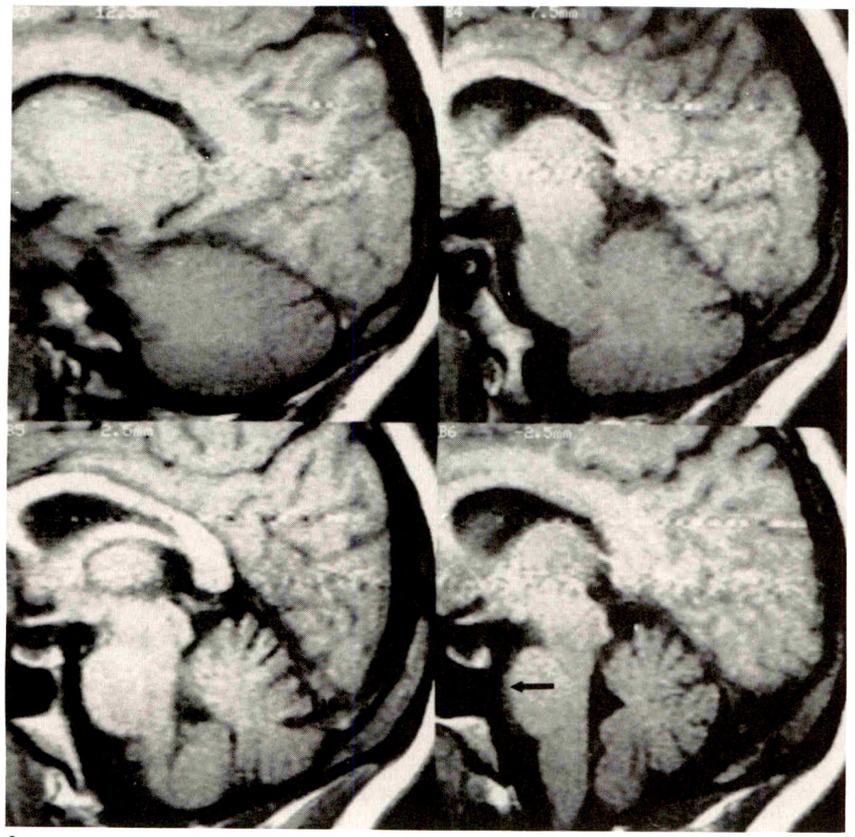
As compared with T2-weighted images, signal changes on T1-weighted images were even less sensitive in the detection of early cerebral ischemia (Fig. 1D). Only three of 19 lesions evaluated before 16 hr and only 12 of 22 evaluated between 16 and 24 hr showed signal abnormalities on the T1-weighted images.

Parenchymal Enhancement Patterns

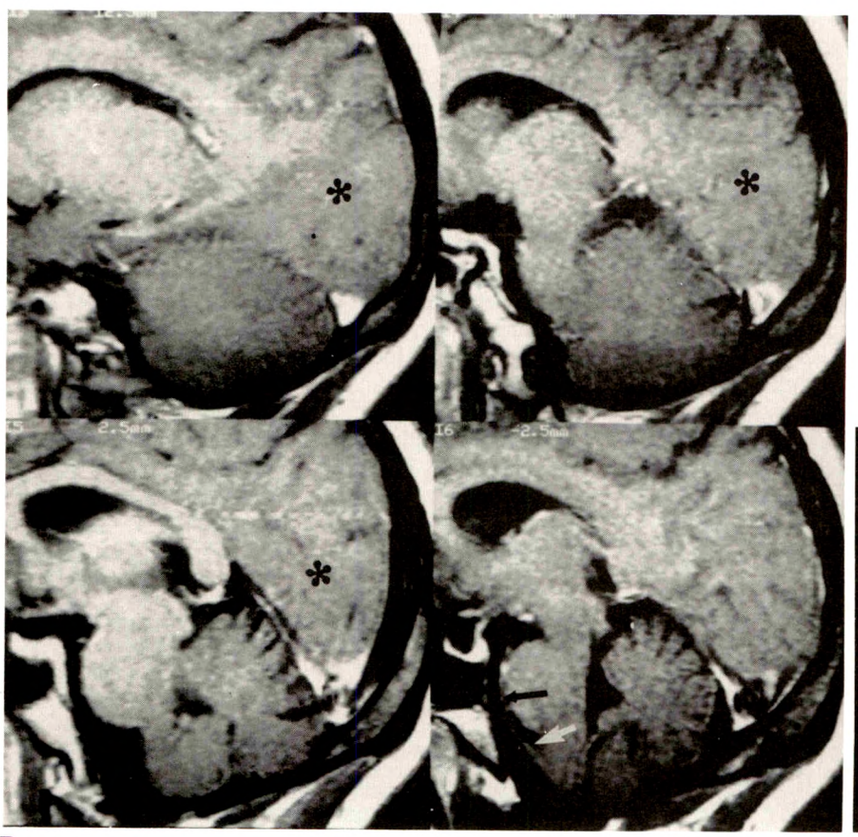
In contrast to the typical gyriform enhancement of cortical infarction seen in the subacute to chronic stages of stroke, enhancement of brain parenchyma was not found in 20 of 25 patients receiving contrast material in this series. However, five of the 25 lesions did show parenchymal enhancement within the first 24 hr; four of these showed a pattern of exaggerated enhancement exceeding the area of signal change on the T2-weighted images. One patient developed acute ischemic symptoms after 2 min of transient balloon occlusion of the ipsilateral internal carotid artery. MR obtained at 2 hr showed a diffuse exaggerated parenchymal enhancement (Fig. 7). An MR study in another patient showed faint enhancement without signal abnormality on T2-weighted images in a watershed distribution after occlusion of the internal carotid artery for treatment of an aneurysm. An enhanced MR examination in a third patient, who presented with acute onset of diminished vision due to occlusion of the proximal internal carotid artery, showed abnormal parenchymal enhancement in the watershed zone of the contralateral hemisphere without signal abnormality on T2-weighted images or clinical sequelae. An MR study in the fourth patient, who had moyamoya disease, showed a lesion with early, exaggerated enhancement in the posterior watershed zone.

Discussion

The detection of acute cerebral ischemia by MR may be dependent on many pathophysiologic factors (Table 2) that are often coexistent. Alteration of normal blood flow is a flow-kinetics phenomenon that should be detected immediately, as was seen in one patient in this series with cardiac arrest. The remaining factors are biophysiologic phenomena that may take time to be appreciated by MR. Sensitivity in detecting ischemia may be increased through the addition of paramagnetic contrast agents, most likely due to either accentuation of the underlying flow derangement or accumulation of abnormal amounts of contrast agent in the ischemic tissue.



A



B



C

Fig. 6.—35-year-old woman with stroke symptoms rapidly progressing from cerebellar dysfunction to unresponsiveness.

A, Precontrast parasagittal T1-weighted images (450/20) obtained 2½ hr after onset show signal isointense with brain in prepontine cistern (*arrow*).

B, Corresponding postcontrast parasagittal images obtained 40 min after *A* show development of massive brain swelling in occipital lobes (*asterisk*) and cerebellum, and progression of a blood clot in the basilar artery (*arrows*).

C, Axial T2-weighted image (2000/100) obtained before contrast administration shows no parenchymal signal abnormality.

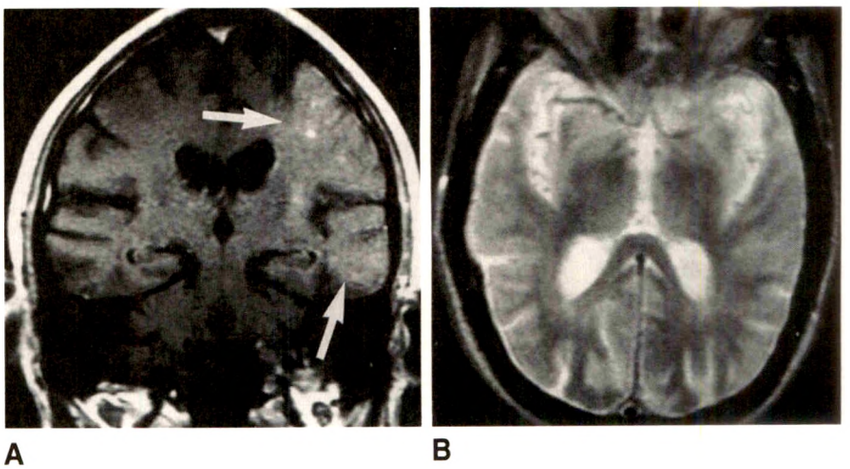


Fig. 7.—67-year-old man who underwent preoperative balloon test occlusion of left internal carotid artery and developed acute ischemic symptoms after 2 min of carotid occlusion. After balloon deflation, preservation of carotid flow was demonstrated angiographically.

***A*, Postcontrast coronal T1-weighted image (583/20) obtained 2 hr after onset shows diffuse parenchymal enhancement of left cerebral hemisphere (*arrows*). Parenchymal morphologic changes (swelling) are noted without evidence of discrete arterial enhancement.**

***B*, Axial T2-weighted image (2000/100) shows no parenchymal signal changes.**

Altered Flow Kinetics

The ability of unenhanced MR imaging to detect absence of flow in large cerebral arteries early in complete thrombotic occlusion has been reported previously [13–15]. Normal arterial structures are generally devoid of intraluminal MR signal due to rapid and/or turbulent flow, the so-called flow-void phenomenon. Normal flow-void phenomenon is seen better on T2-weighted images because of increased susceptibility to motion on long TE sequences and better contrast between the dark vessel and surrounding bright CSF. All lesions with detectable absence of flow void in this series (approximately one third) were demonstrated better with T2 weighting than with T1 weighting.

We have shown that abnormal vascular enhancement by contrast material further improved the ability of MR to detect early cerebral ischemia by accentuating the underlying flow alteration. This could be detected not only in large vessels in both anterior and posterior circulation lesions but also in smaller vessels in distal cortical distributions. However, we were not able to detect enhancement of the terminal arteries supplying isolated deep noncortical lesions, most likely because of their small size. Absence of normal flow void was seen better on T2-weighted images, whereas arterial enhancement was seen better on the enhanced T1-weighted images with respect to the surrounding dark CSF. The contrast agent, therefore, improved the detection of flow derangement in distal cortical branches, which went undetected on the unenhanced images.

Arterial enhancement in stroke has been reported recently [16] and has been attributed to sluggish arterial flow near the infarct. We have encountered cases with arterial enhancement that had angiographic evidence of slow antegrade or retrograde (collateral) flow in the enhancing arteries, while other cases with angiographically proved complete proximal occlusion showed no arterial enhancement in the distal arterial tree when excellent collateral flow was present. Therefore, we also believe that slow flow is the likely mechanism for enhancement of the arterial tree in many of these lesions [17].

In the evaluation of flow alteration in the proximal internal carotid and middle cerebral arteries, we prefer the axial imaging plane because the entire course of these vessels is demonstrated best with the fewest images without significant interference from flow-related enhancement. Optimal evaluation of basilar artery occlusions frequently requires both sagittal T1-weighted imaging and axial T2-weighted imaging [13].

Biophysiologic Phenomena

The other pathophysiologic factors that may result in abnormal MR findings in cerebral ischemia are biophysiologic phenomena (Table 2). The ability of MR to detect parenchymal abnormalities in ischemic stroke caused by these biophysiologic mechanisms depends mostly on anatomic distortion seen best on T1-weighted imaging and/or signal changes seen best on T2-weighted imaging.

T2-weighted images have proved to be sensitive in detecting CNS lesions, such as tumor, on the basis of the abnormal accumulation of fluid that develops over a relatively long period of time. However, the ability of T2-weighted imaging to detect early ischemia appears to be limited. Signal abnormalities on T2-weighted images in this series were not sensitive in detecting ischemia in the first 8 hr after onset and often lagged behind detectable physical flow alterations, abnormal arterial contrast enhancement, and morphologic changes on T1-weighted images. The cause for the delayed development of the signal change on T2-weighted images is unknown. It is probably related to the relatively delayed onset of extracellular swelling or vasogenic edema, which is thought to be caused by the breakdown of the blood-brain barrier (BBB) [10, 18–22]. Experimental work has shown this breakdown does not occur to a significant extent until approximately 6 hr after onset and is then associated with leakage of water as well as proteins and macromolecules into the extracellular and intracellular spaces. The time course of signal change on T2-weighted images found in our series is in accordance with the temporal development of vasogenic

edema. Significant signal change on T2-weighted images, before the development of vasogenic edema, may be limited by relatively insufficient changes in water content (3%) [19], macromolecular shifts, and hydration binding of free water to macromolecules during the first few hours of ischemia (cytotoxic edema phase).

Signal changes on T1-weighted sequences were the most delayed change demonstrated, as expected, and were the least sensitive indicators in the early detection of stroke. This is mostly due to the limited sensitivity of the currently available, relatively T1-weighted pulse sequences in detecting abnormal water accumulation.

Morphologic changes in brain parenchyma demonstrated best on T1-weighted images were early indicators of acute cerebral ischemia and could be seen as early as 2 hr after onset. The occurrence of both abnormal arterial enhancement and morphologic changes (even without signal change) was strongly suggestive of ischemia early in its development. Although the cause of parenchymal morphologic swelling without concomitant signal change is unknown, we speculate that this is related predominantly to the formation of cytotoxic edema. Cytotoxic edema is considered to be the abnormal accumulation of intracellular water that develops in ischemic brain parenchyma as a consequence of decreased availability of ATP and the resultant dysfunction of the Na-K-ATP pump [10, 19, 20, 22, 23]. This occurs within minutes after the induction of experimental ischemia [19]. The excess intracellular fluid is thought to be primarily free water without proteins or macromolecules. The overall shift from the intravascular space at this early stage reportedly results in a modest 3% increase in the amount of parenchymal water. In addition to the relatively small shift in total water during this stage, this free water is not yet bound to macromolecular components. We speculate that this may explain the formation of detectable swelling on T1-weighted images without significant signal changes on T2-weighted images.

Evidence of massive brain swelling was seen to progress rapidly over the course of approximately 1 hr in two patients in this series. The radiologic detection of such dramatic brain swelling in the first few hours of ischemia has not been reported previously. Again, the cause for the shift of such a large amount of water without accompanying signal changes on T2-weighted images is unknown.

Mass effect was usually not detected in isolated noncortical infarcts in our series until signal changes on T2-weighted images were evident. This was probably due to the small size of many isolated noncortical infarcts and to the terminal arteriolar nature of these vascular zones, which lack significant collateral flow. The detection of mass effect is also frequently dependent on the distortion of normal surrounding structures, an indirect sign. The thin, delicate sulci interposed between cortical gyri, on the other hand, are easily distorted by a relatively small amount of cortical edema, and this distortion is easily appreciated by MR. The lack of sulci adjacent to deep brain structures limits the detectability of slight amounts of edema in these areas. In our study, the obliteration of sulci and effacement of gyri in cortical infarctions were usually detected better on the T1-weighted images. This was primarily due to the relatively better contrast between CSF and cortical gyri on the T1-weighted images.

Parenchymal Enhancement Patterns

Most infarcts in our study group did not demonstrate enhancement of brain parenchyma in the first 24 hr after onset of symptoms. This is in agreement with other series that have shown development of typical gyriform enhancement of cortical strokes only in the subacute and chronic (i.e., more than 1–2 weeks) phases [24–27]. The absence of parenchymal enhancement in the acute stage of ischemia is probably related to an inability to deliver sufficient amounts of contrast material to the ischemic area caused by the underlying vascular abnormality and a lack of significant collateral circulation. Those lesions that showed parenchymal enhancement within the first day were usually related to transient vessel occlusion, partial vessel occlusion (i.e., partially intact antegrade flow or partially intact collateral flow), or watershed zone infarct [17]. The mechanism for exaggerated and early enhancement of these types of ischemic lesions is unknown, but probably relates to the abnormal accumulation of contrast material in the presence of an intact supply of contrast material. Possible mechanisms for the local concentration of contrast material include BBB breakdown and/or local hyperemia. The explanation for involvement of a greater area by contrast enhancement than that by signal change on T2-weighted images in these cases is also unknown, but may be indicative of a lesser degree of tissue insult [17].

Limitations

Several limitations of the present study should be noted. The major purpose of this work was to investigate the early MR findings in acute stroke and the time course of their development. Our study population was limited to only those patients with acute clinical symptoms who had MR examinations and showed corresponding MR abnormalities. We have encountered at least three patients (excluded from the present study) with clear neurologic deficits who had no abnormalities on MR imaging. In addition, stroke was often only one of many possible diagnoses in the patients referred to us for MR studies. Clinically, many of these were considered unlikely to have had a stroke and others were lost to follow-up; therefore, we did not attempt to assess the sensitivity, specificity, or accuracy of MR findings early in acute cerebral ischemia. Another limitation stems from the nonuniform temporal distribution of MR examinations in the first 24 hr (Fig. 1). Lack of data points at several time intervals limits more precise determination of the time of onset of several of the MR abnormalities. A prospective and controlled study will be necessary to determine the reliability of MR in detecting early ischemic stroke.

Hemorrhagic lesions were excluded from the study because their mechanism probably differs from that of primary cerebral ischemia. Although T2-weighted images are less

sensitive in the detection of early brain ischemia, we do not suggest eliminating the T2-weighted sequence, as many other diseases may mimic the clinical signs of stroke. In addition, acute parenchymal blood may be detected on T2-weighted images in higher field scanners.

Finally, our results differ slightly from those reported in the imaging of experimental infarcts in other species [9–11, 24]. Whether this is attributable to a difference in vascular anatomy and/or physiology or to different mechanisms of occlusion (gradual or intermittent thrombosis vs abrupt surgical ligation) remains uncertain. Lack of precision in determining the time of occlusion may also contribute to these disparate results.

In conclusion, MR appears to be a useful method for diagnosing early acute cerebral ischemia. Early MR findings include the absence of normal flow void and the presence of arterial enhancement and morphologic changes that may precede detectable signal changes. These early MR signs represent additional evidence of early acute ischemia and further demonstrate the advantages of MR over CT in detecting early ischemic injury. Furthermore, the use of paramagnetic contrast agent is often valuable in the detection and evaluation of acute stroke in its very early stages.

REFERENCES

1. Bryan RN, Wilcott MR, Schneiders NJ, Ford JJ, Dorman HS. Nuclear magnetic resonance evaluation of stroke. *Radiology* **1983**;149:189–192
2. Sipponen JT, Kaste M, Ketonen L, Sepponen RE, Katevuo K, Sivula A. Serial nuclear magnetic resonance (NMR) imaging in patients with cerebral infarction. *J Comput Assist Tomogr* **1983**;7:585–589
3. Sipponen JT. Visualization of brain infarction with nuclear magnetic resonance imaging. *Neuroradiology* **1984**;26:590–594
4. Biller J, Adams HP Jr, Dunn V, Simmons Z, Jacoby CG. Dichotomy between clinical findings and MR abnormalities in pontine infarction. *J Comput Assist Tomogr* **1986**;10:379–385
5. Rothrock JF, Lyden PD, Hesselink JR, Brown JJ, Healy ME. Brain magnetic resonance imaging in the evaluation of lacunar stroke. *Stroke* **1987**;18:781–786
6. Brown JJ, Hesselink JR, Rothrock JF. MR and CT in lacunar infarcts. *AJNR* **1988**;9:477–482, *AJR* **1988**;151:367–372
7. Kinkel PR, Kinkel WR, Jacobs L. Nuclear magnetic resonance imaging in patients with stroke. *Semin Neurol* **1986**;6:43–52
8. Kertesz A, Black SE, Nicholson L, Carr T. The sensitivity and specificity of MRI in stroke. *Neurology* **1987**;37:1580–1585
9. Spetzler RF, Zabramski JM, Kaufman B, Yeung HN. Acute NMR changes during MCA occlusion: a preliminary study in primates. *Stroke* **1983**; 14:185–191
10. Brant-Zawadzki M, Pereira B, Weinstein P, et al. MR imaging of acute experimental ischemia in cats. *AJNR* **1986**;7:7–11
11. McNamara MT, Brant-Zawadzki M, Berry I, et al. Acute experimental cerebral ischemia: MR enhancement using Gd-DTPA. *Radiology* **1986**; 158:701–705
12. Moseley ME, Kucharczyk J, Mintorovitch J, et al. Diffusion-weighted MR imaging of acute stroke: correlation with T2-weighted and magnetic susceptibility-enhanced MR imaging in cats. *AJNR* **1990**;11:423–429
13. Biller J, Yuh WTC, Mitchell GW, Bruno A, Adams HP Jr. Early diagnosis of basilar artery occlusion using magnetic resonance imaging. *Stroke* **1988**;19:297–306
14. Knepper L, Biller J, Adams HP Jr, Yuh W, Ryals T, Godersky J. MR imaging of basilar artery occlusion. *J Comput Assist Tomogr* **1990**;14:32–35
15. Katz BH, Quencer RM, Kaplan JO, Hinks RS, Post MJD. MR imaging of intracranial carotid occlusion. *AJNR* **1989**;10:345–350, *AJR* **1989**;152: 1271–1276
16. Elster AD, Moody DM. Early cerebral infarction: gadopentate dimeglumine enhancement. *Radiology* **1990**;177:627–632
17. Crain MR, Yuh WTC, Greene GM, et al. Cerebral ischemia: evaluation with contrast-enhanced MR imaging. *AJNR* **1991**;12:631–639
18. Hossmann KA, Schuier FJ. Experimental brain infarcts in cats. I: Pathophysiological observations. *Stroke* **1980**;11:583–591
19. Schuier FJ, Hossmann KA. Experimental brain infarcts in cats. II: Ischemic brain edema. *Stroke* **1980**;11:593–601
20. Bell BA, Symon L, Branston MN. CBF and time thresholds for the formation of ischemic cerebral edema, and effect of reperfusion in baboons. *J Neurosurg* **1985**;62:31–41
21. Gotoh O, Asano T, Koide T, Takakura K. Ischemic brain edema following occlusion of the middle cerebral artery in the rat. I: The time courses of the brain water, sodium and potassium contents and blood-brain barrier permeability to ^{125}I-albumin. *Stroke* **1985**;16:101–109
22. Brant-Zawadzki M, Weinstein P, Bartkowski H, Moseley M. MR imaging and spectroscopy in clinical and experimental cerebral ischemia: a review. *AJNR* **1987**;8:39–48
23. Buonanno FS, Pykett IL, Brady TJ, et al. Proton NMR imaging in experimental ischemic infarction. *Stroke* **1983**;14:178–184
24. Imakita S, Nishimura T, Naito H, et al. Magnetic resonance imaging of human cerebral infarction: enhancement with Gd-DTPA. *Neuroradiology* **1987**;29:422–429
25. Imakita S, Nishimura T, Yamada N, et al. Magnetic resonance imaging of cerebral infarction: time course of Gd-DTPA enhancement and CT comparison. *Neuroradiology* **1988**;30:372–378
26. Miyashita K, Naritomi H, Sawada T, et al. Identification of recent lacunar lesions in cases of multiple small infarctions by magnetic resonance imaging. *Stroke* **1988**;19:834–839
27. Muller W, Kramer G, Roder RG, Kuhnert A. Balance of T1-weighted images before and after application of a paramagnetic substance (Gd-DTPA). *Neurosurg Rev* **1987**;10:117–122

Call for Papers on Neuroradiology

On January 1, 1992, The American Roentgen Ray Society and the American Society of Neuroradiology will terminate their agreement whereby manuscripts on neuroradiology submitted to the *AJR* are forwarded to the *AJNR* and selected *AJNR* papers are republished in the *AJR*.

To avoid any lag in the publication of neuroradiologic articles in the *AJR*, the Journal requests authors to submit neuroradiologic manuscripts effective immediately. We plan to expedite publication of these papers. Authors will receive an initial editorial decision in 3–4 weeks, and accepted papers will be published 3 months after revised manuscripts are accepted. This is more than twice as fast as most other journals.

The advantages of this rapid publication time and the *AJR*'s large circulation (24,000) are now available to all authors of neuroradiologic papers. An expanded section on neuroradiology, including review articles, pictorial essays, and commentaries, will accommodate more than the limited number of papers published under the previous agreement.

We invite authors of neuroradiologic articles to submit their papers for original publication in the *AJR* so that the Journal may continue to fulfill its commitment to supply timely and important original information about neuroradiology to general radiologists as well as to those who subspecialize in the field.

Robert N. Berk
Editor-in-Chief

Cerebral Ischemia: Evaluation with Contrast-Enhanced MR Imaging

Martin R. Crain[1]
William T. C. Yuh[1]
George M. Greene[2]
Daniel J. Loes[1]
Tony J. Ryals[1]
Yutaka Sato[1]
Michael N. Hart[3]

Eighty patients with a total of 82 ischemic lesions were examined with contrast-enhanced MR imaging 1 hr to 1 month after onset of symptoms. The studies were reviewed retrospectively to determine the presence of arterial enhancement and the patterns of parenchymal enhancement. Arterial enhancement was often detected on the initial MR examination (45%), was frequently demonstrated in cortical infarction (86%), in some cases preceded the development of signal changes on T2-weighted images, and resolved by 11 days. The presence of arterial enhancement appeared to be a better indicator of clinical severity than was the presence of proximal vessel occlusion on MR or angiographic studies. Two patterns of parenchymal enhancement were seen: progressive enhancement and early and/or intense enhancement. In patients with the progressive pattern, parenchymal enhancement on postcontrast T1-weighted images was rarely seen before 7 days, while signal abnormalities on T2-weighted images were intense during the first few days. The early and/or intense enhancement pattern was usually present within the first 3 days, approximated or exceeded the area and intensity of signal changes on T2-weighted images, and was usually associated with minimal or reversible neurologic sequelae (except when located in or near a watershed zone), suggesting a lesser degree of ischemic insult than was associated with the progressive pattern. Three additional general relationships between MR findings were observed: (1) an inverse relationship between the extent of arterial enhancement and parenchymal enhancement in acute and subacute phases, (2) an inverse relationship between the area of postcontrast parenchymal enhancement and the area of signal change on T2-weighted images in the acute phase, and (3) a direct relationship between arterial enhancement and the degree of signal changes on T2-weighted images in the acute phase.

We conclude that patterns of enhancement appear to reflect the underlying pathophysiology in acute cerebral ischemia and may have prognostic significance. In contrast to results of previous reports, gadopentetate dimeglumine appears to be useful in the MR evaluation of early ischemia and its response to intervention.

***AJNR* 12:631–639, July/August 1991; *AJR* 157:575–583, September 1991**

Received September 28, 1990; revision requested December 7, 1990; revision received February 26, 1991; accepted February 28, 1991.

Presented at the ninth annual meeting of the Society of Magnetic Resonance in Medicine, New York, August 1990.

[1] Department of Radiology, The University of Iowa College of Medicine, Iowa City, IA 52242. Address reprint requests to W. T. C. Yuh.

[2] Department of Surgery, Division of Neurosurgery, The University of Iowa College of Medicine, Iowa City, IA 52242.

[3] Department of Pathology, Division of Neuropathology, The University of Iowa College of Medicine, Iowa City, IA 52242.

0361–803X/91/1573–0575
© American Roentgen Ray Society

The location and time course of enhancement with CT contrast agents in the evaluation of patients with cerebral infarction is well documented [1–4]. Although the use of gadopentetate dimeglumine–enhanced MR imaging has been reported in patients with cerebrovascular disease [5–9], the usefulness of MR contrast agents and the patterns of enhancement that occur, especially early in cerebral ischemia, are not well established. While some investigators have reported that gadopentetate dimeglumine does not improve the sensitivity of MR in acute cerebral ischemia [10], others have suggested that contrast material may be useful in the detection of this entity [8, 11]. Our purpose was to investigate the usefulness of contrast-enhanced MR imaging in the evaluation of acute cerebral ischemia. In particular, we wished to study the degree and pattern of enhancement with respect to location, duration, and temporal progression of ischemia and to relate the findings on enhanced MR images to underlying pathophysiology.

Materials and Methods

Eighty-two ischemic lesions in 80 patients were studied. All patients who presented between November 1988 and February 1990 with symptoms of acute cerebral ischemia (i.e., motor and sensory deficits, loss of consciousness, aphasia) and who also received IV administration of gadopentetate dimeglumine during their MR examination were reviewed retrospectively. Ages ranged from 18 to 89 years (mean, 55 years). There were 44 men and 36 women. The timing of the onset (either the acute onset of symptoms in a previously asymptomatic patient or the rapid progression of intermittent symptoms in a symptomatic patient) was determined from the best available clinical history. The MR time was defined as the interval between the onset of symptoms and the start of the initial MR examination (rounded off to the closest hour). Criteria for inclusion in the final study group included reliably defined onset of acute ischemic symptoms, IV administration of gadopentetate dimeglumine, and MR findings referable to the clinical distribution of ischemia. Patients with intraparenchymal hematoma by initial CT or MR, those without definable clinical symptoms corresponding to MR findings, and those without a reliably defined time of onset were excluded.

All examinations were performed on either a 0.5-T (Picker International, Highland Heights, OH) or a 1.5-T (General Electric, Milwaukee, WI) superconductive scanner. At least one T1-weighted, 350–750/20 (TR range/TE), and one T2-weighted (2000–2300/90–100) spin-echo pulse sequence were obtained with a 3–10-mm slice thickness. There was a 10–50% slice gap in the examinations performed at the higher field strength. At least two orthogonal planes were imaged. Postcontrast imaging was performed immediately after IV injection of 0.1 mmol/kg of gadopentetate dimeglumine (Magnevist, Berlex Laboratories, Inc., Wayne, NJ). Postcontrast pulse parameters and imaging planes were identical with those of the precontrast T1-weighted sequences.

MR examinations were reviewed retrospectively by two radiologists without knowledge of the MR time. Special attention was given to the presence of arterial enhancement, pattern and degree of parenchymal enhancement, parenchymal signal abnormalities on unenhanced images, and vascular distribution of ischemic changes. Vascular distribution was defined as predominant involvement of the anterior cerebral artery (ACA) territory, middle cerebral artery (MCA) territory, or vertebrobasilar circulation. Note was made if abnormal parenchymal signal was located within or near a major watershed zone (watershed infarction). Parenchymal abnormalities were categorized according to location: cortical abnormalities involved predominantly cortical structures with or without involvement of deep structures, and noncortical ones were limited to noncortical structures and included those in the brainstem, subcortical gray matter (basal ganglia and thalamus), and deep white matter. We also categorized the duration of ischemic symptoms using 7 days as the cutoff point between the acute and subacute phases. This definition has been used by other authors [5, 6]. Angiograms were reviewed if they were obtained within 24 hr of the MR examination.

TABLE 1: MR Time (Time from Onset of Ischemic Symptoms to Initial MR Examination)

Time	No. of Lesions
<24 hours	25
2 days	13
3 days	13
4–5 days	10
6–9 days	8
10–14 days	8
≥1 month	5
Total	82[a]

[a] 80 patients.

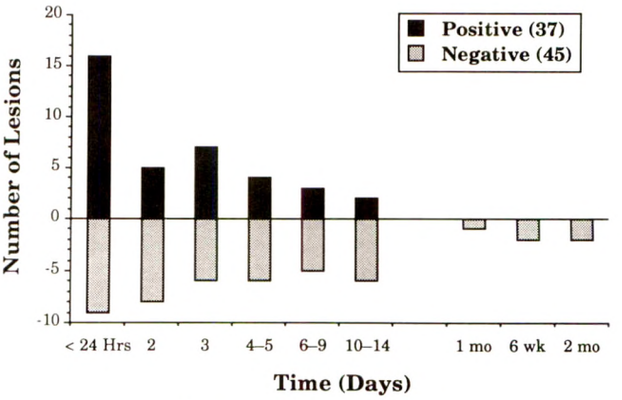


Fig. 1.—Graph depicting the number of lesions that demonstrated arterial enhancement at the time of initial MR examination. Arterial enhancement was frequently detected within the first 24 hr, rarely after 7 days, and not at all after 11 days, suggesting reestablishment of circulation or development of collateral circulation.

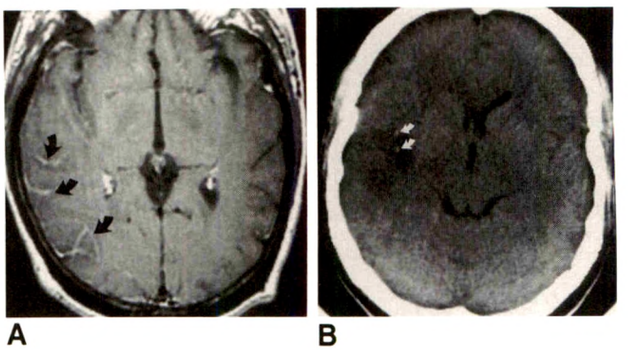


Fig. 2.—Comparison of vascular abnormalities depicted by contrast MR imaging and CT.

***A*, Postcontrast axial T1-weighted image (750/20/1) obtained 3 days after onset shows abnormal arterial enhancement in distribution of right middle cerebral artery (*arrows*). Specifically noted is obvious enhancement of distal peripheral small branches.**

***B*, Axial unenhanced CT image at corresponding level of parietal lobes shows "dense artery sign" (*arrows*) in region of proximal middle cerebral artery. However, no vascular abnormality in distal arterial branches can be appreciated. The extent of the vascular abnormality is much more apparent on enhanced MR image.**

Results

The distribution of the MR times is presented in Table 1. Eleven patients had more than one contrast-enhanced MR examination.

Arterial Enhancement

Arterial enhancement on the initial MR examination was detected in 37 (45%) of 82 ischemic lesions (Figs. 1–5). It was found in 30 (83%) of 36 cortical infarctions, five (16%) of 31 noncortical infarctions, and two (20%) of 10 watershed infarctions (Table 2). The five noncortical lesions with arterial

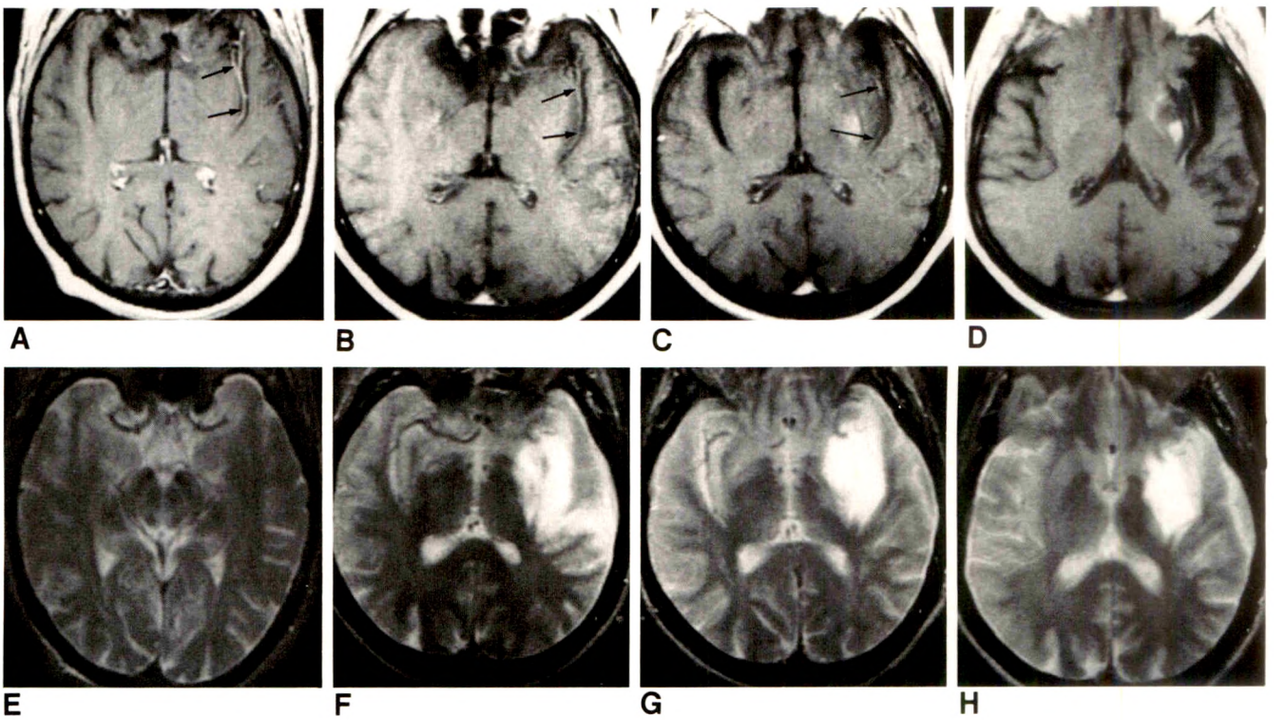


Fig. 3.—Example of early arterial enhancement and progressive parenchymal enhancement in a cortical infarction.

A–H, Postcontrast axial T1-weighted images (750/20) obtained at 2 hr (*A*), 24 hr (*B*), 7 days (*C*), and 3 months (*D*), and the corresponding axial T2-weighted images (2000/100) obtained at the same time intervals (*E–H*) after the onset of acute ischemic symptoms. In typical complete ischemia, arterial enhancement (*arrows*) in distribution of left middle cerebral artery is most prominent at 2 hr (*A*) in the left sylvian fissure, is persistent at 24 hr (*B*), is only partially detected at 7 days (*C*), and is absent at 3 months (*D*). Parenchymal enhancement is absent at 2 hr (*A*) and 24 hr (*B*) and is only faintly seen in left basal ganglia but not in insular cortex at 7 days (*C*). At 3 months (*D*), enhancement is limited to margins of remaining viable tissue in left insular cortex and basal ganglia. Note the apparent inverse relationship between the degrees of arterial and parenchymal enhancement at all stages. The abnormality on T2-weighted images, undetected at 2 hr (*E*), was extensive at 24 hr (*F*) and progressively diminished from 7 days (*G*) to 3 months (*H*). The area of abnormality on T2-weighted images is much greater than that of parenchymal enhancement until the chronic stage.

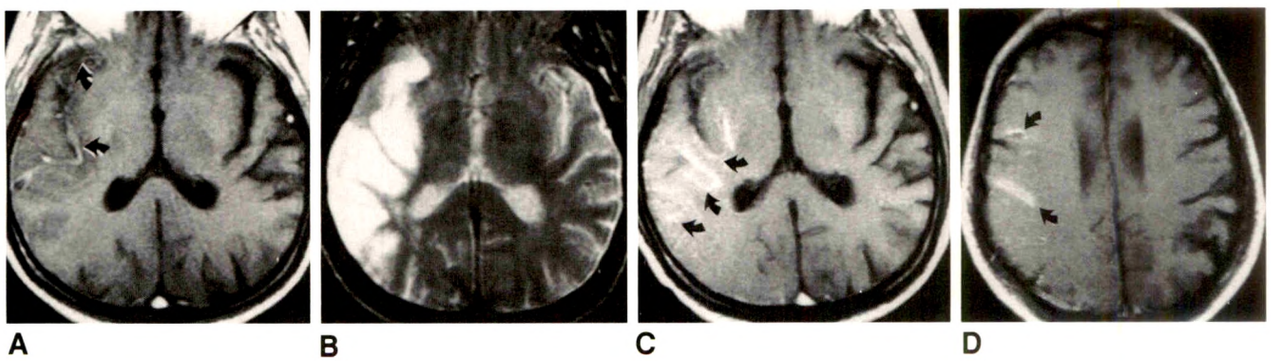


Fig. 4.—Another example of cortical infarction with earlier resolution of arterial enhancement and development of parenchymal enhancement.

A and *B*, Postcontrast axial T1-weighted image (583/20) (*A*) and corresponding T2-weighted image (2000/100) (*B*) obtained within first 24 hr of ischemic symptoms. Arterial enhancement (*arrows*) is demonstrated in distribution of right middle cerebral artery (*A*). Intense signal on T2-weighted images without parenchymal enhancement is present at this time (*A* and *B*). These findings are typical of complete ischemia as seen in Fig. 3.

C and *D*, Follow-up postcontrast axial T1-weighted images (583/20) obtained 7 days after onset of acute ischemic symptoms when arterial enhancement has completely resolved and significant parenchymal gyriform enhancement has developed (*arrows*). The gyriform enhancement in this patient is more prominent than that seen at 7 days in the patient in Fig. 3. This is probably due to earlier reestablishment of circulation or development of collateral circulation.

enhancement were located in the posterior fossa and all were associated with basilar artery enhancement. There was no enhancement of terminal arterial branches in basal ganglia or deep white matter lesions.

Arterial enhancement was most likely to be found if the MR examination was obtained within a few days of the onset of symptoms; it was seen in only two of 15 lesions when the MR examination was obtained after 7 days and was not

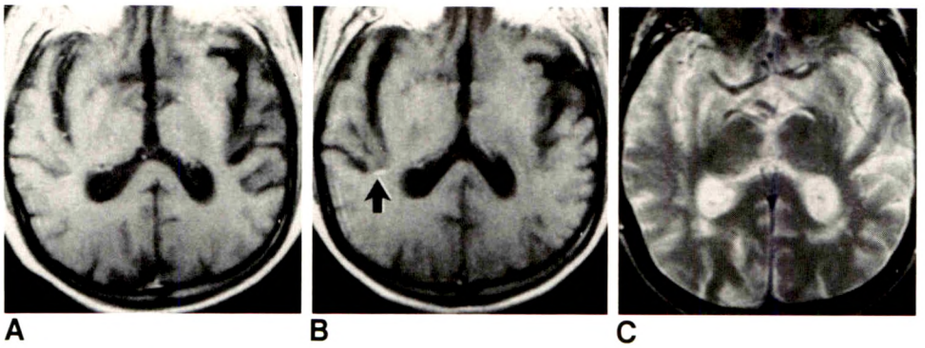


Fig. 5.—Example of rapid resolution of arterial enhancement in a patient with transient neurologic symptoms.

***A* and *B*, Postcontrast T1-weighted images (583/20) obtained 4 hr (*A*) and 24 hr (*B*) after onset of hemispheric ischemic symptoms. Arterial enhancement in distribution of right middle cerebral artery within the sylvian fissure is seen at 4 hr (*A*) but has resolved completely by 24 hr (*B*). Faint parenchymal enhancement near posterior watershed area (*arrow*) can be seen as early as 24 hr, probably due to the early reestablished blood flow to the ischemic region (*B*).**

***C*, Axial T2-weighted image (2000/100) obtained 1 week after onset of symptoms shows minimal signal abnormality, suggesting less severe ischemic tissue insult. The rapid resolution of arterial enhancement paralleled the rapid and complete neurologic recovery of this patient within hours of admission.**

detected after 11 days. In no instance did arterial enhancement occur on a follow-up examination if the initial MR failed to demonstrate this finding.

In patients with arterial enhancement who had multiple MR examinations, the enhancement usually persisted for 7 days, although prompt resolution occurred in two patients (Fig. 5). In both patients, arterial enhancement was present in the first 24 hr but resolved by the second day. Resolution of arterial enhancement paralleled rapid neurologic recovery (within 24–48 hr) in both patients. One developed modest signal abnormality on T2-weighted images that appeared on the second examination at 24 hr and nearly resolved by 1 week (Fig. 5). The other showed no signal change on T2-weighted images on either the initial or follow-up MR examinations up to 3 months after onset.

Eleven patients had angiography within 24 hr of the initial MR examination. Of the six patients who had arterial enhancement, only two had complete proximal occlusion on angiography. All six showed slow antegrade or retrograde flow on the angiogram. One patient with complete angiographic occlusion proximally showed no arterial enhancement on enhanced MR. Complete angiographic proximal vessel occlusion did not relate well to the presence of distal arterial enhancement on MR.

Parenchymal Enhancement

Contrast enhancement of ischemic brain parenchyma followed either of two patterns (Table 2): slowly progressive enhancement (Figs. 3, 4, 6) and early and/or intense enhancement (Figs. 7–9).

Progressive enhancement. Thirty-six cortical lesions (Figs. 2–4) and 31 noncortical lesions (Fig. 6) showed minimal or no parenchymal enhancement on initial MR (Table 2). The areas that did enhance were usually much smaller than the areas

TABLE 2: Summary of Typical Patterns of Enhancement

MR Findings and Outcome	Complete Ischemia (Progressive Enhancement)		Incomplete Ischemia (Early/Intense Enhancement)
	Cortical (n = 36)	Noncortical (n = 31)	Both (n = 15)[a]
Parenchymal enhancement			
Pattern			
Acute (≤7 days)	Usually absent[b] (1/27)[c]	Infrequent[d] (9/30)	Early (10/10)
Subacute (>7 days)	Progressive gyriform	Peripheral→central	Intense (5/5)
Extent (area involved)	Contrast material < T2 signal	Contrast material < T2 signal	Contrast material ≥ T2 signal (13/
Acute	(34/36)	(26/31)	15)
Arterial enhancement			
Acute	Frequent (30/36)	Infrequent[e] (5/31)	Infrequent (2/15)
Clinical outcome	Infarction	Infarction	Reversible/minimal neurologic dysfunction vs irreversible/infarction[f]

[a] Five cases of transient ischemia, 10 cases limited to a watershed zone.
[b] Single case with faint enhancement at 6 days.
[c] Number of positive cases/number of cases imaged.
[d] All enhancing lesions were small and had faint peripheral enhancement.
[e] When positive, usually involved basilar artery.
[f] Infarction in many cases of watershed zone ischemia.

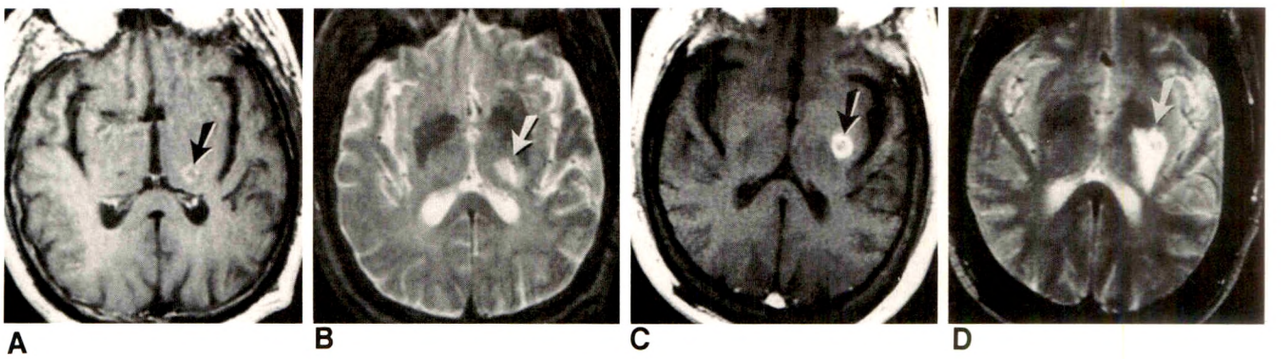


Fig. 6.—Examples of progressive parenchymal enhancement in noncortical infarctions.

A–D, MR images of noncortical infarctions obtained 7 days after onset of symptoms in one patient (*A* and *B*) and 2 weeks after onset of symptoms in another patient (*C* and *D*). Postcontrast axial T1-weighted images (750/20) (*A* and *C*) show that parenchymal enhancement of noncortical infarctions (*arrow*) is faint at the periphery in the early stage (*A*) and later progresses toward the center and becomes more dense (*C*). As in the case of complete cortical ischemia, the areas of signal change (*arrow*) seen on axial T2-weighted images (2000/100) (*B* and *D*) exceed the areas of enhancement in complete noncortical ischemia.

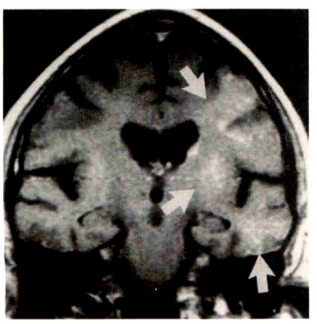
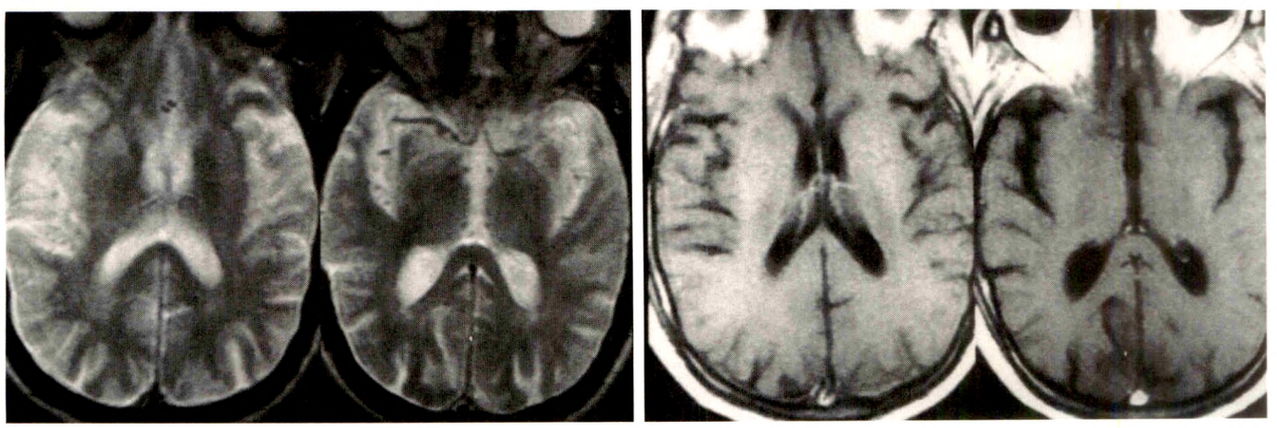


Fig. 7.—Example of early parenchymal enhancement in a patient with transient neurologic symptoms. This patient developed transient left hemispheric symptoms after 2 min of test balloon occlusion of left internal carotid artery.

A, Postcontrast coronal T1-weighted image (583/20) obtained at 2 hr shows diffuse parenchymal enhancement (*arrows*) in distribution of left middle cerebral artery without arterial enhancement. Also noted is enhancement of caudate nucleus.

B, Axial T2-weighted images (2000/100) show no apparent signal change at this time.

C, Postcontrast axial T1-weighted images (583/20) at 24 hr show no evidence of parenchymal or arterial enhancement. No signal abnormality in left middle cerebral artery distribution was present on T2-weighted images at 24 hr (*not shown*). The resolution of parenchymal enhancement by 24 hr parallels the rapid neurologic improvement in this patient. This case demonstrates the inverse relationship between parenchymal enhancement and arterial enhancement, as well as between the areas of parenchymal enhancement and T2 signal abnormality.



of abnormal signal on T2-weighted images. These patients tended to have more severe clinical outcomes than did those with early and/or intense enhancement.

Typical completed cortical infarctions did not develop parenchymal enhancement for about 1 week (Figs. 3 and 4), and signal abnormalities on T2-weighted images predominated in the first weeks. Twenty-six (96%) of 27 cortical lesions showed no parenchymal enhancement when the initial MR examination was obtained within 1 week (Table 2). The only lesion with enhancement before 1 week was seen in a 62-year-old man with minimal gyriform enhancement of an occipital infarction 6 days after the onset of visual symptoms.

After 1 week, thin, faint enhancement of the cortex usually began near the pial surface or margins of the ischemic zone and progressed to thicker, denser gyriform enhancement in the subacute phase (Fig. 4). Not until the subacute to chronic

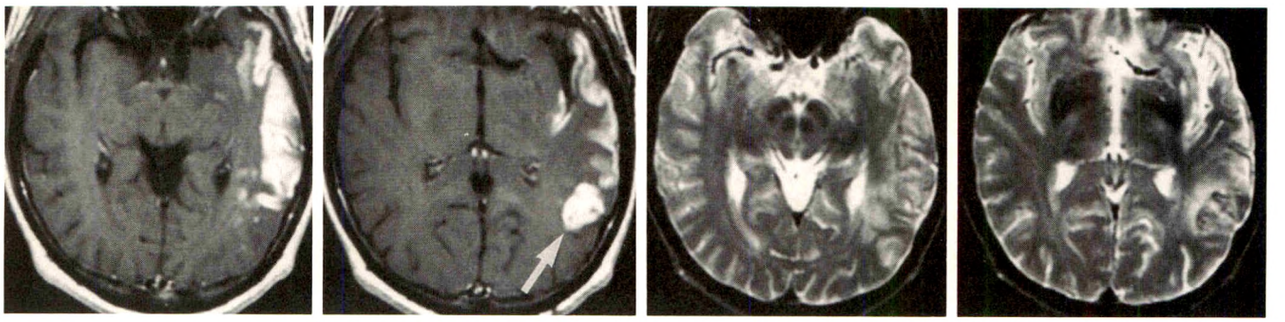


Fig. 8.—Example of early, intense parenchymal enhancement in a patient with reversible ischemic neurologic deficit. MR examination performed 10 days after transient ischemic episode with right-sided weakness and aphasia that resolved almost completely in 2 hr.

***A* and *B*, Postcontrast axial T1-weighted images (700/20) show diffuse, intense cortical enhancement in distribution of left middle cerebral artery without evidence of arterial enhancement.**

***C* and *D*, Corresponding axial T2-weighted images (2000/100) show a much less extensive area of signal abnormality. The enhancement appears more intense near the watershed zone (*B, arrow*), which may reflect greater availability of contrast material in this region. This case again shows that parenchymal enhancement is inversely related to the appearance of arterial enhancement and signal abnormality on T2-weighted images.**

phases were reached did the area of enhancing parenchyma approximate that of the signal change on T2-weighted images, and the enhancement remained moderate in intensity (Fig. 3). Enhancement eventually disappeared in the chronic phase.

Most (21 of 30) noncortical lesions evaluated within 1 week of onset showed no parenchymal enhancement (Fig. 6) (Table 2). In nine lesions enhancement appeared before 1 week and was faint and peripheral. Four of the nine patients had posterior fossa infarctions ranging in age from 1 to 6 days, and three of these presented with intermittent ischemic symptoms preceding the onset of the infarction. The other five had thalamic or basal ganglia infarctions of 48 hr to 7 days duration.

After 1 week, faint peripheral enhancement of noncortical infarctions became dense and thick, similar to the progression seen in cortical lesions (Fig. 6). Later, progression to uniform enhancement of the lesion was seen. As in cortical infarctions, parenchymal enhancement in typical noncortical infarctions usually lagged behind signal abnormality on T2-weighted images in both intensity and area of involvement. However, these lesions were usually much smaller than cortical ischemic lesions.

Early and/or intense enhancement. Fifteen lesions demonstrated a pattern of early and/or intense enhancement; 10 were imaged on MR within the first week of onset (Figs. 7–9) (Table 2). Enhancement was usually noted within the first 2–3 days, and its area equaled or exceeded the area of abnormality on T2-weighted images in most lesions (87%). Only 13% of lesions with this pattern were associated with arterial enhancement (Fig. 9C) (Table 2).

Two distinct groups of patients had lesions with early and/or intense enhancement. One group had minimal symptoms or reversible neurologic deficits (Figs. 7 and 8), and the other group tended to have persistent neurologic deficits (i.e., infarctions) (Fig. 9). In the former group, one patient had onset of hemispheric ischemic symptoms after 2 min of balloon test occlusion of the internal carotid artery (ICA) preoperatively, which almost completely resolved within 2 hr (Fig. 7). Diffuse parenchymal enhancement was seen without signal changes on T2-weighted images at 2 hr and had resolved later. Abnormal signal on T2-weighted images was not demonstrated on the 24-hr, 48-hr, or 7-day follow-up examinations. Another patient with reversible symptoms was an 18-year-old man who collapsed and had right hemiparesis that improved over the first 24–48 hr. An enhanced MR examination at 3 days showed early, intense gyriform enhancement in the left MCA distribution without arterial enhancement, similar to the patient shown in Figure 8. An angiogram obtained at 3 days showed no evidence of vessel occlusion. In a third patient, occlusion of the ICA resulted in acute blindness but no ipsilateral hemispheric clinical symptoms. MR obtained 18 hr after onset of symptoms showed an occluded proximal left ICA without ipsilateral hemispheric abnormality. However, early anterior watershed enhancement was seen in the contralateral (right) hemisphere. A fourth patient had a reversible ischemic neurologic deficit that resolved by 48 hr. Early homogeneous enhancement of the thalamus was demonstrated on MR at 4 days. A fifth patient had had percutaneous balloon occlusion of the ICA for treatment of an aneurysm. The patient developed no neurologic symptoms. An MR obtained 2 hr after the procedure showed faint enhancement without signal change on T2-weighted images in the posterior watershed zone.

The second group with early and/or intense enhancement tended to have more persistent and severe neurologic sequelae than the first, and lesions in these patients were limited to or adjacent to watershed regions (watershed infarctions) (Fig. 9). Five of these patients had MR within 1 week of onset of ischemic symptoms. The area of enhancement equaled or exceeded the size of the area of signal change on T2-weighted images as was seen in transient ischemic lesions, but more intense signal abnormalities were usually present. Five other patients had initial MR examinations between 7 and 14 days after onset of symptoms and also showed an area of intense enhancement equaling or exceeding the area

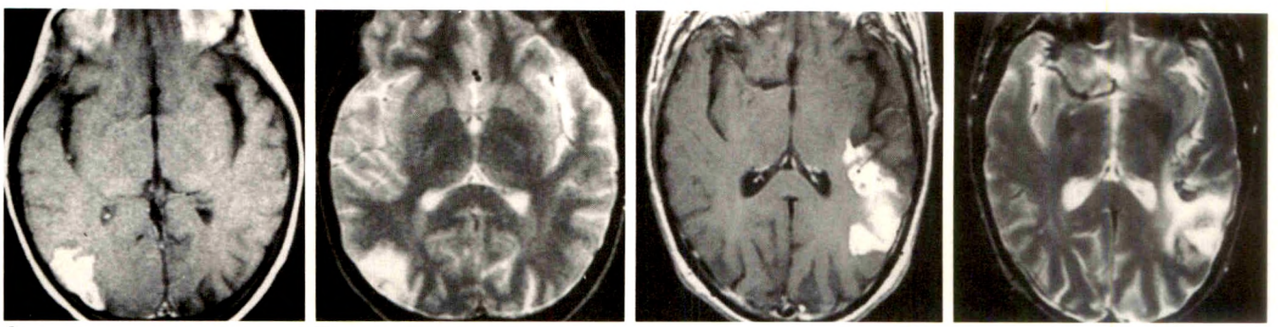


Fig. 9.—Examples of early, intense parenchymal enhancement in region of watershed zones in patients with severe neurologic sequelae. MR examination performed 14 days after gradual onset of symptoms in a patient with hypercoagulable state and angiographic evidence of thrombus in petrous portion of right internal carotid artery.

***A* and *B*, Postcontrast axial T1-weighted image (516/20) (*A*) shows early and intense parenchymal enhancement in right posterior watershed zone without arterial enhancement. The area of enhancement approximates the area of signal abnormality shown on the axial T2-weighted image (2000/100) (*B*).**

***C* and *D*, Postcontrast axial T1-weighted image (750/20) (*C*) of another patient 10 days after onset of acute aphasia with dense residual symptoms shows intense enhancement near watershed zone. Area of enhancement exceeds the extent of signal change on corresponding axial T2-weighted image (2300/90) (*D*). The small area of low signal intensity in posterior aspect of left temporal lobe corresponded to a focus of high signal intensity on precontrast T1-weighted images (not shown) and most likely represents petechial hemorrhage. Arterial enhancement of distal middle cerebral artery branches can also be seen (*C*).**

of the signal abnormality on T2-weighted images. The signal intensity on T2-weighted images in these watershed infarctions related directly to the severity of clinical symptoms.

Discussion

MR has been proved more sensitive than CT in the detection of brain ischemia in its early and chronic stages [11–15]. This has been attributed to the high sensitivity of T2-weighted sequences. However, in our previous study [11], signal changes on T2-weighted images were not usually detected until approximately 8 hr after the onset of symptoms. Brain swelling detected on unenhanced T1-weighted images and the presence of abnormalities in large vessels frequently preceded the development of signal changes on T2-weighted images, improving the sensitivity of unenhanced MR in the detection of early cerebral ischemia.

Previous reports [10] have suggested that gadopentetate dimeglumine does not contribute significantly to the early detection of ischemic stroke. In the present series, findings of arterial and parenchymal enhancement suggest a potential use for contrast material in the detection and evaluation of cerebral ischemia.

Arterial Enhancement

Absence of flow void in major intracranial vessels has been shown to be an indicator of early cerebral ischemia [11, 16]. However, detection of diminished or absent flow in smaller arterial vessels (such as cortical branches of the MCA) may not be appreciated on unenhanced MR images. Recent reports have described a vascular abnormality demonstrated by CT (dense artery sign) [17–19], but this finding may not be as conspicuous as on contrast-enhanced MR images (Fig. 2).

Enhancement of arteries was detected in nearly half the ischemic lesions studied, usually in cortical lesions. Larger arterial size and low signal from surrounding CSF may be the reasons for more frequent detection of arterial enhancement in cortical than in noncortical lesions. Arterial enhancement was rarely detected in isolated noncortical ischemia of the deep white matter or the noncortical gray matter, probably because of the involvement of smaller terminal arterial branches that are not easily detected by either enhanced or unenhanced MR. Therefore, the only noncortical lesions with arterial enhancement were vertebrobasilar circulation lesions with involvement of the large vertebral and basilar arteries.

Theoretically, arterial enhancement should be detectable immediately after the onset of flow alteration, as this is a phenomenon of altered flow kinetics. The earliest arterial enhancement detected in this series was 2 hr after the onset of symptoms (the earliest that we were able to obtain a contrast study). Arterial enhancement may precede the development of parenchymal signal change on T2-weighted images (Fig. 3), suggesting that the addition of gadopentetate dimeglumine may further improve the sensitivity of MR in the detection of certain cases of acute cerebral ischemia in the first few hours after onset [11].

The mechanism of arterial enhancement in cerebral ischemia is unknown. Arterial structures usually lack intraluminal signal owing to rapid and/or turbulent flow, causing the so-called flow-void phenomenon. Slow flow in venous channels may be manifested on contrast-enhanced MR images by an increase of intravascular signal. Arterial enhancement in this series could be seen both in complete proximal occlusion with retrograde collateral flow and in incomplete occlusion with slow antegrade flow on the angiographic examination. Conversely, when rapid flow was maintained distal to an occlusion (either by collateral flow or by a limited "partial" occlusion), arterial enhancement was not demonstrated. Therefore, slow

flow appears to be the primary mechanism for arterial enhancement. Elster and Moody [20] have also recently speculated that sluggish arterial flow near an infarction is responsible for arterial enhancement. Although thrombi within the proximal ICA or basilar artery may enhance with the addition of contrast agent, this is not likely to account for enhancement of the distal vascular tree. Thrombi in our series were seen most frequently as isointense lesions on immediate postcontrast images.

Arterial enhancement was most often detected within the first 24 hr and was not seen after 11 days in this series (Fig. 1). The disappearance of arterial enhancement coincided with the appearance of significant parenchymal enhancement (Figs. 3 and 4). This may be due to the proliferation of collateral vessels [5, 21] or the recanalization of thrombosed vessels in the subacute phase, either mechanism resulting in the reestablishment of fast and/or turbulent flow in distal arterial vessels. It appears that the rate of development of collateral flow affects the time at which arterial enhancement dissipates and parenchymal enhancement develops. An extreme example of this relationship is seen in patients with "incomplete ischemia" (Fig. 7) in whom intense parenchymal enhancement occurs early and arterial enhancement does not develop because of the early reestablishment of flow. The fact that arterial enhancement in completed infarctions dissipates by 7 to 11 days also coincides with the well-documented onset of "luxury perfusion" on contrast-enhanced CT scans at approximately 1 week.

The presence of arterial enhancement appears to be a better indicator of clinical severity than is the presence of proximal vessel occlusion. There were asymptomatic patients in this series with complete proximal large-vessel occlusions who had no arterial enhancement on initial MR studies. These patients had excellent collateral flow on angiographic studies. We also saw two patients with arterial enhancement initially who showed dramatic clinical improvement and rapid resolution of the arterial enhancement (Fig. 5). A potential application of this relationship is in noninvasive monitoring of the response to treatment aimed at reestablishing flow, such as thrombolysis.

Parenchymal Enhancement

Patterns. Previous studies of enhanced MR in ischemic stroke have shown that parenchymal enhancement is not usually seen before 6 days [5, 7], is predominant in the subacute phase (7–30 days), slowly fades in the chronic phase (>30 days) [5, 7], and may persist for 6–8 weeks [22]. Although our data are in agreement with these findings, we have seen two distinct patterns of parenchymal enhancement after the administration of contrast material. In addition to the typical pattern of progressive parenchymal enhancement described previously, we also saw a pattern of early and/or intense parenchymal enhancement (Table 2).

The two patterns appear to reflect pathophysiologic processes similar to those described by Virapongse et al. [5] in a hypothetical model. They divided tissue perfusion during an acute ischemic insult into two categories: complete ischemia (no perfusion) and incomplete ischemia (some perfusion) (Table 2). In their model of complete ischemia, diminished or absent perfusion would result in absence of early parenchymal enhancement owing to a significant interruption of contrast delivery to the ischemic tissue [5]. In our series, cases of complete ischemia tended to show no early parenchymal enhancement while signal abnormalities on T2-weighted images were more intense (Figs. 3, 4, 6). In the model of incomplete ischemia, they predicted that early enhancement may occur because a significant amount of contrast material continues to reach the ischemic tissue. We can substantiate this hypothesis with cases of incomplete ischemia that were characterized by early parenchymal enhancement with limited signal change on T2-weighted images (Figs. 7 and 8).

Three relationships that are compatible with this model of ischemia may be concluded from our observations. As mentioned in the discussion of arterial enhancement, there appeared to be an inverse relationship between arterial enhancement and parenchymal enhancement, with arterial enhancement present in the acute phase of ischemia only when perfusion was absent (complete ischemia). Arterial enhancement dissipated and parenchymal enhancement developed in the subacute phase as collateral flow was established. In the acute phase, the area of parenchymal enhancement also appeared inversely related to the area of signal abnormality on T2-weighted images. Parenchymal enhancement tended to be absent where the area and intensity of signal abnormality on T2-weighted images were greatest, both indicating a severe ischemic insult. A direct relationship between the degree of signal abnormality on T2-weighted images and the presence of arterial enhancement was also apparent in the acute phase of ischemia, with arterial enhancement again only found when the alteration of perfusion was severe (complete ischemia).

Mechanisms. Theoretically, the enhancement of ischemic brain parenchyma by gadopentetate dimeglumine depends on the availability of the contrast agent to the ischemic zone. Two basic sequential steps determine this availability: the adequate vascular delivery of contrast material and abnormal local tissue accumulation of the contrast agent [5, 10, 23].

Parenchymal enhancement can occur only when the delivery of contrast material is intact. In the setting of complete proximal vascular occlusion without preexisting collateral flow (complete ischemia), no early parenchymal enhancement occurs (Figs. 2–4). In incomplete ischemia with early parenchymal enhancement, delivery of contrast material during the acute stage may be maintained with partial vessel occlusion or may be promptly restored after interruption of flow in transient vessel occlusion (Figs. 7–9). In our series, lesions with early enhancement tended to have a better prognosis than did those with complete ischemia, reflecting the intact delivery of gadopentetate dimeglumine in lesser vascular insults. Signal changes on T2-weighted images were also less extensive in the incomplete ischemia cases, again consistent with lesser ischemic insults.

We agree with other authors [5, 7, 9] that progression of parenchymal enhancement in the subacute stages of complete ischemia is due to establishment of collateral blood flow. Delivery of contrast agent may thus resume with the disap-

pearance of arterial enhancement and the development of parenchymal enhancement. The collateral circulation may consist of previously existing vascular channels or proliferation of neovasculature at the border of viable tissue (marginal proliferation) and from the subarachnoid space (transmedullary proliferation). This is supported by the observation that development of gyriform enhancement tends to progress from the outer (pial) surface into the deeper structures and from thinner to thicker areas of involvement. Similarly, enhancement tends to progress from peripheral to central portions of noncortical lesions.

In this and other series [5, 22], enhancement of noncortical infarctions appears to develop earlier (4–7 days) than in cortical infarctions (>7 days). This is probably due to the fact that the blood supply to deep brain structures may have dual sources of supply (between ACA and MCA or between two vertebral arteries) and that there is more viable tissue surrounding these smaller lesions with less distance that the contrast material must penetrate.

Ischemia (Figs. 7 and 8) and infarction (Fig. 9) in or near watershed zones between major arterial distributions often resulted in the early, intense pattern of parenchymal enhancement. We postulate that infarction near these zones represents an equivalent of the incomplete ischemia model with regard to the delivery of contrast material but not the severity of ischemia. Delivery of contrast agent may be maintained by the dual nature of the blood supply from adjacent vascular territories. Therefore, although early and/or intense enhancement of watershed lesions may occur, the underlying insult often results in infarction, and the enhancement pattern is less likely to be predictive of clinical severity and/or reversibility.

After successful delivery of gadopentetate dimeglumine to a zone of ischemia, a subsequent mechanism for greater concentration of contrast material in the ischemic tissue than in normal tissue must be present for the lesion to be depicted by MR imaging. Although enhancement is most likely the result of an immature blood-brain barrier caused by neovascularity in the subacute phase of complete ischemia [5], the mechanism of early parenchymal enhancement is unknown. Breakdown of the blood-brain barrier due to irreversible damage to the vascular endothelium usually does not occur until approximately 6 hr after the insult [24–26], but we have seen cases with abnormal parenchymal enhancement as early as 2 hr (Fig. 7). Either local hyperemia (with blood pooling) caused by dysautoregulation [5] or extravasation of contrast material as a result of endothelial ischemia without frank breakdown of the blood-brain barrier [27, 28] may be postulated as responsible for an increased accumulation of contrast material. In either case, the total amount accumulated will ultimately depend on the overall rate of delivery of contrast agent by the vasculature.

REFERENCES

1. Wing SD, Norman D, Pollock JA, Newton TH. Contrast enhancement of cerebral infarcts in computed tomography. *Radiology* **1976**;121:89–92
2. Inoue Y, Takemoto K, Miyamoto T, et al. Sequential computed tomography scans in acute cerebral infarction. *Radiology* **1980**;135:655–662
3. Pullicino P, Kendall BE. Contrast enhancement in ischaemic lesions. I. Relationship to prognosis. *Neuroradiology* **1980**;19:235–239
4. Wall SD, Brant-Zawadzki M, Jeffrey RB, Barnes B. High frequency CT findings within 24 hours after cerebral infarction. *AJNR* **1981**;2:553–557
5. Virapongse C, Mancuso A, Quisling R. Human brain imaging: Gd-DTPA-enhanced MR imaging. *Radiology* **1986**;161:785–794
6. Imakita S, Nishimura T, Naito H, et al. Magnetic resonance imaging of human cerebral infarction: enhancement with Gd-DTPA. *Neuroradiology* **1987**;29:422–429
7. Imakita S, Nishimura T, Yamada N, et al. Magnetic resonance imaging of cerebral infarction: time course of Gd-DTPA enhancement and CT comparison. *Neuroradiology* **1988**;30:372–378
8. Miyashita K, Naritomi H, Sawada T, et al. Identification of recent lacunar lesions in cases of multiple small infarctions by magnetic resonance imaging. *Stroke* **1988**;19:834–839
9. Muller W, Kramer G, Roder RG, Kuhnert A. Balance of T1-weighted images before and after application of a paramagnetic substance (Gd-DTPA). *Neurosurg Rev* **1987**;10:117–122
10. McNamara MT, Brant-Zawadzki M, Berry I, et al. Acute experimental cerebral ischemia: MR enhancement using Gd-DTPA. *Radiology* **1986**;158:701–705
11. Yuh WTC, Crain MR, Loes DJ, et al. MR imaging of cerebral ischemia: findings in the first 24 hours. *AJNR* **1991**;12:621–629
12. Bryan RN, Wilcott MR, Schneiders NJ, Ford JJ, Dorman HS. Nuclear magnetic resonance evaluation of stroke. *Radiology* **1983**;149:189–192
13. Sipponen JT, Kaste M, Ketonen L, Sepponen RE, Katevuo K, Sivula A. Serial nuclear magnetic resonance (NMR) imaging in patients with cerebral infarction. *J Comput Assist Tomogr* **1983**;7:585–589
14. Rothrock JF, Lyden PD, Hesselink JR, Brown JJ, Healy ME. Brain magnetic resonance imaging in the evaluation of lacunar stroke. *Stroke* **1987**;18:781–786
15. Brown JJ, Hesselink JR, Rothrock JF. MR and CT in lacunar infarcts. *AJNR* **1988**;9:477–482
16. Biller J, Yuh WTC, Mitchell GW, Bruno A, Adams HP Jr. Early diagnosis of basilar artery occlusion using magnetic resonance imaging. *Stroke* **1988**;19:297–306
17. Pressman BD, Tourje EJ, Thompson JR. An early CT sign of ischemic infarction: increased density in a cerebral artery. *AJNR* **1987**;8:645–648
18. Tomsick TA, Brott TG, Chambers AA, et al. Hyperdense middle cerebral artery sign on CT: efficacy in detecting middle cerebral artery thrombosis. *AJNR* **1990**;11:473–477
19. Schuknecht B, Ratzka M, Hofmann E. The "dense artery sign"—major cerebral artery thromboembolism demonstrated by computed tomography. *Neuroradiology* **1990**;32:98–103
20. Elster AD, Moody DM. Early cerebral infarction: gadopentate dimeglumine enhancement. *Radiology* **1990**;177:627–632
21. Goldstein GW, Betz AL. Recent advances in understanding brain capillary function. *Ann Neurol* **1983**;14:389–395
22. Hesselink JR, Press GA. MR contrast enhancement of intracranial lesions with Gd-DTPA. *Radiol Clin North Am* **1988**;26:873–887
23. Brant-Zawadzki M, Berry I, Osaki L, Brasch R, Murovic J, Norman D. Gd-DTPA in clinical MR of the brain: 1. Intraaxial lesions. *AJNR* **1988**;7:781–788
24. Schuier FJ, Hossmann KA. Experimental brain infarcts in cats. II. Ischemic brain edema. *Stroke* **1980**;6:593–601
25. Bell BA, Symon L, Branston MN. CBF and time thresholds for the formation of ischemic cerebral edema, and effect of reperfusion in baboons. *J Neurosurg* **1985**;62:31–41
26. Gotoh O, Asano T, Koide T, Takakura K. Ischemic brain edema following occlusion of the middle cerebral artery in the rat. I. The time courses of the brain water, sodium and potassium contents and blood-brain barrier permeability to ^{125}I-albumin. *Stroke* **1985**;16:101–109
27. Petito CK. Early and late mechanisms of increased vascular permeability following experimental cerebral infarction. *J Neuropathol Exp Neurol* **1979**;38:222–234
28. Rapoport SI. Experimental modification of blood-brain barrier permeability by hypertonic solutions, convulsions, hypercapnia, and acute hypertension. In: Cserr H, Fenel V, Fenstermacher J, eds. *Fluid environment of the brain*. New York: Academic Press, **1975**:61–80

Book Review

Neuroradiology Test and Syllabus, parts 1 and 2. Section editor: Peter E. Weinberg. (Set 28 in the Professional Self-Evaluation and Continuing Education Program.) Reston, VA: American College of Radiology, 926 pp., 1990. $180 for ACR members, $300 for nonmembers, and $150 for residents

I always look forward to publications of the latest American College of Radiology (ACR) syllabus, and I read with great interest this first set devoted solely to neuroradiology (the previous three were on head and neck disorders and thus included both head and neck and neuroradiology). The ACR published its first set (chest disease) in 1972 and has been at it ever since. The professional self-evaluation and continuing education program has been enormously successful (more than 170,000 volumes purchased since its inception). *Neuroradiology*, parts 1 and 2, is the 28th set in the series.

The ACR *Neuroradiology Test and Syllabus* has many of the same notable strengths and weaknesses as the whole series. First (as it is comparatively minor), the bad news: The images in many cases are outdated. In the 32 quiz cases themselves, only one MR image is shown. Several plain radiographs of the skull, unsubtracted cerebral angiograms, and truly ancient CT scans (EMI Mark I with the old water bag, yet!) are shown. In a 1990 publication, with a few exceptions, most of the suggested readings are pre-1988, making the reading list less useful than desirable. The proofreading was spotty, and some slipups in the text have occurred (e.g., Figure 24-4 is printed upside-down). Finally, the explanatory text and the accompanying illustrations occasionally are inconsistent. For example, the syllabus states, "Redundant nerve roots are always associated with spinal stenosis and a block, either complete or partial. The multiple serpiginous filling defects seen on myelography are always situated above the block." Then a supposedly illustrative case of spinal stenosis is shown on the opposite page, where "redundant" nerve roots clearly are seen below the high-grade stenosis as well as above it. Terminology is also loose: There is no such thing as a "partial block." It is either a high-grade stenosis or a block. "Complete block" is also a redundant term. (Picky, picky, but a reviewer has to find a few flaws in order to have credibility. Otherwise, all publications are praised and recommended, making the review basically meaningless.)

Now for the good news. The discussions—in my opinion, the best parts of the series—are wonderful. Several are real tours de force. Tom Naidich and his coauthors have taken great pains to include high-resolution MR images, clinical and intraoperative photographs, gross specimens for radiologic-pathologic correlation, and so forth. For example, the discussion on Chiari malformations is the best I have seen anywhere.

The cases selected span a nice range, from congenital malformations of the brain and spine to vascular disease, infection, traumatic and degenerative disorders, and neoplasms. The explanations are filled with numerous "pearls" and few pitfalls. Although the test questions themselves are not always clear, the discussions are generally excellent. Again, I wish for more state-of-the-art images, but the outstanding strength of the whole ACR series is the meticulous nature of the discussion sections. The *Neuroradiology Test and Syllabus* is no exception.

I cannot think of a target audience that would not benefit greatly from this particular syllabus: residents (both junior and board-eligible), fellows, practicing radiologists, and professors (yes, I learned a thing or two or three from my colleagues). It seems as though everyone who writes any book review concludes with at least a lukewarm recommendation. But trust me—buy this one and you won't be sorry! Even if you do not take the formal evaluation part (25 hr of Category 1 credit are available), it is well worth the investment. Then, don't just put it on your shelf to gather dust, read it.

Anne G. Osborn
University of Utah Medical Center
Salt Lake City, UT 84132

Diagnosis of Acute Cerebral Infarction: Comparison of CT and MR Imaging

R. Nick Bryan[1]
Lucien M. Levy[1]
Warren D. Whitlow[1]
James M. Killian[2]
Thomas J. Preziosi[3]
Joana A. Rosario[1]

The appearance of acute cerebral infarction was evaluated on MR images and CT scans obtained in 31 patients within 24 hr of the ictus; follow-up examinations were performed 7–10 days later in 20 of these patients and were correlated with the initial studies. Acute infarcts were visible more frequently on MR images than on CT scans (82% vs 58%). Proton density– and T2-weighted scans usually demonstrated regions of hyperintensity corresponding to acute infarcts, but proton density–weighted scans often showed better definition of the lesion in terms of regional anatomy. Follow-up MR images and CT scans identified approximately 88% of subacute strokes, 54% of which were better defined and/or larger than on the initial examination. In 20% of lesions, "hemorrhagic" characteristics were seen on at least one examination. CT and MR imaging were comparable in delineating acute hemorrhage, but MR detected more cases with evidence of hemorrhage on follow-up examinations.

MR appears to be more sensitive than CT in the imaging of acute stroke.

***AJNR* 12:611–620, July/August 1991; *AJR* 157:585–594, September 1991**

Although the pathophysiology and diagnosis of stroke have been studied by numerous imaging techniques [1–3], none currently enable precise diagnosis and delineation of acute cerebral infarction. The diagnosis of acute stroke is based primarily on the clinical observation of an acute neurologic deficit and the exclusion of other diagnostic possibilities by CT scanning and metabolic tests [4]. CT often appears normal in the first 24–48 hr [5–8], and may not establish a definitive diagnosis. Physiologic imaging tests such as xenon CT or single-photon emission CT may detect early cerebral perfusion abnormalities that are related to, but not the same as, infarction [9]. Furthermore, these studies have low spatial resolution compared with CT and MR imaging and may be logistically complicated. More sophisticated physiologic imaging examinations such as positron-emission tomography often are not available or practical [10]. MR has been used to evaluate stroke in animal models [11–15], and some studies have reported on MR of stroke in humans [16–22]. Our investigation evaluates the appearance of early stroke on MR, and compares the sensitivities of MR and CT in the detection of this disease.

Subjects and Methods

This prospective study consisted of two parts. First, MR and CT scans were obtained within 24 hr of ictus in patients with a clinical diagnosis of acute stroke. We used the standard clinical criteria for acute stroke, the basis of which is the presentation of a new, measurable neurologic deficit within the previous 24 hr that persists at least 24 hr [4]. Such clinical criteria are estimated to be 90% sensitive. While not definitive, these criteria are often used as a clinical gold standard. Included in this diagnosis would be thrombotic and/or embolic and hemorrhagic or nonhemorrhagic stroke. Subarachnoid hemorrhage usually would not be included. Other selection criteria included willingness of the patients to undergo initial and follow-up CT and MR, their ability to give informed consent, and instrument availability. No

Received July 23, 1990; returned for revision October 1, 1990; revision received January 10, 1991; accepted January 21, 1991.

This work was supported in part by National Institutes of Health grant NS 19056-06.

[1] Neuroradiology Division, Meyer 8-140, The Russell H. Morgan Department of Radiology and Radiological Science, The Johns Hopkins Hospital, 600 N. Wolfe St., Baltimore, MD 21205. Address reprint requests to R. N. Bryan.

[2] Department of Neurology, Baylor College of Medicine, Houston, TX 77030.

[3] Department of Neurology, The Johns Hopkins Hospital, Baltimore, MD 21205.

0361–803X/91/1573–0585
© American Roentgen Ray Society

more than one patient could be in the protocol at any time. Therefore, patients were entered approximately every 2 weeks on a "first-to-fill" basis. Between 1987 and 1989, 44 patients were entered into the protocol. Nine did not complete one or more imaging studies within 24 hr of ictus and were excluded from further analysis. In four others, a final clinical diagnosis of stroke was not made. Fifteen women and 16 men 15–94 years old (median age, 63) with a final diagnosis of stroke completed the first part of the protocol. Twenty of these patients participated in the second part of the study, which consisted of follow-up CT (19 patients) and MR (20 patients) examinations performed 7–10 days following the acute episode. Eleven patients were unable or refused to undergo the second set of examinations despite initial agreement to do so.

Although entry into the study was determined by the initial clinical diagnosis, inclusion in the Results portion of this report was determined by the neurologic discharge diagnosis, which was confirmed by either of the neurologists participating in this study. These neurologists were not the primary attending physicians and did not know the results of the imaging studies.

The CT scans on admission were unenhanced, whereas the follow-up scans were obtained with and without enhancement. CT scans were obtained on either a GE 9800 (General Electric Medical Systems, Milwaukee, WI) or a Siemens DR3 (Siemens Medical Systems Group, Iselin, NJ) scanner with a slice thickness 4–5 mm through the posterior fossa and 8–10 mm supratentorially. MR studies followed the CT examinations as required by the Institutional Review Board. MR examinations included proton density–weighted, 3000–3500/22–35 (TR/TE); T2-weighted, 3000–3500/80–120; and T1-weighted, 500–600/20–35, spin-echo sequences. MR scans were obtained on Siemens 0.5- and 1.0-T and General Electric 1.5-T instruments. All scans were in the axial projection and consisted of 5-mm-thick slices with a 2.0- or 2.5-mm gap, 256 × 256 matrix, and one acquisition for 1.0- and 1.5-T double-echo sequences and two acquisitions for the 0.5-T system. For T1-weighted sequences, four acquisitions were used at 0.5 T and two at 1.0 and 1.5 T. In 16 cases, gradient-echo (GRE) scans, 500/30/90° (TR/TE/flip angle) and 30/15/10°, also were obtained to evaluate T2* effects.

The imaging studies were separated into two sets, initial and follow-up examinations. Film identification was blinded, and the pseudo-randomized (as to patient, type of examination, and date) examinations were presented independently to two observers (both neuroradiologists) for interpretation. The interpreters determined the presence or absence of an acute stroke on the usual clinical basis of a focal region of radiolucency (or increased radiodensity if hemorrhagic) in a vascular pattern on CT with "appropriate" (usually mild) mass effect. On MR studies, the criteria were similar except for the substitution of increased signal intensity on proton density– and T2-weighted images for the radiolucency seen on CT. Lesions were recorded as to location (cortical, subcortical, and posterior fossa, as well as specific regions), size (0–2, 2–5, and >5 cm), and radiodensity and signal intensity (increased, normal, decreased) on CT and MR images, respectively. Clinical information was not initially available for review. For statistical purposes, the locations of the lesions (right vs left hemisphere) seen on MR and CT follow-up studies were used as the gold standard for determining the sensitivity and specificity of both techniques in the initial examination. Each of the 40 hemispheres in the 20 patients who underwent follow-up examinations was treated as a separate entity.

A second interpretation was conducted that compared the initial and follow-up images of each patient as to the location, size, and signal intensity of the lesion. The examinations were interpreted jointly on a third occasion with the addition of clinical information. This resulted in a consensus opinion, which was used for descriptive findings.

Results

Of the 31 patients with acute stroke who underwent initial CT and MR scans, 13 had cerebral cortical strokes, eight had subcortical lesions, seven had combined cortical and subcortical lesions, and three had posterior fossa strokes. The mean time between ictus and CT was 8 hr; between ictus and MR, 12 hr. The numbers and percentages of strokes diagnosed by each of the observers on initial and follow-up CT and MR scans are shown in Table 1. Table 2 shows the percent agreement between the observers. On the basis of the mean of the multiobserver observations of the 31 initial studies, 58% of the initial CT examinations were thought to show an acute stroke as compared with 82% on MR. For the statistical computation of the sensitivity (CT = 59.1%, MR = 88.7%) and specificity for diagnosis of acute stroke (CT = 100%, MR = 91.7%), the combined results of the two interpreters were used only when both initial and follow-up studies had been performed. To determine whether the differences in those values were statistically significant, a chi-square test was applied for both sensitivity (χ^2, 1 df = 7.06) and specificity (χ^2, 1 df = 1.56). At a confidence level of 95% (χ^2 = .95, 1 df = 3.84), there was a statistically significant difference in the sensitivities of CT scanning as compared with MR for the detection of acute stroke. That difference did not hold for specificity.

On the initial MR scans, proton density– *or* T2-weighted images showed the lesions as areas of increased signal intensity in 25 cases (Table 3, Fig. 1). Signal intensities were increased on both proton density– *and* T2-weighted images in 22 cases. In two cases in which the proton-density signal intensity was increased and the T2 signal intensity was thought to be normal, both lesions were cortical. In one case (a pontine lesion), the proton-density signal intensity was normal and the T2 signal intensity was increased. Proton

TABLE 1: CT and MR Studies Diagnosed as Showing Acute Stroke

Observer No./Study	No. Diagnosed/Total No. (%)	
	Initial Studies	Follow-up Studies
1		
CT	21/31 (68)	16/19 (84)
MR	27/31 (87)	19/20 (95)
2		
CT	15/31 (48)	15/19 (79)
MR	24/31 (77)	19/20 (95)
Mean value		
CT	(58)	(82)
MR	(82)	(95)

TABLE 2: Percentage Agreement Between the Two Observers in Interpreting Initial and Follow-up CT and MR Studies in Acute Stroke

Imaging Method	Study Interval	
	Initial	Follow-up
CT	81%	95%
MR	94%	100%

density-weighted images appeared to show slightly better contrast between the lesion and its surroundings than T2-weighted images did. In six cases, neither the proton-density nor the T2 signal intensity was increased. In two of these cases, T2-weighted images showed decreased signal intensity indicative of acute hemorrhage. In both cases there was a corresponding decrease in signal intensity on GRE scans plus an increased radiodensity on CT scans. Both these lesions were typical basal ganglia hematomas approximately 2–3 cm in diameter (Fig. 2). T1-weighted images were the least sensitive in the detection of stroke. On initial examination, only six cases were abnormal, four showing decreased signal intensity and two showing increased signal intensity.

TABLE 3: Signal Intensity of Stroke Lesions (Compared with Normal Hemisphere) on MR Sequences

Examination/ Signal Intensity	PDW	T2W	T1W	GRE
Initial (n = 31)				
Increased	24	22	2	0
Isointense	7	7	25	14
Decreased	0	2	4	2
Follow-up (n = 20)				
Increased	17	17	6	2
Isointense	2	2	9	11
Decreased	1	1	5	1

Note.—PDW = proton-density weighted; T2W = T2 weighted; T1W = T1 weighted; GRE = gradient echo.

On follow-up CT, a mean of 82% of the examinations were thought to show the stroke regions; interobserver variability was minimal. On follow-up MR scans, 95% (19/20) of the lesions were seen and there was no interobserver variability. Of the 20 lesions seen on follow-up MR, 17 were reflected by increased signal intensity on proton density– and T2-weighted images, while decreased signal intensity was seen on proton density– and T2-weighted images in one case. In the latter case, decreased signal intensity was seen on GRE scans also. Two lesions were isointense on proton density– and T2-weighted images. On T1-weighted images, increased signal

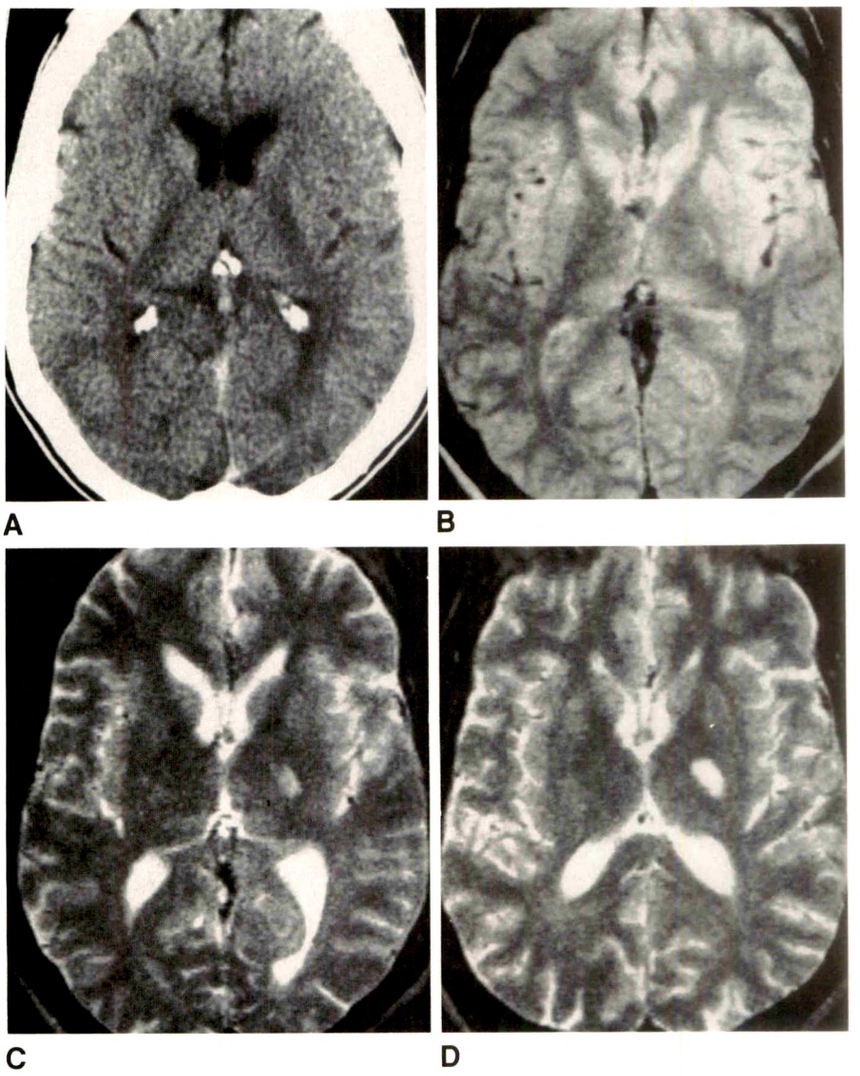


Fig. 1.—Infarct in left posterior limb of internal capsule.

***A*, CT scan 6 hr after ictus is normal.**

***B* and *C*, Proton density–(3000/35) and T2-(3000/105) weighted MR images show infarct as area of increased signal intensity.**

***D*, T2-weighted MR image (3000/105) obtained 7 days after ictus shows better definition of lesion, which is slightly enlarged.**

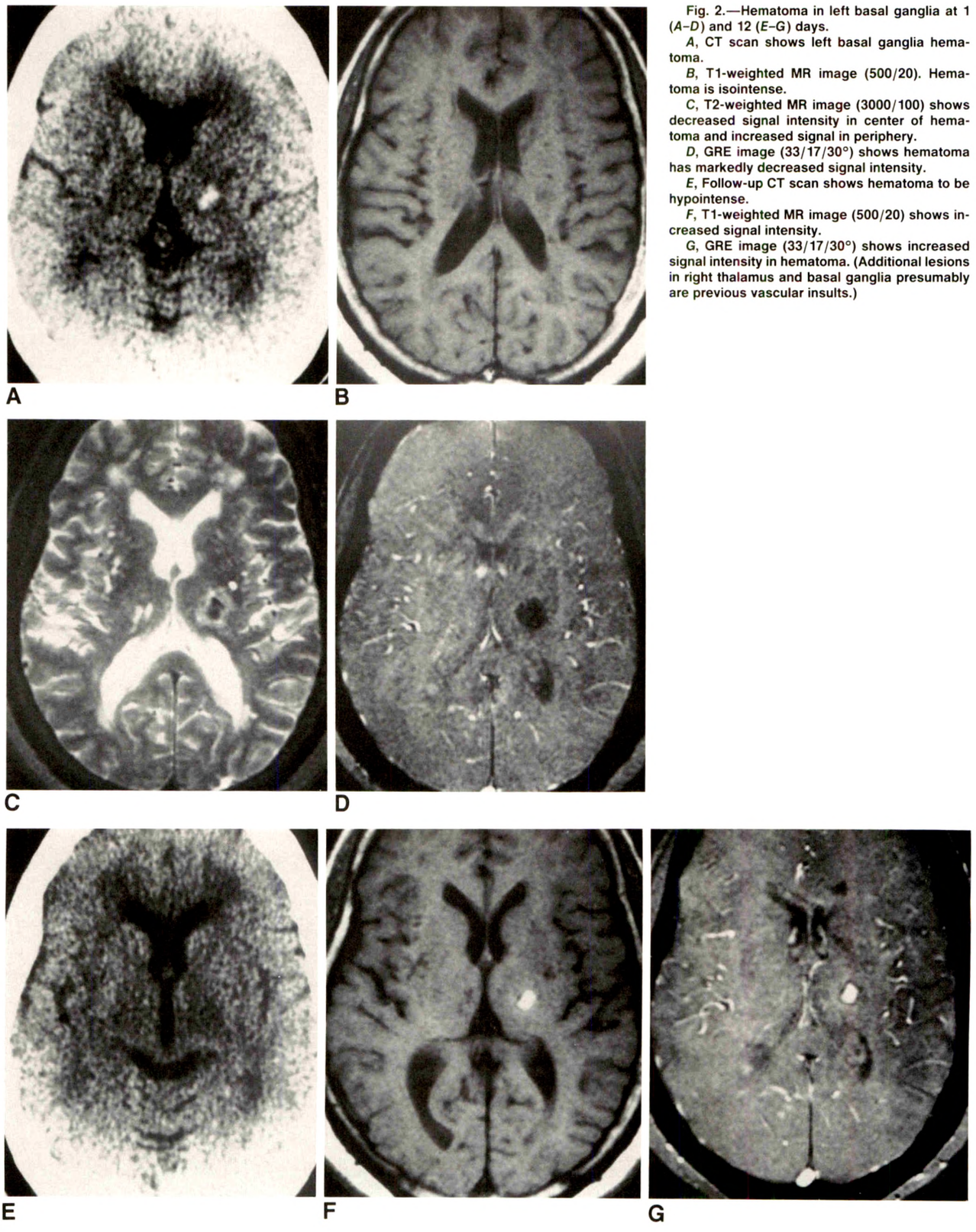


Fig. 2.—Hematoma in left basal ganglia at 1 (*A–D*) and 12 (*E–G*) days.

A, CT scan shows left basal ganglia hematoma.

B, T1-weighted MR image (500/20). Hematoma is isointense.

C, T2-weighted MR image (3000/100) shows decreased signal intensity in center of hematoma and increased signal in periphery.

D, GRE image (33/17/30°) shows hematoma has markedly decreased signal intensity.

E, Follow-up CT scan shows hematoma to be hypointense.

F, T1-weighted MR image (500/20) shows increased signal intensity.

G, GRE image (33/17/30°) shows increased signal intensity in hematoma. (Additional lesions in right thalamus and basal ganglia presumably are previous vascular insults.)

intensity was seen in six lesions while decreased signal intensity was seen in five.

Owing to the nonquantitative evaluation of lesion size, only relative estimates of size and progression could be made (Table 4). On the basis of consensus MR interpretations, 10 lesions initially were 0–2 cm in maximum diameter, nine were 2–5 cm, and seven were larger than 5 cm. In 21 cases in which the same lesions were visible on initial CT and MR studies, the lesions subjectively appeared to be larger on MR in six cases (Fig. 3). Progression in lesion size is probably best assessed by comparing only those lesions in which both initial and follow-up MR studies were performed. Of these 16 cases, four lesions appeared to enlarge, three diminished, and nine showed no change in size.

TABLE 4: Size of Stroke Lesions and Apparent Change in Size on Follow-up Scans

Study/Lesion Size (cm)	Initial Study (No.)	Follow-up Study (No.)			
		Larger	Smaller	No Change	No Follow-up
CT					
0–2	9	5	1	2	1
2–5	8	2	2	0	4
>5	4	0	0	1	3
Not seen	10	3	0	3	4
Total	31	10	3	6	12
MR					
0–2	10	2	0	3	5
2–5	9	2	2	1	4
>5	7	0	1	5	1
Not seen	5	3	0	1	1
Total	31	7	3	10	11

The CT criterion for the presence of "hemorrhage" was increased radiodensity relative to gray matter. On MR, the criteria for hemorrhage were decreased signal intensity on T2-weighted images, increased signal intensity on T1-weighted images, and/or decreased signal intensity on GRE images, all relative to normal white matter.

There was good agreement among observers as to the presence or absence of hemorrhage (Table 5). On initial studies, both interpreters agreed on the presence of two basal ganglia hematomas that were reflected by increased density on CT and decreased signal intensity on T2-weighted and GRE images. There was also agreement about an acute hemorrhagic infarct in the basal ganglia, reflected by increased signal intensity on T1-weighted images (Fig. 4). However, on one CT and one MR examination there was disagreement as

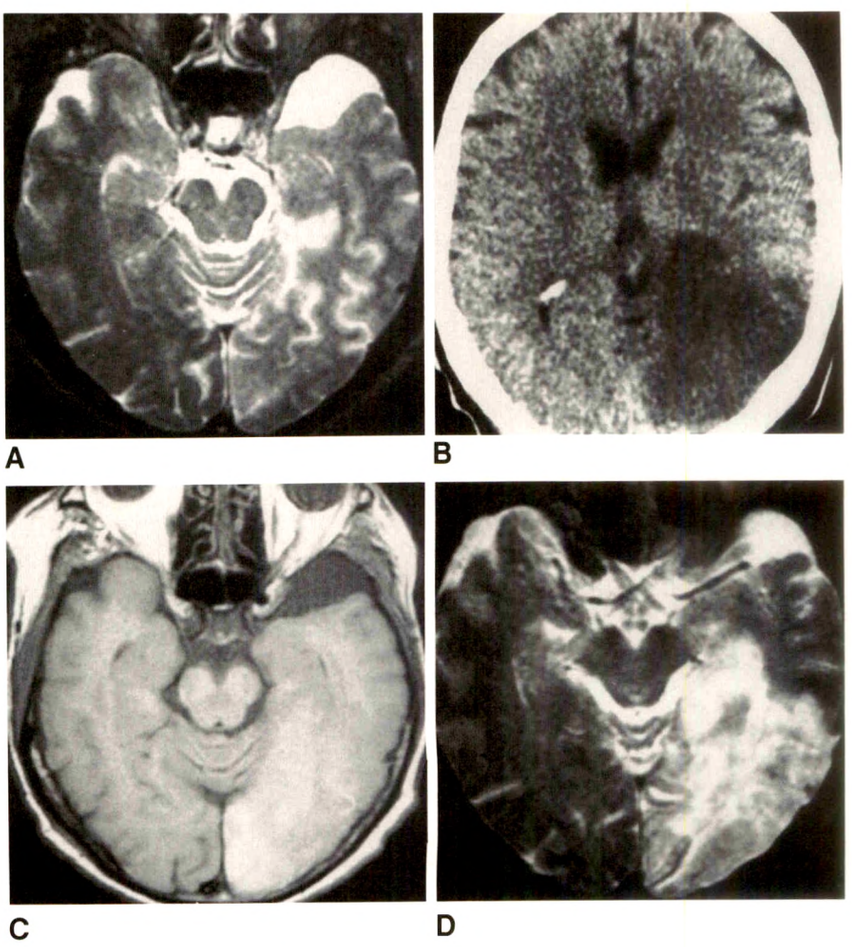


Fig. 3.—Infarct in left occipital lobe at 1 (*A*) and 7 (*B–D*) days appears hemorrhagic and larger on follow-up examinations.

A, T2-weighted MR image (3000/100) shows left occipital lobe infarct with increased signal intensity.

B, Follow-up CT scan shows large infarct.

C, T1-weighted MR image (500/20) shows evidence of hemorrhage with increased signal intensity.

D, T2-weighted MR image (3000/100) shows apparent growth of infarct since initial examination. (Incidental arachnoid cyst in left middle fossa.)

to the presence of hemorrhage. In these cases, the infarcts were radiolucent on CT and showed increased signal intensity on T2-weighted images; however, questionable intermixed regions of increased radiodensity on CT and/or decreased signal intensity on T2-weighted images were seen also. On follow-up examinations, there was disagreement concerning hemorrhage on one CT scan and no disagreement on MR scans.

TABLE 5: Findings of the Observers Concerning the Presence or Absence of Hemorrhagic Infarct on CT and MR

Study/Finding	CT	MR
Initial		
Present	2	3
Absent	28	27
Indeterminate	1	1
Total	31	31
Follow-up		
Present	2	6
Absent	16	14
Indeterminate	1	0
Total	19	20

Note.—Findings are listed as present or absent if the observers agreed on the finding. If the observers disagreed, the finding is listed as indeterminate.

The main discord between CT and MR evidence of hemorrhage was seen in follow-up studies, in which four cases of hemorrhagic signal on MR were reflected by increased signal intensity on T1-weighted images without evidence of increased radiodensity on either the initial or follow-up CT study (Figs. 3 and 4). In none of these four cases was there decreased signal intensity on initial or follow-up T2-weighted or GRE scans. The percentage agreement between the two observers for the detection of hemorrhage varied little between the initial (CT, 97%; MR, 97%) and follow-up (CT, 95%; MR, 100%) studies.

Discussion

Acute infarcts are visible more often on MR than on CT scans. On admission, 82% of MR scans showed abnormality as compared with 58% of CT scans. On follow-up scans, approximately 90% of both CT and MR scans were abnormal. In the one instance in which a "stroke" was detected by CT and not seen on MR, the lesion was a small cortical subarachnoid hemorrhage (Fig. 5). This case illustrates the known limitations of MR in detecting subarachnoid hemorrhage.

This report raises the question of diagnostic criteria. Two were used in the present case. First, for protocol entry and

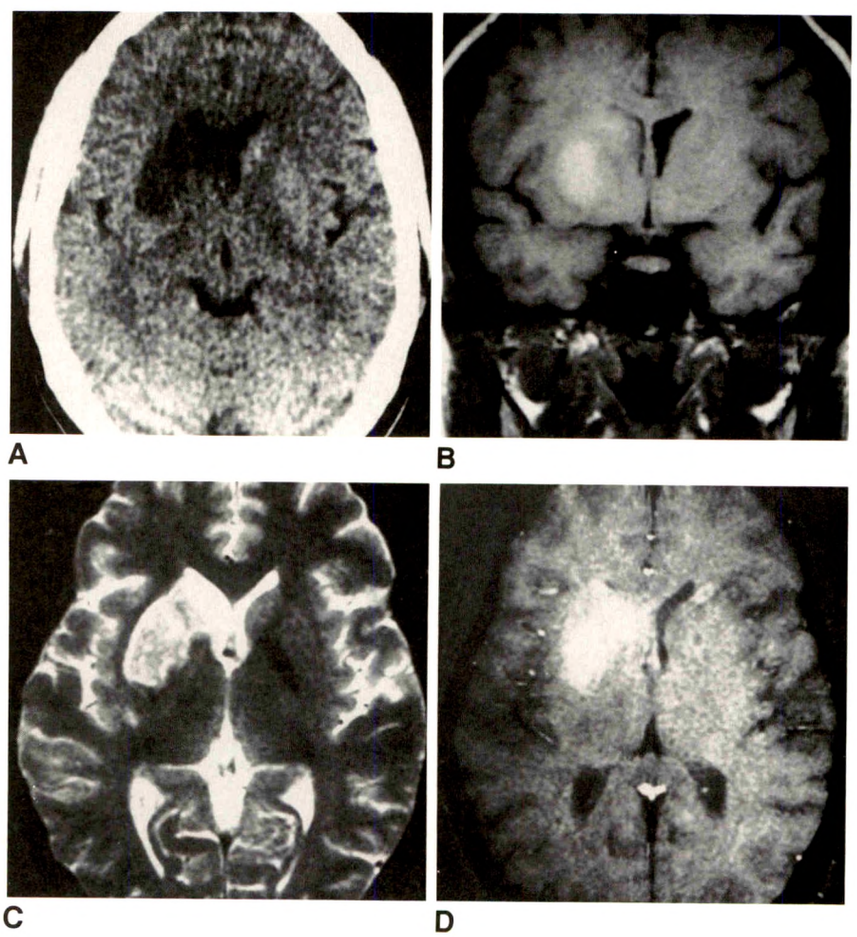


Fig. 4.—Infarct in right basal ganglia shows hemorrhage on MR but not on CT on day 1.
A, CT shows right basal ganglia infarct.
B, T1-weighted coronal MR image (500/20) shows increased signal intensity suggesting hemorrhage.
C and *D*, T2-weighted, 3000/100 (*C*), and GRE, 33/17/30° (*D*), images show infarct but no signal changes definitive of acute hematoma, although heterogeneous signal intensity in lesion on T2-weighted image might raise such a possibility.

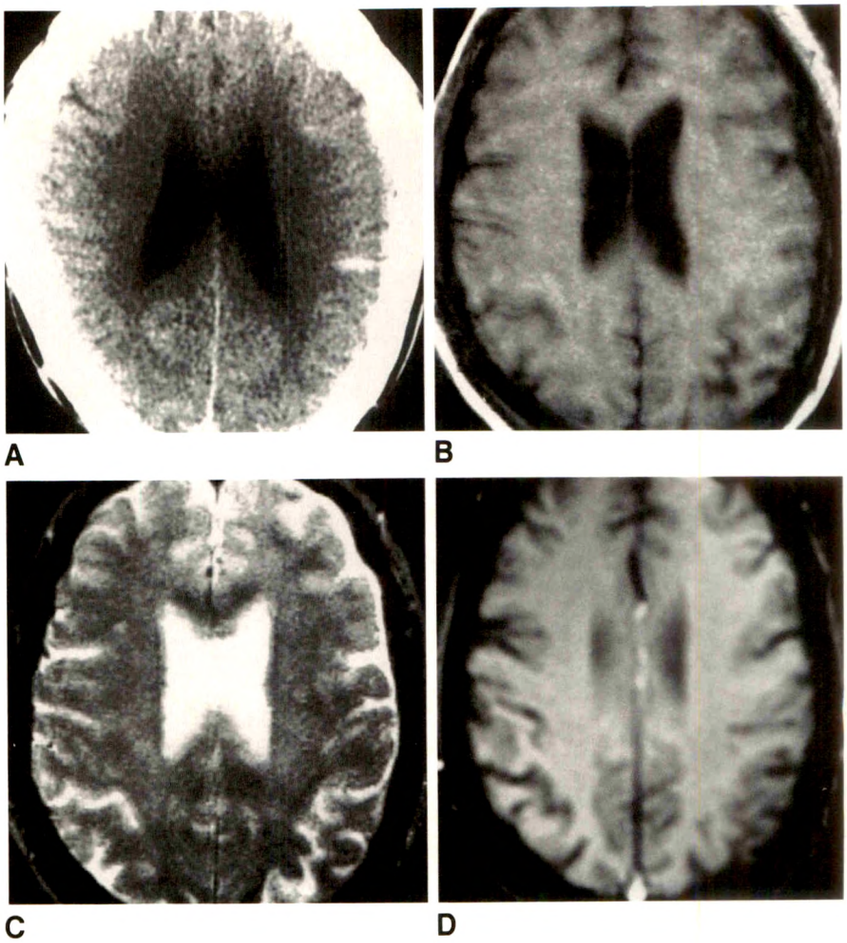


Fig. 5.—Small left cortical subarachnoid hemorrhage was seen on initial CT but not on MR.
***A*, CT scan shows small left cortical subarachnoid hemorrhage.**
***B–D*, T1-weighted, 500/20 (*B*); T2-weighted, 3000/100 (*C*); and GRE, 33/17/30° (*D*), images are all normal.**

descriptive results, we used clinical criteria for stroke diagnosis. This approach is imprecise, but is required for a prospective study since there is no accepted, definitive test for stroke prior to imaging studies. For statistical analysis of sensitivity and specificity, we have restricted our analysis to those cases with a clinical diagnosis of stroke and an abnormal follow-up imaging study. This possibly increases the sensitivity and specificity of CT and MR, since patients with stroke that was not seen on imaging studies (false negative) would be excluded from analysis. Our results and previous reports would suggest that less than 5% of stroke patients fall into this category [5, 6, 8].

Even when possible, the diagnosis of early stroke on CT is often relatively difficult, as the radiographic findings—radiolucency and mass—may be quite subtle, making the diagnosis tentative [8]. This difficulty in diagnosis is reflected in the significant interobserver variability in interpretation of the initial CT scans. This variability nearly disappeared on follow-up scans, by which time the lesions had become obvious.

The CT scans that were abnormal on the first examination appeared to underestimate the size of the lesion as compared with MR, but we have not quantified this discrepancy. The general sensitivity of CT may be higher than observed in this study, since severely ill and uncooperative patients were negatively biased for selection. A high rate of abnormal CT (and MR) findings probably would have been found in such patients. The 58% mean rate for CT in the early detection of stroke is less than that in some other reports [7, 8]. However, no previous reports were prospective studies with blinded interpretations.

On MR imaging, regions of increased signal intensity due to acute infarcts were usually observed on both proton density– and T2-weighted images. The changes on proton density–weighted images were subjectively more conspicuous in three cases. This finding was particularly evident for portions of strokes involving peripheral gray matter. In addition, when structures such as the internal and external capsules, thalamus, and basal ganglia were involved, better anatomic delineation was seen on proton density–weighted images. When a lesion is near a ventricle or subarachnoid space, the presence of CSF makes it difficult to identify the lesion on T2-weighted images since the signal intensities of CSF and the lesion may be similar.

On both initial and follow-up scans, T1-weighted images are the least sensitive for detection of stroke. This is not unexpected owing to the negative mix of T1 and proton-density effects [23].

Our results show a larger infarct, increased signal intensity on proton density– and T2-weighted images, and increased radiolucency on CT on follow-up examinations in approxi-

mately 30% of cases (seven of 20 on the basis of MR size criteria). These are important findings, although not surprising. In addition, 15% of lesions (three of 20) "appeared" between the first and second MR examinations. Thus, despite the sensitivity of MR in the detection of early ischemia, dynamic events occur between the first 24 hr and the subacute follow-up. The significance of this finding is the implication of a larger tissue area "at risk" that is not currently identified on routine MR scans. Explanations for this change in lesion size include infarct extension into the "penumbra," lysis of proximal emboli with reperfusion and/or distal embolization, and spread of secondary edema. Additional clinical, perfusion, metabolic, and angiographic studies are required to determine the precise pathogenesis of these lesions [24–26].

These human clinical results are in keeping with previous reports on the MR appearance of infarction [17–20, 27],

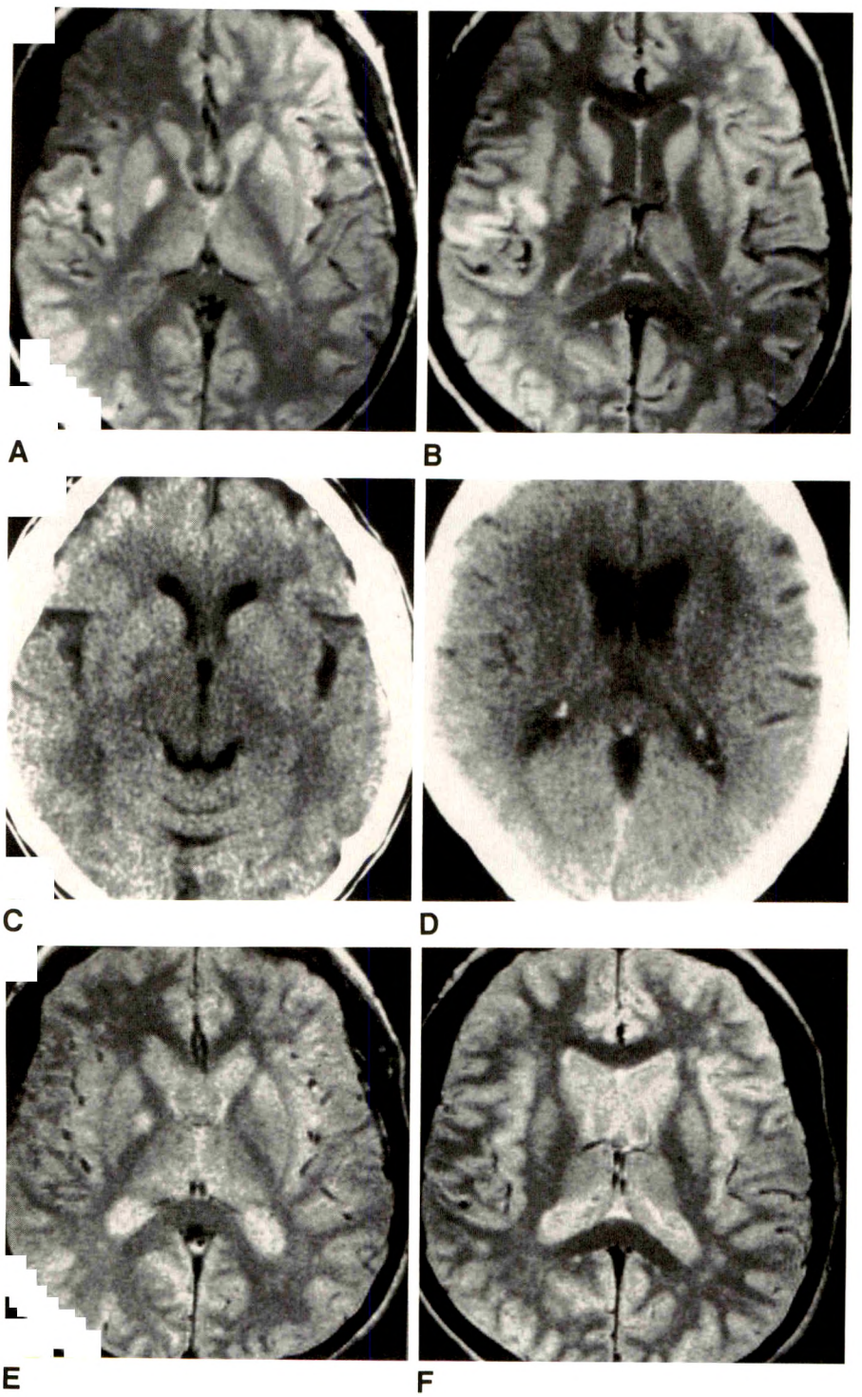


Fig. 6.—Right basal ganglia infarct and apparent right temporal cortical infarct on day 1 (*A* and *B*) with resolution of right cortical findings on follow-up examination on day 7 (*C–F*). Initial CT study was normal.

A and *B*, Proton density–weighted MR images (3000/35), show right basal ganglia and right temporal cortical infarct.

C and *D*, CT now shows infarct in right basal ganglia.

E and *F*, Proton density–weighted MR images (3000/35) show right basal ganglia infarct and resolution of changes in right temporal cortex.

although this earlier work primarily relates to older lesions. Animal experiments indicate that signal changes on conventional spin-echo MR images occur 2–4 hours after ischemic insult [11, 12, 15]. None of our patients was scanned earlier than 4 hr after ictus, but one might not expect to see abnormal MR scans in patients scanned before this time [16].

We believe MR is the most sensitive, accurate, and practical means of imaging acute stroke. However, the significance of the signal changes as well as their relationship to the pathophysiology of acute stroke needs to be clarified. We postulate that the early changes observed on MR reflect changes in intracellular water arising from loss of normal energy homeostasis, subsequent membrane dysfunction (particularly sodium-potassium pumps), increase in intracellular water, associated diminished binding of water, and consequent increase in T1 and T2 [28–32].

In only one case (Fig. 6) did an anatomic region of abnormal MR signal intensity revert to normal. However, our study excluded patients with transient ischemic attacks, and, therefore, we may have underestimated the number of patients in whom MR signal-intensity changes were transient.

Another critical factor in the diagnosis and current management of acute stroke is determination of the presence of a hemorrhagic component. Our results indicate that in the earlier stages of stroke, CI and MR may be equally suited to diagnosing hemorrhage. In the two cases of obvious acute hematoma in our series, typical changes of increased radiodensity on CT and decreased signal intensity on T2 and GRE MR scans were seen (Fig. 2). However, the number of cases of acute hemorrhage in this study is small, and other reports have indicated that acute hemorrhage may not be as obvious on MR as on CT, particularly if GRE scans are not obtained [33]. On the basis of published reports, it is probably not inappropriate to continue to obtain CT scans in the setting of acute stroke, although we believe that more experience with GRE imaging will obviate additional studies [34].

The other main finding related to hemorrhage in stroke is its comparative frequency, as reflected by increased signal intensity on T1-weighted images (Figs. 3 and 4). This type of hemorrhagic signal intensity was seen on follow-up (six of 20) as well as on a few initial (two of 31) MR scans. This hemorrhagic pattern differs from that of the usual hematoma. In particular, it is not associated with decreased signal intensity on T2-weighted images, nor are T2* effects reflected by decreased signal intensity on GRE images. Furthermore, the presence of "methemoglobin" (increased T1-weighted signal intensity) signal on the first day of ischemia is not in keeping with the usual 3- to 4-day process of oxidation of hemoglobin to methemoglobin [35]. These are not frank hematomas, but ischemic lesions with damaged capillary endothelium through which there is leakage, including diapedesis of RBCs, into the surrounding parenchyma; that is, ischemic petechial infarction.

These results suggest that MR offers important capabilities for the clinical evaluation as well as investigation of acute stroke. MR appears to detect ischemic stroke at an earlier stage than CT does and better defines its extent. It also allows differentiation of any associated hemorrhage.

ACKNOWLEDGMENTS

We thank Sharon Norman for data collection and collation and Marge Eddy for manuscript preparation.

REFERENCES

1. Brant-Zawadzki, Weinstein P, Bartkowski H, Moseley M. MR imaging and spectroscopy in clinical and experimental cerebral ischemia: a review. *AJR* **1987**;148:579–588
2. Kricheff IJ. Arteriosclerotic ischemic cerebrovascular disease. *Radiology* **1987**;162:101–109
3. Welch KMA, Levine SR, Ewing JM. Viewing stroke pathophysiology: an analysis of contemporary methods. *Stroke* **1986**;17(6):1071–1077
4. Hachinski V, Norris JW. *The acute stroke*. Philadelphia: Davis, **1985**
5. Inoue Y, Takemoto K, Miyamoto T, et al. Sequential computed tomography scans in acute cerebral infarction. *Radiology* **1980**;135:655–662
6. Hakim AV, Rynder-Cooke A, Melanson D. Sequential computerized tomographic appearance of strokes. *Stroke* **1983**;14:893–897
7. Wall SD, Brant-Zawadzki M, Jeffrey RB, Barnes B. High frequency CT findings within 24 hours of cerebral infarction. *AJR* **1982**;138:307–311
8. Tomura N, Uemura K, Inugami A, et al. Early CT finding in cerebral infarction: obscuration of the lentiform nucleus. *Radiology* **1988**;168:463–467
9. Bushnell DL, Gupta S, MIcoch AG, Romyn A, Barnes WE, Kaplan E. Demonstration of focal hyperemia in acute cerebral infarction with iodine-123 iodoamphetamine. *J Nucl Med* **1987**;28:1920–1923
10. Wise RJS, Rhodes CG, Gibbs JM, et al. Disturbance of oxidative metabolism of glucose in recent human cerebral infarcts. *Ann Neurol* **1983**;14:627–637
11. Bose B, Jones SC, Lorig R, Friel HT, Weinstein M, Little JR. Evolving focal cerebral ischemia in cats: spatial correlation of nuclear magnetic resonance imaging, cerebral blood flow, tetrazolium staining, and histopathology. *Stroke* **1988**;19:28–37
12. Brant-Zawadzki M, Pereira B, Weinstein P, et al. MR imaging of acute experimental ischemia in cats. *AJNR* **1986**;7:7–11
13. Gadian DG, Frackowiak SJ, Crockard HA, et al. Acute cerebral ischaemia: concurrent changes in cerebral blood flow, energy metabolites, pH, and lactate measured with hydrogen clearance and ^{31}P and ^{1}H nuclear magnetic resonance spectroscopy. I. Methodology. *J Cereb Blood Flow Metab* **1987**;7(2):199–206
14. Komatsumoto S, Nioka S, Greenberg JH, et al. Cerebral energy metabolism measured in vivo by 31P-NMR in middle cerebral artery occlusion in the cat—relation to severity of stroke. *J Cereb Blood Flow Metab* **1987**;7:557–562
15. Kucharczyk J, Chew W, Derugin N, et al. Nicardine reduces ischemic brain injury: magnetic resonance imaging/spectroscopy study in cats. *Stroke* **1989**;20:268–273
16. Yuh WTC, Crain MR,Loes DJ, Greene GM, Ryals TJ, Sato Y. MR imaging of cerebral ischemia: findings in the first 24 hours. *AJNR* **1991**;12:621–629
17. Biller J, Adams HP, Dunn V, Simmons Z, Jacoby CG. Dichotomy between clinical findings and MR abnormalities in pontine infarction. *J Comput Assist Tomogr* **1986**;10(3):379–385
18. Brown JJ, Hesselink JR, Rothrock JF. MR and CT of lacunar infarcts. *AJNR* **1988**;9:477–482
19. Bryan RN, Willcott MR, Schneiders NJ, Ford JJ, Derman HS. Nuclear magnetic resonance evaluation of stroke. *Radiology* **1983**;149:189–192
20. DeWitt LD, Kistler JP, Miller DC, Richardson EP, Buonanno FS. NMR-neuropathologic correlation in stroke. *Stroke* **1987**;18(2):342–351
21. Imakita S, Nishimura T, Naito H, et al. Magnetic resonance imaging of human cerebral infarction: enhancement with Gd-DTPA. *Neuroradiology* **1987**;29:422–429
22. Simmons Z, Biller J, Adams HP, Dunn V, Jacoby CG. Cerebellar infarction: comparison of computed tomography and magnetic resonance imaging. *Ann Neurol* **1986**;19(3):291–293
23. Bryan RN, Weathers SW, Blackwell RD. Central nervous system magnetic resonance imaging. In: Appel SH, ed. *Current neurology*. Chicago: Year Book Medical, **1988**:251–294
24. LeBihan D, Breton E, Lallemand D, et al. Separation of diffusion and

perfusion in intravoxel incoherent motion MR imaging. *Radiology* **1988**;168:497–505
25. Grotta JC. Can raising cerebral blood flow improve outcome after acute cerebral infarction? *Stroke* **1987**;18:264–267
26. Figols J, Cervos-Navarro J, Sampaolo S, Ferszt R. Microthrombi in the development of ischemic irreversible brain infarct. In: Cervos-Navarro J, Ferszt R, eds. *Stroke and microcirculation.* New York: Raven, **1987**: 69–74
27. Miyashita K, Naritomi H, Sawada T, et al. Identification of recent lacunar lesions in cases of multiple small infarctions by magnetic resonance imaging. *Stroke* **1988**;19:834–839
28. Erecinska M, Silver IA. ATP and brain function. *J Cereb Flood Flow Metab* **1989**;9:2–19
29. Symon L, Wang A, Momma F. Aspects of cerebral ischemia in humans: clinical correlates of primate thresholds. In: Cervos-Navarro J, Ferszt R, eds. *Stroke and microcirculation.* New York: Raven, **1987**:1–4
30. Plum F. What causes infarction in ischemic brain. The Robert Wartenberg lecture. *Neurology* **1983**;33:222–233
31. Mano I, Levy RM, Crooks LE, Hosobuchi Y. Proton nuclear magnetic resonance imaging of acute experimental cerebral ischemia. *Invest Radiol* **1983**;17:345–351
32. Eleff SM, Schnall MD, Ligetti L, et al. Concurrent measurements of cerebral blood flow, sodium lactate, and high-energy phosphate metabolism using ^{19}F, ^{23}Na, ^{1}H, and ^{31}P nuclear magnetic resonance spectroscopy. *Magn Reson Med* **1988**;7:1–13
33. Edelman RR, Johnson K, Buxton R, et al. MR of hemorrhage: a new approach. *AJNR* **1986**;7:751–756
34. Zyed A, Hayman LA, Bryan RN. MR imaging of inracerebral blood: diversity in the temporal pattern at 0.5 and 1.0 T. *AJNR* **1991**;12:469–474
35. Gomori JM, Grossman RI, Yu Ip C, Asakura T. NMR relaxation times of blood: their dependence on field strength, oxidation state, and cell integrity. *J Comput Assist Tomogr* **1987**;11:684–690

MR Imaging of Primary Trochlear Nerve Neoplasms

Lindell R. Gentry[1]
Rahul C. Mehta[1]
Richard E. Appen[2]
Joel M. Weinstein[2]

We present the clinical, anatomic, and MR imaging findings in six patients with seven primary trochlear nerve neoplasms, as well as the MR and clinical criteria that serve to establish the diagnosis of these rare cranial nerve neoplasms. Three patients had a history of neurofibromatosis and five patients had clinical evidence of a trochlear nerve palsy. Six of seven neoplasms produced localized, fusiform enlargement of the proximal cisternal segments of the trochlear nerves. The lesions that were visible on noncontrast MR scans (T1-, T2-, and proton density-weighted) had signal intensities that were virtually identical to normal brain parenchyma. All lesions showed intense, homogeneous enhancement on contrast-enhanced scans. Contrast-enhanced imaging was necessary for the detection of five of seven lesions and greatly increased the value of the MR study in all six patients.

AJNR 12:707–713, July/August 1991; *AJR* 157:595–601, September 1991

Primary neoplasms arising from pure motor cranial nerves such as the trochlear nerve are rare. To our knowledge just nine primary trochlear nerve neoplasms have been reported in the literature [1–7], only one of which was imaged with MR [1]. Over the last 6 years, since we began to use MR as the primary imaging method for evaluating patients with cranial nerve palsies, we have noticed a striking increase in the number of primary trochlear nerve neoplasms over those encountered during the CT era. We believe this is due to a much greater sensitivity of MR in detecting these typically small lesions. We present our MR experience with the detection and characterization of these rare neoplasms.

Subjects and Methods

During the interval between July 1984 and September 1990, 250 patients studied with MR at our institution were found to have lesions that involved 281 cranial nerves. Fifteen patients in this series had neoplasms that involved the trochlear nerve, six patients had a total of seven primary trochlear nerve neoplasms, and nine patients had neoplasms that secondarily involved that nerve. Five of seven primary lesions and all nine secondary lesions were symptomatic. MR images were obtained with a 1.5-T MR system (Signa, GE Medical Systems, Milwaukee) using T1-weighted (600/20/1–2) (TR/TE/excitations), proton density-weighted (2300–3500/20–30/1), and T2-weighted (2300–3500/90–100/1) noncontrast scans as well as T1-weighted (600/20/1–2) scans after administration of gadopentetate dimeglumine (0.1 mmol/kg). Clinical and imaging findings in seven cases of trochlear nerve neoplasm are presented in Tables 1 and 2, respectively.

Representative Case Reports

Case 1

A 61-year-old man with neurofibromatosis type 2 (NF-2) had a 2-year history of progressive vertical diplopia. His medical history was significant for subtotal resection of a melanotic

Received October 12, 1990; revision requested December 26, 1990; revision received February 6, 1991; accepted February 20, 1991.

[1] Department of Radiology, University of Wisconsin Hospital, E1/336, Clinical Sciences Center, 600 Highland Ave., Madison, WI 53792. Address reprint requests to L. R. Gentry.

[2] Department of Ophthalmology, University of Wisconsin Hospital, Madison, WI 53792.

0361-803X/91/1573-0595
© American Roentgen Ray Society

TABLE 1: Clinical Findings in Seven Cases of Trochlear Nerve Neoplasm

Case No.	Age	Sex	Trochlear Nerve Palsy	Duration of Palsy	MR Follow-up (months)	Surgical Proof	Neurofibromatosis	Other Cranial Nerve Lesions	Other Neoplasms
1	61	M							
Left			Yes	28 mo	8	No	NF-2	Bilateral III, V, VIII	Spinal/peripheral neurofibromas, spinal melanotic schwannoma
Right			No	–	8	No	NF-2	Right VII, Left XII	
2	36	M	No	–	27	No	NF-2	Bilateral VIII	Cranial/spinal meningiomas, brainstem glioma, peripheral/spinal neurofibromas
3	28	M	Yes	2 yr	–	Yes	NF-1	No	Peripheral nerve neurofibromas
4	58	M	Yes	5 yr	12	No	No	No	None
5	64	F	Yes	29 mo	12	No	No	No	None
6	48	M	Yes	9 yr	13	No	No	No	None

Note.—NF-1 = neurofibromatosis type 1, NF-2 = neurofibromatosis type 2.

TABLE 2: Imaging Findings in Seven Cases of Trochlear Nerve Neoplasm

Case No.	Lesion Size (mm^3)	CT Detection	Detection on MR Sequences				Signal Intensity Relative to Brain		
			T1	Proton Density	T2	Enhanced T1	T1	Proton Density	T2
1 Left	20	–	–	R	–	+	NS	Isointense	NS
Right	16	–	–	R	–	+	NS	Isointense	NS
2	16	–	R	R	–	+	Isointense	Isointense	NS
3	8000	+	+	+	+	+	Isointense	Isointense	Isointense
4	32	NP	–	–	–	+	NS	NS	NS
5	16	NP	–	–	–	+	NS	NS	NS
6	192	R	+	–	–	+	Isointense	NS	NS

Note.—MR enhancement pattern was intensely homogeneous in all cases; + = seen; – = not seen; R = seen only retrospectively, after a contrast-enhanced MR scan was performed; NS = not seen; NP = not performed.

schwannoma of a lumbar nerve root 4 years earlier. Neurologic evaluation disclosed a left trochlear nerve palsy, bilateral trigeminal nerve hypesthesias, and mild left facial paresis. Bilateral papilledema was present due to increased intracranial pressure related to elevated CSF protein. Enhanced T1-weighted MR images revealed small bilateral linear enhancing masses in the quadrigeminal plate cistern just posteroinferior to the inferior colliculus of the midbrain (Fig. 1). The elongated lesions were intrinsic to the cisternal segments of the trochlear nerves, just distal to their origin from the midbrain (Fig. 2). Also noted were similar bilateral lesions of the third, fifth, and eighth cranial nerves, as well as a lesion of the right facial nerve. All the cranial nerve neoplasms have remained stable in size over the past year. Surgery is not contemplated at this time because of the minimal symptoms, stable neurologic course, and stable lesion size. In view of the history of NF-2, the cranial nerve lesions most likely represent multiple schwannomas.

Case 3

A 28-year-old man with neurofibromatosis type 1 (NF-1) had a 3-month history of severe intermittent headaches and a 2-year history of vertical diplopia. A plexiform neurofibroma had been resected from his face 2 years earlier. Neurologic examination revealed right trochlear, right trigeminal (third division), and right facial nerve palsies. MR showed a 25 × 20 × 16 mm well-demarcated mass posterior to the inferior colliculus of the midbrain (Fig. 3). The lesion had a signal intensity that was similar to brain parenchyma on all noncontrast pulse sequences. The lesion was located at the point of emergence of the right trochlear nerve from the brainstem. The lesion caused mild hydrocephalus due to aqueductal compression. Contrast-enhanced T1-weighted MR scans revealed intense homogeneous enhancement of the mass (Fig. 3). At right suboccipital craniotomy, the lesion was found to be arising from the right trochlear nerve. The entire mass and involved portions of the trochlear nerve were removed. Histology revealed a schwannoma with mixed focal glial elements. Postoperatively, the patient has done well with the exception of a persistent right trochlear nerve palsy.

Case 6

This 48-year-old man was initially evaluated at another hospital 3 and 9 years earlier, respectively, for two different episodes of vertical diplopia (worse on right gaze), left retroorbital pain, and a left trochlear nerve palsy. Brain CT, MR imaging, and cerebral arteriography were reported to be normal on those occasions. Symptoms improved until 1 year later when he was first evaluated at our hospital for progression of diplopia and retroorbital pain. Neuroophthalmologic examination showed normal visual fields, visual acuity, and pupillary function. A left trochlear nerve palsy was again noted. An MR study revealed a well-defined, elongated mass in the left ambient cistern (Fig. 4). A coronal T1-weighted MR image confirmed that the 12 × 4 × 4 mm mass was intrinsic to the cisternal segment of the left trochlear nerve. The signal intensity of the lesion was similar to normal brain tissue on the T1-weighted scans but was not visible on other precontrast pulse sequences. Intense homogeneous enhancement was noted on postcontrast studies. A review of the old CT scan, obtained 3 years

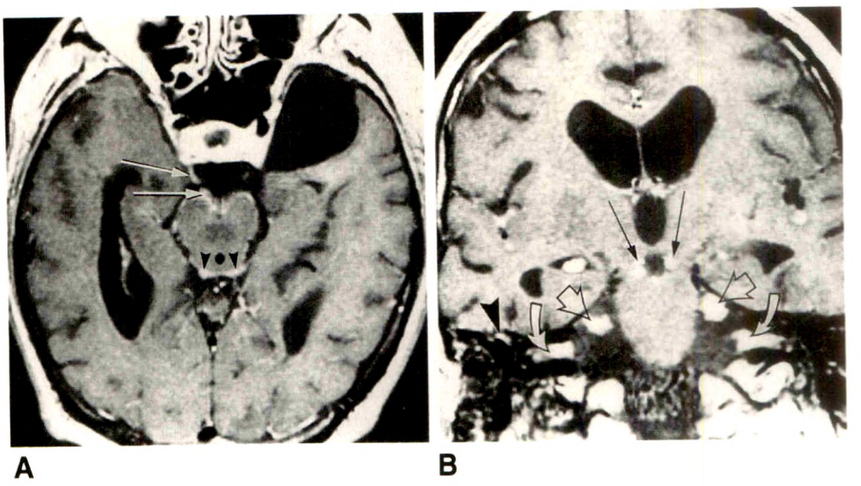


Fig. 1.—Case 1: 61-year-old man with NF-2; the lesions most likely represent multiple cranial nerve schwannomas.

A and *B*, Contrast-enhanced axial (*A*) and coronal (*B*) T1-weighted (600/20) MR scans reveal small bilateral homogeneously enhancing lesions of the proximal cisternal segments of both trochlear nerves (*arrowheads* in *A*). The lesions are located at the site where the trochlear nerves emerge from the midbrain, just posterior and slightly caudal to the inferior colliculus. Also noted are similar lesions of the oculomotor nerve (*long thin arrows*), trigeminal nerve (*open arrows* in *B*), vestibuloacoustic nerve (*curved arrows* in *B*), and right facial nerve (*arrowhead* in *B*).

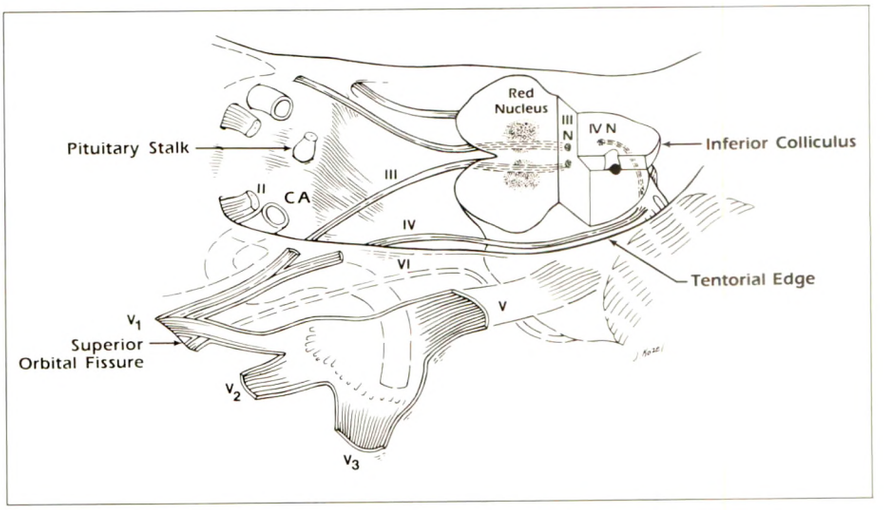


Fig. 2.—Diagram illustrating normal course of fourth cranial nerve. The nerve originates from the trochlear nerve nucleus, just ventrolateral to the cerebral aqueduct and caudad to the oculomotor nerve nucleus. The nerve fibers sweep dorsally around the aqueduct, decussate within the anterior medullary velum, and exit the dorsal surface of the midbrain just below the inferior colliculus, contralateral to the nucleus of their origin. The cisternal segment of the nerve then wraps around the brainstem, successively traversing the quadrigeminal, ambient, crural, and pontomesencephalic cisterns. The cisternal portion of the trochlear nerve is closely related to the tentorium cerebri, and usually is located a few millimeters inferolateral to its free edge. The nerve enters the cavernous sinus by piercing the dura along the lateral clivus, just below the petroclinoidal ligament and between the oculomotor and abducens nerves. The cavernous segment of the nerve runs in the lateral wall of the cavernous sinus, just inferior to the position of the oculomotor nerve. The trochlear nerve enters the orbit through the superior orbital fissure, external to the musculotendinous ring that serves as an attachment for the extraocular muscles.

earlier at another hospital, showed that the trochlear nerve lesion was visible, retrospectively, and had not changed in size. The patient's symptoms improved substantially after the placement of a prism in his eyeglasses. Surgery is not contemplated at the present time because of the minimal neurologic compromise and the significant risks of surgery.

Discussion

The trochlear nerve nucleus is located within the midbrain at the level of the inferior colliculus, just ventrolateral to the cerebral aqueduct (Fig. 2) [8]. The trochlear nerve nucleus gives rise to a group of axons that form a fascicle, which then courses posteroinferiorly around the aqueduct to decussate within the anterior medullary velum just caudad to the inferior colliculus. The trochlear nerve then emerges from the dorsal surface of the lower midbrain contralateral to the nucleus of origin and continues forward around the cerebral peduncle in the ambient cistern slightly inferior to the free edge of the tentorium (Figs. 1 and 2). The trochlear nerve leaves the posterior fossa by piercing the dura along the lateral aspect of the clivus just below the petroclinoidal ligament [8]. The parasellar segment of the trochlear nerve is located within the dura that forms the lateral wall of the cavernous sinus, positioned slightly below the oculomotor nerve [8–10]. It then enters the orbit through the superior orbital fissure, external to the tendinous ring that serves as an attachment site for the extraocular muscles [8].

Neuroophthalmologic evaluation is of great importance in clinical assessment of patients thought to have a trochlear nerve palsy. A true palsy must be differentiated from mechanical restriction of trochlear tendon movement through the trochlear sling (Brown syndrome), primary extraocular muscle abnormalities (e.g., Graves disease), orbital pseudotumor,

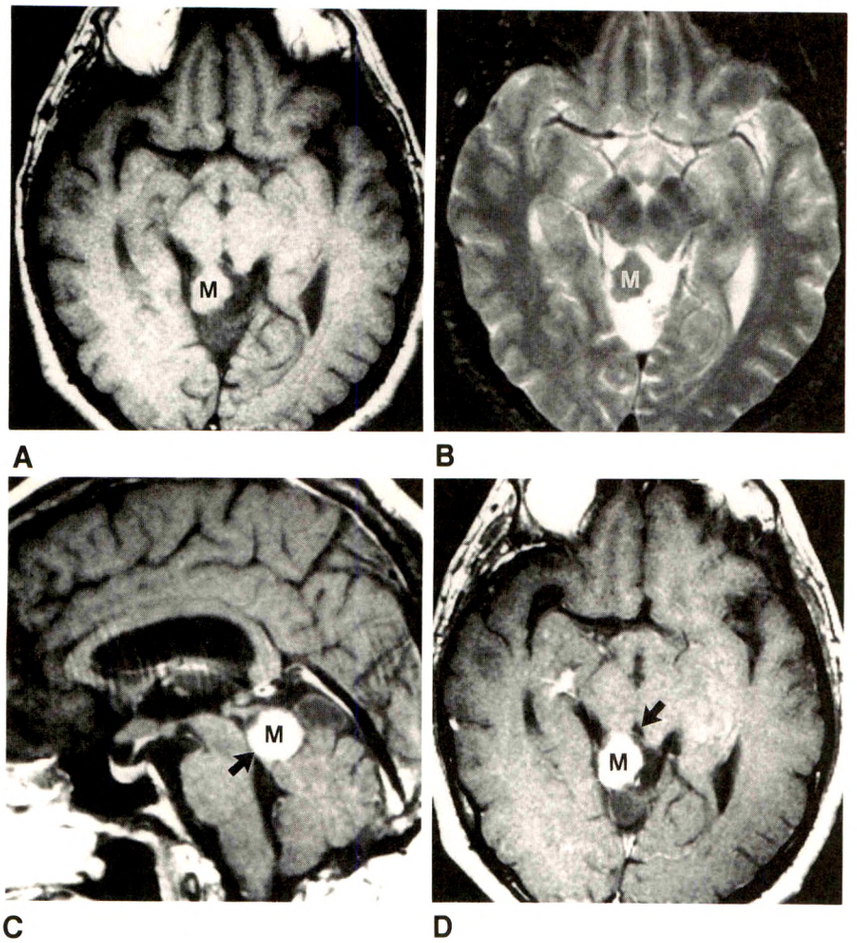


Fig. 3.—Case 3: 28-year-old man with NF-1. *A–D*, Precontrast axial T1- (600/20) (*A*) and T2- (2300/90) (*B*) weighted MR scans, and sagittal (*C*) and axial (*D*) contrast-enhanced T1-weighted (600/20) MR scans. A large soft-tissue mass (M) arises at the site where the right trochlear nerve emerges from the inferior colliculus of the midbrain. Signal intensity of the lesion on noncontrast images is similar to that of normal brain parenchyma. Intense homogeneous enhancement of the lesion is seen on postcontrast scans. The mass lesion causes mild hydrocephalus due to midbrain distortion and aqueductal compression (*arrows*). At surgery, the lesion was noted to originate from the right trochlear nerve. Histopathologic analysis revealed a schwannoma with focal glial elements.

and neuromuscular disease (e.g., myasthenia gravis) [11]. Imaging studies are often required to make this distinction with confidence. The type of visual field deficit and presence of associated palsies of cranial nerves III, V, and VI are often helpful in clinically localizing the site of disease. Because of considerable overlap among the clinical syndromes, however, anatomic delineation of the exact cause of trochlear nerve palsy is usually required.

MR offers considerable advantages over CT for evaluation of suspected cranial nerve abnormalities [12–14]. The superiority of MR results from a greater ability to detect abnormal tissue constituents within cranial nerves, often before there has been significant alteration of nerve morphology, and from improved anatomic depiction of lesions [12–14]. MR also provides a greater potential for increasing the conspicuity of small cranial nerve neoplasms through the use of MR contrast agents (e.g., gadopentetate dimeglumine). For these reasons, MR has become the diagnostic examination of choice at our institution for the evaluation of patients with suspected cranial nerve abnormalities.

The cisternal segment of the normal trochlear nerve is usually seen best with thin-section (3–4 mm), high-spatial-resolution (18–20-cm field of view, 256 × 256 matrix), coronal T1-weighted scans (Fig. 4). This portion of the trochlear nerve can often be traced from its emergence posterior and slightly caudad to the inferior colliculus of the midbrain to the point where it enters the cavernous sinus between the oculomotor and trigeminal nerves. The trochlear nerve is typically found just inferior and medial to the free edge of the tentorium and slightly superior to the position of the preganglionic segment of the trigeminal nerve. Occasionally, the cisternal segment can also be seen on axial images. That segment of the trochlear nerve in the lateral wall of the cavernous sinus can occasionally be identified on coronal T1-weighted images just caudad to the position of the oculomotor nerve and superior to the ophthalmic division of the trigeminal nerve [9, 10]. The orbital and superior orbital fissure segments of the trochlear nerve are not usually visible.

Review of the literature would suggest that primary neoplasms of the trochlear nerve are uncommon. To our knowledge only one case of a primary trochlear nerve neoplasm has been reported since the development of MR imaging [1]. Overall, in the medical literature, only nine cases have been reported [1–7]. Our experience, however, indicates that these lesions may be more common than previously believed. During the last 6 years, when MR was used as the primary

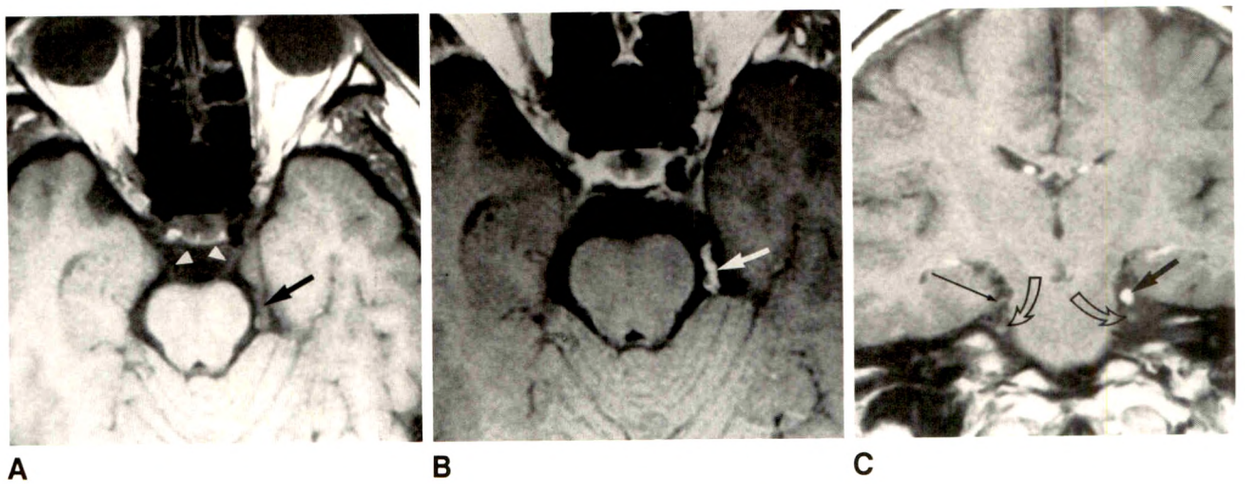


Fig. 4.—Case 6: 48-year-old man with trochlear nerve mass that has remained stable in size for 3 years, indicating that it most likely represents a benign primary neoplasm, the vast majority of which are schwannomas.

***A–C*, Unenhanced axial (*A*) and contrast-enhanced axial (*B*) and coronal (*C*) T1-weighted (600/20) MR scans. A small elongated mass (*straight arrows*) is intrinsic to cisternal segment of left trochlear nerve. The lesion is well-defined, symmetrically expands the trochlear nerve, and shows intense homogeneous enhancement. The normal contralateral trochlear nerve (*long thin arrow* in *C*), oculomotor nerve (*arrowheads* in *A*), and trigeminal nerve (*curved arrows* in *C*) are visualized.**

diagnostic study for evaluation of cranial nerve palsies at our institution, we have identified seven primary trochlear nerve neoplasms. This compares with only one lesion detected at our institution during the previous decade, when CT was used to evaluate this group of patients. We believe that the increase in the number of these lesions in the last 6 years is not merely a chance phenomenon, since four of five lesions were not initially visualized with high-quality CT scans. We believe, rather, that it is a function of the superior ability of MR to detect these typically small neoplasms.

The two main types of benign nerve sheath tumors (schwannomas and neurofibromas) are both thought to be of Schwann cell origin [15]. A comprehensive discussion of the pathologic differences between these two lesions is beyond the scope of this article, although they can easily be distinguished on morphologic and histologic grounds [15]. The schwannoma is the most common type of benign cranial nerve neoplasm [15]. It occurs in two patterns: isolated lesions and multiple schwannomas, as seen in the syndrome of neurofibromatosis [15]. Solitary schwannomas show a strong tendency to involve sensory nerves, and occur predominantly in middle-aged to elderly women [1–7, 15]. Solitary schwannomas most commonly involve the eighth cranial nerve, while other sensory cranial nerves such as the fifth, ninth, and 10th are less commonly involved [15]. Pure motor nerves, such as the trochlear nerve, are thought to be infrequently involved by solitary schwannomas [1–7, 15]. Orbital schwannomas are encountered occasionally, presumably arising from peripheral branches of the nerves to the extraocular muscles [16, 17].

The neurofibroma is the other commonly encountered nerve sheath neoplasm. This lesion usually involves peripheral and spinal nerves. Solitary cranial nerve neurofibromas are thought to rarely (if ever) occur [15]. In fact, some authors assert that there are probably no true examples of isolated cranial nerve neurofibromas in the absence of neurofibromatosis [15]. The vast majority of solitary cranial nerve neurofibromas that have previously been reported in the absence of neurofibromatosis are probably truly schwannomas [15].

Multiple benign nerve sheath tumors are a well-recognized feature of both NF-1 (peripheral neurofibromatosis, or von Recklinghausen disease) and NF-2 (central neurofibromatosis) [15, 18, 19]. With NF-1, involvement of cranial nerves is much less common than involvement of spinal and peripheral nerves; however, multiple benign neoplasms (usually schwannomas) of the cranial nerves are extremely common with NF-2 [15, 19]. These schwannomas may involve any of the cranial nerves, although, quite similar to the situation with solitary schwannomas, sensory nerves are most characteristically affected [15]. Bilateral acoustic nerve schwannomas alone, in fact, are sufficient evidence of NF-2 [15, 18]. Schwannomas of other sensory cranial nerves, such as the fifth, ninth, and 10th, occur less frequently, while pure motor nerves, such as the trochlear, are rarely involved in NF-2 [15].

It is generally believed that cranial nerve schwannomas are most likely to arise at the point where the axonal covering switches from glial elements to Schwann cells [15]. The trochlear nerve junction is usually not more than 0.6 mm away from its emergence from the midbrain [4, 15]. Five of the seven cases in our series arose from this expected location (Figs. 1 and 3). In some cases, however, schwannomas may arise at a distance of several centimeters from the brainstem, anywhere along the course of the nerve (Fig. 4) [1–7, 15]. Imaging of a patient with a trochlear nerve palsy, therefore, must always include the brainstem, ambient cistern, cavernous sinus, and orbit.

Other benign and malignant nerve sheath tumors must also be included in the differential diagnosis of trochlear nerve masses. Benign neoplasms—such as granular cell myoblastomas, neurothekeomas, localized hypertrophic neurofibrosis

(perineurinoma), neurotrophic melanomas, hamartomas, cavernous hemangiomas, and paraganglioma—may potentially affect cranial nerves, although these lesions are exceedingly rare and more commonly affect peripheral nerves [15]. Although the overwhelming majority of cranial nerve sheath tumors are benign, malignant lesions can occur [15]. De novo malignant cranial nerve schwannomas, however, are extremely rare. Benign schwannomas also have a very low propensity to undergo malignant degeneration. When this does occur, it is almost always in patients who have neurofibromatosis [15]. Malignant neurofibromas are more common, but they rarely (if ever) occur outside the setting of neurofibromatosis [15]. A number of patients (2–29%) with neurofibromatosis do eventually develop malignant nerve sheath lesions, but these usually affect peripheral and spinal nerves instead of cranial nerves [15]. Nevertheless, in patients with neurofibromatosis and documented cranial nerve sheath masses, it is important to be aware of the potential for malignant degeneration [15].

A histologic diagnosis was available in only one of our patients (case 3: schwannoma with mixed glial elements); however, the trochlear nerve abnormalities seen in the other cases almost certainly represent benign nerve sheath neoplasms (most likely schwannomas), since these patients have the clinical stigmata of NF-2. The precise pathogenesis is not available for three other lesions in this series although the clinical and radiologic observations strongly suggest that isolated schwannomas are the most likely diagnoses. Other potential causes for intrinsic trochlear nerve abnormalities, however, must also be considered in the differential diagnosis. A wide variety of nonneoplastic processes may produce intrinsic lesions of the cranial nerves for the extraocular muscles [11, 15, 17, 20–22]. The most common entities to be considered in the differential diagnosis include demyelinating diseases, granulomatous meningitis (tuberculous, fungal, sarcoid), carcinomatous meningitis, multifocal viral polyneuritis (e.g., Ramsay-Hunt syndrome) [22], recurrent benign multiple cranial neuropathies [20, 21], and Tolosa-Hunt syndrome [20, 21].

In our cases, demyelinating disease was excluded with reasonable confidence on the basis of clinical data and lack of other lesions on the MR scans. Similarly, granulomatous and neoplastic diseases were excluded on the basis of history and physical examination, clinical evaluation, CSF studies, laboratory analyses, and imaging studies. Postviral polyneuritis was considered unlikely in view of the patients' histories, prolonged symptoms, stable lesion size over time, and the MR scan appearance. Trochlear nerve involvement with the Ramsay-Hunt syndrome is quite uncommon, although cranial nerves other than the seventh and eighth (that is, cranial nerves V, VI, IX, and X) may be involved [22]. Tolosa-Hunt syndrome is a nonspecific inflammatory process of the cavernous sinus that typically affects multiple cranial nerves and presents with a steroid-responsive painful ophthalmoplegia [11, 20, 21]. It was thought to be an unlikely cause of the trochlear nerve lesions in our patients in view of one or more of the following: sparing of other intracavernous cranial nerves, location of the lesions in the cisternal segment of the nerve, lack of painful ophthalmoplegia, and long history of symptoms. Recurrent benign multiple cranial neuropathies is a poorly characterized syndrome that may affect all three ocular motor nerves [11]. Some have postulated that this represents a nonspecific arteritis involving the blood supply to the cavernous portions of the third, fourth, and sixth cranial nerves [11]. This seems to be an unlikely explanation for the isolated lesions of the cisternal segments of the trochlear nerves seen in our patients.

The seven trochlear nerve neoplasms reported here reveal several similar features. Three of six patients had neurofibromatosis and all four lesions in these patients arose near the inferior colliculus and proximal cisternal segments of the trochlear nerves. All primary trochlear nerve neoplasms in this series that were seen on precontrast MR scans revealed signal intensities that were quite similar to normal brain tissue. The precontrast appearance was identical to the more common acoustic schwannomas [12–14]. All seven fourth nerve neoplasms in this report showed intense homogeneous enhancement (Figs. 1, 3, 4), also quite similar to that seen with acoustic schwannomas.

Since primary trochlear nerve neoplasms are benign lesions and surgery is not usually advantageous unless the lesions are large, it is important to make a precise imaging diagnosis [1, 4]. Surgical removal will almost always be associated with persistence or worsening of the trochlear nerve palsy [1, 4]. Surgery, therefore, is usually to be discouraged unless other cranial nerves are in jeopardy, the lesion produces significant mass effect (hydrocephalus, brainstem compression), or there is a suspicion of underlying malignancy. Because of continuous relentless enlargement and a slight possibility of malignant degeneration, however, we believe that it is important to periodically monitor these lesions with follow-up MR scans. This is especially true in patients with the clinical stigmata of NF-1 or NF-2.

On the basis of our experience, we believe the following clinical and MR features are necessary to confidently diagnose a benign primary trochlear nerve neoplasm:

1. Location. The lesion must be intrinsic to the trochlear nerve at some point along its course. This is usually at the point where the trochlear nerve emerges from the brainstem or in the proximal cisternal segment of the fourth nerve.
2. Epicenter. The lesion epicenter must be completely within the trochlear nerve.
3. Margination. These benign lesions must be clearly demarcated from all adjacent structures. Poorly demarcated lesions that extend into adjacent structures raise the possibility of malignant schwannoma, neurofibrosarcoma, or extrinsic malignancies invading the trochlear nerve.
4. Noncontrast MR characteristics. The MR signal intensity of benign trochlear nerve sheath tumors is identical or quite similar to that of normal brain parenchyma.
5. MR contrast enhancement. The lesions typically show intense homogeneous enhancement, identical to that seen with the more common acoustic schwannomas.
6. Multiple cranial nerve lesions or the clinical stigmata of NF-1 or NF-2.
7. Lengthy history of trochlear nerve palsy. The trochlear nerve palsy is usually slowly progressive over a number

of years, since schwannomas and neurofibromas are benign, slow-growing lesions.

8. Stable lesion size over several years.

REFERENCES

1. Tokuriki Y, Yamashita J, Kikuchi H, Asato R, Handa H. Trochlear nerve neurinoma: case report. *Neurol Med Chir* (Tokyo) **1988**;29:70–73
2. King JS. Trochlear nerve sheath tumor: case report. *J Neurosurg* **1976**; 44:245–247
3. Boggan JE, Rosenblum ML, Wilson CB. Neurilemmona of the fourth cranial nerve: case report. *J Neurosurg* **1979**;50:519–521
4. Ho KL. Schwannoma of the trochlear nerve: case report. *J Neurosurg* **1981**;55:132–135
5. Leunda G, Vaquero J, Cebezudo J, Garcia-Uria J, Bravo G. Schwannoma of the oculomotor nerves: report of four cases. *J Neurosurg* **1982**;57: 563–565
6. Yamamoto M, Jimbo M, Takara E, et al. Trochlear neurinoma: case report. *No Shinkei Geka* **1985**;12:493–497
7. Garen PD, Harper CG, Teo C, Johnston IH. Cystic schwannoma of the trochlear nerve mimicking a brain-stem tumor: case report. *J Neurosurg* **1987**;67:928–930
8. Romanes GJ. The central nervous system. In: Romanes GJ, ed. *Cunningham's textbook of anatomy*, 11th ed. London: Oxford University Press, **1972**:581–705
9. Daniels DL, Peck P, Mark L, Pojunas K, Williams AL, Haughton VM. Magnetic resonance imaging of the cavernous sinus. *AJNR* **1985**;6: 187–192
10. Daniels DL, Pech P, Pojunas KW, et al. Trigeminal nerve: anatomic correlation with MR imaging. *Radiology* **1986**;159:577–583
11. Gittinger JW Jr. Nonmyasthenic ophthalmoplegia. In: Lessell S, van Dalen JTW, eds. *Current neuro-ophthalmology*, vol. 2. Chicago: Year Book Medical, **1990**:199–210
12. Daniels DL, Schenck JF, Foster T, et al. Surface-coil magnetic resonance imaging of the internal auditory canal. *AJNR* **1985**;6:487–490
13. Kingsley DPE, Brooks GB, Leung AWL, Johnson MA. Acoustic neuromas: evaluation by magnetic resonance imaging. *AJNR* **1985**;6:1–5
14. New PFJ, Bachow TB, Wismer GL, Rosen BR, Brady TJ. MR imaging of the acoustic nerves and small acoustic neuromas at 0.6 T: prospective study. *AJNR* **1985**;6:165–170
15. Russell DS, Rubinstein LJ. *Pathology of tumours of the nervous system*, 5th ed. Baltimore: Williams & Wilkins, **1989**:533–589
16. Mafee MF, Putterman A, Valvassori GE, Campos M, Capek V. Orbital space-occupying lesions: role of computed tomography and magnetic resonance imaging. An analysis of 145 cases. *Radiol Clin North Am* **1987**;25:529–559
17. Rootman J, Goldberg C, Robertson W. Primary orbital schwannomas. *Br J Ophthalmol* **1982**;66:194–204
18. National Institute of Health Consensus Development Conference. Neurofibromatosis: conference statement. *Arch Neurol* **1988**;45:575–578
19. Aoki S, Barkovich AJ, Nishimura K, et al. Neurofibromatosis types 1 and 2: cranial MR findings. *Radiology* **1989**;172:527–534
20. Kwan ESK, Wolpert SM, Hedges TR III, Laucella M. Tolosa-Hunt syndrome revisited: not necessarily a diagnosis of exclusion. *AJNR* **1987**;8:1067–1072
21. Miller MT, Mafee MF. Computed tomography scanning in the evaluation of ocular motility disorders. *Radiol Clin North Am* **1987**;25:733–752
22. Golden Li, Deeb ZE, deFries H. Atypical findings in cephalic herpes zoster polyneuritis: case reports and radiographic findings. *Laryngoscope* **1990**;5:494–497

Book Review

Gamuts and Pearls in MRI. By Stephen J. Pomeranz. Richmond, VA: William Byrd Press, 273 pp., 1990. $79

Gamuts and Pearls in MRI is a good quick reference source for the practicing radiologist. The author set out to write "a shelf reference that could quickly address issues of MR contraindications, basic protocol, disease appearances, and vignettes of clinical and radiographic information with regard to disease processes that would be easy to locate," and he has succeeded in that goal. It is the kind of book that should be kept in the office as a fast and easy-to-use tool.

The book is based on the author's experience with more than 50,000 cases. About 80% of the material is specific to MR; the other 20% is useful in both MR and other imaging techniques. The gamuts and pearls are intertwined within the book, so do not expect them to be separated into individual chapters. Even so, the material is still straightforward and easy to locate.

The book has seven sections, all divided into category headings. Categories A through E cover the brain (including eight subcategories); ear, nose, and throat, the spine; the temporomandibular joint, and the orbit; the musculoskeletal system; and the knee. Category F is called "Abdomen and Body," but I think this is a misnomer. A better heading would be "Abdomen and Pelvis." The mislabeling becomes even more problematic with the subsection headings. One subsection is titled "Liver, Kidney, Adrenal Glands," but to accurately connote all subcategories of the abdomen, the author would have to include listings for the pancreas, spleen, and gastrointestinal system, which he has not done. Category G is on images and predicaments, with subsections on contraindications, contrast, artifacts, and parameters. I think that "Pearls and Rules of Thumb for MR Scanning" (G-27) has a mistake. Number 2 under this gamut should be reversed to read correctly, "For T1, two or four averages and for T2, one or two averages."

Although the book is well organized and is set up so that it can be used quickly and easily, I think it would be more helpful if page numbers were included at the bottom of each page. As the book stands now, once you find what you were looking for in the table of contents, you still have to flip through pages just to get to the right area of the book, let alone the exact category or subsection. Without page numbers, you never really know exactly where you are in the book; with them, you could look something up in the table of contents and find it much more quickly.

All in all, Pomeranz has written an excellent book. Practicing radiologists will find it helpful and relevant in their everyday working life. I highly recommend it to anyone interested in MR.

Richard E. Rosenthal
Cooper Hospital/University Medical Center
Camden NJ 08103

Analysis of Economics and Use of MR Imaging Units in the United States in 1990

Ronald G. Evens[1]
Ronald G. Evens, Jr.[2]

Personnel from the 72 facilities with the most experience in MR imaging were surveyed, and 45 questionnaires were returned with data to study the economics and use of MR imaging facilities. The data from 1990 were compared with results of studies done in 1985 and 1987. The facilities studied were highly selected, and the data and conclusions are unlikely to be representative of all MR facilities currently operational in the United States. The "typical" MR unit operated about 66 hr per week and imaged 68 patients. Most procedures were examinations of the head and spine (73%), with examinations of bone and joint increasing in frequency (17%). Scheduling delays for both inpatients and outpatients have decreased since 1987, indicating that clinical demand is being met by MR facilities. The global (technical plus professional) charge for an examination was approximately $950, and the charge for IV contrast material was an additional $200. IV contrast material was used in approximately 40% of head and 20% of spine studies. The typical MR unit in 1990 was used to examine more than 3000 patients per year at a charge of approximately $750 each for the technical component. Technical billings for each unit were approximately $2.3 million, and net revenues were almost $1.9 million. We estimate the annual operating cost of an MR unit in 1990 was $1.3 million, so the typical MR unit had an annual net profit of approximately $500,000. This is a considerable improvement from the economic position in 1985, when each MR unit was losing approximately $400,000 annually.

We conclude that experienced MR imaging facilities are now profitable owing to increased efficiency and continually rising charges. We suggest the economic historical pattern demonstrated by MR imaging (large losses initially followed by profitability within several years owing to increased efficiency and higher charges) is a typical pattern for many new technologies with the current medical payment system in the United States.

AJR 157:603–607, September 1991

MR imaging reached a technologic level sufficient for clinical imaging in early 1982. It is now widely available in the United States, and clinically accepted as an important diagnostic procedure. Recent studies show a continuing rapid increase in the number of units available throughout the world, with continued growth in the United States [1–5]. MR units have significant economic impact because each unit has a capital cost of approximately $2.5 million, requires annual operating costs of more than $1 million, and generates billings to patients and their insurers of hundreds of thousands of dollars each year.

As data related to the financial operation of MR imaging equipment are important to radiologists, health-care administrators, planners, politicians, and the public, we performed a survey on three separate occasions of the 72 MR facilities that were operational in the United States in 1984. The three surveys occurred in 1985 [6], 1987 [7], and 1990. The results of the 1990 survey are reported in this article.

Materials and Methods

Only 72 MR imaging installations were operational in the United States before October 1984. The physicians or administrators responsible for these facilities were identified by

Received February 25, 1991; accepted after revision April 15, 1991.

[1] Mallinckrodt Institute of Radiology, Washington University, 510 S. Kingshighway Blvd., St. Louis, MO 63110. Address reprint requests to R. G. Evens.

[2] Iowa Methodist Medical Center, Des Moines, IA 50309.

0361–803X/91/1573–0603
© American Roentgen Ray Society

contacting all equipment manufacturers in 1984. All 72 installations were sent a two-page questionnaire in May 1990, asking for economic and use data for April or May 1990.

After two separate mailings to MR imaging installations, we received 45 responses by August 1990. Two previously active installations responded that they were no longer providing clinical care; accordingly, we obtained data from 45 (64%) of the 70 or fewer active installations (some of the nonresponding facilities could have been nonoperative also). The high percentage of questionnaires returned indicates the interest in this information that physicians and administrators responsible for MR imaging have. The survey questionnaire dealt with detailed questions on the location of the equipment, its use, assigned personnel, and selected economic data. Data from each respondent were entered into a personal computer system for subsequent tabulations and comparisons.

Of the 45 responding MR imaging installations, 30 (67%) were located in hospitals and 15 (33%) in outpatient locations (four owned by radiologists and 11 by nonradiologists). The 45 installations were operating 93 imaging units, which were purchased an average of 3.7 years earlier. The manufacturers of the units were General Electric (30), Siemens (20), Diasonics (16), Technicare (10), and others (17). Radiologists were responsible for all professional interpretations. The average operating Tesla value was 0.97, with 53 units operating at 1.0 T or greater, 13 units at 0.5 T, 17 units at 0.35 T, and 10 units at 0.3 T or less. The mean number of hospital beds was 758.

Results

Data on equipment use are shown in Table 1. The mean schedule delay was 0.9 days for inpatients and 6.9 days for outpatients. Hospital installations had an average of 2.2 operating units per installation and outpatient facilities had an average of 1.8. Twenty-seven of 45 respondents were also responsible for CT imaging; 50% of installations with CT capability reported a decrease in neurologic CT procedures during the last year, whereas only 4% reported a decrease for body CT. The respondents were not asked to quantify any increase or decrease with CT.

The mix of MR imaging procedures by anatomic area is shown in Table 2. All installations reported the use of IV contrast material for select studies, and the use of IV contrast material by anatomic region is shown in Table 2 also. IV contrast material was injected by physicians in 43% of installations, technologists in 40%, and nurses in 17%.

Revenue data on charges for head, spine, bone and joint, and other body procedures are shown in Table 3. Each installation reported its charges as a technical component, professional component, and global charge (the total charge as billed to outpatients). The global charge does not necessarily equal the sum of the means of the technical and professional components, because some installations did not separate charges into technical and professional components,

TABLE 1: Use of MR Imaging Equipment: 1990 Findings

Variable	Mean	SD	Range
Scheduled days/week	5.6	0.78	2–7
Scheduled hours/week	66.0	19.40	10–116
Patients scheduled/day	11.6	3.14	7–20
Patients examined/day	12.1	3.73	7–25
Patients examined and charged/day	11.2	3.51	7–23

TABLE 2: Anatomic Regions Examined by MR Imaging: 1990 Findings

Study/Region	% of All Studies		
	Mean	SD	Range
All studies			
Head	40	15.4	14–80
Spine	33	12.6	10–65
Bone and joint	17	8.3	4–40
Body (other)	10	6.7	0–35
Enhanced studies			
Head	43	25.5	5–95
Spine	21	19.0	0–80
Bone and joint	4	6.7	0–30
Body (other)	6	11.8	0–65

and some installations have a global charge that is different from the sum of their technical and professional components. Table 3 also reports the charge for contrast injection. The revenue reduction factor due to partial payments and bad debts (gross to net revenue) was 21%.

The mean numbers of personnel assigned to an individual MR imaging unit were 1.2 full-time-equivalent (FTE) radiologists, 2.9 FTE technologists, and 1.9 FTE other personnel.

Discussion

We have performed a survey of the economics and use of the first MR imaging systems installed in the United States (those installed between 1982 and October 1984) on three occasions: the first quarter of 1985, the second quarter of 1987, and the second quarter of 1990. Our data do not represent a sample of all current users, but rather the most experienced. Although limited in this respect, the data permit us to evaluate a variety of changes over time in the economics and use of MR imaging units from a large and experienced population of radiologists (Table 4).

The MR facilities studied represent a highly selected group of the first and perhaps the strongest institutions to enter the field of MR imaging. They do not represent all current MR users. For example, these facilities average more than two MR units per facility, whereas it is highly likely that most facilities in 1990 had only one MR unit.

Utilization

MR units studied in this survey were being used 5.6 days per week and 66 hr per week. An average of 12 patients per day, or 68 patients per week, were examined. Assuming 50 working weeks per year, with an allowance for approximately 10 holidays, the mean number of patients examined was 3400 per MR unit. Note that only 3140 patients were billed annually (11.2 patients per day × 5.6 days per week × 50 weeks per year), indicating that some research or other nonbilled activity was taking place. This compares with approximately 1200 patients per unit in 1985 and 2000 in 1987. This dramatic increase from 1987 (55% or approximately an 18% annual increase) is less than the rate of growth between 1985 to 1987, when the increase was approximately 75% annually.

TABLE 3: Charges for MR Imaging Procedures: 1990 Findings

Type of Study/ Type of Charge	Charge ($)		
	Mean	SD	Range
Head			
Technical	750	110.4	560–1054
Professional	212	53.7	140–358
Global	945	116.5	711–1308
Spine			
Technical	766	115.1	490–1054
Professional	215	66.8	120–387
Global	955	142.8	550–1266
Bone and joint			
Technical	742	99.2	560–881
Professional	210	54.4	132–358
Global	932	60.5	540–1200
Body (other)			
Technical	765	105.2	575–1054
Professional	218	60.5	140–358
Global	959	126.9	733–1308
Contrast enhanced			
Technical	203	101.5	25–420
Professional	37	50.2	0–175
Global	210	122.2	35–510

Note.—The "global" charge is the terminology used by many third-party payers for total charge in outpatient procedures. It does not necessarily equal the sum of the technical and professional charges.

TABLE 4: Comparison of MR Imaging Data from 1985, 1987, and 1990

Variable	Mean Value		
	1985	1987	1990
No. of respondents	47	52	45
No. of imaging units	47	74	93
Operation days/week	5.2	5.4	5.6
Scheduled hours/week	55	68	66
Procedures/week	35	58	68
Schedule delay (days)			
Inpatient	1.0	1.6	0.9
Outpatient	5.3	11.4	6.9
Procedure mix (%)			
Head	66	49	40
Spine	11	33	33
Bone and joint	4	6	17
Body (other)	19	12	10
Global charge ($)			
Head	652	713	945
Spine	NA	735	955
Bone and joint	NA	NA	932
Body (other)	702	753	959
Revenue reduction (%)	40	15	21

Note.—The "global" charge is the terminology used by many third-party payers for total charge in outpatient procedures. NA = not available.

The fact that more patients are being examined per unit time now indicates the machines are being used more efficiently. In 1985, installations typically performed 0.6 procedures per hour; this increased to 0.8 procedures per hour in 1987 and slightly more than one procedure per hour in 1990. This decrease in the length of scheduling delay in 1990, compared with prior years, indicates that demand for MR studies is being met better than before (Table 4). The scheduling delay increased between 1985 to 1987, but now has fallen.

In the past, MR imaging has been primarily a neuroradiologic imaging technology, and this trend continues. In 1990, more than 70% of all procedures were related to the head or spine, but this was a proportional decrease from previous years (Table 4). Note the dramatic increase in studies of joints to the extent that 17% of all examinations related to orthopedic problems. While studies of other body regions have decreased as a percentage of studies, the overall number of these studies per MR unit has increased; however, the relative use of MR in the head, spine, and musculoskeletal systems is rising.

The use of IV contrast material for MR imaging is a recent development. No contrast agents were approved for clinical use at the time of the previous studies. In the present study, installations reported that contrast material is commonly used in head and spine studies (Table 2). Whether or not contrast material was used varied among facilities. In some installations, contrast material was never used for spine studies and only rarely used (5%) in head studies. However, in other installations, contrast material was used in as many as 80% of spine and 95% of head studies. This wide range may be associated with the high cost of these contrast materials (current charges are more than $200 per injection) or may be related to differences in patient mix at various institutions. More likely, the difference is related to differing criteria and guidelines for the use of contrast materials. This is the case in other medical procedures (e.g., cardiac catheterization, coronary bypass surgery, stomach and colon endoscopy) with wide variations in the use of contrast media [8, 9]. These data suggest that careful analysis of efficacy of the use of MR contrast media will be important in the future.

Charges and Revenues

The mean technical charge varied slightly by type of study between $742 and $766 (Table 3), with the lower charges related to bone and joint examinations and the higher charges to spine examinations. Professional charges had a similar pattern and varied in a narrow range between $210 and $218. Global charges (i.e., those regularly charged to nonhospital patients) were slightly lower than the total of the technical and professional charges and varied between $932 and $959 (Table 3). All charges have increased since 1987. With the global charge used as an example, head studies have increased from $713 to $945 (Table 4). This 32% increase in a 3-year period is an annual increase of approximately 10% and more than the 5% annual increases that occurred between 1985 and 1987.

The typical charge for an MR examination can be calculated by taking the charge per type of study and weighting each charge by the proportion of that study in the total mix of patient examinations (Table 2). A typical charge for an MR examination in 1990 was a technical charge of $754, a professional charge of $214, and a global charge of $947. A separate charge of $200 or more was made when contrast material was used so that the typical charge for an MR examination is now more than $1000.

Costs

Data from the present survey and experience from the Mallinckrodt Institute [10] allow us to estimate the annual technical cost of operating an MR imaging unit in 1990 (Table 5). Fixed costs, costs that remain constant and are unrelated to the number of procedures performed per day, totaled $731,366 per unit. They include $400,000 for equipment depreciation (mean cost of equipment assumed to be $2 million, depreciated over 5 years by a straight-line method), $29,166 for building depreciation (mean cost of space development is $525,000—3000 square feet of space [6] times a current construction cost of $175 per square foot, depreciated over 18 years by a straight-line method), and $183,000 required for equipment maintenance and cryogens. The nonphysician personnel were assigned current annual salary levels being paid at the Mallinckrodt Institute of Radiology, St. Louis, MO, which totaled $119,200.

Variable costs (costs that change with the number of patient procedures, such as film and supplies) totaled $125,840, assuming an annual volume of 3146 procedures at $40 per procedure. Indirect costs were $228,603, which were estimated by assuming indirect or overhead costs were 50% of fixed and variable costs, excluding depreciation. We used this method previously for estimating the indirect costs of radiologic procedures [6, 7]. Indirect costs comprise many necessary expenses, including fringe benefits, insurance, space maintenance, administrative services, billing, and collection costs. A specific indirect cost rate should be calculated for each MR installation, and we suggested it will approximate 50% of fixed and variable costs [6].

The final cost to consider was the cost of capital. About two thirds of MR installations used capital funds (with an associated cost of the foregone opportunity for other uses of the capital), and about one third of the installations used borrowed funds or leasing (with an associated interest charge). The total capital required for equipment and space was about $2,525,000. We used a factor of 10% annual cost of capital, approximately in the middle of a range between current interest on treasury bills and interest charges for borrowed funds, to estimate a value of $252,500 for the annual capital costs for an MR installation.

The total estimated technical operating costs was $1,338,309 for a typical MR installation.

TABLE 5: Estimate of Annual Technical Costs of MR Imaging for 1990

Type of Cost	Cost ($)
Fixed	
Equipment depreciation	400,000
Building depreciation	29,166
Personnel	119,200
Equipment maintenance	150,000
Cryogens	33,000
Subtotal	731,366
Variable	125,840
Indirect	228,603
Capital	252,500
Total	1,338,309

TABLE 6: Financial Performance of a Typical MR Unit in 1985, 1987, and 1990

Variable	Mean Value		
	1985	1987	1990
No. of respondents	47	52	45
No. of patients billed/year	1260	2024	3140
Typical technical charge ($)	500	589	754
Gross billings[a,b]	630	1193	2372
Net revenues[a,b]	378	1014	1873
Estimated costs[a,b]	820	968	1338
Net profit (loss)[a]	(440)	46	535

[a] In thousands of dollars.
[b] Excluding cost or charge for contrast material.

Economics

Table 6 presents information about the technical operation of a typical MR unit in 1990 compared with 1985 and 1987. Gross billings per unit in 1990 were more than $2.3 million, nearly double the billings in 1987. This is due to a large increase in the number of billed patient examinations per year (a 55% increase in 3 years) and a large increase in the typical technical charge from $589 to $754 (a 28% increase over 3 years). Net revenue per unit (including the reported 21% partial pay/bad debt factor) is now more than $1.8 million annually, a sizeable increase from the previous revenue of approximately $1 million in 1987.

Our current estimate of costs for each unit also has risen to $1,338,309. However, the financial position of each MR unit has improved considerably since 1987, and we estimate that each MR unit in 1990 had an approximate profit of $500,000.

In a 5-year period, MR units have gone from a $400,000 loss (70% of gross billings), to an essentially break-even position in 1987 (a $46,000 gain with gross billings of nearly $1.2 million), to the current favorable position of more than $500,000 profit (a favorable 22% of gross billings). The financial improvement is primarily related to the large increase in the number of examinations performed per unit. However, the increase in technical charges of approximately 9% per year (associated with a reported smaller increase in revenue deductions, from 15% to 21% from 1987 to 1990) is a key factor in the improved net revenues. Although estimated costs have increased 30% in 3 years, this is a lower rate than the increase in revenues. The improved financial position of MR facilities also could be related to the fact that at least some unprofitable facilities were not operational in 1990.

We predict that the favorable economic position of MR units will decline during the next few years because of the reduced demand for MR imaging studies (note the reduced patient scheduling delays in Table 4), the increased number of MR units throughout the United States, the considerable pressure by third-party payers to reduce costs [5, 11–13], and the continued rise in revenue deductions. For example, the 21% revenue reduction rate reported by the respondents in this study is considerably lower than the 31% revenue reductions currently experienced at the Mallinckrodt Institute of Radiology, and the 1990 Medicare reimbursement for the

technical component of an MR head procedure in the St. Louis region was $443, as compared with the technical charge of $750 reported in this study.

Essentially all of our discussion of the economics of MR imaging has centered on technical revenues and costs of MR studies. Data from this survey do not allow an estimate of professional costs, as we did not obtain information regarding radiologists' salaries and other costs of practice. This survey showed that there were 1.2 FTE radiologists per MR unit, and professional billings averaged about $214 per procedure. At 1990 patient volumes, the annual professional gross billings were $673,244 with a net collection of $531,862. Professional charges have risen since 1987 (from $170 per procedure), but not as rapidly as technical charges. Professional charges have increased 26% in the 3-year period, or approximately 8% annually.

Comparison by Location

We compared several economic and use factors according to the location of the MR unit (Table 7). Two thirds of the respondents in our survey were responsible for MR units located in a hospital. Compared with MR units located in outpatient facilities, hospital units examined slightly fewer patients per day, had a longer scheduling delay for outpatients, and had a decidedly different procedure mix. Hospital units were used to examine 50% more head, 30% fewer spine, and 30% fewer bone and joint cases than were outpatient units. The larger percentage of spine and bone and joint examinations in outpatient MR facilities may relate to nonradiologist physician ownership in these facilities, because 11 of the 15 were owned by nonradiologists. The charge for MR examinations performed on hospital units were more than charges in outpatient facilities for all studies. The typical and weighted global charge for hospital units was $967, while the same charge for outpatient facilities was $918.

The comparison of MR imaging use by location has changed since 1987. In 1987, outpatient installations performed a higher percentage of neuroradiologic procedures and had higher charges than hospital locations. In 1990, hospitals were performing a higher percentage of neuroradiologic procedures and had higher charges.

TABLE 7: Comparison of MR Facilities Located in Hospital and Outpatient Settings: 1990 Findings

Variable	Mean Value	
	Hospital	Outpatient
No. of respondents	30	15
MR units/installation	2.2	1.7
No. of patients examined/day	12.1	13.8
Schedule delay for outpatients (days)	8.7	3.7
Procedure mix (%)		
Head	45	30
Spine	29	41
Bone/joint	15	22
Body	11	7
Global charge ($)		
Head	969	903
Spine	973	924
Bone/joint	938	922
Body	981	921
"Typical"	967	918
Revenue deductions (%)	21	21

Conclusions

The 72 oldest MR imaging installations have undergone considerable change in use and economics since 1987, continuing a dynamic pattern since 1985. There have been marked changes in the number of patients examined, mix of patients, revenues, and expenses. Although demand for MR continues, there are suggestions (decreased scheduled hours per week and shorter scheduling delay) that demand is being met by available MR services. The increased volume of examinations and an increase in charges have resulted in an increase in collected technical revenues that is greater than the rise in estimated expenses. The mean, bottom-line, technical financial position of MR imaging units has markedly improved from a considerable loss in 1985 to a nearly break-even position in 1987 to a current, highly favorable economic result. We suggest this economic history for MR is a common pattern for new high-cost technologies in the United States: Initial financial losses progress to a break-even status, with profitability developing in 5–10 years owing to increasing patient demand, operating efficiency, and procedure charges and decreased revenue deductions. However, the recently introduced "bundled" reimbursement systems (diagnosis-related groups) and negotiated payment and discount systems with managed-care third-party providers will dramatically diminish the profitability of MR.

REFERENCES

1. Hillman AL, Schwartz JR. The diffusion of MRI: patterns of siting and ownership in an era of changing incentives. *AJR* **1986**;146:963–969
2. Steinberg EP. The status of MRI in 1986: rates of adoption in the United States and worldwide. *AJR* **1986**;147:453–455
3. Evens RG. The diffusion of MRI in the United States: what is fact and what is speculation. *AJR* **1986**;147:856–857
4. Margulis AR, Crooks LE. Present and future status of MR imaging. *AJR* **1988**;150:487–492
5. Steinberg EP, Anderson GF, Steinwachs DM. Changes in CT utilization between 1982 and 1984: implications for Medicare payment for MR imaging under the prospective payment system. *Radiology* **1987**;165:279–281
6. Evens RG, Jost RG, Evens RG Jr. Economic and utilization analysis of magnetic resonance imaging units in the United States in 1985. *AJR* **1985**;145:393–398
7. Evens RG, Evens RG Jr. Economic and utilization analysis of MR imaging units in the United States in 1987. *Radiology* **1988**;166:27–30
8. Brook RH. Practice guidelines in practicing medicine. Are they compatible? *JAMA* **1989**;262:3027–3030
9. Chassin MR, Brook RH, Park RE, et al. Variations in the use of medical and surgical services by the Medicare population. *N Engl J Med* **1986**;314:285–290
10. Evens RG. Economic costs of nuclear magnetic resonance imaging. *J Comput Assist Tomogr* **1984**;8:200–203
11. Aaron H, Schwartz WB. Rationing health care. The choice before us. *Science* **1990**;247:418–422
12. Muller AG Jr. Shock-wave lithotripsy: assessing a slam-bang technology. *N Engl J Med* **1986**;314:845–847
13. Ginzberg E. High tech medicine and rising health care costs. *JAMA* **1990**;263:1820–1822

Book Review

A Short Textbook of Clinical Imaging. Edited by David Sutton and Jeremy W. R. Young. New York: Springer-Verlag, 856 pp., 1990. $98

This one-volume general textbook is designed as an introduction to clinical imaging for first-year house officers in radiology, and it succeeds admirably. The book is organized by organ system rather than by technology, so it may be more suitable for residents in academic departments that use a similarly organized didactic and clinical approach. For the most part, the illustrations are of high quality, as we have come to expect from Springer-Verlag. In some areas, however, findings are poorly seen because of the high contrast, such as the bladder filling defect in Figure 36.1. Also, the lunate triquetral fusion in Figure 14.2 is mislabeled as a scapholunate fusion. Some of the chest radiographs are quite small, making the identification of subtle pneumothorax, for example, difficult.

Even in such a one-volume introduction, the contributions of several authors are necessary because of the complexity of the discipline, and this book shows both the advantages and disadvantages of such an approach. Experts have discussed their various subspecialties, ensuring accurate reviews of important material; but where the subspecialties overlap, there is perhaps unavoidable confusion. For example, the genitourinary section has an excellent, succinct discussion of reactions to contrast material, but for a related discussion of low-osmolality contrast material, the reader must turn to the chapter on angiography.

Although this book has several contributors, it also has some standardization. Each chapter is an effective mix of text, tables, and illustrations. The text is uniformly readable so that it is possible to peruse a chapter without becoming confused by the format. The tables and lists are useful, but they are not obtrusive, and they do not detract from the editors' intent that this be a true textbook rather than a gamuts approach to differential diagnosis.

Particularly useful are the reviews of mammography and obstetrical sonography. They are models of comprehensive yet terse discussions of their areas. In the musculoskeletal section, the discussion would be more contemporary if it had more emphasis on MR imaging of the knee, particularly normal anatomy and diagnosis of meniscal lesions. Such current topics as imaging of patients who have AIDS also are discussed in the relevant organ system chapters.

This volume not only provides an introduction to diagnostic imaging for junior house officers, as is its intent, but also is sophisticated enough to be a final general review before oral board examinations. It is not to be compared with such multivolume texts as *Radiology*, edited by Taveras and Ferrucci, but rather with such standards as Paul and Juhl's *Essentials of Radiologic Imaging. A Short Textbook of Clinical Imaging* is good enough to invite such comparison, yet different enough in format and approach so that a choice must be made not on the basis of the content, but on personal judgment as to which style is more suitable to the person who will read the text. I think that Sutton and Young have created a new benchmark, and I shall recommend it to all our incoming residents.

Ethan M. Braunstein
Indiana University Hospital
Indianapolis, IN 46223

The Volume and Cost of Radiologic Services in the United States in 1990

Jonathan H. Sunshine[1]
Michael R. Mabry
Swati Bansal

Knowing the total number of radiologic services provided in the United States and their cost is important. This information can, for example, indicate the opportunities available to a radiology practice considering opening a new office or show whether high-technology radiology is, as is widely assumed, an important factor in United States health costs. However, neither the total number of procedures nor their cost is known. We developed two largely independent estimates of each total (one based principally on surveys of radiologists, the other on Medicare data) to cross-validate the estimates and provide an indication of their uncertainty. We estimate that 260–330 million radiologic procedures were performed in the United States in 1990 (including both diagnostic and therapeutic procedures and radiologic procedures performed by nonradiologists) and that payments for these services totaled $19 to $22 billion (including payments for technical components in the hospital setting). This total was approximately 3.5% of national spending on personal health care; high-technology radiology totaled less than half of this amount. The procedures numbered 1.0–1.3 per capita annually, an increase of some 10–40% since 1980. Of the spending total, $10 to $12 billion was paid to physician practices, with a substantial portion of this amount going ultimately to practice expenses, particularly in the office setting.

Our results suggest that spending on high-technology radiology is too small to be a major explanation for the current level of health costs in the United States.

***AJR* 157:609–613, September 1991**

How many radiologic procedures are performed in the United States each year, and how much do they cost? That question is asked by radiologists and by those who deal with business and organizational issues in radiology, such as business managers, manufacturers, and administrators of health maintenance organizations (HMOs). The answers, converted from a national total to per capita figures, can, for example, help tell a radiology practice the opportunities available in opening an office in a new location, indicate what is a suitable capitation rate to charge an HMO, or show what areas are underserved. Unfortunately, however, no useful answers are available. A review of the published literature for the past 5 years identified no estimates of total spending for radiologic services, and the most recent counts of these services [1, 2] refer to the situation as of a decade ago and are somewhat incomplete. The absence of answers is all the more surprising because the growth of high-technology radiology is often cited as classic evidence that technology is a major factor in the rapid growth of health care costs in the United States. Despite this assertion, no one knows the cost of radiology as a whole, to say nothing of the cost of high-technology radiology.

This article provides estimates of the total number of radiologic procedures performed in the United States in 1990 and the cost of these procedures. The estimates cover all radiologic services, including radiation oncology and nuclear medicine, and include radiologic services provided by nonradiologists.

Received February 14, 1991; accepted after revision April 8, 1991.

[1] All authors: Research Department, American College of Radiology, 1891 Preston White Dr., Reston, VA 22091. Address reprint requests to J. H. Sunshine.

0361–803X/91/1573–0609
© American Roentgen Ray Society

Method and Derivation of Estimates

Two largely independent estimates were developed for each of the two totals (number of services and cost) in order to provide cross-validation of the estimates and an indication of the likely magnitude of their uncertainty. This section details the methods of estimating, the major assumptions used in the estimates, and the justification of these assumptions. By making assumptions explicit, we permit readers to test alternatives, if they wish.

One estimate for each total is based on information reported by radiologists themselves, largely through surveys. The other estimate is based on information collected by Medicare, which is the largest payer for radiologic services in the United States. This estimate relies principally on administrative records.

An important assumption used in the Medicare-based estimates is that Medicare pays for one third of radiologic services in the United States. There are two reasons to think this is an accurate assumption. First, previously published data [3] show that this is Medicare's average "market share" for physician specialties (such as radiology), for which Medicare plays a significant role, and radiology is a typical specialty for which Medicare plays a significant role. There is nothing atypical in the patient population of radiology that would make Medicare's role particularly large (as for geriatrics) or particularly small (as for obstetrics and gynecology). Second, and more specifically, the source cited [3], which used careful estimating methods and counted Medicare's deductible, coinsurance, etc., as part of the Medicare market share, has a figure of 28% as Medicare's market share for all specialties compared with 33% for specialties in which Medicare plays a significant role. A recent survey in *Medical Economics* [4], which probably is less accurate (if only because of a low response rate) and probably excludes deductibles, coinsurance, etc., from Medicare's reported market share (specifics are not given, but that would be the natural way to respond to the survey questions), reports a Medicare market share of 24% for all physicians and 29% for radiologists. Both sources show a consistent difference between the all-physician average and the estimate for radiology. Our calculations are based on treating deductibles, etc., as part of Medicare's share, and so one third is the appropriate figure to use.

An important assumption used in both estimates of costs is that in the hospital setting, the total of payments for professional services plus technical services equals 2.5 times the payments for professional services alone. The factor of 2.5 was derived from a detailed comparison of Medicare's professional component payments and its global payments for physicians' radiologic services, with the comparison made separately by CPT-4 (Physician's Current Procedural Terminology) code, carrier locality, and specialty, with each of these separate ratios appropriately weighted.

Details of the four estimates follow.

Radiologist-Based Estimate of the Number of Radiologic Procedures

The 1989 Group Practice Survey of the American College of Radiology found radiologists in diagnostic radiology groups performed an average of 11,800 diagnostic procedures per full-time equivalent (FTE) radiologist. Little change was found from the 1986 Group Practice Survey, so we used 11,800 as the figure for 1990. Unpublished tabulations from the American Medical Association's (AMA's) Physician Masterfile, which lists all United States physicians by self-designated specialty and major professional activity, show that in 1990, there were approximately 21,800 FTE diagnostic radiologists in the United States. (This figure includes nuclear medicine specialists but excludes administrators and researchers as not being in patient care. It counts residents as 0.35 FTE each, following the Graduate Medical Education National Advisory Committee (GMENAC), and counts clinical fellows as 0.65 FTEs.) Multiplying the 21,800 FTE diagnostic radiologists by 11,800 procedures each gives an estimate of 257 million diagnostic procedures performed by radiologists in 1990.

The 1988 Part B Medicare Annual Data (BMAD) Procedure File shows radiation oncology procedures performed by radiologists were 10.3% as numerous as diagnostic procedures performed by radiologists. Medicare serves the elderly, and cancer is a disease of the elderly. Thus, 5% added on for radiation oncology (rather than 10%) is probably more suitable for the overall population. (Even if there were no radiation oncology services for persons under 65, adding on 10% for the elderly works out to adding on approximately 3% for the whole United States population.) Adding 5% to 257 million diagnostic procedures gives an estimate of 270 million radiologic procedures (both diagnostic and therapeutic) performed by radiologists in 1990.

The 1988 BMAD Procedure File shows nonradiologists performed 22.9% as many radiologic procedures as radiologists did. This percentage would not differ for the nonelderly population, so we added 22.9% to 270 million. This gives the estimate of 332 million radiologic procedures performed in the United States in 1990.

Medicare-Based Estimate of the Number of Radiologic Procedures

The 1988 BMAD Procedure File shows a total of 71.6 million radiologic procedures performed on Medicare patients in 1988. The Office of the Actuary, Medicare, reports approximately 91% of Medicare physician claims for a year are processed within 3 months after the end of the year. BMAD includes only those claims for a calendar year that have been processed by March 31 of the following year. Thus, 71.6 million was multiplied by 100/91 to obtain a full Medicare total. We then multiplied by 3 to obtain a total for the whole population, because Medicare accounts for about one third of all radiology. The resulting estimate is 236 million radiologic procedures in 1988. Increasing this by 5% annually, which is the approximate annual growth rate of radiologic procedures, yields an estimate of 260 million radiologic procedures in 1990.

Radiologist-Based Estimate of the Total Cost of Radiologic Services

The AMA's Socioeconomic Survey [5, 6] shows $183,000 was the average after-expense income of a posttraining patient-care radiologist in 1987–1988. The same AMA sources

show average expenses of a radiology practice were $146,000 per "self-employed" radiologist in these years. Given the AMA survey's definition of self-employed (full or part owner of the respondent's main practice), 54% of radiologists said on the survey that they were self-employed. An average of $146,000 in expenses per self-employed radiologist works out to 54% as much, or $79,000, as an average for all radiologists. Adding the expense and income figures shows the AMA data indicate receipts of a radiology practice averaged $262,000 per radiologist in 1987–1988.

To update from this 1987–1988 average to 1990, we increased the practice receipts at 10% annually for 2.5 years because the AMA Socioeconomic Survey shows a 10% annual increase in average total receipts per physician in physician practices (including practice expenses) from 1985 to 1988 for all specialties. (The figure for all physicians was used because there are too few radiologists in the AMA sample to permit an accurate estimate of year-to-year increases for radiologists alone.) The estimate for 1990 was thus $332,000 in practice receipts (including expenses) per radiologist.

Unpublished data from the AMA's Physician Masterfile show 24,300 FTE radiologists in the United States in 1990, including radiation oncologists and nuclear medicine specialists. (The count excludes researchers and administrators as not being in patient care, counts residents as 0.35 FTE each, following GMENAC, and counts clinical fellows as 0.65 FTE each.) Multiplying 24,300 radiologists by $332,000 in practice receipts (including expenses) per radiologist yields $8.07 billion as the estimated total practice receipts of all radiology practices in 1990.

The next step in the estimation process requires breaking down the total of practice receipts by site of service. The 1988 BMAD Procedure File shows the distribution of Medicare-allowed charges of radiology practices was 35.8% in the hospital inpatient setting, 30.1% in the hospital outpatient setting, and 34.0% in the office or other setting. This distribution implies the $8.07 billion in receipts to radiology practices in 1990 consisted of $2.89 billion, $2.43 billion, and $2.74 billion, respectively, from the hospital inpatient, hospital outpatient, and office (and other) settings. (We assume the percent breakdown by setting was the same for all receipts as it was for receipts from Medicare. Again, there is nothing about the difference in population or insurance between Medicare and others to suggest important differences.)

To estimate receipts to physician practices for all radiologic services, including services rendered by nonradiologists, we used 1988 BMAD statistics. BMAD shows that for Medicare, allowed charges for radiologic services of *radiology* practices were 91.8%, 95.0%, and 58.1% of total allowed charges for radiologic services of *all* physician practices (all specialties) in the hospital inpatient, hospital outpatient, and office (and other) settings, respectively. Dividing estimated radiology practice receipts in each site by these percentages gives an estimated total of practice receipts for radiologic services of all physicians of $3.15 billion, $2.56 billion, and $4.72 billion, respectively, in the inpatient, outpatient, and office settings. In total, these amounts add up to approximately $10.4 billion, which is an estimate of total practice receipts (including expenses) of all physician practices from radiologic services.

However, in the hospital setting (both inpatient and outpatient), the costs of radiology also include the hospital's "facility fee" or technical component charge. As noted, we used the assumption that total payments for radiologic services in hospital settings are 2.5 times the professional component (physician's) payment. Making this adjustment to the estimates of payments to physicians found in the preceding paragraph gives estimated total payments for radiologic services of $7.88 billion, $6.40 billion, and $4.72 billion in inpatient, outpatient, and office settings, respectively.

The estimated total cost of radiologic services in 1990 is the sum of these three components, or approximately $19.0 billion.

Medicare-Based Estimate of the Total Cost of Radiologic Services

The 1988 BMAD Procedure File shows total Medicare-allowed amounts payable to physician practices (all specialties) for radiologic services (including radiation oncology and nuclear medicine) were $3.19 billion [7, p. 416]. This amount, of course, includes expenses of the practices. Because BMAD is only about 91% complete, this figure must be multiplied by 100/91 to obtain the full-year figure for 1988. To update to 1990, the 1988 full-year estimate is increased at 10% annually. The result is $4.24 billion.

We added 3% for balance billing (that is, charges above the Medicare "allowed amount"). This assumes that 15% of radiologic claims were balance-billed and that the balance bill was approximately 20% of the allowed amount. (For medicine as a whole, approximately 20% of Medicare claims were balance-billed; radiology is below average [7, pp. 339, 402]. Twenty percent was the ceiling on radiology balance bills in 1990.)

We estimated an average collection rate on Medicare claims of 94%, based on a reported 70% collection rate for Medicare's 20% coinsurance [3]. These adjustments for balance billing and collection rates led to the estimate that total 1990 receipts of physician practices (all specialties) from Medicare-covered radiologic services were $4.1 billion.

This figure was multiplied by 3, since Medicare covers approximately one third of the services of United States physicians, to obtain $12.3 billion as the estimated total 1990 receipts of all physician practices (all specialties) from all radiologic services. This, of course, includes practice expenses as well as physicians' income.

Subsequent steps in the estimating process again require separating figures for different practice sites. The 1988 BMAD Procedure File shows 30.2%, 24.6%, and 45.2% of Medicare-allowed charges for radiologic services rendered by all specialties in, respectively, the hospital inpatient, hospital outpatient, and office (and other) service sites. Multiplying these percentages by $12.3 billion yields estimated receipts of physicians' practices of $3.71 billion, $3.03 billion, and $5.56 billion, respectively, in the three sites. Again, total payments for radiologic services in hospital sites are estimated to be 2.5 times the payments to physicians. Thus, estimated total

payments for radiologic services in 1990 were $9.28 billion, $7.58 billion, and $5.56 billion, respectively, in the inpatient, outpatient, and office (and other) settings.

Again, the estimated total cost of radiologic services in 1990 is the sum of these three components, approximately $22.4 billion.

Discussion

In summary, we estimate that 260–330 million radiologic procedures were performed in the United States in 1990 at a cost of $19 to $22 billion. Radiation oncology and nuclear medicine, as well as diagnostic radiology, are included in these totals, as are all radiologic services provided by nonradiologists. "Cost" refers to the amount patients and third-party payers actually pay for radiologic procedures, not the costs radiologists and hospitals incur in delivering these services or the amount radiologists and hospitals bill. In all settings, costs include both professional component costs (payments mostly for physicians' work) and technical component costs (payments to cover the cost of technologists, equipment, etc.; depending on the setting, these payments may be made to physician practices or to a hospital).

Of total payments, about $10 to $12 billion, or approximately 55%, was paid to physician practices, while the rest went to institutions for technical services. Payments to physician practices are more than the 40% of the total that a familiar Medicare rule of thumb might suggest, principally because payments to practices include the full global payment in noninstitutional settings. Because of practice costs, the net incomes to physicians from radiologic services are substantially less than the total paid to physician practices for these services.

We used two largely independent estimating methods, and thus have two estimates of the number of procedures and of total costs. For both the number of procedures and total costs, the two estimates agree within approximately 25% or less. This reasonable agreement of two independent estimates is strong evidence of the soundness of the estimates. Moreover, there is no apparent bias to either estimating method. For the number of procedures, the estimate based principally on surveys of radiologists is higher than the estimate based principally on Medicare administrative records, while the reverse is true for costs. Again, this is a reassuring finding. A previous study has found that data from surveys generally differ significantly from administrative record data on the same phenomena [8]. In light of this point, the difference between the two estimates for each total is neither surprising nor large.

The difference between the two estimates may be considered a rough measure of the range of uncertainty in our knowledge. However, it is possible that the true figures lie outside the stated range, that is, the low estimate may be too high or the high estimate too low.

Unfortunately, both estimates of costs depend on the assumption that, in the hospital setting, total payments (professional plus technical) are 2.5 times the professional component payments. This common dependence on a major assumption based on a single data source (Medicare) may exaggerate the similarity of the two estimates. Moreover, the statistic that total payments are 2.5 times professional component payments, although the result of a detailed data analysis, is based on payments to physicians. It would have been preferable to know payments actually made to hospitals (not hospitals' billed charges, which hospitals infrequently are actually paid) for technical component services. Such data are not available. Radiologists report that hospital charges are higher than this statistic implies. However, this is an impressionistic observation, and probably is based on billed charges, whereas actual payments to hospitals are substantially less than billed charges. If, in the hospital setting, total payments are actually 3 times professional component payments (not 2.5 times as high), then total spending for radiologic services would be approximately $3 billion more than the stated estimates. If total payments in the hospital setting were actually 3.5 times the professional component payments, then total spending would be approximately $6–7 billion more than the stated estimates.

Sources in the radiologic film industry estimate that approximately 1137 million square feet of film was used in 1990, and they use a rough rule of thumb of 3.3 square feet of film consumed per procedure (Walden AF, personal communication). These figures lead to an estimate of 350 million diagnostic radiologic procedures in 1990. Because this estimate is based on a rather rough estimate of the square footage of film consumed per procedure, we believe our estimates are more accurate. The higher estimate derived from the square footage of film may only indicate that, in actuality, square footage consumed per procedure is higher than 3.3 or that a significant amount of film is wasted. In any case, there are no gross disagreements among the estimates.

Our estimates for the total number of procedures translate into an average of 1.0–1.3 radiologic procedures per capita for the United States population each year. The cost estimates average out to $75–90 per capita in annual spending on radiologic services.

A comparison with previous reports indicates that the number of procedures per capita increased by between 10% and 40% during the 1980s and that the total number of procedures increased by 20–60%. This comparison is made as follows: The two most recent published estimates of the total number of radiologic procedures in the United States are for 1980 [1, 2], and both are based on surveys, principally surveys of hospitals. These two estimates agree within 10% once coverage differences are taken into account, possibly reflecting their similar basis. The authors of the more comprehensive of the two studies judge that it covers approximately 90% of diagnostic imaging procedures, and report a total of 181 million procedures. To make this estimate comparable with those reported in this study requires multiplying by 10/9 to add in the omitted 10% of diagnostic procedures and then adding 5% to include radiation oncology. These adjustments lead to an estimate of approximately 210 million radiologic procedures, or 0.9 procedures per capita, in 1980.

For countries other than the United States, we found no estimates of the total volume or cost of radiologic procedures in the published literature. However, we were provided with extensive unpublished data on Manitoba (MacEwan DW, personal communication). These data show 1.0 radiologic procedures per capita and costs of approximately $60 (in United States dollars) per capita. These findings are consistent with reports that the per capita cost of the Canadian health care system is less than that of the United States system, and that, for physicians' services, the difference lies principally in lower payment levels in Canada rather than in fewer services [9]. However, the differences between Manitoba and the United States average may reflect the relatively rural character of Manitoba.

The $19 to $22 billion estimated cost of radiologic services in 1990 was about 3.5% of total spending on personal health care in the United States in 1990. (Spending on personal health care totaled $531 billion in 1989, the latest year for which government estimates are available; this sum has been growing at approximately 10.5% annually [10, 11]. The category of personal health care refers to all health services and supplies received by individuals. It excludes research costs, public health measures, and insurance administration and profits.)

Spending on high-technology radiology is not enough to account for even a sizeable portion of the high health costs that trouble some observers of health care in the United States. Total spending on health in the United States now exceeds 11% of the gross national product (GNP) [11], while in other Western countries it is in the range of 7–9% of the GNP [12, p. 227]. Thus, persons seeking an explanation of high health costs in the United States are seeking an explanation of some 20–40% of total United States costs. BMAD data indicate that, in total, high-technology radiology—meaning CT, MR imaging, angiography, interventional radiology, and sonography—accounts for less than half of radiology costs. This technology thus accounts for approximately 1.5% of personal health care expenditures. This is not very significant if one is seeking an explanation for 20–40% of personal health care expenditures.

The $10 to $12 billion paid to physician practices in 1990 for radiologic services was 8–9% of the total revenue from practice activities received by all physician practices in the United States. (The government estimates show $117.6 billion received by all physician practices in 1989 and show this figure growing at approximately 12.5% annually [10, 11].)

ACKNOWLEDGMENTS

We thank Dana Friedman for typing the numerous drafts of the manuscript and Douglas MacEwan for data on Manitoba.

REFERENCES

1. Johnson JL, Abernathy DL. Diagnostic imaging procedure volume in the United States. *Radiology* **1983**;146:851–853
2. Bunge RE, Herman CL. *Radiation experience data (RED): documentation and results of the 1980 survey of U.S. hospitals.* Rockville, MD: Center for Devices and Radiological Health, Food and Drug Administration, U.S. Department of Health and Human Services (DHHS publ. No. FDA 86-8253), **1985**:1–54
3. Sunshine JH, Swartzman J. *Medicare's share in U.S. physicians' revenues.* Washington, DC: Physician Payment Review Commission (PPRC background paper No. 89-4), **1989**:1–5
4. Paxton HT, ed. How much cheer do third parties bring you? *Med Economics* **1987**;64(26):108–119
5. Gonzalez ML, ed. *Physician marketplace statistics 1989.* Chicago, IL: American Medical Association, **1989**:51–65
6. Gonzalez ML, ed. *Physician marketplace statistics 1990.* Chicago, IL: American Medical Association, **1990**:61–83
7. Committee on Ways and Means, U.S. House of Representatives. *Medicare reimbursement to physicians. Overview of entitlement programs.* Washington, DC: U.S. Government Printing Office (Ways and Means Committee print 101-29), **1990**:379–428
8. Sunshine JH. How many Americans lack outside sources of payment for health care costs? *J Health Human Resources Admin* **1984**;6(3):341–360
9. Fuchs VR, Hahn JS. How does Canada do it? *N Engl J Med* **1990**;323(13):884–890
10. Office of National Cost Estimates, Health Care Financing Administration. National health expenditures, 1988. *Health Care Financing Rev* **1990**;11(4):1–41
11. U.S. Department of Health and Human Services. *Press release.* December 20, **1990**
12. National Center for Health Statistics. *Health United States, 1989.* Hyattsville, MD: Public Health Service (DHHS Publ. No. (PHS) 90-1232), **1990**

Editorial

Is Plagiarism Ever Insignificant?

Robert N. Berk[1]

In this issue of the Journal, we publish letters [1, 2] concerning the article, "Effective Audiovisual Presentation" by Stuart S. Sagel and Ruth G. Ramsey, which appeared in the January 1991 issue of the *AJR* [3]. In his letter, Dr. Sagel explains why several sentences and phrases in his article were identical or very similar to those published in a paper by Jerome J. Cunningham on the same subject, "One Dozen Ways to Upgrade Your Next Radiologic Presentation," which appeared in the October 1988 issue of *Clear Images* [4]. Because Dr. Sagel failed to cite Dr. Cunningham's article as the source of these duplicated sentences and phrases, the issue of plagiarism rises. This editorial examines the question of whether plagiarism is ever unimportant or excusable.

Webster defines the verb *plagiarize* as "to steal and pass off (the ideas or words of another) as one's own" [5]. In terms of the medical literature, plagiarism occurs when an author copies previously published ideas or words without citing their source, whether those ideas and words were originally expressed by others or by the same author (self-plagiarism).

In the strictest sense, the degree of guilt associated with plagiarism does not vary. Plagiarism is plagiarism, just as theft is theft. However, in a practical sense, the guilt can be mitigated by several factors. The degree of guilt varies in proportion to the significance of the stolen ideas. It is one thing to claim highly original ideas of earthshaking importance as one's own, and another, as in Sagel's case, to copy words simply to illustrate points that are common sense, common knowledge, and familiar to everyone.

The extent of the plagiarism also influences the degree of guilt. Wholesale pirating of an entire manuscript or of whole pages or paragraphs is more serious than the random duplication of a few isolated phrases or sentences.

Finally, plagiarism that is committed knowingly is a greater offense than when it is done unintentionally. As he points out in his letter, Sagel did not mean to deceive, but did so unwittingly because of slovenly scholarship. He failed to record sources of information in the notes on audiovisual presentations that he had gathered over the years, so that ultimately when he came to write about the subject, he could not identify the source or he thought of the material as his own.

Taking all this into consideration, it is clear that mitigating circumstances can make some cases of plagiarism less serious than others. I believe that all of these circumstances apply to this situation with Sagel. Even though some cases can be considered less serious than others, plagiarism is *never* insignificant or excusable. Plagiarism remains, under all circumstances, a serious violation of collegial trust, the fundamental principle on which the integrity of medical journalism depends. For whatever reason it occurs, it is deception and the theft of intellectual property. Whether petty or not, flagrant or not, intentional or not, it is a breech of professional ethics that must be exposed and unreservedly deplored.

REFERENCES

1. Cunningham JJ. Effective audiovisual presentation proper citation of sources (letter). *AJR* **1991**;157:643
2. Sagel SS. Reply. To: Cunningham JJ. Effective audiovisual presentation proper citation of sources (letter). *AJR* **1991**;157:643–644
3. Sagel SS, Ramsey RG. Effective audiovisual presentation. *AJR* **1991**;156:181–187
4. Cunningham JJ. One dozen ways to upgrade your next radiologic presentation. *Clear Images* October **1988**;2(4):20–24
5. *Webster's ninth new collegiate dictionary*. Springfield, MA: Merriam, **1985**

[1] Editor-in-Chief, *American Journal of Roentgenology*, 2223 Avenida de la Playa, Ste. 103, La Jolla, CA 92037-3218. Address reprint requests to R. N. Berk.

 © American Roentgen Ray Society

Meeting News

Society of Computed Body Tomography: 14th Annual Course, April 1991

Elizabeth Whalen[1]

The 14th annual course sponsored by the Society of Computed Body Tomography (SCBT) was held April 15–19, 1991, at the Grand Hyatt Washington, Washington, DC. Experts in cross-sectional imaging offered didactic lectures and informal workshops that provided a practical review and update of the major areas of body CT and MR imaging. The course provided in-depth information on anatomy, imaging techniques, interventional procedures, and correlative imaging. The needs of the practicing radiologist received much attention, and both the lectures and the 32 small-group workshops were clinically oriented. Also included in the meeting were three panel discussions on the topics of thoracic imaging, CT of the gastrointestinal tract, and imaging and interventional methods for pancreatic disease.

Participants were reminded of the upcoming first Summer Practicum sponsored by the SCBT, which will be held in August 1991 at the Keystone Resort in Colorado. The practicum will supply timely, useful information on CT of the body, including its diagnostic and interventional applications and relevant correlations with other imaging methods; MR applications will receive special attention.

AJR space limitations preclude coverage of all the learning opportunities provided by the April 1991 annual course (six days of scientific papers, lectures, workshops, and panel discussions). However, in the following pages, we will summarize the 17 prize-winning presentations of works-in-progress and representative lectures from two of the five review courses.

Prize-Winning Works-in-Progress Presentations

On the day before the courses started, in a members-only meeting moderated by SCBT President Michael Federle (University Hospital of Pittsburgh, PA), 29 papers were presented describing in-progress work in the areas of body CT and MR imaging. A committee of SCBT members selected the best papers for research grant awards. The awards were grouped into three categories: summa cum laude (awarded to three presentations), magna cum laude (four presentations), and cum laude (10 presentations).

Summa Cum Laude

Hounsfield Award.—This award was presented to The Johns Hopkins University, Baltimore, for work done by C. J. Herold, R. H. Brown, R. C. Wetzel, C. A. Hirshman, W. Mitzner, and E. Zerhouni. They are using high-resolution CT (HRCT) on animals to assess pulmonary vascular and airway reactivity to challenges in vivo. The researchers' goal is to increase knowledge of basic lung physiology, which has previously been limited by the inability to clearly show pulmonary parenchymal structures. The lungs challenged with hypoxia showed a decrease in parenchymal density; constriction of vessels in most animals, but unexplained vascular dilatation in other animals; and, surprisingly, airway dilatation. The lungs in the hypervolemic animals showed an increase in parenchymal density, vessel dilatation, and a decrease in area

[1] Contributing editor, *American Journal of Roentgenology*, Ste. 103, 2223 Avenida de la Playa, La Jolla, CA 92037.

Editor's note.—"Meeting News" articles report the highlights of important national radiology meetings. The intent is to provide Journal readers with succinct, substantive, and accurate reviews of topics of current interest, written in a readable fashion and published promptly after the meeting.

The articles will not undergo the peer review usually required of *AJR* publications, nor will they offer a critique of the information provided. The sole purpose of the series is to apprise *AJR* readers of topics of current concern in an interesting and timely fashion.

157:615–621, September 1991 0361–803X/91/1573–0615 © American Roentgen Ray Society

of the airway lumen. Histamine challenge resulted in a decrease in the luminal areas of all airways; however, airway constriction occurred with challenge by saline aerosol, possibly due to stimulation of irritant receptors by the aerosol carrier. These researchers concluded that HRCT can define anatomic correlates and simultaneously show pulmonary vascular and airway reactivity in vivo; as the only imaging method shown so far that may have this capability, this method may be valuable in both experimental and clinical studies.

Lauterbur Award.—This award was given to the Massachusetts General Hospital, Boston, for work being done by S. Saini, P. F. Hahn, P. Reimer, M. Cohen, and J. Wittenberg on ultrafast MR imaging of the liver. Some new developments have made such scanning more practical—ultrafast MR imaging is now feasible on conventional MR imagers. Furthermore, it provides multislice capabilities; improved resolution (standard resolution = 64 × 128, high resolution = 128 × 128, maximum resolution = 128 × 256); and wider pulse sequence options (e.g., spin-echo [SE], inversion recovery [IR], and gradient-echo [GE] sequences). The researchers studied four normal volunteers and 34 patients with various types of liver tumors; fat-suppressed, ultrafast images were obtained at 1.5 T, with a 10-mm slice thickness and a 5-mm gap. Studies were performed with four ultrafast pulse sequences (including two T2-weighted SE, one T1-weighted IR, and one proton density–weighted GE sequence). First, scout images were obtained (21 slices in 6 sec with a high-resolution SE technique in which TE was 26 msec). Second, seven contiguous slices were selected at the level that contained the area of interest. Third, 13 independent acquisitions were obtained. To provide a quantitative assessment of these images, Dr. Saini and his colleagues chose one representative lesion per patient; determined the signal intensity of the liver, spleen, lesion, and noise; and from these data, calculated the differences in contrast among the various imaging sequences. The liver signal-to-noise ratio, the tumor/liver contrast-to-noise ratio, and the spleen-to-liver ratio were highest on high-resolution T2-weighted SE images. The liver signal-to-noise ratio was highest on the ultrafast MR images obtained by a high-resolution SE sequence with a TE of 26 msec; the tumor/liver contrast-to-noise ratio was highest on the high-resolution SE images obtained with a TE of 100 msec. The authors concluded that ultrafast MR imaging of the liver can be performed with a single T2-weighted pulse sequence.

Winthrop Award.—Stanford University, Stanford, CA, received this award for work done by R. J. Herfkins, R. B. Jeffrey, Jr., E. Trefelner, N. J. Pelc, and D. Lucas. Dr. Trefelner presented results of the use of a new cine velocity-encoded pulse sequence to assess aortic dissection. This new pulse sequence results in the acquisition of two images. One is a magnitude image typical of GRASS (gradient-recalled acquisition in the steady state), and the second is a phase-contrast image that allows display of both magnitude and direction of flow within vessels. This can then be displayed in a cine loop, allowing real-time visualization of physiologic flow. An added advantage of this pulse sequence is the ability to calculate not only the flow velocities but the quantitative flow rates as well. In those cases in which a diagnosis of aortic dissection was uncertain on cardiac-gated T1-weighted images alone, the addition of this new cine pulse sequence significantly improved the diagnostic accuracy for aortic dissection. This readily allowed differentiation of true from false lumen and helped in avoiding pitfalls, such as ulcerated plaque, intraluminal thrombus, and intimal hematoma.

Magna Cum Laude

Mallinckrodt Award.—This prize was awarded to the University of Pittsburgh, Pittsburgh, PA, for work being done by T. P. Chambers, G. D. Dodd, W. J. Miller, and R. L. Baron. Dr. Chambers, who gave the presentation, noted that previous studies have shown that nonionic contrast materials produce better hepatic enhancement than do ionic contrast materials. He and his colleagues are in the process of conducting a large-scale prospective study to evaluate this conclusion. Parameters considered include volume, concentration, and administration rate of contrast agent used. Patients are scanned twice, first with one and then with the other contrast agent or different concentrations of the same agent. Preliminary data show that volume of contrast material is directly related to enhancement at all time intervals (i.e., 150 ml of material always produced better contrast enhancement than 100 ml did). The most interesting preliminary finding is that—in contradiction to other studies—ionic contrast material resulted in superior contrast enhancement up to 100 sec after administration (the maximum difference between types of contrast agents occurs 60 sec after administration, when ionic contrast enhancement is 25% higher than nonionic enhancement). The peak enhancement of the two types of contrast agents seems to be identical, but the time to peak enhancement appears to be shorter when an ionic agent is used. These researchers are in the process of continuing this study with more patients and will also compare lesion conspicuity with different contrast parameters (type of agent, volume, concentration).

Stanford University won the magna cum laude award for work being done by R. B. Jeffrey, Jr., N. J. Pelc, and E. Trefelner on optimizing MR angiography of the portal venous system. This paper presented a new technique in which the pulsatility artifacts that typically degrade phase-contrast images were eliminated. This was achieved by the researchers' trying an experimental method in which real-time knowledge of the cardiac cycle was used to select the order for encoding, much like the technique in which EXORCIST (a program for getting rid of ghosts) or ROPE (respiratory-ordered phase encoding) is used to order the phase data within K-space to minimize motion artifacts. A similar technique can be applied to the cardiac cycle so that phase-encoding data is arranged in K-space in such a manner that it will represent only one cardiac cycle, thus producing only one ghost. The use of a high-frequency sort, in combination with no phase wrap, effectively projected this ghost outside of the field of view. When these reviewers compared time-of-flight angiograms, phase-contrast angiograms, and phase-contrast angiograms obtained with this new technique for evaluating the portal venous system, they found improved vessel definition and

static tissue suppression as well as significantly decreased image degradation by artifacts. Because data were acquired in all three orthogonal planes, magnitude and direction maps for all three directions could be created, providing a definite advantage in evaluating patients with varices and shunts. Although the phase-contrast studies take slightly more time, they were thought to provide much more physiologic information than can be realized with current time-of-flight methods.

Manabu Minami from the University of Tokyo, Japan, presented an award-winning paper on dynamic CT of gastric tumors. The patients drank 400 ml of water, received no anticholinergic agents, and had dynamic scanning with contiguous 1-cm-thick slices after IV administration of Omnipaque 350. A multilayered pattern (two or three layers) was seen 1–3 min after contrast administration in the 15 patients with no gastric lesions. The inner layer was markedly enhanced, the intermediate layer had low density, and the outer layer had slightly higher density than did the intermediate layer. In 78 patients with gastric cancer (71 patients later had surgery, and 62 of those had total or partial gastrectomy), dynamic CT enabled detection of 81% of the lesions (detection of 53% of early gastric cancer and 92% of advanced disease). The dynamic CT findings in early gastric cancer included destruction of the multilayered pattern (in 100%) and a thickened gastric wall (in 60%); in advanced gastric cancer, 100% of the cases showed destruction of the multilayered pattern on CT, and 96% showed a thickened gastric wall. In addition, four cases of malignant lymphoma were distinguished from malignant gastric cancer by lymphoma's showing a lack of enhancement in the thickened gastric wall. These results indicate that dynamic CT can distinguish between a normal gastric wall, gastric cancer, and lymphoma.

Optimization of spiral scanning time was discussed by H. Rigauts for H. Rigauts, D. Ooms, G. Marchal, P. Suetens, A. L. Baert, and A. Oosterlinck of the International Research Unit for Radiological Imaging, Leuven, Belgium. Dr. Rigauts and his colleagues used a foam-rubber phantom to investigate the problem of distortion that occurs in spiral spanning, which combines data acquisition with continuous table incrementation. For this scanning technique, resolution depends on slice thickness, incrementation speed, and the method of interpolation. The results of their phantom experiment indicated that, in order to achieve the best resolution with the least distortion, the best parameters are a 5-mm beam width, a 10 mm/sec table incrementation speed, and data interpolation over 180° instead of 360°. Furthermore, image deconvolution can further improve image quality, resulting in spiral-scan image quality that is close to the quality of conventional scans. When asked about the additional time needed to deconvolute images, Dr. Rigauts replied that the normal image reconstruction time is 8 sec/image, but they "have the computer running all night to deconvolute the image."

Cum Laude

Ten presentations were awarded this prize. Each is described briefly below; they are grouped by subject matter.

Hepatic and pancreatic imaging.—B. A. Birnbaum, M. E. Noz, J. Chapnick, J. J. Sanger, A. Megibow, J. C. Weinreb, and E. L. Kramer, of the New York University Medical Center, are developing a method by which findings on single-photon emission CT (SPECT) can be correlated with CT and/or MR findings. The study group consisted of 20 patients with 35 hemangiomas. Lesion size ranged from 1 to 11 cm (mean, 3.5 cm); 11 patients had multiple lesions. First, these investigators reviewed individual slices and selected those that best showed the hemangiomas. Second, intrinsic anatomic landmarks were identified, and these landmarks were occasionally supplemented with landmarks correlating skin surface (CT/MR scans) and edge scatter (SPECT). Third, a warping algorithm was applied, and fourth, landmarks were checked for accuracy. Image registration, or fusion, among the various imaging methods was successful in all cases (50 structural-functional pairs), and region-of-interest analyses provided absolute confirmation of that success. The smallest lesion fused was 1 cm in diameter. The clinical application of such fusion will be the direct superimposition of critical anatomic-pathologic information on CT, MR, and SPECT images; specifically, this method allows detection of very small hemangiomas—particularly those near major intrahepatic vessels that previously have posed diagnostic problems.

An ongoing study correlating hepatic images with resected whole livers is being performed by G. D. Dodd, W. J. Miller, and R. L. Baron of the University of Pittsburgh, PA. Because 600 liver transplantations are performed in their institution each year, they are able to correlate different hepatic imaging techniques with specimens of liver representing many types of hepatic disease, including cirrhosis, fulminate failure, and primary and metastatic neoplasms. Their protocol includes tight control of imaging parameters, prospective reading of all studies, and reporting of all abnormalities on studies. For this presentation, Dr. Dodd reviewed the results from studies of 115 non-Asian patients with cirrhosis. Unenhanced and/or contrast-enhanced CT studies were performed in 102 cases; MR studies included 29 T1-weighted examinations, 28 T2-weighted examinations, and 21 studies in which gadopentetate dimeglumine was administered for contrast enhancement. For malignant lesions, CT accuracy per patient was as follows: unenhanced CT, 65% sensitivity and 69% specificity; enhanced CT, 68% sensitivity and 86% specificity. CT accuracy per lesion was as follows: unenhanced CT, 48% sensitivity and 64% specificity; enhanced CT, 51% sensitivity and 82% specificity. In a subset of high-risk patients, the MR accuracy for lesion detection per patient was as follows: T1-weighted, 79% sensitivity and 93% specificity; T2-weighted, 85% sensitivity and 80% specificity; and gadopentetate dimeglumine–enhanced, 50% sensitivity and 78% specificity. The CT accuracy in the same high-risk patients was 93% sensitivity and 67% specificity. The use of gadopentetate dimeglumine enhancement actually decreased MR tumor sensitivity and specificity. CT arterial portography was nondiagnostic because of poor hepatic enhancement in about 20% of the cases in which it was used. Initial results from this ongoing study indicate that, in patients with advanced cirrhosis, (1) unsuspected malignancy is more common than has been

reported previously, (2) lesions seen on enhanced CT are more likely to be malignant than benign, (3) the addition of MR imaging to the protocol does not increase detection of tumor per patient, (4) the specificity of MR imaging is higher than that of CT in tumor detection, (5) both CT and MR imaging failed to detect a large number (40%) of lesions, and (6) whole-liver pathologic correlation allows more accurate determination of sensitivity and specificity of imaging methods.

Patrick C. Freeny, of the Virginia Mason Clinic, Seattle, compared the results of uniphasic and biphasic bolus injection of 60% iodinated contrast material on CT scans of patients without evidence of liver disease. Patients were given either a uniphasic bolus of 150 ml at 2.5 ml/sec for 60 sec or a biphasic bolus at 2.5 ml/sec for 20 sec and 1 ml/sec for 100 sec. The attenuation of three locations on each scan of the hepatic parenchyma and the attenuation of the aorta and the portal vein were measured. The results were that the uniphasic bolus produced an earlier and higher peak of hepatic enhancement than the biphasic bolus did, and the uniphasic enhancement was sustained at a higher level during the entire scanning sequence than that produced by the biphasic bolus. Dr. Freeny pointed out that the study should be extended to include a comparison of ionic and nonionic agents in a larger number of patients.

D. Ney and E. K. Fishman of The Johns Hopkins University, Baltimore, are working on the creation of three-dimensional (3-D) images of hepatic vessels to aid surgical planning. Use of spiral CT and the volume-rendering technique enables radiologists to produce high-quality 3-D images of hepatic vasculature. 3-D CT images constructed from conventional CT scans have three important deficiencies: motion artifact, inhomogeneous distribution of contrast material, and low, out-of-phase resolution. Helical (spiral) CT, on the other hand, provides continuous scanning with simultaneous table movement, an entire study during one breath-hold (24 sec), and thin slices for good resolution in all directions. To obtain helical CT images, the researchers used the following parameters: 1 sec/revolution, 24-sec total scan time, 4-mm collimation, 4 mm/sec table speed, 170 mAs, 125 kVp, interpolated reconstruction every 2 min, peripheral contrast injection (120 ml of Omnipaque 300 injected at 3 ml/sec), and a 40-sec scan delay. The 3-D images were generated with manual segmentation (which took about 15 min) and volumetric rendering. The resulting 3-D images could be useful in planning and evaluating liver resection. These investigators are pursuing the optimization of acquisition parameters (e.g., contrast administration and longer scan times); automated (rather than manual) segmentation techniques; and an interactive display technique for use as a surgical planning tool.

The staging of chronic pancreatitis was the subject of work being done by P. C. Freeny, P. Malfertheiner, and M. Buchler at the Virginia Mason Clinic, Seattle. Using the 1983 Cambridge Classification, Dr. Freeny and his colleagues rated chronic pancreatitis in 100 patients as mild, moderate, or severe on the basis of CT or ERCP findings. They compared these ratings with the clinical evaluations of the disease (mild, moderate, or severe on the basis of pain, liver function abnormalities, and degree of exocrine and endocrine insufficiency) in the same patients. CT staging agreed with clinical staging in 46% of cases; in most of the disagreements, CT staged the disease higher (11 mild and 40 moderate cases were staged higher by CT, and three moderate cases were staged lower by CT). ERCP staging agreed with clinical staging in 45% of cases; in most of the disagreements, ERCP staged the disease higher (12 mild and 50 moderate cases were staged higher by ERCP, and one moderate and two severe cases were staged lower by ERCP). This study shows that CT and ERCP staging will disagree with clinical staging of chronic pancreatitis in 54–55% of cases and that high staging by CT or ERCP makes up 89–94% of the disagreement. Although 94–100% of the cases of clinically severe disease were correctly staged by ERCP and CT, only 29% of the mild-to-moderate imaging classifications were correct. Dr. Freeny suggested that radiologists need to reevaluate the individual morphologic criteria and to verify their correlations with severity of exocrine/endocrine dysfunction and pain. It may be that the morphologic criteria of chronic pancreatitis are poorly defined and that the morphologic changes being evaluated precede the clinical and functional changes (resulting in higher staging of disease by imaging methods).

Blood-flow measurement.—M. R. Bell, A. W. Stanson, P. F. Sheedy, and J. A. Rumberger (Mayo Clinic, Rochester, MN) are working on the feasibility of ultrafast CT for measuring absolute regional myocardial perfusion in humans (as it has in animals in previous studies). The ability to quantify myocardial perfusion in absolute terms and in a relatively noninvasive manner could have considerable usefulness in assessment and continued treatment of many cardiac patients. The advantages of using ultrafast CT for this purpose include high spatial and temporal resolution (2 mm and 50 msec, respectively). Ultrafast CT scans were obtained on healthy young male volunteers at rest and during a 4-min IV infusion of adenosine with a bolus injection of iopamidol; 20 sequential scans (8-mm-thick slices at four levels) were obtained. The results were analyzed by using operator-defined regions of interest and indicator-dilution curves; myocardial perfusion was calculated by using a flow algorithm developed in Dr. Bell's laboratory. Regional flow at rest appeared uniform across the myocardium and absolute flow increased significantly after adenosine administration; no significant differences in systemic hemodynamics were seen with adenosine infusion (except for small changes in heart rate). No adverse effects occurred as a result of the procedures. In the question-answer session that followed this talk, one of the participants mentioned that problems with beam hardening and scatter limit these results and may explain the slight underestimation of flow reserve obtained in the study.

Another cum laude presentation from the Mayo Clinic (Rochester, MN) was presented by Lilach O. Lerman for L. O. Lerman, M. R. Bell, V. Lahera, J. A. Rumberger, P. F. Sheedy, and J. C. Romero. She described a study of the measurement of renal blood flow with fast CT in a canine model; the ability to measure whole renal, cortical, and medullary blood flow in vivo by a relatively noninvasive method can be useful because alterations in renal blood flow (as well

as cortical and medullary blood flow) and intrarenal distribution of blood may occur in a variety of clinical situations. Fast CT scans were obtained after iohexol administration at baseline, during renal vasodilation, and after recovery of renal blood flow. These investigators found a very good correlation between fast CT and erythrocyte maturation factor (EMF) measurements of renal blood flow, although a consistent overestimation of blood flow by fast CT was observed, which may have been due to filtration of iohexol through the renal tubules. Moreover, cortical blood flow was distinguished from medullary blood flow, and fast CT was able to detect increases in both cortical and medullary blood flow. These results indicate that fast CT is a very promising, relatively noninvasive method for quantifying whole renal blood flow as well as cortical and medullary blood flow.

G. S. Gazelle and J. R. Haaga of Case Western University, Cleveland, OH, are working on a study of the effects of thrombocytopenia and platelet dysfunction in bleeding during aspiration biopsy of the kidney. Using an animal model, these researchers performed kidney biopsies and measured the bleeding by applying dry, preweighed sponges to the biopsy site and then reweighing the sponges after the bleeding had stopped. Before biopsy, the animals had been classified as (1) normal controls, (2) animals with induced thrombocytopenia, and (3) animals that had received IV Venopirin, an experimental water-soluble aspirin. A total of 185 biopsies done with 18- to 22-gauge needles in 12 animals showed that both Venopirin administration and thrombocytopenia resulted in increased bleeding from biopsy—both of these effects were greater with increasing needle size. The implications of these first results are that (1) thrombocytopenia and aspirin do increase the bleeding risk of biopsies, (2) physicians should consider withholding aspirin from the patient for a few days before a biopsy, and (3) platelet function may be more important than thrombin-mediated clot formation in regard to hemostasis with needle biopsy.

Contrast agents.—A pilot study to investigate two new lipophilic paramagnetic contrast agents for possible use in MR imaging was presented by Joseph K. T. Lee of the Mallinckrodt Institute, St. Louis, MO, for J. J. Brown, C. D. Weigers, M. J. Welch, and J. K. T. Lee. Biodistribution, relaxivity, and imaging studies were among the research factors considered. Agents with greater lipophilicity have better affinity to extrarenal organs (e.g., liver, heart), and research has shown that the lipophilicity of DTPA can be increased by substituting agents from phenolic groups for those from carboxylic groups. The two contrast agents studied were a macrocyclic nonadentate ligand (TTCT) and a linear octadentate ligand (HMPMDT). TTCT has high stability constants and nine places to bind gadolinium; it is nonionic and more stable and more lipophilic than DTPA is. HMPMDT has eight places to bind gadolinium and an overall charge of −1; it also is more stable and more lipophilic than is DTPA. Using rats as the experimental model, these researchers obtained relaxation measurements on the gadolinium complexes with these ligands, biodistribution measurements in the rats after administration of the complexes, and 1.0-T MR images before and sequentially up to 30 min after IV administration of the complexes. Gd-DTPA had the highest relaxivity, Gd-HMPMDT had a relaxivity similar to that of Gd-DTPA but lower, and the relaxivity of TTCT (a closed-ring structure) was much lower than those of the other two. One hour after injection, most of both gadolinium compounds had cleared from the body. On MR images, the percentage change in kidney signal intensity was lowest with Gd-TTCT; Gd-DTPA and Gd-HMPMDT showed similar changes in kidney signal intensity, but Gd-DTPA resulted in a slightly faster enhancement. In both liver and heart signal intensity, Gd-HMPMDT produced greater enhancement of longer duration than either of the other two complexes did. Preliminary conclusions from this study are that (1) these two new gadolinium complexes have good relaxivity in vivo and biodistributions that are very similar to that of Gd-DTPA and (2) significant liver, heart, and kidney enhancement is seen with the two new agents.

Computer-assisted training.—Elliot K. Fishman (The Johns Hopkins University, Baltimore) discussed a successful training program for radiologists that can be used by medical students, residents and fellows, and doctors pursuing continuing medical education. The program, called "CT: The Game," runs on a standard Macintosh II computer, and Dr. Fishman estimated that $5000 would buy all the material needed to run the program. Menu-driven, the program asks multiple-choice questions based on CT images reproduced on the screen; the correct answer receives praise, but the programmed response to an incorrect answer may be something like "Ha, ha, ha. . . You must have screwed up somewhere." If the user answers incorrectly, he or she can hit a *Review* button that will put text on the screen with the part that is relevant to the correct answer highlighted. Dr. Fishman and colleagues have now amassed a teaching tool that includes about 2000 CT images (about 72 megabytes); components include a teaching file (i.e., an image, the diagnosis, and facts that can be used to go through cases with students—the user can also turn off the text and use the file as a self-test) and "CT Pearls," which are data bits about relevant CT findings.

Review Course

Formal lectures were presented each morning of the 5 days of the SCBT Annual Course. Forty lectures were presented on the following topics: hepatic imaging, musculoskeletal imaging, thoracic imaging, gastrointestinal and pancreatic imaging, and genitourinary imaging. We are not able to cover all the lectures in the *AJR*, but describe four representative lectures from the first 2 days of the meeting.

Hepatic Imaging

Contrast techniques in hepatic CT.—Michael Bernardino (Emory University, Atlanta) discussed protocol options about

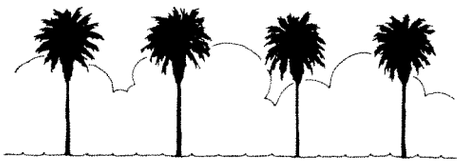
the use of contrast agents, including whether to obtain both pre- and postcontrast scans and whether to administer the contrast material by drip infusion, bolus, or a combination of drip infusion and bolus. This lecture covered dynamic sequential bolus CT, hepatic-specific agents, lipiodol CT, delayed iodine-enhanced CT, and the use of CT angiography (CTA) and CT arterial portography (CTAP). After stating that one can see more lesions and smaller lesions with the dynamic bolus technique, Dr. Bernardino pointed out the two main (potential) pitfalls of this technique: (1) maximum contrast enhancement may not equal maximum tumor detection and (2) the failure of dynamic bolus CT to detect hypervascular lesions (e.g., carcinoids, islet cell tumors, renal cell carcinomas). Liver-specific agents may be on the market within the next 4 years, and studies so far have shown that such agents increase the confidence of diagnosis and help detect most lesions missed by conventional imaging (<3 mm); however, characterizing these small lesions is still problematic (e.g., are they hemangiomas, cysts, or metastases?). Lipiodol CT scanning can be used in conjunction with chemotherapy: 2–5 ml of lipiodol are injected into the hepatic artery, and parenchymal distribution is greater near the tumor. In most cases, delayed iodine-enhanced CT scanning of the liver produces excellent results, with a total IV dose of 60 g of iodinated contrast material, a 4- to 6-hour delay, and subsequent scanning of 8- to 10-mm contiguous slices. When Dr. Bernardino and his colleagues used dynamic CT and delayed iodine-enhanced CT to study 50 patients with hepatic cancer, they found that 58% of the lesions were shown more clearly by delayed iodine-enhanced CT, 31% of the lesions showed no difference, and 11% were shown more clearly on dynamic CT. Finally, Dr. Bernardino discussed using the more aggressive methods, CTA and CTAP, to help define the extent of disease (e.g., liver metastases in colorectal cancer). On CTA, tumors have a dense periphery, but showing the anatomy of cirrhotic livers may be difficult. CTAP is technically easier to perform, but perfusion defects occur and may cause interpretation problems; 15–20% of lesions are not detected on CTAP images. This is still better than other techniques, which can miss up to 50% of hepatic masses. However, CTA and CTAP—the more invasive methods—are more likely to detect small (<1 cm) lesions. In summary, for focal lesion detection, the following CT scanning techniques are most helpful: dynamic incremental CT, delayed iodine-enhanced CT, and CTAP. MR imaging may also be a helpful adjunct to these CT imaging methods.

CT of the spleen.—Problems and appearances in CT scanning of the spleen were discussed by Emil J. Balthazar (Bellevue Hospital, New York). Two of the problems associated with the spleen are (1) the significant variation in size and shape of the normal spleen (e.g., weight of normal spleen ranges from 50 to 400 g, with an average weight of 150 g) and (2) accessory spleens, which are seen in 10–30% of cases in autopsy series, may be solitary or multiple, and enlarge after splenectomy. On CT, a benign splenic cyst is solitary and has a round, unilocular, sharply defined thin wall; 20% of such cysts are congenital (and epithelially lined), 80% are acquired (which have a fibrous capsule and result from previous trauma, liquefying hematoma, or cystic degeneration of infarcts). The possible causes of splenic infarcts include embolization (mostly from heart disease, some from IV drug abuse); arteritis; sickle cell anemia; and occlusion of the splenic artery. CT images of splenic infarcts show nonenhancing, peripheral, wedge-shaped lesions adjacent to the splenic capsule (also seen sometimes as an elongated subcapsular fluid collection that represents subcapsular hemorrhage). Splenic abscess is associated with septicemia (75%), IV drug abuse (10%), and trauma (15%); on CT, splenic abscesses appear as solitary or multiple low-attenuation spherical or ovoid lesions, and the presence of air-fluid or fluid-fluid levels is a very specific sign. Lymphoma is the most common solid tumor of the spleen; CT appearance includes homogeneous enlargement, miliary nodules, multiple masses, and a large solitary mass (large cell lymphoma). CT diagnosis of lymphoma is difficult because sometimes the only finding is splenomegaly. CT examinations can also help detect splenic lesions associated with AIDS: For example, CT findings can indicate Burkitt lymphoma (single or multiple large, lobulated, soft-tissue masses); moniliasis (innumerable, small, low-density lesions involving the entire spleen); tuberculosis (fewer low-density lesions of irregular contour); and *Pneumocystis carinii* (multiple, low-density lesions with upper abdominal lymph nodes that undergo calcification).

Musculoskeletal Imaging

MR imaging of the temporomandibular joint.—Clyde A. Helms (University of California, San Francisco) listed the four clinical indications for MR imaging of the temporomandibular joint (TMJ): pain, tenderness, clicking, and locking. He also noted that physicians sometimes request TMJ imaging for other reasons, such as confirmation of diagnosis for a third-party payer, equivocal clinical diagnoses (20–25% of cases), medicolegal issues, and preoperative planning. MR imaging of the TMJ can show disk position and condition, bony abnormalities, and postoperative changes. In MR imaging of the TMJ, the full open-mouth position should not be used because the disk reduction is determined easily clinically, the meniscal reduction is very temporal, and the position is extremely uncomfortable for the patient. MR parameters for TMJ imaging include the following: 15 slices, 3-mm slice thickness, surface coil, 500/30 (TR/TE), four excitations, sagittal view (only), 30-min examination time, and closed-mouth and *partial* open-mouth positions (closed-mouth position will provide diagnosis for position in all cases, but partial open-mouth position may be necessary to visualize the size and shape of the meniscus). On MR images, the thin intermediate zone is the best determinant of disk position. After discussing grades of TMJ disease and illustrating the MR findings, Dr. Helms summarized by saying that MR imaging is replacing arthrography and CT as the best imaging method for the TMJ—MR imaging provides information about the disk hydration and morphology, both of which correlate with degenerative joint disease and the severity of the disorder.

MR imaging of soft-tissue masses.—The use of MR imaging to detect or exclude clinically suspected soft-tissue masses was discussed by Richard A. McLoud (Mayo Clinic, Rochester, MN). However, MR may fail to detect a lesion when its signal is isointense with its surrounding area; on T1-weighted images, soft-tissue tumors within muscles may be missed, and on T2-weighted images, soft-tissue tumors within fat may be missed. The MR characteristics that help distinguish a benign from a malignant soft-tissue tumor include the following: unlike benign tumors, malignant tumors are poorly marginated, do not respect barriers, grow faster, may be calcified, tend to destroy adjacent bone, have an inhomogeneous density or signal intensity, involve adjacent fat or muscle, and are less homogeneous and larger. Not one of these findings is totally reliable by itself, but if all these factors are considered together and correlated with clinical findings, an 80–85% accuracy rate in predicting malignancy is possible. When soft-tissue masses show a short T1 (bright signal), possible diagnoses include lipoma, nonacute hematoma, hemangioma, gadolinium enhancement, and (rarely) liposarcoma. Low-signal masses on T2 (dark signal) may indicate fibrous tissue (tumor or scar), densely mineralized tissue, or air. A shortened T2 may represent tissue containing hemosiderin, tissue containing iron, or acute hematoma. Benign cysts are characterized by very sharp margins, homogeneous signal intensity, and water-density signal intensity; lipomas are well marginated, have fibrous strands, and have a fat-density signal throughout the tissue. Muscular atrophy is characteristic of hemangioma; other indicators of hemangioma include a nondiagnostic biopsy, a significant amount of fat, variable margination, a signal slightly greater than that of muscle on T1-weighted images, and a signal intensity much greater than that of muscle on T2-weighted images. Included in the MR findings for pigmented villonodular synovitis are intracapsular synovial mass and effusion, dramatic T2 shortening, and absence of heavy calcification; desmoids show variable margination, islands of low signal on T2-weighted sequences, and nonspecific or malignantlike appearance. In these soft-tissue tumors, MR imaging can show extent and size of the tumor, which can contribute significant information for treatment planning; however, both T1- and T2-weighted sequences are needed to avoid missing soft-tissue tumors.



Come to the American Roentgen Ray Society 92nd ANNUAL MEETING

Orlando, FL

Marriott's Orlando World Center
May 10–15, 1992

Scientific Program (200 papers)
Instructional Courses (60 hours)
Categorical Course on Neuroradiology
The Caldwell Lecture
Award Papers
Scientific Exhibits
Social, Golf, and Tennis Programs
Guest Programs

Meeting News

American Roentgen Ray Society: 91st Annual Meeting, May 1991

The 91st annual meeting of the American Roentgen Ray Society was held May 5–10, 1991, at the Sheraton Boston Hotel, Boston, MA. Approximately 200 scientific presentations, 60 instructional courses, and a large and varied selection of scientific and technical exhibits were available to the 2700 attendees. The topic of this year's categorical course was spine and body MR imaging, and the Friday morning symposium was an update on breast imaging. A very successful spouse/companion program on breast cancer screening was provided also. An Introduction to Research seminar, sponsored by the ARRS, AUR, and RSNA, was presented to 40 second-year residents from various institutions.

This review of the 1991 ARRS meeting is intended to provide the reader with a short summary of many of the papers presented in the scientific program. Unfortunately, page limitations do not allow coverage of all presentations or an analysis of them.

Chest Radiology

Dr. Weisbrod, of Toronto, Canada, presented a paper on emphysema associated with talc granulomatosis by M. Rahman, G. L. Weisbrod, S. J. Herman. Talc granulomatosis is associated with IV drug abuse. Radiographic findings include a fine interstitial reticular or micronodular pattern. In chronic cases, areas of conglomeration resembling progressive massive fibrosis develop in the upper lobes. A concomitant finding is severe emphysema, often with bullae. The pathogenesis of the bullous disease in IV substance abusers is unknown, although in the cases presented in this series, all were smokers. However, it appears that the vasculitis and granulomatosis produced by talc may be responsible for the bullous emphysema. Leukocyte sequestration in the lung with subsequent release of proteolytic enzymes may result in parenchymal destruction.

A paper by P. J. LaPrad, F. M. Altman, R. J. Isler, and K. A. Hillman on bedside radiologic and clinical evaluation of aspiration after prolonged mechanical ventilation was presented by Dr. Isler, of Portland, ME. The study demonstrated that aspiration occurs frequently in patients who have been intubated for a long time. Bedside chest radiographs were obtained 1 day after extubation in patients who had been intubated for more than 48 hr. The radiographs were obtained shortly after the patients had swallowed 7 ml of Dionosil. Thirty-two percent of the 50 adult patients showed radiographic evidence of aspiration. The clinical evaluation of risk for aspiration greatly underestimated its actual occurrence. However, when clinical evaluation was combined with radiologic findings, prediction of development of pulmonary complications was accurate. For example, pulmonary complications developed in 89% of the aspirating patients with high-risk clinical evaluations.

The value of gadopentetate dimeglumine enhancement for MR imaging of the chest was discussed by R. Ch. Bittner, of

Editor's note.—"Meeting News" articles report the highlights of important national radiology meetings. The intent is to provide Journal readers with succinct, substantive, and accurate reviews of topics of current interest, written in a readable fashion and published promptly after the meeting.

The articles will not undergo the peer review usually required of *AJR* publications, nor will they offer a critique of the information provided. Presenters did not have the opportunity to review this summary before publication. The sole purpose of the series is to apprise *AJR* readers of topics of current concern in an interesting and timely fashion.

I thank John J. Cronan, Ferris Hall, Donald P. Harrington, B. Leonard Holman, Robert A. Kane, Paul K. Kleinman, Valerie Mandell, Theresa C. McLoud, Peter R. Mueller, Arthur H. Newberg, John F. O'Connor, Daniel H. O'Leary, Daniel I. Rosenthal, Sanjay Saini, Rita Teele, Carl S. Winalski, and Samuel M. Wolpert for contributing to this summary.

Berlin, Germany. Other authors of the paper were J. Gurok, W. Schorner, H. G. Hieckel, and R. Felix. Seventy-six patients with different benign and malignant diseases of the thorax were examined with T1-weighted, T2-weighted, and gadopentetate dimeglumine–enhanced T1-weighted images on both 0.5-T and 1.5-T superconductive MR systems. Correlation was made with CT and surgical findings. It appears that T1-weighted, gadolinium-enhanced images provide the same type of diagnostic information previously provided by T2-weighted images, but with much better spatial resolution. Gadopentetate dimeglumine–enhanced T1-weighted images showed findings equivalent to those on T2-weighted images in the detection of malignant invasion of the chest wall or pleura, in the differentiation of tumor from distal obstructive pneumonitis, and in the detection of remaining tumor after treatment of pulmonary or mediastinal malignant neoplasms with radiation. Enhanced imaging also was useful in diagnosing cystic masses. The advantages of using T1 weighting and gadopentetate dimeglumine enhancement over T2 weighting are threefold: (1) superior spatial resolution; (2) significantly fewer artifacts; and (3) less time for examination.

Mammography

The papers in this scientific session on mammography reflect current interests in breast imaging: costs and cost-benefits, particularly as they relate to screening and needle-aspiration biopsy.

Three papers dealt with the costs of screening mammography. D. D. Dershaw described mobile screening of self-referred women in New York City in a study done by D. D. Dershaw, L. Liberman, P. O'Moore, and B. Smolek. Because many of the women were sponsored by employers, they tended to be relatively young (62% <50 years old). Findings on 88% of 15,000 mammograms were normal. Biopsy was recommended in 1.4%, with carcinoma found in 22% of biopsy samples. At a cost of $65 per screening (based on 10,000 examinations per year), and one carcinoma found per 415 screenings, the authors estimate a cost of $27,000 per cancer detected. Approximately half of the biopsies revealed ductal carcinoma in situ (many of these lesions might never be clinically apparent). The authors compared their data with those of other screening studies and concluded that the cost of detection increases as the age of the screened population decreases.

R. B. Wolk, of Natick, MA, analyzed costs during 3 years of operating a mobile mammographic unit. Costs (excluding the radiologist's interpretation) were $71 per examination during 1990, during which almost 5000 examinations were performed. Costs were proportionally higher in the preceding 2 years, in which fewer patients were examined. Medicare and many other third-party payers contemplate a global screening fee of $55–$60. Dr. Wolk thinks this amount is insufficient to make mobile screening programs economically feasible.

Irena Tocino, of Salt Lake City, UT, provided a cost analysis of screening mammography in different physical environments: hospital, mobile van, or private office. She discussed the hidden costs, such as those relating to quality assurance, accreditation, and continued education. At anticipated future reimbursement rates, some institutions may not wish to, or be able to, offer any screening mammographic service.

Kathleen M. Harris presented data collected by herself and J. P. Hogg, A. Kanbour, M. L. Skolnick, Z. S. Ilkhanipour, M. D. Ganott, and M. J. Staiger, of Pittsburgh, PA, on sonographically guided fine-needle aspiration. R. A. Schmidt, M. Morrow, M. Bibbo, and K. Dowlatshahi, of Chicago, and L. L. Fajardo, of Tucson, AZ, presented similar data on stereotactic needle aspiration biopsy. All showed relatively high sensitivities and specificities for these procedures. However, criteria for selection of patients varied, with many relatively low-suspicion abnormalities undergoing needle aspiration or biopsy. The usefulness of this procedure in selected cases can no longer be questioned; however, costs vs benefits depend on the selection of patients. In this sense, the status of needle biopsy is somewhat similar to the status of screening mammography 15 years ago or screening prostatic sonography today.

Gastrointestinal Radiology

A paper by R. F. Thoeni, D. P. Gorczyca, and H. I. Goldberg, of San Francisco, compared abdominal CT studies performed with different iodine concentrations in nonionic contrast agents and concluded that while parenchymal and vascular enhancement was significantly better at an iodine concentration of 350 mg/ml than at 240 mg/ml (with a constant volume of 180 ml of iohexol), there was no difference in the detection of parenchymal lesions at the different contrast concentrations.

A study by M. J. Lee, P. F. Hahn, J. F. Simeone, N. Papanicolaou, T. Egglin, and P. R. Mueller, of Boston, evaluated and compared the clinical usefulness of CT attenuation, size, and subjective observer interpretation in distinguishing between benign and malignant adrenal masses. Fifty-five patients with 66 adrenal masses were analyzed. Histologic proof was available in five of the 66 masses; the remaining 61 masses were characterized by imaging follow-up (mean, 1.25 years). The subjective observer interpretation was performed by three blinded interpreters using a seven-point scale of certainty. Receiver-operating-characteristic (ROC) analysis was performed on all three methods. The difference in CT attenuation of benign vs malignant masses was highly significant. Size of benign masses ranged from 1.2 to 4.1 cm, whereas malignant masses ranged from 1.5 to 10.0 cm. The area under the ROC curve was significantly larger for CT attenuation than for size or observer interpretation. At 0 H, all lesions were benign (47% sensitivity, 100% specificity). At 10 H, sensitivity increased to 79%, with a specificity of 96%. Therefore, lesions with attenuation from 0 to 10 H are probably benign, but follow-up is recommended. Measurement of CT attenuation proved to be the most clinically useful method to discriminate benign from malignant adrenal masses.

S. L. Dawson, from the group at the Massachusetts General Hospital (other authors: P. R. Mueller, S. Saini, M. J. Lee, J. A. Brink, P. Kelsey, N. Nishioka, R. Schapiro, and J. T. Ferrucci), presented a series of patients with stones in the

common duct that were treated with pulse-dye laser lithotripsy, either through a T-tube or via endoscopic control. Dr. Dawson's group reported excellent success in fragmentation of these large stones, which had not been possible to remove by radiologic and endoscopic methods. He noted that after fragmentation, the numerous small pieces of stones were extracted with a basket or balloon, and that all the endoscopy patients had papillotomy. No significant complications were noted.

B. D. Coley, R. F. Mattrey, M. A. Trambert, K. G. Baker, and E. Heiberg, from San Diego, CA, used manganese dipyridoxal diphosphate (Mn-DPDP) to assess hepatic dysfunction. Mn-DPDP is a paramagnetic contrast agent that is taken up by the hepatocytes and excreted in bile and enhances liver contrast on T1-weighted MR images. It does not diffuse into the extracellular fluid space. This agent was studied in rabbits in which biliary obstruction and hepatitis were induced. Mn-DPDP produced a different enhancement pattern in each group. Hepatitis caused slow but continuous enhancement of the liver and gallbladder, whereas no enhancement was detected in rabbits with biliary obstruction. Dr. Mattrey concluded that this agent may be useful in a clinical setting in patients with biliary obstruction.

A. Tanimoto, Y. Baba, L. Zhao, J. Chen, D. Pouliquen, and D. D. Stark, of Boston, used animal models to assess cell-specific contrast agents in a study of hepatitis induced in rats by oral administration of carbon tetrachloride. In this study, two supraparamagnetic iron oxide preparations and two paramagnetic preparations were studied. Contrary to the expectation that hepatic injury would reduce the uptake of cell-specific agents, results showed unchanged or increased enhancement. Dr. Tanimoto noted that without contrast agents, the T2 value itself was a sensitive indicator of hepatic injury.

Gadolinium-enhanced, fast MR of the liver on a 1.5-T imager was studied by G. S. Gazelle, P. A. Wielopolski, J. R. Haaga, E. N. Haacke, of Cleveland, OH. They used a variation of the RASE (rapid acquisition spin echo) technique. They shortened the TR and TE and used a 170 × 256 matrix and were able to image 20 sections 8-mm thick during a single breath-hold. The images were acquired before, during, and after bolus administration of gadopentetate dimeglumine. Images were compared with CT scans, CT portograms, and sonograms. MR detected all the lesions well and was equal to the other techniques in detecting lesions. The vascular anatomy shown on MR was quite advantageous.

J. B. Kruskal, A. Lunderquist, and M. E. Clouse, of Boston, described a new laboratory technique ("in vivo video microscopy") with which direct visual assessment of hepatic sinusoidal perfusion, cell morphology, and cellular function was shown in live animals. This technique was used to study hepatic response to IV administration of a variety of imaging pharmaceuticals (gadopentetate dimeglumine, perfluorocarbon emulsion Fluosol-43, superparamagnetic iron oxides [SPIO] AMI-25, hepatocyte-specific SPIO). The authors demonstrated the usefulness of this technique in documenting acute (during injection) and chronic (for up to several months) changes in hepatic morphology. For example, compared with saline controls, Fluosol-43 produced hepatocyte swelling and sinusoidal occlusion. Both gadopentetate dimeglumine and Fluosol-43 reduced the phagocytic capacity of Kupffer cells. In contrast, AMI-25 produced adhesion of monocytes to sinusoidal endothelium with subsequent embolization of monocyte cell clusters. The authors noted that it is not possible to make these observations by any other means, including biochemical and histologic tests.

Musculoskeletal Imaging

Knee

R. C. Fritz, C. A. Helms, and H. K. Genant, of San Francisco, studied the MR appearance of normal and abnormal depressions in the tibial plateau. They observed two types of surface osteochondral defects or depressions in the tibial plateau: a posteromedial defect, measuring 4–10 mm (mean, 7 mm), in 100% of patients, best seen on coronal images and representing the site of the insertion of the posterior cruciate ligament; and an anterolateral defect, 1–6 mm (mean, 2 mm), in 95% of patients, just anterior to the insertion of the anterior cruciate ligament and near the anterior attachment of the lateral meniscus. The frequency of these depressions makes them important to recognize in order to differentiate them from abnormalities such as fractures or degenerative subchondral cysts.

T. N. Vahey, D. R. Broome, K. J. Kayes, and K. D. Shelbourne, of Indianapolis, IN, studied the differential MR appearances of acute and chronic complete tears of the anterior cruciate ligament (ACL). They defined an acute tear as less than 70 days old and a chronic tear as more than 6 months old. Acute ACL tears are characterized by ligamentous disruption with edematous changes. These changes may be either a large intraligamentous edematous mass or smaller edematous foci. However, 20% of acute ACL tears lacked identifiable edematous soft-tissue changes. Perhaps a 70-day-old tear is too old to be considered acute. In chronic ACL tears, the ACL was either completely nonvisualized, fragmented but visible, or continuous but with focal angulation. Chronic ACL tears can mimic an intact ACL on MR images by producing a continuous low-intensity band, which may represent fibrous scar tissue. In a high-quality MR study of the knee, nonvisualization of the ACL is diagnostic of a chronic tear.

A retrospective study of axial knee MR was performed by J. S. Swan, M. A. Norris, J. S. Keene, and A. A. De Smet, of Madison, WI, to determine the normal appearance of the patellar articular cartilage and the detectability of chondromalacia patellae (CMP). At arthroscopy, the researchers graded the patellar cartilage of all patients with the Noyes classification. On the basis of the arthroscopic results, MR criteria were developed for the diagnosis of CMP. On axial T1-weighted images, the normal knee has uniform signal intensity. The posterior surface is sharp and the subchondral bone plate is well defined. The cartilage of the patella is of uniform thickness. With CMP, the knee has a low-signal focus, indistinctness, distorted subchondral bone plate, and diffuse or focal cartilage thinning. On axial T2-weighted images, fluid-intensity fissures are present in the cartilage. On axial gradient-echo images, cartilage thinning, focal erosions, foci of

increased or decreased signal, and fluid in the cartilage is shown. T2-weighted axial and sagittal imaging is most specific for CMP, and spin-density and T2-weighted axial imaging is most sensitive. Adding axial images to the knee imaging protocol in those patients with anteromedial knee pain might help differentiate meniscal tears and plica syndromes from CMP.

Nonarticular Bone Imaging

Most papers devoted to nonarticular aspects of bone imaging were concerned with computer applications to the imaging of bone. A number of the presentations were reports of experimental exploration of computer programming used for clinical diagnosis.

A paper by J. R. Crim, J. Sayre, and L. L. Seeger, of Los Angeles, dealt with densitometry of bone by using computer-based digital radiography and dual-energy radiographic absorptiometry. Scans of the lumbar vertebrae L2–L4 and scans of one hip of 16 normal subjects were studied. Spine phantoms also were imaged. The variation of spine phantoms was 0.5%, whereas spine measurements in patients varied as much as 2% in the same subject. A greater variation occurred in the hip. Dr. Crim concluded that the low radiation dose makes dual-energy radiography an appealing screening method, but was cautious about predicting its application to following up response to therapy. A second paper by Drs. Crim and Seeger concerned the pitfalls encountered when using this system. They pointed out that diskogenic sclerosis, osteophytosis, and subtle compression fractures may be difficult to define on these images.

A fascinating presentation of three-dimensional (3-D) reconstruction of skeletal muscle was given by R. McColl for G. Theriault, J. Bowers, J. Fleckenstein, T. Faber, R. McColl, R. Opperman, and R. Peshock, of Dallas, TX. The authors used short-TI inversion recovery (STIR) and T2-weighted MR images (approximately 36 slices per study) to study forearms and thighs before and after exercise. They found that the STIR images were consistently superior to the T2-weighted images, partly because the difficulty of removing the subcutaneous fat signal from the T2-weighted images complicated the program. They also concluded that areas of homogeneous tissue, such as that in the proximal extremities, were better suited to 3-D reconstruction than were the forearm and hand.

T. E. Moore, M. J. Flood, R. A. Robinson, M. H. Kathol, W. T. C. Yuh, and G. Y. El-Khoury, from Iowa City, IA, studied radiographs of 43 patients with posttraumatic osteolysis and stress osteolysis of the clavicle near the acromioclavicular joint and developed a grading system. They also performed MR imaging with and without gadopentetate dimeglumine enhancement and concluded that traumatic osteolysis is a single entity related to repeated microtrauma, but that it is not purely an osteolytic process. They found that the presence of normal bone marrow on MR images suggests a good prognosis and is essential for repair of the osteolytic region.

G. W. Gross and J. M. Boone of Philadelphia, have taught a computer (neural network) to read digitized images of radiographs of forearms with radial fractures. The neural network was able to identify fractures in the training set with excellent performance. We were all depressed to learn that it is entirely possible that a computer may read forearm fractures at least as well as the average radiologist.

M. D. Murphey, J. L. Quale, N. L. Martin, L. T. Cook, and S. J. Dwyer III, of Kansas City, KS, evaluated the application of phosphor-plate radiography to musculoskeletal examinations, including films of the thoracic spine, cervical spine, scoliosis, lateral shoot-through hips, and swimmers views of the cervical spine. They concluded that no significant difference in diagnostic quality existed between screen-film and phosphor-plate examinations and that phosphor-plate imaging was done at approximately 30–50% less radiation dose to the patient. They indicated that the need for repeating images was markedly reduced by the phosphor-plate system because the digital image provided wide latitude and improperly obtained images could often be salvaged at the digital work console.

Fractures

L. P. Davis, D. Guyot, J. Muz, R. Fitzgerald, and G. A. Kling, from Detroit, MI, prospectively studied 14 patients with gunshot wounds to the extremities with radiographs and ^{99m}Tc-labeled methylene diphosphonate bone scans in order to determine the sensitivity of scintigraphy for the detection of fractures. Because fracture from a gunshot wound may be radiographically occult, the extremity is commonly placed in a cast prophylactically, and follow-up radiographs are obtained. If no fracture is detected on the follow-up films, the cast is removed. Of 20 long bones examined, 10 appeared normal on scintigraphy and follow-up radiographs. Of 10 patients whose scintigrams showed fracture, only six patients proved to have fracture on follow-up radiographs (sensitivity 100%, specificity 71%). The soft-tissue damage caused by the bullet was apparent on the scintigrams, and the false-positive examinations occurred when this soft-tissue uptake overlapped on the bone. Orthogonal scintigraphic views were essential in minimizing the false-positive rate. Further work with single-photon emission CT (SPECT) as a method of eliminating overlap is currently underway. Dr. Davis concluded that bone scintigraphy is a sensitive method for the detection of occult fracture from gunshot wounds and that an examination that does not show fracture may eliminate the need for placing a cast on the extremity.

P. J. Fedyshin and R. Daffner of Pittsburgh, PA, retrospectively reviewed the MR findings and radiographic workup of five patients with sacral stress or insufficiency fractures. The patients had confusing clinical findings, and MR was performed in search of malignant lesions or to identify the cause of lower back pain. On MR images, the fractures had low signal intensity on T1-weighted and high signal intensity on T2-weighted images. The signal abnormalities of fractures were on the sacral side, appeared symmetric or asymmetric, and were more linear than would be expected for a neoplasm. Gadopentetate dimeglumine was administered in three cases and the MR images showed mottled enhancement. No soft-tissue masses were identified. Nuclear medicine studies showed fracture in all cases, and CT scans confirmed fracture in all cases. Coincident fracture of the anterior arch on the

pelvis was present in three patients. Plain films were not helpful in the initial evaluation, as findings showing fracture were not present until late in the clinical course. The authors do not recommend the use of MR for suspected sacral insufficiency fracture, but suggest that the sacrum be included in the MR study of the lumbar spine for lower back pain because insufficiency fracture may not be clinically suspected. Scintigraphy and CT are recommended for the evaluation of suspected sacral insufficiency fracture.

M. R. Engle, R. A. McLeod, and K. K. Unni, Rochester, MN, retrospectively reviewed the radiographs and medical records of 140 patients with histologically proved sarcomas arising from previously irradiated bone. The interval between irradiation and sarcoma ranged from 10 months to 55 years (average, 16 years). The 5-year survival rate was only 28%. The common presenting symptoms and signs were pain and/or soft-tissue mass. Radiographic findings included permeative medullary destruction, soft-tissue mass (96%), and cortical destruction (90%). Calcification of tumor matrix was identified in only one third of the cases, and aggressive periosteal reaction was infrequent. Fracture was present in 39%. Comparison films were helpful in differentiating irradiation effects from sarcoma, because the irradiation effects were radiographically stable after 3 years. Cross-sectional imaging techniques were best for detecting soft-tissue masses. The differentiation of infection from postradiation sarcoma was difficult.

Sonography

Seven of the 10 sonography papers dealt with Doppler sonography—duplex, color, or both.

W. H. Horstman, W. D. Middleton, and G. L. Melson, of St. Louis, MO, studied 51 patients who had scrotal inflammatory disease. They used a 7.5-MHz linear array transducer equipped with color to characterize the sonographic features of epididymitis with and without orchitis. They showed that any hypervascularity in the epididymis was abnormal. Spontaneous venous flow in the testis and/or epididymis was another feature of inflammation. Of note was the relative insensitivity of gray-scale imaging in evaluating their patients; the conclusion that color Doppler should be included in the sonographic scrotal examination is supported fully by the data that were presented. The authors did not attempt to consider the differential diagnoses of testicular torsion, torsion of the appendix testis, or tumors.

Dr. Mindy Horrow, of Philadelphia, presented a practical paper in obstetric sonography. She found that a large amniotic sac was a valuable predictor of embryonic death. As a good rule, the diameter of the amniotic sac parallels the crown-rump length of the embryo. When the amniotic sac increases disproportionately, the embryo is not going to survive. All scanning was done with an endovaginal probe in order to visualize the amniotic membrane, the fetal pole, and the chorionic sac.

A carefully designed study was presented by R. C. Nelson, of Atlanta, GA, for V. G. Vassiliades, T. D. Ostrow, J. L. Chezmar, G. L. Hertzler, and R. C. Nelson, on the value of Doppler sonography and CT of the liver for predicting the severity of cirrhosis. The final conclusions were that duplex sonography of the hepatic artery and portal vein was not helpful in predicting the severity of cirrhosis. Nor was it helpful in predicting presence or severity of inflammatory change in the liver. CT scanning also was evaluated to determine whether splenic and hepatic volumes predicted severity of cirrhosis and/or inflammation. No correlation was found on CT.

J. R. Grantham, of Gainesville, FL, investigated the clinical status of 87 patients who had been examined for possible deep venous thrombosis. No patient with normal findings on sonography had subsequent problems that suggested significant deep venous thrombosis of the legs had been missed. The findings support the continued use of sonography as a screening method and the reservation of deep venography for those patients with indeterminate sonograms.

Another practical paper was written by J. F. Whelan, M. H. Barry, J. D. Moir, and G. E. Lund, from St. John, New Brunswick, Canada. They correlated the results from color duplex sonography with angiography in patients who had suspected peripheral vascular disease. Thirty-two patients had a total of 88 hemodynamically significant lesions on angiography. Sensitivity of sonography was 91% and specificity was 97% in this series. Vascular surgeons are now entering the realm of diagnosis by acquiring sonographic units. Radiologists should be expert in the technique of evaluating peripheral arterial disease if they are to serve an adult population. Radiologists would then be in the best position to integrate imaging and to be able to offer angiographic therapeutic options.

Pediatrics

H. L. Mast, J. O. Haller, and M. S. Schiller, of Brooklyn, NY, described 22 children with AIDS and associated pericardial effusion. Nine patients had abnormal cardiac silhouettes, and all had interstitial pulmonary infiltrates or consolidations on radiographs. Histologic changes included myocardial hypertrophy or dilatation, focal cardiomyolysis or myonecrosis, interstitial edema, lymphocytic interstitial infiltrate, or myocardial abscess. One patient had evidence of collapse of the right ventricular wall and a large pericardial effusion on echocardiography. Another had decreased ventricular contractility. The authors stressed the importance of considering pericardial effusion and myocarditis in children with AIDS.

B. C. Dangman and R. L. Lebowitz, of Boston, reviewed six cases of calculi forming on surgical staples in children who had bowel interposition during reconstructive urologic surgery. The stones form in the lumen of the bowel segment on the exposed portion of the staple. The stones may be attached eccentrically to the staple or may pull free and lie within the lumen. The authors think that the appearance is pathognomonic and can easily be differentiated from stones forming from stasis or metabolic derangement.

W. P. Chan, R. G. Miller, P. Lang, S. Majumdar, and H. K. Genant, of San Francisco, studied 14 boys with Duchenne muscular dystrophy by using spin-echo MR imaging. T1- and T2-weighted sequences and fat-saturation techniques were used. The degree of fatty replacement in the calf muscles

was graded and a correlation was found between the degree of fatty replacement and the patient's restrictions in walking and in daily life. The authors suggest that MR is valuable in identifying the extent to which particular muscle groups are involved in Duchenne muscular dystrophy, a factor that may be important in therapeutic interventions such as myoblast implantation.

Nuclear Medicine

In order to determine the relative value of MR imaging and radionuclide bone scanning for the detection of vertebral metastases, M. G. Butler and L. C. Hall, of Cincinnati, OH, performed a retrospective comparison of the two techniques. They found that in 29% of the cases, MR showed abnormalities in areas that were normal on the bone scan. One case of increased activity on bone scintigraphy was due to diskogenic disease that was evident on MR. They suggest that MR is not only more specific than scintigraphy in the detection of vertebral metastases but is more sensitive also.

Gallium-67 scintigraphy appears to be useful in the localization of active extrapulmonary tuberculosis, particularly in patients with fever of unknown origin who live in areas endemic for tuberculosis. S. O. Yang and colleagues, of Pusan, Korea, found that the sensitivity for detection of extrapulmonary tuberculosis was 80%.

In a study designed to determine whether MR, MR spectroscopy, or PET is able to accurately detect cardiac allograft rejection, C. E. Spritzer, T. D'Amico, C. Charles, R. Negro-Vilar, S. Buchanan, J. Berry, and P. Van Tright, of Durham, NC, compared the three techniques in six dogs after heterotopic cardiac transplantation. Although T2 measurements and ^{31}P spectroscopy measurements were abnormal, no differentiation was seen in fluorodeoxyglucose (FDG) uptake. These results do not support the use of PET for diagnosing cardiac allograft rejection but do suggest that MR and MR spectroscopy be used to monitor the development of rejection in cardiac transplantation.

Dynamic PET with FDG and ^{11}C-ACBC (aminocyclobutanecarboxylic acid) appears to be more sensitive than using FDG alone in grading brain tumors. R. Tucker, H. F. Hubner, E. Buonocore, A. Chan, G. T. Smith, A. B. Kliefoth, and B. Keller, of Knoxville, TN, found higher sensitivity with ACBC PET than with FDG alone, but FDG PET is sensitive in identifying radiation necrosis.

Neuroradiology

The overriding message delivered at the diagnostic neuroradiology scientific session was that administration of contrast agents can sometimes mean the difference between a diagnostic and a nondiagnostic MR imaging study. A study done by J. Haustein, W. Bauer, T. Hillbertz, T. Louton, H. P. Niendorf, J. Planitzer, W. Schorner, and P. Schubeus, of Berlin, Germany, showed that doubling the dose of gadopentetate dimeglumine resulted in increased contrast quality compared with studies on the same subjects receiving a standard dose of 0.1 mmol/kg. Although the number of subjects (n = 19) so far enrolled in this multicenter study precluded any generalization about improved diagnosis, the authors clearly expect that diagnostic information increases with increasing dosage.

J. W. West, C. Lee, B. L. Dean, J. E. Kirsch, and V. M. Runge, of Lexington, KY, reported considerable improvement in diagnosis when gadopentetate dimeglumine was used in routine examination of the lower back. Although the use of contrast agents has been well described in the postsurgical spine, its efficacy in studying the nonoperated spine has not been emphasized. Dr. West reported that in 48% of 100 patients studied, a herniated disk could not be excluded on the precontrast study, but could be ruled out on the postcontrast study. Enhancement added information by better delineating anatomy. Also, in 18% of cases, the precontrast study was nondiagnostic because the patient moved, whereas the postcontrast study was diagnostic. The authors stressed the importance of using axial slices with contrast enhancement to determine the presence or absence of disk herniation. They noted that the use of contrast material added 15–20 min to study time, but concluded that the added time, plus the cost of the contrast agent, was offset by the decreased need for subsequent myelography.

Interventional Radiology

Vascular

J. F. Polak, R. L. Bajakian, D. H. O'Leary, M. C. Anderson, and F. A. Jolesz, of Boston, compared two-dimensional (2-D) time-of-flight MR imaging projection angiograms with color Doppler sonography and angiography in 23 patients (42 carotid bifurcations) to evaluate effectiveness in identifying significant carotid artery disease. MR angiography identified significant (≥50%) lumen diameter stenosis with a sensitivity of 0.96 and a specificity of 0.64. Color Doppler sonography, with 1.25 m/sec peak systolic velocity as a threshold, had a sensitivity of 0.96 and a specificity of 0.71. A correlation was found between percent diameter narrowing and the zone of signal loss on MR angiography. A strong correlation was found between angiographic narrowing and color Doppler sonography's peak-systolic velocity. The length of signal loss by MR angiography correlated with peak systolic and peak end-diastolic velocities of blood flow in the internal carotid arteries. MR angiography is comparable to color Doppler sonography for detection of stenosis greater than 50%.

A 3-year experience with the Simpson atherocath for treating arterial stenosis and occlusion was presented by D. Kim for D. Kim, L. E. Gianturco, D. H. Porter, J. B. Siegel, D. E. Orron, K. C. Kent, and J. J. Skillman, of Boston. Fifty-six patients were treated for 74 lesions (54 arterial stenoses and seven occlusions in 48 patients and 13 stenoses in eight patients with in situ vein bypass grafts). The lesions were located in the iliac, superficial femoral, popliteal, and tibial vessels, in addition to in situ grafts. The mean preatherectomy ankle/brachial index (ABI) was 0.66. There were 51 technical successes. Follow-up for a mean of 12 months showed a mean ABI of 0.93 in 51 patients immediately after atherectomy, 0.89 in 36 after less than 3 months, 0.83 in 18 after 4–6 months, 0.81 in 12 after 7–12 months, and 0.76 in 10 after 13–18 months. Complications included three significant groin

hematomas and one pseudoaneurysm. Eight patients had recurrent symptoms and decreased interval ABIs. The authors concluded that use of the Simpson atherocath was effective, with a low complication rate.

The Simon nitinol filter was placed in 271 patients in a multicenter trial performed by D. Kim, C. J. Grassi, D. H. Porter, J. B. Siegel, S. Kleshinski, and M. Simon, of Boston. Placement was successful in all cases. One hundred thirty-six of the patients were followed up for 6 months. Some comparative results in symptomatic vs asymptomatic patients were as follows: three symptomatic patients had recurrent pulmonary embolism (fatal in one patient), vs two asymptomatic; 22 symptomatic patients had occlusion, vs five asymptomatic; no symptomatic patients had penetration, vs two asymptomatic. This filter compares favorably with other IVC filters. Its ease of insertion and compatibility with MR imaging are advantages for its use.

Nonvascular

Uterine arteriovenous malformations (AVMs) have traditionally been treated with hysterectomy. R. Vogelzang and A. Nemcek, of Chicago, reported on four patients with uterine AVMs who were successfully treated with superselective catheterization of the uterine artery and embolization with polyvinyl alcohol sponge or gelatin sponge. All patients had massive uterine bleeding that stopped after embolization. One patient later became pregnant. This series indicates the possibility of avoiding hysterectomy and controlling AVMs with uterine artery embolization.

J. W. Yedlicka, Jr., R. N. Aizpuru, D. W. Hunter, W. R. Castañeda-Zuñiga, and K. Amplatz, of Minneapolis, MN, reported on the potential role of the radiologist in exchanging double-J ureteral stent catheters without cystoscopy. Forty of 41 double-J stent retrievals or exchanges were performed successfully in 22 women and two men. IV sedation was used often. A Foley catheter was used to gain access to the bladder, and a cystogram was performed. A floppy guidewire was placed through the catheter, and the catheter was removed. A guide catheter was then passed over the wire into the bladder. A right-angle snare was passed through the catheter and used to grab the stent. The end of the stent was then pulled through the urethra and a wire was passed through it into the renal pelvis. A new double-J stent was then placed over the wire. The entire procedure took 25 min.

A controversial and very innovative approach to controlling acute lower gastrointestinal bleeding was presented by G. Guy for G. Guy, P. C. Shetty, R. P. Sharma, M. W. Burke, and T. H. Burke, from Detroit, MI. Rather than using the traditional vasopressor to control colonic bleeding, the group used polyvinyl alcohol for direct subselective embolization of the bleeding vessel at the level of the rectal artery. They performed 10 embolizations in nine patients (mean age, 58 years). Three patients bled again at a mean of 9 days later. The colon was monitored endoscopically and only minimal ischemic changes were seen. It was suggested that the authors' success in controlling bleeding without inciting bowel infarction was related to their microvascular catheter technique and the use of permanent occlusion material.

Neurologic

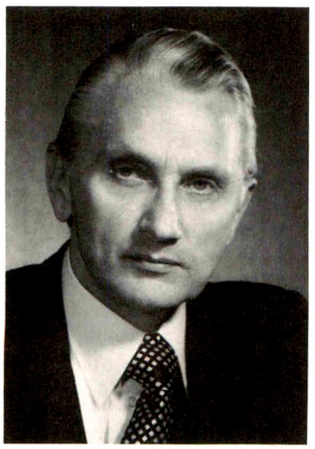
A. D. Bronstein and K. R. Maravilla, of Seattle, presented a paper on the CT and MR appearances of Surgicel and Gelfoam in vitro. The authors indicated that one of the problems with the immediate postoperative CT scans and MR images is the difficulty in distinguishing postoperative bleeding from the surgical changes caused by Surgicel and Gelfoam hemostatis agents. The authors performed phantom studies of samples of Surgicel fabric and powdered Gelfoam, which they imaged under different conditions with both CT and MR. The samples were imaged in air, normal saline, and clotted and heparinized blood. In addition to high-resolution CT, they obtained T1-weighted spin density and T2-weighted MR images. The authors showed that Surgicel saturated with normal saline is hyperdense on CT and hypodense in clotted blood. Gelfoam is isodense in normal saline and hypodense in clotted blood. On MR images, Surgicel is isointense when suspended in normal saline and hyperintense within fresh clotted blood on T1-weighted images and hypointense under both conditions on T2-weighted images. Gelfoam, on the other hand, is hypointense within normal saline or clotted blood on both T1- and T2-weighted images. The authors summarized their paper by indicating that Surgicel and Gelfoam are both less dense than clotted blood on CT, thus suggesting that these materials do not contribute to increased attenuation from blood in the postoperative period. Surgicel, however, appears hyperintense in clotted blood on T1-weighted images; this is the only condition in which the hemostatic agent may contribute to the appearance of postoperative blood.

F. Vanneroy, F. Courtheaux, X. Cornille, J. P. Houtteville, and J. Theron, from Caen, France, used automated percutaneous diskectomy to treat foraminal and extraforaminal lumbar disk herniation. The authors reported a series of 18 cases of posterolateral and lateral disk herniations. They made the point that these lesions are often difficult to diagnose, particularly in the postoperative patient in whom the presence of scar is a significant differential problem. For this purpose, they advocate CT diskography as having fewer false-negative studies than does contrast-enhanced MR. In their 18 patients who had diskectomy, 13 have been followed up for 6 months. Five had excellent results and eight had good clinical results. Percutaneous diskectomy appears to be effective in the correct hands; it is interesting, however, that postdiskectomy CT scans or MR images did not show resolution of the offending disk. Presumably, the symptomatic improvement experienced by these patients is due to a decrease in pressure on the affected nerve root.

J. J. Norconk, G. S. Leight, and C. E. Spritzer, of Durham, NC, studied parathyroid lesion localization with MR imaging, with surgical correlation of their findings. T1-weighted, spin-density, and T2-weighted images were obtained on a 1.5-T system. At surgery, 61 parathyroid adenomas were found in 61 patients. Four hyperplastic glands were resected from one other patient. Prospectively, MR correctly localized 49 adenomas. However, 13 studies were false-negative and three were false-positive. Image quality was suboptimal in seven of the 13 false-negative studies. The authors concluded that MR is accurate for evaluating parathyroid disease.

1991 ARRS Gold Medals

John A. Kirkpatrick, Jr.



Eugene Gedgaudas

Eugene Gedgaudas was born in Lithuania in 1924, where he received his primary and secondary education. In anticipation of the Soviet occupation of Lithuania, he moved to Germany in 1944 and in 1948 graduated in medicine from the University of Munich. The following year, he emigrated to Canada, and for 2 years he worked at the Manitoba Cancer Research Institute in Winnipeg. He subsequently took his internship and radiology residency at St. Boniface Hospital in Winnipeg, including a period at the University of Minnesota under Dr. Leo Rigler. Shortly thereafter, he received his certification in radiology by the Royal College of Physicians and Surgeons of Canada and by the American Board of Radiology.

Gene's professional career in radiology began as an associate radiologist at the St. Boniface Hospital in Winnipeg and a member of the faculty of the University of Manitoba. However, in 1963 he was invited to return to the University of Minnesota as an assistant professor in the Department of Radiology and it was at that institution that he remained for the rest of his professional life, rising through the ranks to become chairman of the department in 1969. He remained in this post for almost 20 years, retiring in July 1986 with the rank of professor emeritus. During his tenure as chairman, he was responsible for an annual complement of over 50 residents circulating through the various teaching hospitals of the University of Minnesota.

That Gene's achievements were not purely academic is revealed by his election to the Senate of the University of Minnesota in 1972 and as chairman of the Council of Clinical Sciences for the 10-year period from 1973 to 1982. His educational endeavors also were noteworthy: on assuming chairmanship of the Department of Radiology, he became responsible for the operation of the famous annual Minnesota Refresher Course begun many years earlier by Leo Rigler; all radiologists in the state were invited by Dr. Gedgaudas to attend the course free of charge. He has been an enormously popular lecturer and has made multiple presentations throughout the world, particularly in the field of cardiovascular disease. Indeed, there are few countries in which his talent as a speaker has not been displayed. His bibliography includes over 50 scientific articles and the very successful book *Cardiovascular Radiology*, of which he is senior author. A clear reflection of the impact he has made on radiologic education over the years was the creation in 1989 of the Vilhelmina and Eugene Gedgaudas Chair in Radiology at the University of Minnesota.

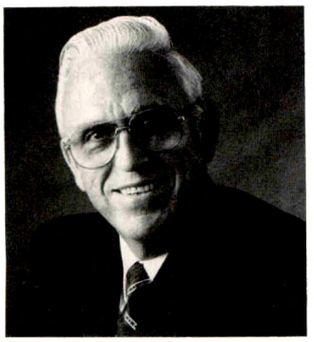
The honors he received during his career in radiology are legion. In 1976, he was the president of the Minnesota Radiological Society, from which organization he received the President's Award in 1986. Within the American Roentgen Ray Society, he became director of instructional courses in 1976 and served with distinction in that capacity until 1984. In that year, he became president-elect of the society and in the following year, its president. In addition, he is an emeritus fellow of the American College of Radiology, an honorary fellow of the Royal Society of Medicine and the Hungarian Radiological Society, a fellow of the International College of Surgeons, and an honorary member of the Rocky Mountain Radiological Society, the Hong Kong Society of Diagnostic Radiologists, and the Singapore Academy of Medicine.

In 1949, Gene married Vilhelmina, a lovely lady whom he met during his medical school days in Munich and who has been his constant companion and love ever since. They have three beautiful daughters.

Dr. Gedgaudas' distinguished career as a medical educator, lecturer, author, and societal leader makes him eminently qualified to receive the gold medal of the American Roentgen Ray Society.

Robert G. Fraser

AJR **157:630–632, September 1991** 0361–803X/91/1573–0630 © American Roentgen Ray Society



Eugene Carl Klatte

Eugene Carl Klatte was born in Indianapolis, IN, on March 19, 1928, and spent his early years in and around Terre Haute, IN. He attended Purdue University and graduated from Indiana University with a baccalaureate degree in chemistry in 1949. He graduated from the Indiana University School of Medicine in 1952 at the top of his class. Membership in Phi Beta Kappa and Alpha Omega Alpha indicates his high level of academic achievement.

He served a rotating internship at the University of Michigan and then 2 years as a captain in the United States Air Force. It was during this tour of service that his wife, Barbara, was afflicted with poliomyelitis. She was then expecting their third child, who proved to be the third of five daughters. Gene and Barbara's love, devotion, and indomitable spirits have enabled them to cope with adversity.

After a residency in radiology at the University of California, San Francisco, Gene was appointed a Picker Scholar in radiologic research and an instructor in radiology at the Indiana University School of Medicine in 1957. He was certified in radiology and nuclear medicine in 1958 by The American Board of Radiology. From 1957 to 1962, he progressed to the rank of associate professor and director of pediatric and cardiovascular radiology. In collaboration with Dr. John A. Campbell, he pioneered in cinefluoroscopy and cineradiography in the evaluation of cardiovascular, genitourinary, and other diseases. This is reflected in an extensive bibliography of publications, book chapters, and exhibits that he has authored and coauthored.

In 1962 Gene was named professor and chairman of the Department of Radiology at Vanderbilt University School of Medicine and in 1971 returned to his alma mater as professor and chairman. In 1979 he was named distinguished professor by Indiana University, one of the highest honors bestowed on a member of the faculty. At both Vanderbilt and Indiana, he has been instrumental in creating superb teaching departments at both undergraduate and postgraduate levels. He has trained more than 250 radiologists, many of whom have gone on to distinguished academic careers.

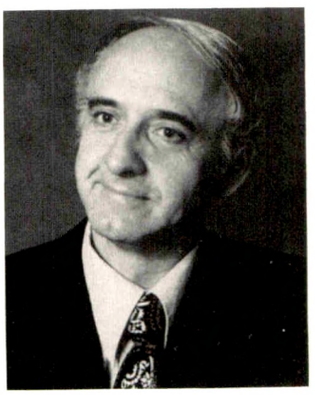
Gene was nominated to the Board of Trustees of The American Board of Radiology from the American Roentgen Ray Society and was elected to that position in 1979. On June 30th of this year, he completed 12 years of service as a trustee and has examined for the board 33 times. He has served on the Executive Committee of the board as well as many of its other committees and has chaired the examination subcommittee on Diagnostic Radiology and the genitourinary radiology category of the oral examination.

He was awarded fellowship in the American College of Radiology in 1970 and was later a member of the Board of Chancellors. He is a member of many other specialty organizations and has served in a leadership role in most. He has served as chairman of the Executive Committee of the Executive Council of the American Roentgen Ray Society and in other capacities. He was a member of the Executive Council of the Society of Chairmen of Academic Radiology Departments (SCARD) and its president in 1972–1973. In 1989, he was awarded the gold medal of the Association of University Radiologists. He has been a reviewer or member of the editorial boards of the *American Journal of Roentgenology*, *Radiology*, and the *Journal of the American Medical Association*.

Under the aegis of the Association of University Radiologists and SCARD, he devised a plan for the resurrection and improvement of the resident-matching program in radiology.

In this short recounting, it is not possible to do justice or to adequately chronicle the multiple contributions this native Hoosier has made throughout his distinguished and stellar professional career as well as in his personal life. In awarding its gold medal to Gene Klatte, the American Roentgen Ray Society bestows appropriate honor on him and does honor to itself.

Kenneth L. Krabbenhoft



Elias G. Theros

Elias G. Theros, a leader in academic radiology, is one of the outstanding and most accomplished radiology teachers of our time. His career has featured unremitting and unselfish teaching services to his students and colleagues throughout the United States and abroad. Lee was born in Hall County, Grand Island, NE, in 1919, of an immigrant father, George Elias Theros of Corinth, Greece, and a mother, Mary Elizabeth Hoffman, from Clearwater, NE. From this midwestern background, Lee has met life's challenges and become a recognized international statesman for radiology.

Lee's academic excellence has its foundation in his Jesuit preparatory school training as a teenager in Omaha at Creighton Prep and continued in Italy at the Royal Conservatory of Music in Rome and Milan (1938–1940). He obtained a B.A. from the University of California, Los Angeles, with highest honors and an M.A. in education from Columbia University. During this education, he was nominated to Phi Beta Kappa in 1947, and subsequently during his medical education at the University of California, Los Angeles, he was elected to Alpha Omega Alpha in 1956 and graduated in 1957. These achievements in education, music, language, and medicine and his abilities as an enthusiastic teacher and leader catapulted him through residency training in radiology at the

National Naval Medical Center, to chairman and registrar, Department of Radiologic Pathology, Armed Forces Institute of Pathology (1966–1976), on to professor, vice chairman, and director of radiologic education at the University of California Medical Center, Los Angeles. He is currently I. Meschan distinguished professor of radiology, Bowman Gray School of Medicine, Wake Forest University, Winston Salem, NC. Lee has received the gold medal from the American College of Radiology (1986) and the Radiological Society of North America (1989).

In early 1940, with war imminent, Lee entered the Navy's officer program. This was the start of a stellar military career spanning over 30 years, with 14 of these as an honored and decorated naval line officer and 16 years as a distinguished medical officer. During his military career, he achieved numerous professional and administrative honors, including many certificates of distinguished service and merit, Army and Navy commendation medals, and the Legion of Merit from the Secretary of the Navy for work in education and medicine in 1974. One of many significant military accomplishments was his duty as a naval intelligence officer during World War II, with assignments throughout the South Pacific as a Japanese translation and interrogation officer and finally as briefing officer and editor of the Far Eastern Desk of the Office of Naval Intelligence, Washington, DC. Lee also managed to become trained in submarine and nuclear occupational medicine, nuclear reactor technology, and health physics, and he qualified in medical officers' deep sea diving.

Lee started his academic career in radiology at the Armed Forces Institute of Pathology (AFIP) in the Department of Radiologic Pathology. The department was founded after World War II and supervised by Colonel Leroy Thompson, who personally selected Lee as his successor at the AFIP. Dr. Theros assumed command in 1966 and worked diligently as the chairman and registrar of the Department of Radiologic Pathology until 1976. During this time Lee built and expanded the AFIP's radiology residency training program. In the initial phase, only a few residents and fellows attended the AFIP course. However, within the first 3 years Lee had increased the staff from three diagnostic radiologists and residents to more than 300 residents trained per year. He was also one of the original persons involved in conceptualizing the American Registry of Pathology (ARP) as it is today and was to be one of the original six ARP distinguished scientists. Lee's administrative excellence and persistence ensured the success of the AFIP program and initiated postgraduate courses, which were among the first cooperative ARP-AFIP ventures.

Continuing medical education was a topic of discussion in the mid 1960s. Lee put together a self-evaluation scientific exhibit "The American College of Radiology Film Quiz" for the 1968 meeting of the Radiological Society of North America. It was an overwhelming success and won the magna cum laude award. With this beginning, Lee and the American College of Radiology launched one of their most successful continuing medical education programs, entitled "American College of Radiology Self-Evaluation and Continuing Education Program" (the "ACR Syllabi"). As editor-in-chief, Lee has supervised the production of more than 30 volumes to date.

Dr. Lee Theros is a unique combination of humanitarian, scholar, teacher, and educator. Achievements in these areas are a testament to his moral worth and concern for others. However, it's Lee's breadth of experience as a vocalist, linguist, educator, naval officer, physician, and radiologist that characterizes the man that we so admire and love. Lee and Ruth (his wife of 48 years) have raised three outstanding children (George, Todd, and Stephanie) of whom they are extremely proud. Countless professional friends and colleagues will be forever in debt to this gentleman and scholar for his warmth and deep abiding concern for all of us.

John E. Madewell

91st Annual Meeting of the ARRS: Secretary's Report

Joseph T. Ferrucci[1]

For the 4th year in succession, a new attendance record was set at the annual meeting of the American Roentgen Ray Society (ARRS), held this year at the Sheraton Boston Hotel, May 5–10, 1991. For 2400 radiologists, all roads led to Boston, where the rich traditions of intellectual and educational excellence provided an ideal setting for the meeting. The continuing record turnouts for this meeting attest to its wide recognition as a splendid educational opportunity in a totally enjoyable atmosphere.

The meeting began officially on Monday morning, May 5, with the installation of John A. Kirkpatrick, Jr., of Boston, as the 91st president of the oldest radiologic society in North America. In an inspiring address, President Kirkpatrick reflected on the tripartite nature of a career in radiology (i.e., clinical care, teaching, and research) and noted the manner in which these activities are woven through daily practice. The opening ceremony continued with a presentation of a series of scientific papers, each of which received a prestigious award. These included the Roscoe E. Miller Award of the Society of Gastrointestinal Radiology, awarded to J. Nelson, F. Starr, E. Schenk, and D. Caldwell for "Percutaneous Transhepatic Portal-Systemic Shunt"; the Society of Uroradiology Award to Henrik S. Thomsen for "Urine Profiles Following Intravenous Diatrizoate and Iohexol in Gentamicin Nephropathy"; ARRS Executive Council Award I to John F. Matthews, Kenneth M. McDonald, Jay N. Cohn, and David W. Hunter for "The Accuracy of MRI in the Estimation of Left Ventricular Mass in Dogs with Hearts Distorted by Localized Myocardial Necrosis"; ARRS Executive Council Award II to Jörg F. Debatin, Charles E. Spritzer, Thomas M. Grist, Craig Beam, Laura Svetkey, Glenn E. Newman, and H. Dirk Sostman for "Renovascular Disease: A Comparison of Time of Flight and Phase-Contrast MR Angiograms with Conventional Angiography"; and the ARRS President's Award to Douglas D. Robertson, Craig M. Mintzer, Barbara N. Weissman, Frederick C. Ewald, Merryl LeBoff, and Myron Spector for "Detection of Distal Femoral Bone Mineral Change Using Visual and Computer Processing of Radiographs and Dual-Energy X-Ray Absorptiometry." The ARRS Executive Council Award papers carried a prize of $1000 and the President's Award paper received $2000 plus an engraved diploma.

The scientific program also began on Monday, having been arranged by Dr. Kirkpatrick and the Scientific Program Committee. There were 17 separate sessions with 188 scientific papers presented. The categorical course was on body and spine MR imaging and was directed by Anton N. Hasso and David D. Stark. This was an outstanding course, with nearly 950 radiologists in attendance during a 16-hr program approved for category 1 credit. The syllabus alone was worth the cost of admission, and for those who did not attend, we urge the purchase of the syllabus while copies are still available, because it provides an excellent review of the current status of body and spine MR imaging.

Two new features of this years meeting were a special symposium for spouses on breast cancer organized by Kay Vydareny, which was attended by more than 180 spouses and companions. In addition, a special program on research careers in radiology was offered to 40 selected second-year residents from across the country in cooperation with the Radiological Society of North America and the Association of University Radiologists. The radiology residents expressed much enthusiasm for the approach and content of this program and uttered astonishment that so many important figures in American radiology were involved in this presentation. Both of these unique special programs will be repeated next year.

The accompanying persons program was supervised by Melvin Clouse and Roy Strand, both of Boston, and was quite well attended. Day tours to Concord and Lexington, Salem and Marblehead, Newport (RI), and Filene's basement drew many eager participants.

The American College of Radiology (ACR) cosponsored luncheons on socioeconomic affairs and again presented timely and informative topics, including "Government Issues" by Gary Price, ACR Director of Government Relations; "Economic Issues" by E. O. Templeton, chairman of the ACR Commission on Economics; "Current Legal Issues" by Thomas W. Greeson, ACR Legal Counsel; and "An Update on ACR Activities" by James M. Moorefield, chairman of the ACR Board of Chancellors.

The annual ARRS golf tournament was held at the Ferncroft Country Club in nearby Danvers, MA. Unfortunately, steady showers in midafternoon prevented some from finishing the course. Not surprisingly, the rest of the week was beautifully sunny. Despite the downpour, ARRS golfing history was made as M. Paul Capp won both the Manges Trophy and the

[1] Secretary, American Roentgen Ray Society. Department of Radiology, Massachusetts General Hospital, 32 Fruit St., Boston, MA 02114.

AJR **157:633–634, September 1991** 0361–803X/91/1573–0633 © American Roentgen Ray Society

Exhibitors Trophy for a low gross. The tennis tournament was held at the Winchester Indoor Tennis Club, Winchester, MA, and the men's singles was won by Morton Burrell and the women's singles by Phyllis Danner. The men's doubles was won by P. C. Shetty and Robert Lascio.

The Friday morning imaging symposium, which has become one of the most popular segments of the ARRS meeting, was directed by Daniel B. Kopans, of Boston, who chose the subject "Current Issues in Breast Imaging." This timely session was extraordinarily well received by the roughly 800 persons attending.

The exhibit space was the largest ever for an ARRS meeting—34,000 square feet—and was shared by technical and scientific exhibitors. A record number of scientific exhibits were shown, with a major increase in the number of front-lighted poster exhibits. The winners of the major awards for exhibits were as follows: the gold medal was awarded to J. Jeffrey Carr, J. C. Reed, R. H. Choplin, and T. L. Pope, Jr., for "Pneumothorax: A Quantitative Study Using Film Screen and Computed Radiography"; silver medals to K. Kawamoto, M. Motooka, N. Hirata, S. Kitagawa, and K. Masuda for "Radiographic Characterization of the Colonic Submucosal Tumor" and W. G. Horstman, W. D. Middleton, and G. L. Nelson for "Color Doppler Ultrasonography of the Scrotum"; and bronze medals to J. T. Surratt and M. J. Siegel for "Imaging of Pediatric Ovarian Lesions," M. T. Benson, K. Dalen, A. Mancuso, H. H. Kerr, A. A. Cacciarelli, and M. Mafee for "Congenital Anomalies of the Brachial Apparatus: Embryology and Pathologic Anatomy," and M. F. Insana, T. J. Hall, J. L. Fishback, S. J. Rosenthal, G. G. Cox, and B. S. Garra for "Interpretation of Ultrasound Properties of Normal Renal Tissues in Terms of Microscopic Anatomy."

On Wednesday morning, the awards session highlighted the week-long activities of the annual meeting. Three distinguished radiologists were presented with ARRS gold medals for outstanding contributions to radiology; they were Eugene Gedgaudas (Minneapolis, MN), Eugene C. Klatte (Indianapolis, IN), and Elias G. Theros (Winston-Salem, NC). These men were all cited for their special leadership roles in American radiology and service to the ARRS.

The Caldwell Lecturer was N. Thorne Griscom, of Boston, whose presentation was entitled "The Long-Term Radiologic Manifestations of Respiratory Problems of Early Life." This was an enlightening summary of a distinguished career of observations in pediatric radiology, emphasizing that successes in pediatric medicine may lead to radiologically visible sequelae in adult life that are of importance for practicing general radiologists.

At the final business meeting of the society, the following officers were elected for 1991–1992: President, John A. Kirkpatrick, Jr. (Boston, MA); President-Elect, A. Everette James, Jr. (Nashville, TN); First Vice President, Andrew K. Poznanski (Chicago, IL); Second Vice President, George R. Leopold (San Diego, CA); Secretary, Joseph T. Ferrucci (Boston, MA); Treasurer, Beverly Wood (Los Angeles, CA); Chairman of the Executive Council, Ralph J. Alfidi (Cleveland, OH); Publications Committee and Editorial Policy Committee, Christopher B. Merritt (New Orleans, LA, 5-year term); Scientific Exhibits Committee, David S. Hartman (Potomac, MD, 5-year term); Committee on Research and Education, Robert R. Hattery (Rochester, MN, 3-year term); and Annual Meeting Committee, Neil H. Messinger (Miami, FL). Theresa C. McLoud was elected as a member of the Executive Council (5-year term).

At the annual business meeting, a major revision of the bylaws and constitution was adopted, bringing the most successful annual meeting of the ARRS to a productive close. Planning has already begun for the 1992 meeting at the Marriott World Center, Orlando, FL, May 10–15, 1992. Orlando promises to be another exciting environment, and the hotel/resort facilities are second to none. We invite attendance by members and guests alike.

The 1991 ARRS Annual Meeting Has Another Record-Setting Year: Administrative Report

Paul R. Fullagar[1]

The 91st annual meeting of the American Roentgen Ray Society (ARRS), held May 5–10, 1991, in Boston, continued the trend of the past three meetings by once again registering record numbers of radiologists in attendance. The growth of the society and the meeting continues, as 403 members were elected into the ARRS during the meeting.

The instructional course chairman, Robert Stanley, provided an outstanding schedule of 60 courses, reaching a total number of 12,627 registrations. This exceeds last year's record by nearly 1400. In addition, the categorical course on spine and body MR imaging, chaired by Anton Hasso and David Stark, had the largest registration of any ARRS categorical course, at 940 participants. The popularity of this course is further reflected in the requests we have received for the separate purchase of the syllabus prepared for course attendees. As is usual, this syllabus is on sale through the American College of Radiology publications division, but we have had to reprint it because the initial quantity has been sold out. The Friday symposium, Breast Imaging Update, chaired by Daniel Kopans, also drew record numbers of participants. The review of registrations indicates that 728 persons attended that session. Between the three course categories, our records indicate that there were 14,295 course attendees, up from the previous record of 12,433.

John Kirkpatrick, president-elect, who chaired the Scientific Program Committee, planned a superb group of scientific sessions, in which 188 papers were presented. The attendance is not recorded at these sessions, but the rooms were generally full throughout the week. Many fine comments were heard about the high quality of these presentations.

Those of you who were fortunate enough to attend and to visit the scientific exhibits saw first hand the results of the work that Reed Dunnick and his committee did in putting together the record number of scientific exhibits. This year saw a large increase in the number of poster board exhibits, and further efforts will be made to encourage this exhibit format in future years. They were outstanding and showed that significant exhibits can be in a variety of formats.

Two major changes in the meeting schedule were attempted this year, and we are glad to report that both were successful. The first occurred on Sunday evening, when a welcoming reception for all registrants was held in the Grand Ballroom. This replaced the former Tuesday night event and was designed to be a true opening reception. Attendance was very high, and the catering staff at the hotel prepared a superb array of food and drink. The second change occurred on Monday morning. After the opening exercises and the installation of John Kirkpatrick as president of the ARRS for 1991–1992, the award papers were presented. This provided for a less crowded schedule on Wednesday, when the gold medals and the Caldwell Lecture were presented. During this Wednesday morning session, John Kirkpatrick, ARRS president, awarded the gold medal of the ARRS to three outstanding radiologists, Eugene Gedgaudas, Eugene Klatte, and Elias Theros. This session then concluded with the Caldwell Lecture, presented by N. Thorne Griscom.

The success of any meeting is the result of the hard work of many volunteers within the membership, and it is unfortunate that space does not permit listing them all by name. Even though that is not possible, those individuals deserve the thanks of all members and staff for their efforts. Their names are, however, listed in the program as committee members and faculty. Certain staff can be named more easily, as they are fewer in number. Certainly Susan Tevens and Cheryl Lancaster deserve my thanks for the year of hard work and attention to detail they provided. Rebecca Haines-Gardner for our publications and Sheila Aubin for on-site meeting management are critical to the meeting success as well. I thank them all.

The 1992 meeting, to be held in Orlando for the first time, promises to be another in a chain of successful meetings. Some unique events are being planned, and we know that this is one meeting you cannot afford to miss. All are invited to attend our 92nd meeting at the Marriott World Center in Orlando, FL, May 10–15, 1992. Why not plan to bring your families and spend some extra time visiting that "other" attraction in Orlando as well? We hope to see you there.

[1] American Roentgen Ray Society, 1891 Preston White Dr., Reston, VA 22091.

AJR **157:635, September 1991** 0361–803X/91/1573–0635 © American Roentgen Ray Society

ARRS Award-Winning Scientific Exhibits, 1991

More than 250 scientific exhibits were displayed at the ARRS 1991 meeting in Boston, MA. The Committee on Awards selected six medal winners and named 37 exhibits for certificates of merit.

Elsewhere in this issue are an application form and instructions for submitting scientific exhibits for the 1992 ARRS meeting in Orlando, FL, May 10–15.

Gold Medal Exhibit

Pneumothorax: a quantitative study using film screen and computed radiography. Carr JJ, Reed JC, Choplin RH, Pope TL Jr. (Winston-Salem, NC).

Measured increments of air were introduced into the right pleural space in three fresh cadavers. Two cadavers had aerated lungs; the third had diffuse air-space consolidations. Serial exams using both film screen and computed radiography were obtained with the cadavers in upright, supine, and left lateral decubitus positions. These studies are compared for pneumothorax detection. Lateral decubitus position is determined to be optimal for detecting minimal pneumothoraces (10 ml), whereas only large pneumothoraces (greater than 100 ml) are reliably identified on supine examinations. Results are compared with those obtained from selected patients in the intensive care unit.

Silver Medal Exhibits

Radiographic characterization of the colonic submucosal tumor. Kawamoto K, Motooka M, Hirata N, Kitagawa S, Masuda K (Fukuoka, Japan).

Findings on double contrast barium enema study in 89 patients with colonic submucosal tumors were compared with the endoscopic and pathologic findings in order to determine the characteristic features of each neoplasm. All tumors were histopathologically confirmed and included malignant lymphoma (21), carcinoid (20), lipoma (14), lymphangioma (10), leiomyosarcoma (6), leiomyoma (4), and others (14). The radiographic findings were classified into five groups. I: Wide-base sessile lesion with gradual sloping and smooth surface, II: wide-base sessile lesion with basal constriction and smooth surface (the surface may have a central depression), III: wide-base sessile lesion with lumpy or lobulated surface, IV: pedunculated or subpedunculated lesion, V: unclassified. The Group I was mainly seen in small lesions of various types of pathology. The Group II was commonly seen in carcinoid or myogenic tumor. The Group III was seen in lymphangioma and hemangioma. The Group IV was seen only in lipoma, lymphangioma, and hemangioma. Adding to this criteria, size, multiplicity, location and the existence of ulceration were also used for the evaluation of the characteristics of each tumor. We concluded that our criteria would be useful in evaluating submucosal tumors radiographically.

Color Doppler ultrasonography of the scrotum. Horstman WG, Middleton WD, Melson GL (St. Louis, MO).

Color Doppler sonography (CDS) is becoming increasingly important in the evaluation of scrotal disorders. This exhibit summarizes our experience with normal volunteers and over 600 patients with a variety of scrotal disorders.

Arterial flow should be detected in all normal testes. In a group of volunteers, centripetal and capsular arteries were visualized in 30/30 testes. These vessels always had a low-resistance waveform (RI .46 to .78, M = .64). Venous flow was seen only in the presence of transtesticular vessels (a normal variant seen in 10–20% of men). Testicular torsion manifests as complete absence or marked decrease in detectable testicular flow. In a series of 28 patients with acute scrotal pain prospectively evaluated with both CDS and scintigraphy, CDS correctly diagnosed 7/7 patients with torsion (100% sensitivity) while scintigraphy diagnosed 6/7 (86% sensitivity). CDS reliably and rapidly distinguished torsion from epididymoorchitis. A detailed analysis of the CDS findings in 51 cases of scrotal inflammation showed hypervascularity in all, detectable venous flow in 18 and decreased arterial RI in 20. In nine cases of epididymitis and eight cases of orchitis, the gray-scale images were normal and the hypervascularity displayed on CDS was the only indication of an inflammatory process. Testicular tumors, on the other hand, were just as easily identified on gray scale as on CDS. Of the 15 tumors seen to date, all <1.5 cm have been hypovascular and >1.5 cm have been hypervascular. Hypervascular tumors may be difficult to distinguish from focal orchitis, therefore, clinical correlation is crucial. Finally, varicoceles appear as peritesticular venous flow that augments with Valsalva and with upright positioning.

We conclude that CDS combines the advantages of both gray-scale sonography and testicular scintigraphy and therefore functions as an all-encompassing scrotal imaging technique.

Bronze Medal Exhibits

Imaging of pediatric ovarian lesions. Surratt JT, Siegel MJ (St. Louis, MO).

Ovarian masses are the most common cause of a genital mass in girls. This exhibit illustrates the sonographic appearances of ovarian lesions in 86 children and describes characteristics of these lesions that can allow a specific diagnosis to be made. The lesions include simple ovarian cysts (n = 16), teratomas (n = 16), hemorrhagic ovarian cysts (n = 11), torsed ovaries (n = 6), malignant ovarian neoplasms (n = 6), tuboovarian abscesses (n = 4), and ectopic pregnancies (n = 3). Useful features in diagnosis are thickness of the wall of the lesion, presence or absence of septa, mural nodule or fat-fluid level, cystic or solid contents, and presence or absence of abnormalities in adjacent organs. Correlation will be made with pathologic specimens and CT scans. Pitfalls in diagnoses also will be illustrated, included extraadnexal masses, such as abscesses, peritoneal fluid, or colonic duplications that may mimic ovarian lesions. Recognition of the normal and abnormal ovary should assist in the interpretation of the pelvic sonogram and CT scan in childhood.

Congenital anomalies of the branchial apparatus: embryology and pathologic anatomy. Benson MT, Dalen K, Mancuso A, Kerr HH, Cacciarelli AA, Mafee M (Royal Oak, MI).

Congenital anomalies of the branchial apparatus may present in a variety of ways, including cysts, sinuses, fistula, or ectopic gland. Both children and adults may be afflicted. These defects involve abnormal migration and incomplete degeneration and include branchial, thymic, and parathyroid anomalies. Using text and diagrams, the embryologic basis and classification systems are discussed. The pathologic anatomy is demonstrated by multiple imaging techniques, including CT, MR imaging, sonography, and fistulography. Understanding the varied radiographic appearances of congenital anomalies of the branchial apparatus is greatly aided by familiarity with their embryologic origins.

Interpretation of ultrasound properties of normal renal tissues in terms of microscopic anatomy. Insana MF, Hall TJ, Fishback JL, Rosenthal SJ, Cox GG, Garra BS (Kansas City, KS).

The echographic appearance of kidneys suggests that the ultrasonic properties vary significantly within normal renal tissues. Measurements and images of the speed of sound, attenuation and backscatter coefficients, and the average scatter size in excised kidneys demonstrate that renal corpuscles are the dominant scattering structure below 5 MHz. Above 5 MHz, the contribution from vessels and/or tubules increases, causing greater anisotropy in scattering and attenuation properties than that observed at lower frequencies. Correlations between ultrasonic properties and light microscopy are used to explain the echographic appearance of normal kidneys in terms of microscopic structure and to identify changes associated with disease.

Certificates of Merit Exhibits

Basal ganglia revisited: neuroimaging in 80 cases with clinical-pathologic correlation. Ho VP, Geyer CA, Ghaed VN, Miletich RS, Smirniotopoulos JG (Washington, DC).

Adhesive arachnoiditis of the spine: myelographic, CT and MR imaging features. Sutton CL, Phillips JG (Charlottesville, VA).

The developmental disorders of the thorax. Heitzman ER, Groskin SA, Randall PA, Katzenstein AL, Scalzetti EM (Syracuse, NY).

The emphysemas: imaging/pathologic features. Foster WL, Gimenez E, Roubidoux M, Sherrier R, Meyer A, Roggli V, Pratt P, Shannon R (Durham, NC).

Tumor recurrence in the postthoracotomy chest: anatomical concepts. Chasen MH, Dunnington JS, Libshitz HI, North LB, Freundlich IM (Houston, TX).

Sonographic image artifacts. Madrazo BL, Shirkhoda A, Hefner LV (Royal Oak, MI).

Color Doppler sonography of erectile dysfunction. Fitzgerald SW, Erickson SJ, Foley WD, Lawson TL, Lipchik EO (Chicago, IL).

Congenital anomalies of the kidney: embryology and radiologic correlation. Jafri SZH, Silva JM, Cacciarelli AA, Madrazo BL, Farah J, Roberts JL (Royal Oak, MI).

Gastrointestinal lymphoma. Smith C, Kubicka RA, Thomas CR Jr. (Chicago, IL).

Computed tomography of bowel wall thickening. Desai RK, Tagliabue JR, Einstein DM, Wegryn S (Cleveland, OH).

A multiplanar imaging atlas of the surgical hepatic segments. Colon E, Meyer CA, Branton P, Ghaed VN (Columbia, MD).

The early diagnosis of life-threatening conditions involving the pediatric chest. Jones JE, Sutton CL, Alford AB, McIlhenny J (Charlottesville, VA).

Traumatic osteolysis of the clavicle. Flood MJ, Moore TE, Robinson RA, Kathol MH, Yuh WTC, El-Khoury GY (Iowa City, IA).

Imaging of the spine in neurofibromatosis. Yaghmai I, Rooholamini SA, Kioumehr F (Sylmar, CA).

Differential MR features of acute and chronic anterior cruciate ligament tears. Broome DR, Kayes KJ, Vahey TN, Shelbourne KD (Indianapolis, IN).

Gd-DTPA-enhanced MRI of musculoskeletal tumors correlated to histology. Geirnaerdt MJA, Bloem JL, Eulderink F, Taminiau AHM (Leiden, The Netherlands).

Complications of total joint replacement. Quale JL, Murphey MD, Martin NL, Bramble JM (Kansas City, KS).

Abnormalities of the sacroiliac joint. Murphey MD, Bramble JM, Wetzel LH, McMillan JH, Batnitzky S (Kansas City, KS).

Radiologic assessment of bone grafting. Murphey MD, Sartoris DJ, Bramble JM (Kansas City, KS).

Percutaneous retrieval of intracardiac catheters and iatrogenic foreign bodies and unknotting of intracardiac catheter knots. Tisnado J, Prasad U, Wilkinson D, Freedman A, Shah S (Richmond, VA).

Technical problems associated with bird's nest vena cava filter placement. Vesely TM, Darcy MD, Hicks ME, Picus D (St. Louis, MO).

Complications of radiation therapy: CT evaluation. Fishman EK, Kuhlman JE (Baltimore, MD).

Clinical experience with a new laser alignment system for consistently high image quality in portable radiography. MacMahon H, Yasillo N, Carlin M (Chicago, IL).

MR imaging in the evaluation of pineal region tumors. Fletcher GP, Miller GM, Scheithauer B (Rochester, MN).

Atypical meningiomas. Buetow PC, Smirniotopoulos JG, Buetow MP (Washington, DC).

Portal vein: pitfalls and oddities. Scanlan KA, Walker D (Madison, WI).

Sonography of the musculoskeletal system. Matamoros A Jr., Anderson JC, Kaplan PA (Omaha, NE).

The natural history of posterior urethral valves in utero. Gilbert EK, Alford BA, Abbitt PL (Charlottesville, VA).

Visceral metastases from melanoma: findings on magnetic resonance imaging. Premkumar A, Sanders L, Marincola F, Feuerstein I, Concepcion R, Schwartzentruber D (Bethesda, MD).

Ultrasonographic anatomy of the left hepatic vein: the feasibility of the live related transplantation. Honda H, Yanaga K, Onitsuka H, Murakami J, Kaneko K, Masuda K (Fukuoka, Japan).

Radiographic and sonographic appearances of thoracic complications of extracorporeal membrane oxygenation (ECMO). Gross GW, Cullen J, Kornhauser MS, Wolfson PJ (Philadelphia, PA).

Computed tomography of the pediatric azygoesophageal recess. Fitzgerald SW, Miller FH, Donaldson JS (Chicago, IL).

Radiographic evaluation of lytic lesions in prehistoric North American Indians. Lichtman JB, Byrne RJ, Blakeley RL, Woodworth R, Varma VA (Atlanta, GA).

A correlative study of MRI, CT, US, and radiographic foreign body detection using an in-vitro turkey model. Shah ZR, Feiglin D, Crass JR, Cohen A, Bellon EM (Cleveland, OH).

Radiological follow-up of treated breast cancer. Cambier L, Kamus E, Cabaret V, Vilain MO (Lille, France).

Objective evaluation of the LGM vena cava filter: early results. Murphy TP, Dorfman GD (Providence, RI).

MR imaging in the presence of inferior vena cava filters. Watanabe AT, Gomes AS, Teitelbaum GP, Roehm JOF, Van Breda A (Los Angeles, CA).

American Roentgen Ray Society New Members

At the 1991 annual meeting of the American Roentgen Ray Society (ARRS) in Boston, 361 applicants were elected to active membership and 36 to international membership. Five hundred forty-five applicants were added to in-training membership during the year preceding the 1991 annual meeting.

Active members of the society must be graduates in good standing of an approved medical or osteopathic school or hold an advanced degree in one of the physical, chemical, or biologic sciences. They must be board certified, active in radiology or one of its branches in the United States or Canada, and sponsored by two ARRS members.

Members-in-training are physicians in a radiology residency or in a postresidency fellowship program.

International members are physicians residing in foreign countries who are active in the science of radiology or allied sciences.

An application form is printed elsewhere in this issue or may be obtained by writing: Paul Fullagar, Executive Director, American Roentgen Ray Society, 1891 Preston White Dr., Reston, VA 22091.

Active Members

William P. Abraham, Monument, CO
Robert H. Ackerman, Boston, MA
Richard A. Ahlstrand, Wichita, KS
E. William Akins, Gainesville, FL
Lino M. Alcasid, Manasquan, NJ
Syed I. Ali, Akron, OH
Jeffrey C. Allard, Miami, FL
Daniel J. Alves, Punta Gorda Isles, FL
Quentin N. Anderson, Golden Valley, MN
Robert C. Andrews, Ogdensburg, NY
Gregory R. Applegate, Pittsburgh, PA
M. Julie Armada, Providence, RI
Thomas L. Arntson, Corona, CA
Farhad Azimi, Fayetteville, NY
Richard J. Bagby, Winter Park, FL
Stewart R. Bakst, Hialeah, FL
Richard S. Bakulski, Andover, MA
Raymond L. Baraldi, Jr., Newtown Square, PA
Robert L. Basista, Alliance, OH
Javier Beltran, Columbus, OH
Matthew J. Bennett, Frederick, MD
Diane K. Bergau, Miami Shores, FL
Howard L. Berman, Chappaqua, NY
William C. Black, Bethesda, MD
Jon J. Bleicher, Council Bluffs, IA
Rano S. Bofill, Man, WV
Mayola C. Walters Boykin, San Antonio, TX
Robert A. Breit, Chicago, IL
G. William Bretz, Dayton, OH
A. Bart Bristow, Kansas City, MO
Bruce Brown, Iowa City, IA
Stephen R. Brown, Severna Park, MD
Michael C. Brunner, Chicago, IL
Kenneth A. Buckwalter, Indianapolis, IN
Michael L. Burke, Albany, NY
Omer L. Burnett, Jr., Tucker, GA
Ted L. Carelock, Garland, TX
Pilar A. Caro, Ardmore, PA
Lynn N. Carlton, Springfield, MO
Walter A. Carpenter, Atlanta, GA
Mark Joseph Carvlin, Washington, DC
William M. Chae, Grosse Pointe Woods, MI
Freydoun Fred Chaffa, Barrington, RI
Gregory Chaljub, Galveston, TX
Evan F. Chambers, Miami, FL
Vijay P. Chandnani, Los Angeles, CA
Paul J. Chang, Iowa City, IA
Dale A. Charletta, Lisle, IL
Riffat R. Chaudary, Belle Mead, NJ
Pauline Woon Lin Chee, Ann Arbor, MI
Elsie Cintron, Rio Piedras, PR
Richard J. Claps, Randolph, NJ
Ramona R. Clark, Santa Barbara, CA
Timothy G. Cloonan, Glendale, AZ
Gilbert H. Cohen, Hollywood, FL
Andrew John Collins, Chapel Hill, NC
Mark B. Collins, Voorheesville, NY
Farhad M. Contractor, Pittsburgh, PA
William F. Conway, Charlottesville, VA
Cirrelda J. Cooper, Great Falls, VA
John L. Cowan, Louisville, KY
William R. Cranley, Wakefield, MA
Philip E. Cranston, Jackson, MS
Jeffrey B. Cutler, Atlanta, GA
Pamela S. Darr, Crowley, LA
Sidney M. Dashefsky, Winnipeg, Man., Canada
Lawrence P. Davis, Detroit, MI
Mark C. Davis, Groton, MA
William John Davros, Washington, DC
John K. Dedic, Burley, ID
Carolyn G. Dedrick, Lexington, MA
A. Chris Degner, Midwest City, OK
Theresa A. DeMarco, Carmichael, CA
Janice J. Dieschbourg, Glenview, IL
Robert A. Duke, Germantown, TN
Fred H. Dunn, Dallas, TX
Michael E. Edwards, Nashville, TN
Howard B. Eisen, Pittsburgh, PA
Brian A. Ellman, Dallas, TX
Scott J. Erickson, Waukesha, WI
Nahid Eshaghi, De Soto, TX
Carl E. Fabian, Miami Shores, FL
Lucia G. Fellows, Burlington, MA
Robert B. Finegold, Novato, CA
Charles F. Fisher, Harlingen, TX
Kendall W. Foster, Jr., East Lansing, MI
Eliot Freeman, Princeton, NJ
Ramon J. Garcia, Port Neches, TX
Michael C. Garovich, Sullivan's Island, SC
Ronald C. Gay, Fayetteville, NC
Jacob M. Gerend, Sheboygan, WI
Mark S. Girson, Dallas, TX
Lori B. Goffner, Long Beach, NY
Liba E. Goldblum, Baltimore, MD
Jacqueline S. Gomberg, Bala Cynwyd, PA
Eduardo R. Gomez, Miami, FL
Philip Goodman, Galveston, TX
William A. Goodrich, Jr., Baytown, TX
Robert E. Gordon, Tyler, TX
Cheryl H. Grandone, Calverton, NY
Suzanne H. Granger, Omaha, NE
David J. Gulliver, Durham, NC
Sudhir B. Guthikonda, Fulton, NY
David B. Handel, Margate, NJ
Anthony J. Hayden, West Newbury, MA
Curtis W. Hayes, Midlothian, VA
Dennis K. Heaston, Provo, UT
Robert W. Henderson, Altadena, CA
Alan Herschman, East Brunswick, NJ
Michael S. Hertzog, Signal Mountain, TN
David C. Hillman, Sevierville, TN
Thomas F. Hirsch, Portland, OR
Ashok B. Jain, Wayne, MI
Nora A. Janjan, Milwaukee, WI
John Oliver Johnson, La Jolla, CA
Gary C. Jones, Hopkinsville, KY
Kenneth E. Jones, Clinton, MO
Louis I. Juravsky, Etna, NH
Paulomi K. Kanzaria, Worcester, MA
Kisan Y. Karapurkar, Dover, DE
Brian Karr, New Orleans, LA
Thomas A. Kavic, Sewickley, PA
Ruben Kier, Orange, CT
Randolph J. Knific, Fort Myers, FL
Phyllis Joy Kornguth, Durham, NC
Charles F. Krecke, East Lansing, MI
John D. Kreinces, Key West, FL
Douglas S. Kuehn, Granger, IN
Sevil J. Kursunoglu, San Diego, CA
Peeler G. Lacey, Laurel, MS
Robert E. Lambiase, East Greenwich, RI
Neela Lamki, Houston, TX
Gary Karnosh Lammert, Cleveland, OH
Stanley P. Laucks, Jr., Red Lion, PA
Thomas A. Layne, Missoula, MT
Clifford S. Levi, Winnipeg, Man., Canada
Laura Liberman, New York, NY
Alexander Ling, Bethesda, MD
Barbara P. Luke, Scarborough, ME
Charles R. Luttenton, Grand Rapids, MI
Robert Maietta, Burlington, MA
B. J. Manaster, Salt Lake City, UT
Daniel M. Marder, Silver Spring, MD
Kenneth L. Margeson, Maitland, FL
David M. Markowitz, New Haven, CT
David S. Martin, St. Louis, MO
Kenneth W. Matasar, Royal Oak, MI
Sam M. Mayerfield, Woodcliff Lake, NJ
C. Douglas Maynard, Winston-Salem, NC
Dennis J. McCabe, Potomac, MD
John C. McDermott, Madison, WI
Mary H. L. McJunkin, Charleston, WV
Todd A. Meister, Baltimore, MD
David S. Mendelson, Scarsdale, NY
Gaston Mendez, Jr., Fort Lauderdale, FL
Timothy J. Micklos, Salt Lake City, UT
Linda M. Miketic, Pittsburgh, PA
Arthur R. Miller, Miami Shores, FL
Barbara Hoeck Miller, Rockville, MD
J. Thomas Miller, Ann Arbor, MI

Leslie Scott Miller, Louisville, KY
Susan Minker, Tucson, AZ
Julie S. Mitnick, New York, NY
Paul L. Molina, Jr., St. Louis, MO
Robert J. Morales, New Orleans, LA
Helen R. Nadel, Vancouver, B.C. Canada
Scott N. Nadel, Chapel Hill, NC
Lawrence M. Neustadter, Voorhees, NJ
Anna R. Nussbaum-Blask, Washington, DC
Gary H. Omell, St. Louis, MO
David A. Oppenheimer, Boulder, CO
John Randolph Osborne, Colorado Springs, CO
Donald D. Owens, Memphis, TN
Chris L. Palaskas, Minnetonka, MN
Edwin L. Palmer III, Lexington, MA
Harriet Joan Paltiel, Cincinnati, OH
Susan M. Pang, Toronto, Ont., Canada
Suman A. Patel, Danielson, CT
Joel F. Platt, Novi, MI
David L. Pohl, St. Louis, MO
Abraham H. Pollack, Brooklyn, NY
Edward K. Poole, Austin, TX
Kevin L. Pope, Fayetteville, AR
Albert R. Porter, Harrisburg, PA
Roy K. Poth, El Paso, TX
Jay J. Protass, Oakland, CA
James M. Quigley, Tampa, FL
Louis E. Rambler, Woodcliff Lake, NJ
Danny C. Rappaport, Gainesville, FL
John D. Rauth, Jr., Wayne, PA
Jonathan G. Reed, Galveston, TX
Steven H. Reid, Greensboro, NC
Laurence Evan Reitman, Plantation, FL
Donald L. Renfrew, Iowa City, IA
Fred W. Riley, Jr., San Antonio, TX
Joseph R. Robbins, Texarkana, TX
Sanford I. Robbins, North Miami Beach, FL
Justo Rodriguez, River Forest, IL
Seyed A. Rooholamini, Sylmar, CA
Norman S. Rosenthal, Burke, VA
Michelle D. Rossmann, Bayside, NY
Thomas D. Rothstein, North Miami Beach, FL
Brian A. Rovira, Olympic Valley, CA
Alla Rozenblit, Eastchester, NY
Marilyn Goske Rudick, Cleveland, OH
Samy F. Saleeb, Mobile, AL
Barbara Heintz Savader, Baltimore, MD
Bernard Schneider, Syracuse, NY
Marlene J. Severson, Fargo, ND
Lalitha Shankar, Islington, Ont., Canada
Robert S. Shapiro, Brooklyn, NY
Jerome J. Sheldon, Miami, FL
Arthur B. Sher, Miami, FL
Ronald C. Sherowsky, Bowling Green, KY
Welland Osborn Short, Tucson, AZ
Anne Adair Singer, Pepper Pike, OH
Chris L. Sistrom, Charlottesville, VA
Carlos J. Sivit, Vienna, VA
Bruce D. Smith, Shaker Heights, OH
Grover R. Smith, Jr., Nashville, TN
Indukumar M. Solanki, Olean, NY
Rhonda R. Stewart, Arlington, VA
Norman A. Stokes, Miami, FL
Janet L. Strife, Cincinnati, OH
Ross T. Sutton, Rochester, MN
Helene M. Tanous, Galveston, TX
Sharlene A. Teefey, Seattle, WA
Jamshid Tehranzadeh, Irvine, CA
Paul W. Templeton, Bethesda, MD
Jeffrey L. Thomasson, St. Louis, MO
Gladys Torres, San Juan, PR
Diane M. Twickler, Dallas, TX
Wenzel G. Vas, St. Louis, MO
Prasad C. Vasireddy, Jacksonville, IL
Thomas J. Vaughan, Lexington, KY
Gregory N. Viscomi, Guilford, CT
Alfred B. Watson, Jr., Sugarland, TX
Mark R. Wax, Hauppauge, NY
Phillip H. Weiss, Moreland Hills, OH
Mitchell S. Whiteman, North Miami Beach, FL
Dennis M. Wilcox, Leawood, KS
Howard R. Wilkov, Fort Lauderdale, FL
Deborah A. Willard, Morgantown, WV
Kathryn J. Wimbish, Birmingham, MI
Merrill K. Winderman, Long Beach, CA
Bernard A. Wirth, Richmond, VA
Robert J. Wittchow, Farmington Hills, MI
Ray M. Woodlief, Richmond, VA
Jules S. Yavil, Merion Station, PA
Duane A. Young, Los Angeles, CA
Jeremy W. R. Young, Baltimore, MD
Solomon G. Zerden, Savannah, GA
Daniel L. Zinn, Brooklyn, NY
Michael Zucker, Los Angeles, CA
Gary S. Zwicky, Peoria, IL
Anatol Zynamon, Ann Arbor, MI

Active Members (Formerly In-Training)

Victor A. Aletich, Gaithersburg, MD
Daniel R. Alzheimer, Great Falls, MT
Stuart A. Aronson, Mount Pleasant, SC
Cheryl J. Avanzato, Bronx, NY
Neil Baron, Windermere, FL
William W. Beckett, Jr., Savannah, GA
Jeffrey R. Bessette, Fort Wayne, IN
James Richard Bognanno, Indianapolis, IN
David J. Brandt, Atlanta, GA
Robert Breger, Brookfield, WI
Andrew D. Bronstein, Bellevue, WA
DeNaye D. Brown, Bowie, MD
Diane K. Brown, Bosier City, LA
Kathleen V. Caldwell, Redlands, CA
Jimmy D. Cardoza, Piedmont, CA
Anne Marie Casey, Fairfax, VA
Patricia E. Cole, New York, NY
Robert R. Conti, Vero Beach, FL
Stanley G. Cooper, Teaneck, NJ
Charles Eugene Cordell, Jr., Mt. Holly, NJ
Norman L. Crocker, Akron, Oh
John Della Badia, Dobbs Ferry, NY
James Kevin DeMarco, Oakland, CA
Roland D. DeMarco, Carmichael, CA
James Denier, Chillicothe, OH
G. Michael Dwyer, Livonia, MI
Karen O. Ehrman, Indianapolis, IN
Angela J. Feyerabend, Denver, CO
Maurice Frank Finnegan, Jr., Peoria, IL
Gregory Scott Foster, Chicago, IL
Thomas W. Free, Sioux Falls, SD
James T. Friedland, Indialantic, FL
Douglas Gardner, Tecumseh, Ont., Canada
John Witherspoon Gilpin, Greenville, SC
Mark C. Glass-Royal, Potomac, MD
Roy Gottlieb, Bethesda, MD
Beth Gross, Jamaica, NY
Robert C. Guay, Jr., Stratford, CT
Lincoln H. Gundersen, LaCrosse, WI
Karen L. Harkens, Fairfield, IA
Curtis L. Harlow, Denver, CO
Jon T. Harman, Indianapolis, IN
Donald A. Harper, FPO Seattle, WA
Connie D. Harrill, Carmel, IN
Lois A. Johnson, Portland, OR
Allen E. Joseph, San Antonio, TX
Rebecca Smith Kennedy, Carrboro, NC
Mitchell A. Klein, Brookfield, WI
Bernard A. Landry, New Orleans, LA
Joseph John Lawrence, Monument, CO
Albert Chun-Jen Lee, Rancho Palos Verdes, CA
Bruce Jay Lehrman, Philadelphia, PA
Marilyn E. Lerner, Riverdale, NY
Robert Michael Liddell, Seattle, WA
Daniel J. Loes, Iowa City, IA
Timothy John Lucas, Mason City, IA
Jeff E. Magnuson, St. Paul, MN
Paul C. Marinelli, Hagerstown, MD
Michael A. Marks, Dunn Loring, VA
Judith C. McGregor, Hickory, NC
Scott A. Mirowitz, St. Louis, MO
Julie K. Mitby, Madison, WI
Lee H. Monsein, Baltimore, MD
Debra L. Monticciolo, Chicago, IL
William David Murphy, Canton, OH
Eduardo M. Nijensohn, Chicago, IL
Richard A. Oria, Houston, TX
Patrick M. O'Toole, Overland Park, KS
Ann Owen, Murfreesboro, TN
John Panaccione, Jacksonville, FL
Robert B. Poliner, Las Vegas, NV
Grant J. Price, Bridgewater, NJ
Yves Y. P. Provost, Arthabaska, Que., Canada
Marc B. Renner, Chelsea, MI
Richard E. Rosenthal, Philadelphia, PA
Gerald Joseph Ross, Philadelphia, PA
Craig G. Rowell, Richmond, VA
Richard F. Rowley, Schenectady, NY
Daniel George Rupley, Baton Rouge, LA
Hajime Sakuma, Mie, Japan
William E. Shiels, Columbia, MD
Anne Marie Shorter, Toronto, Ont., Canada
Gary Michael Smith, Tampa, FL
Stephen M. Smith, Peoria, IL
Nina Soberman, New York, NY
Steven C. Sotile, Baton Rouge, LA
Paul E. Sylvan, Madison, CT
Richard Alexander Szucs, Richmond, VA
Steven J. Taggart, Escondido, CA
James Tagliabue, Highland Heights, OH
Danny S. Tenaschuk, Windsor, Ont., Canada
Wendy Thurston, Toronto, Ont., Canada
Kenneth Tidwell, Jr., Jonesboro, AR
Steven Robert Urbanski, Weatogue, CT
Connie Mitchell Vail, Salt Lake City, UT
Venetia Green Vassiliades, Ann Arbor, MI
Nancy A. T. Wadden, Thornhill, Ont., Canada
Harold S. Walker, Palm Springs, CA
Ivy Warsinski, St. Louis, MO
Larry Ketner West, Little River, SC
Michele S. West, Lutherville, MD
Paula J. Woodward, San Antonio, TX
Robert Worthington-Kirsch, Overbrook Hills, PA

International Members

Yasser A. Abbas, Cairo, Egypt
Peter B. Andersen, Uppsala, Sweden
Jordi S. Andreu, Barcelona, Spain
Francisco J. Avelar, Juarez, Mexico
Sanjay Saran Baijal, Lucknow, India
Leonard Bank, Sydney, Australia
John B. Bingham, London, England
John Chandy, Coventry, England
Albert de Roos, Heemstede, The Netherlands
Zeki Dogan, Istanbul, Turkey
Luis Donoso-Bach, Barcelona, Spain
Alfred Gabmeyer, Eisenstadt, Austria
Joseph Fotsin Gonsu, Yaounde, Cameroon
Eriu J. Haanraadts, Amsterdam, The Netherlands
Joon Koo Han, Seoul, Korea
Man Chung Han, Seoul, Korea
Peter M. Huisman, Amsterdam, The Netherlands
Jung-Gi Im, Seoul, Korea
Kenji Kachi, San Francisco, CA
Tatsumi Kaji, Kawasaki, Japan
Seung H. Kim, Seoul, Korea
Han Joon Koo, Seoul, Korea
Kedia Shankar Lal, Calcutta, India
Antonio Martinez-Noguera, Barcelona, Spain
Kiyoshi Murata, Shiga, Japan
Hiroshi Nishimaki, Kanagawa, Japan
Carmen M. Perez, Barcelona, Spain
Beat Porcellini, Bern, Switzerland
Sheila C. Rankin, Bickley, England
John F. Ratcliffe, Brisbane, Australia
Luis H. Ros, Zaragoza, Spain
Kazuro Sugimura, Izumo, Japan
Hans P. M. Van Heesewijk, Huizen, The Netherlands
Seong-Ku Woo, Chungky Taegu, Korea
Toshio Yamaguchi, Kawasaki, Japan
Motahare Zhianpour, Kerman, Iran

Information and Application for Membership in the American Roentgen Ray Society

General Information

The American Roentgen Ray Society, founded in 1900, has been a forum for progress in radiology since shortly after the discovery of X-rays. From its beginning and continuing to today, the ARRS has been guided by dedication to the goal of the advancement of medicine through the science of radiology and its allied sciences.

The goal of the ARRS is maintained through an annual scientific and educational meeting, and through publication of the *American Journal of Roentgenology*.

The annual meeting consists of instructional courses, scientific sessions, a symposium, scientific exhibits, and commercial exhibits. A special categorical course is also offered. Category I CME credits are available on an hour-for-hour basis.

The monthly *American Journal of Roentgenology* is a highly respected peer review journal with a worldwide subscription base. For over 75 years the *AJR* has been accepted as one of the best specialty journals available in the world, and this reputation grows each month.

A recently developed quarterly ARRS newsletter keeps members informed of events and general Society news.

Application Instructions

Candidates for Active Membership

1. An Active member must be a graduate of an approved medical school or hold an advanced degree in one of the physical, chemical or biological sciences and be certified by the American Board of Radiology, the American Osteopathic Board of Radiology, the Royal College of Physicians of Canada, or document training and credentials that are adequate to qualify for membership. Active members shall actively practice radiology or one of its branches in the United States or Canada. Such members are eligible to participate in all activities of the Society, including membership on committees, and have full voting privileges.
2. Application must be on an official form, signed by the applicant and at least two members of the American Roentgen Ray Society, active or emeritus, in good standing, who endorse the applicant.
3. Application fee is $50 (payable when billed for dues).
4. Annual dues are $150, payable on January 1 of each year following the initial year. First year dues will be invoiced following candidate election at the annual meeting. Of this amount, $50 is for a 1-year subscription to the *American Journal of Roentgenology*, beginning with the July issue following election to membership.
5. Application must be received by February 1 for action during the current year's meeting.

Candidates for In-Training Membership

1. In-training members must be serving in a radiology residency program approved by the Radiology Residency Review Committee, the American Osteopathic Board of Radiology, or the Royal College of Physicians of Canada, or in an approved post-residency fellowship, or be a postgraduate student in an allied science. Training status must be verified by the program director. In-training members have special consideration in fees and subscription rates to the Society journal. Such members cannot hold Society offices or vote.
2. Application must be on an official form and signed by the applicant and by the applicant's training or residency program director.
3. In-training status is limited to a maximum of five years starting with the entrance date into the radiology residency. In the last year, each in-training member will receive an application for active membership from the Society. Those who do not apply for transfer to active membership shall be dropped from membership at the end of the fifth year, but can later apply as a new member through the process outlined for active status.
4. There is no application fee. Annual dues are $25. Membership includes a subscription to the *American Journal of Roentgenology* and admission to the annual meeting without payment of the registration fee.
5. Membership applications will be acted on when received.

International Membership

An international member must meet the qualifications of active membership, but reside and practice in a foreign country. International members shall pay dues and fees, but shall not have the privileges of voting nor of holding elective office.

All Applicants

1. **Do not remit application fee or dues until requested.**
2. **Send completed forms to: American Roentgen Ray Society**
   1891 Preston White Drive
   Reston, Virginia 22091

For ARRS Office Use

Date Rec'd _____

I.D.# _____

AMERICAN ROENTGEN RAY SOCIETY APPLICATION FOR MEMBERSHIP

Date: _____

Category of Membership: (Check One)
- ☐ Active
- ☐ International
- ☐ In-Training

Name (Please Print) _____ Degree(s) _____
First Initial Last

Mailing Address _____ Date of Birth _____
Street/Box

_____ Telephone ( ) _____
City/State/Country Zip Code

A. Education: (List name of institution, years attended, and degree and type received.)

Undergraduate: _____

_____

Graduate (Medical School, Graduate School, etc.):

_____

_____

Postgraduate (Internship, Residency, Fellowship, etc.):

_____

_____

_____

B. Licensure:

Licensed to practice _____ in _____ since _____
(Type) (State, Province, etc.)

C. Appointments/Memberships: (In-Training applicants: skip to Section F on reverse.)

Present Appointments: Academic _____

_____

Hospitals _____

_____

Memberships in Scientific Societies: _____

_____

Offices or Committee Assignments: _____

_____

Government Service (Military or Civilian) _____
(Position) (Years)

Continued on Reverse Side

D. Credentials:

(To be completed by Active and International applicants only.)

I hereby certify that I was issued a certificate of qualification in _____ (Specialty)

in _____ (Year) by the _____ (Name of Qualifying Board)

Other Credentials: _____

Signature: _____

E. References:

(To be completed by Active and International applicants only.)

We, active or emeritus members in good standing of the American Roentgen Ray Society, and acquainted with the applicant, do recommend him/her for membership in the Society. (Two references are required.)

Name (Please Print) 1. _____ 2. _____

Address _____ _____

_____ _____

Signatures: _____ _____

F. IN-TRAINING APPLICANTS MUST COMPLETE THIS SECTION

Credentials:

I certify that I am serving as a Resident/Fellow in _____ (Specialty)

at _____ (Name of Institution). Date program began (begins): _____;

date program to end: _____. I understand that in-training membership is limited to a maximum of 5 years.

Applicant Signature: _____

Verification: (Program Director or Department Chairman *only*)

I certify that the applicant is in training at the institution named and qualifies for enrollment as a member-in-training of the American Roentgen Ray Society.

Name (Please Print) _____

Address: _____

_____

Signature _____

Send completed form to: **American Roentgen Ray Society**
1891 Preston White Drive
Reston, Virginia 22091

Letters

Effective Audiovisual Presentation: Proper Citation of Sources

I was particularly surprised to note that my name did not appear in the Suggested Readings (or bibliography) included in the recent *AJR* article: "Effective Audiovisual Presentation" [1] by Drs. Sagel and Ramsey. The reason for my surprise lies in the fact that no small part of their manuscript consists of blatant plagiarisms taken verbatim or nearly so from my article "One Dozen Ways to Upgrade Your Next Radiologic Presentation" [2] published in 1988.

I enclose a copy of my paper for your reference and two pages of side-by-side "snips" from the two articles which will serve as examples of some of the material "lifted" from my paper without permission or citation.

I am confident you played no knowing role in the matter. I am also confident you will address this issue with the seriousness it deserves because the radiological community will use your response as a measure of how much tolerance you and *AJR* have for intellectual dishonesty and common theft.

Jerome J. Cunningham
The Ohio State University, University Hospitals
Columbus, OH 43210-1228

REFERENCES

1. Sagel SS, Ramsey RG. Effective audiovisual presentation (perspective). *AJR* **1991**;156:181–187
2. Cunningham JJ. One dozen ways to upgrade your next radiologic presentation. *Clear Images* October **1988**;2(4):20–24

Reply

I am responding to the letter from Dr. J. J. Cunningham that some material in our recently published article [1] was taken directly without proper citation from an article he previously published [2]. Although Ruth G. Ramsey is a coauthor of our publication, I wrote the sections of the manuscript under question, and assume full responsibility for the problem. I acknowledge that in several instances Dr. Cunningham's article surely was the source of some cogent phrases and anecdotes used to emphasize potential pitfalls in making audiovisual presentations. He legitimately objects to borrowing without citation and I apologize for not appropriately referencing his article and appreciate the opportunity to correct this omission. I would like to assure the reader that this oversight was related to the unique genesis of my message and flawed behavior in not carefully documenting the source of many of my lecture notes, rather than any deliberate effort to deceive and deprive him of proper credit.

The substance of my contribution to our article goes back more than 10 years before October 1988. Sometime in the late 1970s, I began giving an annual presentation to our residents on this subject. Similar presentations were given to several other academic radiology departments beginning in June 1984. Subsequently, this information was developed into an annual Refresher Course at the Radiological Society of North America given in conjunction with Dr. Ramsey starting in November 1988. Myriad enhancements since about 1978 have occurred to the basic talk. Numerous colleagues and residents, both here and at other institutions, have offered me suggestions, articles, and even books on this topic. Also, I have attended many sessions at national radiologic meetings, as well as a symposium sponsored by Kodak, which addressed proper slide technique and optimal presentation of radiologic material. Valuable information was excerpted and incorporated onto slides for my own lecture. Such informational slide notes, while not shown in the actual lecture, served as valuable reminders of specific ideas and anecdotes during the preparation process. Unfortunately, I never systematically recorded the source of these recommendations onto my slides.

I am almost certain that Dr. Cunningham's published article from October 1988 was originally shown to me by one of our senior residents, who I believe commented at the time on the remarkable similarity of our advice to residents needing to prepare and deliver an audiovisual presentation. Undoubtedly, I was impressed with his lucid phraseology, analogies, and anecdotes, and incorporated some comments directly into my own slide material, again without carefully noting its origin. The article then either was discarded or returned. It never occurred to me to include it in my reference file as few would be able to locate the controlled circulation journal *Clear Images*, and it contained no references; and at the time, I had no intention of publishing an article for which precise attribution would be required.

Our paper was written to convey the advice and admonitions Dr. Ramsey and I had been delivering in lectures to residents and staff for many, many years. To assemble my contribution to our solicited article, I initially reviewed all of my slides and transposed their content into my original rough draft. Then I reviewed my reference file, added more information, and finally searched in the *Index Medicus* for the last 10 years to identify original sources analogous to the usual scientific article I would write. I would like to emphasize that when this literature search was conducted, no article from *Clear Images* ever appeared. With the passage of time and after repeatedly talking about this subject, I was confused about what contentions and phrases had been "borrowed" from others, and which had been my own creation. To my chagrin, even on some controversial points, I was unable to identify references for many of the guidelines. Since the material was intended purely as advice, and no innovative claim for these concepts was intended, the text was not footnoted with specific citations and a short list of "suggested reading" simply was appended to the article. While potentially controversial, I would con-

tend that the rules for effective audiovisual presentation are largely common sense, well accepted, and familiar to many experienced lecturers, and almost all have been published previously in some form.

My sloppy behavior in not scrupulously labeling the sources of material incorporated into my lectures should not be condoned. I intend to be more meticulous in detailing the origin of information in the future. I sincerely regret having offended Dr. Cunningham.

Stuart S. Sagel
Washington University School of Medicine
St. Louis, MO 63110

REFERENCES

1. Sagel SS, Ramsey RG. Effective audiovisual presentation (perspective). *AJR* **1991**;156:181–187
2. Cunningham JJ. One dozen ways to upgrade your next radiologic presentation. *Clear Images* October **1988**;2(4):20–24

Sonography for Mediastinal Lymphoma

The recent article by Wernecke et al. [1] concludes that sonography is "comparable to CT for monitoring patients with mediastinal lymphomas." These authors found that "in all five cases showing discrepancies between sonographic and CT findings, further follow-up indicated that the information obtained at sonography correlated more closely with the clinical outcome" and that "the qualitative criterion (echogenicity) it offers may be a more reliable indicator for vital tumor tissue or clinical outcome than the quantitative criterion (lymph node size) obtained with CT."

I was surprised by the conclusions of this article and confused by its message. The research was done in West Germany, where sonography is apparently more readily available than CT. It is also less expensive. However, in comparison with CT, mediastinal sonography would seem to be more labor and physician intensive, more operator dependent, more difficult to compare with previous and subsequent examinations, and less useful for assessment of certain areas.

Are Wernecke and colleagues describing a useful diagnostic examination of the future, or is the sonographic assessment of mediastinal lymphoma passé on arrival? Is mediastinal sonography being performed for the assessment of lymphoma in the United States? If not, is this because of a presumed lack of accuracy or because CT is readily available? Does esophageal sonography have any role in the assessment of mediastinal lymphoma?

Ferris M. Hall
Beth Israel Hospital
Harvard Medical School
Boston, MA 02215

REFERENCE

1. Wernecke K, Vassallo P, Hoffmann G, et al. Value of sonography in monitoring the therapeutic response of mediastinal lymphoma: comparison with chest radiography and CT. *AJR* **1991**;156:265–272

Reply

We are grateful for Dr. Hall's comments, because they are the first published reaction to our efforts to establish mediastinal sonography as a useful and accurate imaging technique. CT is not much less available in West Germany than it is in the United States. The reasons we perform mediastinal sonography on lymphoma patients even though the technique is more physician intensive and more operator dependent than CT, are the following: (1) Sonography is less expensive than CT. (2) Sonography can detect mediastinal lymphomas with a sufficiently high sensitivity [1]. (3) Sonography is suited for follow-up examinations because of the standardized and reproducible section planes (clearly defined by the narrow size of the acoustic window and mediastinal vessels) [2, 3]. (4) The qualitative criterion (echogenicity) of sonography may be a more reliable indicator for vital tumor tissue or clinical outcome than the quantitative criterion (lymph node size) obtained with CT [2, 3].

One of the main arguments against using mediastinal sonography in lymphoma patients is that sonography is not particularly useful for the assessment of certain areas (subcarinal region, posterior mediastinum, paravertebral region, pulmonary hila and parenchyma, and bone structures). In this respect, CT has an undisputed advantage. The role of mediastinal sonography is not to compete with CT but to be an additional diagnostic method (besides conventional radiography) and therefore reduce the number of CT examinations. In newly diagnosed Hodgkin disease, the superior mediastinal nodes (all nodes of the supraaortic, prevascular, and paratracheal lymph node chains) are involved in 98% of patients with thoracic disease [4]. The sensitivity of sonography in these mediastinal regions (98%, 92%, and 89%) is almost equal to that of CT [1]. Only one of 203 patients with newly diagnosed Hodgkin disease in the series of Castellino et al. [4] had isolated involvement of paravertebral lymph nodes (without concomitant involvement of the superior mediastinal lymph nodes), which could not be assessed by sonography. In our series, we did not miss any mediastinal manifestation of newly diagnosed Hodgkin disease at sonography, but we did miss some mediastinal lymphomas in those regions that are more difficult to assess with sonography. Nevertheless, all lymph nodes undetected by sonography showed a therapeutic response identical to that of those detected and monitored with sonography [2, 3]. One advantage of sonography over CT is that sonography may provide information about vital tumor tissue irrespective of the size of the mediastinal lymph nodes. Sonography can be used to detect lymphomatous involvement of nonenlarged mediastinal lymph nodes [2, 3]. Furthermore, it seems that sonography can be used to differentiate accurately between scar tissue and residual vital tumor [2, 3]. However, further studies with larger groups of patients are necessary to validate these observations.

Mediastinal sonography has substantially improved the radiologic follow-up of lymphoma patients at our hospital. Sonography can be performed in addition to chest radiography in routine follow-up every 3–6 months after therapy. With this protocol, we were able to detect mediastinal recurrence in four patients in 1990 at a very early stage (mediastinal lymphomas 0.8–2.0 cm in diameter).

In our opinion, the main limitation of mediastinal sonography in both West Germany and the United States is not the lack of accuracy but the lack of training and experience in this examination. Mediastinal sonography, although performed since 1984 at our institution, is a relatively new technique and at a stage comparable with that of abdominal sonography in the late 1970s. We are aware of these training problems, but we hope that other institutions will be convinced of the diagnostic efficacy and practicability of this new technique. Mediastinal sonography should not be seen as an exotic tool implemented by some specialized sonographers, but as a widely available and accurate imaging method, when training problems are overcome.

Karl Wernecke
Pierre Vassallo
Peter E. Peters
University of Muenster Medical School
4400 Muenster, Germany

REFERENCES

1. Wernecke K, Vassallo P, Pötter R, Lückener HG, Peters PE. Mediastinal sonography: sensitivity of detection with sonography compared with CT and radiography. *Radiology* **1990**;175:137–143
2. Wernecke K, Vassallo P, Hoffmann G, et al. Value of sonography in monitoring the therapeutic response of mediastinal lymphoma: comparison with chest radiography and CT. *AJR* **1991**;156:265–272
3. Wernecke K. *Mediastinal sonography: examination technique, diagnostic efficiency and value in diagnostic imaging of the mediastinum.* New York: Springer-Verlag, **1991**
4. Castellino RA, Blank N, Hoppe RT, Cho C. Hodgkin disease: contributions of chest CT in the initial staging evaluation. *Radiology* **1986**;160:603–605

Inappropriate Use of Significant Figures

Many of the numerical values stated at radiology meetings and published in the radiologic literature contain too many significant figures. The use of these "extra digits" implies a level of accuracy of these results that is unjustified.

The convention of using significant figures is the practice of rounding off an experimental result so that it contains only the digits of known certainty plus the first uncertain digit [1, 2]. When readings are taken that involve estimation or interpolation, the estimated or interpolated digits are always conceded to be uncertain.

Rules for measured and calculated numerical values can be found in the chapters referenced [1, 2] and can be summarized as follows:

Leading zeros are not significant. For example, 3.1415 and 0.0031415 both are significant to five figures.

Zeros bounded on the right and left by nonzero digits are significant. For example, 6123 and 6003 are both significant to four figures.

The convention of using significant figures is ambiguous when zeros are bounded by digits on the left side only. For example, 200 ml can be significant to one, two, or three figures. One way to avoid this problem is to use scientific notation. For example, 2.00×10^2 ml unambiguously implies three significant figures (trailing zeros are significant), whereas 2×10^2 implies only one significant figure. Another way to avoid this problem is to use a different unit of measurement. Instead of 200 ml, use 0.2 l to imply one significant figure.

When a result is derived from a measured value, the result can not be more accurate than the measured value. For example, New et al. [3] measured a deflection angle on a clip of 57° (i.e., two significant figures of accuracy). The calculated force was given as 3169 dynes (i.e., four significant figures). More appropriate would be 3.2×10^3 dynes. For a value of mass of 160 mg, the forces per gram was then given as 19,863 dynes/g (i.e., five significant figures [3169 divided by 0.16 is 19,806.3, but that is not the subject of this letter]). This result should be reported as 2.0×10^4 dynes/g.

Shellock and Crues [4] report the deflection force on a contraceptive diaphragm as 11,195 dynes (i.e., five significant figures). This implied that the deflection angle as measured on a protractor was 31.695°, when it was admitted that the protractor was accurate to ± 0.5°.

The convention of using significant figures should be observed in order to convey the accuracy of a measured or calculated experimental result.

Nolan J. Kagetsu
New York University Medical Center
New York, NY 10016

REFERENCES

1. Skoog DA, West DM. The evaluation of analytical data. In: *Fundamentals of analytical chemistry*, 2nd ed. New York: Holt, Rinehart & Winston, **1969**:25–58
2. Shoemaker DP, Garland CW, Steinfeld JI, Nibler JW. Treatment of experimental data. In: *Experiments in physical chemistry*, 4th ed. New York: McGraw-Hill, **1981**:25–55
3. New PFJ, Rosen BR, Brady TJ, et al. Potential hazards and artifacts of ferromagnetic and nonferromagnetic surgical and dental materials and devices in nuclear magnetic resonance imaging. *Radiology* **1983**;147:139–149
4. Shellock FG, Crues JV. High-field-strength MR imaging and metallic biomedical implants: an ex vivo evaluation of deflection forces. *AJR* **1988**;151:389–392

Localization of Transected Wire

I would like to comment on the recent letter by Mitnick et al. [1] about the pitfall of inadvertent transection of a breast localization wire. They stated that I have "suggested the routine use of a postlocalization stiffening wire to avoid transection." In fact, I described a postlocalization *needle*, not a wire, to avoid the pitfall of wire transection [2]. The concept of a covering needle is an essential element of one of the spring-hook wire devices in which a stiffening cannula is used, and it is an integral part of the curved J-wire localizer system (Mammalok, North American Instrument, Glens Falls, NY) because both the needle and wire are left in place [3]. As Mitnick et al. correctly state, this reduces the complication of wire transection.

Marc J. Homer
Tufts University
New England Medical Center Hospitals
Boston, MA 02111

REFERENCES

1. Mitnick JS, Vazquez MF, Harris MN, Buchbinder SS. Localization of transected wire (letter). *AJR* **1991**;156:866
2. Homer MJ, Fisher DM, Sugarman HJ. Post-localization needle for breast biopsy of nonpalpable breast lesions. *Radiology* **1981**;140:241–242
3. Homer MJ. Localization of nonpalpable breast lesions with the curved-end retractable wire: leaving the needle in vivo. *AJR* **1988**;151:919–920

Diagnosis of Hemopericardium During Digital Subtraction Angiography

Hemopericardium is a relatively common and potentially lethal complication of penetrating chest trauma. It may be overlooked on the chest radiograph because the resultant increase in cardiac diameter may be subtle, particularly if previous radiographs are not available for comparison. The associated distension of the superior mediastinal venous structures with tamponade may be misinterpreted as evidence of possible arterial injury, leading to a request for angiography. We describe a case of suspected arterial injury in which digital subtraction angiography (DSA) showed features of pericardial tamponade.

A 21-year-old man was stabbed in the left third intercostal space. On admission, he was hemodynamically stable, but a chest radiograph showed superior mediastinal widening that was interpreted as hematoma, possibly due to an arterial injury. On intraarterial DSA, the aortic arch and major arteries appeared normal, but on closer inspection, the cardiac outline could be clearly discerned inside the pericardial outline before the injection of contrast medium (Fig. 1). The distance separating the two structures strongly suggested pericardial fluid, most likely blood. Sonography confirmed a 20-mm-wide pericardial fluid collection. At pericardiotomy, a moderate volume of blood was drained, and a laceration of the pulmonary outflow tract was sutured.

DSA is sensitive to slight differences in radiographic contrast and can show subtle differences in density not necessarily seen on plain

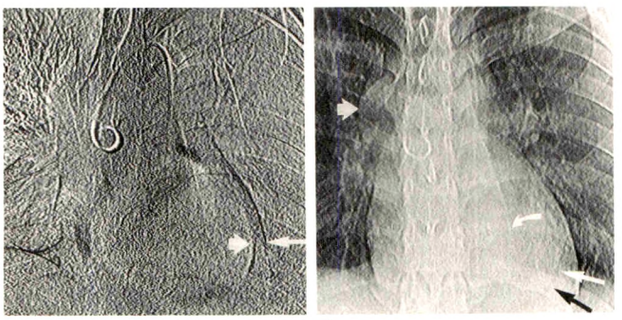


Fig. 1.—Hemopericardium on digital subtraction angiograms.
***A*, Subtracted cardiac image shows epicardial fat (*short arrow*) widely separated from pericardial outline (*long arrow*).**
***B*, Unsubtracted image shows a faint curvilinear lucency representing epicardial fat (*long straight arrows*), distended azygos vein (*short straight arrow*), and a paravertebral hematoma (*curved arrow*).**

radiographs. We think that the appearance on DSA in this case was due to the misregistration of mask and image, which emphasized the epicardial fat layer outlining the myocardium (Fig. 1A). This is analogous to the pericardial band of density sometimes seen on lateral [1] and frontal [2] chest radiographs in the presence of pericardial fluid.

We think this is a useful observation to make on all DSA studies in which concomitant or unsuspected pericardial fluid or hemopericardium may be present. This is especially important in trauma patients, in whom the blood may accumulate rapidly after referral for angiography, with cardiac decompensation following. We stress the importance of not disregarding the cardiac area during viewing of DSA merely because of movement artifact; useful information may be present.

D. J. Solomon
S. Beningfield
Groote Schuur Hospital/University of Cape Town
Cape Town, South Africa

REFERENCES

1. Lane EJ, Carsky EW. Epicardial fat: lateral plain film analysis in normal and pericardial effusion. *Radiology* **1968**;91:1–5
2. Carsky EW, Mauceri RA, Azimi F. The pericardial fat pad sign. *Radiology* **1980**;137:303–308

Choledochal Cyst and Biliary Atresia in the Neonate

The paper by Torrisi et al. [1] misinterprets the accuracy of cholescintigraphy in the diagnosis of biliary atresia. The absence of radionuclide activity in the small bowel is compatible not only with biliary atresia but also with intrahepatic cholestasis, neonatal hepatitis, bile duct paucity, and total parenteral nutrition cholestasis [2]. Additional cholescintigraphs obtained later often show radionuclide activity in the small bowel, thus excluding biliary atresia [2]. The limitations of ^{99m}Tc cholescintigraphy—the short half-life of the radionuclide and its delayed appearance in the small bowel—are well illustrated by Collier et al. [3], who examined five neonates who had hepatitis. Simultaneous studies were done with ^{99m}Tc-p-butyl-iminodiacetic acid and iodine-131 rose bengal. The first technique failed to show a patent biliary tree in three neonates; ^{131}I rose bengal showed a patent biliary tree at 48 hr in two and at 168 hr in one.

I. E. T. Stewart
Hinchingbrooke Hospital
Huntingdon, CAMBS PE18 8NT, United Kingdom

REFERENCES

1. Torrisi JM, Haller JO, Velcek FT. Choledochal cyst and biliary atresia in the neonate: imaging findings in five cases. *AJR* **1990**;155:1273–1276
2. Spivak W, Sarkar S, Winter D, Glassman M, Donlan E, Tucker KJ. Diagnostic utility of hepatobiliary scintigraphy with ^{99m}Tc-DISIDA in neonatal cholestasis. *J Pediatr* **1987**;110:855–861
3. Collier BD, Treves S, Davis MA, Heyman S, Subramanian G, McAfee JG. Simultaneous ^{99m}Tc-p-butyl-IDA and ^{131}I rose bengal scintigraphy in neonatal jaundice. *Radiology* **1980**;134:719–722

Reply

Dr. Stewart is correct in that cholescintigraphy is not *diagnostic* but merely *suggests* the diagnosis of biliary atresia. We did not mean to imply that cholescintigraphy was that specific. The other diseases must be included in the differential diagnosis.

Jean Torrisi
Jack O. Haller
SUNY Health Science Center at Brooklyn
Brooklyn, NY 11203

C-Arm Fluoroscopy

In the November 1990 issue of AJR, Davis et al. [1] describe using a portable C-arm fluoroscopic unit to examine patients with swallowing disorders. I agree that this is an excellent method for examining such patients, and my colleagues and I have been using it for the past 4 years in studies of children with swallowing disorders. However, the portable C-arm fluoroscope is cumbersome to use and has limited image resolution. I wish to draw to the attention of your readers the availability of a commercial C-arm fluoroscopic unit that is attached to a 90/90 tilt table. The unit is produced by Fischer Imaging Corp. (Denver, CO) and is called the Imager. It has a 1000-mA 150-kVp 100-kW generator and is equipped with a 12 × 9 × 6 in. (30 × 23 × 15 cm) image intensifier. The image intensifier can be moved in a craniocaudal and an in and out motion as with any conventional fluoroscopic unit. In addition, it is capable of a full 90° rotation and a 45° craniocaudal tilt.

In addition to its value for studies of patients with swallowing disorders, C-arm fluoroscopy has other distinct advantages. Fit young patients usually can be easily rolled into position, but in many clinical situations, it is advantageous to obtain the desired imaging position by using a C-arm rather than by moving the patient. This is particularly true in infants and children. Some of these situations are as follows: (1) young infants who are swallowing or voiding (they frequently will stop doing this when rolled into an alternative position); (2) children who are intubated; (3) children who are in pain or discomfort after trauma, such as a pelvic fracture or recent surgery; (4) situations in which horizontal-beam imaging with the patient in a prone position (e.g., for identification of a tracheoesophageal fistula) is desirable; (5) any oblique views that can be obtained more easily and accurately by using the C-arm than by rolling the patient into position. (Another advantage of the unit is that craniocaudal tilt can be used when structures of interest overlap, for example, the pyloric antrum.)

In summary, C-arm fluoroscopy offers many distinct advantages. The Fischer Imager is comparable to any conventional fluoroscopic

room and just as easy to use but has the added advantage of having a C-arm.

Mervyn D. Cohen
Indiana University Medical Center
Indianapolis, IN 46202-5200

REFERENCE

1. Davis M, Palmer P, Kelsey C. Use of C-arm fluoroscope to examine patients with swallowing disorders. *AJR* **1990**;155:986–988

Reply

My coauthors and I are gratified that Dr. Cohen agrees with our opinion that C-arm fluoroscopy has a useful place in the diagnosis of swallowing disorders, and we thank him for pointing out other areas in which the C-arm feature is useful.

Although we do not have personal experience with the Fischer Imager, the literature about the unit indicates that it would be a useful addition for a department with adequate space and finances to acquire it. Our point was that most radiology departments now have a portable C-arm unit that can be used advantageously in the diagnosis of swallowing disorders.

Michael Davis
University of New Mexico Medical Center
Albuquerque, NM 87131

Videofluoroscopy in Elderly Patients with Aspiration

Feinberg and Ekberg [1] recently reviewed 50 barium swallow examinations performed in elderly patients who were known to aspirate. The mean age of the patients was 87 years. Dementia was present in 21, stroke in 15, and Parkinson disease in five. The authors concluded that "an accurate and valid assessment of oropharyngeal dysfunction in elderly patients with aspiration is possible," and stated that "critical management decisions regarding dietary alterations, degrees of oral intake, and institution of artificial feeding often depend on the videofluorographic assessment of aspiration."

I commend Feinberg and Ekberg for this lucid discussion of a difficult problem. However, I question their contention that videofluorographic assessment of aspiration in this group of patients often affects management decisions, and I doubt it has much meaningful effect on the lives of most of these elderly patients. The question of efficacy was not addressed in this article, and, to my knowledge, it has not been addressed in any previous publication. Certainly it would be difficult to assess in a controlled fashion.

My own limited experience has been that once such an examination is offered, it is used increasingly in patients whose mental status is severely limited. A patient's ability to tolerate different foods, solids vs liquids, or small vs large boluses often can be assessed better by the astute observer who feeds the patient each day than it can be during the short period of observation in the fluoroscopic suite when artificial radiopaque food materials are used.

Obviously, in selected patients, videofluoroscopic assessment of swallowing function is useful, and I commend Feinberg and Ekberg on their important and continuing contributions in this field.

Ferris M. Hall
Beth Israel Hospital
Harvard Medical School
Boston, MA 02215

REFERENCE

1. Feinberg MJ, Ekberg O. Videofluoroscopy in elderly patients with aspiration: importance of evaluating both oral and pharyngeal stages of deglutition. *AJR* **1991**;156:293–296

Reply

As Dr. Hall points out, the efficacy of swallowing studies has not been established. No large, well-controlled clinical trials have been done that indicate a significant reduction in morbidity or mortality for any age group or specific condition. However, the discipline is relatively new and is still in the descriptive phase, attempting to outline normal and pathologic function and describe the techniques and effects of intervention. As radiologists, we conducted a clinical investigation [1] that we hope will contribute to the scientific basis required for decisions about treatment.

Leading authorities [2, 3] have stressed the need for dynamic imaging in the evaluation of oropharyngeal swallowing disorders. We agree with Dr. Hall's comments on the importance of the clinical evaluation in such cases. The videofluorographic examination gives only a brief view of function under somewhat artificial conditions and may not accurately reflect function or capabilities outside the radiology department. Dysfunction is often intermittent or variable and is affected by levels of alertness, conditioning, and cooperation. The results of the radiologic examination always must be correlated with multiple clinical evaluations before an overall assessment is made.

We strongly support Logemann's recommendation [4] that age should not be a factor in the selection of patients for swallowing therapy. For the frail elderly who have neuropsychiatric illnesses, physical and mental health are often affected by their ability to eat and drink normally. Working as part of a multidisciplinary team, we have participated in the care of hundreds of such patients. As with all new imaging procedures, we first educated referring clinicians about the appropriate role of videofluoroscopy. We do not study patients whose mental status precludes adequate evaluation or patients whose management will not be affected by our results. We think that our clinically correlated radiologic assessment affects patients' quality of life by directly influencing what, how, and if they are fed. Admittedly, we sometimes find ourselves struggling with other team members about what ought to be done when multiple options are available, each with its own benefits and burdens. This situation has provided both a challenge and an opportunity for us as radiologists to assert leadership in shaping attitudes and approaches to this difficult but common problem.

Michael J. Feinberg
Buffalo General Hospital
Buffalo, NY 14203
Olle Ekberg
Malmo General Hospital
Malmo, Sweden

REFERENCES

1. Feinberg MJ, Ekberg O. Videofluoroscopy in elderly patients with aspiration: importance of evaluating both oral and pharyngeal stages of deglutition. *AJR* **1991**;156:293–296
2. Dodds WJ, Logemann JA, Stewart ET. Radiologic assessment of abnormal oral and pharyngeal phases of swallowing. *AJR* **1990**;154:965–974
3. Jones B, Donner MW. Examination of the patient with dysphagia. *Radiology* **1988**;167:319–326
4. Logemann JA. Effects of aging on the swallowing mechanism. *Otolaryngol Clin North Am* **1990**;23:1045–1056

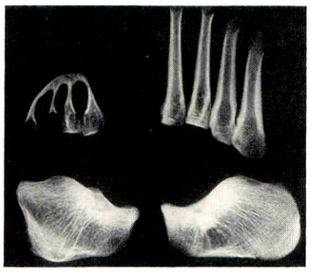


Fig. 1.—Radiograph of dry-bone archeologic specimens shows unilateral ectrodactyly, metatarsal synostosis, and hypoplasia of left foot (*left, top and bottom*). Contralateral bones (*right, top and bottom*) are shown for comparison.

A Rare Form of Metatarsal Synostosis

Congenital anomalies of the feet have been noted in many populations throughout the world [1–3]. One such anomaly, a unique form of metatarsal synostosis accompanied by ectrodactyly (absence of the phalanges), has only recently been discovered. Because of its rarity in clinical and archeologic samples, this case is presented for comparison of gross and radiologic features.

The example is the left foot of a 20- to 25-year-old Eskimo woman from the archeologic site of Tigara at Point Hope, Alaska, dating from approximately A.D. 1400 to 1850. The deformity consists of ectrodactyly, hypoplasia and fusion of the distal second to fifth metatarsals, and mild hypoplasia of the calcaneus (Fig. 1). Radiographs show sclerosis along the lateral shafts of the left second and the right fifth metatarsals and osteoporosis and an irregular trabecular pattern in the calcaneus. This deformity is thought to represent a congenital malformation caused by the inappropriate organization of mesenchyme during the fifth week after conception that is due to a primary defect in the embryonic sensory nerves [4].

Anne Keenleyside
McMaster University
Hamilton, Ontario, Canada L8S 4L9
Robert Mann
Smithsonian Institution
Washington, DC 20560

REFERENCES

1. Fixsen J. Congenital abnormalities of the limbs. *Br J Hosp Med* **1981**;26:194–203
2. Warkany J. *Congenital malformations: notes and comments.* Chicago: Year Book Medical, **1971**
3. Resnick D. Additional congenital or heritable anomalies and syndromes. In: D. Resnick, G Niwayama, eds. *Diagnosis of bone and joint disorders*, 2nd ed. Springfield, IL: Thomas, **1988**:3541–3600
4. McCredie J. Congenital fusion of bones: radiology, embryology and pathogenesis. *Clin Radiol* **1975**;26:47–51

Subluxation of the Humeral Head Associated with Hemarthrosis in a Patient with Hemophilia

Inferior subluxation of the humeral head, pseudodislocation, is caused by hemarthrosis due to a fracture or bleeding disorder. It may be misdiagnosed as a dislocation. Appropriate therapy such as joint aspiration may be delayed if this entity is not recognized. A case of a misdiagnosed pseudodislocation is presented.

A 15-year-old boy was brought to the emergency department for evaluation of a painful right shoulder after a blow to the joint that occurred while he was wrestling. The initial physical examination revealed an erythematous, swollen shoulder with a severely limited range of motion. It was known that the patient had hemophilia. Plain radiographs of the right shoulder showed inferior subluxation of the humeral head, subchondral cysts along the glenoid cavity, and a hemophilic pseudotumor within the humeral metaphysis (Fig. 1). The subluxed humeral head was initially misinterpreted as an anterior dislocation. Widening of the joint space due to hemarthrosis was not recognized, and aspiration of the joint was delayed until the films were interpreted the next day by a radiologist.



Fig. 1.—Anteroposterior radiograph of right shoulder shows subchondral cysts along glenoid cavity, metaphyseal pseudotumor, and subluxation of humeral head.

Hemarthrosis is common among persons who have hemophilia, occurring in 75–90% of them. It is more common in active children than in adults and affects the knee, elbow, hip, and shoulder most often. Joints subjected to repeated stress are involved most frequently, and the initial bout of stress predisposes the joint to subsequent bleeding [1].

Early recognition of pseudodislocation may speed appropriate therapy and prevent painful and improper attempts at reduction.

William H. McCuskey
Mercy Hospital of Pittsburgh
Pittsburgh, PA 15219

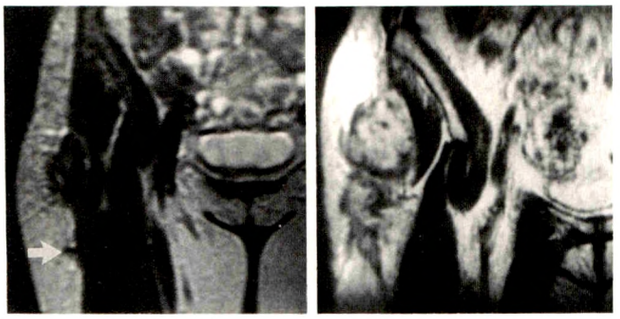
REFERENCE

1. Resnick D, Niwayama G. *Diagnosis of bone and joint disorders*, 2nd ed. Philadelphia: Saunders, **1988**:2497–2520

Paradoxical Signals (Short T2, Long T2) in a Patient with a Soft-Tissue Tumor

A 48-year-old woman had had a nontender mass in the right thigh for several months. MR imaging of the thigh and pelvis (6.5-mm axial and coronal slices) was performed on a 1.5-T General Electric Signa magnet with spin-echo pulse sequences with T1, balanced, and T2 weighting. A 3-cm poorly defined mass with low signal intensity on all sequences was shown in the right thigh, infiltrating the tensor fascia lata (Fig. 1A). A smaller nodular mass was noted inferiorly, suggesting a satellite lesion. Biopsy of the mass revealed a desmoid. Wide local excision of the lesion with tumor-free margins was done. Approximately 2 years later, follow-up MR showed an aggressive 4.0-cm mass infiltrating the muscles adjacent to the right hip (Fig. 1B). The mass had low signal intensity on T1-weighted images and mostly high signal intensity on T2-weighted sequences. Again, biopsy showed a desmoid, and the tumor was removed by wide local excision. Histologic features of the original tumor included a bland proliferation of spindled cells scattered among wavy collagen fibers. The recurrent desmoid had less abundant collagen and greater cellularity.

Most soft-tissue and other masses have a long T2. The significance of masses having a short T2 either before biopsy or after treatment has been the subject of several publications [1, 2]. The questions addressed have been the value of this feature in separating benign



A B

Fig. 1.—Paradoxical signals of a soft-tissue tumor.
***A*, Coronal T2-weighted (2000/80) MR image of pelvis shows a desmoid and satellite lesion (*arrow*) with low signal intensity (short T2) infiltrating subcutaneous fat and muscles of right thigh. Tumor was resected.**
***B*, Follow-up coronal T2-weighted (1900/75) MR image of pelvis obtained 2 years after resection shows recurrent desmoid at site of original tumor. New tumor has mainly high signal intensity (long T2).**

from malignant lesions, in separating recurrent tumors from posttreatment fibrosis, and in predicting tumor histology. The conclusion of one study [1] of soft-tissue tumors with short T2 was that this signal pattern could not be used to separate benign from malignant lesions but could be used to generate a differential diagnosis by predicting histologic compositions of relative acellularity and abundant collagen. De Lange et al. [2] reached a similar conclusion in a study that examined the MR features of suspected recurrent rectosigmoid carcinoma after abdominoperineal resection; rectal masses with short T2 were related to either postoperative or radiation fibrosis or a desmoplastic reaction from recurrent tumor. In contrast, Negendank et al. [3] found that Hodgkin lymphomatous masses that contained dense fibrosis had high signal intensities on T2 sequences as compared with more uniformly cellular and homogeneous non-Hodgkin lymphomas. Some reservations have been expressed about these apparently paradoxical conclusions on fibrosis, including (1) sampling error and (2) possible chemical and structural differences in fibrous tissue associated with lymphomas [4].

The nodules of aggressive fibromatosis may have long or short T2 and may be associated with smaller satellite lesions. Our patient provided us a unique opportunity to study a tumor and its recurrence in the same location approximately 2 years later. Paradoxical T2 signals were obtained for the two masses. Histologic examinations confirmed that both tumors were due to aggressive fibromatosis; however, more collagen and less cellularity was seen in the mass with the short T2. This further confirmed, in a patient serving as her own control, that it is the histologic composition and not the tumor type that influences signal intensity.

Gregg A. Baran
Murali Sundaram
Christine Janney
St. Louis University Medical Center
St. Louis, MO 63110-0250

REFERENCES

1. Sundaram M, McGuire MH, Schajowicz F. Soft-tissue masses: histologic basis for decreased signal (short T2) on T2-weighted MR images. *AJR* **1987**;148:1247–1250
2. de Lange EE, Fechner RE, Wanebo HJ. Suspected recurrent rectosigmoid carcinoma after abdominoperineal resection: MR imaging and histopathologic findings. *Radiology* **1989**;170:323–328
3. Negendank WG, Al-Katib AM, Karanes C, Smith M. Lymphomas: MR imaging contrast characteristics with clinical-pathologic correlations. *Radiology* **1990**;177:209–216
4. Lee JKT, Glazer HS. Controversy in the MR imaging appearance of fibrosis. *Radiology* **1990**;177:21–22

Lateral Meniscus Pseudotear or "Line of Murray"

We noted with interest the recent article by Kaplan et al. [1] on pseudotears of the menisci. We first observed this finding of an equivocal tear about 3 years ago in the posterior horn of the lateral meniscus. We have named it "the line of Murray" after the musculoskeletal radiologist who first observed it. The first few times we noted it, we asked the referring orthopedic surgeon to do an arthroscopic follow-up examination. As none of the entities were tears at surgery, we began to consider this condition a normal variant. Since then, we have seen approximately 30 similar equivocal tears. To our knowledge, surgery has not shown tears in any of these cases.

In our experience, all of these pseudotears have identical characteristics. They are almost always in the posterior horn of the lateral meniscus and on MR have subtle increased signal intensity extending in a thin line down to the inferior articular surface. They are seen on the sagittal proton-density images but not on the T2-weighted images of standard spin-echo sequences (2500/20, 80 [TR/TE]) with normal windowing. With narrow windowing, the line is more easily seen; it abuts but does not clearly break through the inferior articular surface. It is obliquely oriented centrally toward the joint rather than vertically or obliquely and peripherally as in the normal variant caused by the interface with the meniscofemoral ligaments.

Perhaps of interest to the practicing radiologist is that we have seen these with the Signa 1.5-T imager but not with the GE Max 0.5-T imager (General Electric, Milwaukee, WI). We use dedicated knee coils with both systems.

Histologic studies will be of interest. Because of the thin linear characteristic and because we occasionally see pseudotears in young patients, we hypothesized that this might be a developmental variant. In patients in whom the characteristics are similar to the appearance of Figures 1B and 3, rather than that of Figure 2, in the paper of Kaplan et al., we continue to favor this hypothesis. Figure 2 shows a thicker band of signal easily seen on routine windowing; we would more likely consider this myxoid degeneration, which indeed was found histologically in their study. We would like to know if Kaplan et al. have had any cases with the more subtle linear signal for which histologic correlation is available since the study was submitted for publication.

Paul D. Traughber
Saint Alphonsus Regional Medical Center
Boise, ID 83706
University of Utah Medical Center
Salt Lake City, UT 84132
William T. Murray
Saint Alphonsus Regional Medical Center
Boise, ID 83706

REFERENCE

1. Kaplan PA, Nelson NL, Garvin KL, Brown DE. MR of the knee: the significance of high signal in the meniscus that does not clearly extend to the surface. *AJR* **1991**;156:333–336

Reply

On behalf of my coauthors and myself, I thank Drs. Traughber and Murray for their interest in our article [1] on the appearance of equivocal meniscal tears on MR. The experience of Drs. Traughber and Murray is of interest, and it is comforting to know that our results agree with theirs. Unfortunately, we have no histologic information on the numerous patients who had increased linear signal in the posterior horn of the lateral meniscus. There is simply no reason to remove these menisci at arthroscopy, because no tear is detected. Without histologic information, I cannot be certain what is responsible for this finding on MR; the pseudotear may be a normal variant. I think that what is most important is for radiologists to recognize that regardless of the cause, the finding probably has no clinical significance and that no tear will be found at surgery. This recognition will prevent unnecessary surgery.

Phoebe Kaplan
University of Nebraska Medical Center
Omaha, NE 68105

REFERENCE

1. Kaplan PA, Nelson NL, Garvin KL, Brown DE. MR of the knee: the significance of high signal in the meniscus that does not clearly extend to the surface. *AJR* **1991**;156:333–336

Letters are published at the discretion of the Editor and are subject to editing.

Letters to the Editor must not be more than two *double-spaced*, typewritten pages. One or two figures may be included. Abbreviations should not be used. See Author Guidelines, page A5.

Material being submitted or published elsewhere should not be duplicated in letters, and authors of letters must disclose financial associations or other possible conflicts of interest.

Letters concerning a paper published in the *AJR* will be sent to the authors of the paper for a reply to be published in the same issue. Opinions expressed in the Letters to the Editor do not necessarily reflect the opinions of the Editor.

Review of Current Literature

Initials and addresses of corresponding authors are provided in parentheses for each article so that the reader can obtain reprints directly. Abstracts are printed verbatim from each journal.

Gastroenterology

Human gallbladder morphology after gallstone dissolution with methyl *tert*-butyl ether. vanSonnenberg E, Zakko S, Hoffmann AF, et al. (EVS, Dept. of Radiology, University of California, San Diego Medical Center, San Diego, CA 92103). *Gastroenterology* 100:1718–1723, 1991

The effects of methyl *tert*-butyl ether exposure on the human gallbladder in five patients who were treated for gallstones by contact dissolution is described. Two patients underwent cholecystectomy within 1 week of methyl *tert*-butyl ether treatment, one patient 2 weeks after, another 10 weeks after, and one 12 weeks after. Indications for cholecystectomy were bilirubinate stones (resistant to methyl *tert*-butyl ether), catheter dislodgement, bile leakage, and gallstone recurrence (2 patients). Gallstones were dissolved completely in three patients, there was approximately 50% stone reduction in one patient, and no dissolution occurred in the fifth patient. Each gallbladder was examined grossly and histologically. Electron microscopic evaluation was performed in one case. Typical inflammatory findings of chronic cholecystitis were observed in each gallbladder and were most conspicuous in the submucosa; the mucosal and serosal surfaces were intact. Mild acute inflammatory changes were noted in the submucosa in the two patients with the shortest interval between methyl *tert*-butyl ether administration and cholecystectomy. There were no ulcerations in the mucosa and no unusual wall thickening or fibrosis in any patient. These observations support the safety of methyl *tert*-butyl ether perfusion in the human gallbladder; the mild acute changes may be a transient and reversible phenomenon.

Reprinted with permission by the American Gastroenterological Association.

Natural history and prognostic variables in primary sclerosing cholangitis. Farrant JM, Hayllar KM, Wilkinson ML, et al. (JMF, Institute of Liver Studies, King's College Hospital, Denmark Hill, London, England). *Gastroenterology* 100:1710–1717, 1991

The clinical features at the time of presentation and the outcome in 126 patients with primary sclerosing cholangitis were studied to clarify the natural history and prognosis in symptomatic and asymptomatic individuals. The median age of the patients at the time of presentation was 36 years, 62% were male, and 16% were asymptomatic. The median follow-up from time of presentation was 5.8 years. There were more patients who had liver transplants (21%) than patients who died of liver-related disease (16%); the estimated median survival to these end points was 12 years. Cholangiocarcinoma was found in 8 patients and in 23% of those undergoing liver transplantation. Asymptomatic patients had milder disease than symptomatic patients, but in a univariate analysis the presence of symptoms was not prognostically significant. On multivariate analysis, the following independent prognostic factors were found: hepatomegaly, splenomegaly, serum alkaline phosphatase, histological stage, and age. These features were combined to produce a prognostic model that should be valuable in the stratification of patients in clinical trials and in the timing of liver transplantation, particularly in those patients seen soon after presentation.

Reprinted with permission by the American Gastroenterological Association.

Epidemiology of *Helicobacter pylori* in an asymptomatic population in the United States: effect of age, race, and socioeconomic status. Graham DY, Malaty HM, Evans DG, Evans DJ Jr, Klein PD, Adam E (DYG, Dept. of Medicine, Baylor College of Medicine, Houston, TX). *Gastroenterology* 100:1495–1501, 1991

A causative role is now accepted for *Helicobacter* (formerly *Campylobacter*) *pylori* in type B gastritis, and evidence is accumulating that *H. pylori* infection plays a major contributory role in peptic ulcer disease. Preliminary studies have reported that the prevalence of *H. pylori* infection increases with age, but detailed information on the prevalence of the bacteria in any defined population and on the factors that may influence the pattern of distribution remains scanty. In the present study, a sensitive enzyme-linked immunosorbent assay and a [^{13}C]urea breath test were used to investigate the prevalence of *H. pylori* infection among 485 healthy asymptomatic volunteers between the ages of 15 and 80 residing in the Houston metropolitan area. *H. pylori* infection was present in 52%. The prevalence of *H. pylori* infection increased rapidly with age at 1%/yr for the overall population. The frequency of *H. pylori* infection was higher in blacks (70%) than whites (34%) ($P < 0.001$); this difference remained after adjustments were made for age, gender, educational level, income, and use of tobacco or alcohol. *H. pylori* infection was independent of gender but was closely correlated with socioeconomic class. There were significant inverse correlations between age-adjusted frequency of *H. pylori* infection and income and between educational level and *H. pylori* infection. There was no association between *H. pylori* infection and consumption of alcohol or nonsteroidal antiinflammatory drug use or smoking. Having pets was associated with a lower frequency of *H. pylori* infection, but this was highly associated with higher socioeconomic status. The mode(s) of transmission of *H. pylori* is unknown, but the social patterns of *H. pylori* infection are consistent with fecal-oral transmission as one important pathway. Socioeconomic factors seem to determine the age of acquisition.

Reprinted with permission by the American Gastroenterological Association.

Digestive Diseases and Sciences

***Helicobacter pylori* in children with peptic ulcer and their families.** Oderda G, Vaira D, Holton J, et al. (DV, 1st Medical Clinic, University of Bologna, S. Orsola Hospital, Nuove Patologie, Via Massarenti 9, 40138 Bologna, Italy). *Dig Dis Sci* 36(5):572–576, May 1991

Little is known about the source and spread of *Helicobacter pylori*, but transmission from infected family contacts has been suggested. We have therefore investigated 15 children with peptic ulcer and their first-degree relatives for *H. pylori*. Serum anti-*H. pylori* IgG, pepsinogen I, and gastrin levels were measured. Endoscopy was carried out on the children and relatives, and biopsies were taken from the gastric antrum for histology, microbiology, and urease testing. Six of 11 children with duodenal ulcer (55%) and two of four children with gastric ulcer (50%) were positive for *H. pylori*. Fourteen of 16 parents (87%) and eight of 13 siblings (61%) of *H. pylori*-positive children with peptic ulcer were also infected compared with eight of 14 parents (57%) and none of four siblings of *H. pylori*-negative children with peptic ulcer ($P < 0.10$, >0.05, and NS, respectively). The children with *H. pylori*-negative peptic ulcer and negative siblings combined were younger than positive children with peptic ulcer and positive siblings ($P < 0.001$). The reliability of serum anti-*H. pylori* IgG level as a screening test for infection was confirmed. These findings call into question a pathogenetic role for *H. pylori* in some childhood peptic ulceration, but do suggest that person-to-person spread of infection occurs.

Clinical Orthopaedics and Related Research

Diskitis in children. Crawford AH, Kucharzyk DW, Ruda R, Smitherman HC Jr (AHC, Director, Pediatric Orthopaedics, Children's Hospital Medical Center, Elland & Bethesda Aves., Cincinnati, OH 45229). *Clin Orthop* 266:70–79, May 1991

Thirty-six patients diagnosed with diskitis from 1978 to 1988 and followed for an average of 29.2 months were reviewed. The study included 23 boys and 13 girls with an average age of 5.3 years. The initial symptoms varied, but distinct clinical patterns emerged and were identifiable in different age groups. Both the leukocyte count and sedimentation rate were elevated. Routine roentgenograms were positive for intervertebral disk space narrowing in 82% of cases, technetium bone scans positive in 72%, and magnetic resonance imaging positive in all recent cases. Treatment consisted of bed rest for all patients, plaster casts for 50%, antibiotics for 40%, and traction for 23%. Regardless of the treatment combination, the course of the disease in most children is benign. At the completion of the study, all patients were asymptomatic including three children who had recurrences. In spite of being asymptomatic, 74% had persistent roentgenographic changes. The administration of antibiotics appears to be appropriate when indicated, *i.e.*, failure to respond to immobilization. Disk space aspiration or biopsy should be reserved for those cases that are refractory to immobilization and antibiotics.

The Journal of Nuclear Medicine

Optimal iodine-131 dose for eliminating hyperthyroidism in Graves' disease. Nordyke RA, Gilbert FI Jr (RAN, Straub Clinic & Hospital, 888 So. King St., Honolulu, HI 96813). *J Nucl Med* 32:411–416, 1991

Since hypothyroidism is commonplace after treatment of Graves' disease with radioiodine, the goal should be cure of hyperthyroidism rather than avoidance of hypothyroidism. To find the optimal dose to accomplish cure, we treated 605 patients with stepwise increasing doses of 3, 4, 5, 6, 8, and 10 mCi, analyzing the relationship of dose, age, sex, gland weight, and thyroidal uptake to cure. Estimates of cure at doses above 10 mCi were made from the literature. Cure was directly related to dose between 5 and 10 mCi. There was no significant relationship between cure and age (chi-square, $p = 0.74$), sex (chi-square, $p = 0.12$), and 24-hr uptake if over 30% (chi-square for slope, $p > 0.10$). Cure and gland weight had an inverse relationship (chi-square for slope, $0.01 < p < 0.02$). We concluded that the optimal ^{131}I dose for curing hyperthyroidism is approximated by starting with 10 mCi and increasing it for unusually large glands or for special patient circumstances.

Lung thallium-201 uptake during exercise emission computed tomography. Kurata C, Tawarahara K, Taguchi T, Sakata K, Yamazaki N, Naitoh Y (CK, The Third Dept. of Internal Medicine, Hamamatsu University School of Medicine, 3600 Handacho, Hamamatsu 431-31, Japan). *J Nucl Med* 32:417–423, 1991

To test whether the analysis of lung uptake is worth adding to the interpretation of exercise thallium-201 (^{201}Tl) emission computed tomography (ECT), a lung/heart ratio of ^{201}Tl uptake was measured from an anterior image during ECT in 25 clinically normal (Group 1), 91 angiographically normal (Group 2), and 265 subjects with coronary artery disease (Group 3). The mean +2 s.d. of ratios in Groups 1 and 2 were the same (0.37). In Group 3, 80 subjects (30%) with increased ratios (>0.37) had higher frequencies of prior infarction and multivessel disease, more severe left ventricular dysfunction, and ^{201}Tl defects than 185 subjects with normal ratios. Subjects with markedly increased ratios (>0.45) had three-vessel disease more frequently than those with slightly or moderately increased ratios (67% versus 14% or 35%). Thus the measurement of lung/heart ratios may provide information regarding the severity of coronary artery disease and should be added to the routine interpretation of exercise ECT.

Dipyridamole technetium-99m-2-methoxy isobutyl isonitrile tomoscintigraphic imaging for identifying diseased coronary vessels: comparison with thallium-201 stress-rest study. Tartagni F, Dondi M, Limonetti P, et al. (FT, Istituto Malattie Cardiovascolari, Universita' di Bologna, Policlinico S. Orsola-Malpighi, Via Massarenti 9, 40138, Bologna, Italy). *J Nucl Med* 32:369–376, 1991

A same-day double injection protocol employing ^{99m}Tc-methoxyisobutyl isonitrile (MIBI) and myocardial single-photon emission computed tomography (SPECT) for detecting coronary artery disease (CAD) was assessed in 30 patients. SPECT was performed 1 hr after a first injection (250 MBq) of ^{99m}Tc-MIBI, given after 0.56 mg/kg dipyridamole (DPD) infusion. Patients were then reinjected at rest (750 MBq) and were reimaged 1 hr later. Within 1 wk, all patients underwent a complete stress-rest SPECT thallium study. Of the 330 myocardial segments evaluated, 25 were judged ischemic by both techniques, while persistent defects were demonstrated in 50 and in 47 with ^{99m}Tc-MIBI and ^{201}Tl, respectively. Six regions were considered for diseased vessels identification. Sensitivity and specificity for CAD were 100% and 75%, respectively, for both ^{201}Tl and ^{99m}Tc-MIBI. Sensitivity for identification of diseased vessels by ^{201}Tl was 68% for LAD, 89% for RCA, and 80% for LCX as opposed to 75%, 89% and 80%, respectively by ^{99m}Tc-MIBI. Specificity was 93% in both cases for LAD, 73% and 63% for RCA, and 53% and 46% for LCX.

Journal of Ultrasound in Medicine

Evaluation of adnexal masses with transvaginal color ultrasound. Kurjak A, Zalud I, Alfirevic Z (AK, Ultrasonic Institute, University of Zagreb, Pavleka Miskine 64, 41.000 Zagreb, Yugoslavia). *J Ultrasound Med* 10:275–297, June 1991

We evaluated 14,317 asymptomatic or minimally symptomatic women for ovarian carcinoma with transvaginal color Doppler ultrasound. The resistance index was calculated for at least five separate cardiac cycles in each case, and the mean was calculated. We discovered 624 benign adnexal masses: in every case except one the resistance index was >0.40. There were 56 malignant adnexal masses, 16 of which were stage I ovarian cancers. Neovascularization

was found in six of the seven stage I primary neoplasms and in all of the nine stage I secondary ovarian cancers. In all, the RI was ≤0.40. There were 40 advanced ovarian cancers revealed (stage III or IV); 39 showed abnormal colorflow pattern with the resistance index <0.40.

Reprinted with permission by the American Institute of Ultrasound in Medicine.

Journal of Computer Assisted Tomography

Intravascular hematocrit effect in cross-sectional CT imaging. Lin MC, Forrest JV, Mattrey RF, Lasser EC (JVF, Dept. of Radiology, V-114, VA Medical Center, 3350 La Jolla Village Dr., San Diego, CA 92161). *J Comput Assist Tomogr* 15(3):464–466, May/June 1991

Venous fluid–fluid levels were seen on CT or MR of three patients being evaluated for possible thrombosis. In all three cases, further investigation (by ultrasonography, venography, or surgery) revealed the cause of the fluid–fluid level to be slowly flowing blood without thrombosis. On CT done after intravenous contrast medium administration, the nondependent half of the vessel was denser than the dependent half. In an attempt to confirm this MR and CT picture and, particularly, to explain the dense upper half on CT, we conducted an in vitro study. Our study confirmed that when blood with diatrizoate sodium is not clotted and allowed to settle, a similar fluid–fluid level is observed by CT imaging. Our results indicate that an intravascular fluid–fluid level seen on cross-sectional images represents slowly flowing blood, not thrombosis.

Call for Papers on Neuroradiology

On January 1, 1992, The American Roentgen Ray Society and the American Society of Neuroradiology will terminate their agreement whereby manuscripts on neuroradiology submitted to the *AJR* are forwarded to the *AJNR* and selected *AJNR* papers are republished in the *AJR*.

To avoid any lag in the publication of neuroradiologic articles in the *AJR*, the Journal requests authors to submit neuroradiologic manuscripts effective immediately. We plan to expedite publication of these papers. Authors will receive an initial editorial decision in 3–4 weeks, and accepted papers will be published 3 months after revised manuscripts are accepted. This is more than twice as fast as most other journals.

The advantages of this rapid publication time and the *AJR*'s large circulation (24,000) are now available to all authors of neuroradiologic papers. An expanded section on neuroradiology, including review articles, pictorial essays, and commentaries, will accommodate more than the limited number of papers published under the previous agreement.

We invite authors of neuroradiologic articles to submit their papers for original publication in the *AJR* so that the Journal may continue to fulfill its commitment to supply timely and important original information about neuroradiology to general radiologists as well as to those who subspecialize in the field.

Robert N. Berk
Editor-in-Chief

News

The Interamerican College of Radiology

Jack Wittenberg[1]

The Interamerican College of Radiology (Colegio Interamericano de Radiologia [CIR]) was established in 1943 in Buenos Aires, Argentina, as a scientific radiologic organization to "function in countries that pertain to the American Continent." Attesting to its panhemispheric theme, the bylaws state that "the location of the College shall be the country where the President resides." The goals of the organization can functionally be perceived as linking the goals and responsibilities of the American College of Radiology (ACR), the American Board of Radiology, and select radiologic educational societies of North America. Organizationally, the purpose is to "associate the radiologists of the American Continent through their respective national societies, to guard and protect radiology standards and ethics in their respective countries" and to encourage and assist in the formation of national societies of diagnostic radiology in countries presently lacking such societies. Educationally, the development and advancement of radiology is to be accomplished through scientific interchange, which would occur formally during a quadrennial congress of radiology and annual national meetings cosponsored by CIR and a national chapter and through an official scientific journal, *Revista Interamericana de Radiologia*. Furthermore, the bylaws dedicate CIR to coordinating efforts and developing resources that will provide better training opportunities for young physicians in radiology.

At the February 1990 CIR congress in Caracas, Venezuela, Sidney de Souza Almeida of Sao Paulo, Brazil, was elected to the 4-year term of president of CIR. He brings to the organization energy, experience, creativity, and respect. He recently completed a 2-year tenure as president of the Brazilian Society of Radiology. Dr. Almeida has established a renewed commitment to the special mission of CIR by enunciating the following priorities: (1) "To see one America totally integrated in a community of friends searching to increase the value of our specialty to ultimately fulfill the goals of all of us—improved care of the patient." (2) To establish national radiologic societies in countries of the Western Hemisphere where such societies are now absent and to strengthen the federation of national entities that already exist. (3) To reestablish the publication of the College's journal. (4) To establish a network of training centers throughout the Western Hemisphere to which graduate physicians of approved radiologic training programs could be sent to receive previously unavailable or advanced training. (5) To formulate a general curriculum for all residency training programs throughout Latin America, which would include a proposal for the minimal duration of training in each of the major technologic disciplines, and to begin consideration of the feasibility of a standardized resident graduate certification process that could be incorporated by member national societies. (6) To develop a computerized technologic information bank that would allow the archiving of Latin American experiences with newer radiologic technologies; the information would be available to all inquiring members. (7) To develop closer association and become a reference resource for international health organizations such as the World Health Organization and the Pan American Health Organization.

I have just returned from the annual meeting cosponsored by the Brazilian Radiological Society in San Paulo, Brazil, April 14–17. Thematically, emphasis was placed on newer developments in sonography. More than 1000 attendees heard presentations by a distinguished international faculty that were simultaneously translated into English, Spanish, and Portuguese. At the meeting of the CIR board of councillors,

[1]Department of Radiology, Massachusetts General Hospital, Harvard Medical School, Boston, MA 02114. Address reprint requests to J. Wittenberg.

AJR **157:654–655, September 1991** 0361–803X/91/1573–0654 © American Roentgen Ray Society

a review of last year's activities was highlighted by the unprecedented accomplishments as well as the unfulfilled needs and goals. As a result of Dr. Almeida's personal odyssey throughout the hemisphere, 12 national societies have established or renewed their dedication to CIR, and 10 others are in the administrative process of so doing. The training network institutions now number 15 and can be found in major academic centers as geographically diverse as Caracas (Venezuela), Guayaquil (Ecuador), Barcelona (Spain), Monterrey (Mexico), Miami, and Boston. The opportunities for subspecialty training encompass the entire range of technologies, with the expected special attention given to sonography, CT, MR, and interventional techniques. In order to facilitate a more current exchange of information among members, a monthly bulletin in Spanish with English resumes (Organo Informativo Mensual del Colegio Interamericano de Radiologia), published in Brazil, is now being distributed within member countries under the auspices of each of the federated national societies. This publication provides up-to-date information on organizational activities of CIR; scientific meetings scheduled in Latin America; and training opportunities available to college members, academic faculty members, and recent resident graduates. It is not intended to replace the more scientific nature of the *Revista*, whose publication has been suspended because of a lack of funds. Dr. Almeida pointed out that lack of subsidy is also, unfortunately, interfering with maximum use of the opportunities available in the new network of training centers. Although occasionally trainees are being funded by their individual academic institutions or by personal funds, requests from eligible candidates from institutions without such resources are being unmet. Furthermore, educational radiologic materials at both the training and graduate level are sorely lacking or unaffordable, particularly in the poorer countries of South and Central America. A translation of the ACR *Radiological Self-Evaluation Syllabi* into Spanish is one proposal that would provide a vital resource for responding to this deficit.

The importance of having radiologic organizations within the Northern Hemisphere participate in CIR activities is a theme that calls for reemphasis. As with many other current hemispheric political, social, and economic matters, the advantages of integration to the welfare of many of our cultures and societies, including radiologic, are becoming all too apparent. To emphasize this organizational and personal commitment, Dr. Almeida convened a conference in Chicago in December 1990 with Joseph Morasco, chairman of the ACR Committee on International Affairs, and Otha Linton, associate executive director of the ACR. The meeting provided a forum for the delegates of CIR to inform ACR representatives of recent CIR initiatives and to emphasize the critical need for ACR political, scientific, and economic support. Typical of so many recent Pan-American initiatives, the sharing of such resources with less well-endowed southern neighbors will be vital if the present CIR momentum is to be sustained. As pointed out by Dr. Almeida, "We are convinced that only the union of all radiological organizations in the Western Hemisphere countries, independent of political considerations, can best strengthen our specialty and bring about economic, scientific, and ethical union and progress." He encourages all radiologists throughout the hemisphere to participate in this effort through their national societies or councillors and by individual commitments.

News

MRI Visiting Fellowships at UCLA

The Dept. of Radiological Sciences, University of California, Los Angeles, School of Medicine, is offering a new series of 5-day visiting fellowships in MR imaging. The dates for the program are Sept. 9–13, 1991; Oct. 7–11, 1991; Dec. 9–13, 1991; Feb. 3–7, 1992; March 9–13, 1992; April 6–10, 1992; Sept. 14–18, 1992; Oct. 5–9, 1992; and Dec. 7–11, 1992. Recognized experts in MR will present a variety of topics. Category 1 credit: 40 hr. Fee: $1350. Information: Robert B. Lufkin, M.D., Dept. of Radiological Sciences, UCLA School of Medicine, Los Angeles, CA 90024; telephone: (213) 825-7299; fax: (213) 872-2821.

Resident's Review in the Physics and Radiobiology of Diagnostic and Therapeutic Radiology

The Dept. of Radiology, Baylor College of Medicine, Houston, will offer Resident's Review in the Physics and Radiobiology of Diagnostic and Therapeutic Radiology, Sept. 13–15. The course will consist of 20 hr of lecture and discussion organized into 10 sections. Registrants should be familiar with the basic principles of radiologic physics and radiobiology and with the requisite mathematics. Fee: $200. Information: Stewart C. Bushong, Sc.D., F.A.C.R., F.A.C.M.P., Dept. of Radiology, Baylor College of Medicine, One Baylor Plaza, Houston, TX 77030-3498; telephone: (713) 798-4416; fax: (713) 798-5556.

Musculoskeletal MRI

The Dept. of Radiology, Beverly Hills Medical Center, is sponsoring Musculoskeletal MRI, the 1st annual Los Angeles fall conference, Sept. 14–15, at the Loews Santa Monica Beach Hotel, Santa Monica, CA. Program director: Ronald J. Friedman. Faculty: M. Brant-Zawadzki, J. Crues, R. J. Friedman, J. B. Kneeland, and F. G. Shellock. Category 1 credit will be awarded. Fee (through Aug. 1/after Aug. 1): physicians, $275/$310; fellows, residents, interns, and technologists, $175/$210 (letter required). Information: Musculoskeletal MRI, c/o Medical Seminars International, Inc., 18981 Ventura Blvd., Ste. 303, Tarzana, CA 91356; telephone: (818) 774-9077; fax: (818) 774-0244.

Organ Imaging Review

The University of Toronto is sponsoring its annual intensive general radiology course, Sept. 22–27, at the Four Seasons Hotel, Toronto. Radiologic-pathologic correlation will be emphasized. Appropriate use of conventional and advanced imaging techniques and assessment of specific organ systems, including chest, breast, gastrointestinal, genitourinary, musculoskeletal, and CNS, will be discussed. Sonography and radiologic examination of the fetus will be included. Guest faculty: D. Hartman and N. Sadowsky. Category 1 credit: 30 hr. Fee (U.S. dollars/Canadian dollars): physicians, $550/$650; residents and fellows, $360/$425. Information: Edward E. Kassel, M.D., Dept. of Radiology, Faculty of Medicine, Rm. 127, Fitzgerald Bldg., University of Toronto, Toronto, Ontario, Canada M5S 1A8; telephone: (416) 978-6801; fax: (416) 978-6915.

Pediatric Imaging

The Dept. of Radiology, Hospital for Sick Children, University of Toronto, is sponsoring an overview of pediatric imaging, Sept. 27–29, at the Four Seasons Hotel, Toronto. Topics will include congenital anomalies, infections, oncology, trauma, and special procedures for infants and children. Guest faculty: P. Kleinman, R. Lebowitz, and T. Slovis. Fee (U.S. dollars/Canadian dollars): physicians, $320/$375; residents and fellows, $235/$275. Information: Alan Daneman, M.B. Ch., Dept. of Radiology, Faculty of Medicine, Rm. 127, Fitzgerald Bldg., University of Toronto, Ontario, Canada M5S 1A8; telephone: (416) 978-6801; fax: (416) 978-6915.

Tutorial in Portugal

The Dept. of Radiology, The New York Hospital–Cornell Medical Center, is sponsoring a tutorial course at the Hotel Palacio, Estoril, Portugal, Oct. 5–10. Topics to be covered include imaging and interventional radiology. Category 1 credit: 24 hr. Fee: physicians, $475; residents and fellows, $275 (letter required). Information: Radiology Postgraduate Education, Cornell University Medical College, 1300 York Ave., New York, NY 10021; (212) 746-2522.

MR Angiography and MR Imaging of the Cardiovascular System

The Society for Magnetic Resonance Imaging, the Cardiovascular and Interventional Radiological Society of Europe, the European Society of Magnetic Resonance in Medicine and Biology, and SIRM: Sezioni di Radiologia Cardiovascolare ed Interventistica e di Risonanza Magnetica are cosponsoring two meetings in Italy. III International Workshop on Magnetic Resonance Angiography will be held in L'Aquila Oct. 13. Main topics to be discussed are two- and three-dimensional inflow, phase contrast, signal-to-noise ratio and spatial resolution, ultrafast techniques, coils, image presentation, quantita-

tive evaluation, diffusion and perfusion imaging, and clinical applications in different areas. Fee: $100. I Symposium on Magnetic Resonance Imaging of the Cardiovascular System will be held in Rome Oct. 14–16. Techniques and clinical applications of MR angiography and of cardiac MR imaging will be discussed. Fee: $200. Program chairman for both meetings: R. Passariello. Information for both meetings: Paolo Pavone, M.D., Dept. of Radiology, University of L'Aquila, Osp. Collemaggio, 67100 L'Aquila, Italy; telephone: 39-862-26164; fax: 39-862-410997

Radiology/91: Cardiovascular and Interventional Radiology

The Dept. of Radiology, University of Minnesota Medical School, is sponsoring its 54th annual course, Radiology/91: Cardiovascular and Interventional Radiology, Oct. 14–18. The course will be held on the University of Minnesota campus in Minneapolis. Program directors: W. M. Thompson, W. R. Castanedo-Zuniga, D. W. Hunter, J. G. Letourneau, and J. W. Yedlicka, Jr. Category 1 credit: 27.75 hr. Fee: $550. Information: Office of Continuing Medical Education, Radisson Hotel Metrodome, University of Minnesota, 615 Washington Ave., S.E., Ste. 107, Minneapolis, MN 55414; telephone: (612) 626-7600; fax: (612) 626-7766.

New Orleans Fall Radiology Conference

The Dept. of Radiology, School of Medicine in New Orleans, Louisiana State University Medical Center, is sponsoring the New Orleans Fall Radiology Conference, Oct. 28–30, at the Hyatt Regency Hotel, New Orleans. The focus this year will be MR imaging, with special emphasis on the musculoskeletal system, abdomen, and chest. Special sessions will deal with updates in sonography, mammography, and nuclear medicine and in gastrointestinal, pediatric, and interventional radiology. Category 1 credit: 19 hr. Fee: physicians, $440; residents, $295 (letter required). Information: Miss Tammy Garner, LSU School of Medicine, 1542 Tulane Ave., New Orleans, LA 70112; (504) 568-4647.

Computed Body Tomography for the Technologist

The Dept. of Radiology, The Johns Hopkins Medical Institutions, is sponsoring Computed Body Tomography for the Technologist—State of the Art, Nov. 7–10, at the Peabody Orlando Hotel, Orlando, FL. The course will present an integrated approach to the use of body CT. Lectures will be given on normal and pathologic anatomy, with specific emphasis on CT technique and technology. Continuing education credits will be awarded. Fee: $375. Information: Program Coordinator, The Johns Hopkins Medical Institutions, Office of Continuing Education, Turner 20, 720 Rutland Ave., Baltimore, MD 21205; (301) 955-2959.

CT/MRI Head to Toe

The NYU Medical Center, Post-Graduate Medical School, will present the 10th annual CT/MRI Head to Toe, Dec. 15–20, at the Grand Hyatt New York, New York City. The program will be divided into two sections. Part A will be on chest and body CT and MR. Part B will be on CT and MR of the brain, spine, and head and neck. The program will include plenary lectures, workshops, and presentations of clinical cases. Category 1 credit: entire course, 40 hr; part A only, 21 hr; part B only, 19 hr. Fee: entire course $750; part A only, $435; part B only, $375. Information: NYU Medical Center, Post-Graduate Medical School, 550 First Ave., New York, NY 10016; telephone: (212) 263-5295; fax: (212) 263-5293.

Caribbean Cruise—Breast Imaging and MRI at Sea

The Dept. of Radiology, Beverly Hills Medical Center, is sponsoring two courses that will be given during a Caribbean Cruise. The first, Breast Imaging at Sea, will be presented Jan. 11–18, 1992. Faculty: D. Adler and T. Silver. The second, MRI at Sea, will be presented Jan. 18–25, 1992. Topics will include MR imaging of the brain, spine, body, and musculoskeletal system. Faculty: W. G. Bradley, R. Dietrich, and R. J. Friedman. Program director for both courses: Ronald J. Friedman. Category 1 credit will be awarded for both courses. Fee (through Nov. 15/after Nov.15): both courses: physicians, $720/$790; fellows, residents, interns, technologists, and nurses, $620/$690; MR course only *or* breast course only: physicians, $460/$495; fellows, residents, interns, technologists, and nurses, $360/$395. Information: Caribbean Cruise, c/o Medical Seminars International, Inc., 18981 Ventura Blvd., Ste. 303, Tarzana, CA 91356; telephone: (818) 774-9077; fax: (818) 774-0244.

Uroradiology 1992

The Society of Uroradiology will present its 11th annual postgraduate course, Uroradiology 1992, Jan. 13–17, 1992, at the Princess Resort Hotel, Scottsdale, AZ. The course will be a detailed presentation of new developments and basic concepts in urologic imaging and intervention. Information on gynecologic imaging will be included. A major emphasis will be on imaging of the prostate, MR of the urinary tract, the evaluation of impotence, new contrast media, and Doppler and transvaginal sonography. Course director: E. Stephen Amis, Jr. Category 1 credit will be awarded. Information: Dawne Ryals, Ryals and Associates, P. O. Box 1925, Roswell, GA 30077-1925; telephone: (404) 641-9773; fax: (404) 552-9859.

Diagnostic Imaging in Puerto Rico

The Dept. of Radiology, The New York Hospital–Cornell Medical Center, is sponsoring its 17th annual postgraduate course at the Hyatt Regency Cerromar Beach Hotel, Puerto Rico, Jan. 26–31, 1992. The course will review the current status of diagnostic imaging techniques involving various organ systems. Category 1 credit: 22.5 hr. Fee: physicians, $495; residents and fellows, $295 (letter required). Information: Dr. John A. Evans, Director of Radiology Postgraduate Education, Cornell University Medical College, 1300 York Ave., New York, NY 10021; (212) 746-2522.

The American Board of Radiology Examinations

Written examinations for the American Board of Radiology (ABR) are scheduled for Oct. 3–4, 1991; Oct. 1–2, 1992; and Oct. 14–15, 1993. Oral examinations will be held at the Executive West Hotel in Louisville, KY, June 1–5, 1992. The ABR will accept applications for admission to the examinations after July 1, but not later than Sept. 30, in the year *preceding* the year in which the examination is to be taken. For application forms and further information: Office of the Executive Director, The American Board of Radiology, 2301 W. Big Beaver Rd., Ste. 625, Troy, MI 48084.

Meeting and Course Review

For the reader's convenience, a summary of upcoming meetings and courses is provided. Detailed listings are given in the *AJR* issue given in parentheses.

Visiting Fellowships in Interventional Radiology, times arranged, Baltimore (Oct 1990)
Swallowing Center Preceptorship, times arranged, Baltimore (Jan)
Imaging Fellowship, times arranged, Miami Beach, FL (Jan)
Preceptorships in Ultrasound at Johns Hopkins, times arranged, Baltimore (June)
Practicum in Breast Imaging, times arranged, Baltimore (Aug)
World Congress in Ultrasound, Sept. 1–6, Copenhagen (Sept. 1990)
Physics of Diagnostic Radiology, Nuclear Medicine, and Radiation Biology, Sept. 5–8, Sacramento, CA (July)
Pacific Northwest Diagnostic Ultrasound Symposium, Sept. 6–8, Seattle (June)
Registry Preparation Courses for Sonographers: Ultrasound and Doppler Physics, Sept. 7–8, Chicago: Sept. 20–21, Los Angeles; and Oct. 5–6, Dallas; **OB/GYN Ultrasound Review,** Sept. 22, Los Angeles (July)
Abdominal Imaging Review Course, Sept. 7–8, Bethesda, MD (Aug)
International Workshop on Hypertrophic Osteoarthropathy, Sept. 8–11, Dubrovnik, Yugoslavia (Jan)
European Society of Gastrointestinal Radiologists Annual Meeting, Sept. 8–11, Oxford, England (March)
Sonography Update Conference and Exhibit, Sept. 11–13, Coronado (San Diego), CA (May)
Mallinckrodt Institute's 60th Anniversary Celebration, Sept. 12–14, St. Louis (May)
Transrectal Ultrasound in the Diagnosis and Management of Prostate Cancer, Sept. 13–14, Chicago (May)
Diagnostic Ultrasound in Gynecology and Obstetrics and Abdomen, Sept. 13–15, Baltimore (June)
Sonography Registry Review, Sept. 14–15, Coronado (San Diego), CA (May)
European Congress of Radiology 1991, Sept. 15–20, Vienna, Austria (Oct 1990)
MR Imaging Fellowships at LAC/USC Imaging Science Center, Sept. 16–20, Oct. 7–11, and Nov. 4–8, Los Angeles (Feb)
Course on Color Doppler Imaging, Sept. 20–21, Beverly Hills, CA (Aug)
Applied Imaging: A Practical Course, Sept. 22–25, Naples, FL (Aug)
Mammographic Interpretation: A Practical Approach, Sept. 23–26, and Oct. 28–31, Boston (March)
Applied Ultrasound: Accent on Doppler, Sept. 23–26, Laguna Niguel, CA (May)
Diagnosis of Musculoskeletal Disorders, Sept. 25–28, Coronado (San Diego), CA (May)
Dublin 91: Joint Annual Scientific Meeting, Sept. 25–28, Dublin, Ireland (Aug)
Diagnostic Uses of Radiolabeled Monoclonal Antibodies, Sept. 26–27, Washington, DC (June)
International Imaging Course, Sept. 30–Oct. 5, Hong Kong (July)
Magnetic Resonance Imaging 1991: Back to the Future, Oct. 2–5, Cincinnati (July)
Current Concepts of Magnetic Resonance Imaging/Physics, Oct. 3–6, Napa Valley, CA (Aug)
Annual International Body Imaging Congress, Oct. 5–12, Maui, HI (June)
Breast Cancer Diagnosis: State-of-the-Art, Oct. 7–8, New York City (July)
Practical Training in Interventional Radiology, Oct. 7–11 and Nov. 4–8, Lund, Sweden (July)
MR Update: NR and Musculoskeletal, Oct. 7–12, Hilton Head, SC (Aug)
Nuclear Cardiology Symposium and Workshops, Oct. 9–11, Milwaukee, WI (Aug)
MRI: Clinical State of the Art 1991, Oct. 9–12, New York City (July)
Ultrasound: 1991, Oct. 12–13, Sacramento, CA (Aug)
Chest Imaging, Oct. 15–18, Boston (Aug)
Mammography Update 1991, Oct. 17–18, Madison, WI (Aug)
Western Neuroradiological Society Annual Meeting, Oct. 17–20, Laguna Niguel, CA (June)
Michigan Fall Radiology Conference, Oct. 18–19, Royal Oak, MI (Aug)
Progress in Magnetic Resonance Imaging, Oct. 24–25, Cologne, Germany (June)
Neuroradiologic and Musculoskeletal Seminars, Oct. 24–27, Orlando, FL (June)
Advanced Imaging of the Musculoskeletal System, Oct. 26–27, Coronado (San Diego), CA (June)
San Diego Postgraduate Radiology Course, Oct. 28–Nov. 1, Coronado (San Diego), CA (June)
Magnetic Resonance Imaging and CT Update, Oct. 28–Nov. 1, Cambridge, MA (Aug)
Interventional Radiology Course, Nov. 1–3, Coronado (San Diego), CA (July)
Seminar on Bone and Joint Diseases, Nov. 15–17, Scottsdale, AZ (July)
Advanced Seminars in Diagnostic Imaging, Nov. 15–17, Laguna Niguel, CA (Aug)
Diagnosis and Treatment of Bone and Soft-Tissue Tumors, Nov. 21–23, Sacramento, CA (May)
Asian Oceanian Congress of Radiology, Dec. 14–18, New Delhi (July)
International Symposium on Recent Advances in Diagnostic Imaging and Radiation Oncology, March 24–27, 1992, Kathmandu, Nepal (June)
European Symposium on Uroradiology, Aug. 24–27, 1992, Herlev, Denmark (Aug)

AJR carries announcements of courses, symposia, and meetings of interest to its readers if received a minimum of 5 months before the event. There is no charge; receipt of items by the *AJR* Editorial Office is not acknowledged. Submit items for publication typed double-spaced. Provide title, date, location, brief description, sponsor, course directors, fees, category I credit, and address and telephone number for additional information. Faculty from the host institution will not be listed. Guest faculty names will appear **only** if initials are provided. Mail news items to *AJR* Editorial Office, 2223 Avenida de la Playa, Suite 103, La Jolla, CA 92037-3218.

American Roentgen Ray Society:
Officers, Committees, and Membership Information

Officers

President: John A. Kirkpatrick, Jr.
President-elect: A. Everette James, Jr.
1st Vice-president: Andrew K. Poznanski
2nd Vice-president: George R. Leopold
Secretary: Joseph T. Ferrucci, Jr.
Treasurer: Beverly P. Wood

Executive Council: R. N. Berk, M. P. Capp, W. J. Casarella, N. R. Dunnick, R. G. Evens, J. T. Ferrucci, Jr., A. E. James, Jr., J. A. Kirkpatrick, Jr., A. M. Landry, Jr., G. R. Leopold, J. E. Madewell, T. C. McLoud, A. A. Moss, A. K. Poznanski, R. J. Stanley, J. H. Thrall, K. H. Vydareny, N. O. Whitley, B. P. Wood, R. J. Alfidi, chairman

Committees

Editorial Policy: R. N. Berk, E. Buonocore, Melvin M. Figley, C. R. B. Merritt, K. Valji, C. A. Rohrmann, Jr., W. J. Casarella, chairman

Education and Research: R. R. Hattery, C. B. Higgins, B. J. Hillman, R. J. Stanley, W. M. Thompson, N. O. Whitley, chairman

Finance and Budget: R. K. Gedgaudas-McClees, A. A. Moss, J. R. Thornbury, K. H. Vydareny, J. H. Thrall, chairman

Nominating: R. G. Evens, P. J. Fritzsche, A. A. Moss chairman

Publications: E. Buonocore, C. R. B. Merritt, C. A. Rohrmann, Jr., W. J. Casarella, chairman

Membership: J. E. Madewell, T. C. McLoud, A. A. Moss, K. H. Vydareny, chairman

Representatives to Other Organizations

American Board of Radiology: W. J. Casarella, J. A. Kirkpatrick, Jr., L. F. Rogers

American College of Radiology: R. A. Gagliardi, J. E. Madewell, B. L. McClennan, R. J. Stanley

American Medical Association: S. F. Ochsner, delegate; K. L. Krabbenhoft, alternate; K. L. Kidd, CPT Advisory Committee

American National Standards Institute: M. E. Haskin

National Council on Radiation Protection and Measurements: F. D. Miraldi, E. L. Saenger

Armed Forces Institute of Pathology: J. E. Madewell

Meeting Arrangements

Annual Meetings: May 10–15, 1992, Marriott's World Center, Orlando, FL; April 25–30, 1993, Marriott San Francisco, San Francisco, CA

Annual Meeting Committee: J. K. Crowe, N. R. Dunnick, R. R. Lukin, N. H. Messinger, R. J. Stanley, R. D. Steele, Jr., A. M. Landry, Jr., chairman

Instructional Courses: Bruce L. McClennan, associate chairman; R. J. Stanley, chairman

Scientific Program: P. H. Arger, T. B. Hunter, D. Kushner, T. C. McLoud, L. B. Talner, J. H. Thrall, A. E. James, Jr. chairman

Scientific Exhibits: J. R. Haaga, D. S. Hartman, R. G. Ramsey, N. R. Dunnick, chairman

ARRS Membership

An application form is printed in this issue of the Journal. For consideration at the 1992 ARRS meeting, send completed forms before February 1, 1992, to American Roentgen Ray Society, 1891 Preston White Dr., Reston, VA 22091. Active members are graduates of an approved medical or osteopathic school or hold an advanced degree in an allied science. They must practice radiology or work in an associated science in the United States or Canada and be certified by the American Board of Radiology, American Osteopathic Board of Radiology, or Royal College of Physicians of Canada or otherwise adequately document training and credentials. International members are foreign radiologists or scientists who are active in radiology or an allied science. Members-in-training are residents or fellows in radiology or postgraduate students in an allied science. Additional application forms can be obtained from the ARRS offices in Reston, VA.

Business Office

Paul Fullagar, Executive Director, American Roentgen Ray Society, 1891 Preston White Dr., Reston, VA 22091; (703) 648-8992.

American Roentgen Ray Society 92nd Annual Meeting May 10–15, 1992, Orlando, FL Marriott's Orlando World Center

Registration and Hotel Reservations

Forms for advance registration and hotel reservations will be in the February and March 1992 issues of the *AJR*.

Scientific Program

Abstracts of papers to be considered for the program must be submitted by November 1, 1991. Forms on which to submit abstracts are in this issue of the *AJR*. The ARRS Program Committee will select papers and notify authors in early January. The *AJR* has first rights to all papers accepted for presentation at the ARRS meeting. Mail original and five copies to

ARRS President-Elect
c/o Paul R. Fullagar
American Roentgen Ray Society
1891 Preston White Dr.
Reston, VA 22091
Telephone (703) 648-8992

Scientific Exhibits

Proposals for scientific exhibits must reach the Chairman of Exhibits by November 1, 1991. Forms, which may be photocopied, are in this issue of the *AJR*. Send completed form to

N. Reed Dunnick, M.D.
c/o Paul Fullagar
American Roentgen Ray Society
1891 Preston White Drive
Reston, VA 22091
Telephone (703) 648-8992

Refresher Course Program

A summary of the refresher courses will appear in the *AJR* in February along with advance registration forms. Early registration is an advantage in ensuring preferred courses in this popular program.

Local Program

A program of sightseeing, shopping, and entertainment will be developed by the Local Arrangements Chairman. Information and advance registration forms will be in the February issue of the *AJR*.

Residents' Award Papers

The society offers several cash awards for the best scientific papers prepared by residents in radiology. The President's Award has a $2000 prize. There are two Executive Council awards of $1000 each. All are presented at the annual meeting. Papers should be submitted by February 15, 1992, for consideration in this competition. Send entries to

Nancy O. Whitley, M.D.
Dept. of Radiology
University of Maryland Medical Systems Hospital
22 S. Greene St.
Baltimore, MD 21201

Deadlines

Abstracts of papers: November 1, 1991
Scientific exhibit proposals: November 1, 1991
Residents' Award papers: February 14, 1992

Call for Papers

American Roentgen Ray Society 1992 Annual Meeting: May 10–15, 1992, Orlando, FL

ADDRESS OF PRESENTING AUTHOR

Department

Institution

Street

City, State Zip

Phone:

Type title, authors, and abstract in the space provided below. (Instructions are on reverse side of this page. Abstract should not exceed 300 words.)

Select one category: Angio/Interventional Breast Chest CT Gastrointestinal Tract Genitourinary Tract MR Neuroradiology Skeletal Sonography Pediatric

Projection Requirements: 35 mm, single or double (circle one) 16 mm silent film ½'' VHS ¾''

Has this been presented elsewhere? yes no. If yes, please describe on reverse side of this page.

Instructions for Scientific Abstracts

1. Type the information single-spaced. Underline the name of the presenting author. Append as a last line of the abstract any research grant support, if applicable (e.g., Supported by USPHS Grant HE-80144). If the abstract is accepted, it will not be proofread; it will appear exactly as typed. Use the following format:

   MR IMAGING OF THE SPINE AND NECK
   F. S. Lau, M.D., A. N. Kirk, M.D., and R. A. Beck, Ph.D.
   University of California, Bakersfield, Bakersfield, CA 92338

2. Abstracts should include four paragraphs devoted sequentially to the following topics: (1) object or purpose of the study, (2) materials, methods, and procedures, (3) results, (4) significance of the results and conclusions. The text should not exceed 300 words. Specific data are essential. The abstract should be a succinct summary of work done rather than a promissory note.
3. The Program Committee will grade each abstract and determine acceptance. Further information will be forwarded to those whose abstracts are accepted for presentation.

Deadline for submission of abstract is November 1, 1991. Mail abstract and four copies to

ARRS President-Elect
c/o Paul R. Fullagar
American Roentgen Ray Society
1891 Preston White Dr.
Reston, VA 22091
Telephone (703) 648-8992

Call for Scientific Exhibits

American Roentgen Ray Society 1992 Annual Meeting: May 10–15, 1992, Orlando, FL

FOR COMMITTEE USE ONLY

Date Received_____ Application No. _____
Subject_____ Score_____
Rejected_____ Accepted_____
Assigned_____ Space No. _____

Principal Exhibitor's Mailing Address

Name_____ Institution_____

Department_____ Street Address_____ City_____

State_____ Zip Code_____ Telephone: office ( ) _____ home ( ) _____

Names of Exhibitors (List principal exhibitor first and telephone number of each person.)

Last	First	Middle	Telephone	Degree (one only)	Member ARRS?

Title of Exhibit_____

Type abstract single-spaced in the space provided below. (See instructions on the reverse side of this page.)

Instructions for Abstract

The abstract should be a brief paragraph that states the purpose, principal information, and conclusions of the exhibit. Promissory statements are not acceptable. Type single-spaced in the space provided on the reverse side. Brevity is desirable but not at the expense of specific information. **The abstract will appear in the program book as submitted.** Please use typewriter and complete the application form on both sides. List space requirements.

What Type of Exhibit Is Proposed? (Check one and fill in all appropriate blanks.)

_____**Free-standing.** This is a self-contained display created in total by the exhibitor. It may be a fold-open unit, a unit shipped in cases and assembled on site, or a tabletop unit. Linear feet required _____.

_____**Poster Board (backboard panels).** Backboard panels are 4 × 8 ft. (1.2 × 2.5 m). Number of panels required _____. If two panels are needed, there will be a ¼-in. frame separating the panels, thus requiring a separation in the presentation.

_____**Viewbox.** Mounted materials (radiographs and other transparencies) for display on the society's illuminators. Each illuminator is 39.5 × 59.5 in. (100 × 151 cm). Number of illuminators required _____. Materials should not be glass mounted.

Please Indicate Most Appropriate Category.

_____Bone _____Cardiovascular _____Chest_____Gastrointestinal_____Genitourinary _____Breast _____Medical physics
_____Neuroradiology _____Nuclear medicine _____Pediatric_____Radiation oncology_____Sonography

Exhibits will be chosen on the basis of the quality of the abstract and space available. Poster board and computer-based exhibits are encouraged, as they do not require a viewbox.

Signature of Principal Exhibitor_____

Exhibitors will receive instructions for exhibit preparation.

Applications must be received no later than November 1, 1991. Mail original and five copes to

N. Reed Dunnick, M.D.
c/o Paul R. Fullagar
American Roentgen Ray Society
1891 Preston White Dr.
Reston, VA 22091

Telephone: (703) 648-8992

Classified Advertisements

Positions Available

ENDOVASCULAR THERAPIST—The UCLA Dept. of Radiological Sciences has a full-time, assistant professor, tenure-track position. Requirements include California licensure, American Board of Radiology certification, 2-yr neuroradiology fellowship, and 2 yr experience in the job offered and as an academic neuroradiologist. Must have knowledge and experience of endovascular and neuroradiology techniques such as angiography, use of embolic materials, catheters, balloons, and MR, as well as research ability in the area of embolization of cerebral arteriovenous malformations demonstrated by publications. Send application including CV and names and addresses of 3 references to Hooshang Kangarloo, M.D., Chairman, Dept. of Radiological Sciences, UCLA Medical Center, Los Angeles, CA 90024-1721, an EO/AA employer who encourages applications from members of minority groups and women. 9a

MUSCULOSKELETAL RADIOLOGIST—The UCLA Dept. of Radiological Sciences has a full-time, assistant professor, tenure-track position. Requirements include California licensure, American Board of Radiology certification, 2-yr musculoskeletal fellowship, at least 2 yr experience in the job offered, knowledge and experience in musculoskeletal radiology, MRI, arthrography, CT, and nuclear medicine with a strong interest and ability in teaching. Must have research ability demonstrated by publications. Send application including CV and names and addresses of 3 references to Hooshang Kangarloo, M.D., Chairman, Dept. of Radiological Sciences, UCLA Medical Center, Los Angeles, CA 90024-1721, an EO/AA employer who encourages applications from members of minority groups and women. 9a

NORTHERN CALIFORNIA—The Permanente Medical Group, Inc., is seeking a BC radiologist with multimodality interests and fellowship training in MR to join a 12-person group serving a 337-bed, acute-care hospital and 2 outpatient clinics. Teaching opportunities are available with residents of subspecialty services on rotation from Stanford University Hospital, as well as our own medical residents. We have sited a GE 1.5-T MRI system. Competitive salary and excellent benefits. Please send inquiries and CV to Bruce Baker, M.D., Chief, Dept. of Radiology, Kaiser Permanente Medical Center, 900 Kiely Blvd., Santa Clara, CA 95051; (408) 236-4444. EOE. 9–11a

RADIOLOGIST, board-certified preferable, to join staff covering 4 hospitals and an outpatient clinic in southeast Georgia. Skills must include general diagnostic, ultrasound, nuclear medicine, mammography, CT, and special procedures. Salary negotiable. Send letters of inquiry with CV and letters of reference to Office Manager, Regional Diagnostics, P. O. Box 147, Vidalia, GA 30474. 9a

DIAGNOSTIC RADIOLOGIST—Immediate opening at Women's and Children's Hospital in Lafayette, LA. This 93-bed hospital that concentrates on OB-GYN, pediatric, and neonatology services is seeking a BC/BE radiologist. All medical specialties included on staff. Skills include CT scan, mammography, fluoroscopy, and ultrasound. Lafayette, population 95,000, is located almost midway between New Orleans and Houston, TX. The area offers excellent hunting, fishing, and other water sports. Lafayette is known for its authentic Cajun cuisine. Salary and benefits are competitive and generous. Interested applicants should forward CV to Steve Bogacki, Physician Relations, HealthTrust, Inc., P. O. Box 24350, Nashville, TN 37202-4350; (800) 825-3463. No agency calls please. 9ap

SECTION CHIEF, ABDOMINAL IMAGING—The University of Nebraska Medical Center, Dept. of Radiology is recruiting a radiologist to head a section of 2 other GI radiologists. Responsibilities include abdominal CT, abdominal MRI, and traditional GI barium studies. The medical center specializes in tertiary care with emphasis on biliary disease and organ transplantation. The University of Nebraska Medical Center, Dept. of Radiology, currently has 31 faculty members and a very well-equipped dept. This is an academic position requiring strong interest in clinical teaching and research as well as patient care. Academic rank is commensurate with qualifications. Please send inquiries with a CV by Sept. 30, 1991, to Thomas J. Imray, M.D., Professor and Chairman, Dept. of Radiology, University of Nebraska Medical Center, 600 S. 42nd St., Omaha, NE 68198-1045. The University of Nebraska Medical Center is an equal opportunity/affirmative action employer, M/F/H/V. 9a

INTERVENTIONAL RADIOLOGIST—The renowned Geisinger Clinic in Pennsylvania seeks an aggressive associate to develop/manage a new service at the Wyoming Valley Medical Center, its eastern cornerstone. Now 5 M.D.s and 40 techs handle 75,000 exams/yr. Equipment includes MRI, CT, SPECT, and a new angio room with biplane/digital capability. Skills required are basic neuro and angio, renal and peripheral angioplasty (no cardiac), biliary and renal drainage, thrombolytic therapy, and percutaneous biopsy. Responsibilities include administrative leadership, clinical practice (50% IVR, 50% any mix), and some teaching of techs. Call is shared, with general and specialist call equalized. Compensation is competitive with private practice partnership. Benefits include TSAs, insurances, 4 wk vacation/4 wk CME. Geisinger's beautiful new Wyoming Valley Medical campus is located in the western Poconos with affordable housing, excellent schools (12 college/universities), and a family-oriented lifestyle that supports traditional values. For details call Carole Gregory at MedQuest (215) 640-3774 or send CV to P. O. Box MQ, Devault, PA 19432. 9a

THE NATIONAL INSTITUTES OF HEALTH is seeking an interventional radiologist with fellowship training. Resources include 20 fully equipped angiographic rooms and extensive research opportunities with laboratory support available. Would share duties with 2 other senior angiographers. Generous benefit package and appointment at Georgetown University Hospital is included. Interested candidates should contact John L. Doppman, M.D., Dept. of Radiology, National Institutes of Health, Bldg. 10, Rm. 1C-660, Bethesda, MD 20892; (301) 496-5080. 9–11ap

DIAGNOSTIC RADIOLOGIST—Mallinckrodt Institute of Radiology, Washington University, seeks an additional board-certified radiologist with academic interest to staff a satellite hospital of Barnes Hospital in St. Louis. This satellite radiology facility in St. Louis county performs all aspects of diagnostic radiology, including CT, MRI, ultrasound, and nuclear medicine. Equipment is brand new and state-of-the-art. Candidates must be competent in all aspects of diagnostic radiology and must be able to do cross-sectional interventional procedures. Academic rank and salary are dependent on qualifications and previous experience. The institute is conducting research in teleradiology and outcomes research at the satellite facility. Washington University is an equal opportunity employer. Applications from women and minority group members are encouraged. Send CV to R. Gilbert Jost, M.D., Chief of Diagnosis, Mallinckrodt Institute of Radiology, 510 S. Kingshighway Blvd., St. Louis, MO 63110. 9–11ap

DIAGNOSTIC RADIOLOGIST IMMEDIATE OPENING AT ROSE MEDICAL CENTER (RMC), DENVER, CO—An 8-person radiology group is recruiting an additional radiologist with fellowship training in MR and CT. The practice involves all imaging modalities. Highly competitive first yr salary and generous fringe benefit package. Position leads to offer of equal shares in the professional corporation after 1 yr., if mutually agreed upon. RMC is affiliated with the University of Colorado. Contact David W. Wilder, M.D., or Jeffrey A. Levy, M.D.; (303) 320-2256. 9–11ap

RADIOLOGISTS—An innovative health care organization is seeking radiologists to serve communities in rural southern West Virginia. Competitive salary and fringe benefits are offered. A desire and willingness to meet challenges of present-day health care delivery in rural settings is a must. Send confidential resume and inquiries to Box O9, *AJR* (see address this section). 9–11ap

CHIEF, DEPT. OF RADIOLOGY, UNIVERSITY OF CALIFORNIA, SAN FRANCISCO SCHOOL OF MEDICINE, MOUNT ZION HOSPITAL AND MEDICAL CENTER—The University of California, San Francisco (UCSF) is seeking a chief of radiology for Mount Zion Hospital and Medical Center (MZH), 1 of 4 core teaching hospitals. Candidate will be appointed at the level of associate professor or professor of radiology (depending on qualifications) and also serve as vice-chairman of the Dept. of Radiology at UCSF. The Mt. Zion chief of radiology must be an excellent teacher and an experienced administrator who will supervise all clinical, teaching, and research programs in radiology at Mt. Zion. Demonstrated record of ability in clinical and academic research in several modalities such as MRI, ultrasound, CT, and conventional radiology, as well as familiarity with angiography/interventional procedures is desirable. Physician staffing consists of 4 full-time radiologists, fellows in radiology, and radiology residents. Equipment includes Phillips cardiac angio, CGR mammography unit, Acuson ultrasound, Phillips CT (with GE 9800 scanner ordered), and 0.5-T GE MR. A 1.5-T MRI will be on line in the first quarter of 1992. There are 40,000 radiology exams performed annually including 2,000 MRI exams. Mount Zion Hospital has 460 beds. The University of California is an equal opportunity/affirmative action employer. Minority groups, women, and handicapped are encouraged to apply. Send CV to Charles B. Higgins, M.D., Chair, MZH/UCSF Search Committee, Dept. of Radiology, UCSF, San Francisco, CA 94143-0628. 9a

TEXAS, DIAGNOSTIC RADIOLOGIST—Excellent, private-practice opportunity for BC/BE radiologist seeking professional satisfaction and quality of life. Noninvasive procedures; all other modalities except MRI. New equipment in new hospital. Well-trained, congenial medical staff eager to work with radiologist. Great outdoor recreation; hunting and lakes; easy access to stream fishing and snow skiing. Contact Jim Truitt, Physician Resource Network, P. O. Box 37102, Fort Worth, TX 76117-8102; (800) 525-6055. 9–11ap

DIAGNOSTIC RADIOLOGIST—Immediate opening for BC/BE radiologist to join group of 6 in an active practice including 2 hospitals (480 beds) and a multispecialty clinic that performs 110,000 exams/yr. Practice includes substantial CT, nuclear medicine, ultrasound, MRI, angiography, and interventional and is located in a pleasant community on Lake Michigan with easy access to Milwaukee and Chicago. Locums needed in interval. Contact Arnold Strimling, M.D., Dept. of Radiology, St. Mary's Medical Center, 3801 Spring St., Racine, WI 53405; (414) 636-4311. 9ap

DIAGNOSTIC RADIOLOGIST—Board-certified/eligible radiologist with skills in CT, MRI, ultrasound, nuclear medicine, and mammography needed for position with group of 12 young radiologists. Expanding practice is hospital-based, fee-for-service with 2 private-practice offices. Hospital-based practice in 400-bed hospital includes MRI, 2 CT units, modern interventional suite, satellite outpatient imaging center, and breast care center. Private-practice offices include MRI facility and full-service radiology office. Position available July 1992. Interested applicants should submit letter and CV to G. Edward Streubert, M.D., MRI of Bethlehem, Inc., Ste. 105, 95 Highland Ave., Bethlehem, PA 18017. 9–11ap

CHAIRMAN, DEPT. OF DIAGNOSTIC RADIOLOGY, ALBERT EINSTEIN MEDICAL CENTER Albert Einstein Medical Center is a tertiary-care, 600-bed hospital with major affiliations with Temple University School of Medicine. We are now seeking a full-time chairman for the Dept. of Radiology, which includes an independent, fully accredited residency program. The dept. consists of the Divisions of Diagnostic Radiology and Nuclear Medicine. Besides an active general radiology service, it performs studies in ultrasound, CT, body imaging, MRI, mammography, pediatric radiology, and interventional procedures. It has state-of-the-art equipment and an active research program consisting of dedicated MDs and Ph.D. scientists who provide special expertise in radiation biology. The professional staff consists of all full-time, board-certified physicians who hold faculty positions at Temple University School of Medicine. Currently, the dept. performs over 180,000 diagnostic and nuclear medicine exams annually and provides diagnostic services at 2 other satellite locations. The successful candidate must possess strong academic credentials and demonstrate capabilities in patient care, education, research, and administration. He or she would be expected to qualify for an appointment as a full professor and a senior associate chairman of the Department of Radiology at Temple University School of Medicine. Please submit CV to I. Daskal, M.D., Ph.D., Chairman, Dept. of Pathology and Laboratory Medicine, and Chairman, Dept. of Radiology Search Committee, Albert Einstein Medical Center, 5501 Old York Rd., Philadelphia, PA 19141-3098. Equal opportunity employer. 9a

DIAGNOSTIC RADIOLOGIST—Immediate opening for board-certified/eligible radiologist with expertise in CT, MRI, ultrasound, mammography, nuclear medicine, and angiography to join a group of 3 board-certified radiologists. Active ACR-accredited mammography program. 175-bed hospital and private clinic. Excellent living area on the southern Oregon coast with fishing, crabbing, and boating opportunities and only a 4-hr drive for superb skiing. Send inquiries and CV to Michael S. Quinn, M.D., or Norman A. Fiet, M.D., South Coast Radiologists, P.C., 2650 N. 17th St., Coos Bay, OR 97420; (503) 267-5411. 9–10ap

ULTRASOUND/CT/MRI—Opportunity for board-certified radiologist specializing in ultrasound, body CT, and body MRI to pursue an academic career at The New York Hospital-Cornell Medical Center. The dept. provides state-of-the-art equipment, including Acuson ultrasound, GE 9800 CT, and GE Signa 1.5-T MR. A wide variety of ultrasound exams are performed, including abdominal, OB-GYN, color Doppler, small parts, neonatal head, transvaginal, and transrectal. A candidate with prior fellowship in sectional imaging or ultrasound is preferred. Responsibilities include clinlical practice, teaching, and research. Position available 9/1/91. Please send CV to Elias Kazam, M.D., Dept. of Radiology, the New York Hospital-Cornell Medical Center, 525 E. 68th St., New York, NY 10021. 9–12a

FLORIDA—Nuclear medicine and diagnostic radiologists needed for a well-established and progressive group of 14 radiologists in Tampa Bay covering 2 hospitals and outpatient imaging centers. Busy nuclear division with single- and triple-headed SPECT. Nuclear boards or additional fellowship training in interventional radiology or sonography required. Candidate must be willing to cover other areas of diagnostic imaging as well. Competitive first yr salary followed by equitable partnership rate. Send CV to Box O11, *AJR* (see address this section). 9–11ap

COASTAL NORTHERN CALIFORNIA/SAN FRANCISCO BAY AREA—A progressive, diversified group of 16 board-certified diagnostic radiologists, 5 radiation oncologists, and 2 medical oncologists seeks a board-eligible/certified radiologist with some training in MRI and/or neuroradiology. The group serves 4 small- to medium-sized hospitals and a large, outpatient imaging center. The imaging center includes a GE 1.5-T MRI, 9800 Advantage CT, and Acuson ultrasound, as well as CGR mammography, and 3 RF rooms. Competitive salary, 2 yr to full partnership, and excellent benefits. Fast-growing, suburban community 50 min north of downtown San Francisco with sunny Mediterranean climate and very mild winters in the heart of the wine country. Excellent outdoor recreational opportunities. Please send initial inquiry and CV to John J. McGovern, M.D., 121 Sotoyome St., Santa Rosa, CA 95405; (707) 546-4062. 9–2ap

ONCOLOGIC RADIOLOGY/MAMMOGRAPHY The Dana-Farber Cancer Institute and Brigham and Women's Hospital, teaching affiliates of Harvard Medical School, seek a full-time diagnostic radiologist with interests in oncologic radiology and mammography. The 2 hospitals are in close proximity and the radiology dept. at Dana-Farber Cancer Institute is staffed by Brigham and Women's Hospital faculty and residents. The Dana-Farber Cancer Institute is one of the world's leading cancer treatment and research facilities and many opportunities exist for collaborative clinical research in cancer imaging. Please contact Jack E. Meyer, M.D., Director of Diagnostic Radiology, Brigham and Women's Hospital and Dana-Farber Cancer Institute, 75 Francis St., Boston, MA 02115; (617) 732-6269. Brigham and Women's Hospital/Dana-Farber Cancer Institute/Harvard Medical School is an affirmative action/equal opportunity educator and employer. 9–2a

DIAGNOSTIC RADIOLOGIST—Immediate opening leading to partnership in expanding 4-member, hospital-based practice near Boston. Seeking recently trained BC/BE radiologist with skills and experience in general radiology, ultrasound, mammography, CT, and angio/interventional. Interested persons should contact Steven Sitzman, M.D., The Malden Hospital, One Hospital Rd., Malden, MA 02148; (617) 322-7560. 9–11ap

INTERVENTIONAL RADIOLOGIST, ALBUQUERQUE, NM—Well-established, 14-physician group has immediate opening for fellowship-trained vascular interventionalist. Initially, approximately 40–50% of work time will be devoted to interventional procedures; potential exists for additional interventional volume as senior physicians phase down. Practice serves a major hospital within the metropolitan area, 2 MRI centers, 2 outpatient centers, and 3 outlying facilities. All vascular interventional work performed at 1 location. Candidates must have ability and desire to perform both interventional and general radiology procedures. Strong desire to live and work in the southwest is a must. Competitive compensation package. Send CV with references to J. R. Ellison, Executive Director, Radiology Associates of Albuquerque, P.A., 4001 Indian School Rd., N.E., Ste. #300, Albuquerque, NM 87110; (505) 262-1975. 9a

RADIOLOGIST, TYLER, TX—The University of Texas Health Center at Tyler invites applications for a clinical faculty position in the Dept. of Radiology. Some teaching is required, but not publishing or research. A progressive, 4-person dept. practices general radiology (including interventional, MRI, and SPECT) and performs approximately 27,000 exams/yr. New equipment, flexible work hours, very light call, and no weekend schedule. Year-round tennis, golf, and boating are available in addition to excellent schools. Competitive first-yr salary and an unsurpassed benefits package are offered. Send CV to J. R. Shepherd, M.D., University of Texas Health Center at Tyler, P. O. Box 2003, Tyler, TX 75710; (903) 877-7100. The University of Texas Health Center at Tyler is an affirmative action, equal opportunity employer. Minorities are encouraged to apply. 9–11a

MIAMI VETERANS AFFAIRS MEDICAL CENTER is seeking 2 full-time and 1 part-time staff radiologists for its teaching hospital affiliated with the University of Miami School of Medicine. Candidates must board-certified or eligible, with education and experience in CT, MRI, and special procedures. Interested physicians send CV and list of references to Personnel Service (05C3/Jean Little), VA Medical Center, 1201 N.W. 16th St., Miami, FL 33125; (305) 324-4455, ext. 3617. VA is EOE. 9a

DIAGNOSTIC RADIOLOGIST, HAWAII—Excellent opportunity and lifestyle in a multispecialty group servicing west Kauai. Benefits include malpractice insurance, medical plan, life insurance, retirement plan, profit-sharing plan, disability insurance plan, paid vacation, and holidays. Call or send resume to Y. Miyashiro, M.D., Garden Island Medical Group, P. O. Box 669, Waimea, HI 96796; (808) 338-1645 or fax (808) 338-1141. 9ap

POSITION OPEN IMMEDIATELY—A 40-physician, multispecialty clinic serving central and western Kansas, seeks a board-eligible/certified radiologist. Excellent facilities include diagnostic radiography, CT scan, diagnostic ultrasound, nuclear medicine, and MR services. Very competitive salary and benefits. No night or weekend call. An excellent opportunity in a dynamic practice setting. Please send CV to Administrator, Hutchinson Clinic, 2102 N. Waldron, Hutchinson, KS 67502; (316) 669-2626 (collect). 9–11ap

NORTHERN CALIFORNIA—BC diagnostic radiologist sought for medical imaging dept. in a large, multispecialty group practice. Facility features new state-of-the-art equipment, including Phillips CT, SPECT, color Doppler, and mobile 0.5-T MR. Beautiful community in the heart of the wine country, 50 mi. north of San Francisco. Excellent salary and benefits package leading to eligibility for shareholder status. Send CV to Alan Larocque, M.D., Ph.D., Dept. of Medical Imaging, Kaiser Permanente Medical Center, 401 Bicentennial Way, Santa Rosa, CA 95401-2192. EOE. 9–11a

A 4-MEMBER RADIOLOGY GROUP that recently lost 2 physicians to retirement seeks a radiologist to join a rapidly growing practice. Over 70,000 exams. Fifty new physicians and surgeons have joined the staff in the past 2 yr. We are the only radiologists in the medical community serving a 300-bed, regional facility with a service area of 215,000 on Lake Michigan in southwestern Michigan, located only 90 min from Chicago and 30 min from South Bend, IN. Excellent schools and affordable housing. $175,000 first yr salary with second and third yr substantial increases. Full partnership after third yr. Paid malpractice, customary personal insurance, and paid interviewing and relocation expenses. Send CV or call Ken Sammut, Jackson and Coker, Inc., 115 Perimeter Center Pl., Ste. 380 11093, Atlanta, GA 30346; (800) 544-1987. 9a

THE UNIVERSITY OF CALIFORNIA, SAN FRANCISCO, AND ITS AFFILIATE, VA MEDICAL CENTER, FRESNO, are seeking an academically oriented, creative radiologist with demonstrated leadership ability for the position of director of the residency program. Qualifications include board certification in radiology and interest, skill, and background in clinical instruction and research. The central California location offers delightful living conditions and ready access to both coastal and mountain recreational areas. Address inquiries and send CV to Malcolm F. Anderson, M.D., Chief of Radiology, 2615 E. Clinton Ave., Fresno, CA 93703; (209) 228-5358. UCSF is an AA/EOE, M/F/H/V. 9–11a

ARIZONA—VA Medical Center Imaging Service, Prescott, AZ, is accepting applications for a full-time radiologist. Competence and proficiency in interpreting CT scans is required. Prescott is a 217-bed, general medicine hospital with a busy, combined radiology and nuclear medicine service. Prescott is located in the mountains of north central Arizona with a population of 50,000. Commitment and selection is dependent on obtaining and installing a CT scanner. Salary, approximately $80,000, dependent on qualifications. Send CV to Mary M. Poncel, M.D., Chief of Imaging Service, VA Medical Center, Prescott, AZ 86313; (602) 445-4860, ext. 6045, or 776-6045. An equal opportunity employer. 9a

BC DIAGNOSTIC RADIOLOGIST—Affluent practice. Excellent salary, benefits, and early partnership. Investigate now before socialized medicine becomes a reality! Practice at a 395-bed hospital, the second largest in the beautiful state of Delaware, centrally located on the east coast. This is a rapidly expanding, high-powered, group practice. Subspecialty training in interventional, imaging, or neuro desired. Open to F-M with 1–2 yr of postgrad experience. Send resume to or contact Ben Hollander, M.D., Dept. of Radiology, St. Francis Hospital, 7th and Clayton Sts., Wilmington, DE 19805; (302) 421-4300. 9–2ap

NEURORADIOLOGIST—The Dept. of Radiology at Yale University School of Medicine is seeking a neuroradiologist with a strong interest and experience in MR and MR physics for a full-time academic position. Rank is commensurate with experience. Research opportunities are stressed in a strong academic dept. with state-of-the-art radiologic equipment. Candidates must be board-certified or eligible, with fellowship training. Please send CV to Gordon Sze, M.D., Director, Neuroradiology, Dept. of Diagnostic Radiology, Yale University School of Medicine, 333 Cedar St., P. O. Box 3333, New Haven, CT 06510. Yale University is an equal opportunity/affirmative action employer. Applications from women and minority groups are encouraged. Application deadline is Jan. 31, 1992. 9–10a

STAFF RADIOLOGIST—Opportunity for board-certified radiologist at DVA Medical Center, Sepulveda, CA. Recent MRI and interventional radiology training desirable. UCLA-affiliated institution with residency training in medicine, surgery, and psychiatry. Sepulveda is in the beautiful San Fernando Valley, approximately 20 mi. from downtown Los Angeles. Extensive outdoor recreational activities, cultural diversions, fine schools, community colleges, and universities are nearby. Licensure in any state acceptable. Moving expenses authorized. Excellent employment benefits including 30 days paid vacation, 15 days sick leave, liberal education leave, life and health insurance benefits, malpractice insurance, and retirement program. Salary commensurate with experience. Contact or send CV to Ann Esguerra, M.D., Chief of Radiology, DVA Medical Center, Sepulveda, CA 91343; (818) 891-7711. An equal opportunity employer. 9a

HOSPITAL-BASED, BC/BE RADIOLOGIST needed to join newly laid plans for a subregional medical center (campus). Must be proficient in general diagnostic radiology, ultrasound, nuclear medicine, CT, and MRI. Excellent opportunity plus attractive financial package. Located in east, central Montana along the Yellowstone River. Great outdoors for recreation, hunting, and fishing. Excellent education system. Lifestyle is rural and family-oriented. Send CV to Vice-President, Business Services, Holy Rosary Hospital, 2101 Clark, Miles City, MT 59301. 9–11ap

RADIOLOGIST, FLORIDA KEYS—Immediate opening for a BC/BE general diagnostic radiologist. MRI experience desirable. Growing hospital-based practice. Competitive salary leading to partnership. Excellent yr-round climate with exceptional boating, diving, and fishing. Send CV to W. Moccia, M.D., 344 E. Seaview Dr., Marathon, FL 33050; (305) 743-7115. 9–11ap

PHYSICIAN/RADIOLOGIST—Large radiology group with multiple private offices seeks a board-certified radiologist interested in a full-time position. Responsibilities include general radiography. Special training in CT, ultrasound, and nuclear medicine is preferred. Excellent southern New Jersey location. Competitive salary and benefit package. Send CV to RABC, P. O. Box 729, Mt. Holly, NJ 08060. 9–11ap

DIAGNOSTIC RADIOLOGIST—This university-affiliated Veterans Affairs Medical Center in eastern Virginia seeks BC/BE candidates to join our 5-person staff in Nov. 1991. Expertise required in general diagnostic, ultrasound, CT, vascular, and interventional radiology. Position offers opportunity for resident teaching. Please forward CV to C. B. Mahon, M.D., Chief, Radiology Service, Veteran Affairs Medical Center, Hampton, VA 23667. The Dept. of Veterans Affairs is an equal opportunity employer. 9–10a

DIRECTOR OF PEDIATRIC RADIOLOGY—St. Christopher's Hospital for Children seeks a director of radiology to continue the tradition of excellence. The dept. has state-of-the-art imaging equipment that includes CT, MRI, ultrasound, nuclear medicine, and digital subtraction. St. Christopher's Hospital for Children is a new 183-bed, tertiary-care, pediatric hospital in Philadelphia. The Director would assume responsibility for the busy clinical, teaching, and academic activities of the dept. Candidates should be experienced pediatric radiologists with a record of achievement. The position includes an academic appointment in the Dept. of Diagnostic Imaging of Temple University School of Medicine. Please send inquiries to Mark Joffe, M.D., St. Christopher's Hospital for Children, Member of United Hospitals, Inc., Erie Ave. at Front St., Philadelphia, PA 19134-1095. EOE, M/F. 9a

DIAGNOSTIC RADIOLOGIST—BC/BE radiologist wanted to join 2 established radiologists in a hospital-based practice. Candidate must have training/experience in general radiographic procedures, nuclear medicine, CT, ultrasound, mammography, angiography, and MRI. Send inquiries to Maurice Huffman, M.D., 4343 18th Ave., Rock Island, IL 61201. 9–10ap

BC RADIOLOGIST position available to join group of 3 radiologists in a large, multispecialty health-care facility in Seattle. Strong interest and experience in ultrasound, including OB, desired. Strong mammography experience a plus. Diverse patient population includes a mix of managed care and fee-for-service. Outpatient radiology only, limited call, competitive salary, and excellent benefits. Contact Mary Anderson, Pacific Medical Center, 1200 12th Ave. S., Seattle, WA 98144; (206) 326-4100. 8–9ap

THE DEPT. OF DIAGNOSTIC RADIOLOGY, OREGON HEALTH SCIENCES UNIVERSITY, PORTLAND, OR, invites applications for a board-certified musculoskeletal radiologist. Rank will be commensurate with experience and qualifications. Please send CV and references to William Weidner, M.D., Chairman, Diagnostic Radiology, UHN 72, Oregon Health Sciences University, Portland, OR 97201-3098. OHSU is an affirmative action, equal opportunity employer. 8–9a

DIAGNOSTIC IMAGING AND NEURORADIOLOGY, TWO POSITIONS—The 11-member imaging section of Guthrie Clinic–Robert Packer Hospital desires associates with fellowship training and/or expertise in the above areas. The Guthrie Clinic provides tertiary care in the southern tier of New York and the northern tier of Pennsylvania in the beautiful, endless mountains. Outstanding practice opportunities in an environment free of urban hassle. Please send letter of inquiry with CV or call Thomas F. Bednarek, M.D., Chairman, Dept. of Radiology, Guthrie Healthcare System, Sayre, PA 18840; (717) 882-4025. 8–10a

HARTFORD, CT—Position available for board-certified radiologist to join an established group of 8. Practice includes hospital and 4 private offices, all fully equipped, including CT. Mammography and nuclear medicine experience is essential. Competitive starting salary and benefits. Please enclose CV with initial correspondence to Jeffrey Blau, M.D., 40 Hart St., New Britain, CT 06052; (203) 229-2059. 8–10a

DIAGNOSTIC RADIOLOGIST, HOUSTON—Immediate opening for 2 BC/BE radiologists to join 5 BC radiologists associated with a large, internal medicine clinic near the Texas Medical Center. Primarily outpatient practice with regular hours. Also cover adjacent general, medical-surgical hospital. On-site ultrasound, CT, MRI, and nuclear medicine. Experience in angio and interventional is desired. Please send CV to Robert B. Hall, Administrator, Diagnostic Clinic of Houston, 6448 Fannin, Houston, TX 77030; (713) 797-9191. 8–10a

NEURORADIOLOGIST—The Dept. of Radiology at the University of Arkansas for Medical Sciences is seeking a neuroradiologist at the assistant or associate professor rank. Neuroradiology coverage is for 3 hospitals with state-of-the-art equipment including 2 1.5-T MRI units, 5 CT scanners, and 4 angiographic suites. Facility for neurointerventional work is available. Dedicated animal laboratory with advanced NMR spectroscopy units available for research. Candidate must be board-certified and preferably a senior member in ASNR. University of Arkansas for Medical Sciences is an equal opportunity employer. Address inquiries and a current CV to Edgardo Angtuaco, M.D., Chief, Neuroradiology, Dept. of Radiology, University of Arkansas for Medical Sciences, 4301 W. Markham St., Slot 596, Little Rock, AR 72205; (501) 686-6032, (501) 686-6900 (fax). 8–10a

DIAGNOSTIC RADIOLOGIST, NEW MILFORD, CT—A third radiologist is sought for a busy, private practice located in 1 of the most beautiful areas of Connecticut. We provide the full range of diagnostic services for a modern, well-equipped, community hospital. Choice environment; excellent compensation. Send inquiries and CV to Jules White, M.D., New Milford Hospital, 21 Elm St., New Milford, CT 06776; (203) 355-2611, ext. 235. 8–11ap

NEURORADIOLOGIST—Senior ASNR member needed for excellent hospital and imaging center position in Tucson, AZ. Early partnership opportunity. Send CV to Arizona State Radiology, 7250 E. Ventana Canyon Dr., Tucson, AZ 85715. 8–7ap

THE DEPT. OF RADIOLOGY AT WALTER REED ARMY MEDICAL CENTER is recruiting academic radiologists. We need board-certified radiologists to work in this famous and modern health-care center. Our dept. has a residency program consisting of 24 residents and several fellows. Subspecialists are needed in ultrasound, chest, mammography, genitourinary, gastrointestinal, pediatric, CT, MRI, and interventional radiology, as well as general radiology. Excellent opportunity to live in the nation's capital and also become an integral part of a large teaching program. Salaries are competitive and generous. Highly motivated applicants should contact Col. Mark F. Hansen, Radiology Consultant to the Army Surgeon General, Dept. of Radiology, TAMC, HI 96859-5000; (808) 433-6393. 8–7a

THE RADIOLOGY DEPT. AT DWIGHT DAVID EISENHOWER ARMY MEDICAL CENTER is recruiting academic radiologists. The dept. provides a full range of services including angiography, ultrasound, CT (with a new GE 9800 Advantage system), and MRI (with a new 1.5-T GE Signa system). Development is underway for the installation of a digital teleradiology link to area medical facilities. The dept. is also beginning a radiology residency program in affiliation with the program at the Medical College of Georgia in Augusta. With this growth, the dept. has generated a need for several academic diagnostic radiologists. Board-certified diagnostic radiologists with academic credentials and/or experience are urged to apply. Fellowship training is desired, especially in interventional radiology and/or angiography, however candidates at all levels will be considered. Candidates should be particularly interested in patient care, teaching, and research. The medical center is located on Fort Gordon, GA, adjacent to Augusta and is the tertiary-care hospital supporting 9 Army community hospitals of the southeastern region and Puerto Rico. The hospital supports fully accredited residency programs in family practice, general surgery, medicine, orthopedics, pathology, and psychiatry. Salary and benefits are competitive and generous. The medical center is an EO/EEO employer. Please contact Dr. Thomas M. Ralston, LtC., Chief, Radiology Dept., Eisenhower Army Medical Center, Fort Gordon, GA; (404) 791-6245. 8–7a

PEDIATRIC RADIOLOGIST—The Mallinckrodt Institute of Radiology has an opening for a pediatric radiologist. Faculty rank of instructor, assistant, or associate professor will be based on experience. Work site is St. Louis Children's Hospital in a well-equipped pediatric section performing approximately 58,000 studies/yr. Duties include ultrasound, body CT, and general pediatric radiology. MR to be installed on-site within the yr. Interested persons should contact William H. McAlister, M.D., Mallinckrodt Institute of Radiology, 510 S. Kingshighway Blvd., St. Louis, MO 63110. 8–9a

FACULTY POSITION IN ABDOMINAL IMAGING Dartmouth-Hitchcock Medical Center is seeking a faculty member at the associate professor level with experience and interest in abdominal imaging radiology. Clinical responsibility will be in an entirely new 400-bed, clinical facility opening in Oct. 1991 with state-of-the-art instrumentation. Position will involve responsibility for residency training in GI/GU area. Proven record of academic performance including research and teaching with an interest in providing academic guidance for energetic staff of younger radiologists necessary. Interested candidates write with CV to Peter K. Spiegel, M.D., Chairman, Dept. of Diagnostic Radiology, Dartmouth-Hitchcock Medical Center, Hanover, NH 03756. AA/EOE. 9xap

DIAGNOSTIC RADIOLOGIST needed to join an expanding, multimodality breast center located in east Tennessee, near the foothills of the Smoky Mountains. Please send CV to Kamilia Gitschlag, M.D., Bluepointe Pl., 6307 Lonas Dr., Knoxville, TN 37909. 8–9ap

VASCULAR/INTERVENTIONAL RADIOLOGIST, LONG ISLAND, NY—Board-certified radiologist with fellowship training or equivalent experience in vascular/interventional radiology needed to join a 5-member group starting July 1992. Angio suite currently being upgraded to latest state-of-the-art equipment. Must be willing to do most aspects of diagnostic radiology. This well-established practice includes a 325-bed community hospital, a private diagnostic radiology office, and a 1-yr-old MRI facility. Generous salary leading to full partnership. Contact Ira Langer, M.D., 250 Hospital Rd., Patchogue, NY 11722; (516) 475-1030. 8–11ap

PRIVATE PRACTICE IN MIDTOWN MANHATTAN seeks a board-certified diagnostic radiologist with experience and interest in mammography and ultrasound. Send CV to Julie S. Mitnick, M.D., and Bala Subramanyam, M.D., Murray Hill Radiology, 30 E. 40th St., Ste. 1100, New York, NY 10016. 8–9ap

ULTRASOUND STAFF POSITION—The Dept. of Radiology of the Ochsner Clinic is seeking an additional radiologist to meet growing clinical needs in the Section of Ultrasonography. The ultrasound section of the dept. currently performs over 12,000 procedures/yr, including a full range of abdominal, OB/GYN, vascular, operative, interventional, and pediatric studies. State-of-the-art imaging, duplex color Doppler, and intraoperative equipment is available. The individual who joins us in the next few months will have the opportunity to participate in the planning of a major expansion of the facilities of the ultrasound section scheduled to be completed in mid-1992. The dept. is active in teaching and clinical research, with a staff of 22 residents and fellows. Candidates for this position should have fellowship training or a strong background in ultrasonography and be interested in teaching and clinical research as well as patient care. Compensation and benefits are highly competitive. For additional information, contact Christopher R. B. Merritt, M.D., Chairman, Dept. of Radiology, Ochsner Clinic, 1514 Jefferson Highway, New Orleans, LA 70121; (800) 488-2240. 8–9a

HEAD OF MAMMOGRAPHY SECTION—The Dept. of Radiology of the Ochsner Clinic is seeking a radiologist to head a rapidly growing Section of Mammography. Currently over 15,000 mammograms and 500 localization procedures are performed annually. Equipment includes 4 ACR-accredited mammographic units and stereotactic localization equipment. The individual who joins us in the next few months will have the opportunity to participate in the planning of a major expansion of the facilities of the mammography section scheduled to be completed in mid-1992, providing capability for approximately 30,000 procedures annually. The mammography section provides imaging services for a multidisciplinary breast center with a high degree of clinical and research interaction with surgical, medical, and pathology services. The radiology dept. is active in teaching and clinical research with a staff of 22 residents and fellows. Candidates for this position should have fellowship training or a strong background in mammography and be interested in teaching and clinical research as well as patient care. Compensation and benefits are highly competitive. For additional information, contact Christopher R.B. Merritt, M.D., Chairman, Dept. of Radiology, Ochsner Clinic, 1514 Jefferson Highway, New Orleans, LA 70121; (800) 488-2240. 8–9a

ANGIO/INTERVENTIONAL RADIOLOGIST, LANCASTER, PA—Position available immediately for well-trained, enthusiastic, BC/BE angiographer to join diversified group of 19. Stimulating practice includes 550-bed hospital with trauma accreditation, full-service imaging center, 2 MRI facilities, and radiation therapy. The angiography division has 5 technologists working 2 state-of-the-art angio suites. Last yr over 2000 total exams were performed (nearly 300 were interventional procedures including atherectomies). Excellent working relationship with surgical and medical staff. Lancaster is a pleasant, small city, rich in historical tradition, located in a growing county with many cultural and recreational amenities. Beautiful surrounding farms and countryside are in close proximity, yet Philadelphia and Baltimore/Washington are within easy reach. Contact Robert Gress, M.D., Lancaster Radiology Associates, Ltd., Box 3555, Lancaster, PA 17603; (717) 299-4173. 8–9ap

THE DEPT. OF RADIOLOGY AT BROOKE ARMY MEDICAL CENTER, SAN ANTONIO, TX, is recruiting academic radiologists for several divisions of the dept., including ultrasound, chest, skeletal, neuroradiology, general diagnostic, interventional radiology, and mammography. Our dept. offers a fully accredited residency program with 24 residents and 16 attending full-time staff. Numerous consultants from across the country lecture on a continuing and regular basis. The hospital is a modern, tertiary-care center serving Texas, Oklahoma, and Louisiana. A strong residency program, interesting patient population, excellent equipment, teleradiology and digital radiology implementations underway, coupled with a south Texas lifestyle are positive aspects of the practice. Academic credentials and/or experience are necessary. Recently graduated fellows are encouraged to apply. Board certification is mandatory. Candidates should be particularly interested in patient care, teaching, and research. Salary and benefits are competitive and generous. Brooke is an EO/EEO employer. Please contact Dr. Billy E. Cunningham, COL, MC, Assistant Chief, Dept. of Radiology, Brooke Army Medical Center, Fort Sam Houston, TX 78234-6200; (512) 221-8418/8218. 8–7a

DIAGNOSTIC RADIOLOGIST WITH SPECIAL COMPETENCY IN NUCLEAR MEDICINE, LANCASTER, PA—Position available immediately for well-trained, enthusiastic, BC/BE diagnostic radiologist with nuclear medicine interest and expertise to join diversified group of 19. Busy practice includes 550-bed hospital with trauma accreditation, full-service imaging center, 2 MRI facilities, and radiation therapy. Nuclear medicine section has 9 technologists who performed 9500 exams last yr using 6 cameras including 1 SPECT unit. Additional SPECT unit to be added within 6 mo to supplement busy nuclear cardiology program. Lancaster is a pleasant, small city, rich in historical tradition, located in a growing county with many cultural and recreational amenities. Beautiful surrounding farms and countryside are in close proximity, yet Philadelphia and Baltimore/Washington are within easy reach. Contact Robert Basarab, M.D., Lancaster Radiology Associates, Ltd., Box 3555, Lancaster, PA 17603; (717) 299-4173. 8–9ap

TWO RADIOLOGISTS, KANSAS CITY—There is an opening for 2 radiologists, 1 immediately and 1 in July 1992, to join an expanding 4-person group in a 300-bed hospital and a future large, outpatient center. We are looking for a radiologist to head special procedures and the interventional section. The other person could be a general radiologist or have any other subspecialty training. Competitive salary. All benefits lead to early full partnership. Reply to George F. Drasin, M.D., 4949 Rockhill Rd., Kansas City, MO 64110. 8–10ap

DIAGNOSTIC RADIOLOGIST, WASHINGTON—The Moses Lake Clinic is seeking a well-trained diagnostic radiologist to join a group of progressive multispecialty physicians. This is an opportunity to work in a beautiful facility that offers mammography, fluoroscopy, ultrasound, diagnostic radiology, and CT. Competitive compensation, excellent benefit package, located in central Washington. Contact Terry W. Coplin, Administrator, 840 Hill Ave., Moses Lake, WA 98837; (509) 765-0216. 8–10a

IMMEDIATE OPENING FOR BE/BC RADIOLOGIST in a regional hospital with a patient base of 25,000 located in a scenic western Wyoming community. Great outdoor recreation area. Competitive reimbursement. Ultrasound/CT/general radiology. Interested persons contact Paul Sonntag, M.D., P. O. Box 629, Ogden, UT 84402; (801) 625-2092. 8–1ap

ALASKA AREA NATIVE HEALTH SERVICE—Public-service-oriented radiologists needed for cross-cultural health care in Anchorage and Sitka, AK. Salary $85–$95K+, excellent benefits. Medical school loan repayment up to $25K/yr additional. Contact Ken Bartline, RN. (907) 257-1457, collect. Indian Health Service. An equal opportunity employer. 8–1a

CLINICAL DIRECTOR, MRI—MetroHealth Medical Center, a 1,000-bed teaching hospital affiliated with Case Western Reserve University (CWRU), is seeking a clinical director for its MRI section. MHMC is a Level I trauma center providing tertiary care in the Cleveland metropolitan area. The director of MRI will head a major research and clinical service. Responsibilities include overseeing daily operations, research leadership in investigative MR, and development of collaborative ventures with the physics research group and other members of the Dept. of Radiology, hospital, and university. The position provides an excellent opportunity for research and resident education as well as professional development. The Dept. of Radiology is an active, academic dept. with state-of-the-art equipment in angiography, CT, ultrasound, and nuclear medicine and has an approved residency program. The MR section includes a 1.5-T imager (2nd system will be installed by Fall 1991), independent development workstation, 3-D engine (Voxel-Flinger), RF lab, and Starden Titan minicomputer. The research group includes 4 Ph.D. scientists and 4 graduate students. Candidates will be board-certified, have demonstrated experience in MRI research, have dedicated MR training, and be eligible for Ohio medical licensure. The ideal candidate will currently possess an assistant professor or higher rank with administrative experience preferred. MetroHealth Medical Center offers attractive compensation and benefits. The selected candidate will be recommended for a faculty appointment at CWRU School of Medicine commensurate with his/her experience. Interested candidates should forward CV and other pertinent information to Errol M. Bellon, M.D., Director, Dept. of Radiology, MetroHealth Medical Center, 3395 Scranton Rd., Cleveland, OH 44109; fax (216) 459-4072. MetroHealth Medical Center and Case Western Reserve University are equal opportunity employers. 8–10a

MRI/ABDOMINAL IMAGING NEW YORK/NEW JERSEY METROPOLITAN AREA—Board-certified/eligible radiologist needed for a position beginning July 1, 1991. Must have fellowship training in MRI and training in CT, ultrasound, and GI studies. Private practice with 400-bed hospital and outpatient imaging center located in northern New Jersey, near New York City. Send inquiries to James A. Heimann, M.D., Dept. of Radiology, Clara Maass Medical Center, 1 Franklin Ave., Belleville, NJ 07109. 7–12ap

ISRAEL, DIAGNOSTIC RADIOLOGY. Opportunities for 3–4 week or longer working vacations in a number of Israeli medical centers, on a volunteer basis. Positions varied, arrangements flexible. For information contact: Jonathan H. Fish, M.D., 1844 San Miguel Dr., #302, Walnut Creek, CA 94596; (415) 947-0560. 8–10xa

TRAUMA RADIOLOGIST—The State University of New York Health Science Center at Brooklyn seeks to add a board-certified/eligible radiologist to join the Division of Traumatology at Kings County Hospital Center, a 1300-bed tertiary facility and Level I Trauma Center with an international reputation in trauma services. The radiologist is an integral member of the trauma service of the Dept. of Surgery. Opportunities to join ongoing clinical investigations of the use of radiography, CT, angiography/interventional radiology, and ultrasound in the trauma patient are available. Academic rank and salary are commensurate with experience. CV should be addressed to Salvatore J. A. Sclafani, M.D., Dept. of Radiology, Kings County Hospital Center, 451 Clarkson Ave., Brooklyn, NY 11203. An EO/AA employer. 7–9ap

CARDIOVASCULAR AND INTERVENTIONAL RADIOLOGIST—The State University of New York Health Science Center at Brooklyn seeks a board-certified/eligible radiologist with fellowship training in interventional radiology for a faculty position. The institution is a 1700-bed facility, including the Kings County and the State University hospitals. The medical center performs approximately 2000 diagnostic and interventional procedures, including angioplasty, embolization, caval filters, gastrointestinal, genitourinary, and pulmonary interventions. When ongoing renovations are complete, there will be 5 new vascular digital rooms. Research time and facilities are available. Rank and salary are commensurate with qualifications. CV should be addressed to Salvatore J. A. Sclafani, M.D., Kings County Hospital Center, Dept. of Radiology, 451 Clarkson Ave., Brooklyn, NY 11203; (718) 245-4447. An EO/AA employer. 7–9ap

SUPERB PARTNERSHIP POSITION IN LAS VEGAS, NV—Rapidly expanding, 7-member group practice covering 2 full-service imaging centers and a small hospital has an immediate opening. We are looking for an additional board-certified radiologist with an uncommon dedication to excellence in patient care. Our outpatient facilities include 2 MR, 2 CT, angio with a 4-bed recovery area, 5 ultrasound, 5 mammography, 2 SPECT, plus R & F. This is an excellent opportunity for a partnership position with a well-respected group in a growing community. Please send CV to Dr. Mark Winkler, SDMI, 2950 S. Maryland Pkwy., Las Vegas, NV 89109. 5–10a

LARGE, GROWING RADIOLOGY PRACTICE IN CENTRAL NEW JERSEY and adjacent Pennsylvania region seeks diagnostic radiologist with expertise in 1 or more of the following: CT/ultrasound, angio/interventional, or nuclear medicine. Send resume to E. Tarasov, M.D., 838 W. State St., Trenton, NJ 08618. 7–9a

IMMEDIATE OPENING FOR A BC/BE DIAGNOSTIC RADIOLOGIST—Join 1 other as a full-time partner under fee-for-service billing. Ideal family community located in western Pennsylvania, approximately 60 mi. north of Pittsburgh. This is an acute-care hospital with 180 beds doing approximately 30,000–35,000 exams/yr. Need experience in general radiology, some angiography and interventional procedures, ultrasound, CT, MRI (mobile), and mammography services. Applicant should respond as soon as possible with letter of interest and current CV to Wan Jo Kim, M.D., Director of Radiology, St. Francis Hospital of New Castle, 1000 S. Mercer St., New Castle, PA 16101; (412) 656-6011/6116 (before 5 p.m.), (412) 656-0752 (after 5 p.m.). 7–9ap

FACULTY RADIOLOGIST, BODY MRI DIVISION, THOMAS JEFFERSON UNIVERSITY HOSPITAL—The Dept. of Radiology at Thomas Jefferson University Hospital has an opening for a radiologist in an active, body MRI section that encompasses a clinical mix of approximately 50% musculoskeletal and 50% chest/abdomen/pelvis cases. Equipment includes 4 1.5-T GE Signa systems with state-of-the-art and advanced prototype hardware and software. A full-yr body MRI fellowship and/or 1 yr of academic MRI experience is preferred. Clinical cross coverage in ultrasound and/or general radiology also can be incorporated depending on the interests and qualifications of the candidate. Dedicated, non-clinical research time is provided, and the dept. has excellent research facilities and support, including 2 MRI physicists, a radiology animal facility, radiology research funding, and a team of research assistants. Excellent faculty incomes and benefits are offered within a financially secure dept. and university hospital. This is a unique opportunity for an academically oriented MRI radiologist to join a dynamic and rapidly growing dept. Interested candidates should contact Donald G. Mitchell, M.D., Director of MRI, Dept. of Radiology, 1032 Main Bldg., Thomas Jefferson University Hospital, Philadelphia, PA 19107; (215) 955-4809. Jefferson is an equal opportunity/affirmative action employer. 9xa

THE DEPT. OF RADIOLOGY, VIRGINIA COMMONWEALTH UNIVERSITY/MEDICAL COLLEGE OF VIRGINIA, AND THE MCGUIRE VA MEDICAL CENTER, RICHMOND, VA, seek faculty for positions in diagnostic radiology (chest, GI, mammography, CT/ultrasound/MR, musculoskeletal, pediatrics, ER, angio/interventional, and neuroradiology), nuclear medicine, and radiologic physics. MCV is a 1058-bed facility (205 for children) and a Level I trauma center. The McGuire VAMC is an 800-bed facility (pediatrics excluded). ABR certification of eligibility required. Individual should have experience working in a culturally diverse environment. Academic rank and salary commensurate with experience. For position description or to submit CV write or phone A. V. Proto, M.D., Dept. of Radiology, MCV Box 470, Richmond, VA 23298-0470; (804) 786-7212. VCU/MCV is an equal opportunity/affirmative action employer. Women and minorities are encouraged to apply. 8–9ap

THE DEPT. OF RADIOLOGY OF THE CHILDREN'S MEMORIAL HOSPITAL CHICAGO, is seeking a pediatric radiologist. Children's Memorial Hospital is a 265-bed facility, well-equipped with state-of-the-art MR, CT, ultrasound, and nuclear medicine equipment. Currently there are 11 attending radiologists in the dept. Applicants must be certified by the American Board of Radiology and have completed a fellowship in pediatric radiology. Duties include clinical services, teaching, and research. Children's Memorial is affiliated with Northwestern University Medical School. This is a full-time position starting as soon as possible. Please send CV to Andrew K. Poznanski, M.D., Radiologist-in-Chief, Children's Memorial Hospital, 2300 Children's Plaza, Chicago, IL 60614. For inquiries, please call (312) 880-3520. Children's Memorial Hospital and Northwestern University are affirmative action/equal opportunity employers. Hiring is contingent on medical licensure in Illinois. 8–9a

SAN FRANCISCO BAY AREA, DIAGNOSTIC RADIOLOGY—Full-time position available as of July 1992 for BC/BE radiologist to join established group based in growing SF Bay area communities. Competence in all modalities including MRI and angiography required; fellowship training desirable. Contact J. Fish, M.D., c/o Walnut Creek Radiology, 1844 San Miguel Dr., #302, Walnut Creek, CA 94596; (415) 947-0560. 8–10xa

SOUTHERN OREGON—Opportuniy for BC/BE, general diagnostic radiologist to join group of 5 board-certified radiologists. Experience in all modalities desired. Practice includes 2 hospitals and own private office. Competitive starting salary with early full partnership. Excellent lifestyle with many outdoor activities from Pacific Coast to Oregon Cascades. Send CV to Larry Strickland, Administrator, Roseburg Radiologists, P.C., P. O. Box 1547, Roseburg, OR 97478. 8–1ap

RADIOLOGIST—BC/BE radiologist needed to join 2-person practice covering 2 hospitals in the central mountains of Colorado. Ample free time and excellent outdoor recreational opportunities. Contact E. J. Loeffel, M.D., P.O. Box 415, Buena Vista, CO 81211; (719) 539-3782. 7–9ap

OPENING FOR BE/BC DIAGNOSTIC RADIOLOGIST to join a 6-person group in Missoula, a university city of 45,000 located in mountainous western Montana. Looking for a general radiologist with proficiency in MRI, ultrasound, CT, angiography, etc. Administrative skills preferable. Our group of 6 full-time radiologists covers both of Missoula's hospitals (210 and 130 beds). Progressive medical environment with 200 physicians. One yr to full partner income and 2 yr to partnership. Competitive salary. Abundant nearby recreational opportunities include skiing, fishing, backpacking, and hunting. Send CV to Missoula Radiology, Inc., P.O. Box 2039, Missoula, MT 59806. 7–11ap

PEDIATRIC RADIOLOGIST—The Division of Pediatric Radiology, Oregon Health Sciences University, Portland, OR, invites applications for a faculty position available on or about July 1, 1991. Completion of approved fellowship in pediatric radiology and ABR certification required. Send CV to William Weidner, M.D., Diagnostic Radiology, UHN-72, Oregon Health Sciences University, Portland, OR 97201-3098; (503) 494-4498. Equal opportunity, affirmative action employer. 7–9a

THE DEPT. OF RADIOLOGY AT TRIPLER ARMY MEDICAL CENTER, HONOLULU, HI, is recruiting academic radiologists for several divisions of the dept. including ultrasound, chest radiology, skeletal, neuroradiology, general diagnostic radiology, MRI, interventional radiology, and mammography. Our dept. offers a fully accredited residency program with 21 residents and 16 attending full-time staff. Numerous consultants from across the country lecture on a continuing and regular basis. The hospital is a modern, tertiary-care center serving Hawaii and the entire Pacific Basin. A strong residency program, diverse and interesting patient population, excellent equipment, and tropical lifestyle are positive aspects of the practice. Academic credentials and/or experience are necessary. Recently graduated fellows are encouraged to apply. Board certification is mandatory. Candidates should be particularly interested in patient care, teaching, and research. Salary and benefits are competitive and generous. Tripler is an EO/EEO employer. Please contact Dr. Mark F. Hansen, Col., MC, Chief, Dept. of Radiology, TAMC, HI 96859-5000; (808) 433-6393. 7–6a

INDIANAPOLIS, IN—Practice opportunity for a radiologist to serve as medical director of a new, freestanding, privately owned, imaging center with CT and high-field MR. Facility will be managed by and affiliated with the Center for Diagnostic Imaging in Minneapolis, MN. MR experience mandatory. Subspecialty experience in MR desirable. Board certification and ability to obtain licensure in Indiana required. Please send inquiries with CV to Cooper R. Gundry, M.D., Center for Diagnostic Imaging, 5775 Wayzata Blvd., Ste. 190, Minneapolis, MN 55416. All inquiries entirely confidential. No telephone calls please. 7–9ap

FAIRBANKS, AK—Four diagnostic radiologists seek fifth partner for diversified practice including general radiology, ultrasound, nuclear medicine, MRI (GE 1.5-T), and CT (GE 9800). Hospital and office practice. Desirable life-style advantages in a university town. Unlimited access to the outdoors. Excellent salary, benefits, retirement, and vacation. One yr to full partnership. Contact Douglas Hutchinson, M.D., 1919 Lathrop #5, Fairbanks, AK 99701; (907) 452-5092. 8–10ap

IMMEDIATE OPENING IN PALM SPRINGS, CA Radiologist with mammography expertise/specialization needed to join 10-person group in community hospital/office practice. Contact Marvin J. Friedenberg, M.D., Dept. of Radiology, Desert Hospital, 1150 N. Indian, Palm Springs, CA 92262. 9xa

CHEST RADIOLOGIST, CLEVELAND CLINIC FOUNDATION—The Cleveland Clinic Foundation has an opening for a staff position in the Section of Thoracic Imaging. The foundation is a 1000-bed hospital with a large outpatient population and an international referral base. Successful applicants will be involved in all diagnostic modalities, including CT, MRI, and interventional procedures. A strong interest in teaching, research, and patient care is required. Applicants should be board-certified, fellowship-trained, or have equivalent experience. Excellent salary and benefit package. Send CV to Moulay A. Meziane, M.D., Head, Section of Thoracic Imaging, Cleveland Clinic Foundation, One Clinic Center Dr., Cleveland, OH 44195-5021. The Cleveland Clinic Foundation is an equal opportunity employer. 5–10ap

DIAGNOSTIC RADIOLOGIST with skills in CT, MR, interventional, ultrasound, and nuclear medicine needed to join group of 8 board-certified radiologists. Growing practice in eastern Washington at a 228-bed hospital, a new multimodality imaging center, and 2 private offices. Potential for long-term practice is excellent. Top-notch school system, including 3 first-rate universities. Excellent hunting, fishing, boating, and skiing. Contact L. E. Crecelius, M.D., N. 5901 Lidgerwood, Ste. 18B, Spokane, WA 99207; (509) 482-2385. 5–10ap

PRACTICE OPPORTUNITY IN FAST-GROWING LAS VEGAS, NV—Expanding, 6-member radiology group is seeking 2 additional BE/BC radiologists for July 1991 and Jan. 1992. We currently serve 2 hospitals with an outpatient imaging center to open in Jan. 1992. Outstanding salary and benefits package leading to full partnership in 2 yr. Send CV or contact Marc Pomerantz, M.D., Head of Search Committee, 1925 Spode Ave., Henderson, NV 89014; (702) 388-4640. 5–9ap

DIAGNOSTIC RADIOLOGIST, IMMEDIATE OPENING—Ten-person radiology group seeks a diagnostic radiologist with fellowship training, including body MRI/body imaging, to join a busy, hospital-based practice located in rapidly growing north Dallas. GE 1.5-T magnet, Toshiba midfield magnet, 2 GE 9800 scanners, Acuson 128 with color flow Doppler, and new special procedures suite with DSA. Please send CV to Box K54, *AJR* (see address this section). 9xa

UTMB, GALVESTON, TX—The Dept. of Radiology of the University of Texas Medical Branch in Galveston has openings for persons trained and experienced in ultrasonography and mammography. The opportunity for academic advancement is great and benefits are generous. Salaries are competitive and living conditions are desirable. Interested persons should contact Melvyn H. Schreiber, M.D., Chairman, Dept. of Radiology, UTMB, Galveston, TX 77550; (409) 761-1823. UTMB is an equal opportunity M/F/H/V affirmative action employer. UTMB hires only individuals authorized to work in the United States. 4–9a

IMMEDIATE OPENING IN PALM SPRINGS, CA Radiologist with MRI expertise/specialization needed to join 10-person group in community hospital/office practice. Contact Marvin J. Friedenberg, M.D., Dept. of Radiology, Desert Hospital, 1150 N. Indian, Palm Springs, CA 92262. 9xa

BC/BE RADIOLOGIST—Group practice in New Orleans, LA, has a great opportunity leading to partnership. Looking for a radiologist with imaging background or interest in special procedures. Imaging center with 1.5-T GE Advantage System. Excellent hospitals and working conditions. Send CV to B.B.N. & H., 440 General Meyer Ave., Ste. 211, New Orleans, LA 70131; (504) 368-5074. 7–10ap

DALLAS, TX—A 12-member, subspecialty group seeks a board-certified, general radiologist for an immediate opening. Fellowship training preferred, but will consider qualified individual with special expertise. CT/ultrasound, MRI, nuclear medicine, or angiography background particularly helpful. All imaging modalities available (state-of-the-art CT, angio, ultrasound, R & F, SPECT nuclear medicine, and MRI center). Salary and bonuses are excellent. Health and malpractice paid. No buy-in to partnership. Send CV to H. Stuart Peake, M.D., P.O. Box 814129, Dallas, TX 75381; (214) 888-7055. 4–9ap

IMMEDIATE OPENING FOR BC/BE GENERAL RADIOLOGIST with experience in interventional and vascular radiology. Join a group of 4 radiologists in a 160-bed hospital located in Allentown, PA, about 60 mi. northwest of Philadelphia. The daily practice includes all aspects of general radiology, CT, ultrasound, and nuclear medicine. Please call or send CV to Asad Shohadai, M.D., Allentown Osteopathic Medical Center, 1736 Hamilton St., Allentown, PA 18104; (215) 770-8700. 9xa

BOSTON, IMMEDIATE OPENING—Radiologist wanted to join busy, well-established, private-practice group with 4 outpatient facilities. Expertise in ultrasound and mammography. No evening or weekend call. Excellent life-style, partnership opportunity. Send letter and CV to Box E49, *AJR* (see address this section). 6–11ap

DIAGNOSTIC RADIOLOGIST—BC/BE radiologist wanted to join expanding practice of 12 radiologists in northeastern Pennsylvania. Practice includes 3 hospitals (720 beds) and free-standing MRI. Candidate must have experience in angiography and interventional radiology, and be willing to cover other areas of diagnostic imaging. Contact Paul M. Leiman, M.D., Dept. of Radiology, Moses Taylor Hospital, 700 Quincy Ave., Scranton, PA 18501; (717) 963-2601. 8–9ap

THE DEPT. OF RADIOLOGY AT THE UNIVERSITY OF MASSACHUSETTS MEDICAL CENTER in Worcester is seeking a BC/BE general radiologist with a major interest in chest and musculoskeletal radiology. A strong interest in teaching and collaborative clinical research is desired. Rank and salary are commensurate with experience. The medical center is a 370-bed university hospital and medical school located approximately 40 mi. west of Boston. The dept. consists of 22 staff, 13 residents, and 2–4 fellows and does approximately 130,000 exams/yr. The dept. is well-equipped with 2 GE 9800 Quick CT scanners as well as 2 GE 1.5-T MRI scanners in a stand-alone facility and a 2.0-T small-bore unit for animal research. The hospital is a major trauma center and is serviced by 2 Life Flight helicopters. For further information, contact Edward H. Smith, M.D., Professor and Chair, Dept. of Radiology, University of Massachusetts Medical Center, 55 Lake Ave., N., Worcester, MA 01655; (508) 856-3252. UMMC is an equal opportunity/affirmative action employer. 9xa

NORTHERN CALIFORNIA, IMMEDIATE OPENING—Large, diagnostic group seeks BC/BE radiologist to join diversified practice (4 hospitals and 7 offices) on full partnership basis. All modalities available. Send CV or call Andrew Koo, M.D., P.O. Box 9525, San Jose, CA 95157; (408) 244-2100. 7–9ap

Positions Desired

B/C GENERAL RADIOLOGIST, NATIVE NEW YORKER seeks immediate partnership position with hospital-based radiology group. Experienced in all modalities and can perform certain special procedures. Will consider locum tenens to see practice for a week or more. Licenses in New York, Pennsylvania, and Florida. Reply to Box O7, *AJR* (see address this section). 9–10bp

MUSCULOSKELETAL RADIOLOGIST, fellowship-trained at a major university program with over 10 yr experience in all imaging techniques, including CT and MR, seeks a full-time position in an academic or private musculoskeletal radiology practice. Currently an active clinical faculty member at 2 university programs and chief of a bone section in a radiology residency program at a large teaching/county facility (1 of the hospitals covered by our large, private-practice group). Current duties include a significant amount of general radiology. Priorities include high-quality practice of radiology, state-of-the-art equipment, and congenial working environment. Western U.S. preferred, but not mandatory. Enthusiastic, healthy, ABR-certified, mid-40s, and looking for a change. Excellent references. Reply to Box N42, *AJR* (see address this section). 7–9bp

Fellowships and Residencies

MUSCULOSKELETAL IMAGING FELLOWSHIP The Dept. of Diagnostic Radiology and Medical Imaging is offering a 1-yr fellowship in musculoskeletal imaging. The Division of Skeletal Radiology is an integral part of the Henry Ford Bone and Joint Specialty Center. This center represents a unique multispecialty program for clinical and academic excellence in the diagnosis and treatment of musculoskeletal disorders. It comprises the Dept. of Orthopedic Disorders, Dept. of Orthopedic Surgery, Division of Rheumatology, Division of Bone and Mineral Metabolism, Physics Section of the Dept. of Radiology, and the Division of Skeletal Radiology. The group includes recognized experts working closely in the investigation and clinical care of musculoskeletal disorders, providing a fertile environment for education and research. The Division of Skeletal Radiology consists of 3 dedicated osteoradiologists and state-of-the-art imaging technology including polytomography, 3D CT imaging, MRI, musculoskeletal sonography, and arthrography. Ongoing research in imaging includes high-resolution CT, sonography, and other clinical projects. Interested applicants should include CV with letter of inquiry to either Burton I. Ellis, M.D., or Marnix van Holsbeeck, M.D., Dept. of Diagnostic Radiology and Medical Imaging, Division of Musculoskeletal Radiology, Henry Ford Hospital, 2799 W. Grand Blvd., Detroit, MI 48202. 9–11ap

ACCREDITED FELLOWSHIPS IN PEDIATRIC RADIOLOGY AND PEDIATRIC NEURORADIOLOGY—Dept. of Radiology, Children's Hospital Medical Center, Cincinnati, OH, offers 1- or 2-yr accredited (Residency Review Committee for Radiology of ACGME) fellowships in pediatric radiology beginning July 1, 1993. A 1-yr pediatric neuroradiology fellowship program is also offered and may be taken separately or combined with 2 yr of adult neuroradiology fellowship at the University of Cincinnati Medical Center. Children's Hospital Medical Center (CHMC) is a 355-bed institution. The dept. performs over 105,000 radiologic exams/yr in the largest children's hospital and ambulatory practice in the U.S. The dept. has 14 full-time faculty pediatric radiologists, 6 fellows, and many resident trainees. Five pediatric radiology and 2 pediatric neuroradiology fellowship positions are available annually. Training includes all aspects of pediatric imaging including neonatal radiology, neuroimaging, oncologic imaging, ultrasonography, nuclear medicine, CT, MRI, and vascular/interventional procedures. The dept. has an active clinical service with state-of-the-art equipment including digital fluoroscopy; Acuson, AI, and ATL ultrasound units with Doppler and color-flow Doppler capabilities; planar SPECT gamma cameras; GE 9800 Quick CT scanner, 1.5-T GE MRI with spectroscopy; and cardiac catheterization/angiographic suite with digital vascular imaging. The fellowship provides a broad clinical experience in pediatric radiology as well as numerous opportunities to participate in both clinical and basic research. Candidates must be board-certified or qualified in diagnostic radiology and must obtain an Ohio medical license. Salary and fringe benefits are highly competitive. Applications are due before Jan. 1992, with interviews scheduled during the fall and winter of 1991–1992. There are numerous career opportunities in pediatric radiology in both academic and private practice settings. To receive more information about the fellowships at CHMC or careers in pediatric radiology, please contact Donald R. Kirks, M.D., Director, Dept. of Radiology, Children's Hospital Medical Center, Cincinnati, OH 45229-2899; (513) 559-8058. Children's Hospital Medical Center and the University of Cincinnati College of Medicine are affirmative action/equal opportunity employers. 9–5cp

THORACIC RADIOLOGY FELLOWSHIP, MASSACHUSETTS GENERAL HOSPITAL—A 1-yr fellowship beginning July 1, 1992, offers participation in standard film interpretation, CT of the thorax, MRI, and interventional procedures. Opportunity for clinical and academic research. Send inquiries and CV to Theresa C. McLoud, M.D., Dept. of Radiology, Massachusetts General Hospital, Boston, MA 02114. 9cp

VASCULAR AND INTERVENTIONAL RADIOLOGY FELLOWSHIP—The University of South Florida, Dept. of Radiology, will offer a 1-yr fellowship in vascular and interventional radiology beginning July 1, 1992. Clinical experience will include the full range of interventional procedures including vascular, biliary and endourologic procedures, as well as abscess drainage and percutaneous biopsy. The fellow will rotate between the H. Lee Moffitt Cancer Center and Research Institute, the James A. Haley VA Hospital, and the Tampa General Hospital. There is active, ongoing clinical research. Interested candidates contact Steven Morse, M.D., Associate Professor of Radiology, University of South Florida, Director of Vascular Radiology, Moffitt Cancer Center and Research Institute, P. O. Box 280179, Tampa, FL 33682-0179; (813) 972-8425. 9–11cp

ONCOLOGY/MAMMOGRAPHY FELLOWSHIP The Dept. of Radiology at the Dana-Farber Cancer Institute and Brigham and Women's Hospital, Harvard Medical School affiliates, offers a 1-yr fellowship position beginning July 1, 1992. All imaging modalities involved in the diagnosis, staging, and follow-up of patients with malignant disease are integrated into this program. An additional feature is a concentrated experience in the performance of interventional breast diagnostic procedures. Please contact Jack E. Meyer, M.D., Director of Diagnostic Radiology, Brigham and Women's Hospital and Dana-Farber Cancer Institute, 75 Francis St., Boston, MA 02115; (617) 732-6269. Brigham and Women's Hospital/Dana-Farber Cancer Institute/Harvard Medical School is an affirmative action/equal opportunity educator and employer. 9–2c

MARYLAND FELLOWSHIPS—The University of Maryland School of Medicine at Baltimore is accepting applications for fellowships beginning July 1992. One-yr fellowships are available in angio/interventional, skeletal, CT/ultrasound/MR, neuroradiology, trauma and critical care, and pediatrics. The University of Maryland offers competitive salaries, ample time for academic pursuits, and funding for continuing medical education. Board certification in radiology is desired, board eligibility is required. Additional information regarding each fellowship is available by calling toll-free (800) 866-8667 ext. 3477 or direct (301) 328-3477. Send CV to Gerald S. Johnston, M.D., 22 S. Greene St., Baltimore, MD 21201. The University of Maryland is an affirmative action/equal opportunity employer who encourages applications from members of minority groups. 9xcp

FELLOWSHIP IN NEURORADIOLOGY, JULY 1, 1992—The Dept. of Radiology, University of Massachusetts Medical Center offers a 1-yr fellowship position in neuroradiology starting July 1, 1992. Training is offered in neuroangiography, CT, myelography, and MRI. The position involves teaching of medical students and residents with opportunity for research. The University of Massachusetts Medical Center is a 370-bed, university hospital and medical school located in Worcester, 40 mi. west of Boston. The dept. consists of 22 staff, 14 residents, 2–4 fellows, and does approximately 130,000 exams/yr. The hospital is a major trauma center and is serviced by 2 Life Flight helicopters. The dept. is well-equipped with 2 state-of-the-art CT scanners, 2 1.5-T GE MR scanners, as well as 2.0-T small-bore units for animal research. The University of Massachusetts Medical Center is very active academically. Numerous radiologic, clinical, and basic science conferences are scheduled on a daily basis, and there is ample time during the course of the yr to attend many of these presentations. There are many on-going research projects. The fellowship position carries the title of instructor in radiology. For further information, contact Ronald L. Ragland, M.D., Chief, Division of Neuroradiology, University of Massachusetts Medical Center, 55 Lake Ave., N., Worcester, MA 01655; (508) 856-2215. The University of Massachusetts Medical Center is an affirmative action/equal opportunity employer. 9xa

IMAGING FELLOWSHIP—A 1-yr fellowship in ultrasound, MRI, and body CT is available July 1, 1992–June 30, 1993, at a 576-bed teaching hospital. The Dept. of Radiology performs more than 140,000 exams with state-of-the-art equipment. The ultrasound section is responsible for all aspects of sonography including OB-GYN, pediatric, abdominal, and small parts. Extensive training in color flow imaging, duplex Doppler, transvaginal, transrectal techniques, and sonographically guided procedures. Two GE MRI scanners and 2 GE 9800 Quick CT units provide high-volume caseloads in these areas. Opportunities are available for participation in imaging research. For further information, please contact Marcela Bohm-Velez, M.D., Imaging Fellowship Director, West Penn Hospital, 4800 Friendship Ave., Pittsburgh, PA 15224. 5–10c

FELLOWSHIP POSITIONS—The Dept. of Radiology and Radiological Sciences of Vanderbilt University School of Medicine is offering fellowship positions for 1992–1993 in angiography, musculoskeletal radiology, neuroradiology (2), and pediatrics. Research opportunities are available and encouraged. Candidates must be board-certified or qualified in diagnostic radiology and able to obtain a Tennessee medical license. Address inquiries and CV to Martin P. Sandler, M.D., Director, Fellowship Programs, Dept. of Radiology and Radiological Sciences, Vanderbilt University, Nashville, TN 37232-2675. An equal opportunity/affirmative action employer. 7–9cp

FELLOWSHIP POSITIONS AVAILABLE 1992—One-yr fellowships in cross-sectional imaging (includes CT/ultrasound/MRI), angiography/interventional radiology, and MRI at MetroHealth Medical Center, Cleveland, OH, are available starting July 1992. Ideal candidates will have completed an approved diagnostic radiology residency program and have an interest in research as he/she will be responsible for a specific research project during the fellowship. The Dept. of Radiology is an active, academic dept. with state-of-the-art equipment in angiography, CT, ultrasound, and MRI and an approved residency program. MetroHealth Medical Center is a 1000-bed teaching hospital affiliated with Case Western Reserve University and offers attractive compensation and benefits. Interested candidates should forward CV, a letter outlining expectations in the fellowship, and other pertinent information to Errol M. Bellon, M.D., Director, Dept. of Radiology, MetroHealth Medical Center, 3395 Scranton Rd., Cleveland, OH 44109; fax (216) 459-4072. MetroHealth Medical Center and Case Western Reserve University are equal opportunity employers. 8–10c

FELLOWSHIP IN BODY MRI, THOMAS JEFFERSON UNIVERSITY HOSPITAL—The Dept. of Radiology at Thomas Jefferson University Hospital has an unexpected opening for a 1-yr MRI fellow beginning July 1, 1992. This is an active body MRI section that encompasses a clinical mix of approximately 50% musculoskeletal and 50% chest/abdomen/pelvis cases. Equipment includes 4 1.5-T GE Signa systems with state-of-the-art and advanced prototype hardware and software. Ample opportunity for research is provided. The dept. has excellent research facilities and support, including 2 MRI physicists, a radiology animal facility, radiology research funding, and a team of research assistants. Interested candidates should contact Donald G. Mitchell, M.D., Director of MRI, Dept. of Radiology, 1032 Main Bldg., Thomas Jefferson University Hospital, Philadelphia, PA 19107; (215) 955-4809. Jefferson is an equal opportunity/affirmative action employer. 8–1c

MAMMOGRAPHY FELLOWSHIP—Mallinckrodt Institute of Radiology, Washington University Medical Center in St. Louis, MO, has an opening for a 1-yr fellowship in breast imaging starting July 1, 1992. The section performs more than 21,000 mammograms/yr with an active screening program that includes mobile mammography. Adjunctive procedures such as breast needle localization, stereotactic fine-needle aspiration biopsy, galactography, and breast ultrasound are performed in the breast center. For further information, contact Drs. Judy Destouet or Barbara Monsees, Mallinckrodt Institute of Radiology, Washington University Medical Center, 510 S. Kingshighway Blvd., St. Louis, MO 63110; (314) 362-2911. 8–10c

FELLOWSHIP IN BODY CT/MRI AND ULTRASOUND—The Dept. of Radiology of Loyola University Medical Center has 2 1-yr fellowship positions available July 1, 1992. The dept. performs more than 180,000 exams/yr. Fellowship training in all aspects of ultrasound is available. All imaging equipment is state-of-the-art and includes 4 GE 9800 CT scanners, 4 Acuson units, and 2 GE 1.5-T magnets. Candidates must be board-certified/eligible in diagnostic radiology and have an Illinois medical license. For further information, contact Mary Olson, M.D., Dept. of Radiology, Loyola University Medical Center, 2160 S. First Ave., Maywood, IL 60153. 8–11cp

FELLOWSHIPS IN PEDIATRIC RADIOLOGY AND PEDIATRIC NEURORADIOLOGY—The Dept. of Radiology, Children's Hospital Medical Center, Cincinnati, OH, offers 1- or 2-yr fellowships in pediatric radiology beginning July 1, 1993. A 1-yr pediatric neuroradiology fellowship program is also offered and may be taken separately or combined with 1 yr of adult neuroradiology fellowship at the University of Cincinnati Medical Center. Children's Hospital Medical Center (CHMC) is a 355-bed institution. The dept. performs over 105,000 radiologic exams annually in the largest children's hospital and ambulatory practice in the U.S. The dept. has 14 full-time faculty pediatric radiologists, 6 fellows, and many resident trainees. Five pediatric radiology and 1 pediatric neuroradiology fellowship positions are available annually. Training includes all aspects of pediatric imaging: neonatal radiology, neuroimaging, musculoskeletal radiology, cardiovascular and thoracic imaging, abdominal imaging, oncologic imaging, ultrasonography, nuclear medicine, CT, MRI, and vascular/interventional procedures. The dept. has an active clinical service with state-of-the-art equipment as follows: digital fluoroscopy; Acuson, AI, and ATL ultrasound units with Doppler and color flow Doppler capabilities; planar SPECT gamma cameras; GE 9800 Quick CT scanner; 1.5-T GE MRI with spectroscopy; and cardiac catheterization/angiographic suite with digital vascular imaging. The fellowship provides a broad clinical experience in pediatric radiology as well as numerous opportunities to participate in both clinical and basic research. Candidates must be board-certified or board-qualified in diagnostic radiology and must be able to obtain an Ohio medical license. Salary and fringe benefits are highly competitive. Applications are due before Jan. 1992, with interviews scheduled during the fall and winter of 1991–1992. There are numerous career opportunities in pediatric radiology in academic and private practice settings. To receive more information about the fellowships at CHMC or careers in pediatric radiology, please contact Donald R. Kirks, M.D., Director, Dept. of Radiology, Children's Hospital Medical Center, Cincinnati, OH 45229-2899; (513) 559-8058. Children's Hospital Medical Center and the University of Cincinnati College of Medicine are affirmative action/equal opportunity employers. 5–4cp

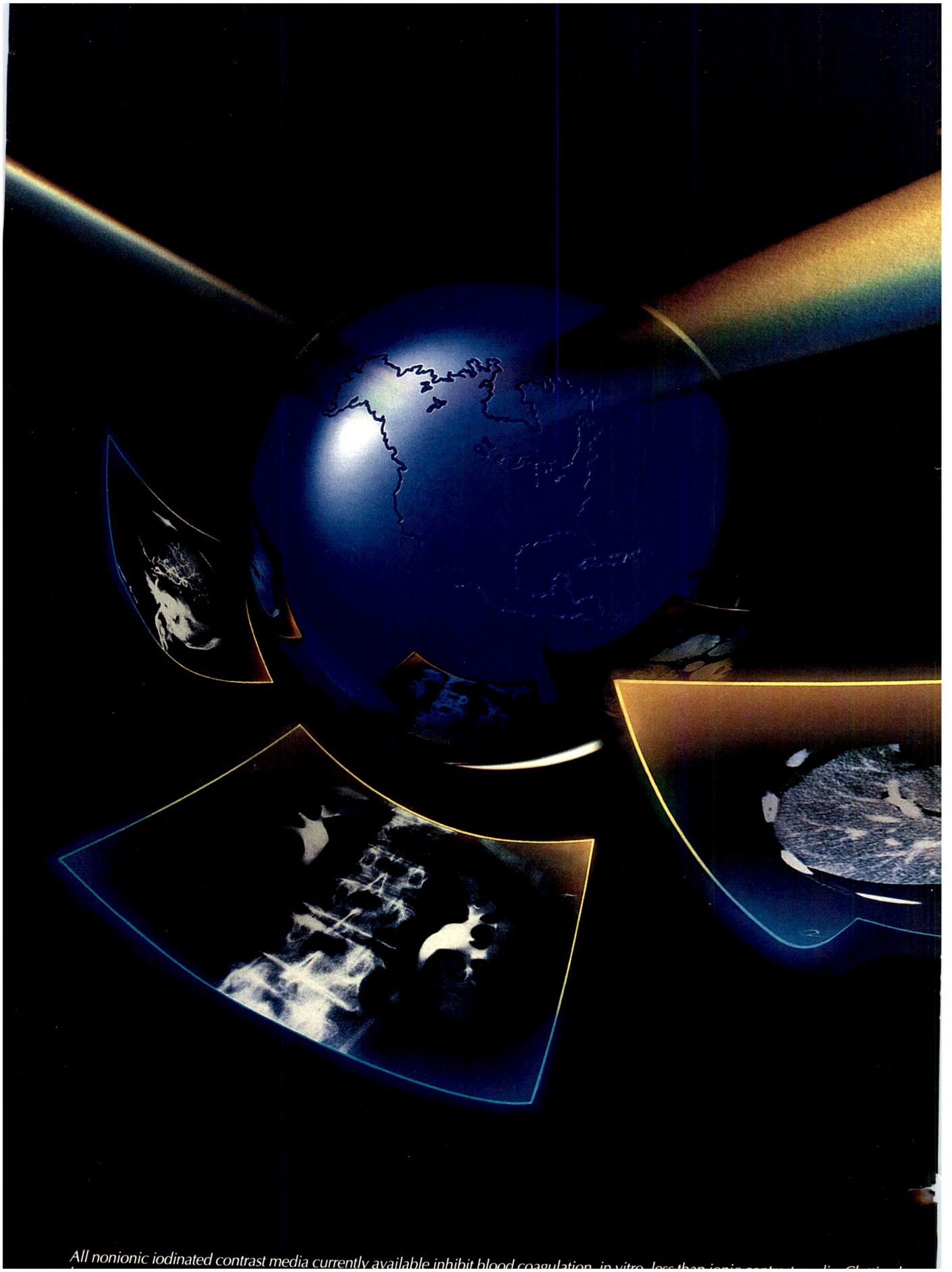
FELLOWSHIPS AT THOMAS JEFFERSON UNIVERSITY HOSPITAL—The Dept. of Radiology at Thomas Jefferson University Hospital in Philadelphia offers the following fellowship programs each yr. Ultrasound/CT/MRI — Jefferson's ultrasound division is 1 of the largest in the world and performs all currently available exams including obstetric, vascular, lithotripsy, invasive, and endoluminal. We also operate 4 GE 1.5-T MRI units and 3 CT scanners. Contact Barry Goldberg, M.D., regarding this program. Cardiovascular/interventional — this division is housed in a new suite containing Philips angio units with DSA and performs the full range of vascular and nonvascular interventional procedures. Contact Geoffrey Gardiner, Jr., M.D. Neuro/ENT radiology — very active clinical services supply a wealth of material to this division, which is housed in a neurosciences imaging center containing all imaging modalities. Contact Carlos Gonzalez, M.D. Breast Imaging — Jefferson's new breast imaging center performs approximately 85 studies/day including ultrasound and needle localizations. Contact Stephen Feig, M.D. Chest — includes biopsies and CT. Contact Robert Steiner, M.D. MRI — a dedicated body MRI program including excellent research opportunities in addition to a large clinical case load. Contact Matthew Rifkin, M.D. Ultrasound — a dedicated ultrasound program. Contact Barry Goldberg, M.D. Musculoskeletal — includes MRI of the musculoskeletal system. Contact David Karasick, M.D. All program directors listed above can be contacted at the Dept. of Radiology, Thomas Jefferson University Hospital, Philadelphia, PA 19107. Jefferson is an equal opportunity/affirmative action employer. 9xc

FELLOWSHIP IN VASCULAR/INTERVENTIONAL RADIOLOGY—The University of Arizona in Tucson has a 1-yr fellowship opening in vascular/interventional radiology beginning July 1, 1992. The full spectrum of vascular and interventional procedures are performed by the section. Tucson is a desirable part of the country, where our competitive salary and reasonable cost of living assure an enjoyable stay as well as an academically productive experience. An informational videotape is available if desired. Applicants must be board-eligible and must submit a recent CV and 3 letters of recommendation including 1 from the program chairman. For further information, please contact Linda Fowler; (602) 694-7136. 8–10cp

BREAST IMAGING FELLOWSHIP—The Susan G. Komen Breast Center in Peoria, IL, affiliated with St. Francis Medical Center, is offering a 1-yr fellowship in breast imaging beginning immediately. St. Francis Medical Center is a 750-bed, general hospital affiliated with the University of Illinois College of Medicine. The center is staffed with 2 radiologists devoted full time to breast imaging. Approximately 20,000 breast imaging studies are performed/yr. This 1-yr fellowship will provide exceptional experience in all aspects of breast imaging, including film/screen mammography and breast ultrasound. The fellow will also acquire skills in interventional procedures including ductography, preoperative localizations, cyst aspirations, and stereotactic needle biopsies (FNA and core biopsies). A 6-wk combined surgery and pathology rotation is provided to acquaint the fellow with surgical concerns in biopsies and mastectomies and to acquire a basic understanding of breast pathology. Opportunity exists and the fellow will be encouraged to participate in research projects relating to breast imaging. Send inquiries with CV to G. W. Eklund, M.D., Medical Director, Susan G. Komen Breast Center, 4911 Executive Dr., Ste. 300, Peoria, IL 61614. 8–10cp



All nonionic iodinated contrast media currently available inhibit blood coagulation, in vitro, less than ionic

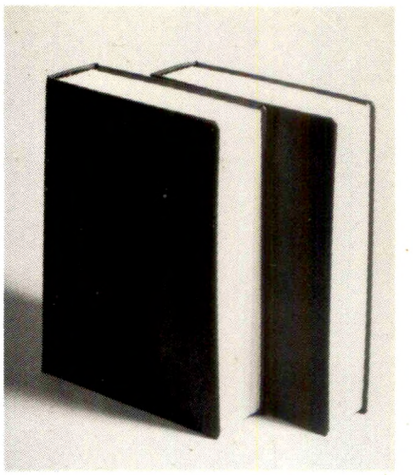


All nonionic iodinated contrast media currently available inhibit blood coagulation, in vitro, less than ionic contrast media. Clinical

AJR: AMERICAN JOURNAL OF ROENTGENOLOGY

Bound Volume Offer

A trouble-free way to keep your reference library up-to-date



As an **AJR: American Journal of Roentgenology** subscriber, you know how much useful information is packed into each issue. But you also probably know how frustrating and time-consuming it can be to try and locate one particular article from a back issue.

Find that back issue quickly and easily

Now you can get a year's worth of articles in bound volume form — a special offer available only to subscribers. So the information you need will be at your fingertips, handsomely preserved and ready for years of future reference.

You get the timely coverage only a journal can provide — penetrating discussions of the topics that interest you most, by the brightest names in your field — with all the durability and convenience of a hard-cover edition. With bound volumes, you'll never again spend frustrating hours sifting through dog-eared back issues, only to discover that the article you need has been torn out. You'll have a year's worth of vital information all arranged and indexed in one sturdy source. And each carefully crafted volume will make a handsome addition to your permanent library.

Send in your paid order by October 31, 1991, and SAVE

Act now and receive the **1991 Bound Volumes** for only $95.00 for all prepaid orders, $2.00 off the regular price of $97.00. (Please add $15.00 to all orders outside the US.) Bound volumes are available for the current year only, and are in addition to the regular subscription price.

We'll help you keep your reference library up-to-date

Once a year, we'll send you a reminder so you can order the latest bound volumes. When you send in your paid order, a set will be reserved for you, to be sent as soon as available on 30-day approval. If you do not want the bound volumes for any reason, simply return them to us within 30 days for a courteous refund. It's that easy.

Williams & Wilkins

P.O. Box 23291 Baltimore, Maryland 21203-9990

Broadway House 2-6 Fulham Broadway London SW6 1AA

EASY ORDERING

Please send me the **AJR: American Journal of Roentgenology 1991 Bound Volumes** at $97.00 ($112.00 outside the US). I understand that I can save $2.00 by sending in my prepaid order (check or charge) by October 31, 1991. I also understand that this offer is in addition to my regular subscription, that it is available only to subscribers, and that I will have the option of ordering bound volumes for subsequent years as long as I remain a subscriber. I will receive my 1991 bound volumes in early 1992.

☐ Check enclosed (payable to Williams & Wilkins) ☐ Bill me

☐ VISA ☐ MasterCard ☐ American Express

Card # Exp. date

Signature/P.O. #

Please pay in US dollars. MD residents, please add 5% sales tax. Orders outside the US must be prepaid in US dollars. Rates subject to change without notice. Canada residents add 7% GST. **All orders must be received by December 31, 1991.** Offer valid while supplies last.

Name

Address

City/State/Zip

Date of order

ORDER FREE BY PHONE.
Call **1-800-638-6423** from anywhere in the US & Canada.

Williams & Wilkins

P.O. Box 23291 Baltimore, Maryland 21203-9990

Broadway House 2-6 Fulham Broadway London SW6 1AA

Volume 157 **American Journal of Roentgenology** September 1991

1991 ARRS PRESIDENTIAL ADDRESS

447 **Reflections on radiology as a career.** *Kirkpatrick JA Jr*

REVIEW ARTICLE

449 **Imaging of vascular complications associated with renal transplants.** *Dodd GD III, Tublin ME, Shah A, Zajko AB*

CARDIOPULMONARY RADIOLOGY

461 **Diffuse pulmonary alveolar hemorrhage after bone marrow transplantation: radiographic findings in 39 patients.** *Witte RJ, Gurney JW, Robbins RA, et al.*

465 **Motion artifact simulating aortic dissection on CT.** *Burns MA, Molina PL, Gutierrez FR, Sagel SS*

469 **Commentary. Current status of mediastinal sonography in the posttreatment evaluation of patients with lymphoma.** *Marglin SI, Laing FC, Castellino RA*

471 **Case report. Torsion of the upper lobe of the lung after surgery: findings on pulmonary angiography.** *Munk PL, Vellet AD, Zwirewich C*

BREAST RADIOLOGY

473 **The American College of Radiology Mammography Accreditation Program.** *McLelland R, Hendrick RE, Zinninger MD, Wilcox PA*

481 **Self-referred mammography patients: analysis of patients' characteristics.** *Reynolds HE, Jackson VP*

GASTROINTESTINAL RADIOLOGY

485 **Altered gallbladder contractility after extracorporeal shock-wave cholecystolithotripsy.** *Rawat B, Fache JS, Burhenne HJ*

491 **Case report. Placement of a metallic biliary endoprosthesis via cholecystostomy.** *Dawson SL, Girard MJ, Saini S, Mueller PR*

495 **Perspective. Primary sclerosing cholangitis: a modified classification of cholangiographic findings.** *Majoie CBLM, Reeders JWAJ, Sanders JB, Huibregtse K, Jansen PLM*

499 **Case report. MR demonstration of edema adjacent to a liver metastasis: pathologic correlation.** *Lee MJ, Saini S, Compton CC, Malt RA*

503 **Pictorial essay. Endorectal sonography in the evaluation of rectal and perirectal disease.** *St. Ville EW, Jafri SZH, Madrazo BL, Mezwa DG, Bree RL, Rosenberg BF*

GENITOURINARY RADIOLOGY

509 **Transurethral balloon dilatation of the prostatic urethra: effectiveness in highly selected patients with prostatism.** *Wasserman NF, Reddy PK, Zhang G, Kapoor DA, Berg P*

513 **Case report. Iliac artery stenosis causing renal allograft-mediated hypertension: angiographic diagnosis and treatment.** *Weigele JB*

517 **Case report. Bilateral testicular infarction caused by epididymitis.** *Eisner DJ, Goldman SM, Petronis J, Millmond SH*

521 **Technical note. Insertion of the Simon nitinol caval filter: value of the antecubital vein approach.** *Kim D, Schlam BW, Porter DH, Simon M*

MUSCULOSKELETAL RADIOLOGY

523 **Cervical paraspinal calcification in collagen vascular diseases.** *Schweitzer ME, Cervilla V, Manaster BJ, et al.*

527 **Diagnosis of osteomyelitis of the foot in diabetic patients: value of ^{111}In-leukocyte scintigraphy.** *Larcos G, Brown ML, Sutton RT*

533 **Photostimulable phosphor digital radiography of the extremities: diagnostic accuracy compared with conventional radiography.** *Wilson AJ, Mann FA, Murphy WA Jr, Monsees BS, Linn MR*

PEDIATRIC RADIOLOGY

539 **Diagnosis of acute pyelonephritis in children: comparison of sonography and ^{99m}Tc-DMSA scintigraphy.** *Björgvinsson E, Majd M, Eggli KD*

545 **Normal length of fetal kidneys: sonographic study in 397 obstetric patients.** *Cohen HL, Cooper J, Eisenberg P, et al.*

549 **Benign hemorrhagic adrenocortical macrocysts in Beckwith-Wiedemann syndrome.** *McCauley RGK, Beckwith JB, Elias ER, Faerber EN, Prewitt LH Jr, Berdon WE*

553 **Parotid enlargement in children seropositive for human immunodeficiency virus: imaging findings.** *Soberman N, Leonidas JC, Berdon WE, et al.*

557 **Case report. Goitrous cretinism manifesting as newborn stridor: CT evaluation.** *Optican RJ, White KS, Effmann EL*

559 **Pictorial essay. Biological classification of soft-tissue vascular anomalies: MR correlation.** *Meyer JS, Hoffer FA, Barnes PD, Mulliken JB*

NEURORADIOLOGY

565 **MR imaging of cerebral ischemia: findings in the first 24 hours.** *Yuh WTC, Crain MR, Loes DJ, Greene GM, Ryals TJ, Sato Y*

575 **Cerebral ischemia: evaluation with contrast-enhanced MR imaging.** *Crain MR, Yuh WTC, Greene GM, et al.*

585 **Diagnosis of acute cerebral infarction: comparison of CT and MR imaging.** *Bryan RN, Levy LM, Whitlow WD, Killian JM, Preziosi TJ, Rosario JA*

595 **MR imaging of primary trochlear nerve neoplasms.** *Gentry LR, Mehta RC, Appen RE, Weinstein JM*

PERSPECTIVES

603 **Analysis of economics and use of MR imaging units in the United States in 1990.** *Evens RG, Evens RG Jr*

609 **The volume and cost of radiologic services in the United States in 1990.** *Sunshine JH, Mabry MR, Bansal S*

EDITORIAL

614 **Is plagiarism ever insignificant?** *Berk RN*

MEETING NEWS

615 **Society of Computed Body Tomography: 14th annual course, April 1991.** *Whalen E*

ARRS 1991 ANNUAL MEETING

623 **Summary of scientific program**
630 **Gold medal recipients.** *Kirkpatrick JA Jr*
633 **Secretary's report.** *Ferrucci JT*
635 **Administrative report.** *Fullagar PR*
636 **Award-winning exhibits**
638 **New members**

OTHER CONTENT

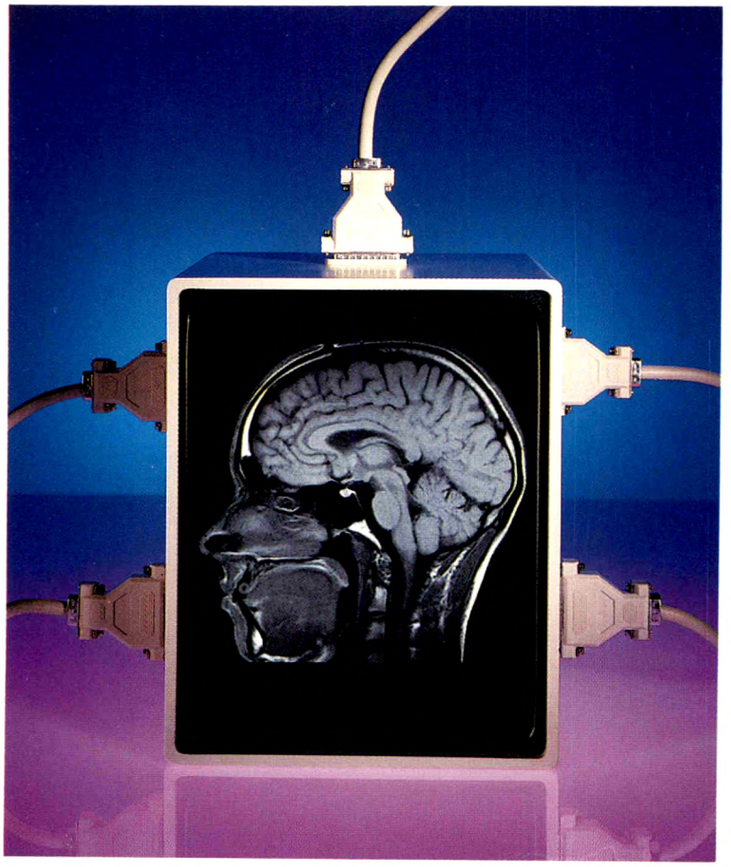
460 **Figley Fellowship announcement**
468 **Radiologic-pathologic conference**
502 **Forthcoming articles**
508 **List of book and videotape reviews**
515 **ARRS 1992 resident award papers information**
574 **Call for papers on neuroradiology**
640 **ARRS membership information and application**
643 **Letters**
651 **Review of current literature**
654 **The Interamerican College of Radiology.** *Wittenberg J*
656 **News**
659 **American Roentgen Ray Society information**
660 **ARRS 1992 meeting announcement, calls for papers and exhibits**
665 **Classified advertisements**
A20 ***AJR* business and subscriber information**
A23 **Guidelines for authors**

AJR

American
Journal of
Roentgenology

October 1991

© Eastman Kodak Company, 1991. 36USC380



Introducing the Kodak Ektascan laser printer model 100 XLP. An advanced digital imaging system that delivers maximum productivity today...and tomorrow.

We created the Ektascan model 100 XLP with features to improve work flow, reduce costs, and increase productivity. You can connect multiple digital modalities such as CT, MRI, and DSA through custom electronic interfaces—and film continuously from each input! Autofilming functions are built in to allow fully automatic operation. The system-designed software incorporated in the 100 XLP will be an important element in your facility's networking strategy. And it will remain compatible with future Kodak products.

An upgrade package allows owners of the Ektascan model 100 to experience these and other 100 XLP advantages. And, of course, the 100 XLP is backed by world-class service that's responsive, comprehensive, and affordable.

Kodak
Official Sponsor of the 1992 Olympic Games

Quality laser imaging from Kodak. Meeting your needs today and setting imaging standards for tomorrow. For details, contact your local Kodak representative.

WE'VE GOT ALL THE RIGHT CONNECTIONS. KODAK

The first choice in quality imaging...worldwide

Kodak

Official Journal of the American Roentgen Ray Society

AJR

American Journal of Roentgenology
Diagnostic Imaging and Related Sciences

Editor-In-Chief Robert N. Berk, *La Jolla, California*
University of California, San Diego
School of Medicine and Medical Center

Editor Emeritus Melvin M. Figley, *Seattle, Washington*

Associate Editor Karim Valji, *San Diego, California*

Associate Editor A. James Barkovich, *San Francisco, California*

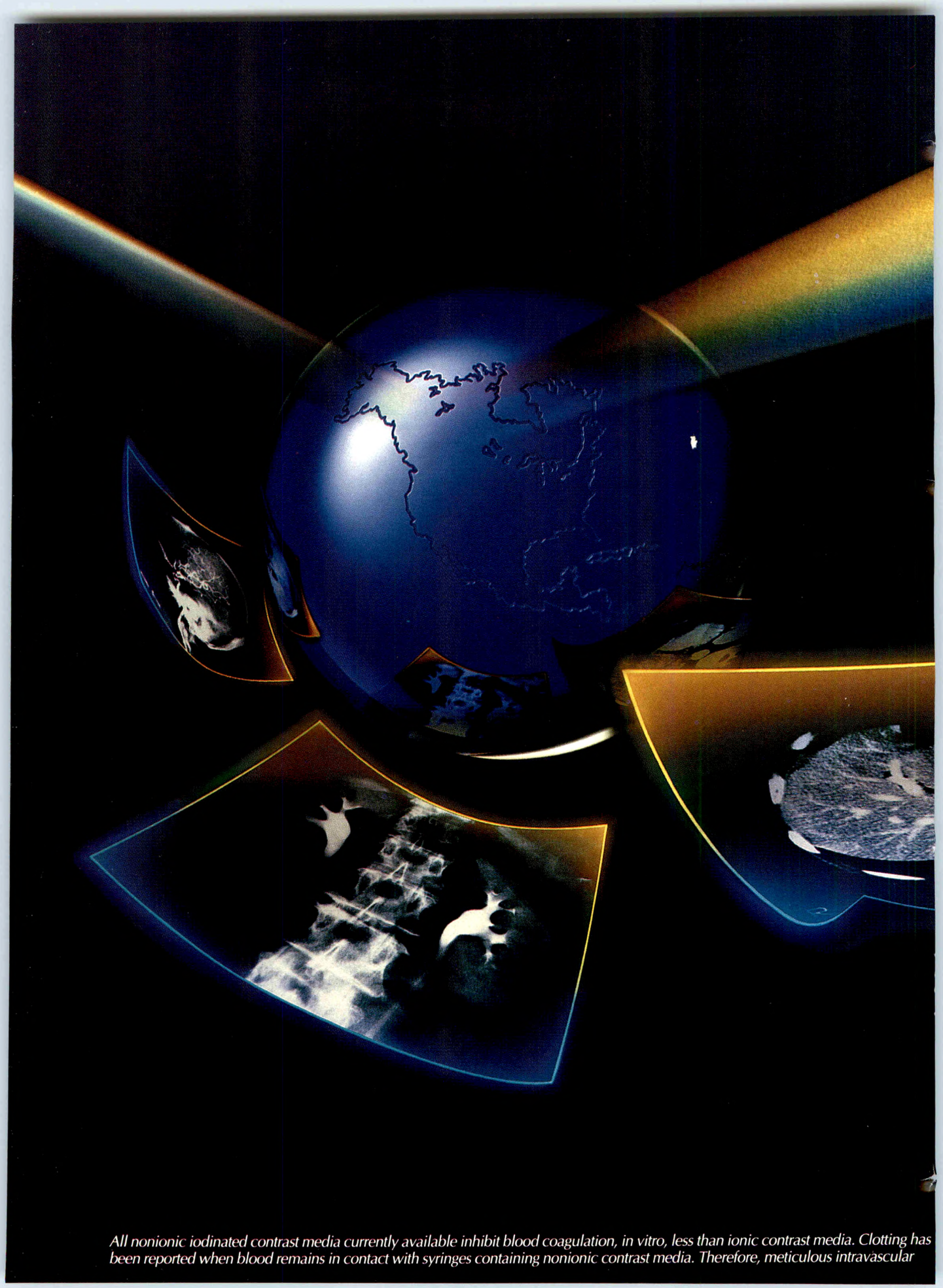
Statistician Charles C. Berry, *San Diego, California*

Editorial Board

John R. Amberg
Ithamar Aviad
Mark E. Baker
Lawrence W. Bassett
Michael A. Bettmann
Felix S. Chew
N. Reed Dunnick
David K. Edwards
Ronald G. Evens
David S. Feigin
Sandra K. Fernbach
Richard H. Gold
William R. Hendee
John R. Hesselink
Charles B. Higgins
Melvyn T. Korobkin
Faye C. Laing
Thomas L. Lawson
Robert G. Levitt
Bruce L. McClennan
Richard P. Moser
Albert A. Moss
Jeffrey H. Newhouse
Donald L. Resnick
Stewart R. Reuter
Charles A. Rohrmann, Jr.
Peter M. Ronai
Sjef H. J. Ruijs
Stuart S. Sagel
David J. Sartoris
Stefan C. Schatzki
William P. Shuman
Edward A. Sickles
Barry A. Siegel
David D. Stark
Edward T. Stewart
Murali Sundaram
Eric vanSonnenberg
Robert K. Zeman

Editorial Staff: Margaret Levene, *managing editor*; Katie L. Spiller, Barbara Rose, Barbara L. Halliburton, and Janine Anderson, *manuscript editors*; Nancy Rydbeck, *office manager*; Sheri Smith, *administrative assistant*; Linda J. Waggoner, *administrative secretary*

AJR, AMERICAN JOURNAL OF ROENTGENOLOGY (ISSN 0361 803X) is the official journal of the American Roentgen Ray Society and is published monthly by Williams & Wilkins, 428 E. Preston St., Baltimore, MD 21202. Annual dues include $50 for journal subscription. Second-class postage paid at Baltimore, MD, and at additional mailing offices. Postmaster, send address changes (Form 3579) to AJR, 428 E. Preston St., Baltimore, MD 21202. Subscription rates $125 ($180 foreign); institutions $135 ($190 foreign); in training $25 ($80 foreign); single copy $18 ($22 foreign). The GST number for Canadian subscribers is 123394371. Airmail rates furnished on request. Indexed by *Current Contents* and *Index Medicus*. Copyright © 1991 by American Roentgen Ray Society.
0361-803X/90$3.00



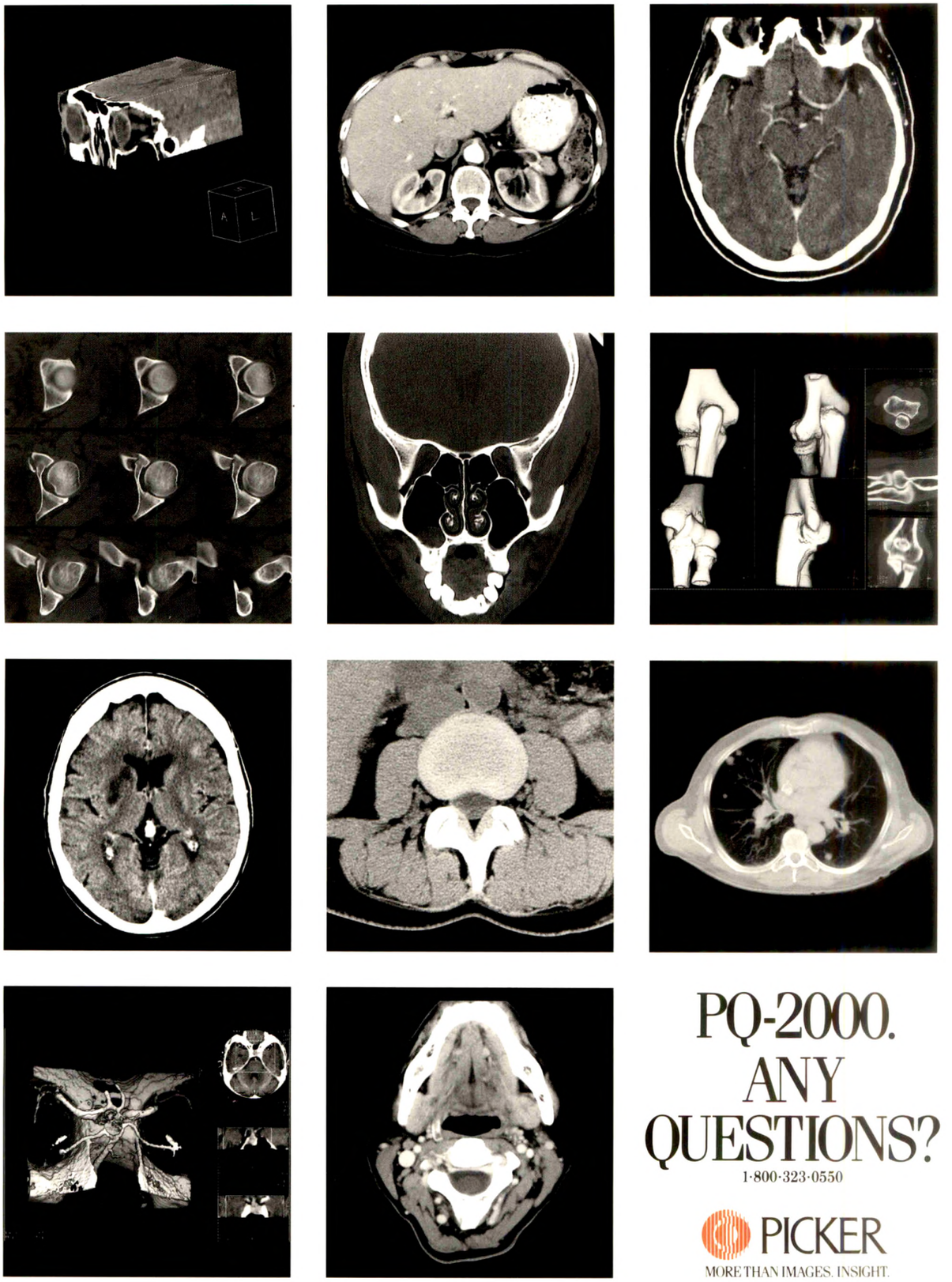
All nonionic iodinated contrast media currently available inhibit blood coagulation, in vitro, less than ionic contrast media. Clotting has been reported when blood remains in contact with syringes containing nonionic contrast media. Therefore, meticulous intravascular

EVERY SIX SECONDS
WE COME UP WITH ANOTHER
IMPRESSIVE ARGUMENT
FOR OWNING THE PQ-2000™.





©1991 Picker International, Inc.



PQ-2000. ANY QUESTIONS?

1·800·323·0550

PICKER

MORE THAN IMAGES. INSIGHT.

When you give blood
you give another birthday,
another anniversary,
another day at the beach,
another night under the stars,
another talk with a friend,
another laugh,
another hug,
another chance.



American Red Cross

Please give blood.

Ad Council

AJR Guidelines for Authors

Address new and revised manuscripts, correspondence, and classified ads to the Editor:

AJR Editorial Office
2223 Avenida de la Playa, Suite 103
La Jolla, CA 92037-3218
Telephone: (619) 459-2229; FAX: (619) 459-8814

Inquiries regarding subscriptions, display advertising, reprints, or permission to republish *AJR* material should be addressed to the publisher:

The Williams & Wilkins Co.
428 E. Preston St.
Baltimore, MD 21202 Telephone: 1-800-638-6423

The *AJR* publishes original contributions to the advancement of medical diagnosis and treatment. Submitted manuscripts should not contain previously published material and should not be under consideration for publication elsewhere.

Manuscript decisions are based on peer review. Reviewers receive manuscripts without title pages to ensure an unbiased review. Statements made in the article, including changes made by the Editor or manuscript editor, are the responsibility of the author and not of the *AJR* or its publisher. Authors will be sent the edited manuscript, galley proof, and proofs of illustrations. If the corresponding author will be unavailable to review galleys, arrangements should be made for a coauthor or colleague to read and return the proof.

The following guidelines are based on instructions set forth in the **Uniform Requirements for Manuscripts Submitted to Biomedical Journals** (*Ann Intern Med* **1988;**108:258–265). Articles will be edited, however, to conform to the individual style of *AJR*.

General Guidelines for Major Papers

Abstract. Clearly state (in 200 words or less) the purpose, methods, results, and conclusions of the study. Include actual data.

Introduction. Briefly describe the purpose of the investigation and explain why it is important.

Methods. Describe the research plan, the materials (or subjects), and the methods used, in that order. Explain in detail how disease was confirmed and how subjectivity in observations was controlled.

Results. Present results in a clear, logical sequence. If tables are used, do not duplicate tabular data in text, but do describe important trends and points.

Discussion. Describe the limitations of the research plan, materials (or subjects), and methods, considering both the purpose and the outcome of the study. When results differ from those of previous investigators, explain the discrepancy.

AUTHOR'S CHECKLIST

For priority handling, complete the following checklist, sign the copyright form on the reverse side of this page, and include both with the manuscript.

_____ Two copies of the manuscript (the original and a photocopy) and two complete sets of figures are submitted. One copy has been retained by the author.

_____ If appropriate, *AJR* Guidelines for case reports, technical notes, pictorial essays, or letters to the Editor have been followed. (See page A33.)

_____ The manuscript, including references, figure legends, and tables, is typed double-spaced on 8½ × 11 in. (21.6 × 27.9 cm) *nonerasable* paper. Right-hand margins are not justified.

_____ All manuscript pages are numbered consecutively beginning with the abstract. Authors' names do not appear on the manuscript pages.

_____ The manuscript is organized as follows: title page, blind title page (title only), abstract, introduction, methods, results, discussion, acknowledgments, references, tables, figure legends, and figures.

_____ Informed consent has been obtained from patients who participated in clinical investigations. If experiments were performed on animals, authors complied with NIH guidelines for use of laboratory animals.

_____ Use of unfamiliar acronyms and abbrevations is kept to a minimum. When abbreviations are used they are defined at first mention, followed by the abbreviation in parentheses.

_____ Metric measurements are used throughout, or the metric equivalent is given in parentheses.

_____ Names and locations (city and state only) of manufacturers are given for equipment and nongeneric drugs.

Title Page

_____ The following information is given: title of article; names and complete addresses (including zip code) of all authors; current addresses of authors who have moved since study; acknowledgment of grant or other assistance. The corresponding author is clearly identified, and a current address, phone number, and FAX number are given.

_____ A blind title page is included in each copy of the manuscript, giving only the title (without the authors' names) for use in the review process.

Abstract

_____ An abstract of approximately 200 words concisely states the purpose, methods, and results of the study in one paragraph. Actual data are included. Conclusions are stated in a second, summary paragraph.

_____ No abbreviations or reference citations are used.

References

_____ References (not to exceed 35) are typed double-spaced starting on a separate page and are **numbered consecutively in the order in which they appear in the text.**

_____ All references are cited in the text and are enclosed in brackets and typed on line with the text (not superscript).

_____ Unpublished data are not cited in the reference list, but are cited parenthetically in the text, for example, (Smith DJ, personal communication), (Smith DJ, unpublished data). This includes papers submitted, but not yet accepted, for publication.

_____ Papers presented at a meeting are not cited in the reference list, but are cited parenthetically in the text (e.g., Smith DJ et al., presented at the annual meeting of the American Roentgen Ray Society, May 1990). After first mention, use (Smith DJ et al., ARRS meeting, May 1990).

_____ Inclusive page numbers (e.g., 333–335) are given for all references.

_____ Journal names are abbreviated according to *Index Medicus*.

_____ Style and punctuation of references follow the format illustrated in the following examples (all authors are listed when six or fewer; when seven or more authors, the first three are listed, followed by "et al."):

Journal article

1. Long RS, Roe EW, Wu EU, et al. Membrane oxygenation: radiographic appearance. *AJR* **1986**;146:1257–1260

Book

2. Smith LW, Cohen AR. *Pathology of tumors*, 6th ed. Baltimore: Williams & Wilkins, **1977**:100–109

Chapter in a book

3. Breon AJ. Serum monitors of bone metastasis. In: Clark SA, ed. *Bone metastases*. Baltimore: Williams & Wilkins, **1983**:165–180

Tables

_____ Each table is typed double-spaced on a separate page without vertical or horizontal rules; each has a short, descriptive title. Tables do not exceed two pages in length and contain at least four lines of data.

_____ Tables are numbered in the order in which they are cited in the text.

_____ Abbreviations are defined in an explanatory note below each table.

_____ Tables are self-explanatory and do not duplicate data given in the text or figures.

_____ All arithmetic (percentages, totals, differences) has been double checked for accuracy, and tabular data agree with data given in the text.

Figures and Legends

_____ Two complete sets of original figures are submitted unmounted in labeled envelopes.

_____ Figures are clean, unscratched, 5 × 7 in. (13 × 18 cm) glossy prints with **white borders.** A separate print is submitted for each figure *part*.

_____ All figure parts relating to one patient have the same figure number.

_____ Each figure is labeled on the back with the figure number and an arrow indicating "top." For black-and-white figures, labeling is done on a gummed label, which is then affixed to the back of the print. **Never** use labels on **color** figures, but write figure number on the back lightly in pencil. *Never* use ink on front or back of any figures.

_____ Authors' names are *not* written on the backs of figures.

_____ Only removable (rub-on) arrows and letters are used on the figures. Symbols are uniform in size and style and are not broken or cracked.

_____ Images are uniform in size and magnification.

_____ Line drawings are done in black ink on a white background. They are professional in quality, and all use the same size type. (Only glossy prints are acceptable.)

_____ Written permission has been obtained for use of all previously published illustrations (and copies of permission letters are included), and an appropriate credit line is given in the legends.

_____ Legends are typed double-spaced, and figure numbers correspond with the order in which the figures are cited in the text.

Transfer of Copyright Agreement, Conflict of Interest Acknowledgment, Certification of Coauthors, and Exclusive Publication Statement

Complete copyright to the article entitled: _____

_____

is hereby transferred to the American Roentgen Ray Society (for United States government employees to the extent transferable), effective if and when the article is accepted for publication in the *American Journal of Roentgenology*. In the case of the authors who are officers or employees of the United States government, the American Roentgen Ray Society recognizes that works prepared by officers or employees of the United States government as part of their official government duties are in the public domain.

Authors reserve all proprietary rights other than copyright, such as patent rights and the right to use all or part of this article in future works of their own. The authors retain the right of replication, subject only to crediting the original source of publication and receiving written permission from the publisher.

Authors guarantee that this manuscript contains no matter that is libelous or otherwise unlawful, invades individual privacy, or infringes any proprietary rights.

Authors understand that they will receive no royalty or other compensation from the American Roentgen Ray Society or the publisher.

Authors guarantee that the editor has been or will be informed of any proprietary or commercial interest or conflicts of interest the authors may have that relate directly or indirectly to the subject of this article.

All authors certify that they have made substantive and specific intellectual contributions to the article and assume public responsibility for its content.

Finally, the authors certify that none of the material in this manuscript has been published previously or is currently under consideration for publication elsewhere.

_____	_____	_____
First author/date	Second author	Third author
_____	_____	_____
Fourth author	Fifth author	Sixth author

This agreement must be signed by all authors in order for the manuscript to be published.

Case Reports

A case report is a brief description of a special case that provides a message that transcends the individual patient.

Format. There is no abstract. The introduction should be a short paragraph giving the general background and the specific interest of the case. No more than one case should be described in detail (similar ones can be mentioned briefly in the discussion). Emphasis should be on the radiologic aspects; clinical information must be limited to that necessary to provide a background for the radiology. The discussion should be succinct and should focus on the specific message and relevance of radiologic methods. A review of the literature is not appropriate.

Length. Maximum of five double-spaced, typewritten pages, including the references but not the title page or figure legends.

References. Maximum of eight.

Figures. Maximum of four, unless the text is shortened accordingly. Legends must not repeat the text.

Tables and Acknowledgments. Not appropriate in case reports.

Technical Notes

A technical note is a brief description of a specific technique or procedure, modification of a technique, or equipment of interest to radiologists.

Format. No abstract, headings, or subheadings are required. If headings are used, they should be a combination of "Case Report," "Materials and Methods," "Results," and "Discussion." A brief one-paragraph introduction should be included to give the general background. Discussion should be limited to the specific message, including the uses of the technique or equipment. Literature reviews and lengthy case reports are not appropriate.

Length. Maximum of five double-spaced, typewritten pages, including the references but not the title page or figure legends.

References. Maximum of eight.

Figures. Maximum of two, unless the text is shortened accordingly.

Tables and Acknowledgments. Not appropriate in technical notes.

Pictorial Essays

A pictorial essay is an article that conveys its message through illustrations and their legends. Unlike other *AJR* articles, which are based on original research, pictorial essays serve primarily as teaching tools, like exhibits at a scientific meeting. They are not encyclopedic book chapters. The abstract should be a short, introductory paragraph.

Length. Maximum of four double-spaced, typewritten pages, including the references but not the title page or figure legends.

References. Maximum of four.

Figures. Maximum of 30 figure *parts*. Number should be as few as necessary to convey the message of the paper.

Tables and Acknowledgments. Not appropriate in pictorial essays.

Letters to the Editor and Replies

Letters to the Editor and Replies should offer objective and constructive criticism of published articles. Letters may also discuss matters of general interest to radiologists. Do not end a letter with a hand-written signature.

Format. All letters should be typed double-spaced on nonletterhead paper, with no greeting or salutation. Name and affiliation should appear at the end of the letter. Titles for letters should be short and pertinent. The title for a reply is simply "Reply."

Length. Maximum of two double-spaced, typewritten pages, including references.

References. Maximum of four.

Figures. Maximum of two.

Tables and Acknowledgments. Not appropriate in Letters to the Editor and Replies.

Opinions, Commentaries, and Perspectives

Opinions, commentaries, and perspectives are special articles dealing with controversial topics or issues of special concern to radiologists.

Format. Include a title page but no abstract. Headings may be used to break up the text.

Length. Maximum of five double-spaced, typewritten pages.

References. Maximum of five.

Tables and Figures. Maximum of four.

Computer Page Articles

Articles published on the computer page deal with practical computer applications to radiology.

Format. Include a title page and an abstract.

Length. Maximum of eight double-spaced, typewritten pages.

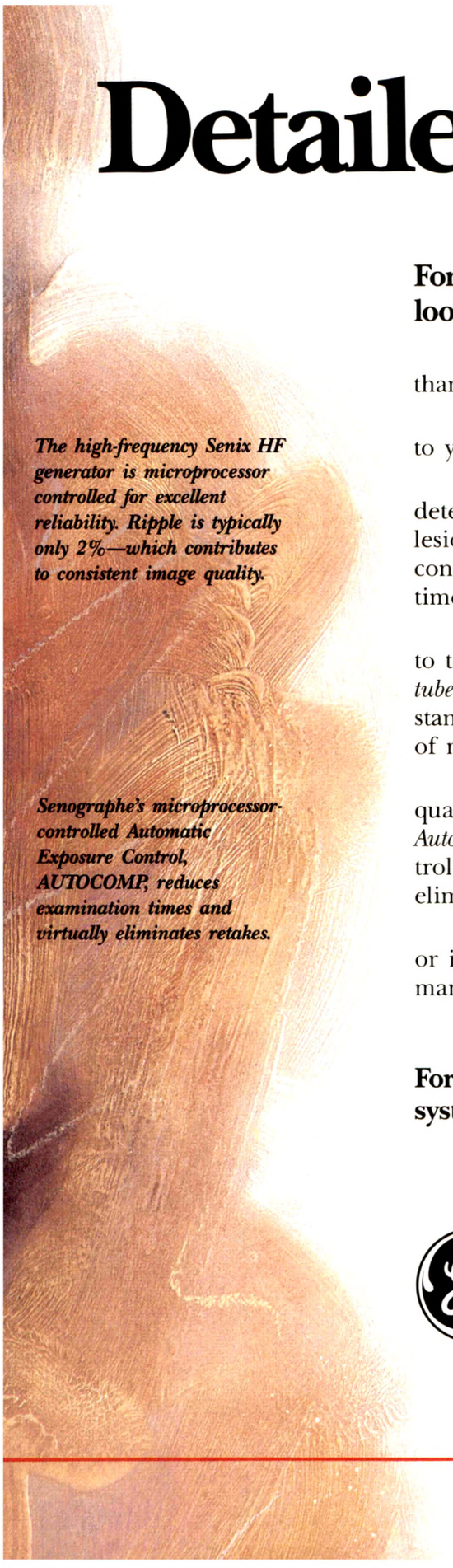
References. Maximum of five.

Figures and Tables. Maximum of five. Computer printouts are not acceptable. Figures must be submitted as 5 × 7 in. glossy prints.

All submissions to the *AJR* must be accompanied by a completed copy of the Author's Checklist and the signed Copyright agreement.


Senographe's dedicated x-ray tube features two focal spots with the highest mAs in the industry—0.3 mm at 100 mA and 0.1 mm at 30 mA—for excellent image quality at low dose.
Pneumatic compression provides "hands free" positioning and consistent, even compression.
Mammography
© Copyright 1989 General Electric Company

Detailed reading



The high-frequency Senix HF generator is microprocessor controlled for excellent reliability. Ripple is typically only 2%—which contributes to consistent image quality.

Senographe's microprocessor-controlled Automatic Exposure Control, AUTOCOMP, reduces examination times and virtually eliminates retakes.

For the finest details in mammography, look to Senographe.

Nothing is more important in mammography than excellent image quality.

And no system is better equipped to give it to you than Senographe® Senix HF™ from GE.

Senographe's finely detailed images let you detect the most subtle microcalcifications and lesions—early and confidently. You get superb contrast and detail, with the shortest exposure times of any system on the market.

This imaging strength stems from attention to technological details. Such as a *dedicated x-ray tube* designed specifically for mammography. And standard *1.85x magnification* for better assessment of microcalcifications and lesion contours.

The Senix *high-frequency generator* boosts image quality by dramatically reducing noise. And *Autocomp*™, our exclusive automatic exposure control, provides constant film density and virtually eliminates retakes.

No matter how you look at it—equipment or image—Senographe is the clear choice in mammography.

For a free brochure on Senographe Senix HF systems, call toll free 1-800-433-5566.

GE Medical Systems

INTRODUCING

PULSE*SPRAY™

PULSED INFUSION SYSTEM



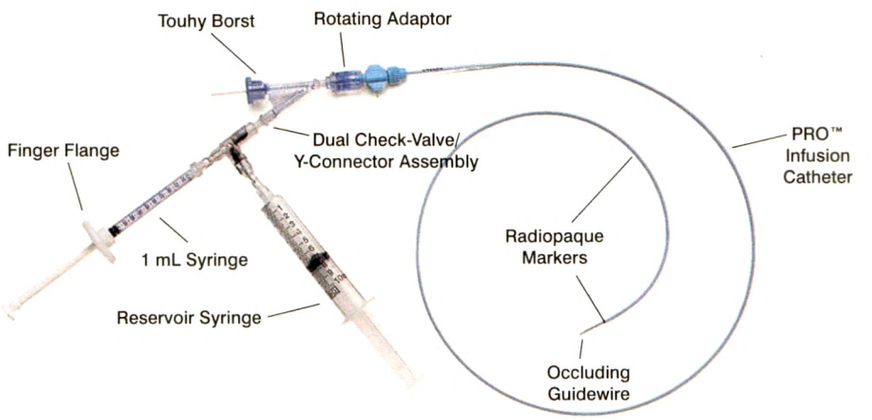
The PULSE*SPRAY™ System is contraindicated for use in the coronary vasculature.

© ANGIODYNAMICS 1991

ANG003

A breakthrough from AngioDynamics specifically developed for the infusion of therapeutic solutions into the peripheral vasculature.

Developed in association with Joseph J. Bookstein, MD, PULSE*SPRAY™ offers:



PRO™ Infusion Catheter (patent pending)

- 5F PRO™ (Pressure Responsive Orifice) Infusion Catheter features slits at 90° intervals around the axis of the catheter.
- Available in both 90 cm and 135 cm lengths, with infusion slit pattern variations of 10 cm and 20 cm.

Unique slit design

- Circumferential slit pattern provides uniform dispersion of the therapeutic solution.

Finger flange

- Conveniently designed finger flange incorporated with the 1 mL tuberculine syringe allows forceful and consistent injection, while offering comfort during the procedure.

Dual check-valve assembly

- Dual check-valve/Y-connector assembly simplifies aspiration and infusion of the therapeutic agent.

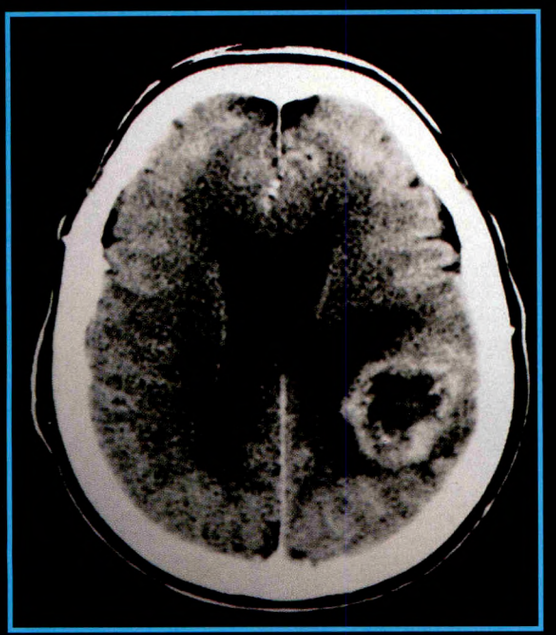
ANGIODYNAMICS™

Division of E-Z-EM, Inc.

AngioDynamics, Division of E-Z-EM, Inc. Glens Falls, NY 12801
1-800-77ANGIO

Distributed in Canada by THERAPEX
Division of E-Z-EM Canada Inc. 1-800-465-5820

L E A D E R S H I





NOW IN CT

SOON IN M

Winthrop has earned universal leadership in nonionic contrast media for CT. Look to us again i MR. For the overall quality of o products, our people, and our commitment to serve. Qualities that help radiology choose Winthrop contrast media first. Now in CT, and soon in MR.

Winthrop
PHARMACEUTICALS

DIAGNOSTIC IMAGING DIVIS

LEADERSHIP IN NONIONIC CONTRA MEDIA

© 1991 Winthrop Pharmaceuticals

63-

Review Article

Hysterosalpingography in the 1990s

Isabel C. Yoder[1] and Deborah A. Hall

All physicians involved in the evaluation and treatment of infertility rely heavily on the information provided by hysterosalpingography. For many years this study has provided images of the lumina of the fallopian tubes that are not available by other diagnostic means, and it also gives the most accurate outline of the uterine cavity. Hysterosalpingography will therefore continue to be a valuable study in the upcoming decade, and it is important now to take account of the many advances in technology that impinge on the execution and interpretation of this study. In this article we first update the continuing debate about elements of the study itself, involving techniques and the choice of contrast material. We also consider surgical advances, such as the widespread use of microsurgical reconstruction of the fallopian tube, that increase the demand for hysterosalpingography. Since radiologists are asked to evaluate the results of surgery, it is essential for them to be familiar with the postoperative appearances of the fallopian tube. Finally, we consider what must be by far the most important development of the 1990s, the continuing integration of hysterosalpingography with new interventional and imaging techniques. Fallopian tube catheterization expands the examination of the fallopian tube and offers new therapeutic applications. Transvaginal sonography and MR imaging have allowed noninvasive exploration of the female pelvis. Correlation of hysterosalpingography and MR imaging is particularly useful in the diagnosis of uterine myomas and congenital uterine duplication anomalies when surgery to preserve or enhance the reproductive capacity of the uterus is indicated. Sonography and MR imaging should be correlated with hysterosalpingography to provide a more efficient diagnostic and therapeutic approach to the common mechanical causes of infertility.

The first hysterosalpingogram was obtained 80 years ago by using bismuth paste as the contrast medium. Since then, the procedure has been a primary tool in the evaluation of infertility, and given today's increasing concern over infertility, it is a procedure that is likely to be more frequently performed. Fortunately, the technique and interpretation of hysterosalpingography have been refined, and the procedure is less painful and diagnostically more accurate than it once was. In this article, we discuss current techniques and use of contrast material in hysterosalpingography. We then review the impact of recent interventional developments, such as fallopian tube catheterization, on hysterosalpingography. Finally, we examine common tubal and uterine abnormalities in the context of the imaging techniques that have become available only in the last decade or so, for example, transvaginal sonography and MR imaging.

Technique

Hysterosalpingography is a procedure that falls within the domain of both radiology and gynecology. Today in the United States, 55% of hysterosalpingograms are obtained by the radiologist and gynecologist working together; only 27% are obtained by the radiologist alone [1]. These circumstances have led to the development of two major techniques. The balloon catheter technique is favored by radiologists [2], and the tenaculum-cannula technique is preferred by gynecologists working alone [3] or with radiologists [4, 5]. We favor the balloon catheter technique (Fig. 1) because it is simple to learn, is comfortable for patients, and facilitates diagnostic maneuvers such as turning patients to oblique and prone positions. Proponents of the cannula technique argue that the balloon may obscure uterine anatomy and may lead to dis-

Received March 13, 1991; accepted after revision May 21, 1991.

[1] Both authors: Department of Radiology, Massachusetts General Hospital, Fruit St., Boston, MA 02114. Address reprint requests to I. C. Yoder.

AJR **157:675–683, October 1991** 0361–803X/91/1574–0675 © American Roentgen Ray Society

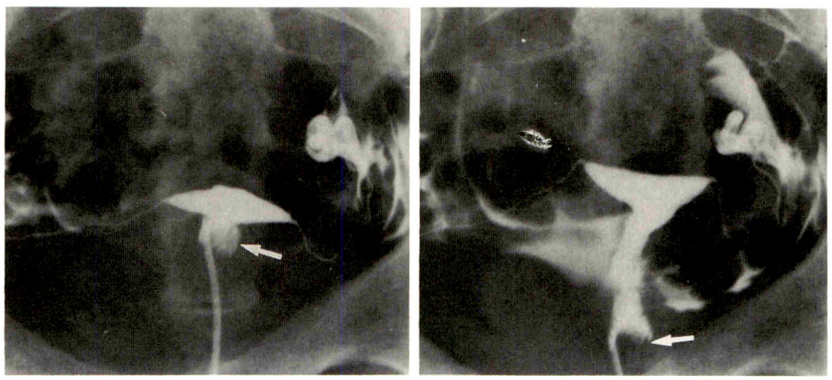


Fig. 1.—Normal balloon catheter hysterosalpingogram in a 36-year-old woman after 1 year of infertility.

A, Anteflexed uterus, foreshortened on anteroposterior view. Foley balloon is inflated within lower cervical canal (*arrow*).

B, After catheter is pulled gently, uterus is straightened and uterine cavity displayed beautifully. Because this maneuver may cause balloon (*arrow*) to pop out of cervical canal, it is usually reserved as final step after all necessary diagnostic films have been obtained. Fallopian tubes are normal in caliber, and free intraperitoneal spill is ample.

comfort after the procedure [6]. In order not to interfere with clear visualization of the uterine cavity, the balloon catheter is inflated within the endocervical canal. This is especially important in the assessment of cervical incompetence, which requires an accurate measurement of the size of the internal cervical os.

Regardless of personal preference, both balloon catheter and cannula techniques produce excellent diagnostic studies, and physicians should be well versed in both of them because circumstances may dictate a specific need for one or the other. For example, balloon catheters allow simultaneous catheterization of a double cervix for better visualization of uterine duplication anomalies. The cannula technique is preferred in the presence of extensive uterine synechiae, because under those circumstances the balloon catheter will be repeatedly expulsed. Physicians also should be aware of refinements in the instruments used for hysterosalpingography. A number of newly developed rigid balloon catheters [7] can be very useful in cannulating patients with cervical stenosis, and a new plastic cannula can be used for the same purpose [8].

After catheter placement, routine spot films are obtained under fluoroscopic control. A normal study may require only five films: a preliminary view of the pelvis, followed by two anteroposterior views and an oblique view of each fallopian tube during instillation of contrast media. Usually, a total of 6–8 ml of contrast material is sufficient, but special circumstances such as an enlarged uterine cavity may warrant larger amounts. The initial anteroposterior spot film is an underfilled view of the uterine cavity to show the presence of small endometrial lesions (Fig. 2A) that are easily obscured by large amounts of contrast media (Fig. 2B). After oblique views of the tubes are obtained, a final anteroposterior view should demonstrate free dispersion of contrast material around bowel loops. Peritoneal adhesions surrounding the tubes may lead to the accumulation of contrast material in a paratubal collection. To aid the detection of paratubal collections, infusion of adequate amounts of contrast media and the use of

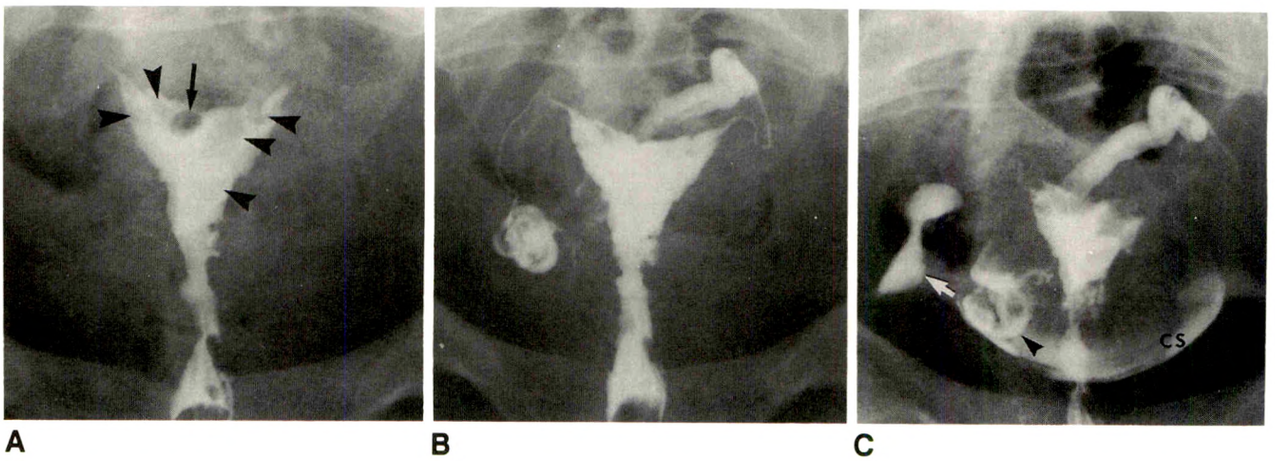


Fig. 2.—Uterine polyps and postoperative peritoneal adhesions in a 38-year-old woman with a long history of infertility. Surgical abdominal myomectomy and uterine suspension were performed 5 years before.

A, Early hysterosalpingogram shows multiple polyps as rounded and oval filling defects in uterine cavity (*arrowheads*) and a solitary air bubble (*arrow*).

B, Further infusion of contrast material fills both fallopian tubes and obscures polyps. Ampullae, although not dilated, appear rigid and in an abnormally medial position.

C, Drainage view shows loculated spill of contrast material (*arrow*), right peritubal halo (*arrowhead*), and some free spill into cul-de-sac (cs). Multiple endometrial polyps were removed at hysteroscopy. Laparoscopy revealed multiple adhesions involving tubes, bowel, and pelvic side wall.

drainage films are very helpful (Fig. 2C). The drainage film is obtained 5–10 min after removal of the uterine catheter and after the patient has been allowed to move around or turn prone.

Technical problems arise when the contrast material does not flow freely into one or both fallopian tubes and there appears to be interstitial tubal obstruction. This may represent a true obstruction or a transient lack of filling due to what is commonly referred to as tubal spasm. Several drugs, such as glucagon and terbutaline, have been used in an attempt to overcome muscular tubal spasm [9]. Our current approach is to try to overcome interstitial obstruction by turning the patient into a prone position and instilling additional contrast material [10]. The normal tube often will fill after this maneuver, and the patient whose tubes remain occluded may become a candidate for fallopian tube catheterization.

Contrast Material

Debate continues between advocates of oil-soluble and those of water-soluble contrast media for hysterosalpingography. The arguments do not center on the diagnostic properties of the agents, because with few exceptions [11], everyone agrees that water-soluble contrast medium provides better uterine and ampullary mucosal detail, and therefore more accurate diagnostic studies [12]. The controversy concerns the therapeutic properties of each contrast medium. Some studies credit oil-soluble contrast medium for higher pregnancy rates after the procedure [13], whereas other studies [14] conclude that there is no statistical difference in pregnancy rates after hysterosalpingography with oil or water-soluble material. Recent animal studies [15, 16] have shown that oil-soluble contrast media result in granulomatous changes and fibrosis on the peritoneal surfaces of the animals tested. Water-soluble contrast material produced either no peritoneal reaction or a mild transitory inflammatory reaction. Clinical studies have shown no advantage to the use of low-osmolality contrast media over conventional contrast media [17].

Therefore, safety and diagnostic factors dictate the use of a conventional water-soluble contrast agent. The concentration of iodine does not need to exceed 30% to provide good detail. We use Sinografin (38% iodine, Squibb), which is slightly more viscous and does not flood the peritoneum as easily as other water-soluble agents do.

Fallopian Tube Catheterization

Obstruction at the interstitial or proximal portion of the fallopian tube precludes evaluation of the distal tube by hysterosalpingography and therefore may make laparoscopy necessary. Fallopian tube catheterization offers an alternative to laparoscopy. It is a method developed by Thurmond et al. [18] to examine the distal tube when hysterosalpingography shows interstitial obstruction of one or both fallopian tubes. Fallopian tube catheterization is a natural extension of hysterosalpingography, but because the procedure is more painful and prolonged than hysterosalpingography, it requires separate scheduling. Patients are placed on oral antibiotics, usually doxycycline, for a few days before and after fallopian tube catheterization. During the procedure, small doses of Versed (Roche Laboratories, Nutley, NJ) and fentanyl are given IV to treat pain as necessary.

Fallopian tube catheterization entails selective catheterization of the ostium of the fallopian tube with an angiographic catheter. The technique was described recently in this journal [19]. Thurmond and Rosch [20] and other authors [21, 22] who perform selective salpingography have reported high rates of success, in the range of 86–98%, in catheterizing occluded tubes. More than half of the distal tubes visualized in this manner appear normal and show free intraperitoneal spill. The remainder show a variety of abnormalities, including peritubal adhesions, hydrosalpinx, salpingitis isthmica nodosa, and postsurgical isthmic stenosis. Endoscopic observation with falloscopy confirms [23] that the guidewire used for tubal cannulation breaks up intraluminal adhesions, and then contrast material flushes mucus plugs from the proximal tubes. Thus, fallopian tube catheterization enjoys both diagnostic and therapeutic properties. The subsequent pregnancy rate varies between 7% [21] and 31% [20] overall, with a significant number of ectopic pregnancies. Tuboplasty, dilatation of the tube with a modified angioplasty balloon catheter as described by Confino et al. [24], does not improve the pregnancy rate (28%) but may prevent tubal reocclusion for longer periods than guidewire cannulation does. Because the balloon catheter used for dilatation has a much larger diameter than the interstitial segment of the tube, it probably breaks up adhesions within the cornu itself and not inside the tube. Furthermore, falloscopy shows that when a fibrotic stricture is present within the proximal tube, both the balloon catheter and the guidewire are completely ineffective in bypassing it [23].

Another successful therapeutic application of selective salpingography has been its use for the direct introduction of gametes and embryos into the fallopian tubes [25]. The procedure depends on the operator's ability to manipulate a transvaginal catheter through the uterotubal ostium and into the isthmus under transvaginal sonographic monitoring [26]. Radiologists may be called on to assist in these fertilization techniques as they become more popular. They require no anesthesia, and gamete intrafallopian transfer results in a 21% live delivery rate, whereas in vitro fertilization with intrauterine embryo transfer has a 12% rate of live deliveries [27].

In summary, fallopian tube catheterization improves on the diagnostic evaluation of the fallopian tube offered by hysterosalpingography, and may have diverse therapeutic applications. Complications of catheterization are similar to complications of hysterosalpingography, and include pain, radiation exposure, infection, and tubal perforation, which is unique to catheterization. Tubal perforation can occur when there is complete fibrotic obstruction of the tubal lumen, but it promptly seals over and has not produced any bleeding or other long-term problems. Prophylactic antibiotics have prevented any septic complications to date [28].

Tubal Abnormalities

The oviduct is a muscular tube measuring 10–14 cm in length. It is divided into the intramural (interstitial), isthmic,

and ampullary portions. The normal mucosa consists of a single layer of columnar epithelium composed of secretory and ciliated cells [29]. The fallopian tube has a limited range of reactions to disease: obstruction and/or dilatation.

Obstruction

Obstruction of the interstitial segment is usually due to infection, such as salpingitis isthmica nodosa, or to endometriosis. Previous salpingectomy and tubal ligation are the most frequent causes of isthmic obstruction of the fallopian tube. Less often, infectious or endometriotic scarring in this portion of the tube may occur. The ampullary portion of the tube is the most commonly obstructed.

Hydrosalpinx

Hydrosalpinx refers specifically to the dilatation of the ampullary segment of the tube that accompanies distal obstruction. The ampulla dilates preferentially because it has a thin muscular wall surrounding a relatively capacious lumen. Hydrosalpinx is usually the sequela of infection with agglutination and fibrosis of the fimbria. It is associated with paratubal adhesions. Gonococcal, chlamydial, and mixed bacterial salpingitis may result in hydrosalpinx. Endometriosis and pelvic surgery may also cause fimbrial adhesions, tubal occlusion, and hydrosalpinx (Fig. 3A). Endometriosis is increasingly a cause of infertility in the older patient who delayed childbearing.

Transvaginal sonography provides a noninvasive view of the dilated fallopian tube but has proved disappointing in its ability to identify the normal tube [30]. A dilated fallopian tube is seen on transvaginal sonography as a tubular structure with a folded configuration and a well-defined echogenic wall [31] (Fig. 3B). Dilated fallopian tubes have to be differentiated from other cystic tubular structures in the pelvis such as bowel loops, which show peristaltic motion; dilated pelvic veins, which have blood flow within them; cystic adnexal masses; and appendicitis [32, 33]. Schlief and Deichert [34] infused SHU 454/Echovist (Schering, Berlin), a new echogenic contrast medium, into the uterus during transvaginal sonography and reliably showed patency of normal fallopian tubes. The advantage of this indirect method is that it spares the patient ionizing radiation. However, it is cumbersome and requires uterine cannulation without giving the accurate anatomic detail of the tube provided by hysterosalpingography.

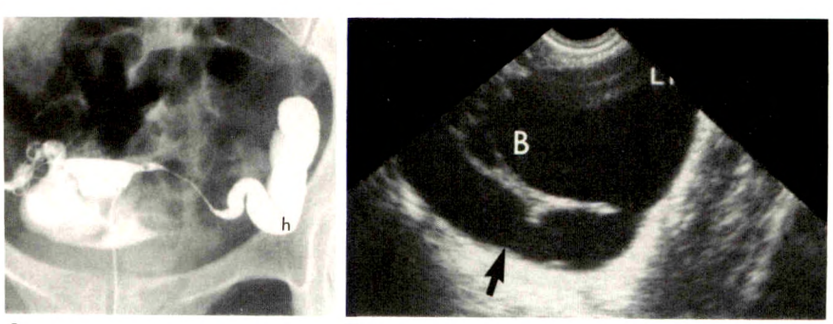
Hysterosalpingography offers the best view of the internal anatomy of the fallopian tube short of direct visualization by falloscopy. Falloscopy is a new microendoscopic technique that enables the surgeon to explore the fallopian tube from the uterotubal ostium to the fimbria through a small flexible hysteroscope [35].

Salpingitis Isthmica Nodosa

The isthmic portion of the tube has a thick muscular wall, and luminal dilatation is very rare. More commonly, the hysterosalpingogram shows multiple small diverticula extending from the isthmic lumen into the wall (Fig. 4). This appearance is characteristic of salpingitis isthmica nodosa. It affects both tubes in 80% of cases [36] and often is associated with proximal obstruction or ampullary dilatation. Fallopian tube catheterization has increased our ability to diagnose salpingitis isthmica nodosa by its ability to fill the isthmic diverticula beyond the proximally occluded tube. These patients have a history of pelvic infection and exhibit a high rate of primary infertility (38%) and ectopic pregnancy (9.4%) [37]. Isthmic diverticulosis identical to salpingitis isthmica nodosa can sometimes be seen in tuberculosis of the fallopian tube. Unlike salpingitis isthmica nodosa, tuberculosis is accompanied by contraction of the ampulla and adnexal calcification.

Fallopian Tube Surgery

Microsurgical techniques allow the successful performance of tubotubal and tubouterine anastomoses. This surgery is commonly executed after diagnosis of an obstructive lesion by hysterosalpingography or for reversal of tubal ligation. Hysterosalpingography before reanastomosis after tubal ligation is considered valuable by some authors [38] and unwarranted by others [39]. In our experience, currently few requests for salpingographic evaluation of tubes are made before reversal of sterilization. However, the demand is increasing for postoperative evaluation of tubes after all types of microsurgical reconstruction. Hysterosalpingography shows the patency of the tube, its length, the degree of narrowing at the site of the anastomosis (Fig. 5), the condition of the ampulla, and the development of paratubal adhesions. Measuring the length of the tube is important, as the viable pregnancy rate is reduced in women with oviducts shorter than 4 cm [40].



A B

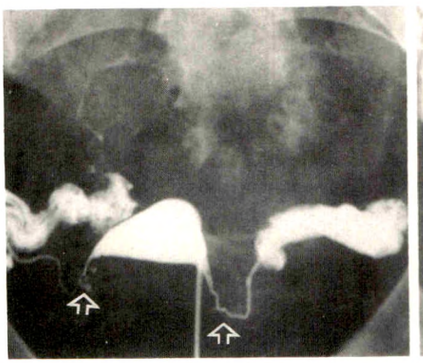
Fig. 3.—Left-sided hydrosalpinx in a 31-year-old woman with secondary infertility after normal delivery 4½ years before.

***A*, Hysterosalpingogram shows dilated and obstructed left fallopian tube (h).**

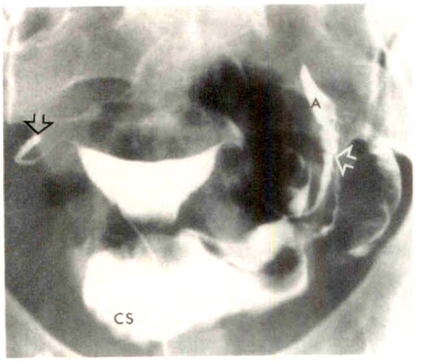
***B*, Transvaginal sonogram obtained 5 days later shows an anechoic tubular structure with linear echoes protruding into its lumen. This represents a dilated left fallopian tube (*arrow*) below an underfilled bladder (B). Laparotomy showed extensive pelvic endometriosis. Fulguration of endometriosis, lysis of adhesions, and left fimbrioplasty for a completely blocked tube were accomplished. Six months later, a pregnancy test was positive.**

Fig. 4.—Salpingitis isthmica nodosa in a 28-year-old woman with 7 years of infertility. Hysterosalpingogram shows bilateral isthmic diverticulosis (*arrows*), more pronounced on right side. Hydrosalpinx is bilateral. Ampullary mucosal pattern is better preserved on right side than on left. Patient had bilateral cuff salpingoplasties and lysis of adhesions. Nodularity of proximal tubes is consistent with salpingitis isthmica nodosa.

Fig. 5.—Hysterosalpingogram after tubal reconstruction in a 33-year-old woman who had a tubotubal reanastomosis after a Pomeroy tubal ligation. One year after surgery, she had not conceived. Hysterosalpingogram shows a nondilated, free-spilling left fallopian tube with marked circumferential narrowing at site of reanastomosis (*white arrow*) and a short and rigid left ampulla (A). Right fallopian tube shows complete isthmic obstruction (*black arrow*) at surgical site. CS = cul-de-sac.



4



5

The normal ciliated cells that line the fimbria and ampulla play a major role in ovum transport. These ciliated cells are destroyed with obstruction and hydrosalpinx. The hysterosalpingogram can be used to determine the success of surgical reconstruction. Increasing dilatation of the ampulla and effacement of its mucosal patterns as shown on hysterosalpingograms is directly correlated with significant decrease of both the percentage of ciliated cells and the pregnancy rate after microsurgical salpingostomy [41]. Donnez and Casanas-Roux [41] report a 48% rate of pregnancy after repair of an occluded nondilated ampulla and a 22% rate of pregnancy in an occluded ampulla distended to a diameter greater than 2.5 cm. If pregnancy does not occur in a reasonable period and the postoperative hysterosalpingogram shows tubal abnormalities, the patient may then be a candidate for in vitro fertilization.

Paratubal Adhesions

Paratubal adhesions are difficult to evaluate by hysterosalpingography. They are the largest source of discrepancy between the results of hysterosalpingography and laparoscopy. Endometriosis, surgery, and pelvic infection are the common sources of adhesions. They cloak the peritoneal surfaces of the tubes and ovaries and disturb the tuboovarian relationship to such an extent that they interfere with ovum capture and transport by the fimbria. Laparoscopy provides direct visualization of adhesions, whereas hysterosalpingography gives only indirect evidence of their presence. The most suggestive salpingographic findings include a convoluted or vertical tube in association with loculated spill of contrast material and peritubal halo effect [42]. The detection of paratubal collections is improved by infusion of adequate amounts of contrast material and the use of drainage films.

Uterine Abnormalities

The normal uterine cavity as shown on hysterosalpingograms is triangular, with a smooth outline. Filling defects within the uterine cavity may be due to air bubbles, polyps, blood clots, adhesions, submucosal myomas, carcinoma, and endometrial hyperplasia. Accurate diagnosis depends on the patient's clinical and surgical history as well as correlation of the hysterosalpingographic findings with findings from other available imaging studies.

Leiomyomas

Uterine myomas are common benign tumors in young women. These tumors may produce symptoms associated with a pelvic mass, menorrhagia, and infertility. Transabdominal or hysteroscopic myomectomy is the surgery of choice to preserve the uterus and future reproductive capacity. Accurate localization of leiomyomas is a prerequisite for conservative surgery. The sonographic diagnosis of uterine fibroids is easily available and inexpensive, but highly inaccurate, with a prospective sensitivity on only 60% [43]. Difficulty in establishing the correct diagnosis is in part due to the variable patterns of echogenicity of fibroids and their frequent exophytic or pedunculated position, which can mimic other pelvic conditions [44].

Hysterosalpingography accurately shows the presence of submucous myomas as smooth filling defects in the uterine cavity (Figs. 6A and 6B) and often suggests the presence of intramural myomas by displacing or enlarging the uterine cavity. However, recent studies show that MR imaging far surpasses both sonography and hysterosalpingography in its ability to identify, localize, and characterize leiomyomas before surgery [45–51]. On T2-weighted images, leiomyomas appear as discrete masses of lesser or greater intensity than the medium-intensity myometrium (Fig. 6C). Histologic analysis shows that on MR images, low-intensity leiomyomas consist of typical whorls of smooth muscle cells with various degrees of fibrosis, whereas high-intensity, inhomogeneous leiomyomas contain various degrees of hyaline, mucinous, hemorrhagic, and myxomatous degeneration [46].

Sonography, hysterosalpingography, and MR imaging have all documented significant decreases in the volume of the uterine cavity and size of fibroids after 2–6 months of therapy with gonadotropin-releasing hormone agonist [52, 53]. Reduction in tumor size is often associated with control of bleeding and normalization of RBC count and hemoglobin. Subsequent myomectomy, therefore, may be clinically safer and technically easier to perform.

In summary, MR imaging is the diagnostic technique of

choice before myomectomy. In order to keep the cost of diagnostic procedures within realistic limits, it is suggested that MR imaging replace all subsequent sonographic examinations in young patients once myomectomy has been chosen as the best form of therapy necessary to preserve reproductive capacity. Hysterosalpingography may be necessary to assess fallopian tube patency, but hysteroscopy may not be needed if MR imaging shows no evidence of submucous myoma.

Adenomyosis

Adenomyosis refers to the presence of endometrium deep within the myometrial wall and hyperplasia of the myometrium around the implants [54]. The disease is more common in women older than 30 who have menorrhagia and dysmenorrhea. On sonograms, adenomyosis has been described as showing a nonspecific uterine enlargement with decreased echogenicity of the myometrium [55]. Rarely, adenomyosis can be diagnosed on hysterosalpingograms when contrast material extends from the uterine cavity into the glands within the myometrium. Characteristic short diverticular outpouchings are then seen along the body or fundus of the uterus (Fig. 7A). T2-weighted MR images of diffuse adenomyosis show thickening of the junctional zone and a poorly marginated low-signal-intensity mass [56] extending diffusely into the myometrium (Fig. 7B). This can usually be differentiated from leiomyomas, which on MR appear as well-circumscribed masses with variable signal intensity [57]. Adenomyosis is a nonresectable disease because it involves the myometrium diffusely and is usually treated by hysterectomy, whereas myomas are encapsulated and can usually be enucleated [58].

Congenital Uterine Anomalies

Congenital anomalies of the uterus are often incidentally diagnosed during an infertility workup but are not usually the

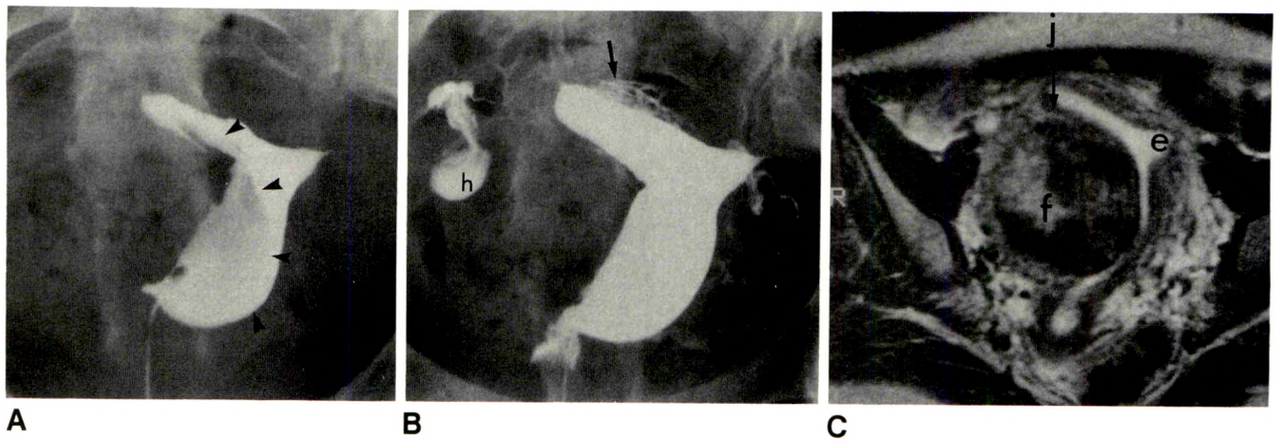


Fig. 6.—Uterine fibroid in a 40-year-old woman with an enlarged uterus and menorrhagia.
A, Hysterosalpingogram shows an enlarged uterine cavity indented along its right wall by a very large, smooth submucosal mass (*arrowheads*).
B, Further infusion of contrast material fills both fallopian tubes and shows mild right hydrosalpinx (h). Intravasation of contrast material into myometrial venous plexus is seen in fundal area (*arrow*) and should not be mistaken for adenomyosis.
C, T2-weighted axial oblique MR image of pelvis shows an 8-cm rounded, hypointense mass with inhomogeneous areas of low intensity occupying entire right myometrial wall. This intramural fibroid (f) is partially submucosal because it disrupts junctional zone (j) and indents into right wall of endometrial cavity (e). Myomectomy yielded an 8-cm fibroid with central myxomatous degeneration. Uterine cavity was entered.

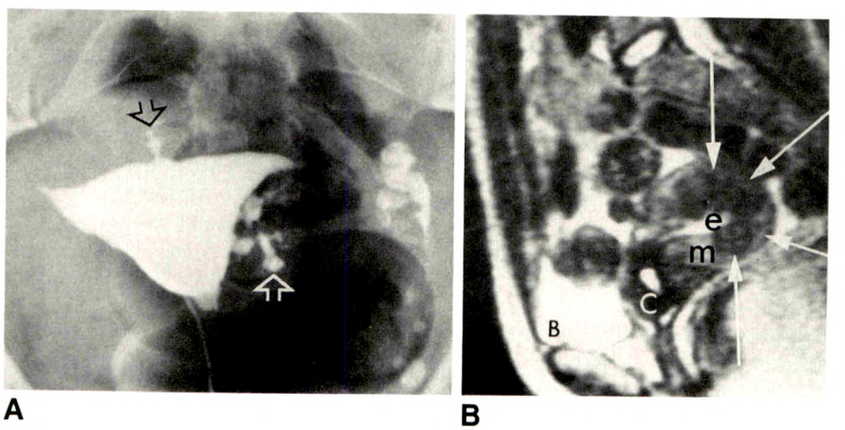


Fig. 7.—Adenomyosis in a 40-year-old infertile woman who had a myomectomy 1 year before. At that time, a uterine wall biopsy revealed adenomyosis.
A, Hysterosalpingogram shows prominent diverticular outpouchings extending into left uterine wall (*white arrow*) and to a lesser extent into fundus (*black arrow*). Although this film suggests isthmic obstruction of right tube, subsequent film with patient prone showed filling of a normal right fallopian tube.
B, Sagittal T2-weighted MR image of pelvis shows a retroflexed uterus. Normal medium-intensity myometrium (m) is replaced by diffuse, lobular, low-intensity adenomyosis (*arrows*) surrounding endometrial cavity. c = cervix, e = endometrium, B = bladder.

cause of primary infertility. Diagnosis before or early in pregnancy allows the clinician to plan for surgical intervention if necessary and for the associated obstetric complications experienced by these patients, including multiple miscarriages, premature labor, and fetal malpresentations [59]. Current imaging techniques such as transvaginal sonography and MR imaging enable us to detect and characterize uterine abnormalities with great accuracy and without the use of ionizing radiation. Hysterosalpingography is still a simple and direct method of diagnosis, but eventually wider availability and decreased cost may make MR imaging the definitive diagnostic tool.

Understanding and diagnosing congenital anomalies depends on knowledge of embryology. The fallopian tubes, uterus, and proximal vagina are embryologically derived from paired müllerian or paramesonephric ducts [60]. The cephalad müllerian ducts form the fallopian tubes and the caudal ducts fuse to form the uterus. Congenital anomalies of the fallopian tube are rare and seldom are demonstrable by hysterosalpingography. They include accessory ostia, multiple lumina, diverticula, duplications, and absence of portions of the tube.

Uterine duplications result from variable lack of fusion of the caudal müllerian ducts. Partial lack of external fusion is seen in the bicornuate uterus, and total failure of fusion is seen in the uterus didelphys, often associated with a vertical vaginal septum. In the septate or subseptate uterus, the caudal ducts have fused but there is total or partial lack of resorption of the medial septum. The unicornuate uterus is a rare anomaly resulting from development of only one müllerian duct and various degrees of atresia of the contralateral system. Up to 23% of women with a genital tract anomaly have a concomitant urinary tract deformity, commonly unilateral renal agenesis or renal ectopia [61].

Septate and Bicornuate Uteri

The hysterosalpingogram can help differentiate between the two most common congenital uterine anomalies, septate and bicornuate uteri. The hysterosalpingogram will show two separate and symmetric cavities in both septate and bicornuate uteri. However, if the angle between the cavities is acute, 75° or less, it is most likely a septate uterus [62] (Fig. 8A). If the contrast-filled horns are widely divergent with an obtuse angle between them, a bicornuate uterus is the more likely diagnosis (Fig. 9A). The differentiation between these two congenital abnormalities is critical, because the septate uterus can easily be corrected by hysteroscopic metroplasty [63]; patients with a bicornuate uterus may require a pregnancy trial before more major abdominal surgery such as a Strassman procedure [59]. Sonography in pregnant patients with uterine septa suggests that their very high rate of miscarriage may be due to implantation on the relatively avascular septum [64]. Sonographic characterization of uterine duplication anomalies in nonpregnant women shows that when abdominal sonography is performed in conjunction with hysterosalpingography, the correct diagnosis can be made in more than 90% of cases [62, 65].

Currently, transvaginal sonography offers an accurate view of the endometrial cavity and may enable a specific diagnosis of uterine duplication independently of the hysterosalpingogram. Careful coronal examination of the fundus during the luteal phase of the cycle will show two distinct endometrial cavity echoes with a thin echogenic septum between them in the septate uterus (Fig. 8B), whereas in the bicornuate uterus the two endometrial echoes will be widely separated by a double thickness of myometrium.

More complex anomalies can be further clarified by MR imaging. MR imaging offers excellent evaluation of uterine anomalies by simultaneous demonstration of external and internal uterine contours [66–68]. On T2-weighted axial images perpendicular to the uterine cavity [69], the septum in a septate uterus is seen as a thin, low-intensity fibrous band separating high-signal endometrial cavities [66]. The intercornual distance is less than 4 cm [68]. In bicornuate and didelphys uteri, a deep external notch is present in the fundus and the uterine horns are more than 4 cm apart. Internally, a thick or double medium-intensity band of myometrium separates the two fundal endometrial cavities (Fig. 9B). Concurrent problems such as a septate vagina, hematocolpos and hematometra, incidental fibroids, and ovarian masses are well shown on MR imaging.

A unicornuate uterus is well seen on hysterosalpingograms; however, MR imaging allows identification of the presence and degree of dilatation of noncommunicating rudimentary horns [68] before laparoscopy.

Diethylstilbestrol (DES) Exposure in Utero

DES exposure in utero causes frequent uterine abnormalities that are well shown of hysterosalpingograms and consist

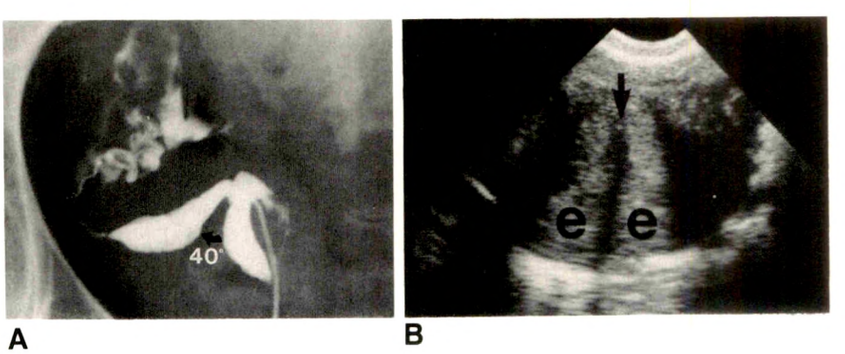


Fig. 8.—Septate uterus in a 28-year-old Russian woman who was told in Russia that she had a "double uterus."

***A*, Hysterosalpingogram shows a deeply septated uterine cavity. Although uterine cavities deviate slightly, angle between them is 40°. Later films showed that both tubes were patent.**

***B*, Coronal transvaginal sonogram of uterus done during luteal phase of cycle shows a very thin septum (*arrow*) separating two distinct and prominent endometrial cavities (e). Patient plans to have hysteroscopic metroplasty before attempting pregnancy.**

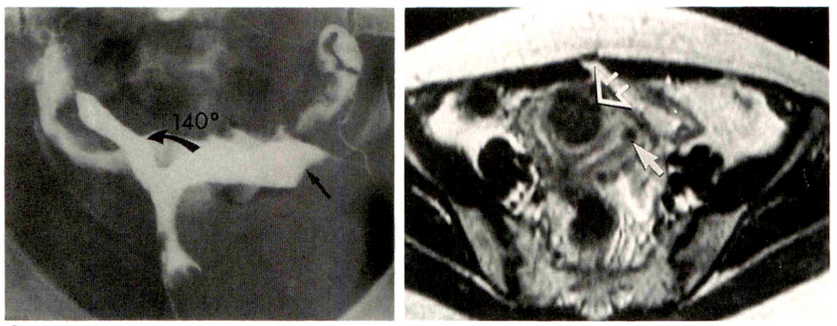


Fig. 9.—Bicornuate uterus in a 41-year-old infertile woman who had a first-trimester miscarriage 2 years before.

***A*, Hysterosalpingogram shows a bicornuate uterus with widely divergent horns. Small concavity of distal left horn (*straight arrow*) suggests a small submucosal fibroid.**

***B*, Axial oblique T2-weighted MR image of pelvis confirms bicornuate configuration of uterus, and in addition shows an unsuspected 4-cm, low-intensity myoma (*open arrow*) within the myometrium separating the two horns and a 1-cm submucosal myoma within distal left horn (*solid arrow*).**

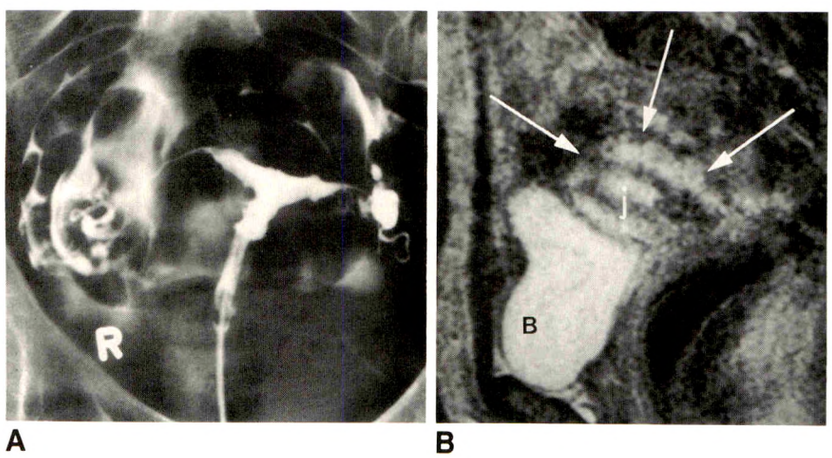


Fig. 10.—32-year-old infertile woman with known diethylstilbestrol exposure in utero who had an irregular uterine cavity at hysteroscopy. Gynecologist questioned presence of submucosal fibroids.

***A*, Hysterosalpingogram shows a T-shaped irregular uterine cavity characteristic of in utero exposure to diethylstilbestrol. Fallopian tubes are normal.**

***B*, Sagittal T2-weighted MR image of uterus shows an anteflexed uterus (*arrows*). Overall size of uterus is smaller than normal, and low-intensity junctional zone (j) of myometrium is slightly thickened and irregular. Irregularities of uterine cavity seen at hysteroscopy and on hysterosalpingogram correlate exactly with irregular junctional zone shown on MR study. In addition, MR image definitely excludes presence of uterine fibroids. B = bladder.**

of irregular constrictions and a T-shaped uterine cavity (Fig. 10A). DES is a synthetic estrogen that was given to pregnant women during the 1950s and 1960s to prevent miscarriage. DES crosses the placenta and exerts a direct effect on the müllerian system of the fetus. As a result, DES daughters, as they are called, show genital tract anomalies that are completely unrelated to fusion anomalies. Women who have vaginal and cervical changes due to DES are more likely to show uterine abnormalities on hysterosalpingography, and abnormal hysterosalpingograms are more often associated with a poor pregnancy outcome [70]. MR images (Fig. 10B) correlate well with the DES changes seen on hysterosalpingography and include hypoplasia of the uterus and cervix, T-shaped cavities, and localized thickening of the junctional zone associated with indentations of the endometrial cavity [71].

REFERENCES

1. Levin DC, Matteucci BS. "Turf battles" over imaging and interventional procedures in community hospitals: survey results. *Radiology* **1990**; 176:321–324
2. Yoder IC. *Hysterosalpingography and pelvic ultrasound: imaging in infertility and gynecology*. Boston: Little, Brown, **1988**:1–35
3. Hunt RB, Siegler AM. *Hysterosalpingography: techniques and interpretation*. Chicago: Year Book Medical, **1990**:5–34
4. Winfield AC, Wentz AC. *Diagnostic imaging of infertility*. Baltimore: Williams & Wilkins, **1987**:9–26
5. Karasick S, Karasick D. *Atlas of hysterosalpingography*. Springfield, IL: Thomas, **1987**:3–30
6. Varpula M. Hysterosalpingography with a balloon catheter versus a cannula: evaluation of patient pain. *Radiology* **1989**;172:745–747
7. Sholkoff SD. Balloon hysterosalpingography catheter. *AJR* **1987**;149: 995–996
8. Margolin FR. A new cannula for hysterosalpingography. *AJR* **1988**;151: 729–730
9. Thurmond AS, Novy M, Rosch J. Terbutaline in diagnosis of interstitial fallopian tube obstruction. *Invest Radiol* **1988**;23:209–210
10. Spring DB, Boll DA. Prone hysterosalpingography. *Radiology* **1980**; 136:235–236
11. Loy RA, Weinstein FG, Seibel MM. Hysterosalpingography in perspective: the predictive value of oil-soluble versus water soluble contrast media. *Fertil Steril* **1989**;51:170–172
12. Lindequist S, Justesen P, Larsen C. Rasmussen F. Diagnostic quality and complications of hysterosalpingography: oil- versus water-soluble contrast media—a randomized prospective study. *Radiology* **1991**;179:69–74
13. Rasmussen F, Lindequist S, Larsen C, Justessen P. Therapeutic effect of hysterosalpingography: oil- versus water-soluble contrast media—a randomized prospective study. *Radiology* **1991**;179:75–78
14. Alper MM, Garner PR, Spence JEH, Quarrington AM. Pregnancy rates after hysterosalpingography with oil- and-water-soluble contrast media. *Obstet Gynecol* **1986**;68:6–9
15. Eisenberg AD, Winfield AC, Page DL, et al. Peritoneal reaction resulting from iodinated contrast material: comparative study. *Radiology* **1989**;172:149–151
16. Moore DE, Segars JH, Winfield AC, et al. Effects of contrast agents on the fallopian tube in a rabbit model. *Radiology* **1990**;176:721–724
17. Davies AC, Kirghley A, Borthwick-Clarke A, Walters HL. The use of low-osmolality contrast medium in hysterosalpingography: comparison with a

conventional contrast medium. *Clin Radiol* **1985**;36:533–536
18. Thurmond AS, Novy M, Uchida BT, Rosch J. Fallopian tube obstruction: selective salpingography and recanalization. *Radiology* **1987**;163:511–514
19. Thurmond AS. Selective salpingography and fallopian tube recanalization. *AJR* **1991**;156:33–38
20. Thurmond AS, Rosch J. Nonsurgical fallopian tube recanalization for treatment of infertility. *Radiology* **1990**;174:371–374
21. Lang EK, Dunaway HE, Roniger WE. Selective osteal salpingography and transvaginal catheter dilatation in the diagnosis and treatment of fallopian tube obstruction. *AJR* **1990**;154:735–740
22. Kumpe DA, Zwerdlinger SC, Rothbarth LJ, Durham JD, Albrecht BH. Proximal fallopian tube occlusion: diagnosis and treatment with transcervical fallopian tube catheterization. *Radiology* **1990**;177:183–187
23. Kerin J, Daykhovsky L, Grundfest W, Surrey E. Falloscopy: a microendoscopic transvaginal technique for diagnosing and treating endotubal disease incorporating guide wire cannulation and direct balloon tuboplasty. *J Reprod Med* **1990**;35:606–612
24. Confino E, Tur-Kaspa I, DeCherney A, et al. Transcervical balloon tuboplasty. A multicenter study. *JAMA* **1990**;264:2079–2082
25. Hughes EG, Shekelton P, Leonie M, Leeton J. Ultrasound-guided fallopian tube catheterization per vaginum: a feasibility study with the use of laparoscopic control. *Fertil Steril* **1988**;50:986–989
26. Fleischer AC, Herbert CM, Hill GA, Kepple DM. Transvaginal sonography: applications in infertility. *Semin Ultrasound CT MR* **1990**;11:71–81
27. Medical Research International and the Society for Assisted Reproductive Technology. The American Fertility Society. In vitro-fertilization-embryo transfer in the United States: 1988 results from the IVF-ET registry. *Fertil Steril* **1990**;53:13–20
28. Thurmond AS, Rosch J, Patton PE, Burry KA, Novy M. Fluoroscopic transcervical fallopian tube catheterization for diagnosis and treatment of female infertility caused by tubal obstruction. *RadioGraphics* **1988**;8:621–640
29. Netter FH. *The Ciba Collection of medical illustrations*, vol. 2. *Reproductive system*. West Caldwell, NJ: Ciba Pharmaceutical Co., **1984**:179–190
30. Timor-Tritsch IE, Rottem S. Transvaginal ultrasonographic study of the fallopian tube. *Obstet Gynecol* **1987**;70:424–428
31. Tessler FN, Perella RR, Fleischer AC, Grant EG. Endovaginal sonographic diagnosis of dilated fallopian tubes. *AJR* **1989**;153:523–525
32. Lande IM, Hill MC, Cosco FE, Kator NN. Adnexal and cul-de-sac abnormalities: transvaginal sonography. *Radiology* **1988**;166:325–332
33. Terry J, Forrest T. Sonographic demonstration of salpingitis: potential confusion with appendicitis. *J Ultrasound Med* **1989**;8:39–41
34. Schlief R, Deichert U. Hysterosalpingo-contrast sonography of the uterus and fallopian tubes: results of a clinical trial of a new contrast medium in 120 patients. *Radiology* **1991**;178:213–215
35. Kerin J, Daykhovsky L, Segalowitz J, et al. Falloscopy: a microendoscopic technique for visual exploration of the human fallopian tube from the utero tubal ostium to the fimbria using a transvaginal approach. *Fertil Steril* **1990**;54:390–400
36. Karasick S, Karasick D, Schilling J. Salpingitis isthmica nodosa in female infertility. *Can Assoc Radiol J* **1985**;35:118–121
37. Creasy JL, Clark RL, Cuttino JT, Groff TR. Salpingitis isthmica nodosa: radiologic and clinical correlates. *Radiology* **1985**;154:597–600
38. Karasick S, Ehrlich S. The value of hysterosalpingography before reversal of sterilization procedures involving the fallopian tubes. *AJR* **1989**;153:1247–1250
39. Groff TR, Edelstein JA, Schenken RS. Hysterosalpingography in the preoperative evaluation of tubal anastomosis candidates. *Fertil Steril* **1990**;53:417–420
40. Rock JA, Guzick DS, Katz E, Zacur HA, King TM. Tubal anastomosis: pregnancy success following reversal of Falope ring or monopolar cautery sterilization. *Fertil Steril* **1987**;48:13–17
41. Donnez J, Casanas-Roux F. Prognostic factors of fimbrial microsurgery. *Fertil Steril* **1986**;46:200–204
42. Karasick S, Goldfarb AF. Peritubal adhesions in infertile women: diagnosis with hysterosalpingography. *AJR* **1989**;152:777–779
43. Gross BH, Silver TM, Jaffe MH. Sonographic features of uterine leiomyomas: analysis of 41 proven cases. *J Ultrasound Med* **1983**;2:401–406
44. Baltarowich OH, Kurtz AB, Parnell RG, Needleman L, Vilaro MM, Goldberg BB. Pitfalls in the sonographic diagnosis of uterine fibroids. *AJR* **1988**;151:725–728
45. Hamlin DJ, Pattersson H, Fitzsimmons J, Morgan LS. MR imaging of uterine leiomyomas and their complications. *J Comput Assist Tomogr* **1985**;9(5):902–907
46. Hricak H, Tscholakoff D, Heinrichs L, et al. Uterine leiomyomas: correlation of MR, histopathologic findings, and symptoms. *Radiology* **1986**;158:385–391
47. Dudiak CM, Turner DA, Patel SK, Archie JT, Silver B, Norusis M. Uterine leiomyomas in the infertile patient: preoperative localization with MR imaging versus US and hysterosalpingography. *Radiology* **1988**;167:627–630
48. Zawin M, McCarthy S, Scoutt LM, Comite F. High-field MRI and US evaluation of the pelvis in women with leiomyomas. *Magn Reson Imaging* **1990**;8:371–376
49. Weinreb JC, Barkoff ND, Megibow A, Demopoulos R. The value of MR imaging in distinguishing leiomyomas from other solid pelvic masses when sonography is indeterminate. *AJR* **1990**;154:295–299
50. Chang YCF, Arrive L, Hricak H. Gynecologic tumor in imaging. *Semin Ultrasound CT MR* **1989**;10(1):29–42
51. Fishman-Javitt MC, Lorecchio JL, Stein HL. The uterus. In: Fishman-Javitt MC, Stein HL, Lovecchio JL, eds. *Imaging of the pelvis: MRI with correlations to CT and ultrasound*. Boston: Little, Brown, **1990**:77–108
52. Donnez J, Sandow J, Schrurs B, Clerckx F, Gillerot S. Treatment of uterine fibroids with implants of gonadotropin-releasing hormone agonist: assessment by hysterography. *Fertil Steril* **1989**;51(6):947–950
53. Zawin M, McCarthy S, Scoutt L, et al. Monitoring therapy with a gonadotropin-releasing hormone analog: utility of MR imaging. *Radiology* **1990**;175:503–506
54. McCarthy S. MR imaging of the uterus. *Radiology* **1989**;171:321–322
55. Bohlman ME, Ensor RE, Sanders RC. Sonographic findings in adenomyosis of the uterus. *AJR* **1987**;148:756–766
56. Mark AS, Hricak H, Heinrichs LRW, et al. Adenomyosis and leiomyoma: differential diagnosis with MR imaging. *Radiology* **1987**;163:527–529
57. Togashi K, Ozasa H, Konishi I, et al. Enlarged uterus: differentiation between adenomyosis and leiomyoma with MR imaging. *Radiology* **1989**;171:531–534
58. Clarke-Pearson DL, Dawood MY. *Green's gynecology: essentials of clinical practice*, 4th ed. Boston: Little, Brown, **1990**:357–372
59. Stein AL, March CM. Pregnancy outcome in women with müllerian duct anomalies. *J Reprod Med* **1990**;35:411–414
60. Golan A, Langer R, Bukovsky I, Caspi E. Congenital anomalies of the müllerian system. *Fertil Steril* **1989**;51:747–755
61. Hamlin DJ, Pettersson H, Ramey SL, Moazam F. Magnetic resonance imaging of bicornuate uterus with unilateral hematometrosalpinx and ipsilateral renal agenesis. *Urol Radiol* **1986**;8:52–55
62. Reuter KL, Daly DC, Cohen SM. Septate versus bicornuate uteri: errors in imaging diagnosis. *Radiology* **1989**;172:749–752
63. Daly DC, Maier DB, Soto-Albors C. Hysteroscopic metroplasty, six year follow-up. *Obstet Gynecol* **1989**;73:201–205
64. Fedele L, Dorta M, Brioschi D, Giudici MN, Candiani GB. Pregnancies in septate uteri: outcome in relation to site of uterine implantation as determined by sonography. *AJR* **1989**;152:781–784
65. Fedele L, Ferrazzi E, Dorta M, Vercillini P, Candiani GB. Ultrasonography in the differential diagnosis of "double" uteri. *Fertil Steril* **1988**;50:361–364
66. Mintz MC, Thickman DI, Gussman D, Kressel HY. MR evaluation of uterine anomalies. *AJR* **1987**;148:287–290
67. Fedele L, Dorta M, Brioschi D, Massari C, Candiani GB. Magnetic resonance evaluation of double uteri. *Obstet Gynecol* **1989**;74:844–847
68. Carrington BM, Hricak H, Nuruddin RN, et al. Müllerian duct anomalies: MR imaging evaluation. *Radiology* **1990**;176:715–720
69. Baumgartner BR, Bernardino ME. MR imaging of the cervix: off-axis scan to improve visualization of zonal anatomy. *AJR* **1989**;153:1001–1002
70. Kaufman RH, Noller K, Adam E, et al. Upper genital tract abnormalities and pregnancy outcome in diethylstilbestrol exposed progeny. *Am J Obstet Gynecol* **1984**;148:973–984
71. Van Gils APG, Tjon A, Tham RTO, Falke THM, Peters AAW. Abnormalities of the uterus and cervix after diethylstilbestrol exposure: correlation of findings on MR and hysterosalpingography. *AJR* **1989**;153:1235–1238

Book Review

Imaging of the Lumbar Spine. By Harry J. Griffiths. Gaithersburg, MD: Aspen, 145 pp., 1991. $79

This text is intended to be a sourcebook for those engaged in the evaluation of patients with lower back pain. The author, Harry J. Griffiths, is a well-known and highly regarded authority on the lumbar spine. He is assisted by contributing authors Richard M. Ellis, an orthopedic internist, and Benjamin C. P. Lee, a neuroradiologist.

The book is divided into 12 chapters. Chapter 1 is an introduction, divided into two parts: clinical management of lower back pain, by Dr. Ellis, and radiologic management, by Dr. Griffiths. The latter has an algorithm for the radiologic workup of a patient with lower back pain and includes suggestions on how the algorithm can be modified, depending on the patient's clinical features and suspected clinical diagnosis.

Chapter 2, "Herniated Discs and Other Related Conditions," was written by Dr. Lee. In addition to describing disk disease, it discusses several other causes of lower back pain; it includes the differential diagnosis of disk disease and epidural and intradural lesions. The chapter is well illustrated, with a large number of high-quality CT scans and MR images, and also serves as a review of the uses of advanced imaging of the lumbar spine.

Chapters 3–11 were written by Dr. Griffiths and constitute the overwhelming majority of the presented material. Topics covered in these chapters include degenerative disk disease, spondylolysis, spondylolisthesis, spinal stenosis, Scheuermann disease and Schmorl nodes, disorders of facet joints, the sacroiliac joints, scoliosis, and spina bifida and other spinal anomalies. These chapters are well written, with material presented in a logical, comprehensive, and readable manner. The pertinent scientific literature is presented in an orderly fashion and nicely summarized when appropriate. Dr. Griffiths supplements the literature with his own considerable experience, a feature that helps put the large amount of data presented into proper perspective. Rather than limiting itself to the radiologic imaging of the lumbar spine, the book contains excellent sections on the history, etiology, pathology, and complications of various disease processes. The chapters are nicely illustrated. Clearly, the emphasis of imaging is on plain film radiography; however, scintigrams, myelograms, CT scans, and MR images are also included.

The final chapter, written by Dr. Ellis, discusses the clinical management of lower back pain. Although the chapter does not discuss radiology, it reviews the assessment of lower back pain from a clinical perspective and the importance of the clinical history and physical examination for proper diagnosis.

The book is logically laid out and is a pleasure to read. Some chapters, such as the one on spinal stenosis, have a large number of CT scans and MR images, although the emphasis is definitely on plain radiographs. This is clearly Dr. Griffiths's bias, as he notes in the introductory chapter that "in patients with mechanical low back problems, plain films will often reveal the answer." Although I share his bias, neuroradiologists and those who are looking for a complete review of imaging of the lumbar spine may be disappointed. For example, the chapter on Scheuermann disease and Schmorl nodes has 26 images, only one of which is a CT scan. Similarly, the chapter on spondylosis has 30 radiologic images: 26 plain radiographs, two scintigrams, one MR image, and one plain tomogram. Frequently, CT and MR examinations of the spine are interpreted without the knowledge of the previous plain film findings. Consequently, it is useful to be familiar with the imaging appearances of many processes that can be readily diagnosed on the basis of plain films. Compared with the overall text, however, this is a minor deficiency.

I recommend this book to all those who are interested in the evaluation of the lumbar spine or involved in the workup of patients with lower back pain. It would be an excellent addition to the academic library of any teaching program. The emphasis placed on fundamentals makes this text ideal for radiology residents, and it should be required reading for them.

Mark J. Kransdorf
Armed Forces Institute of Pathology
Washington, DC 20306-6000

Review Article

Percutaneous Procedures for the Diagnosis and Treatment of Lower Back Pain: Diskography, Facet-Joint Injection, and Epidural Injection

Georges Y. El-Khoury[1] and Donald L. Renfrew

This review discusses the indications, techniques, complications, and results of three percutaneous procedures used to evaluate and treat lower back pain: diskography, facet-joint injection, and epidural injection. Diskography, performed by injection of contrast medium into the nucleus pulposus, is a technique used to determine the cause of lower back pain in patients in whom findings on other imaging studies are normal or conflicting. Injection of steroids and anesthetic into the facet joints of the lumbar spine is useful to diagnose or treat patients with facet syndrome (back pain caused by abnormalities of the facet joints). Injection of steroids and anesthetic agents into the epidural space provides short-term relief, and can sometimes provide permanent relief, of lower back pain.

More than half of the population in the United States suffers from lower back pain at some time, and the annual incidence is at least 5% [1]. The symptom incapacitates up to 20% of workers for long periods (> 4 weeks), absorbs 41% of the cost of workers' compensation, costs society more than $15 billion each year, and has increased much faster than population growth during the past two decades [2]. Only a minority of patients receive a specific diagnosis [2–4]. Unlike the classic model of disease wherein symptoms closely relate to abnormalities detected by imaging procedures [2], patients with back pain may have no abnormalities. On the other hand, asymptomatic persons may manifest striking abnormal findings [5, 6]. In many cases, myelography, CT, and MR fail to answer many questions regarding the diagnosis. In these problem cases, percutaneous procedures such as diskography, facet-joint injection, and epidural injection may be helpful in diagnosis and treatment.

Diskography, injection of contrast medium into the nucleus pulposus, is a diagnostic technique used to evaluate cases of lower back pain in which results of other imaging studies are normal or conflicting. Injection of steroids and anesthetic agents into the facet joints is performed for diagnosis or treatment in patients with the facet syndrome (back pain presumably caused by abnormalities of the facet joints). Injection of steroids and anesthetic agents into the epidural space provides short-term relief, and can sometimes provide permanent relief, of lower back pain.

These controversial procedures have been used for many years. In some centers, they constitute an important part of the evaluation and treatment of lower back pain. Although radiologists are thoroughly trained in percutaneous placement of needles using imaging guidance, these procedures are often performed by nonradiologists. In this review we present the indications, techniques, complications, and results of these procedures.

Diskography

Diskography is purely a diagnostic test, the interpretation and significance of which have evolved during the past few decades. Currently the most important feature of this test is reproduction of the patient's pain [7, 8]. Lindblom, a Swedish

Received March 1, 1991; accepted after revision June 5, 1991.
[1] Both authors: Department of Radiology, The University of Iowa College of Medicine, Iowa City, IA 52242. Address reprint requests to G. Y. El-Khoury.

radiologists, developed lumbar diskography in 1948 [9]. He intended for diskography to complement oil-based myelography. In 1968, Holt [10] performed diskography on asymptomatic volunteers and showed a high false-positive rate (26%). In 1990, Walsh et al. [8] studied diskography in asymptomatic volunteers and patients with lower back pain and had no false-positive results, in striking contrast to Holt's study. During the past two decades, diskography has been used to assess proper needle placement before chemonucleolysis [11].

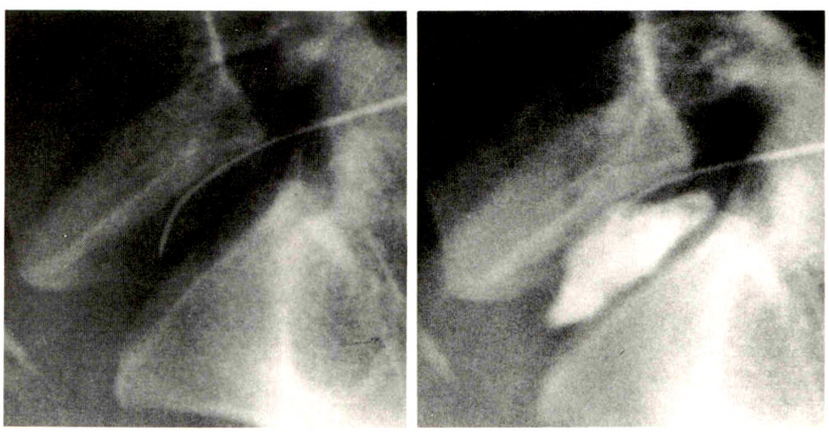
Indications

The indications for diskography have changed since the introduction of CT and MR, which show disk herniation and degeneration noninvasively. The following are cited by advocates as indications for the use of diskography: (1) to diagnose internal disk derangement or disruption [12]; (2) as the last resort in patients with lower back pain in whom results of standard diagnostic procedures are normal; (3) to determine the disk level causing symptoms when multilevel disk degeneration is present [13].

Technique

Lumbar diskography can be performed on an outpatient basis. Informed consent is obtained, and then the patient is premedicated with benzodiazepines or narcotics. Biplane fluoroscopy is used to guide needle placement, and the patient is positioned on the fluoroscopic table either prone or lying on the left side. Lindblom [9] used a transdural midline approach [9], but most operators currently use the posterolateral extradural approach [8, 11, 13]. A double-needle technique is preferred, whereby a 3.5-in. (9 cm), 18-gauge needle (the *guide* needle) is introduced through the skin 10–12 cm from the midline, until its tip lies adjacent to the disk. A 6.0-in. (15 cm), 22-gauge needle (the *insert* needle) is placed through the guide needle and advanced until its tip reaches the center of the disk. For the L5–S1 disk, longer needles may be required. Before the insert needle is introduced, a 45° bend is applied at its distal end so that when it emerges from the guide needle, the insert needle enters the L5–S1 disk transversely in the axial plane (Fig. 1). When the needle tip is confirmed to be within the center of the disk, 0.5–2.0 ml of nonionic contrast material is injected slowly until resistance is met or pain is elicited [8, 11, 13].

The criteria used when interpreting a diskogram include volume of contrast material accepted by the disk, resistance to injection, production of pain, and radiologic appearance [8, 11, 13]. The normal lumbar disk accepts between 0.5 and 1.5 ml of fluid. Injection has a firm end point, and produces no pain. An abnormal disk will accept more than 1.5 ml of fluid and injection does not have a distinct end point [8, 11, 13]. Injection into a symptomatic lumbar disk may reproduce the patient's pain. The morphologic findings are nonspecific, especially in older patients [7]. CT scans are obtained within a few hours after the procedure, primarily to document that the injection went into the nucleus pulposus. After CT scanning, the patient is observed for 1–2 hr and then discharged. Postprocedure instructions to the patient include watching for signs and symptoms of disk infection. Diskitis occurs after diskography in 1–4% of patients, but the frequency of this complication can be decreased by prophylactic antibiotic treatment or by adding antibiotic to the injected material [14].



A B

Fig. 1.—L5–S1 diskogram.
A, Lateral radiograph of L5–S1 disk. Note curvature at end of insert needle.
B, Diskogram of L5–S1 with 1.5 ml of contrast medium. Contrast medium is seen diffusing throughout disk. This pattern suggests disk degeneration.

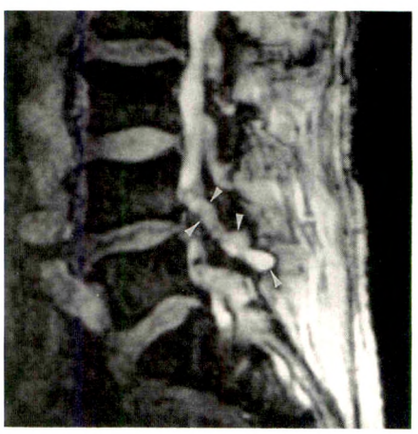


Fig. 2.—Fluid in facet joints. Distended superior synovial recess compressed thecal sac in this 66-year-old man who had progressively severe lower back pain for 10 days. Sagittal T2*-weighted MR image (multiplanar gradient-recalled fast scan [MPGR]; 500/15, flip angle 15°) through medial aspect of facet joints on right side shows fluid-distended superior and inferior recesses at L4–L5 facet joint (*arrowheads*). Patient reported relief from pain after fluid was drained.

Discussion

Advocates of diskography emphasize that the patient's pain will be reproduced in a morphologically abnormal disk [8, 11, 13, 15]. Vanharanta et al. [15] have shown that 77% of patients in whom diskography causes reproduction of pain have anular tears. Anular tears imply disk degeneration that theoretically should be detected by MR. Zucherman et al. [16] reported 18 young patients (mean age, 33 years) with lower back pain and normal MR findings but abnormal findings on diskograms. Kornberg [17] reported similar findings in four patients. In Bernard's series [13] of 190 disks for which MR and diskographic findings were available, the two tests agreed in 89% of the cases. No gold standard was available for cases in which the tests disagreed. Bernard explains the discrepancy on the basis of early disk degeneration; in such early degeneration, the sensitivity of diskography exceeds that of MR. However, others [18, 19] compared diskography with MR and found no advantages gained by performing diskography.

Walsh et al. [8] reported 100% specificity with no false-positive results. In another study, Holt [10] had a 26% false-positive rate. The study by Walsh et al. had the following strengths: (1) a more sophisticated evaluation of response to pain; (2) expert needle placement (2% poor or invalid placement, compared with 25% in Holt's study); and (3) use of less-irritating, nonionic contrast material (iopamidol), compared with ionic contrast material (diatrizoate sodium).

The controversy over diskography has raged for more than 40 years. Despite many studies, two basic questions remain unanswered: (1) does the pain created at diskography causally relate to the patient's symptoms? and (2) can diskography be used to predict the outcome of spinal fusion? Collins et al. [20] operated on 12 patients who had abnormal findings on diskography and MR images. Nine patients improved, and three were unchanged. Some reports [21] seem to indicate that diskography has little value in predicting the outcome of spinal fusion, whereas others [22] support a role for diskography in the diagnosis and treatment of patients with lower back pain. A prospective randomized study may answer this question [23], but has yet to be performed. On the basis of current information, diskography seems to provide information not available by other imaging techniques [8, 13, 18, 19]. Whether the test is truly useful depends on how effective spine fusion is in curing patients who have lower back pain and abnormal results of diskography. Ideally the gold standard should be the clinical response to fusion. Prospective randomized studies are not yet available, and until this issue is settled, the controversy surrounding diskography will continue.

Injection of Steroids and Anesthetic Agents into the Facet Joints

Facet-joint injection with local anesthetic agent and steroids is performed to diagnose and treat what is called the facet syndrome. This syndrome is a poorly defined entity in which pain is thought to originate from the facet joints. The diagnosis is often arrived at by exclusion.

Goldthwait [24] in 1911 suggested that lumbar facet joints may be a source of lower back pain and leg pain. Puttie [25] in 1927 studied facet degeneration in patients with lower back pain and sciatica. In 1976, Mooney and Robertson [26] showed that lower back pain and hip pain can be produced in healthy volunteers by injecting hypertonic saline into facet joints and that this same pain could be obliterated by an injection of local anesthetic. In the same study on patients with chronic lower back pain, the same investigators achieved 62% initial pain relief and 20% long-term relief by injecting local anesthetic and steroids into the facet joints.

Dory [27] attributed pain to distension and inflammation of the synovial capsule, with resultant stimulation of the nociceptive nerve endings. Expanded synovial recesses may compress nerve roots in the spinal canal and neural foramina, which explains the presence of radiculopathy in patients with facet syndrome [27, 28] (Fig. 2). Lippitt [29] attributed pain in the facet syndrome to a combination of synovitis, segmental instability, and degenerative arthritis.

Local anesthetic agents may act on the nociceptive fibers within the synovium, whereas intracapsular corticosteroids may reduce inflammation of the synovium [30]. Inasmuch as the capacity of the lumbar facet joints is only 1-2 ml, facet joint injections of more than 2 ml result in leakage of local anesthetic and corticosteroid from the joint. The drugs may pass laterally, where the innervating branches of the posterior rami pass, or medially into the epidural space or neural foramen [27, 31]. Some of the beneficial effects of facet-joint injection may result from this leakage [31, 32].

Indications

Selection of patients for facet-joint injections and the level of injection are problematic because differentiation between disk disease and facet syndrome can be difficult. Carrera [33] suggested that patients with abnormal facet joints on CT were likely to benefit from the injections, whereas patients with normal facet joints or minimal hypertrophy would not benefit. Destouet et al. [30] stressed that symptoms of facet arthropathy are nonspecific and include lower back pain with radiation into the buttock and thigh. Indications for facet-joint injection include focal tenderness over the facet joints, lower back pain, and sciatica in patients with normal radiologic workup [30]. Other indications include "failed-back" syndrome without recurrent disk herniation or arachnoiditis. The choice of injection level(s) is based on the location of focal tenderness over the joint(s) or the presence of osteoarthritis involving the joints. Lippitt [29] lists the signs of facet syndrome as (1) local paralumbar tenderness; (2) pain on hyperextension; (3) absence of neurologic deficit; (4) absence of root tension signs; and (5) hip, buttock, or back pain when the straight leg is raised.

Regardless of the symptoms, one characteristic that all facet syndrome patients have in common is the relief of pain by local injection of anesthetic [34]. Because local anesthesia does not alter the underlying pathologic changes, Murtagh [34] suggests that facet-joint injections be considered a diagnostic test only; the therapeutic effects of the injection are coincidental and temporary.

Technique

Facet-joint injection in the lumbar spine is a simple and safe procedure that can be performed under fluoroscopic or CT control [33, 34]. The facet joint is both curved and obliquely oriented; the posterior portion of the joint is nearly in the sagittal plane. Most joints can be punctured with the patient either prone or in a shallow anterior oblique position, with the injected side up. The obliquity should be limited to ensure that the most posterior portion of the joint is the part in profile. The posterior aspect of the joint is profiled fluoroscopically, and a 22-gauge spinal needle is advanced vertically into the joint (Fig. 3). Once it is in the joint, position of the needle is checked by injecting 0.5–1.0 ml of nonionic contrast material followed by 3 mg (0.5 ml) of betamethasone and 1.5 ml of 0.25% bupivacaine. Some authors [29, 30] report that distension of the facet joint by contrast material reproduces the patient's pain.

Occasionally facet-joint injection is performed to control pain arising from a defect of the pars interarticularis. Ghelman and Doherty [35] and subsequently other investigators [27, 28, 30] have shown concurrent opacification of a pars defect during facet-joint arthrography. Typically the pars defect communicates with the facet joint above or below the defect (Fig. 4). There are no reported complications from this procedure.

Discussion

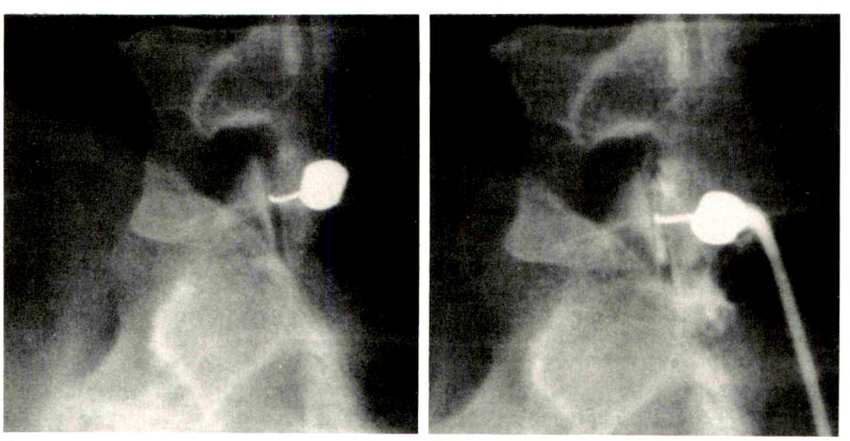
Early studies of facet-joint injection with steroids and anesthetic agents for diagnosis and therapy were encouraging. Carrera [33] reported immediate relief in 13 of 20 patients, and six patients had relief for more than 6 months after a single injection of local anesthetic and corticosteroid. Destouet et al. [30] reported 59% initial improvement and 27% long-term relief. Murtagh [34] reported 94% short-term relief and 54% long-term relief. Forty-three percent of Lippitt's patients showed good to excellent relief of symptoms after facet-joint injection [29]. He concluded that since facet blocking is simple, safe, and cost-effective, the technique should be used in the management of lower back pain.

Many of the early studies were uncontrolled. Lower back pain is usually self-limited and temporary, and the patients may have improved after injection because of the natural history of the disease or the placebo effect. In addition, the large volumes injected in the early investigations almost certainly resulted in capsular rupture with extravasation of local anesthetic and steroids. In 1984, Raymond and Dumas [32], in a study of 25 patients, prevented extravasation by restricting the total volume of fluid injected to 1 ml. Overall relief of pain in their series—16% temporary relief and no long-term relief, differed dramatically from that in other series. Moran et al. [31] restricted injection volume; they achieved only a 13% success rate. In a separate cadaver experiment, they showed extravasation of methylene blue into the epidural space with large-volume injections into the facet joints. Moran et al. [31] suggested that extravasation of injected steroids into the epidural space may relieve the pain in many patients who have large volumes injected into the facet joint.

A study by Lynch and Taylor [36], however, contradicts the work by Raymond and Dumas [32] and Moran et al. [31]. Lynch and Taylor administered two injections of 1 ml of fluid containing corticosteroids in 50 patients. Patients were classified as having both, one, or neither of the injections put into the capsule. The results showed that intraarticular injections were more effective than extraarticular injections for long-term pain relief.

More recent work has challenged the efficacy of facet-joint injection. Jackson et al. [37] performed an elaborate study on 390 patients in which they used intraarticular injections of only 1 ml of 0.5% bupivacaine and 2 mg (0.5 ml) of triamcinolone. The investigators evaluated 127 variables and found that more pain relief was associated with older age, history of lower back pain, normal gait, maximum pain on extension after forward flexion in the standing position, absence of leg pain, muscle spasm, and aggravation of pain when the Valsalva maneuver was performed. The authors concluded, however, that the facet joints were not commonly the single or primary cause of lower back pain in most patients.

In the only prospective, controlled study of facet-joint injection, Lilius et al. [38] studied 109 patients with chronic lower



A B

Fig. 3.—L4–L5 facet-joint injection.

***A*, Spot film with patient turned from prone position in order to profile facet joint being injected (L5–S1). Needle is advanced perpendicularly to joint until its tip is within joint.**

***B*, During injection, contrast material flows away from needle; typically, contrast material collects in superior and inferior recesses and to a lesser extent between articulating facets.**

back pain. The patients randomly received one of three types of injections: (1) corticosteroid and local anesthetic into two facet joints; (2) same mixture around two joints; or (3) physiologic saline into two joints. Sixty-four percent of the patients reported initial relief of pain, and 36% reported benefits persisting up to 3 months. The benefit was independent of the mode of treatment given; results in patients injected with saline were as good as results in those injected with local anesthetic and steroids. These results led the authors to conclude that facet-joint injection is a nonspecific method of treatment and that the good results reflect the tendency for spontaneous remission of the lower back pain. The mode of injection, they thought, did not affect the outcome, but the outcome closely correlated with the results of psychosocial tests [39].

Raymond and Dumas [32] stated that the multiple factors among different investigations of facet-joint injection made "assessment and comprehension in this field an almost impossible task." Although several years have passed, and several additional studies have been performed since they made this statement, evaluation of facet-joint injection remains difficult. It appears that, in general, use of large volumes of fluid during injection substantially increases the relief experienced by patients undergoing facet-joint injection [31, 32]. If facet-joint injection is being used as a therapeutic tool, use of a large volume of injected fluid maximizes relief of pain. If the response to facet-joint injection is used as an indication for surgery, then a problem arises. The favorable response to the injection may be due to epidural or pericapsular leakage of local anesthetic and corticosteroids rather than intracapsular effects. How this relates to the patient's possible response to facet-joint fusion is unknown, as no studies have randomly assigned patients to surgical vs conservative treatment on the basis of results of facet-joint injection.

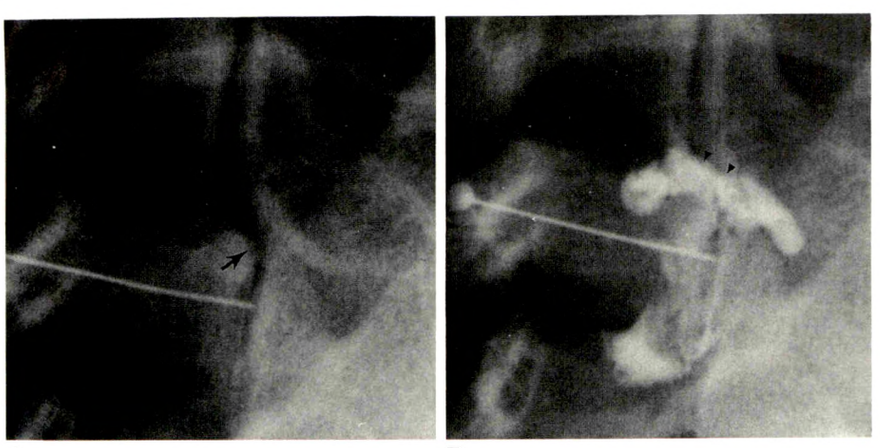
The fact that the only controlled, prospective study [38] comparing injection of local anesthetic and steroids with saline showed no difference in outcome must be of concern to radiologists who perform facet-joint injection. It may be that many of the patients included in this study did not really have facet syndrome. Indeed, immediate pain relief after injection in the facet joint is part of the definition of facet syndrome for several authors. For these authors, the studies of Raymond and Dumas [32], Moran et al. [31], Jackson et al. [37], and Lilius et al. [38], which purport to show little efficacy of facet-joint injection, do not represent a problem with the technique but rather with selection of patients.

Facet-joint injection is currently used as a diagnostic/therapeutic test. When epidural steroid injection has failed, facet-joint injection may determine whether the facets are the cause of a patient's pain. Controversy will no doubt continue regarding the efficacy of facet-joint injections.

Epidural Injection

Epidural injection involves placement of saline, with or without drugs, into the epidural space. Epidural injection of saline [40], anesthetic [41–44], or steroids [45–47] decreases lower back pain and sciatica. Injection of large volumes of saline alone [40, 41] purportedly lyses adhesions in the epidural space [47]. In at least some patients with lower back pain, the nerve roots are inflamed [3, 47–49]. Injection of local anesthetic agents may provide temporary relief from pain by decreasing the sensations arising from the inflamed tissue, or even long-term relief by breaking the pain cycle [47]. Addition of steroid to the anesthetic has been shown to increase efficacy of epidural injection [50], probably by decreasing inflammation in the epidural space. Most recent studies have used a combination of steroids and local anesthetic [51–53].

Pain relief with epidural injection is often temporary. White et al. [53] found that the percentage of patients relieved of



A B

Fig. 4.—Communication between facet joint and a pars interarticularis defect. This communication is important if pars defect is considered a source of lower back pain. Injecting local anesthetic into facet joint could block pain originating in pars defect also.

A, Radiograph shows needle in L5–S1 facet joint and pars defect (*arrow*) superior to joint.

B, After injection of contrast material, both facet joint and pars defect (*arrowheads*) fill simultaneously.

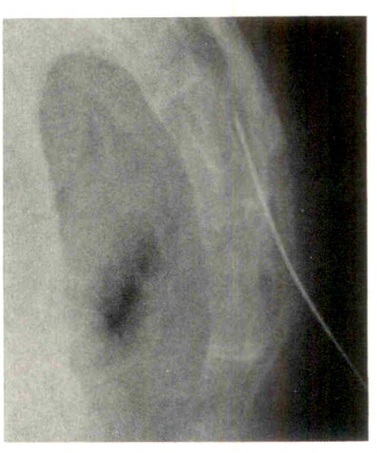


Fig. 5.—Needle position in epidural injection. Lateral spot film shows needle is within sacral canal.

pain decreased from 84% 1 day after injection to 34% 6 months after injection.

Indications

Although some studies suggest that patients with acute herniated nuclei pulposi derive more benefit from epidural injection than do patients with spinal stenosis [52–54], it is difficult to tell whether a given patient with lower back pain will benefit from epidural injection of steroids. This may be because the radiologic abnormalities of patients with lower back pain may not correspond to the actual cause of the patient's distress [2, 4]. Both CT [5] and MR [6] may show findings of herniated nucleus pulposus in asymptomatic volunteers. Similarly, the same degree of spinal stenosis may produce widely varying symptoms [5]. For these reasons, patients with lower back pain, regardless of the putative cause as determined by imaging findings, can be treated with epidural injection.

Technique

The procedure is performed on an outpatient basis and without any specific preparation. Plain films are helpful in determining the location of the sacral hiatus and curvature of the sacrum. If a myelogram or MR study of the lumbar spine is available, these should be studied to assess the inferior extent of the thecal sac. Informed consent is obtained.

The patient's pulse and blood pressure are taken and the patient is placed prone on the fluoroscopic table. The sacral cornua (the borders of the sacral hiatus) and median sacral crest are palpated. The sacral hiatus typically lies at the superior margin of the natal cleft. The skin and subcutaneous tissues down to the periosteum are anesthetized with 1% lidocaine.

A 22-gauge spinal needle is advanced gently in the sacral canal with a twisting motion until its tip reaches just below the S2–S3 level. This is best accomplished by angling the needle along the course of the sacrum. During fluoroscopy with the patient prone, the needle should lie in the sacral canal, which is delineated by the sacral pedicles.

The patient is then rolled into a lateral decubitus position. Observation of the needle position with respect to the spinal canal (Fig. 5) should confirm that the needle tip is within the sacral canal and that the tip is at the S2–S3 level or below. The patient is then turned prone. Two to four milliliters of nonionic contrast material is injected to confirm correct needle placement. Fluoroscopy should show free flow of contrast material away from the needle tip and along the dural sheaths of the sacral nerve roots. Three milliliters (18 mg) of betamethasone followed by either 5–10 ml of sterile saline or 5–10 ml of a diluted 0.25% bupivacaine (1:3 mixture of bupivacaine with normal saline) are injected.

The patient's pulse and blood pressure are taken again. If the patient receives bupivacaine, his or her vital signs and neurocirculatory status are checked every 15 min for 1 hr, the head of the bed is gradually elevated, and the patient must void or ambulate before discharge. Before discharge, the patient receives instructions from the physician or a nurse regarding possible complications. These complications include reactions to contrast material and local anesthetic and infection. In addition, meningitis with neurologic damage has been reported with epidural injection after intrathecal injection of steroids [55]; the technique described earlier helps avoid such intrathecal injection. Transient hypercorticism also may occur after repeated injections of steroids into the epidural space [56].

Discussion

Epidural injection is controversial, with success rates ranging from 23% [44] to 84% [53]. Beliveau [57] found no statistically significant difference between local anesthetic alone and local anesthetic with steroids, whereas Yates [50] found greater pain relief in those patients receiving steroids and local anesthetic than in patients receiving only local anesthetic.

Given the intermittent nature of lower back pain and the placebo effect of an injection, these uncontrolled, unblinded, retrospective studies are not ideal. Dilke et al. [46] performed the first blinded, prospective study of epidural steroid injection in 1973. They found that epidural steroid injection decreased analgesic use and time away from work in patients with an acute herniated nucleus pulposus. Cuckler et al. [54] also performed a blinded, prospective study but came to the conclusion that epidural steroids were not effective in treating lower back pain. The study by Cuckler et al. can be faulted for its selection of an inappropriate "placebo" group (patients given an epidural injection of 5 ml of procaine), the early evaluation of response to injection at 24 hr (particularly considering the placebo), and an overly rigorous requirement for success (75% pain relief). Bush and Hillier [47], in a more recent prospective, blinded trial, found increased relief of pain, improved mobility, and improved quality of life in patients with lower back pain receiving epidural steroids and anesthetic when compared with patients receiving epidural saline.

In 1980, White et al. [53] reported that needle placement without contrast material and fluoroscopic guidance results in inappropriate injection in approximately 25% of cases. The sacral approach, coupled with fluoroscopy and injection of contrast medium, results in technical success in 97% of cases [58]. Because blind needle placement of epidural injections is so often incorrect, the results of studies not documenting needle placement can be questioned. In this regard, it is of interest that only the large series of White et al. [53] proved needle location, and that series had the most success regarding pain relief.

No prospective, blinded study of epidural injection that reports correct drug placement has been published. Such a study would be very helpful in proving whether epidural injections are effective in the treatment of lower back pain. The best summary of the available literature is that such injections, at least in some patients, offer significant but usually temporary pain relief.

REFERENCES

1. Frymoyer JW. Back pain and sciatica. *N Engl J Med* **1988**;318:291–300
2. Haldeman S. Failure of pathology to predict back pain. *Spine* **1990**;15: 718–724
3. Nachemson AL. Advances in low-back pain. *Clin Orthop* **1985**;200: 266–278
4. Modic MT, Ross JS. Morphology, symptoms, and causality. *Radiology* **1990**;175:619–620
5. Wiesel SW, Tsourmas N, Feffer HL, Citrin CM, Patronas N. A study of computer-assisted tomography: I. The incidence of positive CAT scans in an asymptomatic group of patients. *Spine* **1984**;9:549–551
6. Boden SD, Davis DO, Dina TS, et al. Abnormal magnetic-resonance scans of the lumbar spine in asymptomatic patients. *J Bone Joint Surg [Am]* **1990**;72-A:403–408
7. Milette PC, Melanson D. A reappraisal of lumbar discography. *J Can Assoc Radiol* **1982**;33:176–182
8. Walsh TR, Weinstein JN, Spratt KF, Lehmann TR, Aprill C, Sayre H. Lumbar discography in normal subjects: a controlled, prospective study. *J Bone Joint Surg [Am]* **1990**;72-A:1081–1088
9. Lindblom K. Diagnostic puncture of the intervertebral disc in sciatica. *Acta Orthop Scand* **1948**;17:231–239
10. Holt EP. The question of lumbar discography. *J Bone Joint Surg [Am]* **1968**;50-A:720–725
11. Sachs BL, Spivey MA, Vanharanta H, et al. Techniques for lumbar discography and CT/discography in clinical practice. *Appl Radiol* **1989**;18:28–30
12. Crock HV. Internal disc disruption: a challenge to disc prolapse fifty years on. *Spine* **1986**;11:650–653
13. Bernard TN. Lumbar discography followed by computed tomography: refining the diagnosis of low-back pain. *Spine* **1990**;15:690–707
14. Osti OL, Fraser RD, Vernon-Roberts B. Discitis after discography: the role of prophylactic agents. *J Bone Joint Surg [Br]* **1990**;72-B:271–274
15. Vanharanta H, Sachs BL, Spivey MA, et al. The relationship of pain provocation to lumbar disc deterioration as seen by CT/discography. *Spine* **1987**;12:295–298
16. Zucherman J, Derby R, Hsu K, et al. Normal magnetic resonance imaging with abnormal discography. *Spine* **1988**;13:1355–1359
17. Kornberg, M. Discography and magnetic resonance imaging in the diagnosis of lumbar disc disruption. *Spine* **1989**;12:1368–1372
18. Schneiderman G, Flannigan B, Kingston S, Thomas J, Dillin WH, Watkins RG. Magnetic resonance imaging in the diagnosis of disc degeneration: correlation with discography. *Spine* **1987**;12:276–281
19. Gibson MJ, Buckley J, Mawhinney R, Mulholland RC, Worthington BS. Magnetic resonance imaging and discography in the diagnosis of disc degeneration. *J Bone Joint Surg [Br]* **1986**;68-B:369–373
20. Collins CD, Stack JP, O'Connell DJ, et al. The role of discography in lumbar disc disease: a comparative study of magnetic resonance imaging and discography. *Clin Radiol* **1990**;42:252–257
21. Esses SI, Botsford J, Kostuik JP. The role of external spinal skeletal fixation in the assessment of low-back disorders. *Spine* **1989**;14:594–600
22. Linson MA, Williams H. Anterior and combined anteroposterior fusion for lumber disc pain: a preliminary study. *Spine* **1991**;16:143–145
23. Nachemson A. Lumbar discography: where are we today? *Spine* **1989**;14:555–557
24. Goldthwait JE. The lumbosacral articulation: an explanation of many causes of "lumbago, sciatica, and paraplegia." *Boston Med Surg J* **1911**;164:356–372
25. Puttie V. New conceptions in the pathogenesis of sciatic pain. *Lancet* **1927**;2:53–60
26. Mooney V, Robertson J. The facet syndrome. *Clin Orthop* **1976**;115: 149–156
27. Dory MA. Arthrography of the lumbar facet joints. *Radiology* **1981**;140: 23–27
28. Maldague B, Mathurin P, Malghem J. Facet joint arthrography in lumbar spondylosis. *Radiology* **1981**;140:29–36
29. Lippitt AB. The facet joint and its role in spine pain: management with facet joint injections. *Spine* **1984**;9:746–750
30. Destouet JM, Gilula LA, Murphy WA, Monsees B. Lumbar facet injection: indication, technique, clinical correlation, and preliminary results. *Radiology* **1982**;145:321–325
31. Moran R, O'Connell D, Walsh MG. The diagnostic value of facet joint injections. *Spine* **1988**;13:1407–1410
32. Raymond J, Dumas JM. Intraarticular facet block: diagnostic test or therapeutic procedure? *Radiology* **1984**;151:333–356
33. Carrera GF. Lumbar facet injection in low back pain and sciatica: preliminary results. *Radiology* **1980**;137:65–66
34. Murtagh FR. Computed tomography and fluoroscopy guided anesthesia and steroid injection in facet syndrome. *Spine* **1988**;13:686–689
35. Ghelman B, Doherty JH. Demonstration of spondylolysis by arthrography of the apophyseal joint. *AJR* **1978**;130:986–987
36. Lynch MC, Taylor JF. Facet joint injection for low back pain: a clinical study. *J Bone Joint Surg [Br]* **1986**;68-B:138–141
37. Jackson RP, Jacobs RR, Montesano PX. Facet joint injection in low-back pain: a prospective statistical study. *Spine* **1988**;13:966–971
38. Lilius G, Laasonen EM, Myllynen P, Harilainen A, Gronlund G. Lumbar facet joint syndrome: a randomized clinical trial. *J Bone Joint Surg [Br]* **1989**;71-B:681–684
39. Lilius G, Harilainen A, Laasonen EM, Myllynen P. Chronic unilateral low-back pain: predictors of outcome of facet joint injections. *Spine* **1990**;15:780–782
40. Davidson JT, Robin GC. Epidural injections in the lumbosciatic syndrome. *Br J Anaesth* **1961**;33:595–598
41. Evans W. Intrasacral epidural injection in the treatment of sciatica. *Lancet* **1930**;129:1225–1229
42. Kelman H. Epidural injection therapy for sciatic pain. *Am J Surg* **1944**;64:183–190
43. Coomes EN. A comparison between epidural anaesthesia and bed rest in sciatica. *Br Med J* **1961**;1:20–24
44. Goldie I, Peterhoff V. Epidural anesthesia in low-back pain and sciatica. *Acta Orthop Scand* **1968**;39:261–269
45. Lievre JA, Block-Michel H, Attali P. L'injection transsacrée: étude clinique et radiologique. *Bull Soc Med* (Paris) **1953**;73:1110–1117
46. Dilke TFW, Burry HC, Grahame R. Extradural corticosteroid injection in the management of lumbar nerve root compression. *Br Med J* **1973**;2: 635–637
47. Bush K, Hillier S. A controlled study of caudal epidural injections of triamcinolone plus procaine for the management of intractable sciatica. *Spine* **1991**;16:572–575
48. Lindahl O, Rexed B. Histologic changes in spinal nerve roots of operated cases of sciatica. *Acta Orthop Scand* **1951**;20:215–225
49. Garfin SR, Rydevik BL, Brown RA. Compression neuropathy of spinal nerve roots: a mechanical or biological problem? *Spine* **1991**;16:162–166
50. Yates DW. A comparison of the types of epidural injection commonly used in the treatment of low back pain and sciatica. *Rheum Rehab* **1978**;17: 181–186
51. Warr AC, Wilkinson JA, Burn JMB, et al. Chronic lumbosciatic syndrome treated by epidural injection and manipulation. *Practitioner* **1972**;209: 53–59
52. Heyse-Moore GH. A rational approach to the use of epidural medication in the treatment of sciatic pain. *Acta Orthop Scand* **1978**;49:366–370
53. White AH, Derby R, Wynne G. Epidural injections for the diagnosis and treatment of low-back pain. *Spine* **1980**;5:78–86
54. Cuckler JM, Bernini PA, Wiesel SW, et al. The use of epidural steroids in treatment of lumbar radicular pain. *J Bone Joint Surg [Am]* **1985**;67-A: 63–66
55. Dougherty JH, Fraser RAR. Complications involving intraspinal injections of steroids. *J Neurosurg* **1978**;48:1023–1025
56. Stambough JL, Booth RE, Rothman RH. Transient hypercorticism after epidural steroid injection: a case report. *J Bone Joint Surg [Am]* **1984**;66-A:1115–1116
57. Beliveau P. A comparison between epidural anesthesia with and without corticosteroid in the treatment of sciatica. *Rheum Phys Med* **1971**;11: 40–43
58. El-Khoury TY, Ehara S, Weinstein JN, et al. Epidural steroid injection: a procedure ideally performed with fluoroscopic control. *Radiology* **1988**;168:544–557

Book Review

Diagnosis of Diseases of the Chest, 3rd ed., vol 4. By Robert G. Fraser, J. A. Peter Paré, P. D. Paré, Richard S. Fraser, and George P. Genereux. Philadelphia: Saunders, 912 pp., 1991. $90

This is the long-awaited last volume of the ever-expanding "Fraser and Paré" (volume 1 was issued in 1988). It has eight chapters, an appendix comprising a virtual atlas of pleuropulmonary diseases organized into gamuts by radiologic pattern, and a reprinting of the Fleischner Society's glossary of terms and the pulmonary terms and symbols of the American College of Chest Physicians and the American Thoracic Society. This is topped off with the expected comprehensive set of references and a subject index that covers all four volumes. The topics in this volume are varied: drug- and poison-induced pulmonary disease, external trauma, metabolic and idiopathic pulmonary diseases, diseases of the pleura and the mediastinum, the diaphragm and chest wall, and an unusual chapter on diseases in which the chest radiograph is normal.

Countless illustrations are combined into 306 generously sized figures. Most of these are chest radiographs of excellent quality, but certain topics have had the attention of pathologist Richard Fraser, who has contributed excellent photomicrographs and a few photographs of pathologic specimens. The inclusion of Gough whole-lung sections would be useful in some chapters. CT has made a tentative appearance in the series. Although the technique is mentioned frequently in the text, the number and quality of the CT scans clearly lag behind the current state of the art. MR imaging is acknowledged to have promise in diseases of the mediastinum, but readers will have to refer to more specialized MR texts for examples.

Of course, any reviewer can find some problems with the attention paid to various topics; sickle cell disease, for example, gets a shorter discussion than many exceedingly rare entities. Pleural plaques, surely an important topic, are heavily outweighed by the rare fibrous pleural tumors. The discussion of the important differential diagnosis of pneumomediastinum, pneumothorax, and pneumopericardium is inadequate, and pneumopericardium is not even a primary entry in the index.

Some recommendations are a little obsolete. For example, biopsy of a scalene lymph node is recommended for sarcoidosis because bronchoscopic biopsy would be "blind." I think that fiberoptic bronchoscopy is really the technique of choice now. For identification of a mediastinal goiter, the ease and speed of CT is ignored, and the old-fashioned approach of radionuclide scanning is cited.

Some discussions leave out important considerations. For example, in the discussions of both aortic dissection and aortic laceration, CT is advocated without any mention of the need to avoid exceeding the patient's tolerance for contrast material because angiography subsequently will be required. I was disappointed by the section on interstitial fibrosis; the role of diffuse alveolar damage and the relationship of adult respiratory distress syndrome in pathogenesis are ignored. Even the relationship to collagen diseases is not made clear. Not all such patients have small lungs, and lymphangiomyomatosis does *not* look like usual interstitial pneumonia. Nor is desquamative interstitial pneumonia uniformly distributed pathologically.

The massive size of the entire four-volume work has resulted in coverage of diseases or findings in more than one place; duplication is common, with a paucity of cross-referencing, except in the index. The short summary of a topic in one place may distract the reader from finding the more definitive discussion elsewhere. Some indexing problems have crept in: "Asbestosis" is absent; no "fibrosis" or "interstitial fibrosis" is listed directly under "asbestos-related disease"; and "asbestos" is not listed under "fibrosis, interstitial." "Ankylosing spondylitis" refers to more entries than does "spondylitis, ankylosing"; neither index entry lists the associated interstitial fibrosis.

This book is generally the first place to turn for answers to specific questions and for an entry into the medical literature. It is detailed and comprehensive enough that sections can be read as thoughtful essays on many important topics, although it has a little too much straight reporting of questionably relevant research results. I am not aware of any other book that attempts to combine so much text and graphic information on chest diseases, so it is fair to say that it is incomparably successful. If you are put off by the errors in spelling and grammar found in so many modern textbooks, you will be delighted by the quality of the writing and proofreading of this opus. If you own the previous volumes, you will want this one; if you do not have access to it in a convenient library, see your bank about a loan.

Paul J. Friedman
University of California, San Diego
La Jolla, CA 92093

Chronic Diffuse Infiltrative Lung Disease: Comparison of Diagnostic Accuracy of High-Resolution and Conventional CT

Ann N. Leung[1]
Catherine A. Staples[2]
Nestor L. Müller[1]

We compared the accuracies of high-resolution CT (HRCT) and conventional CT in determining the specific diagnoses in 75 consecutive patients with chronic diffuse infiltrative lung disease. Without knowledge of clinical or pathologic data, two reviewers independently assessed three separate sets of CT scans in random order: three HRCT scans, three 10-mm collimation CT scans obtained at the same levels as the HRCT scans, and a complete conventional CT scan. The HRCT scans were obtained at the level of the aortic arch, tracheal carina, and 1 cm above the right hemidiaphragm by using 1.5-mm collimation and a high spatial resolution algorithm. Observers gave the most likely diagnosis along with their degree of diagnostic confidence. The correct diagnosis, irrespective of confidence level, was reached with 71% of the HRCT scans and with 72% of both the corresponding 10-mm and complete conventional CT scans. Confidence level 1 (definite) was reached with 49% of HRCT scans, 31% of corresponding 10-mm scans, and 43% of complete conventional CT examinations; the correct diagnosis was made in 92%, 96%, and 94% of those examinations, respectively. In none of the patients were findings on the limited HRCT scan normal when findings on the conventional CT scan were abnormal.

We conclude that in most patients with chronic infiltrative lung disease a specific diagnosis can be made by obtaining a limited number of HRCT scans.

AJR 157:693–696, October 1991

High-resolution CT (HRCT) allows detailed delineation of the pulmonary parenchyma by minimizing partial volume averaging and increasing spatial resolution. Anatomic detail comparable to that seen on gross inspection of tissue is achieved [1]. A number of studies have shown the advantages of HRCT compared with conventional CT in the assessment of patients with chronic diffuse infiltrative lung disease [2, 3]. However, the use of HRCT is not standardized, and its role as a complement to conventional CT or as an independent study has not been defined clearly [4–6]. The aim of this study was to compare the accuracy of HRCT with that of conventional CT in the determination of specific diagnoses in patients with diffuse infiltrative lung disease.

Materials and Methods

All patients who had a diagnosis of a specific variety of chronic diffuse infiltrative lung disease at our institution between July 1986 and October 1989 and in whom both conventional CT and HRCT scans had been obtained were included in a retrospective study. Seventy-five patients, 41 men and 34 women, with a mean age of 52 years (range, 24–86 years) met these criteria.

The 75 cases in the study included a total of 14 different pathologic entities. Twenty patients had sarcoidosis; 15 had lymphangitic carcinomatosis; 12 had usual interstitial pneumonia; seven had silicosis; four had extrinsic allergic alveolitis; four had bronchiolitis obliterans organizing pneumonia; three had lymphangioleiomatosis; two each had lymphoma, alveolar proteinosis, and bronchoalveolar carcinoma; and one each had desquamative inter-

Received February 19, 1991; accepted after revision April 23, 1991.

[1] Department of Radiology, University of British Columbia and Vancouver General Hospital, 855 W. 12th Ave., Vancouver, B.C., Canada V5Z 1M9. Address reprint requests to N. L. Müller.

[2] Department of Radiology, University of British Columbia and St. Paul's Hospital, Vancouver, B.C., Canada V6Z 1Y6.

0361–803X/91/1574–0693
© American Roentgen Ray Society

stitial pneumonia, eosinophilic granuloma, coccidiodomycosis, and lymphoid hyperplasia in rheumatoid arthritis. Definitive pathologic diagnosis based on the results of either transbronchial or open lung biopsy was available in all cases except the seven cases of silicosis.

All CT scans were obtained on a General Electric 9800 scanner (GE Medical Systems, Milwaukee, WI). Contiguous 10-mm collimation scans were obtained from lung apices to bases; three additional 1.5-mm collimation scans were obtained at the level of the aortic arch, tracheal carina, and 1 cm above the right hemidiaphragm. These HRCT scans were obtained at 120 kVp and 360–420 mAs; retrospective targeting of the thin-section scans was performed with a field of view of 20 or 25 cm and a high-spatial-resolution (bone) algorithm [7]. All scans were obtained at end-inspiratory lung volumes and photographed at window levels and widths appropriate for lung parenchyma (level, −600 to −700 H; width, 1000–2000 H) and mediastinum (level, 30–50 H, width, 350–500 H).

Three separate sets of images of each patient (set 1 = three HRCT scans; set 2 = the three corresponding 10-mm scans; set 3 = complete conventional CT scan) were assessed in random order by two independent observers who had no knowledge of clinical or pathologic data other than the age and sex of the patient. Approximately every 2 weeks, each of the two observers received a package containing 20–25 sets of images, a randomized mixture of HRCT scans and conventional CT scans. In the unlikely event that the randomization would lead to two different kinds of CT scans of the same patient being present in the same package, the second set was removed and again randomized. Interpreting the findings on the basis of previously published data on the CT appearances of chronic diffuse infiltrative lung disease [2, 3, 8–25], each observer listed the most likely diagnosis with the level of diagnostic confidence (1 = definite, 2 = probable, 3 = possible).

The percentage of correct diagnoses of each set or combination of sets represents the sum of the correct interpretations by the two observers divided by the total number of interpretations. The percentage of correct diagnoses was statistically compared between sets and set combinations by using the chi-square test.

Results

The correct first-choice diagnosis, irrespective of the degree of confidence, was made with 71% of the HRCT scans and with 72% of both the corresponding 10-mm and complete conventional CT images (Fig. 1). The HRCT interpretations were most accurate in the diagnosis of lymphangitic carcinomatosis (100%) and usual interstitial pneumonia (92%) (Fig. 2). The difference between the diagnostic accuracy of the limited HRCT study and that of the complete conventional CT study was not statistically significant ($p > .05$). The diagnostic accuracy of the combination of the HRCT scans and a complete conventional CT study (82/150) was not significantly improved ($p > .05$, chi-square test) over the diagnostic accuracy of HRCT scans alone (68/150).

A diagnosis with a high confidence level (level 1) was reached with 49% of the HRCT scans, 31% of the corresponding 10-mm scans, and 43% of the complete conventional CT scans. This diagnosis was correct in 92%, 96%, and 94% of scans, respectively. The increased confidence of diagnosis with HRCT as compared with conventional CT was due to the greater ease in diagnosing lymphangitic carcinomatosis ($p < .01$, chi-square test).

Discussion

HRCT is clearly superior to conventional CT in the morphologic delineation of pulmonary parenchyma [1–6]. However, because of the inherent nature of HRCT, the long examination time and high doses of radiation preclude routine complete HRCT examination of the lungs.

At present, no consensus exists about the best use of HRCT in the assessment of patients with chronic diffuse infiltrative lung disease [4, 6]. Two alternatives have been advocated: HRCT as an adjunct to a complete conventional CT scan and used only in selected areas to define abnormalities better [4] and HRCT as an independent, limited examination with slices obtained at various intervals (range, 1–4 cm) [5, 15].

Our results support the use of a limited number of HRCT scans in the initial assessment of patients with chronic diffuse

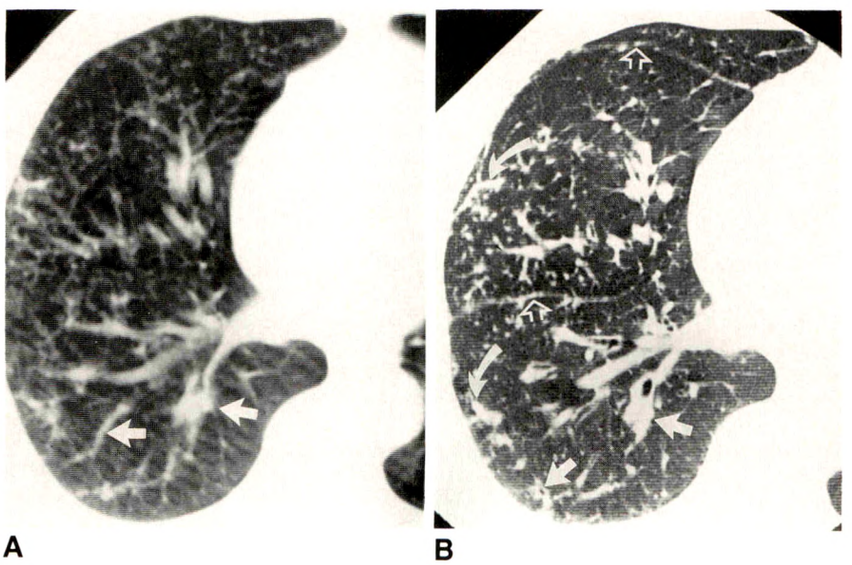
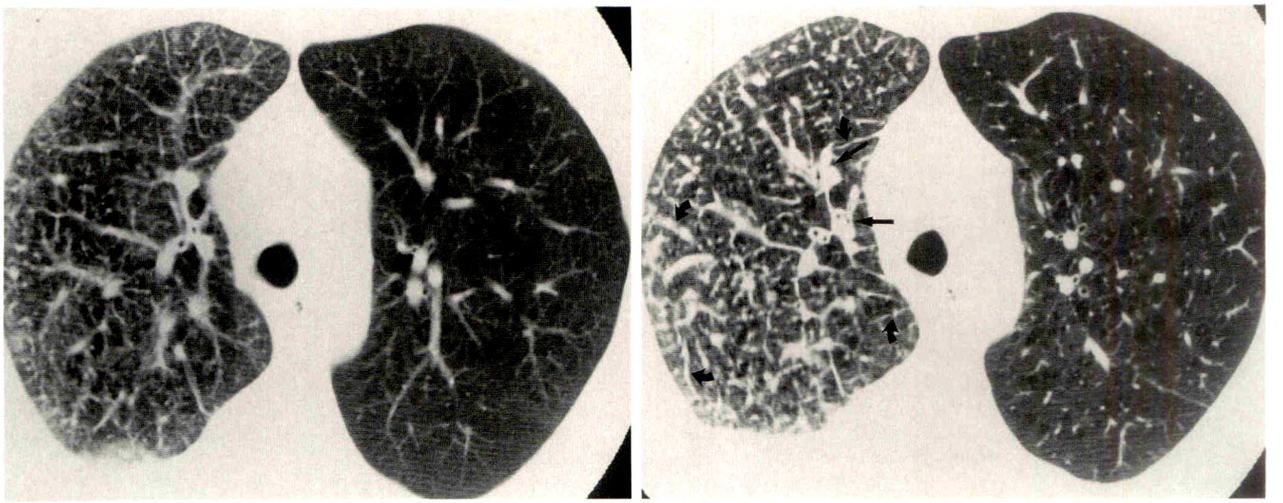


Fig. 1.—62-year-old man with sarcoidosis.
A, 10-mm collimation CT scan shows small nodules, some in a peribronchovascular distribution (*arrows*).
B, Corresponding 1.5-mm high-resolution CT scan targeted to right lung better delineates nodules and their relationship to bronchovascular bundles (*straight solid arrows*), interlobular septa (*curved arrows*), and interlobar fissures (*open arrows*).



A B

Fig. 2.—67-year-old woman with lymphangitic carcinomatosis.
A, 10-mm collimation CT scan shows unilateral, right-sided, diffuse, increased density and multiple linear opacities extending more peripherally than normal.
B, Corresponding 1.5-mm high-resolution CT scan shows linear densities representing uneven nodular thickening of bronchovascular bundles (*straight arrows*) and interlobular septa (*curved arrows*). Presence of multiple polygonal arcades with nodular thickening is highly suggestive of lymphangitic carcinomatosis.

infiltrative lung disease [4, 5, 15]. We found that with only three HRCT scans, one obtained of each of the three lung zones, diagnostic accuracy comparable to that of complete conventional CT scanning can be achieved. Surprisingly, the combination of complete conventional CT scanning plus HRCT did not significantly improve the diagnostic accuracy. Mathieson et al. [3] studied 118 patients with chronic diffuse infiltrative lung disease, 66 of whom had HRCT, and concluded that HRCT was superior in the assessment of diseases that cause predominantly irregular opacities but that conventional CT was superior in the assessment of small nodular opacities. In their study, they did not analyze the HRCT scans independently from the conventional CT scans, but compared the scans side-by-side and determined the ease with which the abnormalities could be seen. Because nodular opacities were easier to distinguish from vessels on conventional CT than on high-resolution CT scans, they recommended that both conventional and HRCT scans be obtained in the initial assessment of patients with chronic diffuse infiltrative lung disease.

In our study, in which HRCT and the conventional CT scans were analyzed separately, it was clear that, although small nodular opacities are easier to distinguish from vessels on the conventional CT scans, they are clearly identified on the HRCT scans also. This is in agreement with recent studies that show that HRCT scans can be used to identify clearly and characterize small nodular opacities in sarcoidosis [15] and various pneumoconioses [26]. Remy-Jardin et al. [27] have suggested that HRCT actually may be more sensitive than conventional CT is in the detection of small nodules, although it may be difficult to distinguish between small nodules and vessels. In our study, we found no significant difference in the diagnostic accuracy of HRCT and that of conventional CT in the assessment of patients with small nodular opacities such as those caused by sarcoidosis and silicosis.

HRCT has greater spatial resolution and thus allows better assessment of parenchymal detail than does conventional CT [2–7]. The greater confidence in making a specific diagnosis in patients with chronic infiltrative lung disease in the present study was due to the greater ease in identifying interlobular septal thickening in lymphangitic carcinomatosis. This has been demonstrated before by several investigators [2–4, 17]. As with any technique, observer experience influences confidence in interpreting HRCT scans. Until recently, we believed that conventional CT was necessary in the initial assessment of all patients with chronic infiltrative lung disease [3, 28, 29]. The results of our study, however, show that a similar diagnostic accuracy can be obtained with a limited number of HRCT scans.

We conclude that in most patients with chronic diffuse infiltrative lung disease, the correct diagnosis can be made by obtaining a limited number of HRCT scans. Our protocol included HRCT scans at only three levels: aortic arch, tracheal carina, and 1 cm above the right hemidiaphragm, with the patient supine. Obviously, with such a limited examination, focal parenchymal abnormalities may be overlooked, the patchy distribution of many diffuse infiltrative lung diseases may not be appreciated, and small nodules may be missed between high-resolution sections [3, 4, 9, 16, 17]. Therefore, we think that although the limited HRCT protocol allows accurate diagnosis, a greater number of HRCT scans is necessary for adequate and sufficient evaluation of the extent of disease and activity. The optimal number may depend on the clinical situation. In certain cases, a focused search strategy based on the known or suspected distribution of disease

may be indicated. At our institution, we currently obtain 1.5-mm collimation scans every 10 mm from the lung apices to bases in the initial assessment of patients with chronic infiltrative lung disease.

REFERENCES

1. Meziane MA, Hruban RH, Zerhouni EA, et al. High resolution CT of the lung parenchyma with pathologic correlation. *RadioGraphics* **1988**;8: 27–54
2. Zerhouni EA, Naidich DP, Stitik FP, Khouri NF, Siegelman SS. Computed tomography of the pulmonary parenchyma. Part 2. Interstitial disease. *J Thorac Imag* **1985**;1:54–64
3. Mathieson JR, Mayo JR, Staples CA, Müller NL. Chronic diffuse infiltrative lung disease: comparison of diagnostic accuracy of CT and chest radiography. *Radiology* **1989**;171:111–116
4. Webb WR, Müller NL, Zerhouni EA. High-resolution CT of the lungs: current clinical uses. *Perspect Radiol* **1989**;2:61–69
5. Gamsu G, Klein JS. High resolution computed tomography of diffuse lung disease. *Clin Radiol* **1989**;40:554–556
6. Naidich DP. Pulmonary parenchyma high-resolution CT: to be or not to be. *Radiology* **1989**;171:22–24
7. Mayo JK, Webb WR, Gould R, et al. High-resolution CT of the lungs: an optimal approach. *Radiology* **1987**;163:507–510
8. Bergin CJ, Müller NL. CT of interstitial lung disease: a diagnostic approach. *AJR* **1987**;148:8–15
9. Müller NL, Miller RR, Webb WR, Evans KG, Ostrow DN. Fibrosing alveolitis: CT-pathologic correlation. *Radiology* **1986**;160:585–588
10. Müller NL, Staples CA, Miller RR, Vedal S, Thurlbeck WM, Ostrow DN. Disease activity in idiopathic pulmonary fibrosis: CT and pathologic correlation. *Radiology* **1987**;165:731–734
11. Bergin CJ, Müller NL, Vedal S, Chan-Yeung M. CT in silicosis: correlation with plain films and pulmonary function tests. *AJR* **1986**;146:477–483
12. Kuhlman JE, Fishman EK, Hamper VM, Knowles M, Siegelman SS. The computed tomographic spectrum of sarcoidosis. *RadioGraphics* **1989**;9:449–466
13. Müller NL, Kullnig P, Miller RR. The CT findings of pulmonary sarcoidosis: analysis of 25 patients. *AJR* **1989**;152:1179–1182
14. Müller NL, Mawson JR, Mathieson JR, Abboud R, Ostrow DN, Champion P. Sarcoidosis: correlation of extent of disease at CT with clinical, functional, and radiographic findings. *Radiology* **1989**;171:613–618
15. Brauner MW, Grenier P, Mompoint D, Lenoir S, DeCremeoux H. Pulmonary sarcoidosis: evaluation with high-resolution CT. *Radiology* **1989**;172: 467–471
16. Stein MG, Mayo J, Müller NL, Aberle DR, Webb WR, Gamsu G. Pulmonary lymphangitic spread of carcinoma: appearance on CT scans. *Radiology* **1987**;162:371–375
17. Munk PL, Müller NL, Miller RR, Ostrow DN. Pulmonary lymphangitic carcinomatosis: CT and pathologic findings. *Radiology* **1988**;166:705–709
18. Silver SF, Müller NL, Miller RR, Lefcoe MS. Hypersensitivity pneumonitis: evaluation with CT. *Radiology* **1989**;173:441–445
19. Müller NL, Guerry-Force ML, Staples CA, et al. Differential diagnosis of bronchiolitis obliterans with organizing pneumonia and usual interstitial pneumonia: clinical, functional, and radiologic findings. *Radiology* **1987**;162:151–156
20. Müller NL, Staples CA, Miller RR. Bronchiolitis obliterans organizing pneumonia: CT features in 14 patients. *AJR* **1990**;154:983–987
21. Rappaport DC, Weisbrod GL, Herman SJ, Chamberlain DW. Pulmonary lymphangioleiomyomatosis: high-resolution CT findings in four cases. *AJR* **1989**;152:961–964
22. Godwin JD, Müller NL, Takasugi JE. Pulmonary alveolar proteinosis: CT findings. *Radiology* **1988**;169:609–613
23. Templeton PA, McLoud TC, Müller NL, Shepard JO, Moore EH. Pulmonary lymphangioleiomyomatosis: CT and pathologic findings. *J Comput Assist Tomogr* **1989**;13:54–57
24. Moore ADA, Godwin JD, Müller NL, et al. Pulmonary histiocytosis X: comparison of radiographic and CT findings. *Radiology* **1989**;172: 249–254
25. Brauner NW, Grenier P, Mouelhi MM, Mompoint D, Lenoir S. Pulmonary histiocytosis X: evaluation with high-resolution CT. *Radiology* **1989**;172:255–258
26. Akira M, Higashihara T, Yokoyama K, et al. Radiographic type p pneumoconiosis: high-resolution CT. *Radiology* **1989**;171:117–123
27. Remy-Jardin M, Degreef JM, Beuscart R, Voisin C, Remy J. Coal worker's pneumoconiosis: CT assessment in exposed workers and correlation with radiographic findings. *Radiology* **1990**;177:363–371
28. Müller NL, Miller RR. State of the art: Computed tomography of chronic diffuse infiltrative lung disease. Part 1. *Am Rev Respir Dis* **1990**;142:1206–1215
29. Müller NL, Miller RR. State of the art: Computed tomography of chronic diffuse infiltrative lung disease. Part 2. *Am Rev Respir Dis* **1990**;142:1440–1448

Paraquat Poisoning: Findings on Chest Radiography and CT in 42 Patients

Jung-Gi Im[1]
Kyung Soo Lee[2]
Man Chung Han[1]
Sung Jin Kim[1]
In One Kim[1]

The purpose of this study is to describe the radiologic manifestations of paraquat-induced pulmonary damage, with special emphasis on the sequential changes seen with this condition. Paraquat is a herbicide that has toxic effects on the lungs, liver, and kidneys. Progressive respiratory failure is a frequent cause of death. We analyzed retrospectively 42 patients with a history of paraquat ingestion and abnormal findings on chest radiographs. Radiographic changes during the first week after ingestion included diffuse consolidation (26/39), pneumomediastinum with or without pneumothorax (15/39), and cardiomegaly with widening of the superior mediastinum (8/39). Small cystic and linear shadows began to appear at the end of the first week and were the preponderant parenchymal abnormality after 2–4 weeks. Focal honeycombing was the major parenchymal abnormality after 4 weeks. High-resolution CT of the lung 9 months after paraquat exposure revealed localized fibrosis containing small cysts.

Our study shows that the pulmonary manifestations of paraquat poisoning begin with air-space consolidation, which then leads to end-stage lung.

AJR 157:697–701, October 1991

Paraquat (1,1′-dimethyl-4,4′-bipyridylium dichloride) is a widely used herbicide that has toxic effects on the lungs, liver, and kidneys. More than 200 deaths due to paraquat ingestion were reported in the first two decades after its widespread use began in 1958 [1–3]. Since 1978, we were able to find reports of more than 700 deaths due to paraquat poisoning [4–18]. Death from paraquat poisoning was primarily caused by progressive pulmonary damage with respiratory failure [19]. To our knowledge, findings on chest radiographs, especially the sequential changes that occur in long-term survivors, have not been described in detail [20]. Awareness of these findings is important because in some cases the history of paraquat ingestion may not be evident at the time of presentation [21]. We describe the findings on chest radiographs and CT, emphasizing the sequential abnormalities that are visible on radiographs and their clinical implications.

Materials and Methods

The chest radiographs, obtained during the past 5 years at two university hospitals, of 91 patients who had ingested ($n = 87$) or inhaled ($n = 4$) paraquat were reviewed. Radiographs of 49 patients did not show abnormalities. Of these patients, 35 died within 2 days after ingestion due to renal or multiorgan failure. Forty-two patients (46%) had radiographic abnormalities. Of these patients, 36 ingested undiluted Gramoxone (24.5% paraquat), 27 to commit suicide and nine accidentally. The remaining six patients were members of two families who repeatedly ate soy sauce and soybean paste that contained a high concentration of paraquat (265–1009 mg/kg).

Twenty-three patients were men and 19 were women. Age ranged from 11 to 69 years, with a mean of 35 years. The estimated amount of ingested paraquat, in the 21 suicide patients whose data are available, ranged from 15 ml to 200 ml, with a mean of 55 ml. In the group who accidentally ingested paraquat, six of nine had taken a mouthful of paraquat and

Received February 5, 1991; accepted after revision March 21, 1991.

This work was supported in part by research funds from Seoul National University Hospital.

[1] Department of Diagnostic Radiology, Seoul National University Hospital, 28 Yongon-dong, Chongno-gu, Seoul 110-744, Korea. Address reprint requests to J. G. Im.

[2] Department of Radiology, Soonchunhyang School of Medicine, Chonan, Korea.

0361–803X/91/1574–0697
© American Roentgen Ray Society

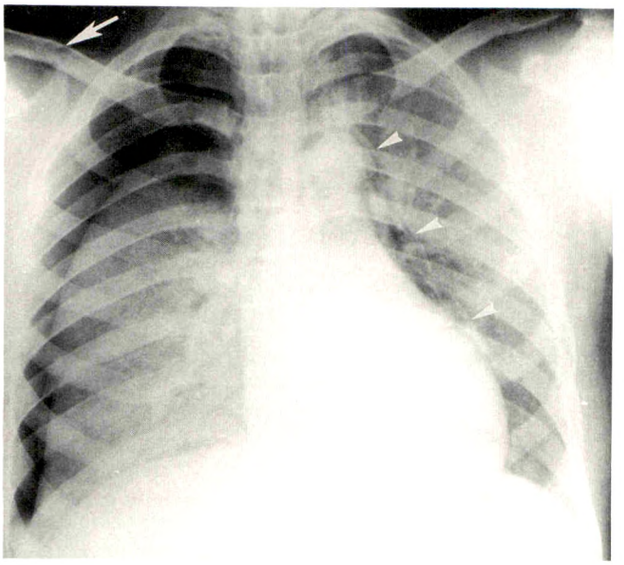


Fig. 1.—18-year-old man who ingested 200 ml of paraquat. Soon after ingestion he vomited and became comatose. Chest radiograph obtained 3 days after ingestion shows diffuse consolidation. Note pneumomediastinum (*arrowheads*), pneumothorax, and subcutaneous emphysema (*arrow*).



Fig. 2.—30-year-old man 15 days after ingestion of 50 ml of paraquat. Coned-down view of right lower lung shows multiple cystic and linear shadows.

had spat it out immediately. Chest radiographs were obtained within 7 days of ingestion in 41 patients. Radiographic follow-up, at 1- to 5-day intervals for 2 weeks and at 1- to 2-week intervals thereafter, was done in 28 patients. Total length of follow-up ranged from 1 day to 9 months, with a mean of 20 days.

High-resolution CT scans were obtained in two patients, 11 and 15 days after ingestion in one and 9 months after ingestion in the other. Scans were made with a GE 9800 scanner (General Electric Medical Systems, Milwaukee, WI) (1.5-mm collimation, 140 kVp, 170 mA, 2 sec, bone algorithm, retrospective retargeting with 20-cm field of view).

Results

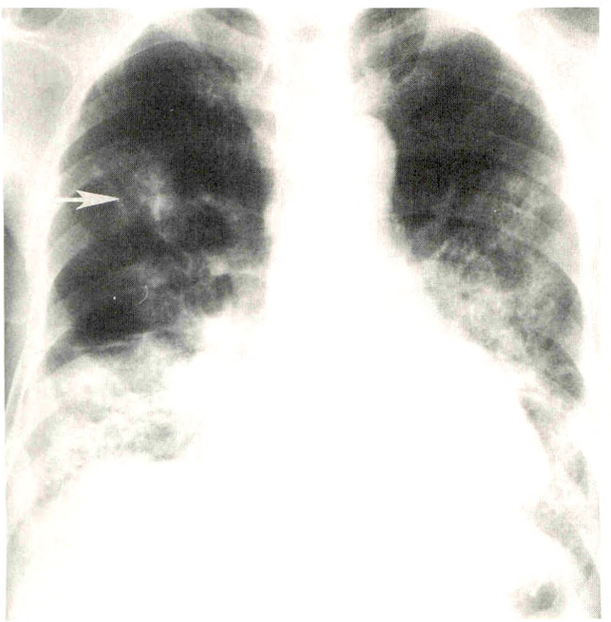
There were three patterns of pulmonary abnormalities seen on the chest radiographs: (1) diffuse air-space consolidation, (2) diffuse cystic and linear shadows, and (3) focal interstitial opacities containing small cysts. The most common early finding was diffuse consolidation seen in 29 patients (69%, Fig. 1, Table 1). The consolidative lesions appeared within the first 7 days after ingestion in 26 patients. Consolidation evolved into a small cystic (2–9 mm) and linear pattern in eight patients (Figs. 2 and 3). These small cysts appeared 15 days after ingestion in four of the eight patients (Table 1). Only six patients were radiographed after 28 days, and all showed multifocal interstitial opacities, containing small cysts (Figs. 4 and 5, Table 1). These chronic interstitial opacities were associated with loss of lung volume and large thin-walled cysts (Fig. 4).

In one patient, high-resolution CT, done 11 days after ingestion, showed diffuse air-space consolidation that contained small cystic and tubular shadows, suggestive of dilated bronchioles and small bronchi. The consolidated lung decreased in size on follow-up high-resolution CT 4 days later (Fig. 3). High-resolution CT done 9 months after ingestion revealed localized fibrotic areas within otherwise normal lung (Fig. 5).

TABLE 1: Findings on Chest Radiographs in 42 Patients with Paraquat Poisoning

Findings	No. of Patients at Each Period (Days) After Poisoning					
	0–2 (n = 20)	3–7 (n = 23)	8–14 (n = 15)	15–28 (n = 7)	>28 (n = 6)	Total (n = 42)
Pulmonary lesions						
Air-space consolidation	13	13	3	0	0	29
Small cysts	0	2	2	4	0	8
Focal interstitial opacities	0	0	0	0	6	6
Pneumomediastinum	6	9	2	0	0	17
Pneumothorax	3	4	0	1	1	9
Subcutaneous emphysema	3	8	0	0	0	11
Cardiomegaly with widening of superior mediastinum	4	4	2	1	0	11
Pleural effusion	0	2	2	1	0	5

Note.—Each number indicates the number of patients who had newly developed findings on radiographs within the given period.



A



B

Fig. 3.—69-year-old man who accidentally ingested a mouthful of paraquat and spat it out immediately.

***A*, Chest radiograph 11 days after ingestion shows diffuse consolidation associated with cystic and tubular lucencies. Note bilateral small pleural effusions. Arrow indicates level of scan in *B*.**

***B*, High-resolution CT scan of right upper lung 15 days after ingestion shows localized honeycombing (*arrows*). Surrounding lung is normal.**

Pneumomediastinum occurred in 17 patients, in 15 of them within 7 days of paraquat ingestion (Table 1). All 17 patients died within 3 days of appearance of pneumomediastinum. In three patients, pneumomediastinum was the only radiographic abnormality. Pneumomediastinum was frequently associated with pneumothorax (nine patients) and subcutaneous emphysema (11 patients; Fig. 1).

Cardiomegaly and widening of the superior mediastinum appeared in 11 patients, usually within 7 days of paraquat ingestion. This time course corresponded to the period of acute renal failure. In five patients, pleural effusions were seen (Table 1).

The clinical symptoms and signs were related to the local corrosive effect of paraquat; these included sore throat and difficult swallowing ($n = 38$), nausea or vomiting ($n = 21$), and epigastric pain ($n = 20$). Respiratory symptoms occurred in 33 patients.

The mortality rate for the suicidal group was 96% (26/27) and that of the accidental-ingestion group was 40% (6/15), which yields an overall mortality rate of 76% (32/42). Patients in the suicidal group survived from 1 to 51 days (mean, 8.0 days), and those in the accidental-ingestion group survived from 8 to 17 days (mean, 11 days). The major causes of death were respiratory failure in 20 patients, renal failure in four, and multiorgan failure in eight. A higher mortality rate was observed in those patients in whom the abnormalities shown on radiographs appeared earlier and were more severe.

Discussion

The toxic effects of paraquat are thought to result from oxygen radicals that destroy the cell membrane [22–24]. Organ damage by paraquat depends on the balance between oxygen radicals and tissue levels of oxygen and antioxidants. Organ-specific damage to the lungs is caused by both lower concentration of the antioxidants and higher concentration of oxygen within the lung [23, 24]. Rose et al. [25] showed that paraquat accumulates within the lung in concentrations 10 to 90 times higher than that in circulating blood.

Early pathologic findings in the lung include thickening of the alveolar walls by edema, hemorrhage, and inflammatory cells. Some of the alveoli fill with fluid and large amounts of fibrin [26–29]. Late pathologic findings include pulmonary fibrosis and microcysts [22, 27].

We have demonstrated a characteristic time course in pulmonary damage from paraquat ingestion. In the first 7 days after ingestion, the preponderant radiographic abnormality was diffuse consolidation. Cystic (2–9 mm) and linear opacities then appeared within the consolidated lung during the next 7 days, and this pattern was the preponderant finding after 2 weeks (Fig. 2). Beyond 1 month, focal honeycomb lung was the principal abnormality.

On high-resolution CT, remarkable topographic variation was seen in the severity of pulmonary damage. The same regional variability has been described in pathologic descriptions of paraquat lung toxicity [22]. Regional variation of fibrotic pulmonary lesions may be caused by local variation in the concentration of antioxidants or oxygen in the tissues. The distribution of pulmonary lesions on high-resolution CT of paraquat-induced pulmonary fibrosis in our patients was different from that described in idiopathic pulmonary fibrosis. Paraquat-induced pulmonary fibrosis involves the central regions of the lung, whereas idiopathic pulmonary fibrosis primarily involves the lung periphery.

About 60% of marijuana used in the United States is grown in Mexico, and 20% of this contains paraquat [30, 31].

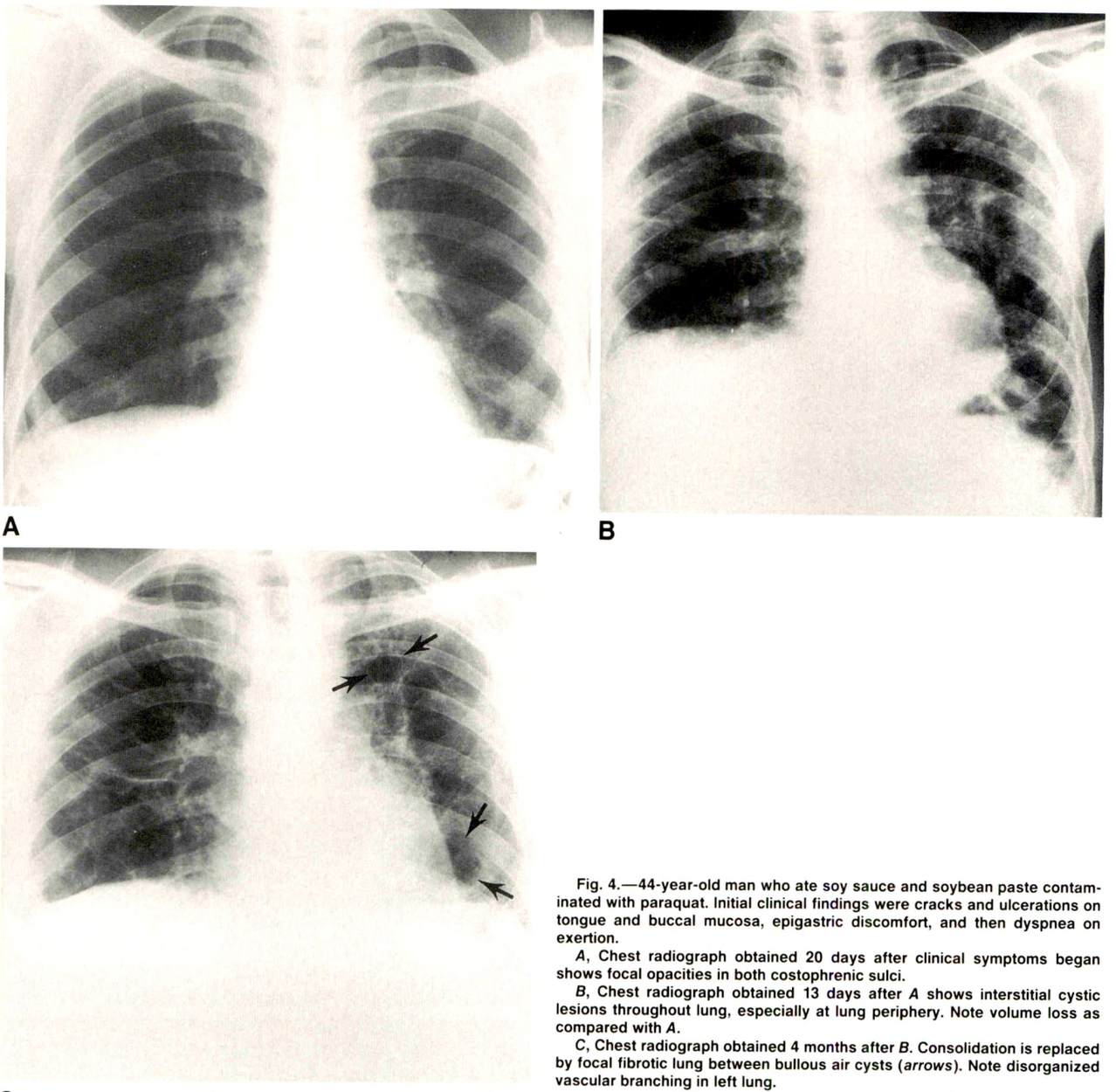


Fig. 4.—44-year-old man who ate soy sauce and soybean paste contaminated with paraquat. Initial clinical findings were cracks and ulcerations on tongue and buccal mucosa, epigastric discomfort, and then dyspnea on exertion.

A, Chest radiograph obtained 20 days after clinical symptoms began shows focal opacities in both costophrenic sulci.

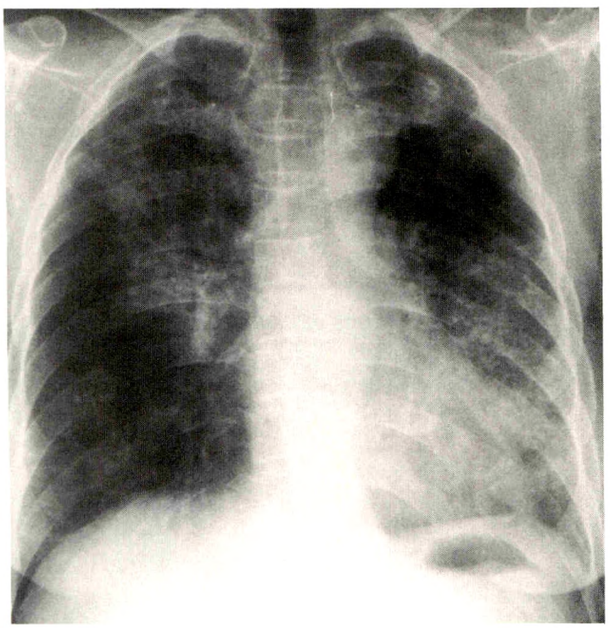
B, Chest radiograph obtained 13 days after *A* shows interstitial cystic lesions throughout lung, especially at lung periphery. Note volume loss as compared with *A*.

C, Chest radiograph obtained 4 months after *B*. Consolidation is replaced by focal fibrotic lung between bullous air cysts (*arrows*). Note disorganized vascular branching in left lung.

Combustion tests indicate that approximately 0.2% of the paraquat on marijuana passes into the inhaled smoke. In contaminated marijuana, Landrigan et al. [32] estimated that marijuana smokers could inhale up to 500 μg of paraquat per year, a dose judged to represent a health hazard. However, no cases of paraquat poisoning have been recognized among marijuana smokers.

Early symptoms after paraquat ingestion are a burning sensation in the throat, abdominal pain, vomiting, and diarrhea. The local corrosive effect of paraquat causes ulcerations on the tongue, buccal mucosa, and the esophagus [18, 26, 27]. Esophageal perforation can lead to death before pulmonary toxicity becomes manifest. The absence of caustic burns in the upper digestive tract indicates a good prognosis [19].

The radiographic signs of esophageal perforation include pneumomediastinum and subcutaneous emphysema. Pneumomediastinum suggests a poor prognosis for the patient. All 17 patients in our series and two patients in the series of Ackrill et al. [33] died within 3 days of its appearance. However, we do not have radiologic or pathologic proof that the pneumomediastinum was caused by esophageal rupture. Pneumomediastinum may result from pulmonary interstitial emphysema. However, no definite evidence of pulmonary interstitial emphysema was observed in our cases.



A



B

Fig. 5.—64-year-old woman who had repeatedly ingested small amounts of paraquat from contaminated soy sauce and soybean paste. Initial clinical findings were cracks on tongue and buccal mucosa, swallowing difficulty, and dyspnea.

***A*, Chest radiograph obtained 9 months after ingestion shows multifocal areas of honeycombing.**

***B*, High-resolution CT scan obtained 2 days after *A*. Multiple focal areas of fibrosis (*arrows*) with cystic and tubular lucencies. Surrounding lung is almost normal, except for some hyperinflation.**

In summary, the pulmonary manifestations of paraquat poisoning have a typical time course, beginning with diffuse consolidation, which evolves several days later into cystic lesions. Focal fibrotic lesions are the chronic manifestation of paraquat toxicity. Awareness of the sequential pattern on radiographs might be critical in the diagnosis of paraquat poisoning when the history of ingestion is vague.

REFERENCES

1. Campbell S. Paraquat poisoning. *Clin Toxicol* **1968**;1:245–249
2. Paraquat poisoning. *Lancet* **1971**;2:1018–1019
3. Davies DS, Hawksworth GM, Bennett PN. Paraquat poisoning. *Proc Eur Soc Toxicol* **1977**;18:21–26
4. Rebello G, Mason JK. Pulmonary histological appearance in fatal paraquat poisoning. *Histopathology* **1978**;2:53–66
5. Proudfoot AT, Stewart MS, Levitt T, Widdop B. Paraquat poisoning: significance of plasma-paraquat concentrations. *Lancet* **1979**;18:330–332
6. Howard JK. Recent experience with paraquat poisoning in Great Britain: a review of 68 cases. *Vet Hum Toxicol* **1979**;21:213–216
7. Conso F. Paraquat poisoning: experience of Poison Control Centers in France. *Vet Hum Toxicol* **1979**;21:112–113
8. Matsumoto T, Matsumori H, Kuwabara N, Fukuda Y, Ariwa R. A histopathological study of the liver in paraquat poisoning: an analysis of fourteen autopsy cases with emphasis on bile duct injury. *Acta Pathol Jpn* **1980**;30:859–870
9. Wohlfahrt DJ. Paraquat poisoning in Papua New Guinea. *P N G Med J* **1981**;24:164–168
10. Tabei K, Asano Y, Hosoda S. Efficacy of charcoal hemoperfusion in paraquat poisoning. *Artif Organs* **1982**;6:37–42
11. Bismuth C, Dally S, Schermann JM, Gaultier M, Fournier PE. Paraquat poisoning: prognostic and therapeutic evaluation in 28 patients. *Nouv Presse Med* **1982**;11:3239–3244
12. Frelon JH, Merigot P, Garnier R, Bismuth C, Efthymiou ML. Prognostic factors in acute paraquat poisoning: a retrospective study of cases registered by the Poison Control Center of Paris in 1981. *Toxicol Eur Res* **1983**;5:163–169
13. Addo E, Poon-King T. Leucocyte suppression in treatment of 72 patients with paraquat poisoning. *Lancet* **1986**;1:1117–1120
14. Ninomura N. Histopathological analysis of pulmonary findings of 40 autopsy cases in paraquat poisoning. *Nippon Kyobu Shikkan Gakkai Zasshi* **1986**;24:437–446
15. Onyon LJ, Volans GN. The epidemiology and prevention of paraquat poisoning. *Hum Toxicol* **1987**;6:19–29
16. Harsanyi L, Nemeth A, Lang A. Paraquat (gramoxone) poisoning in southwest Hungary, 1977–1984: toxicological and histological aspects of group intoxication cases. *Am J Forensic Med Pathol* **1987**;8:131–134
17. Suzuki K, Takasu N, Arita S, et al. A new method for predicting the outcome and survival period in paraquat poisoning. *Hum Toxicol* **1989**;8:33–38
18. Lee JK, Lee SH, Kim DS, Lee BC, Chon JH. Clinical observation of paraquat poisoning in 35 cases. *J Korean Med Assoc* **1989**;32:1323–1330
19. Bismuth C, Garnier R, Band FJ, Muszynski J, Keyes C. Paraquat poisoning: an overview of the current status. *Drug Saf* **1990**;5:243–251
20. Bier RK, Osborne IJT. Pulmonary changes in paraquat poisoning. *Radiology* **1978**;127:308
21. Fernando R, Harendra De Silva DG, Amarasena TS. An unusual case of fatal accidental paraquat poisoning. *Forensic Sci Int* **1990**;44:23–26
22. Thurlbeck WM, Thurlbeck SM. Pulmonary effect of paraquat poisoning. *Chest* **1976**;69:276–280
23. Bus JS, Cagen SZ, Olgaard M, Gibson JE. A mechanism of paraquat toxicity in mice and rats. *Toxicol Appl Pharmacol* **1976**;35:501–513
24. Smith LL. Mechanism of paraquat toxicity in lung and its relevance to treatment. *Hum Toxicol* **1987**;6:31–36
25. Rose MS, Lock EA, Smith LL, Wyatt I. Paraquat accumulation: tissue and species specificity. *Biochem Pharmacol* **1976**;25:419–423
26. Bullivant CM. Accidental poisoning by paraquat: report of two cases in man. *Br Med J* **1966**;1:1272–1273
27. Mattew H, Logan A, Woodruff MFA, Heard B. Paraquat poisoning-lung transplantation. *Br Med J* **1968**;3:759–763
28. Copland GM, Kolin A, Shulman HS. Fatal pulmonary intraalveolar fibrosis after paraquat ingestion. *N Engl J Med* **1974**;291:290–292
29. Vieira DN, de Azevedo-Bernarda R. Paraquat poisoning: pulmonary lesions. *J Toxicol Clin Exp* **1989**;9:177–186
30. Whalen RP. Paraquat toxicity: background report. *NY State J Med* **1978**;78:1308
31. Smith RJ. Poisoned pot becomes burning issue in high places. *Science* **1978**;200:417–418
32. Landrigan PJ, Powell KE, James LM, Taylor PR. Paraquat and marijuana: epidemiologic risk assessment. *Am J Public Health* **1983**;73:784–788
33. Ackrill A, Hasleion PS, Rakton AJ. Oesophageal perforation due to paraquat. *Br Med J* **1978**;1:1252–1253

Book Review

Management of Cardiothoracic Trauma. Edited by Stephen Z. Turney, Aurelio Rodriguez, and R. Adams Cowley. Baltimore: Williams & Wilkins, 417 pp., 1990. $69

The editors and contributing authors of this book have both individually and as a group vast hands-on experience in caring for the victims of chest trauma. They have drawn heavily on this personal, practical knowledge and on the extensive current literature on trauma to compile this compact, accessible volume. Many fine books are already available that describe various aspects of the diagnosis and treatment of trauma, but few deal exclusively with chest trauma, and fewer still focus primarily on the management of patients who have these injuries.

One of this book's strengths is that the editors have included chapters on topics that figure importantly in the management of trauma patients but that do not, strictly speaking, relate directly or exclusively to the diagnosis and treatment of thoracic injuries. The chapters that discuss the use of anesthesia in patients who have chest trauma (chapter 5), the treatment (active and prophylactic) of infections in patients with thoracic trauma (chapter 7), the place of heart-assist devices in the management of patients with chest trauma (chapter 8), and the diagnosis and treatment of tracheoinnominate artery fistula (chapter 20) are interesting and instructive and contain information of significant practical value that is rarely included in standard trauma textbooks.

Another desirable feature of this work is the detailed way in which the treatment of specific injuries is discussed. For example, one of the authors gives step-by-step instructions for the repair of aortic lacerations. He begins with the preoperative preparation of the patient and includes advice on the selection of the most appropriate incision site and on where and how to cross-clamp the aorta, and warns about what complications to watch for. Controversial aspects of therapy (e.g., the role of nonoperative, conservative management of esophageal perforation) are also discussed in a rational, balanced fashion.

This volume does have several shortcomings. Some are intentional, some are largely unavoidable, and others are simply lamentable. Because the focus of this book is the *management* of chest injuries, little space is devoted to the biomechanics and pathophysiology of thoracic wounds. This is unfortunate. These topics are intrinsically interesting, and an understanding of the basic physical and physiologic processes involved in chest trauma can provide physicians with the insights necessary to anticipate the presence of certain types of injuries in specific clinical settings. This understanding can also provide them with the knowledge necessary to treat those injuries in the most efficient and physiologically appropriate manner.

Inconsistent writing styles are a fact of life in books that have more than one author, and this book is no exception. Most of the contributors write clearly and intelligibly; others, unfortunately, do not. Algorithms seem to be an essential component of current medical texts. At times, they can help organize and give form to lengthy, complex sequences of diagnostic and therapeutic maneuvers; more often, however, they look more impressive than they are. Most of the algorithms and flow charts in this book are redundant at best and hopelessly confusing at worst. Fortunately, they do not detract significantly from the text.

The last, and to my mind the least excusable, problem with this book is the truly terrible quality of the radiographs it contains. It is abundantly clear that this volume was written for clinicians and not for radiologists, but this does not mean that the images that appear on its pages can or should be so small and so poorly selected and reproduced that they are totally uninterpretable.

I recommend this book without reservation to anyone interested in learning about the treatment of thoracic injuries. It is not, however, a comprehensive textbook of thoracic trauma. It does not contain detailed information about the biomechanics and pathophysiology of chest injuries, and despite a thorough chapter on the radiologic evaluation of chest trauma, its radiographs are of such poor quality that they are effectively worthless. Prospective buyers should be aware of the limitations and the strengths of this book and should carefully consider their specific professional needs before purchasing a copy for their libraries or offices.

Stuart A. Groskin
SUNY Health Science Center at Syracuse
Syracuse, NY 13210

Diagnosis and Localization of Laceration of the Thoracic Duct:
Usefulness of Lymphangiography and CT

Peter B. Sachs[1]
Margaret G. Zelch[1]
Thomas W. Rice[2]
Michael A. Geisinger[1]
Barbara Risius[1]
Gary K. Lammert[1]

The usefulness of lymphangiography and CT in the diagnosis and localization of laceration of the thoracic duct was evaluated in 12 patients with chylothorax or chylous ascites after surgery. Bipedal lymphangiography was performed in all 12 patients. The last four patients studied also had CT after lymphangiography. Seven patients had abnormal findings on lymphangiograms; five with leaks from the thoracic duct, one with a lymphocele in a nephrectomy bed, and one with obstructed intestinal lymphatic vessels after thoracotomy. Five patients had no evidence of lymphatic leakage. CT in one patient with evidence of a leak on lymphangiography showed extravasation of contrast medium into the mediastinum and pleural space. CT in three patients with no abnormalities on lymphangiography also showed no abnormalities. Four of the five thoracic duct lacerations and the lymphocele were confirmed surgically. The diagnosis of obstructed intestinal lymphatic vessels was supported clinically. Four of the five patients with normal findings on lymphangiograms had resolution of their pleural effusions and no evidence of recurrence during a follow-up period of 1–27 months. One patient with normal findings on lymphangiography had an alternative diagnosis established at surgery.

Laceration of the thoracic duct was accurately diagnosed and localized with lymphangiography, which allowed definitive surgical repair. CT was of little additional value in diagnosing these injuries.

AJR 157:703–705, October 1991

The prevalence of laceration of the thoracic duct ranges from an average of 0.5% to as high as 2.0% in selected series. The mortality rate in untreated postoperative chylothorax can approach 50%, and morbidity can be severe, including cardiorespiratory compromise, dehydration, nutritional deficiencies, and immunosuppression [1–10].

Because of frequent anatomic variations in the lymphatic system, precise localization before definitive surgical repair is necessary. The usefulness of lymphangiography in the evaluation of patients with suspected thoracic duct laceration was studied in 12 patients. Four of the patients had CT scanning after lymphangiography in an attempt to determine if CT is of additional value in the diagnosis and localization of lymphatic injury.

Subjects and Methods

Twelve patients were studied for possible lymphatic leakage between 1984 and 1990. The patients (nine men, three women) ranged in age from 31 to 74 years, with a mean of 60 years. All patients had undergone thoracic or abdominal surgery from 3 days to 9 months before undergoing lymphangiography. Operations performed included pulmonary lobectomy (three patients), esophagectomy (two patients), thoracic or abdominal aneurysm repair (two patients), pneumonectomy, thoracotomy for mediastinal lymph node resection, pleurodesis,

Received April 11, 1991; accepted after revision May 10, 1991.

[1] Department of Diagnostic Radiology, The Cleveland Clinic Foundation, One Clinic Ctr., 9500 Euclid Ave., Cleveland, OH 44195-5103. Address reprint requests to M. G. Zelch.

[2] Department of Thoracic and Cardiovascular Surgery, The Cleveland Clinic Foundation, One Clinic Ctr., 9500 Euclid Ave., Cleveland, OH 44195-5066.

0361–803X/91/1574–0703
© American Roentgen Ray Society

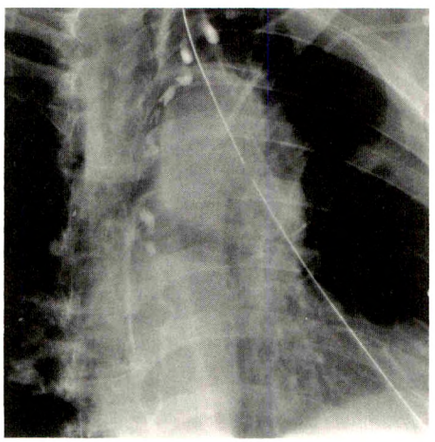


Fig. 1.—Lymphangiogram of 58-year-old man with pleural effusion after left lung lobectomy shows a normal thoracic duct.

dissection of the left side of the neck, and nephrectomy. Clinical presentations included chylothorax (six patients), chylous ascites (two patients), and milky, nonchylous pleural effusions (four patients).

Lymphangiography was performed according to the technique described by Clouse and Wallace [11]. After cannulation of a lymphatic vessel on the dorsum of each foot, 7–10 ml of ethiodized oil, followed by 7–10 ml of saline, was injected into each lower extremity. If only one lymphatic channel could be cannulated, 10–15 ml of contrast material and 10–15 ml of saline were injected via that extremity. A frontal view of the pelvis and frontal and lateral views of the abdomen and chest were obtained approximately 1–2 hr after injection. Additional radiographs were obtained until the thoracic duct had been seen in its entirety and no leak was identified, or as needed to establish the presence, location, and size of a leak. Additional projections also were obtained as needed. All radiographs were reviewed by two radiologists independently. At least one of the radiologists had no clinical information when the study was reviewed. A leak was defined as a collection of contrast medium outside the confines of normal lymphatic channels that enlarged over time.

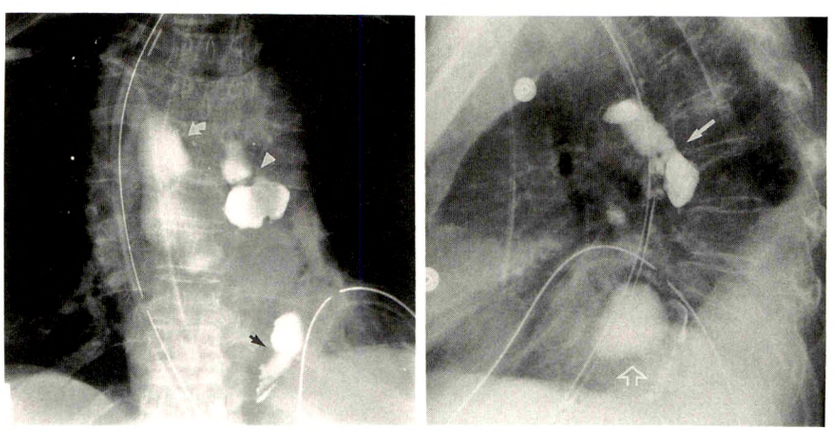
In the last four patients studied, CT scans of the chest without oral or IV contrast material were obtained immediately after lymphangiography was completed. Serial axial scans through the entire chest of contiguous 10-mm slices were obtained. The scans were interpreted independently by at least two radiologists. At least one of the radiologists was unaware of the results of lymphangiography when the CT scan was reviewed.

Six of the 12 patients had surgery after the imaging studies were completed. The remaining six patients were followed up clinically for 1–27 months, with a mean follow-up of 11 months.

Results

Twelve lymphangiograms were obtained in 12 patients. No lymphatic leakage was identified in five of the 12 patients (Fig. 1). A leak from the thoracic duct was seen in five of the 12 patients (Figs. 2 and 3). A lymphocele in a nephrectomy bed was identified in one patient. In the last patient, although no leak was seen, lymphangiographic evidence of lymphatic obstruction explained the patient's chylous ascites. Both reviewers agreed on the results of lymphangiography in all cases. No complications occurred after lymphangiography in any of the 12 patients.

The thoracic duct was ligated in four of the five patients with lymphangiographic evidence of a leak. The site of leakage as determined by lymphangiography was found to be correct in all four cases when the leak was surgically repaired. None of the four had recurrence of chylothorax after surgery. The fifth patient with a documented leak had spontaneous resolution of his chylothorax after lymphangiography and died 11 months later without recurrence of the chylothorax. The presence of a lymphocele in a postnephrectomy patient was confirmed during exploratory laparotomy. The patient died 1 month later of unrelated causes. The patient with evidence of



A B

Fig. 2.—Thoracic duct laceration in 68-year-old woman with chylothorax after esophagectomy.
A, Anteroposterior lymphangiogram shows extravasation of contrast medium from thoracic duct (*arrowhead*) with accumulation in mediastinum (*curved arrow*) and pleural space (*black arrow*).
B, Lateral lymphangiogram again shows extensive leakage from thoracic duct (*solid arrow*) and contrast medium accumulating in pleural space posteriorly (*open arrow*).

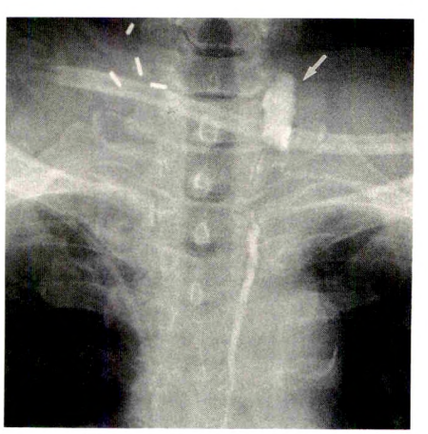


Fig. 3.—Thoracic duct laceration in an unusual location in a 65-year-old woman with left-sided chylothorax after dissection of left side of neck. Anteroposterior lymphangiogram shows leakage from apex of thoracic duct (*arrow*).

intestinal lymphatic obstruction as the cause of his chylous ascites required repeated paracenteses until his death 27 months after diagnosis.

Of the five patients in whom no leak was shown, the pleural effusions resolved spontaneously in two, after multiple thoracenteses in one, after pleurodesis in one, and after repair of a postgastroplasty anastomotic leak in one. None of these patients had recurrence of the effusion during follow-up periods of 1–27 months (mean, 11 months).

CT confirmed the lymphangiographic results in three patients without lymphangiographic evidence of a leak. CT was performed in only one patient with a lymphangiographically documented leak and confirmed the presence of a leak. In addition, it verified that the leak communicated with the pleural space.

Discussion

Thoracic duct laceration has been reported after a variety of percutaneous and surgical procedures. Translumbar aortography has been reported to cause chylothorax in 0.15% of cases [1]. Esophagectomy (0.5–0.9% prevalence) [2]; repair of congenital cardiac defects such as ventricular septal defect, anomalous pulmonary venous return, patent ductus arteriosus, and coarctation (0.2–0.5%) [3]; pneumonectomy [4]; gastrectomy [5]; thoracic aneurysm repair [6]; valve replacement [7]; and coronary bypass surgery [8] have all resulted in chylothorax.

The nature of the fluid can be determined by analysis of triglyceride content and an electrophoretic pattern characteristic of chylomicrons [2]. Initial therapeutic maneuvers include repeated thoracenteses, thoracostomy drainage, pleurodesis, and thoracic duct rest. Total parenteral nutrition and a diet of medium-chain triglycerides may reduce the flow of lymph. If these interventions fail or, as is the case with most of the patients in our series, lymphatic leakage persists despite the presence of a chest tube or surgical drain, surgical ligation must be undertaken [2, 4, 5, 6, 10]. A number of imaging techniques have been used to diagnose and localize thoracic duct laceration. Direct visualization at surgery via ductography or injection of dye into the esophagus is possible but is time-consuming and results in bothersome staining of tissues in the surgical field [12]. CT scanning may provide indirect evidence of leak, with visualization of low-density fluid collections [13]. Recently, a technique has been described for opacification of the thoracic duct after the oral ingestion of ethiodized oil for CT scanning [14]. Nuclear lymphangiography may be useful in selected cases [15].

However, thoracic duct anatomy varies considerably, and two or more main ducts are present in up to 50% of patients [4]. Thus, lymphangiography allows precise anatomic localization before definitive repair. Additionally, it helps exclude those with false-positive chylous effusions due to esophageal or gastric leaks, such as our patient with an anastomotic leak after gastroplasty [2]. In all cases in this series, the lymphangiographic findings were confirmed either surgically or clinically.

Concurrent CT scanning has not proved to be useful in our limited experience. Although the lymphangiographic findings were confirmed in all four patients who had CT scans, the scans added no additional information. If enough serial chest radiographs are obtained during lymphangiography, the precise level of the leak can be determined from the radiographs. Similarly, in no case was a lymphangiogram with normal findings found to be falsely normal by subsequent CT. Although a technique has been described for direct opacification of the thoracic duct for CT scanning alone, our surgeons find the multiplanar spatial localization allowed by lymphangiography to be preferable. Additionally, many postoperative patients are not candidates for the oral ingestion of ethiodized oil and a 50% fat emulsion as required by CT [14].

Although some of the five patients with normal findings may actually have had leaks that were not detected by lymphangiography, all had resolution of their effusion or chylothorax without surgery. Thus, a lymphangiogram that shows leakage appears to identify patients with a large leak who will probably require surgical intervention. This is supported by the two patients with abdominal lymphatic abnormalities as documented by a lymphangiogram suggesting leakage. Neither had resolution of their leak with conservative therapy.

Lymphangiography remains the imaging procedure of choice in the diagnosis and localization of thoracic duct laceration.

ACKNOWLEDGMENT

The authors acknowledge Chris Turay for assistance in preparation of the manuscript.

REFERENCES

1. Edixhoven PJ, Sluzewski H. Chylothorax following "high" translumbar aortography. *Neth J Surg* **1980**;32:167–170
2. Lam H, Lim STK, Wong J, Ong GB. Chylothorax following resection of the oesophagus. *Br J Surg* **1979**;66:105–109
3. Higgins CB, Mulder DG. Chylothorax after surgery for congenital heart disease. *J Thorac Cardiovasc Surg* **1971**;61:411–418
4. Van Mulders A, Lacquet LM, Van Mieghem W, Deneffe G. Chylothorax complicating pneumonectomy. *Thorax* **1984**;39:954–955
5. Van Der Vliet JA, Van Der Linden CJ, Greep JM. Chylothorax after gastric resection. *Neth J Surg* **1985**;37:16–19
6. Servelle M, Nogues C, Soulie J, Andrieux JB, Terhedebrugge R. Spontaneous, post-operative and traumatic chylothorax. *J Cardiovasc Surg* **1980**;21:475–486
7. Joyce LD, Lindsay WG, Nicolott DM. Chylothorax after median sternotomy for intrapericardial surgery. *J Thorac Cardiovasc Surg* **1976**;71:476–480
8. Czarnecki DJ, Kehoe ME, Tector AJ. Lymphangiographic evaluation of chylothorax after myocardial revascularization. *AJR* **1988**;151:1054–1055
9. Cevese PG, Vecchioni R, D'Amico DF, et al. Postoperative chylothorax. *J Thorac Cardiovasc Surg* **1975**;69:966–971
10. Ngan H, Fok M, Wong J. The role of lymphography following thoracic surgery. *Br J Radiol* **1988**;61:1032–1036
11. Clouse ME, Wallace S. *Lymphatic imaging: lymphography, computed tomography and scintigraphy*, 3rd ed. Baltimore: Williams & Wilkins, **1985**:111–119
12. Heilman RD, Collins VP. Identification of laceration of the thoracic duct by lymphangiography. *Radiology* **1963**;81:470–472
13. Watanabe AT, Jeffrey RB. CT diagnosis of traumatic rupture of the cisterna chyli. *J Comput Assist Tomogr* **1987**;11:175–176
14. Day DL, Warwick WJ. Thoracic duct opacification for CT scanning. *AJR* **1985**;144:403–404
15. Rice TW, Kirsh JC, Schachter IB, Goldberg M. Simultaneous occurrence of chylothorax and subarachnoid pleural fistula after thoracotomy. *Can J Surg* **1987**;30:256–258

AJR

AMERICAN JOURNAL OF ROENTGENOLOGY

MELVIN M. FIGLEY FELLOWSHIPS IN RADIOLOGY JOURNALISM 1992

The American Roentgen Ray Society announces two one-month fellowships in radiology journalism in the La Jolla editorial office of the AJR. Board-certified radiologists with special academic promise are invited to apply.

PURPOSE

The purpose of the fellowship is (1) to stimulate bright young radiologists to continue with an academic career, to accelerate their progress, and to stimulate their interest in good radiology journalism and (2) to improve the quality of radiology journals by teaching the fundamentals of medical journalism to academicians, training manuscript reviewers and future editors, and providing core teachers of medical journalism in radiology departments around the country.

CURRICULUM

The fellows will be taught the fundamentals of medical writing, manuscript preparation, peer review, manuscript editing, the ethics of scientific journalism, and journal publication and printing in personal tutorials given by the AJR editors and editorial staff through hands-on experience in the editorial office. They will visit Williams & Wilkins in Baltimore to observe the publication and printing process.

STIPEND

The successful candidates will each be awarded $10,000, which includes the cost of travel to La Jolla and Baltimore, living expenses for the month, and an honorarium.

APPLICATIONS

Candidates should apply in writing to Robert N. Berk, M.D., Editor-in-Chief, AJR Editorial Office, 2223 Avenida de la Playa, Suite 103, La Jolla, CA 92037. The letter must include a curriculum vitae and a description of the candidate's goals during the fellowship. Letters of recommendation from his or her department chairman and one other senior person are required. Deadline for receipt of applications is Nov. 1, 1991. The successful candidates will be notified Dec. 2, 1991.

Pictorial Essay

Normal Anatomy of the Thoracic Inlet as Seen on Transaxial MR Images

Birgit im Spring[1] and Mark L. Schiebler[1,2]

The thoracic inlet can now be studied with high-resolution MR imaging. Recent advances in fold-over suppression (antialiasing software) allow for small fields of view without the usual problems of aliasing from the shoulders. This pictorial essay shows the normal anatomy that can be seen in this area on transaxial MR images. The vagus, phrenic, and recurrent laryngeal nerves can be seen as discrete entities. MR imaging can be used more often for pathologic conditions involving the lower portion of the neck and the thoracic inlet.

MR imaging has been used often to evaluate the brachial plexus, lower portion of the neck, and upper portion of the thorax [1–6]. MR imaging has become an important technique for the evaluation of the thoracic inlet for four major reasons. First, it provides excellent soft-tissue contrast. Second, it has multiplanar capabilities. Third, MR imaging is free from beam-hardening artifacts from the shoulders that limit CT in this area. Last, with gradient-echo (GRE) techniques, MR imaging can be used to evaluate the vascular anatomy of the thoracic inlet [7]. With the introduction of 10-mT/m gradient coils and newer antialiasing software, routine high-quality images of the brachial plexus and thoracic inlet can be obtained with the send-receive body coil. This pictorial essay illustrates the normal transverse anatomy of the thoracic inlet with special attention to the small nerves and arteries in this important region. Other planes are not depicted because of the problem of volume averaging of adjacent structures with these small nerves. There is anatomic variation in patients, and some

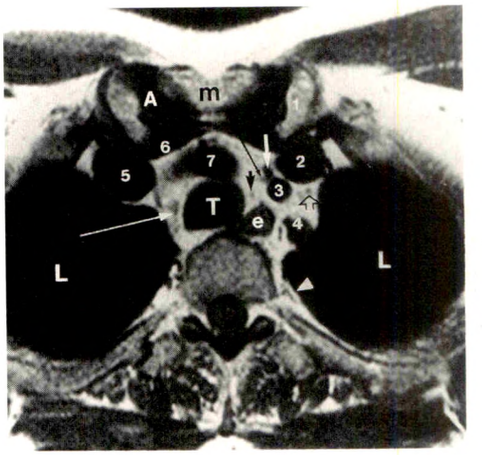


Fig. 1.—Level of manubrioclavicular junction. Transaxial MR image (SE 600/20, 3 mm thick, four excitations, 205 × 256 matrix) at level of manubrium (m) and clavicular articulation (A). Left clavicular head (1) and left brachiocephalic vein (2) are seen anterior to left common carotid artery (3) and left subclavian artery (4). Thyrocervical trunk (*short white arrow*) is seen anterior to left common carotid artery. Right brachiocephalic vein (5) lies posterior to insertion of sternohyoid muscle (6) on posterior aspect of manubrium. Probable site of left vagus nerve (*long solid black arrow*) is in carotid sheath medial to left common carotid artery. Immediately anterior to trachea (T) lies brachiocephalic artery (7). Left sympathetic ganglion (*arrowhead*) is seen next to the costovertebral junction. Lung cupulae (L) are seen as regions totally devoid of signal. Esophagus (e) also can be seen. Probable site of left phrenic nerve (*open black arrow*) can be seen posterior to left brachiocephalic vein (2). Probable site of right vagus nerve (*long white arrow*). Left recurrent laryngeal nerve (*short black arrow*).

Received February 11, 1991; accepted after revision May 10, 1991.

[1]Department of Radiology, University of North Carolina at Chapel Hill, CB 7510, Chapel Hill, NC 27599-7510.

[2]Present address: Division of Magnetic Resonance Imaging, Department of Radiology, Hospital of the University of Pennsylvania, 3400 Spruce St., Philadelphia, PA 19104.

AJR **157:707–710, October 1991** 0361–803X/91/1574–0707 © American Roentgen Ray Society

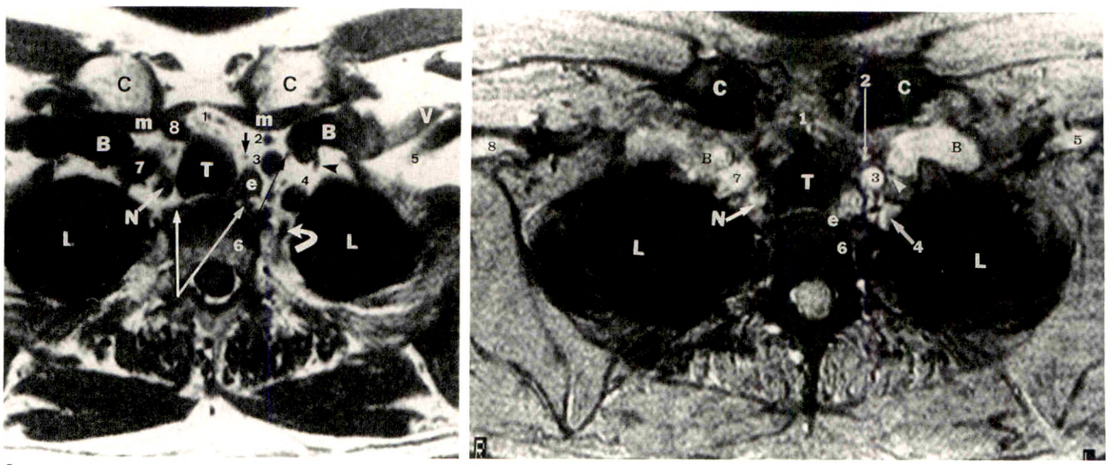


Fig. 2.—Level of sternal notch.

A, MR image (SE 600/20, 3 mm thick, four excitations, 205 × 256 matrix) at sternal notch. Cupulae of lungs (L) can be seen easily along with heads of both clavicles (C). Right paratracheal lymph node (N) may be seen at this level between trachea (T) and right subclavian artery (7). Brachiocephalic veins (B) are formed from junction of subclavian veins and internal jugular veins. Sternohyoid muscles (m) are seen anterior to inferior thyroid vein (1). Probable site of left inferior thyroid artery can be appreciated (2), along with left common carotid artery (3) and left subclavian artery (4). Probable site of left recurrent laryngeal nerve (*short black arrow*) and posterior aspect of thoracic duct (*curved white arrow*) are also seen. Note juxtaposition of axillary artery (5) and vein (V) in fatty tissues of left axilla. Probable site of left vagus nerve (6) is between left common carotid artery and left brachiocephalic vein. Note how this nerve has moved laterally at this more superior level because carotid sheath is now in a more lateral location. Right subclavian artery (7) lies just posterior to right brachiocephalic vein. Right common carotid artery (8) lies just posterior to sternohyoid muscles. Note anterior insertion at thoracic duct into left brachiocephalic vein (*arrowhead*). Longus colli muscles (*long straight white arrows*) are small at this level.

B, Axial MR flow image (GRE 958/15/30°, 5 mm thick, two excitations, 128 × 256 matrix) shows GRE appearance of same level shown in *A*. Heads of clavicles (C), inferior thyroid vein (1), and thyrocervical trunk (2) can be seen, along with left common carotid artery (3) and left subclavian artery (4). Left axillary artery (5), left side of vertebral body (6), and right subclavian artery (7) are seen. Probable site of left vagus nerve is also seen between left brachiocephalic vein and left common carotid artery (*arrowhead*). Because of intrinsically long T2* times of esophageal mucosa (e) and lymph nodes (N), these structures also appear as high-signal regions on this T2*-weighted image. Right axillary artery (8) lies in fat of axilla. Trachea (T), brachiocephalic veins (B), and lungs (L) can be seen.

major vessels and nerves may not be seen exactly at the same levels depicted on this pictorial essay.

Materials and Methods

All images are from a conventional 1.5-T Philips Gyroscan MR imaging device. Spin-echo (SE) images (e.g., 600/20 [TR/TE]) and GRE images (e.g., 958/15/30° [TR/TE/flip angle]) were obtained. The slice thickness varied from 3 to 5 mm. The number of excitations varied from two to four. The field of view was 270 mm. This imager was equipped with 10-mT/m gradients. Presaturation pulses were used to decrease any contaminating in-flow enhancement from unsaturated blood flowing into the imaging plane. The imaging matrix varied from 128 to 205 × 256. No contrast material was used to highlight the flowing blood on the GRE images.

These MR images were all from one patient. Each of the anatomic structures in this essay was identified by comparing these MR images with photographs of cryosections and drawings of the neck and thoracic inlet regions from an atlas [8]. Because these MR images were not from a cadaver with corresponding cryotome anatomic sections, the exact identification of these small nerves could not be proved with certainty.

Results

Manubrioclavicular Junction

At this level, the brachiocephalic artery in this patient lies directly anterior to the trachea (Fig. 1). The left carotid and

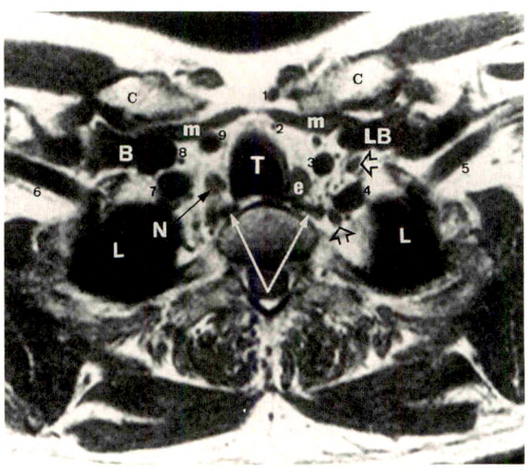


Fig. 3.—Level of thoracic duct. Transaxial MR image (SE 600/20, 3 mm, four excitations, 205 × 256 matrix) shows left anterior jugular vein (1) separated from small left inferior thyroid vein (2) by sternohyoid muscle (m). Left common carotid artery (3) is anterior and medial to left subclavian artery (4). Junction of left internal jugular vein with left subclavian vein forms proximal left brachiocephalic vein (LB). Axillary vein is anterior and runs parallel to left axillary artery (5). Right axillary artery (6) and right subclavian artery (7) are posterior to right brachiocephalic vein (B). Right paratracheal lymph node (N) is seen at this level along with esophagus (e). Cupulae of both lungs are seen as well (L). Right inferior thyroid vein (8), right common carotid artery (9), and thoracic duct (*open arrows*) also are seen. Longus colli muscles are now well seen (*long white arrows*). C = clavicle, T = trachea, B = junction of right subclavian vein with right internal jugular vein to form proximal portion of right brachiocephalic vein.

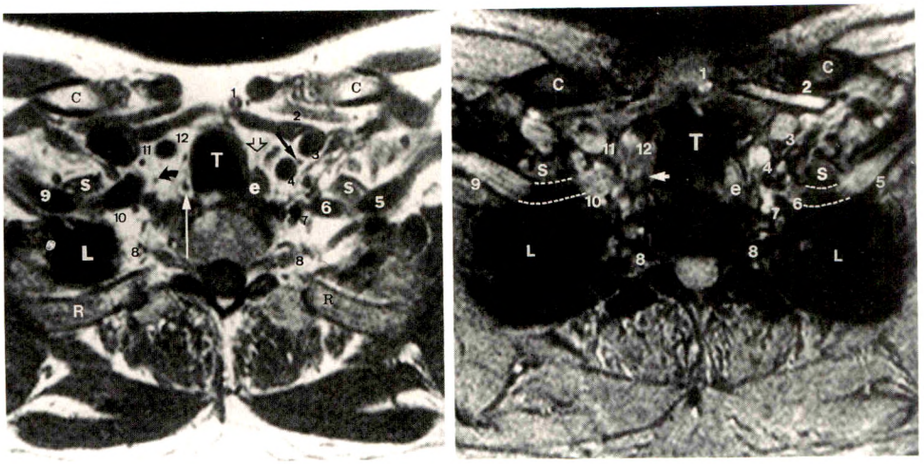


Fig. 4.—Thoracic inlet.

A, Transaxial MR image (SE 600/20, 3 mm, four excitations, 205 × 256 matrix) shows second rib (R), esophagus (e), and left recurrent laryngeal nerve (*open arrow*). Vessels seen at this level include left anterior jugular vein (1), left jugular venous arch (2), left internal jugular vein (3), left common carotid artery (4), third part of left subclavian artery (5), proximal left subclavian artery (6), left vertebral artery origin (7), T2 nerve root ganglia (both right and left) (8), third part of right subclavian artery (9), proximal right subclavian artery (10), right internal jugular vein (11), and right common carotid artery (12). Probable sites of normal right inferior parathyroid gland (*white arrow*) and of left vagus nerve in carotid sheath (*straight solid black arrow*) are shown. Probable site of right recurrent laryngeal nerve is just medial to subclavian artery (*curved arrow*). C = clavicle, S = anterior scalene muscle, T = trachea, L = lung.

B, Field-echo MR image at thoracic inlet shows left anterior jugular vein (1), left jugular venous arch (2), left internal jugular vein (3), left common carotid artery (4), third portion of left subclavian artery (5), proximal left subclavian artery (6), left vertebral artery (7), T2 nerve root ganglia (8), third portion of right subclavian artery (9), and proximal right subclavian artery (10). Right brachiocephalic vein (11) and right common carotid artery (12) are also seen. Lung cupulae appear much larger on field-echo images than on routine spin-echo images (*A*) owing to magnetic susceptibility difference between air in lung and protons of apical thoracic soft tissue. Nonvisualized course of subclavian artery is highlighted by *broken white lines*. Probable site of normal right inferior parathyroid gland is of low signal intensity on this image (*arrow*). C = clavicle, S = anterior scalene muscle, T = trachea, L = lung, e = esophagus.

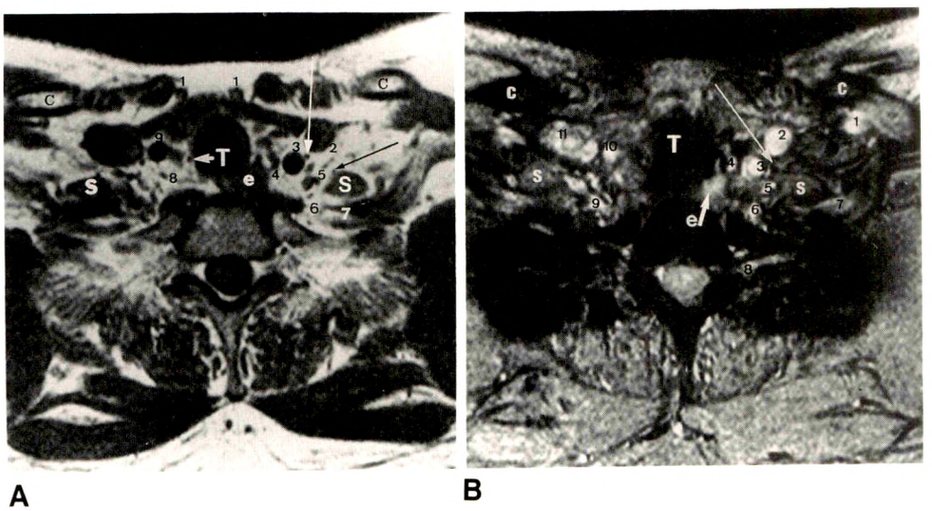


Fig. 5.—Level of costovertebral junction of first rib.

A, Transaxial MR image (SE 600/20, 3 mm, four excitations, 205 × 256 matrix) shows right and left anterior jugular veins (1); left internal jugular vein (2); left common carotid artery (3); left inferior thyroid artery (4); left thyrocervical trunk (5); left vertebral artery (6); left subclavian artery, second portion (7); right inferior thyroid artery (8); and right common carotid artery (9). Probable site of left phrenic nerve is immediately anterior to anterior scalene muscle (*black arrow*), and probable site of right recurrent laryngeal nerve is just lateral to trachea (*short white arrow*). Probable site of left vagus nerve is between left jugular vein and left common carotid artery (*long white arrow*). Clavicle (C), anterior scalene muscle (S), trachea (T), and esophagus (e) are seen also.

B, Transaxial MR flow image (968/15/30°, 5 mm thickness, two excitations, 128 × 256 matrix) shows vessels with a high signal intensity: left external jugular vein (1), left internal jugular vein (2), left common carotid artery (3), left inferior thyroid artery (4), left thyrocervical arterial trunk (5), left vertebral artery (6), third portion of left subclavian artery (7) immediately posterior and lateral to anterior scalene muscle (S), CSF surrounding nerve root sheath of left first thoracic nerve root ganglion (8), right vertebral artery (9), right common carotid artery (10), and right internal jugular vein (11). Note that esophagus (e) is also of high signal intensity because of presence of mucosal water and an increase in its T2* time compared with surrounding tissues. *Long white arrow* shows probable site of left vagus nerve to be of low signal intensity, proving that this is not a vascular structure. C = clavicle, T = trachea.

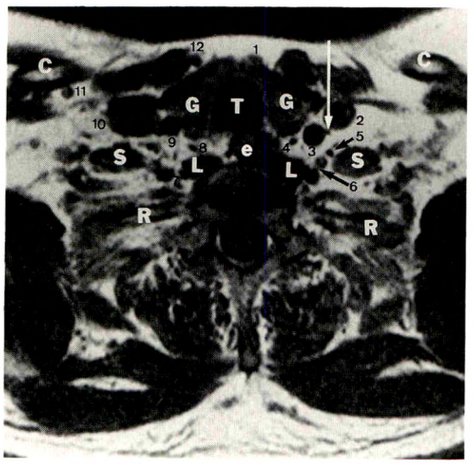


Fig. 6.—Level of C7–T1 disk space. Transaxial MR image (SE 600/20, 3 mm, four excitations, 205 × 256 matrix) shows medial aspect of sternohyoid muscle (1) anterior to thyroid gland (G). Left internal jugular vein (2) and left common carotid artery (3) are surrounded by fat. Probable site of left vagus nerve lies between these two structures (*white arrow*). Left inferior thyroidal artery (4) can be seen anterior to left longus colli muscle (L) along with left thyrocervical trunk (5), which is anterior to anterior scalene muscle (S). Left vertebral artery and vein are paired structures at this level (6) (*long black arrow* points between them; artery is posterior and medial to vein). Right vertebral artery (7) is small in this patient. Right inferior thyroidal artery (8) is anterior to right longus colli muscle and lateral to esophagus (e). Right common carotid artery (9) is adjacent to large right internal jugular vein (10). Right external jugular vein (11) and right anterior jugular vein (12) are seen also. Superior aspect of this patient's first ribs are seen (R). C = clavicle, T = trachea.

subclavian arteries are seen at approximately the 2 and 4 o'clock positions with respect to the trachea. Directly anterior to the left common carotid artery is the left brachiocephalic vein. The origin of the left thyrocervical trunk is seen arising from the left common carotid artery. The vagus, phrenic, and recurrent laryngeal nerves also can be seen.

Sternal Notch

The brachiocephalic artery has bifurcated into the right subclavian artery and the right common carotid artery (Fig. 2). The longus colli muscles anterior to the vertebral bodies are small and diminutive. At this level, the axillary artery is parallel to the axillary vein. The brachiocephalic veins are being formed by the junction of the internal jugular and subclavian veins. The thoracic duct also can be appreciated.

Level of Thoracic Duct

At this level, the thoracic duct can be seen on high-resolution MR images along with the axillary artery and vein (Fig. 3). The anterior jugular vein is seen anterior to the strap muscles.

Level of Thoracic Inlet

This is a very important level because of the possibility of the scalenus anticus syndrome (Fig. 4). Fast field echoes at this level cause in-plane saturation of the horizontal portions of the subclavian artery and axillary artery, and so the horizontal portions of those vessels are shown less well with GRE techniques. The jugular venous arches and the origin of the left vertebral artery can be seen at this level.

Level of First Rib

This level is important because of the relationship of the anterior scalene muscle and the subclavian artery (Fig. 5). Directly anterior to the vertebral artery and vein lies the thyrocervical trunk. Also, the phrenic nerve can be seen anterior to the anterior scalene muscle at this level. The vagus nerve runs between the left common carotid artery and the left internal jugular vein.

C7–T1 Disk Space

At this level, the loops of the left thyrocervical trunk are seen just anterior to the anterior scalene muscle (Fig. 6). The nondominant right vertebral artery also is seen.

REFERENCES

1. Swensen St J, Ehman RL, Brown LR. Magnetic resonance imaging of the thorax. *J Thorac Imaging* **1989**;4:19–33
2. Stark DD, Moss AA, Gamsu G, Clark OH, Godding GAW, Webb WR. Magnetic resonance imaging of the neck. Part I: Normal anatomy. *Radiology* **1984**;150:447–454
3. Stark DD, Moss AA, Gamsu G, Clark OH, Godding GAW, Webb WR. Magnetic resonance imaging of the neck. Part II: Pathologic findings. *Radiology* **1984**;150:455–462
4. Blair DN, Rapaport ST, Sostman HD, Blair OC. Normal brachial plexus: MR imaging. *Radiology* **1987**;165:673–677
5. Vock P, Owens A. Computed tomography of the normal and pathological thoracic inlet. *Eur J Radiol* **1982**;2:187–193
6. Zylak CJ, Pallie W, Pirani M, Wandtke JC, Kothari K. Anatomy and computed tomography: a correlative module on the cervico-thoracic junction. *RadioGraphics* **1983**;3:478–530
7. Spritzer C, Gamsu G, Sostman D. Magnetic resonance imaging of the thorax: techniques, current applications, and future directions. *J Thorac Imaging* **1989**;4:1–18
8. Cahill DR, Orland MJ, Reading CC, eds. *Atlas of cross-sectional anatomy: with CT and MR images*, 2nd ed. New York: Wiley-Liss, **1990**:3–9

Localization and Needle Aspiration of Breast Lesions:
Complications in 370 Cases

Mark A. Helvie[1]
Debra M. Ikeda
Dorit D. Adler

A prospective study of the immediate complications of 370 consecutive breast-imaging procedures (203 wire localizations and 167 radiographically or sonographically guided fine-needle aspirations) is reported. Vasovagal reactions occurred in 27 (7%) of 370 cases, ranging in severity from syncope (four of 370, 1%) to mild light-headedness. These vasovagal reactions were independent of procedure type or use of local anesthesia, but were more common in younger patients. Other complications included prolonged (5 min or longer) bleeding (three of 370, 1%) and extreme pain (two of 370, 1%). One patient was found to have malignant hypertension.

We conclude that wire localizations and imaging-guided aspirations are generally well tolerated procedures. However, vasovagal reactions are frequent enough to warrant close observation of patients. Radiologists and breast-imaging personnel should be able to recognize and treat vasovagal reactions.

AJR 157:711–714, October 1991

Preoperative wire localization of impalpable breast lesions is a widely practiced procedure that is an integral component in the early detection of breast carcinoma. Image-directed fine-needle aspiration of breast lesions also is commonly used. Although these procedures are generally considered safe and well tolerated, few studies have documented the frequency of immediate complications resulting from such procedures. We report the results of a prospective study to determine the type and frequency of immediate complications associated with invasive breast-imaging procedures.

Subjects and Methods

Immediate complications of mammographic procedures were studied prospectively for 12 months (October 1989–October 1990). We performed 370 procedures, including 203 preoperative wire localizations and 167 radiographically or sonographically guided fine-needle aspirations. Various methods for wire localizations and fine-needle aspiration were used during the study period (Table 1), and each of the radiologists performing the procedure was free to determine which method was used.

Wire localizations were performed by using either coordinate-grid [1] or stereotactic [2] radiographically guided methods, freehand methods [3], or rarely by using sonographic guidance [4]. Patients were seated for all radiographically guided procedures and for some freehand wire localizations. They were supine for other freehand or sonographically guided placement. All wire localizations were performed with either a 21-gauge spring hookwire (Kopans Spring Hookwire, Cook, Bloomington, IN) or a curved-end retractable wire (Homer Mammalok, Namic, Glens Falls, NY). A dedicated mammography processor requiring 3.5 min to develop radiographs was used. Mammographic procedures were performed with a General Electric 500T or 600T (equipped with stereotactic adaptor, Columbia, MD). A Hitachi 310EUB (Hitachi Medical Corp., Tokyo, Japan) real-time sonographic unit with a 7.5-MHz linear transducer was used for all sonographically directed procedures.

Fine-needle aspiration was most frequently used to evaluate impalpable, low-suspicion nodules detected by mammography that were not simple cysts on sonography. Occasionally

Received February 25, 1991; accepted after revision May 15, 1991.

[1] All authors: Department of Radiology, University of Michigan Medical Center, 1500 E. Medical Center Dr., Rm. TC2910, Ann Arbor, MI 48109-0326. Address reprint requests to M. A. Helvie.

0361–803X/91/1574–0711
© American Roentgen Ray Society

fine-needle aspiration was used also for suspicious mammographic lesions to provide material for preoperative cytology. Positioning of the patient and approaches were similar to those used for wire localizations [5–7]. Freehand aspirations of palpable lesions were excluded from this study. All aspirations were done with standard 22-gauge beveled needles. Four passes were routinely made for each lesion unless cystic fluid was obtained, in which case a single pass was made and a pneumocystogram was attempted.

Local anesthesia (lidocaine 1% administered with a 27-gauge needle) was used at the discretion of the attending radiologist for both wire localization and fine-needle aspiration. Fifty-three percent (196/370) of the women received local anesthesia.

Wire localizations were done in the morning, with the women having been instructed not to eat before surgery. Patients undergoing fine-needle aspiration were not given specific dietary instructions and were scheduled for the late morning or afternoon. On entering the mammographic suite, patients were greeted by a registered nurse who obtained an initial blood pressure measurement and answered questions. A radiologist then explained the procedure and began the examination. While waiting for film processing, the nurse or physician remained in the room, conversing with and observing the patient. Tabulated procedural data included the type and length of examination, use of local anesthesia, type of immediate complication (if any), and whether the procedure was prematurely terminated. Complications recorded included bleeding, extreme pain, vomiting, abnormal blood pressure, and vasovagal (vasodepressor) reactions that ranged from mild light-headedness to syncope. The radiologist performing the examination documented all complications. All documented vasovagal reactions required interruption of procedure and/or treatment of the patient. Minimal symptoms, such as light-headedness that did not require treatment, were not formally considered a complication. Patients were never unattended until they were discharged from the breast-imaging clinic.

Results

The women ranged in age from 28 to 92 years (median, 55 years). The median time for all procedures was 28 min (range, 5–110 min). Fine-needle aspirations (median time, 25 min) were minimally faster than wire localization (median time, 30 min). The number and type of immediate complications for the various breast procedures are listed in Table 1. Vasovagal reactions were the most common untoward event, occurring in 27 procedures (7%). The severity of these reactions varied from frank syncope (four women, 1%) to mild light-headedness. Initial blood pressure measurement did not help predict those patients who would experience syncope, because all readings were normal in this group. The four women with syncope ranged in age from 37 to 63 years (mean, 47 years). Two women experienced syncope while the breast was being compressed, even before the needle was inserted. The third woman fainted after the first pass, and the fourth fainted at the completion of fine-needle aspiration. Procedures were terminated prematurely in two additional women undergoing fine-needle aspiration because of vasovagal reactions (without syncope). Hence, a total of five (1%) of 370 procedures were terminated prematurely because of vasovagal reactions. The 22 remaining women who had vasovagal reactions improved clinically after supportive treatment, allowing completion of the procedure.

The age of the 23 women with mild vasovagal reactions without syncope (median, 49 years) was slightly younger than that for the study population as a whole (median, 55 years). Two of these women had low initial blood pressure measurements (94/62 and 98/62 mm Hg, respectively) that were considered their normal baseline.

The use of local anesthesia did not affect the frequency of vasovagal reactions. Fifty-six percent of 27 women who had vasovagal reactions had received local anesthesia, similar to 53% of the total study population also given anesthesia. No patient with frank syncope had been given local anesthesia.

The frequency of vasovagal reactions generally paralleled the frequency of procedure type (Table 2). All 27 vasovagal reactions were treated in the breast-imaging clinic with simple supportive measures, including placing the patient supine and elevating her legs. In no case was there a need for IV fluid, medications, or referral to the emergency department. Even the women experiencing frank syncope responded rapidly to such supportive measures. All fainting episodes were recognized by the breast-imaging staff, and no patient was injured as a result of a fall.

TABLE 1: Procedure Type vs Complications in 370 Cases

Procedure	Complications					
	None (n = 335)	Vasovagal (n = 27)	Bleeding (n = 3)	Pain (n = 2)	Other[a] (n = 3)	Total (n = 370)
Wire localizations (n = 203)						
Coordinate grid	157	12	1	2	1	173
Freehand	15	1	1	0	0	17
Stereotactic	9	2	0	0	0	11
Sonographic	2	0	0	0	0	2
Fine-needle aspirations (n = 167)						
Coordinate grid	98	7	0	0	2	107
Stereotactic	41	4	0	0	0	45
Sonographic	13	1	1	0	0	15

[a] Malignant hypertension, nausea, Ménétrier disease.

TABLE 2: Frequency of Procedure vs Frequency of Vasovagal Reactions

Procedure	Total No. (%) of Procedures (n = 370)	Total No. (%) of Reactions (n = 27)
Wire localizations		
Coordinate grid	173 (47)	12 (44)
Freehand	17 (4)	1 (4)
Stereotactic	11 (3)	2 (7)
Sonographic	2 (1)	0 (0)
Fine-needle aspirations		
Coordinate grid	107 (29)	7 (26)
Stereotactic	45 (12)	4 (15)
Sonographic	15 (4)	1 (4)

Mild but prolonged bleeding averaging 23 min (range, 5–45 min) in duration occurred in three women. None of these women had a known bleeding diathesis nor did they require further treatment after cessation of the bleeding. The hook-wire appeared to traverse a small vein in the woman with 45 min of bleeding, possibly inhibiting clot formation.

The most subjective assessment, an unusual amount of pain, was experienced by two women, both of whom received local anesthesia. Both procedures were completed without difficulty.

One procedure was never started when unexpected extreme elevation of blood pressure (250/130 mm Hg) was noted by the nurse before the study started. The procedure was rescheduled and completed uneventfully at a later date, after successful treatment with antihypertensive medications.

Discussion

Invasive mammographically or sonographically directed breast procedures are commonly performed. Such procedures are expected to continue to increase in frequency as mammographic screening expands. Despite extensive radiologic literature devoted to wire localization and fine-needle aspiration, little has been specifically written regarding immediate complications of such procedures [4, 6–19]. Gisvold and Martin [8] did note "some problems" with vasovagal reactions and hematoma formation, but the actual frequency was not reported. A single vasovagal reaction during 47 wire localizations [9] and one hematoma due to arterial injury during 96 fine-needle aspirations [10] have been described.

Discomfort during routine mammography has been reported by Jackson et al. [20], who report the results of a survey of patients. Eleven percent of women surveyed felt that the test was very uncomfortable and 3% found it to be intolerable. In fact, 4% of women stated they would not return for routine mammography. It could be anticipated that even more women would react negatively to invasive procedures, which often require longer compression time, additional mammographic views, and the insertion of needles. Additionally, these women would be expected to be more anxious because an abnormality has been discovered.

Our study confirms the commonly held opinion that breast imaging procedures are generally safe and well tolerated. We did, however, identify a significant minority (7%) of patients who had mild to severe vasovagal reactions. Interestingly, two of four women who had vasodepressor syncopal episodes did so before any needle puncture, implying that anxiety and anticipation (in addition to pain and discomfort) play a role in these reactions. This may explain why the use of local anesthesia did not reduce the frequency of vasovagal reactions. These responses occurred independently of procedure type (fine-needle aspiration vs wire localization), suggesting that preexisting factors associated with the patient contribute to their occurrence. Because anxiety can contribute to vasovagal reactions, some physicians, other than ours, premedicate some patients with antianxiety medications before the procedures. The efficacy of this treatment is important to study.

Vasovagal reactions and vasovagal (vasodepressor) syncope are well-known phenomena and are the leading cause of syncope [21]. Such reactions are initiated by a host of causes, including stress, emotional upset, pain, injury, blood loss, and surgery. Clinically, mild prodromal signs and symptoms are frequently obvious before frank syncope. These include light-headedness, nausea, diaphoresis, pallor, yawning, and sighing. Syncope usually occurs from an upright position. The pathophysiology of vasodepressor syncope is not completely understood, but involves peripheral arterial vasodilation and secondary bradycardia, which leads to hypotension and depressed cardiac output, resulting in cerebral hypoperfusion and subsequent syncope [21–24]. Management involves placing the patient in a recumbent position with legs elevated and removing the initiating stimulus [21].

Because vasovagal reactions occur during invasive breast procedures, patients should be attended at all times by persons trained to recognize and treat such problems. These persons should know how to release the patient's breast from compression if the technologist is not present. Additionally, a bed or examining table and equipment for monitoring blood pressure should be readily available. Because vasodepressor syncope is unusual when the patient is recumbent, persons who perform wire localizations or aspirations with the patient in this position can expect fewer reactions [15]. Ideally, compression time should be as short as possible. Although it is speculative, those centers that use faster processors than our 3.5-min extended unit may have fewer reactions because of the shorter compression time.

Initial blood pressure recordings provided a useful baseline, but they were not helpful in predicting who would faint. Although one patient's procedure was cancelled because of marked hypertension, the yield (0.3%) is probably too low to recommend routine initial blood pressure measurements. Selected blood pressure measurements could be obtained in patients known to have hypertension.

We conclude that wire localizations and fine-needle aspirations are generally well tolerated in the immediate periprocedural period. However, vasovagal reactions are frequent enough to warrant close observation of patients during such procedures. Radiologists and breast-imaging personnel should be able to recognize and treat these reactions.

REFERENCES

1. Kopans DB, Lindfors K, McCarthy KA, Meyer JE. Spring hookwire breast lesion localizer: use with rigid-compression mammographic systems. *Radiology* **1985**;157:537–538
2. Lovin JD, Parker SH, Jobe WE, Leuthke JM, Hopper KD. Stereotactic percutaneous breast core biopsy, technical adaptation and initial experience. *Breast Dis* **1990**;3:135–143
3. Feig SA. Localization of clinically occult breast lesions. *Radiol Clin North Am* **1983**;21:155–170
4. Fornage BD, Faroux MJ, Simatos A. Breast masses: US-guided fine-needle aspiration biopsy. *Radiology* **1987**;162:409–414
5. Novak R. Position-controlled needle aspiration biopsy at mammography. *Fortschr Geb Rontgenstr Nuklearmed Erganzungsband* **1979**;131: 659–661
6. Löfgren M, Andersson I, Bondeson L, Lindholm K. X-ray guided fine-needle aspiration for the cytologic diagnosis of nonpalpable breast lesions. *Cancer* **1988**;61:1032–1037
7. Löfgren M, Andersson I, Lindholm K. Stereotactic fine-needle aspiration for cytologic diagnosis of nonpalpable breast lesions. *AJR* **1990**;154: 1191–1195
8. Gisvold JJ, Martin JK. Prebiopsy localization of nonpalpable breast lesions. *AJR* **1984**;143:477–481
9. Goldberg RP, Hall FM, Simon M. Preoperative localization of nonpalpable breast lesions using a wire marker and perforated mammographic grid. *Radiology* **1983**;146:833–835
10. Hann L, Ducatman BS, Wang HH, Fein V, McIntire JM. Nonpalpable breast lesions: evaluation by means of fine-needle aspiration cytology. *Radiology* **1989**;171:373–376
11. Homer MJ. Localization of nonpalpable breast lesions: technical aspects and analysis of 80 cases. *AJR* **1983**;140:807–811
12. Meyer JE, Kopans DB, Stomper PC, Lindfors KK. Occult breast abnormalities: percutaneous preoperative needle localization. *Radiology* **1984**;150:335–337
13. Homer MJ, Pile-Spellman ER. Needle localization of occult breast lesions with a curved-end retractable wire: technique and pitfalls. *Radiology* **1986**;161:547–548
14. Rosenberg AL, Schwartz GF, Feig SA, Patchefsky AS. Clinically occult breast lesions: localization and significance. *Radiology* **1987**;162:167–170
15. Dowlatshahi K, Gent HJ, Schmidt R, Jokich PM, Bibbo M, Sprenger E. Nonpalpable breast tumors: diagnosis with stereotactic localization and fine-needle aspiration. *Radiology* **1989**;170:427–433
16. Ciatto S, Del Turco MR, Bravetti P. Nonpalpable breast lesions: stereotactic fine-needle aspiration cytology. *Radiology* **1989**;173:57–59
17. Evans WP, Cade SH. Needle localization and fine-needle aspiration biopsy of nonpalpable breast lesions with use of standard and stereotactic equipment. *Radiology* **1989**;173:53–56
18. Azavedo E, Auer G, Svane G. Stereotactic fine-needle biopsy in 2594 mammographically detected non-palpable lesions. *Lancet* **1989**;1: 1033–1036
19. Helvie MA, Baker DE, Adler DD, Andersson I, Naylor B, Buckwalter KA. Radiographically guided fine-needle aspiration of nonpalpable breast lesions. *Radiology* **1990**;174:657–661
20. Jackson VP, Lex AM, Smith DJ. Patient discomfort during screen-film mammography. *Radiology* **1988**;168:421–423
21. Sobel BE, Roberts R. Hypotension and syncope. In: Braunwald E., ed. *Heart disease*, 3rd ed. Philadelphia: Saunders, **1988**:889–890
22. Glick G, Yu PN. Hemodynamic changes during spontaneous vasovagal reactions. *Am J Med* **1963**;34:42–51
23. Epstein SE, Stampfer M, Beiser GD. Role of the capacitance and resistance vessels in vasovagal syncope. *Circulation* **1968**;37:524–533
24. Martin JB, Ruskin J. Faintness, syncope, and seizures. In: Wilson JD, Braunwald E, Isselbacher KJ, et al., eds. *Harrison's principles of internal medicine*. New York: McGraw-Hill, **1991**:134–135

Phylloides Tumor: Findings on Mammography, Sonography, and Aspiration Cytology in 10 Cases

Wolfgang Buchberger[1]
Karin Strasser[1]
Kurt Heim[2]
Elisabeth Müller[2]
Hans Schröcksnadel[2]

Phylloides tumor is a rare fibroepithelial breast tumor that occasionally has unpredictable clinical behavior. In nine cases of histologically benign tumors and one case of malignant phylloides tumor, the findings on physical examination, mammography, sonography, and aspiration biopsy were correlated retrospectively with the histologic diagnosis of resected specimens. Mammograms showed a round or lobulated benign-appearing opacity in nine cases; one small tumor was missed mammographically. Sonography depicted all tumors as mostly solid masses. Sonographic features included low-level internal echoes, either uniform or scattered; smooth contours; and no significant posterior shadowing. Intramural cysts were shown in six cases. Neither mammography nor sonography allowed reliable differentiation between benign and malignant phylloides tumors. Aspiration biopsy permitted accurate diagnosis of seven benign tumors. The malignant phylloides tumor was classified as a malignant tumor, but the definite differentiation from a carcinoma could not be made. Two histologically benign phylloides tumors were misdiagnosed as carcinomas.

Although uncommon, phylloides tumor should be considered in the differential diagnosis of mammographically benign-appearing breast masses, especially if sonography shows intramural cysts within a well-defined solid lesion. Aspiration cytology is unreliable because of the inhomogeneity of the tumor; both intraoperative frozen section and permanent sections are needed for correct histologic diagnosis.

AJR 157:715–719, October 1991

Phylloides tumor is a rare breast tumor that accounts for 0.3% to 1.0% of all breast neoplasms [1]. The histologic appearance is similar to that of an intracanalicular fibroadenoma, but phylloides tumor has more stromal cellularity and proliferation. Osseous and chondroid metaplasias of the stroma and epithelium occur [2]. Differentiation of benign, malignant, and borderline tumors is based on microscopic findings [3].

The prevalence of local recurrences is similar for both the histologically benign and the malignant forms and is probably a function of inadequate excision. The recurrence rate is 16–28% after mastectomy or wide-wedge resection and 28–46% after simple enucleation of the tumor [4, 5]. Repeated relapses are common. The prevalence of distant metastases at initial diagnosis is between 3% and 12% [6]. The tumor metastasizes via the vascular route; about two thirds of metastases are to the lungs, fewer are to the bone, liver, and myocardium [7]. Phylloides tumor occurs mostly in women in their fifth or sixth decade, and occasionally in women younger than 20 years old [5, 8, 9]. A few cases in males with gynecomastia have been described. The main clinical finding is a palpable mass, quite often of remarkably large size. The growth of the tumor extends sometimes over several years; periodic remission and sudden growth are typical [10].

Large phylloides tumors usually are diagnosed correctly on the basis of mammographic findings because of their size and benign-looking appearance. In smaller tumors, differential diagnosis includes cysts, fibroadenomas, and even well-circum-

Received January 8, 1991; accepted after revision April 30, 1991.

[1] Department of Radiology, University of Innsbruck, Anichstraße 35, A-6020 Innsbruck, Austria. Address reprint requests to D. W. Buchberger.

[2] Department of Gynecology and Obstetrics, University of Innsbruck, Anichstraße 35, A-6020 Innsbruck, Austria.

0361–803X/91/1574–0715
© American Roentgen Ray Society

scribed carcinomas. According to the literature [4, 11], mammography cannot be used to differentiate benign from malignant phylloides tumor. Sonography and aspiration cytology have gained importance in breast diagnosis (12–14], but little information about their value in the diagnosis of phylloides tumor is available. The purpose of our study was to describe the sonographic findings of the tumor and to evaluate the use of sonography and aspiration cytology as additional tools in the diagnosis.

Materials and Methods

All tumors coded as phylloides tumor, cystosarcoma phylloides, giant fibroadenoma, or sarcoma of the breast and diagnosed between 1981 and 1990 were selected from the files of the University of Innsbruck Hospital. Ten tumors that met the histologic criteria of phylloides tumor were evaluated retrospectively. For each of the cases, preoperative mammograms were reviewed, and the descriptive features of the tumors were recorded. The descriptive features included tumor location, size, shape and contour, and the presence or absence of a halo or microcalcifications. All mammography had been performed with a dedicated breast unit (Mammomat; Siemens, Erlangen, Germany) with a 0.4-mm target in a molybdenum anode, 0.03-mm molybdenum filter, and 60-cm target-receptor distance. Craniocaudal, mediolateral, and oblique projections were obtained routinely by using a grid and an appropriate film-screen combination (Ortho MA film and Min R screen; Kodak Pathé, Chalons sur Saone, France).

Breast sonography had been performed with real-time instruments (Picker LSC 7000 and LSC 9500, Hitachi Medical Corp., Tokyo, Japan) with 5-MHz convex and 7.5-MHz linear transducers. The scans had been recorded either with a multiformat camera or on videoprints. The descriptive sonographic features of each lesion, including shape, contour, internal echo strength and distribution, sound attenuation or enhancement effects, and the presence of intramural cysts, were recorded on data sheets.

The original histologic slides from surgical resection specimens were reviewed by an oncologic pathologist. The tumors were classified histologically as benign phylloides tumor, recurrent benign phylloides tumor, fibroadenoma with transition to benign phylloides tumor, or malignant phylloides tumor.

In each case, at least one aspiration biopsy of the tumor had been performed. The aspiration was guided clinically in nine cases and sonographically in one; 21-gauge, 40-mm-long standard needles and 10-ml syringes were used. Depending on the size of the tumor, two or three passes were done. Aspirates were expelled on glass slides, fixed with a spray, and stained by the Papanicolaou method. The cytologic smears were reevaluated retrospectively by an experienced cytologist and correlated with the pathohistologic diagnosis.

Results

The tumors had occurred in women between 18 and 50 years old (mean age, 38 years). Each patient had had a mobile palpable mass that had been present for 3 weeks to 8 months. None had had palpable axillary nodes or skin or nipple involvement. The tumor diameter varied between 2.0 and 12.5 cm; most were medium sized to large. Five were located in the left breast, and five in the right; multiple or bilateral tumors were not found.

Histology

Six tumors were classified as benign phylloides tumor, one as recurrent benign phylloides tumor, two as fibroadenoma with transition to benign phylloides tumor, and one as malignant phylloides tumor. The malignant tumor had been treated by radical mastectomy. Five years later, no local recurrence or metastasis was apparent. The eight benign phylloides tumors had been treated by lumpectomy; one showed local recurrence within 1 year. Distant metastasis did not occur in the histologically benign cases.

Mammography

On mammograms, nine of 10 tumors were sharply defined, round or lobulated opacities (Figs. 1A and 2A). In five cases, a clear halo was seen around the mass. One small tumor (1.3 × 1.3 × 2.0 cm) was missed on mammography and was shown only on sonography. None of the tumors showed any calcifications. Secondary signs of malignancy, such as perifocal edema, engorgement of vessels, disruption of perifocal structures, skin thickening, or nipple retraction were absent. No enlarged axillary nodes were shown on the mammograms. The only malignant tumor was distinctly lobulated and well circumscribed (Fig. 3A).

Sonography

On sonograms, all 10 neoplasms were seen as well-defined masses with low-level echoes (Table 1). In three cases, the tumor was surrounded by an echogenic rim (Fig. 2B). Only three of 10 tumors had homogeneous internal echoes; the rest had a nonuniform pattern, with mostly weak scattered echoes and a few echogenic spots. Five lesions showed posterior enhancement and none had acoustic attenuation. In six cases, intramural cysts with a diameter between 3 and 10 mm were apparent. They were round or ovoid with smooth walls, usually multiple, and marginally located (Fig. 1B). The malignant phylloides tumor was lobulated with rather smooth contours and had inhomogeneous internal echoes but no posterior shadowing (Fig. 3B).

Cytology

Seven of the nine histologically benign tumors prospectively were classified cytologically as benign. In two of the benign tumors, the initial cytologic diagnosis was "malignant, probably carcinoma." A review of the original slides of these two cases with knowledge of the histology showed that the smears contained nearly exclusively dense clusters of epithelial cells with enlarged nuclei, which had led to a false diagnosis of carcinoma. The malignant phylloides tumor was diagnosed correctly as malignant, but a definite differentiation from a carcinoma could not be made.

Discussion

Numerous authors [11, 15, 16] have tried to correlate the gross and histologic features of phylloides tumor with its

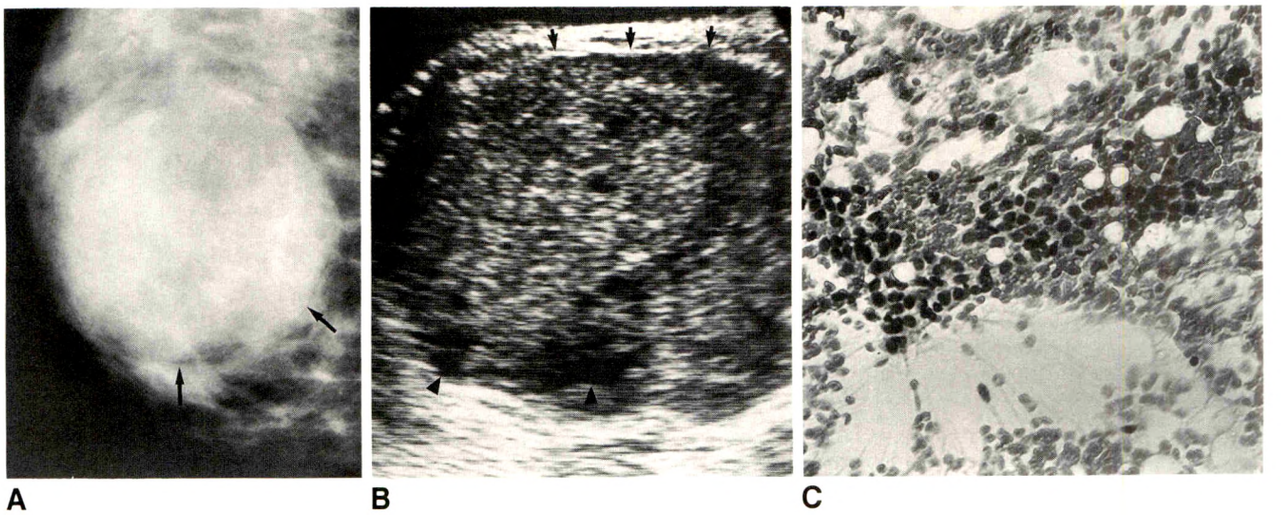


Fig. 1.—Benign phylloides tumor.
A, Mediolateral mammogram of right breast shows a round, slightly lobulated, sharply defined mass surrounded by a clear halo (*arrows*).
B, Transverse sonogram shows a well-circumscribed solid mass with an inhomogeneous echo pattern and slight, posterior enhancement. Lesion is partially surrounded by an echogenic rim (*arrows*) and contains small, echo-free cystic spaces (*arrowheads*).
C, Photomicrograph of cytologic smear shows dense clusters of hyperplastic epithelial cells and stromal cells with no signs of atypia.

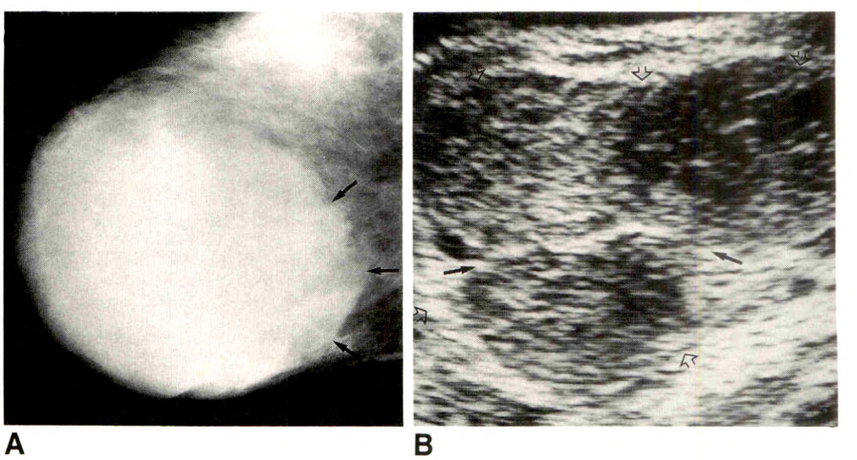


Fig. 2.—Benign phylloides tumor.
A, Mediolateral mammogram of right breast shows a huge mass that had been clinically apparent for 8 months. Mass is surrounded partially by a clear halo (*arrows*) and partially obscured by dense breast tissue.
B, Transverse sonogram shows a solid mass composed of two nodules separated by an echogenic septum (*solid arrows*) and surrounded by an echogenic rim (*open arrows*).

clinical behavior. Most advocate the division of phylloides tumors into histologically benign, malignant, and borderline categories. Recurrences are frequent in both the benign and the malignant types [4, 5]. Metastasis occurs mainly in malignant and borderline tumors, but metastatic spread from histologically benign tumors has been described [11]. On the other hand, only 29% of the histologically malignant tumors metastasize [5]. Thus, classification of phylloides tumors according to the histology seems to be justified, although the clinical behavior of the tumor is unpredictable.

One of the difficulties with the cytologic diagnosis lies in the similarity of phylloides tumor and fibroadenoma. The stromal proliferation typical for phylloides tumor is not always demonstrable in the cytologic smear. In malignant phylloides tumor, the cells of the stroma show distinct cell and nuclear polymorphia and increased mitotic activity; this is not true for the epithelial cells [17, 18]. For this reason it is important to obtain smears that contain both stromal cells and epithelial cells. We have found that it is not always possible to obtain both types of cells, even if multiple aspirations are performed. False results of aspiration cytology in our study were all due to inadequate cytologic samples. In one case, only degenerated cell material from cysts within the tumor was obtained; in two other cases, the smears contained nearly exclusively hyperplastic duct epithelial cells, but no stromal cells. In general, the diagnostic value of aspiration cytology is limited because of the inhomogeneity of the tumor, and aspiration cytology should not replace intraoperative wedge biopsy. The mammographic findings in phylloides tumor are variable and extend from small to medium-sized smoothly marginated masses to huge tumors occupying practically the entire breast [19]. Hamartomas (angiomyolipomas) may resemble phyl-

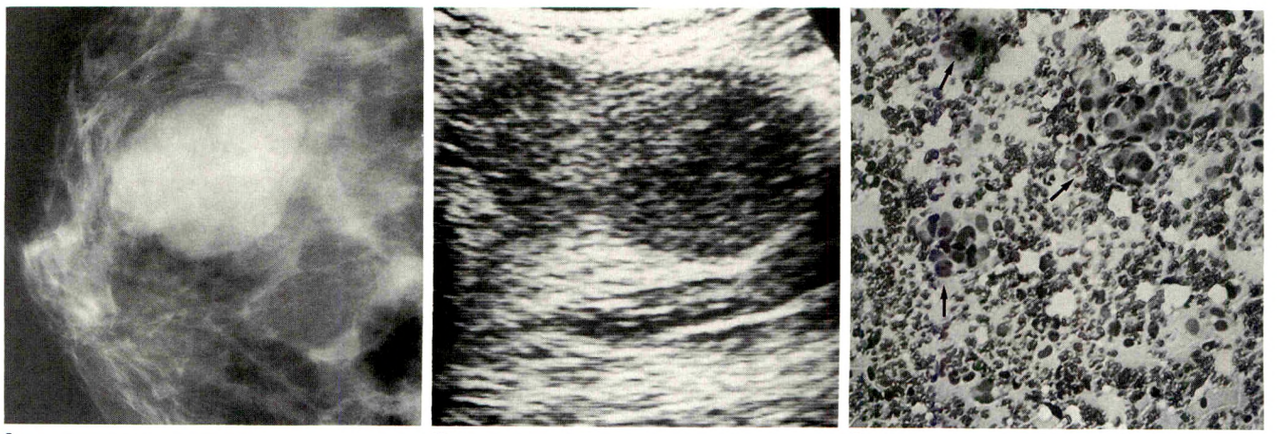


Fig. 3.—Malignant phylloides tumor.
A, Mediolateral mammogram of right breast shows a well-circumscribed, lobulated mass.
B, Sagittal sonogram shows a solid mass with coarse internal echoes and smooth margins. No posterior acoustic shadowing is noted.
C, Photomicrograph of cytologic smear shows numerous RBCs and small groups of stromal cells with enlarged, polymorphous and hyperchromatic nuclei (*arrows*).

TABLE 1: Descriptive Sonographic Criteria of 10 Cases of Phylloides Tumor

Descriptive Criteria	No. of Cases
Shape	
Round	1
Oval	2
Lobulated	7
Contour	
Smooth	10
Irregular	0
Echogenic rim	3
Internal echoes	
Weak (< fat)	6
Intermediate (= fat)	4
Strong (> fat)	0
Uniform	3
Scattered	7
Intramural cysts	6
Posterior shadowing	0
Sound enhancement	5

loides tumor, but these lesions usually show evidence of fat by mammography. If the tumors are small, fibroadenomas, cysts, and well-circumscribed carcinomas (medullary, mucinous, and rarely invasive and in situ ductal carcinomas) should be considered in the differential diagnosis. Only a few authors [20–22] have reported on the sonographic appearance of phylloides tumor. Their experiences are similar to our's. They described well-defined masses with weak uniform or scattered internal echoes.

Single or multiple, round or cleftlike cystic spaces are characteristic but not pathognomonic. Occasionally, intramural cystic structures, representing focal necrosis or degeneration, can be observed in other well-circumscribed tumors, such as medullary carcinomas or fibroadenomas [23, 24]. As in other studies [22], no reliable sonographic criteria for differentiation between benign and malignant phylloides tumors could be found. Inhomogeneous internal echoes were demonstrable in both the malignant and benign tumors. On the other hand, the malignant phylloides tumor was well-circumscribed and showed no posterior shadowing.

In summary, phylloides tumor is an uncommon lesion of the breast with a high prevalence of local recurrences and the capacity for metastasis. The tumors manifest themselves clinically as palpable masses of variable size and mammographically as localized opacities without signs of malignancy. Sonographic findings can be used to differentiate with certainty cysts from solid tumors. The demonstration of cystic structures within a well-circumscribed solid lesion with weak internal echoes should suggest phylloides tumor. Neither mammography nor sonography can be used to differentiate reliably between malignant and benign phylloides tumors. Aspiration cytology gives better results but is also unreliable. The diagnosis should be verified by examination of an intraoperative frozen section. Because of the inhomogeneous structure of the tumor, a fairly reliable prognosis with regard to its biological behavior is possible only after careful studies of the entire resected material have been done.

REFERENCES

1. Ariel L. Skeletal metastases in cytosarcoma phylloides. *Arch Surg* **1961**;82:275–280
2. The World Health Organization. The WHO histological typing of breast tumors, 2nd ed. *Am J Clin Pathol* **1982**;78:806–816
3. Al-Jurf A, Hawk WA, Crile G. Cystosarcoma phylloides. *Surg Gynecol Obstet* **1978**;146:358–364
4. Mc Crea E, Johnston C, Keramati B. Cystosarcoma phylloides. *South Med J* **1986**;79:543–547
5. Pietruszka ML, Barnes L. Cystosarcoma phylloides: a clinicopathologic analysis of 42 cases. *Cancer* **1978**;41:1974–1983
6. Lester J, Stout AP. Cystosarcoma phylloides. *Cancer* **1954**;7:335–353
7. Kessinger A, Foley JF, Lemon HM, Miller DM. Metastatic cystosarcoma

phylloides: a case report and review of the literature. *J Surg Oncol* **1972**;4:131–147
8. Haagensen CD. *Diseases of the breast*, 3rd ed. Philadelphia: Saunders, **1986**:284–312
9. Hart WR, Bauer RC, Oberman HA. Cystosarcoma phylloides: a clinicopathologic study of twenty-six hypercellular stromal tumors of the breast. *Am J Clin Pathol* **1978**;70:211–216
10. Blickert-Toft M, Hart Hansen JP, Hart Hansen O, Schiodt T. Clinical course of cystosarcoma phylloides related to histologic appearance. *Surg Gynecol Obstet* **1975**;140:929–933
11. Norris HJ, Taylor HB. Relationship of histologic features to behavior of cystosarcoma phylloides: analysis of ninety-four cases. *Cancer* **1967**;20:2090–2099
12. Bassett LW, Kimme-Smith C, Sutherland LK, Gold RH, Sarti D, King W. Automated and hand-held breast US: effect on patient management. *Radiology* **1987**;165:103–108
13. Fornage BD, Faroux MJ, Simatos A. Breast masses: US-guided fine-needle aspiration biopsy. *Radiology* **1987**;162:409–414
14. Griffith CN, Kern WH, Mikkelsen WP. Needle aspiration cytologic examination in the management of suspicious lesions of the breast. *Surg Gynecol Obstet* **1986**;162:142–144
15. Ward RM, Evans HL. Cystosarcoma phylloides: a clinicopathologic study of 26 cases. *Cancer* **1986**;58:2282–2289
16. Contarini O, Urdaneta LF, Hagan W, Stephenson SE. Cystosarcoma phylloides of the breast: a new therapeutic proposal. *Am J Surg* **1982**;48:157–163
17. Stawicky ME, Hsiu JG. Malignant cystosarcoma phylloides: a case report with cytologic presentation. *Acta Cytol* **1978**;23:61–64
18. Micoli P, Iacconi P, Roncella M. Les tumeurs phylloides du sein. *Acta Chir Belg* **1985**;85:128–132
19. Wolfe JN. *Xeroradiography of the breast*, 2nd ed. Philadelphia: Saunders, **1982**:243
20. Kobayashi T. *Clinical ultrasound of the breast*. New York: Plenum, **1978**;50–51, 130–132
21. Jellins J, Hughes C, Ryan J, Reeve T, Kossoff G. A comparative evaluation of a case of cystosarcoma phylloides: ultrasound, xeroradiography and thermography. *Radiology* **1977**;124:803–804
22. Cole-Beuglet C, Soriano R, Kurtz AB, Meyer JE, Kopans DB, Goldberg BB. Ultrasound, X-ray-mammography and histolopathology of cystosarcoma phylloides. *Radiology* **1983**;146:481–486
23. Harper AP, Kelly-Fry E, Noe JS, Bies JR, Jackson VP. Ultrasound in the evaluation of solid breast masses. *Radiology* **1983**;146:731–736
24. Hackelöer BJ, Duda V, Lauth G. *Ultraschallmammographie*. New York: Springer, **1986**:50

American Roentgen Ray Society
Residents' Award Papers, 1992

The ARRS announces competition for the 1992 President's Award and two Executive Council Awards for the best papers concerning the clinical application of the radiologic sciences.

Awards

The winner of the President's Award will receive a certificate and a $2000 prize. The winners of the two Executive Council Awards will each be given a certificate and a prize of $1000. The winners will be announced on March 16, 1992. Winning papers will be presented at the ARRS annual meeting at Marriott's Orlando World Center, Orlando, FL, May 10–15, 1992. Winning papers will be submitted for early publication in the *American Journal of Roentgenology*. All other papers will be returned to the authors.

Regulations

Eligibility is limited to residents or fellows in radiology who have not yet completed 4 years of approved training in a radiologic discipline. A letter from the resident's department chairman attesting to this status must accompany the manuscript. The resident must be the sole or senior author and be responsible for all or most of the project.

Submitted manuscripts must not exceed 5000 words and have no more than 10 illustrations. Four copies of the manuscript and illustrations are required. Submitted manuscripts should not contain previously presented or published material and should not be under consideration for publication elsewhere.

Deadline for submissions is February 14, 1992. Send papers to

Nancy O. Whitley, M.D.
Chairman, Committee on Education & Research
American Roentgen Ray Society
Department of Radiology
University of Maryland Medical Systems Hospital
22 S. Greene St.
Baltimore, MD 21201

Before and After

Stefan C. Schatzki[1]

Andy Warhol is one of America's best-known and, at the same time, most controversial artists. Four years after his death, the disagreement continues between his admirers, who consider Warhol an important and innovative artist who was honored by many international museums, and his detractors, who think his work is unoriginal and commercial. Andy Warhol was the leader of the pop art movement that began in the 1960s and is represented today in every major museum of modern art. Warhol made a career of reproducing famous images and products in order to advance his own reputation. He used the fame of his subjects to promote his works of art, which have become recognized and valued throughout the world of modern art.

Andrew Warhola was born about 1930 in Pennsylvania (Warhol purposely obscured the details of his birth). As a teenager he attended the Carnegie Institute of Technology in Pittsburgh and soon thereafter moved to New York, where he became a successful and well-known commercial illustrator. His first solo exhibition was in 1952. The pop art era began in 1960, when Warhol began to produce multiple copies of widely known subjects. Dick Tracy, Popeye, and Superman were early comic strip subjects. These soon were followed by those images that ensured his early fame, particularly Campbell's Soup cans, Coca-Cola bottles, and dollar bills. These were shown either as single objects or as multiple similar objects with subtle variations. His portraits of Elvis Presley, Elizabeth Taylor, and his first *Marilyns* date from this period. These portraits, like much of his work, were largely Warhol's interpretation of existing, available images of his subjects. His many gallery shows and first museum show confirmed his star in the artistic firmament.

In 1965, he abruptly retired from painting and produced underground movies for the next several years. However, 7 years later, in 1972, his painting career was reborn. Using many different techniques, Warhol created a large body of work. His portraits of many of the best-known women and men of the day remain an important part of his legend and include such figures as Mao Zedong, Jimmy Carter, Mick Jagger, Liza Minelli, Albert Einstein, Queen Elizabeth, and Marilyn Monroe.

During these years of immense international popularity, Warhol remained at the center of a social culture that revolved around modern art in New York City. Fame continued until his sudden death after a cholecystectomy in February 1987.

Warhol produced three versions of *Before and After*. This image has been widely reproduced, becoming one of the many familiar Warhol images. *Before and After* uses an illustration from an advertisement for cosmetic surgery. As was true of most of Warhol's work, the message is clear. The mature woman on the left with a severely aquiline nose has been miraculously transformed by surgery to a young, girlish woman. Warhol has borrowed, blown up, and slightly altered the existing image and has used our culture's clichés about beauty. Warhol makes no attempt to reveal his own personal ideas about the subject matter, but the work merely serves as a mirror for the artifacts of our culture.

Warhol's art was intended to provoke. Almost everything he did was calculated to win attention, and his insatiable appetite for fame remains a source of controversy. He was determined to make the art world accept him on his terms. Warhol's pop images reveal something about our culture without revealing a great deal about the artist. In addition, Warhol rejected the uniqueness of art by producing multiple copies of virtually identical works of art. His studio was even called the "Factory."

Four years after his death, Andy Warhol remains a personal and artistic enigma. As may be true for most popular art, it will be many years before a decision can be made on whether Andy Warhol's art represents unique, innovative creations of his time or merely clever, successful commercialism.



Andy Warhol (1930?–1987). *Before and After 3*, 1962. Synthetic polymer on canvas, 74 × 100 in. Whitney Museum of American Art, New York; gift of Charles Simon.

[1] Department of Radiology, Mount Auburn Hospital, 330 Mount Auburn St., Cambridge, MA 02238.

AJR **157:720, October 1991** 0361–803X/91/1574–0720 © American Roentgen Ray Society

Value of Dual-Energy CT in Differentiating Focal Fatty Infiltration of the Liver from Low-Density Masses

Vassilios Raptopoulos[1,2]
Andrew Karellas[1]
Jeffrey Bernstein[3,4]
Frank R. Reale[5]
Chris Constantinou[6]
John K. Zawacki[3]

Focal (irregular, partial) fatty infiltration of the liver may simulate neoplastic or other hypodense masses on CT. On the basis of previous observations of the phenomenon that differences in X-ray attenuation diminish with increasing energy of X-rays used, we performed a preliminary study to determine if dual-energy CT could be used to discriminate between fatty infiltration and hypodense liver masses. Dual-energy CT at 140 and 80 kVp was performed in 14 patients undergoing liver biopsy and in seven control subjects with presumedly normal liver. Attenuation measurements were taken, and the changes in attenuation between 140 and 80 kVp were calculated. The mean changes in attenuation were 3.5 H for normal liver (n = 7), 2.5 H for hypodense liver masses (n = 6), 13 H for fatty liver (n = 5), 0.3 H for fatty liver combined with hemochromatosis or hemosiderosis (n = 3), and 2 H for the spleen (n = 18). The change in attenuation increased as the fat content in the liver increased. Analysis of variance showed a statistically significant difference ($p < .001$) between fatty liver and the other groups. A difference greater than 10 H was unique to fatty infiltration.

These results suggest that dual-energy CT may help to differentiate focal fatty infiltration of the liver from low-density neoplastic or other lesions, but only if the iron content of the liver is not increased.

AJR 157:721–725, October 1991

Although advanced fatty infiltration of the liver is easily recognized by CT, a satisfactory quantitative method has not been described and early fatty liver changes may not be detected [1–4]. In addition, focal (irregular, partial, nodular) fatty infiltration of the liver may simulate neoplastic or other low-density parenchymal masses [5–13].

In CT scans obtained at various X-ray energies, the CT attenuation of bone mineral, measured in Hounsfield units, decreases with increasing X-ray energy (kVp), although there is little change in the attenuation of soft tissues or water [14–16]. Accordingly, dual-energy CT has been proposed for noninvasive quantification of liver iron deposition [17]. We did a preliminary study to determine if the opposite response would be observed in fatty infiltration of the liver. We expected the attenuation of fatty liver to increase with increasing kVp and to remain about the same in normal or hypodense, non–fat-containing, liver. If this is the case, dual-energy CT can be used to differentiate focal fatty infiltration from liver masses.

Subjects and Methods

Dual-energy CT was performed in eight consecutive ambulatory patients who had liver biopsy for presumed hepatocellular disease and in 13 persons who served as control subjects: six patients with hypodense liver masses and seven volunteers with presumedly normal liver.

Of the eight patients with hepatocellular disease, five were men and three were women; their mean age was 42 years. After the biopsy, but before the patients were discharged, dual-energy CT was done at the level of the biopsy. Conventional guidelines were followed

Received January 3, 1991; accepted after revision April 8, 1991.

[1] Department of Radiology, University of Massachusetts Medical Center, Worcester, MA 01655.

[2] Present address: Department of Radiology, Beth Israel Hospital, 330 Brookline Ave., Boston, MA 02215. Address reprint requests to V. Raptopoulos.

[3] Division of Gastroenterology, University of Massachusetts Medical Center, Worcester, MA 01655.

[4] Present address: 14201 Laurel Park Dr., Suite 226, Laurel, MD 20707.

[5] Department of Pathology, University of Massachusetts Medical Center, Worcester, MA 01655.

[6] Department of Radiation Oncology, Brocton Hospital, 680 Centre St., Brocton, MA 02402-3395.

0361–803X/91/1574–0721
© American Roentgen Ray Society

for the biopsies: the needle entry site was at the anterior axillary line, at least two intercostal spaces of dullness on percussion below the diaphragm, and the needle course was directed cephalad, toward the xiphoid process. A 16-gauge suction biopsy needle was used, providing a specimen approximately 2 cm long and 1 mm in diameter. Scanning was performed at a single level, assessed to be at the location from where the biopsy specimen was taken by considering the location of the needle entry and the cephalad angle used. CT density measurements were taken from the center of the right lobe, and the mean attenuation of an area 4–6 cm^2 was obtained. Because of the potential complicating factor of hematoma or postbiopsy edema interfering with accurate measurements of the tissue, the attenuation measurements were compared with those of other nearby and remote regions. In the absence of considerable discrepancies in density numbers, the obtained value was considered to be representative of the biopsy sample.

All biopsy material was stained with conventional H and E and iron stains and whatever else was deemed necessary for pathologic diagnosis. The estimation of the amount of fat in the specimen was visual and was done by counting the percentage of the number of cells containing fat. This was done both at the time of the biopsy and also at the end of the study. This percentage was given in increments of 25% and was so appraised by an experienced pathologist who had no knowledge of the CT results. Additional significant findings were also reported, including the presence of cirrhosis, chronic active hepatitis, toxic injury, metastatic disease, hemochromatosis, or hemosiderin deposits.

One control group consisted of six patients with hypodense liver masses that measured more than 3 cm in diameter. This group comprised three men and three women with mean age of 56 years. Five had metastatic disease and had conventional suction biopsy with large-bore needles (16 gauge in three and 18 gauge in two patients). The primary tumors included carcinoma of the lung ($n = 2$), colon ($n = 2$), and uterine cervix ($n = 1$). The sixth patient had a large hepatic hemangioma proved by fine- (22-gauge) needle biopsy and a 12-month follow-up. The biopsies were done with CT guidance, and dual-energy CT was done at the level chosen just before the biopsy. The mean density of a homogeneous area at the center of the mass measuring 4–6 cm^2 was obtained. Histologic examination was done as in the group of patients with hepatocellular disease.

The other control group consisted of seven normal volunteers, also scanned at a single level. This group comprised four men and three women with mean age of 34 years. It was presumed that there was no fatty infiltration in their livers. This, of course, is a conjecture and would require biopsy for confirmation. However, liver biopsy in normal asymptomatic subjects is prohibitive because of the risks. Therefore, stringent criteria were used for inclusion in this control group. These subjects had no history of liver disease; their alcohol consumption was minimal, if any (no more than two drinks a week); they were not receiving any medications; and they did not have any condition predisposing to fatty infiltration, such as diabetes or obesity. In addition, they had no predisposing intrinsic or extrinsic factor that could increase the iron deposition in the liver (for example, blood transfusions). CT attenuation measurements were taken from the center of the right lobe of the liver in an area 6 cm^2.

Measurements were also take from 2-cm^2 areas of the aorta ($n = 21$), from the subcutaneous fat ($n = 21$), and from the spleen, where measurements were taken from areas 4–6 cm^2 ($n = 18$; the spleen was not included on the image in two patients and another had had a splenectomy).

All scans were obtained with a conventional GE 9800 scanner (General Electric, Milwaukee, WI). The patients were scanned at a single level only, and 1-cm-thick sections were taken once with 140 kVp and 120 mA and again with 80 kVp and 170 mA. The milliamperage varied according to energy used for partial compensation of the quantum mottle at the lower energy. There was also some variation in the field of view, which was adjusted so that the whole body section would fit into the circle of reconstruction. In general, the subjects in this study were of average size. The field of view was set between 38 and 40 cm in 15; in the remaining six subjects, it was increased up to 44 cm to allow for differences in patient size. For each subject, the field of view was constant for the scans taken with the two different energies.

The linearity of tissue attenuation values and the precision of calibration were tested with a prototype phantom placed on each subject's abdomen. The phantom was made of Lucite and had five tubes, four of which contained decreasing concentrations of iron dextran solutions (2.0, 1.0, 0.5, and 0.2 g of iron per 100 ml of dextran) and one of which contained a 10% ethyl alcohol solution. We chose this phantom because iron in the form of iron dextran has been used before and has proved to be efficacious in quantitative dual-energy CT of liver iron in animals [17]. The mean densities of 2-cm^2 areas at the center of the phantom tubes were measured.

Density measurements in Hounsfield units were taken from regions of interest (ROIs) in the phantom, liver, spleen, aorta, and adipose tissue. The mean attenuation of each ROI in scans obtained at 140 kVp (H_{140}) and 80 kVp (H_{80}) was recorded, and the difference (ΔH) was calculated where

$$\Delta H = H_{140} - H_{80}. \quad (1)$$

Care was exercised to measure homogeneous regions in the liver and other tissues. The areas of ROI measured between 2 and 6 cm^2, depending on the homogeneity, shape, and size of the structures. However, for each paired measurement, it was identical in size, shape, and location. The ROI did not include the periphery of the structures measured to avoid erroneous measurements related to volume averaging. Variations in the field of view, size, location, and shape of ROIs may influence the single-energy measurements because of their impact on beam-hardening effects, scatter, geometry, and centering. Because these factors were kept constant intraindividually, we assumed that in a particular patient these effects were comparable at high and low energies and, thus, canceled out on the dual-energy calculations [15]. Higher variations in quantum statistics are present in all dual-energy techniques. However, quantum statistics are more critical in imaging than in quantitative techniques.

The pathologist who examined the liver biopsy samples and the radiologist who made the CT measurements were not aware of the other's findings. Statistical analysis of the data was done with a commercially available computer software program (CSS: Complete Statistical System, StatSoft, Tulsa, OK).

Results

The phantom measurements showed a direct linear relationship between iron concentration and CT attenuation values at both 80 and 140 kVp. As expected, the slope was steeper with the 80-kVp than with the 140-kVp technique (Table 1, Fig. 1). This resulted in an energy-dependent change in CT attenuation, which was inversely but linearly related to the iron concentration (Fig. 1). There were also changes in attenuation with the 10% alcohol solution in the phantom and the adipose tissue of our patients. These changes in attenuation reflected those with the iron dextran solutions of 1g/dl and 2g/dl, respectively (Table 1). These results are comparable to previously reported results with dual-energy CT [14, 17].

TABLE 1: CT Attenuation of Adipose Tissue and of Phantom with Tubes Containing Various Concentrations of Iron Dextran Solutions and Alcohol, Placed on 21 Patients

Substance	Mean Attenuation ± SD (Range)		
	140 kVp	80 kVp	ΔH
Iron dextran (g Fe/dl dextran)			
2.0	92 ± 8 (72 to 103)	121 ± 11 (100 to 144)	−29 ± 8 (−52 to −19)
1.0	47 ± 8 (21 to 58)	58 ± 10 (31 to 71)	−11 ± 4 (−16 to 3)
0.5	24 ± 10 (−6 to 37)	23 ± 11 (−7 to 40)	1 ± 4 (−6 to 8)
0.2	9 ± 8 (−16 to 22)	1 ± 11 (−30 to 17)	8 ± 4 (1 to 16)
Alcohol	−4 ± 8 (−20 to 16)	−13 ± 7 (−39 to −4)	9 ± 6 (4 to 29)
Adipose tissue	−104 ± 23 (−123 to −4)	−131 ± 22 (−153 to −39)	27 ± 7 (5 to 35)

Dual-energy CT was done in eight patients with hepatocellular disease who had liver biopsy. They all had some degree of fatty infiltration. Depending on the biopsy findings, they were separated into two groups: patients without (n = 5) and with (n = 3) accompanying iron deposition. In the first group, the mean CT attenuation of the liver increased from 10 to 23 H when scanning at 80 and 140 kVp, respectively (Table 2). The mean change was 13 H, and the change in CT attenuation increased as the fat content increased (Table 2). One patient had minimal fatty infiltration, and the change in attenuation resembled the values of the upper limits of the control subjects (Fig. 2). Patients with fatty infiltration estimated to be greater than 25% showed a distinct change in attenuation (greater than 10 H), which was significantly greater than that of the control subjects. Because of the limited number or patients studied, the threshold of fatty infiltration that could be detected by dual-energy CT could not be determined.

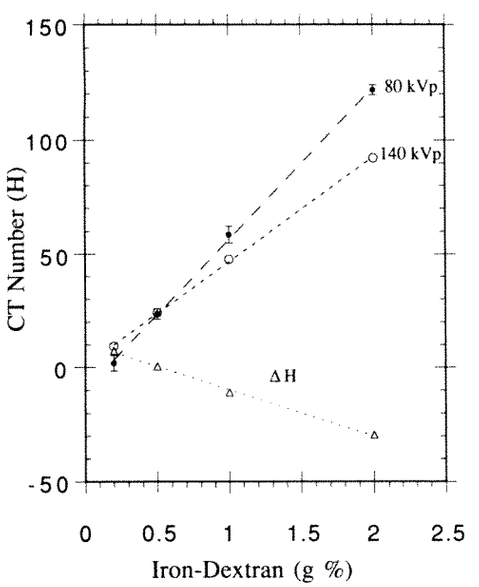


Fig. 1.—CT attenuation as a function of iron dextran concentration for 80 and 140 kVp. There is a linear increase in attenuation with increasing iron concentration (r = .999 for all lines), and slope is steeper with 80 kVp (increased sensitivity). ΔH is difference in measurements between scanning with high and low energies. Each point represents mean value of phantom for all scans. Brackets on 80-kVp line represent ±1 SE. Uncertainties of other points were comparable and omitted for clarity.

The second group included two patients with less than 25% fatty infiltration and +3 hemosiderin deposits and another patient with estimated 25–50% fatty infiltration and hemochromatosis. The mean change in attenuation (0.3 H)

TABLE 2: Mean CT Attenuation of Fatty Liver and Control Substances in 21 Patients

Substance	No. of Patients	Mean Attenuation			p Value
		140 kVp	80 kVp	ΔH	
Normal liver	7	52.0	48.5	3.5	.014
Spleen	18	40.5	38.5	2.0	.005
Aorta	21	38.0	36.5	1.5	NS
Liver mass	6	34.5	32.0	2.5	.081
Fatty liver + iron	3	49.3	49.0	0.3	NS
Fatty liver (% fat)[a]	5	23.0	10.0	13.0	.04
<25		47.5	41.0	6.5	
25–50		33.5	22.0	11.5	
25–50		41.0	30.0	11.0	
50–75		−8.5	−22.5	14.0	
>75		0.5	−20.0	20.5	
Adipose tissue	21	−104.0	−131.0	27.0	.0001

Note.—NS = not significant. Fatty liver + iron = combination of fatty liver and iron deposition.

[a] Actual values from the five patients with fatty liver but without iron depositions. Two patients had livers with 25–50% fat

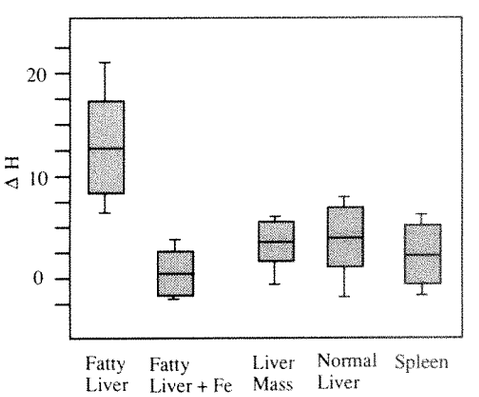


Fig. 2.—Box plots of means, means ± SD, and ±95% range of energy-related (140 or 80 kVp) change (ΔH) in CT attenuation of fatty liver, fatty liver and iron deposits, hypodense liver masses, normal liver, and spleen. Values of fatty liver are discrete, whereas those of other substances overlap.

was significantly lower ($p < .001$) when compared with that in patients with fatty infiltration but without hepatic iron deposits.

In the control groups, the change in attenuation was significantly smaller than that observed in patients with non–iron-containing fatty infiltration (Fig. 2). No fat was present in any of the hypodense liver masses, and it was presumed that no fat was in the liver of our normal volunteers, or in the aorta and spleen of all patients. The mean changes in density of hypodense liver masses and presumed normal liver were 2.5 and 3.5 H, respectively, whereas that of presumed normal spleen was 2 H and that of the aorta was 1.5 H (Table 2). Analysis of variance showed that the mean changes in attenuation among these control subjects and the patients with combined fat and iron deposition were not significantly different. However, a significant difference was found in mean change in attenuation of all of these four groups of patients and the patients with non–iron-containing fatty liver ($p < .001$). Conversely, on single-energy CT, the range of attenuation measurements of liver masses scanned with 80 or 140 kVp was not significantly different from that of fatty infiltration estimated to have less than 50% fat (Table 2).

Discussion

The results of this study suggest that dual-energy CT could be useful in the evaluation of hypodense liver lesions. When scanned with 80 and 140 kVp, fatty infiltration of the liver exhibits greater change in attenuation values than do normal liver and hypodense masses. A change greater than 7 H was suggestive of and greater than 10 H was unique to fatty infiltration.

The ability of dual-energy CT to discriminate fatty from nonfatty hypodense liver can be attributed to the inherent higher sensitivity of the low-energy X-ray beam to the various densities, providing higher contrast (Fig. 1), and the improved accuracy of the dual-energy approach itself. The CT attenuation of soft tissues is relatively independent of beam quality, and that of water is by definition 0 for all energies. However, the attenuation of fat is not independent of the beam energy because of its larger hydrogen content and its considerably lower density [15]. The low-energy scan is used to improve subject contrast, whereas the higher-energy scan is used as a reference value within the region to normalize the low-energy values. The dual-energy normalization is known to enhance differentiation between various types of tissues in quantitative CT [14–17]. Thus, when using dual-energy CT, the difference in attenuation of fat (ΔHF) is greater than that of liver (ΔHL) and hypodense liver masses (ΔHM) (Table 2):

$$\Delta HF > \Delta HL \approx \Delta HM. \quad (2)$$

In a region of the liver with fatty infiltration, the attenuation (HFL) may fall in the range of attenuations of hypodense liver masses:

$$HFL = \alpha HF + (1 - \alpha)HL = HM, \quad (3)$$

where HF, HL, and HM are the CT attenuation numbers for fat, liver, and hypodense mass, respectively, and α is the volume fraction of fat. Considering the attenuation coefficient of the tissues, at high energies, different combinations of liver-fat and liver-mass tissue may yield virtually identical CT numbers. Therefore, discrimination is not possible. Based on their basic attenuation properties, the discrimination between varying fractions of liver and mass tissue is only marginally higher at low energies. However, increasing concentrations of fat shows marked decrease in the CT number at low energies [15]. Fat-containing regions are expected to produce lower attenuation values than do normal liver or hypodense liver masses, although they could produce comparable attenuation values at high energies. The lower attenuation, however, may be within the range of a hypodense liver mass. Still, the change in attenuation of fatty liver (ΔHFL) would be greater than that of liver masses:

$$\Delta HFL = \alpha\Delta HF + (1 - \alpha)\Delta HL > \Delta HM. \quad (4)$$

High-density substances have an opposite effect, and it has been shown in dogs that the combined parenchymal/iron attenuation decreases with increasing kVp [17]. In our cases, infiltration with both fat and iron had a neutralizing effect with no attenuation changes on dual-energy CT, similar to normal liver.

Although advanced fatty infiltration of the liver is easily recognized by CT, direct attenuation measurements have proved unreliable [4, 17, 18]. Accurate quantification of fat content may be of clinical importance in persons susceptible to fatty infiltration. These include patients with diabetes mellitus, obesity, and alcohol or other substance abuse. It may also be important to monitor fatty response to or recovery from fatty response of the liver to various drug treatments, hyperalimentation, toxic materials, blunt liver trauma, and other catastrophes [5–13, 19–23]. In our study, there was a tendency of dual-energy CT to follow the degree of fatty infiltration more closely than direct CT attenuation measurements. Although the validity of these findings is limited by the small number of patients and lack of follow-up studies, these results warrant further investigation.

Dual-energy CT may also be helpful in cases of focal fatty infiltration of the liver, which may result in confusing or misleading CT images, because focal fatty infiltration may be mistaken for neoplastic or inflammatory conditions [5–13, 19]. In general, neoplastic and inflammatory conditions do not contain fat and change little in attenuation with dual-energy CT. However, fatty metamorphosis of the liver can rarely be seen in hepatocellular carcinoma and may be confused with focal fatty changes, especially when the tumor is small [24]. In such a situation, dual-energy CT could not help.

We encountered a number of cases with fatty liver combined with increased hepatic iron deposits. The combination of fat and iron could create problems in the use of dual-energy CT. We showed that the technique cannot detect fatty infiltration in the presence of hemochromatosis or hemosiderosis. Conversely, it cannot detect hemochromatosis or hemosiderosis in the presence of fatty infiltration of the liver. This

would suggest that the method is helpful only when attenuation changes. A number of patients with known primary cancer have both fatty infiltration (due to chemotherapy, diet, etc.) and increased iron deposits (due to hemosiderin deposits from blood transfusions). Theoretically, a specific low-attenuation mass in this group of patients would have similar attenuation at two energies, and thus dual-energy CT would not discriminate this occurrence from metastasis. In such situations, however, the single-energy attenuation values may be adequate, because the relatively hypodense regions would be at a range of densities similar to that of normal liver, whereas the surrounding parenchyma would have higher than normal attenuation. In addition, postprocessing CT techniques, similar to those proposed for determination of the composition of bone, may be helpful [15, 16]. To this purpose, special phantom development and the three-equation three-unknown method could be used to separate the various components of the mixed liver tissue (HFLI) [16]:

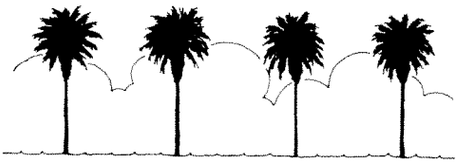
$$HFLI = \alpha HF + \beta HL + \gamma HI, \quad (5)$$

where HFLI is mixture of fatty liver and α, β, and γ are the volume fractions of fat, liver, and iron, respectively. This analysis, however, needs to be investigated.

Our results suggest a potential role for dual-energy CT of fatty infiltration of the liver. Additional studies are needed to validate these findings and to substantiate the potential for quantifying the degree of fatty infiltration.

REFERENCES

1. Ducommun JC, Goldberg HI, Korobkin M, Moss AA, Kressel HY. The relations of liver fat to computed tomography numbers: a preliminary experimental study in rabbits. *Radiology* **1979**;130:511–513
2. Kawata R, Sakata K, Kunieda T, Saji S, Doi H, Nozawa Y. Quantitative evaluation of fatty liver by computed tomography in rabbits. *AJR* **1984**;142:741–746
3. Piekarski J, Goldberg HI, Royal SA, Axel L, Moss AA. Difference between liver and spleen CT numbers in the normal adult: its usefulness in predicting the presence of diffuse liver disease. *Radiology* **1980**;137:727–729
4. Bydder GM, Chapman RWG, Harry D, Bassan L, Sherlock S, Kreel L. Computed tomography attenuation values in fatty liver. *J Comput Tomogr* **1981**;5:33–35
5. Mulhern CB Jr, Arger PH, Coleman BG, Stein GN. Nonuniform attenuation in computed tomography study of the cirrhotic liver. *Radiology* **1979**;132:399–402
6. Scott WW Jr, Sanders RC, Siegelman SS. Irregular fatty infiltration of the liver: diagnostic dilemmas. *AJR* **1980**;135:677–671
7. Halvorsen RA, Korobkin M, Ram PC, Thompson WM. CT appearance of focal fatty infiltration of the liver. *AJR* **1982**;139:277–281
8. Yates CK, Streight RA. Focal fatty infiltration of the liver simulating metastatic disease. *Radiology* **1986**;159:83–84
9. Baker MK, Wenker JC, Cockerill EM, Ellis JH. Focal fatty infiltration of the liver: diagnostic imaging. *RadioGraphics* **1985**;5:923–939
10. Baker ME, Silverman PM. Nodular focal fatty infiltration of the liver: CT appearance. *AJR* **1985**;145:79–80
11. Tang-Barton P, Vas W, Weissman J, Salimi Z, Patel R, Morris L. Focal fatty liver lesions in alcoholic liver disease: a broadened spectrum of CT appearances. *Gastrointest Radiol* **1985**;10:133–137
12. Kawashima A, Suehiro S, Murayama S, Russel WJ. Focal fatty infiltration of the liver mimicking a tumor: sonographic and CT features. *J Comput Assist Tomogr* **1986**;10:329–331
13. Adkins MC, Halvorsen RA, duCrest RP. CT evaluation of atypical hepatic fatty metamorphosis. *J Comput Assist Tomogr* **1990**;14:1013–1015
14. Cann CE. Quantitative CT for determination of bone mineral density: a review. *Radiology* **1988**;166:509–522
15. Rao GU, Yaghmai I, Wist AO, Arora G. Systematic errors in bone-mineral measurements by quantitative computed tomography. *Med Phys* **1987**;14:62–69
16. Goodsitt MM, Rosenthal DI, Reinus WR, Coumas J. Two postprocessing CT techniques for determining the composition of trabecular bone. *Invest Radiol* **1987**;22:209–215
17. Goldberg HI, Cann CE, Moss AA, Ohto M, Brito A, Federle M. Noninvasive quantitation of liver iron in dogs with hemochromatosis using dual-energy CT scanning. *Invest Radiol* **1982**;17:375–380
18. Levi C, Gray JE, McCullough EC, Hattery RR. The unreliability of CT numbers as absolute values. *AJR* **1982**;139:443–447
19. Pardes JG, Haaga JR, Borkowski G. Focal hepatic fatty metamorphosis secondary to trauma. *J Comput Assist Tomogr* **1982**;6:769–771
20. Nomura F, Ohnishi K, Ochiai T, Okuda K. Obesity-related nonalcoholic fatty liver: CT features and follow-up studies after low-calorie diet. *Radiology* **1987**;162:845–847
21. Bashist B, Hecht HL, Harley WD. Computed tomographic demonstration of rapid changes in fatty infiltration of the liver. *Radiology* **1982**;142:691–692
22. Ludwig J, Viggiano TR, McGill DB, Ott BJ. Nonalcoholic steatohepatitis: Mayo Clinic experiences with a hitherto unnamed disease. *Mayo Clinic Proc* **1980**;55:434–438
23. McKee CM, Weir PE, Foster JH, Murnaghan GA, Callender ME. Acute fatty liver of pregnancy and diagnosis by computed tomography. *Br Med J* **1986**;292:291–292
24. Yoshikawa J, Matsui O, Takashima T, et al. Fatty metamorphosis in hepatocellular carcinoma: radiologic features in 10 cases. *AJR* **1988**;151:717–720



Come to the American Roentgen Ray Society 92nd ANNUAL MEETING

Orlando, FL

Marriott's Orlando World Center
May 10–15, 1992

Scientific Program (200 papers)
Instructional Courses (60 hours)
Categorical Course on Neuroradiology
The Caldwell Lecture
Award Papers
Scientific Exhibits
Social, Golf, and Tennis Programs
Guest Programs

Differentiation Between Hemangiomas and Metastases of the Liver with Ultrafast MR Imaging: Preliminary Results with T2 Calculations

Mark A. Goldberg[1]
Sanjay Saini
Peter F. Hahn
Thomas K. Egglin
Peter R. Mueller

We studied the efficacy of T2 measurements at high field strength in distinguishing between liver hemangiomas and hepatic metastases when an ultrafast (single-excitation) MR imaging technique is used. Fourteen patients with known liver tumors were imaged in a 2.0-T prototype ultrafast MR scanner with a spin-echo (infinite TR and TE of 30–340 msec) pulse sequence. Each image was obtained with a total data acquisition time of 20 msec. T2 calculations for hepatic metastases (n = 6) showed a mean of 79.3 ± 13.5 msec, whereas hemangiomas (n = 8) showed a T2 of 139.8 ± 18.8 msec (p < .0001). T2 values of lesions had a smaller relative standard deviation than previously reported, and the range of T2 values of hemangiomas (119–181 msec) and metastases (68–103 msec) did not overlap.

Our preliminary results suggest that T2 calculations with ultrafast MR imaging may be useful for differentiating hemangiomas from metastases. We hypothesize that T2 values obtained from ultrafast MR images are more reliable than those obtained from conventional MR images, primarily because of the elimination of T1 information and effects of motion on image signal intensity.

AJR 157:727–730, October 1991

Because of the high rate of benign cavernous hemangiomas in the general population [1], their differentiation from malignant tumors (metastases and hepatocellular carcinoma) remains an important goal in liver cancer imaging [2]. With MR imaging, a variety of morphologic [3] and quantitative criteria [4–11] have been advanced to allow tissue characterization. Quantitative techniques have included lesion-to-liver contrast-to-noise ratios [5], lesion-to-liver signal intensity ratios [7, 9, 11], and image-derived T2 relaxation time calculations [4, 6, 8, 10].

At high field strength (1.5 T), a statistically significant difference between the mean T2 of hemangiomas and solid liver tumors has been shown [6, 8, 10]. Hence, T2 cutoff values (thresholds) have been advocated to differentiate hemangiomas from metastases or hepatomas [6, 8, 10]. Unfortunately, although mean T2 times of hemangiomas and metastases show clear separation, T2 values of hypervascular metastases are relatively long and often overlap the relatively short T2 values of fibrotic hemangiomas. Thus, for individual lesions, this overlap precludes the use of T2 cutoff values as a sole differentiating criterion [4, 6–12].

Several factors influence T2 calculations derived from conventional spin-echo images. These include the effects of motion [13], volume averaging [13], T1 contamination, flow-related even-echo rephasing [14], imperfections in RF pulse profile [15–17], magnetic field inhomogeneity [15, 18], and sampling only two or three points for relaxation time calculations [15]. We hypothesized that the adverse effects of many of these factors are decreased with ultrafast MR imaging, which should result in more precise estimation of T2 times. Therefore, we undertook this study to determine the usefulness of using T2 values derived from ultrafast MR images for distinguishing between liver hemangiomas and metastases.

Received February 26, 1991; accepted after revision April 19, 1991.

[1] All authors: Department of Radiology, Massachusetts General Hospital, 32 Fruit St., Boston, MA 02114. Address reprint requests to S. Saini.

0361–803X/91/1574–0727
© American Roentgen Ray Society

Subjects and Methods

Fourteen patients known to have liver tumors had ultrafast MR imaging. The group included eight patients with cavernous hemangiomas and six patients with metastases. The 10 men and four women were 40–80 years old (mean age, 59 years). The patients had mass lesions in the liver that had been detected previously on either CT or sonography. Four patients (two with hemangiomas and two with metastases) had histologic proof based on percutaneous needle biopsies. In the remaining cases, pathologic classification was based on correlative imaging with CT and/or sonography in combination with at least 1 year of follow-up. In the six patients with metastases, the primary lesions were pancreatic carcinoma in one, colonic carcinoma in two, lung carcinoma in one, lymphoma in one, and small-bowel carcinoid in one.

Ultrafast MR imaging was undertaken on a 2.0-T prototype scanner (Advanced NMR Systems, Woburn, MA) with the spin-echo instant scan technique, which has been described previously [19, 20]. Single-slice imaging was performed in the transverse plane with a 10- or 5-mm slice thickness. A fat-suppression technique, with a narrow-bandwidth 180° refocusing pulse tuned to the water resonance frequency, was used to obtain the images from which the T2 calculations were done. Images had a rectangular data matrix of 128 frequency-encoded steps and 64 phase-encoded steps. With a 22.5- by 45-cm rectangular field of view, the spatial resolution for these initial studies was approximately 4 × 4 mm.

Before patients were imaged, a phantom was scanned for calibration of signal intensity measurements. Patients were then imaged with the following protocol. The entire liver was first scanned with single-slice spin-echo acquisitions (infinite TR, 30-msec TE). Each slice was followed by incremental table movement, which was equal to the thickness of the preceding slice. A specific anatomic level through a liver tumor was then identified for further nonincremental (single-level) imaging. For each of these images, the patient was instructed to take breaths of uniform inspiratory effort, so that the several independently acquired images at different TEs could be obtained at a nearly identical anatomic level. Between four and 11 images were obtained with progressively longer TEs, which increased by steps of 30 msec until at visual inspection no discernible signal was present in the liver and/or lesion. In every case, images were obtained with at least these TEs: 30, 60, 90, and 120. Images were obtained with a single excitation, and no signal averaging was done. For each image, the data acquisition time was 20 msec. Interscan delay between sequential images was at least 2 min (120,000 msec). Thus, each image had a very long, essentially infinite TR.

Quantitative analysis was performed with calculation of T2 relaxation times. For this, tissue signal intensity was measured with manually contoured regions of interest (ROIs) on the liver tumor and adjoining normal liver. All lesions analyzed were larger than 2 cm. For liver tumors, the ROI included as large an area of the lesion as possible, and a similar-sized ROI was used to measure signal intensity from the adjacent normal liver. T2 calculations were derived from an equation of the general form:

$$SI = k \times \exp(-TE/T2)\,[1 - \exp(-TR/T1)],$$

where SI = signal intensity. A linear graph was constructed by using a semilogarithmic plot of ln(SI) vs TE (Fig. 1). With data obtained at multiple TEs, a linear fit was performed and T2 calculated from the slope of the regression line. For each lesion, and adjacent normal liver, a multiple point fit was performed by using data from between four and 11 images, each obtained at a different TE. The calculated T2 times of hemangiomas and metastases were statistically compared by using the unpaired Student's t test.

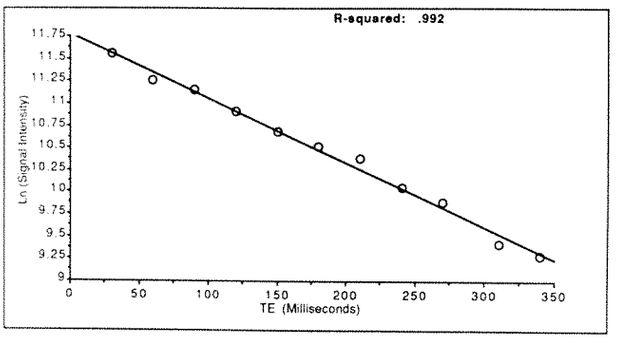


Fig. 1.—T2 calculation. Graph of natural logarithm (Ln) of image signal intensity vs TE. Data are from a colonic metastasis. Ultrafast MR imaging allows T2 calculation from a multiple point fit. Lesion signal shows monoexponential decay, and T2 time is slope of line that provides a linear fit.

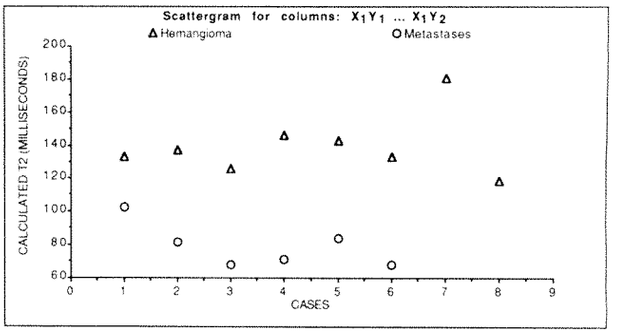


Fig. 2.—Scatterplot of T2 values calculated from ultrafast MR images for hemangiomas and metastases. Note that these data do not overlap.

Results

The mean T2 of liver was 43.7 ± 6.5 msec. In the eight patients with hemangiomas, the calculated mean T2 value was 139.8 ± 18.8 msec. The 95% confidence interval for the mean was 102–178 msec. For the six patients with metastases, the mean T2 was 79 ± 13.5 msec with a 95% confidence range of 52–106 msec (Fig. 2). The shortest T2 for a hemangioma was 119 msec and the longest T2 for a metastasis was 103 msec (small-bowel carcinoid). Thus, there was no overlap between T2 times of metastases and hemangiomas. The difference between the mean T2 values of metastases and hemangiomas was statistically significant ($p < .0001$).

Discussion

The precise relationship between T2 values derived from imaging experiments and the true T2 relaxation time of living tissues is not easily defined, but considerable error is believed to exist [10, 15–18]. Sources of error include imperfections in RF pulse and slice profiles, magnetic field inhomogeneity, motion-related artifacts, volume averaging, and even-echo rephasing [14–18]. Nonetheless, in the context of liver imaging, T2 quantification has been shown to be reproducible [4–6, 8, 10]. However, in practice, T2 values are of limited value

because of the large overlap in the range of T2 relaxation times of liver hemangiomas and metastases [10].

We hypothesize that ultrafast MR imaging offers certain advantages in calculating T2 relaxation times. Most importantly, ultrafast MR imaging eliminates the T1 component from the tissue signal intensity because the TR is infinite [21]. Thus, the information analyzed is purely T2 weighted, and calculations of T2 based on image signal intensity should be more accurate. Reproducibility also should be considerably enhanced, because the adverse effects of a number of additional variables (particularly those related to gross motion) that affect the signal intensity and hence the T2 calculation are reduced. For example, it has been estimated that the liver may move up to 2 cm with each respiratory cycle. Thus, tissues moving in and out of the imaging plane will affect T2 measurements because of the volume averaging of different tissue types (i.e., normal liver and lesions). As liver has a relatively short T2 time, volume averaging of lesions and normal liver will result in reduced estimates of lesion relaxation times.

In addition to the advantage of extremely short data acquisition times (20 msec), which eliminates effects of motion, an important source of error in T2 estimation results from RF pulse imperfections and static field inhomogeneity. These effects are compounded in pulse sequences in which multiple echoes [16–18] are obtained. In multiecho pulse sequences, even-echo rephasing also produces significant errors in T2 calculation when slow flow is present within the region of interest [14]. The ultrafast MR imaging technique overcomes many of these limitations in T2 calculations from conventional pulse sequences. For example, because the ultrafast pulse sequence used only a single 90–180° RF pulse pair with the 180° pulse being non-slice selective, signal degradation due to imperfection in RF pulses and magnetic field inhomogeneity is greatly reduced. Furthermore, the ultrafast technique efficiently allows T2 calculations to be based on many more (as many as 11 in this series) data points (each at a different TE). In contrast, T2 calculations in prior reports were usually based on two [4, 6–8, 10, 12] or occasionally three [5, 9] data points that were obtained from a single multiecho pulse sequence. More data points are thought to reduce the error in the T2 estimate (Fig. 1.)

On the basis of relaxation theory, T1 relaxation times increase as field strength is increased, but T2 relaxation times are not significantly affected [22]. In practice, however, image-derived T2 value shortening is observed at higher field strength. It is thought that this is because of exaggerated effects of RF pulse imperfections, suboptimal slice profiles, and magnetic field inhomogeneity [10, 15–18]. Indeed, the calculated T2 values for hemangiomas and liver that have been reported in the literature confirm this when results at high field strength (1.5 T) are compared with results of studies at 0.35 or 0.6 T [5–12] (Table 1). Given the considerations above, one would expect the calculated T2 values at 2.0 T to be decreased compared with previous high-field-strength observations. However, mean T2 values for hemangiomas in this study are substantially higher than those previously reported at high field strength. Although no other study at field strengths greater than 1.5 T has been done, our result of 139.8 ± 18.8 msec at 2.0 T is compared with prior results at 1.5 T of 85.6 ± 26.3 msec [10], 85.3 ± 21.2 msec [6], and 88.6 ± 20.0 msec [8]. We believe that our findings, which are contrary to those predicted, confirm the presence of an inherent advantage in ultrafast scanning in performing T2 calculations as predicted by the arguments above.

TABLE 1: Comparison of T2 Values Reported at Different Field Strengths

Field Strength/ Reference	Mean T2 ± SD (msec)	
	Hemangioma	Liver
0.35		
Li et al. [7]	93.0 ± 43.0	47.0 ± 13.0
Ohtomo et al. [4]	100.0 ± 30.0	46.0 ± 6.0
Ohtomo et al. [6]	101.6 ± 25.8	46.2 ± 5.4
Schmidt et al. [12][a]	100.0 ± 46.0	46.0 ± 8.0
0.6		
Egglin et al. [9]	143.0 ± 51.0	NA
Stark et al. [5]	150.0 ± 45.0	58.0 ± 9.0
1.5		
Lombardo et al. [10]	85.6 ± 26.3	NA
Ohtomo et al. [6]	85.3 ± 21.2	36.7 ± 3.7
Ohtomo et al. [8]	88.6 ± 20.0	NA
2.0		
This article	139.8 ± 18.8	43.7 ± 6.5

Note.—NA = not available.

[a] T2 times are interpolated from bar graphs.

Although the mean T2 value of liver is in close agreement with the T2 value as reported by Bottomley et al. [15], this technique may be less effective in measuring the T2 times of tissues with relatively short T2s [23]. Thus, in the data acquisition period of 20 msec, signal decay may be significant for the liver (T2 of approximately 43 msec) but will be less important for tissues such as hemangiomas (T2 of approximately 140 msec) and metastases (T2 of approximately 80 msec).

Comparison of the mean T2 values for metastases obtained with this technique with mean T2 values of metastases reported in the literature is more difficult because of differences in populations of patients. For example, it is well known that certain hypervascular metastatic lesions have considerably longer T2 relaxation times than do other metastatic lesions. The differing proportion of such patients in a given population would bias any attempt at comparison [3, 7, 10]. However, given these limitations, it is important to note that our preliminary results showed no overlap in the calculated T2 relaxation times of hemangiomas (range, 119–181 msec) and liver metastases (range, 68–103 msec). Indeed, even at 2 SD from the mean, the overlap was very small in the range of T2 values for hemangiomas (range, 102–178 msec) and metastases (range, 52–106 msec). We believe that this benefit was due to the relatively smaller standard deviation compared with those reported in previous T2 measurements of hemangiomas at high field strength.

We acknowledge that our study population is small and included only one patient with a metastatic lesion that is typically hypervascular (carcinoid). As a result, it is possible that the excellent separation achieved may in part be due to the small number of hypervascular metastases (with longer

T2 values) in the study group. For these reasons, our results must be considered preliminary, and further investigation is necessary to validate our initial findings.

Further limitations of the technique described in this article include the use of unique, nonconventional scanning equipment [21, 24]. In addition, imaging capability was limited to the axial plane, and only single-slice acquisitions were possible. Anatomic resolution in this prototype imager was also less than on conventional scanners, and this would adversely (owing to volume averaging) affect T2 calculations of small tumors. Thus, patients with lesions smaller than 2 cm were not included in the study. Experiments are currently underway on new ultrafast scanning equipment [25]. Advantages of the new system include compatibility with conventional 1.5-T imaging equipment, improved image resolution, thinner slices, and the ability to perform multislice multiplane acquisitions.

In conclusion, our preliminary results suggest that ultrafast MR imaging may offer unique advantages in quantitative T2 analysis compared with conventional spin-echo experiments. As a result, T2 calculations may serve as a highly useful diagnostic criterion in distinguishing liver hemangiomas from metastases. Although these preliminary results are based on a small data set, we believe the findings are clinically important, and confirmatory studies are underway with the new 1.5-T ultrafast MR imaging equipment.

ACKNOWLEDGMENT

We thank Richard Rzedzian for assistance in manuscript preparation.

REFERENCES

1. Karhunen PJ. Benign hepatic tumours and tumour like conditions in men. *J Clin Pathol* **1986**;39:183–188
2. Ferrucci JT. Liver tumor imaging: current concepts. *AJR* **1990**;155:473–484
3. Wittenberg J, Stark DD, Forman BH, et al. Differentiation of hepatic metastases from hepatic hemangiomas and cysts by using MR imaging. *AJR* **1988**;151:79–84
4. Ohtomo K, Itai Y, Furui S, Yashiro N, Yoshikawa K, Iio M. Hepatic tumors: differentiation by transverse relaxation time (T2) of magnetic resonance imaging. *Radiology* **1985**;155:421–423
5. Stark DD, Felder RC, Wittenberg J, et al. Magnetic resonance imaging of cavernous hemangioma of the liver: tissue-specific characterization. *AJR* **1985**;145:213–222
6. Ohtomo K, Itai Y, Yoshikawa K, Kokubo T, Iio M. Hepatocellular carcinoma and cavernous hemangioma: differentiation with MR imaging. Efficacy of T2 values at 0.35 and 1.5 T. *Radiology* **1988**;168:621–623
7. Li KC, Glazer GM, Quint LE, et al. Distinction of hepatic cavernous hemangioma from hepatic metastases with MR imaging. *Radiology* **1988**;169:409–415
8. Ohtomo K, Itai Y, Yoshida H, Kokubo T, Yoshikawa K, Iio M. MR differentiation of hepatocellular carcinoma from cavernous hemangioma: complementary roles of FLASH and T2 values. *AJR* **1989**;152:505–507
9. Egglin TK, Rummeny E, Stark DD, Wittenberg J, Saini S, Ferrucci JT. Hepatic tumors: quantitative tissue characterization with MR imaging. *Radiology* **1990**;176:107–110
10. Lombardo DM, Baker ME, Spritzer CE, Blinder R, Meyers W, Herfkens RJ. Hepatic hemangiomas vs metastases: MR differentiation at 1.5 T. *AJR* **1990**;155:55–59
11. Itoh K, Saini S, Hahn PF, Imam N, Ferrucci JT. Differentiation between small hepatic hemangiomas and metastases on MR images: importance of size-specific quantitative criteria. *AJR* **1990**;155:61–66
12. Schmidt HC, Tscholakoff D, Hricak H, Higgins CB. MR image contrast and relaxation times of solid tumors in the chest, abdomen, and pelvis. *J Comput Assist Tomogr* **1985**;9:738–748
13. Ehman RL, Kjos BO, Hricak H, Brasch RC, Higgins CB. Relative intensity of abdominal organs in MR images. *J Comput Assist Tomogr* **1985**;9:315–319
14. Kucharczyk W, Brant-Zawadzki M, Lemme-Plaghos L, et al. MR technology: effect of even-echo rephasing on calculated T2 values and T2 images. *Radiology* **1985**;157:95–101
15. Bottomley PA, Hardy CJ, Argersinger RE, Allen-Moore G. A review of 1-H nuclear magnetic resonance relaxation in pathology: are T1 and T2 diagnostic? *Med Phys* **1987**;14(1):1–37
16. Majumdar S, Orphanoudakis SC, Gmitro A, O'Donnell M, Gore JC. Errors in the measurements of T2 using multiple-echo MRI techniques. I. Effects of radiofrequency pulse imperfections. *Magn Reson Med* **1986**;3:397–417
17. Crawley AP, Henkelman RM. Errors in T2 estimation using multislice multiple-echo imaging. *Magn Reson Med* **1987**;4:34–47
18. Majumdar S, Orphanoudakis SC, Gmitro A, O'Donnell M, Gore JC. Errors in the measurements of T2 using multiple-echo MRI techniques. II. Effects of static field inhomogeneity. *Magn Reson Med* **1986**;3:563–574
19. Rzedzian RR, Pykett II. Instant images of the human heart using a new, whole-body MR imaging system. *AJR* **1987**;149:245–250
20. Pykett IL, Rzedzian RR. Instant images of the body by magnetic resonance. *Magn Reson Med* **1987**;5:563–571
21. Saini S, Stark DD, Rzedzian RR, et al. Forty-millisecond MR imaging of the abdomen at 2.0 T. *Radiology* **1989**;173:111–116
22. Wehrli FW. The basics of MR contrast. In: Atlas SW, ed. *Magnetic resonance imaging of the brain and spine.* New York: Raven, **1991**:23–38
23. Macovski A, Meyer C. Gradient power and T2 considerations in rapid imaging (abstr). In: *Book of abstracts: Society of Magnetic Resonance in Medicine 1987*, vol. 1. Berkeley, CA: Society of Magnetic Resonance in Medicine, **1987**:449
24. Stehling MK, Howseman AM, Ordige RJ, et al. Whole-body echo-planar MR imaging at 0.5 T. *Radiology* **1989**;170:257–264
25. Cohen MS, Weisskoff RM. Ultrafast imaging. *Magn Reson Imaging* **1991**;9:1–37

Detection of Hepatic Masses in Patients with Carcinoma:
Comparative Sensitivities of Sonography, CT, and MR Imaging

Karl Wernecke[1]
Ernst Rummeny[1]
Georg Bongartz[1]
Pierre Vassallo[1]
Dietmar Kivelitz[1]
Werner Wiesmann[1]
Peter E. Peters[1]
Berthold Reers[2]
Maximilian Reiser[1]
Wilfried Pircher[2]

To evaluate the sensitivity of sonography, CT, and MR imaging in the detection of hepatic masses in carcinoma patients, we conducted a prospective study of 75 consecutive patients with gastrointestinal tumors who were admitted for surgical resection of the primary tumor. Sonography was performed with convex transducers of 3.5 and 5.0 MHz. Three noninvasive CT techniques were used: unenhanced CT scans, the incremental bolus dynamic scanning technique, and delayed scanning 4–6 hr after bolus injection of 60 g of iodine. MR images (1.5 T) were acquired as presaturated T1- and T2-weighted spin-echo sequences and as breath-holding fast low-angle shot (FLASH) 60° and FLASH 15° sequences. As it is difficult to distinguish benign from malignant masses solely on the basis of morphologic criteria, the techniques for each imaging method were designed to detect and not to characterize hepatic lesions. Each examination was interpreted blindly, and the results were compared with surgical findings, intraoperative sonography, and biopsy of the liver as the gold standard. All focal hepatic masses verified at surgery, malignant or benign, were included in the analysis. Sixty-five (68%) of 95 focal hepatic masses were detected by CT, 60 lesions (63%) by MR, and 50 lesions (53%) by sonography. Although lesions 1–2 cm were shown almost equally well by CT and MR (74% and 77%, respectively), the detection rate of smaller lesions (<1.0 cm) decreased more drastically with MR (31%) than with CT (49%). Sonography had a sensitivity of only 20% with the smaller lesions. All imaging techniques had a sensitivity of 100% for focal hepatic masses larger than 2.0 cm.

Our results show that CT has a higher overall sensitivity (68%) than MR and sonography for the detection of focal hepatic masses. When the results of the three procedures are combined, the overall sensitivity is 77%. This is unsatisfactorily low, as CT and MR have a size threshold of about 1.0 cm and are relatively unreliable for the detection of smaller lesions.

AJR 157:731–739, October 1991

Single-institution and cooperative studies have shown a 20–40% 5-year survival rate in carcinoma patients in whom colorectal metastases have been resected from the liver [1–5]. Proper selection of patients for this surgical procedure requires accurate preoperative determination of the number, size, and location of the metastases. The results of several comparative studies of various imaging techniques for the detection of liver metastases are controversial [6–13] (Weyman PJ et al., presented at the annual meeting of the Radiological Society of North America, November 1986).

The purpose of this study was to evaluate the sensitivity of sonography, CT, and MR in the detection of focal hepatic masses in the prospective assessment of 75 consecutive patients undergoing surgery of gastrointestinal tumors. Surgical examination, intraoperative sonography, and biopsy of the liver were used as the gold standard for the diagnoses. Despite advances in hepatic CT and MR imaging, it is difficult to make a specific (benign or malignant) diagnosis solely on the basis of morphologic criteria, because most liver tumors have spectra of morphologic patterns that overlap. For this reason, the techniques for each imaging method

Received December 4, 1990; accepted after revision April 26, 1991.

[1] Institute of Clinical Radiology, University of Münster Medical School, Albert-Schweitzer-Str. 33, D-4400 Münster, Germany. Address reprint requests to K. Wernecke.

[2] Clinic of Surgery, University of Münster Medical School, D-4400 Münster, Germany.

0361–803X/91/1574–0731
© American Roentgen Ray Society

were designed to detect and not to characterize focal hepatic masses, and all lesions verified at surgery, malignant or benign, were included in the analysis.

Subjects and Methods

A prospective blinded study was conducted in 88 consecutive patients admitted within a period of 18 months for surgical removal of a primary gastrointestinal tumor. All patients had sonographic, CT, and MR examinations of the liver for initial staging and preoperative evaluation. In 13 patients, surgery was postponed or abandoned for various reasons (extended disease, distant metastases, presurgical chemotherapy), and these patients were excluded from the study.

The study population therefore included 75 patients (23 women, 52 men) in whom the liver was examined at surgery by visual inspection, thorough palpation, intraoperative sonography, and biopsy. The patients were 30–80 years old (mean, 58 years). The primary tumors originated from the colon and rectum (n = 15), esophagus (n = 16), pancreas (n = 13), stomach (n = 30), and small bowel (n = 1). Preoperative diagnostic examinations were generally performed within 2 days of one another. Surgery was carried out 1–17 days (mean, 3.6 days) after the last examination.

The findings of each examination were documented according to a standard protocol including number, size, and location of hepatic lesions. Information on previous imaging results was withheld. The liver was mapped according to the concept of Mukai et al. [14], identifying four segments (posterior and anterior segment of the right lobe, medial and lateral segment of the left lobe), which are differentiated with reference to the main branches of the hepatic veins on the axial tomograms. For clear and reproducible location of foci, detected hepatic lesions were marked on axial diagrams of the liver.

Sonographic Examination Technique

Sonography was performed with convex transducers of 3.5 and 5.0 MHz (LSC 9500, Picker International, Munich, Germany). All examinations were done by two experienced radiologists. The liver was examined first by using a subcostal approach in the sagittal and paraaxial planes. As a rule, the right hepatic lobe then was examined also with a lateral approach through the intercostal spaces. In slender patients, transducers of 5.0 MHz also were used for better resolution. No patient was excluded from sonography because of extreme obesity or marked fatty degeneration of the liver.

CT Examination Technique

All CT scans were obtained with the same imaging system (Philips Tomoscan 350) by using contiguous 9-mm sections through the entire liver. Three noninvasive CT techniques were used. Unenhanced CT scans of the liver were obtained first. Subsequently, patients were examined by using the incremental bolus dynamic scanning technique, with IV bolus injection of 60 g of iodine (200 ml Ultravist-300, Schering, Berlin, Germany), a scanning time of 4.8 sec, an interscan delay of 7.0 sec, and a scanning rate of five scans/min. The first, most cranial scan of the liver was obtained after an IV bolus injection of 30 g of iodine; the remaining scans were obtained during repeated manual bolus injections of an additional 30 g of iodine. The entire liver was scanned in 2.4-4.0 min (12–20 sections), depending on the size of the liver and the scanning time used. Delayed scanning was performed 4–6 hr after IV administration of contrast material. This delayed scanning technique is different from that described by Nelson et al. [12], who administered contrast material directly into the liver through both the hepatic artery and the portal vein. One patient could not be studied by incremental bolus dynamic CT and delayed CT because of an adverse reaction to the contrast medium. Although all but one of the 75 patients had incremental bolus dynamic CT, three lesions in the dome of the liver in three patients were not included on the scans because of slight differences in the centering of the patients.

MR Examination Technique

MR imaging was performed at 1.5 T (Magnetom, Siemens). The pulse sequences used were optimized for our MR system to obtain MR images of the liver with optimal anatomic resolution. All images were obtained in the axial plane with a section thickness of 10 mm by using four spin-echo (SE) sequences: T1-weighted SE 800/15/4 (TR/TE/excitations), proton density–weighted SE 2000/15/2, T2-weighted SE 800/70/4 or 2, and T2-weighted SE 2000/70/4 or 2. In addition, for all patients, fast imaging was done by using the fast low-angle shot (FLASH) technique. T1-weighted FLASH images, 100/6/60° (TR/TE/flip angle), and T2*-weighted images, 80/10/15°, were obtained. In order to reduce artifacts due to pulsatile flow, proximal and distal presaturation pulses were applied in all pulse sequences.

All 75 patients had the SE 800/15 and SE 800/70 sequences. In two patients, the SE 2000/15 and SE 2000/70 sequences were not performed because of limited examination time. In one patient, the SE 2000/15 and SE 2000/70 sequences were technically inadequate (motion artifacts) and were excluded from the lesion-by-lesion analysis.

All patients had the FLASH 60° sequence; in one instance, one lesion in the dome of the liver was not included in the examination. Toward the end of the study, the FLASH 15° sequence was omitted in 27 patients, because this sequence had already been proved insensitive for the detection of hepatic lesions.

Intraoperative Examination of the Liver

At laparotomy, the entire liver was visually inspected and bimanually palpated for the presence of intrahepatic lesions. In order to ensure careful intraoperative examination of lesions, the surgeon and the attending radiologist were informed about the results of all presurgical examinations. For examination of deep parenchymal areas, intraoperative sonography with a special operative probe (electronic 5.0-MHz transducer) was performed by an experienced radiologist. Biopsy or excision of the lesion was performed to confirm the diagnosis. When multiple lesions were identical visually or on sonography, only one lesion was sampled by biopsy. For this reason, the majority of deeply located lesions less than 1 cm in diameter were not biopsy proved.

In nine of 75 patients who were examined intraoperatively, sonography of the liver could not be performed because of technical difficulties. In these patients, follow-up CT was performed 6–8 months after surgery to confirm the presence or absence of hepatic metastases in deep parenchymal areas. Two of these nine patients had three deeply located metastases that increased in size between preoperative and follow-up examinations. The other seven patients had no hepatic lesions on either examination.

Evaluation of the Results

Intraoperative visual inspection, manual palpation, and sonography of the liver were used as the gold standard in this study. At the end of the study, the results of the presurgical imaging techniques were compared with the intraoperative findings. The results were evaluated with reference to single lesions and to individual patients.

Lesion-by-Lesion Analysis

In 32 of 75 patients, hepatic lesions were detected intraoperatively. In patients with five lesions or fewer (n = 21 patients), all lesions (total: n = 40) were included in the analysis. In patients with more than five lesions (n = 11 patients), only five foci were included in the lesion-by-lesion analysis. In two of the 11 patients, none of the lesions documented on intraoperative examination protocols could be detected with any of the preoperative imaging techniques. In nine patients with more than five lesions documented on preoperative imaging protocols, only five foci clearly identified as to size and location by intraoperative examination protocols were selected for comparison. Thus, 95 lesions verified at surgery were included in the lesion-by-lesion analysis. Our primary intent was to assess detection rate and not to characterize the focal lesions. Therefore, the examination techniques for each imaging method were designed to detect and not to characterize hepatic lesions. For this reason, all hepatic lesions verified at surgery, benign or malignant, were included in the analysis. Seventy-four (78%) of the 95 hepatic lesions were metastases and 21 were benign. The benign lesions included 10 cysts, four hemangiomas (all verified by biopsy), and two biopsy-proved focal fatty infiltrations of the liver. In two patients with superficially located and histologically verified hemangiomas, five other deeply located lesions were detected intraoperatively that had identical morphology on sonography. Although the real nature of these lesions remains unproved, they probably represented hemangiomas. Preoperative imaging techniques and additional follow-up CT studies over 6 months did not show these subcentimeter lesions, supporting our assumption of benign foci. Eleven of 21 benign lesions were 1.0 cm or less in diameter, and 18 benign lesions were smaller than 2.0 cm.

For each imaging technique, each lesion seen was characterized as true positive, false positive, or false negative. The sensitivity of each imaging technique was subsequently determined. The specificity could not be calculated because it is not possible to determine the number of true-negative hepatic lesions.

Patient-by-Patient Analysis

An evaluation with reference to the individual patient was performed for each imaging technique on the basis of one of three therapeutically relevant findings: (1) no hepatic lesions detected, (2) resectable hepatic lesions detected, and (3) nonresectable hepatic lesions detected. According to generally accepted surgical guidelines, patients were considered as surgically treatable if only one hepatic lobe was involved and not more than three metastases were detected [5].

We characterized the decision made for each patient as either true or false positive or as true or false negative, and the sensitivity and specificity were calculated for each imaging technique. In the patient-by-patient analysis, the specificity for each imaging technique could be calculated because the number of patients with true-negative results (absence of hepatic lesions) could be determined. The results were analyzed for statistically significant differences by means of the McNemar test.

Results

Lesion-by-Lesion Analysis

The results of the lesion-by-lesion analysis with each imaging technique are shown in Table 1. Sixty five (68%) of 95 lesions were detected by CT, 60 lesions (63%) by MR, and 50 lesions (53%) by sonography. No statistically significant differences were noted between the overall sensitivity of CT and MR.

The incremental bolus dynamic scanning technique was the most sensitive (67%) of the three CT techniques used (Figs. 1 and 2). Among the six different MR sequences, T2-weighted sequences (SE 800/70 and SE 2000/70) and the T1-weighted FLASH 60° sequence had the highest sensitivities (50%, 51%, and 51%, respectively; Fig. 2). The sensitivity of each individual MR sequence was significantly inferior to that of incremental bolus dynamic CT.

The detection of lesions with each technique as a function of lesion size is given in Table 2. All three imaging techniques showed identical sensitivity (88%) for lesions 2–5 cm in diameter. The two lesions missed by all techniques were 2.0 cm in diameter. Thus, all imaging techniques had a sensitivity of 100% for lesions greater than 2.0 cm. With lesions 1–2 cm in diameter, the detection rates of CT (74%) and MR (77%) decreased by 14% and 11%, respectively. The detection rate achieved by sonography was only 61% in this range of lesion sizes. For lesions less than 1 cm in diameter, the sensitivity of MR decreased significantly more (detection rate, 31%) than

TABLE 1: Lesion Detection by Sonography, CT, and MR

Imaging Technique	No. of Patients	No. of Lesions	True Positive	False Negative	False Positive	% Sensitivity
Sonography	34	95 [21]	50 [10]	45 [11]	0	53 [48]
Unenhanced CT	33	90	46	44	1	51
Incremental bolus dynamic CT	30	91	61	30	1	67
Delayed CT	33	94	50	44	2	53
CT (overall)	34	95 [21]	65 [12]	30 [9]	2	68 [57]
SE 800/15	34	95	32	63	1	34
SE 800/70	34	95	48	47	0	50
SE 2000/15	31	80	13	67	0	16
SE 2000/70	31	80	41	39	0	51
FLASH 15°	25	57	3	54	0	5
FLASH 60°	34	94	48	46	0	51
MR (overall)	34	95 [21]	60 [6]	35 [15]	1	63 [29]

Note.—SE = spin-echo, FLASH = fast low-angle shot. Numbers in brackets represent benign lesions; 74 of the 95 hepatic lesions were metastases, and 21 were benign. Significance of difference between CT (overall) and sonography: $p < .008$; between CT (overall) and MR (overall): $p > .168$.

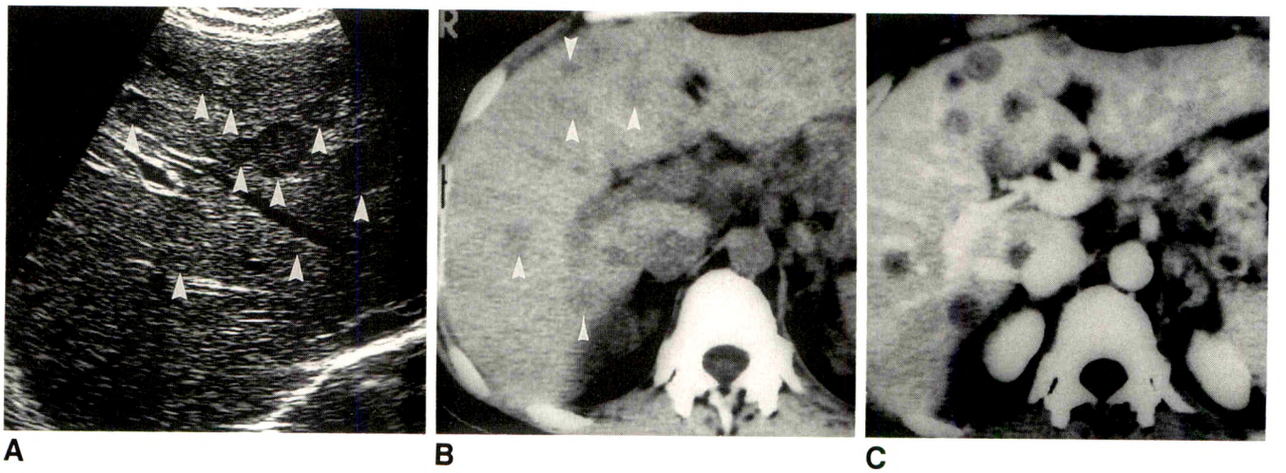


Fig. 1.—Visualization of hepatic metastases (adenocarcinoma of stomach) by sonography and various CT scanning techniques.
A, Subcostal paraaxial sonogram shows multiple target lesions (*arrowheads*) 0.8–2.0 cm in diameter.
B, On unenhanced CT scan, only a few large metastatic lesions (*arrowheads*) are faintly visible.
C, On incremental bolus dynamic CT scan, large metastases and additional smaller lesions can be clearly detected.

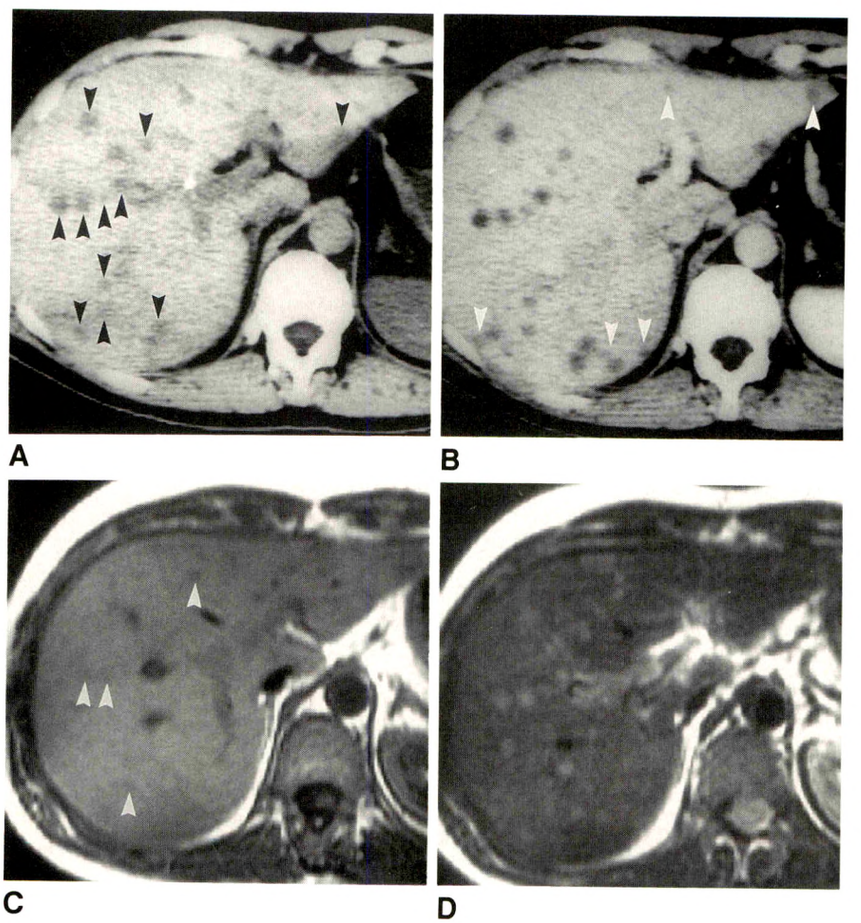


Fig. 2.—Visualization of small hepatic metastases (adenocarcinoma of pancreas) by various CT and MR imaging techniques.
A, Unenhanced CT scan shows multiple metastases (*arrowheads*) 1.0 cm in diameter in both hepatic lobes.
B, On incremental bolus dynamic CT scan, additional small lesions (*arrowheads*) can be detected in left lobe and posterior segment of right lobe.
C, On T1-weighted SE 800/15 MR image, only few metastatic lesions (*arrowheads*) are faintly visible.
D, On T2-weighted SE 800/70 MR image, multiple small metastases are shown in right lobe and medial segment of left lobe. Three lesions in lateral segment of left lobe, shown on incremental bolus dynamic CT scan (*B*), were not detected.

TABLE 2: Lesion Detection According to Size

Imaging Technique	No. (%) [No. (%) Benign]				
	Total	<1 cm	1–2 cm	2–5 cm	5–10 cm
Sonography	50/95 [10/21]	7/35 (20) [4/11 (36)]	24/39 (61) [3/7 (43)]	15/17 (88) [2/2 (100)]	4/4 (100) [1/1 (100)]
Unenhanced CT	46/90	14/35 (40)	16/34 (47)	12/17 (71)	4/4 (100)
Incremental bolus dynamic CT	61/91	16/34 (47)	27/37 (73)	14/16 (87)	4/4 (100)
Delayed CT	50/94	13/35 (37)	21/39 (54)	12/16 (75)	4/4 (100)
CT (overall)	65/95 [12/21]	17/35 (49) [5/11 (45)]	29/39 (74) [4/7 (57)]	15/17 (88) [2/2 (100)]	4/4 (100) [1/1 (100)]
SE 800/15	32/95	6/35 (17)	14/39 (36)	9/17 (53)	3/4 (75)
SE 800/70	48/95	8/35 (23)	24/39 (61)	13/17 (76)	3/4 (75)
SE 2000/15	13/80	1/28 (4)	5/31 (16)	4/17 (23)	3/4 (75)
SE 2000/70	41/80	3/28 (11)	20/31 (64)	15/17 (88)	3/4 (75)
FLASH 15°	3/57	0/20	2/27 (7)	1/9 (11)	0/1
FLASH 60°	48/94	9/35 (26)	22/38 (58)	13/17 (76)	4/4 (100)
MR (overall)	60/95 [6/21]	11/35 (31) [2/11 (18)]	30/39 (77) [1/7 (14)]	15/17 (88) [2/2 (100)]	4/4 (100) [1/1 (100)]

Note.—SE = spin-echo, FLASH = fast low-angle shot. Significance of the difference in sensitivity between CT and MR for lesions smaller than 1 cm: $p < .042$; between CT and sonography: $p < .030$. Seventy-four of the 95 hepatic lesions were metastases, and 21 were benign.

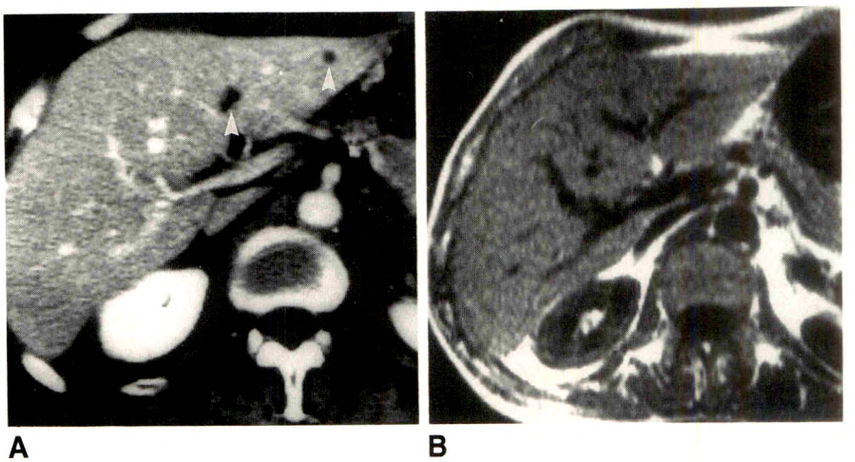


Fig. 3.—Small metastases (adenocarcinoma of stomach) in left hepatic lobe shown by CT, but not by MR.

***A*, Incremental bolus dynamic CT scan shows two small metastases (1.5 and 1.0 cm in diameter, *arrowheads*) in left hepatic lobe.**

***B*, On T1-weighted FLASH 60° image and on other MR sequences (*not shown*), these lesions were not detected.**

that of CT (49%) (Figs. 2 and 3). Sonography gave the poorest results, with a sensitivity of only 20% (7/35 lesions).

In the detection of small foci, incremental bolus dynamic CT scanning again showed the highest sensitivity (47%, Figs. 1 and 2). Among the MR sequences used, the SE 800/70 and FLASH 60° sequence were clearly superior to the SE 2000/70 sequence (sensitivities, 23% and 26%, respectively, vs 11%).

The lesion detection rates as a function of anatomic location are shown in Table 3. The detection rates of CT and MR were identical in lesions of the right hepatic lobe (75%). In the left hepatic lobe, the detection rate of MR (43%) decreased more than that of CT (57%, Figs. 2 and 3). The detection rate of sonography was approximately 15% lower than the rate for CT for both the right (58%) and the left (43%) hepatic lobes. False-positive findings occurred with CT (two lesions) and MR (one lesion), but not with sonography. The false-positive CT findings were due to misinterpretation of vascular structures. The false-positive MR finding turned out to be an imaging artifact.

Table 4 lists the sensitivity values for sonography, different combinations of CT techniques, MR sequences, and combinations of all three imaging techniques. These results suggest that delayed CT, which poses problems in planning and is time-consuming, can be omitted because the combination of incremental bolus dynamic CT and unenhanced CT will already result in an overall sensitivity of 67%. Of the MR techniques, the best combination of three pulse sequences would combine SE 800/70, SE 2000/70, and FLASH 60° (overall sensitivity, 62%); the best combination of two pulse sequences would be the SE 800/70 and FLASH 60° sequences (overall sensitivity, 60%). It is important to note that

TABLE 3: Lesion Detection by Location

Imaging Technique	No. of Lesions	No. Detected (%) [No. (%) Benign]	
		Right Lobe	Left Lobe
Sonography	95	35/60 (58) [6/12 (50)]	15/35 (43) [4/9 (44)]
Unenhanced CT	90	34/57 (60)	12/33 (36)
Incremental bolus dynamic CT	91	43/57 (75)	18/34 (53)
Delayed CT	94	35/59 (59)	15/35 (43)
CT (overall)	95	45/60 (75) [8/12 (67)]	20/35 (57) [4/9 (44)]
SE 800/15	95	26/60 (43)	6/35 (17)
SE 800/70	95	37/60 (62)	11/35 (31)
SE 2000/15	80	12/51 (23)	1/29 (3)
SE 2000/70	80	32/51 (63)	9/29 (31)
FLASH 15°	57	2/36 (6)	1/21 (5)
FLASH 60°	94	37/59 (63)	11/35 (31)
MR (overall)	95	45/60 (75) [5/12 (42)]	15/35 (43) [1/9 (11)]

Note.—SE = spin-echo, FLASH = fast low-angle shot. Seventy-four of the 95 hepatic lesions were metastases, and 21 were benign.

TABLE 4: Calculated Sensitivity Values for Sonography and Various Combinations of CT Techniques and MR Pulse Sequences and for Combinations of All Three Imaging Techniques

Imaging Techniques	No. (% Sensitivity)
Sonography	50/95 (53)
CT (overall)	65/95 (68)
Unenhanced CT + incremental bolus dynamic CT	64/95 (67)
Unenhanced CT + delayed CT	55/95 (58)
Incremental bolus dynamic CT + delayed CT	64/94 (68)
MR (overall)	60/95 (63)
SE 800/70 + SE 2000/70 + FLASH 60°	59/95 (62)
SE 2000/70 + FLASH 60°	54/95 (57)
SE 2000/70 + SE 800/70	54/95 (57)
SE 800/70 + FLASH 60°	57/95 (60)
Combination of different imaging techniques	
Sonography + CT + MR	73/95 (77)
Sonography + CT	71/95 (75)
Sonography + MR	67/95 (70)
CT + MR	69/95 (73)

Note.—SE = spin-echo, FLASH = fast low-angle shot. Seventy-four of the 95 hepatic lesions were metastases, and 21 were benign.

the total detection rate reaches an optimum of only 77%, even if all three imaging techniques are combined. Combined sonography and CT had a total detection rate of 75%.

Patient-by-Patient Analysis

The results of the patient-by-patient analysis are shown in Tables 5 and 6. The therapeutic consequences of the findings about the presence or absence of metastases and resectability were better answered by CT (72%) than by MR (55%) or sonography (50%). The sensitivity of combined CT and sonography was 78%.

Discussion

Cross-sectional imaging techniques play an essential role in proper selection of patients for hepatic surgery. However, controversy exists about the selection of the single best imaging technique or the most appropriate combination of different techniques [6–13] (Weyman et al., RSNA, November 1986).

Three possible factors are responsible for inconsistent results among comparative studies. First, different CT techniques (scanning time and administration of contrast material), MR techniques (pulse sequences, scanning parameters), and hardware are used. Second, many studies have no proper gold standard for determination of the actual diagnoses. Third, those studies with an appropriate gold standard are based on relatively small numbers of patients. In order to compensate for these small numbers, lesion-by-lesion analyses of as many as 20 metastases per patient were performed. It is well known that no sonographic, CT, or MR technique can be judged the best or poorest for any patient. Metastases with identical histologic findings may, for obscure reasons, be shown better by the one imaging technique in one patient and by another technique in the next. If up to 20 lesions per patient are included in a lesion-by-lesion analysis, statistics may be strongly biased in favor of one specific technique if those lesions happen to be particularly well detected by that method.

In an attempt to avoid these influences, we adhered to the following rules in the study design: (1) examination of a comparatively large number of patients with a gold standard adapted to the conditions of a clinical study, (2) inclusion of no more than five foci per patient in the lesion-by-lesion analysis, and (3) additional patient-by-patient analysis with reference to therapeutic consequences.

Our results show that CT has the highest sensitivity in the lesion-by-lesion analysis, with an overall detection rate of 68%. The advantages of CT as compared with other cross-sectional imaging techniques consisted mainly in the higher detection rate of smaller lesions (<1.0 cm diameter) and lesions located in the left hepatic lobe (Tables 2 and 3, Figs. 2 and 3). Whereas foci 1–2 cm in diameter are imaged almost equally well by CT and MR, the detection rate of smaller lesions (<1.0 cm) decreased more drastically with MR (31%) than with CT (49%). Both methods detected lesions in the right hepatic lobe better (sensitivity of both techniques, 75%) than they did those in the left lobe; MR was clearly inferior to CT for lesions in the left lobe (CT, 57%; MR, 43%; Figs. 2 and 3).

The superior detection rate of CT with small lesions might be attributed to several factors. CT is still distinguished by better resolution and lower susceptibility to artifacts. However, one definite advantage of CT is that the images are acquired during breath-holding, whereas most of our MR images are taken during normal respiration. With the MR technique, it can be imagined that small lesions may disappear because of averaging with respiratory movements. The superior sensitivity of FLASH 60° images, which are acquired during breath-holding, compared with the SE images supports this hypothesis (Table 2). Unfortunately, currently available

TABLE 5: Patient-by-Patient Analysis: Correlation of Presurgical Sonography, CT, and MR with Intraoperative Findings

Imaging Study/Finding	Operative Finding		
	No Lesions	Resectable Hepatic Lesions	Unresectable Hepatic Lesions
Sonography			
No lesions	43 TN	8 FN	3 FN
Resectable hepatic lesions	0 FP	6 TP	5 FN
Unresectable hepatic lesions	0 FP	0 FP	10 TP
CT			
No lesions	41 TN	5 FN	3 FN
Resectable hepatic lesions	2 FP	9 TP	1 FN
Unresectable hepatic lesions	0 FP	0 FP	14 TP
MR			
No lesions	43 TN	8 FN	4 FN
Resectable hepatic lesions	0 FP	5 TP	2 FN
Unresectable hepatic lesions	0 FP	1 FP	12 TP

Note.—TN = true negative, FN = false negative, FP = false positive, TP = true positive.

TABLE 6: Patient-by-Patient Analysis: Sensitivity and Specificity of Each Imaging Technique and of Combinations of the Three Imaging Techniques

Imaging Method(s)	No. (% Sensitivity)	No. (% Specificity)
CT	23/32 (72)[a]	41/43 (95)
Sonography	16/32 (50)[a]	43/43 (100)
MR	17/31 (55)[a]	43/44 (98)
Sonography + CT	25/32 (78)	41/43 (95)
Sonography + MR	20/31 (64)	43/44 (98)
CT + MR	23/31 (74)	41/44 (93)
Sonography + CT + MR	25/31 (81)	41/44 (93)

[a] Significance of the difference in sensitivity between CT and MR: $p > .1$; between CT and sonography: $p > .138$.

FLASH sequences have a much lower power of spatial resolution than the SE sequences do, which markedly limits their use in the detection of smaller foci. The low sensitivity of MR for focal lesions in the left lobe may be due in part to obscuring effects of flow-related artifacts from the aorta and the heart.

Of the three CT techniques used, incremental bolus dynamic CT had the highest sensitivity (67%) (Figs. 1 and 2). The high detection rates of delayed CT reported by other research groups [8, 15] could not be reproduced in our study. This discrepancy may be due to the different ways of administering contrast medium. Nelson et al. [11] and Miller et al. [8] administered contrast material directly into the liver through both the hepatic artery and the portal vein. This may have caused more effective opacification of the reticuloendothelial system than IV administration, which was used in our study, would produce. The results of our study indicate that the detection rate with delayed CT after IV administration of 60 g of iodine is not significantly higher than that with unenhanced CT (Table 1). The detection rate with CT can be improved by combining incremental bolus dynamic CT with unenhanced CT (Fig. 4) or with the more time-consuming delayed CT (Table 4). In our study, four of the 65 lesions detected by CT were not shown by incremental bolus dynamic CT; this probably resulted from strong contrast enhancement due to tumor vascularity causing blending of the lesion with surrounding liver tissue. Three of these four lesions were detected by unenhanced CT (Fig. 4).

Of the six MR sequences used, the T2-weighted SE sequences (SE 800/70 and SE 2000/70) and the T1-weighted FLASH 60° sequence taken during breath-holding were the most sensitive (50%, 51%, and 51%, respectively). A combination of these three sequences showed 59 of 60 hepatic lesions detected by all MR sequences (Table 4).

Sonography, although performed by radiologists with considerable experience, produced by far the poorest results. The size threshold of reliable detection is clearly higher in sonography than in the other techniques. Although lesions more than 2 cm in diameter are detected with an absolutely identical sensitivity of 100% by all three methods, the decrease in detection rate of sonography (61%) for lesions 1–2 cm was more than 10% lower than that of CT (74%) and MR (77%). The drop in sensitivity of sonography became even more pronounced with lesions less than 1 cm in diameter (20%).

Combined sonography, CT, and MR yielded a sensitivity of 77%. The best combination of two procedures was sonography with CT, showing an overall sensitivity of 75% (Table 4). These data show that although CT had the highest overall sensitivity, it was not the best technique in every patient and that sonography and MR might have an important adjuvant role in improving both the rate and confidence of detection of focal hepatic lesions (Fig. 5). However, even when the information from all techniques was combined, the overall sensitivity was only 77%, as CT and MR have a size threshold of about 1.0 cm and are relatively unreliable for the detection of smaller lesions.

In the patient-by-patient evaluation, the superiority of CT became even more apparent, although the differences in sensitivity between the three imaging techniques were not statistically significant (Table 6). The therapeutically relevant data on absence or presence and resectability of metastases were more often correct with CT (72%) than with MR (55%) or sonography (50%). Even in the patient-by-patient analysis,

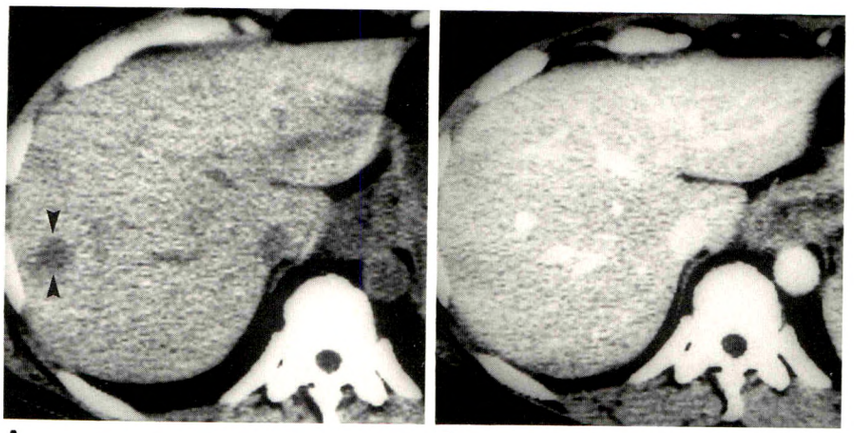


Fig. 4.—Vanishing metastasis (adenocarcinoma of esophagus) on incremental bolus dynamic CT scans.
A, Unenhanced CT scan shows metastasis (2.0 cm in diameter, *arrowheads*) in right hepatic lobe.
B, On incremental bolus dynamic CT scan, lesion shown in *A* could not be detected because of strong enhancement of metastasis.

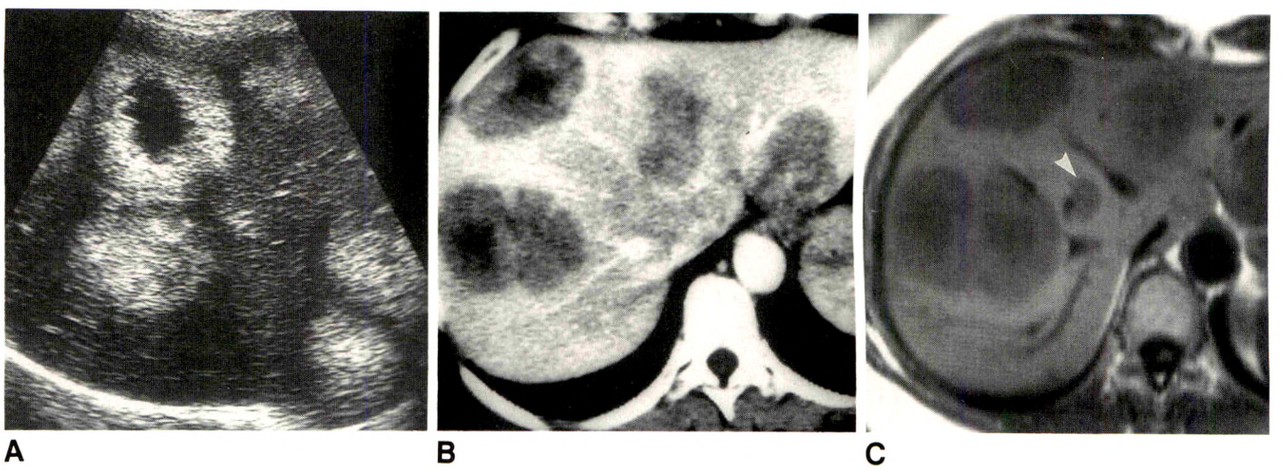


Fig. 5.—Multiple hepatic metastases (adenocarcinoma of colon): small lesion shown by MR, but not by CT or sonography.
A, Subcostal paraaxial sonogram shows multiple large hyperechoic metastases, which partly show hypoechoic central necrosis.
B, Incremental bolus dynamic CT scan shows multiple large metastases with central necrosis in both hepatic lobes.
C, On T1-weighted SE 800/15 MR image, an additional small metastasis (1.5 cm in diameter, *arrowhead*) was detected that could not be seen on CT and sonography.

the overall sensitivity when all techniques were combined was only 81% (Table 6).

One criticism may be raised with respect to this study: the use of surgical examination of the liver at laparotomy and intraoperative sonography as the gold standard. A more accurate standard would be to use the results of pathologic examination of all or a portion of the liver, but it is difficult to acquire data on a large series of patients undergoing such resections. In two studies that compared surgical assessment of the liver with autopsy results, macroscopic metastatic disease was present in the liver in only 3–5% of patients considered free of hepatic metastasis at laparotomy [16, 17]. The deep, central portions of the liver cannot be adequately palpated, and we have used intraoperative sonography to examine these areas more thoroughly. Direct surgical examination of the liver at laparotomy in combination with intraoperative sonography is regarded as the standard against which any other result should be tested [18]. However, reliability of the chosen gold standard and accuracy statistics decreases with the size of the lesion. The combination of surgical examination and intraoperative sonography may miss lesions less than 1 cm in diameter that are too small to be seen and/or overcalls such lesions proved only by association with larger lesions.

Twenty-one (22%) of 95 hepatic lesions included in this study were benign. We did not exclude benign lesions for several reasons. Our primary intent was to assess detection rate of hepatic lesions, not to characterize the focal lesions. Therefore, the examination techniques for each imaging method were designed to detect and not to characterize hepatic lesions. This approach agrees with other studies that have compared the detection rates of different imaging techniques [12, 13]. In a prospective blinded study of detection rates, benign lesions should not be excluded retrospectively.

Although detection of benign lesions seems to be irrelevant to the task of finding liver metastases, data on detection of these lesions are also clinically relevant. Prospective differentiation from metastatic lesions with certainty remains a problem, and their detection consequently influences clinical management. This is particularly true for lesions less than 1 cm in diameter (11 of 21 benign lesions in our study), which are too small to have distinctive morphologic features with any of the three imaging techniques. Importantly, CT detected more benign lesions than MR did. In fact, more benign lesions, particularly those smaller than 2.0 cm in diameter, were missed by MR (Tables 1–3). Liver metastases from gastrointestinal carcinomas are almost always hypovascular. The results of this study may include a predominance of hypovascular metastases and cannot be extrapolated to include hypervascular metastases from other tumors. Hypervascular lesions may behave differently and may be more subtle on dynamic CT scans than on unenhanced CT scans (Fig. 4) [19].

Although our results may seem somewhat pessimistic about the current clinical usefulness of MR in the evaluation of hepatic lesions, they should be placed in the proper perspective. MR is a relatively new technique, and significant technical improvements can be expected. MR images obtained in this study showed the highest lesion-liver contrast on T2-weighted SE sequences, as reported previously [20]. Additional technical developments may favor T1-weighted pulse sequences, as recommended for low- and mid-field systems, with fast and ultrafast imaging techniques at high field strength [21, 22]. In addition, the administration of contrast agents (gadopentetate dimeglumine, superparamagnetic iron oxide particles) also may improve the detection rate for focal hepatic lesions.

At present, however, we conclude that the question about the precise number, size, and location of focal hepatic lesions before hepatic resection is best answered by CT, which offers the highest overall sensitivity of all noninvasive imaging techniques.

REFERENCES

1. Adson MA, Van Heerden JA, Adson MH, Wagner JS, Ilstrup DM. Resection of hepatic metastases from colorectal cancer. *Arch Surg* **1984**;119: 647–651
2. Wagner JS, Adson MA, Van Heerden JA, Adson MH, Ilstrup DM. The natural history of hepatic metastases from colorectal cancer: comparison with resective treatment. *Ann Surg* **1984**;199:502–508
3. Hughes KS, Sugarbaker PH. Treatment of metastatic liver tumors. In: Rosenberg SA, ed. *Surgical cure of metastatic cancer*. Philadelphia: Lippincott, **1987**:125–164
4. Sugarbaker PH, Kemeny N. Management of metastatic liver cancer. *Adv Surg* **1988**;22:1–55
5. Adson MA. Resection of liver metastases—when is it worthwhile? *World J Surg* **1987**;11:511–520
6. Glazer GM, Aisen AM, Francis IR, Gross BH, Gyves JW, Ensminger WD. Evaluation of focal hepatic masses: a comparative study of MRI and CT. *Gastrointest Radiol* **1986**;11:263–268
7. Matsui O, Takashima T, Kadoya M, et al. Liver metastases from colorectal cancers: detection with CT during arterial portography. *Radiology* **1987**;165:65–69
8. Miller DL, Simmons JT, Chang R, et al. Hepatic metastasis detection: comparison of three CT contrast enhancement methods. *Radiology* **1987**;165:785–790
9. Stark DD, Wittenberg J, Butch RJ, Ferrucci JT. Hepatic metastases: randomized, controlled comparison of detection with MR imaging and CT. *Radiology* **1987**;165:399–406
10. Curati WL, Halevy A, Gibson RN, Carr DH, Blumgart LH, Steiner RE. Ultrasound, CT, and MRI comparison in primary and secondary tumors of the liver. *Gastrointest Radiol* **1988**;13:123–128
11. Nelson RC, Chezmar JL, Steinberg HV, et al. Focal hepatic lesions: detection by dynamic and delayed computed tomography versus short TE/TR spin echo and fast field echo magnetic resonance imaging. *Gastrointest Radiol* **1988**;13:115–122
12. Nelson RC, Chezmar JL, Sugarbaker PH, Bernardino ME. Hepatic tumors: comparison of CT during arterial portography, delayed CT, and MR imaging for preoperative evaluation. *Radiology* **1989**;172:27–34
13. Reinig JW, Dwyer AJ, Miller DL, Frank JA, Adams GW, Chang AE. Liver metastases: detection with MR imaging at 0.5 and 1.5 T. *Radiology* **1989**;170:149–153
14. Mukai JK, Stack CM, Turner DA, et al. Imaging of surgically relevant hepatic vascular and segmental anatomy. Part 1. Normal anatomy. *AJR* **1987**;149:287–292
15. Bernardino ME, Erwin BC, Steinberg HV, Baumgartner BR, Torres WE, Gedgaudas-McClees RK. Delayed hepatic CT scanning: increased confidence and improved detection of hepatic metastases. *Radiology* **1986**;159:71–74
16. Hogg L, Pack GT. Diagnostic accuracy of hepatic metastases at laparotomy. *Arch Surg* **1956**;72:251–252
17. Gray BN. Surgeon accuracy in the diagnosis of liver metastases at laparotomy. *Aust N Z J Surg* **1980**;50:524–526
18. Boldrini G, de Gaetano AM, Giovannini I, Castagneto M, Colagrande C, Castiglioni G. The systematic use of operative ultrasound for detection of liver metastases during colorectal surgery. *World J Surg* **1987**;11: 622–627
19. Bressler EL, Alpern MB, Glazer GM, Francis IR, Ensminger WD. Hypervascular hepatic metastases: CT evaluation. *Radiology* **1987**;162:49–51
20. Foley WD, Kneeland JB, Cates JD, et al. Contrast optimization for the detection of focal hepatic lesions by MR imaging at 1.5 T. *AJR* **1987**;149:1155–1160
21. Stark DD, Wittenberg J, Edelmann RR, et al. Detection of hepatic metastases: analysis of pulse sequence performance in MR imaging. *Radiology* **1986**;159:365–370
22. Edelmann RR, Wallner B, Singer A, Atkins DJ, Saini S. TurboFLASH: method for breath-hold MR imaging of the liver with flexible contrast. *Radiology* **1990**;177:515–521



The Radiology Outreach Foundation (ROF) is a nonprofit corporation whose goal is to help disadvantaged countries improve their health care by providing radiology equipment, books, consultation, education, and training to their practitioners. This assistance is on an application basis that is independent of political, ethnic, or religious orientation of the grantee. It depends on the need of the people and the ability of the ROF to meet that need. The ROF is approved by the U.S. Internal Revenue Service as a tax-exempt organization. It is endorsed by the following radiologic societies:

American Association of Women Radiologists
American College of Radiology
American Roentgen Ray Society
Association of University Radiologists
Radiological Society of North America
Society of Chairmen of Academic Radiology Departments
Society for Pediatric Radiology
European Society of Pediatric Radiology

All donations to the ROF are tax deductible. Persons who would like to contribute financially to the ROF, would be interested in being a visiting professor, would like to send books or journals to any of the institutions supported by the ROF, or would like further information about the ROF should write to

Charles A. Gooding, M.D.
President
Radiology Outreach Foundation
3415 Sacramento St.
San Francisco, CA 94118 USA

Pictorial Essay

MR Imaging in Hydatid Disease

Walther von Sinner,[1] Lambertus te Strake,[1] David Clark,[2] and Hassan Sharif[2]

Hydatid cysts may develop anywhere in the body as a result of the presence of a viable parasite (*Echinococcus granulosus*). Depending on the condition of the parasite, the host reaction, and therapy, the hydatid cyst will degenerate and may eventually collapse, leaving an area of calcification in the host tissue. The purpose of this pictorial essay is to demonstrate the use of MR imaging in the diagnosis of the various stages of hydatid disease and in monitoring response to therapy.

Echinococcus granulosus is a zoonosis of worldwide distribution. Humans may become infested after ingesting parasitic eggs directly, from contact with dogs, or indirectly, from contaminated water or food. Hatched parasitic embryos migrate through the intestinal mucosa and enter venules and lymphatics. The liver filters 60–70% of the embryos and the lungs, 15–25%; 10–15% will reach other organs via the systemic circulation. Embryos that are not destroyed transform into small cysts that will grow 2–3 cm each year. The wall of the parasitic cyst consists of a germinal layer (endocyst) and a laminated proteinaceous membrane (ectocyst). The host reacts against the cyst by forming a dense fibrous capsule (pericyst), which contains blood vessels that provide nutrients to the parasite. The natural history of the hydatid cyst shows that the disease is a dynamic entity with different manifestations depending on the degree and severity of degenerative changes of the parasite. Effective new drugs are now available to treat hydatid disease medically. We demonstrate the use of MR in diagnosing simple and complicated hydatid cysts and in monitoring the results of chemotherapy.

Stages of Development of Hydatid Cysts

Simple Viable Hydatid Cyst

The wall of the intact viable hydatid cyst consists of two layers: (1) parasitic membranes consisting of gelatin and proteinaceous material and (2) an outer layer consisting of dense fibrous capsule from reactive host tissue.

In the intact cyst, these layers cannot be separated on MR images. On T1-weighted spin-echo (SE) images, the cyst wall is isointense relative to the fluid in the cyst and appears on T2-weighted images as a low-intensity rim surrounding the homogeneous high-signal cyst contents (Fig. 1). In the liver, the low-intensity rim is a nonspecific finding and has been described in a number of other benign and malignant conditions [1].

Hydatid Cyst with Daughter Cysts

On T1-weighted images, the viable daughter cysts may be isointense or slightly hypointense compared with the contents ("hydatid sand") of the mother cyst (Fig. 2). Daughter and mother cysts are isointense on T2-weighted images. The development of daughter cysts is an early sign of degeneration of the mother cyst.

Hydatid Cyst with Detached Parasitic Membranes

The presence of detached membranes is a sign of more severe degeneration and rupture of the parasitic membranes

Received January 22, 1991; accepted after revision April 24, 1991.

[1] Department of Radiology, MBC #28, King Faisal Specialist Hospital & Research Centre, P.O. Box 3354, Riyadh 11211, Saudi Arabia. Address reprint requests to W. von Sinner.

[2] Department of Radiology, Riyadh Military Hospital, Riyadh, Saudi Arabia.

AJR **157:741–745, October 1991** 0361–803X/91/1574–0741 © American Roentgen Ray Society

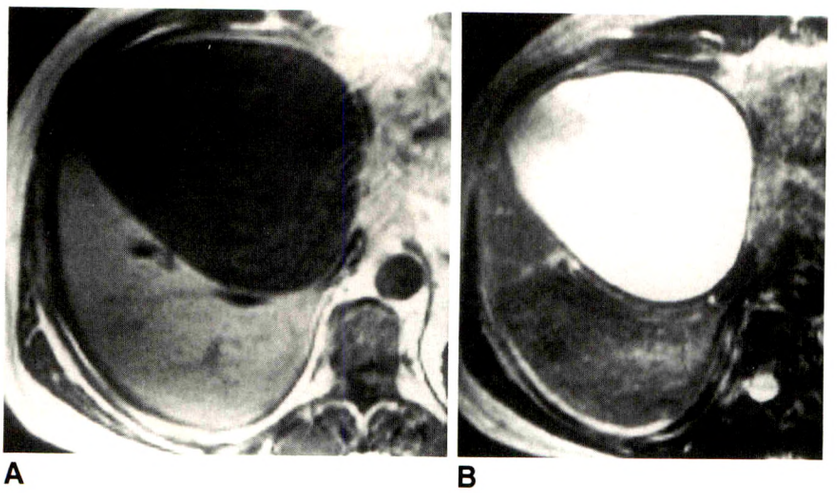


Fig. 1.—Simple viable hydatid cyst of liver.
A, T1-weighted MR image (SE 733/20). Cyst wall is isointense relative to cyst contents.
B, T2-weighted MR image (SE 2000/100). Cyst wall, consisting of both intact parasitic membranes and pericyst, is of low signal intensity compared with high signal of cyst contents.

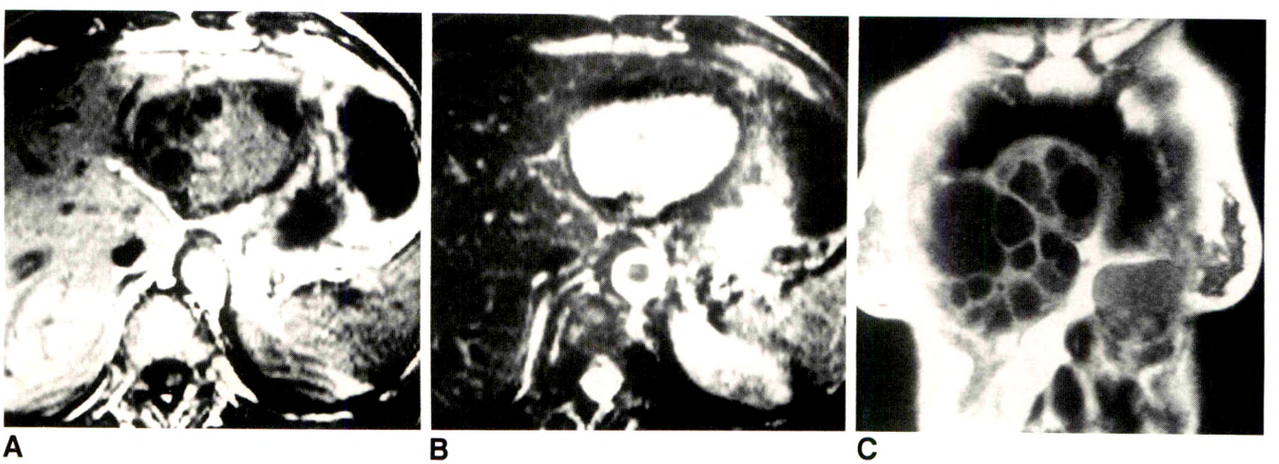


Fig. 2.—Hydatid liver cyst containing daughter cysts.
A, T1-weighted MR image (SE 640/20) shows multiple daughter cysts containing low-intensity fluid compared with intermediate signal of hydatid sand of mother cyst.
B, T2-weighted MR image (SE 2000/100). Contents of mother cyst and daughter cyst have same high signal intensity.
C, Coronal T1-weighted MR image (SE 640/20) in patient with large subdiaphragmatic hydatid cyst containing multiple daughter cysts.

[2]. These membranes are seen floating within the cyst and appear dark on both T1- and T2-weighted images (Fig. 3). The pericyst is also dark on T2-weighted images, but tends to be isointense relative to normal liver tissue on T1-weighted images.

Intrahepatic Rupture of a Hydatid Cyst

The next stage in the process of degeneration of the hydatid cyst is the rupture of the pericyst. The cyst contents are no longer contained by the pericyst and spill into the surrounding parenchyma [2–4]. During this process, bile ducts and veins may be eroded, releasing cyst contents into the biliary system or the blood stream. On MR images, rupture of the cyst is easily recognized as an area of discontinuity of the low-intensity cyst wall (Fig. 4).

External Rupture of Hydatid Cyst

External rupture of a cyst occurs when both the wall of the cyst and the capsule of the organ harboring the cyst rupture [2–4]. In a hepatic cyst, contents will spill into the peritoneal cavity, leading to extensive intraperitoneal seeding (Fig. 5).

Complicated Hydatid Disease of the Lung

In the lung, the cyst may rupture into the bronchial tree. The patient will cough up cyst contents that may be aspirated, causing extensive reactive pneumonitis. MR may show communication between the bronchial tree and the cyst (Fig. 6).

End-Stage Calcified Cyst

During the course of the disease, spontaneous collapse and calcification of the cyst may occur, leaving an area of

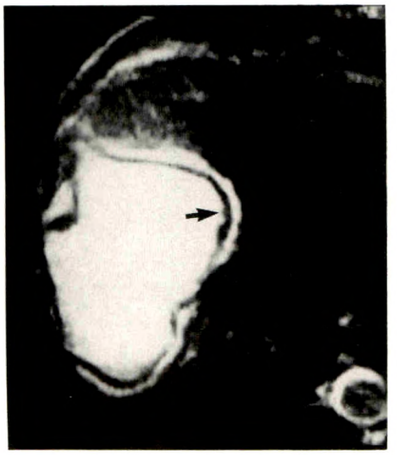


Fig. 3.—Hydatid liver cyst with detached parasitic membranes on T2-weighted MR image (SE 2000/100). Both detached parasitic membranes (*arrow*) and pericyst are of low intensity.

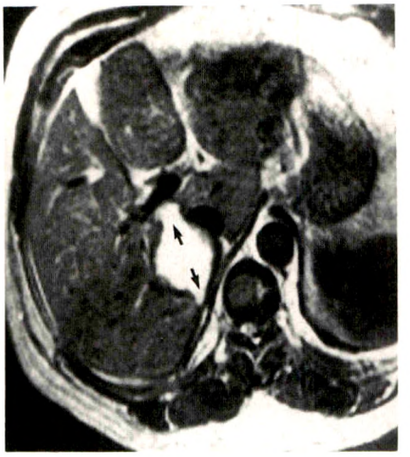


Fig. 4.—Intrahepatic rupture of liver cyst on MR image (SE 2100/50). Low-intensity pericyst is disrupted, and fluid contents spill into liver parenchyma (*arrows*).

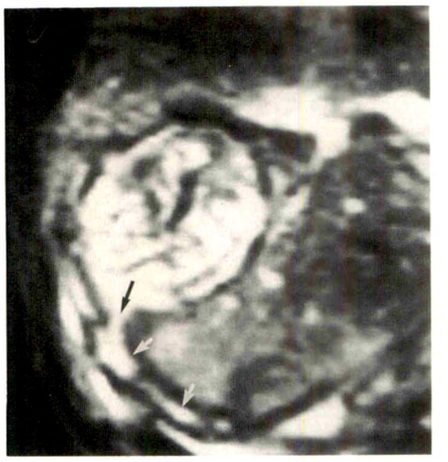


Fig. 5.—External rupture of liver cyst. T2-weighted MR image (SE 2000/100) shows disruption of low-intensity rim of pericyst (*black arrow*) with spillage of fluid into perihepatic space (*white arrows*). (Reprinted with permission from von Sinner [2].)

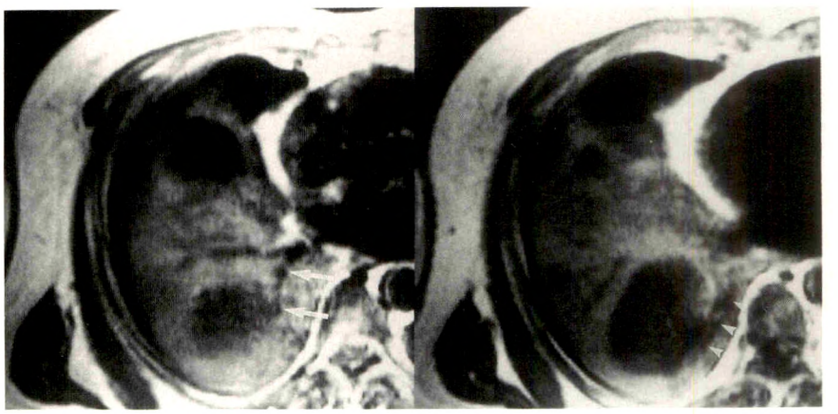


Fig. 6.—Complicated hydatid cyst of lower lobe of right lung. MR image (SE 950/20) shows lower lobe bronchi in close contact with cyst wall (*arrows and arrowheads*). Spread of cyst contents into lower lobe caused infiltrates and reactive pneumonitis.

calcification in the host tissue. Partial calcifications of the cyst wall are degenerative changes that may be seen with both living and dead parasites. Calcifications are better appreciated on CT, although they may be suggested on MR by an area of signal dropout (Fig. 7).

Response to Treatment of Hepatic Parenchymal Reaction to Hydatid Disease

Albendazole, in combination with praziquantel, is a new, powerful drug for the treatment of hydatid disease. The regression in size of hydatid cysts and the changes in the host tissue during chemotherapy can be adequately assessed by MR (Fig. 8).

Hydatid Disease Outside the Lungs and Liver

Hydatid disease may occur anywhere in the body. Some typical examples of cysts at locations other than the liver or the lungs are illustrated (Figs. 9–12).

Spread of Hydatid Disease Across the Diaphragm

The spread of hydatid disease across the diaphragm is a known complication that is well shown on sagittal MR scans (Fig. 9).

Musculoskeletal Involvement of Hydatid Disease

MR imaging is a useful technique in determining the extent of bone involvement and soft-tissue extension (Fig. 10). The appearance of hydatid disease in bone is not specific and may mimic tumors or other inflammatory conditions.

Cardiac Hydatid Disease

Cardiac hydatid disease may be due to hematogenous spread or rupture of a lung cyst. ECG-gated MR imaging allows accurate assessment of the location of a cardiac cyst and its relation to valves, ventricular septum, and myocardium (Fig. 11).

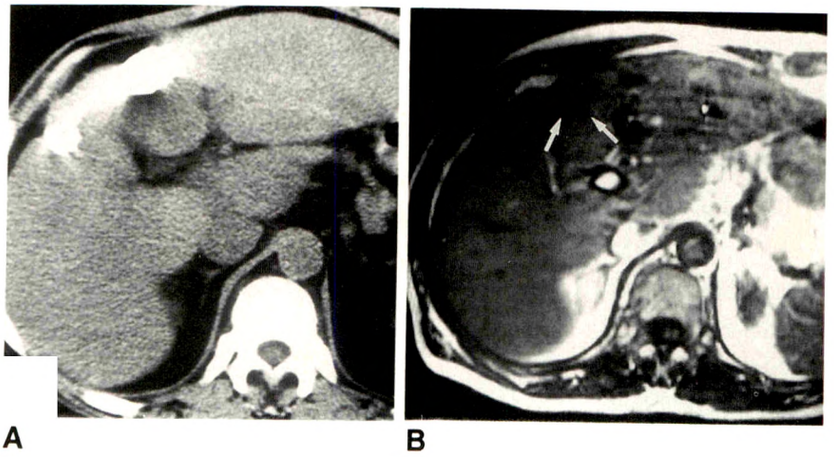


Fig. 7.—End-stage collapsed calcified liver cyst.

A, CT shows two calcifications in liver.

B, T1-weighted MR image (SE 733/120) shows only larger calcified cyst as an area of signal dropout (*arrows*).

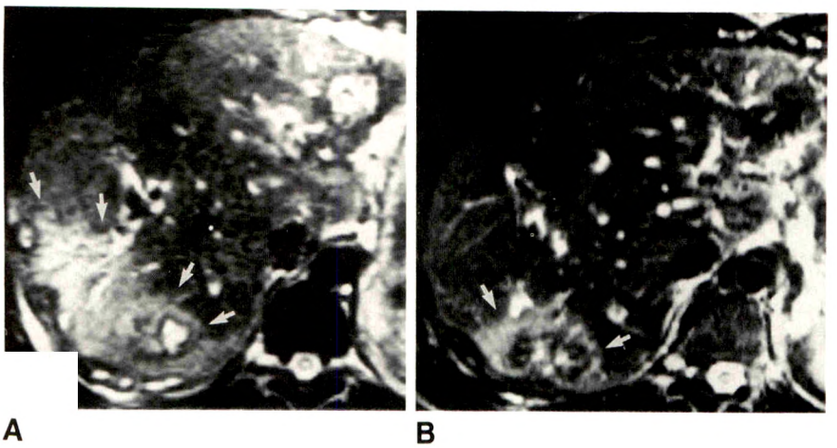


Fig. 8.—Monitoring of response to albendazole treatment.

A, MR image (SE 2100/100) obtained before treatment with albendazole. Excelient contrast resolution of MR allows delineation of extensive reactive edematous changes in liver surrounding hydatid cyst (*arrows*).

B, MR image (SE 2000/100) obtained after treatment shows decrease of size of hydatid cysts and of surrounding reactive changes (*arrows*).

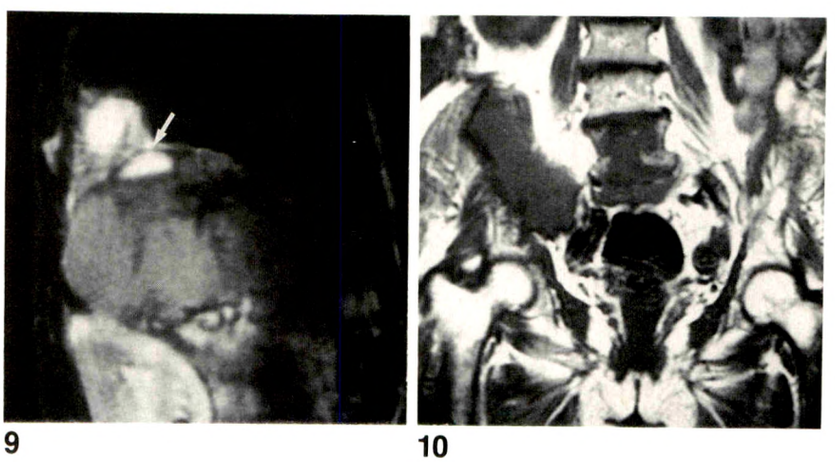


Fig. 9.—Subphrenic and supradiaphragmatic spread of hydatid cysts. T2-weighted sagittal MR image (SE 2000/100). Multiplanar imaging capability and excellent contrast resolution of MR allow differentiation among supradiaphragmatic lung cyst with surrounding reactive pulmonary changes, left hemidiaphragm (*arrow*), and subphrenic cyst.

Fig. 10.—Hydatid cyst of bone. Coronal T1-weighted MR image (SE 533/20) shows extensive involvement of lower lumbar spine, sacrum, and right iliac bone with soft-tissue extension.

Hydatid Disease of the Brain

Hydatid cysts of the brain are rare, and they may reach a large size before the patient becomes symptomatic. On MR, the diagnosis is easily suggested by the presence of a cyst with a low-intensity rim (Fig. 12).

Discussion

When treating hydatid disease, it is important to realize that the hydatid cyst represents a living organism. Like other organisms, it ages, undergoes degeneration, and eventually may die. The host attempts to contain the cyst by forming a

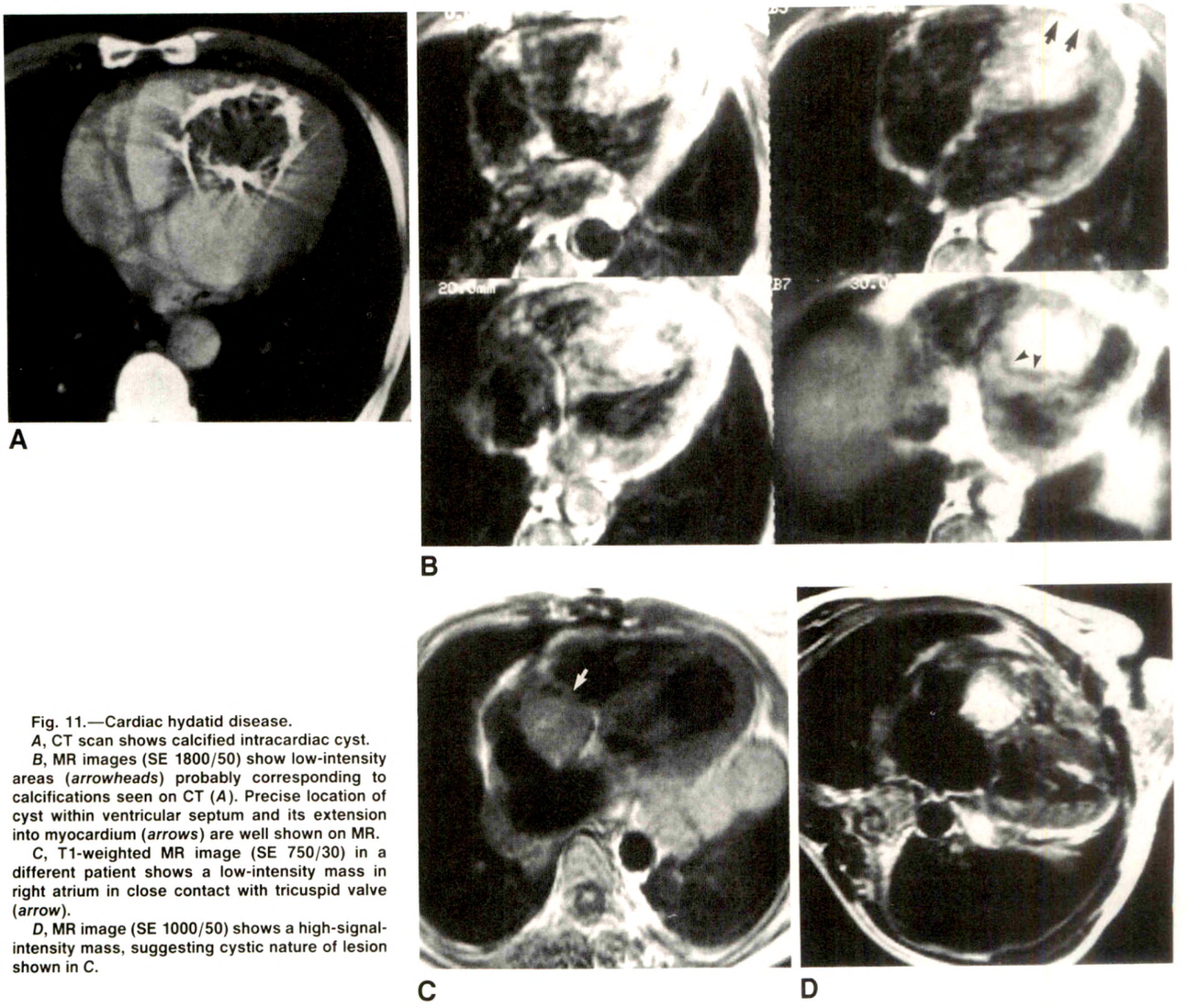


Fig. 11.—Cardiac hydatid disease.
A, CT scan shows calcified intracardiac cyst.
B, MR images (SE 1800/50) show low-intensity areas (*arrowheads*) probably corresponding to calcifications seen on CT (*A*). Precise location of cyst within ventricular septum and its extension into myocardium (*arrows*) are well shown on MR.
C, T1-weighted MR image (SE 750/30) in a different patient shows a low-intensity mass in right atrium in close contact with tricuspid valve (*arrow*).
D, MR image (SE 1000/50) shows a high-signal-intensity mass, suggesting cystic nature of lesion shown in *C*.

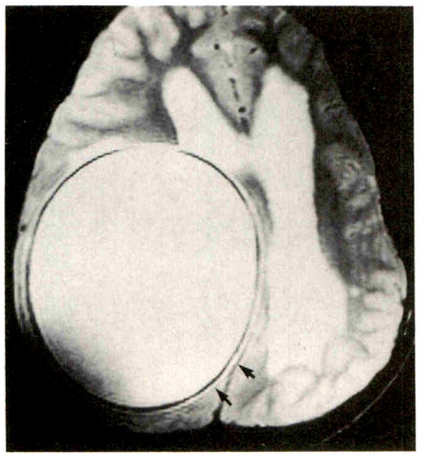


Fig. 12.—Simple hydatid cyst of brain. T2-weighted MR image (SE 2000/40) shows low-intensity rim of cyst wall surrounded by high-signal-intensity reactive changes in compressed brain consistent with gliosis (*arrows*).

dense fibrous capsule around the parasitic membrane. Surgical removal of the hydatid cyst was until recently the only treatment. However, imidazole compounds combined with praziquantel taken orally have proved to be effective in destroying the germinal layer of the parasite, thus inducing or accelerating the natural process of degeneration and death of the cyst. MR is capable of adequately demonstrating all features of hydatid disease, with the exception of calcifications. MR also is useful in monitoring the response to treatment.

REFERENCES

1. Hahn PF, Stark DD, Saini S, et al. The differential diagnosis of ringed hepatic lesions in MR imaging. *AJR* **1990**;154:287–290
2. von Sinner WN. Ultrasound, CT, and MRI of ruptured and disseminated hydatid cysts. *Eur J Radiol* **1990**;11:31–37
3. Lewall DB, McCorkell SJ. Rupture of echinococcal cysts: diagnosis, classification, and clinical implications. *AJR* **1986**;146:391–394
4. Lupetin AR, Dash N. Intrahepatic rupture of hydatid cyst: MR findings. *AJR* **1988**;151:491–492

Forthcoming Articles

SPECIAL ARTICLE

Perspective. AIDS risk and risk reduction in the radiology department. *Wall SD, Olcott EW, Gerberding JL*

CONTRAST MEDIA

Acute reactions to intravascular contrast media: types, risk factors, recognition, and specific treatment. *Bush WH, Swanson DP*

REVIEW ARTICLE

Radiologic assessment of impotence: angiography, sonography, cavernosography, and scintigraphy. *Rosen MP, Schwartz AN, Levine DFJ, Greenfield AJ*

Commentary. The arteriolar component of impotence: a possible paradigm shift. *Bookstein JJ, Valji K*

CARDIOPULMONARY RADIOLOGY

Pictorial essay. Defects of the interventricular septum of the heart: en face MR imaging in the oblique coronal plane. *Yoo S-J, Lim T-H, Park I-S, Hong CY, Song MG, Kim SH*

Case report. Bronchopulmonary sequestration: dynamic, ultrafast, high-resolution CT evidence of air trapping. *Stern EJ, Webb WR, Warnock ML, Salmon CJ*

GASTROINTESTINAL RADIOLOGY

The radiologic diagnosis of Barrett esophagus: importance of mucosal surface abnormalities on air-contrast barium studies. *Glick SN, Teplick SK, Amenta PS*

Disseminated histoplasmosis: abdominal CT findings in 16 patients. *Radin DR*

Primary sclerosing cholangitis: value of cholangiography to determine the prognosis. *Craig DA MacCarty RL, Wiesner RH, Grambsch PM, LaRusso NF*

Pictorial essay. CT imaging in acquired abnormalities of the spleen. *Taylor AJ, Dodds WJ, Erickson SJ, Stewart ET*

Case report. Color Doppler sonography in a case of splenic hemangioma: value of compressing the tumor. *Niizawa M, Ishida H, Morikawa P, Naganuma H, Masamune O*

Percutaneous drainage of hepatic abscesses: comparison of results in abscesses with and without intrahepatic biliary communication. *Do H, Lambiase RE, Deyoe L, Cronan JJ, Dorfman GS*

Case report. Multiple intrahepatic portal-hepatic venous shunts: treatment with steel-coil embolization. *Okada Y, Endo T, Kusano S, Yoshida M*

GENITOURINARY RADIOLOGY

Detection of renal stones with real-time sonography: effect of transducers and scanning parameters. *Kimme-Smith C, Perrella RR, Kaveggia LP, Cochran S, Grant EG*

Imaging of the renal arteries: value of MR angiography. *Debatin JF, Spritzer CE, Grist TM, et al.*

Arteriovenous malformations of the kidneys: diagnosis and follow-up with color Doppler sonography in six patients. *Takebayashi S, Aida N, Matsui K*

Case report. Nonobstructing periureteric venous ring: diagnosis with conventional and three-dimensional reconstruction CT. *Dillon EH, Camputaro C*

Transitional cell carcinoma of the bladder: patterns of recurrence after cystectomy as determined by CT. *Ellis JH, McCullough NB, Francis IR, Grossman HB, Platt JF*

Case report. Testicular microlithiasis: sonographic features with pathologic correlation. *Smith WS, Brammer HM, Henry M, Frazier H*

MUSCULOSKELETAL RADIOLOGY

Review. Noninvasive measurements of bone mass, structure, and strength: a review of current methods and experimental techniques. *Faulkner KG, Glüer, C-C, Majumdar S, Lang P, Engelke K, Genaft HK*

MR of the labral capsular complex: normal variations. *Neumann CH, Petersen SA, Jahnke AH*

Pictorial essay. Hallux rigidus deformity: radiologic assessment. *Karasick D, Wapner KL*

Case report. Localized Castleman disease: development of skeletal lymphoma within 5 years. *Buckley JG, Sundaram M*

PEDIATRIC RADIOLOGY

Review. Drug-related complications in infants and children: imaging features. *Kassner EG*

Review. Sonography of the biliary tract in infants and children. *Haller JO*

Fetal abdominal wall mass detected on prenatal sonography: gastroschisis vs omphalocele. *Perrella RR, Ragavendra N, Tessler FN, Boechat I, Crandall B, Grant EG*

Technical note. MR angiography of vascular grafts in children. *Fillmore DJ, Yucel EK, Briggs SE, Steinberg FL, Waltman AC*

NEURORADIOLOGY

Review. Proton MR spectroscopy in multiple sclerosis: value in establishing diagnosis, monitoring progression, and evaluating therapy. *Richards TL*

The prevalence and location of metastases from ocular melanoma: an imaging study in 110 patients. *Lorigan JG, Wallace S, Mavligit GM*

MR imaging of malignant uveal melanoma: role of pulse sequence and contrast agent. *Mihara F, Gupta KL, Murayama S, Lee N, Bond JB, Haik BG*

Optimization of techniques in screening CT of the sinuses. *Babbel R, Harnsberger HR, Nelson B, Sonkens J, Hunt S*

Maternal cocaine abuse: the spectrum of radiologic abnormalities in the neonatal CNS. *Heier LA, Carpanzano CR, Mast J, Brill PW, Winchester P, Deck MDF*

Chronic acquired hepatic failure: MR imaging of the brain at 1.5 T. *Brunberg JA, Kanal E, Hirsch W, Van Thiel DH*

COMPUTER PAGE

Computer page. A PC-based semiautomated reporting system. *Schwartz LH, Brill PW, Winchester P*

MEDICOLEGAL REPORT

Radiology practices' contracts with hospitals, 1989–1990: a representative sample survey. *Sunshine J, Chan WC, Kassing PJ*

COMMENTARY

Understanding ROC curves: a graphic approach. *Brismar J*

Gallstone Lithotripsy: Results When Number of Stones Is Excluded as a Criterion for Treatment

Robert K. Zeman[1]
William J. Davros[1]
Jo Anne Goldberg[1]
Daryl Fanney[1]
Leslie E. Forer[1]
Brian S. Garra[1]
Wendelin S. Hayes[1]
Steven C. Horii[1]
Cirrelda J. Cooper[1]
Paul M. Silverman[1]
Edward L. Cattau, Jr.[2]
Firas Al-Kawas[2]

The Siemens Lithostar Plus protocol (Siemens Medical Systems, Iselin, NJ) allows investigators to perform gallstone lithotripsy on patients regardless of the number of stones they have, provided the stones occupy less than 50% of the gallbladder lumen. The purpose of this study was to determine the interrelationships between stone burden, fragmentation response, and stone-free rates when treatment is not limited to three stones or fewer. Of 200 patients initially examined, 80 (40%) underwent lithotripsy. The mean number of treatments per patient was 2.1, and the mean number of shock waves per patient was 7386. In 60 patients in whom 6-month follow-up was available, the overall stone-free rate, based on actual results, was 32% (19/60). The stone-free rates for solitary stones, two or three stones, and four or more stones were 50%, 12%, and 26%, respectively. Regardless of number of stones, patients who ultimately became stone free had significantly smaller mean fragment size (0.25 cm) 2 weeks after lithotripsy than did those who did not become stone free (0.51 cm). Retrospective volume analysis showed that seven (47%) of 15 patients with multiple stones occupying less than 2000 mm^3 were stone free; none became stone free when this volume was exceeded.

Lithotripsy remains a practical option for patients with solitary stones. Comparable stone-free rates to those achieved for solitary stones can be obtained in patients with multiple stones, regardless of their number, provided treatment is aggressive and the stone aggregate is less than 2000 mm^3.

AJR 157:747–752, October 1991

In spite of the persistent investigational status of gallstone lithotripsy and the wave of enthusiasm for laparoscopic cholecystectomy, lithotripsy remains an option for patients who are steadfastly against surgery or in whom the laparoscopic approach to cholecystectomy is not feasible [1]. In the United States, patients must have a patent cystic duct and limited stone burden to qualify for gallstone lithotripsy. Although the means of limiting stone burden is controversial, most protocols, including that used by investigators for Dornier Medical Systems (Marietta, GA) [2–4], restrict treatment to patients with three or fewer stones. The Siemens Lithostar Plus (Siemens Medical Systems, Iselin, NJ) clinical trial in the United States currently places no specific limitation on the number of gallstones that can be treated by lithotripsy in any one patient. Instead this protocol specifies that the gallstones cannot occupy more than 50% of the gallbladder lumen and secondarily limits the total cross-sectional area of the stone burden to 9 cm^2 or less.

The purpose of the current study was to determine the interrelationships between stone burden, fragmentation response, and stone-free rates when treatment was not specifically limited to patients with three or fewer stones. Toward this end, the results of screening 200 patients and performing lithotripsy on 80 patients are presented, with results of 6 months of follow-up in 60 patients.

Received April 23, 1991; accepted after revision June 5, 1991.

[1] Department of Radiology, Georgetown University Medical Center, 3800 Reservoir Rd., N.W., Washington, DC 20007. Address reprint requests to R. K. Zeman.

[2] Department of Medicine, Gastroenterology Division, Georgetown University Medical Center, 3800 Reservoir Rd., N.W., Washington, DC 20007.

0361–803X/91/1574–0747
©American Roentgen Ray Society

Subjects and Methods

Selection of Patients

The entire list of inclusion and exclusion criteria for potential lithotripsy candidates is shown in Table 1. Patients were recruited via marketing brochures sent to affiliated referring physicians and households in our immediate metropolitan area after hospital contact. The specific inclusion and exclusion criteria were not publicized as part of marketing to avoid biasing referrals. The initial visit included gathering of medical history (to confirm symptoms) and physical examination followed by a sonographic examination and plain film of the abdomen. The fasting patient was examined with state-of-the-art real-time sonography at 3.5 or 5.0 MHz. The maximal gallbladder dimensions and cross-sectional area (determined electronically) were recorded on a single long-axis view. The number of stones, maximal stone diameter, and maximal cross-sectional area of each stone were noted also. For oval or oblong stones, two dimensions were recorded. The cumulative stone area (sum of maximal areas of a patient's stones), cumulative stone diameter (sum of stone diameters of a patient's stones), and mean stone diameter (cumulative diameter/number of stones) were tabulated for each patient. To qualify for the protocol, the patients' stones had to have a total cross-sectional area less than 9 cm^2 and occupy less than 50% of the gallbladder lumen. This provided a crude yet easily measured upper limit of stone burden that was eligible for treatment.

Nineteen patients had more than 10 stones. Because counting the stones was difficult in 10 of these patients [5], the actual number of stones had to be determined by correlating sonography with the patient's subsequent oral cholecystogram. The remaining nine patients had stones exceeding the requirements of the protocol for sonographic cross-sectional area. The caliber of the common hepatic duct was measured and the upper abdomen was studied for abnormalities that might be in the path of the shock wave during lithotripsy. Plain abdominal radiographs were scrutinized for evidence of gallstone calcification. To qualify for treatment, stones must be minimally calcified (3-mm rim or nidus) or noncalcified.

If the patient qualified on the basis of symptoms, sonography, and plain abdominal radiographs, then oral cholecystography (OCG) was performed in the standard fashion after a single or double 3-g dose of Telepaque (Winthrop Pharmaceuticals, New York). In those patients who qualified and opted to have lithotripsy, the volume of their stone burden was specifically calculated on the basis of a consensus of three observers reviewing the baseline sonogram and oral cholecystogram. Although not a protocol requirement, this was done to study any possible relationship between stone volume and treatment outcome. Calculation was based on the formula for a sphere or ellipse, depending on the stone's shape. In five qualified patients with more than 10 stones, the volume was calculated on the basis of an ellipse surrounding the cluster of stones. For those patients who qualified and decided to pursue lithotripsy, a chest radiograph, EKG, urinalysis, blood count, and blood chemistry analysis, including measurements of transaminase, alkaline phosphatase, bilirubin, and amylase levels were performed.

TABLE 1: Inclusion and Exclusion Criteria for Potential Lithotripsy Candidates

Inclusion Criteria
History of biliary colic
Total stone area 9 cm^2 or less
Total stone burden not more than 50% of gallbladder volume
At least one stone ≥5 mm
Stones radiolucent or minimally calcified (3 mm or less nidus or rim) on radiograph
Normal pretreatment laboratory values
Stones can be sonographically targeted
Patent cystic duct
Exclusion Criteria
Patients younger than 18 years of age
Pregnant women or nursing mothers
Patients classified as Anesthesia Risk Group V
Patients with
Uncorrectable coagulopathy
Porcelain gallbladder
Air-containing structure or calcification in blast path
Acute cholangitis or pancreatitis
Stones in common bile duct
Contraindication to ursodiol

Lithotripsy Treatment Protocol

After informed consent was obtained, patients who conformed to the treatment qualifications were randomized to 2 weeks of pretreatment with ursodiol (Actigall, Ciba-Geigy, Summit, NJ) or no pretreatment. All patients were given ursodiol after lithotripsy as a single bedtime dose (8–10 mg/kg). Each patient underwent lithotripsy as an outpatient and received light, IV sedation for the treatment. Lithotripsy was performed with the Siemens Lithostar Plus with the patient in an oblique (usually left posterior oblique) position. This is an electromagnetic lithotriptor with power settings ranging from one to nine and corresponding to 220–780 bar. The number of shock waves at each power setting was recorded in order to calculate a weighted mean power setting for each treatment. Neither cardiac nor respiratory gating was used. The treatment strategy was to target on the largest stone or fragments, gradually increasing the power setting. Continuous real-time targeting was done with an in-line 3.5-MHz ultrasound probe that can manually be rotated to display axial and sagittal planes. Each treatment was limited to 4000 shock waves. The protocol goal was to produce fragments less than 5 mm in diameter; at our institution, patients with 5-mm fragments were retreated. Patients were allowed to have up to six individual lithotripsy treatments. If retreatment was necessary, the protocol allowed retreatment within 48 hr, but at our institution a 2-week interval was used.

Follow-up Evaluation

At the conclusion of the lithotripsy treatment, gallbladder sonography, blood count, clean catch urinalysis, and blood chemistry analysis, including measurements of transaminase, alkaline phosphatase, bilirubin, and amylase levels, were performed. These were repeated 2 weeks, 3 months, and 6 months after lithotripsy. In the patients who had multiple treatments, the elapsed time interval was calculated from the last treatment. The frequency of stone-free patients was tabulated; life table or actuarial analysis, which tends to overestimate stone-free trend, was not used. Complications immediately after the procedure, delayed adverse events, and the number of patients undergoing cholecystectomy during the 6-month data collection period also were recorded. Although 80 patients have been treated, stone characteristics and fragmentation data in this report are based on 60 patients in whom 6-month follow-up is available.

Results

Data on Selection of Patients

Of the 200 patients, 132 were women and 68 were men. The mean age was 49.2 ± 11.0 years. The screening evalu-

ation resulted in 106 (53%) of 200 patients being qualified for lithotripsy. If patients with more than three stones or with minimal calcification were excluded, only 61 patients (31%) would have qualified for treatment. If 3 cm had been imposed as the upper limit of cumulative stone diameter, an additional 18 patients would have been excluded, further reducing the qualifying rate to 22%. Twenty-six patients (13%) who qualified elected not to have lithotripsy. This resulted in a total of 80 patients (40% of those evaluated) actually having the treatment. Opting for cholecystectomy was the most common reason for a qualified patient not to have lithotripsy. This occurred in 12 of the 26 patients who elected not to have lithotripsy.

Overall Treatment Characteristics and Outcome

The 6-month follow-up group consisted of 38 women and 22 men. The mean age was 49.7 ± 12.0 years. The mean weight was 177.4 ± 40.0 lbs. There was an average of 5.7 stones per patient (SD, 10.8) with a mean cumulative diameter of 3.14 ± 2.50 cm. The mean individual stone diameter was 1.10 ± 0.06 cm. The stone burden, as assessed by cumulative volume, had a mean of 1910 ± 1666 mm^3. The mean number of shock waves per patient was 7386 ± 4684 at a weighted mean power setting of 5.6 ± 1.3. The mean number of treatments per patient was 2.1 ± 1.2 (range, 1–6). Contrary to the type of learning curve (with diminishing retreatment) that might have been expected, retreatment rate rose during the course of the study. Stone fragmentation occurred in 59 of 60 patients. The largest mean fragment size 2 weeks after the last treatment was 0.46 cm.

Among the 60 patients who were treated and followed up for 6 months, 19 (32%) are stone free. Pretreatment with ursodiol had no statistically significant impact on whether or not a patient became stone free. Included in the 19 stone-free patients are three with minimal calcification. Six other patients with minimal calcification are not stone free 6 months after treatment. Because the treated group of patients with calcified stones was so small, no statistically significant trends were present. One patient who was stone free on two successive sonograms had a stone less than 1 mm in diameter recur 6 months after treatment (after 3 months of ursodiol therapy). Five patients underwent cholecystectomy because of inability to reduce the stones or residual fragments to less than 5 mm in diameter. One patient underwent cholecystectomy 3 days after acute cholecystitis developed. She had 5- to 8-mm fragments and was awaiting retreatment.

In addition to the patient who had subacute cholecystectomy, two patients (3%) required ERCP and sphincterotomy for fragments in the common bile duct. One of these patients ultimately became stone free. There were 21 patients (35%) with hematuria immediately after the procedure. Two patients had gross hematuria and 19 had microscopic hematuria (15 of 19 patients with less than 10 RBCs per high-power field). Among the patients with microscopic hematuria, six patients were menstruating and had microscopic hematuria on prelithotripsy urinalysis. Hematuria resolved by 2 weeks after lithotripsy in all but six patients. Five of these six were clear by 3 months after treatment. The remaining patient with persistent hematuria had cystoscopy, and a low-grade transitional cell carcinoma was found. Neither clinical nor chemical pancreatitis developed in any patients.

Outcome vs Number of Stones

For purposes of analysis, patients were divided into three groups on the basis of their number of stones. The groups consisted of patients with solitary stones, two or three stones, and four or more stones (Fig. 1). Of those patients with solitary stones, 12 (50%) of 24 were stone free 6 months after lithotripsy. Two (12%) of the 17 patients with two or three stones were stone free after 6 months. Five (26%) of 19 patients with four or more stones became stone free (Fig. 1). The treatment parameters (mean number of shock waves, mean number of treatments, weighted mean power setting) were (7483, 2.1, 5.7) for the solitary-stone group, (7445, 2.05, 5.92) for the two-or-three-stone group, and (7239, 2.1, 5.3) for the four-or-more-stone group. These parameters did not differ significantly. Nine patients had minimally calcified stones; three became stone free.

Relationship Between Stone Number, Diameter, and Volume

The individual and cumulative stone diameters are plotted against the number of stones in Figure 2. The largest solitary stone that was treated was 2.4 cm in diameter (7256 mm^3). With increasing numbers of stones, the cumulative diameter increases. For patients with four or more stones, the mean cumulative diameter was 5.1 cm (Fig. 2). Because the protocol requirements set an arbitrary upper limit on stone cross-sectional area, the data show that in patients with multiple stones, the stones individually tended to be small, that is, only 0.6 cm in the four-or-more group. Individual and cumulative stone volume vs stone number are plotted in Figure 3.

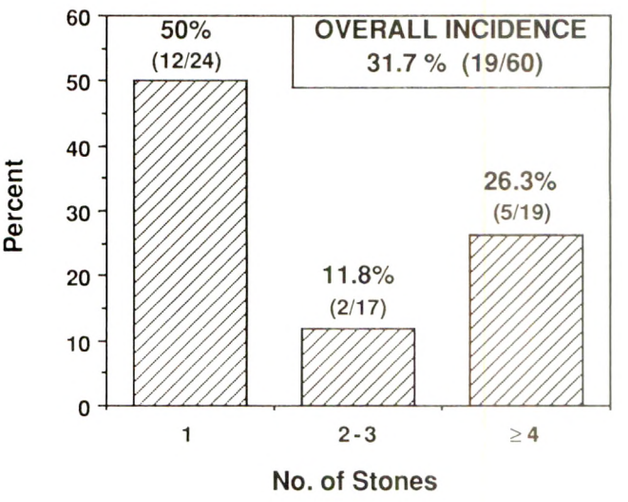


Fig. 1.—Cumulative stone-free rate at 6 months.

This plot shows that the individual volume of stones in patients with multiple stones also tends to be small and less than the volume of solitary stones. More importantly, it shows a mean cumulative volume of 1888 mm^3 for patients with four or more stones. This was significantly less ($p < .0001$) than the cumulative volumes for the solitary (2642 mm^3) or two-to-three-stone groups (2796 mm^3).

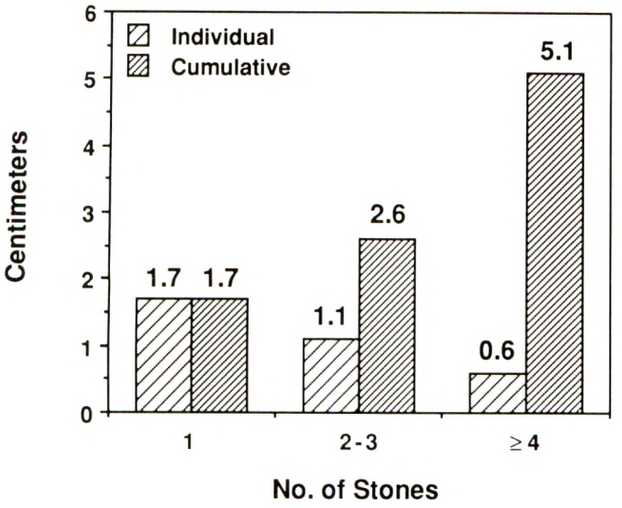


Fig. 2.—Mean individual and cumulative stone diameter vs number of stones. Although individual stone diameters become smaller with increasing number of stones, cumulative (added) diameters of stones are greater. If cumulative diameter were used as the only indicator of stone burden, patients with four or more stones would have the heaviest stone burden (5.1 cm). (SD range, 0.5–3.2 cm).

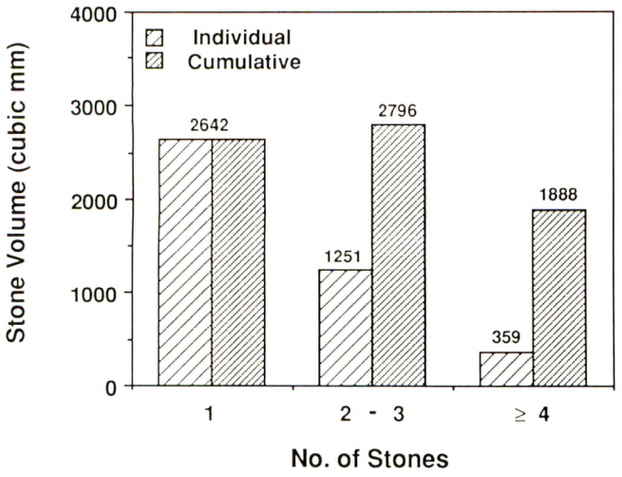


Fig. 3.—Stone volume vs number of stones. Individual and cumulative stone volumes are plotted for each stone group. Patients with solitary stones had a greater cumulative volume than did patients with four or more stones. The solitary-stone group was of comparable cumulative volume to the two-to-three-stone group. Individual stones in the four-or-more group were the smallest, and this group had the smallest cumulative volume. Individual volumes all statistically differed ($p < .001$ or less) between the three stone groups. Cumulative volumes did not differ between solitary- and two-to-three-stone groups, but both of these differed from the four-or-more-stone group ($p < .0001$).

Although a wide range of cumulative volumes was found in patients with single stones who became stone free (Fig. 4), the cumulative volume in stone-free patients with multiple stones was always less than 2000 mm^3. Seven (47%) of the 15 patients with a cumulative stone volume of 2000 mm^3 or less became stone free. A similar analysis showed no useful trends relating cumulative diameter to stone-free status in patients with multiple stones.

Fragment Size Diminution and Clearance

Solitary stones showed the most dramatic reduction in size from an initial mean diameter of 1.70 cm to 0.42 cm 2 weeks after lithotripsy (Fig. 5). From 2 weeks to 6 months, the mean fragment size was further reduced from 0.42 cm to 0.18 cm. Patients with two or three stones showed a moderate reduction in stone diameter after 6 months (from 1.1 to 0.4 cm) but still had larger fragments than did patients with solitary stones or with four or more stones. The patients with four or more stones had the least absolute reduction in stone size. Their stones reduced from 0.60 to 0.49 cm 2 weeks after lithotripsy. Even after 6 months of ursodiol treatment, their mean diameter was 0.32 cm.

The patients who became stone free by 6 months after lithotripsy had a mean largest fragment size of 0.25 cm 2 weeks after lithotripsy. This differed significantly ($p < .001$) from the 2-week mean fragment size (0.51 cm) of the patients who did not become stone free by 6 months. Twenty-two patients had fragments less than 0.35 cm on their 2-week sonogram. Thirteen became stone free after 6 months. Ten of 13 initially had solitary stones, the remaining three had multiple stones. Of the 38 patients with fragments greater than 0.35 cm after 2 weeks, only six became stone free. Three of these six had four or more stones. The incidence of stone-free patients showed a progressive rise in all categories

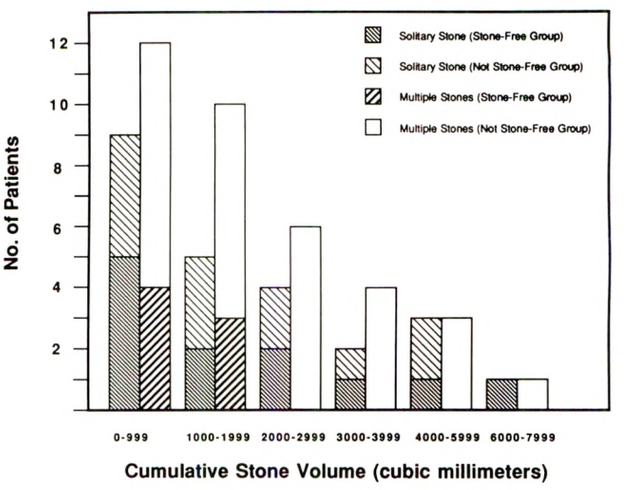


Fig. 4.—Relationship between number of stones, cumulative stone volume, and stone-free status. Histogram shows single-stone patients became stone free over the entire range of stone volume treated in this series. Seven of 15 multiple-stone patients with cumulative stone volumes less than 2000 mm^3 became stone free within 6 months; none above this volume became stone free.

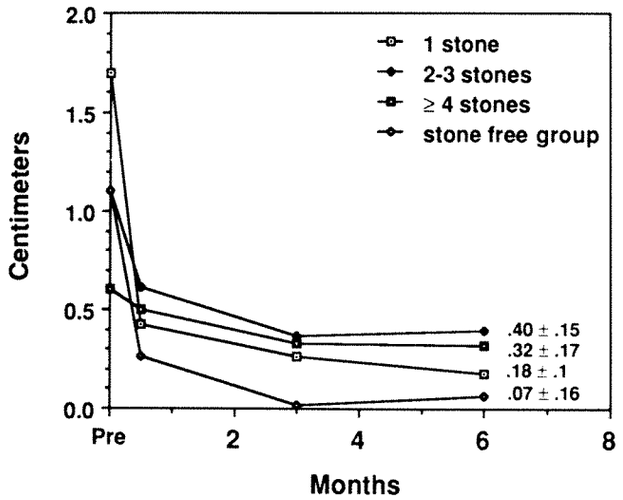


Fig. 5.—Largest stone or fragment size vs time. Stone and fragment diameters recorded as largest dimension are plotted before lithotripsy (pre) and 2 weeks, 3 months, and 6 months after lithotripsy. Those patients that ultimately became stone free had smallest fragments (0.25 cm) 2 weeks after lithotripsy (SD range, 0.06–0.19 cm). Stone-free group dimensions include one patient with recurrence.

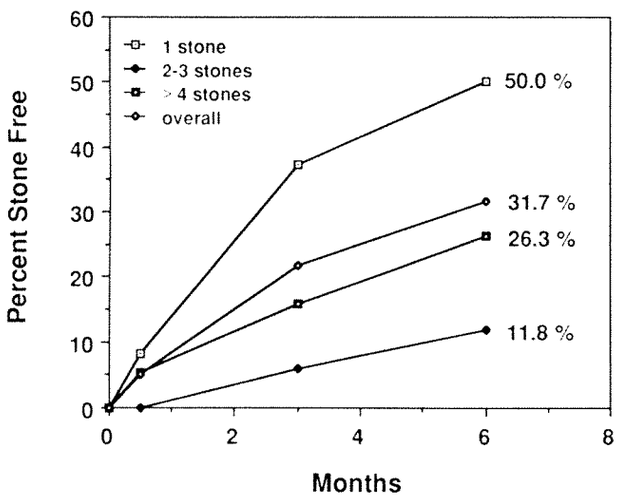


Fig. 6.—Stone-free rate vs time. Number of stone-free patients progressively rose during 6-month study. Sample size for each stone group is shown in Figure 1.

during the 6-month study (Fig. 6). One patient who had been stone free had stone recurrence after 6 months.

Discussion

Our data shed light on the complex relationship between stone burden, selection of patients, and treatment outcome. By not limiting treatment to patients with three stones or fewer, 53% of potential candidates were qualified for lithotripsy. This is a dramatically higher qualifying rate than has been reported when treatment is limited by stone number [5]. Eighty patients (40%) actually had lithotripsy, and among 60 with 6 months follow-up, the stone-free rate was 32%. This was slightly higher than the 26% stone-free rate reported by Torres and colleagues in their subgroup of 62 patients with noncalcified stones of similar size and volume who received adjunctive ursodiol therapy [2]. In that trial, treatment was limited to those patients with three stones or fewer.

There are many different ways of looking at how stone burden relates to treatment outcome. Besides stone number, we retrospectively analyzed the effect of individual stone diameter, cumulative stone diameter, and cumulative stone volume on outcome. Counting and measuring stones may be difficult unless careful sonographic sections through the gallbladder are obtained and correlation with OCG is performed [6, 7]. As in other series, solitary stones responded uniquely well to lithotripsy [2–4]. Our 6-month 50% stone-free rate in this group proved not to be a function of stone diameter or volume. This may in part be due to population selection because the largest single stone treated in this series was 2.4 cm in diameter (7256 mm^3). We do not know if larger stones would have fared so well.

In patients with multiple stones, the specific number of stones and their cumulative diameter did not relate to outcome. Patients with four or more stones had the largest cumulative diameters but became stone free more often than did patients with two or three stones. As others have suggested [8] from in vitro studies, cumulative volume was more useful than diameter in predicting outcome. No patients with multiple stones and a cumulative volume greater than 2000 mm^3 became stone free within 6 months of treatment. Forty-seven percent of patients with multiple stones less than 2000 mm^3 became stone free within 6 months. Thus, by careful selection of patients with multiple stones (based on volume, not stone number) it is possible to achieve stone-free rates comparable to those of single stones.

Regardless of whether solitary or multiple stones are treated, production of the smallest possible fragments results in the most rapid stone clearance. The patients who became stone free after 6 months had much smaller fragments (mean, 0.25 cm) than did their counterparts who were not stone free (mean, 0.51 cm), when fragments were measured 2 weeks after treatment. This suggests that when many protocols were designed, the goal of achieving a 0.5-cm fragment was not adequate and that finer fragmentation would have produced better stone-free rates after 6 months. At our institution, patients with 0.5-cm fragments underwent an additional lithotripsy treatment to try to achieve smaller fragments. In order to produce small fragments, the stone must be exposed to a yet unknown cumulative amount of energy and cavitation effects [9–11]. Both the device's power setting and the number of repetitive shock waves contribute to this cumulative result. Electromagnetic lithotriptors like the Lithostar are intrinsically less powerful than are spark-gap devices such as the Dornier. Our ability to perform up to six treatments per patient and administer 4000 shock waves per treatment allowed us to produce smaller fragments than could Dornier investigators, who were limited to two treatments of 1500 shock waves each with the MPL 9000 [2]. Other authors also have stressed the need for aggressive treatment [12–14], be it via device power or number of shock waves.

Patients with solitary stones had stone volumes comparable to those in patients with two or three stones but had much smaller fragments and higher stone-free rates. Why do patients with single stones respond so well to lithotripsy in clinical and in vitro studies [2–4, 8]? The reason may not lie solely in the number of targets. It may reflect the necessity of punching through less-pigmented rims and rings to reach homogeneous cholesterol plates in one stone vs two or three stones of equal volume [15]. Once the cholesterol-rich interior is exposed, the stone is more easily fragmented and the fragments become more vulnerable to ursodiol effects. Unfortunately, since this study did not include a group treated with drugs only, the relative contribution of ursodiol cannot be confirmed. Similarly, data in this series were insufficient to confirm the deleterious effects of stone calcification on pulverization [15, 16].

Conclusions

By not restricting gallstone lithotripsy to patients with three or fewer stones, 40% (80/200) of those patients who had diagnostic examination ultimately were treated. After 6 months of follow-up in 60 patients, the overall stone-free rate was 32%. This appears to be the result of our aggressive approach to treatment (mean, 7386 shock waves and 2.1 treatments per patient). In spite of aggressive treatment, lithotripsy was safe, with few clinically significant complications. Regardless of their initial number of stones, those patients who became stone free had significantly smaller fragments 2 weeks after lithotripsy (0.25 cm) than did those patients who did not become stone free (0.51 cm). Fifty percent of solitary-stone patients were stone free after 6 months. A comparable stone-free rate (47%) was achieved in patients with multiple stones, provided their cumulative volume was less than 2000 mm^3. On the basis of this experience, lithotripsy remains a practical option for the treatment of solitary gallstones and multiple stones of limited cumulative volume, regardless of number.

REFERENCES

1. Zeman RK, Al-Kawas F, Benjamin SB. Gallstone lithotripsy: is there still cause for optimism? *Radiology* **1991**;178:33–35
2. Torres WE, Steinberg HV, Davis RC, Baumgartner BR, Nelson RC, Casarella WJ. Extracorporeal shock wave lithotripsy of gallstones: results and 6 month follow-up in 141 patients. *Radiology* **1991**;178:509–512
3. Schoenfield LJ, Berci G, Carnolvale RI, et al. The effect of ursodiol on the efficacy and safety of extracorporeal shock-wave lithotripsy of gallstones: the Dornier National Biliary Lithotripsy Study. *N Engl J Med* **1990**;323:1239–1244
4. Albert MB, Fromm H, Borstelmann R, Shehan CM, Gicking R. Successful outpatient treatment of gallstones with piezoelectric lithotripsy. *Ann Intern Med* **1990**;113:164–166
5. Brink JA, Simeone JF, Mueller PR, Richter JM, Prien EL, Ferrucci JT. Physical characteristics of gallstones removed at cholecystectomy: implications for extracorporeal shock-wave lithotripsy. *AJR* **1988**;151:927–931
6. Garra BS, Davros WJ, Lack EE, Horii SC, Zeman RK. Visibility of gallstone fragments using ultrasound and fluoroscopy: implications for monitoring of gallstone lithotripsy. *Radiology* **1990**;174:343–347
7. Torres WE, Baumgartner BR, Jones MT, Steinberg HV, Peterson JE. Comparison of ultrasonography and oral cholecystography in biliary lithotripsy: Part I—screening patients. *Invest Radiol* **1991**;26:633–635
8. Torres WE, Baumgartner BR, Jones MT, Nelson RC. Biliary lithotripsy: an in vitro analysis of gallstone fragmentation for equivalent stone volumes. *Radiology* **1990**;177:507–509
9. Schachler R, Sauerbruch T, Wosiewitz U, et al. Fragmentation of gallstones using extracorporeal shockwaves: an in vitro study. *Hepatology* **1988**;8:925–929
10. Staritz M, Rambow A, Mildenberger P, et al. Second-generation extracorporeal shockwaves for gallstone lithotripsy: in vitro experiments and clinical relevance. In: Ferrucci JT, Delius M, Burhenne HJ, eds. *Biliary lithotripsy*. Chicago: Year Book Medical, **1989**:43–61
11. Zeman RK, Davros WJ, Goldberg J, et al. Cavitation effects during lithotripsy: II. Clinical observations. *Radiology* **1990**;177:163–166
12. Burhenne HJ, Becker CD, Malone DE, Rawat B, Fache JS. Biliary lithotripsy: early observations in 106 patients. *Radiology* **1989**;171:363–367
13. Fache JS, Rawat B, Burhenne HJ. Extracorporeal cholecystolithotripsy without oral chemolitholysis. *Radiology* **1990**;177:719–721
14. Sackmann M, Pauletzki J, Sauerbruch T, Holl J, Schelling G, Paumgartner G. The Munich gallbladder lithotripsy study: results of the first 5 years with 711 patients. *Ann Intern Med* **1991**;114:290–296
15. Zeman RK, Marchand T, Davros WJ, Garra BS, Glass-Royal M, Soloway RD. Gallstone fragmentation during biliary lithotripsy: effect of stone composition and structure. *AJR* **1991**;156:493–499
16. Rawat B, Burhenne HJ. Extracorporeal shockwave lithotripsy of calcified gallstones: work in progress. *Radiology* **1990**;175:667–670

Gallbladder Contractility: Variation in Normal Subjects

Jennifer J. Donald[1]
J. Stephen Fache
Anne R. Buckley
H. Joachim Burhenne

Gallbladder contractility can be quantified radiologically, but it is not known whether the degree of contraction exhibited by a person's gallbladder varies from day to day. Thirty healthy volunteers were studied with sonography on three separate occasions to determine the variation of individual gallbladder contractility. Using the ellipsoid method, we measured gallbladder volume after an overnight fast (fasting gallbladder volume) and between 45 and 60 min after a standard fatty meal (residual gallbladder volume). Percentage gallbladder contraction was calculated by dividing the difference between the fasting and residual gallbladder volumes by the fasting gallbladder volume and multiplying by 100. The 90 studies in 30 subjects exhibited a wide range of values: fasting gallbladder volume from 1.9 to 45.5 ml, residual gallbladder volume from 0.1 to 21.0 ml, and percentage gallbladder contraction from −10% to 99%. Within each subject, fasting gallbladder volume measurements varied from 1.5 to 26.2 ml (mean ± two standard deviations, 10.3 ± 5.1 ml) and residual gallbladder volume from 0.3 to 15.4 ml (5.1 ± 3.8 ml). Percentage gallbladder contraction varied from 6% to 87% (28% ± 18%). In 60% of the subjects, percentage gallbladder contraction values varied by more than 20%, and in 20% of the subjects it varied by more than 40%.

These data show that a wide variation exists within a normal person in the degree of gallbladder contraction exhibited from one day to another, and a single test for gallbladder contraction can be misleading.

AJR 157:753–756, October 1991

Several imaging tests are available to measure gallbladder contraction after a fatty meal, but little is known about whether the degree of contraction exhibited in a single study is reproducible and representative. Sonography is a well-established technique for the measurement of gallbladder volumes and provides a means of assessing gallbladder contraction after administration of a cholecystokinetic agent. Unlike oral cholecystography and scintigraphy, sonography is quick and simple and requires no radiation exposure. The accuracy and validity of the sonographic technique were first reported by Everson et al. [1], who used the sum-of-cylinders method, and subsequently confirmed by Dodds et al. [2], who used the simple and less time-consuming ellipsoid method. More recently it has been shown that the sonographic demonstration of a contracting gallbladder after a fatty meal can reliably be used to indicate cystic duct patency, as the results correlate closely with gallbladder opacification on oral cholecystography [3] (McGrath FP et al., presented at the Third International Interdisciplinary Symposium on Biliary Lithotripsy, September 1990).

To assess variation in gallbladder contraction within a person, we examined 30 healthy volunteers on three separate occasions. The study was not done to assess the value of contractility as a diagnostic test for acalculous cholecystitis or biliary dyskinesia.

Subjects and Methods

Thirty healthy volunteers (15 men, 15 women; mean age, 33 years [range, 22–65 years]) were recruited from the radiology department. Subjects were excluded if they had a history

Received March 7, 1991; accepted after revision April 23, 1991.

[1] All authors: Department of Radiology, University of British Columbia and Vancouver General Hospital, 855 W. 12th Ave., Vancouver, B.C., Canada V5Z 1M9. Address reprint requests to H. J. Burhenne.

0361–803X/91/1574–0753
© American Roentgen Ray Society

of biliary disease, previous gastric surgery or vagotomy, diabetes mellitus, or if they had gallstones. All examinations were performed by a single observer using a Diasonics Wide-Vu unit equipped with a 5-MHz transducer. After an overnight fast of 8–12 hr (including water and cigarettes), the gallbladder volume was measured before (fasting gallbladder volume) and 45–60 min after (residual gallbladder volume) a standard fatty meal consisting of 60 ml of Neo-Cholex (Horner Inc., Ville Mont-Royal, Quebec, Canada). We had previously established that 45–60 min after this fatty meal is the best time for assessment of maximal gallbladder contraction (McGrath FP et al., Biliary Lithotripsy Symposium, September 1990). Longitudinal and axial cross-sectional images of the gallbladder were made in duplicate, so as to obtain maximal gallbladder length and width. Volume measurements were made by using the ellipsoid formula: volume = 0.52 (width × height × length). Percentage gallbladder contraction was calculated from the equation (fasting gallbladder volume − residual gallbladder volume)/fasting gallbladder volume, multiplied by 100%. This procedure was repeated on three separate occasions (day 0, day 1, and day 7) on each subject.

Individual variations in the three studies done on each subject (i.e., difference between maximal and minimal value) in fasting gallbladder volume, residual gallbladder volume, and percentage gallbladder contraction were calculated. The degree of correlation between the fasting gallbladder volume, residual gallbladder volume, and percentage gallbladder contraction was evaluated. Physical data on each subject included weight and height, from which a body mass index (weight in kilograms/[height in meters]^2) was calculated. The degree of correlation between each subject's body mass index and fasting gallbladder volume, residual gallbladder volume, and percentage gallbladder contraction was calculated. Differences between the sexes were analyzed statistically by using Student's t test.

Results

Gallbladder volume measurements varied widely in the 90 studies, with fasting gallbladder volume and residual gallbladder volume values ranging from 1.9 to 45.5 ml (mean ± two standard deviations, 19.0 ± 9.0 ml) and 0.1 to 21.0 ml (mean, 5.9 ± 4.2 ml), respectively (Figs. 1–3). Within each subject, differences in fasting gallbladder volume ranged from 1.5 to 26.2 ml (mean, 10.3 ± 5.1 ml) and residual gallbladder volume differences ranged from 0.3 to 15.4 ml (mean, 5.1 ± 3.8 ml). Overall percentage gallbladder contraction varied from −10% to 99% (mean, 69% ± 19%; Fig. 4), with differences within a subject of 6% to 87% (mean, 28% ± 18%; Fig. 5). Variations of percentage gallbladder contraction greater than 5%, 10%, 20%, and 40% occurred in 100%, 93%, 60%, and 20% of the subjects, respectively (Fig. 6).

Body mass index showed a significant positive (one-tailed significance, .001) correlation with fasting gallbladder volume ($r = .55$) but showed no significant correlation with residual gallbladder volume ($r = .34$) or percentage gallbladder contraction ($r = -.01$). Residual gallbladder volume showed a significant negative (one-tailed significance, .001) correlation

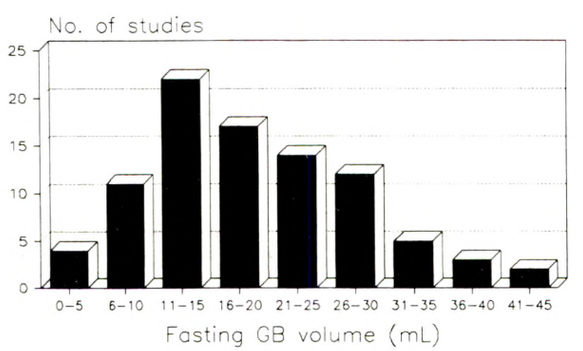


Fig. 1.—Distribution of gallbladder (GB) volumes in fasting subjects: 90 studies in 30 subjects, three studies per subject.

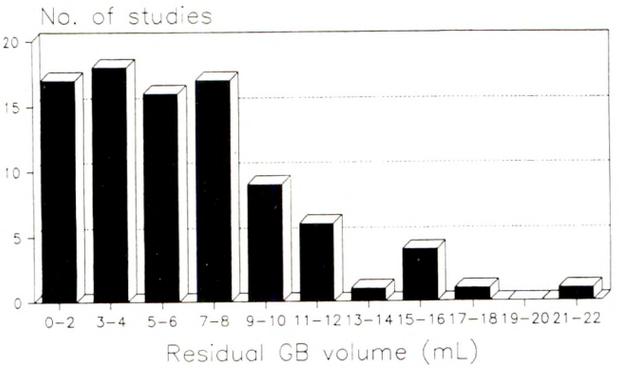


Fig. 2.—Distribution of residual gallbladder (GB) volumes (45–60 min after a fatty meal): 90 studies in 30 subjects, three studies per subject.

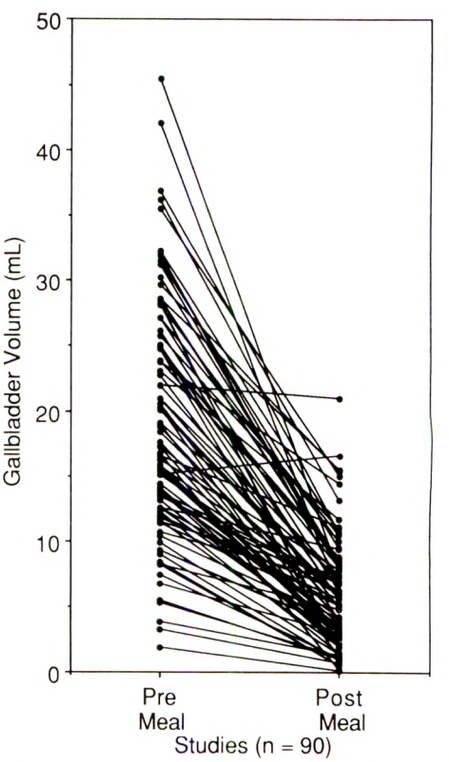


Fig. 3.—Gallbladder volumes before and after a fatty meal. Inspection indicates that in all but one of 90 studies gallbladder volume decreased after fatty meal.

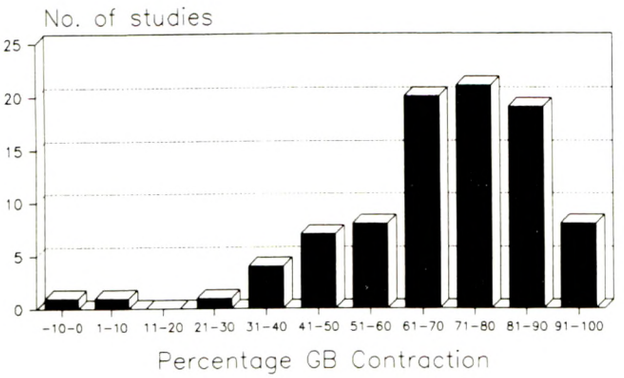


Fig. 4.—Distribution of percentage gallbladder (GB) contraction values: 90 studies in 30 subjects, three studies per subject.

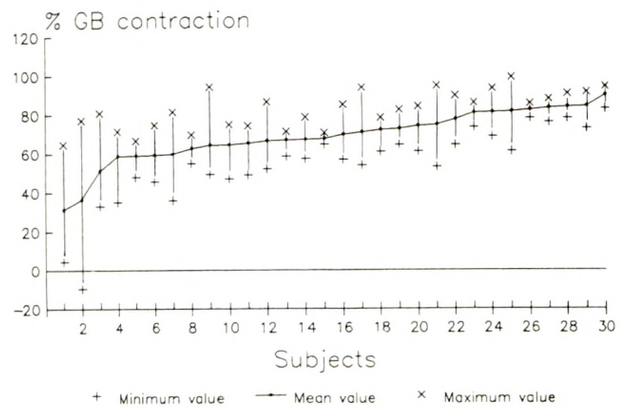


Fig. 5.—Variation within each subject in gallbladder (GB) contractility. Spread of minimal and maximal percentage gallbladder contraction values are plotted about the mean for each subject.

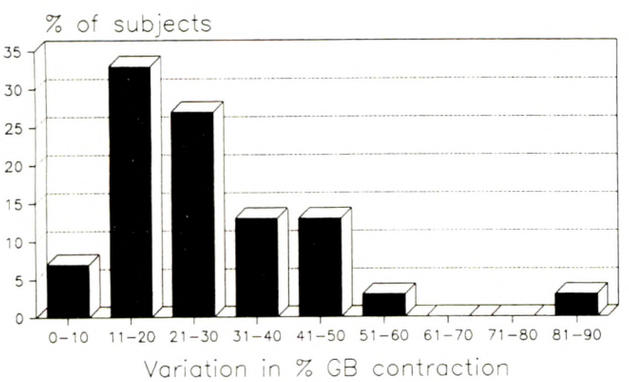


Fig. 6.—Distribution of each subject's variation in percentage gallbladder (GB) contraction. Inspection indicates that 40% of subjects varied by up to 20%, a further 40% of subjects varied between 21% and 40%, and remaining 20% of subjects varied by more than 41%.

with percentage gallbladder contraction (r = −.75). No significant correlation was found between fasting gallbladder volume and percentage gallbladder contraction (r = .03). Fasting gallbladder volume and residual gallbladder volume showed a significant positive (one-tailed significance, .001) correlation (r = .56).

In the 15 men, the values of fasting gallbladder volume, residual gallbladder volume, and percentage gallbladder contraction ranged from 1.9 to 45.5 ml (mean, 20.8 ml), 0.1 to 15.5 ml (mean, 5.8 ml) and 46% to 99% (mean, 73%), respectively. The corresponding values in the 15 women were 3.8–31.5 ml (mean, 16.8 ml), 0.5–21.0 ml (mean, 6.0 ml) and −10%–94% (mean, 63%). Male subjects had significantly higher fasting gallbladder volumes than female subjects did (p = .02), but no significant difference between the sexes was found in the residual gallbladder volume (p = .53) and percentage gallbladder contraction (p = .11).

Discussion

Despite the use of radiologic gallbladder volume measurements before and after a standard fatty meal as a means of quantifying gallbladder contractility, the individual reproducibility has not been well studied.

Gallbladder physiology is complex, with both intrinsic and extrinsic factors affecting its kinetics. In the fasting state, the gallbladder repeatedly undergoes partial emptying and refilling in conjunction with the migrating motor complex cycle of the small bowel. During the second half of the duodenal migrating motor complex cycle, the gallbladder contracts about 40% [4]. Postprandial gallbladder contraction has an immediate cephalic phase regulated by excitatory cholinergic vagal nerves and a more prolonged phase generated by endogenous cholecystokinin, released by entry of nutrients into the duodenum [5].

A number of factors that modify gallbladder kinetics have been identified. Fasting gallbladder volume values have been shown to be higher in males than in females [6], in pregnant patients [7], and in patients taking the oral contraceptive pill [7]. During the ovulatory cycle, increased fasting gallbladder volume and residual gallbladder volume with slower gallbladder emptying have been reported on days 21 and 22 when compared with days 12 and 13 in the same subject [8]. These findings have not been confirmed by other workers, who showed no differences in gallbladder kinetics throughout the ovulatory cycle [7, 9]. Conflicting data also have been reported in patients after vagotomy, but the major influence seems to be on the timing rather than the magnitude of fat-stimulated gallbladder contraction when compared with that in normal control subjects [8, 10–12]. Body habitus is also known to alter gallbladder dynamics, with both obese and nonobese large people having significantly greater fasting gallbladder volume and residual gallbladder volume values with slower gallbladder emptying rates than normal-sized control subjects do [13, 14]. In most gallstone patients, gallbladder motility has been shown to be impaired with increased fasting gallbladder volume and decreased gallbladder emptying [15–20], but whether this is a primary or secondary abnormality remains to be determined [20].

Our data in normal subjects show a wide variation in gallbladder volumes (fasting gallbladder volume and residual gallbladder volume) and percentage gallbladder contraction when evaluated between subjects and within an individual.

These findings are contrary to those of Everson et al. [1], who examined 16 healthy women on two consecutive days and reported only "modest daily variations." Despite the fact that a number of the known factors detailed here have not been addressed in this study, the variations remain significant, even allowing for a 10% intraobserver error in gallbladder volume measurements [1, 2]. Ninety-three percent of our subjects showed differences greater than 10% between their recorded percentage gallbladder contractions. Variations of greater than 20% and 40% occurred in 60% and 20% of the subjects, respectively. The exact clinical importance of these findings is uncertain, but as the subjects were healthy volunteers, it almost certainly represents a normal physiological variation rather than any abnormality. Kishk et al. [20] reported a normal range of fractional gallbladder emptying of 47–91% (mean, 67%) with a value of less than 44% indicating two standard deviations below the mean. Although in our study a mean value of gallbladder contraction of 69% is not dissimilar, five (17%) of the 30 subjects in eight (9%) of the 90 studies were found to have values below a 44% contraction level.

An essential inclusion criterion for gallstone treatment with either oral dissolution agents and/or biliary lithotripsy is the demonstration of a patent cystic duct. We have previously shown that use of a minimum sonographic value of 20% gallbladder contraction as a cut-off level is as accurate as oral cholecystography in determining cystic duct patency and therefore patients' eligibility for biliary lithotripsy (McGrath FP et al., Biliary Lithotripsy Symposium, September 1990). With this criterion, two of the 90 events we studied would have fallen below this level of required contraction. This occurred in two different subjects, but on repeated examination, percentage gallbladder contraction was found to be greater than 20% in both subjects. Therefore, two of the 30 normal subjects would have been falsely excluded from biliary lithotripsy on the basis of a single assessment of gallbladder contraction. In a number of institutions, gallstone treatment protocols require oral cholecystography to prove cystic duct patency. We can assume from our findings that this technique also will be subject to a false-exclusion rate. In patients with gallbladder calculi in whom the gallbladder kinetics are known to be impaired, the false-exclusion rate may be higher, but this needs to be confirmed with further studies. Currently, we advise a second examination in such patients, who are otherwise eligible for nonoperative treatment.

These data show that the degree of gallbladder contraction varies widely within a person, and a single recording may be misleading. However, in most patients, use of a contraction value of 20% as a cutoff level to indicate cystic duct patency remains justifiable as a means of assessing eligibility for either oral dissolution therapy or biliary lithotripsy.

REFERENCES

1. Everson GT, Braverman DZ, Johnson MJ, Kern F Jr. A critical evaluation of real-time ultrasonography for the study of gallbladder volume and contraction. *Gastroenterology* **1980**;79:40–46
2. Dodds WJ, Groh WJ, Darweesh RMA, Lawson TL, Kishk SMA, Kern MK. Sonographic measurement of gallbladder volume. *AJR* **1985**;145:1009–1011
3. Bellamy PR, Hicks A. Assessment of gallbladder function by ultrasound: implications for dissolution therapy. *Clin Radiol* **1988**;39:511–512
4. Takahashi I, Kern MK, Dodds WJ, Hogan WJ, Sarna SK, Hoh Z. Contraction pattern of opposum gallbladder during fasting and after feeding. *Am J Physiol* **1986**;250:G227–G235
5. Ryan JP. Motility of the gallbladder and biliary tree. In: Johnson LR, ed. *Physiology of the gastrointestinal tract*. New York: Raven Press, **1981**: 473–474
6. Fried GM, Ogden WD, Fagan CJ, et al. Comparison of cholecystokinin release and gallbladder emptying in men and in women at estrogen and progesterone phases of the menstrual cycle. *Surgery* **1984**;95:284–289
7. Everson GT, McKinley C, Lawson M, Johnson M, Kern F Jr. Gallbladder function in the human female: effect of the ovulatory cycle, pregnancy, and contraceptive steroids. *Gastroenterology* **1982**;82:711–719
8. Braun B, Dormeyer HH. Changes in gallbladder motor function during the female cycle—a risk factor leading to gallstone formation? *Klin Wochenschr* **1982**;60:1357–1362
9. Kern F Jr, Everson GT, DeMark B, et al. Biliary lipids, bile acids, and gallbladder function in the human female: effects of pregnancy and the ovulatory cycle. *J Clin Invest* **1981**;68:1229–1242
10. Fisher RS, Rock E, Malmud LS. Cholinergic effects on gallbladder emptying in humans. *Gastroenterology* **1985**;89:716–722
11. Masclee AA, Jansen JB, Driessen WM, Geuskens LM, Lamers CB. Effect of truncal vagotomy on cholecystokinin release, gallbladder contraction, and gallbladder sensitivity to cholecystokinin in humans. *Gastroenterology* **1990**;98:1338–1344
12. Shaffer EA. The effect of vagotomy on gallbladder function and bile composition in man. *Ann Surg* **1982**;195:413–418
13. Vezina WC, Paradis RL, Grace DM, et al. Increased volume and decreased emptying of the gallbladder in large (morbidly obese, tall normal, and muscular normal) people. *Gastroenterology* **1990**;98:1000–1007
14. Kucio C, Besser P, Jonderko K. Gallbladder motor function in obese versus lean females. *Eur J Clin Nutr* **1988**;42:121–124
15. Shaffer EA, McOrmond P, Duggan H. Quantitative cholescintigraphy: assessment of gallbladder filling and emptying and duodenogastric reflux. *Gastroenterology* **1980**;79:899–906
16. Fischer RS, Stelzer F, Rock E, Malmud LS. Abnormal gallbladder emptying in patients with gallstones. *Dig Dis Sci* **1982**;27:1019–1024
17. Thompson J, Fried GM, Ogden WD, et al. Correlation between release of cholecystokinin and contraction of the gallbladder in patients with gallstones. *Ann Surg* **1982**;195:670–675
18. Forgacs JC, Masey MN, Murphy GM, Dowling RH. Influence of gallstones and ursodeoxycholic acid therapy on gallbladder emptying. *Gastroenterology* **1984**;87:299–307
19. Pomeranz IS, Shaffer EA. Abnormal gallbladder emptying in a subgroup of patients with gallstones. *Gastroenterology* **1985**;88:787–791
20. Kishk SMA, Darweesh RMA, Dodds WJ, et al. Sonographic evaluation of resting gallbladder volume and postprandial emptying in patients with gallstones. *AJR* **1987**;148:875–879

Pictorial Essay

CT Appearance of Splenic Injuries Managed Nonoperatively

Huy M. Do[1] and John J. Cronan

This essay illustrates the appearance of the traumatized spleen on CT scans obtained during the course of conservative treatment. Although the CT appearance of acute rupture of the spleen has been adequately described, little has been reported about the appearance of the spleen as it heals after trauma. Examples of CT studies of splenic injuries illustrate the various changes in appearance over time in the traumatized spleen that is treated nonoperatively.

Materials and Methods

We reviewed the medical records and abdominal CT scans of 12 patients 5–32 years old (mean, 18 years) with splenic injuries who had CT studies of the abdomen obtained at presentation with injury and at follow-up examinations between 1985 and 1989. Representative cases were selected for this essay. Patients in whom splenic injuries were treated with surgery were excluded from this study.

Results

Initial CT features of splenic trauma are subcapsular hematomas, intrasplenic hematomas, splenic lacerations, and, rarely, splenic infarcts [1]. Subcapsular hematomas appear as lenticular, low-density fluid collections that flatten or indent the lateral margin of the spleen. Intrasplenic hematomas appear as irregular low-density areas within the spleen (Figs. 1A and 2A). The CT findings of splenic lacerations vary more than those of subcapsular hematomas. They include indistinct splenic margins, low-density fracture lines, inhomogeneous splenic parenchyma, perisplenic hematoma, and free fluid in the peritoneal cavity (Figs. 1A, 2A, and 3A). Splenic lacerations may occur with or without subcapsular hematomas. Splenic infarcts appear as wedge-shaped, unenhancing areas with the apices pointing toward the splenic hilum (Fig. 4A). They develop after devascularization as a result of trauma.

Intraperitoneal fluid and perisplenic hematoma usually resolve within 2–4 weeks [2]. Subcapsular or intrasplenic hematoma evolves during a period of weeks to months. Within 1–2 days of bleeding, CT attenuation values of splenic hematomas may be equal to or greater than that of the splenic parenchyma [3]. During the next few weeks, CT attenuation values of splenic hematomas gradually decrease and become less than that of the normal spleen [4]. Sharply defined margins develop in the hematomas as they diminish. This maturation of the hematomas is the result of lysis of clotted blood and resorption of fluid, protein, and necrotic debris (Figs. 1 and 2). Several months may be required for complete resolution of the hematomas. In some patients, the final sequela may be a chronic splenic pseudocyst containing serous fluid [5].

Splenic hematomas may become infected and form abscesses. Fifteen percent of splenic abscesses are associated with trauma (Fig. 3) [5]. CT is helpful in the early detection of splenic abscess, demonstrating a well-defined, low-density

Received August 2, 1990; accepted after revision May 2, 1991.

[1] Both authors: Department of Diagnostic Imaging, Rhode Island Hospital and Brown University Program in Medicine, Providence, RI 02902. Address reprint requests to J. J. Cronan.

AJR **157:757–760, October 1991** 0361–803X/91/1574–0757 © American Roentgen Ray Society

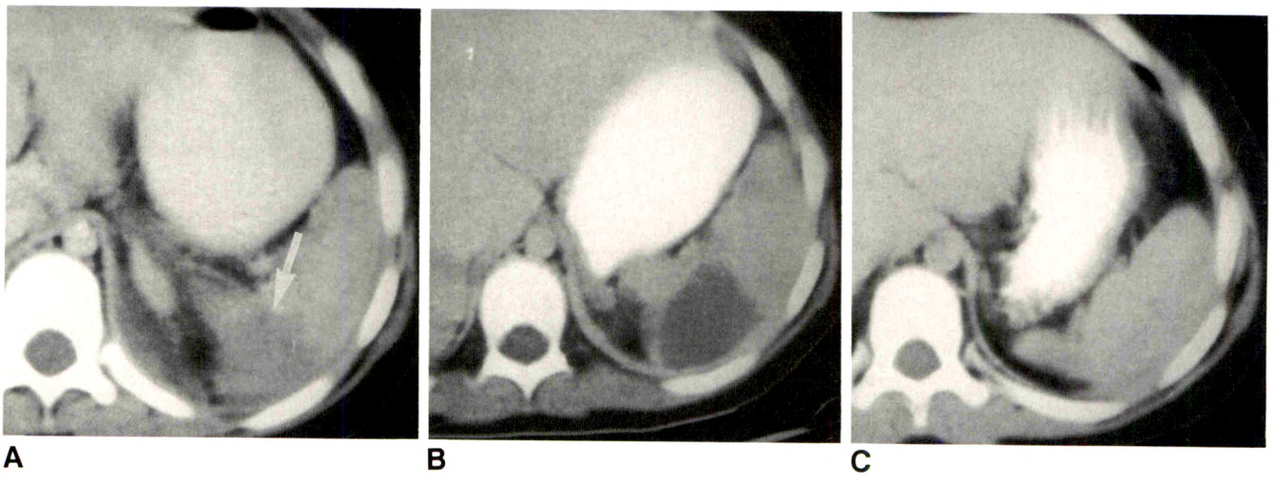


Fig. 1.—10-year-old boy injured in a motor vehicle accident.
A, CT scan shows splenic laceration and large, low-density intrasplenic hematoma (*arrow*) in posterior portion of spleen.
B, After 9 days, hematoma is organized, with well-defined border.
C, 5 months after initial injury, spleen appears normal without evidence of residual hematoma.

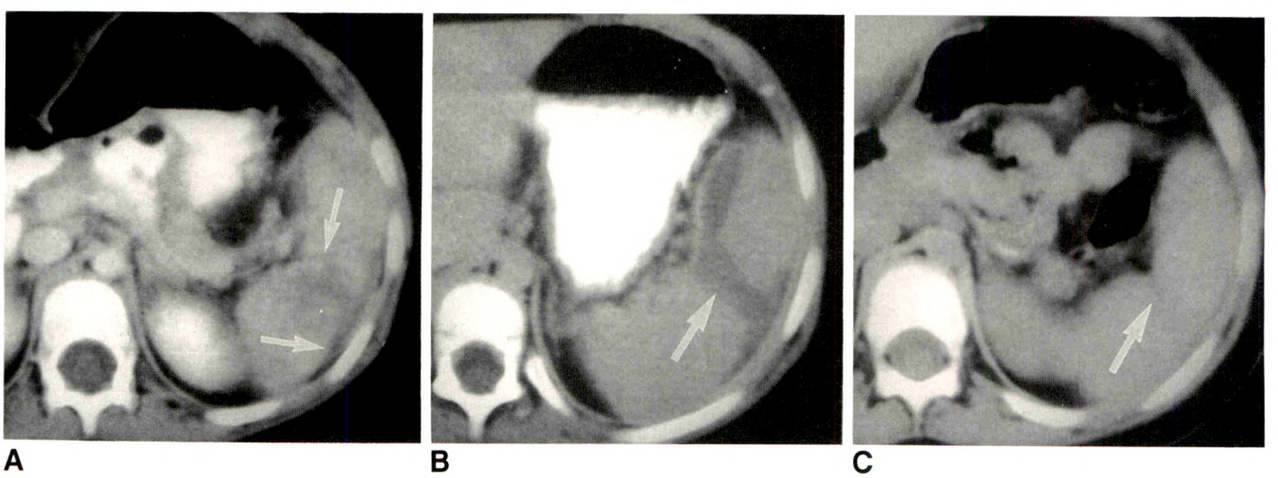


Fig. 2.—Splenic laceration in a 5-year-old girl injured in a motor vehicle accident.
A, Initially, CT scan shows both lenticular subcapsular hematoma and poorly defined intrasplenic hematoma (*arrows*).
B, 1 week later, communicating hematomas (*arrow*) are more organized and now occupy midportion of spleen.
C, Splenic fracture (*arrow*) is still evident 1 month later, but spleen appears well healed with virtual resorption of hematomas.

focal area within the spleen. Gas may or may not be seen within the abscess cavity.

Splenic infarcts resolve over a period of several months (Fig. 4). The time needed for resolution of splenic lacerations seen on CT varies, depending on the size and depth of the tear. Small peripheral lacerations may take several weeks to resolve, whereas deeper tears may require months to disappear [2].

Discussion

CT has proved to be a sensitive technique in establishing the presence and extent of acute injuries to the spleen [1, 6]. In our experience, CT has also been beneficial in documenting the healing process of the spleen. The pattern and duration of healing depend on the nature and severity of the initial injury, with parenchymal injuries taking longer to

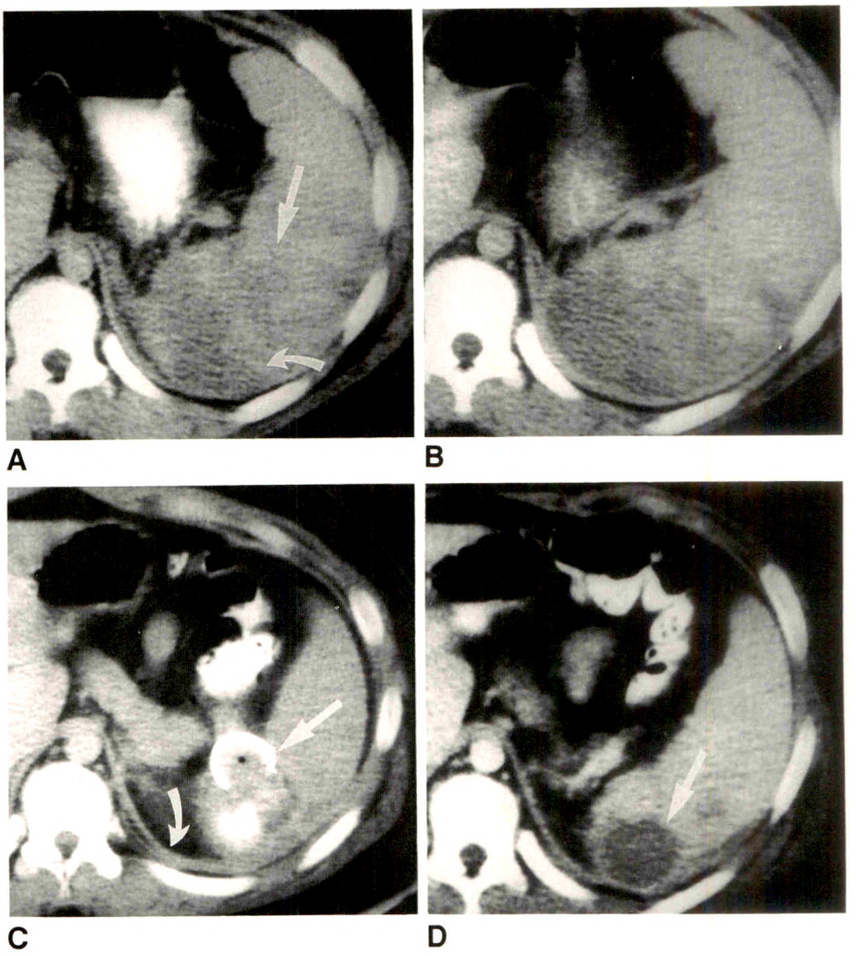
Fig. 3.—16-year-old boy injured in bicycling accident. Patient was discharged after 1 week of nonoperative treatment, but returned 6 weeks later with recurrent fever and pain in left upper abdomen.

A, Initial CT scan shows lacerations (*straight arrow*) throughout midspleen and subcapsular hematoma (*curved arrow*) posteriorly.

B, 1 week later, subcapsular hematoma is better defined.

C, CT scan 6 weeks later shows well-defined, low-attenuation fluid collection posteriorly. Percutaneous aspiration confirmed this to be a posttraumatic abscess. After placement of sump catheter (*straight arrow*), cavity size is markedly reduced. There is also some left pleural reaction (*curved arrow*).

D, Follow-up CT scan obtained 1 month after drainage shows unenhancing residual pseudocyst (*arrow*). Color Doppler sonography and dynamic CT showed that it was not a pseudoaneurysm. The patient was asymptomatic.



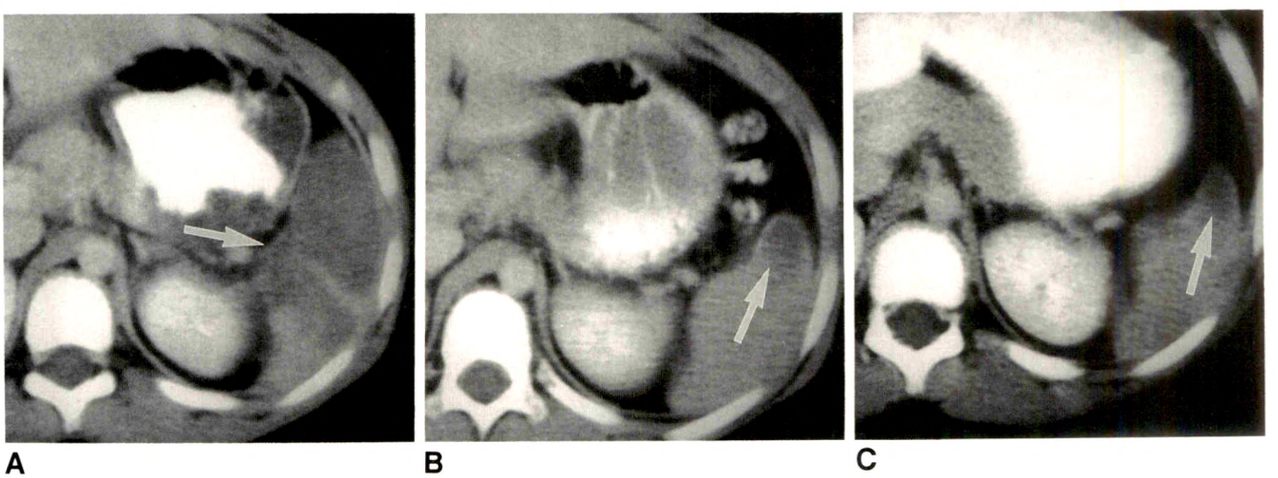


Fig. 4.—Traumatized spleen in a 10-year-old boy who fell on his left side.
A, Initial CT scan shows a large, low-attenuation, wedge-shaped infarct affecting anterior half of spleen (*arrow*).
B and *C*, CT studies obtained after 2 (*B*) and 5 (*C*) months show significant liquefaction and marked reduction in size of infarct (*arrows*).

return to normal than perisplenic or intraabdominal fluid collections do [2].

Successful outcome of conservative management of patients with splenic trauma is defined as the resolution of abnormalities found on initial CT scans, along with relief of any signs and symptoms that might indicate the need for intervention (e.g., orthostatic hypotension, falling hematocrit, abdominal distension, or left shoulder pain). The evolution of these abnormalities can be assessed by serial CT scans. Deterioration in a patient's clinical status may signal that conservative management is unsuccessful. Follow-up CT scans in these patients may reveal worsening of the initial CT findings [4].

The changes in the CT findings in patients treated conservatively should not be misconstrued as changes indicating the need for intervention. Although delayed rupture is an important feature of splenic trauma that should be recognized promptly, the value of CT scans repeated at regular intervals after splenic trauma remains unproved [6]. Nevertheless, the various manifestations of splenic healing should not be mistaken for nonhealing or new hemorrhage of the spleen. Intervention in these cases is not indicated unless there is worsening of the initial injuries and deterioration in the patient's clinical status [4].

REFERENCES

1. Federle MP, Griffiths B, Minagi H, Jeffrey RB. Splenic trauma: evaluation with CT. *Radiology* **1987**;162:69–71
2. Lupien C, Sauerbrei EF. Healing in the traumatized spleen: sonographic investigation. *Radiology* **1984**;151:181–185
3. Jeffrey RB, Laing FC, Federle MP, Goodman PC. Computed tomography of splenic trauma. *Radiology* **1981**;141:729–732
4. Mirvis SE, Whitley NO, Gens DR. Blunt splenic trauma in adults: CT-based classification and correlation with prognosis and treatment. *Radiology* **1989**;171:33–39
5. Faer MJ, Lynch RD, Lichtenstein JE, Madewell JE, Feigin DS. RPC from the AFIP. *Radiology* **1980**;134:371–376
6. Jeffrey RB. CT diagnosis of blunt hepatic and splenic injuries: a look to the future. *Radiology* **1989**;171:17–18

LIST OF BOOK REVIEWS

684 **Imaging of the Lumbar Spine.** *Griffiths HJ*
692 **Diagnosis of Diseases of the Chest, 3rd ed., vol. IV.** *Fraser RG, Paré JAP, Paré PD, Fraser RS, Genereux GP*
702 **Management of Cardiothoracic Trauma:** *Turney SZ, Rodriguez A, Cowley RA, eds.*
768 **Atlas of Oral Diagnostic Imaging.** *Higashi T, Shiba JKC, Ikuta H*
776 **Morphologic and Fuctional MR of the Kidneys and Adrenal Glands.** *Krestin GP*
784 **Imaging of the Pelvis: MRI with Correlations to CT and Ultrasound.** *Fishman-Javitt MC, Stein HL, Lovecchio JL, eds.*
834 **Comparative Cardiac Imaging: Function, Flow, Anatomy, and Quantitation.** *Brundage BH, ed.*
842 **Practical MRI Atlas of Neonatal Brain Development.** *Barkovich AJ, Truwit CI*
850 **Manual of Clinical Magnetic Resonance Imaging, 2nd ed.** *Heiken JP, Brown JJ, eds.*
866 **Essentials of Neuroimaging.** *Kirkwood JR*

The Value of Barium as a Gastrointestinal Contrast Agent in MR Imaging: A Comparison Study in Normal Volunteers

Pablo R. Ros[1]
Richard M. Steinman[1]
Gladys M. Torres[1]
Sharon S. Burton[1]
John L. Panaccione[1,2]
Daniel C. Rappaport[1]
Susan P. McGorray[3]

Preliminary data suggest that barium sulfate suspension is a potentially useful negative gastrointestinal contrast agent for MR imaging. To evaluate this hypothesis in a controlled fashion, abdominal and pelvic MR studies of 10 normal volunteers were performed before and after both oral (600–900 ml) and rectal (400 ml) administration of barium. Standard spin-echo coronal T1-, axial T1-, proton density–, and T2-weighted images were obtained at 1.5 T. Images obtained were randomized and interpreted by three observers, who evaluated bowel visualization and delineation of normal anatomy. Bowel segments evaluated were stomach, duodenum, proximal small bowel, proximal colon, distal colon, and rectum. Anatomic structures examined were pancreatic head, pancreatic body, pancreatic tail, retroperitoneum, spleen, liver, pelvic side walls, uterus, vagina, bladder, prostate, and seminal vesicles. Data concerning barium tolerance and safety were recorded. Descriptive, percent change, and kappa statistics were analyzed. Pairwise agreement techniques and repeated measures analysis of variance were performed. This statistical assessment showed a significant improvement in both bowel visualization (59–123% improvement, depending on the segment) and delineation of normal anatomy (23–68% improvement, depending on the structure) after barium administration, particularly on T1-weighted images. In addition, barium was a well-tolerated and safe contrast agent that did not produce artifacts.

Our results show that barium sulfate is a useful negative gastrointestinal contrast agent for MR because it improves bowel visualization and delineation of abdominal anatomy, particularly on T1-weighted sequences.

AJR **157:761–767, October 1991**

Preliminary data, both in vitro and in vivo, suggest that commercially available barium sulfate suspensions may be useful oral contrast materials for MR [1, 2] (Parikh AM, Mezrich RS, presented at the annual meeting of the Society of Magnetic Resonance in Medicine, August 1988; Ballinger R et al., SMRM, August 1990). Barium sulfate is a particularly appealing potential gastrointestinal contrast agent for MR imaging because it has a long-standing record of safety, tolerance by patients, low cost, and wide availability.

No data are currently available from a well-controlled, randomized, prospective series comparing MR images before and after administration of barium in the same subjects. Although the safety and tolerance of barium used in conjunction with diagnostic radiographs is well known, we thought that it was necessary to document any potential unusual effects of barium interacting within a strong magnetic field.

Therefore, the purpose of this study was twofold: (1) to assess the potential of oral and rectal barium sulfate as a gastrointestinal MR contrast agent for visualizing bowel segments (e.g., bowel visualization or opacification) and delineating normal abdominal and pelvic anatomy and (2) to assess tolerance by patients and the potential side effects of oral and rectal barium administration in MR.

Received February 21, 1991; accepted after revision May 21, 1991.

Presented at the annual meeting of the Society of Gastrointestinal Radiologists, Carlsbad, CA, February 1991, and recipient of the 1990 Society of Gastrointestinal Radiologists Research Award.

[1] Department of Radiology, Box J-374, JHMHC, University of Florida College of Medicine, Gainesville, FL 32610-0374. Address reprint requests to P. R. Ros.

[2] Present address: Department of Radiology, Methodist Hospital, Jacksonville, FL 32209.

[3] Department of Statistics, University of Florida College of Medicine, Gainesville, FL 32610-0374.

0361–803X/91/1574–0761
© American Roentgen Ray Society

Subjects and Methods

Ten normal volunteers (seven men and three women 25–53 years old) participated in the study. All were healthy, with no history of gastrointestinal disease, prior surgery, or allergy to barium. Each subject underwent abdominal and pelvic MR imaging before and after administration of barium, both orally and rectally. The unenhanced images served as controls for images obtained after oral and rectal administration of barium.

The oral contrast agent used was a 95% barium sulfate suspension (E-Z-pake, E-Z-EM, Inc., Westbury, NY) mixed to 60% weight/weight (w/w). The rectal contrast agent used was a 97% barium sulfate suspension (Sol-O-pake, E-Z-EM, Inc.) mixed to 66% w/w.

All volunteers drank 600–900 ml barium administered in three aliquots of 300 ml each (60 min, 30 min, and immediately before the scan). In addition, all volunteers received 400 ml barium as an enema.

Imaging was performed in all cases with a 1.5-T Signa unit (General Electric, Milwaukee, WI). Standard spin-echo sequences were used: coronal T1-weighted images, 600/20 (TR/TE); axial T1-weighted images, 600/20; axial proton-density-weighted images, 2700/30; and axial T2-weighted images, 2700/80, were obtained with a 256 × 256 or 256 × 128 matrix, two excitations, 5- to 10-mm slice thickness, and 0.5- to 2-mm gap. These variations pertain to differences between pulsing sequences or planes, because identical imaging protocols were used in all cases.

Tolerance to barium was evaluated by recording spontaneous comments by the subjects immediately after imaging and 24 hr later.

All images obtained were separated into unenhanced and enhanced sets, so that for any given volunteer studied, two image sets (unenhanced and enhanced) were created. These 20 sets were then provided to each of the three blinded evaluators in a random sequence, which underwent rerandomization between interpreters. The independent observers analyzed all images without knowledge of whether barium was administered. The parameters evaluated were (1) bowel marking or opacification, defined as the degree of visualization of contrast material within the bowel, and (2) delineation of normal anatomy, defined as the distinctness of normal anatomic structures of the abdomen and pelvis (including bowel and solid organs). The six bowel segments analyzed were stomach, duodenum, proximal colon, distal colon, and rectum. The 12 anatomic structures studied were pancreatic head, pancreatic body, pancreatic tail, retroperitoneum, spleen, liver, pelvic side walls, uterus, vagina, bladder, prostate, and seminal vesicles. Each item analyzed was given a value on a scale of 1–5: 1 = no marking/delineation, 2 = poor marking/delineation (<20%), 3 = fair marking/delineation (20–50%), 4 = good marking/delineation (50–80%), and 5 = excellent marking/delineation (>80%).

Computer-coded evaluation forms were analyzed descriptively (mean, standard deviation, range, and percent change), for trends and for variability between interpreters.

For each item analyzed (six bowel segments and 12 anatomic structures), descriptive statistics were calculated for the evaluators independently and as a pooled score of all evaluators combined. For all items, percent change scores comparing responses made before and after barium administration were calculated with regard to MR pulse sequence and plane. Summary scores were calculated from the individual bowel and anatomy grades. Kappa statistics [3, 4], based on the degree of improvement for all items, were used to assess overall agreement between evaluators. Summary scores were calculated from the individual bowel and anatomy grades. Repeated measures analyses of variance were performed to assess differences due to evaluator, MR pulse sequence/plane, presence (or absence) of barium, and interactions between these factors.

Specifically, bowel and anatomy summary scores were calculated for each combination of evaluator, MR pulse sequence/plane, and presence of barium. Bowel scores were calculated for bowel marking, and consisted of the sum of the six bowel segments considered for each of the 10 volunteers. Anatomy scores were calculated in an identical manner, and consisted of the sum of the scores for the 12 anatomic structures examined for the 10 subjects, and for each combination of evaluator, MR pulse sequence, and presence of barium.

At the component level, we focused on the amount of change for each response before and after barium administration. We evaluated this variable in both continuous and categorical fashions. The categories of worse, same, and better were calculated, and pairwise agreement was determined for the evaluators by using the kappa statistic.

Results

The summary scores indicated consistent improvement with barium administration for each MR pulse sequence/plane studied and each evaluator, although the magnitude of improvement varied. Grouping all scores for each evaluator's responses showed a consistent trend of improvement after barium administration for all pulse sequences evaluated irrespective of anatomic region. A repeated measure analysis of variance was performed, and significant effects ($p < .01$) due to barium administration and pulse sequence/plane were observed for both bowel opacification (marking) and anatomy. Also, effects due to evaluator and evaluator–barium administration interaction were noted.

To illustrate these results, Table 1 displays the means and standard deviations of the anatomy scores by evaluator, MR pulse sequence, and presence of barium.

Next we considered variability between interpreters. The tested hypothesis, no agreement between interpreters ($\kappa = 0$), vs agreement between interpreters ($\kappa > 0$) was evaluated. Kappa statistics were calculated, where z corresponds to the hypothesis test (Table 2). While these statistics are significantly different ($p < .01$) from 0 (no agreement), they do not indicate strong agreement.

Percent change scores were calculated for each item. These scores are particularly sensitive to improvements in

TABLE 1: Means and Standard Deviations of Anatomy Scores

Interval/MR Sequence	Mean Anatomy Score (SD)		
	Observer 1	Observer 2	Observer 3
Before barium			
Axial T1 weighted	36.4 (3.6)	28.4 (5.2)	31.4 (2.0)
Coronal T1 weighted	29.0 (2.9)	23.8 (4.1)	24.4 (3.0)
T2 weighted	28.9 (2.2)	21.0 (2.7)	28.7 (2.7)
Proton-density weighted	33.3 (3.4)	25.6 (4.4)	30.0 (4.1)
After barium			
Axial T1 weighted	42.4 (3.8)	45.2 (2.8)	36.2 (2.9)
Coronal T1 weighted	31.6 (2.8)	34.7 (4.4)	27.2 (2.8)
T2 weighted	31.0 (2.5)	40.7 (4.7)	31.3 (3.8)
Proton-density weighted	35.5 (9.6)	41.2 (4.1)	31.9 (6.2)

Note.—Twelve anatomic structures in 10 subjects were evaluated for delineation of normal anatomy on the basis of a 1–5 scale: 1 = no delineation, 2 = poor delineation (<20%), 3 = fair delineation (20–50%), 4 = good delineation (50–80%), and 5 = excellent delineation (>80%). The maximum mean score possible per observer was 46.5.

TABLE 2: Variability Among Interpreters

Observer	κ	SE	z	p
1 vs 2	.055	.018	3.134	<.01
1 vs 3	.248	.027	9.213	<.01
2 vs 3	.084	.017	4.854	<.01

quality, if initial assessment was poor. Detailed results are given in bar graph format (Figs. 1 and 2) with pre- and postbarium scores displayed for each pulse sequence and plane used (coronal T1-weighted images, axial T1-weighted images, axial T2-weighted images, and axial proton density–weighted images), as well as major parameters (bowel marking and anatomy; Figs. 1 and 2, respectively).

Improved marking or opacification of bowel and enhanced delineation of upper abdominal and pelvic structures were observed with all pulse sequences and planes (Figs. 3–9). The only exception was imaging of the vagina with T1-weighted coronal images, which displayed decreased visualization after barium was administered (Fig. 2A). It should be noted, however, that axial T1-weighted images, T2-weighted images, and proton density–weighted images (Figs. 2B–2D) showed improvement of vaginal delineation after barium administration.

In general, the structures that benefited most (greatest percent change) from barium administration were the rectum and distal colon (Fig. 6). Additionally, the duodenum, stomach, and proximal small bowel displayed significantly improved visualization after barium administration (Figs. 4, 5, 7, and 8). Axial T1-weighted images displayed consistent improvement with maximal postbarium scores for all anatomic regions evaluated (Fig. 2). Although T1-weighted images improved significantly after barium was administered, it may be interesting to note that visualization of the uterus and vagina was most improved with T2-weighted images obtained after barium administration (Figs. 2C and 9) and visualization of the

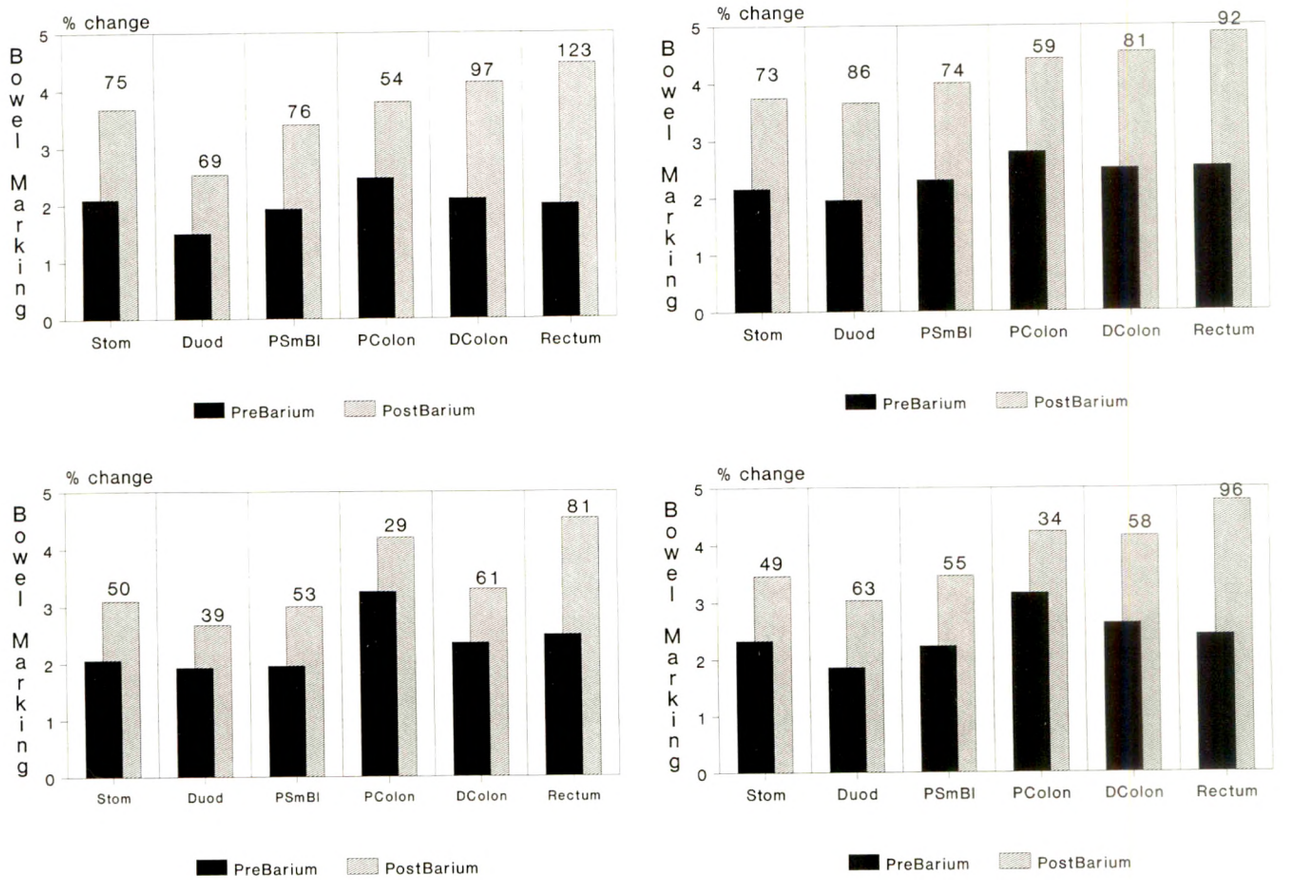


Fig. 1.—Effect of barium on MR bowel marking. In each graph, percent change in bowel marking, or opacification, is given by bowel segment.
***A*, Coronal T1-weighted image.**
***B*, Axial T1-weighted image.**
***C*, Axial T2-weighted image.**
***D*, Axial proton density–weighted image.**
Stom = stomach, Duod = duodenum, PSmBl = proximal small bowel, DColon = distal colon.

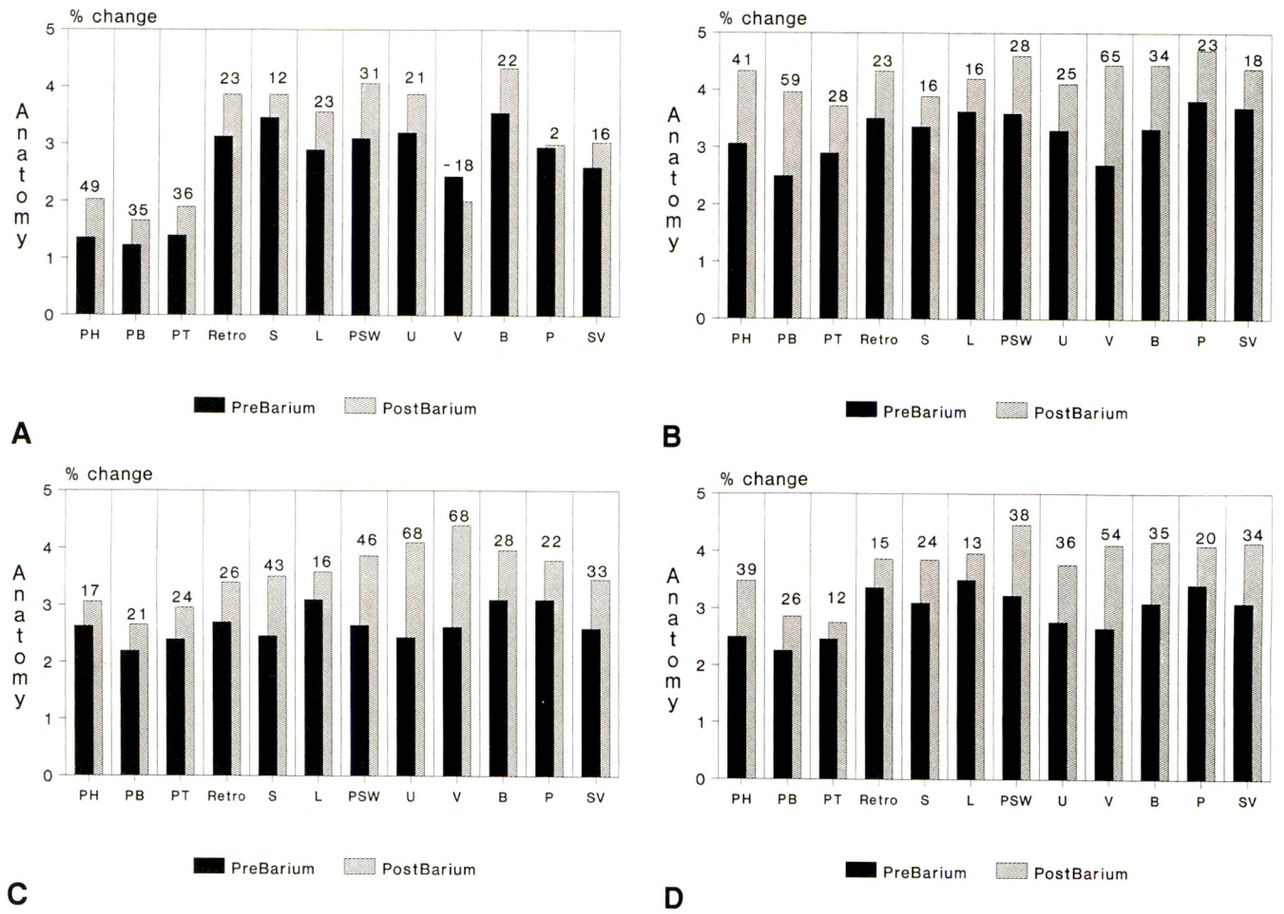


Fig. 2.—Effect of barium on MR delineation of anatomy. In each graph, percent change in delineation of anatomy is given by anatomic structure.
A, Coronal T1-weighted image.
B, Axial T1-weighted image.
C, Axial T2-weighted image.
D, Axial proton density–weighted image.
PH = pancreatic head, PB = pancreatic body, PT = pancreatic tail, Retro = retroperitoneum, S = spleen, L = liver, PSW = pelvic side walls, U = uterus, V = vagina, B = bladder, P = prostate, SV = seminal vesicles.

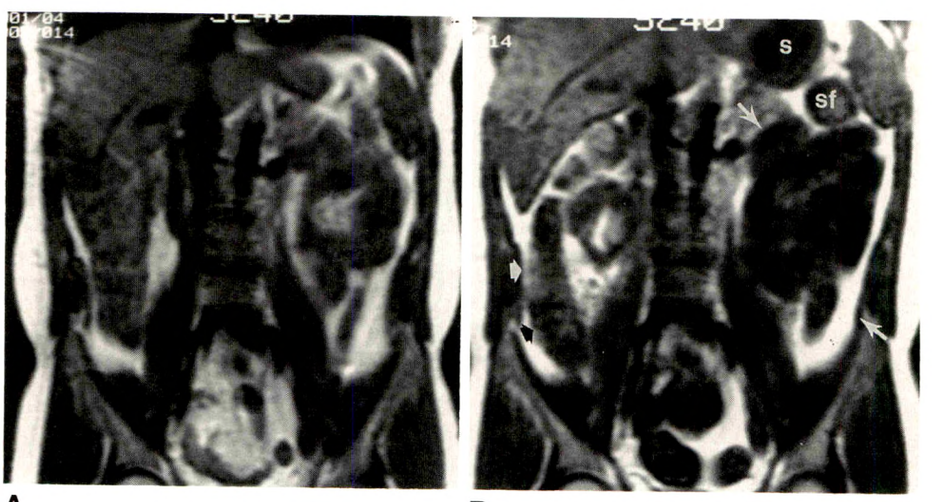


Fig. 3.—Coronal T1-weighted MR images of abdomen.
A, Before barium administration, superior border of liver is indistinct, as are splenic flexure, ascending colon, and stomach.
B, After barium administration, delineation of proximal small bowel (*long arrows*), pelvic bowel, ascending colon (*short arrows*), splenic flexure (sf), stomach (s), and inferior border of liver is improved.

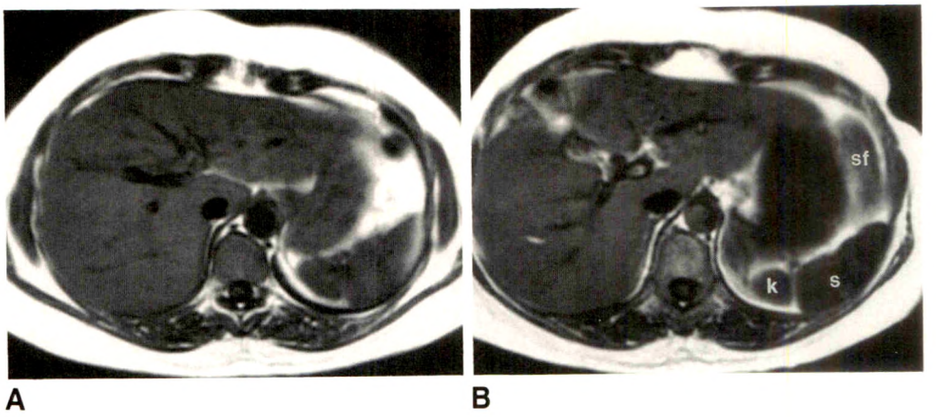


Fig. 4.—Axial T1-weighted MR images of upper abdomen (stomach and left upper quadrant).

A, On prebarium T1-weighted image, stomach appears somewhat collapsed and contains normal gastric secretions. Gastric wall cannot be distinguished.

B, On postbarium image, stomach appears distended. This may allow, as in this case, clearer delineation of upper pole of kidney (k), spleen (s), most lateral portion of left lobe of liver, and splenic flexure of colon (sf).

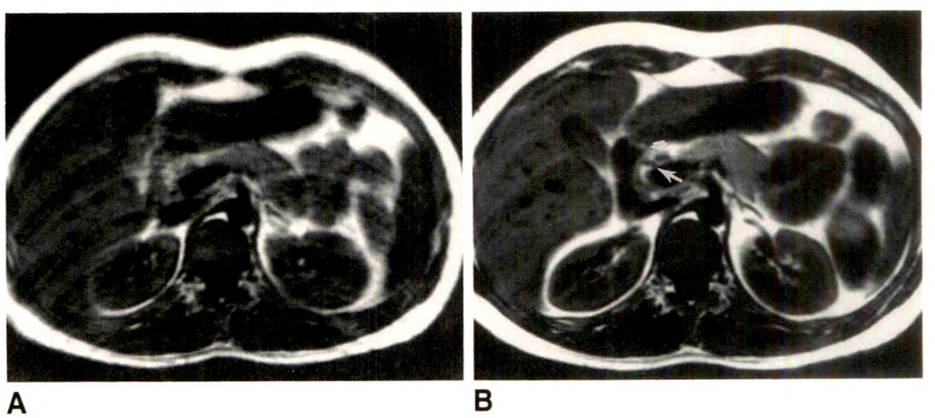


Fig. 5.—Axial T1-weighted MR images of duodenum/pancreas.

A and *B*, Compared with prebarium MR image (*A*), good marking of duodenal sweep and proximal jejunum is seen after administration of barium (*B*). Duodenum and proximal small bowel are also well delineated, with good visualization of adjacent structures, such as portal vein, body of pancreas, and left adrenal gland. Note how hepatic artery (*long arrow*) and common bile duct (*short arrow*) can be identified.

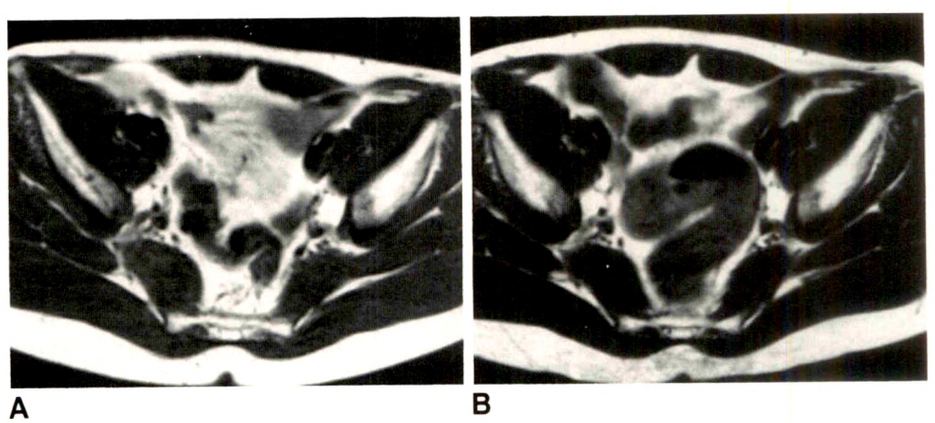


Fig. 6.—Axial T1-weighted MR images of sigmoid colon.

A and *B*, Sigmoid colon is identified well on images obtained before (*A*) and after (*B*) barium administration. However, after rectal administration of barium, sigmoid colon shows opacification, with improved delineation of pelvic side walls.

seminal vesicles and pelvic side walls was most improved with proton density–weighted images (Fig. 2D).

As expected, anatomic structures that were not near bowel structures and that were well imaged before barium administration displayed modest improvement after barium administration (liver and retroperitoneum) (Fig. 2). On the postbarium images, no artifacts were specifically related to barium administration.

The secondary effects observed were nausea in four patients, cramps in three, and mild constipation in two. All patients recovered fully without therapeutic intervention. These symptoms were similar to those produced by the administration of barium for gastrointestinal examinations other than MR. Therefore, it appears that MR does not produce specific secondary effects for barium administered orally or rectally.

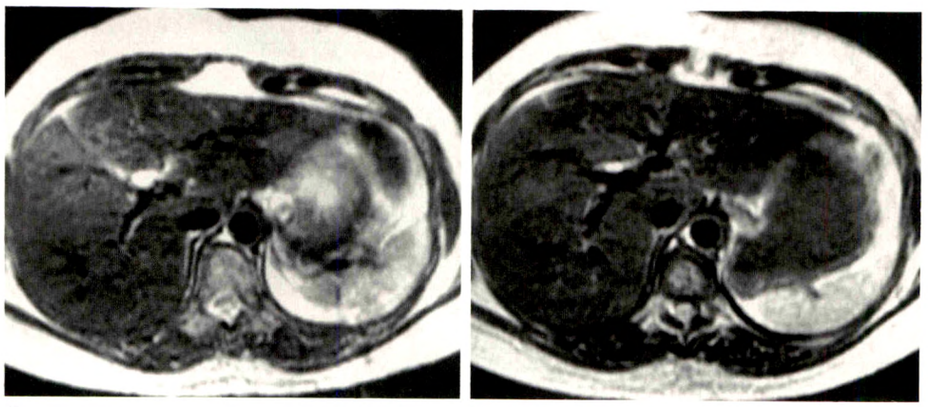


Fig. 7.—Axial T2-weighted MR images of stomach and left upper quadrant.

A, On prebarium image, ghost artifacts from residual gastric contents deteriorate visualization of structures in left upper quadrant, such as spleen and lateral segment of left lobe of liver.

B, After contrast administration, low intensity of barium allows better visualization of spleen and left lobe of liver, predominantly by reduction of ghost artifacts. Gastric wall can be easily identified; note negative contrast effect of barium on this heavily T2-weighted image.

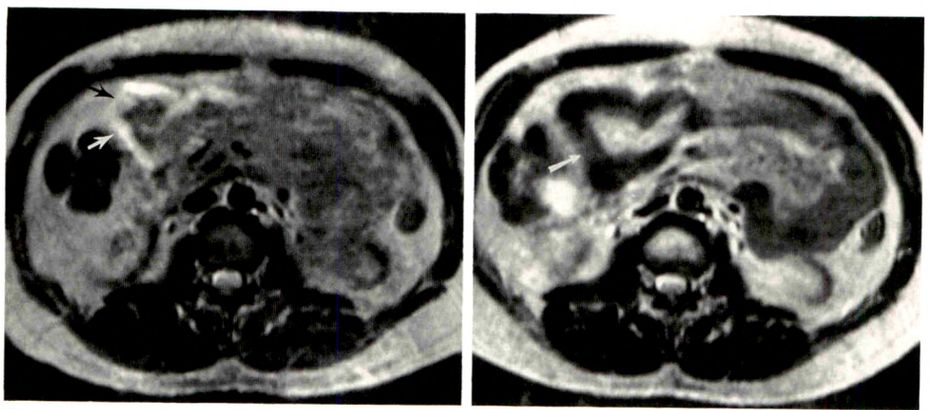


Fig. 8.—Axial T2-weighted MR images of proximal small bowel.

A, On prebarium image, bowel marking and delineation of bowel from mesentery are poor. High intensity results from enteric secretions (*arrows*).

B, After administration of barium, enhanced marking and delineation of bowel compared with surrounding structures are seen. Ghosting in this image is mildly reduced by negative contrast effect of barium (*arrow*).

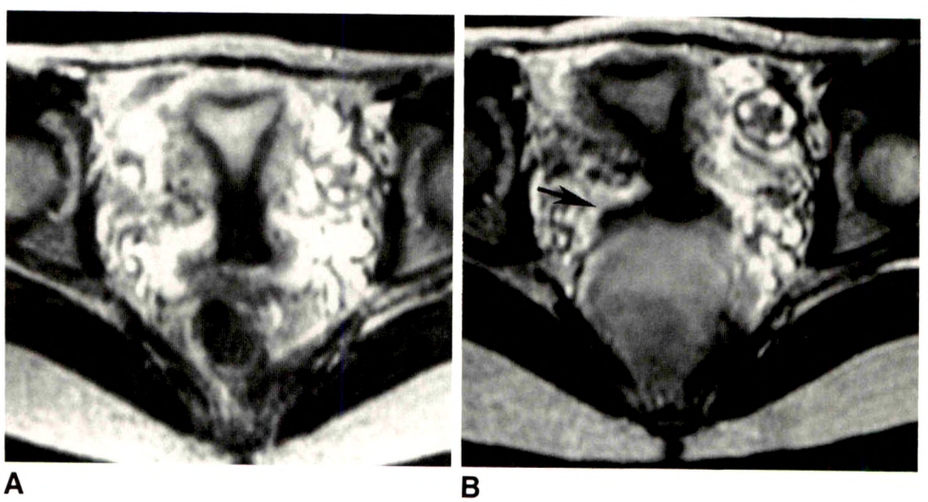


Fig. 9.—Axial T2-weighted MR images of uterus.

A and *B*, Although uterus is well seen on images obtained before (*A*) and after (*B*) barium administration, postbarium study shows that by filling rectum with contrast material and thus displacing uterus anteriorly, vaginal fornix (*arrow*) is delineated better than on prebarium image.

Discussion

This study, designed to evaluate the effect of barium as a gastrointestinal contrast agent, demonstrates a statistically significant improvement in bowel opacification and delineation of abdominal and pelvic structures in almost all pulse/plane sequence combinations analyzed.

It is not well known why barium sulfate produces a negative contrast effect. Barium is a diamagnetic substance, which in aqueous suspension eliminates signal by the following pro-

posed mechanisms: (1) magnetic susceptibility at particle-water interphase (primarily a T2 shortening effect) and (2) particle replacement of water by barium, which contains no hydrogen.

The negative contrast effect of barium is well maintained in bowel segments that are distant from its entry point, such as the jejunum or ileum, where peristalsis and mixture with enteric secretions might dilute it. This may be due to the intrinsic composition of the commercially available barium sulfate suspensions used, which contain additives designed to produce uniform opacification of the gastrointestinal tract.

Regarding tolerance and safety, our results demonstrate that the secondary effects attributable to barium during MR examination are mild and not appreciably different from those observed during routine gastrointestinal barium examinations. Therefore, barium may be a useful negative gastrointestinal contrast agent, with a wide margin of tolerance and safety, and with potential reactions that in complicated cases (obstruction, perforation, allergy, etc.) are well known in the radiologic literature. No artifacts attributable to barium that would decrease its efficacy as an MR gastrointestinal contrast agent were noted. An additional advantage of barium used as an MR gastrointestinal contrast agent is that MR examinations may be performed after upper gastrointestinal examination or barium enema, thus providing an alternative to abdominal CT studies.

Thus, barium sulfate appears to be a useful negative contrast agent for MR imaging because it improves bowel marking and delineation of abdominal anatomy, particularly on T1-weighted sequences.

REFERENCES

1. Burton SS, Ros PR, Torres GM, et al. Barium-MRI of the pancreas: initial experience. *Radiology* **1989**;173(P):517
2. Storm BL, Li KCP, Tart RP, et al. Barium sulfate suspension as an oral contrast agent in MR imaging: initial clinical results. *Radiology* **1989**;173(P):522
3. Kramer MS, Feinstein AR. The biostatistics of concordance. *Clin Pharmacol Ther* **1981**;29;111–123
4. Fleiss JL. *Statistical methods for rates and proportions*, 2nd ed. New York: Wiley, **1981**:212–236

Book Review

Atlas of Oral Diagnostic Imaging. By Tomomitsu Higashi, Jimmy K. Chen Shiba, and Hiroyuki Ikuta. St. Louis: Ishiyaku EuroAmerica, 270 pp., 1990. $42.50

This book is liberally illustrated and appears to be addressed to the dental profession. The style of the authors is unusual and enjoyable in that everything is in outline form or concisely written. All radiographs or other clinical material is accompanied by line diagrams that are clearly labeled. This makes it extremely interesting for the novice to understand the findings in each radiograph.

The book is divided into 12 chapters, each composed of 10–15 pages. It encompasses everything in the oral cavity, from dental abnormalities and congenital lesions through inflammatory disease, benign tumors, malignant diseases of the paranasal sinuses, and diseases of the salivary glands. Each chapter finishes with a one- to three-page summary in outline form, giving differential diagnosis in a 1, 2, 3 fashion or comparing two problem entities such as benign vs malignant maxillary sinus disease.

The first chapter covers anomalies and technique. It is broken down into anomalies of number, then position, and finally size and shape. This chapter is clearly illustrated and quite complete. Probably the most enjoyable thing about the third chapter is the excellent illustrations and line diagrams showing common dental pathologic changes. If incidental pathologic changes are present on other teeth on the illustration, the author wisely addresses the issue. Unfortunately, this chapter is only five pages long. The fourth chapter covers inflammatory disease and is done reasonably well. The later pages of the chapter cover the differential diagnosis of osteomyelitis from malignancies. The CT studies leave much to be desired.

The highlight of the book is chapter 5 on odontogenic cysts. It follows the usual format of panoramic views or transoral views coupled with line drawings that are well labeled. In this chapter, the authors have several references to the use of xeroradiography, which they overrate. The chapter is 55 pages well spent. Radiologists will enjoy chapter 8, on non-odontogenic tumors, because we seldom get an opportunity to see high-quality transoral views of mandibular lesions. Unfortunately CT scans and MR images are not included. The author of this chapter is enthusiastic about the uses of technetium nuclear scanning, which is not entirely justified. He boldly states that the presence of malignant tumor within the maxillary sinus can be ruled out when no appreciable uptake of gadolinium occurs.

After the authors leave the mandible and maxillae to discuss sinuses, salivary glands, and temporomandibular joints, the book becomes considerably less interesting. Several CT scans of marginal quality are included, and the plain films of sinuses and temporomandibular joints do not really show the pathologic changes. Only one attempt is made at an MR image, and this is entirely unsatisfactory. Although chapter 14 discusses salivary glands, the tumors that are illustrated are massive types of tumors that actually represent end-stage disease. This is probably suitable for introduction to a novice but has little clinical bearing. One of the final chapters on trauma is good basic material but contains nothing about modern management of fractures of the mandible.

In summary, the authors are to be congratulated on their style of writing, which presents a lot of information in a small space. It is an attempt to follow the lines of one of the best books on differential diagnosis of oral lesions, which was written by Norman K. Wood and Paul W. Goaz and published by Mosby. The authors state that the book was written for dental students and general dental practitioners. I think the authors cannot include any other groups in their audience unless they greatly expand the material in the first eight chapters. They also state that they have included new diagnostic imaging techniques such as CT and MR, but this is not entirely true. Radiologists will have to be content with books written by Mancuso, Bergeron, Som, and Delbalso for these imaging techniques.

William Hanafee
University of California, Los Angeles
Los Angeles, CA 90024-1721

Enteral Feeding Tubes: Placement by Using Fluoroscopy and Endoscopy

David J. Ott[1]
Huitt E. Mattox[2]
David W. Gelfand[1]
Michael Y. M. Chen[1]
Wallace C. Wu[2]

Fluoroscopy and endoscopy are both effective for guiding placement of enteral feeding tubes, but the relative advantages and limitations of the two methods are less clear. Consequently, we studied 104 consecutive patients referred for primary fluoroscopic placement of a Frederick-Miller feeding catheter. Success rate, fluoroscopic and room times, and tube position were determined. Unsuccessful fluoroscopic placement was followed immediately by an endoscopic attempt. The success rate for fluoroscopic placement was 90% (94/104), with the tube placed into the jejunum in 53% and into the duodenum in 47%. The fluoroscopic and room times for successful fluoroscopic placements were 8.6 ± 5.6 min (mean ± SD) and 21.7 ± 8.4 min, respectively. For the 10 unsuccessful placements, the fluoroscopic and room times were 16.2 ± 5.4 min (mean ± SD) and 45.6 ± 18.4 min, respectively. Both time differences were significant statistically. Endoscopic placement was successful in all seven patients in whom it was attempted, with a mean time of 13.4 min. The tubes placed endoscopically were in the jejunum in 29% and in the duodenum in 71%.

Our results show that fluoroscopic and endoscopic placement of enteral feeding tubes is highly effective. Fluoroscopic time in successful cases is usually less than 15 min. Endoscopic placement of feeding tubes is successful after fluoroscopic failure.

AJR 157:769–771, October 1991

Enteral feeding has become an important means of providing nutritional support to seriously ill patients [1]. As infusion of feeding solutions beyond the pylorus presumably lessens the chance of aspiration, placement of enteral tubes into the duodenum or preferably into the jejunum is a major goal [2]. A variety of nasoenteral tubes are available, and techniques for their placement include blind approaches that use periodic abdominal films to verify placement or fluoroscopic and endoscopic methods [2–12]. Between 1983 and 1990, direct fluoroscopic placement of enteral catheters at our institution increased from none to over 400 procedures annually (Fig. 1).

Directed placement of enteral tubes with fluoroscopy or endoscopy has been recommended to expedite the procedure [2, 6, 8, 10–12]. Both methods have been successful and have permitted rapid enteric intubation and immediate feeding of the patient. However, the relative advantages and limitations of the use of fluoroscopy and endoscopy for this purpose are less clear. As a result, we compared the success of fluoroscopic and endoscopic placement of the Frederick-Miller feeding catheter (Cook Inc., Bloomington, IN) in 104 consecutive patients [5].

Materials and Methods

During a 4-month period, 104 consecutive patients were referred for primary fluoroscopic placement of an enteral feeding tube. The group consisted of 46 women and 58 men with a mean age of 66 years (range, 19–100 years). The Frederick-Miller catheter (8-French, 120-

Received March 18, 1991; accepted after revision April 18, 1991.

[1] Department of Radiology, Bowman Gray School of Medicine, Wake Forest University, Winston-Salem, NC 27103. Address reprint requests to D. J. Ott.

[2] Department of Medicine, Bowman Gray School of Medicine, Wake Forest University, Winston-Salem, NC 27103.

0361–803X/91/1574–0769
© American Roentgen Ray Society

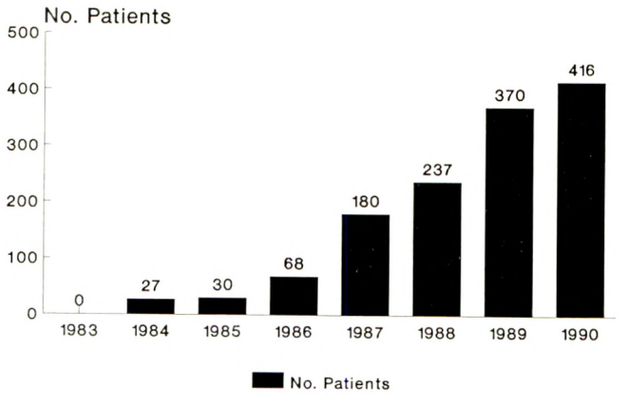


Fig. 1.—Bar graph shows marked annual increase in number of fluoroscopic feeding tube placements at our institution between 1983 and 1990.

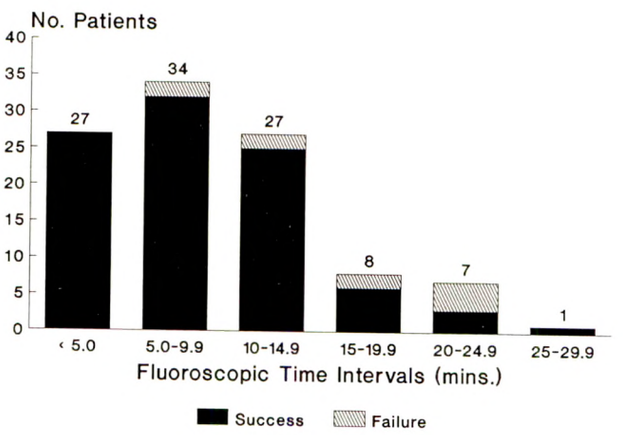


Fig. 2.—Stacked bar graph of successful and failed fluoroscopic feeding tube placements during 5-min intervals.

cm length; Teflon-coated guidewire) was used in all patients. After selection and preparation of a naris, the catheter was placed transnasally while the patient was supine and passed into the gastric antrum under fluoroscopic guidance. The patient was then turned to the left posterior oblique position, and supported by a bolster if needed, for further manipulation of the catheter through the pylorus and into the distal duodenum or jejunum. The success rate for fluoroscopic placement beyond the pylorus, fluoroscopic and total room times, and tube position were determined. Fluoroscopists varied in their experience and included radiology residents at different levels of training and, less often, faculty specialized in gastrointestinal radiology.

Unsuccessful fluoroscopic placement was followed immediately by an endoscopic attempt. A modified Frederick-Miller tube with the closed distal tip clipped off was passed transnasally and recovered from the mouth. An Olympus GIF-XQ10 endoscope (Olympus Corp., Lake Success, NY) was then advanced into the distal duodenum, avoiding excessive gastric insufflation. A 4-m, 0.035-in. Teflon-coated floppy-tipped guidewire (Wilson-Cook Medical, Inc.,Winston-Salem, NC) was placed into the duodenum via the biopsy channel of the endoscope, which was withdrawn, leaving the guidewire in place. The guidewire was transferred from the mouth to the nose by using the Frederick-Miller catheter as a transfer tube. The feeding catheter was then advanced over the guidewire into the small bowel. Duration of the procedure was recorded, and tube position was determined by fluoroscopic observation or plain radiography.

Results

The fluoroscopic success rate was 90% (94/104), with the tip of the Frederick-Miller catheter placed into the distal duodenum in 44 patients (47%) and into the jejunum in 50 patients (53%). The fluoroscopic and room times in the successful placements were 8.6 ± 5.6 min (mean ± SD) and 21.7 ± 8.4 min, respectively. In the 10 unsuccessful procedures, the mean fluoroscopic and room times were 16.2 ± 5.4 min and 45.6 ± 18.4 min, respectively. Both time differences were significant statistically ($p < .01$). Unsuccessful attempts increased proportionately for fluoroscopic times above 15 min (Fig. 2). No complications occurred in this group of patients.

The main reasons for terminating the unsuccessful fluoroscopic procedures were patients' discomfort or persistent looping of the catheter in the stomach. Endoscopic placement was attempted in seven of the 10 patients in whom fluoroscopic placements were unsuccessful and was successfully completed in all patients without complications. The mean endoscopic time was 13.4 min, and the tip of the modified Frederick-Miller catheter was placed into the duodenum in five (71%) patients and into the jejunum in two (29%). Endoscopy was not used in the remaining three patients because of clinical considerations or unavailability of the endoscopic team.

Discussion

The advantages of enteral over parenteral feeding and the administration of solutions into the small bowel rather than the stomach to prevent reflux and aspiration have increased the demand for placement of enteral feeding tubes [3, 4, 6]. Blind placement of feeding tubes with weighted tips followed by plain films of the abdomen to document their position is often done initially. However, this method is less effective than fluoroscopic or endoscopically guided techniques and is more time consuming [3, 4]. We evaluated fluoroscopic placement of the Frederick-Miller catheter and assessed the use of a specific endoscopic method of placing a modified tube if the fluoroscopic attempt failed.

The Frederick-Miller tube is a soft, flexible, fine-bore (8-French) catheter with a nonweighted tip that facilitates radiologic positioning as compared with alternative tubes with weighted tips [5]. The end of the catheter is closed and contains a small embedded metal plug, which is easily seen fluoroscopically. A Teflon-coated guidewire is packaged with the catheter. The technique used for fluoroscopic placement of the Frederick-Miller tube is similar to that described for hypotonic duodenography and enteroclysis. The use of water-soluble contrast material to identify anatomy or metoclopramide hydrochloride to stimulate peristalsis may assist in advancement of the tube, especially through the pylorus.

Our fluoroscopic success rate for placement of the Frederick-Miller catheter was 90%, similar to the 93% success reported in the original description of this tube [5]. However,

the mean fluoroscopic time in our study was 8.6 min for successful placement compared with 3.3 min found in the original report. This time difference most likely reflects the variable experience of radiology residents at different levels in their training, who were primarily responsible for performing this procedure. Other types of fluoroscopically guided nasoenteric tubes, particularly the Entriflex catheter (Biosearch Medical Products, Somerville, NJ), have shown comparably high success rates [2, 8].

Unsuccessful fluoroscopic placements required approximately twice the fluoroscopic and room times as the successful placements did, with more failures occurring in the 15–20 min fluoroscopic time interval. A similar experience has been observed with the Entriflex tube, in which successful placements were accomplished in less than 10 to 15 min [2, 8]. These studies indicate that enteric intubation by using fluoroscopy and an appropriate catheter is achieved in 90% or more of patients, usually within 5–10 min. We think that prolonging fluoroscopy beyond 15 min is unlikely to produce success and an alternative approach should be chosen, such as endoscopy.

A variety of endoscopic methods have been described for placement of enteral feeding tubes [10–12]. The technique that we have used combines endoscopic placement of a guidewire and a modified Frederick-Miller catheter. This technique has been safe, effective, and rapid. Endoscopic placement was successful in all seven patients in whom it was attempted, with a mean time for the procedures of only 13.4 min. This experience is similar to other recent reports indicating that endoscopy is an excellent option for placement of feeding tubes [11, 12]. A difference between our successful fluoroscopic and endoscopic placements was the final location of the catheter tip. The tip of the Frederick-Miller tube was placed in the jejunum more reliably with fluoroscopy (53%) than with endoscopy (29%). Duodenal placements may be associated with gastric reflux or retrograde migration of the tube into the stomach. Thus, the duration of the duodenal placement may be shorter, but further study is needed to determine the relevance of this factor [8].

In conclusion, our results and other reports have shown that fluoroscopic and endoscopic placement of enteral tubes have a high success rate. In order to avoid undue radiation exposure to the radiologist and patient, a fluoroscopic time limit of 15 min is suggested because success is unlikely beyond that time. Endoscopic placement of feeding tubes by using guidewire-assisted techniques has been successful after unsuccessful fluoroscopic placement and may be used as an initial method of enteric intubation. In patients unable to be transported safely to the radiology department, endoscopic placement of the feeding tube is an excellent option, although the use of portable fluoroscopy is also possible. We have adopted endoscopy rather than bedside fluoroscopy, particularly in patients in the intensive care unit who are unstable or who require anesthesia.

REFERENCES

1. Silk DBA, Rees RG, Keohane PP, Attrill H. Clinical efficacy and design changes of "fine bore" nasogastric feeding tubes: a seven-year experience involving 809 intubations in 403 patients. *J Parenter Enteral Nutr* **1987**;11:378–383
2. Grant JP, Curtas MS, Kelvin FM. Fluoroscopic placement of nasojejunal feeding tubes with immediate feeding using a nonelemental diet. *J Parenter Enteral Nutr* **1983**;7:299–303
3. Ramos SM, Lindine P. Inexpensive, safe and simple nasoenteral intubation: an alternative for the cost conscious. *J Parenter Enteral Nutr* **1986**;10:78–81
4. Thurlow PM. Bedside enteral feeding tube placement into duodenum and jejunum. *J Parenter Enteral Nutr* **1986**;10:104–105
5. Frederick PR, Miller MH, Morrison WJ. Feeding tube for fluoroscopic placement. *Radiology* **1982**;145:847
6. Prager R, Laboy V, Venus B, Mathru M. Value of fluoroscopic assistance during transpyloric intubation. *Crit Care Med* **1986**;14:151–152
7. Woodall BH, Winfield DF, Bisset GS III. Inadvertent tracheobronchial placement of feeding tubes. *Radiology* **1987**;165:727–729
8. Gutierrez ED, Balfe DM. Fluoroscopically guided nasoenteric feeding tube placement: results of a 1-year study. *Radiology* **1991**;178:759–762
9. Lewis BS, Mauer K, Bush A. The rapid placement of jejunal feeding tubes: the Seldinger technique applied to the gut. *Gastrointest Endosc* **1990**;36:139–141
10. Chung RSK, Denbesten L. Improved technique for placement of intestinal feeding tube with the fiberoptic endoscope. *Gut* **1976**;17:264–266
11. Pleatman MA, Naunheim KS. Endoscopic placement of feeding tubes in the critically ill patient. *Surg Gynecol Obstet* **1987**;165:69–70
12. Rives DA, LeRoy JL, Hawkins ML, Bowden TA Jr. Endoscopically assisted nasojejunal feeding tube placement. *Am Surg* **1989**;55:88–91

Books Received

Receipt of books is acknowledged as a courtesy to the sender. Books considered of sufficient interest are reviewed as space permits. If the book has been reviewed in the *AJR*, the date of its review is given in parentheses.

Tissue Characterization in MR Imaging. Clinical and Technical Approaches. Edited by H. Peter Higer and Gernot Bielke. New York: Springer-Verlag, 340 pp., 1990. $149 (7/91)

Atlas of Interventional Radiology. By Constantin Cope, Dana R. Burke, and Steven G. Meranze. Philadelphia: Lippincott, 325 pp., 1990. $89.50 (7/91)

Magnetic Resonance Imaging of the Pediatric Brain. An Anatomical Atlas. By G. Salamon, C. Raynaud, J. Regis, and C. Rumeau. New York: Raven, 350 pp., 1990. $105 (7/91)

Atlas of Normal and Variant Angiographic Anatomy. By Saadoon Kadir. Philadelphia: Saunders, 544 pp., 1991. $95 (7/91)

RSNA Today, Vol. 4, No. 4. Oak Brook, IL: The Radiological Society of North America, 1990. $55; by subscription, 6 issues annually at $185 for RSNA members and $225 for nonmembers (VHS videotape) (8/91)

Clinical Radiology of the Breast. By Eric J. Roebuck. Oxford, England: Heinemann (distributed by Butterworths, Stoneham, MA), 273 pp., 1990. $75, softcover (8/91)

MRI of the Wrist and Hand. By Murray A. Reicher and Leland E. Kellerhouse. New York: Raven, 203 pp., 1990. $89 (8/91)

Thyroid Disease. Endocrinology, Surgery, Nuclear Medicine, and Radiotherapy. Edited by Stephen A. Falk. New York: Raven, 670 pp., 1990. $125 (8/91)

Therapeutic Endoscopy and Radiology of the Gut, 2nd ed. Edited by John R. Bennett and Richard H. Hunt. Baltimore: Williams & Wilkins, 386 pp., 1990. $120 (8/91).

The Radiologic Clinics of North America. Imaging of Joints. Guest editor: Jeremy J. Kaye. Philadelphia: Saunders, September 1990;28(5):905–1138. $25; by subscription, 6 issues annually for $93 (8/91)

CT and MRI of the Genitourinary Tract. Edited by Stanford M. Goldman and Olga M. B. Gatewood. (Vol. 13 in Contemporary Issues in Computed Tomography.) New York: Churchill Livingstone, 323 pp., 1990. $79.95 (8/91)

Radiology in the Management of Cancer. Edited by R. J. Johnson, B. Eddleston, and R. D. Hunter. New York: Churchill Livingstone, 472 pp. 1990. $125 (8/91).

Physics and Instrumentation of Diagnostic Medical Ultrasound. By Peter Fish. New York: Wiley, 250 pp., 1990. $34.50 (8/91)

The Lungs. Edited by B. Corrin. (Vol. 5 of Systemic Pathology, 3rd ed. General editor: W. St C. Symmers.) New York: Churchill Livingstone, 467 pp., 1990. $159 (8/91)

Atlas of Roentgenographic Measurement, 6th ed. By Theodore E. Keats. St. Louis: Mosby–Year Book, 710 pp., 1990. $89.95 (9/91)

Neuroradiology Test and Syllabus, parts 1 and 2. Section editor: Peter E. Weinberg. (Set 28 in the Professional Self-Evaluation and Continuing Education Program.) Reston, VA: American College of Radiology, 926 pp., 1990. $180 for ACR members, $300 for nonmembers, and $150 for residents (9/91)

The Language of Fractures, 2nd ed. By Robert Jordan Schultz. Baltimore: Williams & Wilkins, 333 pp., 1990. $49.95 (9/91)

Magnetic Resonance Imaging of Carcinoma of the Urinary Bladder. By Jelle O. Barentsz, Frans M. J. Debruyne, and Sjef H. J. Ruijs. Boston: Kluwer, 121 pp., 1990. $120 (9/91)

RSNA Today, Vol. 4, No. 5. Oak Brook, IL: The Radiological Society of North America, 1990. $55; by subscription, 6 issues annually at $185 for RSNA members and $225 for nonmembers (VHS videotape) (9/91)

A Short Textbook of Clinical Imaging. Edited by David Sutton and Jeremy W. R. Young. New York: Springer-Verlag, 856 pp., 1990. $98 (9/91)

Textbook of Uroradiology. By N. Reed Dunnick, Ronald W. McCallum, and Carl M. Sandler. Baltimore: Williams & Wilkins, 505 pp., 1991. $125 (9/91)

MRI of the Musculoskeletal System, 2nd ed. Edited by Thomas H. Berquist. New York: Raven, 545 pp., 1990. $130 (9/91)

Detection and Treatment of Early Breast Cancer. By Ian Fentiman. Philadelphia: Lippincott, 272 pp., 1990. $69.50 (9/91)

The Radiologic Clinics of North America. Interventional Radiology of the Biliary Tract. Guest editor: H. Joachim Burhenne. Philadelphia: Saunders, November 1990;28(6):1139–1313. $25; by subscription, 6 issues annually for $93 (9/91)

Obstetrics and Gynecology. (Vol. 1 in Diagnostic Medical Sonography. A Guide to Clinical Practice.) Edited by Mimi C. Berman. Philadelphia: Lippincott, 768 pp., 1991. $85 (9/91)

Gamuts and Pearls in MRI. By Stephen J. Pomeranz. Richmond, VA: William Byrd Press, 273 pp., 1990. $79 (9/91)

Progress in Cardiology, 4/1. Edited by Douglas P. Zipes and Derek J. Rowlands. Philadelphia: Lea & Febiger, 138 pp., 1991. $39.50

Conceptual Basis for Calculations of Absorbed-Dose Distributions. Recommendations of the National Council on Radiation Protection and Measurements. (NCRP Report No. 108.) Bethesda, MD: National Council on Radiation Protection and Measurements, 234 pp., 1991. $22

Case Report

Systemic *Yersinia enterocolitica* Infection Associated with Iron Overload and Deferoxamine Therapy

Peter W. Abcarian[1] and Barbara E. Demas

Since the discovery of *Yersinia enterocolitica* as a human pathogen in 1939 [1], several reports have appeared in the medical and pediatrics literature describing systemic yersiniosis in the setting of iron overload, particularly in those patients undergoing iron-chelation therapy [2–4]. Although the vast majority of infections caused by *Y. enterocolitica* produce a self-limited gastroenteritis and mesenteric adenitis, patients with underlying diseases causing iron overload are at particular risk for serious, often fatal systemic infection. We present a case of systemic yersinial infection in a child with thalassemia major who was being treated with deferoxamine, in order to alert radiologists to the unique relationship between *Y. enterocolitica* and excessive iron stores in conjunction with deferoxamine therapy.

Case Report

A 5-year-old boy with transfusion-dependent β-thalassemia major treated with daily subcutaneous deferoxamine injections and monthly blood transfusions had a 5-day history of abdominal pain. The pain began in the epigastrium, subsequently localized to the right lower quadrant and was associated with anorexia, diarrhea, and fever (body temperature, 40°C). On examination in the emergency department he was in moderate distress, had marked tenderness in the right lower quadrant, and had an elevated leukocyte count with a left shift.

A sonogram showed an abnormally thick-walled, noncompressible loop of small bowel in the right lower quadrant with associated hypoechoic and slightly enlarged mesenteric lymph nodes. The appendix was not visualized as a discrete structure and no appendicolith was detected. Diagnostic considerations included acute appendicitis and infectious terminal ileitis with mesenteric adentis.

A Hypaque (Winthrop Pharmaceuticals, New York, NY) enema showed that the cecum was nondistensible and scalloped along its medial margin, suggesting mass effect from adenopathy and/or cecal inflammation. The ileocecal valve was prominent. The appendix was not visualized. Reflux of contrast material into the terminal ileum showed mild luminal narrowing and effacement of the mucosa of the ileum (Fig. 1A).

During surgery, purulent cloudy fluid was found in the peritoneal cavity. The appendix was inflamed, without perforation, and the ileum was normal. An appendectomy was performed. Pathologic evaluation of the specimen showed marked and acute inflammation involving much of the mucosa and extending through the wall with fibrinous deposits and abscess formation on the peritoneal surface.

Blood cultures obtained in the emergency department and peritoneal fluid cultures obtained at the time of surgical resection grew *Y. enterocolitica*.

Postoperative management consisted of supportive measures, including IV triple antibiotics and fluid replacement, blood transfusions, and discontinuation of deferoxamine iron-chelation therapy. The patient's course was complicated by persistent fevers, abdominal distension, and pulmonary edema. Repeated cultures of blood were negative for *Y. enterocolitica*.

Serial CT examinations of his abdomen were obtained because of concern for pericecal abscess. Four days after surgery, a CT study showed multiple sites of intraabdominal lymphadenopathy, including pericecal, mesenteric, periceliac, portacaval, peripancreatic, retrocaval, and retrocrural regions. The lymph nodes appeared low in attenuation with densely enhancing peripheral rims and were believed to

Received March 11, 1991; accepted after revision April 25, 1991.

[1] Both authors: Department of Radiology, University of California, San Francisco, San Francisco General Hospital, 1 × 57, 1001 Potrero Ave., San Francisco, CA 94110. Address reprint requests to B. E. Demas.

AJR 157:773–775, October 1991 0361–803X/91/1574–0773 © American Roentgen Ray Society

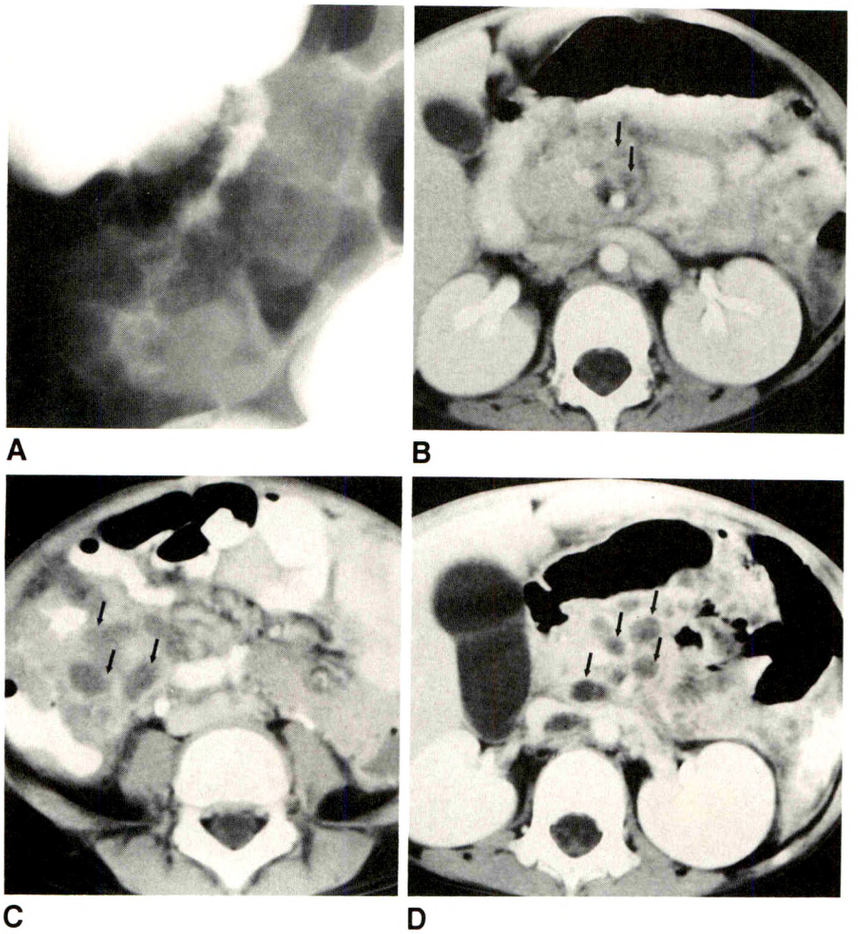


Fig. 1.—*A*, Spot film of terminal ileum reveals luminal narrowing, scalloping of ileal contour, and effacement of mucosal detail.

B, Contrast-enhanced CT scan at level of proximal superior mesenteric artery shows enlarged, low-density mesenteric lymph nodes (*arrows*).

C, CT scan obtained at same time as *B* shows wall of ascending colon is markedly thickened and bulky; necrotic lymph nodes (*arrows*) are present next to terminal ileum and ileocecal valve.

D, CT scan obtained 8 days after appendectomy, in presence of clinical signs of continued systemic infection, shows increased extent of mesenteric adenopathy (*arrows*).

be inflamed and centrally necrotic. Phlegmonous changes were noted in the pericecal region without abscess formation (Figs. 1B and 1C). The liver and spleen were enlarged, and small bilateral pleural effusions were present. CT done 8 days after surgery showed increased adenopathy and multiple sites of bowel wall thickening, involving the terminal ileum, cecum, hepatic flexure, and sigmoid colon (Fig. 1D). Fifteen days after surgery, a third CT scan revealed persistence of the colonic wall thickening without abscess formation or change in the intraabdominal adenopathy. Stool was negative for *Clostridium difficile* toxin.

Sixteen days after surgery, the fever had abated, and the abdominal distension had resolved. The patient tolerated a regular diet. Three days later, IV antibiotics were discontinued, and the patient was discharged with oral antibiotics.

Discussion

Y. enterocolitica is a Gram-negative coccobacillus with worldwide distribution that is a common cause of gastroenteritis and mesenteric adenitis in children and adolescents. Reported complications have included severe enterocolitis involving the ileocecal region [5], appendicitis [6], small-bowel gangrene [7], intestinal perforation [8], peritonitis [9], hepatic and splenic abscesses [5, 10], chronic abscess formation in the right inguinal region [11], and fatal septicemia [5, 11]. Infection in the normal host is typically self-limited, usually requiring no medical therapy. In patients with iron overload, however, virulence is enhanced and systemic infection with high morbidity and mortality rates may ensue [12].

The pathogenesis of the infection relates to the role of iron as an essential growth factor [13, 14]. Bacteria acquire iron by producing and releasing high-affinity chelators called siderophores, which bind and solubilize ferric iron. The iron/siderophore complexes enter bacterial cells after binding to specific receptors. Deferoxamine is a bacterial siderophore obtained from *Streptomyces piloce* that is used as a chelating agent in the treatment of acute iron toxicity and of chronic iron overload states. *Y. enterocolitica* is unusual among bacteria in that it requires iron for growth and has receptors for siderophores, but cannot produce siderophores endogenously [15]. Within the lumen of the gut, where siderophores are abundant, *Y. enterocolitica* has no difficulty obtaining iron and is able to proliferate relatively freely. Within human tissues where free iron is scant, *Y. enterocolitica* competes with host iron-binding proteins and its growth is naturally restricted.

Systemic *Yersinia* infection occurs almost exclusively in patients with iron overload treated with chelating agents,

which act as exogenous siderophores. The clinical presentation of this infection can be insidious and may resemble a variety of types of gastrointestinal inflammatory and infectious processes. The imaging features as described in this case report initially simulate those of simple appendiceal inflammation; disease progression may lead to development of intraperitoneal abscesses and distant visceral infection. The CT findings described here of progressive bowel wall thickening, bulky necrotic adenopathy, and secondary peritoneal and pleural effusions after appendectomy and initiation of antibiotic therapy attest to the need for aggressive and expectant treatment when systemic yersiniosis is considered probable. Once systemic infection develops, it is generally agreed that iron-chelation therapy with deferoxamine should be discontinued and IV antibiotic therapy started promptly. The patient we have described recovered partly because of the timely recognition of the relationship between systemic *Yersinia* infection, iron overload, and deferoxamine therapy.

REFERENCES

1. Schleifstein JI, Coleman MB. An unidentified organism resembling *B lignieri* and *Past. pseudotuberculosis*, and pathogenic for man. *NY State J Med* **1939**;39:1749–1753
2. Robbins-Browne RM, Prpic JK. Effects of iron and desferrioxamine on infections with *Yersinia enterocolitica*. *Infect Immun* **1985**;47:774–779
3. Kelly DA, Jani B, Wright V, Rossiter M, Walker-Smith JA. *Yersinia* enterocolitis in iron overload. *J Pediatr Gastroenterol Nutr* **1987**;6:643–645
4. Masters AP, Hopkinson RB. *Yersinia enterocolitica* septicaemia. *Intensive Care Med* **1988**;14:585–587
5. Scharnetzky M, Konig R, Lakomek M, Tillman W, Schroter W. Prophylaxis of systemic yersinosis in thalassaemia major. *Lancet* **1984**;1:791
6. Swaminathan MC, Harmon MC, Melman IJ. A review: *Yersinia enterocolitica*. *J Appl Bacteriol* **1982**;52:151–183
7. Leino RE, Renvall SY, Lipasti JA, Toivanen AM. Small bowel gangrene caused by *Yersinia enterocolitica* III. *Br Med J* **1980**;280:1419
8. Browning G, Weir W. Intestinal perforation associated with *Yersinia enterocolitica* infection. *Br Med J* **1985**;290:1872
9. Bradford WD, Noce PS, Gutman LT. Pathologic features of enteric infection with *Yersinia enterocolitica*. *Arch Pathol* **1974**;98:17–22
10. Leighton PM, MacSween HM. *Yersinia* hepatic abscesses subsequent to long-term iron therapy. *JAMA* **1987**;257:964–965
11. Chiu HY, Flynn DM, Hoffbrand AV. Infection with *Yersinia enterocolitica* in patients with iron overload. *Br Med J* **1986**;292:97
12. Robbins-Browne RM, Rabson AR, Koornhof HJ. Generalised infection with *Yersinia enterocolitica* and the role of iron. *Contrib Microbiol Immunol* **1979**;5:277–282
13. Weinberg E. Iron and infection. *Microbiol Rev* **1978**;42:45–66
14. Ward CG. Influence of iron on infection. *Am J Surg* **1986**;151:291–295
15. Perry RD, Brubaker RR. Accumulation of iron by yersiniae. *J Bacteriol* **1979**;137:1290–1298

Book Review

Morphologic and Functional MR of the Kidneys and Adrenal Glands. By Gabriel P. Krestin. New York: Field & Wood (distributed by Norton, New York), 109 pp., 1991. $115

Morphologic and Functional MR of the Kidneys and Adrenal Glands is divided into six chapters and includes both spectroscopy and imaging. All of the chapters except chapter 2 were written by Krestin, which provides a uniformity of style and content. The first chapter reviews the principles of fast gradient-echo imaging. The physical principles are simplified and clearly stated. This chapter provides a good review of the physics needed to understand and interpret MR studies. As such, it should be useful both for practicing physicians and for residents learning MR.

The chapter on spectroscopy was contributed by a guest author, but it also provides a good review of the basic principles. The discussion of phosphorous-31 spectroscopy is well done, but little clinical material is available for review. This paucity of clinical data is even more obvious in the sections on the spectroscopy of sodium, carbon, and hydrogen compounds. So little clinical information is available on spectroscopy that I am surprised it is included in a book on clinical applications of MR.

Chapter 3 reviews the normal anatomy and physiology of the kidney and adrenal glands with regard to MR imaging. A thorough review of the anatomy is not attempted, but comments on the anatomic features pertinent to MR imaging are included. Contrast-enhanced studies are one of the strengths of this book, and the discussion of renal physiology is particularly useful. The fourth and fifth chapters are devoted to renal lesions, and the sixth chapter addresses adrenal diseases. Each of these last three chapters begins with a brief review of pertinent clinical and pathologic information that is followed by a specific discussion of the MR appearance of the lesions. The chapters conclude with a brief recapitulation of the key points.

The material is as up-to-date as a book can be, and much information on dynamic contrast-enhanced studies of the kidneys and adrenal glands is included. Even so, I could find only seven references published more recently than 1988. The book has ample high-quality illustrations, although they are skewed toward the use of fast scanning techniques.

In general, I am pleased with the quality of this textbook. It is clearly written, the information is current and accurate, and the MR images are of excellent quality. However, I am disappointed in the scope of the book. Because it is limited to the adrenal glands and kidneys, more imaging sequences could be included. It is biased toward fast scanning techniques and limits or excludes other clinically useful examination sequences. One of the most important contributions of MR, the assessment of venous extension of renal or adrenal carcinomas, is not emphasized. Little information is included on fat-suppression techniques.

The cost of the book, approximately $1.00 per page, is high, and I suspect that most radiologists would rather spend their money for either a more general MR book or a textbook of uroradiology that includes MR imaging. It is an excellent review, however, for physicians specifically interested in this topic.

N. Reed Dunnick
Duke University Medical Center
Durham, NC 27710

Percutaneous Biopsy of Left Adrenal Masses: Prevalence of Pancreatitis After Anterior Approach

Naomi M. Kane[1]
Melvyn Korobkin[1]
Isaac R. Francis[1]
Leslie E. Quint[1]
Philip N. Cascade[1,2]

Acute pancreatitis is an unusual but recognized complication of percutaneous aspiration biopsy of the pancreas. As the pancreatic tail is located anterior to the left adrenal gland, percutaneous biopsy of a left adrenal mass via the anterior approach may result in needle passage through the tail of the pancreas with subsequent potential development of pancreatitis. To evaluate this risk, we retrospectively reviewed 48 CT-directed percutaneous aspiration biopsies of left adrenal masses done between 1984 and 1989 at two institutions. Positioning of the patient, the course of the needle, the number of needle passes, and the size of the needle were analyzed. Thirty-three (69%) of 48 biopsies of a left adrenal mass were performed by using the anterior approach. The pancreas was traversed by one or more needles in 32 of 33 cases. Biopsies were performed with 20- to 22-gauge needles, and the number of needle passes varied widely. The medical records of the 33 patients in whom the anterior approach was used also were reviewed for complications. Acute pancreatitis, which required 11–13 days of hospitalization, developed in two patients (6%). None of the other 31 patients suffered a complication.

We conclude that the pancreatic tail is routinely traversed by the biopsy needle when biopsy of a left adrenal mass is done via the anterior approach and that severe acute pancreatitis can occur as a result.

AJR 157:777–780, October 1991

Percutaneous fine-needle aspiration biopsy of an adrenal mass has been shown to be a simple and safe procedure to establish or exclude the presence of metastatic carcinoma [1–4]. Although initial reports advocated a posterior approach with the patient prone as the shortest and most direct route to an adrenal mass, the risk of pneumothorax from transgression of the posterior costophrenic sulcus of the lung has led to advocacy of alternative routes of access [1–5]. For right adrenal masses, a transhepatic approach has been used successfully [2–4]. For a left adrenal mass, both an ipsilateral decubitus posterior approach and a direct anterior approach have been advocated [4, 5].

As the tail of the pancreas often lies in a transaxial plane at or near the left adrenal gland, there is a theoretical risk of pancreatic injury when aspirating a left adrenal mass from the anterior approach. Recent reports of percutaneous aspiration biopsies of abdominal masses in general, and of pancreatic masses in particular, suggest a small but important risk of severe acute pancreatitis whenever a percutaneous biopsy needle traverses normal pancreatic tissue [6–13]. As we have performed most of our percutaneous biopsies of left adrenal masses from the anterior approach with the patient supine, we reviewed our large experience with this procedure to determine: (1) how often the biopsy needle appears to traverse the pancreatic parenchyma, (2) how often there is clinical evidence of severe acute pancreatitis, and (3) whether there are other identifiable features of these biopsies that appear to increase the risk of severe pancreatitis.

Received April 5, 1991; accepted after revision May 31, 1991.

[1] Department of Radiology, University of Michigan Hospitals, 1500 E. Medical Center Dr., Ann Arbor, MI 48109-0326. Address reprint requests to N. M. Kane (TC 2910).

[2] Department of Radiology, Sinai Hospital, 6767 W. Outer Dr., Detroit, MI 48235.

0361–803X/91/1574–0777
© American Roentgen Ray Society

Materials and Methods

All CT-directed percutaneous aspiration biopsies of left adrenal masses performed from 1984 to 1989 at the University of Michigan Hospitals and Sinai Hospital of Detroit were included in this retrospective analysis. The CT studies were reviewed to determine the needle path and whether or not the pancreas was traversed. The medical records of those patients in whom the anterior approach was used were reviewed for biographic data; reason for biopsy; final cytologic diagnosis; biopsy needle type, size, and number of passes; and recorded immediate and delayed complications.

Biopsies were performed at another time, after diagnostic CT had been performed. The technique and needle size for the biopsies were selected by the radiologist performing the procedure. Biopsy was performed via the tandem-needle technique after the localizing scans were obtained. Cytologic specimens were prepared and reviewed immediately by a cytopathologist. The use of additional needle passes was determined by whether or not the cytopathologist had received adequate tissue to make a diagnosis.

Forty-eight CT-guided aspiration biopsies of a left adrenal mass were performed in 47 patients (one patient had two biopsies, 10 months apart). Thirty-three (69%) of 48 were performed by using the anterior approach with the patient supine; nine, the posterior approach with the patient in the left lateral decubitus position; and six, the posterior approach with the patient prone.

The number of needle passes was documented in fourteen (42%) of 33 patients; six (18%) of 33 had one to three needle passes, and eight (24%) of 33 had four to six needle passes. Twenty of the procedures were performed with 22-gauge needles, one with a 21-gauge needle, one with a 20-gauge needle, four with both 20- and 22-gauge needles, and seven patients had no documentation as to needle size. When documented, Chiba and spinal needles were used in all cases, except one, when a 20-gauge Franseen was used. Adequate adrenal cellular material was obtained for evaluation in 32 of 33 cases.

Review of patients' status at the time of the aspiration biopsy showed that 13 (39%) of 33 were inpatient, 17 (52%) were outpatient, and the status of the remaining three (9%) was unknown. Inpatients generally were returned to their hospital room for observation. Outpatients were observed in the radiology department for various lengths of time, and although not documented, this usually ranged from 2 to 4 hr.

Results

Of the 33 left adrenal masses that were sampled by using the anterior approach, the needle traversed the pancreas in 32 (97%, Fig. 1). Two (6%) of 33 patients suffered complications. According to their charts, none of the other 31 patients had a delayed complication.

The first complication occurred in a 30-year-old woman with a history of melanoma who had a biopsy of a 4-cm left adrenal mass (Fig. 2) as an outpatient. One pass was made with a 22-gauge needle and was followed by two passes with a 20-gauge needle. Cytologic analysis showed normal adrenal cells. Approximately 2 hr after the procedure, her blood pressure dropped. Supportive measures were instituted, and she was admitted to the hospital. A second abdominal CT examination showed a small amount of fluid in the perirenal space around the left adrenal gland. Three days later, a third CT examination showed development of intraperitoneal fluid and a large amount of fluid in the left anterior pararenal area surrounding the tail of the pancreas (Fig. 2). Serum amylase and lipase values were markedly elevated, peaking at 540 IU (normal, 23–100 IU) and 4990 IU (normal, 4–24 IU), respectively, 2 days after the procedure, and then both progressively declined. The patient slowly improved and was discharged 11 days after the biopsy with a clinical diagnosis of resolving acute pancreatitis.

The second complication occurred in a 72-year-old woman with breast cancer and bilateral adrenal masses who had a CT-guided biopsy as an inpatient. Obesity and a severe spinal deformity due to rheumatoid spondylitis made the anterior approach with the patient supine the most feasible one. The left adrenal gland was chosen for biopsy because the mass was larger on that side. Approximately six passes with a 20-gauge Chiba needle were performed (cytology negative for neoplasm). Approximately 10 hr after the procedure, the patient complained of acute abdominal pain and exhibited mild diffuse tenderness and had rebound on physical examination. Examinations performed at that time revealed a markedly elevated amylase level (3660 IU), an elevated WBC count ($15{,}600/\mu l^3$), and pleural effusion. The patient was treated conservatively with IV fluids and gastrointestinal tract intubation. She required two units of blood because of a drop in hemoglobin level. She was discharged from the hospital 13 days after the procedure. A pancreatic pseudocyst was seen on follow-up CT performed 5 and 11 months later (Fig. 3).

Discussion

Adrenal masses can be sampled by biopsy from the posterior approach with the patient prone, but their proximity to the posterior costophrenic sulcus of the lung leads to the risk of pneumothorax [1]. A pneumothorax can usually be avoided by using a more lateral approach or by angling the needle upward from a more caudal point of entry by using simple triangulation methods [8, 9]. Alternatively, the lung can often be avoided by using the posterior approach when the patient is in the ipsilateral decubitus position [5]. This elevates the

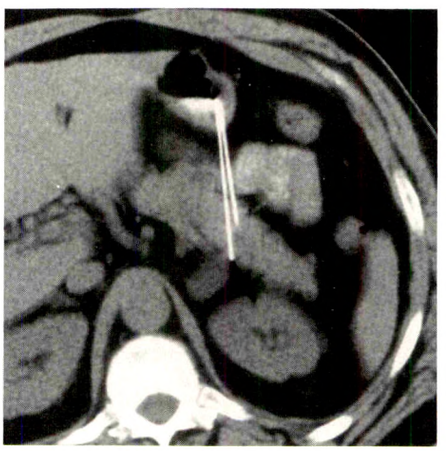


Fig. 1.—CT scan shows tandem needles traversing pancreas before reaching left adrenal mass.

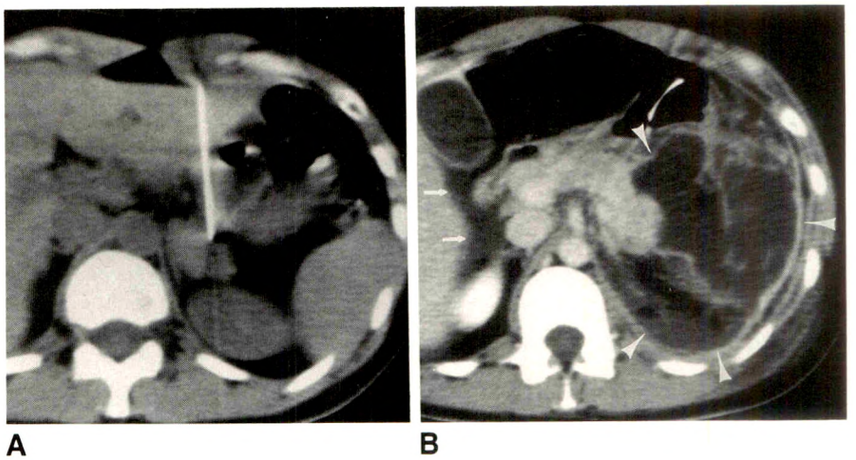


Fig. 2.—30-year-old woman with history of melanoma and 4-cm left adrenal mass (cytology negative for malignancy).

A, CT scan shows needle traversing pancreas with tip in left adrenal mass.

B, CT scan 3 days after aspiration biopsy shows development of a large peripancreatic fluid collection (*arrowheads*) and intraperitoneal fluid (*arrows*) in hepatorenal fossa.

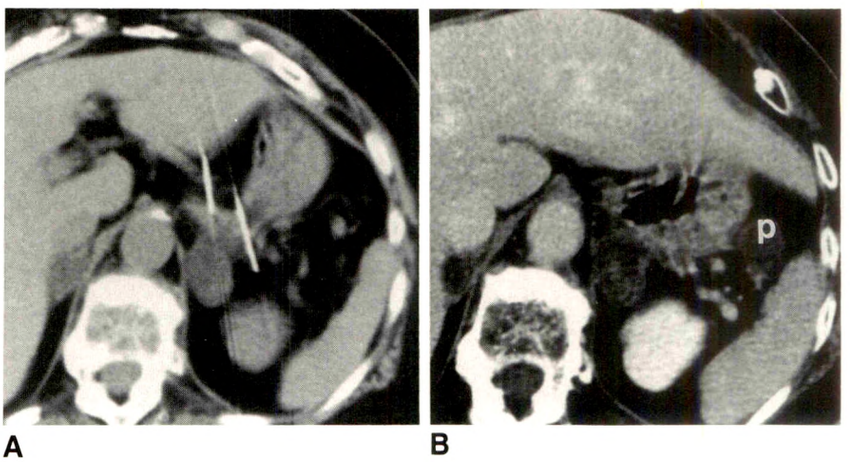


Fig. 3.—72-year-old woman with breast cancer and bilateral adrenal masses (cytology negative for malignancy).

A, CT scan shows two 20-gauge Chiba needles traversing pancreas.

B, CT scan obtained 11 months later shows a pseudocyst (p).

dependent hemidiaphragm and reduces respiratory motion on that side. However, a more direct and technically simpler approach to a left adrenal mass is through the anterior abdominal wall while the patient is supine. When this approach is used, the needle often crosses bowel, liver, or pancreas. It is generally acceptable to traverse the gastrointestinal tract or liver in the immunocompetent patient when performing percutaneous fine-needle aspiration biopsies of abdominal masses [8, 10, 11]. Because the left adrenal gland is posterior to the pancreas and in, or adjacent to, the same transaxial plane, it is not surprising that it is often traversed while a biopsy needle is being positioned from this approach. Our study clearly documents that the biopsy needle passes through the tail or body of the pancreas in almost all patients in whom the anterior approach is used.

Although we have used the anterior approach in most of our patients, a review of prior publications on percutaneous biopsy of a left adrenal mass revealed that the posterior approach is more often preferred because it allows the shortest distance from the surface to the adrenal lesion. We do not know of any published reports that document acute pancreatitis after percutaneous biopsy of a left adrenal mass. Zornoza et al. [14] took biopsy samples of all 12 left adrenal lesions from the posterior approach without reported complication. Pagani [2] used the paraspinous approach in all 22 CT-guided left adrenal biopsies, also without reported complication. Bernardino et al. [4] approached 21 of 27 left adrenal masses posteriorly; the other six were approached anteriorly through the left hepatic lobe when safe access could not be obtained posteriorly. Two of 27 patients had a decrease in the hematocrit, but it is not stated from which approach the biopsy was done [4]. The absence of a resultant pneumothorax was attributed to the choice of a transhepatic route on the right side and an anterior approach in selected examples on the left side when aspirating an adrenal mass. Charboneau et al. [8], in their biopsies of 55 consecutive left adrenal lesions, used the anterior approach with the patient supine in only four "because of surrounding stomach, colon, and spleen," without mention of any complication. The Mayo Clinic reported a 5% complication rate (four of 75) for all adrenal biopsies [12].

Percutaneous biopsy of pancreatic masses also is considered a safe and effective procedure, although complications, including acute pancreatitis, have been reported. Mueller et al. [6] have recently described the development of acute pancreatitis after fine-needle biopsy when attempting to sam-

ple small pancreatic lesions (3-cm diameter or smaller). In their review of 184 percutaneous pancreatic biopsies, severe pancreatitis developed in five cases (3%). All five of these patients had an initial imaging diagnosis of masses of 3-cm diameter or smaller, but the pancreas proved normal in three of five patients at surgery ($n = 2$) or at clinical follow-up ($n = 1$). They attributed the complication of acute pancreatitis to the unavoidable puncture of normal pancreas, whereby direct injury to the main pancreatic duct or one of its branches led to leakage of pancreatic enzymes. In a review of over 75,000 cases accrued from both the literature and from a multiinstitutional survey, Smith [13] reported five of 33 deaths were from postbiopsy pancreatitis, and in each of these five, no pancreatic tumor was found, although a pancreatic mass was suggested by imaging studies. Another such case of fatal necrotizing pancreatitis also has recently been reported [7]. Four passes with a 22-gauge spinal needle were made into a minimally enlarged pancreatic head. Twenty-four hours later the patient complained of abdominal discomfort and at laparotomy, necrotizing pancreatitis was diagnosed. At autopsy, no malignant tumors were found in the pancreas [7]. These reports, in addition to our results, clearly suggest a small but important risk of severe acute pancreatitis when a percutaneous biopsy needle traverses normal pancreatic tissue.

The mortality rate from traumatic or postoperative pancreatitis is reported at 20–60%. Early complications are shock, respiratory disorders, gastrointestinal bleeding, hypocalcemia, and jaundice. Late complications of acute pancreatitis include pseudocyst formation, abscess, and pancreatic ascites. In our series, acute pancreatitis requiring 11–13 days of hospitalization developed in two (6%) of 32 patients. None of the 32 patients had a preexisting underlying pancreatic abnormality. Multiple factors determine the risks of complication after any interventional procedure. The number of needle passes and size of needles used, biopsy techniques, inexperienced operators, or uncooperative patients are among the key factors. In this study these factors were not thought to play a role because the biopsies were performed by experienced radiologists on cooperative patients and only small-gauge needles were used. Although the precise cause of acute pancreatitis in our two patients is unknown, we presume it resulted from laceration of ductal structures. It is also unclear why pancreatitis did not develop in the other patients in whom the needle traversed the pancreatic tail. As serum enzyme levels were not routinely measured, it is feasible that biochemical but subclinical pancreatitis could have developed in some of these other patients.

In summary, severe acute pancreatitis is an infrequent but important complication of percutaneous aspiration biopsy of a left adrenal mass via the anterior approach with the patient supine. The pancreatic tail is routinely traversed during this procedure, probably lacerating a ductal structure in a small proportion of patients. Whenever technically feasible, we recommend that percutaneous biopsy of a left adrenal mass be performed from the posterior approach. It is usually easier to treat a pneumothorax resulting from the posterior approach than to treat pancreatitis caused by the anterior approach.

ACKNOWLEDGMENTS

The authors thank Bernard Naylor, cytopathologist, for meticulous record keeping and Carol O'Connor for manuscript preparation.

REFERENCES

1. Heaston DK, Handel DB, Ashton PR, Korobkin M. Narrow gauge needle aspiration of solid adrenal masses. *AJR* **1982**;138:1143–1148
2. Pagani JJ. Normal adrenal glands in small cell lung carcinoma: CT-guided biopsy. *AJR* **1983**;140:949–951
3. Berkman WA, Bernardino ME, Sewell CW, Price RB, Sones PJ Jr. The computed tomography-guided adrenal biopsy: an alternative to surgery in adrenal mass diagnosis. *Cancer* **1984**;53:2098–2103
4. Bernardino ME, Walther MM, Phillips VM, et al. CT-guided adrenal biopsy: accuracy, safety, and indications. *AJR* **1985**;144:67–69
5. Heiberg E, Wolverson MK. Ipsilateral decubitus positions for percutaneous CT-guided adrenal biopsy. *J Comput Assist Tomogr* **1985**;9:217–218
6. Mueller PR, Miketic LM, Simeone JF, et al. Severe acute pancreatitis after percutaneous biopsy of the pancreas. *AJR* **1988**;151:493–494
7. Evans WK, Ho CS, McLoughlin MJ, Tao LC. Fatal necrotizing pancreatitis following fine-needle aspiration biopsy of the pancreas. *Radiology* **1981**;141:61–62
8. Charboneau JW, Reading CC, Welch TJ. CT and sonographically guided needle biopsy: current techniques and new innovations. *AJR* **1990**;154:1–10
9. Wittenberg J, Mueller PR, vonSonnenberg E, Ferrucci JT. Percutaneous tumor biopsy. In: Ferrucci JT, Wittenberg J, eds. *Interventional radiology of the abdomen*. Baltimore: Williams & Wilkins, **1981**:111–155
10. Gazelle GS, Haaga JR. Guided percutaneous biopsy of intraabdominal lesions. *AJR* **1989**;153:929–935
11. Ferrucci JT, Wittenberg J, Mueller PR, et al. Diagnosis of abdominal malignancy by radiologic fine-needle aspiration biopsy. *AJR* **1980**;134:323–330
12. Welch TJ, Sheedy PF, Johnson CD, Johnson CM, Stephens DH. CT-guided biopsy: prospective analysis of 1,000 procedures. *Radiology* **1989**;171:493–496
13. Smith EH. Complication of percutaneous abdominal fine-needle biopsy. *Radiology* **1991**;178:253–258
14. Zornoza J, Ordonez N, Bernardino ME, Cohen MA. Percutaneous biopsy of adrenal tumors. *Urology* **1981**;18:412–416

Case Report

Castleman Disease of the Adrenal Gland: MR Imaging Features

Jörg F. Debatin,[1] Charles E. Spritzer, and N. Reed Dunnick

Castleman disease is a benign lymphoid neoplasm. Although it can arise wherever lymphoid tissue is found, it most frequently manifests in the thorax. The adrenal glands are only rarely involved [1].

MR imaging can be used to distinguish benign from malignant causes of adrenal masses. However, not all lesions can be distinguished by using MR, even with contrast enhancement [2, 3]. We present a case of a benign Castleman tumor of the hyaline vascular type affecting an adrenal gland that has the MR imaging signal and enhancement characteristics of a malignant lesion.

Case Report

A 43-year-old woman with a long history of arterial hypertension underwent excretory urography for hematuria. A right-sided suprarenal mass was found, and subsequent CT examination confirmed a right adrenal mass measuring 4.7 × 3.0 × 3.2 cm (Fig. 1A). Laboratory analysis showed the lesion was not hyperfunctioning.

The mass was stable for 3 years until July 1990, when it increased in size to 5.5 × 6.1 × 5.8 cm. An MR examination showed the mass was hypointense to liver on T1-weighted images and uniformly hyperintense on T2-weighted images (Figs. 1B and 1C). The calculated T2 value obtained from a multislice, two-echo image (2500/40, 80 [TR/TE]) was 70 msec (Fig. 1D). After IV administration of gadopentetate dimeglumine, the mass showed a more than threefold increase in its signal intensity and relatively slow washout (Fig. 1E). Ten minutes after contrast administration, the signal intensity of the mass was still twice as high as before contrast injection (Figs. 1E–1G). The calculated T2 value and contrast enhancement characteristics were consistent with a malignant tumor of the adrenal gland.

During laparotomy, a dark yellow tumor, measuring 5 × 6 cm, that had replaced the right adrenal gland was resected en bloc. Histologic examination revealed giant lymph node hyperplasia (Castleman disease) of the hyaline vascular type. Surrounding lymph nodes were normal, and the postoperative convalescence was uneventful.

Discussion

Castleman disease is a benign proliferation of mature lymphocytes and/or plasma cells, with preservation of the lymph node architecture [1]. Also referred to as giant lymph node hyperplasia, this benign lymphoid neoplasm was first reported by Castleman and Towne [4] and was thought to represent hyperplasia of mediastinal lymph nodes. Two distinct histologic patterns are recognized. The hyaline vascular variety, accounting for up to 90% of Castleman tumors, is usually asymptomatic [5]. Histologically, this type is characterized by small, flat, concentrically layered, follicle-centered cells, extensive capillary proliferation, and defacement of lymphoid sinuses. Various amounts of hyaline tissues encase the proliferated capillaries [5].

The plasma cell subtype is a much less common form of Castleman tumor and is characterized by the presence of sheets of mature plasma cells [5]. The follicle centers are normal, without evidence of vascularization or hyalinization. About half these patients have systemic signs and symptoms; the most common are anemia, fever, fatigue, hyperglobulinemia, and hypoalbuminemia.

Whereas the hyaline vascular subtype is usually a solitary lesion between 1.5 and 16.0 cm in size, the plasma cell

Received March 11, 1991; accepted after revision April 30, 1991.

[1] All authors: Radiology Department, Box 3808, Duke University Medical Center, Erwin Rd., Durham, NC 27710. Address reprint requests to N. R. Dunnick.

AJR 157:781–783, October 1991 0361–803X/91/1574–0781 © American Roentgen Ray Society

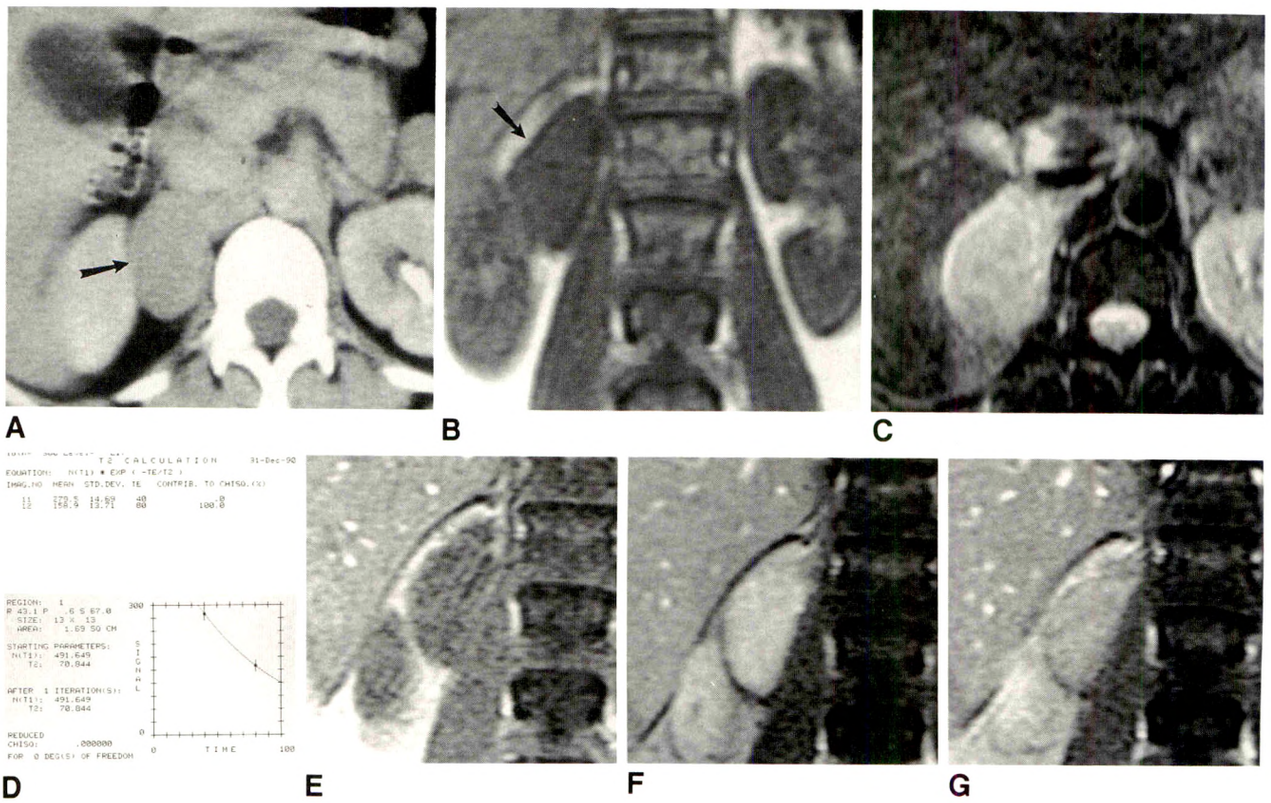


Fig. 1.—*A*, Contrast-enhanced CT scan shows a 4.7 × 3.2 cm right adrenal mass (*arrow*). Mass is of homogeneous attenuation without evidence of calcification, necrosis, or hemorrhage.

B, Coronal T1-weighted (500/20) MR image shows a large right adrenal mass (*arrow*) characterized by homogeneous signal mildly hypointense to that of hepatic parenchyma.

C, Axial T2-weighted (2500/80) MR image shows a uniformly hyperintense right adrenal mass.

D, Absolute T2 value of adrenal lesion was 70.8 msec.

E–G, Coronal spoiled gradient-recalled echo images (28/5, flip angle 45°) obtained before (*E*), 3 min after (*F*), and 10 min after (*G*) IV administration of gadopentetate dimeglumine (0.1 mmol/kg) show rapid contrast enhancement and relatively slow washout of paramagnetic contrast agent from right adrenal mass.

subtype may be either focal or multifocal [1, 5]. Complete surgical resection is the treatment of choice and is generally curative. As in this case, Castleman tumors may enlarge over time [1].

Castleman disease occurs most often in young, otherwise healthy patients. Males and females are equally affected [1] and range in age from 8 to 66 years. Castleman tumors may occur in almost any area in which lymphoid tissue is normally found [1]. Of the 400 reported cases [6], 70% involved the thorax, 40% the neck, 12% the abdomen, and 4% the axilla. Most intraabdominal lesions are located in the pelvic, mesenteric, and perinephric regions [7], but they have been described throughout the abdomen.

The only other report of Castleman disease involving the adrenal gland described a voluminous retroperitoneal tumor in an asymptomatic 47-year-old woman. Histologic examination of the surgical specimen showed adrenal hyperplasia associated with an adrenal myelolipoma adherent to a Castleman tumor [8]. It is conceivable that in that case, and in the present case, the Castleman tumor may have originated from lymphoid tissue in the adrenal periphery and subsequently extended into the adrenal gland itself.

The MR appearance of Castleman disease in the abdomen has not been described. In our patient, the signal characteristics were similar to those reported in adrenal lymphoma: hypointense compared with hepatic parenchyma on T1-weighted images and hyperintense on T2-weighted images [3].

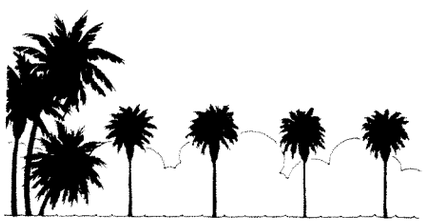
Several investigators reported that most lesions (80%) with a T2 value greater than 60 msec are malignant [2]. According to this criterion, the calculated T2 value of 70 msec indicated a malignant cause. Similarly, the prompt increase in signal intensity after the IV injection of gadopentetate dimeglumine and the delayed washout of the paramagnetic contrast agent from the lesion strongly suggest a malignant cause according to criteria reported by Krestin et al. [3]. This may be a reflection of the extensive capillary proliferation typical of Castleman tumors of the hyaline vascular form. The homogeneity of the signal characteristics before and after contrast administration was unusual for a malignant tumor. In a me-

tastasis or a primary adrenal carcinoma of this size, areas of cystic degeneration and tumor necrosis are expected.

This case emphasizes that signal intensities and enhancement characteristics of MR cannot be applied to all adrenal lesions. Castleman tumor of the adrenal gland has to be added to the list of exceptions to the rule that benign adrenal masses have a relatively short T2 and only mild enhancement with quick washout after administration of gadopentetate dimeglumine.

REFERENCES

1. Keller AR, Hochholzer L, Castleman B. Hyaline-vascular and plasma-cell types of giant lymph node hyperplasia of the mediastinum and other locations. *Cancer* **1972**;29:670–683
2. Baker ME, Blinder R, Spritzer C, Leight GS, Herfkens RJ, Dunnick NR. MR evaluation of adrenal masses at 1.5 T. *AJR* **1989**;153:307–312
3. Krestin GP, Steinbrich W, Friedmann G. Adrenal masses: evaluation with fast gradient-echo MR imaging and Gd-DTPA enhanced dynamic studies. *Radiology* **1989**;171:675–680
4. Castleman B, Towne VW. Case records of the Massachusetts General Hospital: case 40011. *N Engl J Med* **1954**;250:26–30
5. Goldberg MA, Deluca SA. Castleman's disease. *Am Fam Physician* **1989**;49:151–153
6. Fizzera G. Castleman's disease: more questions than answers. *Hum Pathol* **1985**;3:202–205
7. Ebisana S, Yamauchi T, Fukani T, Ohkawa T. Retroperitoneal Castleman's disease: a case report and brief review of tumors of the pararenal area. *Urol Int* **1989**;44:169–172
8. Seniuta P, Cazenave-Mahe JP, Le Treut A, Trojani M. Adrenal myelolipoma and Castleman's pseudotumor: a case of association in a retroperitoneal tumor (review). *J Urol (Paris)* **1989**;95:511–514



Scientific Program (200 papers)
Instructional Courses (60 hours)
Categorical Course on Neuroradiology
The Caldwell Lecture
Award Papers
Scientific Exhibits
Social, Golf, and Tennis Programs
Guest Programs

Come to the American Roentgen Ray Society

92nd

ANNUAL MEETING

Orlando, FL

Marriott's Orlando World Center
May 10–15, 1992

Book Review

Imaging of the Pelvis. MRI with Correlations to CT and Ultrasound. Edited by Marcia C. Fishman-Javitt, Harry L. Stein, and John L. Lovecchio. Boston: Little, Brown, 303 pp., 1990. $85

When MR imaging first came on the scene, some predicted that it would play a major role in pelvic imaging. In many community hospitals, though, neurologic and musculoskeletal applications predominate, as sonography and CT remain effective techniques for imaging the pelvis. This book shows how and when MR imaging can complement and supplement the results of other imaging techniques.

The editors, aided by an able group of contributors, have prepared detailed, copiously illustrated discussions of normal and pathologic anatomic findings in the male and female reproductive organs, bladder, rectum, and perirectal area. Other chapters discuss physics; comparison of clinical efficacy of MR, CT, and sonography; issues in the evaluation of MR technology; and future applications. Obstetric MR is not included. The authors and the publisher are especially to be commended for the excellent quality of the MR images and illustrations. The images are well chosen and carefully captioned and labeled; only a few show their age in this rapidly progressing field. The text is appropriately annotated with reasonably up-to-date references. The prose is clean and readable. The chapter on issues in the evaluation of MR technology is a gem. It consists of a discussion of the essentials of statistical methods and the pitfalls to be avoided in evaluating clinical research papers. I am glad the editors included this section. Although many of us have a deep fear of mathematics, especially statistics, we cannot judge the merits of published investigations without recourse to mathematics. To help our patients and our referring clinicians, we all must be able to recognize flawed methodology and statistical analysis that lead to meaningless, or worse, misleading results.

The book's greatest success is in visually depicting what MR can do in pelvic imaging. The analyses of relative advantages of MR vs sonography and CT are less successful. The information in these chapters could have been integrated more succinctly and effectively into the rest of the text. The chapter on physics, although adequate, is an unnecessary duplication of other published work. The authors do not seek to oversell MR especially, as is the case in scrotal and prostatic imaging, for which other techniques are strong.

This work complements general MR texts and will be useful to many who are involved in cross-sectional imaging. The quality and breadth of the images alone are worth the purchase price. The book has hidden bonuses and few disappointments. I recommend it to all those who interpret MR images.

J. Eric Blum
Akron City Hospital
Akron, OH 44309

Case Report

Cystic Carcinoma of the Prostate: Findings on Transrectal Sonography

Christine H. Llewellyn[1,2] and Lowrey H. Holthaus[1,3]

Prostatic carcinoma is the most common type of cancer in American males (followed closely by lung cancer), with an incidence of slightly over 100,000 new cases per year [1]. Although carcinoma of the prostate may have a variety of sonographic appearances, it typically is seen as a solid hypoechoic nodule in the peripheral zone of the gland [2]. A solitary, large, macroscopic, cystic space associated with carcinomatous wall nodularity is a rare entity that has not been previously reported in the imaging literature. We report two such cases of cystic carcinoma of the prostate as demonstrated with transrectal sonography.

Case Report

A 68-year-old man had signs and symptoms of bladder-outlet obstruction, including diminished force of stream and dribbling. Digital rectal examination revealed an enlarged prostate with a fluctuant mass in the right lobe. The serum level of prostate-specific antigen was 32 ng/ml (normal, 0–4 ng/ml). The serum level of acid phosphatase was within normal limits.

Transrectal axial and sagittal sonograms were obtained by using the Hitachi EUB-450 scanner fitted with a 6.5-MHz angled end-fire probe (Hitachi Medical Corporation, Tarrytown, NY). This scanner does not come equipped with an endorectal probe condom for fluid instillation. Sonography showed that the prostate was rotated anteriorly and to the left by a 4.5-cm exophytic cystic mass arising from the posterior aspect of the right lobe. Fronds of solid tissue projected into the cystic component of this mass (Figs. 1A and 1B). The patient had a sonographically guided biopsy of the solid component of the mass; an 18-gauge needle and the Biopty spring-loaded biopsy gun (Bard Urological Division, Covington, GA) were used. A 20-gauge needle then was used to aspirate approximately 20 ml of dark-brown fluid from the cystic component of the mass. Examination of the biopsy specimen showed a moderately well differentiated adenocarcinoma with an endometrioid pattern. Tissue stains for prostate-specific antigen and prostatic acid phosphatase confirmed that it was a primary prostatic tumor. The results of cytologic examination of the fluid were normal. Cultures of the fluid were negative.

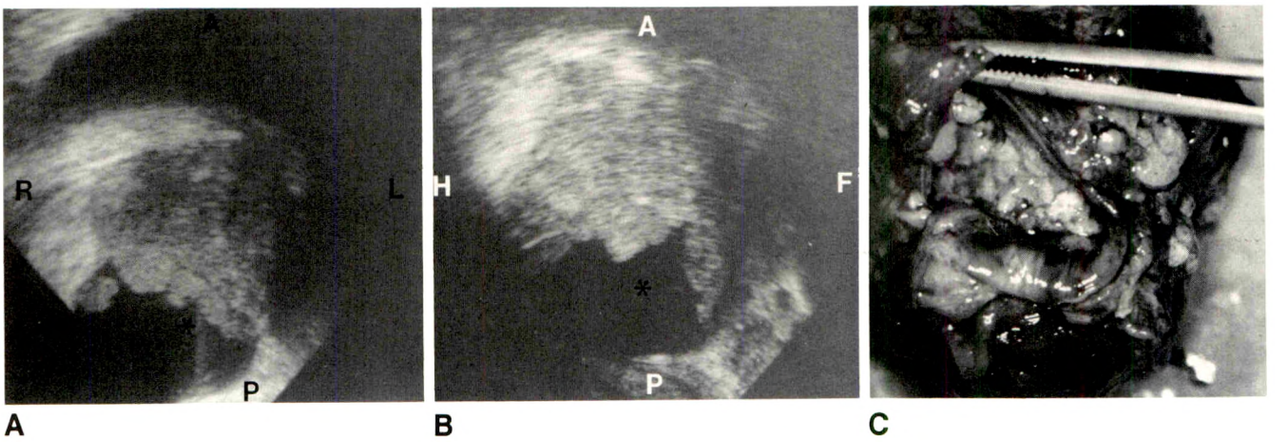
The patient had a radical prostatectomy. The final pathologic diagnosis was moderately well differentiated adenocarcinoma of the prostate with cyst formation. Only a few small areas showed endometrioid carcinoma. The cyst had smooth walls, except that portion in which tumor projected from underlying prostatic tissue (Fig. 1C). Tumor was not present within the smooth portions of the cyst wall. The patient had an uneventful recovery.

Discussion

Cystic carcinoma of the prostate occurs as a predominantly cystic mass with wall nodularity. The solid wall components pathologically represent the tumor. This appearance is drastically different from the appearance of typical prostatic cancer, which occurs as an entirely solid mass, reflecting the pathologic appearance of closely spaced acini. The association of a solitary, large, cystic space with any form of prostatic carcinoma is rare. Belter and Dodson [3] reported a case of papillary adenocarcinoma associated with a 4- to 5-cm cavity that had a shaggy lining. Papillary adenocarcinoma is synon-

Received February 21, 1991; accepted after revision April 29, 1991.
[1] Radiology Service (114), Hunter Holmes McGuire Veterans Administration Medical Center, 1201 Broad Rock Blvd., Richmond, VA 23249.
[2] Present address: Department of Radiology, Chippenham Medical Center, 7101 Jahnke Rd., Richmond, VA 23225.
[3] Present address: Department of Radiology, Medical College of Virginia Hospitals, Box 615, MCV Station, Richmond, VA 23298.

 0361–803X/91/1574–0785 © American Roentgen Ray Society



A B C

Fig. 1.—*A* and *B*, Transrectal axial (*A*) and right sagittal (*B*) sonograms of prostate show large cystic mass (*asterisk*) with anterior solid components in posterior lobe. A = anterior, P = posterior, R = right, L = left, H = head, F = foot.
C, Gross surgical specimen with posterior cyst wall elevated shows tumor nodules projecting into cyst cavity.

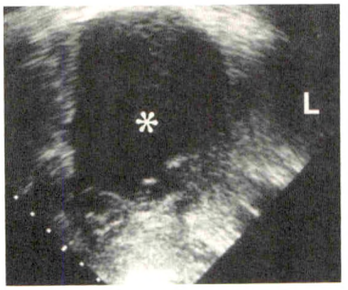


Fig. 2.—Transrectal axial sonogram of prostate shows large cystic mass (*asterisk*) with posterior irregular low-level echoes. L = left.

ymous with endometrioid carcinoma, which was originally thought to arise from the prostatic utricle but has subsequently been shown to be of prostatic acinar origin and usually, as in our case, also is associated with a typical carcinoma in the prostate [4]. It is not typically associated with a large cystic space, but it is of interest that our case showed a few similar foci.

We subsequently had another patient who had had transrectal sonography, pelvic CT, and MR imaging for staging of prostatic adenocarcinoma, all of which showed an 8-cm predominantly cystic mass of the prostate containing wall irregularity (Fig. 2). At surgery, this also was found to be an adenocarcinoma of the prostate with cyst formation. Pathologically, no papillary features were reported.

Most reported cystic lesions of the prostate in the imaging literature are benign; they include müllerian duct cysts, prostatic utricle cysts, ejaculatory duct cysts, cystic degeneration in benign prostatic hypertrophy, prostatic retention cysts, cavitary prostatitis, and prostatic abscess [5, 6]. The only case reported in association with a tumor described urothelial carcinoma in the defect after surgical removal of an adenoma. As nearly all of these lesions appear as true simple cysts, the only sonographic differential diagnosis is a prostatic abscess. The clinical presentation should help differentiate these two entities.

In evaluating these lesions, as with other tumors that contain cystic components, it is important to do a biopsy on the solid components of the tumor for an accurate diagnosis. Cytologic evaluation of the bloody fluid aspirated from the anechoic space of the first case showed no tumor cells. Pelvic CT examination was useful in the second case to confidently delineate the large cystic component of the tumor from the urinary bladder.

REFERENCES

1. Cotran RS, Kumar V, Robbins SL. *Robbin's pathologic basis of disease*, 4th ed. Philadelphia: Saunders, **1989**:1121–1125
2. Rifkin MD, Dahnert W, Kurtz AB. State of the art: endorectal sonography of the prostate gland. *AJR* **1990**;154:691–700
3. Belter LF, Dodson AI. Papillomatosis and papillary adenocarcinoma of prostatic ducts: a case report. *J Urol* **1970**;104:880–883
4. Kissane JM, ed. *Anderson's pathology*, 9th ed. St. Louis: Mosby, **1990**:907–915
5. Nghiem HT, Kellman GM, Sandberg SA, Craig BM. Cystic lesions of the prostate. *RadioGraphics* **1990**;10:635–650
6. Gevenois PA, Van Sinoy ML, Sintzoff SA, et al. Cysts of the prostate and seminal vesicles: MR imaging findings in 11 cases. *AJR* **1990**;155:1021–1024

Case Report

Diagnosis of Gestational Trophoblastic Disease: Value of Endovaginal Color Flow Doppler Sonography

Robert K. Desai[1] and Andrea L. Desberg

The early diagnosis of invasive trophoblastic disease is important in the successful treatment of this disease. Standard pulsed Doppler sonography and transabdominal color flow sonography have been used in the diagnosis of gestational trophoblastic disease, including the identification of invasive trophoblastic disease [1, 2]. We report the early diagnosis of an invasive mole with endovaginal color flow sonography, which showed vascular invasion of the myometrium.

Case Report

A 32-year-old woman was examined for a possible molar pregnancy. The estimated gestational age of the fetus was 12 weeks. On physical examination, the size of the uterus was compatible with a 12-week gestation. The β-human chorionic gonadotropin (β-HCG) level of 134,000 mIU/ml (134,000 IU/l) was elevated. Transabdominal sonography disclosed no intrauterine gestation but did reveal the presence of an enlarged uterus with hyperechoic endometrial contents. Endovaginal examination showed numerous small, rounded anechoic spaces within the uterus, consistent with a diagnosis of molar pregnancy (Fig. 1A). As expected, pulsed Doppler examination revealed no evidence of blood flow within these anechoic spaces. The patient subsequently underwent suction curettage. The pathologic diagnosis was complete hydatidiform mole.

One week after evacuation, the β-HCG titer was 18,000 IU/l. Approximately 1 week later, the titer had fallen to 3500 IU/l. Three weeks after evacuation, the β-HCG level rose to 28,450 IU/l, and the diagnosis of an invasive molar pregnancy was entertained. Transabdominal sonography showed a slightly enlarged uterus of mildly increased echogenicity. No anechoic or hypoechoic spaces were seen. Images obtained showed multiple serpiginous anechoic channels throughout the central region of the uterus (Fig. 1B). Nearly all of these channels showed prominent blood flow on subsequent endovaginal color Doppler flow imaging (Fig. 1C), and several demonstrated extension into the myometrium, an appearance considered to represent vascular invasion. Pulsed Doppler sampling disclosed arterial waveforms of high amplitude and low pulsatility (Fig. 1D). A CT scan of the chest and abdomen obtained 3 days later to evaluate for metastatic disease revealed two small pulmonary nodules and a solitary low-attenuation mass within the liver. Sonographic examination of the liver showed the hepatic lesion to be hyperechoic. MR examination of the liver was subsequently performed to differentiate between metastasis and cavernous hemangioma. The MR characteristics were incompatible with cavernous hemangioma, and a presumptive diagnosis of metastatic disease was made. Multiagent chemotherapy was promptly started with a concomitant decline in the patient's β-HCG titer.

Discussion

Transabdominal sonography is the most common method of evaluating the gravid female pelvis. Its use in determining the status of the developing fetus is well established. Sonography is also of value when gestational trophoblastic disease is a diagnostic consideration. The typical sonographic appearance of a molar pregnancy is of an enlarged uterus with a hyperechoic endometrial echo complex, which may contain multiple hypoechoic and anechoic spaces and, according to previous studies, is best shown in the second trimester of pregnancy [3]. These spaces have been shown to represent vesicles and hemorrhagic spaces [4, 5].

Although quite difficult to demonstrate, invasive trophoblastic disease may be identified infrequently by the sonographic visualization of myometrial invasion by echogenic tumor [6]. Angiographic evaluation of invasive moles demonstrates enlarged spiral arteries feeding vesicular spaces and prominent arteriovenous shunting [2]. The use of duplex Doppler sonography has been shown to aid further in the diagnosis of invasive trophoblastic disease by detecting these abnormal vessels, which demonstrate a spectral waveform typical for a

Received March 18, 1991; accepted after revision May 10, 1991.

[1] Both authors: Department of Diagnostic Radiology, A21, Cleveland Clinic Foundation, 9500 Euclid Ave., Cleveland, OH 44195. Address reprint requests to R. K. Desai.

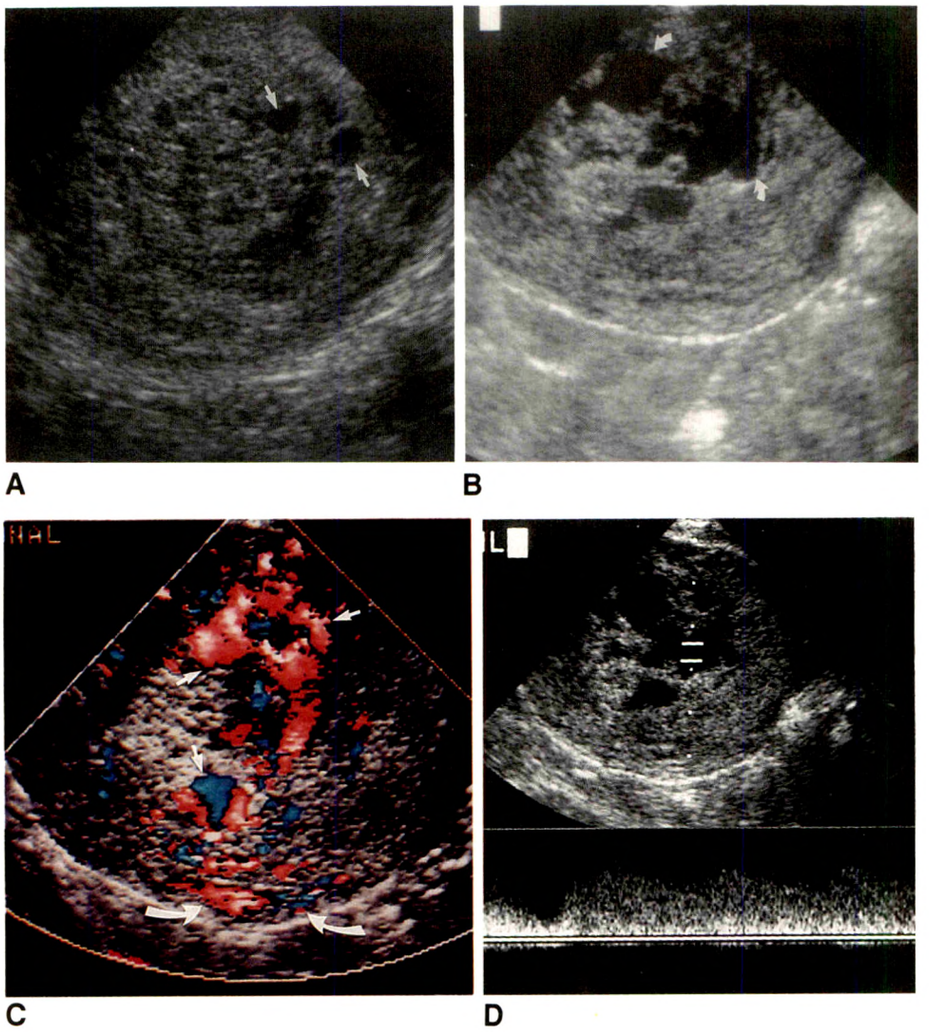


Fig. 1.—*A*, Coronal endovaginal sonogram of uterus. Multiple anechoic spaces (*arrows*) in uterus represent complete hydatidiform mole.

***B*, Coronal endovaginal sonogram of uterus shows multiple anechoic spaces (*arrows*).**

***C*, Coronal, endovaginal, color Doppler flow sonogram of uterus shows multiple blood vessels with rapid blood flow (*straight arrows*). Several of these vessels extend through myometrium to periphery of uterus (*curved arrows*).**

***D*, Coronal pulsed Doppler sonogram of vascular spaces. Doppler waveform indicates turbulent, high-velocity arterial blood flow with large diastolic component (low-impedance system).**

low-impedance system [1, 7]. Transabdominal color Doppler flow sonography has been used to evaluate invasive molar pregnancies. As expected, high-velocity blood flow is shown within the anechoic channels [2]. The use of transabdominal color Doppler flow imaging, however, requires the tumor to be of sufficient size and have large enough vessels to be adequately studied. Demonstration of vascular invasion of the myometrium has not been shown with transabdominal color Doppler flow sonography.

In the case reported, transabdominal sonographic evaluation performed 3 weeks after evacuation of the uterus to remove a molar pregnancy showed only a mildly enlarged uterus with a minimally increased echogenic pattern centrally without visible vesicles or anechoic channels. Subsequent endovaginal sonography showed the uterine contents in better detail, revealing multiple anechoic channels and spaces typically seen with trophoblastic disease. Better visualization was attributed to the superior resolution of the high-frequency endovaginal transducer. Color flow endovaginal imaging showed high-velocity blood flow through most of these spaces, and waveform analysis confirmed the presence of a low-impedance system. Importantly, color flow imaging disclosed the presence of vascular invasion of the myometrium. These findings allowed an early diagnosis of invasive trophoblastic disease, which led to the search for metastatic disease and to the prompt initiation of chemotherapy. Accordingly, we believe that the use of endovaginal color Doppler flow imaging is valuable in the early diagnosis of invasive trophoblastic disease.

REFERENCES

1. Taylor KJ, Schwartz PE, Kohorn EI. Gestational trophoblastic neoplasia: diagnosis with Doppler ultrasound. *Radiology* **1987**;165:445–448
2. Shimamoto K, Sakuma S, Ishigaki T, Makino N. Intratumoral blood flow: evaluation with color Doppler echography. *Radiology* **1987**;165:683–685
3. Woodward RM, Filly RA, Callen PW. First trimester molar pregnancy: nonspecific ultrasonographic appearance. *Obstet Gynecol* **1980**;55[suppl]:31S
4. Hussain S, Ansari A. Ultrasonic patterns in trophoblastic disease. *Clin Radiol* **1982**;33:593–597
5. Fleisher AC, James AE, Krause DA, Millis JB. Sonographic patterns in trophoblastic disease. *Radiology* **1978**;126:215–220
6. Munyer TP, Callen PW, Filly RA, Bragg CA, Jones HW. Further observations on the sonographic spectrum of gestational trophoblastic disease. *JCU* **1981**;9:349–358
7. Hata T, Hata K, Senoh D. Doppler ultrasound assessment of tumor vascularity in gynecologic disorders. *J Ultrasound Med* **1989**;8:309–314

Indications for Radiography in Patients with Acute Ankle Injuries:
Role of the Physical Examination

Ann G. Auletta[1]
William F. Conway[1]
Curtis W. Hayes[1]
Donald F. Guisto[2]
Alfred S. Gervin[2]

A prospective study was performed to test the hypothesis that a thorough physical examination can eliminate the need for a large number of radiographs obtained in patients with acute ankle trauma. Two hundred one patients were seen in the emergency department for acute ankle trauma and referred to the department of radiology for ankle radiographs. Radiology residents performed a brief but thorough physical examination of the ankle in all 201 patients. Solely on the basis of a strict set of physical examination criteria (examination for gross deformity, instability, crepitation, focal bony tenderness, severe soft-tissue tenderness, moderate or severe soft-tissue swelling, and ecchymosis), the radiologists determined whether or not the radiographs were indicated. All patients, irrespective of the physical examination, underwent ankle radiography, and the results were correlated with those of the physical examination. On the basis of the results of the physical examinations, 101 (50%) of the radiologic studies were not indicated. In only one of these patients was a fracture seen on radiographs. The radiograph in this case showed a small avulsion fracture of the dorsal aspect of the talus that was clinically insignificant (no cast or surgery was required).

Our results suggest that a brief but thorough physical examination can eliminate the need for a large percentage of radiographs ordered in patients with acute ankle trauma.

***AJR* 157:789–791, October 1991**

According to studies published in both the United States and Great Britain, ankle injuries account for approximately 10% of all visits to the emergency department [1, 2]. Ankle fractures are detected in approximately 13% of these cases [3, 4]. Consensus is growing that the radiologic evaluation of the injured ankle has superseded the physical examination as the method to detect fractures in many institutions, and particularly in crowded inner-city emergency departments [5]. Reasons for this change in medical practice include the large number of patients, lack of follow-up, expectations of patients, and medicolegal concerns [6–8]. Consequently, we undertook a prospective study to determine if a brief but thorough physical examination could reduce the need for radiologic examinations in patients with acute ankle trauma.

Received January 28, 1991; accepted after revision April 16, 1991.

Presented at the annual meeting of the American Roentgen Ray Society, Washington, DC, May 1990.

[1] Department of Radiology, Box 615 MCV Station, Medical College of Virginia, Richmond, VA 23298-0615. Address reprint requests to W. F. Conway.

[2] Department of Surgery, Medical College of Virginia, Richmond, VA 23298.

0361–803X/91/1574–0789
© American Roentgen Ray Society

Subjects and Methods

The study group consisted of 201 patients who were referred from a level I trauma emergency department to the radiology department for ankle radiographs from April to August 1989. There were 109 men and 92 women 11–72 years old (average, 32 years).

Of the 201 patients, 151 were examined by resident clinical physicians (with varying degrees of orthopedic experience) in the emergency department before referral to radiology. Forty-five patients were referred directly to radiology by nonphysician triage personnel without an examination by a physician. In five cases, it was unclear if a physician had examined the patient before referral to radiology.

Only patients who had ankle trauma for less than 24 hr before coming to the emergency department were included. In addition, only patients who were fully alert, English speaking,

and not pregnant were included. Patients with multiple trauma, abnormal neurovascular findings, open wounds, possible septic joints, or a history of malignancy or diabetes mellitus were excluded. Once in the radiology department, patients were reinterviewed and reexamined by the radiology resident (10 first- and second-year residents were involved in the study). These residents were unaware of the results of any physical examination that might have been performed by emergency department personnel prior to referral for radiographs.

Before the study, radiology residents were given formal instruction in the inspection and palpation of the traumatized ankle. Despite its thoroughness, this examination, including a brief interview of the patient, required less than 5 min to perform.

Gross deformity, instability or crepitation, focal bony tenderness, severe soft-tissue tenderness, moderate or severe soft-tissue swelling, and ecchymosis were all considered indicative of potential clinically significant injuries. Special attention was given to distinguishing bony from soft-tissue tenderness. The deltoid, fibulocalcaneal, and anterior and posterior talofibular ligaments were all individually palpated, as were the lateral and medial malleoli, the base of the fifth metatarsal, and the dorsal talus.

In both the initial physical examination and final radiologic evaluation, ankle injuries were considered clinically significant if the injury required open or closed manipulation and/or long-term immobilization in a cast. At our institution, this includes mostly fractures and dislocations, because acute ligamentous injuries are not treated surgically and are only rarely treated by immobilization in a cast. Clinically insignificant injuries were those that were treated conservatively, that is, with weight-bearing as tolerated, elevation, nonsteroid antiinflammatory medications, and/or an Ace wrap.

Solely on the basis of the physical examination, the radiology resident was required to indicate, on a preprinted questionnaire before the radiographs were made if (1) a clinically significant bony injury was suspected, (2) a clinically significant soft-tissue injury was suspected, (3) it was unclear whether a clinically significant injury was present, or (4) no clinically significant injury was suspected. If the radiology resident believed that a clinically significant injury was present (whether it was of bony or soft-tissue origin) or was uncertain, the patient was classified as having adequate indications for radiography. If the radiology resident believed that no clinically significant injury was present, the patient was classified as having inadequate indications for radiography. The residents were instructed to be conservative in their evaluations and were told that *no clinically significant injury* meant that they were confident by virtue of the physical examination that no significant injury was present.

Regardless of the evaluation by the radiology resident, all patients received a full set of ankle radiographs including anteroposterior, lateral, and mortise views. All studies were then evaluated by a staff radiologist who was blinded to the results of the physical examination. For purposes of this study, outcome was considered complete with the interpretation of the radiograph and categorization of the findings as clinically significant or insignificant.

Results

On the basis of the results of physical examination, 100 of the 201 patients in this study had adequate indications for ankle radiography. Of these patients, 30 (30%) had an abnormality on the radiographs that required manipulation and/or immobilization in a cast. Twenty-nine had fractures, and one had a chronic tear of the deltoid ligament that was acutely exacerbated and required casting. No other patient had a soft-tissue injury that led to orthopedic intervention. Seventy of the 100 patients had no radiographic evidence of significant bony or soft-tissue injury and were treated conservatively.

One hundred one patients (50%) were classified as having inadequate indications for radiographs of the ankle on the basis of the physical examination. Of these, only one had a fracture; this was a minimal avulsion fracture of the dorsal aspect of the talus that was treated conservatively. The remaining 100 patients had no radiologic evidence of a significant bony or soft-tissue injury.

Of the 151 patients who were actually examined by a physician before referral to radiology, 74 (49%) were classified as having adequate indications for radiographs of the ankle. Twenty-three (31%) of those patients had an injury that required orthopedic intervention. Seventy-seven patients (51%) were classified as having inadequate indications for radiographs (all of these patients had injuries that could be treated conservatively). This group included the previously described patient with an avulsion fracture of the dorsal talus.

Forty-five patients (22%) were sent directly to radiology by nonphysician triage personnel without the benefit of physical examination. Twenty-one (47%) of these patients had adequate indications for radiographs; of this group, six (29%) had a clinically significant injury requiring orthopedic intervention. Twenty-four patients (53%) were classified as having inadequate indications for ankle radiographs. None of these had clinically significant injuries.

Discussion

Only half of the patients who were referred for ankle radiography had a physical examination performed by radiology residents that indicated a need for ankle radiographs. No patients in whom indications for radiography were inadequate on the basis of the radiologist's physical examination had a clinically significant ankle injury (95% confidence interval: .960, 1.0 [9]). In none of these cases did radiographs change the clinical management. These findings suggest that a brief but thorough physical examination can eliminate the need for a large percentage of ankle radiographs in patients with acute ankle injuries.

It is important to note that some patients who presented to the emergency department with acute ankle trauma were never sent for radiographs. Emergency department physicians believed the injuries in these patients were insignificant, and they were treated conservatively. Additionally, clinicians (with the exception of the chairman of the emergency department) were unaware that the study was ongoing. This prevented unintentional bias in the patient referral pattern for radiography, but it also led to incomplete record keeping. Thus, we do not know the exact number of patients treated without the diagnostic aid of radiographs. We were also unable to ascertain the criteria used by emergency department personnel in ordering radiographs.

Approximately 75% of the patients were referred for ankle radiographs after examination by a resident emergency department physician. Radiographs on the others were requested by nonphysician triage personnel without the aid of a physical examination. No significant difference was found

in the percentage of indicated studies ordered by these two groups (51% vs 53%, respectively; 95% confidence interval: 0.197, −0.157 [9]). In addition, no difference was seen in the percentage of clinically significant injuries detected on radiographs (15% vs 13%, respectively; 95% confidence interval: 0.145, −0.105 [9]). These data suggest that either the emergency department physician performed an inadequate physical examination or failed to act on the results of an adequate examination.

DeLacey et al. [1] stated that if the maxim of "no swelling, no radiographs" were applied, the number of radiographs of the ankle could be reduced by two thirds. Our study indicates that if a policy of "no significant physical examination findings, no radiographs" had been implemented, the number of radiographs in this specific patient population could have been reduced by 50%. Overall reduction probably would have been lower if all patients (i.e., multiple trauma) had been included in the study.

Many studies, in both the United States and Great Britain [1, 3–6, 10–12], have addressed the issue of overuse of radiology in the evaluation of acute ankle trauma. Yet, these studies have had limited impact on clinical practice; overuse of ankle radiographs in patients with acute ankle trauma persists. This issue takes on special significance in this day of cost containment and limited resources. The cost in terms of money, radiation exposure, and decreased efficiency is substantial.

Even though the study was performed by radiologists, we do not advocate that radiologists routinely take medical histories and perform physical examinations on patients with traumatized ankles. Rather, we think that clinical physicians or physicians' assistants, with their additional clinical training and experience, should be performing this task. It must be emphasized, however, that whoever performs the physical examination should be well trained in its intricacies. Without such training, accuracy is limited.

In conclusion, our study confirms that requesting radiographs on the basis of a properly performed physical examination can substantially reduce the number of radiographs obtained for evaluation of acute ankle trauma without affecting the quality of patients' care.

REFERENCES

1. DeLacey GJ, Bradbrooke S. Rationalizing requests for x-ray examination of acute ankle injury. *Br Med J* **1979**;1:1597–1598
2. Warren RA, Ferguson DG. Why do accident and emergency doctors request x-rays? *Arch Emerg Med* **1984**;3:143–150
3. Cockshott WB, Jenken JK, Pui M. Limiting the use of routine radiography for acute ankle injuries. *Can Med Assoc J* **1983**;129:129–131
4. Dunlop MG, Beattie TF, White GI, Raab GM, Doull RI. Guidelines for selective radiological assessment of inversion ankle injuries. *Br Med J* **1986**;293:603–605
5. Vargish T, Clarke WR, Young RA, Jensen A. The ankle injury—indications for the selective use of x-rays. *Injury* **1982**;14:507–512
6. Brand DA, Frazier WH, Kohlhepp WC, et al. A protocol for selecting patients with injured extremities who need x-rays. *N Engl J Med* **1982**;306:333–339
7. Hall FM. Overutilization of radiologic examination. *Radiology* **1978**; 120:443–448
8. Grover K. X-ray examination for legal protection. *JAMA* **1980**;244:1436–1437
9. Berry CC. A tutorial on confidence intervals for proportions in diagnostic radiology. *AJR* **1990**;154:477–480
10. Brooks SC, Potter BT, Rainey JB. Inversion injuries of the ankle: clinical assessment and radiographic review. *Br Med J* **1981**;282:607–608
11. Garfield JS. Is radiological examination of the twisted ankle necessary? *Lancet* **1960**;2:1167–1169
12. Montague AP, McQuillan RF. Clinical assessment of apparently sprained ankle and detection of fracture. *Injury* **1985**;545–546

Radiation-Induced Osteochondroma

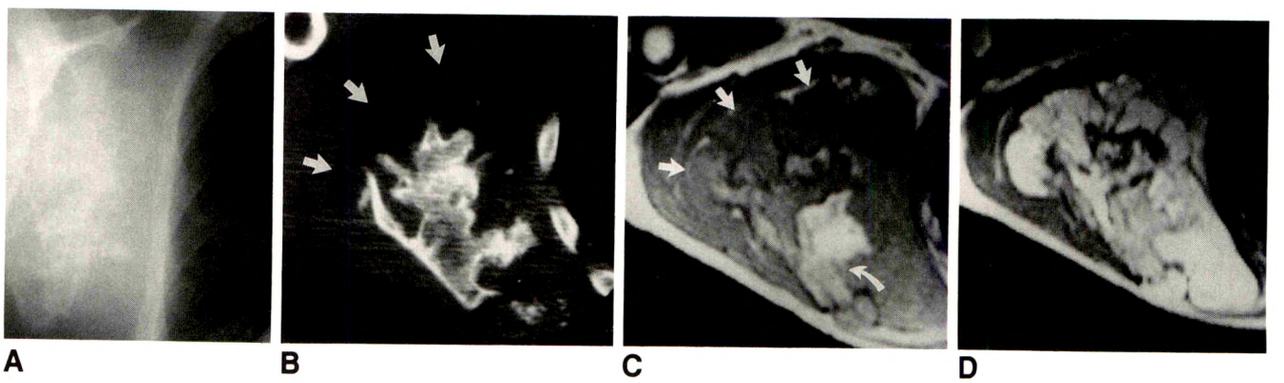
Felix S. Chew[1] and Ralph Weissleder

A 25-year-old man had a painless winged scapula. He had had prophylactic therapeutic irradiation (approximately 20 Gy) to the lungs for Wilms tumor in early childhood; the irradiated field included both scapulae. Plain films showed an ossified or calcified mass involving the right scapula, displacing the scapula away from the thoracic cage (Fig. 1). CT showed a broad-based exophytic lesion arising from the anterior surface of the scapula, containing mature bone, calcified cartilage, and extensive peripheral areas without mineralization. Attenuation numbers in the nonmineralized portions were consistent with cartilage. T2-weighted MR imaging showed bright signal throughout the nonmineralized portions of the lesion. Subtotal scapulectomy was performed. The gross specimen had cartilaginous nodules on the anterior surface. The cut specimen showed a stalk of mature bone with its cortex and medullary cavity continuous with the underlying scapula. Although the thickness of the cartilage cap was greater than 1 cm, microscopic examination revealed normal bone and mature hyaline cartilage with no malignant features. The final pathologic diagnosis was radiation-induced osteochondroma. Because of its large size, the lesion had evidently been present for many years.

Osteochondromas (benign osteocartilaginous exostoses) are outgrowths of bone that initially are covered by a cartilage cap. Arising from cartilage at active epiphyseal plates, they are not considered true neoplasms but rather are aberrations of normal growth. Osteochondromas may arise after a variety of traumas to the perichondrial ring of the growing physis, including therapeutic irradiation [1]. Osteochondromas after irradiation are identical in all respects to those that occur spontaneously and have a prevalence of approximately 6–12% [2, 3]. Malignant degeneration to chondrosarcoma in this circumstance is extremely rare. When necessary to relieve mechanical problems, the treatment is surgical excision. Osteochondromas do not recur.

REFERENCES

1. Langerskiold A, Edgren W. Initiation of chondrodysplasia by localized roentgen ray injury: an experimental study of bone growth. *Acta Chir Scand* **1950**;99:353–373
2. Libshitz HI, Cohen MA. Radiation-induced osteochondromas. *Radiology* **1982**;142:643–647
3. Jaffe N, Ried HL, Cohen M, McNeese MD, Sullivan MP. Radiation induced osteochondroma in long-term survivors of childhood cancer. *Int J Radiat Oncol Biol Phys* **1983**;9:665–670



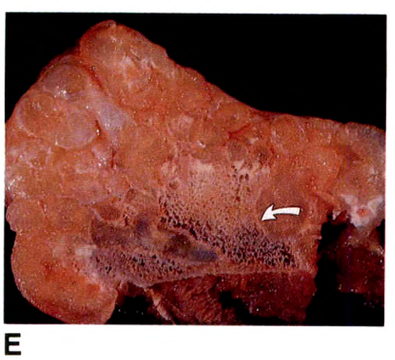


Fig. 1.—Radiation-induced osteochondroma.
***A*, Radiograph shows mineralized lesion of scapula.**
***B*, CT scan shows a partially calcified mass (*arrows*) with an ossified stalk arising from anterior aspect of scapula.**
***C*, Proton density–weighted axial MR image shows bright signal in marrow cavity of stalk (*curved arrow*). Mass is partially outlined by fat (*arrows*).**
***D*, T2-weighted axial MR image shows bright signal in nonmineralized portions of lesion.**
***E*, Cut surface of gross specimen (axial orientation) shows ossified stalk (*arrow*) arising from scapula with nodules of cartilage on the surface. Note concave contour where lesion abutted chest wall (*top*).**

From the weekly radiologic-pathologic correlation conferences conducted by Jack Wittenberg. Pathology editor: Andrew E. Rosenberg. Radiology editors: Felix S. Chew, Daniel P. Barboriak, William E. Palmer, Daniel I. Rosenthal.

[1] Both authors: Department of Radiology, Massachusetts General Hospital and Harvard Medical School, 32 Fruit St., Boston, MA 02114. Address reprint requests to F. S. Chew.

Pictorial Essay

Sonography of the Normal Elbow

Lori L. Barr[1] and Diane S. Babcock

Sonography was performed in 30 normal patients, neonatal to 45 years old, to illustrate our technique for complete and rapid examination of the elbow joint. Sonography is an easy, noninvasive method of evaluating the articulating surfaces, tendinous insertions, and supporting soft tissues of the elbow joint. Reliable identification of both normal and diseased anatomy is possible at all ages. Familiarization with the sonographic appearance of the six elbow ossification centers aids in sonographic interpretation.

Several investigators have described the usefulness of sonography in the examination of the normal elbow joint [1], effusion [2], fat pads [3], and loose bodies [4, 5]. We describe a technique for complete and rapid examination of the elbow joint. We examined 30 patients with no history of elbow symptoms or injury. Five patients in each of six age groups were scanned: 0–2 years, 2–5 years, 5–10 years, 10–15 years, 15–25 years, and 25–45 years. In patients less than 2 years old, the periarticular structures were visible when a 7.5-MHz linear-array transducer was used. In older patients, a 5.0-MHz linear-array transducer provided optimal visualization and was used to identify the various muscle groups surrounding the elbow.

Technique

The examination begins with the patient supine, the arm resting comfortably at the side, the forearm supinated, and the wrist halfway between pronation and supination (Figs. 1A and 2A). Additional views are obtained with the wrist in supination (Figs. 3A, 4A, and 5A) and from a posterior approach with 180° arm elevation, 90° flexion, and slight abduction (Figs. 6A and 7A). Acoustic gel is used as the coupling medium.

Discussion

The first drawing in each figure demonstrates both the arm and transducer positions used. The second drawing reveals the anatomic structures visible from reflection of the ultrasound beam [6]. To demonstrate the two extremes of ossification, an adult elbow and a neonatal elbow are shown. The radiographic appearance of the normal ossification centers has been well documented by several investigators. Our discussion is based on the work of Brodeur et al. [7]. Skeletal maturation in girls is more rapid than in boys, with the capitellum becoming visible at about 4–6 months of age in girls (as late as 18 months in boys) and with complete skeletal maturation achieved by 15 years in girls (16 years in boys).

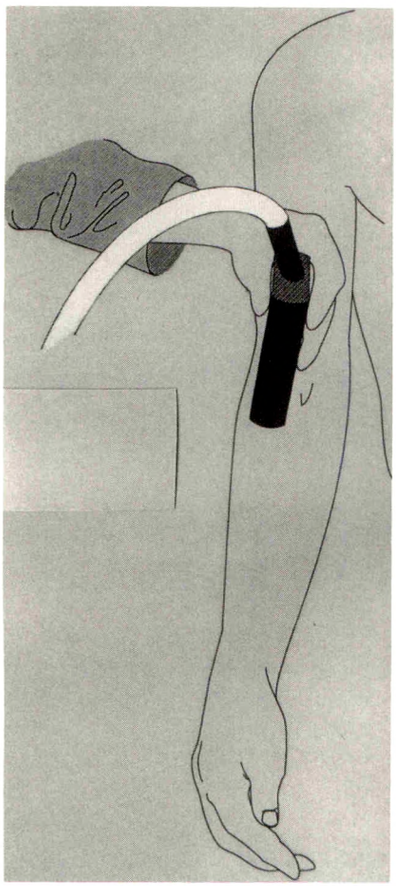
The ossifying epiphyses begin as spherical, ovoid, or irregular sites of calcium deposition within the cartilaginous preformed bone ends. These are detectable on both radiographs or sonograms [8].

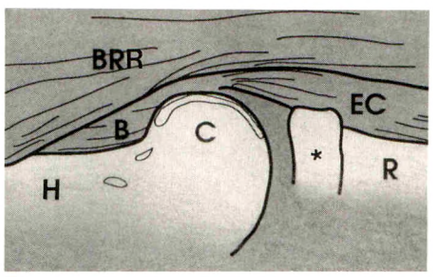
On sonograms, the cartilaginous epiphysis appears as a smoothly marginated hypoechoic matrix with small echogenic reflectors randomly interspersed. No posterior shadowing is present. Early epiphyseal enchondral bone formation leads to a decrease in the through-transmission of the ultrasound beam and gradually increased reflectivity of the cortical margin as the bone continues to increase in density. The amount of

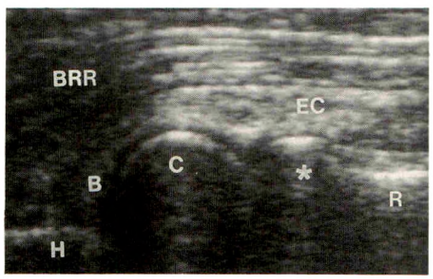
Received December 24, 1990; accepted after revision May 29, 1991.

[1] Both authors: Department of Radiology, Children's Hospital Medical Center and The University of Cincinnati College of Medicine, Elland & Bethesda Aves., Cincinnati, OH 45229-2899. Address reprint requests to L. L. Barr.

AJR **157:793–798, October 1991** 0361–803X/91/1574–0793 © American Roentgen Ray Society







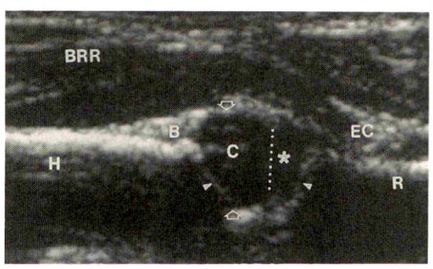


Fig. 1.—Anterior: anterior longitudinal view of lateral aspect of elbow. This plane allows best visualization of radiohumeral articulation and capitellum. A longitudinal view of the radial head is seen.

A, Drawing illustrates neutral position of hand for anterior scanning. Transducer is aligned with radiohumeral articulation along lateral aspect of elbow.

B, Drawing of structures visible on sonograms. Most superficial muscle is brachioradialis muscle. In this plane, biceps brachii muscle appears continuous with extensor carpi radialis muscle group. These two muscles overlap each other, but their relationship is oblique to ultrasound beam in scan plane, and they may appear to be continuous. Anterior cortex of humeral metaphysis appears as an echogenic interface perpendicular to ultrasound beam. Bulbous capitellum articulates with fovea of radial head (*asterisk*). Anterior cortex of radial metaphysis is slightly diagonal to ultrasound beam.

C, Sonogram in adult. Most superficial muscle visible is brachioradialis muscle. Extensor carpi radialis muscle group and visible portion of biceps brachii muscle appear inseparable in this patient. Capitellum (C) and radial head (*asterisk*) are ossified and physes are fused. Shaft of humerus intersects abruptly with curved capitellum. Anterior aspect of radial head is perpendicular to ultrasound beam, and radial metaphysis is slightly diagonal in orientation.

D, Sonogram in neonate. Fascial planes separate brachioradialis muscle, biceps brachii muscle, and extensor carpi radialis muscle. Longer segment of humeral shaft is visible. Rounded capitellum (*arrows*) and radial head (*asterisk*) are not yet ossified and are impossible to distinguish (*dots*). Both appear hypoechoic with moderately echogenic reflectors interspersed. No posterior shadowing is seen. Physes (*arrowheads*) of distal humerus and proximal radius (R) appear as obliquely oriented echogenic lines. A percentage of ultrasound beam traverses bones, giving a vague outline of muscles along posterior aspect of elbow.

Key to Abbreviations Used in Figures

A	anconeus muscle
B	biceps brachii muscle
BR	brachialis muscle
BRR	brachioradialis muscle
C	capitellum
CEM	common extensor muscle group of forearm
CF	common flexor muscle group of forearm
EC	extensor carpi radialis muscle group
ECR	extensor carpi radialis longus muscle
ED	extensor digitorum muscle
F	flexor muscles of forearm
FD	flexor digitorum profundus muscle
FP	fat pad
H	humerus, humeral shaft, humeral metaphysis
LE	lateral epicondyle of humerus
ME	medial epicondyle of humerus
O	olecranon
PT	pronator teres muscle group
R	radius, radial head, radial shaft, radial physis, radial metaphysis
S	supinator muscle
T	tendon of common extensor or flexor muscle group of forearm
TBR	triceps brachii muscle
TN	trochlear notch
Tr	trochlea of humerus
U	ulna

Fig. 2.—Anterior: anterolateral longitudinal sonogram. This view displays tendinous origin of common forearm extensor muscle group, which is prone to injury (lateral epicondylitis).

A, Drawing shows slight obliquity necessary to align transducer along long axis of common extensor muscle group of forearm. Note that hand remains neutrally positioned.

B, Drawing of structures visible on sonograms. Superficially, brachioradialis muscle is identified. Visible portion of biceps brachii muscle is seen as a separate structure from common forearm extensor muscle group, which is not limited to but includes extensor carpi radialis muscle. Common forearm extensor muscle group arises from a common tendon attached to lateral epicondyle of humerus. Radial head is oblique in this projection.

C, Sonogram in adult. Brachioradialis muscle is superficial to biceps brachii muscle. Lateral epicondyle appears as smoothly marginated, curved echogenic line from which common tendon arises. Tendon is less echogenic than lateral epicondyle but more echogenic than common forearm extensor muscle, which flares after passing over oblique radial head. Radial head is ossified, echogenic, and demonstrates posterior shadowing. High-frequency ultrasound beam is attenuated; therefore, no structures are identified deep to bone.

D, Sonogram in neonate. Brachioradialis muscle is just below skin surface. Biceps brachii muscle demonstrates separate fascial planes from common forearm extensor muscle group. Common forearm extensor muscle group appears as a flared structure arising from echogenic common tendon, which arises from hypoechoic lateral epicondyle of neonate. Oblique portion of unossified radial head and radial shaft is diagonally oriented just below narrow neck of common forearm extensor muscle group tendon. A portion of triceps muscle and supinator muscle can be seen in this patient.

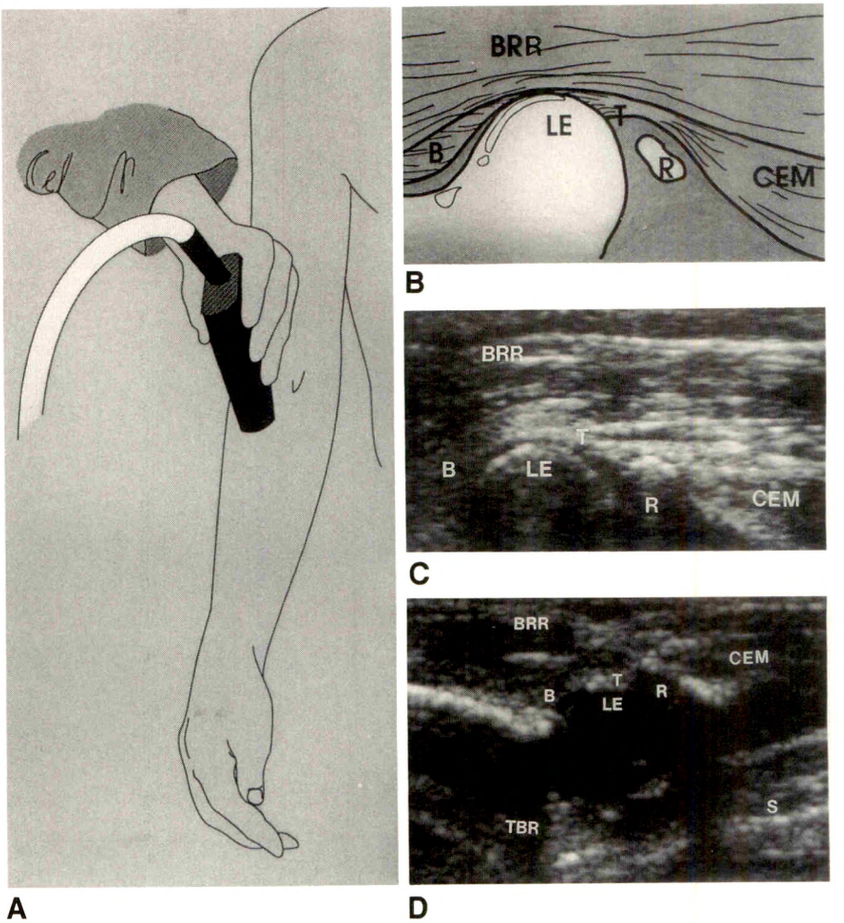


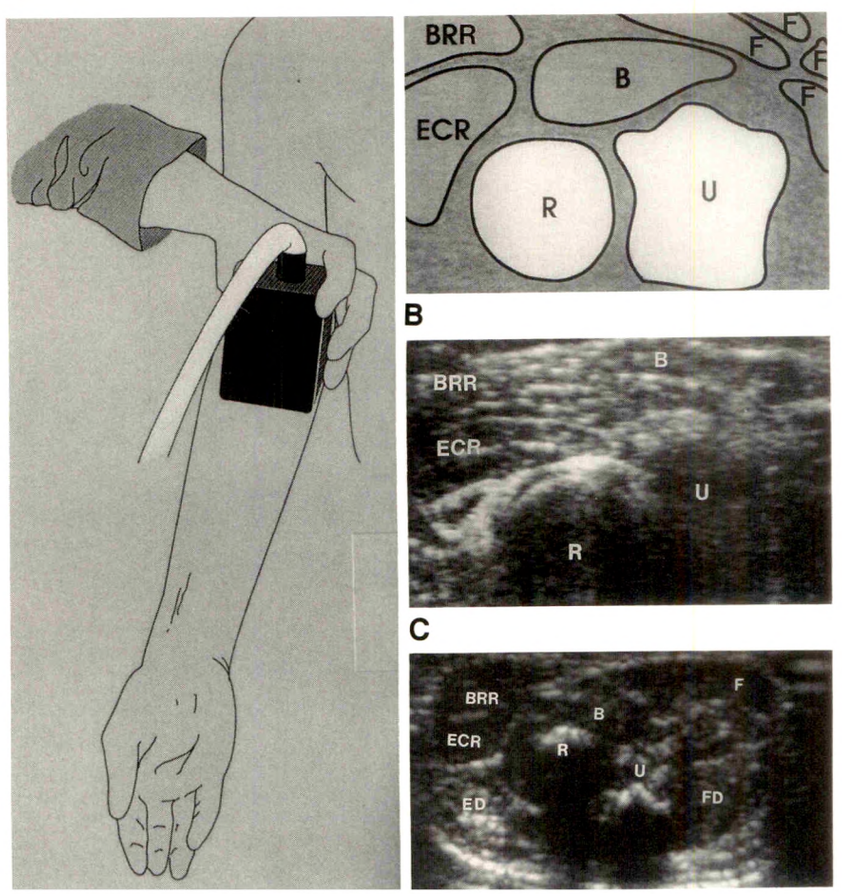
Fig. 3.—Anterior: inferior transverse sonogram. This plane is useful for evaluation of radioulnar articulation and for watching supination and pronation of proximal radius.

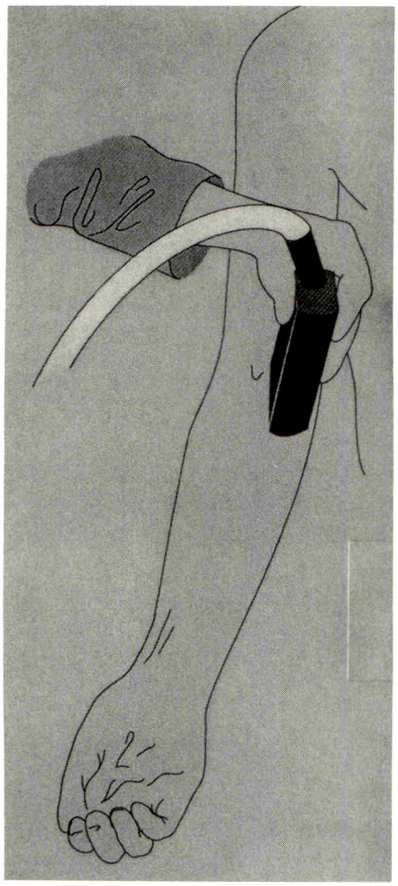
A, Drawing shows transverse orientation of transducer, so that side of image on viewer's left is assigned to lateral aspect of elbow joint. Hand is supinated.

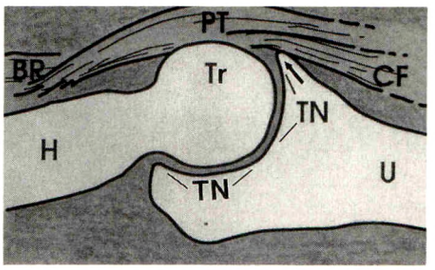
B, Drawing of structures visible on sonograms. Brachioradialis muscle is most superficial lateral muscle. Deep to brachioradialis muscle is extensor carpi radialis longus muscle. Biceps muscle is superficial to radioulnar articulation. Because this view is designed to evaluate radial head and radioulnar articulation, superficial forearm flexor muscles, which are located medially, are not always identified. Radial head is rounded and rotates with hand supination and pronation. Because surface of ulna closest to transducer is irregular and oblique to ultrasound beam, surface of bone is indistinct.

C, Sonogram in adult. Brachioradialis muscle is seen superficially along lateral aspect of forearm. Biceps brachii muscle is seen in midline superficial to radioulnar articulation. Although anterior articular surface of radial head appears as a smooth echogenic line, anterior surface of ulna is irregular and not clearly seen. Instead, a vague area of posterior shadowing is seen deep to poorly defined echogenic area. Transverse diameter in adult does not allow clear visualization of forearm flexor muscles in this patient. Posterior shadowing from bones limits evaluation to antecubital fossa.

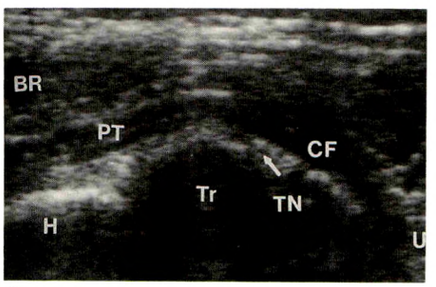
D, Sonogram in neonate. Elbow is small enough in transverse diameter that forearm flexor muscles are identified superficially along medial aspect of the forearm. Laterally, brachioradialis muscle is seen superficial to extensor carpi radialis muscle. Posterior shadowing is identified from radial physis and ulna. Increased ultrasound beam penetration in neonate allows visualization of extensor digitorum muscle and flexor digitorum profundus muscle in posterior aspect of forearm.



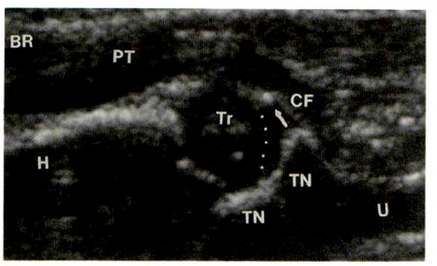




B



C



D

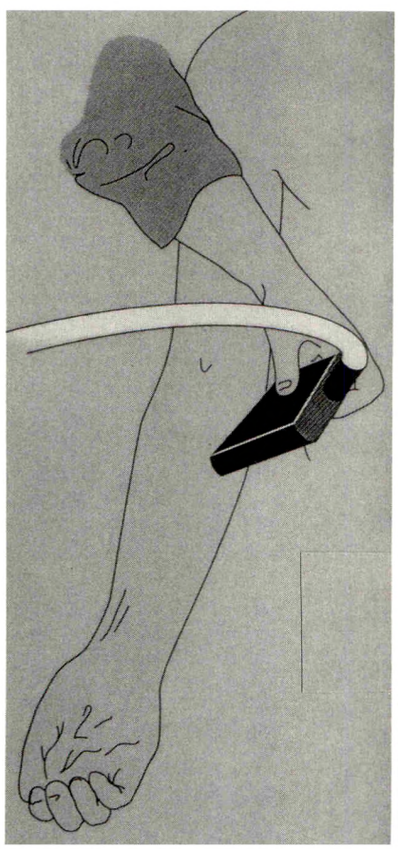
Fig. 4.—Anterior: anterior longitudinal sonogram of medial aspect of elbow. This view is useful for visualization of ulnohumeral articulation and coronoid process of ulna.

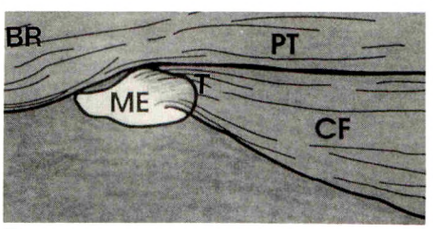
A, Drawing shows transducer aligned longitudinally along long axis of ulna to visualize ulnohumeral articulation. Hand is supinated.

B, Drawing of structures visible on sonograms. Most superficial muscle in distal arm is brachialis muscle. Pronator teres muscle arises from the humeral shaft and courses anterior to ulnohumeral articulation. Trochlea of humerus articulates within trochlear notch of ulna. Coronoid process (*arrow*) is pointed protuberance of ulna. Origin of common forearm flexor muscle group is not seen in this projection. Posterior aspect of pronator teres muscle is inseparable from proximal portion of common forearm flexor muscle group.

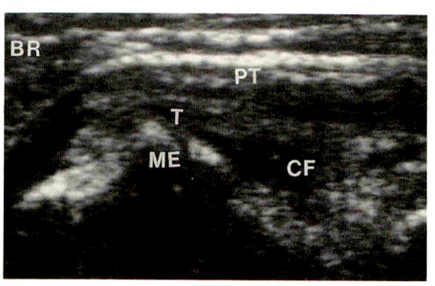
C, Sonogram in adult. Brachialis muscle is superficial to common forearm flexor muscle group, which blends with posterior aspect of pronator teres muscle. Diagonal orientation of humeral shaft blends with rounded trochlea. Coronoid process (*arrow*) is seen as echogenic angulated structure abutting inferior aspect of trochlea. High-frequency ultrasound beam is attenuated along anterior surface of humerus and ulna.

D, Sonogram in neonate. Brachialis muscle is identified proximal to ulnohumeral articulation. Pronator teres muscle spans elbow joint. Proximal portion of common forearm flexor muscle group appears relatively anechoic, becoming more echogenic as muscle flares at level of ulnar metaphysis. Entire trochlear notch is visible because trochlea is not ossified. Coronoid process (*arrow*) is unossified as well and appears hypoechoic. *Dotted line* outlines separation between unossified trochlea and unossified coronoid process.





B



C

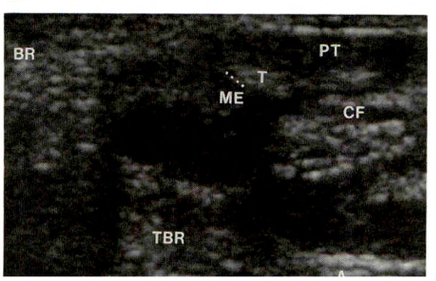


Fig. 5.—Anterior: anteromedial longitudinal sonogram. This view is designed to visualize common tendon from which forearm flexor muscle group arises.

A, Drawing shows that with hand in supination, transducer is slightly oblique to match long axis of common forearm flexor muscle group arising from common tendon attached to medial epicondyle.

B, Drawing of structures visible on sonograms. Most superficial muscle deep to skin is pronator teres. This muscle is inseparable from distal portion of brachialis muscle in distal arm in this scan plane. Medial epicondyle is irregular ovoid structure from which tendon of common forearm flexor muscles arises. Tendon of common flexor muscle group of forearm is not as long or narrow as tendon of common extensor muscle group on lateral aspect of arm. Common flexor muscle group of forearm flares as it extends down into forearm.

C, Sonogram in adult. Brachialis muscle and pronator teres muscle are seen superficially. Muscles are clearly separated from each other in this patient. Medial epicondyle is ossified and echogenic, with posterior shadowing. Tendon from which common flexor muscle group of forearm arises is more echogenic than surrounding muscular tissue. Superficial to tendinous origin is pronator teres muscle, which is clearly separated from brachialis muscle in this patient.

D, Sonogram in neonate. Brachialis muscle and pronator teres muscle are superficial to medial epicondyle. In this patient, the two muscles are inseparable from each other. Medial epicondyle is not ossified and appears hypoechoic without posterior shadowing. Tendon is more echogenic than either medial epicondyle or common forearm flexor muscle group, which flares shortly after tendinous origin. *Dots* outline interface between unossified medial epicondyle and tendon. Through-transmission allows visualization of anconeus muscle and triceps brachii muscle in por-

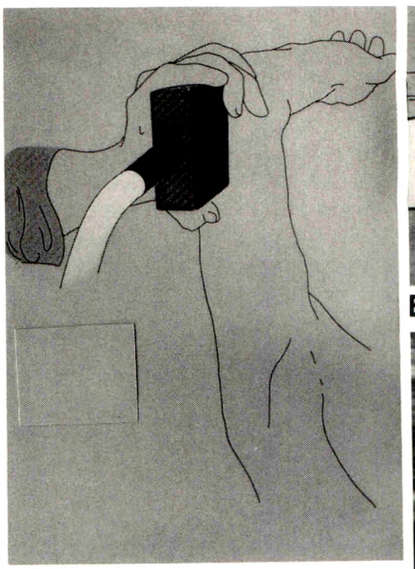
Fig. 6.—Posterior: midline longitudinal sonogram. This plane is useful in evaluating distal humerus and displacement of posterior fat pad indicating fluid in joint.

A, Drawing shows that for posterior scanning, arm is elevated 180° next to patient's head and elbow flexed 90°. Transducer should be oriented so that proximal portion of arm is oriented to viewer's left on image.

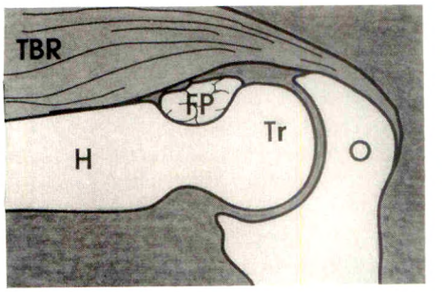
B, Drawing of structures visible on sonograms. Triceps brachii muscle is just deep to skin surface and spans elbow joint. Humeral shaft is slightly diagonal in orientation to scan plane. Fat pad is identified in olecranon fossa of distal humerus. Bulbous trochlea articulates with trochlear notch of olecranon of ulna.

C, Sonogram in adult. Patient cooperation allows alignment of long axis triceps brachii muscle and humeral shaft with ultrasound beam. Fat pad is more echogenic than surrounding muscle but remains less echogenic than olecranon fossa of humerus. Mature olecranon fossa is deeper than that in infant. Mature trochlea appears as an echogenic line distal to fat pad. Fully ossified olecranon is located slightly superior and distal to trochlea.

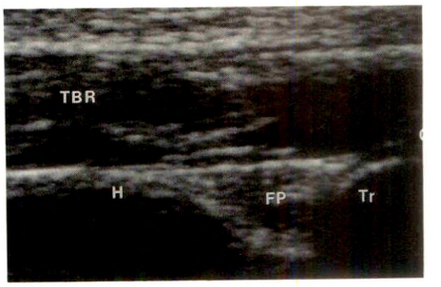
D, Sonogram in neonate. Both triceps muscle and humeral shaft are oriented diagonally to ultrasound beam. Fat pad is more echogenic than surrounding muscle but less echogenic than olecranon fossa of humerus in which it lies. Trochlea is unossified and appears hypoechoic. Its surface is less echogenic than humeral shaft or olecranon fossa. Olecranon of ulna is also unossified and has a less echogenic surface.



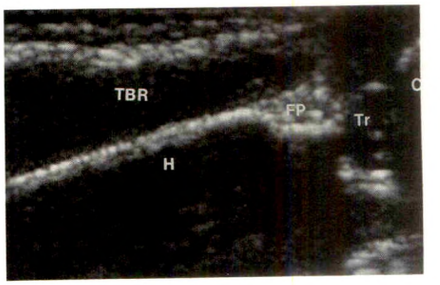
A



B



C



D

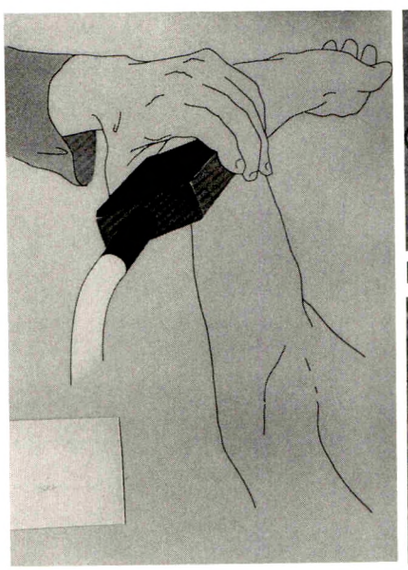
Fig. 7.—Posterior: superior transverse sonogram. This view is useful in identifying fluid in joint and displacement of fat pad. Epicondylar injuries may also be detected.

A, Drawing shows that arm remains in same position and transducer is oriented transversely at level of posterior fat pad in olecranon fossa of distal humerus.

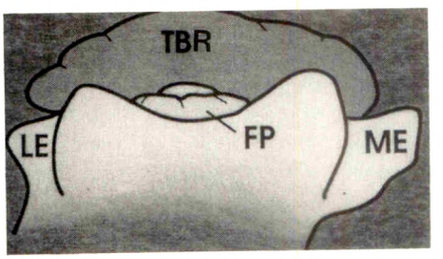
B, Drawing of structures visible on sonograms with side of image to viewer's left assigned to lateral aspect of elbow joint. Deep to skin, triceps brachii muscle is identified. Echogenic fat pad lies within olecranon fossa of humerus. Lateral epicondyle is located to left of screen, and medial epicondyle, which is slightly more prominent, is seen to viewer's right.

C, Sonogram in adult. Triceps brachii muscle is noted superficially. Echogenic fat pad is identified in deep olecranon fossa associated with skeletal maturity. Much of ultrasound beam is attenuated at irregular surfaces of lateral epicondyle and medial epicondyle.

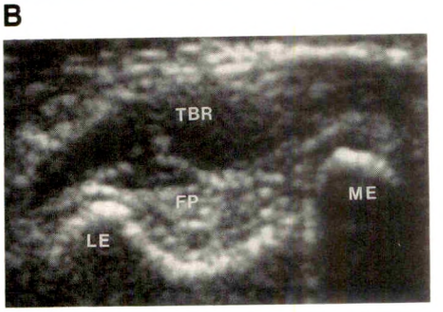
D, Sonogram in neonate. Neonate's arm is so narrow in transverse diameter that contact is not maintained through length of transducer face. Triceps brachii muscle is deep to skin and superficial to echogenic fat pad. Note shallow appearance of olecranon fossa before skeletal maturation. Unossified lateral epicondyle has a smoothly curved echogenic surface continuous with lateral aspect of olecranon fossa, but no posterior shadowing is identified. Unossified medial epicondyle appears to have a more tightly curved surface, which is not as smooth and does not have posterior shadowing either.



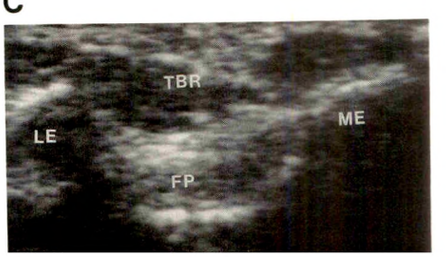
A



B



C



posterior shadowing likewise increases with ossification. Of the six elbow epiphyses, four begin ossification in a spherical pattern; the exceptions are the lateral epicondyle, which is ovoid, and the radial head, which is disk-shaped.

The first ossifying epiphysis at the elbow is the capitellum, which also varies most in appearance. In all cases, some ossification of the capitellum is visible by age 2 years. Capitellar fusion is complete by 13–14 years. The capitellum is best evaluated by anterior longitudinal views of the lateral aspect of the elbow.

The medial epicondylar epiphysis is best evaluated by an anterior or anteromedial longitudinal view; ossification begins at about 4 years and is complete at 15–16 years. Medial epicondylar epiphyseal injuries constitute approximately 10% of all childhood elbow fractures [7]. The tendon for the common forearm flexor muscles arises from the medial epicondyle. Therefore, the medial view is the most useful for evaluation of tendinous injury (medial epicondylitis).

Ossification of the radial head epiphysis begins at about 5 years and is complete by 15–16 years. The epiphysis and physis are best examined by anterolateral longitudinal and anteroinferior transverse sonograms. The latter view facilitates real-time evaluation of the motion of the proximal radius when the elbow is examined with the hand in pronation and supination. The radial head ossification center is disk-shaped.

The trochlear epiphysis begins ossification at about 8 years and is completely ossified by 15–16 years. It is best evaluated with anteromedial longitudinal and posterior midline longitudinal views. Prior to ossification, the articulation within the trochlear notch is sonographically visible. Posterior shadowing after enchondral bone formation obscures the joint at approximately 10 years.

The olecranon epiphysis appears at about 9 years and fuses at 14 years. It is best evaluated by posterior midline longitudinal views. If injury is suspected, the epiphysis may be viewed in the transverse plane by extension of the arm and posterior positioning of the transducer. Concomitant deepening of the olecranon fossa as the olecranon epiphysis matures is seen on the posterior superior transverse sonogram. This view is helpful in evaluating fluid in the elbow joint with displacement of the fat pad toward the transducer and out of the olecranon fossa.

The lateral epicondylar epiphysis begins ossifying at about 10 years and is complete at 14 years. It is best evaluated by anterior anterolateral longitudinal sonograms, in which transducer obliquity allows visualization of the common forearm extensor muscle group tendon that is attached to the lateral epicondyle. Skeletal and tendinous injuries of the lateral aspect of the elbow are common. Comparison with the asymptomatic elbow is often helpful in detecting acute soft-tissue injuries not visible on radiographs. The ossification center of the lateral epicondyle is normally ellipsoid to linear.

Sonography is an easy, noninvasive method of evaluating the articulating surfaces, tendinous insertions and supporting soft tissues of the elbow joint. Reliable identification of both normal anatomy and pathology is possible at all ages. Familiarization with the sonographic appearance of the six elbow ossification centers aids in sonographic interpretation.

REFERENCES

1. Fornage BD. *Ultrasonography of muscles and tendons*. New York: Springer-Verlag, **1989**
2. Koski JM. Ultrasonography of the elbow joint. *Rheumatol Int* **1990**;10: 91–94
3. Miles KA, Lamont AC. Ultrasonic demonstration of the elbow fat pads. *Clin Radiol* **1989**;40:602–604
4. Seltzer SE, Finberg HJ, Weissman BN. Arthrosonography—technique, sonographic anatomy, and pathology. *Invest Radiol* **1980**;15:19–28
5. Giannini S, Lipparini M, Della Villa S, et al. Ultrasonography in pathological conditions of muscles, tendons and joints. *Ital J Orthop Traumatol* **1987**;13:253–259
6. Williams PL, Warwick R. *Gray's anatomy*. 36th ed. Philadelphia: Saunders, **1980**
7. Brodeur AE, Silberstein MJ, Graviss ER. *Radiology of the pediatric elbow*. Boston: Hall Medical, **1981**
8. Harcke HT, Lee MS, Sinning L, et al. Ossification center of the infant hip: sonographic and radiographic correlation. *AJR* **1986**;147:317–321

Osteoarthritis of the Knee:
Comparison of Radiography, CT, and MR Imaging to Assess Extent and Severity

Wing P. Chan[1]
Philipp Lang[1]
Michael P. Stevens[2]
Kenneth Sack[2]
Sharmila Majumdar[1]
David W. Stoller[1]
Christa Basch[3]
Harry K. Genant[1,2]

Although conventional radiography is the method most frequently used for monitoring progression of osteoarthritis, it may not show osteoarthritic changes of the knee until late in the disease, and it may show involvement of only one or two compartments in patients who have tricompartmental disease. We compared radiography, CT, and MR imaging for assessing the extent and severity of osteoarthritis of the knee in 20 patients. Radiography included posteroanterior weight-bearing, true lateral, and sunrise patellar projections. Axial CT scans were reformatted in sagittal and coronal planes. MR imaging consisted of spin-echo (600–800/20; 2000/60, 120 [TR/TE]), and gradient-echo (600/30, $\theta = 30°$) sequences. The severity of osteoarthritic changes was graded from 0 to 3. MR frequently showed tricompartmental cartilage loss when radiography and CT showed only bicompartmental involvement in the medial and patellofemoral compartments. In the lateral compartment, MR showed a higher prevalence of cartilage loss (60%) than radiography (35%) and CT (25%) did. In the medial compartment, CT and MR showed osteophytes in 100% of the knees, whereas radiography showed osteophytes in only 60%. Notably, radiography often failed to show osteophytes in the posterior medial femoral condyle. On MR images, meniscal degeneration or tears were found in all 20 knees studied. Partial and complete tears of the anterior cruciate ligament were found in three and seven patients, respectively.

MR is more sensitive than radiography and CT for assessing the extent and severity of osteoarthritic changes and frequently shows tricompartmental disease in patients in whom radiography and CT show only bicompartmental involvement. MR imaging is unique for evaluating meniscal and ligamentous disease related to osteoarthritis.

AJR 157:799–806, October 1991

Osteoarthritis frequently affects the knee and can cause profound changes in the surrounding bone and soft tissues. These changes include cartilage loss, subchondral sclerosis, osteophytosis, subchondral cysts, and meniscal degeneration [1–5]. Radiographs can show osteoarthritic changes of the bone; however, soft-tissue involvement may not be appreciated. CT is superior to conventional radiography because it provides a tomographic assessment of soft-tissue and osseous changes.

MR imaging has direct multiplanar imaging capability and provides a higher soft-tissue contrast than CT does. MR imaging is established as a noninvasive tool for evaluating pathologic changes in the articular cartilage, menisci, and ligaments of the knee [6–13].

In this study, we compared radiography, CT, and MR imaging for assessing the extent and severity of osteoarthritis of the knee. Twenty consecutive patients with osteoarthritis of the knee were examined prospectively with radiography, CT, and MR imaging. The severity of the osteoarthritic changes was graded for each imaging technique.

Received February 20, 1991; accepted after revision April 16, 1991.

[1] Department of Radiology, University of California, San Francisco, 505 Parnassus Ave., San Francisco, CA 94143. Address reprint requests to H. K. Genant.

[2] Department of Medicine, University of California, San Francisco, 505 Parnassus Ave., San Francisco, CA 94143.

[3] Syntex Laboratories, Inc., 3401 Hillview Ave., Palo Alto, CA 94303.

0361–803X/91/1573–0799
© American Roentgen Ray Society

Materials and Methods

Selection of Patients

Twenty patients (11 women and nine men), 42 to 73 years old (mean, 58 years), with clinical and radiologic evidence of osteoarthritis of the knee were studied prospectively as part of a clinical drug trial to monitor the effects of nonsteroidal antiinflammatory drug therapy on osteoarthritis. In each patient, one knee was evaluated with radiography, CT, and MR imaging. A requirement for inclusion in the study was that patients had knee pain and knee joint effusion for at least 1 month. For patients with bilateral disease, the knee clinically determined to have the most severe disease was selected for study.

Imaging Techniques

Radiography of the knee consisted of posteroanterior weight-bearing, true lateral non-weight-bearing, and sunrise patellar projections [1, 2, 14]. Posteroanterior weight-bearing radiographs were obtained with the knee in 20° flexion to orient the tibial plateau orthogonal to the X-ray beam.

Axial CT was performed with a GE CT/T 9800 unit. We used a scanning time of 2 sec, 140 kVp, 70 mA, and a vertical gantry. A 34.5-cm field of view (FOV) with a 512 × 512 matrix was used. Slice thickness was 3 mm. Scans were obtained contiguously. The patient was supine, with both extremities parallel and the ankles and the knees taped together. The knees were placed in 30° flexion [5]. Images were reformatted in sagittal and coronal planes by using a slice thickness of 3 mm with no interslice gap.

MR imaging was performed on a 1.5-T Signa system (General Electric, Milwaukee, WI) with a transmit-and-receive extremity coil. A spin-echo sequence was used to obtain images in three orthogonal planes. Repetition time (TR) varied from 600 to 800 msec, and echo time (TE) was 20 msec for all three planes. Axial images were generated also by using a spin-echo technique with a TR of 2000 msec and TEs of 60 and 120 msec. Additionally, gradient-echo images were obtained with a TR of 600 msec, a TE of 30 msec, and a flip angle θ of 30° in axial and sagittal planes. For all cases, the slice thickness was 5 mm, the image matrix varied from 256 × 192 to 256 × 256, and FOV ranged from 14 to 16 cm. Spin-echo and gradient-echo images were acquired with two excitations. The interval between radiography, CT, and MR did not exceed 2 weeks for any of the patients.

Interpretation of the Images

Image analysis included evaluation of four diagnostic parameters: cartilage loss, subchondral sclerosis, osteophytes, and subchondral cysts. MR also was used to evaluate the menisci and ligaments. The extent of the disease was evaluated separately for the medial, lateral, and patellofemoral compartments. The severity of the osteoarthritic changes of the knee was graded from 0 to 3. The severity of cartilage loss was judged as 0 = normal; 1 = mild, or 1–33% decrease in cartilage thickness; 2 = moderate, or 34–66% decrease in cartilage thickness; and 3 = severe, or 67–100% decrease in cartilage thickness. Subchondral sclerosis was noted as 0 = absent; 1 = mild, or localized eburnation (or mild localized signal reduction on MR); 2 = moderate increase in density (or moderate localized signal reduction on MR); 3 = severe, widespread sclerosis (or severe extensive signal reduction on MR) [2]. Osteophytes were graded as 0 = absent; 1 = small beaklike osteophyte; 2 = intermediate-size osteophyte, between those of grades 1 and 3; 3 = proliferative or mushroomlike osteophyte [15]. Subchondral cysts were evaluated as 0 = absent; 1 = one to two small cysts; 2 = single large or multiple small cysts; or 3 = many large cysts [2]. In the event of nonuniform involvement of a single compartment, the most severe degree of change was used for grading. Meniscal changes were graded by MR as 0 = no tear; 1 = focal or globular intrasubstance increased signal intensity that did not extend to the articular surface; 2 = horizontal, linear intrasubstance increased signal intensity that extended from periphery of the meniscus but did not involve an articular surface; and 3 = increased signal intensity communicating or extending to at least one articular surface [7]. Ligamental changes were evaluated as no tear, partial tear, and complete tear.

All images were assessed in a joint reading by three of the authors, and a consensus interpretation was reached. Twenty sets of radiographs; axial and reformatted coronal and sagittal CT scans; and axial, coronal, and sagittal MR images were interpreted in random patient sequence. First, 20 sets of radiographic films were interpreted, and the scoring forms were collected by another author. After 2 weeks, 20 sets of CT films were interpreted by the same readers. The readers had no knowledge of the radiographic scoring forms. Two weeks after the CT evaluation, MR images were interpreted by using the same method.

Statistical Analysis

Rank-order correlations were calculated by using Kendall's tau (τ) for pairwise combinations: radiography vs CT, radiography vs MR, CT vs MR. Four diagnostic parameters were compared among the techniques. Kendall's correlation coefficients (τ) were corrected for "ties" before the p values were obtained [16]. The null hypothesis was rejected at the 95% or 99% confidence level, and p values of .05 or less and .01 or less, respectively, were considered significant.

Results

Cartilage Loss

Bicompartmental cartilage loss was seen frequently on radiographs (12 knees) and on CT (14 knees). On MR, however, tricompartmental cartilage loss predominated (nine knees) (Fig. 1). This discrepancy was caused by cartilage loss in the lateral compartment, which was detected by MR imaging but not by radiography and CT (Fig. 1).

In the medial compartment, the occurrence rate of grade 3 cartilage loss was higher on both radiography and MR (nine knees, 45%, each) than on CT (three knees, 15%; Table 1). In the lateral compartment, the overall occurrence rate of cartilage loss on MR (12 knees, 60%) was markedly greater than that on radiography (seven knees, 35%) and CT (five knees, 25%; Fig. 2). In the patellofemoral compartment, all techniques showed a similar occurrence rate and severity of cartilage loss (Table 1, Fig. 3).

The correlation between radiography and CT reached statistical significance in the lateral ($\tau = 0.5836$, $p = .0003$) and patellofemoral ($\tau = 0.5487$, $p = .0007$) compartments. Similarly, in the lateral and patellofemoral compartments, correlation between CT and MR was also significant ($\tau = 0.3711$, $p = .0222$ and $\tau = 0.3987$, $p = .014$, respectively), although it was not as strong as that between radiography and CT. The correlation between radiography and MR was statistically significant in the medial ($\tau = 0.7142$, $p = .0001$) and lateral compartments ($\tau = 0.4004$, $p = .0136$).

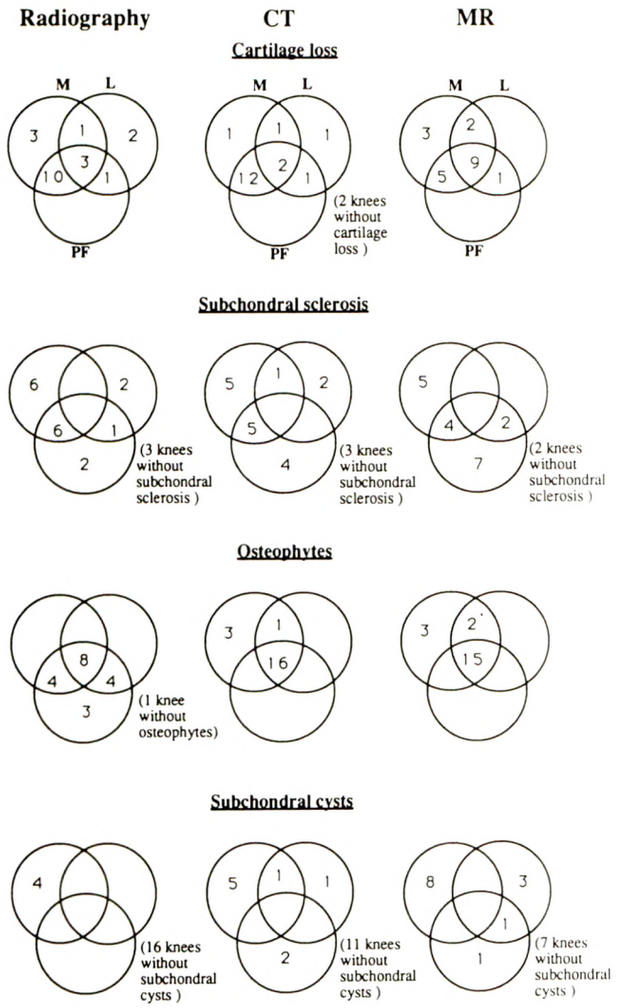


Fig. 1.—Compartmental distribution of changes in knee as determined by radiography, CT, and MR in 20 patients with osteoarthritis of the knee. Overlapping portions of circles indicate number of knees in which more than one compartment was abnormal. Note that for cartilage loss, MR imaging frequently shows tricompartmental involvement when radiography and CT show primarily bicompartmental disease. Similarly, in detecting osteophytes, both CT and MR show tricompartmental involvement more often than radiography does. Unicompartmental distribution predominates for both subchondral sclerosis and subchondral cysts. M = medial compartment, L = lateral compartment, PF = patellofemoral compartment.

Subchondral Sclerosis

Unicompartmental subchondral sclerosis was seen frequently on radiography (10 knees), CT (11 knees), and MR (12 knees; Figs. 1 and 4). In the medial and lateral compartments, both radiography and CT showed a higher occurrence rate of subchondral sclerosis than MR did. In the patellofemoral compartment, subchondral sclerosis was observed more frequently on MR (13 knees, 65%) than on radiography (nine knees, 45%) and on CT (nine knees, 45%; Table 1).

The correlation between radiography and CT, radiography and MR, and CT and MR was statistically significant ($p \leq .05$) for subchondral sclerosis in all compartments.

Osteophytes

With radiography, both bicompartmental and tricompartmental osteophytosis was observed frequently (eight knees). With CT and MR imaging, however, tricompartmental osteophytosis predominated (16 and 15 knees, respectively; Figs. 1 and 5).

In the medial compartment, both CT and MR showed a markedly higher occurrence rate (20 knees, 100%) of osteophytes than radiography did (12 knees, 60%). In the lateral compartment, the occurrence rate of osteophytes on CT and MR (17 knees, 85%) was also greater than on radiography (12 knees, 60%). In the patellofemoral compartment, however, radiography showed a higher occurrence rate (19 knees, 95%) of osteophytes than CT (16 knees, 80%) and MR (15 knees, 75%) did (Table 1).

The correlation between radiography and CT, radiography and MR, and CT and MR was statistically significant ($p \leq .05$) for osteophytes in all compartments.

Subchondral Cysts

Unicompartmental formation of subchondral cysts was observed frequently on radiography (four knees), CT (eight knees), and MR (12 knees; Fig. 1). In all compartments, both CT and MR showed a higher occurrence rate of subchondral cysts than radiography did (Table 1, Fig. 6).

The correlation between CT and MR was statistically significant for subchondral cysts in the medial ($\tau = 0.7445$, $p = .0001$) and the patellofemoral compartments ($\tau = 0.9864$, $p = .0001$).

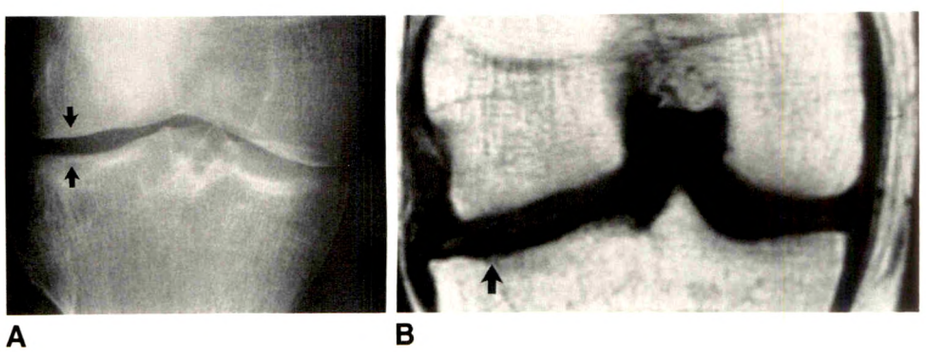


Fig. 2.—*A*, Conventional radiograph of knee shows mild widening of joint space in lateral compartment (*arrows*). *B*, MR image (SE 600/20) shows focal grade 3 cartilage defect in lateral compartment (*arrow*). Note that width of joint space in *A* does not provide accurate information on cartilage loss.

TABLE 1: Occurrence Rates and Severity of Osteoarthritic Changes on Radiographs (RG), CT Scans, and MR Images of the Knee in 20 Patients

Grade	Medial			Lateral			Patellofemoral		
	RG	CT	MR	RG	CT	MR	RG	CT	MR
Cartilage loss									
0	3	4	1	13	15	8	6	5	5
1	4	5	3	3	1	2	3	7	5
2	4	8	7	2	2	4	8	4	6
3	9	3	9	2	2	6	3	4	4
Subchondral sclerosis									
0	8	9	11	17	17	18	11	11	7
1	10	7	3	1	3	0	6	5	11
2	1	4	5	2	0	2	2	3	0
3	1	0	1	0	0	0	1	1	2
Osteophytes									
0	8	0	0	8	3	3	1	4	5
1	5	10	10	4	9	6	9	8	7
2	3	3	3	2	5	6	4	5	4
3	4	7	7	6	3	5	6	3	4
Subchondral cysts									
0	16	14	12	20	18	16	20	18	18
1	3	5	5	0	1	3	0	1	0
2	1	1	3	0	1	1	0	1	2
3	0	0	0	0	0	0	0	0	0

Meniscal Abnormalities

In the anterior horn of the medial meniscus, MR showed grade 1 meniscal pathologic changes in three patients, grade 2 changes in one, and grade 3 changes in 16. In the posterior horn of the medial meniscus, grade 1 changes were seen in one knee and grade 3 changes in 19 knees (Fig. 7).

In the lateral meniscus, grade 1, 2, and 3 changes in the anterior horn were shown in four, six, and 10 knees, respectively. In the posterior horn of the lateral meniscus, grade 1 changes were shown in two knees, grade 2 changes in three, and grade 3 changes in 15.

Ligamentous Changes

For the anterior cruciate ligament, MR showed no tears in 10 knees, partial tears in three, and complete tears in seven. For the posterior cruciate ligament, partial tears were found in two knees and a complete tear in one knee. No tears were detected in the medial or lateral collateral ligaments.

Discussion

Osteoarthritis is characterized pathologically by cartilage loss, subchondral sclerosis and cyst formation, and osteo-

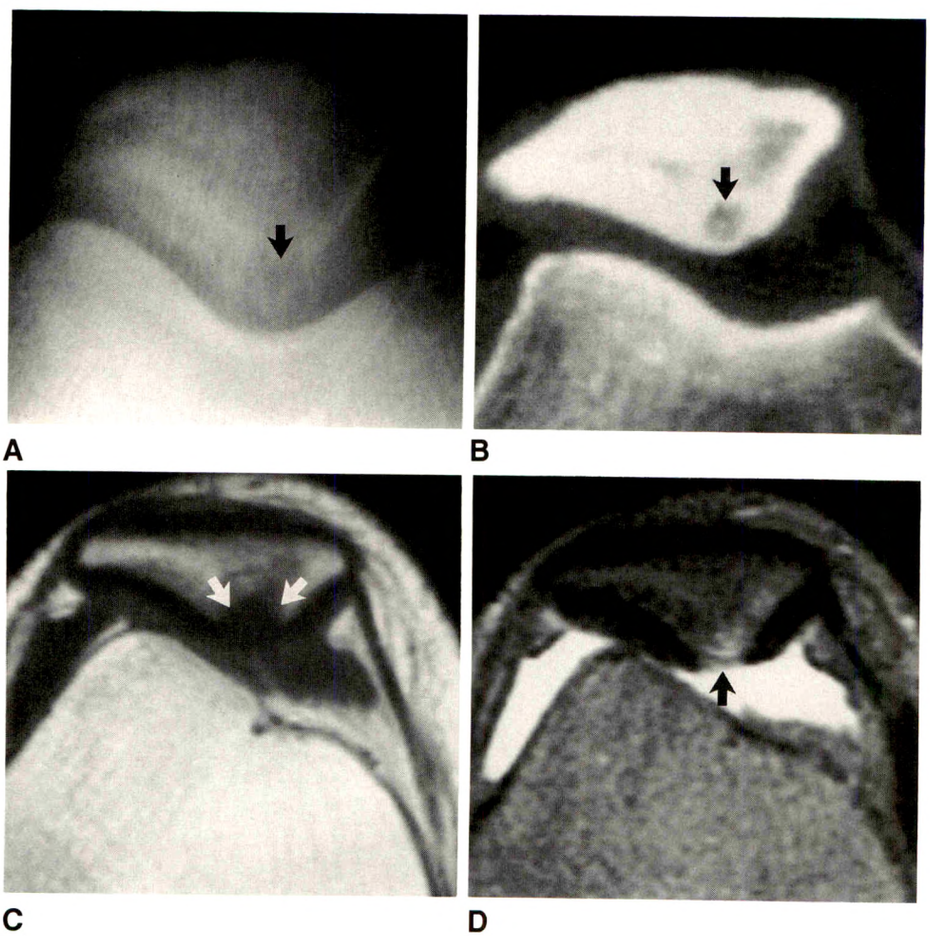


Fig. 3.—*A*, Conventional radiograph (sunrise patellar projection) of knee does not show joint-space narrowing in patellofemoral compartment. Note incidental small, radiolucent area at apex of patella (*arrow*).

***B*, Axial CT scan shows thickness of cartilage is difficult to evaluate on CT. Note small cyst at patellar apex (*arrow*).**

***C* and *D*, T1-weighted (*C*, SE 600/20) and T2-weighted (*D*, SE 2000/60) MR images. On T2-weighting (*D*), cartilage denudation and grade 3 cartilage loss at patellar apex are shown (*arrow*), which cannot be detected on radiography and CT. Note, small cyst at patellar apex is seen as low-intensity area on T1-weighted image (*arrows* in *C*).**

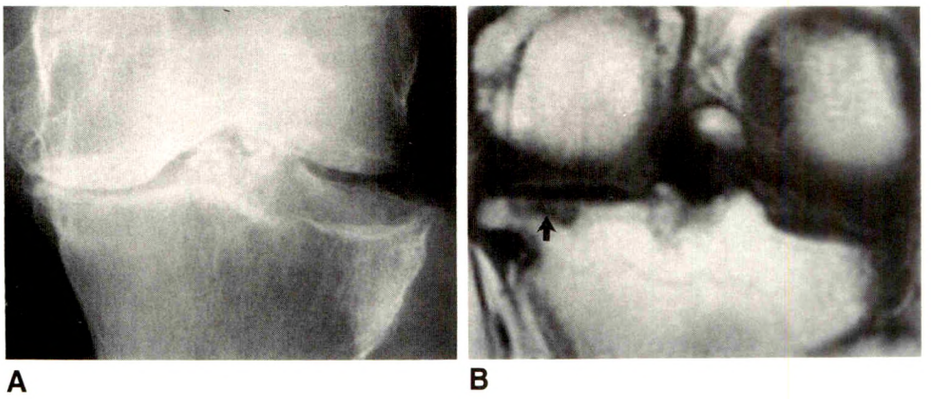


Fig. 4.—*A*, Conventional radiograph shows subchondral sclerosis, narrowing of joint space, and osteophytosis.
B, MR image (SE 600/20) shows subchondral sclerosis as an area of low signal intensity (*arrow*) in medial compartment extending into high-signal-intensity marrow space.

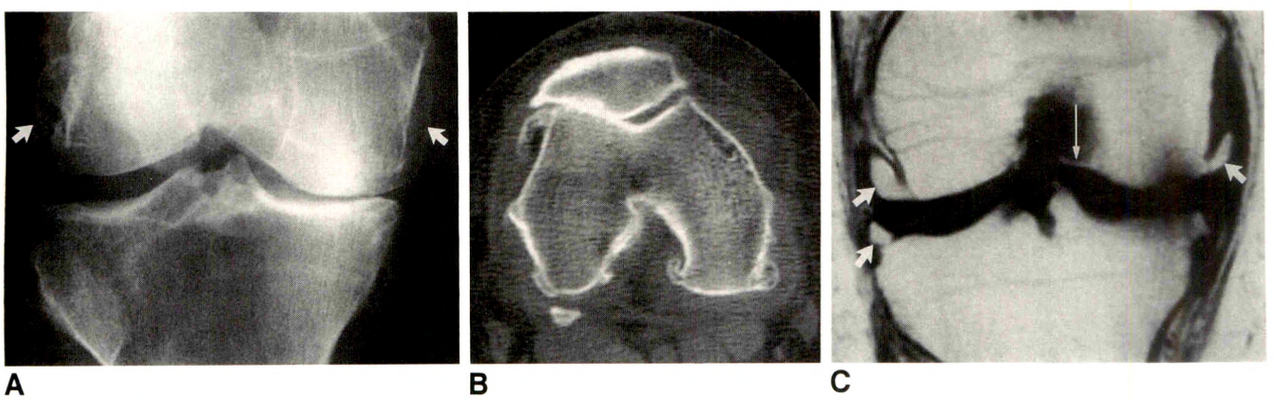


Fig. 5.—*A*, Conventional radiograph shows formation of osteophytes (*arrows*) in medial and lateral compartments.
B, CT scan shows marked osteophytosis in both medial and lateral compartments. Osteophytosis is particularly accentuated in posterior femoral condyles.
C, MR image (SE 600/20) confirms advanced osteophytosis in medial and lateral femoral condyles and in tibial plateau (*thick arrows*). Note beaklike intercondylar osteophyte (*thin arrow*) at medial femoral condyle, which was not detected by radiography.

phytosis [1–5]. Radiography has been the primary method for monitoring the progression of these changes in the knee [17]. Unfortunately, osteoarthritic changes may not be detected on radiographs until late in the disease. The use of radiography is limited in clinical drug trials designed to assess the influence of therapies on the progression of osteoarthritis. Similar to previous animal studies [3], the results of our in vivo investigation in humans indicate that MR imaging is more sensitive than radiography and CT for detecting osteoarthritic joint changes and is unique for assessing soft-tissue changes related to osteoarthritis.

Cartilage

Cartilage loss appeared frequently and to a severe degree in the medial compartment (Table 1). The occurrence rate of grade 3 medial cartilage loss was markedly lower on CT than that observed on radiography and MR (Table 1). With radiography, cartilage is assessed indirectly by evaluating the width of the joint space on weight-bearing projections [1, 2, 14]. With MR, the cartilage is evaluated directly. Cartilage appears as an intermediate to high-signal-intensity line next to the low-intensity subchondral bone [3, 12, 13]. CT does not provide a direct assessment of cartilage [18] because soft-tissue contrast is not as great as that seen on MR. CT also is limited in the accurate evaluation of the width of the joint space as an indirect sign of cartilage thickness because the patient is not in weight-bearing position during the study. These differences may explain the lower sensitivity of CT compared with radiography and MR in detecting cartilage loss.

In the lateral compartment, MR was more sensitive than radiography or CT in showing cartilage loss (Table 1). Our MR findings correspond with pathologic studies that report abnormal cartilage not only in the medial but also in the lateral compartments of the knees of patients with osteoarthritis [1, 2]. Radiography primarily detects cartilage loss in the medial compartment. This may be because cartilage loss in the medial compartment causes the lateral joint space to open 1–2 mm as weight is shifted medially [14]. Joint-space widening in the lateral compartment as seen on radiographs, therefore, does not necessarily reflect the actual thickness of the cartilage (Fig. 2). This may account for the lower frequency and severity of cartilage loss in the lateral compartment

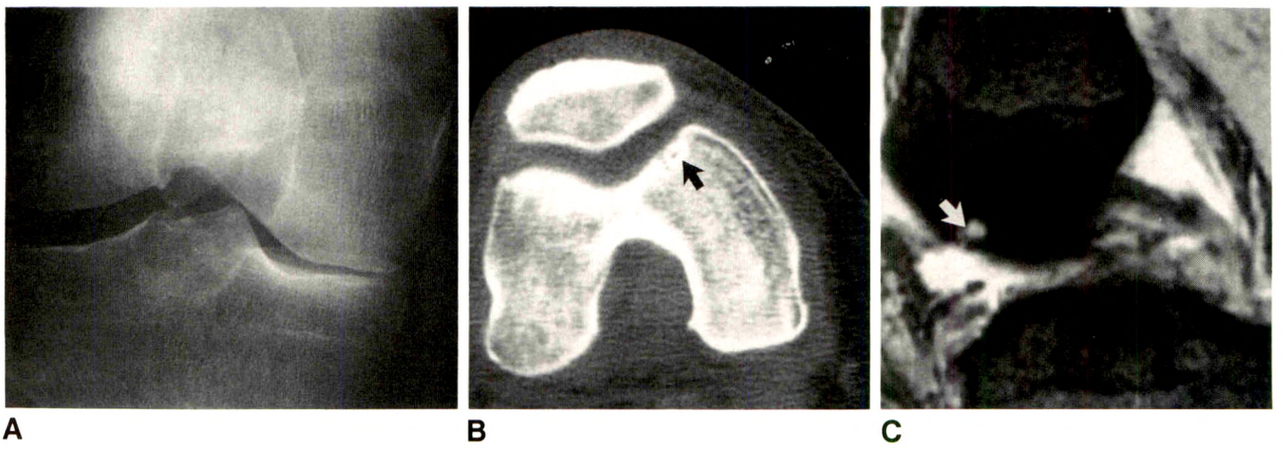


Fig. 6.—*A*, Conventional radiograph does not show any signs of subchondral cyst formation.
B, CT scan shows a small subchondral cyst (*arrow*) in medial femoral condyle, which is surrounded by a thin sclerotic halo.
C, On T2*-weighted gradient-echo MR image (600/30/30°), subchondral cyst (*arrow*) has high signal intensity. Cyst can be differentiated easily from surrounding normal marrow, which has low signal intensity.

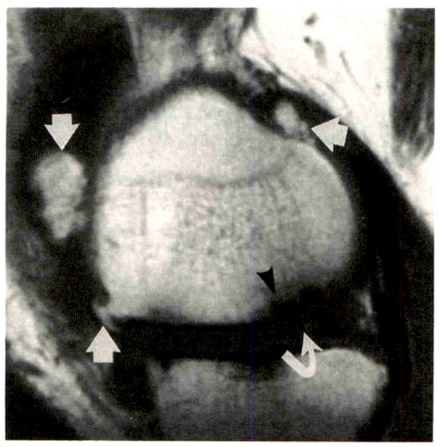


Fig. 7.—MR image (SE 600/20) shows marked osteophytosis (*straight arrows*) and subchondral sclerosis (*arrowhead*) corresponding to osteoarthritic changes. Posterior horn of medial meniscus has a grade 3 tear with maceration (*curved arrow*).

discernible on radiography, and it also may explain the higher occurrence rate of tricompartmental cartilage loss on MR compared with radiography (Fig. 1).

Detection of cartilage loss in the lateral compartment on MR imaging may have a direct impact on surgical treatment. Among patients in whom radiography showed cartilage loss only in the medial compartment, a unicompartmental prosthetic device has been used in many centers for surgical treatment [19]. However, when cartilage loss is detected in both the medial and lateral compartments on MR imaging, a total knee joint prosthesis appears preferable [20].

Subchondral Sclerosis

Radiography and CT show subchondral sclerosis as areas of increased density and attenuation. On MR, these areas of increased bone density have low signal intensity on all sequences because of the lack of resonating protons. Because both subchondral sclerosis and subchondral bone are characterized by low signal intensity, delineation of sclerotic regions that were located immediately adjacent to the subchondral bone was sometimes difficult on MR. This may explain why MR had less sensitivity than radiography and CT in detecting early grade 1 subchondral sclerosis (Table 1). However, once sclerotic areas extended deeper from the joint margin into the high-signal-intensity marrow cavity on T1-weighted images, detection was facilitated on MR (Fig. 4). Because marrow fat has a short T1-relaxation time and resultant high signal intensity on short TR/TE sequences, detection of low-intensity sclerotic areas within the bone marrow was best on these imaging sequences.

In the patellofemoral compartment, radiography and CT were limited for assessing subchondral sclerosis. Osteophytes that project over the patellofemoral compartment and overlapping parts of the patella and femur may make radiographic evaluation of this area difficult [1].

Osteophytes

Osteophytosis is thought to be a reparative response associated with early osteoarthritis [5]. Osteophytes were the most prevalent CT and MR abnormalities. This suggests that osteophytosis is a valuable diagnostic sign for osteoarthritis of the knee. Osteophytes were not detected on radiographs in eight knees (40%) in the medial compartment and in eight knees (40%) in the lateral compartment. In many cases, osteophytes were overlapped by adjacent anterior and posterior bony structures evident on radiographs (Fig. 5).

Osteophytosis appeared frequently and to a severe degree in the posterior femoral condyle of the medial compartment. When osteophytes were present in only one condyle, it was almost always the posterior medial femoral condyle. This suggests that osteophytosis of the knee may begin at this site [15]. A small osteophyte in that location usually remains undetected on radiography, but it is detected easily on transaxial CT and MR (Fig. 5), indicating that tomographic, thin-section imaging techniques with multiplanar imaging capability significantly improve the diagnostic sensitivity.

Interestingly, in the patellofemoral compartment, CT and MR were less sensitive than radiography (Table 1). On radiography, the lateral projection provided more information for detecting osteophytes than the sunrise patellar projection did. Osteophytes usually were found in the superior and inferior margins of the patellar facets on lateral radiographs. Sagittal CT reformations and sagittal MR images were difficult to evaluate for the presence of osteophytes in the patella. This may be due to the lower spatial resolution of CT in the reformatted sagittal plane as compared with the original axial plane. In addition, a prominent partial volume effect in the sagittal plane on both CT and MR may contribute to the difficulties in interpretation.

Subchondral Cysts

Subchondral cysts result from focal bone resorption in an area of high intraarticular pressure that is frequently associated with cartilage loss [5]. In all imaging techniques, subchondral cysts were shown most often in the medial compartment (Table 1). On radiographs, subchondral cysts frequently were missed. This may be related to local osteopenia or sparse trabeculae producing radiolucent areas below the articular surface and thereby obscuring the cysts. Many small subchondral cysts were detected by CT and MR because of the techniques' tomographic nature and multiplanar imaging capability.

The value of MR imaging was enhanced further by using T2*-weighted gradient-echo sequences (Fig. 6). Subchondral cysts showed high signal intensity when these pulse sequences were used, and differentiation from adjacent low-signal-intensity normal marrow and subchondral bone was good (Fig. 6). The high signal intensity of subchondral cysts on this imaging sequence may be caused by joint fluid filling the defect. The low signal intensity of the surrounding normal marrow may be related to inhomogeneous magnetic susceptibility at the interface of bone marrow and trabecular bone [21].

In some cases, MR showed the synovial fluid tract leading to the cysts (Fig. 6). This correlates with the hypothesis by Freund that intrusion of synovial fluid is an important pathogenetic factor in the formation of subchondral cysts [5].

Meniscal Abnormalities

MR showed a high prevalence of meniscal degeneration (Fig. 7) in osteoarthritis, similar to findings in earlier animal studies [3]. This suggests a strong relationship between meniscal abnormalities and degenerative joint disease. In the standing adult, the weight-bearing line normally passes from the center of femoral head through the center of both knees and ankles. Any condition that leads to angular deformity will result in a shift of force per unit area in the knee [5]. A varus angulation of the knee, for example, will increase the weight-bearing load across the medial compartment, thereby intensifying the biomechanical stress on the cartilage there [1, 5]. In our study, degeneration of the medial meniscus was seen more often than lateral meniscal degeneration. This may explain the frequent finding of varus deformity seen in osteoarthritis of the knee. Further studies including pathologic-anatomic correlation are needed to determine whether meniscal degeneration is (1) the underlying pathogenetic principle of osteoarthritis or (2) a result of changes in the joint related to osteoarthritis.

Ligaments

The prevalence of tears of the anterior cruciate ligament (10 knees) on MR imaging was greater than that of tears of the posterior cruciate ligament (three knees). Tears and resultant insufficiency of the anterior cruciate ligament are known to cause osteoarthritic changes in the affected knee [22]. Anterior cruciate ligament tears frequently were associated with medial compartmental disease. This association may result from increased mechanical stresses in the medial compartment of the unstable knee.

Study Limitations

Our investigation was limited by the relatively small number of patients. Study of larger populations is desirable to determine the prevalence of osteoarthritic changes for each technique more precisely. Arthroscopic or surgical confirmation of the imaging results was not available in any of the patients. The high diagnostic yield of MR imaging in detecting osteoarthritic changes may be limited, therefore, by false-positive and false-negative results that cannot be reliably excluded in the absence of a gold standard. However, surgery and arthroscopy could not be performed in our volunteer subjects because of the invasiveness of the procedures. In addition, surgery and arthroscopy can be used as a gold standard for cartilage loss, osteophytosis, and meniscal and ligamentous disorders only. Subchondral cysts and subchondral sclerosis as well as grade 1 and 2 meniscal degeneration cannot be detected arthroscopically and surgically. With respect to cartilage loss and soft-tissue changes, previous studies have emphasized the high correlation between MR and arthroscopy [3, 6–8, 11–13].

Our data may overestimate the sensitivity of radiography for detecting osteoarthritic changes, because patients were selected on the basis of both clinical and radiologic findings. However, the clinician responsible for the selection of patients was not involved in the interpretation of the different imaging studies. The sensitivity of radiography in detecting intercondylar changes, in turn, may be improved when tunnel views are added. In general, better results on radiographs can be

expected when additional projections are obtained to supplement the standard views.

Conclusions

On the basis of this preliminary cross-sectional investigation, MR imaging is more sensitive than conventional radiography and CT in showing the joint changes caused by osteoarthritis. We conclude the following: (1) MR frequently detects tricompartmental disease when radiography and CT show only bicompartmental involvement. (2) The finding of normal joint spaces on radiographs does not exclude cartilage loss, which can be shown by MR. (3) Osteoarthritis frequently is associated with meniscal pathologic changes and tears of the anterior cruciate ligament. Both may be contributing causes of osteoarthritis. MR imaging is the only noninvasive diagnostic tool that can be used to evaluate meniscal and ligamentous abnormalities related to osteoarthritis. (4) MR is a sensitive tool for detecting early osteoarthritic changes. MR appears to be particularly useful for noninvasive longitudinal monitoring of osteoarthritis in studies that assess the efficacy of treatments for osteoarthritis.

REFERENCES

1. Ahlback S. Osteoarthritis of the knee: a radiographic investigation. *Acta Radiol Suppl* (Stockh) **1968**;277:7–72
2. Thomas RH, Resnick D, Alazraki NP, Daniel D, Greenfield R. Compartmental evaluation of osteoarthritis of the knee: comparative study of available diagnostic modalities. *Radiology* **1975**;116:585–594
3. Sabiston CP, Adams ME, Li DKB. Magnetic resonance imaging of osteoarthritis: correlation with gross pathology using an experimental model. *J Orthop Res* **1987**;5:164–172
4. Pataki A, Fries R, Ochsner K, Witzemann E. Qualitative radiographic diagnosis of osteoarthritis of the knee joint in the C57BL mouse. *Agents Actions* **1987**;22:123–130
5. Resnick D, Niwayama G. Degenerative disease. In: Resnick D, Niwayama G, eds. *Diagnosis of bone and joint disorders*, 2nd ed. Philadelphia: Saunders, **1988**:1442–1458
6. Braunstein EM, Brandt KD, Albrecht M. MRI demonstration of hypertrophic articular cartilage repair in osteoarthritis. *Skeletal Radiol* **1990**;19:335–339
7. Stoller DW, Martin C, Crues JV III, Kaplan L, Mink JH. Meniscal tears: pathologic correlation with MR imaging. *Radiology* **1987**;164:731–735
8. Crues JV III, Mink JH, Levy TL, Lotysch M, Stoller DW. Meniscal tears of the knee: accuracy of MR imaging of the knee: first 144 cases. *Radiology* **1987**;164:445–448
9. Reicher MA, Rauschning W, Gold RH, et al. Magnetic resonance imaging of the knee joint. Clinical update I. Injuries to menisci, patellar tendon and cruciate ligaments. *Radiology* **1987**;162:547–553
10. Mink JH, Levy T, Crues JV III. Tears of the anterior cruciate ligament and menisci of the knee: MR imaging evaluation. *Radiology* **1988**;167:769–775
11. Lee JK, Yao L, Phelps CT, et al. Anterior cruciate ligament tears: MR imaging compared with arthroscopy and clinical tests. *Radiology* **1988**;166:861–864
12. Konig H, Sauter R, Deimling M, Vogt M. Cartilage disorders: comparison of spin-echo CHESS, and FLASH sequence MR images. *Radiology* **1987**;164:753–758
13. Reiser MF, Bongartz G, Erlemann R, et al. Magnetic resonance in cartilaginous lesions of the knee joint with three-dimensional gradient-echo imaging. *Skeletal Radiol* **1988**;17:465–471
14. Leach RE, Gregg T, Siber FJ. Weighted-bearing radiography in osteoarthritis of the knee. *Radiology* **1970**;97:265–268
15. Kindynis P, Haller J, Kang HS, et al. Osteophytosis of the knee: anatomic, radiographic, and pathologic investigation. *Radiology* **1990**;174:841–846
16. Kendall MG, Stuart A. *The advanced theory of statistics*, vol 2. New York: Hafner, **1967**:302–304
17. Altman RD, Fries JF, Bloch DA, et al. Radiographic assessment of progression in osteoarthritis. *Arthritis Rheum* **1987**;30:1214–1225
18. Hernandez RJ, Poznanski AK. CT evaluation of pediatric hip disorders. *Orthop Clin North Am* **1985**;16:513–542
19. Macintosh DL. Hemiarthroplasty of the knee using a space occupying prosthesis for painful varus and valgus deformities. *J Bone Joint Surg [Br]* **1958**;48-B:1431–1435
20. Goldberg VM, Figgie MP, Figgie HE III, Heiple KG, Sobel M. Use of a total condylar knee prosthesis for treatment of osteoarthritis and rheumatoid arthritis. *J Bone Joint Surg [Am]* **1988**;70-A:802–811
21. Davis CA, Genant HK, Dunham JS. The effects of bone on proton NMR relaxation times of surrounding liquids. *Invest Radiol* **1986**;21:472–477
22. Kannus P, Jarvinen M. Posttraumatic anterior cruciate ligament insufficiency as a cause of osteoarthritis in a knee joint. *Clin Rheumatol* **1989**;8:251–260

Diagnosis of Osteomyelitis in the Presence of Soft-Tissue Infection and Radiologic Evidence of Osseous Abnormalities: Value of Leukocyte Scintigraphy

Arnold F. Jacobson[1,2]
John D. Harley[2,3]
Benjamin A. Lipsky[4]
Roger E. Pecoraro[4]

To evaluate the usefulness of ^{111}In-leukocyte scintigraphy for identifying osteomyelitis in the presence of soft-tissue infection, we prospectively studied 45 bone sites adjacent to soft-tissue infection in patients with abnormal findings on radiographs and ^{99m}Tc bone scans that were suggestive of osteomyelitis. ^{111}In-leukocyte scans were analyzed in terms of the intensity of abnormal uptake and its location relative to bone. The diagnosis of osteomyelitis was established from results of percutaneous bone biopsy culture (n = 35), histologic examination of surgical specimens (n = 8), and clinical follow-up (n = 2). Osteomyelitis was present at 22 sites, including 16 of 18 sites with increased leukocyte uptake in bone, resulting in a sensitivity of 73%, specificity of 91%, and positive predictive value of 89% for this finding. Osteomyelitis was present at four of 17 sites with predominantly soft-tissue localization of leukocyte activity in the region of bone, none of seven sites with normal leukocyte scans, and two of three sites with diminished leukocyte uptake in bone. Although not helpful in distinguishing infectious from noninfectious bone abnormalities, 3- and especially 24-hr bone scans viewed in conjunction with leukocyte studies provided important correlation to aid in estimating the location of focal abnormal leukocyte uptake.

The finding of soft-tissue infection with increased uptake of labeled leukocytes that extends to involve adjacent bone strongly suggests concurrent osteomyelitis. When the presence of abnormal leukocyte uptake in bone is uncertain, additional imaging and possibly biopsy may be required to establish or exclude the diagnosis of osteomyelitis.

AJR 157:807–812, October 1991

Noninvasive confirmation of the presence of osteomyelitis in bone contiguous to an area of soft-tissue infection is often difficult [1, 2]. Bone radiography and ^{99m}Tc bone scintigraphy are commonly used to evaluate sites of suspected osteomyelitis, but findings with both techniques are often nonspecific [3–7]. Scintigraphy with ^{67}Ga-citrate [3, 8, 9] and ^{111}In-labeled leukocytes [3, 7, 9–13] improves specificity for diagnosis of osteomyelitis, with leukocytes also showing high sensitivity in recent reports [7, 12, 13]. Studies comparing the radiographic and scintigraphic techniques used to identify osteomyelitis are numerous [3–17]. However, few previous studies were done prospectively, included imaging of all patients with all techniques under consideration, and had the presence or absence of osteomyelitis confirmed microbiologically or histologically in most of their cases [13, 14, 16].

To clarify the usefulness of leukocyte scintigraphy for detecting osteomyelitis in patients with concurrent soft-tissue infection, we prospectively studied a consecutive series of patients in whom abnormal findings on plain radiographs and ^{99m}Tc bone scans were suggestive of osteomyelitis. ^{111}In-leukocyte scans were obtained, followed as appropriate by percutaneous needle biopsy or surgical excision and clinical follow-up in all cases to establish the diagnosis.

Subjects and Methods

During a 3-year interval, 50 patients with 52 plain radiographs with findings suggestive of osteomyelitis (focal bone destruction or osteopenia, cortical disruption, or periosteal reaction)

Received January 22, 1991; accepted after revision May 29, 1991.

This work was supported by the Veterans Health Services and Research Administration of the Department of Veterans Affairs.

[1] Department of Nuclear Medicine Section (115), Department of Veterans Affairs Medical Center, 1660 S. Columbian Way, Seattle, WA 98108. Address reprint requests to A. F. Jacobson.

[2] Department of Radiology, University of Washington Medical Center, Seattle, WA 98195.

[3] Department of Radiology, Department of Veterans Affairs Medical Center, Seattle, WA 98108.

[4] Department of Medical Service, Department of Veterans Affairs Medical Center, Seattle, WA 98108, and Department of Medicine, University of Washington Medical Center, Seattle, WA 98195.

0361–803X/91/1574–0807
©American Roentgen Ray Society

were prospectively identified for possible participation in this study. ^{99m}Tc bone scintigraphy was performed first, and if findings were abnormal, leukocyte scintigraphy and percutaneous needle biopsy were scheduled. Three patients who did not have leukocyte scintigraphy, two with normal findings on bone scans, and one not studied because of scheduling difficulties were excluded. Of the remaining 48 patients (49 sites), 44 patients with 45 sites associated with clinically apparent soft-tissue infections were included in the study.

Forty-four men 28–79 years old (mean, 62 years) were studied. Thirty-six had diabetes, one of whom was studied on two separate occasions for suspected osteomyelitis at different locations in the same foot. All studies were performed in conjunction with protocols approved by the University of Washington Human Subjects Review Board, and informed consent was obtained for all patients. Osteomyelitis was clinically suspected on the basis of abnormal radiographic findings and either a recently developed soft-tissue infection (n = 13) or a chronic or recurrent soft-tissue ulcer, abscess, or draining sinus (n = 32). Radiographic findings alone were not considered sufficient to establish the diagnosis of osteomyelitis in the majority of cases. Sites of suspected involvement were foot, 37; ankle, two; fibula, one; femur, one; pelvis, three; and hand, one. Patients had received at most only short regimens (<2 weeks) of antibiotic therapy immediately before being studied, but none was currently taking antibiotics at the time of either leukocyte scintigraphy or bone biopsy.

All patients had three- or four-phase bone scans after injection with 925–1110 MBq (25–30 mCi) of ^{99m}Tc-methylene diphosphonate. Imaging was done with a large-field-of-view gamma camera equipped with a low-energy high-resolution collimator. All studies included dynamic 4-sec/frame flow imaging over the area in question, followed by blood-pool images 5–10 min after injection and delayed static imaging 3–4 hr after injection. Delayed images at 24 hr were obtained in 41 studies to provide better bone localization with decreased soft-tissue activity. The 3-hr images were typically acquired for 250,000–600,000 counts, 24-hr images for 50,000–100,000 counts.

Leukocytes were labeled with 18.5–37.0 MBq (0.5–1.0 mCi) of ^{111}In-oxine by using the methods previously described [18, 19]. In most cases, leukocyte labeling was done either on the same day as the bone scan, with cells reinjected after 3-hr bone imaging (n = 31), or on the day after 24-hr bone imaging (n = 11). Imaging was performed 18–24 hr after reinjection of the labeled cells by using a large-field-of-view gamma camera equipped with a medium-energy collimator and dual 20% energy windows for the 173- and 247-keV ^{111}In photopeaks. Images were typically acquired for 200,000 counts or 10 min, whichever occurred first. When leukocyte imaging was done immediately after 24-hr bone imaging, identical views were obtained sequentially without moving the patient or the gamma camera whenever possible, and a 10% window was used for the lower-energy ^{111}In photopeak to minimize the contribution of residual ^{99m}Tc activity to the ^{111}In images. On the basis of previous measurements at representative count rates, the contribution of ^{99m}Tc photons to the ^{111}In images was less than 10%. A 10% ^{99m}Tc window was used for images when significant ^{111}In downscatter was identified, primarily those in which the liver and spleen were in the field of view. The 24-hr bone images obtained on the same day as leukocyte images were acquired by using the medium-energy collimator.

All available clinical, radiographic, and scintigraphic information was used in reaching decisions concerning whether to perform percutaneous bone biopsy and the biopsy site and direction of approach. Thirty-eight bone biopsies were performed, including two at sites chosen on the basis of scintigraphic and follow-up radiographic studies rather than on the basis of the initial clinical evaluation. Of seven sites not sampled by biopsy, four had relatively unimpressive bone radiographs and bone scans and normal or equivocal leukocyte images, and three were presumptively treated for osteomyelitis.

Percutaneous bone biopsy was performed under fluoroscopic guidance with a 17-gauge Ostycut needle (Bard/Angiomed, Bard Urological Division, Covington, GA). The needle path was chosen to avoid traversing infected soft tissues. Specimens were submitted for aerobic and anaerobic culture. For small bones, only a single pass with the biopsy needle was made, which in some instances returned only an aspirate of bone. In 11 patients, in addition to specimens for culture, bone cores were obtained and submitted for histologic examination. No morbidity was associated with any of the biopsies performed. The diagnosis of osteomyelitis required either a positive bone culture or histologic findings showing both necrosis and neutrophils.

All scintigraphic studies were reviewed and scored by an experienced nuclear medicine physician without knowledge of biopsy and/or histologic results. All four phases of the bone scintigraphic images, and the leukocyte images, were scored on a five-level scale: −1 = decreased, 0 = normal, +1 = mildly increased, +2 = moderately increased, and +3 = markedly increased when compared with an adjacent or contralateral uninvolved bone site. The approach of scoring uptake relative to normal sites such as the liver or bone marrow could not be used because most studies included only images of the feet. In addition, the location of abnormal leukocyte uptake in the area of suspected osteomyelitis was rated as either definitely involving bone or predominantly involving soft tissue with bone involvement uncertain. For the purposes of this tabulation, leukocyte studies with minimal, nonfocal asymmetric uptake and abnormal focal accumulation only at sites distant from the area in question were categorized as normal (score 0).

All patients except one had clinical follow-up for a minimum of 6 months. One patient died 2 months after being studied, but an autopsy included histologic examination of the biopsy site. Twelve patients had follow-up bone and/or leukocyte scans, and 15 patients, including five who had not undergone percutaneous bone biopsy, had surgical resections or amputations of affected limbs as a result of chronic ulcers, persistent soft-tissue infections, peripheral vascular disease, or other sites of bone infection. Absence of osteomyelitis was considered confirmed if the patient had no clinical, radiologic, or histopathologic evidence of recurrence or progression at the suspected site during the follow-up interval.

Results

Of 45 sites with focal increased tracer accumulation on the 3- to 4-hr bone scan images, regional blood flow and blood pool were increased in 43 (96%). Focal increased leukocyte uptake was seen in the area of 35 (78%) of these sites, and focal decreased uptake was seen in three (7%) sites (Table 1).

Of the 38 bone biopsies, 31 were performed within 1 day of leukocyte imaging, and six others were done within 5 days. In one patient, the biopsy was done 35 days after leukocyte imaging, with a positive biopsy culture for *Staphylococcus epidermidis* obtained after conservative local care and antibiotic therapy had not produced improvement in a sacral decubitus ulcer in the region of bone. Of seven patients who did not have biopsy, two had normal leukocyte scans, two had increased leukocyte uptake that did not appear to involve the bone under investigation, and three were presumptively treated for osteomyelitis on the basis of clinical, scintigraphic, and radiographic findings.

Twenty-two patients had bone infection, confirmed by bone biopsy culture in 16 (Fig. 1) and histology and/or culture of surgical specimens in six. Of these last six patients, one, who had abnormal bone and leukocyte scans (Fig. 2) but a bone biopsy culture showing no growth twice during a 4-month interval, required amputation of the involved foot 3 weeks after the second set of scans, with histologic findings of suppurative inflammation extending into bone. Two other patients with biopsy cultures showing no growth had surgical

TABLE 1: Interpretations of 45 Leukocyte Scintigraphic Studies Performed in 44 Patients

Leukocyte Uptake Score/ Location	No. of Studies	Osteomyelitis	
		Present	Absent
−1: Decreased			
Bone involvement present	3	2	1
0: Normal	7	0	7
+1: Mildly increased			
Bone involvement present	3	3	0
Soft-tissue predominance	7	3	4
+2: Moderately increased			
Bone involvement present	9	8	1
Soft-tissue predominance	9	1	8
+3: Markedly increased			
Bone involvement present	6	5	1
Soft-tissue predominance	1	0	1
Total	45	22	23

Note.—Bone involvement was defined as focal increased leukocyte activity extending into bone as visually defined in coordination with the ^{99m}Tc bone scan. Soft-tissue predominance was defined as focal increased leukocyte activity in soft-tissue without clearly visualized extension into bone.

exploration of foot wounds within 1 week of the biopsies that revealed histologic evidence of osteomyelitis. One patient, whose leukocyte scan showed discrete soft-tissue uptake that did not appear to extend to bone, did not have a biopsy; 2 weeks later, the involved foot was amputated because of gangrene, with histologic examination showing widespread bone destruction. Two patients with markedly abnormal findings on bone and leukocyte scans were presumptively treated for osteomyelitis, but had surgery after this treatment produced no response. Histologic examination of specimens obtained at surgery confirmed the diagnosis of osteomyelitis.

There was no evidence of osteomyelitis during clinical follow-up of 23 suspected sites, 19 with biopsy cultures showing no growth and four that were not sampled by biopsy. Further histologic examination of seven sites (including two that had not been sampled), six after amputations and one at autopsy, revealed no evidence of osteomyelitis.

Results for diabetic and nondiabetic patients were similar, with osteomyelitis present at 18 of 37 sites in the diabetic and four of eight sites in the nondiabetic group. In light of this

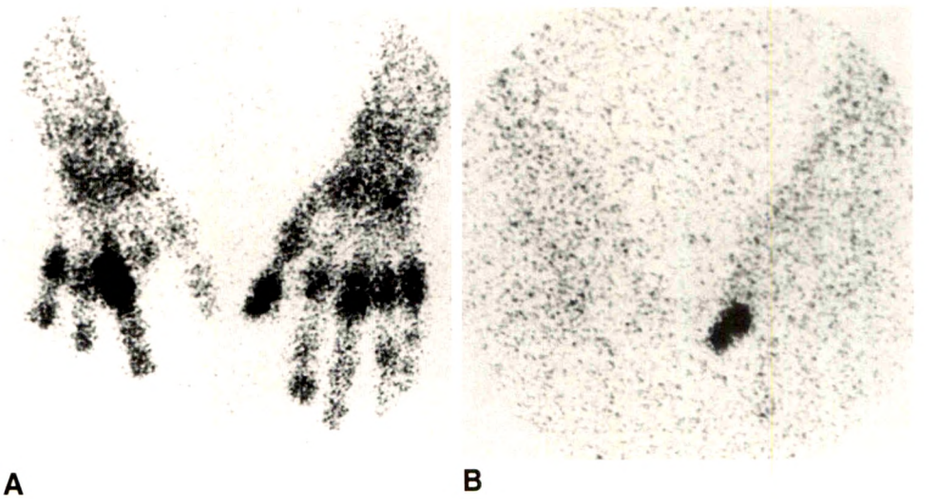


Fig. 1.—True-positive leukocyte scan and bone biopsy culture.

***A* and *B*, 24-hr bone (*A*) and leukocyte (*B*) scintigrams of hands of 56-year-old diabetic patient with draining ulcer at tip of right thumb show intense uptake in distal right first phalanx. Biopsy culture grew *Staphylococcus aureus*. Bone image shows increased uptake in multiple neuropathic joints, which do not show increased accumulation of leukocytes.**

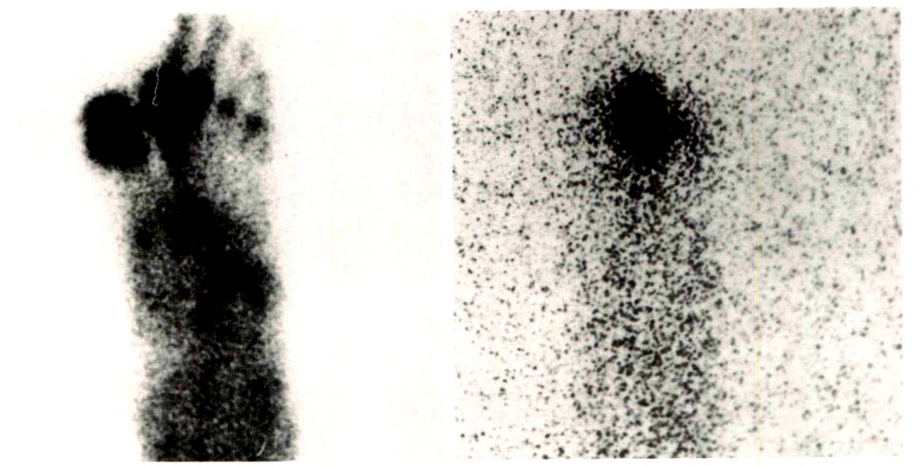


Fig. 2.—True-positive leukocyte scan; false-negative bone biopsy culture.

***A* and *B*, Bone (*A*) and leukocyte (*B*) scintigrams show intense uptake in second and third metatarsal heads. Biopsies on two occasions showed no growth, but eventual amputation because of nonhealing plantar ulcer revealed histologic evidence of bone changes consistent with chronic osteomyelitis.**

finding and the relatively small number of nondiabetic patients, the results are not subdivided in terms of the presence or absence of diabetes.

Scintigraphic Analysis

The intensity of abnormal uptake on the ^{99m}Tc bone scan was +2 or greater on the delayed images in 19 (86%) of 22 sites with and 19 (83%) of 23 sites without osteomyelitis. Increased regional blood flow did not distinguish bone infection from noninfectious processes affecting bone; two sites of osteomyelitis showed no significant increased flow, possibly as a result of impaired vascular supply, whereas all 23 abnormal scans in patients without osteomyelitis showed increased regional flow.

Among the 45 leukocyte scans, 16 (89%) of 18 studies with definite focally increased uptake in bone proved to represent osteomyelitis, whereas none of the seven patients with no significant increased uptake at the sites in question had osteomyelitis (Table 1). Of the two patients with +2 or greater false-positive leukocyte uptake, one had a large ulcer of the heel with apparent extensive bony reaction in the adjacent calcaneus but no osteomyelitis (Fig. 3), and the other received 6 weeks of antibiotic therapy despite a biopsy culture with no growth. Follow-up leukocyte scanning in the latter patient showed significantly less increased uptake, and rebiopsy of the bone in question resulted in negative cultures for infection.

Sites with mildly increased (+1) leukocyte uptake with uncertain bone involvement, and those with decreased (−1) activity compared with expected normal marrow uptake, showed intermediate prevalence of osteomyelitis. Of seven leukocyte scans with +1 uptake in the area of but not definitely localizable to bone, osteomyelitis was present in three cases (43%) (Table 1) (Fig. 4). Diminished leukocyte accumulation represented osteomyelitis in two of three patients.

Using the conservative criterion that only definite increased leukocyte accumulation in bone represented osteomyelitis, we found that leukocyte scintigraphy had a sensitivity of 73%, a specificity of 91%, and a positive predictive value of 89%. Classifying any study with increased leukocyte uptake in the area of suspected bone involvement as positive for osteomyelitis yielded a sensitivity of 91%, a specificity of 30%, and a positive predictive value of 57%.

Discussion

In the presence of significant soft-tissue abnormalities, particularly in the feet, scintigraphic evaluation of sites of possible bone infection can be difficult [12, 20, 21]. A normal bone scan virtually excludes osteomyelitis, but this is relatively uncommon in patients with abnormal bone radiographs. The increase in regional blood flow and equilibrium blood pool activity typically observed on three-phase bone scintigraphy is also of limited diagnostic value in the presence of soft-tissue lesions, because such hyperemia is commonly seen regardless of the extent of bone involvement. Both ^{111}In-leukocyte and ^{67}Ga-citrate scintigraphy have been used extensively in conjunction with ^{99m}Tc bone imaging to increase specificity over bone imaging alone for diagnosing osteomyelitis. In direct comparisons, labeled leukocytes have proved equivalent or superior to gallium [3, 9, 14], although it has been suggested that gallium is better than labeled leukocytes for imaging chronic infection [10]. Given that the presence of neutrophils is required for the histopathologic diagnosis of osteomyelitis, any reduction in sensitivity of leukocyte imaging for detection of chronic bone infection may merely reflect the difficulty of identifying a lesser degree of uptake than is present in an earlier, more acute stage. In addition, as patients with peripheral vascular disease and diabetes typically constitute a significant proportion of those studied for suspected osteomyelitis [10–13], decreased blood flow to the extremities and possible impaired leukocyte responsiveness probably limit the sensitivity achievable with leukocyte scintigraphy.

In our series, all patients had regional soft-tissue infection or inflammation, the majority of which had been present for more than 1 month, and at least minimal changes on bone radiographs and scintigrams. Although inclusion of only patients with abnormal bone radiographs and scans might appear to introduce significant bias into our data, abnormalities on plain radiographs are usually the initial findings that suggest osteomyelitis, a circumstance under which we found bone scans to be abnormal more than 90% of the time. In this selected but not atypical population, definite increased bone uptake of leukocytes was highly associated with osteomyelitis (16/18; 89%). Osteomyelitis was less common in the absence of such localization (6/27; 22%), but only when there was no increased leukocyte uptake anywhere in the vicinity

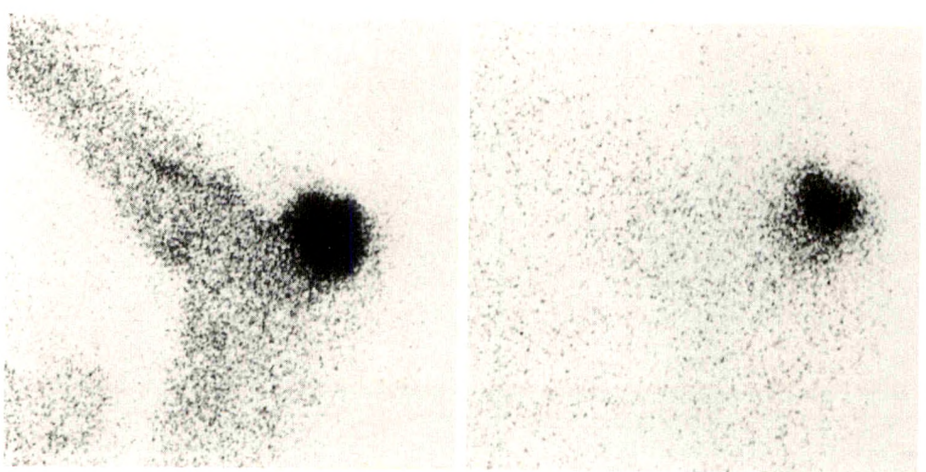


Fig. 3.—False-positive leukocyte scan; true-negative bone biopsy culture.

***A* and *B*, Lateral 24-hr bone (*A*) and leukocyte (*B*) scintigrams of foot of patient with long-standing ulcer of right heel show intense uptake in right calcaneus. Bone biopsy showed no growth. Follow-up bone and leukocyte scans after wound healing were both normal.**

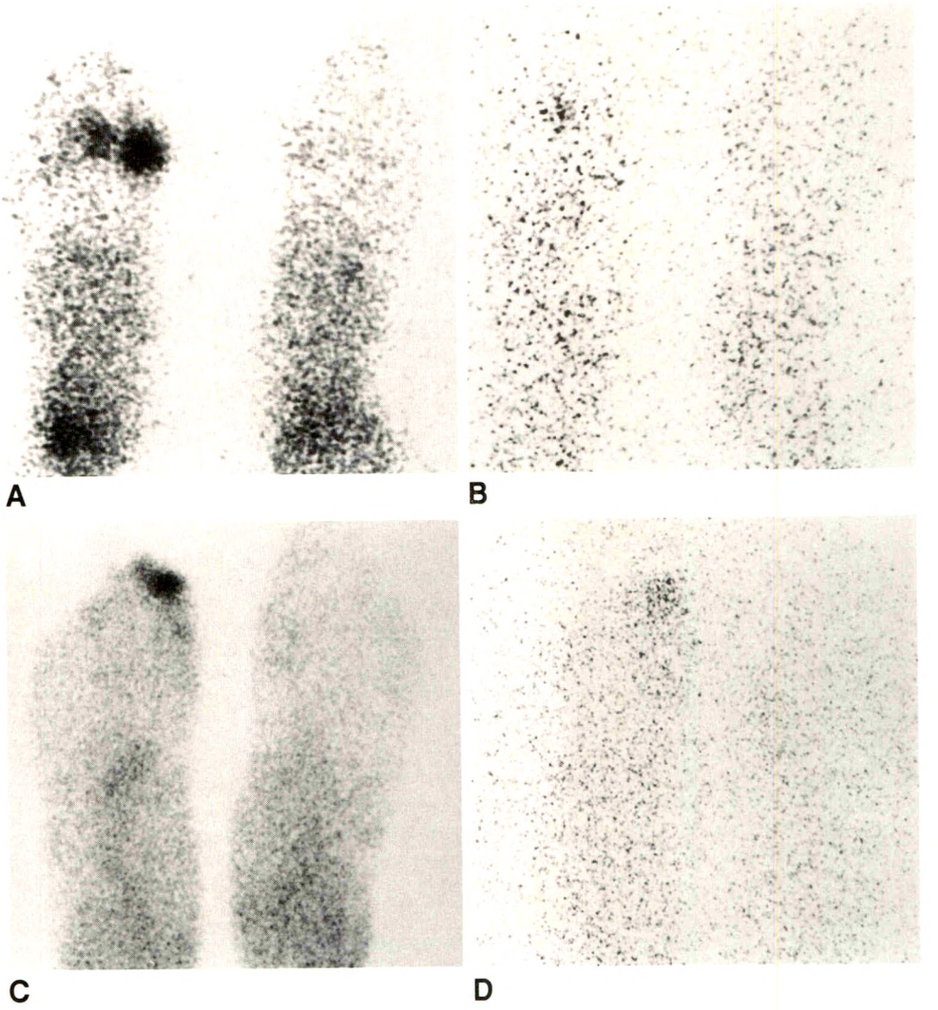


Fig. 4.—Positive and negative biopsy cultures in two patients with mildly increased leukocyte uptake, soft-tissue predominance.

A–D, Plantar scintigrams from two patients with chronic plantar foot ulcers show focally increased uptake on 24-hr (*A*) and 3-hr (*C*) bone images and mildly increased leukocyte uptake (*B* and *D*). Biopsy culture was positive for *Staphylococcus epidermidis* in right second metatarsal head (*A* and *B*) and negative for infection in right great toe (*C* and *D*).

of the site under investigation could the diagnosis of osteomyelitis be excluded with certainty. Periostisis may have been responsible for the two cases with false-positive leukocyte uptake in bone, and chronicity of infection may have contributed to false-negative findings.

The majority of persons in our series were diabetic patients with foot infections, a problematic group that has been studied extensively both retrospectively and prospectively [7, 11, 13, 21–25]. The most common sites in question were metatarsal bones adjacent to plantar ulcers ($n = 11$) and toe tufts ($n = 8$). Seven of nine metatarsal bones and six of eight toe tufts that were sampled by biopsy had negative cultures. Two metatarsals with negative cultures were shown to be infected at subsequent surgery, indicative of the limited sampling that can reduce the diagnostic accuracy of the needle biopsy technique. Nevertheless, clinical and surgical follow-up in the remaining cases indicated that the changes seen radiographically probably resulted from osteolysis of bone due to vascular insufficiency or neuropathy [24]. All phases of the bone scan were abnormal in all 13 cases with biopsies that showed no growth, whereas leukocyte scans showed no increased uptake in four and predominantly soft-tissue uptake in seven. Although noninfectious bone destruction such as that caused by neuropathic osteoarthropathy typically results in abnormalities on three-phase bone scintigraphy, increased uptake of labeled leukocytes is seen only infrequently [11, 13, 25–27].

The association of osteomyelitis and diminished bone uptake of labeled leukocytes has been observed previously [28, 29]. Both active and healed osteomyelitis can have this appearance [29], as can noninfectious processes, such as vertebral compression fractures and metastatic disease [28, 29]. Diminished leukocyte uptake reflects destruction of a site of normal marrow where labeled leukocytes would be expected to accumulate, and thus is most often observed in the spine, pelvis, and proximal femora. Biopsy may be necessary to establish the cause of such photopenic defects, although MR imaging of marrow may provide an alternative noninvasive means for further examination of such patients [30].

In our experience, bone scintigraphy is more valuable for localization of sites of bony abnormality than for diagnosis of a cause. Although 24-hr bone images frequently provide better anatomic definition than those obtained at 3 hr, no study was rated normal on the early but abnormal on the later views. The true value of the 24-hr images was in providing spatial orientation for the leukocyte images acquired serially in the identical projections. For imaging in a location with essentially no bone marrow such as the feet, it is extremely difficult to assess the extent of soft-tissue uptake of leukocytes with respect to involvement of adjacent bone. This is

particularly true when abnormal leukocyte uptake is modest (score +1) or nonfocal. Although use of a radioactive marker to outline the foot or use of a flood source to obtain a combined emission/transmission image can sometimes be helpful, the combined bone/leukocyte imaging approach remains the most readily available and convenient means to examine the relative spatial relations of sites of soft-tissue and bone infection [13, 17]. In no instance did residual ^{99m}Tc activity interfere with interpretation of ^{111}In-leukocyte images.

We found leukocyte scintigraphy somewhat less sensitive and specific than reported in several recent series [7, 11–13]. This discrepancy may in part reflect differences in characteristics of patients and diagnostic criteria. In one series with a sensitivity of 97% and specificity of 82%, only 15% of patients had soft-tissue injuries or infections [12]. In another series with a sensitivity of 100% and specificity of 83%, the diagnosis was based on examination of a bone specimen in only 43% (15/35) patients [13], compared with 96% (43/45) of our cases. In one review [7], less than half as many leukocyte scans were obtained as bone scans (46 vs 94), and in another [11], only 13 patients were studied. As noted earlier, we concur with Schauwecker et al. that sequential 24-hr bone and leukocyte imaging [17], along with leukocyte acquisitions in orthogonal planes [13], is helpful in localizing leukocyte uptake to soft tissue or bone. However, given the limited resolution of many low-count ^{111}In leukocyte images, we remain uncertain that sensitivity and specificity approaching 100% can be routinely achieved in difficult cases such as diabetic patients with foot infections and chronic noninfectious bone disease.

In summary, the presence of an active infectious process in soft tissue adjacent to bone makes it difficult to achieve both high sensitivity and specificity for the diagnosis of osteomyelitis with ^{111}In-leukocyte scintigraphy. The finding of definite increased uptake in bone on leukocyte scans has a high positive predictive value (89%) but a somewhat lower sensitivity (73%), whereas absence of increased leukocyte uptake in or near bone makes the diagnosis of osteomyelitis very unlikely. In those instances in which increased leukocyte uptake is subtle or cannot be localized exclusively to soft tissue, the diagnosis of osteomyelitis is less certain, and further imaging, such as CT [31] or MR [30], should be considered. Our experience indicates that percutaneous bone biopsy can be performed safely and without morbidity, even in the foot of the diabetic patient, so we suggest that this technique be used as necessary to confirm the findings of noninvasive imaging studies.

REFERENCES

1. Cotran RS, Kumar V, Robbins SC. The musculoskeletal system. In: Robbins SC, ed. *Pathologic basis of disease*, 4th ed. Philadelphia: Saunders, **1989**:1320–1322
2. Waldvogel FA, Papageorgion PS. Osteomyelitis: the past decade. *N Engl J Med* **1980**;303:360–370
3. Al-Sheikh W, Sfakianakis GN, Mnaymneh W, et al. Subacute and chronic bone infections: diagnosis using In-111, Ga-67 and Tc-99m MDP bone scintigraphy, and radiography. *Radiology* **1985**;155:501–506
4. Tumeh SS, Aliabadi P, Weissman BN, McNeil BJ. Disease activity in osteomyelitis: role of radiography. *Radiology* **1987**;165:781–784
5. Segall GM, Nino-Murcia M, Jacobs T, Chang K. The role of bone scan and radiography in the diagnostic evaluation of suspected pedal osteomyelitis. *Clin Nucl Med* **1989**;14:255–260
6. Yuh WTC, Corson JD, Baraniewski HM, et al. Osteomyelitis of the foot in diabetic patients: evaluation with plain film, ^{99m}Tc-MDP bone scintigraphy, and MR imaging. *AJR* **1989**;152:795–800
7. Keenan AM, Tindel NL, Alavi A. Diagnosis of pedal osteomyelitis in diabetic patients using current scintigraphic techniques. *Arch Intern Med* **1989**;149:2262–2266
8. Tumeh SS, Aliabadi P, Weissman BN, McNeil BJ. Chronic osteomyelitis: bone and gallium scan patterns associated with active disease. *Radiology* **1986**;158:685–688
9. Merkel KD, Brown ML, Dewanjee MK, Fitzgerald RH. Comparison of indium-labeled-leukocyte imaging with sequential technetium-gallium scanning in the diagnosis of low-grade musculoskeletal sepsis. *J Bone Joint Surg [Am]* **1985**;67-A:465–476
10. Schauwecker DS, Park HM, Mock BH, et al. Evaluation of complicating osteomyelitis with Tc-99m MDP, In-111 granulocytes, and Ga-67 citrate. *J Nucl Med* **1984**;25:849–853
11. Maurer AH, Millmond SH, Knight LC, et al. Infection in diabetic osteoarthropathy: use of indium-labeled leukocytes for diagnosis. *Radiology* **1986**;161:221–225
12. McCarthy K, Velchik M, Alavi A, Mandell GA, Esterhai JL, Goll S. Indium-111–labeled white blood cells in the detection of osteomyelitis complicated by a pre-existing condition. *J Nucl Med* **1988**;29:1015–1021
13. Schauwecker DS, Park HM, Burt RW, Mock BH, Wellman HN. Combined bone scintigraphy and indium-111 leukocyte scans in neuropathic foot disease. *J Nucl Med* **1988**;29:1651–1655
14. Esterhai JL, Goll SR, McCarthy KE, et al. Indium-111 leukocyte scintigraphic detection of subclinical osteomyelitis complicating delayed and nonunion long bone fractures: a prospective study. *J Orthop Res* **1987**;5(1):1–6
15. Wukich DK, Abreu SH, Callaghan JJ, et al. Diagnosis of infection by preoperative scintigraphy with indium-labeled white blood cells. *J Bone Joint Surg [Am]* **1987**;69-A:1353–1360
16. Van Nostrand D, Abreu SH, Callaghan JJ, Atkins FB, Stoops HC, Savory CG. In-111–labeled white blood cell uptake in noninfected closed fracture in humans: prospective study. *Radiology* **1988**;167:495–498
17. Schauwecker DS. Osteomyelitis: diagnosis with In-111–labeled leukocytes. *Radiology* **1989**;171:141–146
18. McAfee JG, Thakur MC. Survey of radioactive agents for *in vitro* labeling of phagocytic leukocytes. I. Soluble agents. *J Nucl Med* **1976**;17:480–487
19. Gilbert BR, Cerqueira MD, Vea HW, Nelp WB. Indium-111 labeled leukocyte uptake: false-positive results in non-infected pseudoaneurysm. *Radiology* **1986**;153:761–763
20. Froehlich JW, Swanson D. Imaging of inflammatory processes with labeled cells. *Semin Nucl Med* **1984**;14(2):128–140
21. Seldin DW, Heiken JP, Feldman F, Alderson PO. Effect of soft-tissue pathology on detection of pedal osteomyelitis in diabetics. *J Nucl Med* **1985**;26:988–993
22. Bamberger DM, Daus GP, Gerding DN. Osteomyelitis in the feet of diabetic patients. *Am J Med* **1987**;83:653–660
23. Park HM, Wheat LJ, Siddiqui AR, et al. Scintigraphic evaluation of diabetic osteomyelitis: concise communication. *J Nucl Med* **1982**;23:569–573
24. Zlatkin MB, Pathria M, Sartoris DJ, Resnick D. The diabetic foot. *Radiol Clin North Am* **1987**;25:1095–1105
25. Eymontt MJ, Alavi A, Dalinka MK, Kyle GC. Bone scintigraphy in diabetic osteoarthropathy. *Radiology* **1981**;140:475–477
26. Techner LM, Eiser CA, Laine W. Indium-111 imaging in osteomyelitis and neuroarthropathy. *J Am Podiatr Med Assoc* **1986**;76:23–29
27. Splittgerber GF, Spiegelhoff DR, Buggy BP. Combined leukocyte and bone imaging used to evaluate diabetic osteoarthropathy and osteomyelitis. *Clin Nucl Med* **1989**;14:156–160
28. Datz FL, Thorne DA. Cause and significance of cold bone defects on indium-111 labeled leukocyte imaging. *J Nucl Med* **1987**;28:820–823
29. Gilles CP, Cerqueira MD, Jacobson AF. The clinical significance of photopenia in bone on indium-111 leukocyte scintigraphy (abstr). *J Nucl Med* **1989**;30:1749
30. Mason MD, Zlatkin MB, Esterhai JL, Dalinka MK, Velchik MG, Kressel HY. Chronic complicated osteomyelitis of the lower extremity: evaluation with MR imaging. *Radiology* **1989**;173:355–359
31. Sartoris DJ, Devine S, Resnick D, et al. Plantar compartmental infection in the diabetic foot. The role of computed tomography. *Invest Radiol* **1985**;20:772–784

Pictorial Essay

Abnormalities of the Foot in Patients with Diabetes Mellitus: Findings on MR Imaging

Timothy E. Moore,[1] William T. C. Yuh,[1] Mary H. Kathol,[1] Georges Y. El-Khoury,[1] and John D. Corson[2]

The MR appearances of foot problems in patients with diabetes mellitus are illustrated. MR has been found to be effective in the diagnosis of osteomyelitis, the most common indication for imaging the feet of diabetic patients. MR has the ability to image numerous pathologic processes, especially subtle soft-tissue changes, that are not detectable with other imaging methods.

Patients spend more days in hospital for foot complications than for any other aspect of diabetes mellitus [1]. The principal factors in diabetic foot disease are vascular insufficiency and peripheral neuropathy, which may result in isolated ischemic or neuropathic changes. Frequently, the combination of both complications leads to the development of osteomyelitis. The diagnosis of osteomyelitis is a common clinical problem and the most frequent reason for imaging the feet of diabetic patients. Traditionally, radiographs and nuclear medicine studies have been used most often. More recently, MR has been found to have good specificity and sensitivity in the diagnosis of osteomyelitis [2], and we have noted a steady increase in the numbers of diabetic patients referred for MR studies of the foot. Because of the multifactorial nature of diabetic foot disease, numerous disease processes, especially subtle soft-tissue changes, often are not detectable with other imaging methods. The detection of some of these abnormalities may result in significant alterations in management of the patient's care. In this essay, we illustrate the MR appearances of problems in the foot in patients with diabetes mellitus.

Edema

Diffuse high signal in the soft tissues on T2-weighted (e.g., 2033/100 [TR/TE]) or short TI inversion recovery (STIR) (e.g., 2000/170 [TR/TI]) images is common and is our most frequent positive finding when imaging the feet of diabetic patients. It is usually seen in the plantar compartments that lie between the plantar aponeurosis and the metatarsus (Fig. 1). In many cases, the likely cause of the increased signal is

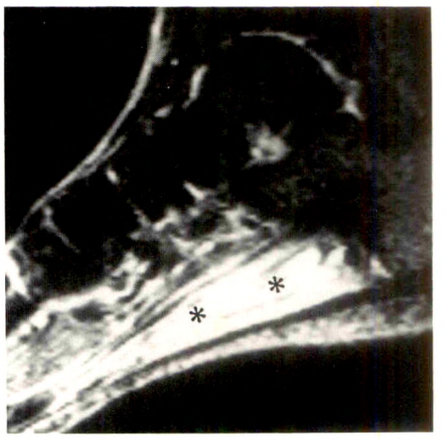


Fig. 1.—Subaponeurotic edema. Sagittal STIR MR image (2000/170) shows a diffuse increase in subcutaneous tissues and high signal (*asterisks*) deep to plantar aponeurosis in region of flexor digitorum brevis muscle. This pattern of edema is common in diabetic patients.

Received February 12, 1991; accepted after revision May 2, 1991.
Presented at the annual meeting of the American Roentgen Ray Society, Washington, DC, May 1990.
[1]Department of Radiology, The University of Iowa College of Medicine, Iowa City, IA 52242. Address reprint requests to T. E. Moore.
[2]Department of Surgery, The University of Iowa College of Medicine, Iowa City, IA 52242.

AJR 157:813–816, October 1991 0361–803X/91/1574–0813 © American Roentgen Ray Society

edema, as the signal does not correspond with clinically suspected soft-tissue infection. However, the increased signal is a nonspecific finding that may be difficult to differentiate from infection, which is known to have a predilection for this site in diabetic patients [3].

Localized Soft-Tissue Fluid Collections

Localized soft-tissue fluid collections may represent either regions of localized cellulitis, abscesses, or sinus tracts. T1-weighted imaging (e.g., 600/20 [TR/TE]) and either T2-weighted or STIR imaging without enhancement show a nonspecific localized region of high signal, usually close to an ulcer. However, the addition of a T1-weighted sequence after administration of gadopentetate dimeglumine may be helpful, as cellulitis and the walls of abscesses and sinuses enhance, whereas pus typically does not (Figs. 2 and 3).

Joint Effusions

Another frequent nonspecific finding is increased intraarticular fluid. This often involves the ankle or subtalar joints, which are typically some distance from ulcers or other sites of clinical infection (Fig. 4). None of our patients had confirmed

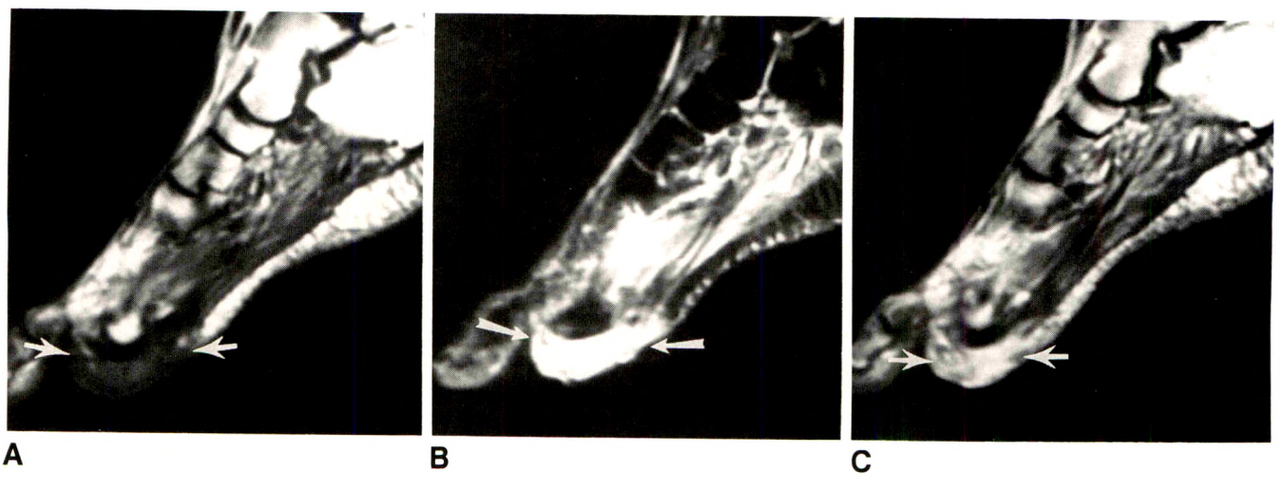


Fig. 2.—Cellulitis. MR study performed to rule out metatarsal osteomyelitis in a 41-year-old woman with an ulcer beneath first metatarsal head.
A, Sagittal T1-weighted MR image (600/20) shows low signal (*arrows*) in subcutaneous fat beneath second metatarsal head.
B, STIR image (2000/170) corresponding to *A* shows high signal (*arrows*) beneath second metatarsal head.
C, T1-weighted image (600/20) after IV administration of contrast material shows slightly inhomogeneous enhancement (*arrows*) beneath metatarsal head. This suggests a soft-tissue inflammatory process with no central unenhancing abscess or sinus cavity. Marrow signal is normal in all three images.

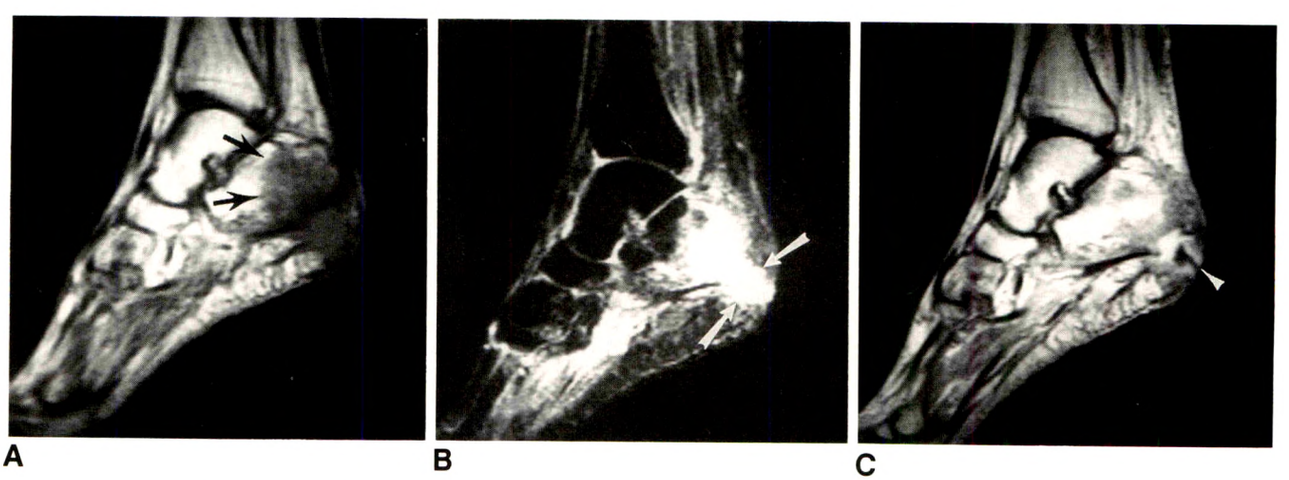


Fig. 3.—Osteomyelitis and abscess with open sinus tract.
A, Sagittal T1-weighted MR image (600/20) shows low signal (*arrows*) from marrow in calcaneus caused by osteomyelitis. Note adjacent region of low signal in subcutaneous fat of heel.
B, Sagittal STIR image (2000/170) corresponding to *A*. High signal in calcaneal marrow, corresponding to low signal in *A*, is caused by osteomyelitis. Localized region of high signal (*arrows*) in soft-tissue of heel, corresponding to low signal in *A*, may represent either cellulitis or abscess.
C, Sagittal T1-weighted image (600/20) after IV injection of gadopentetate dimeglumine shows enhancement of soft-tissue inflammatory process in heel, but lack of enhancement of central region with track to skin surface (*arrowhead*). This confirmed clinical suggestion of abscess with open draining sinus.

septic arthritis, although evidence of adjacent osteomyelitis or ulcers should raise this possibility.

Fluid in the Tendon Sheath

A small quantity of fluid in tendon sheaths is a frequent observation although of uncertain significance. However, infected tenosynovitis must be suspected when the tendon sheath is grossly distended and close to ulcers or other clinical evidence of infection (Fig. 5). In a review of 14 MR studies, Beltran et al. [4] suspected infected tenosynovitis in the feet of four diabetic patients, but it was confirmed in only one.

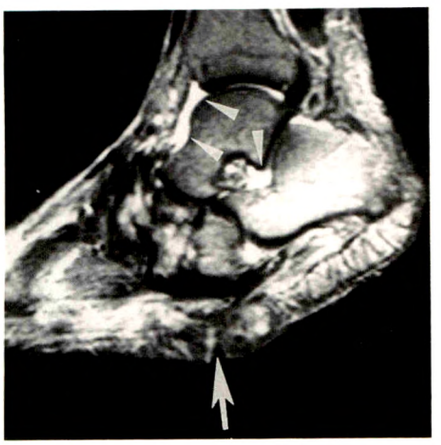


Fig. 4.—Deformity from neuroarthropathy in a 58-year-old man with long-standing diabetic neuroarthropathy. Sagittal T2-weighted MR image (2033/100) of foot shows collapse of midtarsus along weight-bearing vector of tibia. As a result, cuboid has become major weight-bearing bony prominence of foot and therefore a site of ulcer formation (*arrow*). Note ankle and subtalar joint effusions (*arrowheads*).

Ulcers

The identification of ulcers in MR studies is useful because ulcers serve as pointers to areas in which osteomyelitis or abscesses may occur. Ulcers are commonly found beneath weight-bearing bony prominences such as the metatarsal heads and the calcaneal tuberosity (Fig. 6), or the cuboid if the midtarsus has collapsed because of neuroarthropathy (Fig. 4).

Osteomyelitis

Decreased marrow signal on T1-weighted images and increased signal on T2-weighted or STIR images are the typical findings in active osteomyelitis [5]. Because the signal characteristics reflect increased marrow fluid, the same findings may be found with neuropathic fractures, making interpretation difficult (Fig. 7). Proximity to a typical ulcer site and the presence of adjacent abnormal soft-tissue signal favor osteomyelitis as a cause of abnormal marrow signal (Fig. 6).

Neuroarthropathy

Neuroarthropathy may produce deformities such as hammer toes or collapse of the midtarsus along the weight-bearing vector of the tibia (Fig. 4). Chronic neuroarthropathy may show decreased signal in the marrow on all imaging sequences. Beltran et al. [4] have described these findings. However, we have found that acute spontaneous neuropathic fractures may show decreased signal in the marrow on T1-weighted images and high signal on T2-weighted images. These signal characteristics are similar to those discussed above for osteomyelitis (Fig. 7). Old ununited fracture lines also have low signal on T1- and T2-weighted images, but adjacent marrow signal is normal (Fig. 6).

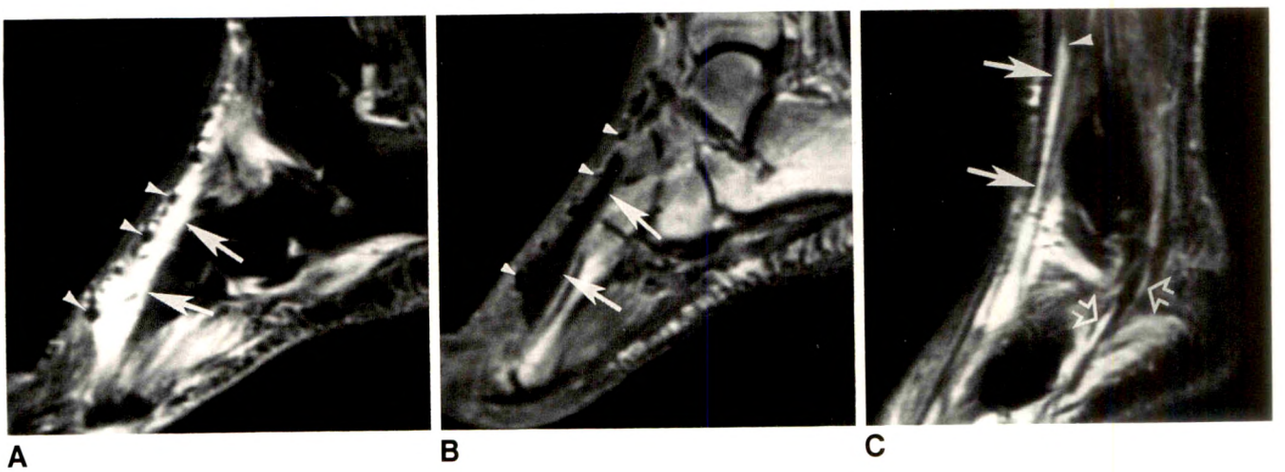


Fig. 5.—Tenosynovitis.

***A*, Sagittal STIR MR image (2000/170) shows high signal (*arrows*) in dorsal soft tissues that corresponds anatomically to common synovial sheath for tendons of extensor digitorum longus. Small rounded regions of low signal intensity (*arrowheads*) on all sequences represent bubbles of gas also seen on plain radiographs (*not shown*) and presumably caused by gas-forming organisms, although patient was already on antibiotics and culture was negative.**

***B*, Sagittal T1-weighted image (600/20) corresponding to *A* after IV injection of gadopentetate dimeglumine shows that distended extensor digitorum longus sheath (*arrows*) does not enhance, indicating that it contains fluid. Subsequent debridement of overlying necrotic tissue exposed tendons surrounded by pus. *Arrowheads* indicate gas bubbles.**

***C*, Sagittal STIR image (2000/170) lateral to *A* and *B* shows high signal intensity in extensor digitorum longus tendon (*solid arrows*) extending as far as musculotendinous junction (*arrowhead*). High signal surrounding peroneal tendons (*open arrows*) indicates tendon sheath fluid but not necessarily infection.**

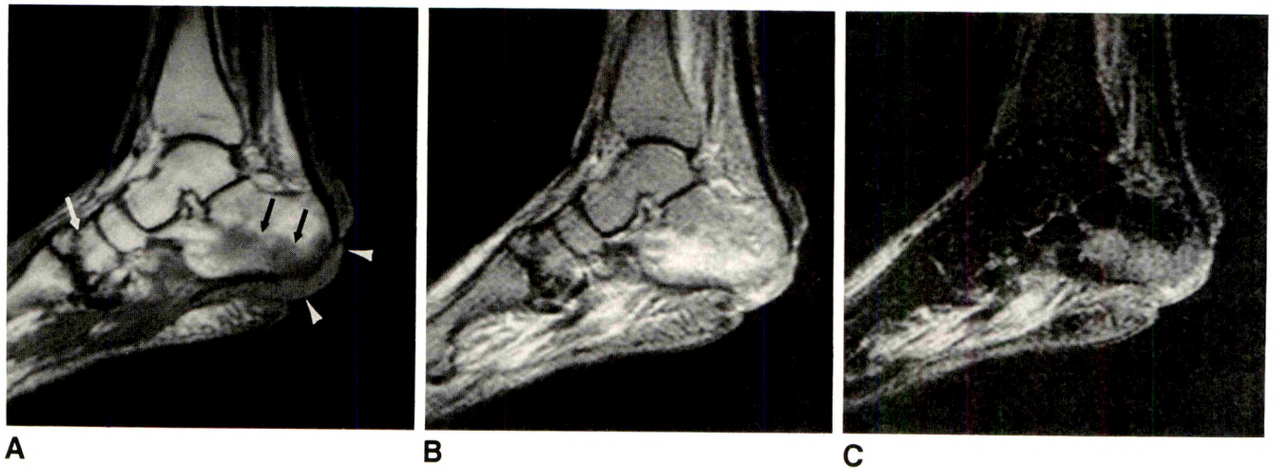


Fig. 6.—Osteomyelitis and large open ulcer.

A, Sagittal T1-weighted MR image (683/20) shows open ulcer (*arrowheads*) overlying weight-bearing prominence of calcaneus. Low signal intensity within calcaneus (*black arrows*) is caused by osteomyelitis. An old ununited neuropathic fracture of medial cuneiform bone (*white arrow*) was confirmed on radiograph (*not shown*).

B, Sagittal T2-weighted MR image (2033/100) corresponding to *A* shows increased signal in ulcer that continues into calcaneus. This is typical course in diabetic osteomyelitis, in which infection spreads directly from ulcers to underlying bone.

C, Sagittal STIR image (2000/125) shows findings similar to those on T2-weighted MR image (*B*), but high signal from osteomyelitis is more easily detected against background of low-signal normal bone marrow.

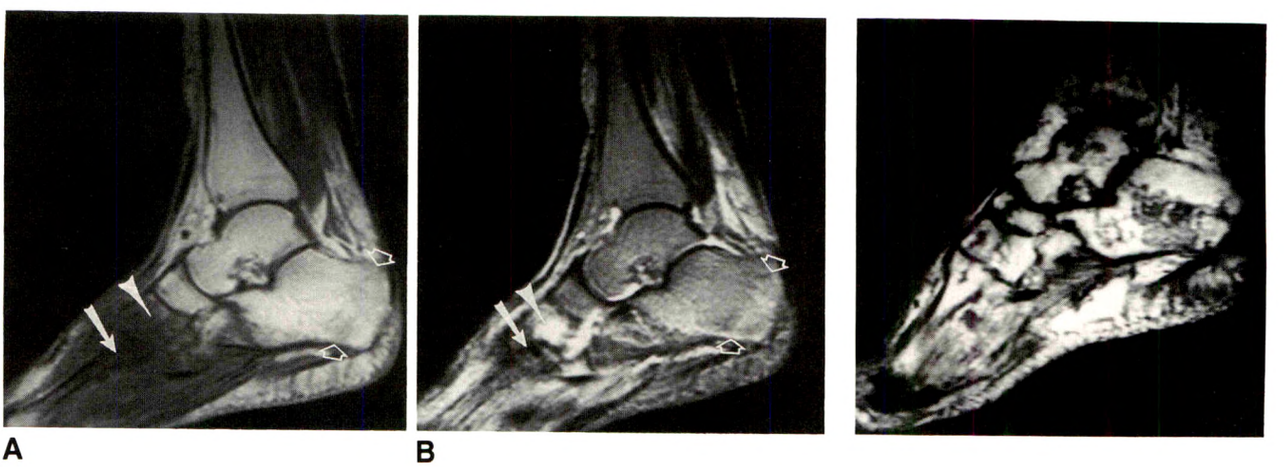


Fig. 7.—Bone marrow signal changes of early neuroarthropathy in a 29-year-old diabetic woman with peripheral neuropathy but no clinical evidence of infection.

A and *B*, Sagittal T1-weighted (600/20, *A*) and T2-weighted (2050/100, *B*) MR images show decreased signal intensity in base of second metatarsal (*solid arrows*) on both T1- and T2-weighted images, consistent with fracture callus that was seen on radiographs taken on same day (*not shown*). There is decreased signal intensity in middle cuneiform bone on T1-weighted image but increased signal on T2-weighted image (*arrowheads*). This is consistent with edema from spontaneous microfractures of neuroarthropathy. Differential diagnosis should include osteomyelitis, although site and clinical setting make this less likely in this case. Subsequent radiographs showed advancing changes of neuroarthropathy, which included cuneiform bones. Calcaneal fracture line (*open arrows*) is seen as band of decreased signal intensity on T1-weighted image and increased signal on T2-weighted image. This was also faintly visible on radiographs.

Fig. 8.—Bone marrow infarction. Sagittal T1-weighted MR image (600/20) in elderly diabetic patient with femoral grafts for ischemia shows numerous geographic regions of low signal intensity in tarsal bones. These findings are typical of bone marrow infarction, although this case was not biopsy proved.

Bone Infarcts

Despite the frequency of severe ischemic disease in the limbs of diabetic patients, we have found bone infarction to be surprisingly uncommon (Fig. 8).

REFERENCES

1. Gibbons GW, Eliopoulous GM. Infection of the diabetic foot. In: Kozak GP, Campbell D, Hoar CS, et al., eds. *Management of diabetic foot problems*. Philadelphia: Saunders, **1984**:97–102
2. Yuh WTC, Corson JD, Baraniewski HM, et al. Osteomyelitis of the foot in diabetic patients: evaluation with plain film, ^{99m}Tc-MDP bone scintigraphy, and MR imaging. *AJR* **1989**;152:795–800
3. Sartoris DJ, Devine S, Resnick D, et al. Plantar compartmental infection in the diabetic foot: the role of computed tomography. *Invest Radiol* **1985**;20:772–784
4. Beltran J, Campanini DS, Knight C, McCalla M. The diabetic foot: magnetic resonance imaging evaluation. *Skeletal Radiol* **1990**;19:37–41
5. Tang JSH, Gold RH, Bassett LW, Seegar LL. Musculoskeletal infection of the extremities: evaluation with MR imaging. *Radiology* **1988**;166:205–209

Case Report

Septic Arthritis of the Hip: A Complication of a Rectal Tear Associated with Pelvic Fractures

Andrea B. Magen,[1] Richard P. Moser, Jr., Cathleen A. Woomert, and Michaela A. I. Guidici

Pelvic fractures are serious, potentially life-threatening medical emergencies. If encountered, complications usually result from coexistent neurovascular or genitourinary injury. Scant literature pertaining to pelvic fracture and associated intestinal lesions is available [1]. We describe the imaging findings in a patient who sustained multiple pelvic fractures after a ditch cave-in and subsequently had persistent pain in the lower abdomen with accompanying fever and leukocytosis. Gastrografin (Squibb Diagnostics, New Brunswick, NJ) enema revealed a rectal tear with extravasation of contrast material into the retroperitoneum and left hip joint. To our knowledge, this is the first description of a septic joint due to communication between the rectum and hip joint resulting from rectal tear caused by pelvic trauma or fracture.

Case Report

A 59-year-old male construction worker was transferred to our hospital 2 days after sustaining multiple pelvic fractures in a ditch cave-in. Accompanying radiographs showed a vertical fracture of the left sacral ala, comminuted fractures of the left iliac wing and acetabulum, and fractures of the left superior and inferior pubic rami (Fig. 1).

The patient's hematocrit decreased from 31 to 22 in the 2 days after his injury, so abdominal and pelvic CT scans were obtained. CT confirmed the presence of the pelvic fractures, and showed a massive pelvic hematoma that deviated the rectum, bladder, and left ureter anteriorly, superiorly, and to the right (Fig. 1C). After multiple blood transfusions, the hematocrit rose to 29. In the next 2 days, he complained of persistent tenderness in the left lower abdomen. Mild fever and leukocytosis were attributed to right lung infiltration and/or atelectasis, which was visible on the chest radiograph. The discomfort in the left lower abdomen persisted. Therefore, on the second day of hospitalization at our institution, a Gastrografin enema was performed. The enema revealed a rectal tear below the peritoneal reflection, with extravasation of contrast material into the retroperitoneum and left hip joint (Fig. 1D).

The discomfort in the left lower abdomen, fever, and leukocytosis were attributed to septic arthritis of the left hip. After percutaneous aspiration of the left hip joint yielded a small amount of pus, the patient was taken to surgery, during which the left hip and retroperitoneum were copiously irrigated and a diverting colostomy was performed. Blood cultures subsequently grew Gram-negative rods, and Gram stains of the hip aspirate and pelvic hematoma showed both Gram-negative rods and Gram-positive cocci and rods. Despite the diverting colostomy, the intermittent discomfort in the left lower abdomen was persistent. Continued pain and appearance of gradually increasing osteolytic destruction of the left hip on radiographs were consistent with evolving osteomyelitis.

Discussion

Pelvic fracture is a serious occurrence. Rectal laceration is a rare associated finding [1–5]. Coexistent urologic injury, including bladder rupture and tears of the ureters or urethra are more frequent complications of pelvic trauma [6, 7]. Septic arthritis has been described as resulting from urologic trauma [6, 7] and complicating diverse nontraumatic causes such as Crohn disease, diverticulitis, and uterine abscess [5–8]. To the best of our knowledge, however, our case is the first report of communication between a lacerated colon (caused by trauma) and the hip joint.

In our case, a contrast enema showed a communication, via an adjacent pelvic hematoma, between a rectal tear and

Received March 26, 1991; accepted after revision May 10, 1991.

[1]All authors: Department of Radiology, Penn State University Hospital, The Milton S. Hershey Medical Center, 500 University Dr., Hershey, PA 17033. Address reprint requests to R. P. Moser, Jr.

AJR 157:817–818, October 1991 0361–803X/91/1574–0817 © American Roentgen Ray Society

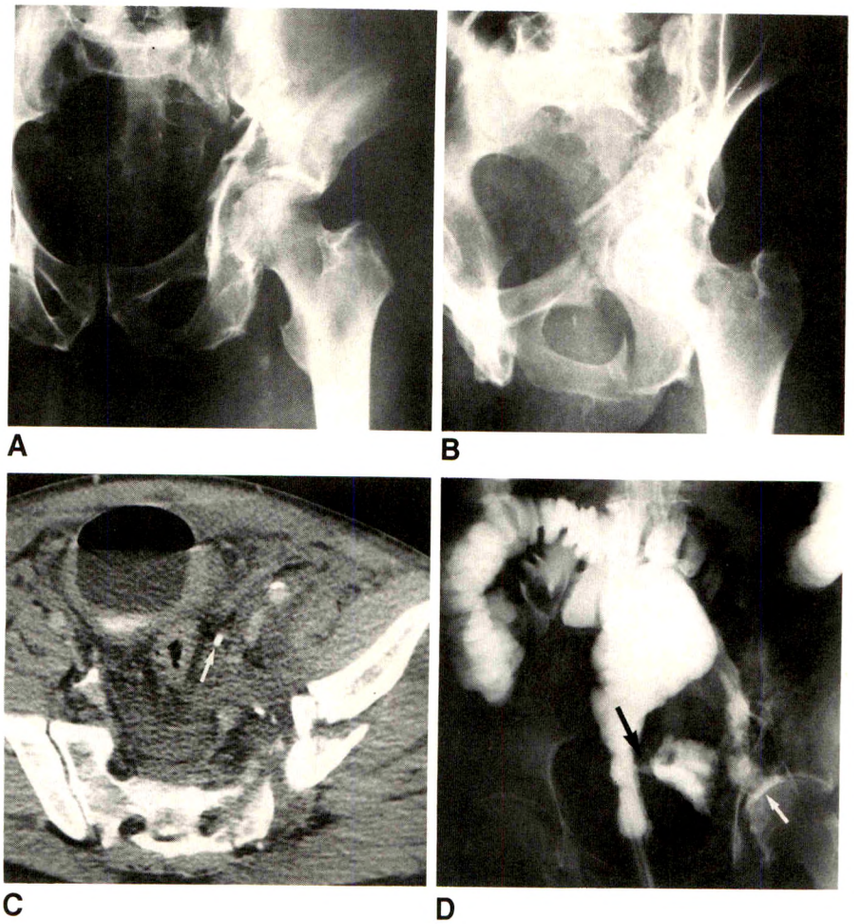


Fig. 1.—*A* and *B*, Anteroposterior (*A*) and right posterior oblique (*B*) radiographs show a vertical fracture through left sacral ala, comminuted fractures of left iliac wing and left acetabulum, fractures of left superior and inferior pubic rami, and an "overlapping" fracture of right pubic ramus, near symphysis.

C, Soft tissue–window axial CT scan shows fractures of left hemipelvis; an adjacent complex hematoma; and displacement of rectum, urinary bladder, and left ureter (*arrow*) anteriorly, superiorly, and to right.

D, Gastrografin enema shows extravasation of contrast material (*black arrow*) through rectal tear below peritoneal reflection, leaking into left pelvic hematoma and then into left hip joint (*white arrow*).

an intraarticular acetabular fracture. Once the rectal serosa was disrupted, colonic bacteria spread through the adjacent hematoma along the iliopsoas muscle and subsequently into the incompetent hip joint capsule. The cause of the tear remains speculative. Because of the rapid time course, vascular compromise with resulting bowel necrosis seems unlikely. More likely, the rectal tear resulted from a shearing injury unrelated to the pelvic fracture. Although no residual bony fragments were identified adjacent to the lacerated bowel, it is conceivable that the rectum was torn by a fragment of fractured bone.

ACKNOWLEDGMENTS

We thank Elizabeth E. Frauenhoffer for analyzing the pathologic specimens, Constance Gardner-Hornyak for expert word processing, and John Biondo for preparation of the prints.

REFERENCES

1. Moore JR. Pelvic fracture: associated intestinal and mesenteric lesions. *Can J Surg* **1966**;9:253–261
2. Buchanan JR. Bowel entrapment by pelvic fracture fragments: a case report and review of the literature. *Clin Orthop Rel Res* **1980**;147:164–166
3. Peltier LF. Complications associated with fractures of the pelvis. *J Bone Joint Surg [Am]* **1965**;47-A:1060–1069
4. Perry JF Jr. Pelvic open fractures. *Clin Orthop Rel Res* **1980**;151:41–45
5. Smith WS, Ward RM. Septic arthritis of the hip complicating perforation of abdominal organs. *JAMA* **1966**;195:170–172
6. Bacilla PR Jr, Corces A, Nimtyongskul P. Septic hip in pelvic fracture with urologic trauma: case report. *J Trauma* **1990**;30:1600–1602
7. Cooke CP III, Levinsohn EM, Baker BE. Septic hip in pelvic fractures with urologic injury: a case report, review of the literature and discussion of the pathophysiology. *Clin Orthop Rel Res* **1980**;147:253–257
8. Shreeve DR, Ormerod LP, Dunbar EM. Crohn's disease with fistulae involving joints. *J R Soc Med* **1982**;75:946–948

Arteriopathy and Coarctation of the Abdominal Aorta in Children with Mucopolysaccharidosis: Imaging Findings

Donna B. Taylor[1, 2]
Susan I. Blaser[1]
Patricia E. Burrows[1]
David A. Stringer[1, 3]
Joe T. R. Clarke[4]
Paul Thorner[5]

Eight children with mucopolysaccharidosis I (MPS I), representing 33% of all children with MPS I seen at our institution during an 18-year period, developed hypertension. Five of these hypertensive children also exhibited symptoms of aortic coarctation. The radiographic evaluation of four of these children with MPS I (three with Hurler syndrome, MPS I H, and one with Scheie disease, MPS I S) and arteriopathy affecting the thoracic aorta, abdominal aorta, and visceral and renal arteries is presented. Hypertension developed in all four children before they were 4 years old; three had differences between upper- and lower-extremity blood pressures. Irregular narrowing of the abdominal aorta with either multiple minor asymmetric wall lesions (n = 2) or abrupt concentric narrowing (n = 2) was present in all children as shown by aortography (n = 3), sonography (n = 3), MR imaging (n = 2), and/or autopsy (n = 1). A variety of other vessels also were involved, including the ascending aorta (n = 1) and vertebral (n = 1), axillary (n = 1), intercostal (n = 2), lumbar (n = 2), mesenteric (n = 3), renal (n = 2), and iliac arteries (n = 3). Autopsy in one child demonstrated thickened heart valves, narrowing of the coronary arteries, and irregularity of the aorta due to deposition of mucopolysaccharide material within the intima.

Our series demonstrates various facets of the arteriopathy of MPS I as shown by sonography, MR imaging, and angiography.

AJR 157:819–823, October 1991

Significant vascular disease may develop at an early age in children with mucopolysaccharidosis I (MPS I) [1]. Previous reports have emphasized the lesions in the coronary arteries, cardiac valves, endocardium, myocardium, and aorta [2–5], but not involvement of the thoracic and abdominal aorta and visceral and renal arteries. We describe various manifestations of the arteriopathy as shown by sonography, MR imaging, and angiography.

Materials and Methods

Between January 1972 and January 1990, 24 infants and children with MPS I were clinically examined at our institution. The diagnosis of MPS I was confirmed in all cases by showing severe deficiency of alpha-L-iduronidase activity in peripheral blood leukocytes and/or cultured skin fibroblasts. The classification into MPS I H (Hurler-syndrome), MPS I S (Scheie syndrome), or MPS I H/S (Hurler-Scheie syndrome) was based on the clinical findings.

Blood pressure measurements were obtained in all 24 patients during initial examination and on follow-up visits. Arterial hypertension developed in eight of these patients. Five of eight hypertensive children had clinical evidence of coarctation of the aorta, with strong brachial and weak femoral pulses and a significant blood pressure difference between the upper and lower extremities.

Only one child had symptoms of intermittent claudication. Four hypertensive children, 4.5–10.0 years old, underwent imaging of the aorta. Three had MPS I H and one had MPS I S. All had systemic hypertension and three had clinical evidence of coarctation of the aorta. The other four children were not evaluated because of their poor clinical condition when hyperten-

Received October 22, 1990; accepted after revision April 9, 1991.

Presented as a poster at the annual meeting of the European Society for Pediatric Radiology, Munich, Germany, May 1990.

[1] Department of Radiology, The Hospital for Sick Children and University of Toronto, 555 University Ave., Toronto, Ontario, Canada M5G 1X8. Address reprint requests to P. E. Burrows.

[2] Present address: Department of Radiology, Royal Perth Hospital, Box X2213, G.P.O., Perth, West Australia 6001.

[3] Present address: Department of Radiology, British Columbia Children's Hospital, 4480 Oak St., Vancouver, B.C., Canada V6H 3V4.

[4] Departments of Genetics and Pediatrics, The Hospital for Sick Children and University of Toronto, Toronto, Ontario, Canada M5G 1X8.

[5] Department of Pathology, The Hospital for Sick Children and University of Toronto, Toronto, Ontario, Canada M5G 1X8.

0361–803X/91/1573–0819
© American Roentgen Ray Society

sion developed. The following vascular imaging studies were done: sonography, MR, and angiography in one patient; sonography and angiography in one; MR and sonography in one; and angiography alone in one. Gray-scale sonography was performed with a 5-MHz transducer on an Acuson 125 unit. Doppler studies were performed in two patients with a 3.5-MHz transducer. A 1.5-T General Electric MR scanner was used to obtain spin-echo images of the thoracic and abdominal vessels in sagittal, coronal, and axial planes in two patients. IV administration of Nembutal sodium (Abbott Laboratories, Ltd., Toronto) for sedation was required for one of these MR studies, and all angiograms were obtained under general anesthesia. Anesthetization was performed carefully since patients with MPS may have upper airway obstruction and cord compression at the craniocervical junction due to mucopolysaccharide deposition. Two children have died of their disease since being examined; an autopsy was performed on one.

Results

The clinical features of the four children who underwent vascular imaging are summarized in Table 1. All three children with MPS I H had developmental delay, but the child with MPS I S was intellectually normal. Systemic hypertension was present in all four patients, and in three of these it was difficult to control with medication. In case 2, hypertension developed after a general anesthetic was administered for insertion of a ventriculoperitoneal shunt to treat extraventricular obstructive hydrocephalus. The hypertension remained difficult to control. Differences between upper- and lower-extremity blood pressures were documented in cases 1–3. Subsequent imaging confirmed the presence of one or more marked stenoses within the thoracoabdominal aorta (Figs. 1–4). Only one child (case 1) had claudication; discomfort in his legs was caused by walking and relieved immediately by rest. The other three patients may not have communicated their discomfort because of immobility and/or intellectual impairment.

The sites of arterial involvement in each child are summarized in Table 1. The ascending aorta was abnormal in one patient, with supravalvular stenosis and poststenotic dilatation (Fig. 4B). Irregular wall lesions were present in the aortic arch in two patients. The descending thoracic aorta showed asymmetric wall lesions in three patients with occlusion and irregularity of multiple intercostal arteries.

All children had involvement of the abdominal aorta consisting of multiple minor asymmetric wall lesions and/or abrupt concentric narrowing. Two patients had occlusion of lumbar arteries. In three patients, the major visceral arteries, including the celiac trunk, superior and inferior mesenteric arteries, and renal arteries, had stenoses of their origins and/or irregular wall lesions in peripheral branches. Narrowing of the iliac arteries was seen in three patients. MR was performed 2 years after angiography in one child and demonstrated progression of abdominal aortic obstruction (Fig. 1). Autopsy in one patient showed thickening of the cardiac valve leaflets and diffuse narrowing of the coronary arteries. Yellowish streaks were noted on the intimal surface of the ascending aorta, just above the aortic valve. On microscopic examination, mucopolysaccharide was seen expanding the intima of the coronary arteries (Fig. 4B) and the endocardium of cardiac valve leaflets. Foamy macrophages and myointimal cells were present within the aortic intima.

TABLE 1: Summary of Clinical and Radiologic Findings in Children with Mucopolysaccharidosis I (MPS I)

Case No.	Age (yr)	Type of MPS I	Symptoms	Locations of Lesions on Imaging Studies		
				Sonography	MR	Angiography
1	8.5	I S	Hypertension, coarctation, claudication	Aorta, distal to superior mesenteric artery	Aorta, distal to superior mesenteric artery; iliac arteries	Infrarenal aorta, origins of iliac/lumbar arteries
2	4	I H	Hypertension, coarctation	Aorta, proximal to superior mesenteric artery	MR not performed	Thoracoabdominal aorta, origins of intercostal/lumbar/celiac/renal arteries, distal superior mesenteric artery, peripheral renal arteries
3	7	I H	Hypertension, coarctation	Axillary artery; aorta, distal to superior mesenteric artery; superior mesenteric artery	Arch, distal thoracic/suprarenal aorta to bifurcation, superior mesenteric artery, iliac arteries	Angiography not performed
4	5	I H	Hypertension	Sonography not performed	MR not performed	Supravalvular, descending thoracic, supra- and infrarenal aorta; proximal subclavian and vertebral arteries; origins of intercostal/lumbar/iliac arteries; superior and inferior mesenteric arteries; peripheral renal artery

Note.—MPS I S = Scheie syndrome; MPS I H = Hurler syndrome.

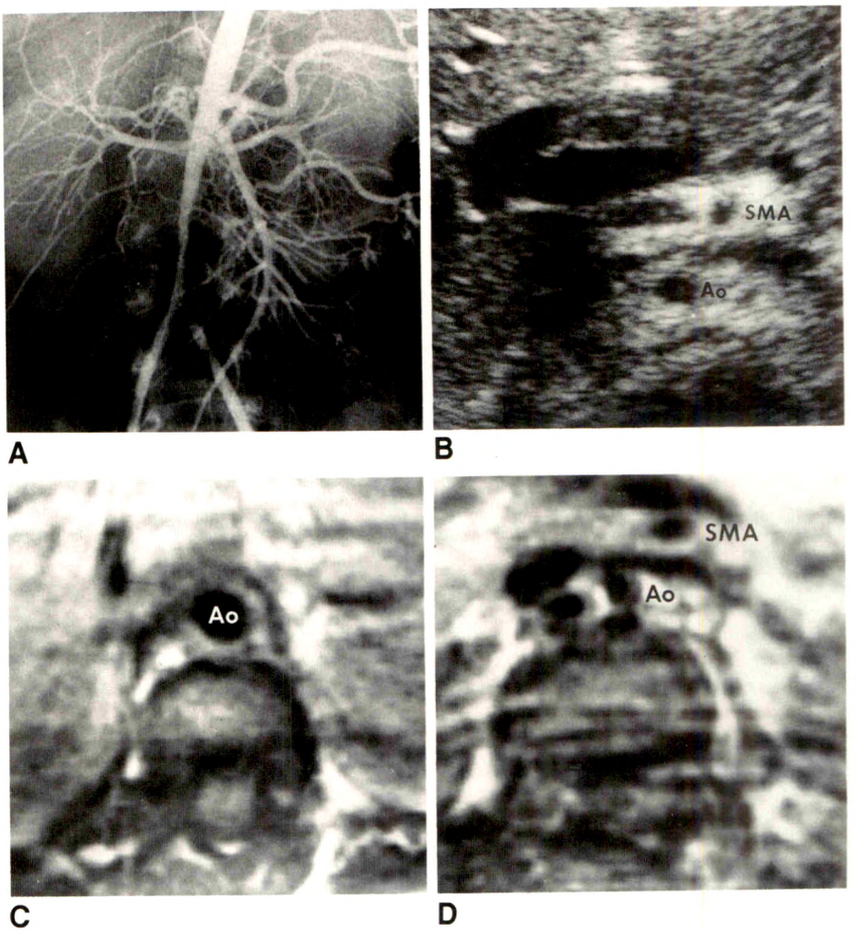


Fig. 1.—Aortography, sonography, and MR imaging in case 1, an 8.5-year-old boy with mucopolysaccharidosis I S.

A, Abdominal aortogram shows abrupt infrarenal aortic narrowing extending to and involving origins of iliac arteries. Irregular narrowing also involves proximal lumbar arteries.

B, Transverse sonogram. Lumens of aorta (Ao) and superior mesenteric artery (SMA) are of similar caliber.

C and *D*, Axial T1-weighted MR images obtained above celiac axis (*C*) and at level of left renal vein (*D*) show progressive narrowing of abdominal aorta (Ao). Severe narrowing and apparent wall thickening is at level of left renal vein.

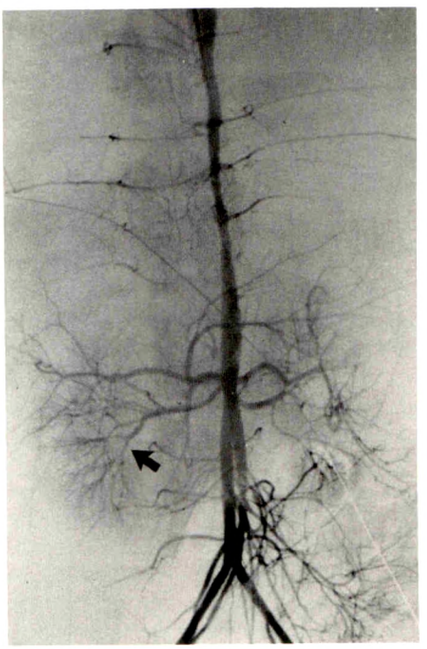


Fig. 2.—Aortography in case 2, a 4-year-old boy with mucopolysaccharidosis I H. Aortography performed via axillary artery shows severe, irregular, and diffuse narrowing of suprarenal thoracoabdominal aorta, with occlusion of multiple intercostal arteries, and focal stenosis of proximal superior mesenteric artery. Note also caliber changes involving branches of renal arteries (*arrow*).

Discussion

The MPS diseases are a group of inherited disorders characterized by a deficiency of lysosomal enzymes. In MPS I, alpha-L-iduronidase deficiency leads to intralysosomal storage of dermatan and heparan sulfate in different tissues, resulting in characteristic neurologic, skeletal, cardiovascular, and visceral changes [1]. The clinical spectrum of MPS I is highly variable. All have a deficiency of the same alpha enzyme (α L-iduronidase); however, there are at least three clinically and genetically distinct variants [6]. The Hurler syndrome (MPS I H) is characterized by severe somatic and neurologic involvement with mental retardation. Death usually occurs by 10–12 years of age. In contrast, children with Scheie syndrome (MPS I S) have much milder skeletal and visceral problems and no primary neurologic involvement. These children are frequently of normal intelligence and may live into adulthood. A clinically intermediate form has also been described (I H/S) [6].

Hypertension, often refractory to treatment, has been reported in up to 32% of patients with MPS I [7]. Two possible mechanisms are occlusive disease of the aorta and renal arteries and chronic upper airway obstruction. Hypertension may, as in one of our children, be triggered by interventional procedures or surgery, but the reason for this is unknown.

Cardiovascular disease has been documented in all forms of MPS [1]. Narrowing of the coronary arteries is thought to be most severe in Hurler syndrome (MPS I H) and Hunter syndrome (MPS II) [8] and, although extensive, is usually

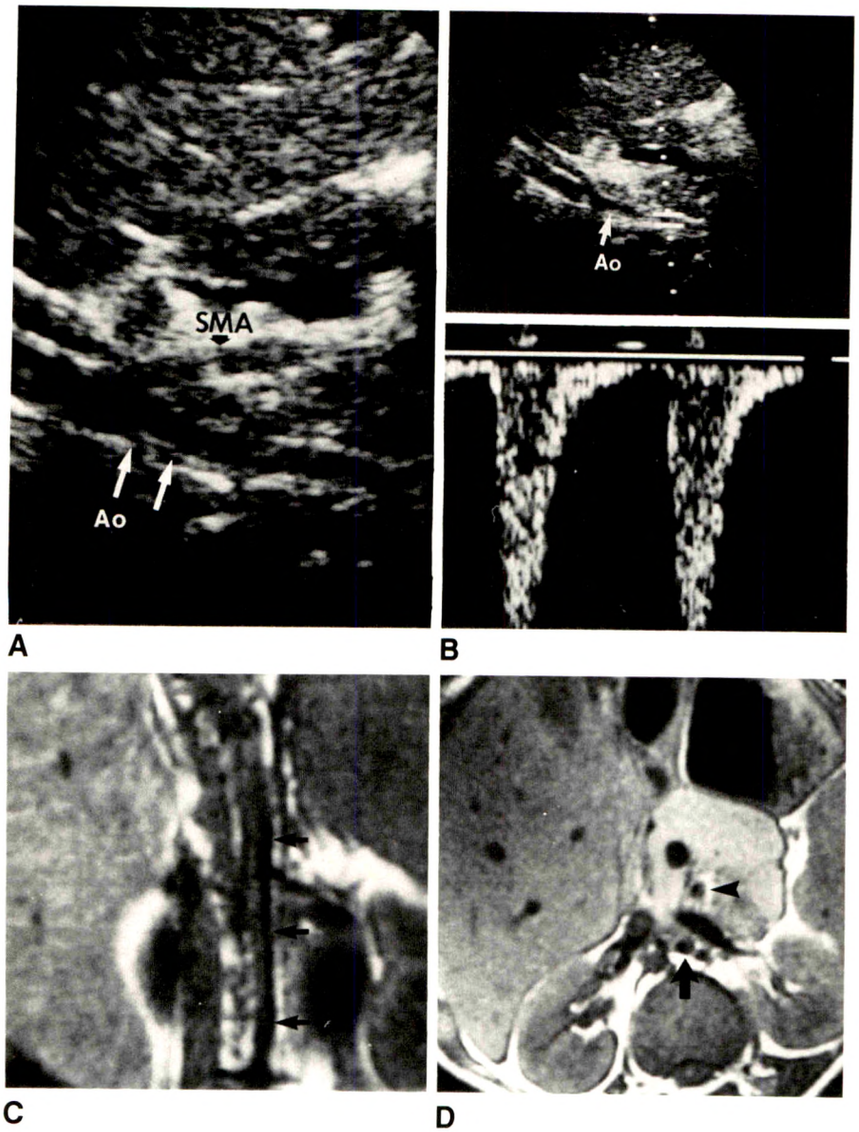


Fig. 3.—Sonography and MR imaging in case 3, a 7-year-old boy with mucopolysaccharidosis I H.

A, Sagittal sonogram shows abrupt aortic narrowing (*arrows*) below origin of superior mesenteric artery (SMA). Diameter of aorta (Ao) is similar to that of superior mesenteric artery.

B, High-frequency shifts on Doppler sonogram confirm luminal stenosis.

C, T1-weighted coronal MR image shows diffuse, severe narrowing (*arrows*) of abdominal aorta.

D, T1-weighted axial MR image. Note 2- to 3-mm lumen of suprarenal aorta (*arrow*) and small lumen of superior mesenteric artery (*arrowhead*), with vessel wall thickening.

asymptomatic. A clear-cut history of angina pectoris has been reported in only one patient with MPS I H [8]. The lack of reported symptoms may be related to the inability of many of these children to communicate, although none of our patients had clinical or ECG evidence of myocardial ischemia.

Involvement of the aorta and other large vessels has been mentioned in previous reports [4, 7]. In a review by Krovertz et al. [7] of published autopsy findings in 58 patients with Hurler syndrome, aortic plaques were recorded in 15 patients and generalized arterial involvement in five others. One of the 15 had aortic narrowing and stenosis of the origin of the left subclavian artery. Renteria et al. [4] found multiple yellow and fibrous atherosclerotic plaques within the aorta of all six of their MPS I patients. Similar lesions were seen in the carotid arteries and branches of the renal and hepatic arteries.

Autopsies of MPS I patients have shown the arterial narrowing to be caused by the deposition of "Hurler plaque" within the intima and inner portion of the media of the large and medium-sized arteries [2, 4]. These lesions differ from atherosclerotic plaques in that electron microscopy shows marked proliferation of vacuolated myointimal (Hurler) cells and macrophages; these cells contain nondegradable mucopolysaccharide within markedly distended lysosomes. Massive proliferation of collagen and elastic fibers is also present [4].

Few radiologic reports have described the visceral arterial findings in MPS I. Schmidt et al. [9] reported the radiologic findings in two patients with MPS I H/S at 20 and 40 years of age. Neither was hypertensive nor had clinical evidence of vascular disease. Severe aortic narrowing such as that observed in our patients has been reported in only one previous case, an 8-year-old child with MPS VII (β-glucuronidase deficiency) [10]. Clinical findings included hypertension and symptoms of coarctation. Angiography suggested concentric narrowing of the aorta below the origins of the renal arteries, as was seen in three of our children.

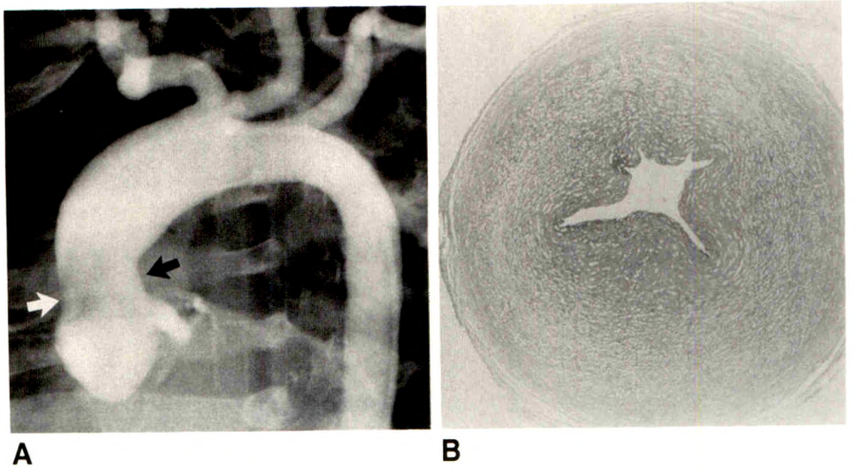


Fig. 4.—Aortography and pathologic examination in case 4, a 5-year-old boy with mucopolysaccharidosis I H.

A, Arch aortogram shows mild focal supravalvular aortic stenosis (*arrows*) and dilatation of ascending aorta. Incidentally noted is common origin of innominate and left carotid arteries.

B, Cross section of coronary artery shows marked stenosis due to expansion of subintimal region. Material in subintima stains positively for acid mucopolysaccharide. (Colloidal iron–PAS, original magnification, ×65)

Our series includes the use of several different imaging techniques to evaluate the major vessels. An important consideration in the selection of the imaging technique is the need for sedation. Chronic upper airway obstruction is common in MPS I [11], making sedation both riskier and less effective (owing to excessive chest movement with upper airway obstruction) than in normal children. These patients may also require larger than usual doses of sedative drugs [7]. Although Krovertz et al. [7] did not report any complications related to sedation of their patients, one of our patients developed stridor and desaturation after IV sedation for the MR examination; he responded to airway suctioning and oxygen administration.

Sonography has the advantage of rarely requiring sedation. The limitations of this technique include inability to show the descending thoracic aorta and inability to visualize the lower abdominal aorta owing to overlying bowel gas. In our patients, sonography showed stenoses of the aorta and axillary arteries. Echocardiography has been used in other patients to evaluate the cardiac valves [5]. MR imaging showed aortic narrowing and vessel wall thickening with great precision in our patients. Disadvantages of this technique include its high cost, the need to change metallic tracheostomy tubes to plastic ones before scanning, and the need for sedation. Advantages include the ability to image, as part of the same examination, the other organ systems involved, such as the spine, the brain and meninges, and the heart. Angiography is currently the only technique that can show the full extent of the arteriopathy, especially the involvement of visceral branches.

The role of surgical or transcatheter treatment of vascular disease in these patients has not yet been determined. Such therapy may be appropriate in those symptomatic children with a relatively good general prognosis (those with MPS I H/S and MPS I S). The patient with MPS VII and aortic narrowing reported by Beaudet et al. [10] underwent aortic bypass surgery. Although the aorta was described as friable, no intraoperative difficulties were reported. Cardiac valve replacement has also been successfully undertaken in patients with MPS I [12, 13].

Our study indicates that aortic narrowing may be more common in patients with MPS I than previously thought, contributing to the development of hypertension and claudication, although symptoms are rarely reported. Some form of vascular imaging is indicated in patients with MPS I and symptomatic aortic or visceral arterial narrowing to document the cause of the hypertension and to direct treatment. Both sonography and MR imaging can identify obstructive aortic lesions, and can be used in initial screening of follow-up examinations in patients with MPS. Angiography probably should be reserved for those children in whom treatment is being considered, or in whom delineation of disease of the aortic branches is clinically indicated.

ACKNOWLEDGMENTS

We thank Sandra Leung, Deborah Villeneuve, Carolyn MacDonald, and Susan Scorizzi for manuscript preparation.

REFERENCES

1. McKusick VA, Neufeld EF. The mucopolysaccharide storage diseases. In: Stanbury JB, Wyngaarden JB, Fredrickson DS, eds. *The metabolic basis of inherited disease*, 4th ed. St Louis, MO: Mosby, **1972**:521–686
2. Goldfischer S, Coltoff-Schiller B, Biempica L, Wolinsky H. Lysosomes and the sclerotic arterial lesion in Hurler's disease. *Hum Pathol* **1975**;6: 633–637
3. Brosius FC, Roberts WC. Coronary artery disease in the Hurler syndrome. *Am J Cardiol* **1981**;47:649–653
4. Renteria EG, Ferrans VJ, Roberts WC. The heart in Hurler syndrome. *Am J Cardiol* **1976**;38:487–500
5. Gross DM, Williams JC, Caprioli C, Dominguez B, Howell R. Echocardiographic abnormalities in the mucopolysaccharide storage diseases. *Am J Cardiol* **1988**;61:170–176
6. Roybicek M, Gehler J, Spranger J. The clinical spectrum of alpha-L-iduronidase deficiency. *Am J Med Genet* **1985**;20:471–481
7. Krovertz LJ, Lorincz AE, Schiebler GL. Cardiovascular manifestations of the Hurler syndrome. *Circulation* **1965**;31:132–141
8. Craig WS. Gargoylism in a twin brother and sister. *Arch Dis Child* **1954**;29:293–295
9. Schmidt H, Ullrich K, Von Lengerki HJ, Kleine M, Bramswig J. Radiological findings in patients with mucopolysaccharidosis 1 H/S (Hurler-Scheie syndrome). *Pediatr Radiol* **1987**;17:409–414
10. Beaudet AL, DiFerrante WM, Ferry GD, Buford LN, Mullins CE. Variation in the phenotypic expression of beta-glucuronidase deficiency. *J Pediatr* **1975**;86:388–394
11. Shapiro J, Strome M, Crocker AC. Airway obstruction and sleep apnea in Hurler and Hunter syndromes. *Ann Otol Rhino Laryngol* **1985**;94:458
12. Wilson CS, Mankin HT, Pluth JR. Aortic stenosis and mucopolysaccharidosis. *Ann Intern Med* **1980**;92:496–498
13. Butman SM, Karl L, Copeland JG. Combined aortic and mitral valve replacement in an adult with Scheie's disease. *Chest* **1989**;96:209–210
14. Butman SM, Karl L, Copeland JG. Combined aortic and mitral valve replacement in an adult with Scheie's disease. *Chest* **1989**;96:209–210

Memorial

John W. Turner, 1912–1991



The death of John W. Turner on May 4, 1991, brought to a close the illustrious career of one who arguably could be considered the dean of radiologists in Western Massachusetts, and the medical community lost one of its most erudite, creative, and congenial colleagues. He had practiced the specialty of radiology in this area since 1938, fashioning a career replete with honors—locally, nationally, and internationally—and demonstrating standards of excellence that inspired great respect and emulation among his peers.

A native of Smithfield, TX, Dr. Turner was educated at Baylor University, the University of Texas, and the Baylor College of Medicine, where he was elected to Alpha Omega Alpha Honorary Medical Society. His postgraduate training included a rotating internship at Parkland Hospital in Dallas and then a fellowship in radiology at the University of Michigan (1937–1938) under Dr. Fred Jenner Hodges, who said that John typified the "finest example of the University of Michigan (radiology) graduate program." In 1938, John became a diplomate of the American Board of Radiology, and he migrated to Massachusetts, ostensibly for 1 year. Fortunately for the greater Springfield community, it became a 53-year expedition in excellence.

World War II interrupted Dr. Turner's private career, and he became the chief of radiology at the AAF Navigation School, San Marcos, TX, and the chief of radiology and regional consultant, Tucson, AZ (1942–1946). After the war years, he returned to the Springfield area to become radiologist at Western Massachusetts Hospital (1938–1957); chief of radiology, Wesson Memorial Hospital (1951–1977); associate professor of nuclear medicine, University of Connecticut (1976–1982); chief of medical imaging, Wesson Memorial Unit, Baystate Medical Center (1977–1981); clinical professor of radiology, Springfield Technical Community College (1974–1991); cochairman, Department of Radiology, Baystate Medical Center (1977); and chairman emeritus, Department of Radiology, Baystate Medical Center (1981–1991).

Throughout his career, Dr. Turner was a dedicated student of his specialty and maintained a constant awareness of the expanding parameters of its scope. This led to his developing the first nuclear medicine facility in Western Massachusetts in 1953 at the Wesson Memorial Hospital, resulting in his endorsement by the American College of Radiology as a diplomate of the American Board of Nuclear Medicine in 1972. He received fellowship honors in the American College of Radiology in 1946 and in the American College of Nuclear Medicine in 1974.

Dr. Turner's interest and involvement in cancer detection and treatment are indicated by his long association with the American Cancer Society; he was a director of the Massachusetts division from 1961 to 1991 and served as its president in 1977–1978. His awareness of the advancing technology in radiotherapeutic techniques led to the installation of the first cobalt unit in this area in 1957. In recognition of his outstanding contribution to the control of cancer, he was awarded a bronze medal by the American Cancer Society in 1970. Beyond these efforts in the diagnosis and treatment of lung cancer and other respiratory diseases related to smoking, his personal crusade to eliminate the hazards of tobacco usage gained him worldwide recognition.

As an academician, Dr. Turner's devotion to teaching was unceasing. In addition to his lectures at Springfield Technical Community College and on the hospital scene, John especially enjoyed the one-on-one tutoring experiences with medical students and residents. Over the years, the records of the students under his tutelage who took the national board examinations were most creditable; on several occasions, they had the top grades in the country. His teaching sessions continued after his retirement in 1989.

Dr. Turner is survived by his wife, Oma, to whom he was married for almost 54 years, and by his son, John G. Turner, who is the father of one daughter and three sons. Of special delight to John and Oma was the arrival of a great-grandson during the past year.

Dr. Turner's reputation as an academician and clinician was enhanced by a delicately dry sense of humor that blended so well with his kindness, compassion, and patience. He left an ineradicable heritage of professional excellence and moral integrity.

Kenneth L. McEwen
Springfield, MA 01103

Review Article

Response of Osteosarcoma and Ewing Sarcoma to Chemotherapy: Imaging Evaluation

Barry D. Fletcher[1]

The importance of diagnostic imaging in evaluating therapeutic response of bone sarcomas has increased with the use of chemotherapy administered before radiation therapy or surgery. The information provided by imaging studies is used to estimate prognosis; modify preoperative chemotherapy; and plan radiation therapy, surgery, and postoperative chemotherapy. This review examines the value and illustrates some pitfalls of traditional imaging methods, including conventional radiography, angiography, CT, and radionuclide scintigraphy, and discusses recent efforts to monitor therapy by using MR imaging and MR spectroscopy.

Dramatic improvement in the survival of patients with osteosarcoma and Ewing sarcoma during the past two decades can be attributed to the use of aggressive chemotherapy. Short-term disease-free survival rates have risen from approximately 10% for Ewing sarcomas and 20% for osteosarcomas before the use of adjuvant chemotherapy to at least 50% for Ewing sarcomas and even higher for osteosarcomas [1–4]. In the absence of chemotherapy, these two highly malignant tumors quickly metastasize even when adequate local control has been achieved. Drug treatment before surgery or radiation allows immediate delivery of a maximum dose to the primary tumor and any overt or occult metastatic disease that may be present. This strategy also presents the opportunity to assess the efficacy of various chemotherapeutic agents before adding other therapeutic procedures.

Precise clinical and radiologic methods of evaluating the primary lesion are necessary to select appropriate sites for excisional or needle biopsy, to plan surgical procedures so that resection can be achieved with adequate tumor margins, and to assess response to therapy. Clinical methods of monitoring response to treatment primarily rely on physical findings and biochemical markers [5]. The standard definitions for partial response (50% or greater reduction in tumor size) and complete response (complete disappearance of tumor) are subject to error and are difficult to apply to lesions arising in bone [6]. Estimates of volumetric changes based on diagnostic imaging studies are more reliable than clinical methods, but they do not always predict histopathologic response [7]. Because assessment of gross anatomic changes offers limited insight into the cellular alterations of malignant tissue, more refined techniques are needed to monitor the status of tumors during treatment and to predict response.

Osteosarcoma and Ewing sarcoma together account for the majority of musculoskeletal sarcomas diagnosed in patients of all ages and nearly 90% of those occurring in children and adolescents. Treatment of osteosarcoma usually consists of chemotherapy prior to surgical resection and postoperative chemotherapy. For Ewing sarcoma, chemotherapy precedes radiation therapy and/or surgery, which are followed by additional chemotherapy. However, primary surgical excision is frequently the treatment of choice for other malignant bone and soft-tissue neoplasms. The search for more sensitive

Received February 13, 1991; accepted after revision May 29, 1991.
This work was supported in part by National Cancer Institute grant PO1 CA 23099, Cancer Support (CORE) grant P30 CA 21765, and the American Lebanese Syrian Associated Charities.
[1] Department of Diagnostic Imaging, St. Jude Children's Research Hospital, 332 N. Lauderdale, P.O. Box 318, Memphis, TN 38101-0318. Address reprint requests to B. D. Fletcher.

AJR **157:825–833, October 1991** 0361–803X/91/1574–0825 © American Roentgen Ray Society

methods of monitoring treatment of osteosarcoma and Ewing sarcoma is especially important because response to the initial chemotherapy is one of the most reliable predictors of outcome [8, 9].

Histopathologic examination is the most accurate method of evaluating initial tumor response, which, in the case of osteosarcoma, is considered good if the remaining number of viable cells is less than 10% and poor if it exceeds 10% [8, 10–13]. The extent of the initial response may influence subsequent chemotherapy and the choice of surgical procedures, especially if limb-sparing surgery is an option. This review considers traditional methods of assessing therapeutic response and discusses the new option of using MR imaging (Table 1).

Conventional Radiography

Conventional radiography, essential for evaluating bone sarcomas, remains the most useful imaging technique for developing differential diagnoses, detecting pathologic fractures, and gauging tumor aggressiveness. Radiographs cannot be used to indicate accurately the extent of medullary involvement or to delineate soft-tissue masses unless the masses are heavily calcified.

Radiographic changes during initial chemotherapy of osteosarcomas loosely correlate with histologic grades [14]. Most drug-sensitive osteosarcomas show decreased bulk and increased ossification of the mass with formation of a peripheral bony shell [15–17], which is also evident on CT (Fig. 1). The irregular bony architecture appears more organized and less aggressive [17]. Destructive changes sometimes are seen; however, in the intraosseous component of the tumor, these may be due to liquefaction and necrosis rather than tumor growth [14] (Fig. 2). Other misinterpretations are also possible. For example, reductions in tumor size may be underestimated or overestimated on plain films, and increased extraosseous calcification and formation of a peripheral calcific shell have been observed in almost as many nonresponsive as responsive tumors [18]. Unlike osteosarcomas, responsive Ewing sarcomas do not form tumor bone, although frequently, the typical "onion skin" periosteal new bone in the extraosseous component of the mass will solidify. This reactive bone becomes incorporated into the remodeled cortex during chemotherapy or radiotherapy. The medullary cavity also may become heavily trabeculated [19].

Radionuclide Studies

A variety of radiopharmaceuticals are available for imaging bone tumors. Although radionuclide studies do not provide anatomic detail, semiquantitative analyses of tumorous activity can be performed because uptake of the labeled compound depends on cellular or other physiologic functions. Bone scintigraphy with ^{99m}Tc-labeled bone-seeking phosphate compounds, such as methylene diphosphonate (MDP), is used for detecting metastases at initial presentation and during follow-up of osteosarcomas and Ewing sarcomas [20, 21]. Bone scans (Figs. 1E and 1F) are less helpful for evaluating the primary tumor because they offer restricted spatial resolution and often exaggerate the extent of the tumor [22].

A complete three-phase examination includes rapid, dynamic images of local blood flow obtained at intervals of a few seconds during and after administration of the radiopharmaceutical and then static blood-pool or tissue-phase images [23]. A whole-body scan showing osseous uptake is obtained approximately 2 hr later. Some success in evaluating the response to treatment by using a combination of radiographs and skeletal scintigrams has been reported [24], but even three-phase studies may not predict response correctly [7].

TABLE 1: Imaging Signs of Chemotherapeutic Response

Imaging Study	Osteosarcoma	Ewing Sarcoma
Conventional radiography/CT	Increased tumor ossification, peripheral ossification	Disappearance of soft-tissue mass; cortical, medullary sclerosis
Radionuclide studies		
^{99m}Tc-MDP	Decreased activity	Decreased activity
^{67}Ga	Decreased activity	Decreased activity
^{201}Tl	Decreased activity	Decreased activity
Angiography	Disappearance of tumor vessels	Not done
MR imaging		
T1-weighted	No change	No change
T2-weighted	Increased signal suggests necrosis	Increased marrow signal, disappearance of soft-tissue mass
Enhanced with gadopentetate dimeglumine	No enhancement in necrotic regions	No soft-tissue enhancement
Dynamic enhanced	Decreased time-intensity curve slopes	Decreased slope of residual mass
^{31}P MR spectroscopy	Increased PCr/Pi; decreased pH, PME, and PDE	Increased PCr/Pi; decreased pH, PME, and PDE

Note.—PCr = phosphocreatine; Pi = inorganic phosphate; PME = phosphomonoester; PDE = phosphodiester.

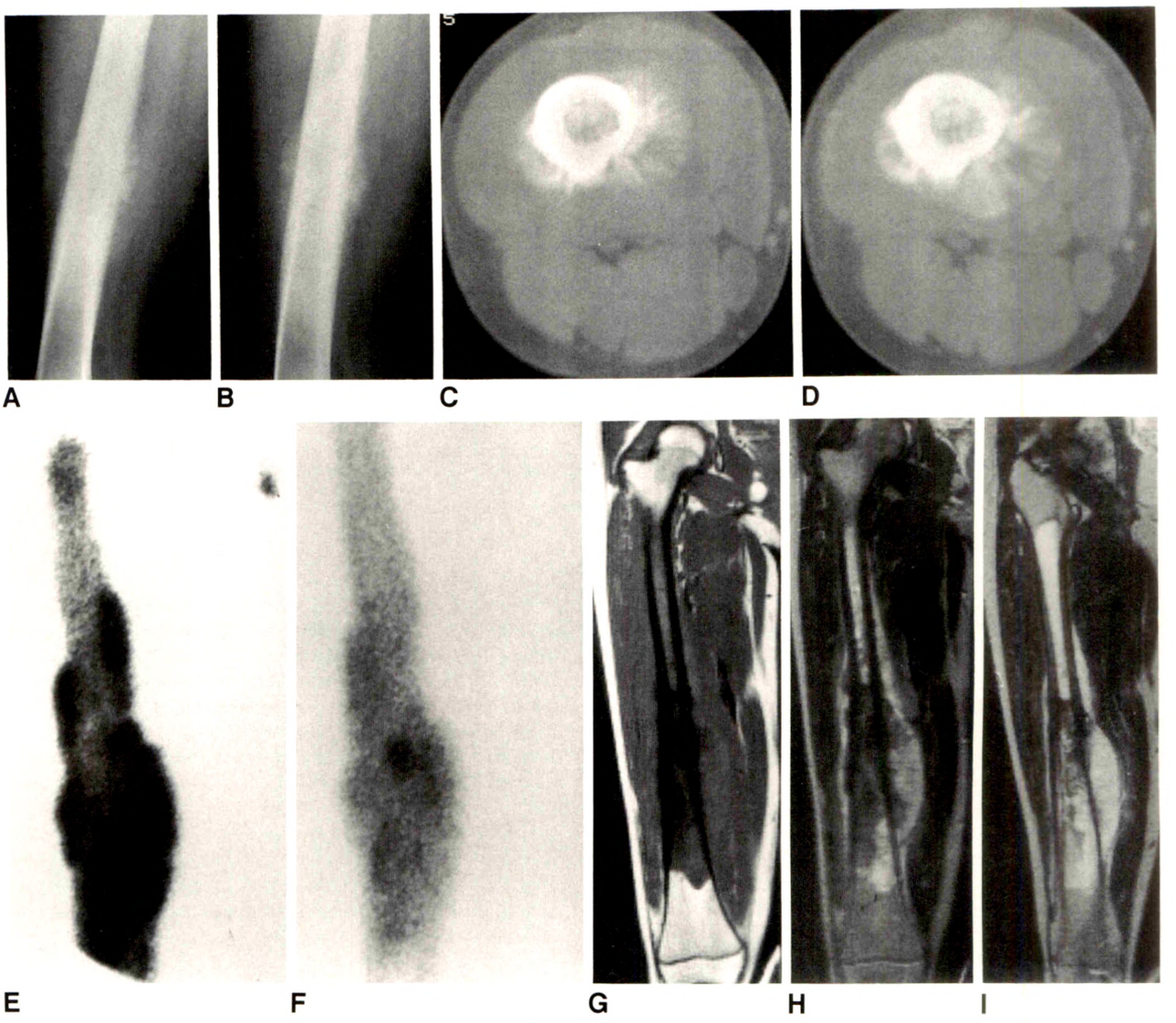


Fig. 1.—Osteosarcoma of femur with 100% histologic response in a 15-year-old girl.

A, Initial radiograph shows "sunburst" pattern of periosteal new bone formation extending from middle of femoral shaft.

B, Radiograph obtained after completion of first cycle (5 weeks) of chemotherapy shows soft-tissue ossification has increased slightly and appears more organized.

C and *D*, Contrast-enhanced CT scans obtained before (*C*) and after (*D*) chemotherapy show changes comparable to those seen on plain radiographs. Ossification of medulla and of soft-tissue mass is apparent. Ossified soft-tissue mass is well defined after treatment.

E and *F*, ^{99m}Tc-MDP bone scintigrams obtained before (*E*) and after (*F*) chemotherapy show decreasing uptake of radionuclide and no change in extent of its distribution.

G, coronal T1-weighted MR image, 440/19 (TR/TE), obtained before chemotherapy shows longitudinal extent of bone marrow involvement, which was not changed after chemotherapy. Soft-tissue component of tumor is similar in intensity to adjacent normal muscle.

H and *I*, Coronal T2-weighted MR images (2500/90) obtained before (*H*) and after (*I*) therapy show soft-tissue mass is relatively intense compared with hypointense muscle. Signal-deprived regions in medulla and soft-tissue mass correspond to areas of bone formation seen on CT scans. Chemotherapy slightly decreased extent of soft-tissue mass. Intensity of lesion increased.

Dynamic studies of ^{99m}Tc-MDP uptake have been used to distinguish good from poor responses to chemotherapy [25, 26]. Rapid serial scintigrams are used to measure activity in the tumor, which is compared with the activity in normal contralateral bone. Frequent sampling of venous blood determines plasma clearance of the radionuclide. Reductions in regional plasma clearance of more than 20% are considered significant and indicate tumor necrosis.

^{67}Ga-citrate is bound to plasma proteins, especially transferrin, and normally is distributed to the skeleton, liver, and soft tissues within 24–72 hr after administration. It is taken up avidly by Ewing sarcomas, osteosarcomas, and other

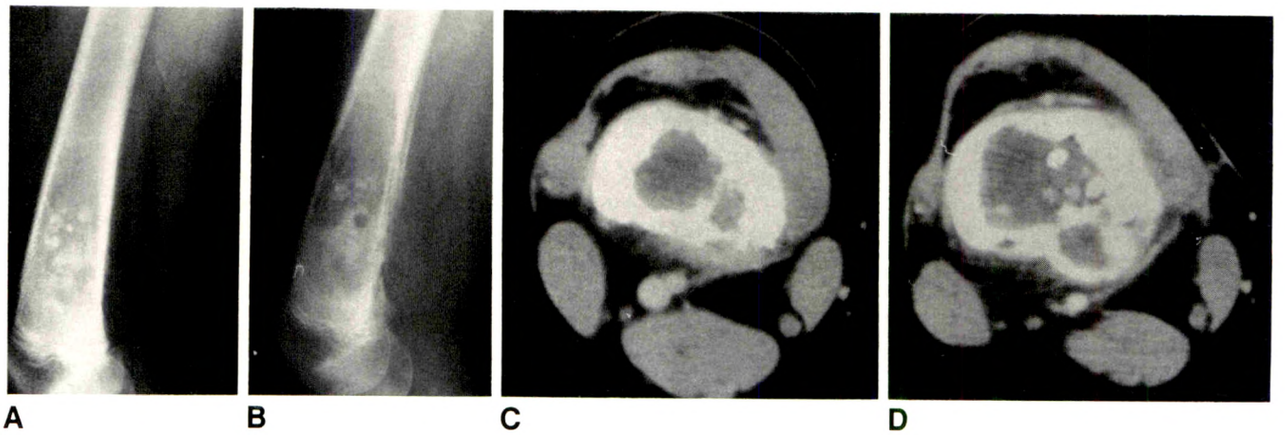


Fig. 2.—13-year-old boy with osteosarcoma.
A, Lateral radiograph of femur shows destructive lesion of medullary cavity with rounded areas of bone formation.
B, After 9 weeks of chemotherapy, tumor has extended beyond cortex posteriorly, and medullary component of lesion has enlarged.
C, Initial CT scan shows increased attenuation of medullary cavity and thick, irregular cortex.
D, After 9 weeks of chemotherapy, tumor expands posteriorly, and thigh muscles are atrophic. Histologic examination of resected specimen confirmed 100% necrosis. Posterior lesion was due to hemorrhagic necrosis.

benign and malignant bone tumors [27]. Uptake of ^{67}Ga more closely defines the actual tumor than does the ^{99m}Tc bone scan [28]. The ratios expressing uptake of gallium in tumor and in normal tissues significantly decrease in responsive osteosarcomas [29]. These responses occur somewhat earlier and are shown more consistently on gallium scans than on technetium scans.

Gallium scintigrams are probably most helpful for monitoring treatment response of Ewing sarcoma when findings on bone scintigraphy remain abnormal and no pathologic fracture is present. Under these conditions, normal findings on a gallium study suggest that no residual malignant disease is present [30]. As a routine follow-up procedure, gallium scintigraphy is inconvenient, because the studies require several days to be completed.

Thallium-201 has affinity for a variety of neoplasmas (Fig. 3) [31]. Its uptake is related to sodium-potassium pump activity, and because of its rapid clearance from the blood and lack of accumulation in nonneoplastic bone, ^{201}Tl appears to reflect actual tumor burden more accurately than scintigrams obtained with either ^{99m}Tc-MDP or ^{67}Ga-citrate [32]. Thallium scans may be more accurate than gallium or bone scans in indicating the course of disease, but they have not been widely used for this purpose [33].

Angiography

Because osteosarcomas are highly vascular, arteriography usually shows abundant neovascularity and capillary tumor stain [15, 34, 35]. Their soft-tissue components frequently can be opacified angiographically, and vessels in the less-well-differentiated portions of the tumor tend to be more irregular and disorganized than vessels in histologically less malignant regions [36]. Direct arteriography with conventional or digital imaging [37], which is required for optimal visualization of small tumor vessels, usually is reserved for patients receiving intraarterial treatment or for evaluation before limb salvage procedures.

Rapid disappearance of tumor vessels is associated with favorable response to chemotherapy, and persistent tumor vascularity suggests poor response [34]. In one study comparing osteosarcomas before and after chemotherapy, angiograms and histopathologic analyses corresponded for both responsive and nonresponsive tumors [18]. In another, larger series, angiograms enabled identification of most nonresponsive tumors, but many responsive tumors falsely were considered to be nonresponsive [34].

CT

CT provides a cross-sectional view of sarcomas arising from long bones, and its superior contrast resolution permits better visualization of the extraosseous soft-tissue masses and involved bone marrow. Calcifications also are detected more readily on CT. Changes in the CT appearance of the soft-tissue mass during successful treatment of osteosarcoma are analogous to those observed on plain films: decreased tumor size, increased intratumoral calcifications, and formation of a peripheral calcific rim [38, 39] (Figs. 1C, 1D, 3B, and 3C). In responsive tumors, however, CT may not show significant changes in the extent or attenuation of marrow disease, and active tumor cannot be differentiated from intramedullary necrosis [38] (see Figs. 2C and 2D). As with radiographs, CT scans may show increased ossification and formation of a peripheral bony shell in both nonresponsive and responsive tumors. In Ewing sarcomas, CT can show sclerosis and detect changes in the soft-tissue component of the tumor, allowing detailed study of the evolution of the tumor [40].

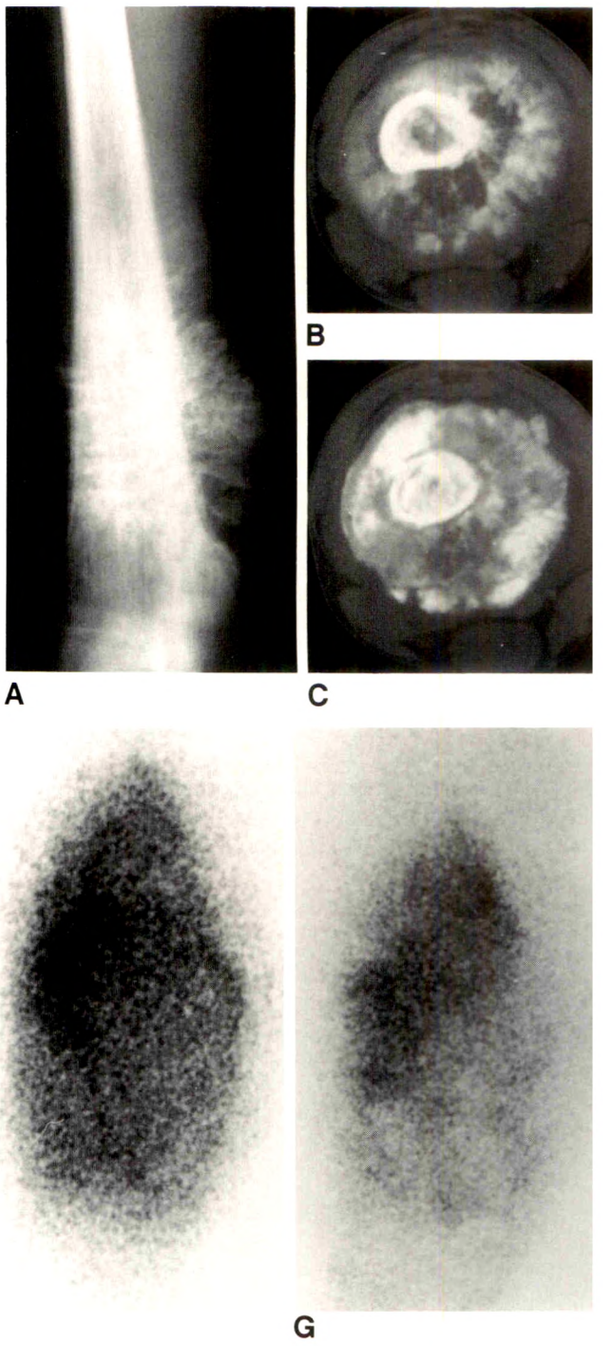
Fig. 3.—20-year-old man with clinical response to chemotherapy for osteosarcoma.

A, Anteroposterior radiograph obtained at diagnosis shows a large, bone-forming tumor of distal femur.

B and *C*, CT scans before (*B*) and after (*C*) chemotherapy show some increase in intramedullary and soft-tissue ossification with therapy but little change in transverse diameter of tumor.

D and *E*, ^{99m}Tc-MDP bone scintigrams before (*D*) and after (*E*) chemotherapy show decrease in radioactivity of tumor.

F and *G*, ^{201}Tl scintigrams before (*F*) and after (*G*) chemotherapy show considerable reduction in radionuclide uptake with chemotherapy, suggesting widespread tumorous necrosis.



MR Imaging

On MR images, the intensity of a given tissue is a function of the concentration of hydrogen atoms (protons) resonating within the imaged volume and of the longitudinal (T1) and transverse (T2) relaxation times, which, in turn, depend on the biophysical state of the water molecules of the tissue [41]. Many studies have shown the superiority of MR over CT for evaluating the medullary and soft-tissue components of bone sarcomas [42–49]. Malignant tumors have low signal on T1-weighted images and are usually isointense relative to muscle (Fig. 1G). Because of their high water content, most tumors are more intense than their tissue of origin on T2-weighted images. Involvement of bone marrow usually is shown best on T1-weighted images, on which the normally bright signal of the marrow fat is replaced by the less intense signal of the tumor (see Fig. 1G). Images of the entire length of the midshafts of affected long bones are obtained to detect

ith signal intensities of tumor, edema, and hemor-
] (e.g., Figs. 1H and 1I).

ts at correlating changes in MR signal intensity with
ave been somewhat conflicting. One group of inves-
52] observed four different patterns on T1- and T2-
images obtained after preoperative chemotherapy
arcomas: dark, mottled or speckled, homogeneous,
c. Other investigations [7, 53], which combined
omas, Ewing sarcomas, and other tumors, corre-
reases in T2-weighted signal intensity of the soft-
ss and favorable histologic response after preoper-
motherapy. Peritumoral, or paratumoral, edema,
ears on T2-weighted images as a rim of high signal
surrounding or adjacent to the tumor margins [52],
decrease with response to chemotherapy. In an-

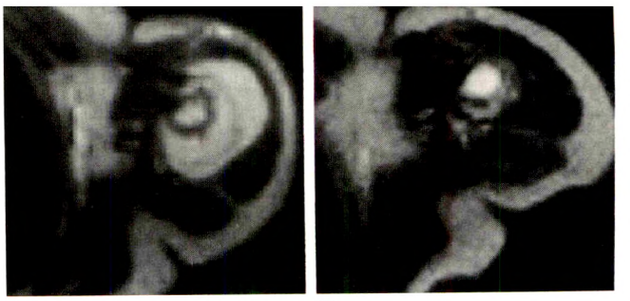


Fig. 4.—*A* and *B*, Transverse T2-weighted MR images, 2500/90 (TR/TE), of a 6-year-old girl with Ewing sarcoma of proximal humerus obtained before (*A*) and after (*B*) 6 weeks of chemotherapy show decrease in diameter of soft-tissue mass and increased intensity of marrow cavity.



destruction. On enhanced T1-weighted images, signal intensity remains low in avascular, necrotic regions of tumor and increases in viable tissue (Fig. 5). Although the fibrous and sclerotic portions of a tumor do not enhance, enhancement of nonmalignant, well-vascularized granulation tissue within a mass and peritumoral edema can lead to overestimations of the amount of residual malignant tissue [7, 60].

Dynamic MR studies, which use rapid gradient-echo imaging of a single section of tumor after injection of gadopentetate dimeglumine, have been used to distinguish benign and malignant musculoskeletal tumors [60] and to assess response to therapy [7, 61]. Tumor signal intensity is plotted from serial images obtained at 15- to 20-sec intervals, and the slope of the resultant time-intensity curve is calculated. Steeper slopes (>30%) suggest the presence of viable tumor. More gradual increases in signal intensity are seen in necrotic areas, but also in cystic regions and in cartilaginous and myxomatous tissue [60]. Overall, tumors sensitive to drugs show slower uptake of gadopentetate dimeglumine after preoperative chemotherapy than nonresponsive lesions do. The rapid uptake of the contrast agent by malignant tissues may be due to increased vascularity and more rapid perfusion of the agent through an expanded interstitial space [62].

Metabolic Imaging and Analysis

In vivo human MR spectroscopy is still an experimental technique, but it is being performed frequently on clinical high-field MR systems that are used for imaging also. Certain biologically important nuclei resonate at different RFs when placed in a magnetic field and excited at their characteristic frequencies. Studies of animal tumors by using high-field magnets have shown alterations with treatment of phosphorous-31 spectra that may reflect change in tumor oxygenation and provide earlier indications of chemotherapeutic response than conventional methods do [63, 64]. Studies of human musculoskeletal tumors have been confined mostly to analyses of ^{31}P spectra. At magnetic field strengths appropriate for humans, it is difficult to obtain a strong enough signal to resolve spectral peaks from tumor without contamination of the data by signals from normal muscle or fat. Currently, only semiquantitative measurements of metabolites are possible.

With musculoskeletal tumors, surface coils often can be used to achieve more efficient signal recovery. MR spectroscopy with surface coils has been used in several small series of human bone sarcomas and other malignant tumors [65–72]. The findings indicated that ^{31}P spectra are not specific for individual tumor types [67] but can be used to distinguish benign from malignant tumors [68]. The spectral pattern of malignant musculoskeletal sarcomas consists of elevated inorganic phosphate (Pi) and phosphomonoester (PME) resonances and relatively low phosphocreatine (PCr) resonances compared with surrounding muscle. Especially high levels of PCr, PME, and phosphodiesters (PDE), compared with β-nucleotide triphosphate, have been observed in large tumors with extensive necrosis [71]. Spectral changes associated with chemotherapy are sometimes contradictory, but responsive tumors usually show reversal of the pretreatment findings, with an increase in the PCr/Pi ratios, although several investigators have observed increased Pi concentrations during chemotherapy [66, 69]. Decreases in PME, PDE, and tumor pH also have been observed [65–67, 69].

A recent study is remarkable for the diversity of spectra observed in histologically similar malignant tumors [72]. Drug-responsive sarcomas, however, had lower PDE/PME ratios before chemotherapy and a larger increase in this ratio during the first cycle of chemotherapy than did nonresponsive tumors. These findings suggest a prognostic role for ^{31}P spectroscopy if these values remain consistent in a larger patient population.

Positron emission tomography (PET) with ^{18}F-2-fluoro-2-deoxy-D-glucose has been used for metabolic imaging of musculoskeletal neoplasms, mainly soft-tissue sarcomas. Uptake of this radioactive glucose analogue reflects glucose use, and high-grade tumors have been found to take up more of this analogue than low-grade lesions do [73, 74]. The ability to observe changes in glucose metabolism may offer a new method to quantify response to therapy, but no PET studies of musculoskeletal tumor response are yet available.

Conclusions

Response to chemotherapy is produced by subtle, fundamental alterations in tumor biology and ultimately is assessed by means of histologic estimations of tumor cell necrosis. Precise interim evaluations of chemotherapeutic success or failure cannot be made on the basis of changes in tumor bulk alone, but are important for further treatment planning and prognosis. Older imaging methods that use conventional radiography, CT, and radionuclide scintigraphy are important for initial diagnosis and staging, but changes demonstrated on these studies are difficult to quantify and do not always reflect alterations in tumor activity.

MR imaging is strongly recommended for follow-up evaluation of malignant lesions of the bone and may replace CT for this purpose. Analysis of signal intensity changes on T2-weighted images is particularly useful for monitoring the chemotherapeutic response of Ewing sarcoma. Although contrast enhancement does not provide more tumor/nontumor contrast than T2-weighted images do and increases the intensity of both malignant and reactive tissues, lack of contrast uptake is a precise indicator of tumor necrosis. Dynamic, enhanced MR images may permit more accurate estimations of tumor viability, but further trials of this new technique are needed. MR spectroscopy is capable of demonstrating metabolic changes in responsive tumors, but its clinical usefulness has yet to be determined. Finally, preliminary PET investigations suggest that this method also has the potential to detect the effects of chemotherapy in malignant tumors.

ACKNOWLEDGMENTS

I thank William H. Meyer, H. Lynn Magill, and June S. Taylor for advice and Ann Morris for editorial assistance.

REFERENCES

1. Zucker JM, Henry-Amar M, Sarrazin D, Blache R, Patte C, Schweisguth O. Intensive systemic chemotherapy in localized Ewing sarcoma in childhood: a historical trial. *Cancer* **1983**;52:415–423
2. Link MP, Goorin AM, Miser AW, et al. The effect of adjuvant chemotherapy on relapse-free survival in patients with osteosarcoma of the extremity. *N Engl J Med* **1986**;314:1600–1606
3. Eilber F, Giuliano A, Eckardt J, Patterson K, Moseley S, Goodnight J. Adjuvant chemotherapy for osteosarcoma: a randomized prospective trial. *J Clin Oncol* **1987**;5:21–26
4. Jürgens H, Exner U, Gadner H, et al. Multidisciplinary treatment of primary Ewing's sarcoma of bone: a 6-year experience of a European cooperative trial. *Cancer* **1988**;61:23–32
5. Miller AB, Hoogstraten B, Staquet M, Winkler A. Reporting results of cancer treatment. *Cancer* **1981**;47:207–214
6. Moertel CG, Hanley JA. The effect of measuring error on the results of therapeutic trials in advanced cancer. *Cancer* **1976**;38:388–394
7. Erlemann R, Sciuk J, Bosse A, et al. Response of osteosarcoma and Ewing sarcoma to preoperative chemotherapy: assessment with dynamic and static MR imaging and skeletal scintigraphy. *Radiology* **1990**;175:791–796
8. Rosen G, Caparros B, Huvos AG, et al. Preoperative chemotherapy for osteogenic sarcoma: selection of postoperative adjuvant chemotherapy based on the response of the primary tumor to preoperative chemotherapy. *Cancer* **1982**;49:1221–1230
9. Oberlin O, Patte C, Demeocq F, et al. The response to initial chemotherapy as a prognostic factor in localized Ewing's sarcoma. *Eur J Clin Oncol* **1985**;21:463–467
10. Salzer-Kuntschik M, Delling G, Beron G, Sigmund R. Morphological grades of regression in osteosarcoma after polychemotherapy: study COSS 80. *J Cancer Res Clin Oncol* **1983**;106 [suppl]:21–24
11. Huvos AG, Rosen G, Marcove RC. Primary osteogenic sarcoma: pathologic aspects in 20 patients after treatment with chemotherapy en bloc resection, and prosthetic bone replacement. *Arch Pathol Lab Med* **1977**;101:14–18
12. Raymond AK, Chawla SP, Carrasco CH, et al. Osteosarcoma chemotherapy effect: a prognostic factor. *Semin Diagn Pathol* **1987**;4:212–236
13. Picci P, Bacci G, Campanacci M, et al. Histologic evaluation of necrosis in osteosarcoma induced by chemotherapy: regional mapping of viable and nonviable tumor. *Cancer* **1985**;56:1515–1521
14. Smith J, Heelan RT, Huvos AG. Radiographic changes in primary osteogenic sarcoma following intensive chemotherapy: radiological-pathological correlation in 63 patients. *Radiology* **1982**;143:355–360
15. Chuang VP, Benjamin R, Jaffe N, et al. Radiographic and angiographic changes in osteosarcoma after intraarterial chemotherapy. *AJR* **1982**;139:1065–1069
16. Riebel T, Lassrich MA, Kumpan W. Roentgenologic follow-up in primarily conservatively treated osteogenic sarcoma. *J Cancer Res Clin Oncol* **1983**;106[suppl]:38–42
17. Den Heeten GJ, Thijn CJP, Kamps WA, Koops HS, Oosterhuis JW, Oldhoff J. The effect of chemotherapy on osteosarcoma of the extremities as apparent from conventional roentgenograms. *Pediatr Radiol* **1986**;16:407–411
18. Kumpan W, Lechner G, Wittich GR, et al. The angiographic response of osteosarcoma following pre-operative chemotherapy. *Skeletal Radiol* **1986**;15:96–102
19. Taber DS, Libshitz HI, Cohen MA. Treated Ewing sarcoma: radiographic appearance in response, recurrence, and new primaries. *AJR* **1983**;140:753–758
20. Gilday DL, Eng B, Ash JM, Reilly BJ. Radionuclide skeletal survey for pediatric neoplasms. *Radiology* **1977**;123:399–406
21. McKillop JH, Etcubanas E, Goris ML. The indications for and limitations of bone scintigraphy in osteogenic sarcoma: a review of 55 patients. *Cancer* **1981**;48:1133–1138
22. Sty JR, Starshak RJ, Miller JH. *Pediatric nuclear medicine*. Norwalk, CT: Appleton-Century-Crofts, **1983**:4
23. Holder LE. Clinical radionuclide bone imaging. *Radiology* **1990**;176:607–614
24. Riebel Von T, Knop J, Winkler K, Delling G. A comparison of radiological and isotope examinations of osteosarcomas for evaluating the effectiveness of preoperative chemotherapy. *ROFO* **1986**;145:365–372
25. Sommer H-J, Knop J, Heise U, Winkler K, Delling G. Histomorphometric changes of osteosarcoma after chemotherapy: correlation with ^{99m}Tc methylene diphosphonate functional imaging. *Cancer* **1987**;59:252–258
26. Knop J, Delling G, Heise U, Winkler K. Scintigraphic evaluation of tumor regression during preoperative chemotherapy of osteosarcoma: correlation of ^{99m}Tc-methylene diphosphonate parametric imaging with surgical histopathology. *Skeletal Radiol* **1990**;19:165–172
27. Frankel RS, Jones AE, Cohen JA, Johnson KW, Johnston GS, Pomeroy TC. Clinical correlations of ^{67}Ga and skeletal whole-body radionuclide studies with radiography in Ewing's sarcoma. *Radiology* **1974**;110:597–603
28. Simon MA, Kirchner PT. Scintigraphic evaluation of primary bone tumors: comparison of technetium-99m phosphonate and gallium citrate imaging. *J Bone Joint Surg [Am]* **1980**;62-A:758–764
29. Yeh SDJ, Rosen G, Caparros B, Benua RS. Semiquantitative gallium scintigraphy in patients with osteogenic sarcoma. *Clin Nucl Med* **1984**;9:175–183
30. Estes DN, Magill HL, Thompson EI, Hayes FA. Primary Ewing sarcoma: follow-up with Ga-67 scintigraphy. *Radiology* **1990**;177:449–453
31. Hisada K, Tonami N, Miyamae T. Clinical evaluation of tumor imaging with ^{201}Tl chloride. *Radiology* **1978**;129:497–500
32. Sehweil AM, McKillop JH, Milroy R. Mechanism of ^{201}Tl uptake in tumours. *Eur J Nucl Med* **1989**;15:376–379
33. Ramanna L, Waxman A, Binney G, Waxman S, Mirra J, Rosen G. Thallium-201 scintigraphy in bone sarcoma: comparison with gallium-67 and technetium-MDP in the evaluation of chemotherapeutic response. *J Nucl Med* **1990**;31:567–572
34. Carrasco CH, Charnsangavej C, Raymond AK, et al. Osteosarcoma: angiographic assessment of response to preoperative chemotherapy. *Radiology* **1989**;170:839–842
35. Jaffe N, Knapp J, Chuang VP, et al. Osteosarcoma: intra-arterial treatment of the primary tumor with *cis*-diammine-dichloroplatinum II (CDP). Angiographic, pathologic and pharmacologic studies. *Cancer* **1983**;51:402–407
36. Lagergren C, Lindbom A, Soderberg G. The blood vessels of osteogenic sarcomas: histologic, angiographic and microradiographic studies. *Acta Radiol* **1961**;55:161–176
37. Paushter DM, Borkowski GP, Buonocore E, Belhobek GH, Marks KE. Digital subtraction angiography for preoperative evaluation of extremity tumors. *AJR* **1983**;141:129–133
38. Mail JT, Cohen MD, Mirkin LD, Provisor AJ. Response of osteosarcoma to preoperative intravenous high-dose methotrexate chemotherapy: CT evaluation. *AJR* **1985**;144:89–93
39. Shirkhoda A, Jaffe N, Wallace S, Ayala A, Lindell MM, Zornoza J. Computed tomography of osteosarcoma after intraarterial chemotherapy. *AJR* **1985**;144:95–99
40. Vanel D, Contesso G, Couanet D, Piekarski JD, Sarrazin D, Masselot J. Computed tomography in the evaluation of 41 cases of Ewing's sarcoma. *Skeletal Radiol* **1982**;9:8–13
41. Mitchell DG, Burk DL Jr, Vinitski S, Rifkin MD. The biophysical basis of tissue contrast in extracranial MR imaging. *AJR* **1987**;149:831–837
42. Zimmer WD, Berquist TH, McLeod RA, et al. Bone tumors: magnetic resonance imaging versus computed tomography. *Radiology* **1985**;155:709–718
43. Aisen AM, Martel W, Braunstein EM, McMillin KI, Phillips WA, King TF. MRI and CT evaluation of primary bone and soft tissue tumors. *AJR* **1986**;146:749–756
44. Bohndorf K, Reiser M, Lochner B, Feaux de La Croix W, Steinbrich W. Magnetic resonance imaging of primary tumours and tumour-like lesions of bone. *Skeletal Radiol* **1986**;15:511–517
45. Boyko OB, Cory DA, Cohen MD, Provisor A, Mirkin D, DeRosa GP. MR imaging of osteogenic and Ewing's sarcoma. *AJR* **1987**;148:317–322
46. Pettersson H, Gillespy T III, Hamlin DJ, et al. Primary musculoskeletal tumors: examination with MR imaging compared with conventional modalities. *Radiology* **1987**;164:237–241
47. Sundaram M, McGuire MH, Herbold DR. Magnetic resonance imaging of osteosarcoma. *Skeletal Radiol* **1987**;16:23–29
48. Gillespy T III, Manfrini M, Ruggieri P, Spanier SS, Pettersson H, Springfield DS. Staging of intraosseous extent of osteosarcoma: correlation of preoperative CT and MR imaging with pathologic macroslides. *Radiology* **1988**;167:765–767
49. Bloem JL, Taminiau AHM, Eulderink F, Hermans J, Pauwels EKJ. Radiologic staging of primary bone sarcoma: MR imaging, scintigraphy, angiog-

raphy, and CT correlated with pathologic examination. *Radiology* **1988**;169:805–810
50. Sundaram M, McGuire MH, Schajowicz F. Soft-tissue masses: histologic basis for decreased signal (short T2) on T2-weighted MR images. *AJR* **1987**;148:1247–1250
51. Sanchez RB, Quinn SF, Walling A, Estrada J, Greenberg H. Musculoskeletal neoplasms after intraarterial chemotherapy: correlation of MR images with pathologic specimens. *Radiology* **1990**;174:237–240
52. Pan G, Raymond AK, Carrasco CH, et al. Osteosarcoma: MR imaging after preoperative chemotherapy. *Radiology* **1990**;174:517–526
53. Holscher HC, Bloem JL, Nooy MA, Taminiau AHM, Eulderink F, Hermans J. The value of MR imaging in monitoring the effect of chemotherapy on bone sarcomas. *AJR* **1990**;154:763–769
54. Vanel D, Lacombe M-J, Couanet D, Kalifa C, Spielmann M, Genin J. Musculoskeletal tumors: follow-up with MR imaging after treatment with surgery and radiation therapy. *Radiology* **1987**;164:243–245
55. Frouge C, Vanel D, Coffre C, Couanet D, Contesso G, Sarrazin D. The role of magnetic resonance imaging in the evaluation of Ewing sarcoma: a report of 27 cases. *Skeletal Radiol* **1988**;17:387–392
56. Lemmi MA, Fletcher BD, Marina NM, et al. Use of MR imaging to assess results of chemotherapy for Ewing sarcoma. *AJR* **1990**;155:343–346
57. Brasch RC, Weinmann H-J, Wesbey GE. Contrast-enhanced NMR imaging: animal studies using gadolinium-DTPA complex. *AJR* **1984**;142:625–630
58. Carr DH, Brown J, Bydder GM, et al. Gadolinium-DTPA as a contrast agent in MRI: initial clinical experience in 20 patients. *AJR* **1984**;143:215–224
59. Weinmann H-J, Brasch RC, Press W-R, Wesbey GE. Characteristics of gadolinium-DTPA complex: a potential NMR contrast agent. *AJR* **1984**;142:619–624
60. Erlemann R, Reiser MF, Peters PE, et al. Musculoskeletal neoplasms: static and dynamic Gd-DTPA–enhanced MR imaging. *Radiology* **1989**;171:767–773
61. Hanna SL, Fletcher BD, Fairclough DL, Le A. Use of dynamic Gd-DTPA enhanced MRI in musculoskeletal malignancies. *Magn Reson Imaging* **1990**;8[suppl]:9
62. Vaupel P, Kallinowski F, Okunieff P. Blood flow, oxygen and nutrient supply, and metabolic microenvironment of human tumors: a review. *Cancer Res* **1989**;49:6449–6465
63. Ng TC, Evanochko WT, Hiramoto RN, et al. ^{31}P NMR spectroscopy of *in vivo* tumors. *J Magn Reson* **1982**;49:271–286
64. Steen RG. Response of solid tumors to chemotherapy monitored by *in vivo* ^{31}P nuclear magnetic resonance spectroscopy: a review. *Cancer Res* **1989**;49:4075–4085
65. Nidecker AC, Muller S, Aue WP, et al. Extremity bone tumors: evaluation by P-31 MR spectroscopy. *Radiology* **1985**;157:167–174
66. Ross B, Helsper JT, Cox IJ, et al. Osteosarcoma and other neoplasms of bone: magnetic resonance spectroscopy to monitor therapy. *Arch Surg* **1987**;122:1464–1469
67. Semmler W, Gademann G, Bachert-Baumann P, Zabel H-J, Lorenz WJ, van Kaick G. Monitoring human tumor response to therapy by means of P-31 MR spectroscopy. *Radiology* **1988**;166:533–539
68. Negendank WG, Crowley MG, Ryan JR, Keller NA, Evelhoch JL. Bone and soft-tissue lesions: diagnosis with combined H-1 MR imaging and P-31 MR spectroscopy. *Radiology* **1989**;173:181–188
69. Redmond OM, Stack JP, Dervan PA, Hurson BJ, Carney DN, Ennis JT. Osteosarcoma: use of MR imaging and MR spectroscopy in clinical decision making. *Radiology* **1989**;172:811–815
70. Dewhirst MW, Sostman HD, Leopold KA, et al. Soft tissue sarcomas: MR imaging and MR spectroscopy for prognosis and therapy monitoring. *Radiology* **1990**;174:847–853
71. Zlatkin MB, Lenkinski RE, Shinkwin M, et al. Combined MR imaging and spectroscopy of bone and soft tissue tumors. *J Comput Assist Tomogr* **1990**;14:1–10
72. Koutcher JA, Ballon D, Graham M, et al. ^{31}P NMR spectra of extremity sarcomas: diversity of metabolic profiles and changes in response to chemotherapy. *Magn Reson Med* **1990**;16:19–34
73. Kern KA, Brunetti A, Norton JA, et al. Metabolic imaging of human extremity musculoskeletal tumors by PET. *J Nucl Med* **1988**;29:181–186
74. Adler LP, Blair HF, Williams RP, et al. Grading liposarcomas with PET using [^{18}F]FDG. *J Comput Assist Tomogr* **1990**;14:960–962

Book Review

Comparative Cardiac Imaging. Function, Flow, Anatomy and Quantitation. Edited by Bruce H. Brundage. Rockville, MD: Aspen, 561 pp., 1990. $115

This text is unique in that the editor, Dr. Brundage, has brought together 56 different contributors to discuss cardiac imaging as organized by disease process rather than technique. Of these 56, 10 are radiologists, and seven more have joint appointments with radiology departments. The remainder are cardiologists and cardiovascular surgeons.

The text includes 45 chapters separated into nine parts. Only part 1 deals with techniques per se. It is composed of four chapters that discuss echocardiography and Doppler techniques, cardiovascular nuclear medicine techniques, and technical aspects of cardiac CT and MR imaging. Thus, the reader is introduced to the basics and the differences in the various techniques before beginning analysis of the disease processes.

Part 2 deals with coronary artery disease and is composed of 15 chapters, which make up the largest portion of the entire text. Chapter 6, on coronary arteriography, is especially well done, with excellent illustrations, helpful diagrams, and anatomic descriptions. It covers a large topic concisely and accurately. The all-important chapter on contrast media discusses the physiologic effects of contrast media as well as the current controversy over ionic vs nonionic media. Florence Sheehan's chapter discusses using contrast ventriculograms to measure left ventricular function and compares the methods used most commonly to analyze wall motion. Chapters 5 and 9 provide a fine discussion of digital angiography for anatomy and myocardial perfusion. Chapter 10 illustrates echocardiographic evaluation of the left ventricle with excellent anatomic diagrams for positioning of the transducer and examples of two-dimensional and M-mode images. The limitations of echocardiography are offered honestly. Chapters 11–13 provide the input of nuclear medicine into infarct-avid scintigraphy, determination of myocardial perfusion by using planar thallium-201 imaging at rest and during exercise, and evaluation of left ventricular function by using radionuclide imaging. Chapters 14–17 describe using CT (both conventional and, especially, ultrafast) to evaluate acute myocardial infarction, myocardial blood flow, left ventricular function with exercise, and left ventricular aneurysms with or without thrombus. The ultrafast CT technique requires the use of IV contrast medium but provides excellent anatomic and functional information. Chapter 18 states that MR imaging for the evaluation of coronary artery disease holds promise but has not yet reached widespread clinical application. Chapter 19 provides the indirect and direct methods for evaluation of coronary artery bypass grafts and leaves no doubt that selective graft angiography currently is the gold standard.

Part 3 is composed of six chapters on the various means of assessing valvular heart disease. The value of radionuclide blood-pool imaging for evaluation of valvular heart disease is the least helpful. Dynamic MR is the newest method and shows great potential.

Part 4, on primary myocardial disease, is the second largest portion of the text and is composed of seven chapters. Part 5 has four chapters on pericardial disease, and part 6 has three chapters on congenital heart disease. Of interest, none of the last three chapters (part 6) describes contrast angiocardiograms in congenital heart disease. Instead two-dimensional echocardiography with Doppler imaging, ultrafast CT, and MR are touted. Charles Higgins's chapter confirms that MR can be used to define anatomic anomalies of the heart and great vessels as well as to evaluate function by using gradient refocused techniques. The noninvasive nature of MR makes it ideal for monitoring severe cardiovascular anomalies and following up postoperative status in children.

Part 7 consists of one delightful chapter on imaging of cardiac tumors. It is short and sweet, concise and complete. Part 8 provides four chapters on the great vessels. Chapter 45 composes the final part 9, which discusses the comparative safety of the cardiac imaging techniques and brings all the previous chapters into proper perspective.

Most of the text is well organized and comprehensive, with excellent references and comparisons. When compared with other current texts, this book is broader in scope because it includes all cardiac imaging techniques, not just two or three. However, its emphasis on disease process, rather than technique, does allow some redundancy. Because it has multiple contributors, the style of writing varies throughout the text. However, the summary at the end of each chapter brings everything together.

Several criticisms can be made. Early in the text are four pages of colored illustrations. Only the first page is pertinent to the adjacent chapter. The others refer to later chapters in the text. This is inconvenient for the reader but certainly easier and less expensive for the publishers. Second, almost 50% of the illustrations are from previous publications. When new illustrations are offered, they are excellent and demonstrative, especially the MR images and echocardiograms. The tables and diagrams are helpful and easily interpreted.

In summary, this is one of the top books on comparative cardiac imaging techniques. I highly recommend it for any and all libraries in academic and clinical departments that deal with cardiac imaging.

Patricia A. Randall
SUNY Health Science Center at Syracuse
Syracuse, NY 13210

Case Report

Distal Aortopulmonary Window with Aortic Origin of the Right Pulmonary Artery and Interruption of the Aortic Arch (Berry Syndrome): Diagnosis by MR Imaging

Shi-Joon Yoo,[1] Hye Young Choi,[1] In-Sook Park,[2] Chang Yee Hong,[2] Meong Gun Song,[3] and Sam Hyun Kim[3]

Aortopulmonary window is an uncommon congenital malformation characterized by a windowlike communication between the ascending aorta and the pulmonary arterial trunk in the presence of separate aortic and pulmonary valves. The defects have been classified into proximal, distal, and total types according to the location of the defect [1–4]. Berry et al. [2] recognized the association of the distal type of aortopulmonary window with aortic origin of the right pulmonary artery and hypoplasia or interruption of the aortic arch as a specific syndrome. Correct preoperative diagnosis and detailed anatomic depiction of each component of this association are important. We report a case in which each component of this rare association was defined precisely by using MR imaging.

Case Report

A 45-day-old male neonate was admitted because of respiratory distress and cyanosis, which had developed a few days after his birth. He had been born after 36 weeks of uneventful gestation. On physical examination, the body weight was 3500 g, the pulse rate was 156 beats per minute, and respirations were 70/min. The blood pressures of the right and left arms were 90/48 mm Hg and 100/41 mm Hg, respectively. Those of the right and left legs were 64/45 mm Hg and 69/43 mm Hg, respectively. Auscultation of the heart revealed accentuation of the first and second heart sounds and a grade 3/6 systolic murmur at the base of the heart. The ECG showed left ventricular hypertrophy. The chest radiographs showed a cardiothoracic ratio of 70% and increased pulmonary vascularity.

ECG-gated MR imaging was performed on a 1.5-T MR unit (Signa, General Electric Medical Systems, Milwaukee, WI). Multiplanar images with a slice thickness of 3 or 4 mm were obtained by using spin-echo, multislice technique with an echo time (TE) of 20 msec and a repetition time (TR) of 600 msec. No intracardiac anomaly was seen. The ascending aorta and main pulmonary arterial trunk arose from their respective ventricles and were related normally to each other. A large defect 12 mm in diameter was present between the ascending aorta and the distal main pulmonary artery, approximately 8 mm above the semilunar valves. The exact site of the defect was best shown on oblique coronal images, which were equivalent to the angiographic right anterior oblique view (Fig. 1A). The oblique axial image that traversed the orifices of the right and left pulmonary arteries clearly showed the spatial relationship between the aortopulmonary window and the pulmonary arterial orifices (Fig. 1B). The aortopulmonary window involved the left posterior wall of the ascending aorta, and the right pulmonary artery was separated from the left pulmonary artery and arose from the posterior wall of the ascending aorta. The left pulmonary artery was a direct continuation of the main pulmonary arterial trunk. The oblique sagittal image, which was equivalent to the angiographic left anterior oblique view, showed the interrupted aortic arch distal to the origin of the left subclavian artery (Fig. 1C). More steeply oblique sagittal images showed the connection of the roof of the main pulmonary arterial trunk and the proximal descending aorta by a small patent ductus arteriosus (Fig. 1D). These MR findings were more precise and objective than the findings of two-dimensional echocardiography, which was performed before and after the MR imaging.

The patient had two-stage corrective surgery on the basis of the MR imaging and echocardiographic findings alone, without the need for cardiac catheterization and angiocardiography. At the first-stage operation, the interrupted aortic arch was reconstructed by using a 10-mm Goretex tube (Gore and Associates, Inc., Flagstaff, AZ) interposition graft, and the patent ductus arteriosus was ligated. Ten days after the first operation, tunneling of the right pulmonary artery to the main pulmonary artery was performed by using a Dacron patch through a transaortic approach, and a separate pericardial patch was applied to the vertically incised margins of the anterior wall of the ascending aorta. The postoperative course was uneventful. At follow-up when he was 6 months old, the patient was doing well.

Discussion

The distal type of aortopulmonary window is a communication between the left posterolateral wall of the ascending aorta and the pulmonary arterial bifurcation [1–4]. Such defects are closely related to the orifice of the right pulmonary

Received March 12, 1991; accepted after revision May 2, 1991.
[1] Department of Diagnostic Radiology, University of Ulsan, Asan Medical Center, Kang-Dong P.O. Box 145, Seoul 134-600, Korea.
[2] Department of Pediatrics, University of Ulsan, Asan Medical Center, Kang-Dong P.O. Box 145, Seoul 134-600, Korea.
[3] Department of Thoracic Surgery, University of Ulsan, Asan Medical Center, Kang-Dong P.O. Box 145, Seoul 134-600, Korea.

 0361–803X/91/1574–0835 © American Roentgen Ray Society

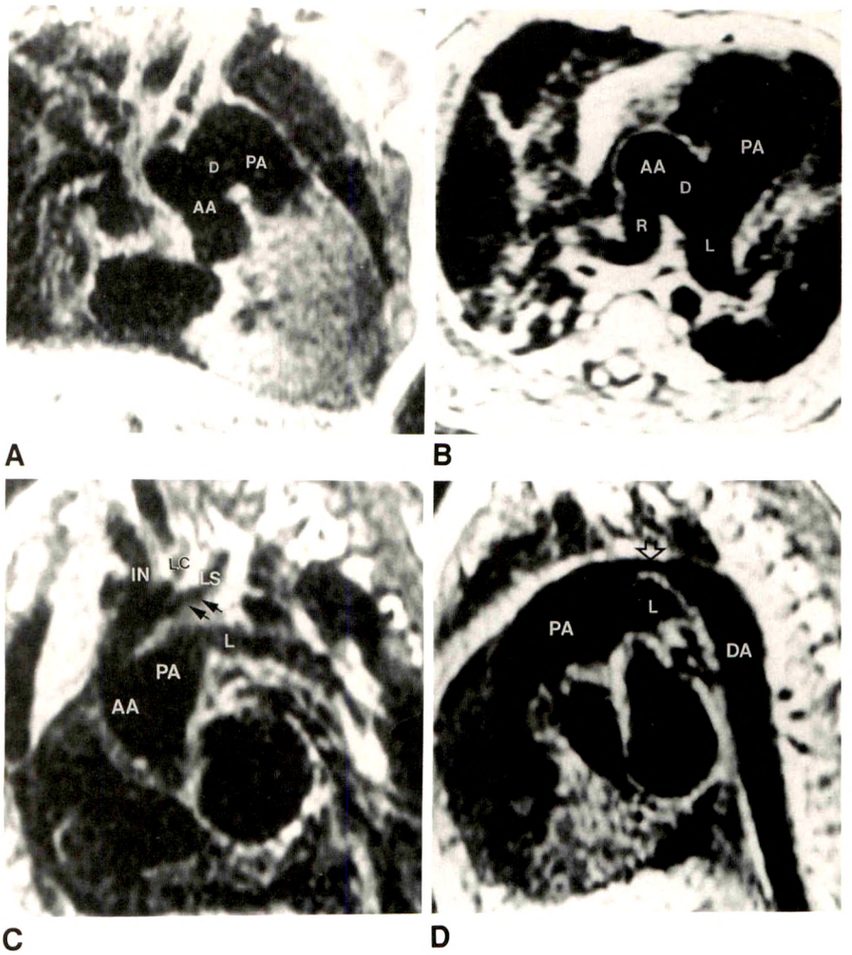


Fig. 1.—*A*, Oblique coronal MR image equivalent to angiographic right anterior oblique view shows a large aortopulmonary window (D) between distal ascending aorta (AA) and distal pulmonary artery (PA).

***B*, Oblique axial MR image shows an aortopulmonary window (D) and anomalous origin of right pulmonary artery (R) from posterior wall of ascending aorta (AA). L = left pulmonary artery.**

***C*, Oblique sagittal MR image equivalent to angiographic left anterior oblique view shows interruption of aortic arch (*arrows*) distal to origin of left subclavian artery (LS). IN = innominate artery, LC = left common carotid artery.**

***D*, More steeply oblique sagittal MR image shows a small patent ductus arteriosus (*arrow*). DA = descending aorta.**

artery, which may be separated from the orifice of the left pulmonary artery in various degrees [1–5]. Frequently, the right pulmonary artery straddles the aortopulmonary window or originates completely from the posterior wall of the ascending aorta. Berry et al. [2] have recognized the frequent association of the distal type of aortopulmonary window with hypoplasia or interruption of the aortic arch when the right pulmonary artery arises separately from the ascending aorta. They have related the development of the obstructive lesion of the aortic arch in the distal type of aortopulmonary window to the diminished blood flow to the aortic isthmus caused by direct diversion of the aortic blood flow into the right pulmonary artery during fetal life. They have characterized the association as a specific syndrome rather than a random coincidence.

Surgical correction of this complex anomaly requires both repair of the hypoplastic or interrupted aortic arch and septation of the aortopulmonary window, with exclusion of the right pulmonary arterial orifice from the aorta [2]. Because simple patch tunneling for the second procedure may create supravalvular aortic stenosis, patch tunneling with enlargement of the aorta by using an anterior patch or detachment and connection of the right pulmonary artery to the main pulmonary arterial trunk is mandatory [2]. The success of this complicated repair depends on the meticulous design of each step of the procedure before surgery. Hitherto, this syndrome has been diagnosed on the basis of angiographic and echocardiographic studies [2, 6].

This case illustrates the advantage of MR imaging in depicting the detailed anatomy of this complex syndrome, which includes the exact site of origin of the right pulmonary artery from the posterior wall of the ascending aorta and the spatial relationship between the aortopulmonary window and the right pulmonary arterial orifice. When coupled with two-dimensional and Doppler echocardiographic studies, MR imaging, with its wide field of view and capability to image the heart and great vessels in any desired plane, will obviate angiocardiographic confirmation.

REFERENCES

1. Mori K, Ando M, Takao A, Ishikawa S, Imai Y. Distal type of aortopulmonary window: report of 4 cases. *Br Heart J* **1978**;40:681–689
2. Berry TE, Bharati S, Muster AJ, et al. Distal aortopulmonary septal defect, aortic origin of the right pulmonary artery, intact ventricular septum, patent ductus arteriosus and hypoplasia of the aortic isthmus: a newly recognized syndrome. *Am J Cardiol* **1982**;49:108–116
3. Blieden LC, Moller JH. Other left-to-right shunts. In: Moller JH, Neal WA, eds. *Fetal, neonatal, and infant cardiac disease.* Norwalk, CT: Appleton & Lange, **1990**:433–450
4. Kusche LM, Van Mierop LHS. Anatomy and pathogenesis of aorticopulmonary septal defect. *Am J Cardiol* **1987**;59:443–447
5. Braunlin E, Peoples WM, Fredom RM, Fyler DC, Goldblatt A, Edwards JE. Interruption of the aortic arch with aortopulmonary septal defect: an anatomic review. *Pediatr Cardiol* **1982**;3:329–335
6. Mendoza DA, Ueda T, Nishioka K, et al. Aortopulmonary window, aortic origin of right pulmonary artery, and interrupted aortic arch: detection by two-dimensional and color Doppler echocardiography in an infant. *Pediatr Cardiol* **1986**;7:49–52

Optimizing Brain MR Imaging Protocols with Gadopentetate Dimeglumine: Enhancement of Intracranial Lesions on Spin-Density- and T2-Weighted Images

Francis W. Wessbecher[1]
Kenneth R. Maravilla
Robert W. Dalley

To determine whether long TR MR imaging is best performed before or after IV administration of gadopentetate dimeglumine, we obtained spin-density- and T2-weighted images before and after contrast administration in 21 patients with known intracranial enhancing lesions. Of 25 lesions demonstrating enhancement on T1-weighted sequences, 21 showed mild or moderate enhancement on spin-density-weighted sequences and 20 showed mild enhancement on T2-weighted sequences. Importantly, no spin-density or T2 information was obscured by the administration of gadopentetate dimeglumine, and no T2 shortening effects were visible. Two new foci of enhancement were visible on postcontrast spin-density- and T2-weighted images that were missed on postcontrast T1-weighted images and on precontrast spin-density- and T2-weighted studies. Visualization of new areas of enhancement is the main advantage provided by the long TR images obtained after IV injection of gadopentetate dimeglumine. The most likely reason for the appearance of these newly visualized lesions is thought to be delayed enhancement. This imaging protocol also allows the display of adjacent edema or gliosis and enhancing lesions on a single image. Additionally, in three cases, posterior fossa phase-shift artifacts raised the suspicion of an enhancing lesion on postcontrast T1-weighted images, but the cerebellum was shown to be normal on the postcontrast spin-density- and T2-weighted studies.

On the basis of our results, we recommend obtaining long TR images after rather than before the administration of gadopentetate dimeglumine in patients with intracranial enhancing lesions.

***AJNR* 12:675–679, July/August 1991; *AJR* 157:837–841, October 1991**

Several reports have documented the importance of gadopentetate dimeglumine in MR imaging of the brain [1–5]. Although enhancing lesions in the brain are best demonstrated on postcontrast T1-weighted images, long TR pulse sequences (i.e., spin-density- and T2-weighted images) remain essential to identify many nonenhancing abnormalities with increased water content, such as low-grade tumors or areas of edema, infarction, or demyelination. It has been recognized that some contrast enhancement occurs with spin-density-weighted imaging sequences [3]; however, little attention has been directed toward the relative advantages or disadvantages of combining contrast administration with long TR pulse sequences. In view of this, we undertook a study to compare pre- and postcontrast spin-density- and T2-weighted images to determine whether it is more advantageous to obtain long TR images before or after the administration of contrast material. Our aims were to determine the frequency with which contrast enhancement was discernible on spin-density- and T2-weighted images and whether such enhancement provided any additional information to that obtained with postcontrast T1-weighted images. We also analyzed the postcontrast long TR images to determine whether any new areas of enhancement were detected and, most importantly, whether any spin-density or T2 information was obscured after administration of gadopentetate dimeglumine.

Received July 23, 1990; revision requested November 11, 1990; revision received January 30, 1991; accepted February 17, 1991.

Presented at the annual meeting of the Society of Magnetic Resonance Imaging, Washington, DC, February 1990.

[1] All authors: Department of Radiology SB-05, University of Washington Medical Center, Seattle, WA 98195. Address reprint requests to K. R. Maravilla.

0361–803X/91/1574–0837
© American Roentgen Ray Society

Materials and Methods

Twenty-one randomly selected patients with a variety of intracranial lesions that had demonstrated enhancement on previous CT or MR examinations were studied prospectively. Nine patients had recurrent gliomas, three patients had metastatic lesions, two patients had postoperative enhancement, two patients had meningiomas, one patient had a low-grade glioma, one patient had an inflammatory lesion, one patient had a pineal germinoma, one patient had a venous angioma, and one patient had an acute demyelinating plaque. Of the three patients with metastatic disease, one patient had three lesions while the other two patients had two lesions each. Thus, a total of 25 enhancing lesions were identified in the study population.

All patients were examined on a 1.5-T MR unit (GE, Milwaukee, WI). Imaging sequences prior to contrast injection consisted of sagittal and axial T1-weighted sequences, 600/20/2 (TR/TE/excitations), followed by axial spin-density- and T2-weighted images (2700/30–80/1). Following IV administration of 0.1 mmol/kg of gadopentetate dimeglumine (Magnevist, Berlex, Inc., Wayne, NJ), the axial T1-weighted and the axial long TR sequences were repeated with identical imaging parameters. Postcontrast images were completed within 20 min of injection. Slice thickness was 5 mm with a 2.5-mm interslice gap and 256 × 192 matrix.

All studies were reviewed by three neuroradiologists in a nonblinded fashion; a consensus opinion was reached as to the presence or absence of enhancement on each pulse sequence. Enhancement was graded as mild, moderate, or marked. Pre- and postcontrast spin-density- and T2-weighted images were compared to determine the degree of enhancement and the location and extent of all pathologic findings, both enhancing as well as nonenhancing. The enhanced spin-density- and T2-weighted images were also compared with the postcontrast T1-weighted images to determine if any areas of enhancement were obscured or if any additional areas of enhancement were identified on the long TR images. The presence and extent of

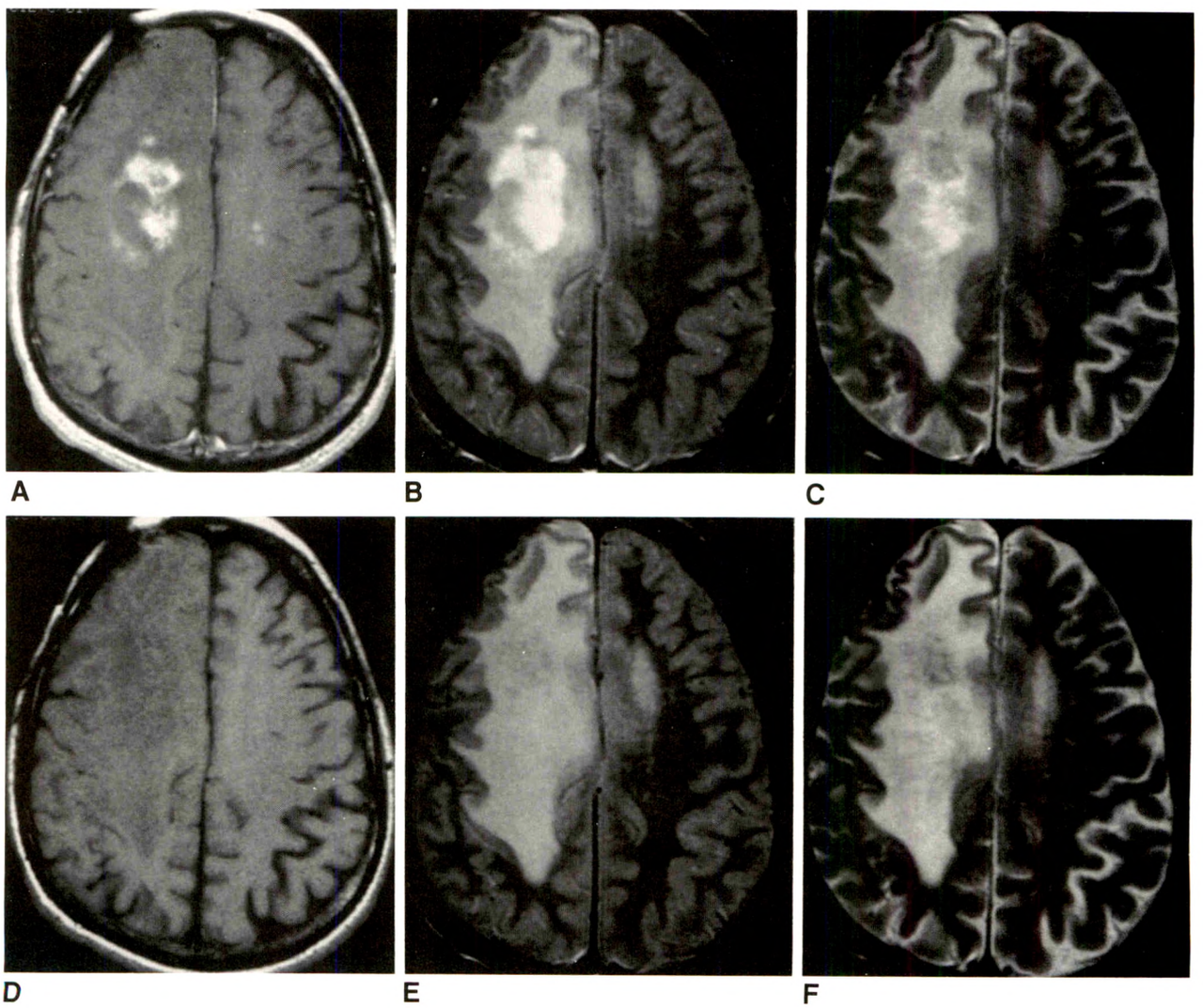


Fig. 1.—Patient with recurrent astrocytoma.
A–F, Postcontrast T1-weighted (*A*), spin-density-weighted (*B*), and T2-weighted (*C*) MR images distinguish enhancement of underlying lesion from adjacent edema as compared with unenhanced T1-weighted (*D*), spin-density-weighted (*E*), and T2-weighted (*F*) images.

nonenhancing abnormalities (such as edema or gliosis) were also evaluated on pre- and postcontrast long TR images to determine if contrast administration had any effect on these abnormalities.

Results

In this series of 21 patients, 25 enhancing lesions were identified on T1-weighted postcontrast MR images. Most of these lesions also demonstrated enhancement on the long TR pulse sequences. Twenty-one of 25 lesions enhanced on spin-density-weighted images and 20 of 25 lesions showed some perceptible enhancement on T2-weighted images. Of the four lesions that showed no discernible enhancement on postcontrast spin-density- or T2-weighted images there was only mild enhancement on postcontrast T1-weighted images. All lesions that demonstrated moderate to marked enhancement on the postcontrast T1 sequence also showed enhancement on the postcontrast long TR sequence.

In 14 of 16 cases with significant associated edema, concurrent visualization of the enhancing nidus of the lesion as well as the adjacent edema was possible on both the postcontrast spin-density- and T2-weighted images (Fig. 1). In these cases, nidus identification was generally not possible on the precontrast spin-density- and T2-weighted images. In six of nine cases with proved recurrent astrocytoma, the postcontrast spin-density- and T2-weighted images allowed improved differentiation of the enhancing recurrent tumor from an adjacent postsurgical cavity when compared with the precontrast spin-density- and T2-weighted images. In two cases with intracerebral hemorrhage, the postcontrast spin-density- and T2-weighted images showed an enhancing lesion that proved to be the origin of the hemorrhage. These lesions were not seen on precontrast long TR images, although they were seen on the postcontrast T1-weighted images.

Most importantly, direct comparisons of pre- and postcontrast long TR images demonstrated that no spin-density or T2 information was obscured after the administration of gadopentetate dimeglumine. Despite the theoretical concern that the T2 shortening effect of contrast medium might obscure pathologic changes, this did not occur in any of our cases. As expected, enhancement on the spin-density-weighted images was either equal to or, in most cases, less than that observed on T1-weighted images. Also as expected, more marked enhancement was observed on the spin-density-weighted images than on the corresponding T2-weighted images.

In two cases, new areas of enhancement were visualized on the postcontrast long TR pulse sequences that were not visualized on the postcontrast T1-weighted images. In one case of recurrent astrocytoma, spin density- and T2-weighted images demonstrated a new finding of dural enhancement (Fig. 2). In another patient with metastases from a renal cell carcinoma, spin-density images demonstrated enhancement within a hemorrhagic tumor that was not evident on enhanced T1 images. The visualization of these new areas of enhancement was the single most important advantage to obtaining the long TR pulse sequences after rather than before contrast administration. These new abnormalities are most likely related to delayed enhancement within these lesions rather than to increased sensitivity of the spin-density sequences to contrast enhancement.

We also noted three cases in which suspicious or equivocal lesions within the brainstem or cerebellum were seen on enhanced T1-weighted images. These were later proved to represent posterior fossa phase-shift artifacts and not pathologic abnormalities. In all three cases, these suspicious areas of abnormality were shown to be entirely normal on the postcontrast spin-density- and T2-weighted images that were

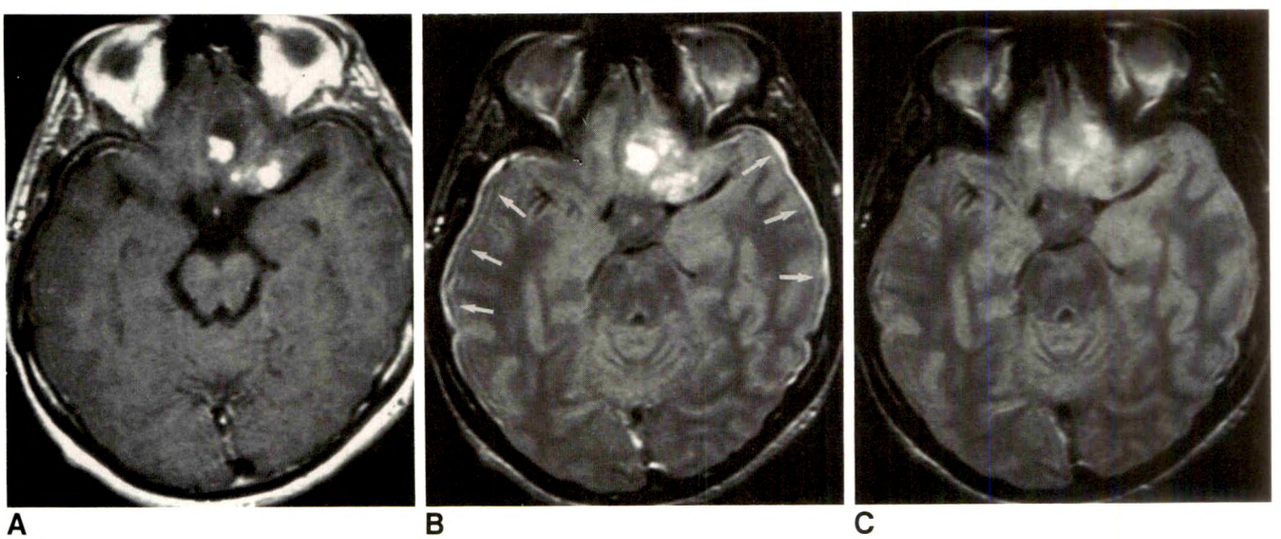


Fig. 2.—*A–C*, Lesion enhancement in patient with recurrent astrocytoma is demonstrated on postcontrast T1-weighted image (*A*) and postcontrast spin-density-weighted image (*B*). In addition, postcontrast spin-density-weighted image shows a new finding of bilateral dural enhancement (*arrows*) as compared with precontrast spin-density-weighted image (*C*). Finding was not apparent on *A*, and is most likely the result of delayed enhancement of the dura.

obtained with flow-compensation techniques (Fig. 3). These findings were later confirmed by follow-up MR imaging in all three cases.

Discussion

In clinical practice, long TR images are sometimes obtained and evaluated to determine whether contrast material should be administered. In addition, a small portion of MR brain examinations are performed to investigate such entities as chronic multiple sclerosis plaques that do not require further characterization by the administration of contrast material. Clearly, the results of this study will have little impact on either of these subsets of MR examinations. However, in an ever-increasing percentage of cases, it is known before the start of the MR examination that the clinical considerations can only be addressed with the use of contrast material. It is for this group of cases that our study was designed. While the most commonly used protocol consists of unenhanced T1 and long TR sequences followed by a T1-weighted enhanced examination, our study demonstrates several advantages to obtaining the long TR images after rather than before contrast administration.

There are two major reasons for the common practice of obtaining spin-density- and T2-weighted images before the administration of contrast medium. First, since the predominant effect of gadopentetate dimeglumine at the clinically used dosage is T1 shortening [6], there is no obvious advantage to obtaining T2-weighted images after its administration. Second, at high concentrations, gadopentetate dimeglumine has an additional effect of T2 shortening that could theoretically mask T2 abnormalities by causing a "paradoxical" decrease in signal intensity [6].

In the present study, contrast enhancement was visible in the vast majority of cases on both spin-density- and T2-weighted images. This enhancement was either equal to or, in most cases, less than that observed on T1-weighted images. The predominant mechanism for this enhancement is the residual T1 effects that are present on the spin-density-weighted and, to a much lesser degree, the T2-weighted images caused by incomplete recovery of the longitudinal magnetization vector during the finite TR interval of 2700 msec. This residual T1 effect is amplified by the use of a high-field-strength magnet (1.5 T), which prolongs the T1 relaxation time of tissues compared with a low- or mid-field-strength MR system. Although the T1 information displayed on these spin-density-weighted images would be demonstrated better by a T1-weighted image obtained at the same time, the spin-density images provide the advantage of displaying both contrast enhancement and T2 information on a single image. This improves the appreciation of the spatial relationships between different components of a pathologic entity, such as tumor nidus or edema. Most significantly, no T2 shortening effects were observed in our study. Direct comparisons of the pre- and postcontrast long TR images demonstrated that no spin-density or T2 information was obscured after the administration of contrast material. Nonenhancing abnormalities such as edema and gliosis were equally well shown on the pre- and postcontrast long TR sequences in all cases. Thus, equivalent T2 information can be obtained with both pre- and postcontrast imaging.

We also analyzed these studies to determine if additional abnormalities could be identified on the postcontrast long TR images. New lesions with enhancement were defined in two of our 21 patients on the postcontrast spin-density- and T2-weighted images that were definitely not present on the precontrast long TR images or on the short TR images, with or without contrast enhancement. In one case, bilateral areas of postoperative dural reaction with enhancement were noted, and in another case an enhancing metastatic lesion adjacent to an area of hemorrhage was noted. These findings are most likely the result of delayed enhancement within these lesions, a phenomenon noted previously on MR images of intracranial disease [7, 8]. It should be noted that in this study the postcontrast long TR images were always acquired after the postcontrast T1-weighted images. Thus, a delay of approxi-

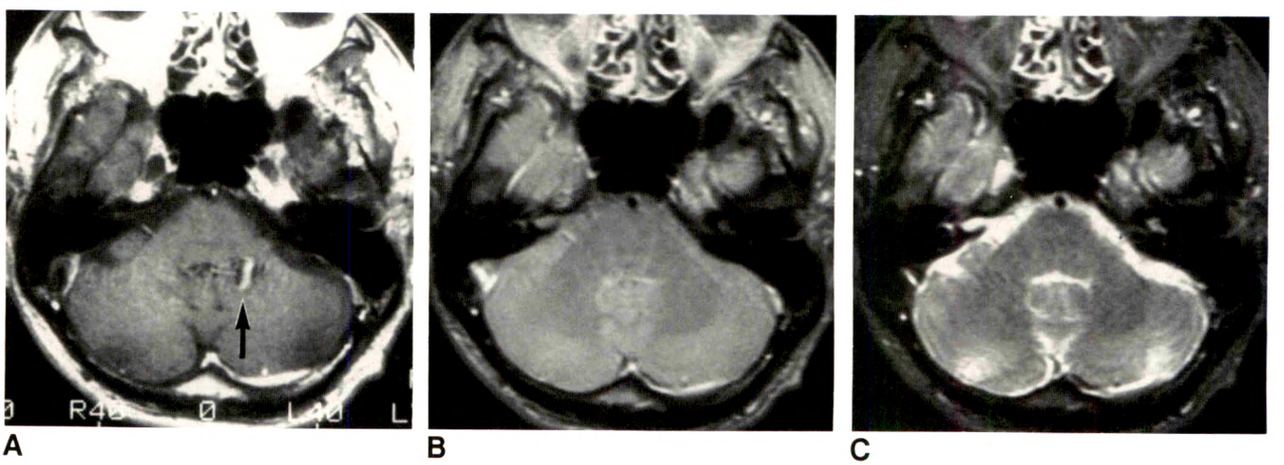


Fig. 3.—*A–C*, Postcontrast T1-weighted image (*A*) shows area of increased signal (*arrow*) adjacent to fourth ventricle, representing flow-related artifact. Postcontrast spin-density-weighted (*B*) and T2-weighted (*C*) images show that this area is normal and confirm that the finding is an artifact.

mately 10–15 min occurred between the time of contrast injection and the acquisition of long TR images, and a relative delay of 7–10 min occurred between postcontrast T1- and T2-weighted images. Our results indicate that the delay necessitated by obtaining postcontrast long TR images can provide additional diagnostic information without prolonging the overall imaging time for the patient. This was the main advantage to obtaining the long TR images after rather than before contrast administration. While information similar to that found in our two patients could probably be obtained by using delayed postcontrast T1-weighted sequences, such a protocol would add to the imaging time.

Another major advantage of the flow-compensated postcontrast long TR images is the improved differentiation of lesions from posterior fossa phase-shift artifacts on enhanced T1-weighted sequences. These artifacts are caused by misregistration of signal from enhanced flowing blood in the sigmoid and lateral sinuses that propagates across the brainstem and/or cerebellum along the phase-encoding axis. When these artifacts fortuitously reinforce one another, they may simulate enhancing lesions on postcontrast T1-weighted images, causing a confusing diagnostic dilemma. The routine use of flow-compensation techniques on postcontrast T1-weighted images has been proposed to eliminate these artifacts [9]. However, in our experience, the use of these techniques has not been entirely successful for several reasons. First, flow-compensating, gradient-moment-nulling techniques reduce the number of slices possible for a given TR, thus precluding coverage of the entire head with the use of a single, short TR sequence. This limitation can be rectified by either increasing TR, which has the disadvantage of reducing the T1-weighting of the image, or performing two separate axial T1 sequences to cover the entire head, which has the disadvantage of increasing the examination time. Second, flow compensation produces increased signal within superficial veins due to improved refocusing of signal from enhanced, slow-flowing blood. This can sometimes mimic leptomeningeal enhancement. Third, flow compensation increases signal from CSF due to reduced pulsation-related signal loss. This results in decreased image contrast between CSF and brain. Finally, and most importantly, the flow compensation used with our scanner is only a first-order (velocity) correction. Although velocity-compensated techniques reduce posterior fossa phase-shift artifacts, they do not completely eliminate them, since residual artifacts are still produced as a result of acceleration and "jerk" motions of flowing blood. For these reasons, and because of our own previous experiences, we do not routinely use gradient-moment-nulling techniques on postcontrast T1-weighted images.

Long TR images, on the other hand, show significantly fewer of these artifacts through a combination of gradient-moment-nulling techniques (used routinely with our long TR imaging sequences in the head and spine), prolonged echo-delay time that results in a fewer number of flowing protons remaining within the imaging volume between application of the 90° and 180° RF pulses, and decreased signal from blood due to T2 decay effects. Thus, absence of increased signal on the long TR images can clarify an area of suspicion on an enhanced T1-weighted study. The presence of increased signal on both sequences would confirm a lesion. This point is valid, since postcontrast long TR images, as demonstrated by this study, show enhancement in virtually all lesions that have moderate or intense enhancement on T1-weighted images. The only cases that did not show enhancement on the long TR studies had only mild degrees of enhancement on the corresponding postcontrast T1 weighted images. Thus, routine use of postcontrast long TR imaging protocols will help to identify posterior fossa artifacts with a greater degree of certainty.

Conclusions

In view of the findings that contrast enhancement is visible on spin-density- and T2-weighted sequences in most cases and that no T2 information is obscured by gadopentetate dimeglumine, our results indicate several advantages for obtaining spin-density- and T2-weighted images after rather than before contrast administration. The primary advantages are improved detection of some lesions that enhance slowly because of slow blood-brain-barrier leakage and improved differentiation between enhancing lesions and flow-related phase-shift artifacts in the posterior fossa. Importantly, the total MR examination time is not prolonged. This imaging protocol also provides the ability to display both enhancing lesions and edema or gliosis on a single image. Therefore, the recommended imaging protocol for cranial MR imaging with gadopentetate dimeglumine consists of a sagittal localizing sequence and a baseline T1-weighted axial sequence before contrast administration, followed by axial T1-, spin-density-, and T2-weighted images after the administration of contrast material. Additional supplemental views can be added as needed.

REFERENCES

1. Brant-Zawadzki M, Berry I, Osaki L, Brasch R, Murovic J, Norman D. Gd-DTPA in clinical MR of the brain. 1: Intraaxial lesions. *AJNR* **1986**;7:781–788
2. Berry I, Brant-Zawadzki M, Osaki L, Brasch R, Murovic J, Newton T. Gd-DTPA in clinical MR of the brain: 2. Extraaxial lesions and normal structures. *AJNR* **1986**;7:789–793
3. Hesselink J, Healy M, Press G, Brahme F. Benefits of Gd-DTPA for MR imaging of intracranial abnormalities. *J Comput Assist Tomogr* **1988**; 12:266–274
4. Runge V, Carollo B, Wolf C, Nelson K, Gelblum D. Gd-DTPA: A review of clinical indications in central nervous system magnetic resonance imaging. *Radiographics* **1989**;9:929–958
5. Runge V, Schaible T, Goldstein H, et al. Gd-DTPA: Clinical efficacy. *Radiographics* **1988**;8:147–159
6. Runge V, Clanton J, Herzer W, et al. Intravascular contrast agents suitable for magnetic resonance imaging. *Radiology* **1984**;153:171–176
7. Virapongse C, Mancuso A, Quisling R. Human brain infarcts: Gd-DTPA-enhanced MR imaging. *Radiology* **1986**;161:785–794
8. Grossman R, Gonzalez-Scarano F, Atlas S, Galetta S, Silberberg D. Multiple sclerosis: gadolinium enhancement in MR imaging. *Radiology* **1986**;161:721–725
9. Richardson D, Elster A, Williams D. Gd-DTPA-enhanced MR images: accentuation of vascular pulsation artifacts and correction by using gradient-moment nulling (MAST). *AJNR* **1990**;11:209–210

Book Review

Practical MRI Atlas of Neonatal Brain Development. By A. James Barkovich and Charles L. Truwit. New York: Raven, 75 pp., 1990. $26, softcover

This short atlas has four sections ("chapters"). Section 1, "Normal Brain Myelination," has MR images showing myelination at 31 weeks and 34 weeks of gestation and at 1, 3, 4, 6, 8, 10, 12, 15, 18, and 24 months of age. Section 2, "Normal Postnatal Development of the Corpus Callosum," has MR images that show the corpus callosum at 31 and 35 weeks of gestation; at 1, 4, 6, 7, 9, and 10 months of age; and at 15 years of age. Section 3, "Normal MR Development of the Bone Marrow of the Skull," has MR images of bone marrow at 3 and 13 months and at 4, 5, 10, and 16 years of age. Section 4, "Normal MR Development of Brain Iron," has MR images of the brain at 4, 13, and 25 years of age.

Each section provides little introductory text. The whole atlas has only five pages of text and only one reference to the first author's textbook, *Pediatric Neuroimaging*, which happens to be a good one. The atlas has 121 illustrations in 31 figures and three tables.

This book is part of the recent crop of short atlases that deal with various aspects of radiology. It contains carefully selected illustrations that depict the normal appearance of the developing brain, primarily in the first 2 years of life. Such information is usually not easily obtainable in textbooks, and an exhaustive search is needed to extract it from the published articles in the journals. It is this gap that this atlas successfully fills. The MR changes that occur in a rapidly developing brain can be misinterpreted as pathologic lesions unless the person who interprets the images is reasonably familiar with the normal changes. This fact is well known to experienced neuroradiologists and to those physicians who deal with imaging of the brains of infants and children. For these physicians, this atlas may not have much of interest. However, for those radiologists and physicians who regularly interpret MR images of adults but have only rare exposure to MR images of the brains of infants and children, this atlas would provide a prompt reference. Further information can be obtained then by referring to the textbook written by the first author.

I recommend this atlas to general radiologists and other physicians who do not regularly interpret MR images of infants and children. Those radiology residents and fellows who are not exposed sufficiently to imaging of the brain in infants and children would find this atlas handy. Radiology departmental libraries should own a copy of it.

Mohammad Sarwar
Doctors Hospital
Dallas, TX 75218

Intracerebral Gangliogliomas in Patients with Partial Complex Seizures: CT and MR Imaging Findings

D. Tampieri[1]
R. Moumdjian
D. Melanson
R. Ethier

The clinical and radiologic findings in 19 patients with partial complex seizures and surgically proved intracerebral gangliogliomas were reviewed to characterize the radiologic features of these lesions. The CT and MR findings were not specific. On CT the gangliogliomas can be hypodense with no enhancement and they often have calcifications. On MR these tumors have a wide variety of signals. In five of our cases the tumor had a high-intensity signal with a cystlike component on proton density– and T2-weighted images. In five cases the lesion had an inhomogeneously intense signal on proton density–weighted images and high signal intensity on T2-weighted images. The tumor had high-intensity signal on both proton density– and T2-weighted images in four patients. Finally, in two cases the MR findings were normal.

We recommend MR as the examination of choice for patients with partial complex seizures because it allows an artifact-free evaluation of the temporal region. However, CT should also be performed in order to recognize calcifications that may be missed on the MR examination.

***AJNR* 12:749–755, July/August 1991; *AJR* 157:843–849, October 1991**

Gangliogliomas are rare, slow-growing, relatively benign neoplasms consisting of a mixture of adult ganglion cells and glial tumor cells. They are often responsible for a prolonged clinical course, characterized primarily by seizures. To better define the imaging characteristics of these tumors, we reviewed the clinical and radiologic findings in 19 patients presenting with partial complex seizures who were subsequently found to have surgically proved gangliogliomas.

Materials and Methods

From January 1987 to August 1990, 19 patients, 11 men and eight women, 7 to 44 years old (mean age, 21 years), were referred to our institute for intractable partial complex seizures (PCoS). PCoS are one of the features found in temporal lobe epilepsy. They often, but not always, start with motor arrest typically followed by oroalimentary automatism lasting less than 1 min, which in turn is followed by post-ictal confusion and amnesia [1]. These patients received a complete clinical and radiologic work-up and underwent surgery for removal of intracerebral space-occupying lesions histologically proved to be gangliogliomas. EEG findings, skull radiographs, and CT scans were available for all patients. CT examinations were performed with an EMI scanner 1010 and a GE 9800 Quick scanner. In eight cases the CT scans were obtained without contrast enhancement; in six cases the examinations were performed after injection of contrast medium. Five patients had both plain and enhanced CT examinations. Eighteen patients were studied by MR imaging; in one patient (case 4) the examination was stopped because the boy had a seizure. In five cases, the MR examinations were performed with a Philips Gyroscan 0.5-T unit, and T1-weighted, 500/30/2 (TR/TE/excitations), proton density–weighted, and T2-weighted (1500/30,60/2) images were obtained. In 13 cases, a 1.5-T unit was used, and T1-weighted (500/30/2), proton density–weighted, and T2-weighted (2100/30,60/2) images were obtained. Proton density– and T2-weighted images were obtained in axial and coronal views in all cases. T1-weighted images

Received October 19, 1990; revision requested November 30, 1990; revision received February 1, 1991; accepted February 4, 1991.

[1] All authors: Department of Diagnostic Radiology, Montreal Neurological Hospital and Institute, 4801 University St., Montreal, Quebec, Canada H3A 2B4. Address reprint requests to D. Tampieri.

0361–803X/91/1574–0843
© American Roentgen Ray Society

TABLE 1: Clinical and Electroencephalographic Findings

Case No.	Age (years)	Sex	Type of Seizures	Age at Onset (years)	Free Interval (years)	Frequency of Attacks	EEG Focus	Tumor Location
1	7	M	PCoS + left fms	11 months	6	4/day	R temp	R temp
2	11	F	PCoS + 1 gen	3	8	2–3/week	R posterior temp/ occ	R posterotemp
3	12	M	PCoS	2	10	–	L temp	L temp
4	12	M	PCoS	3 months	11	6/year	L temp	L temp
5	14	M	PCoS + da	11	3	–	L temp	L temp
6	15	F	PCoS + gen	5	10	Frequent	L temp	L temp
7	16	F	PCoS	8	8	8–10/month	R + L temp	L temp
8[a]	17	M	PCoS	14	3	–	L temp	L frontoopercular
9	17	F	PCoS	6	11	1/week	R temp	R temp
10	18	M	PCoS	12	6	10/month	R temp	R temp
11[b]	21	M	PCoS	2	19	10/month	L temp	L temp
12	25	M	PCoS + gen	9	16 (PCoS)/8 (gen)	12/month	L temp	L temp
13	25	F	PCoS	12	13	–	R temp	R temp
14	27	M	PCoS + gen	10	17	4/yr (gen)	R temp	R temp
15	27	F	PCoS + abs	16	11	3/month (abs)	R abn	R temp
16	32	M	PCoS + gen	21	11	2/year	R abn	R frontoopercular
17	33	F	PCoS	13	20	2/day	L abn	L temp
18	34	F	PCoS + gen	8	26	3/day	R temp	R temp
19	44	M	PCoS + gen	31	13	1/month	R temp	R temp

Note.—PCoS = partial complex seizures, fms = focal motor seizures, gen = generalized seizures, da = drop attacks, abs = absence episodes, R = right, L = left, temp = temporal lobe, occ = occipital lobe, abn = abnormality.

[a] Previous partial resection in another center.

[b] Previous partial corticectomy and partial amygdalo-hippocampectomy.

were available only in seven cases. None of the MR studies were contrast enhanced, since this study was carried out before the clinical use of gadopentetate dimeglumine in Canada.

Results

Clinical and EEG Findings (Table 1)

The familial and medical histories were unremarkable in 16 patients in our series. One patient (case 5) was born 3 weeks post-term without any evidence of perinatal sequela. Another patient (case 18) was suffering from Rosenthal syndrome caused by deficiency of factor XI. A 33-year-old woman (case 17) developed PCoS after an episode reported as encephalitis at age 13.

All the patients were referred for intractable PCoS. In seven cases, these episodes were associated at an older age with tonic-clonic seizures and secondary generalization. Case 1 presented with PCoS and left focal motor seizures. In one patient (case 5) the PCoS were associated with drop attacks, and in another (case 15) with absences, characterized by short episodes of loss of contact without automatism.

The age of onset of seizure disorders ranged from 3 months to 31 years. The frequency of the attacks, when specified, ranged from four attacks per day to two per year at the time of admission.

All the patients had a prolonged clinical course with an important free interval between the onset of the seizures and the radiologic diagnosis. This time interval ranged from 3 to 26 years (mean, 11½ years).

The EEGs showed epileptiform abnormality in all the cases in our series.

In seven patients the EEG reports described an abnormal discharge with a right temporal focus, and in seven cases the focus was found in the left temporal region. In case 7 the abnormal discharge was from both temporal lobes, and in case 2 the abnormality was from the right posterior tempo-rooccipital area. In only three patients (cases 15, 16, and 17) did the EEG demonstrate an abnormal discharge lateralized to one cerebral hemisphere with no evidence of focal anomalies.

Radiologic Findings (Table 2)

Skull Radiographs. In no case did the plain films reveal any evidence of raised intracranial pressure or mass effect with displacement of the calcified pineal gland. In four patients flocular calcifications were visualized in the middle cranial fossa on the same side of the lesion. In cases 8 and 11, the plain films documented the previous craniotomy.

CT Scans. The CT findings were available in all cases. In 15 patients it was positive: four lesions (cases 1, 4, 15, 16) were hypodense (Figs. 1 and 2); two lesions (cases 7 and 8) were ring-enhancing (Fig. 3), and in six patients (cases 2, 3, 6, 9, 10, 13) the examination demonstrated only calcifications (Fig. 4). Two CT studies (cases 14 and 18) showed asymmetry of the temporal horn (Fig. 5), the larger being on the tumoral side, and in case 12 the CT study demonstrated only a prominent left hippocampus. In three cases (5, 17, 19) the examination was negative, and, finally, in case 11 there was only evidence of the previous surgery.

MR Images. Seventeen MR examinations were completed and available and the tumor was identified in 15 patients

TABLE 2: Radiologic Findings

Case No.	Age (years)	Sex	Skull	CT		MR			Location
				Plain	Enhanced	T1	Proton Density	T2	
1	7	M	Neg	Hypodense	–	–	↑is + cystlike	↑is + cystlike	R temp
2	11	F	Neg	Calcifications	No enh	–	–	–	R posterotemp
3	12	M	Calcifications	Calcifications	No enh	–	Inh is + cyst-like	Inh is + cyst-like	L temp
4	12	M	Neg	Hypodense	–	–	–	–	L temp
5	14	M	Neg	Neg	–	↓is	Inh is	↑is	L temp
6	15	F	Neg	Calcifications	No enh	–	↑is	↑is	L temp
7	16	F	Neg	–	Ring enh	Iso is	↑is + cystlike	↑is + cystlike	L temp
8[a]	17	M	Prev. cranio-otomy	–	Ring enh + calcification	–	↑is + cystlike	↑is + cystlike	L frontoopercular
9	17	F	Calcification	Calcification	No enh	Iso is	↑is + small void sig	↑is + small void sig	R temp
10	18	M	Calcifications	–	Calcifications	–	Inh is	↑is	R temp
11[b]	21	M	Prev. cranio-otomy	Prev. surgery	–		Prev. surgery		L temp
12	25	M	Neg	–	Prominent hippocampus	Iso is	↑is	↑is	L temp
13	25	F	Calcifications	Calcifications	–	–	Inh is + void sig	↑is + void sig	R temp
14	27	M	Neg	Asymmetric temporal horn R > L	–	Asymmetric temporal horn R > L	Neg	Neg	R temp
15	27	F	Neg	–	Hypodense	Hypo is + cystlike	↑is + cystlike	↑is + cystlike	R temp
16	32	M	–	Hypodense	No enh	–	Inh is	↑is	R frontoopercular
17	33	F	Neg	Neg	–	–	Neg	Neg	L temp
18	34	F	Neg	Asymmetric temporal horn R > L	–	↓is	Inh is	↑is	R temp
19	44	M	Neg	–	Neg	–	↑is	↑is	R temp

Note.—neg = negative examination, – = examination not done, no enh = no enhancement after injection, inh is = inhomogeneously intense signal, iso is = isointense signal, hypo is = hypointense signal, ↑is = high-intensity signal, ↓is = low-intensity signal, void sig = void signal, R = right, L = left, temp = temporal lobe.

[a] Previous partial resection in another center.

[b] Previous partial corticectomy and partial amygdalo-hippocampectomy.

(88%). One MR examination (case 17) was negative; one (case 14) showed the right temporal horn to be larger than the left (Fig. 5); and one (case 11) demonstrated prior surgery but no evidence of residual tumor.

The gangliogliomas demonstrated a wide variety of signals. In five patients (cases 1, 3, 7, 8, 15) the lesion had a signal similar to CSF on proton density–weighted images and higher than CSF on T2-weighted images (Figs. 1–3). In five cases the tumor had an inhomogenously intense signal on proton density-weighted images that became hyperintense on the T2-weighted images (cases 5, 10, 13, 16, 18). Finally, the lesion had a high-intensity signal on both proton density- and T2-weighted images in four patients (cases 6, 9, 12, 19).

MR detected calcifications in only two patients (cases 9 and 13) (Fig. 4). T1-weighted images were available in only seven patients: they showed the lesions to be isointense in three cases, hypointense in two cases, and isointense with CSF in one case (Fig. 2).

Discussion

The first description of gangliogliomas was given by Courville in 1930 [2]. The term ganglioglioma clearly defines the structure of these uncommon tumors as a mixture of nerve cells and glial elements. They constitute just 0.4% of all CNS tumors [3, 4]. This percentage has been reported to be as high as 4.3% [5] and 7.6% [6] in studies that factor out the adult population, reflecting the fact that this tumor is more common among children. The tumors do not have any sex predilection, but some authors report a predominance in males [2, 7]. Gangliogliomas can occur in any number of locations in the CNS, and can involve both brain and spinal cord; however, the most common locations in the adult population seem to be the temporal lobe and the floor of the third ventricle [3, 8]. In the present series we included only lesions causing PCoS, and for this reason a preference for the temporal lobe, particularly the hippocampal gyrus, was found.

In childhood, gangliogliomas seem to occur more frequently in the medulla and spinal cord [9] and the differential diagnosis with the more benign gangliocytoma has to be considered. This latter tumor, rarely supratentorial [10, 11] and purely neuronal without a glial component, is an extremely rare entity, accounting for 0.1% of intracranial tumors [12] with a slight male predilection [13], and it cannot be radiologically differentiated from ganglioglioma.

The clinical course suggests that gangliogliomas are slow-growing neoplasms, and a malignant transformation is very uncommon. When it happens it is usually the glial element that is responsible for the change [14]. Metastasis in the CNS

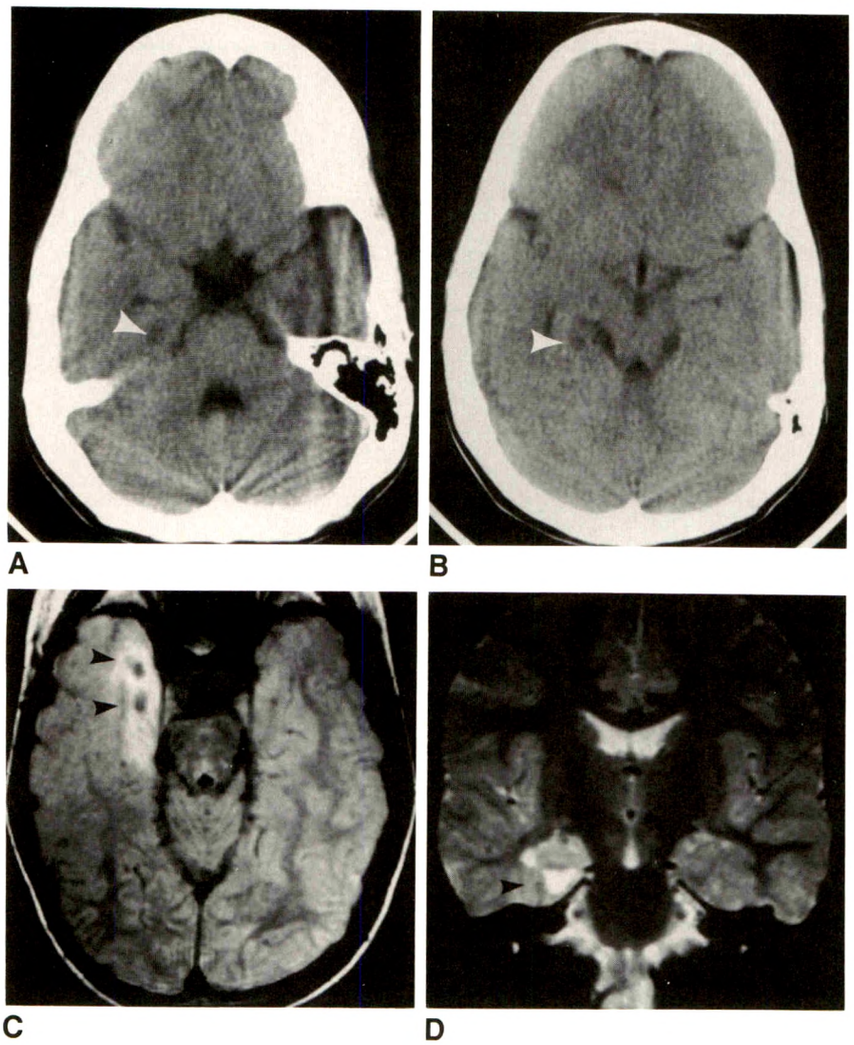


Fig. 1.—Case 1.
A and *B*, Unenhanced CT scans show two small, poorly defined areas of hypodensity (*arrowheads*).
C, Axial proton density–weighted (2100/30/1) MR image better defines the lesion, which appears as two low-intensity cystlike areas surrounded by a high-intensity signal in right temporomesial region (*arrowheads*).
D, Coronal T2-weighted (2100/80/1) MR image of tumor shows increased signal intensity. Cystlike component is surrounded by high-intensity signal, which involves the cortex and adjacent white matter (*arrowhead*).

appears to be exceptional [14]. Some authors have also raised the possibility that gangliogliomas are hamartomatous lesions since they have been found in temporal lobes of patients with a long history of seizures [15] and because collections of heterotopic gray matter similar to ganglioglioma can cause seizures [16]. Nowadays, the literature seems to agree that gangliogliomas are true neoplasms and their removal has to be attempted [5, 17].

The EEG findings usually suggest the focal abnormality that must be confirmed by the imaging findings. Radiologically, gangliogliomas do not have a specific appearance. Calcifications can be visualized on a skull radiograph in 10% of patients [18]. Although the skull radiograph is a superfluous examination, it was performed in all our patients and we observed four cases (21%) with flocular calcifications in the middle cranial fossa.

CT findings also are nonspecific. Gangliogliomas are usually hypodense [19] with calcifications [20]. In our series CT scans were positive in 12 patients (63%); six of them (32%) demonstrated only abnormal calcifications, and the other six showed a wide variety of findings. In no case in our series did CT demonstrate edema or mass effect.

In a small series [21] of four patients studied with MR imaging, two lesions had a cystic appearance while the other two displayed an increased signal on T1-weighted images and a decreased signal on T2-weighted images. The authors did not try to explain these findings. In a larger series of 14 patients reported by Castillo et al. [22] there were four cystic lesions (low signal on T1-weighted images and high signal on T2-weighted images) and 10 solid masses that demonstrated high-intensity signal on T2-weighted images. The authors did not mention whether the cystic nature of the lesions observed on MR was confirmed later at surgery.

In our series, gangliogliomas presented different signals because of their heterogeneous components of glial and neuronal cells associated with calcifications. In five (29%) of the 17 patients who were studied with MR imaging, the gangliogliomas had a cystlike component (Figs. 1 and 2) and

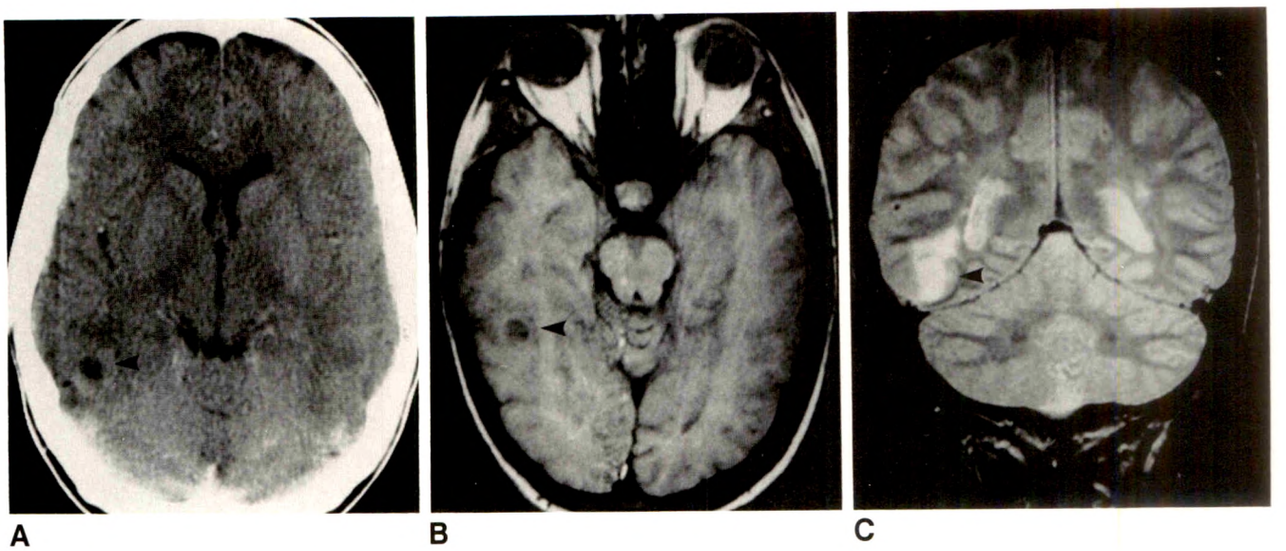


Fig. 2.—Case 15.
A, Enhanced CT scan shows well-defined hypodense nonenhancing lesion (*arrowhead*).
B and *C*, T1-weighted (500/30/1) (*B*) and T2-weighted (2100/80/1) (*C*) MR images show cystlike tumor (*arrowhead*) in right inferotemporal gyrus surrounded by some edema.

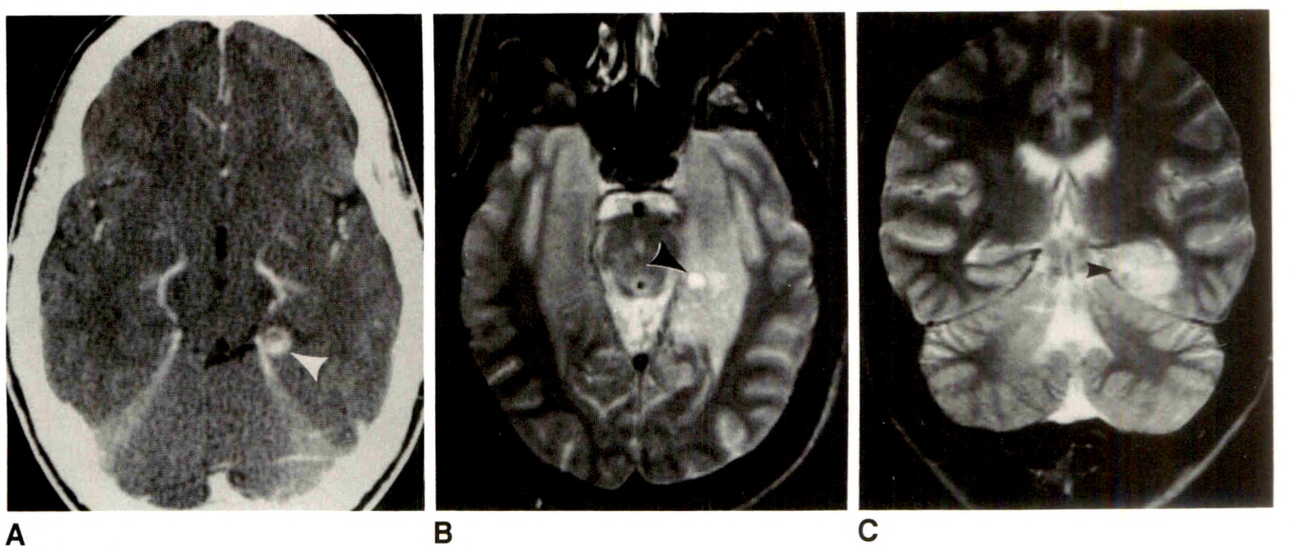


Fig. 3.—Case 7.
A, Enhanced CT scan shows ring-enhancing lesion (*arrowhead*) in left posterior parahippocampal region.
B and *C*, Axial (*B*) and coronal (*C*) T2-weighted (2100/80/1) MR images enable complete evaluation of the tumor, which involves the left hippocampus and parahippocampus gyri. The ganglioglioma has a high-intensity signal and a central cystlike nodule (*arrowheads*), which corresponds to the ring-enhancing lesion seen on the enhanced CT scan.

in five patients (29%) the lesions displayed inhomogeneous signal on proton density-weighted images and high-intensity signal on T2-weighted images. Finally, in four cases (24%) the tumors had high signals on both proton density- and T2-weighted images. In only two patients (12%) was MR able to detect calcifications (Fig. 4). We prefer to use the term cystlike appearance to describe the MR characteristic of a well-defined area with signal intensity similar to CSF on proton density-weighted images and higher than CSF on T2-weighted images. This is because the content of the lesions is not fluid but solid; therefore, it cannot be drained but has to be removed, as was the case in the patients in our series.

MR failed to show the tumor in two (12%) of the 17 cases. Owing to their frequent attacks of seizures and their EEG results, these patients eventually underwent temporal lobectomy; the histologic reports revealed the presence of the

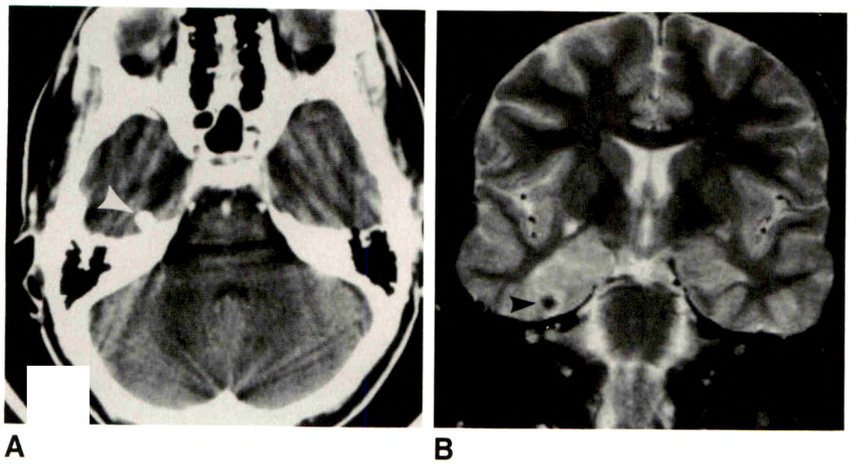


Fig. 4.—Case 9.
A, Contrast-enhanced CT scan shows flocculer calcification (*arrowhead*) in right middle cranial fossa.
B, Coronal T2-weighted (2100/80/1) MR image confirms presence of calcification (*arrowhead*) in right fusiform gyrus and shows a hyperintense signal that involves the amygdala, hippocampus and parahippocampus gyri, and adjacent white matter.

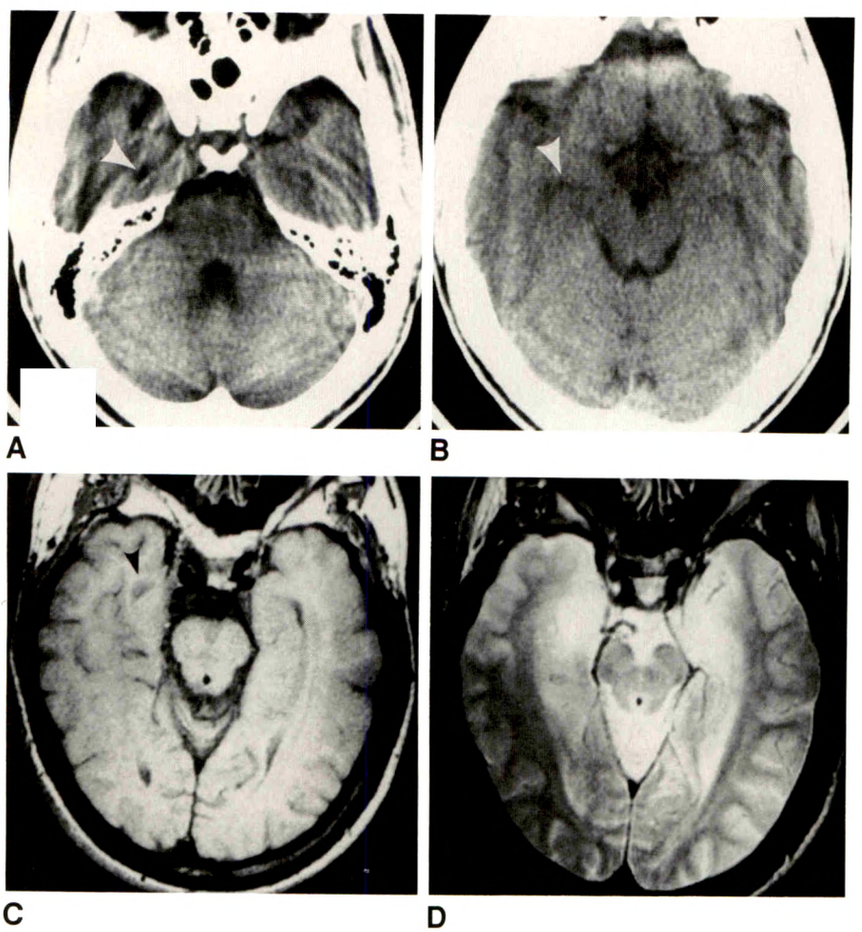


Fig. 5.—Case 14.
A–D, Unenhanced CT scans (*A* and *B*) and T1-weighted (500/30/1) MR image (*C*) show slight asymmetry of temporal horn, with right (*arrowhead*) larger than left. T2-weighted (2100/80/1) MR shows no evidence of the ganglioglioma discovered later at surgery in the right temporal lobe.

lesion. The CT and MR findings in these patients demonstrated an asymmetry of the temporal horns in one patient (case 14) and were completely normal in the other (case 17).

In conclusion, gangliogliomas are uncommon lesions, but their presence has to be considered in patients with a long history of uncontrollable seizures. Since most of these tumors are located in the middle cranial fossa, MR is the examination of choice because it allows images free from bone artifact. Nevertheless, false-negative diagnoses are possible and we think that CT should also be performed in order to detect calcification, which can be missed on MR.

REFERENCES

1. Commission on Classification and Terminology of the International League Against Epilepsy. Proposal for revised classification of epilepsies and epileptic syndromes. *Epilepsia* **1989**;30:389–399
2. Courville CB. Ganglioglioma: tumor of the central nervous system; review of the literature and report of two cases. *Arch Neurol Psychiatry* **1930**;24:439–491
3. Zulch KJ. *Brain tumors: their biology and pathology*, 2nd ed. New York: Springer, **1965**
4. Cox JD, Zimmerman HM, Haughton VM. Microcystic ganglioglioma treated by partial removal and radiation therapy. *Cancer* **1982**;50:473–477
5. Sutton LN, Packer RJ, Rorke LB, et al. Cerebral gangliogliomas during childhood. *Neurosurgery* **1983**;13:124–128
6. Johannsson JH, Rekate HL, Roessmann U. Gangliomas: pathological and clinical correlation. *J Neurosurg* **1981**;54:48–63
7. Rommel T, Hamer J. Development of ganglioglioma in computed tomography. *Neuroradiology* **1983**;24:237–239
8. Zulch KJ. *Progress in neurological surgery*. Chicago: Yearbook, **1968**
9. Albright L, Byrd RP. Ganglioglioma of the entire spinal cord. *Child's Brain* **1980**;6:274–280
10. Dom R, Brucher JM. Hamartoblastoma (gangliocytome diffus) unilateral de l'écorce cérébrale associé à une dégénérescence soudanophile de la substance blanche du côté opposé. *Rev Neurol* (Paris) **1969**;120:307–318
11. Kawamoto K, Yamanouchi Y, Suwa J, Kurimoto T, Matsumura H. Ultrastructural study of a cerebral gangliocytoma. *Surg Neurol* **1985**;24:541–549
12. Roski RA, Roessmann U, Spetzler RF, Kaufman B, Nulsen FE. Clinical and pathological study of dysplastic gangliocytoma: a case report. *J Neurosurg* **1981**;55:318–321
13. Altman NR. MR and CT characteristics of gangliocytoma: a rare cause of epilepsy in children. *AJNR* **1988**;9:917–921
14. Russel DS, Rubinstein LJ. *Pathology of tumors of the nervous system*. London: Arnold, **1989**:289–306
15. Cavanagh JB. On certain small tumors encountered in the temporal lobe. *Brain* **1958**;81:389–405
16. Layton DD. Heterotopic cerebral gray matter as an epileptogenic focus. *J Neuropathol Exp Neurol* **1962**;21:244–249
17. Garrido E, Becker LF, Hoffman HJ, et al. Gangliogliomas in children: a clinicopathological study. *Child's Brain* **1978**;4:339–346
18. Katz MC, Kier EL, Schechter MM. The radiology of gangliogliomas and ganglioneuromas of the central nervous system. *Neuroradiology* **1972**;4:69–73
19. Zimmerman RA, Bilaniuk LT. Computed tomography of intracerebral gangliogliomas. *J Comput Assist Tomogr* **1979**;3:24–30
20. Dorne HL, O'Gorman AM, Melanson D. Computed tomography of intracranial gangliogliomas. *AJNR* **1986**;7:281–285
21. Denierre B, Stinchnoth FA, Hori A, Spoerri O. Intracerebral gangliogliomas. *J Neurosurg* **1986**;65:177–182
22. Castillo M, Davis PC, Takei Y, Hoffman JC. Intracranial ganglioglioma: MR, CT, and clinical findings in 18 patients. *AJNR* **1990**;11:109–114

Book Review

Manual of Clinical Magnetic Resonance Imaging. A Practical Guide to Conducting Magnetic Resonance Imaging Examinations of the Head and Body, 2nd ed. Edited by Jay P. Heiken and Jeffrey J. Brown. New York: Raven, 192 pp., 1991. $35, softcover

This text is designed to help practicing radiologists and radiologic technologists understand some of the basic concepts underlying the MR imaging techniques routinely used by current practitioners of clinical MR imaging. The text has several notable highlights and omissions. The first two thirds of the work is devoted to didactic discussions of the principles and techniques of MR imaging; the last third is devoted exclusively to listings of suggested pulse sequence protocols for numerous anatomic regions of interest and diagnostic considerations. The discussions on the underlying physics are generally concisely and clearly written, but the authors tend to presuppose a moderate level of understanding of some of these concepts. Intermingled within these discussion, however, are some disturbing minor glitches. For example, the authors state a given number of protons that will align with the field B_0 without taking the opportunity to describe the dependence of this number on the magnitude of the B_0 being used. The signal-to-noise ratio of quadrature coils is described inaccurately as being linearly improved as compared with linearly polarized RF fields; it is actually improved by the square root ratio of the number of coils used relative to the region of interest. In the section on flow effects, loss of high-velocity signals is said to increase with increased slice thickness; actually, the reverse is true.

The book also has little discussion of proton density and its relevance to diagnostic clinical MR for such entities as multiple sclerosis. Most of the text, instead, is devoted to the more typical T1- and T2-oriented discussions. The book has virtually no graphs or discussions on the effect of flip-angle modifications on the resultant image; gradient-echo imaging techniques are mentioned only briefly in the text and in the suggested protocols. This is highly unusual, as use of gradient-echo imaging techniques with lower flip angles for spine imaging is nearly ubiquitous in clinical practice, even if only as part of a screening series. Similarly, the book has virtually no discussion of and protocols for three-dimensional Fourier transform techniques, with the concomitant advantages and disadvantages. MR angiographic sequences and their underlying principles are not covered, despite the immense progress and growth in the clinical applications of this technique.

The section on pulse sequence protocols in the last third of the text is the least useful aspect of this book. The protocols are perhaps useful for general informational purposes, but they have little clinical applicability to a scanner that may be used by anyone interested in perfecting his or her own technique. It is generally almost universally easier to obtain from the manufacturer a rather comprehensive listing of "suggested" pulse sequence protocols used by any of many experienced so-called luminary sites that use the same equipment, thus allowing users to take the most advantage of the system-specific capabilities—and limitations—of their own particular equipment. This should eliminate the need to devote a third of the text to yet another opinion on the appropriate manner in which to scan a particular region of interest with no particular system and static magnetic field strength. (For example, the authors themselves suggest a rather liberal doubling of the number of data acquisitions, and therefore study time, if an imaging system with a static field strength of <1 T is used.)

The discussion of safety considerations of MR environments is inadequate. The authors erroneously state on two occasions that to date no occurrence of localized heating has been reported with prostheses of any kind. Localized heating and thermal injury associated with numerous implants, objects, or electrically conductive devices certainly have been reported. Later in the same chapter, the authors themselves report a third-degree burn caused by MR imaging. Furthermore, the factor of the mass of a ferromagnetic object as a major determinant of the mechanical forces and torque that it might experience in the imaging environment is inadvertently omitted from the discussion of such items.

In summary, I think that most of the MR practitioners at the roughly 2000 (not 3000, as claimed in the preface) clinical MR sites in the United States might benefit from many of the discussions in this text and might find it a useful reference for a rapid review of some of the concepts covered. It has sufficient omissions of what now is or shortly will be considered state-of-the-art, current MR imaging, however. Consequently, I think that many will find its breadth of scope somewhat wanting and will complete the text still hungry for more depth for most topics covered.

Emanuel Kanal
University of Pittsburgh, School of Medicine
Pittsburgh NMR Institute
Pittsburgh, PA 15213

MR Imaging of Reversible Cyclosporin A–Induced Neurotoxicity

Charles L. Truwit[1]
Charles P. Denaro[2]
John R. Lake[3]
Teresa DeMarco[4]

Neurotoxicity is a recognized complication of cyclosporin A (CsA) therapy in patients undergoing organ transplantation. It is most commonly manifested by fever, seizures, and altered mental status. Cortical blindness and speech and motor disturbances can also occur. Changes seen in cerebral white matter on imaging studies are nonenhancing areas of hypoattenuation on CT and T2 prolongation on MR. We report three cases of CsA-induced neurotoxicity in which reversible changes were observed in the cerebral white matter. In the first patient, CsA neurotoxicity occurred 1 week following orthotopic liver transplantation. In the second patient, CsA neurotoxicity coincided with an episode of severe systemic hypertension 4 weeks after cardiac transplantation. The third patient experienced seizures 1 month after heart/lung transplantation for cystic fibrosis. A current theory postulates a relationship between diminished serum cholesterol and CsA neurotoxicity. This theory, however, does not satisfactorily address all cases of CsA neurotoxicity. In particular, serum cholesterol measurements were normal in cases 2 and 3 and probably were normal in case 1, despite diminished cholesterol levels preoperatively.

Although the matter of CsA-induced neurotoxicity remains unresolved, we suggest that endothelin, a newly described neuropeptide that causes intense vasoconstriction and that has been implicated in cerebral vasospasm, may potentiate CsA-induced damage to endothelium and promote CsA neurotoxicity.

***AJNR* 12:651–659, July/August 1991; *AJR* 157:851–859, October 1991**

Received September 5, 1990; revision requested October 15, 1990; revision received February 26, 1991; accepted March 1, 1991.

C. P. Denaro is a Merck International Fellow.

The opinions expressed herein are those of the authors and do not necessarily reflect those of the U.S. Army or the Department of Defense.

[1] Department of Radiology, Neuroradiology Section, Box 0628, University of California, San Francisco, 505 Parnassus Ave., San Francisco, CA 94143, and Army Medical Department, U.S. Army Academy of Health Sciences, HSHA-GPS, Fort Sam Houston, TX 78234-6100. Address reprint requests to C. L. Truwit at the Department of Radiology, Fitzsimons Army Medical Center, Aurora, CO 80045-5001.

[2] Division of Clinical Pharmacology and Experimental Therapeutics, University of California, San Francisco, San Francisco, CA 94143.

[3] Department of Medicine, Liver Transplantation Service, University of California, San Francisco, San Francisco, CA 94143.

[4] Department of Medicine, Cardiac Transplantation Service, University of California, San Francisco, San Francisco, CA 94143.

0361-803X/91/1574-0851
© American Roentgen Ray Society

Cyclosporin A (CsA)-induced neurotoxicity has been reported to occur in up to 35% of patients undergoing orthotopic liver transplantation [1, 2]. It has also been reported in patients undergoing renal, bone marrow, and cardiac transplantation [1, 2]. It is most commonly manifested by seizures and altered mental status [1, 3, 4]. Cortical blindness and speech and motor disturbances can occur also [2, 5–7]. Changes seen in cerebral white matter on imaging studies include areas of hypoattenuation on CT and T2 prolongation on MR [1, 2, 5, 6]. We report three cases of CsA-induced neurotoxicity in which reversible changes were observed in the cerebral white matter.

Case Reports

Case 1

A 50-year-old woman with cryptogenic cirrhosis and overt, chronic hepatic encephalopathy underwent orthotopic liver transplantation. Postoperatively, she was treated with 750 mg of CsA orally twice a day until postoperative day 3, when the dose was increased to 1 g orally twice a day. Bile drained via a T tube was refed via a nasogastric tube. IV magnesium sulfate was given on postoperative days 3, 4, 5, and 7 to compensate for hypomagnesemia, as noted in Table 1. An initial dose of methylprednisolone, 750 mg, was given intraoperatively. This was followed by a postoperative regimen of prednisone, 40 mg four times a day for the first 6 days, which was subsequently tapered. Other medications included azathioprine,

TABLE 1: Pre- and Postoperative Laboratory Values in Case 1

Day	BP (mm Hg)	Temp. (°C)	Hct. (%)	CsA (μg/l)	Mg^{++} (mg/dl)	Chol. (mg/dl)	Alk. Phos. (U/dl)	Bilirubin (mg/dl)	AST (U/l)	Creatinine (mg/dl)
−88					2.3[a]	46	241[a]	2.7 (1.4)[a]	91[a]	1.6[a]
−87						40	198[a]	2.5 (1.4)[a]	76[a]	1.6[a]
−86						44	195[a]	2.4[a]	73[a]	1.5[a]
−80					2.0	58				1.5
−14							220	2.9	91	1.3
0	140/80	35.8 R	21.2		2.1		245	14.9	76	2.1
1	170/90	37.2 R	22.7	<25	1.3, 1.2[b]		52, 54[b]	1.7, 2.2[b]	600, 727[b]	1.6, 1.4, 1.5, 1.7, 1.7[b]
2	165/90	37.2 R	21.5	<25	1.2		76	2.9	785	1.4, 2.0, 2.0, 2.0[b]
3	180/80	37.2	28.2	37	1.0		66	3.8	960	1.7, 1.8, 1.6, 1.6[b]
4	185/90	36.9	29.7	48	1.6		105	6.1 (5.2)	355	1.6, 1.8[b]
5	185/90	37.0	33.0	78			147	5.8	88	1.6
6	180/90	36.9	32.6	253			167	7.1	88	1.6
7[c]	160/86	36.7	34.9	401	1.1		194	8.6 (6.5)	57	1.5
	180/110	37.2								
8										1.4
9				75			213	3.6	34	1.2
10				178			256	3.2	34	1.3
11				64			246	2.6	29	1.2
12				231			259	1.9	27	1.3
21				220			358	1.1	40	1.4

Note.—Day 0 = day of operation; −88 = 88 days before surgery. Values for blood pressure (BP) and oral or rectal (R) temperature (Temp.) are the highest recorded during that 24-hr period. Hematocrit (Hct.) values are the lowest recorded during that 24-hr period. Cyclosporin A (CsA) was measured by high-performance liquid chromatography, whole blood; the therapeutic range is 50–400 μg/dl. Normal ranges for magnesium (Mg^{++}), alkaline phosphatase (Alk. Phos.), total bilirubin (values for direct bilirubin are in parentheses), aspartate transferase (AST), and creatinine are 1.6–2.7 mg/dl (magnesium), 41–133 U/l (alkaline phosphatase), 0.1–1.2 mg/dl (total bilirubin), 0.1–0.3 mg/dl (direct bilirubin), 7–39 U/l (aspartate transaminase), and 0.5–1.4 mg/dl (creatinine). Chol. = cholesterol. Albumin measured 3.2 mg/dl on day 9 and 3.9 mg/dl on day 21 (normal, 3.4–4.7 mg/dl).

[a] These values were measured at an outside laboratory. Normal values were 1.9–2.5 mg/dl (magnesium), 39–177 U/l (alkaline phosphatase), 0.1–1.2 mg/dl (total bilirubin), 0.1–0.25 mg/dl (direct bilirubin), 0–31 U/l (aspartate transaminase), and 0.5–0.9 mg/dl (creatinine).

[b] Serial values, same day, in chronologic order.

[c] First set of data was obtained on the ward, before seizures; the second set was obtained after seizures.

Minnesota antilymphocyte globulin, gancyclovir, sucralfate, nystatin, multivitamins, folate, thiamine, morphine sulfate, nifedipine, acetaminophen, and diphenhydramine. T-tube cholangiographic findings on postoperative day 6 were normal. The following day, the patient had two focal seizures, manifested by head jerking to the right and staring episodes. No visual changes were reported. On the day of the seizures, the patient was afebrile and normotensive. The seizures were treated with standard doses of IV phenytoin and diazepam. Serum CsA was 401 μg/l, as measured by whole-blood, high-performance liquid chromatography assay. Although at the upper limit of the therapeutic range for CsA, the level had risen precipitously over 2 days, from 78 to 401 μg/l.

CT revealed bilateral, nonenhancing areas of hypoattenuation in the occipital white matter (Fig. 1A). MR the following day demonstrated bilateral nonenhancing areas of T2 prolongation in the occipital white matter (Fig. 1B). No petechial hemorrhage was apparent. Because the clinical findings and imaging features suggested CsA-induced neurotoxicity, CsA was withheld for 2 days. No further seizures occurred, and CsA was restarted on postoperative day 9 at 200–300 mg orally twice a day. There were no further complications. Peak blood pressure and temperature and preoperative and postoperative laboratory values are listed in Table 1. Of note, preoperative serum cholesterol measurements ranged from 40 to 58 mg/dl. No postoperative cholesterol measurements were obtained. However, fresh frozen plasma was administered during the perioperative period. Postoperative serum creatinine values were normal. On postoperative day 23 (16 days after the seizures), T2-weighted MR examination revealed complete resolution of the white matter lesions (Fig. 1C).

Case 2

A 36-year-old man underwent cardiac transplant following 19 months of refractory dilated cardiomyopathy due to cardiac sarcoidosis. The peri- and postoperative periods were unremarkable until 4 weeks after transplantation, when the patient awoke with confusion, headache, change of vision, and anxiety. The day before admission, he had felt well and had walked the 18 holes of a golf course. The patient's medications included 400 mg of CsA twice a day, acyclovir, prednisone, diltiazem, captopril, magnesium supplement, ranitidine, aspirin, ferrous sulfate, Colace, clotrimazole, and trimethoprim/sulfamethoxazole.

In the emergency department, the patient was found to be markedly hypertensive (210/110 mm Hg) and was noted to have a gaze palsy. He had a generalized seizure that was treated with phenytoin. Nifedipine was administered for control of blood pressure. Clinically, the history of hypertension, confusion, and seizures suggested CsA neurotoxicity. The CsA level on admission was 348 μg/l; 4 days earlier, it was 392 μg/l. CsA was withheld, and the levels promptly decreased to 271, 188, and 169 μg/l, respectively, over the next 3 days. Serum cholesterol, magnesium, and creatinine were normal. Laboratory data and vital signs are listed in Table 2.

Ophthalmologic evaluation on the day of admission revealed subtle bilateral central scotomata that were diminished on reexamination 3½ hr later. Unenhanced CT revealed bilateral foci of decreased attenuation involving occipital white matter. MR the following day revealed nonenhancing areas of T2 prolongation in the same areas (Figs. 2A–2C). Minimal cortical involvement was suggested as well. The CT and MR findings were consistent with the clinical suspicion

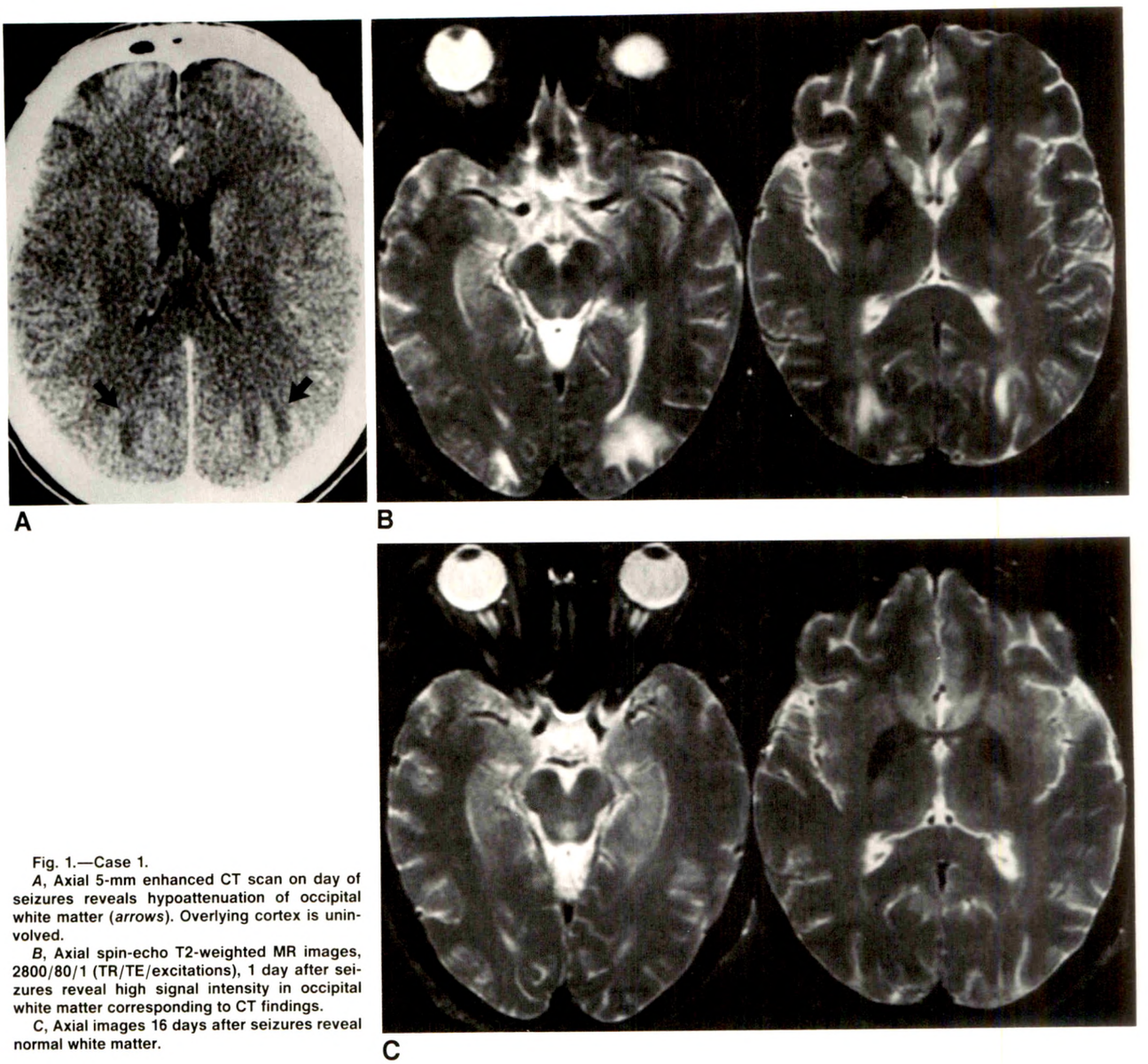


Fig. 1.—Case 1.
***A*, Axial 5-mm enhanced CT scan on day of seizures reveals hypoattenuation of occipital white matter (*arrows*). Overlying cortex is uninvolved.**
***B*, Axial spin-echo T2-weighted MR images, 2800/80/1 (TR/TE/excitations), 1 day after seizures reveal high signal intensity in occipital white matter corresponding to CT findings.**
***C*, Axial images 16 days after seizures reveal normal white matter.**

of CsA neurotoxicity. Follow-up T2-weighted images 3 days later revealed nearly complete resolution of the abnormalities (Figs. 2D–2F).

Case 3

A 33-year-old woman underwent heart/lung transplantation for cystic fibrosis. Intraoperatively, a prolonged period of cardiopulmonary bypass was needed. The postoperative course was unremarkable except for an episode of moderate cardiac rejection and of mild pulmonary rejection on postoperative day 5; these were treated with methylprednisolone. The patient had no history of seizures. Medications included 100 mg of CsA three times a day, Imuran, prednisone, Pancrease, ranitidine, terfenadine, metoclopramide, magnesium supplementation, nystatin, and albuterol inhaler.

On postoperative day 29, the patient experienced generalized seizures with right arm involvement that were preceded by severe headache. Blood pressure at that time was 125/81 mm Hg, and CsA level was 636 μg/l. (Therapeutic CsA at that institution was 75–300 μg/l). Phenytoin therapy was instituted with a loading dose and was maintained at 300 mg orally every night. CsA was temporarily withheld. Admission CT demonstrated multiple areas of hypoattenuation in the cerebral white matter. MR 4 days later, on postoperative day 33, confirmed the CT findings (Figs. 3A–3C). Follow-up MR 12 days later revealed nearly complete resolution of the white matter lesions (Figs. 3D–3F). Phenytoin therapy was continued until postoperative day 63. Over the ensuing weeks, CsA levels were elevated sporadically (511 and 742 μg/l on postoperative days 66 and 72, respectively, as noted in Table 3). No seizures occurred during this period, although the patient did experience headaches.

TABLE 2: Pre- and Postoperative Laboratory Values in Case 2

Day	BP (mm Hg)	Temp. (°C)	Hct. (%)	CsA (μg/l)	Mg^{++} (mg/dl)	Chol. (mg/dl)	Alk. Phos. (U/l)	Bilirubin (mg/dl)	AST (U/l)	Creatinine (mg/dl)
−5			37.6	321	1.7		83	0.8	29	1.1
−1			38.0	392	1.6					1.4
0	210/110	37.1	39.3	348	1.6					1.2
1	200/90	36.6	36.3	271	1.8					1.1
2	180/80	36.9	40.6	188	1.8	181[a]	91	0.5	25	1.1
3	120/80	36.5		169						1.3
4	110/75	37.3	43.9	225			102	0.7	24	1.2
5	135/75	37.0	36.8	231	22.3, 1.8[b]				22	1.1
6	135/65	37.0	36.1	161	1.7				28	0.9

Note.—Day 29 = day of cyclosporin A toxicity. Values for blood pressure (BP) and temperature (Temp.) are the highest recorded during that 24-hr period. Hematocrit (Hct.) values are the lowest recorded during that 24-hr period. Cyclosporin A (CsA) was measured by high-performance liquid chromatography, whole blood; the therapeutic range is 50–400 μg/l. Normal ranges for magnesium (Mg^{++}), alkaline phosphatase (Alk. Phos.), total bilirubin, aspartate transaminase (AST), and creatinine are 1.6–2.7 mg/dl (magnesium), 41–133 U/l (alkaline phosphatase), 0.1–1.2 mg/dl (total bilirubin), 7–39 U/l (aspartate transaminase), and 0.5–1.4 mg/dl (creatinine). Chol. = total cholesterol.

[a] High-density lipoprotein cholesterol = 51 mg/dl; low-density lipoprotein cholesterol = 105 mg/dl.

[b] Serial values, same day, in chronologic order.

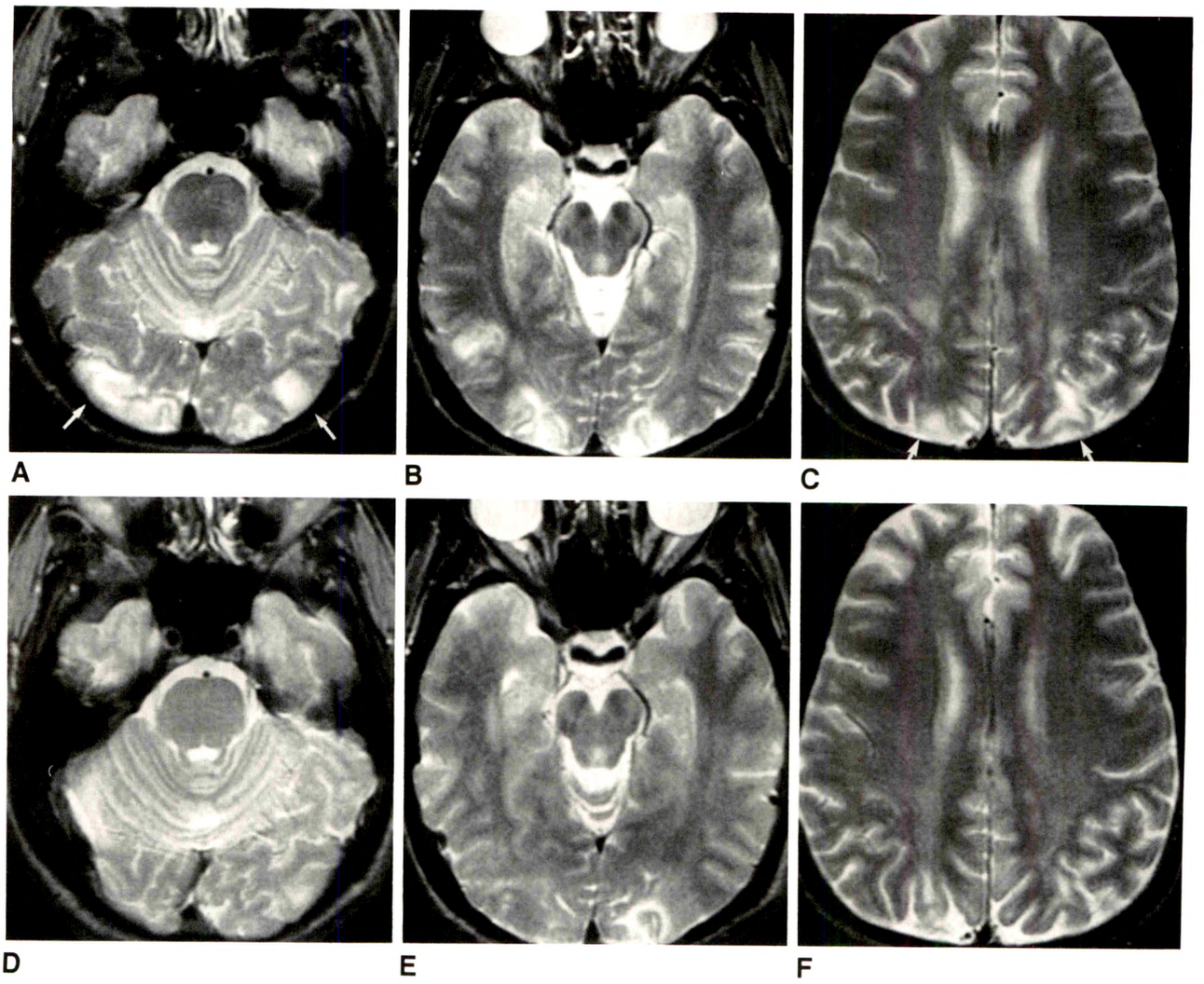


Fig. 2.—Case 2.

A–C, Axial spin-echo T2-weighted MR images, 2800/80/1 (TR/TE/excitations), 1 day after admission reveal hyperintense signal in occipital and to a lesser extent posterior temporal and parietal white matter (*arrows*). No abnormalities were detected on T1-weighted images (not shown), either before or after administration of contrast material. Unenhanced CT scans (*not shown*) on day of admission revealed similar lesions.

D–F, Follow-up images 3 days later show nearly complete resolution of white matter abnormalities.

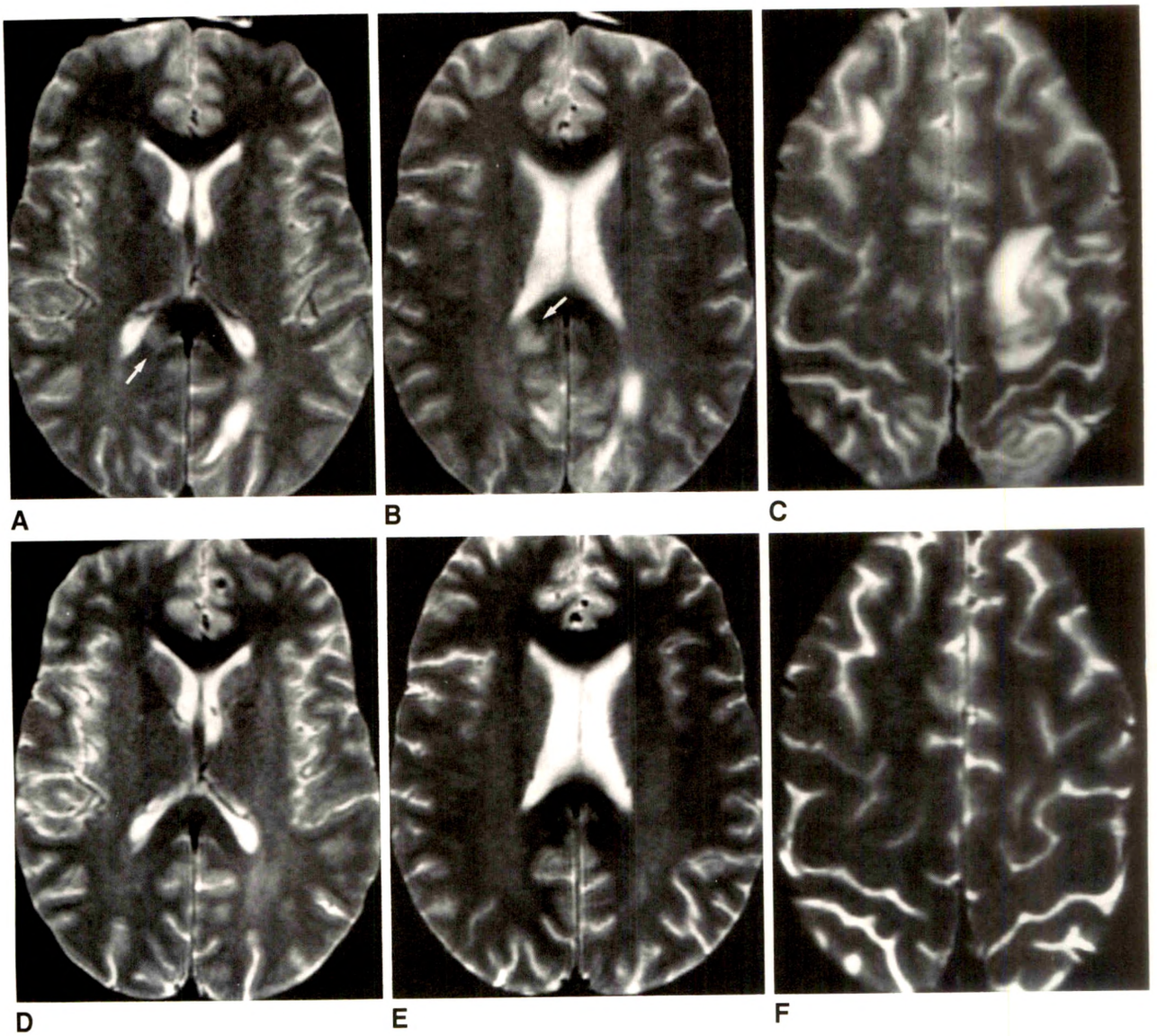


Fig. 3.—Case 3.
***A–C*, Axial spin-echo T2-weighted MR images, 2500/80/1 (TR/TE/excitations), 4 days after initial episode of cyclosporin A neurotoxicity reveal multiple foci of hyperintensity in subcortical white matter, as well as in right splenium (*arrows*).**
***D–F*, Follow-up T2-weighted images (2308/80/1) 12 days later reveal complete resolution of white matter abnormalities.**

On postoperative day 84, the patient had a generalized tonic clonic seizure, again with right arm involvement. The CsA level was 116 μg/l at the time of readmission. MR revealed recurrent subcortical white matter lesions of the cerebral hemispheres, as well as new lesions of the corpus callosal genu and splenium and the midbrain and pons (Figs. 4A–4C). Smudgy enhancement of some of the lesions was suggested on enhanced images. Phenytoin therapy was reinstituted. No further seizures occurred, but headache persisted. Given the therapeutic levels of CsA, it was unclear whether these seizures were related to CsA or to some other clinical condition, including infection and hypoxic-ischemic insult due to the long duration of cardiopulmonary bypass. Blood and CSF analyses were negative, and infection was excluded as the source of the seizures and MR findings. Finally, follow-up MR on postoperative day 99 revealed complete resolution of the white matter changes (Figs. 4D and 4E). A few questionable foci of either pial or cortical contrast enhancement were still apparent.

Discussion

The introduction of CsA in the late 1970s has resulted in a substantial decrease in the rate of rejection of organ transplants. Its use, however, is not without significant adverse effects. Most common are dose-related nephrotoxicity and hypertension. Neurotoxicity has been reported as well, and usually manifests as seizures, visual impairment, confusion, quadriparesis, drowsiness, or coma [7–12]. Although CsA

TABLE 3: Postoperative Laboratory Values in Case 3

Day	BP (mm Hg)	Temp. (°C)	Hct. (%)	CsA (μg/dl)	Mg^{++} (mEq/dl)	Chol. (mg/dl)	Alk. Phos. (U/l)	Bilirubin (mg/dl)	AST (U/l)	Creatinine (mg/dl)
24				176	2.0	122	87	0.7	100	0.9
29	125/81	36.8	31.1	636		146	113	0.7	14	1.2
30	100/60	37.2	28.5	64		139	97	0.5	14	0.8
31	120/70	36.7	34.7	49	1.9	151	114	0.6	11	0.8
32	115/70	36.8	32.5	110						0.8
33	130/90	36.5	34.2	126						0.9
34	134/84	36.6	31.4	279						0.6
35	120/70	36.9	31.4	190	1.1	183	120	0.4	<7	0.6
42			31.6	104		181	121	0.2	8	0.6
63	140/90		32.4	121		199	116	0.2	23	0.6
66				511						
70	130/90		35.5	165		239	94	0.3	14	0.9
72				742						
73				108						
79				351						
84			38.5	116		263	102	0.7	24	1.0
96			32.1	187						

Note.—Day 29 = day of cyclosporin A toxicity. Values for blood pressure (BP) and temperature (Temp.) are the highest recorded during that 24-hr period. Hematocrit (Hct.) values are the lowest recorded during that 24-hr period. Cyclosporin A (CsA) was measured by fluorescent polarization, serum; the therapeutic range is 75–300 μg/l. Normal ranges for magnesium (Mg^{++}), alkaline phosphatase (Alk. Phos.), total bilirubin, aspartate transaminase (AST), and creatinine are 1.6–2.7 mg/dl (magnesium), 43–122 U/l (alkaline phosphatase), 0.2–1.0 mg/dl (total bilirubin), 5–35 U/l (aspartate transaminase), and 0.5–1.4 mg/dl (creatinine). Chol. = cholesterol.

neurotoxicity typically occurs within the first month of therapy, toxicity may appear within the first hours to days or several months after the onset of CsA therapy.

Several reports of CsA neurotoxicity have included neuroimaging findings [1, 2, 5, 6]. Typical findings include white matter hypoattenuation on CT and hyperintensity on T2-weighted MR images. Less commonly, hemorrhage has been reported. Wilson et al. [5] reported a case of reversible cortical blindness due to CsA neurotoxicity. CT revealed bilateral hypoattenuation of the occipital white matter that was also apparent on follow-up MR 3 weeks later. Their patient ultimately succumbed to transplant rejection, and autopsy was performed. Pathologic specimens revealed mild pallor of the white matter and a few scattered macrophages among nerve fibers. Irregular swelling of myelin sheaths and mild astrocytosis were evident. Additionally, these investigators reported small resolving petechiae and a few minute demyelinating lesions characteristic of progressive multifocal leukoencephalopathy. Their description, however, reflects the findings 8.5 months following transplantation and, in particular, 3.5 months following a completely normal ophthalmologic examination.

As the findings of Wilson et al. [5] reflect only subtle foci of demyelination within a broader picture of myelin pallor, it is unlikely that acute demyelination is the source of the CT and MR signal abnormalities. One explanation would involve an acute toxic insult of undetermined origin resulting in axonal swelling and increased water. This is supported by the hypoattenuation seen on CT, the prolonged T2 relaxation seen on MR, and the absence of gadopentetate dimeglumine enhancement on MR and iodinated contrast enhancement on CT. Alternatively, vascular spasm might initiate mild, reversible ischemia. This is supported by the occasional incomplete reversal of white matter changes as well as the infrequent reports of hemorrhagic lesions associated with CsA-induced neurotoxicity.

Another interesting question relates to the site of predilection for CsA neurotoxicity. Although scattered reports suggest that CsA neurotoxicity can occur in almost any location within the brain, including the posterior fossa and supratentorial white matter, a frequent region of insult is the occipital white matter, resulting in seizures or reversible changes in visual acuity, sometimes severe enough to cause reversible cortical blindness [1, 2, 4–7]. Although watershed ischemic changes may be related, it is possible that an as yet undefined selective vulnerability of the occipital white matter is responsible for the frequent association of CsA neurotoxicity with occipital lesions. As similar findings have been noted in *cis*-platinum–induced neurotoxicity, eclampsia, and acute hypertensive encephalopathy, it is possible that selective vulnerability of the occipital white matter plays a role in these disorders as well [13–15].

Some reported cases of CsA neurotoxicity have been correlated with elevated levels of CsA and/or its metabolites. However, many cases occur in the face of apparently normal (therapeutic) blood CsA levels [4, 16]. In light of these more problematic cases, several authors have sought to correlate CsA neurotoxicity with other factors, including hypomagnesemia, aluminum overload, high-dose methylprednisolone therapy, and elevated levels of CsA metabolites [8, 10–12, 16, 17]. To date, these theories have not been substantiated.

Another theory was suggested by de Groen et al. [4], who noted an inverse relationship between CsA neurotoxicity and serum cholesterol, which binds CsA in the serum. Within the blood, the vast majority of CsA either is carried by erythrocytes or is bound to lipoproteins, especially low- (LDL) and high-density lipoproteins [18]. Only a small fraction (<10%) of CsA is unbound. Thus, a small shift of the equilibrium between

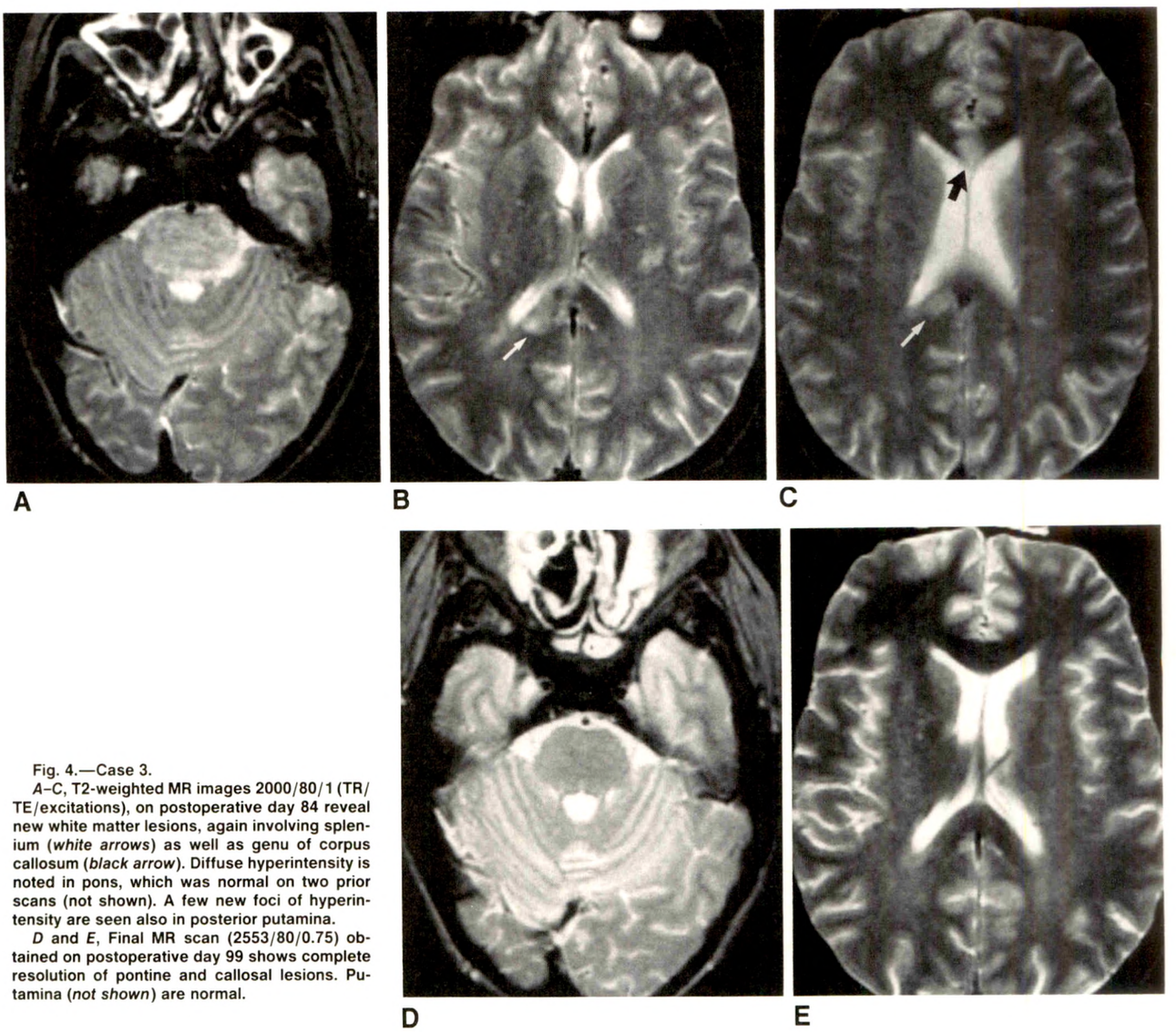


Fig. 4.—Case 3.

A–C, T2-weighted MR images 2000/80/1 (TR/TE/excitations), on postoperative day 84 reveal new white matter lesions, again involving splenium (*white arrows*) as well as genu of corpus callosum (*black arrow*). Diffuse hyperintensity is noted in pons, which was normal on two prior scans (not shown). A few new foci of hyperintensity are seen also in posterior putamina.

D and *E*, Final MR scan (2553/80/0.75) obtained on postoperative day 99 shows complete resolution of pontine and callosal lesions. Putamina (*not shown*) are normal.

erythrocyte-CsA, LDL-bound CsA, and free CsA could significantly alter the small fraction of free CsA. Such a change is suspected in cases of depressed cholesterol, where a diminished binding capacity would be present. In the face of a depressed binding capacity, de Groen et al. suggested an increased fraction of unbound (unmeasured) CsA would be present. As the current clinical assays of CsA measure total concentration, any increase in the free fraction would be undetected by routine testing.

In a subsequent report, however, de Groen [19] revised part of this theory, noting that dedicated assays of unbound CsA had failed to correlate with changes in total serum cholesterol. Instead, he hypothesized an increased concentration of bound CsA per LDL particle (in the case of diminished LDL), resulting in increased delivery of CsA to astrocytes, accounting for neurotoxicity. This theory also invokes diminished cholesterol as the underlying factor in CsA neurotoxicity. However, not all patients with CsA neurotoxicity have diminished serum cholesterol levels.

Our first patient (case 1) had presumed CsA neurotoxicity in temporal association with several factors. Serum magnesium levels were chronically depressed, despite replacement therapy and fairly constant serum creatinine levels. CsA levels rose precipitously between postoperative days 5 and 7 to a level of 401 mg/dl, most likely consequent to increased absorption of CsA. Despite the rapid rise, a concentration of 401 mg/dl is often a nontoxic level in the immediate postoperative period of liver transplantation. No serum cholesterol measurements were obtained during the hospitalization period, although markedly diminished preoperative serum cholesterol was noted. In most liver transplantation patients, serum cholesterol rapidly reaches normal levels within the first few postoperative days because of the large perioperative infusions of plasma. Nevertheless, we cannot know

whether the serum cholesterol in this patient remained depressed or had increased to normal levels by postoperative day 7, the day of CsA neurotoxicity.

In case 2, serum CsA levels were within the therapeutic range, and the serum cholesterol, creatinine, and magnesium levels were normal. In case 3, although serum CsA was elevated at the time of initial neurotoxicity, serum cholesterol, creatinine, and magnesium levels were not depressed. It is unlikely, therefore, that the cholesterol hypothesis applies to these cases.

The second patient had systemic hypertension at the time of CsA neurotoxicity, although not to the levels seen in acute hypertensive encephalopathy (HE). In HE, diastolic blood pressure measurements typically surpass 130 mm Hg [15]. HE is hypothesized to result from a loss of cerebral autoregulation, focal vasodilatation, and breakdown of the blood-brain barrier (BBB) with extravasation of serum proteins and water [15, 20–22]. CsA neurotoxicity, on the other hand, occurs at lower blood pressures, even if elevated. As a result, loss of cerebral autoregulation most likely does not apply. Rather, we suggest that CsA neurotoxicity may be consequent to focal vasoconstriction, which may be mediated by the release of endothelin (ET), a new neuropeptide.

ET is a potent diffusible vasoconstrictive substance, first characterized in 1988 [23]. ET is a 21-amino acid peptide elaborated by endothelial cells that appears to act on vascular smooth muscle. It may have a significant role in the development of vasospasm, and may play a pivotal role in CsA neurotoxicity. Specific binding sites for ET have been identified in several areas of the human brain, including the cerebellum, hippocampal formation, diencephalon, and choroid plexus [24–26].

Clinically, increased plasma ET levels correlate with several conditions, including cardiogenic shock, hypertension (case 2), orthotopic liver transplantation (case 1), and acute myocardial infarction [27]. Conditions in which ET is postulated to play a role include sepsis, coronary artery spasm, vasculitis, toxemia of pregnancy, and CsA nephrotoxicity [27]. ET has also been implicated in vasospasm following subarachnoid hemorrhage, as it has been isolated in the CSF of patients with subarachnoid hemorrhage [28, 29]. We suspect that ET also may be involved in the development of CsA neurotoxicity and that a similar mechanism may be operative in the reversible CNS effects of eclampsia.

In the kidney, CsA has been shown to disrupt endothelial integrity, which induces increased release of ET [30]. Two in vitro studies have reported the stimulatory effect of CsA on ET release [30, 31]. In addition, CsA-induced increases in ET-1 binding site density in mice cardiac cell membranes have been reported [32]. Given the significant cerebral vasoconstrictive properties of ET, it is not unreasonable to suggest similar effects of CsA on CNS release and binding of ET.

In the CNS, integrity of the BBB normally restricts movement of both CsA and ET. However, in many patients on CsA, conditions exist that disrupt the BBB and permit access of both CsA and ET to otherwise protected sites in the CNS. Under conditions of hepatic encephalopathy, an increase in the permeability of the BBB has been observed experimentally [19]. Clinically, the patient described in case 1 had multiple episodes of overt hepatic encephalopathy before transplantation.

A possible mechanism of BBB disruption involves elevation of plasma cholestanol, consequent to a deficiency of the hepatic enzyme 26-hydroxylase [19]. Increased cholestanol may alter the integrity of the BBB. Princen et al. [33] recently found potent inhibition of the same hepatic enzyme by CsA in rats. It is possible that such a mechanism disrupts the BBB in CsA neurotoxicity; if so, it could help explain CsA neurotoxicity in nonhepatic transplant patients, as in cases 2 and 3.

If endothelial integrity were disrupted, CsA could gain access to astrocytes, ET could gain access to cerebral vascular smooth muscle resulting in vasoconstriction and vasospasm, and elevated circulating ET could promote systemic hypertension. Under such conditions, local ischemia, and consequent white matter edema, would be possible. If severe enough, petechial or confluent parenchymal hemorrhages could ensue. Since the white matter lesions seen in CsA neurotoxicity are not seen after subarachnoid hemorrhage, vasospasm alone would seem to be inadequate to promote such lesions. We suspect a synergistic effect of both ET and CsA may be operative in CsA neurotoxicity. Unfortunately, ET assays are not yet readily available at our institution. As a result, we do not as yet have direct evidence of elevated ET at the time of CsA neurotoxicity.

Three cases of CsA-induced neurotoxicity are reported. Analysis of these cases fails to support the suggested relationship between diminished serum cholesterol and CsA neurotoxicity. The notion that underlying chronic hepatic encephalopathy increases permeability of the BBB may, however, apply. Elevated levels of ET during the first week after orthotopic liver transplantation may have contributed to the development of vasospasm in case 1. In case 2, severe systemic hypertension, perhaps consequent to CsA therapy and coupled with elevated levels of ET, may have resulted in cerebral vasoconstriction and/or vasospasm. In other words, CsA-induced hypertension, coupled with disruption of the BBB, could promote local ischemia with the development of white matter edema. In the third case, markedly elevated levels of serum CsA correlate with the initial episode of CsA neurotoxicity. Although systemic hypertension was not present, the markedly elevated levels of CsA may have promoted ET-mediated cerebral vasospasm resulting in neurotoxicity.

Despite numerous theories, including our hypothesis, the matter of CsA-induced neurotoxicity remains unsettled. We recognize the speculative nature of our hypothesis about the relationship between CsA and ET, particularly without direct evidence of elevated levels of ET at the time of neurotoxicity. We are hopeful that further study will offer additional insights into this fascinating and, fortunately, transient disorder.

ACKNOWLEDGMENTS

We thank Michael Ross for case 3 and David Norman for reviewing the manuscript.

REFERENCES

1. Lloveras J-J, Larrue V, Suc E, Fourtanier G, Durand D. Leucoencephalopathy after cyclosporine in a liver transplant. *Clin Transplant* **1990**;4: 58–62
2. Rubin AM, Kang H. Cerebral blindness and encephalopathy with cyclosporin A toxicity. *Neurology* **1987**;37:1072–1076
3. Wilczek H, Ringden O, Tyden G. Cyclosporine-associated central nervous system toxicity after renal transplantation. *Transplantation* **1985**;39:110
4. De Groen PC, Aksamit AJ, Rakela J, Forbes GS, Krom RAF. Central nervous system toxicity after liver transplantation: the role of cyclosporine and cholesterol. *N Engl J Med* **1987**;317:861–866
5. Wilson SE, de Groen PC, Aksamit AJ, Wiesner RH, Garrity JA, Krom RAF. Cyclosporin A–induced reversible cortical blindness. *J Clin Neuro Ophthalmol* **1988**;8(4):215–220
6. Lane RJM, Roche SW, Leung AAW, Greco A, Lange LS. Cyclosporin neurotoxicity in cardiac transplant recipients. *J Neurol Neurosurg Psychiatry* **1988**;51:1434–1437
7. Noll RB, Kulkarni R. Complex visual hallucinations and cyclosporine. *Arch Neurol* **1984**;41:329–330
8. Boogaerts MA, Zachee P, Verwilghen RL. Cyclosporin, methylprednisolone, and convulsions. *Lancet* **1982**;2:1216–1217
9. Atkinson K, Biggs J, Darveniza P, Boland J, Concannon A, Dodds A. Cyclosporine-associated central nervous system toxicity after allogenic bone marrow transplantation. *Transplantation* **1984**;38(1):34–37
10. Durrant S, Chipping PM, Palmer S, Gordon-Smith EC. Cyclosporin A, methylprednisolone, and convulsions. *Lancet* **1982**;2:829–830
11. Joss DV, Barrett AJ, Kendra JR, Lucas CF, Desai S. Hypertension and convulsions in children receiving cyclosporin A. *Lancet* **1982**;1:906
12. Thompson CB, Sullivan KM, June CH, Thomas ED. Association between cyclosporin neurotoxicity and hypomagnesemia. *Lancet* **1984**;2:1116–1120
13. Kattah JC, Potolicchio SJJ, Kotz HL, Kolsky MP, Thomas D. Cortical blindness and occipital lobe seizures induced by *cis*-platinum. *Neuroophthalmology* **1987**;7(2):99–104
14. Coughlin WF, McMurdo SK, Reeves T. MR imaging of postpartum cortical blindness. *J Comput Assist Tomogr* **1989**;13(4):572–576
15. Hauser RA, Lacey M, Knight MR. Hypertensive encephalopathy: magnetic resonance imaging demonstration of reversible cortical and white matter lesions. *Arch Neurol* **1988**;45:1078–1083
16. Kunzendorf U, Brockmoller J, Jochimsen F, Keller F, Walz G, Offermann G. Cyclosporin metabolites and central-nervous-system toxicity. *Lancet* **1988**;1:1223
17. Nordal KP, Talseth T, Dahl E, et al. Aluminum overload, a predisposing condition for epileptic seizures in renal-transplant patients treated with cyclosprin? *Lancet* **1985**;2:153–154
18. Sgoutas D, MacMahon W, Love A, Jerkunica I. Interaction of cyclosporin A with human lipoproteins. *J Pharm Pharmacol* **1986**;38:583–588
19. De Groen PC. Cyclosporine, low-density lipoprotein, and cholesterol. *Mayo Clin Proc* **1988**;63:1012–1021
20. Jesperson CM, Rasmussen D, Hennild V. Focal intracerebral oedema in hypertensive encephalopathy visualized by computerized tomographic scan. *J Intern Med* **1989**;225:349–350
21. Kwong YL, Yu YL, Lam KSL, Woo E, Ma JTC, Huang CY. CT appearance in hypertensive encephalopathy. *Neuroradiology* **1987**;29:215
22. Gibby WA, Stecker MM, Goldberg HI, et al. Reversal of white matter edema in hypertensive encephalopathy. *AJNR* **1989**;10[suppl]:S78
23. Yanagisawa M, Kurihara H, Kimura S, et al. A novel potent vasocontrictor peptide produced by vascular endothelial cells. *Nature* **1988**;332:411–415
24. Hoyer D, Waeber C, Palacios JM. $^{[125I]}$Endothelin-1 binding sites: autoradiographic studies in the brain and periphery of various species including humans. *J Cardiovasc Pharmacol* **1989**;13[Suppl 5]:S162–165
25. Koseki C, Imai M, Hirata Y, Yanagisawa M, Masaki T. Autoradiographic distribution in rat tissues of binding sites for endothelin: a neuropeptide. *Am J Physiol* **1989**;256:R858–R866
26. Kadel KA, Heistad DD, Faraci FM. Effects of endothelin on blood vessels of the brain and choroid plexus. *Brain Res* **1990**;518:78–82
27. Lerman A, Hildebrand FLJ Jr, Margulies KB, et al. Endothelin: a new cardiovascular regulatory peptide. *Mayo Clin Proc* **1990**;65:1441–1445
28. Ide K, Yamakawa K, Nakagomi T, et al. The role of endothelin in the pathogenesis of vasospasm following subarachnoid haemorrhage. *Neurol Res* **1989**;11:101–104
29. Fujimori A, Yanagisawa M, Saito A, et al. Endothelin in plasma and cerbrospinal fluid of patients with subarachnoid hemorrhage. *Lancet* **1990**;336(8715):633
30. Kon V, Sugiura M, Inagami T, Harvie BR, Ichikawa I, Hoover RL. Role of endothelin in cyclosporine-induced glomerular dysfunction. *Kidney Int* **1990**;37:1487–1491
31. Nakahama H. Stimulatory effect of cyclosporine A on endothelin secretion by a cultured renal epithelial cell line, LLC-PK1 cells. *Eur J Pharmacol* **1990**180:191–192
32. Nayler WG, Gu XH, Casley DJ, Panagiotopoulos S, Liu J, Mottram PL. Cyclosporine increases endothelin-1 binding site density in cardiac cell membranes. *Biochem Biophys Res Commun* **1989**;163(3):1270–1274
33. Princen HMG, Meijer P, Hofstee B, Havekes LM, Kuipers F, Vonk RJ. Effects of cyclosporin A (CsA) on LDL-receptor activity and bile acid synthesis in hepatocyte monolayer cultures and in vivo in rat (abstr). *Hepatology* **1987**;7:1109

Call for Papers on Neuroradiology

On January 1, 1992, The American Roentgen Ray Society and the American Society of Neuroradiology will terminate their agreement whereby manuscripts on neuroradiology submitted to the *AJR* are forwarded to the *AJNR* and selected *AJNR* papers are republished in the *AJR*.

To avoid any lag in the publication of neuroradiologic articles in the *AJR*, the Journal requests authors to submit neuroradiologic manuscripts effective immediately. We plan to expedite publication of these papers. Authors will receive an initial editorial decision in 3–4 weeks, and accepted papers will be published 3 months after revised manuscripts are accepted. This is more than twice as fast as most other journals.

The advantages of this rapid publication time and the *AJR*'s large circulation (24,000) are now available to all authors of neuroradiologic papers. An expanded section on neuroradiology, including review articles, pictorial essays, and commentaries, will accommodate more than the limited number of papers published under the previous agreement.

We invite authors of neuroradiologic articles to submit their papers for original publication in the *AJR* so that the Journal may continue to fulfill its commitment to supply timely and important original information about neuroradiology to general radiologists as well as to those who subspecialize in the field.

Robert N. Berk
Editor-in-Chief

Value of Subtraction Images in the Detection of Hemorrhagic Brain Lesions on Contrast-Enhanced MR Images

Soheil L. Hanna[1]
James W. Langston
Suzanne A. Gronemeyer

Contrast-enhanced T1-weighted MR images are known to improve the detection and conspicuity of CNS lesions; however, lesion enhancement may be indistinguishable from contiguous hemorrhagic areas of intrinsically increased signal intensity. In a series of cranial MR studies in 22 pediatric oncologic patients with evidence of subacute hemorrhage, we found that subtracting the unenhanced from the enhanced T1-weighted images was essential in 14 of the cases to visualize and/or characterize the enhanced tissue in the presence of adjacent hemorrhage. In six patients, a nodular pattern of enhancement suggestive of tumor was detected and/or outlined only after subtraction. In eight patients, linear benign-appearing enhancing margins were seen clearly only after subtraction. In the remaining eight patients, the presence and shape of enhancement was verified with subtraction.

Subtraction is a useful, simple, and rapid postprocessing procedure that does not increase scan time or require modification of standard pulse sequences. Subtraction separates the enhanced areas from adjacent bright hemorrhage.

***AJNR* 12:681–685, July/August 1991; *AJR* 157:861–865, October 1991**

The benefit of gadopentetate dimeglumine–enhanced T1-weighted MR imaging in detecting brain tumors in children and adults has been reported [1, 2]. Contrast-enhanced MR imaging has also been found useful in detecting residual tumor and gliosis in postoperative patients [3]. However, it may be difficult or impossible to detect the presence or distinguish the shape of the enhanced region from adjacent bright subacute hemorrhage. In 22 cranial MR studies with evidence of subacute hemorrhage, we applied a simple subtraction technique that we have successfully used to evaluate contrast-enhanced MR images of musculoskeletal tumors [4]. Using the standard digital image subtraction software on our scanner, we subtracted the unenhanced T1-weighted images from the corresponding images obtained after administration of gadopentetate dimeglumine. The purpose of this study was to evaluate the use of image subtraction with contrast-enhanced MR imaging of hemorrhagic brain lesions.

Patients and Methods

During a 2-year period from August 1988 to July 1990, 93.3% of 829 pediatric oncologic patients with symptoms of intracranial disease due to known or suspected primary or secondary brain neoplasia were studied with cranial MR imaging before and after enhancement with gadopentetate dimeglumine. Of those, 22 patients had MR evidence of subacute hemorrhage. Subjects included six girls and 16 boys ranging in age from 9 months to 18 years (mean, 9.6 years). Their diagnoses are included in Table 1. Eleven of the 22 patients were examined 1 to 3 weeks after tumor resection to exclude residual tumor. Of the remaining 11 patients, one was examined for evaluation of a hemorrhagic primary tumor, five for known hemorrhagic metastases, and five for parenchymal hemorrhage with suspected underlying neoplasia. All studies were performed after obtaining written informed consent from the

Received September 17, 1990; revision requested December 21, 1990; revision received January 15, 1991; accepted January 23, 1991.

This work was supported in part by the National Cancer Institute, Cancer Center Support (CORE) grant P30CA21765 and by the American Lebanese Syrian Associated Charities.

[1]All authors: Department of Diagnostic Imaging, St. Jude Children's Research Hospital, 332 N. Lauderdale, P.O. Box 318, Memphis, TN 38101, and Department of Radiology, University of Tennessee, Memphis, TN. Address reprint requests to J. W. Langston.

0361–803X/91/1574–0861
© American Roentgen Ray Society

TABLE 1: MR Subtraction Results in 22 Patients with Intracranial Hemorrhage

Case No.	Age (years)	Diagnosis	Postoperative Enhancement			Shape Determined Only After Subtraction		Imaging Impression
			Y/N	No. of Weeks Postop.	Seen Only After Subtraction	Y/N	Shape	
1	15	A	Yes	3	Yes	Yes	Linear	No tumor
2	3	M	Yes	2	No	Yes	Nodular	Residual
3	0.75	A	Yes	3	Yes	Yes	Linear	No tumor
4	15	A	Yes	3	No	No	Linear	No tumor
5	3	M	Yes	1	No	Yes	Linear	No tumor
6	10	GBM	Yes	2	No	Yes	Nodular	Residual[a]
7	13	GBM	Yes	2	No	Yes	Nodular	Residual
8	6	A	Yes	3	No	Yes	Linear	No tumor
9	4	E	Yes	2	Yes	Yes	Linear	No tumor
10	7	PNET	Yes	2	No	No	Linear	No tumor
11	7	GC	Yes	1	No	Yes	Nodular	Residual
12	9	ALL	No	–	Yes	Yes	Linear	No tumor
13	15	ALL	No	–	Yes	Yes	Linear	No tumor
14	5	ALL	No	–	Yes	Yes	Linear	No tumor
15	6	M	No[c]	–	Yes	Yes	Nodular	Tumor[b]
16	6	NB	No	–	Yes	Yes	Nodular	Tumor
17	15	RD	No	–	No	No	Nodular	Tumor
18	17	OS	No	–	No	No	Nodular	Tumor
19	17	OS	No	–	No	No	Nodular	Tumor
20	18	OS	No	–	No	No	Nodular	Tumor
21	3	M	No[c]	–	No	No	Nodular	Tumor
22	1	NB	No	–	No	No	Nodular	Tumor

Note.—A = astrocytoma, ALL = leukemia, E = ependymoma, GBM = glioblastoma multiforme, GC = gliomatosis cerebri, M = medulloblastoma, NB = neuroblastoma, OS = osteosarcoma, PNET = primitive neuroectodermal tumor, RD = rhabdoid.

[a] Biopsy proved GBM.

[b] Biopsy and serologically proved visceral larva migrans.

[c] Hemorrhage in remote location from surgical site.

patients or their guardians and with approval of the institutional clinical trials review committee. The MR studies of all 22 patients showed intracranial regions with increased signal intensity on T1- and T2-weighted images consistent with methemoglobin [5]. The presence of subacute blood made the visual detection of possible intrinsic or adjacent enhancement difficult.

The MR examinations were performed on a 1.0-T Magnetom scanner (Siemens Medical Systems, Iselin, NJ). Routine evaluation included sagittal and transverse T1-weighted, 550/15/2 (TR/TE/excitations), images and double-echo spin-density and T2-weighted (2500/25–90/1) transverse images. A 256 × 256 matrix, 25-cm field of view, and section thickness of 5 mm with a 1-mm interslice gap were used in all sequences. Gadopentetate dimeglumine (Berlex Laboratories, Cedar Knolls, NJ) at a dose of 0.1 to 0.2 mmol/kg was then administered slowly via a previously installed vascular access device or peripheral IV route without moving the patient. Five min after administering the contrast material, transverse T1-weighted sequences were repeated using the same imaging parameters as those used for the precontrast transverse T1-weighted sequences. The transmitter and receiver attenuator values were held constant between the pre- and postcontrast images as were the gray scale adjustments.

Corresponding unenhanced and enhanced anatomic slices showing bright blood and possible adjacent enhancement were chosen for subtraction. The pre- and postcontrast images were reviewed on the monitor to determine if motion had occurred between the unenhanced and enhanced T1-weighted images. In a few cases, slight in-plane motion was noted, and the images were pixel-shifted in the appropriate horizontal and/or vertical direction to correct image alignment. Subtraction was then performed by displaying the contrast-enhanced image and electronically subtracting the unenhanced image on a pixel-by-pixel basis using the image subtraction function available as standard software on our system. Production of the subtracted image was typically completed in 10 sec. The resultant images reflected the enhancement provided by contrast material alone after subtraction of all unenhanced areas.

To determine the clinical utility of subtraction technique, we visually evaluated the unenhanced and enhanced T1-weighted images for the presence or absence of enhancement and the shape (linear or nodular) of the enhancing region, and then compared these findings with the subtracted images. Subtraction was considered useful if previously undetected enhancement was seen and/or the configuration of the enhancing region was better delineated.

Results

Subtraction was successfully performed in all 22 cases. None of the subtracted images showed uncorrectable misregistration due to rotatory patient head movement.

All 22 cases showed enhancement either around or within the subacute hemorrhagic areas. Subtraction improved contrast between the enhanced areas and adjacent bright subacute hemorrhage on all 22 patients, revealing only the enhanced regions contrasted against a muted background.

In eight of the 22 cases, subtraction was essential in the detection of enhancement, which was otherwise not visible because of the adjacent subacute hemorrhage. In six of the remaining 14 cases in which the presence of enhancement was visually detected without subtraction, subtraction was

necessary to differentiate a linear from a nodular pattern (Table 1).

A benign-appearing linear and peripheral pattern of enhancement was found in 10 cases, eight of which could only be separated from the adjacent subacute hemorrhage by subtraction. In the remaining 12 cases, a nodular enhancing configuration suggestive of tumor was present.

The subtracted images outlined the enhanced postoperative margins in all 11 postsurgical cases. Seven had a linear enhancement pattern consistent with gliosis or blood-brain barrier disruption, thus suggesting absence of residual tumor. Residual focal nodular enhancement was demonstrated in the remaining four patients (Fig. 1). In the second group (Table 1, cases 12–16), which included five patients with parenchymal hemorrhage who were studied to determine if underlying neoplasia was present, subtraction was necessary to demonstrate metastatic-like nodular enhancement in two patients as the underlying cause of hemorrhage (Fig. 2). In the remaining three patients, subtraction confirmed absence of associated nodular enhancement. In the third group, including six patients (Table 1, cases 17–22) with known intracranial hemorrhagic malignancy, the subtracted images highlighted the enhanced tumor component permitting more accurate measurement of tumor extent and subsequent monitoring of tumor response to therapy.

On the basis of the findings from the subtracted images, two patients underwent a stereotaxic biopsy procedure. One patient (case 6) had an enhanced nodular area at the resection margins that was precisely outlined only after subtraction; biopsy confirmed the presence of residual glioblastoma multiforme (Fig. 1). The other patient (case 15), treated for medulloblastoma, had unenhanced T1-weighted images showing several hundred small, bright, parenchymal brain lesions. Subtraction disclosed that only three lesions enhanced, thus providing guidance for the subsequent biopsy, which aided in the serologic diagnosis of visceral larva migrans infection.

Discussion

Contrast-enhanced MR imaging has proved very useful for evaluating intracranial abnormalities [1], including pediatric brain tumors [2]. Contrast enhancement enables detection of areas with abnormal vasculature and/or disrupted blood-brain barrier and thus permits more accurate assessment of tumors than does unenhanced MR imaging alone, especially when separation of tumor from surrounding edema is difficult [1, 2]. Furthermore, contrast-enhanced T1-weighted images are useful in morphologically differentiating residual tumor from nonhemorrhagic postoperative gliosis and encephalomalacia, since all may have similar signal characteristics prior to contrast administration [3]. Typically, a linear pattern of enhancement around the margins of resection is more consistent with gliosis or blood-brain barrier disruption, while a focal nodular configuration is more consistent with residual tumor [3].

Not infrequently, the presence of bright subacute hemorrhage prevents appreciation of contiguous enhanced regions of similar increased signal intensity. The lack of contrast between bright blood and adjoining bright enhancement is caused by shortening of the T1 relaxation time of the contrast-enhanced areas to an extent comparable to the shortening due to methemoglobin in contiguous hemorrhagic regions [5]. Several diagnostic problems may be caused by this lack

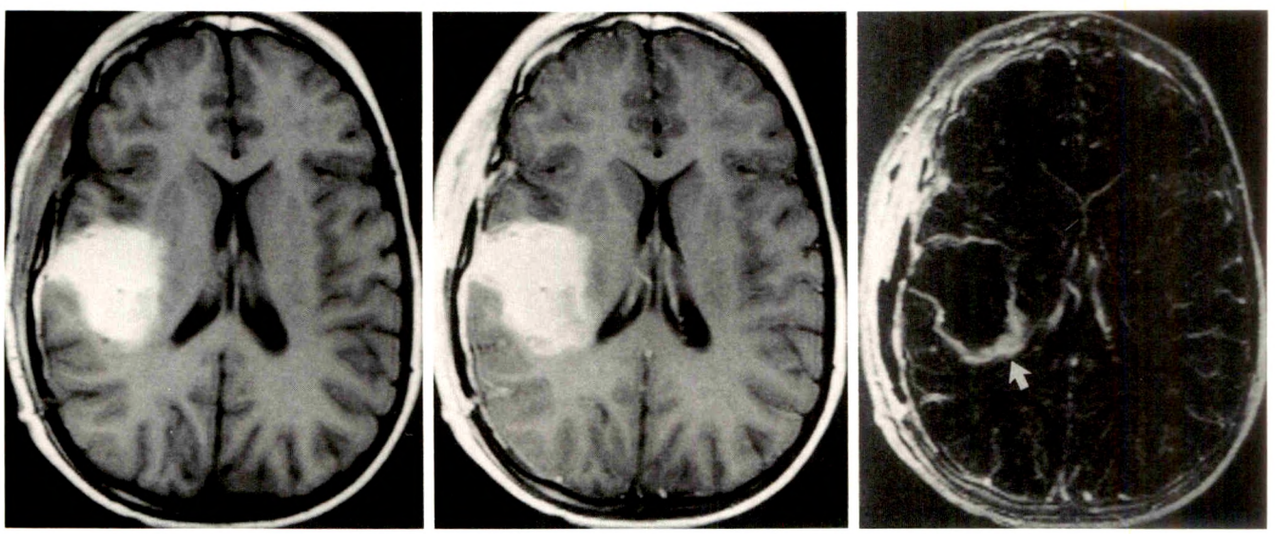


Fig. 1.—Postoperative MR images of a 10-year-old patient with right temporal glioblastoma multiforme.
A, Unenhanced transverse T1-weighted (550/15) image shows right postsurgical changes with a hyperintense area consistent with subacute hemorrhage.
B, Contrast-enhanced T1-weighted (550/15) image of same slice shows enhancement about the margins of resection that is difficult to distinguish from adjacent hemorrhage.
C, Subtraction of *A* from *B* clearly shows posteromedial nodular enhancement (*arrow*) consistent with residual tumor, which was confirmed by biopsy.

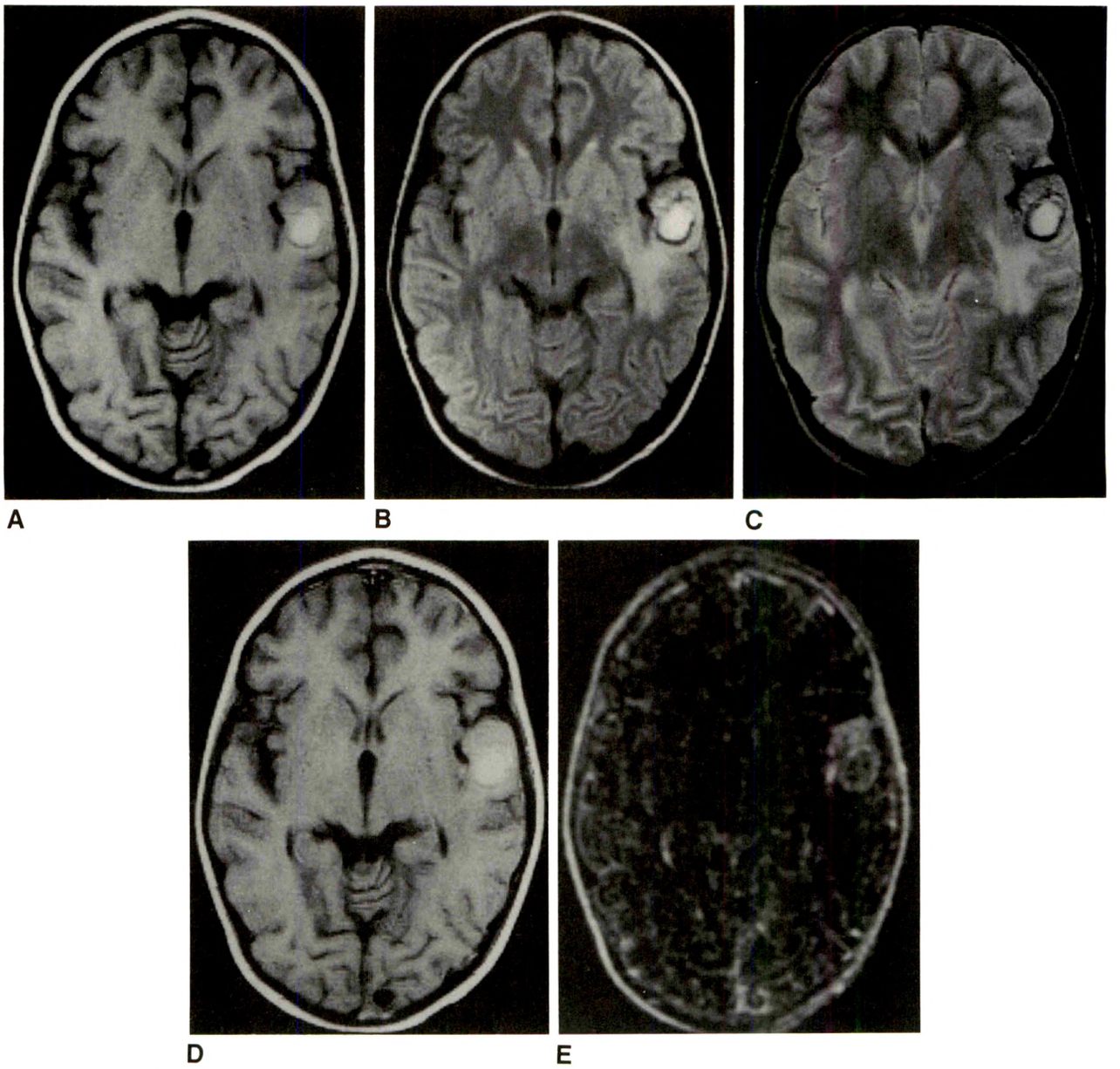


Fig. 2.—Six-year-old patient with known retroperitoneal neuroblastoma.

A–C, Unenhanced transverse T1-weighted (550/15) (*A*) proton-density-weighted (2500/25) (*B*), and T2-weighted (2500/90) (*C*) images obtained at same level show a left temporal lesion consistent with subacute hemorrhage.

D, Contrast-enhanced T1-weighted (550/15) image does not clearly show enhancement.

E, Subtraction of *A* from *D* shows adjacent anterior nodular enhancement, suggesting that tumor caused the hemorrhage.

of contrast. First, it may preclude precise discernment of the enhanced boundaries of hemorrhagic malignant neoplasms and thereby prevent the accurate measurement of tumor extent necessary for monitoring tumor response to therapy. Second, the presence of postoperative subacute hemorrhage may prevent delineation of the surgical margins and subsequent differentiation of contiguous enhanced residual tumor from gliosis or blood-barrier disruption. Third, the occurrence of cerebral parenchymal hemorrhage in patients with known systemic oncologic diseases such as the leukemias mandates exclusion of possible underlying enhanced neoplasm that could be masked by hemorrhage.

In theory, enhancement can be confirmed by measuring the mean signal intensity of regions of interest directly from the enhanced and unenhanced images, but this does not provide information about the shape of the enhanced region. Further-

more, quantifying signal intensities requires prior detection of sites of abnormality, which is not always possible. Subtraction can be performed more rapidly than can mean signal intensity measurements and also shows lesions that would otherwise have been missed (Fig. 2). Additionally, subtraction provides a global perception of the morphologic features of the enhanced regions that is necessary to distinguish a nodular from a linear configuration. This is demonstrated in Figure 1C, where the subacute blood has been subtracted, leaving linear enhanced resection margins consistent with gliosis or blood-brain barrier disruption [3]. However, by revealing the inner border of the enhanced lesion with subtraction, a nodular pattern of enhancement was readily visible posteromedially, prompting us to perform a stereotaxic biopsy that confirmed the presence of residual tumor. Other uses of subtraction in cranial MR imaging include differentiation of enhanced calvarial metastases from adjacent bright fatty marrow [6].

Subtraction may not be possible when rotatory head motion occurs in the interval between the pre- and postcontrast sequences producing uncorrectable misregistration of the subtracted images [4]; however, we did not encounter this problem in our series. Secure stabilization of the subject's head and consecutive acquisition of the unenhanced and enhanced T1-weighted images decrease the likelihood of motion.

In summary, image subtraction is a simple, rapid, postprocessing procedure that does not increase scan time or require modification of standard T1-weighted pulse sequences. Subtraction can differentiate enhancement from adjacent subacute hemorrhage and thus increase the level of confidence when the shape of the enhancing area is clearly demonstrated. Our experience indicates that without subtraction, intracranial lesions may be missed.

REFERENCES

1. Hesselink JR, Healy ME, Press GA, Brahme FJ. Benefits of Gd-DTPA for MR imaging of intracranial abnormalities. *J Comput Assist Tomogr* **1988**;12:266–274
2. Powers TA, Partain CL, Kessler RM, et al. Central nervous system lesions in pediatric patients: Gd-DTPA-enhanced MR imaging. *Radiology* **1988**;169:723–726
3. Bird CR, Drayer BP, Medina M, Rekate HL, Flom RA, Hodak JA. Gd-DTPA-enhanced MR imaging in pediatric patients after brain tumor resection. *Radiology* **1988**;169:123–126
4. Hanna SL, Langston JW, Gronemeyer SA, Fletcher BD. Subtraction technique for contrast-enhanced MR images of musculoskeletal tumors. *Magn Reson Imaging* **1990**;8:213–215
5. Atlas SW, Grossman RI, Gomori JM, et al. Hemorrhagic intracranial malignant neoplasms: spin-echo MR imaging. *Radiology* **1987**;164:71–77
6. West MS, Russell EJ, Breit R, Sze G, Kim KS. Calvarial and skull base metastases: comparison of nonenhanced and Gd-DTPA-enhanced MR images. *Radiology* **1990**;174:85–91

Book Review

Essentials of Neuroimaging. By J. Robert Kirkwood. New York: Churchill Livingstone, 497 pp., 1990. $89.95

As noted by the author in the preface to *Essentials of Neuroimaging*, there has been lacking for some time a single manageable introductory text suitable for those just starting to explore the complex world of neuroimaging. This need is eliminated with the availability of *Essentials of Neuroimaging*.

Divided into 14 chapters (techniques and anatomy; cerebrovascular disease; intracranial aneurysms and subarachnoid hemorrhages; arteriovenous malformations; cranial tumors; cranial tumors in children and adolescents; head trauma; infections; white matter disease; atrophy, aging, and dementia; hydrocephalus; congenital abnormalities of the brain; spine; and spinal trauma), this text provides the essential facts (and more) for readers who require basic information about the capabilities, limitations, and indications for use of the numerous imaging techniques now available for examining the brain and spinal cord. In addition, a wealth of useful information is provided on the cause, pathophysiology, clinical manifestations, and prognosis of most disease states that will be encountered by those who have to apply and interpret neuroimaging studies. Generally splendid illustrations, clear and concise writing, availability of key references for further reading, and the use of abundant tables and boxed material to underscore key points complement well the basic knowledge supplied in the text.

Complicated topics such as the basis for the appearance of intraparenchymal hematomas on MR imaging and congenital abnormalities of the brain are presented so that the reader is not submerged in details but instead is given basic information that is adequate either for initial application in practice or for the building of subsequent understanding. Controversial topics such as the role of diskography in the diagnosis of disk herniation are identified as such and are presented in a balanced manner. I find no fault with the index.

In a few instances, I found information that differs from what I provide my students. For example, with the availability of current MR techniques, is angiography still the definitive diagnostic test for thrombosis of intracranial veins or dural sinuses? Are venous angiomas an uncommon form of vascular malformations? And, is the risk of neural injury greater with injection of contrast medium into the costocervical trunk than is the case with any other vasculature? These issues are much more a matter of personal experience and preference than of substance and do not at all detract from the value of this book. For a book of this length and complexity, it is remarkable that so few editorial errors occurred. Flaws of this nature are not significant; the use of "density" for "intensity" on page 31 and "cortic vein" for "cortical vein" on page 95 are examples.

Essentials of Neuroimaging is a marvelous book, and it should be in the hands of any physician who is starting to perform or interpret imaging of the brain and spinal cord. Trainees in radiology, neurology, and neurosurgery will all find cover-to-cover reading of this text of great value. It will also be of considerable use as a quick reference to those who although not involved full time in neuroimaging are called on from time to time to use and apply these techniques. The book is also perfectly suited as a source for selected reading by medical students. Kirkwood is to be congratulated for providing this excellent text.

Charles M. Strother
University of Wisconsin
Madison, WI 53792

Neurologic Involvement in Behcet Disease: Imaging Findings in 16 Patients

M. Banna[1]
K. El-Ramahi[2]

Behcet disease is a rare multisystem immune-related vasculitis that is prevalent in Japan, the Middle East, and many Mediterranean countries. In our study population of 36 patients with Behcet disease, 16 (44%) had CNS involvement. CT was noncontributory, except in a single patient with dural sinus thrombosis. MR imaging in nine patients showed foci of high signal intensity on T2-weighted images within the brainstem, the basal ganglia, and the cerebral hemispheres in that order of frequency. Unlike the plaques associated with multiple sclerosis, Behcet lesions show no predilection for the periventricular regions.

***AJNR* 12:791–796, July/August 1991; *AJR* 157:867–872, October 1991**

Neurologic manifestations of Behcet disease (neuro-Behcet) have been reported in 10–25% of patients. These are nonspecific and include loss of vision, diplopia, nystagmus, cranial nerve palsies, speech disorders, cerebellar signs, and cerebral and spinal sensory and motor disturbances. In general, three patterns of neurologic manifestations have been observed: a brainstem syndrome, a meningoencephalitic syndrome, and an organic confusion syndrome [1].

CT is of little diagnostic help in patients with neuro-Behcet disease. In most cases the CT findings are normal, equivocal, or nonspecific. In a few cases, CT may reveal small foci of low attenuation in the brainstem, basal ganglia, thalami, or cerebral hemispheres [2, 3]. These foci may show homogeneous or patchy enhancement following injection with contrast medium. The more chronic cases are associated with atrophy, especially of the brainstem [4, 5]. Rarely, the disease may manifest as a mass lesion simulating an intraaxial neoplasm [6].

There have been a few isolated reports of MR findings in neuro-Behcet disease [3, 6]. We describe our observations in 16 patients with this disorder and discuss the radiologic differential diagnosis.

Patients and Methods

During the past 10 years, 36 cases of Behcet disease were seen at a major tertiary referral center in the Kingdom of Saudi Arabia. The age and sex distribution of these patients are shown in Fig. 1. The mean age was 28.2 years. The youngest patient was a boy 15 years old, and the oldest, a woman of 54 years. There were 29 males and seven females; a sex ratio of 4:1 in favor of males. The frequency of disease manifestations is shown in Fig. 2. Involvement of the nervous system occurred in 16 patients (44%); of these, 10 (62.5%) had symptoms and signs referrable to the brainstem, two (12.5%) presented with meningoencephalitis, two with pseudotumor cerebri, and two had spinal cord symptoms. The high rate of occurrence of neurologic manifestations is attributable to the referral pattern of our hospital. A total of 21 CT scans, nine MR scans, and four cerebral angiograms were performed on these patients; the type of tests depended on whether the patient was seen before or after the availability of MR in our institution, and up to six CT scans were obtained on some of the patients at different intervals.

Received July 26, 1990; revision requested October 5, 1990; revision received January 8, 1991; accepted January 14, 1991.

[1] Department of Radiology, King Faisal Specialist Hospital, P.O. Box 3354, Riyadh 11211, Saudi Arabia. Address reprint requests to M. Banna.

[2] Department of Medicine, King Faisal Specialist Hospital, Riyadh 11211, Saudi Arabia.

0361–803X/91/1574–0867
© American Roentgen Ray Society

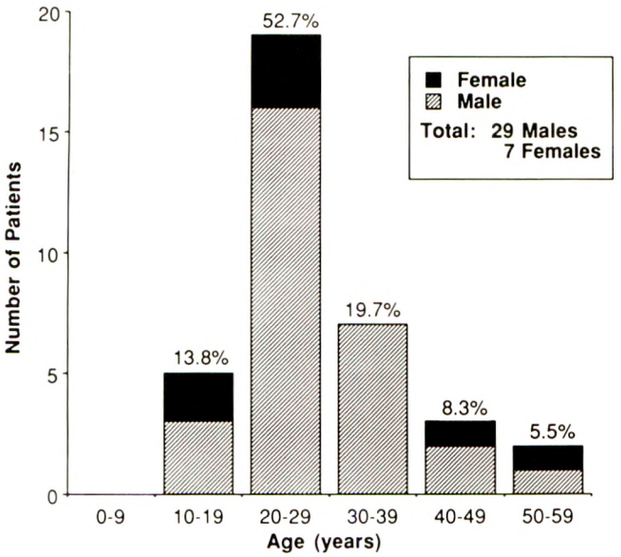


Fig. 1.—Age and sex distribution of 36 patients with Behcet disease who constituted study population.

MR studies were performed on a 1.5-T Vista scanner (Picker, Inc., Solon, OH). The scanning parameters were as follows: 600/20/2 (TR/TE excitations), 2000/40–80/2, and a 7-mm slice thickness. Both T1- and T2-weighted scans were obtained in the axial plane first, and this was supplemented by scans in the sagittal and/or coronal planes depending on the findings. The additional scans were obtained by using a T2-weighted sequence and a slice thickness of 4 mm.

Results

Of the 21 CT scans, only two showed equivocal findings suggestive of brainstem atrophy. Of the four cerebral angiograms, two showed conclusive evidence of dural venous sinus thrombosis. The findings on MR were abnormal in nine patients in whom there was clinical evidence of CNS involvement. All showed abnormal high-signal-intensity foci on T2-weighted images. On the T1-weighted images (600/20), only two lesions 3–5 mm in size were seen as areas of low signal intensity, but smaller lesions that were evident on T2 were not apparent on T1. On the long TR dual-echo pulse sequence, the lesions were seen on both the early and late echoes. Although the late echo (2000/80) gave more tissue contrast, small lesions in the vicinity of the CSF spaces were detected more readily on the early T2 (2000/40) proton-density images. On these, Behcet lesions had higher signal intensity than CSF. Selected examples of the lesions are shown in Figures 3 and 4. The distribution is summarized in Table 1. Following treatment with corticosteroids alone or in combination with immunosuppressive drugs, the lesions decreased in size; in some patients, they disappeared (Fig. 5). Dural venous sinus thrombosis occurred in two patients. The findings on MR were definite in one of these cases and probable in the other (Fig. 6). MR studies in five additional patients with no neurologic deficit were normal.

Discussion

Behcet disease was first described by Hulusi Behcet (1889–1948) of Istanbul University. In 1937 Behcet published his observations on two patients with a triple-symptom complex of recurrent oral and genital ulcerations and ocular inflammation, which he attributed to viral infection [7]. During the 50 years or so that followed Behcet's description, two important facts came to light. First, Behcet disease is not a viral infection, but a multisystem immune-related vasculitis characterized by periods of remission and exacerbation with an unpredictable prognosis. Second, involvement of other systems may occur concomitant with, but more often some months or years following, a complete or incomplete triple-symptom complex. This may manifest as erythema nodosum, polyarthritis, thrombophlebitis, arterial occlusions, pulmonary infarc-

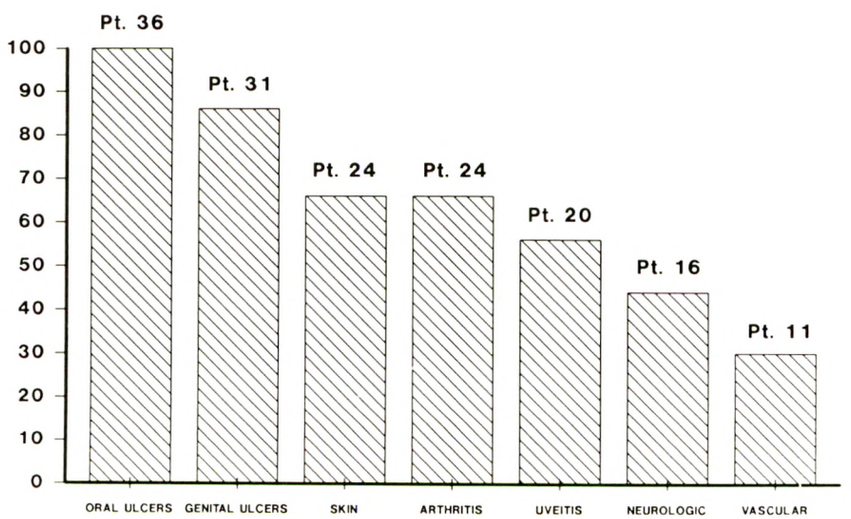


Fig. 2.—Clinical manifestations of 36 patients with Behcet disease who constituted study population.

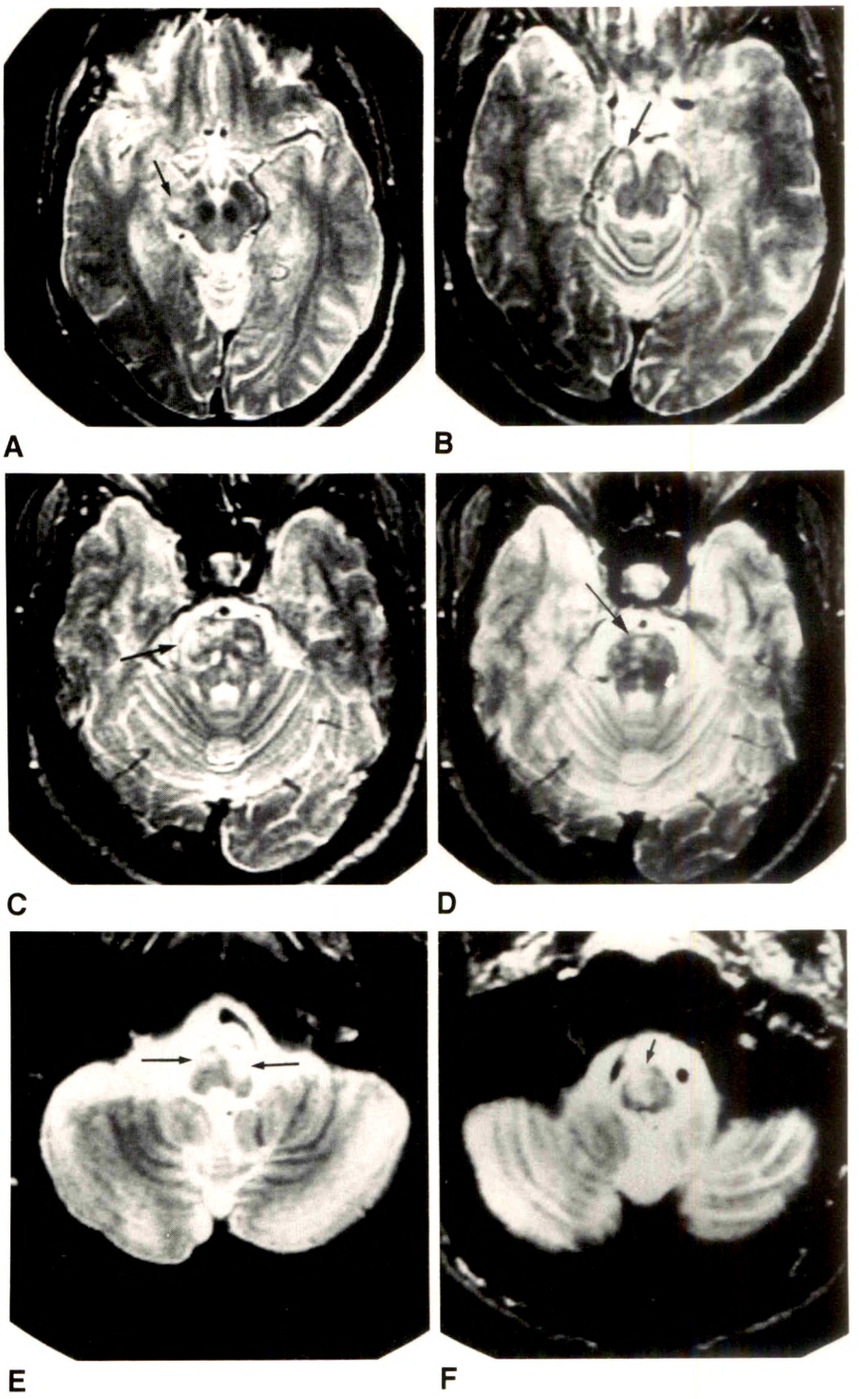
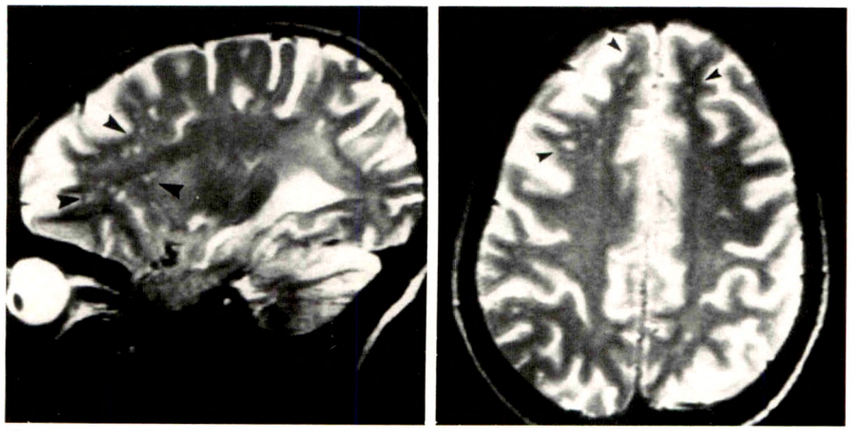


Fig. 3.—*A–F*, Axial T2-weighted MR images (2000/80) from different patients showing multiple Behcet foci (*arrows*) within midbrain (*A* and *B*), pons (*C* and *D*), and medulla (*E* and *F*). Note predilection of lesions for ventral portion of brainstem.

tion, ulcerative colitis, portal hypertension, or neurologic, cardiac, or renal complications. One or more systems may be involved in the same patient [7, 8].

The majority of patients with Behcet disease are young adults, but the disease has been reported in neonates [9] and in subjects over 70 years of age. It is two to four times more common in males. A few familial cases have been recorded [7, 8].

Although Behcet disease is generally rare, it is prevalent in Japan and many Mediterranean and Middle Eastern countries [7–11]. Its incidence in these regions varies from place to place, but in only a few localities does it exceed 10 cases per



A B

Fig. 4.—*A* and *B*, T2-weighted MR images (2000/80) showing Behcet lesions within cerebral hemispheres.

A, Sagittal image shows clusters of Behcet foci within frontal lobe (*arrowheads*).

B, Axial section above the level of lateral ventricles shows that, unlike the plaques that occur with multiple sclerosis, Behcet lesions (*arrowheads*) have no predilection for periventricular area.

TABLE 1: Distribution of Behcet Lesions Within the Brain in Nine Patients

Case No.	Brainstem[a]			Thalami	Corpus Striatum		Cerebral Cortex				Cerebellum
	Medulla	Pons	Midbrain		Caudate	Lentiform	Frontal	Parietal	Temporal	Occipital	
1	+	+	+	−	−	−	−	−	−	−	−
2	+	−	−	−	−	−	−	−	+	−	−
3	−	−	+	+	−	−	−	−	−	−	−
4	−	−	−	−	+	−	−	−	−	−	−
5	+	+	−	−	−	−	−	+	−	−	−
6	−	+	−	−	−	−	+	+	−	−	−
7	+	+	+	−	−	+	−	−	−	−	−
8	−	+	+	−	−	−	−	−	−	−	−
9	Dural venous thrombosis										

[a] Note frequent involvement of the brainstem.

100,000 of the population [8]. It is a less well known entity in Europe and North America [7, 8].

Despite the lapse of more than half a century since the original description of Behcet disease, it remains an enigmatic condition with regard to origin, geographic distribution, and clinical course. Pathologic studies on autopsy cases are few and came principally from Japan. The basic brain lesion, according to Japanese researchers, is a chronic relapsing inflammatory cellular infiltration around venules and capillaries and occasionally around arteries. Macroscopically, these appear as foci of brain softening, which affect the brainstem more frequently than elsewhere. As the lesions become more chronic, there is excessive gliosis, atrophy, and in some cases thickening and fibrosis of the meninges [8]. It is believed that the inflammatory reaction is brought about by human leukocyte antigens generated by many factors, which might be environmental, genetic, or otherwise. Venous thrombosis occurs in approximately one third of patients with Behcet disease [12]. The vena cava and the portal vein are the most common sites, and involvement of the dural venous sinuses is rare. Venous thrombosis may be precipitated in some patients by high fibrinogen levels, but in many cases the exact mechanism is unknown [12].

The MR findings in neuro-Behcet disease consist of small foci of high signal intensity on T2-weighted images, which are iso- or hypointense relative to brain on T1-weighted images. The lesions may be circular, linear, crescentic, or irregular, and occur most frequently within the brainstem, especially around the cerebral peduncles and in the pons. The thalamus and basal ganglia are second in frequency and similar foci may be seen in the cerebral hemispheres, the spinal cord, or the cerebellum. They most likely represent inflammatory cellular infiltration, demyelination, and edema, which may diminish in size in response to corticosteroids alone or in combination with immunosuppressive drugs.

Cerebral angiography of patients with neuro-Behcet disease usually shows no evidence of arteritis and most abnormalities are attributed to venous thrombosis. However, at least one case has been recorded in which cerebral angiography revealed widespread areas of stenosis and ectasia of the anterior middle cerebral arteries [12].

In the absence of a clear history of genital or oral ulcers, the diagnosis of neuro-Behcet disease could be extremely difficult. From a radiologic viewpoint, the differential diagnosis includes four main entities: multiple sclerosis, brainstem infarction, rhomboencephalitis, and dilated perivascular spaces.

Multiple sclerosis and neuro-Behcet disease have many features in common. They are both disseminated, demyelinating, and inflammatory diseases of unknown origin, but clear-cut cases can be differentiated on the basis of clinical history and serum and CSF findings [14]. Multiple sclerosis is a disease of white matter, and these plaques occur more

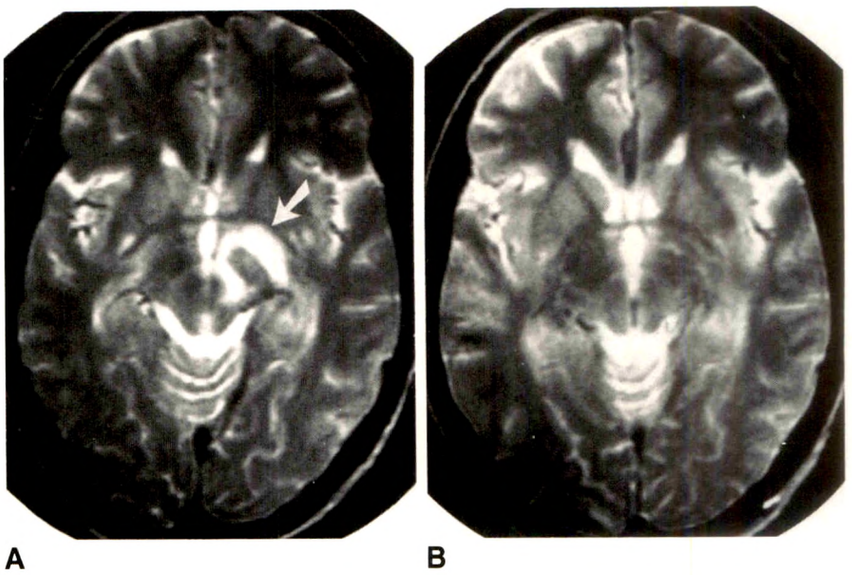


Fig. 5.—T2-weighted MR images (2000/80) showing response of Behcet lesions to corticosteroids.

A, Axial image shows marked involvement of midbrain in region of left cerebral peduncle and thalamus (*arrow*).

B, Corresponding section after 3 weeks of treatment shows almost complete resolution of the lesion.

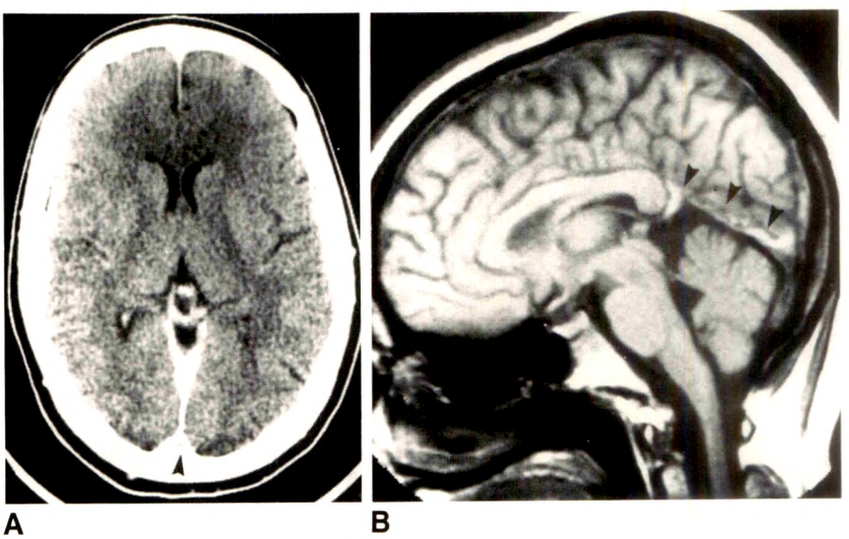


Fig. 6.—CT and MR images showing dural venous sinus thrombosis in Behcet disease.

A, Axial contrast-enhanced CT scan shows filling defect within confluence of dural sinuses (*arrowhead*).

B, Sagittal T1-weighted MR image (600/20) shows high signal intensity of clotted blood within vein of Galen and straight sinus (*arrowheads*).

frequently in the periventricular regions. Behcet lesions, on the other hand, may involve the white and gray matter, and are much more common within the brainstem.

Lacunar infarction from arteriosclerotic disease occurs in an older group of patients with evidence of cerebrovascular disease elsewhere. To date, sizable brain infarction due to occlusion of major cerebral arteries has not been reported in Behcet disease.

Rhomboencephalitis is a rare entity in which there is acute inflammation, which for no known reason is almost always limited to the brainstem. It appears as areas of high signal intensity on T2-weighted images and can be differentiated from Behcet disease by the clinical history and the CSF findings [15, 16].

Dilatation of perivascular spaces is an anatomic variant, which may be seen in the brainstem as punctate high-density foci in the substantia nigra and the cerebral peduncles. These may be unilateral or bilateral and they most likely represent perivascular spaces around penetrating branches of the collicular arteries [17].

ACKNOWLEDGMENTS

We are grateful to Z. Kawi, S. Bohlega, and A. Dalaan for allowing us to include their cases in our study; Gary Pammer and his staff for the photographic work; and Catherine Devane and Catherine Healy for their secretarial assistance.

REFERENCES

1. Serdaroglu P, Yazici H, Ozdemir C, Yurdakul S, Bahar S, Aktin E. Neurologic involvement in Behcet's syndrome. A prospective study. *Arch Neurol*

1989;46:265–269
2. Williams AL, Haughton VM, Saxena VK, Albers JW. Computed tomography in Behcet's disease. *Radiology* **1979**;131:403–404
3. Patel DV, Neuman MJ, Hier DB. Reversibility of CT and MR findings in neuro-Behcet's disease. Case Report. *J Comput Assist Tomogr* **1989**;13:669–673
4. Herskovitz S, Lipton RB, Lantos G. Neuro-Behcet's disease: CT and clinical correlates. *Neurology* **1988**;38:1714–1720
5. Litvan I, Roig C, Rovira A, Ruscalleda J. Behcet's syndrome masquerading as tumor. *Neuroradiology* **1987**;29:103
6. Wildhagen K, Meyer GJ, Stoppe G, Heintz P, Deicher H, Hundeshagen H. PET and MR imaging in a neuro-Behcet syndrome. *Eur J Nucl Med* **1989**;15:764–766
7. Plotkin GR, Calabro JJ, O'Duffy JD. *Behcet's disease: a contemporary synopsis*. New York: Futura, **1988**
8. Inaba G. *Behcet's disease. Pathogenetic mechanism and clinical future.* Tokyo: University of Tokyo Press, **1982**
9. Lewis MA, Priestley BL. Transient neonatal Behcet's disease. *Arch Dis Child* **1986**;61:805–806
10. Rahman A, Mousa M, Marafie AA, Rifai KM, Dajani AI, Mukhtar MM. Behcet's disease in Kuwait, Arabia. A report of 29 cases and a review. *Scand J Rheumatol* **1986**;15:310–332
11. Dalaan AA, Balaa SA, Ramahi KE, Rajapakse CNA. Behcet's disease in Saudi Arabia. *Ann Saudi Med* **1989**;9:353–359
12. Bartlett ST, McCarthy WJ III, Palmer AS, Flinn WR, Bergan JJ, Yao JST. Multiple aneurysms in Behcet's disease. *Arch Surg* **1988**;123:1004–1008
13. Zelenski JD, Capraro JA, Holden D, Calabrese LH. Central nervous system vasculitis in Behcet's syndrome: angiographic improvement after therapy with cytotoxic agents. Brief Report. *Arthritis Rheum* **1989**;32:217–220
14. Motomura S, Tabira T, Kuroiwa Y. A clinical comparative study of multiple sclerosis and neuro-Behcet's syndrome. *J Neurol Neurosurg Psychiatry* **1980**;43:210–213
15. Just M, Kramer G, Higer HP, Thomke F, Pfannenstiel P. MRI of Listeria rhombencephalitis. *Neuroradiology* **1987**;29:401–402
16. Yaqub BA, Al-Deeb SM, Daif AK, et al. Bickerstaff brainstem encephalitis. A grave non-demyelinating disease with benign prognosis. *J Neurol Sci* **1990**;96:29–40
17. Elster AD, Richardson DN. Focal high signal on MR scans of the midbrain caused by enlarged perivascular spaces: MR-pathologic correlation. *AJNR* **1990**;11:1119–1122

Technical Note

Percutaneous Retrieval of an Embolized Arterial Sheath

D. W. Marcuzzi[1] and R. J. Chisholm[2]

Percutaneous retrieval of intravascular foreign bodies is a relatively common procedure. Many techniques have been described [1–3], and new methods for the nonsurgical extraction of a wide variety of fragments of catheters and guidewires, malpositioned embolization coils, and other foreign bodies continually are being developed [4, 5]. We describe a new technique for percutaneous retrieval of an embolized fragment of a femoral arterial sheath set.

Case Report

A 67-year-old woman with coronary artery disease had coronary angiography through a Check-flo sheath set (VCFW 7.0-38, Cook Inc., Bloomington, IN) via the right femoral artery. When the angiographic catheter was inserted over a guidewire, resistance was encountered at the tapered end of the sheath, and the sheath inadvertently was separated from the Check-flo portion and advanced intraarterially. The catheter and guidewire were withdrawn, and an abdominal radiograph showed the inferior flared end of the sheath caught in the right common iliac artery and the tapered superior end positioned in the abdominal aorta, at the level of the L1 vertebral body. A second 7-French arterial sheath was inserted, and the coronary angiogram was completed uneventfully.

The patient was transferred to the radiology department. A 9-French sheath set was introduced into the left femoral artery. Tight coning of the fluoroscopic image was necessary, because the embolized sheath was barely visible. In order to prevent its distal migration, the embolized sheath was stabilized near its flared end with grasping forceps inserted from the right side of the groin. No attempt was made to change the position of the embolized sheath; it was grapsed lightly but securely to avoid arterial damage and compression of its lumen. A 0.038-in. (0.1 cm) guidewire (Glidewire, Terumo, Piscataway, NJ) was passed also from the right side of the groin through the lumen of the embolized sheath and into the upper portion of the abdominal aorta. This took roughly 10 min of manipulation. The end of the guidewire then was snared with a basket inserted through the left femoral artery and gently pulled back out through the sheath in the left femoral artery. The grasp on the embolized sheath was released, and as the guidewire was pulled out of the left side of the groin, the embolized sheath gently migrated distally in the right iliac artery until the tapered end was positioned at the aortic bifurcation. The guidewire thus entered the right femoral artery, passed through the lumen of the embolized sheath, and crossed the aortic bifurcation to exit from the left side. The embolized sheath was removed by pushing it out through the left femoral sheath with a multipurpose catheter approaching from the right. The embolized sheath was flexible enough to pass around the bifurcation over the guidewire with little difficulty. Hemostasis was achieved easily after the bilateral sheath sets were removed.

Discussion

The shape and position of the embolized sheath in this case presented a unique problem. The outside diameter of the shaft was 8-French, but the diameter of the flared end was 14-French. In addition, the edge of the flare was quite sharp and tended to catch on the vessel wall if it was the leading edge during extraction. An attempt at simple basket removal through the right femoral sheath or through the vessel wall directly would have been difficult or impossible and might have seriously damaged the artery, necessitating surgical repair. Extraction with the tapered end leading was ideal. The flared end was advantageous, however, because it facilitated placement of the guidewire through its lumen. If

Received March 7, 1991; accepted after revision April 23, 1991.
[1] Department of Diagnostic Imaging, St. Michael's Hospital, 30 Bond St., Toronto, Ontario M5B 1W8, Canada. Address reprint requests to D. W. Marcuzzi.
[2] Division of Cardiology, St. Michael's Hospital, 30 Bond St., Toronto, Ontario M5B 1W8, Canada.

AJR **157:873–874, October 1991** 0361–803X/91/1574–0873 © American Roentgen Ray Society

we had been unsuccessful with the guidewire and grasping forceps alone, we would have used a curved-tip catheter to direct the guidewire.

The embolized sheath was stabilized with the grasping forceps carefully, because the teeth of the forceps can easily damage intimal surfaces. Fluoroscopic control is necessary to ensure that the orientation of forceps with respect to the fragment is satisfactory. Apposition of the jaws should be halted once slight resistance by the fragment is felt. Further compression will compress the lumen of the fragment and may result in injury to the arterial wall. Although we introduced the grasping forceps through the right side of the groin in our case, a contralateral approach most likely would have been as effective.

Placement of the guidewire through the lumen of the embolized sheath was the key to its successful extraction, and technically the most difficult. Grasping the guidewire from the contralateral side and pushing the embolized sheath across was simple. If, during the cardiac catheterization, the initial introducing guidewire had been left in place through the embolized sheath, completion of the coronary angiogram could have been performed just as easily, and subsequent extraction of the embolized sheath would have been simplified. This principle can be applied in other cases of embolized foreign bodies.

REFERENCES

1. Dotter CT, Keller FS, Rosch J. Transluminal catheter removal of foreign bodies from the cardiovascular system. In: Abrams HL, ed. *Abrams angiography*, vol. 3, 3rd ed. Boston: Little, Brown, **1983**:2395–2399
2. Gerlock AJ, Mirfakhraee M. Retrieval of intravascular foreign bodies. *J Thorac Imaging* **1987**;2:52–60
3. Kadir S, Athanasoulis C. Percutaneous retrieval of intravascular foreign bodies. In: Athanasoulis C, Green R, Pfister R, Robertson G, eds. *Interventional radiology*. Philadelphia: Saunders, **1982**:379–390
4. Grabeuwoeger F, Dock W, Piuterits F, Appel W. Fixed intravascular foreign bodies: a new method for removal. *Radiology* **1988**;167:555–556
5. Gurley JC, Booth DC, Hixon C, Smith MD. Removal of retained intracoronary percutaneous transluminal coronary angioplasty equipment by a percutaneous twin guidewire method. *Cathet Cardiovasc Diagn* **1990**; 19:251–256

Meeting News

Society of Thoracic Radiology Ninth Annual Meeting and Postgraduate Course, May 1991

Elizabeth Whalen[1]

The ninth annual meeting and postgraduate course of the Society of Thoracic Radiology was held May 13–17, 1991, at the Four Seasons Hotel—Yorkville, Toronto, Ontario, Canada. The meeting consisted of five sections: a postgraduate course, scientific sessions, a research symposium, workshops, unknown cases of the day, and the annual Benjamin Felson Lecture. The postgraduate course included seven plenary sessions that provided detailed reviews of state-of-the-art techniques in cardiopulmonary radiology (MR Imaging and CT of the Thorax, Cardiovascular Imaging, Chest Roentgenology—The Art, Chest Neoplasms, Immune Deficiency Infections, Pediatric Thoracic Radiology, and Diffuse Lung Disease) and two scientific sessions featured 33 presentations of original scientific investigations in thoracic imaging and intervention. Two annual highlights of the meeting were the Scanlon Memorial Research Symposium (a 2-hr discussion of digital radiography of the thorax) and the Benjamin Felson Annual Lecture, this year featuring Robert J. Ginsberg (Memorial Sloan-Kettering Institute, New York) speaking about the limitations of surgical resection for lung carcinoma. Speakers from seven different countries participated, and their levels of experience ranged from residents to experienced expert radiologists.

Because of *AJR* space limitations, we cannot include coverage of all the activities provided at this 5-day meeting. However, we have summarized the following: 10 of the presentations of original scientific research, six of the up-to-date reviews given in the postgraduate plenary sessions, and the Felson Lecture.

Presentations of Original Scientific Research

Most of the 33 short scientific presentations concerned thoracic CT or chest radiography. Our page limitations do not allow summaries of the others, which were on thoracic sonography, biopsy techniques, and urokinase treatment of empyema.

Conventional CT of the Thorax

J. R. Standen, R. J. Knudsen, K. Rehm, W. T. Kaltenborn, and D. E. Knudson (University of Arizona, Tucson) prospectively studied the assessment of emphysema with CT in 64 patients. Emphysema is abnormal, permanent enlargement of air spaces distal to the terminal bronchioles, with destruction of the walls of the bronchioles but without fibrosis. Both smokers and nonsmokers were among the 64 subjects, pulmonary function test results were correlated with CT findings, and some patients were followed up for as long as 20 years. CT scans were obtained of 8-mm sections during both inspiration and expiration; CT measurements were used to arrive at a "pixel-index": the percentage of all pixels with a CT density between −900 and −1024 H. Several of the patients with normal lungs had a high inspiratory pixel index; the

[1] Contributing editor, *American Journal of Roentgenology*, Ste. 103, 2223 Avenida de la Playa, La Jolla, CA 92037.

Editor's note.—"Meeting News" articles report the highlights of important national radiology meetings. The intent is to provide Journal readers with succinct, substantive, and accurate reviews of topics of current interest, written in a readable fashion and published promptly after the meeting.

The articles will not undergo the peer review usually required of *AJR* publications, nor will they offer a critique of the information provided. The sole purpose of the series is to apprise *AJR* readers of topics of current concern in an interesting and timely fashion.

AJR **157:875–881, October 1991** 0361–803X/91/1574–0875 © American Roentgen Ray Society

researchers labeled these cases as "disappearing emphysema" when the inspiratory densities were −900 to −1024 H but the expiratory densities were normal. All of the patients with disappearing emphysema were asymptomatic and had normal diffusing capacity and spirometry, leading the researchers to think that this phenomenon might be related to an early stage of emphysema or a higher risk of emphysema; future studies will focus on careful follow-up of these patients and on determination of the limits of normal lung density and the effects of aging and asthma. If disappearing emphysema does prove to be an early form of the disease, these CT measurements will be an objective way to measure it, will enable quantification of the disease early in its cycle, may add to information about the natural history of emphysema, and may help indicate interventions (e.g., smoking cessation) that could prevent or delay the development of the disease.

The CT assessment of broncholithiasis was the subject of a study by D. J. Conces, R. D. Tarver, and V. A. Vix (Indiana University). An uncommon disease, broncholithiasis often presents a diagnostic challenge; it is characterized by peribronchial or endobronchial calcified lymph nodes. CT findings were reviewed in 15 patients with broncholithiasis (all patients lived in a region of endemic histoplasmosis). Ten of these patients had endobronchial lymph nodes, and five had peribronchial lymph nodes. Cough was the most common sign (13 patients). Other signs and symptoms included hemoptysis (six), chest pain (three), and sputum-producing cough (three). Chest radiographs showed calcified lymph nodes in 11 patients, atelectasis in nine, infiltrates in two, and peripheral calcified granulomatosis in four. Of the 14 bronchoscopies performed, only five showed broncholiths, seven showed bronchial distortion, and three showed bronchial blood; the bronchus was obscured in two cases. CT scans showed calcified lymph nodes in all 15 patients. Changes due to bronchial obstruction were seen on the CT scans (atelectasis in 10, bronchiectasis in four, infiltrates in four, and air trapping in one). No soft-tissue masses were seen in any of the patients. In the 10 patients with endobronchial calcified lymph nodes, CT results indicated the location of six correctly, and in the five patients with peribronchial calcified lymph nodes, CT located four correctly (the errors in location were due to the effects of volume averaging). These researchers conclude that bronchoscopy is definitely necessary for the diagnosis of broncholithiasis and that the combination of bronchoscopic and CT results should be sufficient to suggest the diagnosis of broncholithiasis.

High-Resolution CT

Pulmonary fibrosis in dyspneic smokers as evaluated by high-resolution CT (HRCT) was the focus of a study presented by Jeffrey R. Galvin for J. R. Galvin, P. J. Chang, D. S. Schwartz, M. Mori, R. A. Helmers, W. Stanford, and G. W. Hunninghake, of the University of Iowa, Iowa City. In 10 smokers with pulmonary fibrosis who were referred for evaluation of new or worsening dyspnea, chest radiography, pulmonary function tests, and HRCT were performed. Spirometry and lung volumes were often normal despite severe dyspnea; chest radiographs provided a reasonable assessment of fibrosis but underestimated the severity of emphysema (and agreement of interpretation of radiographic severity of emphysema was poor: kappa scores ranged from .14 to .38). Although HRCT resulted in reliable quantification of emphysema that showed a good correlation with pulmonary function measurements of airway obstruction, HRCT results did not quantify fibrosis as effectively. These researchers therefore tried to assess fibrosis severity by using an automated measurement of fractal dimension; this calculation process is simple to use and automate, results in a single quantitative measure, and has the features and advantages of statistical, structural, and spectral methods. The fractal dimension of a normal lung proved to be 1.3, whereas the fractal dimension of a fibrotic lung was 1.7; also, the fractal dimension directly correlated with lung volume, and, as the fractal dimension increased, flow rates increased. Considering the results of this preliminary study, the researchers concluded that smokers with both dyspnea and radiographic evidence of fibrosis may have pulmonary function results that do not reflect the severity of damage. However, HRCT reliably measures emphysema severity and, by use of fractal dimensions, can provide a useful representation of fibrosis.

Jung-Gi Im discussed HRCT findings of fresh and healing lesions in pulmonary tuberculosis that were collected by J.-G. Im, J. H. Lee, Y. S. Shim, J. M. Ahn, and M. C. Han, of Seoul National University, Seoul, Korea. The objective of the study was to use HRCT (15-mm collimation, 20-cm field of view) to describe pretreated lesions and then sequential changes with chemotherapy in 31 patients with newly diagnosed tuberculosis. The HRCT findings in patients before treatment were small (2–4 mm), centrilobular branching in 26 patients; larger (5–6 mm) fuzzy nodules in 21; lobular consolidations in 20; cavities in 18; thickened interlobular septa in 14; and large branching lesions in five. Posttreatment follow-up was obtained in 21 of these patients; HRCT showed that (1) the small centrilobular lesions disappeared and left lobular emphysema with a central dot and minimal distortion of the bronchovascular bundle, (2) lobular consolidations resolved from the periphery with more bronchovascular distortion and emphysema, (3) thickening of interlobular septa disappeared without residue, and (4) treatment caused some effects in cavities, including thinning of walls with minimum distortion and fibrotic bands with marked distortion. In these patients, HRCT showed disease at the lobular level and provided helpful information about ongoing healing activity.

A patient who has conventional HRCT is exposed to 120–140 mGy. To investigate whether a lower dose impairs image quality, C. V. Zwirewich, J. R. Mayo, and N. L. Müller, of Vancouver, Canada, compared 1.5-mm-collimation, 2-sec images obtained in high-dose HRCT studies (200 mA [400 mAs]) with those obtained in low-dose HRCT studies (20 mA [40 mAs]). Without knowledge of HRCT technique, three observers evaluated the scans of 31 patients for demonstration of pulmonary anatomy (vessels, bronchi, secondary nodules), pathology (interstitial disease, air-space disease, and bronchiectasis), and the presence of linear stratification artifacts. The McNemar statistical test for significance was used to assess whether the quality of high-dose HRCT images was significantly better than that of the low-dose HRCT images.

In a large percentage of patients, the two techniques resulted in the same quality of visualization of vessels, segmental and lobar bronchi, secondary pulmonary nodules, reticulation, honeycomb cysts, and thickened interlobular septa. In three cases, high-dose images revealed ground-glass opacities or emphysema not seen on low-dose images, but the evidence for these was subtle even at 400 mAs. Although artifacts were more prominent on images acquired with the low-dose technique, the two techniques yielded images with equal visual quality in 97% of cases. Overall, low-dose HRCT seems to have potential usefulness, especially in young patients and for follow-up studies. However, high-dose HRCT remains preferable for initial examinations because of the few cases in which mild emphysema and ground-glass opacity were seen only with the high-dose technique and because artifacts were more prominent on low-dose HRCT.

Ultrafast CT

J. J. Geraghty, W. Stanford, J. R. Galvin, and K. S. Landas, of the University of Iowa Hospitals and Clinics, Iowa City, performed a canine study to determine the usefulness of ultrafast CT in the diagnosis of peripheral pulmonary embolisms. In seven deeply anesthetized mongrel dogs, three 7-by 15-mm gelatin-sponge emboli were introduced into the right femoral vein; after administration of 60 ml of contrast media, 3-mm axial ultrafast CT scans were obtained. All dogs were sacrificed after scanning, and the locations of the emboli were recorded by a pathologist: 19 emboli were in the third and fourth division pulmonary arteries, and two emboli were in more proximal pulmonary arteries. In the reviews of the ultrafast CT scans by three chest radiologists, all 21 emboli were identified unequivocally; moreover, the locations determined by the radiologists correlated exactly with pathologic findings. The researchers concluded that ultrafast CT can demonstrate reliably the presence and location of gelatin-sponge emboli; their plans for further research in this area include studies of in vivo blood clots, different sizes of emboli, and the possible role of three-dimensional imaging.

J. Bormann, W. Stanford, R. Stenberg, M. Winniford, J. R. Galvin, K. S. Bernbaum, and C. Talman, of the University of Iowa Hospitals and Clinics, Iowa City, investigated using ultrafast CT to evaluate coronary artery calcification and correlated those findings with coronary artery stenosis as shown by quantitative angiography. Areas with >70% stenosis were considered to have significant stenosis. In each of 50 patients, 20 axial, contiguous, 3-mm, unenhanced, ultrafast CT scans of the proximal 2 cm of each coronary artery were obtained and interpreted by three radiologists. The area of calcification was determined by software inherent to the system and the density grade was based on Hounsfield units. A calcium score was calculated as follows: calcium score = area of calcification × density grade. For 37 sites (17 with stenosis), calcium scores failed to predict a significant stenosis at the calcification site (for patients older than 60 years, however, the correlation between calcium score and presence of lesion approached significance). Calcium was found in 92 vessels, 33 of which had stenosis, but the calcium-score sums in any individual vessel were not predictive of stenosis in that vessel. However, for the sums of the scores within the left main coronary artery, a significant ($p < .014$) difference was found between calcium scores of vessels with stenosis and calcium scores of vessels without stenosis. Because of the great variation in calcium scores, the sums of all calcium scores for a patient did not correlate with significant stenosis in that patient (40 patients with calcium, 23 with stenosis). These researchers concluded that calcium scores obtained from ultrafast CT were not helpful in predicting stenosis, except in the left main coronary artery.

Chest Radiography

To evaluate clinically the use of computed radiography in imaging lung cancer, E. Itouji, K. Yamasaki, E. Sakai, M. Kusumoto, S. Adachi, and M. Kono, of Kobe University, Kobe, Japan, compared conventional radiographs with plain computed radiographs, image-processed (tomographic) computed radiographs, and energy-subtraction computed radiographs in five patients with lung cancer (three with peripheral lung cancer and two with hilar lung cancer). Twenty-three radiologists from 15 university hospitals rated the computed radiographs on the following scale: 1 = inferior to conventional radiography, 2 = slightly inferior to conventional radiography, 3 = equal to conventional radiography, 4 = slightly superior to conventional radiography, and 5 = superior to conventional radiography. The following results were found for the evaluation of lung anatomy: scores for energy-subtraction computed radiography were better than those for conventional radiography in the bronchus and paratracheal strips and equal for other anatomic structures studied; scores for computed radiography tomography were better than those for conventional tomography; and scores of high-pass processed computer radiography were better than those for conventional radiography. In peripheral lung cancer, images obtained with energy-subtraction technique had the best scores; in hilar lung cancer, images obtained with computed radiographic tomography were judged as showing anatomy and pathology better than images generated by the other three techniques.

M. L. Rosado-de-Christenson (Armed Forces Institute of Pathology, Washington, DC) presented a 40-year retrospective study done by M. L. Rosado-de-Christenson, R. D. Pugatch, M. Koss, and J. Galobardes, of patients with thymolipoma, which is a rare thymic neoplasm of unknown etiology. From 1950 to 1990, 25 pathologically proved cases of thymolipoma were referred for radiologic studies; radiographs were obtained in all 25, CT scans were obtained in nine, and MR images were obtained in two. In only one of these 25 cases was thymolipoma considered in the prospective differential diagnosis. Radiographic locations of the thymolipomas were the anterior inferior mediastinum in 20 and the anterior superior mediastinum in five; 14 were unilateral and 11 were bilateral. In 10 patients, the thymolipoma conformed to the cardiac silhouette and looked like cardiomegaly; in eight patients, the neoplasm extended along the diaphragm, mimicking diaphragmatic elevation on lateral views. Other radiographic findings included hyperlucency in 12 cases, large sizes (occupying more than one-third of a hemithorax) in 10 cases, lack of diaphragmatic silhouetting in five cases; and

mobility or positional change in shape in six cases. Fat density was seen in the mass in eight of the nine CT studies (in six, the pattern was an even mixture of fat and soft-tissue density; in two, the pattern was predominantly fat density). The contiguity of the thymolipoma with the thymus was also seen on CT. Contiguity with the thymus and the mixture of fat and soft tissue characterized these neoplasms on the two MR studies also; coronal MR images of the diaphragm were useful. Dr. Rosado-de-Christenson suggested that thymolipoma should be part of the differential diagnosis when patients who are asymptomatic or minimally symptomatic have a paracardiac mass that simulates cardiomegaly or drapes along the hemidiaphragm with lack of diaphragmatic silhouetting; the diagnosis is supported by MR or CT evidence of fat in the mass. Although surgery cannot be avoided, a specific diagnosis with important anatomic information can be suggested preoperatively.

A study comparing the subjective judgments of expert radiologists with analysis by Bayesian theory was done by J. W. Gurney, J. A. McKay, and D. Lyddon of the University of Nebraska Medical Center, Omaha. Radiographs from 66 patients with lung lesions (44 malignant and 22 benign) were evaluated by the radiologists and by using Bayesian analysis to determine the likelihood of malignancy. To obtain the Bayesian likelihood ratios, the researchers reviewed the literature and derived 15 characteristics associated with malignancy (four of the top five malignant signs were radiographic) and 21 characteristics associated with benignity (five of the top six were radiographic signs). In this group of patients, the patients with malignant tumors tended to be older and to have smoked more than those with benign tumors; furthermore, the size of the malignant tumors was not significantly different from the size of the benign tumors. The experts rated the likelihood of malignancy on a scale of 0 to 100, and receiver-operating-characteristic (ROC) analysis was used to assess the ability of each observer to differentiate benign from malignant masses. For both expert and Bayesian likelihood scores, success in recognizing malignant lesions was not affected by knowledge of clinical history. Without the aid of clinical history, the area under the ROC curve for radiologists was 66–67 and for Bayesian analysis it was 80–81; when information on the patients' clinical histories was provided, the areas under the ROC curves were 68–71 for radiologists and 81 for Bayesian analysis. Use of Bayes' theorem and likelihood ratios was significantly better than expert subjective opinion in judging the malignancy of a lung lesion. Dr. McKay and her colleagues conclude that the use of Bayesian analysis can improve the accuracy of a radiologist's subjective recognition of the benign or malignant nature of lung tumors.

Plenary Session on MR Imaging and CT of the Thorax

MR Imaging

John Mayo (University of British Columbia, Vancouver, B.C., Canada) presented a discussion of practical physics and pulse sequences in thoracic MR. MR imaging can be complementary to CT and can help with problematic diagnoses; MR imaging is a noninvasive method in which no ionizing radiation is used, and it provides increased soft-tissue contrast and multiplanar capacity. Modification of standard pulse sequences are needed to overcome two limitations of thoracic MR imaging: slow acquisition compared with physiologic motion and low signal-to-noise ratio of lung parenchyma. Dr. Mayo briefly described the pulse-sequence parameters (TR/TE), imaging plane, and sequence modifiers (cardiac gating, respiratory compensation, flow compensation, and presaturation) to overcome artifacts. He discussed the application of each of these parameters to imaging the chest wall, mediastinum, vascular structures, and lung parenchyma. For chest wall and mediastinum imaging, suggested parameters include T1-weighted imaging (TR = 1 R-R interval, TE = 20 msec, and two to four excitations) and proton-density/T2-weighted imaging (TR = 2–3 R-R intervals, TE = 20/80 msec, and two excitations); respiratory compensation and presaturation should always be used, but flow compensation should be used with caution because it decreases vascular contrast. T1-weighted images (TR = 1 R-R, TE = 20 msec, two to four excitations, and respiratory compensation) without flow compensation should be used for vascular MR imaging to provide maximum flow contrast (with dark blood). Ultrafast spin-echo or gradient-echo sequences are effective for further evaluation of intravascular masses. Finally, MR imaging of the lung parenchyma is still at the research stage. A major problem is that the air/soft-tissue interfaces in inflated lung induce magnetic field inhomogeneity that causes rapid signal loss and results in the failure of conventional MR sequences to show lung parenchyma. Researchers have suggested using very short echo delays, with either gradient-echo or spin-echo sequences to limit the amount of signal loss, or using Carr-Purcell-Mibloom-Gill (CPMG) sequences, which partially compensate for the loss of phase coherence. However, even with conventional MR imaging, abnormal lung with thickened lobular septa and pleural effusions can be seen. In addition, infiltrated lung parenchyma (e.g., alveolitis) can be seen.

MR imaging of the lung parenchyma was discussed further by Colleen J. Bergin (Stanford University, Stanford, CA). Dr. Bergin noted the following five obstacles that must be overcome or minimized for successful imaging: low proton density of the lung, a relatively short T2, susceptibility effects, motion artifacts, and diffusion/perfusion effects. Possible solutions to these challenges include the following: for a short T2 relaxation time, susceptibility effects, and signal loss from diffusion/perfusion, the echo time must be short relative to T2 (TE <15 msec); for superimposed motion artifacts, using multiple excitations, fat saturation, and respiratory compensation is helpful. Dr. Bergin emphasized that in MR imaging of the lung, respiratory compensation is essential, as it decreases respiratory motion artifacts without increasing the imaging time or decreasing the coverage. She also described an ultrashort TE projection reconstruction MR technique developed at Stanford that may help to overcome some of the limitations in imaging lung parenchyma. This sequence uses an echo time shorter than 1 msec.

High-Resolution CT

Use of high-resolution CT (HRCT) in the differential diagnosis of chronic diffuse infiltrative lung disease was the topic of a presentation by Nestor L. Müller (University of British Columbia, Vancouver, Canada). His HRCT technique consists of thin-section CT, 1- to 2-mm collimation, with a high-frequency resolution reconstruction algorithm, at 1-cm intervals through the chest. HRCT shows parenchymal detail and characterizes abnormalities much better than does conventional CT; also, HRCT can clarify radiographic diagnoses and characterize abnormalities seen on radiographs, thereby allowing correct prospective diagnoses. Although HRCT cannot replace the chest radiograph as the diagnostic method of choice, it accurately reflects the macroscopic morphologic features of lung disease and provides useful supplementary information. Dr. Müller reviewed the HRCT findings for the six abnormalities characteristic of diffuse infiltrative lung disease: thickened interlobular septa, intralobular linear opacities, cystic air spaces, small nodules, ground-glass opacities, and air-space consolidation. (1) If thickened interlobular septa are smooth on HRCT, they suggest edema; if nodular, they suggest tumor or sarcoidosis; and, if irregular, they suggest fibrosis. (2) The characteristic distribution of intralobular, linear opacities is in the subpleural lung regions and lower lung zones in idiopathic pulmonary fibrosis and fibrosing alveolitis associated with collagen vascular disease and is central, along the bronchovascular bundles (leading to a central clustering of bronchi and vessels), in sarcoidosis. Asbestosis can be recognized by the combination of subpleural lines, parenchymal bands, thickened interlobular septa and intralobular core structures in association with pleural plaques. (3) Cystic air spaces are most common in lymphangioleiomyomatosis (air spaces surrounded by relatively normal lung parenchyma, cyst diameter = 2 mm to 5 mm, cyst wall thickness = barely perceptible to 2 mm, and involves lungs diffusely); pulmonary histiocytosis X (has nodular component, involves upper two-thirds of lungs, and spares the costophrenic angles); and idiopathic pulmonary fibrosis (honeycombing surrounded by areas of fibrosis in the subpleural regions and lung bases). (4) Sarcoidosis, silicosis, and coal-worker's pneumoconiosis are characterized by pulmonary nodules (diameter: 1–10 mm). In sarcoidosis, noncaseating granulomas are present along the lymphatics, mainly along the bronchovascular bundles; in silicosis, the nodules are usually more numerous in the posterior aspect of the upper lung zones. (5) A ground-glass pattern (bilateral patchy areas of hazy, increased density) is characteristic of subacute extrinsic allergic alveolitis (50% of these patients have poorly defined 1- to 5-mm nodules), pulmonary alveolar proteinosis (HRCT shows thickening of the interlobular septa), and active alveolitis in idiopathic pulmonary fibrosis. (6) Air-space consolidation differs from the ground-glass pattern because vascular markings cannot be identified and air bronchograms may be present. Predominantly subpleural air-space consolidation suggests chronic eosinophilic pneumonia (peripheral distribution can be seen on HRCT even when not seen on radiographs), and in bronchiolitis obliterans organizing pneumonia, the pattern can be identical to that of chronic eosinophilic pneumonia or consist of patchy unilateral or bilateral areas of air-space consolidation and small nodular opacities. Air-space consolidation may also be seen in bronchioalveolar carcinoma and lymphoma (these should be considered when the consolidation progresses over several months). Results of HRCT—when considered with clinical history, physical findings, and results of both pulmonary function tests and chest radiographs—may be very helpful in making the differential diagnosis in chronic diffuse infiltrative lung disease.

Philip A. Templeton (University of Maryland Medical Systems, Baltimore) investigated whether HRCT can further improve diagnostic information and confidence in cases of focal lung disease. The technique used at his institution includes standard CT scanning followed by selected HRCT scans (using 1- to 2-mm collimation, contiguous scans, a single breath-hold technique, and either a high spatial frequency reconstruction algorithm or a modification of the algorithm) through the abnormality. For example, if chronic cough is the patient's problem, thin-section CT has a sensitivity of 96% and a specificity of 93% for diagnosing bronchiectasis; HRCT is especially effective in recognizing cylindrical or varicose bronchiectasis, whereas conventional CT finds the cystic form effectively. In persistent atelectasis or recurrent infection, HRCT can clarify the cause (e.g., aspirated popcorn). Because only 70% of the segmental bronchi are seen routinely on conventional CT scans, it is useful to supplement those scans with contrast-enhanced 2- to 5-mm collimation scans through the hila (moreover, the thin-section scans avoid the problems of partial volume averaging). HRCT can also help characterize carcinoids, usually located at the lobar bronchial bifurcation; on the high-resolution images, the diagnostic features of these tumors can be seen (e.g., smooth borders, bronchial splaying, marked enhancement with IV contrast, and, in about 50% of cases, calcification). When small solitary pulmonary nodules (<2 cm) are seen on CT scans (nodules >3 cm are usually malignant), they can be classified by using HRCT densitometry, with 164 H as the cutoff point between malignant and benign tumors; no contrast material is used in this procedure because iodinated contrast media and/or partial volume averaging can artificially elevate the Hounsfield units. Other important applications of HRCT in focal lung disease include early detection of infection (e.g., pulmonary aspergillosis) in immunocompromised hosts by recognition of the CT halo sign (a halo of low attenuation surrounding one or more areas of mass consolidation); anatomic localization of pulmonary lesions via clear delimitation of fissures; and improved biopsy planning by HRCT indication of the safest approach and how vessel perforation can be avoided.

Plenary Session on Chest Neoplasms

Lung Cancer Imaging

Robert D. Pugatch (Armed Forces Institute of Pathology, Washington, DC) focused his talk on the "who, when, and why" of lung cancer imaging. Radiologic protocols for lung cancer vary depending on the prevailing surgical attitudes,

previous experience with CT, the ongoing results with CT, and local patterns of referral. A literature review of studies of CT of lung carcinoma shows sensitivities ranging from 29% to 95%, specificities from 46% to 100%, criteria for nodal enlargement from 5 mm to 2 cm, and various recommendations about when CT should be performed; in addition, many studies do not make clear if or how CT results were correlated with pathologic and/or surgical findings. If an ideal study could be performed, it would include a histologic diagnosis, complete clinical and laboratory results, a review of findings on chest radiographs, and a determination of how CT influenced decision-making. Which patients with lung cancer should be imaged? Dr. Pugatch gave this list: include all patients with non–small-cell, operable lung cancer; exclude patients with obvious N3 or T4 cancer; and include patients with lung cancer staged as T1 N0 M0. How should radiologists image patients with lung cancer? For imaging lung cancer, conventional radiography is specific but not sensitive; conventional tomography has been tried but, for the most part, has been abandoned as not useful; gallium scanning is not used; and invasive vascular imaging is rarely used. Therefore, routine CT should be considered in these patients, and Dr. Pugatch suggested that chest CT scans should always be hanging in the operating room during surgery on these patients; also, MR imaging is a good problem-solving tool and sometimes nicely complements CT. Why should CT be performed in these patients? To this date, surgery is the only means to cure lung cancer, and an updated CT staging system helps in distinguishing between local invasion (N2 disease) and nonresectable tumors. Furthermore, institutions aggressively treating patients with lung cancers in which the mediastinum is involved are finding that such treatment along with adjuvant chemotherapy is increasing 5-year survival in these patients from less than 10% to a rate approaching 40%. By interpretation of CT scans, radiologists can inform surgeons of the status of the mediastinum and indicate that mediastinal involvement is no longer an automatic indication of nonresectability. CT results can be used to guide transthoracic needle biopsies and Wang needle biopsies, to help plan mediastinoscopy or limited thoracotomy, to indicate which patients are surgical candidates, to evaluate tumor response to therapy, and to aid in planning radiation therapy. False-positive CT findings remain a problem; these can be caused by errors of interpretation (mistakes, confusion of normal vascular structures and lymph nodes, and anatomic variants) or by lymph node hyperplasia (postobstructive pneumonia, lobar collapse, and previous granulomatous disease). Therefore, the positive predictive value of CT of the mediastinum is only about 75%, but its negative predictive value is 90%. In summarizing the use of CT to evaluate the mediastinum in patients with lung cancer, Dr. Pugatch suggested that most positive results on CT require histologic confirmation, but, in most patients with normal CT findings, no further preoperative staging is necessary.

Radiation-Induced Changes

Changes in the thorax caused by radiation therapy were discussed by Herman I. Libshitz (M.D. Anderson Hospital, Houston, TX). He noted that radiation-induced changes do not observe anatomic boundaries but generally affect irradiated areas only. The measurable factors that influence the radiographic appearance of radiation-induced changes include lung volume; field shape; dose (number of fractions and time, as well as number of rad given); date of end of radiation therapy; and other therapies used. In his discussion, the radiation dose was assumed to be 200 rad/day on 5 days/week. The likelihood of radiation pneumonitis developing in a patient is related to total dose as follows: less than 3000 rad, not likely; 3000–3500 rad, possible; and 3500–3999 rad, probable; at doses of 4000 rad or more, radiation pneumonitis almost always occurs. The time of appearance of radiation pneumonitis is about 8 weeks (sometimes as little as 6 weeks) after completion of therapy with 3000–3500 rad. The high point of radiation fibrosis is generally 3–4 months after completion of treatment; the fibrosis begins to retract after that and becomes stable at 9–12 months after the completion of therapy. Despite lack of clinical correlation to date, Dr. Libshitz believes very strongly that radiation pneumonitis always leads to radiation fibrosis. Four patterns of CT appearance of radiation-induced lung change have been noted: homogeneous consolidation (thought to represent an early minimal but general radiation pneumonitis); patchy consolidation (the CT analog of radiation pneumonitis seen on chest radiographs); discrete consolidation (either nearly uniform pneumonitis or pneumonitis evolving into radiation fibrosis or incompletely retracted pneumonitis); and solid consolidation (the CT counterpart to radiation fibrosis seen on conventional studies). In the differential diagnosis of radiation pneumonitis, timing and location play significant roles (e.g., changes seen outside the irradiated area or earlier than 6 weeks after completion of therapy are probably not radiation induced). Cardiac injuries caused by radiation therapy include acute or chronic pericarditis, pancarditis, myocardial fibrosis, conduction and valvular abnormalities, and coronary artery disease. For radiation-induced pericarditis—the injury most frequently identified as clinically significant—general assumptions about the timing of the changes should be revised and long-term studies are needed; at this point, the best estimates are as follows: at 4–12 months after completion of therapy, 60% of the changes are apparent; at 12–24 months, another 20% are evident; and the last 20% are seen more than 2 years after completion of therapy. The most dangerous cardiac injury due to radiation therapy is pancarditis, which can lead to chronic heart failure. The timing for radiation-induced changes in the bony thorax is very different from that of cardiac and lung changes; the minimum time for appearance of bony changes is 2–3 years after therapy. Two examples showed how long these changes take to develop: radiation-induced rib fractures occurred in a patient 5 years after a mastectomy and radiotherapy and had still not healed 30 years later (painless radiation-induced rib fractures are generally not dangerous and may be accompanied by callous formations that should not be confused with osteosarcoma) and a much more destructive radiation-induced sarcoma that usually occurs 10–15 years after therapy and is seen in up to 0.5% of patients (in one case, the sarcoma developed 50 years after radiation therapy). Radiation-induced sarcomas have occurred in patients who have

received as low a dose as 3000 rad in therapy; the radiologist should suspect development of a sarcoma when rapid change is seen in an area of radiation osteitis. In general, the chest radiograph and the history (timing and dose) of radiation therapy for each patient are the keys that allow radiologists to accurately diagnose radiation-induced thoracic changes.

The Benjamin Felson Lecture: Lung Cancer—The Limits of Resection

In the annual Felson Lecture, Robert J. Ginsberg (Memorial Sloan-Kettering, New York) discussed the role of surgery in the advanced stages of lung carcinoma (T3–T4, N2–N3, M1). Dr. Ginsberg emphasized that incomplete resection invariably fails to cure lung cancer and that palliative resection is rarely palliative—the operative morbidity for stage III lung cancer is nearly double that for stage I lung cancer. Also addressed in the lecture was the usefulness of radiation therapy and chemotherapy as adjuvants to surgery in more advanced disease. Success of surgery in patient survival depends on the node and tumor status. Adjuvant radiotherapy and chemotherapy have not improved survival. In Pancoast tumor, preoperative radiotherapy is the rule despite no evidence that this improves survival rates. Postoperatively, adjuvant brachytherapy (^{125}Io seeds and ^{192}Ir afterload) may be used. Four large studies show that sleeve pneumonectomy (in which the whole carina is removed to obtain safe margins) has achieved a 15–23% 5-year survival rate with an operative mortality of 11–29%. For N2 operative disease, defined as involvement by ipsilateral nodes and/or subcarinal nodes, six 1985 studies (in which the number of cases ranged from 79 to 218) showed 5-year survival rates of 23–39% (the one exception to this range was a 1.4% 5-year survival for patients with adenocarcinoma who had had incomplete resection). Adverse factors affecting survival in these patients included incomplete resection, age over 60 years, multiple N2 disease levels, pneumonectomy, and adenopathy.

Dr. Ginsberg reviewed recent combined data from two institutions at which he has done research: 112 patients were treated with neoadjuvant chemotherapy (criteria for inclusion: non–small-cell carcinoma, N2 inoperable disease, histologic confirmation, no N3 or M1 disease, patient medically fit for surgery). Some response was seen in 71%; complete response was seen in 8% (10 patients were judged by pathologic criteria to have no tumor left after resection—eight cases of complete response were seen on preoperative radiologic studies). In 80 patients who had resections (23 pneumonectomies, 50 lobectomies, and seven operations in which lesser resections were done) the operative mortality rate was 4.5%. The overall treatment-related mortality rate was 7.2%. Dr. Ginsberg quoted other nonsurgical studies in which radiotherapy (4000 rad) has resulted in a radiologic partial response rate of 50% and a radiologic complete response rate of up to 25% in patients with similar stage disease.

T4 tumors invading the esophagus, pulmonary arteries, atrium, nerves, trachea, and carina are possibly resectable and occasionally curable; however, tumors invading the vertebral body, heart, superior vena cava, and aorta have been found to be incurable. Sleeve pneumonectomy can cure 20% of stage IIIB, T4 N0 tumors, but patients must be selected very carefully; with careful selection, resection of T4 tumors of the vertebral body can relieve pain and impending paralysis, but no 5-year survival has been shown so far.

In the treatment of all cases of advanced lung cancer, selection of patients is key, because operative mortality rates can be high. Dr. Ginsberg's "take-home message" about these patients was "Select, then resect."

Letters

Optical Character Recognition for Storing Literature References

In a recent issue of *AJR*, Lossef and Schwartz [1] describe a computerized literature reference system based on the technology of optical character recognition (OCR). However, for good reasons, similar methods are not yet realistic. Hand-held scanners usually produce scans of inferior quality for OCR purposes and place a great burden on the recognition software to compensate. Achieving sufficiently aligned scans is difficult, software must be adjusted to handle skewed characters, and scanning full-sized pages is excessively time-consuming. Even if an expensive desktop scanner is available, the accuracy of OCR software varies incredibly, depending on the recognition method [2].

Trainable software uses pattern-matching recognition algorithms to compare every character image to the already known images of letters and numbers in a typeface. Although simple in concept, pattern-matching OCR has considerable disadvantages in practice. Initially, tedious training sessions in which the image of each character is displayed and the user types the corresponding letter must be repeated for each font separately. Omnifont software uses topologic recognition algorithms that distinguish characters irrespective of a character's shape; each character is decomposed into its elements, and the result is compared with information in the character data base of the software. Omnifont packages are more accurate, especially for complex documents with multiple columns and embedded illustrations.

Elements of type design that make text more readable, such as tight kerning and ligatures, create many problems, particularly with trainable packages. High error rates (more than 10%) result in text that is inordinately laborious to correct afterward. The most common proofreading tool, the spell-checker of a word processor, cannot discover misrecognized punctuation marks, substitution errors that result in apparently legitimate words, and spacing errors. Although dedicated grammar checkers attempt to correct these problems, text and especially numeric information must be checked manually.

OCR requires that the computer have substantial processing power and memory-handling capabilities; every page is loaded into memory, text is separated from figures and ordered properly, and the typeface is recognized by the aforementioned complex algorithms. Illustrations can be included in the plain-text files, but this process involves additional software. Obviously, the whole task of retrieving and storing an article becomes extremely complex for the average user. Moreover, incorporated photographs simply do not preserve the necessary radiologic information.

The literature reference systems have become computerized, but the death of paper is being greatly exaggerated. The idea of taking the image of a document and converting it into working text, as well as transforming drawers jammed with reprints and photocopies into searchable word-processing and data-base files, is attractive. Nevertheless, until OCR technology matures, the only real alternative seems to be the electronic publishing of scientific journals on compact disk.

Stavros Mussurakis
Royal Hallamshire Hospital,
Sheffield, United Kingdom

REFERENCES

1. Lossef SV, Schwartz LH. Computerized literature reference system: use of an optical scanner and optical character recognition software. *AJR* **1990**;155:617–619
2. Grunin L. OCR software moves into the mainstream. *PC Magazine* **1990**;9(18):299–356

Reply

Dr. Schwartz and I appreciate the comments of Dr. Mussurakis. However, we have found that optical scanners with a resolution of 400 dots per inch (dpi) have been sufficient for optical character recognition. In fact, this is an evolving technology, and scanners with resolutions of 800 dpi are now available for a price similar to the cost of the scanner originally used when our article [1] was submitted. Also, improvements in software programs for optical character recognition have made the programs easier to use and more accurate. We agree that electronic publishing of the medical literature on compact disks with read-only memory would be ideal. However, until this is widely available, optical scanning is a useful technology.

Steven V. Lossef
Georgetown University Hospital
Washington, DC 20007-2197

REFERENCE

1. Lossef SV, Schwartz LH. Computerized literature reference system: use of an optical scanner and optical character recognition software. *AJR* **1990**;155:617–619

European Radiology Journals

I read with interest Schütte's review [1] of the current status and perspectives of European radiology. His list of the most important European radiologic journals does not include the German journal *ROFO*. The journal was founded in 1897 and is affiliated with the German Roentgen Ray Society, which currently has 3600 members. Circulation includes 3100 full-cost subscriptions. The journal is mainly in German, but articles in English are published also. Another German journal, *Radiologe*, also includes English papers and is worthy of mention as well.

Rolf W. Günther
University of Technology
D-5100 Aachen, Germany

REFERENCE

1. Schütte HE. Europe 1992: Consequences for European health care and radiology (commentary). *AJR* **1990**;155:1321–1325

Mammography and Malpractice

I commend Potchen et al. [1] on their recent commentary on mammographic malpractice problems in the United States. However, I disagree with a number of their unreferenced statements: "In general, radiologists will recommend six to eight biopsies per cancer detected. . . . Most people agree that a positive predictive value between 10% and 20% is appropriate for screening mammography. . . . Many studies proclaim the need to do biopsies of suspicious lesions at a rate of six to eight biopsies per cancer found to maximize the potential for the cure of nonpalpable breast cancer."

The average positive predictive value (PPV) of cancer for biopsies of nonpalpable breast lesions detected at mammography in the United States is about 20–25%, or one in four to five biopsies [2]. Larger series and those performed by more experienced mammographers generally have higher PPVs, whereas earlier and smaller series have lower PPVs [2–4]. It is true that PPVs as low as 10% have been recommended [5]. On the other hand, some think that a PPV of more than 40% is acceptable [2, 6]. By implying a PPV standard of only 10%–20%, considerably lower than what is currently used in the United States, Potchen et al. may have inadvertently increased the medicolegal risks and anxiety of many experienced mammographers.

How frequently biopsies are actually performed for nonpalpable, probably benign, breast lesions detected at mammography is determined by the expertise of the mammographer and his or her perceived malpractice environment [2–4]. I think that these factors, as much as the use of needle biopsy, explain why the PPV for cancer in surgical breast biopsies is as high as 60%–70% in Sweden and 40%–57% in the Netherlands [7].

I also dissent from the final recommendation by Potchen et al. [1] that radiologists "add a disclaimer on your reports that a normal mammogram does not exclude cancer when a palpable mass is present." I consider such a standard disclaimer a variant of the once-common statement that mammography can never exclude cancer. Perhaps in the early years of mammography such disclaimers were reasonable, but this technique has been around for two decades, and its limitations should be known by all physicians. Cancer cannot be excluded on the basis of any imaging examination, but this fact is not routinely stated on the chest film report of smokers or on the barium enema report of patients with occult blood in the stool. I am skeptical that such reporting practices provide much medicolegal protection, although I defer to Dr. Potchen and other legal experts on this matter.

Ferris M. Hall
Beth Israel Hospital
Harvard Medical School
Boston, MA 02115

REFERENCES

1. Potchen EJ, Bisesi MA, Sierra AE, Potchen JE. Mammography and malpractice (commentary). *AJR* **1991**;156:475–480
2. Hall FM, Storella JM, Silverstone DZ, Wyshak G. Nonpalpable breast lesions: recommendations for biopsy based on suspicion of carcinoma at mammography. *Radiology* **1988**;167:353–358
3. Brenner RJ, Sickles EA. Acceptability of periodic follow-up as an alternative to biopsy for mammographically detected lesions interpreted as probably benign. *Radiology* **1989**;171:645–646
4. Hall FM. Mammographic second opinions prior to biopsy of nonpalpable breast lesions. *Arch Surg* **1990**;125:298–299
5. Moskowitz M. Impact of a priori medical decisions on screening for breast cancer. *Radiology* **1989**;171:605–608
6. Ciatto S, Cataliotti L, Distante V. Nonpalpable lesions detected with mammography: review of 512 consecutive cases. *Radiology* **1987**; 165:99–102
7. Kopans DB, Swann CA. Observations of mammographic screening and false-positive mammograms. *AJR* **1988**;150:785–786

Reply

My coauthors and I applaud Dr. Hall's untiring efforts to enhance awareness that improved skills in diagnostic radiology can decrease the number of surgical biopsies done for mammographically detected breast cancer. We wholeheartedly support this effort, and we wish to do nothing to decrease the importance and effect of his message. Our commentary [1] is intended to do no more than describe a phenomenon and its implications.

The issue of positive predictive value (PPV) and its implications in medical malpractice is more complicated than can be addressed in the space available for this response. The concern that our paper [1] will increase medicolegal risks is not warranted. Our restatement of the literature does not establish a standard of care. Standards are established by medical experts during trial of a specific case. No single reference is all encompassing, nor will it prevail. No single biopsy rate or range is appropriate as a standard of care for an individual malpractice case. Of more concern is the observation that the interpretation of cancer as "normal" is far more likely than a false-positive diagnosis to result in litigation.

The average PPV for biopsies of nonpalpable breast lesions detected at mammography in the United States is uncertain at best. Hall et al. [2] state, "Recent published series show an 11%–36% rate of carcinoma in breast biopsy specimens obtained from mammographically apparent but nonpalpable lesions." The PPV for carcinoma in that series was 30% (119 of 400). In the 40 series we reviewed in preparation of our commentary, the number of cancers per biopsy ranged from the extreme 3.5% (two of 56) at a university hospital to 75.7% [3, 4]. The most recently published series [5] found one cancer in every 6.33 biopsies. The PPV in any case depends heavily on the type of mammographic abnormality that signaled the need for surgical biopsy. Any effort to claim a single norm for all situations is probably inappropriate. No standard exists that should be applied to all cases. Dr. Hall's experience is with a large hospital-based clinical practice with biweekly conferences at which recent mammograms and pathologic reports of corresponding breast biopsies are reviewed. This may be the most appropriate way to do mammography; however, this method is not the norm in community hospitals, where most mammography is practiced. It may be unreasonable to hold all radiologic practices to the standard exemplified by Dr. Hall's excellent work. We agree with Dr. Hall [2] that more experienced mammographers recommend fewer biopsies that have negative results. Perhaps the message is that fewer radiologists should attempt to interpret mammograms.

Dr. Hall's statement that the expertise of the mammographer is more important than the use of needle biopsy is not supported by the evidence in the literature. In our survey of 40 reported series, the

best results were clearly obtained by those clinicians who used the triple-diagnosis approach. They depend on the outcome of fine-needle aspiration biopsy of a nonpalpable lesion to determine which mammographic abnormality warrants surgical biopsy. In the most recent series from the Karolinska hospital in Stockholm [6], mammographers have been able to attain a rate of seven cancers for every eight surgical biopsies performed.

Dr. Hall's last paragraph, although of interest, is not a valid position. The most common malpractice litigation involving mammographies arises when the referring physician defends his or her action by stating that the mammogram was read as normal, thereby implicating the radiologist. This may be diminished by the caveat we suggest. Dr. Hall thinks that this should be known by all physicians. We have observed that what should be known by all physicians is not necessarily what all physicians know. Our efforts were an attempt to identify the legal risk of radiologists involved in the interpretation of mammograms.

E. James Potchen
Michigan State University
East Lansing, MI 48824

REFERENCES

1. Potchen EJ, Bisesi MA, Sierra AE, Potchen JE. Mammography and malpractice (commentary). *AJR* **1991**;156:475–480
2. Hall FM, Storella JM, Silverstone DZ, Wyshak G. Nonpalpable breast lesions: recommendations for biopsy based on suspicion of carcinoma at mammography. *Radiology* **1988**;167:353–358
3. Lang NP, Talbert GE, Shewmake KB, et al. The current evaluation of nonpalpable breast lesions. *Arch Surg* **1987**;122:1389–1391
4. Azavedo E, Svane G, Auer G. Stereotactic fine-needle biopsy in 2594 mammographically detected non-palpable lesions. *Lancet* **1989**;1:1033–1036
5. Kessler HB, Rimer BK, Devine PJ, Gatenby RA, Engstrom PE. Corporate-sponsored breast cancer screening at the work site: results of a statewide program. *Radiology* **1991**;179:107–110
6. Azavedo E, Svane G. Radiologic aspects of breast cancers detected through a breast cancer screening program. *Eur J Radiol* (in press)

The commentary by Potchen et al. [1] is current and informative. The following comments are in reference to various points in that commentary.

There is no anatomic breast designation such as the "left upper quadrant." Standard nomenclature for identification by quadrants includes left breast, upper inner or upper outer quadrant, and so forth.

I disagree that radiologists who recommend fewer than three biopsies per cancer will have a high false-negative rate. In fact, it should be expected that *dedicated* highly experienced mammographic radiologists will practice with a sufficiently high predictive value that they will be able to call findings that closely and thus decrease false-positive overcalls significantly.

Radiologists should be encouraged to specify in their reports biopsy and biopsy preceded by needle localization, when appropriate. The suggestion that "it is usually preferable to recommend a surgical consultation rather than a biopsy" seems inappropriate and dilutes the role of radiologists as consultants. If it should be determined that "extenuating circumstances" exist, then obviously and reasonably the surgeon has every right to cancel or postpone the biopsy.

Although the authors suggest that "a radiologist who accepts self-referred patients should see that a breast examination is performed," they indicate neither the rationale for the physical examination nor who should perform it. Only experienced, skilled clinicians, nurses, or physician assistants should do breast physical examinations, and most radiologists certainly do not fall into any of these categories. Additionally, as most of the self-referred patients are having screening mammogaphy, there seems to be little or no indication for physical examination at that time. The screening study is being done to detect subclinical disease, and therefore physical examination plays little, if any, part.

Finally, although I agree with the authors' recommendation for verbal communication to the referring physician, I suggest that this be taken a step further. Specifically, when the report includes the word "carcinoma," the verbal communication and typed report should be followed by transmission of that report via certified mail, return receipt requested [2]. This should, at least somewhat, protect the interests of all parties, but most importantly, and especially, the patient.

Gerald Edelstein
Hahnemann University Hospital
Philadelphia, PA 19102

REFERENCES

1. Potchen EJ, Bisesi MA, Sierra AE, Potchen JE. Mammography and malpractice (commentary). *AJR* **1991**;156:475–480
2. Edelstein G. Communication problems after mammographic screening (letter). *Radiology* **1989**;173:879

Reply

My coauthors and I appreciate Dr. Edelstein's comments and his appropriate correction of our designation of left upper quadrant. We are impressed by his stated ability to obtain fewer than three biopsies per cancer without a high false-negative rate. We have had to rely on our experience and that of others who have published their results. Of the 40 published series we reviewed in preparation of our paper, we found only five [1–5] with a biopsy rate less than three biopsies per cancer. In none of these series was the mammogram the sole study used to recommend a surgical biopsy. In four of these series, the investigators relied on the cytologic results of a fine-needle biopsy in addition to the mammogram as the indication for surgical biopsy. The fifth series [3] used a multitechnique approach of mammography, sonography, thermography, and, most importantly, physical examination revealing a palpable mass. In that series, 7% of the cancers were missed on mammography. We consider this a high false-negative rate. The results published in the literature suggest that reducing the number of biopsies per cancer to fewer than three by using mammography without cytologic studies markedly increases the false-negative rate. Obviously this problem can be overcome by using mammography plus fine-needle stereotaxic aspiration cytology to select those patients who need a surgical biopsy because of suspected breast cancer. The addition of fine-needle aspiration markedly augments the capacity to decrease the number of "unnecessary" surgical biopsies.

We agree that a dedicated highly experienced mammographer can decrease the number of false-positive overcalls significantly. We do not think that all false-positive overcalls can be safely eliminated. Hall et al. [6] have suggested an approach by which they could have increased their positive predictive value from the 30% they experienced to 41% by not performing biopsies of calcified lesions in their minimally suspicious group and of masses in their minimally and slightly suspicious groups. This alternative criterion for biopsy would have resulted in missing six of 127 carcinomas, but only one of those was invasive. Ciatto et al. [7] state that using a similar change in biopsy criteria, they could improve their positive predictive value from 30% to 51% and increase their false-negative rate by only 1.8%. These considerations suggest that it may be feasible to do better than the published biopsy rates, and we eagerly await the results of the use of these alternative algorithms in prospective studies.

We recommend surgical consultation or cytologic evaluation of a mammographically suspicious lesion to primary physicians rather than surgical biopsy per se because we think that the triple-diagnosis approach (mammography, clinical examination, and cytology) for

selecting patients for biopsy is the most effective and efficient means to detect early breast cancer while minimizing unnecessary surgical biopsies. This involves a multidisciplinary team (radiologists, pathologists, and surgeons) in deciding which patient needs a surgical biopsy. In addition to being good medical care, this approach should decrease the risk of malpractice litigation.

E. James Potchen
Michigan State University
East Lansing, MI 48824

REFERENCES

1. Azavedo E, Svane G, Auer G. Stereotactic fine-needle biopsy in 2594 mammographically detected non-palpable lesions. *Lancet* **1989**;1:1033–1036
2. Andersson I, Andren L, Hildell J, Linell S, Ljungqvist U, Pettersson H. Breast cancer screening with mammography: a population-based, randomized trial with mammography as the only screening mode. *Radiology* **1979**;132:273–276
3. van Dam PA, Van Goethem ML, Kersschot E, et al. Palpable solid breast masses: retrospective single- and multimodality evaluation of 201 lesions. *Radiology* **1988**;166:435–439
4. Lamb J, Anderson TJ, Dixon MJ, Levack P. Role of fine needle aspiration cytology in breast cancer screening. *J Clin Pathol* **1987**;40:705–709
5. Arnesson LG, Fagerberg G, Grontoft O, Lundstrom B. Surgical biopsy of non-palpable mammary lesions: technique and results. *Acta Chir Scand* **1986**;152:97–101
6. Hall FM, Storella JM, Silverstone DZ, Wyshak G. Nonpalpable breast lesions: recommendations for biopsy based on suspicion of carcinoma at mammography. *Radiology* **1988**;167:353–358
7. Ciatto S, Cataliotti L, Distante V. Nonpalpable lesions detected with mammography: review of 512 consecutive cases. *Radiology* **1987**;165:99–102

Anaphylactic Reactions to Latex Balloons

I read with interest the article by Gelfand [1], "Barium Enemas, Latex Balloons, and Anaphylactic Reactions." Allergy to latex products used in medical devices has been underestimated. Recognition of this complication prompts us to consider the possibility of similar problems with permanent implantable devices such as latex detachable balloons, which are used increasingly in interventional radiology for vascular embolization. I am not aware of any reported case of an anaphylactic reaction that was due to a latex detachable balloon. Although data indicate that fatal anaphylactic reactions to latex are rare, latex detachable balloons used in intimate contact with vessels and blood should be a concern. Furthermore, latex detachable balloons are implanted permanently and after placement cannot be withdrawn without surgery. Using a latex detachable balloon for embolization may create a permanent source of allergy in atopic patients, which may pass unnoticed.

Further development of the presumably less allergenic silicone detachable balloons is advisable. These balloons are far more expensive than latex detachable balloons, are not as elastic, and are less permeable. Silicone balloons compare favorably with latex balloons for duration of useful expanded time within the blood vessels, for permanent occlusion.

Although it is too early to say that use of latex balloons should be abandoned, more information on anaphylaxis and latex should be accumulated by the manufacturers of detachable balloons and discussed with interventional radiologists. A total switch to silicone devices may be inconvenient but may result in safer embolization procedures.

Renan Uflacker
Hosp. Beneficencia Portuguesa
Sao Paulo, SP, 01323, Brazil

REFERENCE

1. Gelfand DW. Barium enemas, latex balloons, and anaphylactic reactions. *AJR* **1991**;156:1–2

Retained E-Z-EM Balloon Barium Enema Tip

An enema tip (Super XL System with a silicone retention cuff, E-Z-EM, Inc., Westbury, NY) was introduced into a 43-year-old man for an air-contrast barium enema examination. At the end of the study, the retention cuff, which had been inflated in the patient, did not deflate. A surgeon had to be called in to remove the inflated balloon under local anesthesia.

The balloon was sent to the manufacturer. On the basis of an investigation at the company, a spokesperson for E-Z-EM wrote that they think that the lower tie of the cuff might have moved past the airway when the tip was being positioned in the patient. Thus, air in the inflated cuff had no outlet. The spokesperson indicated that a training session was held with supervisors and operative personnel to make them aware of the incident and the importance of securing the cuff tightly.

Ashwin C. Kesaria
Firelands Community Hospital
Sandusky, OH 44870

Percutaneous Needle Puncture for Treatment of Ileal Obstruction Caused by Migration of a Gastrostomy Tube

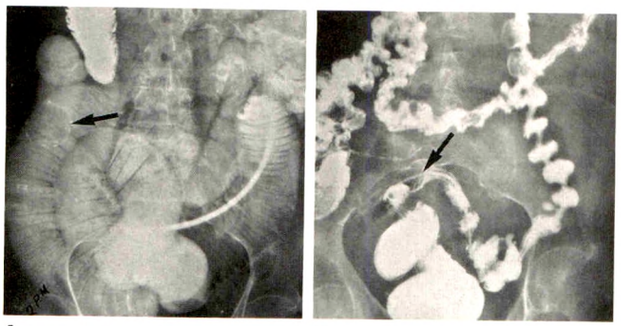
A rare complication of percutaneous gastrostomy is obstruction of the gastric outlet or duodenum caused by migration of the catheter balloon into the duodenum [1]. We describe a case in which a gastrostomy tube migrated into the distal small bowel and caused an obstruction. The obstruction was relieved by percutaneous puncture of the balloon.

A 70-year-old woman was admitted to the hospital for treatment of sepsis. One year before admission she had had percutaneous endoscopic gastrostomy for administration of enteral nutrition. The original gastrostomy tube was replaced with a 12-French Foley catheter. The catheter functioned well until 1 week after admission, when the external clamp was repositioned. The morning after the repositioning, the catheter was no longer visible.

Abdominal radiographs obtained with the patient supine did not show the missing catheter. A second Foley catheter was placed through the mature gastrocutaneous fistula. Barium (150 ml) was injected through the new catheter to determine if the first Foley catheter had been retained. Dilated fluid-filled loops of small bowel were seen to the level of the distal ileum, where a round filling defect obstructed the flow of barium (Fig. 1A). Suction overnight via the second Foley catheter did not relieve the high-grade partial obstruction of the small bowel.

The balloon of the first Foley catheter was deflated percutaneously under fluoroscopic guidance by using a 21-gauge Chiba needle. With an audible pop, the round filling defect disappeared, and barium flowed into the colon. The next day the first Foley catheter had progressed beyond the ileocecal valve and into the colon (Fig. 1B). Within 2 days, the patient passed the tube via the rectum.

Our case differs from previously reported cases of migration of a gastrostomy tube because the balloon port of the Foley catheter was not accessible to allow deflation by that route. In this respect, our case resembles the cases of intestinal obstruction caused by Cantor, Harris, and Miller-Abbott oral feeding tubes [2]. The thin-walled latex or rubber weight-bearing balloons of these tubes may enlarge within



A B

Fig. 1.—Ileal obstruction caused by a migrating gastrostomy tube.
***A*, Small-bowel follow-through examination shows multiple dilated loops of small bowel to level of distal ileum, where obstructing balloon of a Foley catheter is seen (*arrow*).**
***B*, Follow-up film obtained 1 day after percutaneous deflation of obstructing balloon shows passage of catheter into colon (*arrow*) and resolution of small-bowel obstruction.**

bowel because of the permeability of the wall of the tube, enteric luminal pressure, and the different compositions of gases in the balloon and enteric gases [3]. Treatment of obstruction caused by a migrating tube has included bowel decompression by suction via a second tube to reverse the effects of luminal pressure, rupture of the balloon by pulling on the tube, and percutaneous deflation [4]. When these fail, a laparotomy must be performed.

In our case, the catheter with the balloon deflated was small and pliable enough to pass through the ileocecal valve. Thus, simple percutaneous puncture of the balloon allowed resolution of this uncommon complication of tube gastrostomy.

Roger K. Harned II
Judith L. Chezmar
Emory University School of Medicine
Atlanta, GA 30322

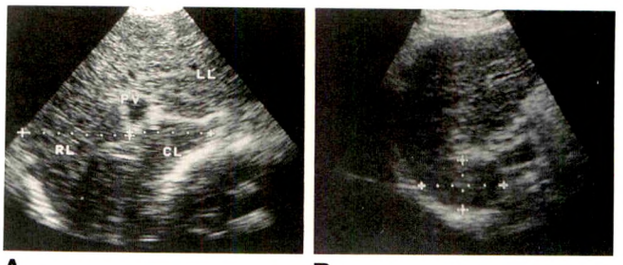
REFERENCES

1. Sheman ML, Cosgrove MJ, Dennis JM. Gastrostomy tube migration. *Am Surg* **1973**;39:122–123
2. Smoger RS, Rosen RJ, Teplick SK, Mandell GA, Teplick JG. Small bowel obstruction caused by distension of the Cantor tube balloon. *AJR* **1980**;135:612–613
3. Fricke FJ, Niewodowski MA. Hazardous gaseous distension of intestinal balloons. *JAMA* **1976**;235:2611–2613

Hepatic Sarcoidosis as a Cause of Hypertrophy of the Caudate Lobe: Sonographic Findings

In a pictorial essay published in the *AJR* [1], hepatic cirrhosis and Budd-Chiari syndrome are the only examples shown of diffuse hepatic disease that results in hypertrophy of the caudate lobe of the liver. We report on a patient with hepatic sarcoidosis in whom shrinkage of the right lobe of the liver and enlargement of the caudate lobe suggested hepatic cirrhosis, a diagnosis that was not confirmed by laparoscopy and biopsy. To our knowledge, sarcoidosis has not been reported before as a cause of enlargement of the caudate lobe.

A 60-year-old man had fatigue, general malaise, hepatosplenomegaly, elevated serum levels of transaminases (aspartate aminotransferase, 62 U/l; alanine aminotransferase, 45 U/l), cholestasis (alkaline phosphatase, 1417 U/l; γ-glutamyl transferase, 495 U/l), and dysproteinemia (albumin, 3.2 g/dl [32 g/l]; γ-globulins, 1.9 g/dl [19 g/l]). He had no history of alcohol abuse, hepatitis, or use of hepatotoxic drugs. Sonography was performed with a 3.5-MHz curved-array transducer after the patient had fasted overnight. The sonograms showed an enlarged liver with well-defined enlargement of both the caudate and left lobes and shrinkage of the right lobe (Fig. 1). The caudate-to-right-lobe ratio [2] was 0.74, and the ratio of the three-dimensional caudate index to the right-lobe diameter [3] was 12.5 cm^2. Both values suggested cirrhosis. Such a diagnosis seemed corroborated by the presence of finely irregular liver margins, coarse parenchymal echotexture (i.e., large, bright, and scattered liver echoes), and evidence of portal hypertension (dilated main portal trunk, collateral vessels along the greater gastric curvature). Splenomegaly with homogeneous echostructure was noted also. At laparoscopy, no cirrhosis of the liver was apparent. Histologic examination of biopsy samples from both lobes of the liver showed sarcoid noncaseating granulomas in portal and periportal areas surrounded by marked fibrosis; no cirrhotic nodular regeneration was seen.



A B

Fig. 1.—Hypertrophy of the caudate lobe caused by hepatic sarcoidosis.
***A*, Transverse sonogram at level of portal vein (PV) bifurcation shows hypertrophy of caudate lobe (CL) of liver and shrinkage of right lobe (RL). LL = left lobe.**
***B*, Longitudinal sonogram shows caudate lobe. Note fine wavy outline of liver and coarse parenchymal echotexture.**

Dodds et al. [1] have hypothesized that the caudate lobe originates from a small portion of both hepatic lobes as a result of a rightward rotation of the fetal liver around and behind the mesentery of the ductus venosus. This explains why the vascular supply of the caudate lobe comes from both hepatic arteries and both portal veins. In addition, caudate venous drainage bypasses the hepatic veins, as small communicating veins connect the caudate lobe directly to the inferior vena cava. Such a unique vascular system allows the caudate lobe to have comparatively better oxygenation than the other hepatic segments in diffuse liver diseases that cause derangement of either arterioportal inflow (hepatic cirrhosis) or venous outflow (Budd-Chiari syndrome).

Giampiero Francica
Giorgio Cozzolino
Universita' di Napoli
80131 Napoli, Italy
Antonio Giorgio
Ospedale "D. Cotugno"
Napoli, Italy

REFERENCES

1. Dodds WJ, Erickson SJ, Lawson TL, Stewart ET. Caudate lobe of the liver: anatomy, embryology, and pathology. *AJR* **1990**;154:87–93
2. Harbin WP, Robert NJ, Ferrucci JT Jr. Diagnosis of cirrhosis based on regional changes in hepatic morphology: a radiological and pathological analysis. *Radiology* **1980**;135:273–283
3. Hess CF, Schmiedl U, Koelbel G, Knecth R, Kurtz B. Diagnosis of liver cirrhosis with US: receiver-operating characteristic analysis of multidimensional caudate lobe indexes. *Radiology* **1989**;171:349–351

High Serum Level of Alkaline Phosphatase Is Not a Contraindication for Embolization of the Hepatic Artery in Liver Cancer

Embolization of the hepatic artery for palliation of unresectable liver tumors is being evaluated in a number of institutions [1]. A high serum level of alkaline phosphatase (45 King-Armstrong units/dl [SI units, 320 U/l], or 19 mmol/hr·l) is usually regarded as a contraindication for the procedure [2, 3].

My colleagues and I have used transcatheter embolization in 85 patients with hepatic neoplasms. Retrospective analysis showed that seven of the 85 had increased levels of alkaline phosphatase in their serum before the embolization: range, 20 mmol/hr·l (340 U/l) to 28 mmol/hr·l (476 U/l); mean, 22 ± 3 mmol/hr·l (374 ± 51 U/l). All seven tumors (two primary and five metastatic) were unresectable and occupied 20–70% of liver volume. Gelatin sponge particles and steel coils were used to occlude the hepatic artery. No complications developed. Serum levels of alkaline phosphatase returned to normal in five patients 1–3 weeks after the embolization. In the other two patients, the level of the enzyme increased slightly after the embolization but returned to normal by 5–7 weeks after treatment.

We agree with Delcour and Struyven [4] that all existing contraindications for embolization of the hepatic artery, including high serum level of alkaline phosphatase, are relative. The possibility of embolization should be considered on an individual basis for each patient.

Pavel G. Tarazov
Central Research Institute of Roentgenology and Radiology
Leningrad, U. S. S. R.

REFERENCES

1. Allison DJ, Jordan H, Hennesy O. Therapeutic embolization of the hepatic artery: a review of 75 procedures. *Lancet* **1985**;1:595–598
2. Powell-Tuck J, McIvor J, Reynolds KW, Murray-Lyon IM. Prediction of early death after therapeutic hepatic arterial embolization. *Br Med J* **1984**;288:1257–1259
3. Carrasco CH, Charnsangavej C, Ajani J, Samaan NA, Richli W, Wallace S. The carcinoid syndrome: palliation by hepatic artery embolization. *AJR* **1986**;147:149–154
4. Delcour CP, Struyven JL. Interventional radiology in oncology. *Eur J Cancer Clin Oncol* **1988**;24:815–819

MR and CT Diagnosis of Intracranial Lipoma

Intracranial lipomas are rare. The most common variety is a lipoma of the corpus callosum. It is thought that the tumor arises from an embryologic anomaly caused by failure of absorption of the primitive meninges. Other midline defects may be present, such as agenesis of the corpus callosum, myelomeningocele, and spina bifida. Other common intracranial locations for lipomas include the pericallosal quadrigeminal plate and tuber cinereum [1].

Our patient, a 20-year-old man, was admitted because of seizures. The results of a physical examination were normal. Radiographs showed a central radiolucency with curvilinear calcifications shaped like parentheses. CT (Fig. 1A) showed an interhemispheric lesion with a density similar to that of fat near the genu of the corpus callosum with peripheral calcification. Two other small similar lesions were seen in the lateral ventricles. MR (Figs. 1B–1D) showed a midline high-intensity lesion on T1 sequences that was less intense on T2 sequences. The corpus callosum could not be detected. Two other lesions with the same signal intensity on both T1 and T2 sequences were detected in the body of the right ventricle and left trigone. This workup confirmed the presence of an interhemispheric lipoma with agenesis of the corpus callosum and associated intraventricular lipomas.

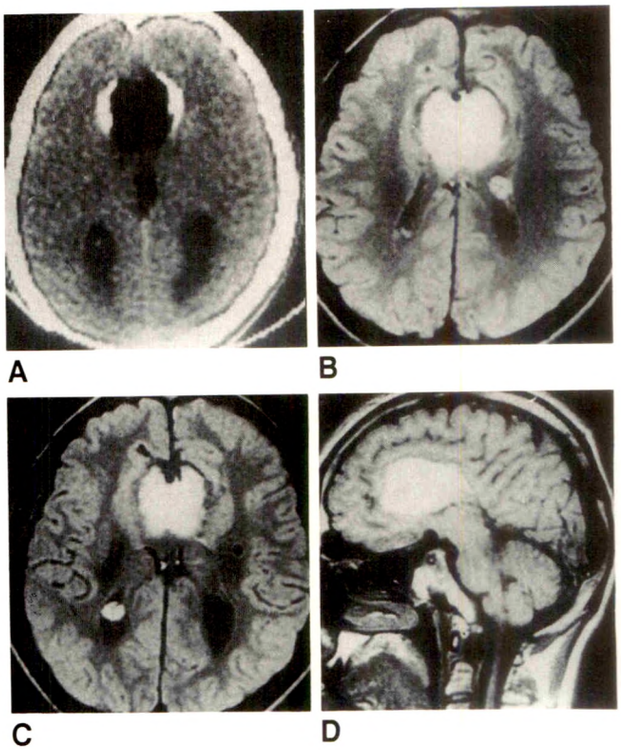


Fig. 1.—Intracranial lipoma.
***A*, CT scan shows curvilinear calcified lesions with a central hypodense component.**
***B and C*, Axial T1-weighted MR images (2500/25) show three high-intensity lesions in midline, body of right ventricle, and left trigone. Intensity of lesions decreased on T2-weighted images (*not shown*).**
***D*, Parasagittal MR image shows a high-intensity lesion. Corpus callosum could not be detected.**

Intracranial lipomas may be asymptomatic; however, seizures, mental retardation, behavioral disorders, and headache are common findings. Diagnosis made on the basis of CT and MR findings depends on the demonstration of the characteristic fat density on CT and signal intensities on MR [2, 3]. CT may show marginal calcifications not seen on MR. Nevertheless, MR is the procedure of choice for evaluation of the corpus callosum because of the capacity to obtain direct coronal and sagittal images without the need for reconstruction. It is particularly useful in showing associated agenesis of the corpus callosum and vascular encasement. Sonography may be useful in making the diagnosis in neonates [4]; the site and echogenic appearance are characteristic. Differential diagnosis includes other midline diseases, such as dermoid cysts, teratomas of the corpus callosum, and other tumors, especially germinomas.

G. Rubio
C. Garcia Guijo
J. J. Mallada
Clinica Puerta de Hierro
Madrid, Spain

REFERENCES

1. Atlas SW, Zimmerman RA, Bilaniuk LT, et al. Corpus callosum and limbic system: neuroanatomic MR evaluation of developmental anomalies. *Radiology* **1986**;160:355–362
2. Nabawi P, Dobben GD, Mafee M, Espinosa GA. Diagnosis of lipoma of the corpus callosum by CT in five cases. *Neuroradiology* **1981**;21:159–162

3. Olm M, Blesa R, Ribera G, Cardenal C. Lipoma of the corpus callosum: CT and MR for diagnosis. *AJR* **1988**;151:613–614
4. Fisher RM, Cremin BJ. Lipoma of the corpus callosum: diagnosis by ultrasound and magnetic resonance. *Pediatr Radiol* **1988**;18:409–410

Unusual Spread of Sinonasal Carcinoma via the Eustachian Tube into the Middle and External Ear

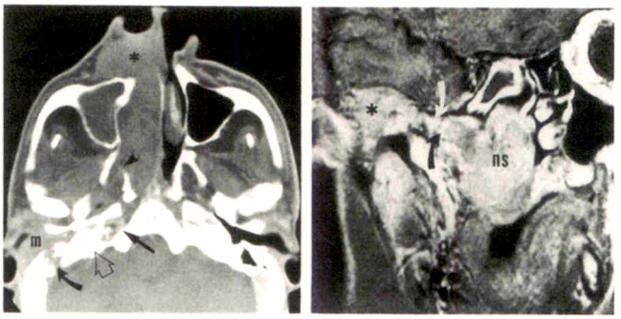
A 49-year-old man had had pain in his right ear, drainage, and nasal swelling for 6 months. Physical findings included complete obliteration of the right nasal cavity by a tender mass that protruded from the right naris and deformed the nasolabial fold. A purulent mass completely filled the right external auditory canal. Contrast-enhanced CT showed a large mass filling the right nasal cavity and extending posteriorly to the nasopharynx. The internal structures of the right ear were intact, but the middle and external ear contained tumor, and destruction of the ossicles and erosion of the mastoid were present (Fig. 1A). Gadolinium-enhanced MR imaging showed that the tumor extended from the nasopharynx to the right middle ear (Fig. 1B). Biopsies of the masses in the nasopharynx and middle ear showed adenocarcinoma. At surgery, extension via the eustachian tube was found; the lesion was unresectable. The patient had intraarterial chemotherapy, and CT 1 month after therapy showed that the mass had decreased considerably in size.

Adenocarcinoma is an uncommon malignancy of the sinonasal cavity, accounting for approximately 4%–8% of tumors in that location [1]. In the sinonasal region, adenocarcinomas more commonly involve the ethmoid and maxillary sinuses [1].

Initially these tumors expand the sinonasal spaces, but as the tumors enlarge, bone erosion occurs. Nodal metastasis also can develop [2].

Malignancies of the head and neck extend via the following mechanisms: (1) direct extension, (2) lymphatic extension, (3) blood-borne extension, and (4) perineural spread. Direct extension may occur along the airway (path of least resistance), along the musculofascial planes, or by direct erosion of bone. In the nasopharynx, lymphatic metastasis generally occurs in the direction of drainage (first order of drainage is the lateral pharyngeal node of Rouviere). Occasionally, we have seen retrograde lymphatic spread. Blood-borne extension manifests itself as distant metastases (brain, lungs, and liver). Extension along the perineural spaces is common with tumors of glandular origin [3].

In this case, the bulk of the tumor was in the nasal cavity. Protrusions into the nasopharynx and naris are examples of spread via the airway. An unusual finding was the presence of tumor in the middle and external ear with no obvious involvement of the inner ear. The only plausible explanation for this phenomenon is mucosal extension via the eustachian tube, which in this case was confirmed surgically. We are not aware of any other cases in which such extension has been documented.



A B

Fig. 1.—Spread of sinonasal carcinoma via eustachian tube.
***A*, Axial CT scan (bone windows) shows mass (*asterisk*) in right nasal cavity extending anteriorly through naris and posteriorly into nasopharynx and eroding medial pterygoid plate (*arrowhead*). Bowing of medial wall of right maxillary sinus and of nasal septum is evident. Structures of internal ear (*open arrow*) are intact, indicating that no contiguous extension through bone is present. Questionable erosion of medial aspect of petrous bone (*straight arrow*) is seen. Tumor (m) is seen in middle and external ear, with destruction of ossicles and erosion of mastoid (*curved arrow*).**
***B*, Oblique (parallel to course of eustachian tube) gadolinium-enhanced T1-weighted MR image shows largest bulk of tumor (ns) is in nasopharynx, extending along region of eustachian tube (*arrows*) into middle ear (*asterisk*).**

Mauricio Castillo
Ya Yen Lee
University of Texas Medical School at Houston
Houston, TX 77026

REFERENCES

1. Dillon WP, Mancuso AA. The oropharynx and nasopharynx. In: Newton TH, Hasso AN, Dillon WP, eds. *Computed tomography of the head and neck*. New York: Raven, **1988**:10.42–10.44
2. Som PM. Lymph nodes of the neck. *Radiology* **1987**;165:593–600
3. Lee YY, Castillo M, Nauert C. Intracranial perineural metastasis of adenoid cystic carcinoma of head and neck. *J Comput Tomogr* **1985**;9:219–223

Letters are published at the discretion of the Editor and are subject to editing.

Letters to the Editor must not be more than two *double-spaced*, typewritten pages. One or two figures may be included. Abbreviations should not be used. See Author Guidelines, page A13

Material being submitted or published elsewhere should not be duplicated in letters, and authors of letters must disclose financial associations or other possible conflicts of interest.

Letters concerning a paper published in the *AJR* will be sent to the authors of the paper for a reply to be published in the same issue. Opinions expressed in the Letters to the Editor do not necessarily reflect the opinions of the Editor.

Review of Current Literature

Initials and addresses of corresponding authors are provided in parentheses for each article so that the reader can obtain reprints directly. Abstracts are printed verbatim from each journal.

The New England Journal of Medicine

A controlled study of inhaled pentamidine for primary prevention of *Pneumocystis carinii* pneumonia. Hirschel B, Lazzarin A, Chopard P, et al. (BH, Division des Maladies infectieuses, Hopital Cantonal Universitaire, CH 1211 Geneva 4, Switzerland). *N Engl J Med* 324(16):1079–1083, April 1991

Background. Current recommendations for prophylaxis of *Pneumocystis carinii* pneumonia (PCP) are based on data from patients who have had at least one episode of PCP (secondary prevention). We designed a study to determine the efficacy and side effects of inhaled pentamidine in the primary prevention of PCP.

Methods. Two hundred twenty-three patients seropositive for human immunodeficiency virus (HIV) who had the acquired immunodeficiency syndrome (AIDS) but not PCP, who had advanced AIDS-related complex, or who had less than 0.2×10^9 CD4-positive lymphocytes per liter received either 300 mg of pentamidine isethionate or 300 mg of sodium isethionate every 28 days by inhaler. The proportion of patients surviving without PCP was analyzed with the log-rank test as a function of time spent in the trial, according to the intention to treat with either placebo or pentamidine.

Results. The third of five planned interim analyses showed a significant difference in the occurrence of PCP, with 8 cases in the pentamidine group and 23 in the placebo group (nominal P value = 0.0021). There were no deaths within 60 days of the diagnosis of PCP and no significant differences in survival between groups. Approximately 53 inhalations were needed to prevent one episode of pneumonia. Thirty-eight of 114 patients given pentamidine (33 percent) and 7 of 109 given placebo (6 percent) had moderate-to-severe coughing during inhalations (two-tailed $P < 0.00001$), which caused 4 patients given pentamidine (3.5 percent) to discontinue taking it.

Conclusions. A dose of 300 mg of aerosolized pentamidine given every four weeks was well tolerated and 60 to 70 percent effective in preventing a first episode of PCP in patients with HIV infection.

Hyperhomocysteinemia: an independent risk factor for vascular disease. Clarke R, Daly L, Robinson K, et al. (I. Graham, Dept. of Cardiology, Adelaide Hospital, Peter St., Dublin 8, Ireland). *N Engl J Med* 324(17):1149–1155, April 1991

Background. Hyperhomocysteinemia arising from impaired methionine metabolism, probably usually due to a deficiency of cystathionine β-synthase, is associated with premature cerebral, peripheral, and possibly coronary vascular disease. Both the strength of this association and its independence of other risk factors for cardiovascular disease are uncertain. We studied the extent to which the association could be explained by heterozygous cystathionine β-synthase deficiency.

Methods. We first established a diagnostic criterion for hyperhomocysteinemia by comparing peak serum levels of homocysteine after a standard methionine-loading test in 25 obligate heterozygotes with respect to cystathionine β-synthase deficiency (whose children were known to be homozygous for homocystinuria due to this enzyme defect) with the levels in 27 unrelated age- and sex-matched normal subjects. A level of 24.0 μmol per liter or more was 92 percent sensitive and 100 percent specific in distinguishing the two groups. The peak serum homocysteine levels in these normal subjects were then compared with those in 123 patients whose vascular disease had been diagnosed before they were 55 years of age.

Results. Hyperhomocysteinemia was detected in 16 of 38 patients with cerebrovascular disease (42 percent), 7 of 25 with peripheral vascular disease (28 percent), and 18 of 60 with coronary vascular disease (30 percent), but in none of the 27 normal subjects. After adjustment for the effects of conventional risk factors, the lower 95 percent confidence limit for the odds ratio for vascular disease among the patients with hyperhomocysteinemia, as compared with the normal subjects, was 3.2. The geometric-mean peak serum homocysteine level was 1.33 times higher in the patients with vascular disease than in the normal subjects ($P = 0.002$). The presence of cystathionine β-synthase deficiency was confirmed in 18 of 23 patients with vascular disease who had hyperhomocysteinemia.

Conclusions. Hyperhomocysteinemia is an independent risk factor for vascular disease, including coronary disease, and in most instances is probably due to cystathionine β-synthase deficiency.

Measurement of prostate-specific antigen in serum as a screening test for prostate cancer. Catalona WJ, Smith DS, Ratliff TL, et al. (WJC, 4960 Audubon Ave., St. Louis, MO 63110). *N Engl J Med* 324(17):1156–1161, April 1991

Background. Prostate-specific antigen (PSA) is secreted exclusively by prostatic epithelial cells, and its serum concentration is increased in men with prostatic disease, including cancer. We evaluated its usefulness in the detection and staging of prostate cancer.

Methods. We measured serum PSA concentrations in 1653 healthy men 50 or more years old. Those with PSA values ≥ 4.0 μg per liter then underwent rectal examination and prostatic ultrasonography. Ultrasound-directed prostatic needle biopsies were performed in the men with abnormal findings on rectal examination, ultrasonography, or both. The results were compared with those in 300 consecutively studied men 50 or more years old who underwent ultrasound-directed biopsy because of symptoms or abnormal findings on rectal examination.

Results. Serum PSA levels ranged from 4.0 to 9.9 μg per liter in 6.5 percent of the 1653 men (107). Nineteen of the 85 men in this group (22 percent) who had prostatic biopsies had prostate cancer. Serum PSA levels were 10.0 μg per liter or higher in 1.8 percent of

the 1653 men (30). Eighteen of the 27 men in this group (67 percent) who had prostatic biopsies had cancer. If rectal examination alone had been used to screen the men who had biopsies, 12 of the 37 cancers (32 percent) would have been missed. If ultrasonography alone had been used to screen these men, 16 of the 37 cancers (43 percent) would have been missed. Serum PSA measurement had the lowest error rate of the tests, and PSA measurement plus rectal examination had the lowest error rate of the two-test combinations.

Conclusions. The combination of measurement of the serum PSA concentration and rectal examination, with ultrasonography performed in patients with abnormal findings, provides a better method of detecting prostate cancer than rectal examination alone.

Dysphagia in patients with the post-polio syndrome. Sonies BC, Dalakas MC (MCD, Neuromuscular Diseases Section, NINDS, NIH, Rm. 4N248, Bldg. 10, Bethesda, MD 20892). *N Engl J Med* 324(17):1162–1167, April 1991

Background and Methods. Dysphagia may develop in some patients many years after an attack of acute paralytic poliomyelitis. To identify clinical or subclinical signs of oropharyngeal dysfunction, we examined 32 patients (mean age, 48.9 years) with the post-polio syndrome (defined by new weakness in the limbs). Of the 32 patients, 14 had symptoms of new swallowing difficulties, and 18 were asymptomatic in this respect; 12 had a history of bulbar involvement during acute poliomyelitis. Swallowing function was assessed objectively by ultrasonography, videofluoroscopy, and an oral motor index score for 10 components of oral function.

Results. All but 1 of the 32 patients, regardless of whether they had new symptoms or previous bulbar involvement, had some abnormality on detailed testing of oropharyngeal function; only 2 patients had any signs of aspiration. The mean oral motor index score (a quantitative measure of oral sensorimotor function) in the patients was higher than that in age-matched normal subjects ($P < 0.001$). Videofluoroscopy showed abnormalities of varying severity, including unilateral bolus transport through the pharynx, pooling in the valleculae or pyriform sinuses, delayed pharyngeal constriction, and impaired tongue movements. On ultrasonography, the mean (±SD) duration of wet swallows was significantly longer in the symptomatic patients than in the asymptomatic patients (2.67 ± 0.70 vs. 1.65 ± 0.42 seconds). The four patients who were reexamined two years later had objective signs of worsening oropharyngeal function and corresponding new symptoms.

Conclusions. In patients with the post-polio syndrome, the bulbar muscles often have clinical or subclinical signs of dysfunction. These abnormalities suggest that in bulbar neurons there is a slowly progressive deterioration similar to that in the muscles of the limbs.

Preoperative transcatheter closure of congenital muscular ventricular septal defects. Bridges ND, Perry SB, Keane JF, et al. (J. E. Lock, Cardiology Dept., Children's Hospital, 300 Longwood Ave., Boston, MA 02115). *N Engl J Med* 324: 1312–1317, May 1991

Background. Surgical repair of muscular ventricular septal defects, particularly those associated with complex heart lesions, carries a higher risk of reoperation and death than the repair of membranous defects. Closing a muscular defect through an incision in the systemic ventricle may cause late ventricular dysfunction. In a collaborative approach to this problem, we undertook preoperative transcatheter closure of muscular ventricular septal defects remote from the atrioventricular and semilunar valves, followed by the surgical repair of associated conditions.

Methods. In 12 patients selected jointly by a cardiologist and a cardiac surgeon, we attempted preoperative transcatheter umbrella closure of 21 defects. Half the patients had associated complex heart lesions; the others had had pulmonary-artery banding to reduce the amount of *left-to-right shunting*. Half had severe ventricular septal deficiency.

Results. All 21 defects were successfully closed without major complications. Subsequent cardiac surgery for associated conditions in 11 of the 12 patients resulted in a mean pulmonary-to-systemic flow ratio of 1.1, indicating minimal residual left-to-right shunting; 1 patient awaited surgical repair. No deaths, reoperations, or late complications have occurred after a follow-up of 7 to 20 months.

Conclusions. A collaborative approach using transcatheter closure followed by the surgical repair of associated cardiac lesions may decrease rates of operative mortality, reoperation, and left ventricular dysfunction in patients with muscular ventricular septal defects.

Risk factors for falls as a cause of hip fracture in women. Grisso JA, Kelsey JL, Strom BL, et al. (JAG, Clinical Epidemiology Unit, University of Pennsylvania, 317R Nursing Education Bldg, 420 Service Dr., Philadelphia, PA 19104-6095). *N Engl J Med* 324:1326–1331, May 1991

Background. Although even in the elderly most falls are not associated with fractures, over 90 percent of hip fractures are the result of a fall. Few studies have assessed whether the risk factors for falls are also important risk factors for hip fracture.

Methods. To examine the importance of risk factors for falls in the epidemiology of hip fracture, we performed a case-control study of 174 women (median age, 80 years) admitted with a first hip fracture to 1 of 30 hospitals in New York and Philadelphia. Controls, matched to the case patients according to age and hospital, were selected from general surgical and orthopedic surgical hospital services. Information was obtained by direct interview.

Results. As measured by the odds ratio, increased risks for hip fracture were associated with lower-limb dysfunction (odds ratio = 1.7; 95 percent confidence interval, 1.1 to 2.8), visual impairment (odds ratio = 5.1; 95 percent confidence interval, 1.9 to 13.9), previous stroke (odds ratio = 2.0; 95 percent confidence interval, 1.0 to 4.0), Parkinson's disease (odds ratio = 9.4; 95 percent confidence interval, 1.2 to 76.1), and use of long-acting barbiturates (odds ratio = 5.2; 95 percent confidence interval, 0.6 to 45.0). Of the controls, 44 (25 percent) had had a recent fall. The case patients were more likely than these controls to have fallen from a standing height or higher (odds ratio = 2.4; 95 percent confidence interval, 1.0 to 5.7). Of those with hip fracture the younger patients (<75 years old) were more likely than the older ones (≥75 years old) to have fallen on a hard surface (odds ratio = 1.9; 95 percent confidence interval, 1.04 to 3.7).

Conclusions. A number of factors that have been identified as risk factors for falls are also associated with hip fracture, including lower-limb dysfunction, neurologic conditions, barbiturate use, and visual impairment. Given the prevalence of these problems among the elderly, who are at highest risk, programs to prevent hip fracture should include measures to prevent falls in addition to measures to slow bone loss.

Chest

Expiratory computed tomography for assessment of suspected pulmonary emphysema. Knudson RJ, Standen JR, Kaltenborn WT, et al. (RJK, Division of Respiratory Sciences, University of Arizona College of Medicine, Tucson, AZ 85724). *Chest* 99(6):1357–1366, June 1991

Results of computed tomography of the lung performed at two levels in upper lung zones at full inspiration and full expiration were compared with results of tests of ventilatory function, lung mechanics, and single breath carbon monoxide diffusing capacity in 64 subjects, many of whom had some form of airflow obstruction. From the CT scans, the mean percentage of pixels in the range −900 to −1,024 Hounsfield units, or pixel index, was determined for each subject. The highest correlations of pixel index with physiologic variables consistent with a diagnosis of emphysema were observed for CT taken at full expiration. In some subjects, the inspiratory CT would give a "false positive" for emphysema when the hyperaeration observed at inspiration was not observed at expiration. We believe that the CT scan taken at full expiration can effectively reveal the abnormal permanent enlargement of airspaces which defines emphysema and provides a noninvasive method of assessing lung morphology in the living human subject.

Clinics in Chest Medicine

Noninfectious pulmonary diseases masquerading as community-acquired pneumonia. Gross TJ, Chavis AD, Lynch JP III (TJG, Division of Pulmonary and Critical Care Medicine, Dept. of Internal Medicine, University of Michigan Medical Center, Ann Arbor, MI). *Clin Chest Med* 12(2):363–394, June 1991

A wide spectrum of pulmonary disorders may manifest clinical and radiographic features consistent with infectious pneumonitis. Bronchiolitis obliterans, eosinophilic pneumonia, hypersensitivity pneumonitis, pulmonary vasculitis, alveolar hemorrhage, and alveolar proteinosis all may be difficult to distinguish from community-acquired pneumonia. The salient clinical features of these disorders are reviewed in this article. In addition, specific diagnostic and therapeutic approaches that may aid in differentiating these unusual diseases from the pulmonary infections they mimic are outlined.

Gastroenterology

Scintigraphic measurement of regional gut transit in idiopathic constipation. Stivland T, Camilleri M, Vassallo M, et al. (TS, Gastroenterology Research Unit, Mayo Clinic, Rochester, MN). *Gastroenterology* 101:107–115, 1991

In this study, total gut transit and regional colonic transit in patients with idiopathic constipation were measured scintigraphically. Eight patients with severe constipation were studied, none of whom had evidence of abnormal function of the pelvic floor. ^{99m}Tc-radiolabeled Amberlite resin particles (average diameter, 1 mm: Sigma Chemical Co., St. Louis, MO) with a mixed meal were used to assess gastric emptying and small bowel transit; similar particles labeled with ^{111}In were ingested in a coated capsule that dispersed in the ileocecal region. These were used to quantify colonic transit. Five healthy volunteers were also studied. Two patients showed delayed gastric emptying and two had slow small bowel transit. Seven of the eight patients had slow colonic transit. In five, delay affected the whole colon ("pancolonic inertia"); in two, transit in the ascending and transverse colon was normal, but solids moved through the left colon slowly. Mean colonic transit was also measured using radiopaque markers; this technique identified the patients with slow transit, as shown by measurements of overall colonic transit by simultaneous scintigraphy. However, estimated transit through the ascending and transverse colons was considerably shorter by the radiopaque marker technique. In conclusion, idiopathic constipation is characterized by either exaggerated reservoir functions of the ascending and transverse colons and/or impairment of propulsive function in the descending colon. Particle size may influence the result of regional colonic transit tests. Transit delays in other parts of the gut suggest that, in some patients, the condition may be a more generalized motor dysfunction.

Reprinted with permission by the American Gastroenterological Association.

Cost-effectiveness of extracorporeal shock-wave lithotripsy versus cholecystectomy for symptomatic gallstones. Bass EB, Steinberg EP, Pitt HA, et al. (EBB, Dept. of Medicine, The Johns Hopkins University School of Medicine, Baltimore, MD). *Gastroenterology* 101: 189–199, 1991

To evaluate the cost-effectiveness of extracorporeal shock-wave lithotripsy vs. cholecystectomy for symptomatic gallstones, a model was constructed that projects charges and survival for both treatments. For a 45-year-old woman with one small stone, treatment with extracorporeal shock-wave lithotripsy rather than cholecystectomy is projected to result in an average gain of only 3 days of life and an average increase in direct medical charges of $1729 over 5 years of follow-up. The resulting marginal cost-effectiveness of extracorporeal shock-wave lithotripsy vs. cholecystectomy is $216,000 of extra charges per year of life gained with extracorporeal shock-wave lithotripsy. Extracorporeal shock-wave lithotripsy is projected to be much more cost-effective for elderly than for young patients (10–20-fold difference), but considerably less cost-effective for multiple stones than a single stone (2–4-fold difference), and less cost-effective for women than men (twofold difference). Adjusting for effects of morbidity on quality of life, extracorporeal shock-wave lithotripsy is projected to have slightly better quality-adjusted survival than cholecystectomy for the small subset of patients with one stone (by 8 to 43 days at 5 years) but not for young patients with multiple stones. It is concluded that decisions about appropriate use of extracorporeal shock-wave lithotripsy should consider the effects of patient characteristics on clinical and economic outcomes.

Reprinted with permission by the American Gastroenterological Association.

Digestive Diseases and Sciences

Collagenous colitis pathophysiologic considerations. Stampfl DA, Friedman LS (LSF, Jefferson Medical College, 1025 Walnut St., Philadelphia, PA 19107). *Dig Dis Sci* 36(6):705–711, June 1991

Collagenous colitis, a cause of watery diarrhea characterized by a distinctive band of collagen under the surface epithelium of the colon, has been recognized with increasing frequency in recent years. The pathophysiology of collagenous colitis remains obscure. The thickening of the subepithelial collagen layer may be a response to chronic inflammation or a local abnormality of collagen synthesis. The precise mechanism of the diarrhea in collagenous colitis is also unclear, and it has not been possible to link the diarrhea directly to the excess collagen deposition. The relationship between collagenous colitis and lymphocytic colitis, another type of microscopic colitis, remains to be defined: elucidating the relationship between the two disorders may provide clues to the pathophysiology of both.

Gastrointestinal Endoscopy

The gastroenterologist: physician or technician? DiSario JA, Waring JP, Sanowski RA, Wadas DD (RAS, Gastroenterology, Carl J. Hayden Veterans Administration Medical Center, 7th St. and Indian School Rd., Phoenix, AZ 85012). *Gastrointest Endosc* 37(3):315–318, 1991

Concern exists about perceived overuse of gastrointestinal endoscopic procedures. To determine the portion of the current practice of gastroenterology that is procedure related or purely cognitive, we compared 303 consultations from two practices. One-hundred and eighty-seven patients were in a Veterans Affairs Medical Center and 116 in a private group practice. Sixty-five percent of the consultations resulted in an endoscopic procedure. Patients referred for abnormal barium studies (100%), percutaneous endoscopic gastrostomy placement (97%), and gastrointestinal bleeding (83%) were most likely to have a procedure. Sixty-nine percent of consultations from medical specialties had endoscopy compared with 44% from surgical specialties and 45% from other specialties. There were no differences noted between the two practices. We conclude that gastroenterology is predominantly a procedure-oriented subspecialty. Procedures are performed most commonly on patients referred for conditions that are likely to require endoscopic biopsy or therapeutics and on patients referred from medical specialists.

Minute lesions of the rectum and sigmoid colon in patients with Crohn's disease. Okada M, Maeda K, Yao T, Iwashita A, Nomiyama Y, Kitahara K (MO, Dept. of Internal Medicine and Gastroenterology, Fukuoka University Chikushi Hospital, 377-1 Ohaza-Zokumyoin, Chikushino-shi, Fukuoka 818, Japan). *Gastrointest Endosc* 37(3):319–324, 1991

Sigmoidoscopy with a spray of 0.1% indigocarmine was performed on 20 patients with Crohn's disease whose main lesions were located proximal to the transverse colon and on 10 age-matched healthy volunteers. Minute lesions such as aphthoid lesions, areas of erythema, and small ulcers were found in 90% of patients with Crohn's disease and in 0% of healthy volunteers ($p < 0.001$). Among the minute lesions, aphthoid lesions were found in the highest incidence (85%). It was difficult to determine the presence of aphthoid lesions

without the spray of indigocarmine, which facilitated detection. Histologically, granulomas were found in 15% of patients with Crohn's disease. Aphthoid lesions were not associated with superficial erosions and lymphoid follicles. The presence of aphthoid lesions in the rectum and sigmoid colon would be a strong indication of the presence of Crohn's disease.

Endoscopic biopsy technique for acquiring larger mucosal samples. Levine DS, Reid BJ (DSL, Division of Gastroenterology RG-24, University of Washington, 1959 N.E. Pacific St., Seattle, WA 98195). *Gastrointest Endosc* 37(3):332–337, 1991

Biopsies of the esophagus, stomach, and intestine are most often obtained using the traditional advance-and-close method with flexible endoscopes by extending an open forceps several millimeters beyond the endoscope tip to sample the mucosa, all under direct vision. We developed an alternative "turn-and-suction" endoscopic biopsy technique that permits the acquisition of larger mucosal samples. The biopsy forceps is advanced into the lumen, opened, and withdrawn backward until it is flush with the endoscope tip. Next, the endoscope tip is turned gently into the wall while air is suctioned from the lumen, and the biopsy forceps is very slightly advanced and then closed, usually without direct visualization. After straightening the endoscope tip, the biopsy is obtained by withdrawing the forceps and avulsing a superficial mucosal sample. By using this new method, we have safely taken over 10,000 biopsies without complications in endoscopic surveillance research protocols in patients at risk for gastrointestinal cancer. To compare the sizes of biopsies obtained with these two techniques, histologic sections of 341 mucosal samples from 12 patients with chronic ulcerative colitis were studied retrospectively. The mean greatest length of biopsy sections using the traditional technique was 4.72 mm, and using our new technique was 7.35 mm (56% longer). The turn-and-suction endoscopic biopsy method is best applied when flat mucosa is randomly sampled to seek microscopic pathologic changes that are not visible endoscopically, and may be advantageous for various nonhistologic research analyses of gastrointestinal mucosa which are limited by tissue quantity.

Endoscopic ultrasound in pancreatic tumor diagnosis. Rösch T, Lorenz R, Braig C, et al. (TR, II Medizinische Klinik und Poliklinik der Technischen Universität, Klinikum Rechts der Isar Ismaningerstrasse 22, D-8000, Munich 80, Germany). *Gastrointest Endosc* 37(3):347–352, 1991

In a prospective study from 1988 to 1990, 132 patients with suspected pancreatic tumor were examined with endoscopic ultrasound (EUS), transabdominal ultrasound (US), computed tomography (CT), and ERCP. The final diagnosis of 102 pancreatic tumors of different origin (76 malignant and 26 inflammatory tumors) and the exclusion of a pancreatic tumor in 30 patients was made by operation (N = 47), puncture (N = 36), autopsy (N = 3), or follow-up of a mean of 51 weeks (N = 46). Sensitivity and specificity in pancreatic tumor diagnosis were significantly higher for EUS (99% and 100%) than for US (67%/40%) and CT (77%/53%) and equal to ERCP (sensitivity 90%). This was even more obvious in small pancreatic tumors of 3 cm and less. However, as with the other imaging procedures, EUS was not able to differentiate reliably malignant from inflammatory pancreatic masses (accuracy 76% for malignancy and 46% for focal inflammation). From analysis of the endosonographic pattern of pancreatic tumors, no consistent morphologic features were identified which could have been specifically attributed to malignant or inflammatory masses. Our results show that EUS is superior to US and CT and equal to ERCP in pancreatic tumor diagnosis. In contrast to the indirect evidence obtained by ERCP, EUS provides direct visualization of tumor size and shape in almost all patients examined. Thus, EUS should be considered early in the evaluation of patients with suspected pancreatic tumors.

Clinical Orthopaedics and Related Research

Fractures of the spine in diffuse idiopathic skeletal hyperostosis. Paley D, Schwartz M, Cooper P, Harris WR, Levine AM (AML, Section of Spinal Surgery, Division of Orthopedic Surgery, University of Maryland, 22 S. Greene St., Baltimore, MD 21201). *Clin Orthop* 267: 22–32, June 1991

Fractures of the spine in diffuse idiopathic skeletal hyperostosis (DISH) have rarely been reported. Only four cases could be found in the world literature. Eight new cases with nine fractures are reported in this study. The critical features are the frequent delays in diagnosis (three of eight patients) and the high rate of immediate and delayed neurologic deficit (seven of eight patients). Two fracture patterns occurred in this group. The first type occurred through the midportion of an ankylosed segment of the spine and involved the vertebral body (five fractures). The second type occurred at the top or bottom of a fused segment (four fractures). The latter were disk disruptions or odontoid fractures. This is a marked difference from spinal fractures in ankylosing spondylitis, in which the majority are transdiskal fractures. The difference can be explained on the basis of the different pathology of these two disease processes. Careful evaluation of patients with DISH who sustain trauma is critical. Treatment of this rare injury should be early stabilization of the spine to avoid complications of nonunion, deformity, neurologic injury, and death.

The Journal of Urology

A prospective study of urologist-performed sonographic evaluation of the urinary tract in patients with prostatism. Reisman EM, Kennedy TJ, Roehrborn CG, McConnell JD (EMR, Division of Urology, The University of Texas Southwestern Medical Center, Dallas, TX). *J Urol* 145:1186–1191, June 1991

In this study 171 consecutive patients hospitalized for prostatectomy were prospectively evaluated by urologist-performed transabdominal ultrasound. The urologist-sonographers were blinded to the results of an excretory urogram (IVP) performed and interpreted by radiologists. All significant upper tract pathology (4 renal cell carcinomas and 1 transitional cell carcinoma of the renal pelvis) identified by an IVP also was detected by ultrasonography. Of 5 clinically silent stones seen on an IVP 4 were identified by sonography. There were 13 patients (7.6%) with severe contrast medium allergies or renal failure who were readily evaluated with ultrasonography. Urologist-performed sonography can safely replace an IVP for routine evaluation of the urinary tract before prostatectomy. Moreover, sonography provided significant additional data on prostate size and post-void residual. However, the cost-effectiveness of upper tract imaging in patients before prostatectomy may be questioned.

Journal of Ultrasound in Medicine

Sonographic recognition of intraparenchymal regenerating nodules using high-frequency transducers in patients with cirrhosis. Giorgio A, Francica G, de Stefano G, Aloisio T, Pierri P, Amoroso P (AG, Viale Colli Aminei 491, 80131 Napoli, Italy). *J Ultrasound Med* 10:355–360, July 1991

In 38 patients with cirrhotic liver, an ultrasound examination was carried out by using 3/3.5-, 5-, and 7.5-MHz transducers sequentially in order to identify hypoechoic intraparenchymal regenerating nodules ≤20 mm. Twenty healthy subjects and 35 patients with noncirrhotic chronic liver disease were scanned as controls. Focal lesions were disclosed in five patients: one case turned out to be a small hepatocellular carcinoma; regenerating nodules were diagnosed as such in four cases by means of surgery,[1] laparoscopy,[1] and fine needle biopsy.[2] At a follow-up needle biopsy one year later, one of these nodules proved to be malignant. Use of high-frequency transducers offered little aid to the diagnosis of small nodules. In only one case were multiple lesions revealed with a 7.5-MHz probe but not with 3- and 5-MHz probes. It seems that intraparenchymal regenerating nodules are rarely seen with the available technology, and their recognition cannot be recommended as a reliable ultrasound diagnostic marker of liver cirrhosis.

Reprinted with permission by the American Institute of Ultrasound in Medicine.

News

Conference on Coronary Artery Disease

Saint Mary's Regional Medical Center is sponsoring Coronary Artery Disease: Current Concepts in Pathogenesis and Non-Invasive Diagnosis, Oct. 3, at Harrah's Hotel and Casino, Reno, NV. This half-day conference will focus on the latest technologies, practices, and questions relating to prevention, diagnosis, and treatment of coronary artery disease. Category 1 credit: 6 hr. Fee: $75. Information: Lisa Laughlin, Manager, Community Relations and Outreach, Saint Mary's Regional Medical Center, 235 W. 6th St., Reno, NV 89520-0108; (702) 789-3126.

Pittsburgh Conference on Interventional Radiology

The Western Pennsylvania Hospital, Pittsburgh, will present The Pittsburgh Conference: An International Symposium on Interventional Radiology, Oct. 4–6, at the Westin William Penn Hotel, Pittsburgh. The conference will cover the latest advances in interventional radiology, with emphasis on the newest techniques. Course directors: Harvey L. Neiman and Gordon K. McLean. Category 1 credit: 14.5 hr. Fee: physicians, $475; residents, fellows, and technologists, $295. Information: Dept. of Continuing Medical Education; The Western Pennsylvania Hospital, 4800 Friendship Ave., Pittsburgh, PA 15224; (412) 578-6926.

Yale Clinical MRI

The Dept. of Radiology, Yale University School of Medicine, will present Yale Clinical MRI, Oct. 21–23, at the Yale–New Haven Hospital MRI Center, New Haven, CT. Topics will include neurologic, musculoskeletal, and abdominal applications of MR imaging. Enrollment will be limited to 20 persons. Category 1 credit: 21.5 hr. Fee: physicians, $575; residents, fellows, and technologists, $400. Information: Office of Post-Graduate and Continuing Medical Education, Yale University School of Medicine, 333 Cedar St., P. O. Box 3333, New Haven, CT 06510; (203) 785-4578.

CT and MR Imaging of the Brain, Head, Neck, and Spine

The Dept. of Diagnostic Radiology, Rush–Presbyterian–St. Luke's Medical Center will present its 18th annual course on CT and MR imaging of the brain, head, neck, and spine, Oct. 24–25, at the Hyatt Suites Hotel, Chicago. Category 1 credit: 15 hr. Information: Michael S. Huckman, M.D., Rush–Presbyterian–St. Luke's Medical Center, 1653 W. Congress Parkway, Chicago, IL 60612; (312) 942-5781.

Nuclear Medicine Update

The Dept. of Radiology, Division of Nuclear Medicine, Emory University School of Medicine, will present Nuclear Medicine Update: Infection, Bone, Renal, Cardiac, Brain, Hepatobiliary, Endocrine, and Lung Imaging, with Emphasis on SPECT, Dec. 9–11, at the Ritz-Carlton Buckhead, Atlanta, GA. The course will include a review of several areas of clinical nuclear medicine and a presentation of recent developments in each. All clinical presentations will emphasize patient case material. Course directors: Naomi P. Alazraki, Ernest V. Garcia, and Andrew Taylor, Jr. Category 1 credit: 18.5 hr. Fee: $500. Information: Continuing Medical Education, Emory University School of Medicine, 1440 Clifton Rd., N.E., 111-A WHSCAB, Atlanta, GA 30322; telephone: (404) 727-5695; fax: (404) 727-5667.

Current Topics in Nuclear Medicine Technology

The Dept. of Radiology, Division of Nuclear Medicine, Emory University School of Medicine, will present Current Topics in Nuclear Medicine Technology, Dec. 11–13, at the J. W. Marriott at Lenox, Atlanta, GA. The course is designed to help nuclear medicine technologists develop a better understanding of (1) the clinical usefulness and technical aspects of new imaging agents (Sestamibi, Teboroxime, and MAG3) and new pharmacologic stress agents (dipyridamole and adenosine) and (2) the current role of the imaging procedures presented and the appropriate use of the methods in given clinical situations. Course directors: Donald B. Faulkner and James R. Galt. Continuing education credit: 1.5 CEUs or 15 contact hr; VOICE credits are pending. Fee: $325. Information: Continuing Medical Education, Emory University School of Medicine, 1440 Clifton Rd., N.E., 111-A WHSCAB, Atlanta, GA 30322; telephone: (404) 727-5695; fax: (404) 727-5667.

Park City 1992: MRI Update

The Dept. of Radiological Sciences, University of California, Los Angeles, is sponsoring the 3rd annual Park City 1992: MRI Update at the Sundance Film Festival, Jan. 25–29, 1992, at the Yarrow Hotel, Park City, UT. Program directors: Robert B. Lufkin and Wendy Smoker. Faculty: W. Bradley, R. Dietrich, R. Lufkin, W. Smoker, and L. Teresi. Category 1 credit: 20 hr. Fee: physicians, scientists, and company representatives, $445; nurses, technologists, and residents, $395. Information: Robert B. Lufkin, M.D., 12961 Mulholland Dr., Beverly Hills, CA 90210; (213) 825-7299.

Course on Positron Emission Tomography

The Division of Nuclear Medicine and Biophysics, University of California, Los Angeles, will present Positron Emission Tomography: Clinical Applications and Practical Considerations, Jan 26–29, 1992, at the Dana Point Resort, Dana Point, CA. Key topics to be covered include new clinical applications in cardiology, neurology, and oncology; image interpretation; reimbursement and costs; competing clinical techniques (e.g., positron emission tomography [PET], single-photon emission CT, MR imaging); and lowering health care with PET. Fee: physicians (through/after Dec. 23, 1991), $495/$595; fellows, residents, and technologists, $395. Information: Wendy Hagar, UCLA Postgraduate PET Course, Nuclear Medicine B2-086 CHS, 10833 Le Conte Ave., Los Angeles, CA 90024-1721; (213) 825-2724.

Society of Gastrointestinal Radiologists Annual Meeting

The Society of Gastrointestinal Radiologists will hold its 21st annual meeting and postgraduate course Feb. 16–21, 1992, at the Hyatt Regency Grand Cypress, Orlando, FL. Information: Lynne K. Tiras, CMP, International Meeting Managers, Inc., 4550 Post Oak Pl., Ste. 248, Houston, TX 77027; telephone: (713) 965-0566; fax: (713) 960-0488.

Advanced Clinical Magnetic Resonance Imaging

Harvard Medical School is sponsoring Advanced Clinical Magnetic Resonance Imaging, Feb. 17–21, 1992, at the Hyatt Regency Waikoloa Resort Hotel, Hawaii. The course will be presented by faculty from Brigham and Women's Hospital; Massachusetts General Hospital; Beth Israel Hospital; and Keio University, Tokyo, Japan. Key topics to be covered include fast spin-echo, echoplanar, three-dimensional, interventional, and cardiac MR imaging; advances in mid-field imaging; diffusion and perfusion; MR angiography; and turboflash imaging. Program director: Ferenc A. Jolesz. Category 1 credit: 20 hr. Fee: $650. Information: Harvard Med-CME, P. O. Box 825, Boston, MA 02117; (617) 432-1525.

MR Angiography and Imaging of the Head, Spine, and Musculoskeletal System

The Medical College of Wisconsin is offering MR Angiography and Imaging of the Head, Spine, and Musculoskeletal System, the sixth course in the series MRI Update 1992, Feb. 17–21, 1992, at the Westin La Paloma Resort, Tucson, AZ. The course will cover both basic concepts and current applications of MR. Program chairmen: Victor Haughton, Robert Quencer, Thomas Naidich, and Joachim Seeger. Category 1 credit: 25 hr. Fee: through Dec. 31, 1991, $495; after Dec. 31, 1991, $545. Information: Marti Carter, Course Coordinator, Continuing Medical Education, Inc., 11011 W. North Ave., Milwaukee, WI 53226; (414) 771-9520.

Sun Valley Imaging Meeting

The 8th annual Sun Valley Imaging Meeting will be held Feb. 23–29, 1992, at the Sun Valley Lodge, Sun Valley, ID. The course will review important aspects and the latest developments in body imaging and intervention. Speakers: P. L. Cooperberg, W. R. Lees, E. A. Lyons, A. Megibow, B. McClennan, N. Muller, and R. Filly. Category 1 credit: 20 hr. Fee: $515. Information: Diane Robert, Dept. of Radiology, St. Paul's Hospital, 1081 Burrard St., Vancouver, B.C., Canada V6Z 1Y6; telephone: (604) 631-5026; fax: (604) 631-5283.

AFIP Neuroradiology Review Course

The Armed Forces Institute of Pathology (AFIP), the American Registry of Pathology, and the American College of Radiology are sponsoring the 7th annual AFIP Neuroradiology Review Course, Feb. 29–March 1, 1992, at the Hyatt Regency Bethesda, Bethesda, MD. The purpose of the course is to review basic concepts in neuroradiology, with an emphasis on pathologic correlation and pathophysiology. As before, the course will immediately precede the annual AFIP Neuropathology Course, which will be held at the same hotel and will begin on March 2, 1992. Course directors: James G. Smirniotopoulos and Frances M. Murphy. Category 1 credit: 13 hr. Information: Education Division, Armed Forces Institute of Pathology, Washington, DC 20306-6000; (301) 427-5620.

The American Board of Radiology Examinations

Written examinations for the American Board of Radiology (ABR) are scheduled for Oct. 3–4, 1991; Oct. 1–2, 1992; and Oct. 14–15, 1993. Oral examinations will be held at the Executive West Hotel in Louisville, KY, June 1–5, 1992. The ABR will accept applications for admission to the examinations after July 1, but not later than Sept. 30, in the year *preceding* the year in which the examination is to be taken. For application forms and further information: Office of the Executive Director, The American Board of Radiology, 2301 W. Big Beaver Rd., Ste. 625, Troy, MI 48084.

Meeting and Course Review

For the reader's convenience, a summary of upcoming meetings and courses is provided. Detailed listings are given in the *AJR* issue given in parentheses.

Swallowing Center Preceptorship, times arranged, Baltimore (Jan)
Imaging Fellowship, times arranged, Miami Beach, FL (Jan)
Preceptorships in Ultrasound at Johns Hopkins, times arranged, Baltimore (June)
Practicum in Breast Imaging, times arranged, Baltimore (Aug)
International Imaging Course, Sept. 30–Oct. 5, Hong Kong (July)
Magnetic Resonance Imaging 1991: Back to the Future, Oct. 2–5, Cincinnati (July)
Current Concepts of Magnetic Resonance Imaging/Physics, Oct. 3–6, Napa Valley, CA (Aug)
Registry Preparation Courses for Sonographers: Ultrasound and Doppler Physics, Oct. 5–6, Dallas (July)
Tutorial in Portugal, Oct. 5–10, Estoril, Portugal (Sept)
Annual International Body Imaging Congress, Oct. 5–12, Maui, HI (June)
Breast Cancer Diagnosis: State-of-the-Art, Oct. 7–8, New York City (July)
MR Imaging Fellowships at LAC/USC Imaging Science Center, Oct. 7–11 and Nov. 4–8, Los Angeles (Feb)
Practical Training in Interventional Radiology, Oct. 7–11 and Nov. 4–8, Lund, Sweden (July)
MRI Visiting Fellowships at UCLA, Oct. 7–11, 1991; Dec. 9–13, 1991; Feb. 3–7, 1992; March 9–13, 1992; April 6–10, 1992; Sept. 14–18, 1992; Oct. 5–9, 1992; and Dec. 7–11, 1992; Los Angeles (Sept)
MR Update: NR and Musculoskeletal, Oct. 7–12, Hilton Head, SC (Aug)

Nuclear Cardiology Symposium and Workshops, Oct. 9–11, Milwaukee, WI (Aug)
MRI: Clinical State of the Art 1991, Oct. 9–12, New York City (July)
Ultrasound: 1991, Oct. 12–13, Sacramento, CA (Aug)
MR Angiography and MR Imaging of the Cardiovascular System: angiography workshop, Oct. 13, L'Aquila, Italy; cardiovascular symposium, Oct. 14–16, Rome (Sept)
Radiology/91: Cardiovascular and Interventional Radiology, Oct. 14–18, Minneapolis (Sept)
Chest Imaging, Oct. 15–18, Boston (Aug)
Mammography Update 1991, Oct. 17–18, Madison, WI (Aug)
Western Neuroradiological Society Annual Meeting, Oct. 17–20, Laguna Niguel, CA (June)
Michigan Fall Radiology Conference, Oct. 18–19, Royal Oak, MI (Aug)
Progress in Magnetic Resonance Imaging, Oct. 24–25, Cologne, Germany (June)
Neuroradiologic and Musculoskeletal Seminars, Oct. 24–27, Orlando, FL (June)
Advanced Imaging of the Musculoskeletal System, Oct. 26–27, Coronado (San Diego), CA (June)
New Orleans Fall Radiology Conference, Oct. 28–30, New Orleans (Sept).
Mammographic Interpretation: A Practical Approach, Oct. 28–31, Boston (March)
San Diego Postgraduate Radiology Course, Oct. 28–Nov. 1, Coronado (San Diego), CA (June)
Magnetic Resonance Imaging and CT Update, Oct. 28–Nov. 1, Cambridge, MA (Aug)
Interventional Radiology Course, Nov. 1–3, Coronado (San Diego), CA (July)
Computed Body Tomography for the Technologist, Nov. 7–10, Orlando, FL (Sept)
Seminar on Bone and Joint Diseases, Nov. 15–17, Scottsdale, AZ (July)
Advanced Seminars in Diagnostic Imaging, Nov. 15–17, Laguna Niguel, CA (Aug)
Diagnosis and Treatment of Bone and Soft-Tissue Tumors, Nov. 21–23, Sacramento, CA (May)
Asian Oceanian Congress of Radiology, Dec. 14–18, New Delhi (July)
CT/MRI Head to Toe, Dec. 15–20, New York City (Sept)
Caribbean Cruise—Breast Imaging and MRI at Sea: breast imaging, Jan. 11–18, 1992; MR imaging, Jan. 18–25, 1992 (Sept)
Uroradiology 1992, Jan. 13–17, 1992, Scottsdale, AZ (Sept)
Diagnostic Imaging in Puerto Rico, Jan. 26–31, 1992, Cerromar Beach Hotel, Puerto Rico (Sept)
International Symposium on Recent Advances in Diagnostic Imaging and Radiation Oncology, March 24–27, 1992, Kathmandu, Nepal (June)
European Symposium on Uroradiology, Aug. 24–27, 1992, Herlev, Denmark (Aug)

AJR carries announcements of courses, symposia, and meetings of interest to its readers if received a minimum of 5 months before the event. There is no charge; receipt of items by the *AJR* Editorial Office is not acknowledged. Submit items for publication typed double-spaced. Provide title, date, location, brief description, sponsor, course directors, fees, category I credit, and address and telephone number for additional information. Faculty from the host institution will not be listed. Guest faculty names will appear **only** if initials are provided. Mail news items to *AJR* Editorial Office, 2223 Avenida de la Playa, Suite 103, La Jolla, CA 92037-3218.

ERRATUM

The name of the fifth author of the article "Radiocontrast-associated renal dysfunction: a comparison of lower-osmolality and conventional high-osmolality contrast media," *AJR* July 157:59–65, was misspelled. The correct spelling is Nogah Haramati. We regret this error.

American Roentgen Ray Society 92nd Annual Meeting May 10–15, 1992, Orlando, FL Marriott's Orlando World Center

Registration and Hotel Reservations

Forms for advance registration and hotel reservations will be in the February and March 1992 issues of the *AJR*.

Scientific Program

Abstracts of papers to be considered for the program must be submitted by November 1, 1991. Forms on which to submit abstracts are in this issue of the *AJR*. The ARRS Program Committee will select papers and notify authors in early January. The *AJR* has first rights to all papers accepted for presentation at the ARRS meeting. Mail original and five copies to

A. Everette James, Jr., M.D.
c/o Paul Fullagar
American Roentgen Ray Society
1891 Preston White Drive
Reston, VA 22091
Telephone (703) 648-8992

Scientific Exhibits

Proposals for scientific exhibits must reach the Chairman of Exhibits by November 1, 1991. Forms, which may be photocopied, are in this issue of the *AJR*. Send completed form to

N. Reed Dunnick, M.D.
c/o Paul Fullagar
American Roentgen Ray Society
1891 Preston White Drive
Reston, VA 22091
Telephone (703) 648-8992

Refresher Course Program

A summary of the refresher courses will appear in the *AJR* in February along with advance registration forms. Early registration is an advantage in ensuring preferred courses in this popular program.

Local Program

A program of sightseeing, shopping, and entertainment will be developed by the Local Arrangements Chairman. Information and advance registration forms will be in the February issue of the *AJR*.

Residents' Award Papers

The society offers several cash awards for the best scientific papers prepared by residents in radiology. The President's Award has a $2000 prize. There are two Executive Council awards of $1000 each. All are presented at the annual meeting. Papers should be submitted by February 15, 1992, for consideration in this competition. Send entries to

Nancy O. Whitley, M.D.
Dept. of Radiology
University of Maryland Medical Systems Hospital
22 S. Greene St.
Baltimore, MD 21201

Deadlines

Abstracts of papers: November 1, 1991
Scientific exhibit proposals: November 1, 1991
Residents' Award papers: February 14, 1992

Call for Papers

American Roentgen Ray Society 1992 Annual Meeting: May 10–15, 1992, Orlando, FL

ADDRESS OF PRESENTING AUTHOR

Department

Institution

Street

City, State Zip

Phone:

Type title, authors, and abstract in the space provided below. (Instructions are on reverse side of this page. Abstract should not exceed 300 words.)

Select one category: ____Angio/Interventional ____Breast ____Chest ____CT ____Gastrointestinal Tract ____Genitourinary Tract ____MR ____Neuroradiology ____Skeletal ____Sonography ____Pediatric

Projection Requirements: ____35 mm, single or double (circle one) ____16 mm silent film ____½''VHS ____¾''

Has this been presented elsewhere? ____yes ____no. If yes, please describe on reverse side of this page.

Instructions for Scientific Abstracts

1. Type the information single-spaced. Underline the name of the presenting author. Append as a last line of the abstract any research grant support, if applicable (e.g., Supported by USPHS Grant HE-80144). If the abstract is accepted, it will not be proofread; it will appear exactly as typed. Use the following format:

   MR IMAGING OF THE SPINE AND NECK
   F. S. Lau, M.D., A. N. Kirk, M.D., and R. A. Beck, Ph.D.
   University of California, Bakersfield, Bakersfield, CA 92338

2. Abstracts should include four paragraphs devoted sequentially to the following topics: (1) object or purpose of the study, (2) materials, methods, and procedures, (3) results, (4) significance of the results and conclusions. The text should not exceed 300 words. Specific data are essential. The abstract should be a succinct summary of work done rather than a promissory note.
3. The Program Committee will grade each abstract and determine acceptance. Further information will be forwarded to those whose abstracts are accepted for presentation.

Deadline for submission of abstract is November 1, 1991. Mail abstract and four copies to

A. Everette James, Jr., M.D.
c/o Paul R. Fullagar
American Roentgen Ray Society
1891 Preston White Dr.
Reston, VA 22091
Telephone (703) 648-8992

Call for Scientific Exhibits

American Roentgen Ray Society 1992 Annual Meeting: May 10–15, 1992, Orlando, FL

FOR COMMITTEE USE ONLY

Date Received_____ Application No. _____
Subject_____ Score_____
Rejected_____ Accepted_____
Assigned_____ Space No. _____

Principal Exhibitor's Mailing Address

Name_____ Institution_____

Department_____ Street Address_____ City_____

State_____ Zip Code_____ Telephone: office ( ) _____ home ( ) _____

Names of Exhibitors (List principal exhibitor first and telephone number of each person.)

Last	First	Middle	Telephone	Degree (one only)	Member ARRS?

Title of Exhibit_____

Type abstract single-spaced in the space provided below. (See instructions on the reverse side of this page.)

Instructions for Abstract

The abstract should be a brief paragraph that states the purpose, principal information, and conclusions of the exhibit. Promissory statements are not acceptable. Type single-spaced in the space provided on the reverse side. Brevity is desirable but not at the expense of specific information. **The abstract will appear in the program book as submitted.** Please use typewriter and complete the application form on both sides. List space requirements.

What Type of Exhibit Is Proposed? (Check one and fill in all appropriate blanks.)

_____**Free-standing.** This is a self-contained display created in total by the exhibitor. It may be a fold-open unit, a unit shipped in cases and assembled on site, or a tabletop unit. Linear feet required _____.

_____**Poster Board (backboard panels).** Backboard panels are 4 × 8 ft. (1.2 × 2.5 m). Number of panels required _____. If two panels are needed, there will be a ¼-in. frame separating the panels, thus requiring a separation in the presentation.

_____**Viewbox.** Mounted materials (radiographs and other transparencies) for display on the society's illuminators. Each illuminator is 39.5 × 59.5 in. (100 × 151 cm). Number of illuminators required _____. Materials should not be glass mounted.

Please Indicate Most Appropriate Category.

_____Bone _____Cardiovascular _____Chest_____Gastrointestinal_____Genitourinary _____Breast _____Medical physics
_____Neuroradiology _____Nuclear medicine _____Pediatric_____Radiation oncology_____Sonography

Exhibits will be chosen on the basis of the quality of the abstract and space available. Poster board and computer-based exhibits are encouraged, as they do not require a viewbox.

Signature of Principal Exhibitor_____

Exhibitors will receive instructions for exhibit preparation.

Applications must be received no later than November 1, 1991. Mail original and five copes to

N. Reed Dunnick, M.D.
c/o Paul R. Fullagar
American Roentgen Ray Society
1891 Preston White Dr.
Reston, VA 22091

Telephone: (703) 648-8992

American Roentgen Ray Society:
Officers, Committees, and Membership Information

Officers

President: John A. Kirkpatrick, Jr.
President-elect: A. Everette James, Jr.
1st Vice-president: Andrew K. Poznanski
2nd Vice-president: George R. Leopold
Secretary: Joseph T. Ferrucci, Jr.
Treasurer: Beverly P. Wood

Executive Council: R. N. Berk, M. P. Capp, W. J. Casarella, N. R. Dunnick, R. G. Evens, J. T. Ferrucci, Jr., A. E. James, Jr., J. A. Kirkpatrick, Jr., A. M. Landry, Jr., G. R. Leopold, J. E. Madewell, T. C. McLoud, A. A. Moss, A. K. Poznanski, R. J. Stanley, J. H. Thrall, K. H. Vydareny, N. O. Whitley, B. P. Wood, R. J. Alfidi, chairman

Committees

Editorial Policy: R. N. Berk, E. Buonocore, Melvin M. Figley, C. R. B. Merritt, K. Valji, C. A. Rohrmann, Jr., W. J. Casarella, chairman

Education and Research: R. R. Hattery, C. B. Higgins, B. J. Hillman, R. J. Stanley, W. M. Thompson, N. O. Whitley, chairman

Finance and Budget: R. K. Gedgaudas-McClees, A. A. Moss, J. R. Thornbury, K. H. Vydareny, J. H. Thrall, chairman

Nominating: R. G. Evens, P. J. Fritzsche, A. A. Moss, chairman

Publications: E. Buonocore, C. R. B. Merritt, C. A. Rohrmann, Jr., W. J. Casarella, chairman

Membership: J. E. Madewell, T. C. McLoud, A. A. Moss, K. H. Vydareny, chairman

Representatives to Other Organizations

American Board of Radiology: W. J. Casarella, J. A. Kirkpatrick, Jr., L. F. Rogers

American College of Radiology: R. A. Gagliardi, J. E. Madewell, B. L. McClennan, R. J. Stanley

American Medical Association: S. F. Ochsner, delegate; K. L. Krabbenhoft, alternate; K. L. Kidd, CPT Advisory Committee

American National Standards Institute: M. E. Haskin

National Council on Radiation Protection and Measurements: F. D. Miraldi, E. L. Saenger

Armed Forces Institute of Pathology: J. E. Madewell

Meeting Arrangements

Annual Meetings: May 10–15, 1992, Marriott's World Center, Orlando, FL; April 25–30, 1993, Marriott San Francisco, San Franciso, CA

Annual Meeting Committee: J. K. Crowe, N. R. Dunnick, R. R. Lukin, N. H. Messinger, R. J. Stanley, R. D. Steele, Jr., A. M. Landry, Jr., chairman

Instructional Courses: Bruce L. McClennan, associate chairman; R. J. Stanley, chairman

Scientific Program: P. H. Arger, T. B. Hunter, D. Kushner, T. C. McLoud, L. B. Talner, J. H. Thrall, A. E. James, Jr., chairman

Scientific Exhibits: J. R. Haaga, D. S. Hartman, R. G. Ramsey, N. R. Dunnick, chairman

ARRS Membership

An application form is printed in the August issue of the Journal. For consideration at the 1992 ARRS meeting, send completed forms before February 1, 1992, to American Roentgen Ray Society, 1891 Preston White Dr., Reston, VA 22091. Active members are graduates of an approved medical or osteopathic school or hold an advanced degree in an allied science. They must practice radiology or work in an associated science in the United States or Canada and be certified by the American Board of Radiology, American Osteopathic Board of Radiology, or Royal College of Physicians of Canada or otherwise adequately document training and credentials. International members are foreign radiologists or scientists who are active in radiology or an allied science. Members-in-training are residents or fellows in radiology or postgraduate students in an allied science. Additional application forms can be obtained from the ARRS offices in Reston, VA.

Business Office

Paul Fullagar, Executive Director, American Roentgen Ray Society, 1891 Preston White Dr., Reston, VA 22091; (703) 648-8992.

Classified Advertisements

Positions Available

RADIOLOGIST/CARDIOVASCULAR/INTERVENTIONAL RADIOLOGY—The Dept. of Radiology at the University of Minnesota has a full-time position available in the cardiovascular/interventional radiology section at the rank of tenure-track assistant professor beginning as soon as possible. At the assistant professor level, minimum requirements are board-certification in radiology, a minimum of 1 yr postresidency specialty training in cardiovascular/nonvascular interventional radiology, and a demonstrated involvement in quality research accepted or published in peer-reviewed journals. Responsibilities will include all facets of cardiovascular/interventional radiology as well as graduate and undergraduate medical instruction. Research performance will be strongly encouraged and evaluated. Salary is negotiable and competitive and is dependent on past scholarly productivity and post-M.D. experience. Applicants must be licensed or able to obtain a license to practice medicine in the state of Minnesota before appointment date. Applications will be accepted through Oct. 31, 1991. Send letters to William M. Thompson, M.D., Professor and Chairman, Dept. of Radiology (Box 292 UMHC), University of Minnesota, 420 Delaware St., S.E., Minneapolis, MN 55455. The University of Minnesota is an equal opportunity educator and employer. 10a

A MULTISPECIALTY MEDICAL GROUP has an immediate need for a radiologist. Excellent benefit package, guaranteed salary with incentive, all expenses paid first yr, with partnership opportunity for the future. Direct inquiries or send CV to Penny Phillips, Malone and Hogan Clinic, 1501 W. 11th Pl., Big Spring, TX 79720; (915) 267-6361. 10–3a

INTERVENTIONAL RADIOLOGIST—Well-established community hospital and imaging center–based practice in New York capitol district seeks fellowship-trained interventional radiologist. Individual should have expertise and interest in all aspects of interventional radiology including thrombolytic therapy. Ultramodern-equipped practice with state-of-the-art new biplane angiography suite. Practice emphasizes subspecialty expertise in all aspects of diagnostic imaging, performing 100,000 exams/yr. Excellent compensation package leading to lucrative full partnership. Send CV to Michael E. Berlow, M.D., Dept. of Medical Imaging, Albany Memorial Hospital, 600 Northern Blvd., Albany, NY 12204. 10–11ap

NEURO/INTERVENTIONAL RADIOLOGIST The College of Physicians and Surgeons of Columbia University is searching for a junior or senior staff radiologist for neuro/interventional radiology. Salary and academic rank will be commensurate with experience and qualifications. Responsibilities include patient care, teaching, and supervising residents for junior staff level. In addition, research and demonstrated academic ability are required for senior staff level. Requirements include board-eligibility or certification and at least 2 yr of interventional experience for senior staff level. New York state medical license required; narcotics license desirable. Please send resume to Philip O. Alderson, M.D., Dept. of Radiology, 622 W. 168th St., New York, NY 10032. Columbia University is an affirmative action/equal opportunity employer. 10ap

NEURO/GENERAL RADIOLOGIST—Exceptional private-practice opportunity created by involuntary departure of neuroradiologist. 350-bed community hospital with all modalities including 1.5-T MRI and new DSA. Full benefits, 1 yr to partnership, excellent salary, and liberal time off. Contact John Lacika, M.D., 1406 N. 6th Ave., St. Cloud, MN 56303; (612) 255-5619. 10–12ap

NEURORADIOLOGIST—Well-established community hospital and imaging center–based practice in Albany, NY, seeks fellowship-trained neuroradiologist. Applicants should have expertise and interest in all aspects of neuroradiology with particular emphasis on MRI. Interests in other aspects of radiology, particularly cross-sectional imaging, desirable. Ultramodern-equipped practice including 2 high-field Siemens MRI units and MRA capability, new biplane angiography suite, and 2 Siemens CT scanners. Practice emphasizes subspecialty expertise in all aspects of diagnostic imaging, performing 100,000 exams/yr. Capitol district community with abundant cultural, recreational, and educational opportunities. Excellent compensation package leading to lucrative full partnership. Send CV to Michael E. Berlow, M.D., Dept. of Medical Imaging, Albany Memorial Hospital, 600 Northern Blvd., Albany, NY 12204. 10–11ap

CALIFORNIA CENTRAL COAST—Established group has an opening for a general radiologist skilled in angiography, CT, MRI, and ultrasound to practice in 2 community hospitals, an MRI center, and a multispecialty clinic. Pediatric radiology experience a plus. Competitive compensation with opportunity for advancement to full partner. This is an excellent opportunity to join an expanding practice in a beautiful community along California's central coast. Please contact Managing Partner, Radiology Associates of SLO, P. O. Box 8129, San Luis Obispo, CA 93403-8129. 10–11ap

LARGE, DYNAMIC RADIOLOGY PRACTICE in central New Jersey and adjacent Pennsylvania region seeks diagnostic radiologist with expertise in 1 or more of the following: CT/ultrasound, angio/interventional, or nuclear medicine with cardiac emphasis. Outstanding opportunity for well-qualified person. Send resume to E. Tarasov, M.D., 838 W. State St., Trenton, NJ 08618. 10–12a

NORTHWEST ROCKY MOUNTAINS—Highly respected, 8 person group with strong subspecialty interests seeks highly qualified radiologist. Fellowship or academic experience preferred. Body imaging/MRI, nuclear medicine with boards, or ABR special competency strongly desired. Position includes all aspects of radiology. Practice is located in Boise, ID, which has many recreational and cultural amenities. Reply to Paul Traughber, M.D., or J. Tim Hall, M.D., Dept. of Radiology, St. Alphonsus Regional Medical Center, 1055 N. Curtis Rd., Boise, ID 83706; (208) 378-2161. 10–1ap

FLORIDA, BE/BC DIAGNOSTIC RADIOLOGIST needed to join group in the Orlando area. Will cover 2 hospitals and 1 outpatient clinic. Interventional or neuroradiology a plus. For more information, call or send your CV to Dee Dee Ralston, HealthTrust, Inc., 4525 Harding Rd., Nashville, TN 37205; (800) 825-3463 (24 hr). 10ap

RADIOLOGISTS—Vacancies exist for board-certified/eligible radiologists, including chief of the radiology service, at this 473-bed medical center with a 180-bed nursing home care unit. We are affiliated with Temple University and Hahnemann University School of Medicine, Episcopal Hospital, Philadelphia, PA, and have active residency programs. We offer an attractive wage and bonus, paid malpractice insurance, vacation/sick leave, health/life insurance, and retirement package including tax-deferred savings plan. Wilkes-Barre, located near Pocono Mountain resort areas and a 2-1/2 hr drive to New York City and Philadelphia, offers an unprecedented selection of cultural activities, educational institutions, and a variety of affordable residential areas. Contact William K. Grossman, M.D., Chief of Staff, VAMC, 1111 East End Blvd., Wilkes-Barre, PA 18711; (717) 824-3521, ext. 7207. EOE. 10a

STAFF RADIOLOGISTS—The College of Physicians and Surgeons of Columbia University is searching for junior or senior staff radiologists with a subspecialty interest in chest radiology to begin July 1992 or earlier. Salary and academic rank will be commensurate with experience and qualifications. Responsibilities include patient care, teaching, and supervising residents for junior staff level, and include research for senior staff level. Requirements include board-eligibility or certification in diagnostic radiology, completion of an accredited radiology residency for instructor level, and at least 1 yr experience or completion of a fellowship in chest radiology with demonstrated academic ability for more senior staff levels. New York state medical license required; narcotics license desirable. Please send resume to Philip O. Alderson, M.D., Dept. of Radiology, 622 W. 168th St., New York, NY 10032. Columbia University is an affirmative action/equal opportunity employer. 10ap

GENERAL/INTERVENTIONAL RADIOLOGISTS The College of Physicians and Surgeons of Columbia University is searching for junior and senior staff radiologists at our Allen Pavilion division to do general radiology and to perform interventional procedures part-time (e.g., stent placements, biopsies, tube checks, and pulmonary or peripheral angiograms). Salary and academic rank will be commensurate with experience and qualifications. Responsibilities include patient care, teaching, and supervising residents. Requirements include board-eligibility or certification in diagnostic radiology for junior staff level; board-certification and at least 2 yr of experience for more senior staff levels. New York state medical license required; narcotics license desirable. Please send resume to Philip O. Alderson, M.D., Dept. of Radiology, 622 W. 168th St., New York, NY 10032. Columbia University is an affirmative action/equal opportunity employer. 10ap

THE DEPT. OF RADIOLOGY OF THE CHILREN'S MEMORIAL HOSPITAL, CHICAGO, is seeking a third pediatric neuroradiologist. The Division of Neuroradiology has 3 positions including the director. There is 1 fellowship position per yr as well as a fellow rotating from Northwestern Memorial Hospital. The dept. has an active clinical service with state-of-the-art equipment as follows: 2 CT scanners (a GE 9800 Quick CT scanner, and a Philips LX), a 1.5-T GE Signa MRI, Acuson ultrasound units, and Siemens Angiostar with biplane digital imaging. Applicants must be certified by the American Board of Radiology and have completed a fellowship in neuroradiology. Duties include clinical services, teaching, and research. The institution has very active neurosurgery and neurology services with 4 full-time neurosurgeons. The Children's Memorial Hospital is affiliated with Northwestern University Medical School, and the candidate selected would have an appointment in the Dept. of Radiology at Northwestern University. Please send CV to Andrew K. Poznanski, M.D., Radiologist-in-Chief, Children's Memorial Hospital, 2300 Children's Plaza, Chicago, IL 60614. For inquiries, please call (312) 880-3520. Children's Memorial Hospital and Northwestern University are affirmative action/equal opportunity employers. Hiring is contingent on medical licensure in Illinois. 10–11a

OPENING FOR BC/BE RADIOLOGIST with cross-sectional imaging (MRI/CT/ultrasound) fellowship or equivalent experience to join 8-member hospital-based group in Pensacola, FL. Position open Jan. 1992 (possible to hold open until July 1992). Teaching involved. 380-bed hospital/100,000+ procedures/yr. Send CV to Harry Cramer, M.D., P.O. Box 9210, Pensacola, FL 32513-9210. 10–1ap

BODY IMAGING FACULTY POSITION—The Dept. of Radiology at the Albany Medical College is recruiting for a board-certified radiologist in the section of body imaging. This section is responsible for body MRI (2 high-field units), CT (3 GE), and ultrasound (4 Acuson with color Doppler capability). Some general body imaging is also performed. Candidates should have some interest in the newer cross-sectional modalities, but responsibilities are flexible. A new, financially secure Dept. of Radiology and new hospital have recently been completed. Albany Medical College is a private institution situated in northeastern New York with a significantly high quality of life. It is adjacent to the Saratoga–Lake George area, the Berkshires (Tanglewood), and the Adirondack and Catskill Mountains. All interested parties should contact Matthew D. Rifkin, M.D., Professor and Chairman, Dept. of Radiology, Albany Medical Center, Albany, NY 12208; (518) 445-3277. 10a

ANGIOGRAPHER FACULTY POSITION—The Dept. of Radiology at the Albany Medical College is searching for a board-certified radiologist for its cardiovascular and interventional radiology section. Academic and hospital appointment, from assistant to full professor, will be commensurate with qualifications. A new hospital and financially secure radiology dept. have just been completed. The CVIR section is an active, dynamic part of the Dept. of Radiology presently engaged in all aspects of interventional techniques. Albany Medical College is a private institution situated in northeastern New York with a significantly high quality of life. It is adjacent to the Saratoga–Lake George area, the Berkshires (Tanglewood), and the Adirondack and Catskill Mountains. All interested parties should contact Matthew D. Rifkin, M.D., Professor and Chairman, Dept. of Radiology, Albany Medical College, Albany, NY 12208; (518) 445-3277. 10a

DIAGNOSTIC RADIOLOGISTS, FULL-TIME OR LOCUM TENENS, ALASKA AND GEORGIA Managed Health Care, Ltd., operates radiology services at military hospitals throughout the U.S. and is currently seeking radiologists at Ft. Wainwright, Fairbanks, AK, and Ft. Benning, Columbus, GA. The position at Ft. Wainwright offers a full-time, $210,000 compensation package or locum tenens $750/day. Board certification is required. The position at Ft. Benning offers a full-time, $185,000 compensation or locum tenens $700/day. Board eligibility or certification is required. Positions are immediate. Licensure required in 1 of the 50 states to qualify. Please call collect for further information. David A. Descoteau, Managed Health Care, Ltd., 6140 Scarborough Way, Columbia, MD 21044; (301) 992-1443. 10ap

STAFF RADIOLOGISTS—The College of Physicians and Surgeons of Columbia University is searching for junior and senior general diagnostic radiologists at our Allen Pavilion division with special interest and/or expertise in all aspects of abdominal imaging (genitourinary, gastrointestinal, and ultrasound/CT). Interventional experience (e.g., abscess drainage, percutaneous biopsy) desirable but not required. Salary and academic rank will be commensurate with experience and qualifications. Responsibilities include patient care, teaching, and supervising residents. Requirements include board-eligibility or certification in diagnostic radiology and completion of an accredited radiology residency for junior staff level; at least 1 yr experience or fellowship in abdominal imaging for senior staff level. New York state medical license required; narcotics license desirable. Please send resume to Philip O. Alderson, M.D., Dept. of Radiology, 622 W. 168th St., New York, NY 10032. Columbia University is an affirmative action/equal opportunity employer. 10ap

PEDIATRIC RADIOLOGIST—A full-time faculty position, Dept. of Radiology, Children's Hospital Medical Center, Cincinnati, OH, at academic rank of assistant professor to professor, Dept. of Radiology and Pediatrics, University of Cincinnati College of Medicine, is available Jan 1, 1992. Salary and fringe benefits are highly competitive; salary is based on academic rank and experience. Candidates must be certified in diagnostic radiology by the American Board of Radiology or its equivalent, must have completed a fellowship in pediatric radiology, and must be eligible for active membership in the Society for Pediatric Radiology. Duties include clinical service, teaching, and research. Professional coverage includes conventional radiography, ultrasonography, CT, MRI, nuclear medicine, vascular/interventional, and digital radiography. The candidate must have a demonstrated interest and qualifications in basic and/or clinical pediatric imaging research. Children's Hospital Medical Center and University of Cincinnati are affirmative action/equal opportunity employers. Address inquiry and CV to Donald R. Kirks, M.D., Director, Dept. of Radiology, Children's Hospital Medical Center, Cincinnati, OH 45229-2899; (513) 559-8058. 10ap

DIAGNOSTIC RADIOLOGIST—A 5-person group seeks a BC/BE diagnostic radiologist. MRI available. Located in northwest Indiana (greater Chicago metropolitan area). 80,000 diagnostic imaging procedures/yr. Excellent compensation commensurate with qualifications. Reply to Box P80, *AJR* (see address this section). 10–11ap

NORTHERN CALIFORNIA—The Permanente Medical Group, Inc., is seeking a BC radiologist with multimodality interests and fellowship training in MR to join a 12-person group serving a 337-bed, acute-care hospital and 2 outpatient clinics. Teaching opportunities are available with residents of subspecialty services on rotation from Stanford University Hospital, as well as our own medical residents. We have sited a GE 1.5-T MRI system. Competitive salary and excellent benefits. Please send inquiries and CV to Bruce Baker, M.D., Chief, Dept. of Radiology, Kaiser Permanente Medical Center, 900 Kiely Blvd., Santa Clara, CA 95051; (408) 236-4444. EOE. 9–11a

COASTAL NORTHERN CALIFORNIA/SAN FRANCISCO BAY AREA—A progressive, diversified group of 16 board-certified diagnostic radiologists, 5 radiation oncologists, and 2 medical oncologists seeks a board-eligible/certified radiologist with some training in MRI and/or neuroradiology. The group serves 4 small- to medium-sized hospitals and a large, outpatient imaging center. The imaging center includes a GE 1.5-T MRI, 9800 Advantage CT, and Acuson ultrasound, as well as CGR mammography, and 3 RF rooms. Competitive salary, 2 yr to full partnership, and excellent benefits. Fast-growing, suburban community 50 min north of downtown San Francisco with sunny Mediterranean climate and very mild winters in the heart of the wine country. Excellent outdoor recreational opportunities. Please send initial inquiry and CV to John J. McGovern, M.D., 121 Sotoyome St., Santa Rosa, CA 95405; (707) 546-4062. 9–2ap

TEXAS, DIAGNOSTIC RADIOLOGIST—Excellent, private-practice opportunity for BC/BE radiologist seeking professional satisfaction and quality of life. Noninvasive procedures; all other modalities except MRI. New equipment in new hospital. Well-trained, congenial medical staff eager to work with radiologist. Great outdoor recreation; hunting and lakes; easy access to stream fishing and snow skiing. Contact Jim Truitt, Physician Resource Network, P. O. Box 37102, Fort Worth, TX 76117-8102; (800) 525-6055. 9–11ap

DIAGNOSTIC RADIOLOGIST IMMEDIATE OPENING AT ROSE MEDICAL CENTER (RMC), DENVER, CO—An 8-person radiology group is recruiting an additional radiologist with fellowship training in MR and CT. The practice involves all imaging modalities. Highly competitive first yr salary and generous fringe benefit package. Position leads to offer of equal shares in the professional corporation after 1 yr., if mutually agreed upon. RMC is affiliated with the University of Colorado. Contact David W. Wilder, M.D., or Jeffrey A. Levy, M.D.; (303) 320-2256. 9–11ap

RADIOLOGISTS—An innovative health care organization is seeking radiologists to serve communities in rural southern West Virginia. Competitive salary and fringe benefits are offered. A desire and willingness to meet challenges of present-day health care delivery in rural settings is a must. Part- or full-time positions are available. Arrangements may also be made to accommodate continued residence outside West Virginia. Send confidential resume and inquiries to Box O9, *AJR* (see address this section). 10–11ap

DIAGNOSTIC RADIOLOGIST—Immediate opening leading to partnership in expanding 4-member, hospital-based practice near Boston. Seeking recently trained BC/BE radiologist with skills and experience in general radiology, ultrasound, mammography, CT, and angio/interventional. Interested persons should contact Steven Sitzman, M.D., The Malden Hospital, One Hospital Rd., Malden, MA 02148; (617) 322-7560. 9–11ap

DIAGNOSTIC RADIOLOGIST—Immediate opening for board-certified/eligible radiologist with expertise in CT, MRI, ultrasound, mammography, nuclear medicine, and angiography to join a group of 3 board-certified radiologists. Active ACR-accredited mammography program. 175-bed hospital and private clinic. Excellent living area on the southern Oregon coast with fishing, crabbing, and boating opportunities and only a 4-hr drive for superb skiing. Send inquiries and CV to Michael S. Quinn, M.D., or Norman A. Fiet, M.D., South Coast Radiologists, P.C., 2650 N. 17th St., Coos Bay, OR 97420; (503) 267-5411. 9–10ap

POSITION OPEN IMMEDIATELY—A 40-physician, multispecialty clinic serving central and western Kansas, seeks a board-eligible/certified radiologist. Excellent facilities include diagnostic radiography, CT scan, diagnostic ultrasound, nuclear medicine, and MR services. Very competitive salary and benefits. No night or weekend call. An excellent opportunity in a dynamic practice setting. Please send CV to Administrator, Hutchinson Clinic, 2102 N. Waldron, Hutchinson, KS 67502; (316) 669-2626 (collect). 9–11ap

DIAGNOSTIC RADIOLOGIST—Mallinckrodt Institute of Radiology, Washington University, seeks an additional board-certified radiologist with academic interest to staff a satellite hospital of Barnes Hospital in St. Louis. This satellite radiology facility in St. Louis county performs all aspects of diagnostic radiology, including CT, MRI, ultrasound, and nuclear medicine. Equipment is brand new and state-of-the-art. Candidates must be competent in all aspects of diagnostic radiology and must be able to do cross-sectional interventional procedures. Academic rank and salary are dependent on qualifications and previous experience. The institute is conducting research in teleradiology and outcomes research at the satellite facility. Washington University is an equal opportunity employer. Applications from women and minority group members are encouraged. Send CV to R. Gilbert Jost, M.D., Chief of Diagnosis, Mallinckrodt Institute of Radiology, 510 S. Kingshighway Blvd., St. Louis, MO 63110. 9–11ap

TEXAS, DIAGNOSTIC RADIOLOGIST—Excellent, private-practice opportunity for BC/BE radiologist seeking professional satisfaction and quality of life. Noninvasive procedures; all other modalities except MRI. New equipment in new hospital. Well-trained, congenial medical staff eager to work with radiologist. Great outdoor recreation; hunting and lakes; easy access to stream fishing and snow skiing. Contact Jim Truitt, Physician Resource Network, P. O. Box 37102, Fort Worth, TX 76117-8102; (800) 525-6055. 9–11ap

ONCOLOGIC RADIOLOGY/MAMMOGRAPHY The Dana-Farber Cancer Institute and Brigham and Women's Hospital, teaching affiliates of Harvard Medical School, seek a full-time diagnostic radiologist with interests in oncologic radiology and mammography. The 2 hospitals are in close proximity and the radiology dept. at Dana-Farber Cancer Institute is staffed by Brigham and Women's Hospital faculty and residents. The Dana-Farber Cancer Institute is one of the world's leading cancer treatment and research facilities and many opportunities exist for collaborative clinical research in cancer imaging. Please contact Jack E. Meyer, M.D., Director of Diagnostic Radiology, Brigham and Women's Hospital and Dana-Farber Cancer Institute, 75 Francis St., Boston, MA 02115; (617) 732-6269. Brigham and Women's Hospital/Dana-Farber Cancer Institute/Harvard Medical School is an affirmative action/equal opportunity educator and employer. 9–2a

RADIOLOGIST, TYLER, TX—The University of Texas Health Center at Tyler invites applications for a clinical faculty position in the Dept. of Radiology. Some teaching is required, but not publishing or research. A progressive, 4-person dept. practices general radiology (including interventional, MRI, and SPECT) and performs approximately 27,000 exams/yr. New equipment, flexible work hours, very light call, and no weekend schedule. Year-round tennis, golf, and boating are available in addition to excellent schools. Competitive first-yr salary and an unsurpassed benefits package are offered. Send CV to J. R. Shepherd, M.D., University of Texas Health Center at Tyler, P. O. Box 2003, Tyler, TX 75710; (903) 877-7100. The University of Texas Health Center at Tyler is an affirmative action, equal opportunity employer. Minorities are encouraged to apply. 9–11a

THE NATIONAL INSTITUTES OF HEALTH is seeking an interventional radiologist with fellowship training. Resources include 20 fully equipped angiographic rooms and extensive research opportunities with laboratory support available. Would share duties with 2 other senior angiographers. Generous benefit package and appointment at Georgetown University Hospital is included. Interested candidates should contact John L. Doppman, M.D., Dept. of Radiology, National Institutes of Health, Bldg. 10, Rm. 1C-660, Bethesda, MD 20892; (301) 496-5080. 9–11ap

ULTRASOUND/CT/MRI—Opportunity for board-certified radiologist specializing in ultrasound, body CT, and body MRI to pursue an academic career at The New York Hospital-Cornell Medical Center. The dept. provides state-of-the-art equipment, including Acuson ultrasound, GE 9800 CT, and GE Signa 1.5-T MR. A wide variety of ultrasound exams are performed, including abdominal, OB-GYN, color Doppler, small parts, neonatal head, transvaginal, and transrectal. A candidate with prior fellowship in sectional imaging or ultrasound is preferred. Responsibilities include clinical practice, teaching, and research. Position available 9/1/91. Please send CV to Elias Kazam, M.D., Dept. of Radiology, the New York Hospital-Cornell Medical Center, 525 E. 68th St., New York, NY 10021. 9–12a

DIAGNOSTIC RADIOLOGIST—Board-certified/eligible radiologist with skills in CT, MRI, ultrasound, nuclear medicine, and mammography needed for position with group of 12 young radiologists. Expanding practice is hospital-based, fee-for-service with 2 private-practice offices. Hospital-based practice in 400-bed hospital includes MRI, 2 CT units, modern interventional suite, satellite outpatient imaging center, and breast care center. Private-practice offices include MRI facility and full-service radiology office. Position available July 1992. Interested applicants should submit letter and CV to G. Edward Streubert, M.D., MRI of Bethlehem, Inc., Ste. 105, 95 Highland Ave., Bethlehem, PA 18017. 9–11ap

FLORIDA, NUCLEAR MEDICINE AND DIAGNOSTIC RADIOLOGISTS needed for a well-established and progressive group of 14 radiologists in Tampa Bay covering 2 hospitals and outpatient imaging centers. Busy nuclear division with single- and triple-headed SPECT. Nuclear boards or additional fellowship training in interventional radiology or sonography required. Candidate must be willing to cover other areas of diagnostic imaging as well. Competitive first yr salary followed by equitable partnership route. Send CV to Box O11, *AJR* (see address this section). 9–11ap

OPENING FOR BE/BC DIAGNOSTIC RADIOLOGIST to join a 6-person group in Missoula, a university city of 45,000 located in mountainous western Montana. Looking for a general radiologist with proficiency in MRI, ultrasound, CT, angiography, etc. Administrative skills preferable. Our group of 6 full-time radiologists covers both of Missoula's hospitals (210 and 130 beds). Progressive medical environment with 200 physicians. One yr to full partner income and 2 yr to partnership. Competitive salary. Abundant nearby recreational opportunities include skiing, fishing, backpacking, and hunting. Send CV to Missoula Radiology, Inc., P.O. Box 2039, Missoula, MT 59806. 7–11ap

MRI/ABDOMINAL IMAGING NEW YORK/NEW JERSEY METROPOLITAN AREA—Board-certified/eligible radiologist needed for a position beginning July 1, 1991. Must have fellowship training in MRI and training in CT, ultrasound, and GI studies. Private practice with 400-bed hospital and outpatient imaging center located in northern New Jersey, near New York City. Send inquiries to James A. Heimann, M.D., Dept. of Radiology, Clara Maass Medical Center, 1 Franklin Ave., Belleville, NJ 07109. 7–12ap

IMMEDIATE OPENING IN PALM SPRINGS, CA Radiologist with MRI expertise/specialization needed to join 10-person group in community hospital/office practice. Contact Marvin J. Friedenberg, M.D., Dept. of Radiology, Desert Hospital, 1150 N. Indian, Palm Springs, CA 92262. 10xa

IMMEDIATE OPENING IN PALM SPRINGS, CA Radiologist with mammography expertise/specialization needed to join 10-person group in community hospital/office practice. Contact Marvin J. Friedenberg, M.D., Dept. of Radiology, Desert Hospital, 1150 N. Indian, Palm Springs, CA 92262. 10xa

VASCULAR/INTERVENTIONAL RADIOLOGIST, LONG ISLAND, NY—Board-certified radiologist with fellowship training or equivalent experience in vascular/interventional radiology needed to join a 5-member group starting July 1992. Angio suite currently being upgraded to latest state-of-the-art equipment. Must be willing to do most aspects of diagnostic radiology. This well-established practice includes a 325-bed community hospital, a private diagnostic radiology office, and a 1-yr-old MRI facility. Generous salary leading to full partnership. Contact Ira Langer, M.D., 250 Hospital Rd., Patchogue, NY 11722; (516) 475-1030. 8–11ap

DIAGNOSTIC RADIOLOGIST, WASHINGTON—The Moses Lake Clinic is seeking a well-trained diagnostic radiologist to join a group of progressive multispecialty physicians. This is an opportunity to work in a beautiful facility that offers mammography, fluoroscopy, ultrasound, diagnostic radiology, and CT. Competitive compensation, excellent benefit package, located in central Washington. Contact Terry W. Coplin, Administrator, 840 Hill Ave., Moses Lake, WA 98837; (509) 765-0216. 8–10a

TWO RADIOLOGISTS, KANSAS CITY—There is an opening for 2 radiologists, 1 immediately and 1 in July 1992, to join an expanding 4-person group in a 300-bed hospital and a future large, outpatient center. We are looking for a radiologist to head special procedures and the interventional section. The other person could be a general radiologist or have any other subspecialty training. Competitive salary. All benefits lead to early full partnership. Reply to George F. Drasin, M.D., 4949 Rockhill Rd., Kansas City, MO 64110. 8–10ap

THE DEPT. OF RADIOLOGY AT BROOKE ARMY MEDICAL CENTER, SAN ANTONIO, TX, is recruiting academic radiologists for several divisions of the dept., including ultrasound, chest, skeletal, neuroradiology, general diagnostic, interventional radiology, and mammography. Our dept. offers a fully accredited residency program with 24 residents and 16 attending full-time staff. Numerous consultants from across the country lecture on a continuing and regular basis. The hospital is a modern, tertiary-care center serving Texas, Oklahoma, and Louisiana. A strong residency program, interesting patient population, excellent equipment, teleradiology and digital radiology implementations underway, coupled with a south Texas lifestyle are positive aspects of the practice. Academic credentials and/or experience are necessary. Recently graduated fellows are encouraged to apply. Board certification is mandatory. Candidates should be particularly interested in patient care, teaching, and research. Salary and benefits are competitive and generous. Brooke is an EO/EEO employer. Please contact Dr. Billy E. Cunningham, COL, MC, Assistant Chief, Dept. of Radiology, Brooke Army Medical Center, Fort Sam Houston, TX 78234-6200; (512) 221-8418/8218. 8–7a

THE RADIOLOGY DEPT. AT DWIGHT DAVID EISENHOWER ARMY MEDICAL CENTER is recruiting academic radiologists. The dept. provides a full range of services including angiography, ultrasound, CT (with a new GE 9800 Advantage system), and MRI (with a new 1.5-T GE Signa system). Development is underway for the installation of a digital teleradiology link to area medical facilities. The dept. is also beginning a radiology residency program in affiliation with the program at the Medical College of Georgia in Augusta. With this growth, the dept. has generated a need for several academic diagnostic radiologists. Board-certified diagnostic radiologists with academic credentials and/or experience are urged to apply. Fellowship training is desired, especially in interventional radiology and/or angiography, however candidates at all levels will be considered. Candidates should be particularly interested in patient care, teaching, and research. The medical center is located on Fort Gordon, GA, adjacent to Augusta and is the tertiary-care hospital supporting 9 Army community hospitals of the southeastern region and Puerto Rico. The hospital supports fully accredited residency programs in family practice, general surgery, medicine, orthopedics, pathology, and psychiatry. Salary and benefits are competitive and generous. The medical center is an EO/EEO employer. Please contact Dr. Thomas M. Ralston, LtC., Chief, Radiology Dept., Eisenhower Army Medical Center, Fort Gordon, GA; (404) 791-6245. 8–7a

SUPERB PARTNERSHIP POSITION IN LAS VEGAS, NV—Rapidly expanding, 7-member group practice covering 2 full-service imaging centers and a small hospital has an immediate opening. We are looking for an additional board-certified radiologist with an uncommon dedication to excellence in patient care. Our outpatient facilities include 2 MR, 2 CT, angio with a 4-bed recovery area, 5 ultrasound, 5 mammography, 2 SPECT, plus R & F. This is an excellent opportunity for a partnership position with a well-respected group in a growing community. Please send CV to Dr. Mark Winkler, SDMI, 2950 S. Maryland Pkwy., Las Vegas, NV 89109. 5–10a

THE DEPT. OF RADIOLOGY AT WALTER REED ARMY MEDICAL CENTER is recruiting academic radiologists. We need board-certified radiologists to work in this famous and modern health-care center. Our dept. has a residency program consisting of 24 residents and several fellows. Subspecialists are needed in ultrasound, chest, mammography, genitourinary, gastrointestinal, pediatric, CT, MRI, and interventional radiology, as well as general radiology. Excellent opportunity to live in the nation's capital and also become an integral part of a large teaching program. Salaries are competitive and generous. Highly motivated applicants should contact Col. Mark F. Hansen, Radiology Consultant to the Army Surgeon General, Dept. of Radiology, TAMC, HI 96859-5000; (808) 433-6393. 8–7a

IMMEDIATE OPENING FOR BE/BC RADIOLOGIST in a regional hospital with a patient base of 25,000 located in a scenic western Wyoming community. Great outdoor recreation area. Competitive reimbursement. Ultrasound/CT/general radiology. Interested persons contact Paul Sonntag, M.D., P. O. Box 629, Ogden, UT 84402; (801) 625-2092. 8–1ap

DIAGNOSTIC RADIOLOGIST, NEW MILFORD, CT—A third radiologist is sought for a busy, private practice located in 1 of the most beautiful areas of Connecticut. We provide the full range of diagnostic services for a modern, well-equipped, community hospital. Choice environment; excellent compensation. Send inquiries and CV to Jules White, M.D., New Milford Hospital, 21 Elm St., New Milford, CT 06776; (203) 355-2611, ext. 235. 8–11ap

FACULTY POSITION IN ABDOMINAL IMAGING Dartmouth-Hitchcock Medical Center is seeking a faculty member at the associate professor level with experience and interest in abdominal imaging radiology. Clinical responsibility will be in an entirely new 400-bed, clinical facility opening in Oct. 1991 with state-of-the-art instrumentation. Position will involve responsibility for residency training in GI/GU area. Proven record of academic performance including research and teaching with an interest in providing academic guidance for energetic staff of younger radiologists necessary. Interested candidates write with CV to Peter K. Spiegel, M.D., Chairman, Dept. of Diagnostic Radiology, Dartmouth-Hitchcock Medical Center, Hanover, NH 03756. AA/EOE. 10xap

BC DIAGNOSTIC RADIOLOGIST—Affluent practice. Excellent salary, benefits, and early partnership. Investigate now before socialized medicine becomes a reality! Practice at a 395-bed hospital, the second largest in the beautiful state of Delaware, centrally located on the east coast. This is a rapidly expanding, high-powered, group practice. Subspecialty training in interventional, imaging, or neuro desired. Open to F-M with 1–2 yr of postgrad experience. Send resume to or contact Ben Hollander, M.D., Dept. of Radiology, St. Francis Hospital, 7th and Clayton Sts., Wilmington, DE 19805; (302) 421-4300. 9–2ap

PHYSICIAN/RADIOLOGIST—Large radiology group with multiple private offices seeks a board-certified radiologist interested in a full-time position. Responsibilities include general radiography. Special training in CT, ultrasound, and nuclear medicine is preferred. Excellent southern New Jersey location. Competitive salary and benefit package. Send CV to RABC, P. O. Box 729, Mt. Holly, NJ 08060. 9–11ap

NEURORADIOLOGIST—Senior ASNR member needed for excellent hospital and imaging center position in Tucson, AZ. Early partnership opportunity. Send CV to Arizona State Radiology, 7250 E. Ventana Canyon Dr., Tucson, AZ 85715. 8–7ap

DIAGNOSTIC RADIOLOGIST with skills in CT, MR, interventional, ultrasound, and nuclear medicine needed to join group of 8 board-certified radiologists. Growing practice in eastern Washington at a 228-bed hospital, a new multimodality imaging center, and 2 private offices. Potential for long-term practice is excellent. Top-notch school system, including 3 first-rate universities. Excellent hunting, fishing, boating, and skiing. Contact L. E. Crecelius, M.D., N. 5901 Lidgerwood, Ste. 18B, Spokane, WA 99207; (509) 482-2385. 5–10ap

DIAGNOSTIC RADIOLOGIST, IMMEDIATE OPENING—Ten-person radiology group seeks a diagnostic radiologist with fellowship training, including body MRI/body imaging, to join a busy, hospital-based practice located in rapidly growing north Dallas. GE 1.5-T magnet, Toshiba midfield magnet, 2 GE 9800 scanners, Acuson 128 with color flow Doppler, and new special procedures suite with DSA. Please send CV to Box K54, *AJR* (see address this section). 10xa

IMMEDIATE OPENING FOR BC/BE GENERAL RADIOLOGIST with experience in interventional and vascular radiology. Join a group of 4 radiologists in a 160-bed hospital located in Allentown, PA, about 60 mi. northwest of Philadelphia. The daily practice includes all aspects of general radiology, CT, ultrasound, and nuclear medicine. Please call or send CV to Asad Shohadai, M.D., Allentown Osteopathic Medical Center, 1736 Hamilton St., Allentown, PA 18104; (215) 770-8700. 10xa

BOSTON, IMMEDIATE OPENING—Radiologist wanted to join busy, well-established, private-practice group with 4 outpatient facilities. Expertise in ultrasound and mammography. No evening or weekend call. Excellent life-style, partnership opportunity. Send letter and CV to Box E49, *AJR* (see address this section). 6–11ap

CHEST RADIOLOGIST, THOMAS JEFFERSON UNIVERSITY HOSPITAL—The Dept. of Radiology at Jefferson has an opening for a thoracic radiologist at either the junior or senior level. The position encompasses plain film radiography, CT, and percutaneous thoracic interventions. Involvement in mammography, other general diagnostic areas, and ultrasound can also be incorporated, depending on the interests of the candidate. Dedicated, nonclinical research time is provided, and the dept. has excellent research facilities and support. Our chest radiology practice is expanding rapidly and close working relationships are maintained with pulmonary medicine and thoracic surgery. Teaching is also emphasized, with a large residency program and a thoracic radiology fellowship. Excellent faculty income and benefits. This is a fine opportunity for a radiologist with academic interests to join a dynamic and rapidly growing dept. Interested candidates should contact David C. Levin, M.D., Chairman, Dept. of Radiology, Thomas Jefferson University Hospital, Philadelphia, PA 19107; (215) 955-7264. Jefferson is an equal opportunity/affirmative action employer. 10xa

HOSPITAL-BASED, BC/BE RADIOLOGIST needed to join newly laid plans for a subregional medical center (campus). Must be proficient in general diagnostic radiology, ultrasound, nuclear medicine, CT, and MRI. Excellent opportunity plus attractive financial package. Located in east, central Montana along the Yellowstone River. Great outdoors for recreation, hunting, and fishing. Excellent education system. Lifestyle is rural and family-oriented. Send CV to Vice-President, Business Services, Holy Rosary Hospital, 2101 Clark, Miles City, MT 59301. 9–11ap

NORTHERN CALIFORNIA—BC diagnostic radiologist sought for medical imaging dept. in a large, multispecialty group practice. Facility features new state-of-the-art equipment, including Phillips CT, SPECT, color Doppler, and mobile 0.5-T MR. Beautiful community in the heart of the wine country, 50 mi. north of San Francisco. Excellent salary and benefits package leading to eligibility for shareholder status. Send CV to Alan Larocque, M.D., Ph.D., Dept. of Medical Imaging, Kaiser Permanente Medical Center, 401 Bicentennial Way, Santa Rosa, CA 95401-2192. EOE. 9–11a

NEURORADIOLOGIST—The Dept. of Radiology at Yale University School of Medicine is seeking a neuroradiologist with a strong interest and experience in MR and MR physics for a full-time academic position. Rank is commensurate with experience. Research opportunities are stressed in a strong academic dept. with state-of-the-art radiologic equipment. Candidates must be board-certified or eligible, with fellowship training. Please send CV to Gordon Sze, M.D., Director, Neuroradiology, Dept. of Diagnostic Radiology, Yale University School of Medicine, 333 Cedar St., P. O. Box 3333, New Haven, CT 06510. Yale University is an equal opportunity/affirmative action employer. Applications from women and minority groups are encouraged. Application deadline is Jan. 31, 1992. 9–10a

DIAGNOSTIC RADIOLOGIST—This university-affiliated Veterans Affairs Medical Center in eastern Virginia seeks BC/BE candidates to join our 5-person staff in Nov. 1991. Expertise required in general diagnostic, ultrasound, CT, vascular, and interventional radiology. Position offers opportunity for resident teaching. Please forward CV to C. B. Mahon, M.D., Chief, Radiology Service, Veteran Affairs Medical Center, Hampton, VA 23667. The Dept. of Veterans Affairs is an equal opportunity employer. 9–10a

FAIRBANKS, AK—Four diagnostic radiologists seek fifth partner for diversified practice including general radiology, ultrasound, nuclear medicine, MRI (GE 1.5-T), and CT (GE 9800). Hospital and office practice. Desirable life-style advantages in a university town. Unlimited access to the outdoors. Excellent salary, benefits, retirement, and vacation. One yr to full partnership. Contact Douglas Hutchinson, M.D., 1919 Lathrop #5, Fairbanks, AK 99701; (907) 452-5092. 8–10ap

CHEST RADIOLOGIST, CLEVELAND CLINIC FOUNDATION—The Cleveland Clinic Foundation has an opening for a staff position in the Section of Thoracic Imaging. The foundation is a 1000-bed hospital with a large outpatient population and an international referral base. Successful applicants will be involved in all diagnostic modalities, including CT, MRI, and interventional procedures. A strong interest in teaching, research, and patient care is required. Applicants should be board-certified, fellowship-trained, or have equivalent experience. Excellent salary and benefit package. Send CV to Moulay A. Meziane, M.D., Head, Section of Thoracic Imaging, Cleveland Clinic Foundation, One Clinic Center Dr., Cleveland, OH 44195-5021. The Cleveland Clinic Foundation is an equal opportunity employer. 5–10ap

BC/BE RADIOLOGIST—Group practice in New Orleans, LA, has a great opportunity leading to partnership. Looking for a radiologist with imaging background or interest in special procedures. Imaging center with 1.5-T GE Advantage System. Excellent hospitals and working conditions. Send CV to B.B.N. & H., 440 General Meyer Ave., Ste. 211, New Orleans, LA 70131; (504) 368-5074. 7–10ap

CLINICAL DIRECTOR, MRI—MetroHealth Medical Center, a 1,000-bed teaching hospital affiliated with Case Western Reserve University (CWRU), is seeking a clinical director for its MRI section. MHMC is a Level I trauma center providing tertiary care in the Cleveland metropolitan area. The director of MRI will head a major research and clinical service. Responsibilities include overseeing daily operations, research leadership in investigative MR, and development of collaborative ventures with the physics research group and other members of the Dept. of Radiology, hospital, and university. The position provides an excellent opportunity for research and resident education as well as professional development. The Dept. of Radiology is an active, academic dept. with state-of-the-art equipment in angiography, CT, ultrasound, and nuclear medicine and has an approved residency program. The MR section includes a 1.5-T imager (2nd system will be installed by Fall 1991), independent development workstation, 3-D engine (Voxel-Flinger), RF lab, and Starden Titan minicomputer. The research group includes 4 Ph.D. scientists and 4 graduate students. Candidates will be board-certified, have demonstrated experience in MRI research, have dedicated MR training, and be eligible for Ohio medical licensure. The ideal candidate will currently possess an assistant professor or higher rank with administrative experience preferred. MetroHealth Medical Center offers attractive compensation and benefits. The selected candidate will be recommended for a faculty appointment at CWRU School of Medicine commensurate with his/her experience. Interested candidates should forward CV and other pertinent information to Errol M. Bellon, M.D., Director, Dept. of Radiology, MetroHealth Medical Center, 3395 Scranton Rd., Cleveland, OH 44109; fax (216) 459-4072. MetroHealth Medical Center and Case Western Reserve University are equal opportunity employers. 8–10a

FACULTY RADIOLOGIST, BODY MRI DIVISION, THOMAS JEFFERSON UNIVERSITY HOSPITAL—The Dept. of Radiology at Thomas Jefferson University Hospital has an opening for a radiologist in an active, body MRI section that encompasses a clinical mix of approximately 50% musculoskeletal and 50% chest/abdomen/pelvis cases. Equipment includes 4 1.5-T GE Signa systems with state-of-the-art and advanced prototype hardware and software. A full-yr body MRI fellowship and/or 1 yr of academic MRI experience is preferred. Clinical cross coverage in ultrasound and/or general radiology also can be incorporated depending on the interests and qualifications of the candidate. Dedicated, nonclinical research time is provided, and the dept. has excellent research facilities and support, including 2 MRI physicists, a radiology animal facility, radiology research funding, and a team of research assistants. Excellent faculty incomes and benefits are offered within a financially secure dept. and university hospital. This is a unique opportunity for an academically oriented MRI radiologist to join a dynamic and rapidly growing dept. Interested candidates should contact Donald G. Mitchell, M.D., Director of MRI, Dept. of Radiology, 1032 Main Bldg., Thomas Jefferson University Hospital, Philadelphia, PA 19107; (215) 955-4809. Jefferson is an equal opportunity/affirmative action employer. 10xa

DIAGNOSTIC IMAGING—The 11-member imaging section of Guthrie Clinic–Robert Packer Hospital desires an associate with fellowship training and/or expertise in the above area. The Guthrie Clinic provides tertiary care in the southern tier of New York and the northern tier of Pennsylvania in the beautiful, endless mountains. Outstanding practice opportunities in an environment free of urban hassle. Please send letter of inquiry with CV or call Thomas F. Bednarek, M.D., Chairman, Dept. of Radiology, Guthrie Healthcare System, Sayre, PA 18840; (717) 882-4025. 8–10a

HARTFORD, CT—Position available for board-certified radiologist to join an established group of 8. Practice includes hospital and 4 private offices, all fully equipped, including CT. Mammography and nuclear medicine experience is essential. Competitive starting salary and benefits. Please enclose CV with initial correspondence to Jeffrey Blau, M.D., 40 Hart St., New Britain, CT 06052; (203) 229-2059. 8–10a

DIAGNOSTIC RADIOLOGIST, HOUSTON—Immediate opening for 2 BC/BE radiologists to join 5 BC radiologists associated with a large, internal medicine clinic near the Texas Medical Center. Primarily outpatient practice with regular hours. Also cover adjacent general, medical-surgical hospital. On-site ultrasound, CT, MRI, and nuclear medicine. Experience in angio and interventional is desired. Please send CV to Robert B. Hall, Administrator, Diagnostic Clinic of Houston, 6448 Fannin, Houston, TX 77030; (713) 797-9191. 8–10a

NEURORADIOLOGIST—The Dept. of Radiology at the University of Arkansas for Medical Sciences is seeking a neuroradiologist at the assistant or associate professor rank. Neuroradiology coverage is for 3 hospitals with state-of-the-art equipment including 2 1.5-T MRI units, 5 CT scanners, and 4 angiographic suites. Facility for neurointerventional work is available. Dedicated animal laboratory with advanced NMR spectroscopy units available for research. Candidate must be board-certified and preferably a senior member in ASNR. University of Arkansas for Medical Sciences is an equal opportunity employer. Address inquiries and a current CV to Edgardo Angtuaco, M.D., Chief, Neuroradiology, Dept. of Radiology, University of Arkansas for Medical Sciences, 4301 W. Markham St., Slot 596, Little Rock, AR 72205; (501) 686-6032, (501) 686-6900 (fax). 8–10a

SOUTHERN OREGON—Opportuniy for BC/BE, general diagnostic radiologist to join group of 5 board-certified radiologists. Experience in all modalities desired. Practice includes 2 hospitals and own private office. Competitive starting salary with early full partnership. Excellent lifestyle with many outdoor activities from Pacific Coast to Oregon Cascades. Send CV to Larry Strickland, Administrator, Roseburg Radiologists, P.C., P. O. Box 1547, Roseburg, OR 97478. 8–1ap

SAN FRANCISCO BAY AREA, DIAGNOSTIC RADIOLOGY—Full-time position available as of July 1992 for BC/BE radiologist to join established group based in growing SF Bay area communities. Competence in all modalities including MRI and angiography required; fellowship training desirable. Contact J. Fish, M.D., c/o Walnut Creek Radiology, 1844 San Miguel Dr., #302, Walnut Creek, CA 94596; (415) 947-0560. 8–10xa

ALASKA AREA NATIVE HEALTH SERVICE—Public-service–oriented radiologists needed for cross-cultural health care in Anchorage and Sitka, AK. Salary $85–$95K+, excellent benefits. Medical school loan repayment up to $25K/yr additional. Contact Ken Bartline, RN. (907) 257-1457, collect. Indian Health Service. An equal opportunity employer. 8–1a

THE DEPT. OF RADIOLOGY AT TRIPLER ARMY MEDICAL CENTER, HONOLULU, HI, is recruiting academic radiologists for several divisions of the dept. including ultrasound, chest radiology, skeletal, neuroradiology, general diagnostic radiology, MRI, interventional radiology, and mammography. Our dept. offers a fully accredited residency program with 21 residents and 16 attending full-time staff. Numerous consultants from across the country lecture on a continuing and regular basis. The hospital is a modern, tertiary-care center serving Hawaii and the entire Pacific Basin. A strong residency program, diverse and interesting patient population, excellent equipment, and tropical lifestyle are positive aspects of the practice. Academic credentials and/or experience are necessary. Recently graduated fellows are encouraged to apply. Board certification is mandatory. Candidates should be particularly interested in patient care, teaching, and research. Salary and benefits are competitive and generous. Tripler is an EO/EEO employer. Please contact Dr. Mark F. Hansen, Col., MC, Chief, Dept. of Radiology, TAMC, HI 96859-5000; (808) 433-6393. 7–6a

DIAGNOSTIC RADIOLOGIST—BC/BE radiologist wanted to join 2 established radiologists in a hospital-based practice. Candidate must have training/experience in general radiographic procedures, nuclear medicine, CT, ultrasound, mammography, angiography, and MRI. Send inquiries to Maurice Huffman, M.D., 4343 18th Ave., Rock Island, IL 61201. 9–10ap

ISRAEL, DIAGNOSTIC RADIOLOGY. Opportunities for 3–4 week or longer working vacations in a number of Israeli medical centers, on a volunteer basis. Positions varied, arrangements flexible. For information contact: Jonathan H. Fish, M.D., 1844 San Miguel Dr., #302, Walnut Creek, CA 94596; (415) 947-0560. 8–10xa

OREGON—Opportunity for BC/BE radiologist to join 7 BC radiologists in growing practice in the Portland metropolitan area. Training/expertise in all aspects of radiology including MRI is required. The practice includes 2 suburban hospitals, an outpatient clinic, and a new multimodality outpatient imaging clinic. Competitive compensation with generous fringe package and partnership in 2 yr. Send letter and CV to Jon C. Sewell, M.D., P.O. Box 227, Oregon City, OR 97045; (503) 655-1439. 10xa

Positions Desired

EXPERIENCED, YOUNG, FACULTY INTERVENTIONALIST (ABR, SCVIR) seeks private-practice position leading to full partnership. Can perform general radiology, including MRI, ultrasound, and CT. Prefer medium-sized to large hospital in urban or suburban location. Available March 1992. Reply Box P82, *AJR* (see address this section). 10–11bp

RADIOLOGIST, UNIVERSITY TRAINED—Previous angiographic interventional fellowship. Extensive angio/interventional experience (25 yr). Over 1000 angioplasties. Reasonable proficiency in modern imaging modalities. Presently holding responsible position in university-affiliated hospital. Please reply to Box P84, *AJR* (see address this section). 10–12bp

R3 OR R4 RADIOLOGY RESIDENCY—University of Iowa–trained radiologist through R3 yr seeks additional training at R3 or R4 level immediately. M. D. Tempel, M.D., 4550 Louisiana St., #A, San Diego, CA 92116. 10bp

B/C GENERAL RADIOLOGIST, NATIVE NEW YORKER seeks immediate partnership position with hospital-based radiology group. Experienced in all modalities and can perform certain special procedures. Will consider locum tenens to see practice for a week or more. Licenses in New York, Pennsylvania, and Florida. Reply to Box O7, *AJR* (see address this section). 9–10bp

Fellowships and Residencies

FELLOWSHIP IN MAMMOGRAPHY—The Emory University, Dept. of Radiology, offers a 6- or 12-mo fellowship in mammography. Approximately 17,000 mammograms are performed annually through a 600-bed university hospital, a 900-bed county hospital, and an outpatient clinic. Clinical activities would include extensive training in all aspects of mammography, breast ultrasound, stereotactic fine-needle aspirations, and biopsy. Candidates should be eligible for Georgia medical licensure. Contact Beth Kruse, M.D., Section of Radiology, The Breast Imaging Center, 1327 Clifton Rd. N.E., Atlanta, GA 30322; (404) 248-4446. Emory University is an equal opportunity/affirmative action employer. 10–1cp

FELLOWSHIP IN VASCULAR/INTERVENTIONAL RADIOLOGY 1992—The University of New Mexico has an unexpected opening for a 1-yr fellowship in vascular/interventional radiology beginning July 1, 1992. We perform all noncardiac diagnostic angiography, including neuroangiography, as well as a wide variety of vascular and nonvascular interventional procedures, with state-of-the-art equipment at the University Hospital (a level 1 trauma center) and the VA/Air Force Hospital. Applicants must have passed the ABR written exam, be eligible for ABR certification, and be eligible for medical licensure in the state of New Mexico. We are an equal opportunity employer. Contact Jerry King, M.D., Dept. of Radiology, University of New Mexico School of Medicine, 915 Camino Salud, N.E., Albuquerque, NM 87131; (505) 272-2439. 10–12c

VASCULAR AND INTERVENTIONAL RADIOLOGY FELLOWSHIP—The University of Arkansas for Medical Sciences is offering a 1-yr fellowship in vascular and interventional radiology starting July 1, 1992. Training includes all aspects of angiography and vascular and nonvascular interventions. Ample clinical material is available at a university hospital, a large veterans' hospital, and a children's hospital. Active vascular and nonvascular research programs are in place. Stipend and fringe benefits are competitive. Candidates must be board-certified or eligible in diagnostic radiology. Applications should include a current CV and 3 letters of reference. For further information, please contact David R. McFarland, M.D., Dept. of Radiology/556, University of Arkansas for Medical Sciences, 4301 W. Markham, Little Rock, AR 72205; (501) 686-6910. The University of Arkansas for Medical Sciences is an equal opportunity educator and employer. 10–12c

FELLOWSHIP IN ULTRASOUND/CT/ANGIO-INTERVENTIONAL—A 1-yr fellowship program is available beginning July 1992 at Lehigh Valley Hospital Center (LVHC) in Allentown, PA. LVHC is a 492-bed, acute-care, university-affiliated hospital. The fellowship program offers training in CT (head and body), ultrasound, angiography (neuro and visceral), and interventional radiology. MRI experience is also available. For further information, contact Robert Kricun, M.D., Dept. of Radiology, Lehigh Valley Hospital Center, P.O. Box 689, Allentown, PA 18105. 10–12cp

ANGIO/INTERVENTIONAL RADIOLOGY FELLOWSHIP—A 1-yr fellowship program is available beginning July 1992 at Harper Hospital/Wayne State University in Detroit, MI. Harper Hospital is a 700-bed, tertiary-care facility situated on the campus of the Detroit Medical Center. Approximately 2000 procedures were performed last yr. Participation in the clinical management of patients is emphasized. This fellowship includes training in all phases of diagnostic angiography and interventional techniques. This includes arterial and venous thrombolysis, angioplasty, arterectomy, intravascular stents, as well as all biliary and urologic techniques. We perform biopsy and drainage procedures under multiple modalities. Current research interests include percutaneous placement of venous access ports and hepatic arterial chemoembolizations. For further information, please contact Marc L. Kahn, M.D., Dept. of Radiology, Vascular/Interventional Division, 3900 John R, Detroit, MI 48201; (313) 745-2606. 10c

FELLOWSHIP IN ABDOMINAL IMAGING—The University of Arizona, Dept. of Radiology, is presently accepting applications for a 1-yr fellowship in body imaging (MR, CT, and ultrasound) beginning July 1, 1992. The fellowship provides a high volume of diagnostic evaluations in these modalities and experience in cross-sectional and interventional techniques. Strong clinical program provides ample opportunity for research. The fellowship is open to candidates who have completed an accredited residency training program. Interested applicants should send CV and cover letter to Evan Unger, M.D., UAHSC, Dept. of Radiology/MRI, 1501 N. Campbell Ave., Tucson, AZ 85724. The UA is an equal opportunity/affirmative action employer. 10cp

NEURORADIOLOGY FELLOWSHIP POSITION A 1- or 2-yr neuroradiology fellowship is available in the Dept. of Radiology at the Albany Medical College. The section of neuroradiology is situated in a new dept. and new hospital and is responsible for all aspects of neuroradiology. Two high-field MRI, 3 CT, and excellent myelographic and angiography rooms are in use. The fellowship encompasses all clinical aspects of neuroradiology with ample opportunities for research. Albany Medical College is a private institution situated in northeastern New York with a significantly high quality of life. It is adjacent to the Saratoga–Lake George area, the Berkshires (Tanglewood), and the Adirondack and Catskill Mountains. All interested parties should contact Matthew D. Rifkin, M.D., Professor and Chairman, Dept. of Radiology, Albany Medical College, Albany, NY 12208; (518) 445-3277 or William Wagle, M.D., Director of Neuroradiology; (518) 445-3338. 10c

ANGIOGRAPHY AND INTERVENTIONAL RADIOLOGY FELLOWSHIP POSITION—A 1-yr fellowship in angiography and interventional radiology is available in the Dept. of Radiology at the Albany Medical College. The section of angiography and interventional radiology is responsible for the full gamut of interventional procedures and is situated in a new dept. and new hospital. The fellowship encompasses all clinical aspects of cardiovascular and interventional radiology with ample opportunities for research. Albany Medical College is a private institution situated in northeastern New York with a significantly high quality of life. It is adjacent to the Saratoga–Lake George area, the Berkshires (Tanglewood), and the Adirondack and Catskill Mountains. All interested parties should contact Matthew D. Rifkin, M.D., Professor and Chairman, Dept. of Radiology, Albany Medical College, Albany, NY 12208; (518) 445-3277 or Mohammed Sarrifizadeh, M.D., Interventional Radiology Section; (518) 445-3393. 10c

BODY IMAGING FELLOWSHIP POSITION—A 1 yr fellowship in body imaging is available in the Dept. of Radiology at the Albany Medical College. The body imaging section is responsible for all aspects of body imaging, but the fellowship emphasizes ultrasound (4 Acuson with color Doppler), CT (3 new GE units), and MRI (2 high-field units), which includes musculoskeletal MRI. Clinical experience and expertise is emphasized, but opportunities for research are ample. Albany Medical College is a private institution situated in northeastern New York with a significant quality of life. It is adjacent to the Saratoga–Lake George area, the Berkshires (Tanglewood), and the Catskill Mountains. All interested parties should contact Matthew D. Rifkin, M.D., Professor and Chairman, Dept. of Radiology, Albany Medical Center, Albany, NY 12208; (518) 445-3277 or James C. Peters, M.D., Section of Body Imaging; (518) 445-3277. 10c

FELLOWSHIP IN MUSCULOSKELETAL IMAGING—A position is available July 1, 1991, to June 30, 1992, for a board-certified radiologist to obtain advanced training and undertake research in musculoskeletal imaging at the Johns Hopkins Hospital. The experience includes MRI, CT, 3-D imaging, and conventional studies. Johns Hopkins Hospital has an active emergency service and serves as a regional pediatric trauma center. The fellow may participate in and extend ongoing research projects in 3-D imaging, using the Pixar Imaging Computer, and studies of osteoporosis and bone remodeling using the latest dual energy X-ray absorptiometry. MRI equipment includes high-field-strength research units as well as 2 1.5-T General Electric units for clinical studies. Body CT studies are performed on Siemens DR H and PLUS scanners, with over 14,000 body studies done yearly. The fellow will work closely with 2 experienced musculoskeletal radiologists. Interested parties should contact George Saba II, M.D., The Johns Hopkins Hospital, Dept. of Radiology, 600 N. Wolfe St., Baltimore, MD 21205; (301) 955-7700. 10–12c

FELLOWSHIPS AT THOMAS JEFFERSON UNIVERSITY HOSPITAL—The Dept. of Radiology at Thomas Jefferson University Hospital in Philadelphia offers the following fellowship programs each yr. (1) Ultrasound/CT/MRI — Jefferson's ultrasound division is 1 of the largest in the world and performs all currently available exams including obstetric, vascular, lithotripsy, invasive, and endoluminal. We also operate 4 GE 1.5-T MRI units and 3 CT scanners. Contact Barry Goldberg, M.D., regarding this program. (2) Cardiovascular/interventional — this division is housed in a new suite containing Philips angio units with DSA and performs the full range of vascular and nonvascular interventional procedures. Contact Geoffrey Gardiner, Jr., M.D. (3) Neuro/ENT radiology — very active clinical services supply a wealth of material to this division, which is housed in a neurosciences imaging center containing all imaging modalities. Contact Carlos Gonzales, M.D. (4) Breast Imaging — Jefferson's new breast-imaging center performs approximately 85 studies/day including ultrasound and needle localizations. Contact Stephen Feig, M.D. (5) Chest — includes biopsies and CT. Contact Robert Steiner, M.D. (6) MRI — a dedicated body MRI program including excellent research opportunities in addition to a large clinical case load. Contact Donald Mitchell, M.D. (7) Ultrasound — a dedicated ultrasound program. Contact Barry Goldberg, M.D. (8) Musculoskeletal — includes MRI of the musculoskeletal system. Contact David Karasick, M.D. All program directors listed above can be contacted at the Dept. of Radiology, Thomas Jefferson University Hospital, Philadelphia, PA 19107. Jefferson is an equal opportunity/affirmative action employer. 10xc

FELLOWSHIP—The College of Physicians and Surgeons of Columbia University is searching for a board-certified or eligible junior radiologist to participate in a 1-yr mammography fellowship to begin July 1, 1992. Fellowship involves intensive exposure to mammography reading and techniques, including needle localization and biopsy, in a large and growing mammography service in a major academic medical center. Experience with breast ultrasound also will be obtained. A large mammography teaching file will be available to the fellow. Time also will be spent in general ultrasound, particularly as it relates to the female pelvis and breast. Requirements include board-eligibility or certification in diagnostic radiology. New York state medical license required; narcotics license desirable. Please send resume to Philip O. Alderson, M.D., Dept. of Radiology, Columbia-Presbyterian Medical Center, 622 W. 168th St., New York, NY 10032. Columbia University is an affirmative action/equal opportunity employer. 10cp

A FELLOWSHIP IN ULTRASOUND AND BODY CT/MRI is available July 1, 1992, to June 30, 1993, at The New York Hospital-Cornell Medical Center. The dept. provides state-of-the-art equipment, including Acuson ultrasound, GE 9800 CT, and GE Signa 1.5-T MR. Wide variety of ultrasound exams include abdominal, OB-GYN, color Doppler, small parts, neonatal head, transvaginal, and transrectal. Applicants should be ABR-eligible or certified. Send CV to Elias Kazam, M.D., Dept. of Radiology, The New York Hospital–Cornell Medical Center, 525 E. 68th St., New York, NY 10021. 10–1c

NEURORADIOLOGY FELLOWSHIP—Two yr beginning July 1, 1992. Exposure to all aspects of clinical/academic neuroradiology. Participation in research/training. Send cover letter/CV to John R. Jinkins, M.D., Director, Neuroradiology Section, The University of Texas Health Science Center, 7703 Floyd Curl Dr., San Antonio, TX 78284-7800. The University of Texas Health Science Center at San Antonio is an affirmative action/equal opportunity employer. 10–12cp

FELLOWSHIP IN NEURORADIOLOGY—A fellowship position in neuroradiology is available July 1, 1992, in the Dept. of Radiology at New England Medical Center Hospitals, Boston, MA. The Boston Floating Hospital for Children is an integral part of the New England Medical Center Hospitals. The center is the teaching unit of Tufts University School of Medicine. The program is for 1 or 2 yr and includes both adult and pediatric case material. The fellow will be trained in the technique and interpretation of carotid and vertebral angiography as well as myelography. CT and MRI of the head and spine form major components of the neuroradiology service as does interventional neuroradiology. The facilities include state-of-the-art MRI and CT scanners. Neuroradiologic services at the New England Medical Center Hospitals are carried out in liaison with the Depts. of Neurology, Neurosurgery, and Pediatric Neurology. Joint radiologic and clinical conferences are held frequently, and within a short time, the applicants will have considerable exposure to an array of neuroradiologic material. The Dept. of Neuropathology also runs conferences, allowing correlation to be made between radiologic interpretation and pathology. The fellowship program is accredited by the Accreditation Council for Graduate Medical Education. Interested applicants should call (617) 956-6333 or write to Samuel M. Wolpert, M.D., Professor of Radiology and Neurology, Director, Neuroradiology Fellowship Program, Dept. of Radiology, 750 Washington St., Boston, MA 02111. 10–11cp

MUSCULOSKELETAL IMAGING FELLOWSHIP The Dept. of Diagnostic Radiology and Medical Imaging is offering a 1-yr fellowship in musculoskeletal imaging. The Division of Skeletal Radiology is an integral part of the Henry Ford Bone and Joint Specialty Center. This center represents a unique multispecialty program for clinical and academic excellence in the diagnosis and treatment of musculoskeletal disorders. It comprises the Dept. of Orthopedic Disorders, Dept. of Orthopedic Surgery, Division of Rheumatology, Division of Bone and Mineral Metabolism, Physics Section of the Dept. of Radiology, and the Division of Skeletal Radiology. The group includes recognized experts working closely in the investigation and clinical care of musculoskeletal disorders, providing a fertile environment for education and research. The Division of Skeletal Radiology consists of 3 dedicated osteoradiologists and state-of-the-art imaging technology including polytomography, 3D CT imaging, MRI, musculoskeletal sonography, and arthrography. Ongoing research in imaging includes high-resolution CT, sonography, and other clinical projects. Interested applicants should include CV with letter of inquiry to either Burton I. Ellis, M.D., or Marnix van Holsbeeck, M.D., Dept. of Diagnostic Radiology and Medical Imaging, Division of Musculoskeletal Radiology, Henry Ford Hospital, 2799 W. Grand Blvd., Detroit, MI 48202. 9–11ap

FELLOWSHIPS IN PEDIATRIC RADIOLOGY AND PEDIATRIC NEURORADIOLOGY—The Dept. of Radiology, Children's Hospital Medical Center, Cincinnati, OH, offers 1- or 2-yr fellowships in pediatric radiology beginning July 1, 1993. A 1-yr pediatric neuroradiology fellowship program is also offered and may be taken separately or combined with 1 yr of adult neuroradiology fellowship at the University of Cincinnati Medical Center. Children's Hospital Medical Center (CHMC) is a 355-bed institution. The dept. performs over 105,000 radiologic exams annually in the largest children's hospital and ambulatory practice in the U.S. The dept. has 14 full-time faculty pediatric radiologists, 6 fellows, and many resident trainees. Five pediatric radiology and 1 pediatric neuroradiology fellowship positions are available annually. Training includes all aspects of pediatric imaging: neonatal radiology, neuroimaging, musculoskeletal radiology, cardiovascular and thoracic imaging, abdominal imaging, oncologic imaging, ultrasonography, nuclear medicine, CT, MRI, and vascular/interventional procedures. The dept. has an active clinical service with state-of-the-art equipment as follows: digital fluoroscopy; Acuson, AI, and ATL ultrasound units with Doppler and color flow Doppler capabilities; planar SPECT gamma cameras; GE 9800 Quick CT scanner; 1.5-T GE MRI with spectroscopy; and cardiac catheterization/angiographic suite with digital vascular imaging. The fellowship provides a broad clinical experience in pediatric radiology as well as numerous opportunities to participate in both clinical and basic research. Candidates must be board-certified or board-qualified in diagnostic radiology and must be able to obtain an Ohio medical license. Salary and fringe benefits are highly competitive. Applications are due before Jan. 1992, with interviews scheduled during the fall and winter of 1991–1992. There are numerous career opportunities in pediatric radiology in academic and private practice settings. To receive more information about the fellowships at CHMC or careers in pediatric radiology, please contact Donald R. Kirks, M.D., Director, Dept. of Radiology, Children's Hospital Medical Center, Cincinnati, OH 45229-2899; (513) 559-8058. Children's Hospital Medical Center and the University of Cincinnati College of Medicine are affirmative action/equal opportunity employers. 5–4cp

ACCREDITED FELLOWSHIPS IN PEDIATRIC RADIOLOGY AND PEDIATRIC NEURORADIOLOGY—Dept. of Radiology, Children's Hospital Medical Center, Cincinnati, OH, offers 1- or 2-yr accredited (Residency Review Committee for Radiology of ACGME) fellowships in pediatric radiology beginning July 1, 1993. A 1-yr pediatric neuroradiology fellowship program is also offered and may be taken separately or combined with 2 yr of adult neuroradiology fellowship at the University of Cincinnati Medical Center. Children's Hospital Medical Center (CHMC) is a 355-bed institution. The dept. performs over 105,000 radiologic exams/yr in the largest children's hospital and ambulatory practice in the U.S. The dept. has 14 full-time faculty pediatric radiologists, 6 fellows, and many resident trainees. Five pediatric radiology and 2 pediatric neuroradiology fellowship positions are available annually. Training includes all aspects of pediatric imaging including neonatal radiology, neuroimaging, oncologic imaging, ultrasonography, nuclear medicine, CT, MRI, and vascular/interventional procedures. The dept. has an active clinical service with state-of-the-art equipment including digital fluoroscopy; Acuson, AI, and ATL ultrasound units with Doppler and color-flow Doppler capabilities; planar SPECT gamma cameras; GE 9800 Quick CT scanner, 1.5-T GE MRI with spectroscopy; and cardiac catheterization/angiographic suite with digital vascular imaging. The fellowship provides a broad clinical experience in pediatric radiology as well as numerous opportunities to participate in both clinical and basic research. Candidates must be board-certified or qualified in diagnostic radiology and must obtain an Ohio medical license. Salary and fringe benefits are highly competitive. Applications are due before Jan. 1992, with interviews scheduled during the fall and winter of 1991–1992. There are numerous career opportunities in pediatric radiology in both academic and private practice settings. To receive more information about the fellowships at CHMC or careers in pediatric radiology, please contact Donald R. Kirks, M.D., Director, Dept. of Radiology, Children's Hospital Medical Center, Cincinnati, OH 45229-2899; (513) 559-8058. Children's Hospital Medical Center and the University of Cincinnati College of Medicine are affirmative action/equal opportunity employers. 9–5cp

MAMMOGRAPHY FELLOWSHIP—Mallinckrodt Institute of Radiology, Washington University Medical Center in St. Louis, MO, has an opening for a 1-yr fellowship in breast imaging starting July 1, 1992. The section performs more than 21,000 mammograms/yr with an active screening program that includes mobile mammography. Adjunctive procedures such as breast needle localization, stereotactic fine-needle aspiration biopsy, galactography, and breast ultrasound are performed in the breast center. For further information, contact Drs. Judy Destouet or Barbara Monsees, Mallinckrodt Institute of Radiology, Washington University Medical Center, 510 S. Kingshighway Blvd., St. Louis, MO 63110; (314) 362-2911. 8–10c

FELLOWSHIP IN BODY CT/MRI AND ULTRASOUND—The Dept. of Radiology of Loyola University Medical Center has 2 1-yr fellowship positions available July 1, 1992. The dept. performs more than 180,000 exams/yr. Fellowship training in all aspects of ultrasound is available. All imaging equipment is state-of-the-art and includes 4 GE 9800 CT scanners, 4 Acuson units, and 2 GE 1.5-T magnets. Candidates must be board-certified/eligible in diagnostic radiology and have an Illinois medical license. For further information, contact Mary Olson, M.D., Dept. of Radiology, Loyola University Medical Center, 2160 S. First Ave., Maywood, IL 60153. 8–11cp

FELLOWSHIP IN NEURORADIOLOGY, JULY 1, 1992—The Dept. of Radiology, University of Massachusetts Medical Center offers a 1-yr fellowship position in neuroradiology starting July 1, 1992. Training is offered in neuroangiography, CT, myelography, and MRI. The position involves teaching of medical students and residents with opportunity for research. The University of Massachusetts Medical Center is a 370-bed, university hospital and medical school located in Worcester, 40 mi. west of Boston. The dept. consists of 22 staff, 14 residents, 2–4 fellows, and does approximately 130,000 exams/yr. The hospital is a major trauma center and is serviced by 2 Life Flight helicopters. The dept. is well-equipped with 2 state-of-the-art CT scanners, 2 1.5-T GE MR scanners, as well as 2.0-T small-bore units for animal research. The University of Massachusetts Medical Center is very active academically. Numerous radiologic, clinical, and basic science conferences are scheduled on a daily basis, and there is ample time during the course of the yr to attend many of these presentations. There are many on-going research projects. The fellowship position carries the title of instructor in radiology. For further information, contact Ronald L. Ragland, M.D., Chief, Division of Neuroradiology, University of Massachusetts Medical Center, 55 Lake Ave., N., Worcester, MA 01655; (508) 856-2215. The University of Massachusetts Medical Center is an affirmative action/equal opportunity employer. 10xc

FELLOWSHIP POSITIONS—The Dept. of Radiology, University of Arkansas for Medical Sciences, Little Rock, AR, has openings for fellowships to begin July 1992. Positions are available in body imaging/intervention, neuroradiology, vascular and interventional radiology, and pediatric radiology. Eligible candidates must be board-certified or eligible for certification in diagnostic radiology and should be eligible for licensing in the state of Arkansas. Interested candidates should contact the program directors: imaging/intervention — Teresita L. Angtuaco, M.D., or Steven K. Teplick, M.D.; neuroradiology — Edgardo J. C. Angtuaco, M.D.; vascular and interventional radiology — Ernest J. Ferris, M.D.; pediatric radiology — Joanna J. Siebert, M.D. All program directors listed above can be contacted at the Dept. of Radiology, University of Arkansas for Medical Sciences, Slot 556, 4301 W. Markham St., Little Rock, AR 72205; (501) 686-5740. The University of Arkansas for Medical Sciences is an affirmative action/equal opportunity employer. 10c

BREAST IMAGING FELLOWSHIP—The Susan G. Komen Breast Center in Peoria, IL, affiliated with St. Francis Medical Center, is offering a 1-yr fellowship in breast imaging beginning immediately. St. Francis Medical Center is a 750-bed, general hospital affiliated with the University of Illinois College of Medicine. The center is staffed with 2 radiologists devoted full time to breast imaging. Approximately 20,000 breast imaging studies are performed/yr. This 1-yr fellowship will provide exceptional experience in all aspects of breast imaging, including film/screen mammography and breast ultrasound. The fellow will also acquire skills in interventional procedures including ductography, preoperative localizations, cyst aspirations, and stereotactic needle biopsies (FNA and core biopsies). A 6-wk combined surgery and pathology rotation is provided to acquaint the fellow with surgical concerns in biopsies and mastectomies and to acquire a basic understanding of breast pathology. Opportunity exists and the fellow will be encouraged to participate in research projects relating to breast imaging. Send inquiries with CV to G. W. Eklund, M.D., Medical Director, Susan G. Komen Breast Center, 4911 Executive Dr., Ste. 300, Peoria, IL 61614. 8–10cp

FELLOWSHIPS AT THOMAS JEFFERSON UNIVERSITY HOSPITAL—The Dept. of Radiology at Thomas Jefferson University Hospital in Philadelphia offers the following fellowship programs each yr. Ultrasound/CT/MRI — Jefferson's ultrasound division is 1 of the largest in the world and performs all currently available exams including obstetric, vascular, lithotripsy, invasive, and endoluminal. We also operate 4 GE 1.5-T MRI units and 3 CT scanners. Contact Barry Goldberg, M.D., regarding this program. Cardiovascular/interventional — this division is housed in a new suite containing Philips angio units with DSA and performs the full range of vascular and non-vascular interventional procedures. Contact Geoffrey Gardiner, Jr., M.D. Neuro/ENT radiology — very active clinical services supply a wealth of material to this division, which is housed in a neurosciences imaging center containing all imaging modalities. Contact Carlos Gonzalez, M.D. Breast Imaging — Jefferson's new breast imaging center performs approximately 85 studies/day including ultrasound and needle localizations. Contact Stephen Feig, M.D. Chest — includes biopsies and CT. Contact Robert Steiner, M.D. MRI — a dedicated body MRI program including excellent research opportunities in addition to a large clinical case load. Contact Matthew Rifkin, M.D. Ultrasound — a dedicated ultrasound program. Contact Barry Goldberg, M.D. Musculoskeletal — includes MRI of the musculoskeletal system. Contact David Karasick, M.D. All program directors listed above can be contacted at the Dept. of Radiology, Thomas Jefferson University Hospital, Philadelphia, PA 19107. Jefferson is an equal opportunity/affirmative action employer. 10xc

MRI FELLOWSHIP AVAILABLE 1992—One-yr fellowships in MRI at MetroHealth Medical Center, Cleveland, OH, are available starting July 1992. Ideal candidates will have completed an approved diagnostic radiology residency program and have an interest in research as he/she will be responsible for a specific research project during the fellowship. The Dept. of Radiology is an active, academic dept. with state-of-the-art equipment in angiography, CT, ultrasound, and nuclear medicine and an approved residency program. The MR section includes a 1.5-T imager (2nd system will be installed in Fall 1991), independent development workstation, 3-D engine (Voxel-Flinger), RF lab, and Starden Titan minicomputer. The research group includes 4 Ph.D. scientists and 4 graduate students. MetroHealth Medical Center is a 1000-bed teaching hospital affiliated with Case Western Reserve University and provides tertiary care in the Cleveland metropolitan area. Interested candidates should forward CV, a letter outlining expectations in the fellowship, and other pertinent information to Errol M. Bellon, M.D., Director, Dept. of Radiology, MetroHealth Medical Center, 3395 Scranton Rd., Cleveland, OH 44109; fax (216) 459-4072. MetroHealth Medical Center and Case Western Reserve University are equal opportunity employers. 8–10c

FELLOWSHIP IN VASCULAR/INTERVENTIONAL RADIOLOGY—The University of Arizona in Tucson has a 1-yr fellowship opening in vascular/interventional radiology beginning July 1, 1992. The full spectrum of vascular and interventional procedures are performed by the section. Tucson is a desirable part of the country, where our competitive salary and reasonable cost of living assure an enjoyable stay as well as an academically productive experience. An informational videotape is available if desired. Applicants must be board-eligible and must submit a recent CV and 3 letters of recommendation including 1 from the program chairman. For further information, please contact Linda Fowler; (602) 694-7136. 8–10cp

VASCULAR AND INTERVENTIONAL RADIOLOGY FELLOWSHIP—The University of South Florida, Dept. of Radiology, will offer a 1-yr fellowship in vascular and interventional radiology beginning July 1, 1992. Clinical experience will include the full range of interventional procedures including vascular, biliary and endourologic procedures, as well as abscess drainage and percutaneous biopsy. The fellow will rotate between the H. Lee Moffitt Cancer Center and Research Institute, the James A. Haley VA Hospital, and the Tampa General Hospital. There is active, ongoing clinical research. Interested candidates contact Steven Morse, M.D., Associate Professor of Radiology, University of South Florida, Director of Vascular Radiology, Moffitt Cancer Center and Research Institute, P. O. Box 280179, Tampa, FL 33682-0179; (813) 972-8425. 9–11cp

FELLOWSHIP POSITIONS AVAILABLE 1992—One-yr fellowships in cross-sectional imaging (includes CT/ultrasound/MRI), angiography/interventional radiology, and MRI at MetroHealth Medical Center, Cleveland, OH, are available starting July 1992. Ideal candidates will have completed an approved diagnostic radiology residency program and have an interest in research as he/she will be responsible for a specific research project during the fellowship. The Dept. of Radiology is an active, academic dept. with state-of-the-art equipment in angiography, CT, ultrasound, and MRI and an approved residency program. MetroHealth Medical Center is a 1000-bed teaching hospital affiliated with Case Western Reserve University and offers attractive compensation and benefits. Interested candidates should forward CV, a letter outlining expectations in the fellowship, and other pertinent information to Errol M. Bellon, M.D., Director, Dept. of Radiology, MetroHealth Medical Center, 3395 Scranton Rd., Cleveland, OH 44109; fax (216) 459-4072. MetroHealth Medical Center and Case Western Reserve University are equal opportunity employers. 8–10c

IMAGING FELLOWSHIP—A 1-yr fellowship in ultrasound, MRI, and body CT is available July 1, 1992–June 30, 1993, at a 576-bed teaching hospital. The Dept. of Radiology performs more than 140,000 exams with state-of-the-art equipment. The ultrasound section is responsible for all aspects of sonography including OB-GYN, pediatric, abdominal, and small parts. Extensive training in color flow imaging, duplex Doppler, transvaginal, transrectal techniques, and sonographically guided procedures. Two GE MRI scanners and 2 GE 9800 Quick CT units provide high-volume caseloads in these areas. Opportunities are available for participation in imaging research. For further information, please contact Marcela Bohm-Velez, M.D., Imaging Fellowship Director, West Penn Hospital, 4800 Friendship Ave., Pittsburgh, PA 15224. 5–10c

MUSCULOSKELETAL RADIOLOGY FELLOWSHIP—Applications are now being accepted for a musculoskeletal fellow position for 1992 at the Cleveland Clinic Foundation (CCF). CCF is a 1000-bed, tertiary-care, teaching medical center with a large radiology residency program. Local, national, and international patients provide an interesting and varied mix of bone pathology. Training includes all aspects of musculoskeletal radiology including MR, CT, arthrography, biopsy, bone densitometry, and a large plain film experience. Fellowship includes patient care, teaching, and research. There is a close working relationship with the orthopedic, rheumatology, and endocrinology depts. There are presently 4 musculoskeletal staff in the section. For further information, please contact Bradford J. Richmond, M.D., Head, Section of Musculoskeletal Radiology, Desk A-21, 9500 Euclid Ave., Cleveland, OH 44195; (216) 444-3931. 5–10c

FELLOWSHIP IN BODY MRI, THOMAS JEFFERSON UNIVERSITY HOSPITAL—The Dept. of Radiology at Thomas Jefferson University Hospital has an unexpected opening for a 1-yr MRI fellow beginning July 1, 1992. This is an active body MRI section that encompasses a clinical mix of approximately 50% musculoskeletal and 50% chest/abdomen/pelvis cases. Equipment includes 4 1.5-T GE Signa systems with state-of-the-art and advanced prototype hardware and software. Ample opportunity for research is provided. The dept. has excellent research facilities and support, including 2 MRI physicists, a radiology animal facility, radiology research funding, and a team of research assistants. Interested candidates should contact Donald G. Mitchell, M.D., Director of MRI, Dept. of Radiology, 1032 Main Bldg., Thomas Jefferson University Hospital, Philadelphia, PA 19107; (215) 955-4809. Jefferson is an equal opportunity/affirmative action employer. 8–1c

ONCOLOGY/MAMMOGRAPHY FELLOWSHIP The Dept. of Radiology at the Dana-Farber Cancer Institute and Brigham and Women's Hospital, Harvard Medical School affiliates, offers a 1-yr fellowship position beginning July 1, 1992. All imaging modalities involved in the diagnosis, staging, and follow-up of patients with malignant disease are integrated into this program. An additional feature is a concentrated experience in the performance of interventional breast diagnostic procedures. Please contact Jack E. Meyer, M.D., Director of Diagnostic Radiology, Brigham and Women's Hospital and Dana-Farber Cancer Institute, 75 Francis St., Boston, MA 02115; (617) 732-6269. Brigham and Women's Hospital/Dana-Farber Cancer Institute/Harvard Medical School is an affirmative action/equal opportunity educator and employer. 9–2c

RADIOLOGY RESIDENCY POSITION—Unexpected immediate opening for an R3- or R4-radiology resident commencing July 1991 at Sacred Heart Medical Center (SHMC) in Spokane, WA. SHMC is a large, 650-bed tertiary-care hospital with a state-of-the-art radiology dept. The 11-member faculty are all fellowship trained. Residency program currently includes 2 residents/yr. Please direct all inquires to Royce L. Zobell, M.D., Program Director, Dept. of Radiology, Sacred Heart Medical Center, W. 101 8th Ave., TAF-C9, Spokane, WA 99220; (509) 455-3020. 10xcp

Tutorials/Courses

CARIBBEAN CRUISE—BREAST IMAGING AT SEA—Jan. 12–19, 1992. Faculty: Drs. Dorit Adler and Terry Silver. CME I. Medical Seminars International, 18981 Ventura Blvd., Ste. 303, Tarzana, CA 91356; (818) 774-9077. 9–12d

CARIBBEAN CRUISE—MRI AT SEA—Jan. 19–26, 1992. Faculty: Drs. William G. Bradley, Rosalind Dietrich, and Ronald J. Friedman. CME I. Medical Seminars International, 18981 Ventura Blvd., Ste. 303, Tarzana, CA 91356; (818) 774-9077. 9–12d

AJR Classified Advertisements Information

Box Responses and Address for Ad Placement

Write Box _____, *AJR*, 2223 Avenida de la Playa, Suite 103, La Jolla, CA 92037-3218; Telephone: (619) 459-2229; FAX: (619) 459-8814.

How to Place an Ad

AJR accepts classified advertising for Positions Available, Positions Desired, Fellowships and Residencies, and Tutorials/Courses. Ads are accepted by mail or FAX.

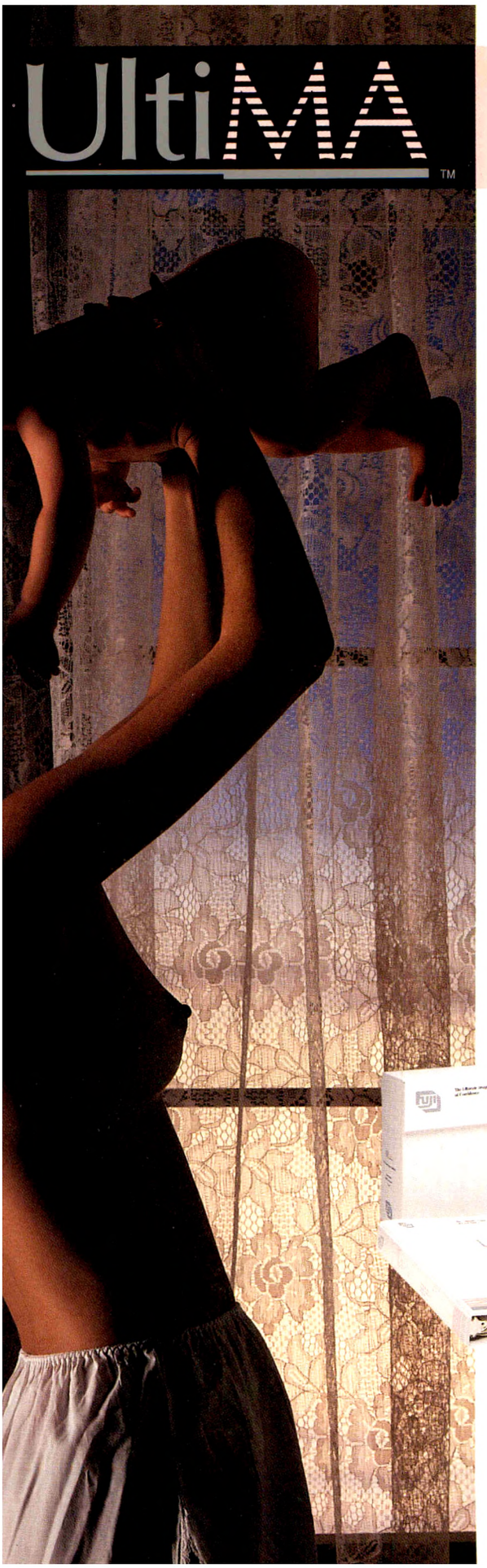
Rates: $6.00/line with a $30 minimum charge. Box service is $10 additional for each month the ad appears. There are discounts for multiple insertions: 10% for 2–3 insertions; 20% for 4 or more. To estimate lines, count all words and divide by 7.

Billing: Ads *must* be prepaid, or advertisers will be billed after the ad appears *providing* a purchase order number is submitted with the advertising copy. Terms are net 30 days.

Deadlines: 6 weeks prior to issue date. For specific deadlines, telephone the *AJR* editorial office.

Estimating Ad Charges

Line charge: divide total words by 7 and multiply by $6.00	$
Multiple insertions? If so, multiply by number	×
Subtotal	$
Discount applies to two or more insertions. Subtract 10% if ad appears 2–3 months; 20% if 4 months or more	−
Subtotal	$
Box response requested? If so, multiply number of months by $10.00	+
Approximate advertising charge	$



The Ultimate Image of Confidence.

Fuji introduces UltiMA... the ultimate imaging systems for mammography.

Here are the mammography systems you have been waiting for. Fuji has created UltiMA to provide you and your patients with the assurance that ultimate imaging technology is employed for every breast exam.

No other system can surpass the image quality and diagnostic information delivered by the unique combination of UltiMA films, intensifying screens, cassettes and Computed Radiography.

Fuji's UltiMA Quality Assurance Management Program provides further confidence that the UltiMA systems deliver the ultimate in image quality.

For further details, contact your Fuji representative today, or call 1-800-431-1850, (In CT 353-0300).



A new way of seeing things.

REVIEW ARTICLES

675 **Hysterosalpingography in the 1990s.** *Yoder IC, Hall DA*
685 **Percutaneous procedures for the diagnosis and treatment of lower back pain: diskography, facet-joint injection, and epidural injection.** *El-Khoury GY, Renfrew DL*

THORACIC RADIOLOGY

693 **Chronic diffuse infiltrative lung disease: comparison of diagnostic accuracy of high-resolution and conventional CT.** *Leung AN, Staples CA, Müller NL*
697 **Paraquat poisoning: findings on chest radiography and CT in 42 patients.** *Im J-G, Lee KS, Han MC, Kim SJ, Kim IO*
703 **Diagnosis and localization of laceration of the thoracic duct: usefulness of lumphangiography and CT.** *Sachs PB, Zelch MG, Rice TW, Geisinger MA, Risius B, Lammert GK*
707 **Pictorial essay. Normal anatomy of the thoracic inlet as seen on transaxial MR images.** *Spring Bi, Schiebler ML*

BREAST RADIOLOGY

711 **Localization and needle aspiration of breast lesions: complications in 370 cases.** *Helvie MA, Ikeda DM, Adler DD*
715 **Phylloides tumor: findings on mammograhy, sonography, and aspiration cytology in 10 cases.** *Buchberger W, Strasser K, Heim K, Müller E, Schröcksnadel H*

GASTROINTESTINAL RADIOLOGY

721 **Value of dual-energy CT in differentiating focal fatty infiltration of the liver from low-density masses.** *Raptopoulos V, Karellas A, Bernstein J, Reale FR, Constantinou C, Zawacki JK*
727 **Differentiation between hemangiomas and metastases of the liver with ultrafast MR imaging: preliminary results with T2 calculations.** *Goldberg MA, Saini S, Hahn PF, Egglin TK, Mueller PR*
731 **Detection of hepatic masses in patients with carcinoma: comparative sensitivities of sonography, CT, and MR imaging.** *Wernecke K, Rummeny E, Bongartz G, et al.*
741 **Pictorial essay. MR imaging in hydatid disease.** *von Sinner W, te Strake L, Clark D, Sharif H*
747 **Gallstone lithotripsy: results when number of stones is excluded as a criterion for treatment.** *Zeman RK, Davros WJ, Goldberg JA, et al.*
753 **Gallbladder contractility: variation in normal subjects.** *Donald JJ, Fache JS, Buckley AR, Burhenne HJ*
757 **Pictorial essay. CT appearance of splenic injuries managed nonoperatively.** *Do HM, Cronan JJ*
761 **The value of barium as a gastrointestinal contrast agent in MR imaging: a comparison study in normal volunteers.** *Ros PR, Steinman RM, Torres GM, et al.*
769 **Enteral feeding tubes: placement by using fluoroscopy and endoscopy.** *Ott DJ, Mattox HE, Gelfand DW, Chen MYM, Wu WC*
773 **Case report. Systemic *Yersinia enterocolitica* infection associated with iron overload and deferoxamine therapy.** *Abcarian PW, Demas BE*

GENITOURINARY RADIOLOGY

777 **Percutaneous biopsy of left adrenal masses: prevalence of pancreatitis after anterior approach.** *Kane NM, Korobkin M, Francis IR, Quint LE, Cascade PN*
781 **Case report. Castleman disease of the adrenal gland: MR imaging features.** *Debatin JF, Spritzer CE, Dunnick NR*
785 **Case report. Cystic carcinoma of the prostate: findings on transrectal sonography.** *Llewellyn CH, Holthaus LH*
787 **Case report. Diagnosis of gestational trophoblastic disease: value of endovaginal color flow Doppler sonography.** *Desai RK, Desberg AL*

MUSCULOSKELETAL RADIOLOGY

789 **Indications for radiography in patients with acute ankle injuries: role of the physical examination.** *Auletta AG, Conway WF, Hayes CW, Guisto DF, Gervin AS*
793 **Pictorial essay. Sonography of the normal elbow.** *Barr LL, Babcock DS*
799 **Osteoarthritis of the knee: comparison of radiography, CT, and MR imaging to assess extent and severity.** *Chan WP, Lang P, Stevens MP, et al.*
807 **Diagnosis of osteomyelitis in the presence of soft-tissue infection and radiologic evidence of osseous abnormalities: value of leukocyte scintigraphy.** *Jacobson AF, Harley JD, Lipsky BA, Pecoraro RE*
813 **Pictorial essay. Abnormalities of the foot in patients with diabetes mellitus: findings on MR imaging.** *Moore TE, Yuh WTC, Kathol MH, El-Khoury GY, Corson JD*
817 **Case report. Septic arthritis of the hip: a complication of a rectal tear associated with pelvic fractures.** *Magen AB, Moser RP Jr, Woomert CA, Guidici MAI*

PEDIATRIC RADIOLOGY

819 **Arteriopathy and coarctation of the abdominal aorta in children with mucopolysaccharidosis: imaging findings.** *Taylor DB, Blaser SI, Burrows PE, Stringer DA, Clarke JTR, Thorner P*
825 **Review. Response of osteosarcoma and Ewing sarcoma to chemotherapy: imaging evaluation.** *Fletcher BD*
835 **Case report. Distal aortopulmonary window with aortic origin of the right pulmonary artery and interruption of the aortic arch (Berry syndrome): diagnosis by MR imaging.** *Yoo S-J, Choi HY, Park I-S, Hong CY, Song MG, Kim SH*

NEURORADIOLOGY

837 **Optimizing brain MR imaging protocols with gadopentetate dimeglumine: enhancement of intracranial lesions on spin-density- and T2-weighted images.** *Wessbecher FW, Maravilla KR, Dalley RW*
843 **Intracerebral gangliogliomas in patients with partial complex seizures: CT and MR imaging findings.** *Tampieri D, Moumdjian R, Melanson D, Ethier R*
851 **MR imaging of reversible cyclosporin A–induced neurotoxicity.** *Truwit CL, Denaro CP, Lake JR, DeMarco T*
861 **Value of subtraction images in the detection of hemorrhagic brain lesions on contrast-enhanced MR images.** *Hanna SL, Langston JW, Gronemeyer SA*
867 **Neurologic involvement in Behcet disease: imaging findings in 16 patients.** *Banna M, El-Ramahi K*

VASCULAR RADIOLOGY

873 **Technical note. Percutaneous retrieval of an embolized arterial sheath.** *Marcuzzi DW, Chisholm RJ*

MEETING NEWS

875 **Meeting news. Society of Thoracic Radiology ninth annual meeting and postgraduate course, May 1991.** *Whalen E*

OTHER CONTENT

706 **Figley Fellowship announcement**
719 **ARRS 1992 residents' award papers information**
720 **Medicine in American art**
746 **Forthcoming articles**
760 **List of book reviews**
772 **Books received**
792 **Radiologic–pathologic conference**
824 **Memorial, John W. Turner**
860 **Call for papers on neuroradiology**
882 **Letters**
889 **Review of current literature**
893 **News**
896 **ARRS 1992 meeting announcement, calls for papers and exhibits**
901 **American Roentgen Ray Society information**
902 **Classified advertisements**
A14 ***AJR* business and subscriber information**
A31 **Guidelines for authors**